*Irradiated Polyethylene III—Evidence for an Ionic Mechanism in Allyl-free Radical Formation**

I. AUERBACH

Radiation interacting with polyethylene forms alkyl ions which in turn provide allyl-free radicals. Charge and radical migration mechanisms are considered for the processes whereby reactivity is transferred from the initial alkyl ion to the allyl radical site. The following observations provide evidence for a charge migration mechanism. (1) An ionic mechanism which would involve a charge migration process would be expected to be intramolecular in character whereas a radical mechanism would not be restricted to intramolecular migration. Statistical models are considered for charge and radical migration and compared with experimental results. The comparative results favour a charge migration process. (2) The G values for vinyl decay in polyethylene and for the polymerization of lower molecular weight 1-olefins, which are known to undergo ionic rather than radical reactions, are sufficiently close to suggest that the same mechanisms are operative in both materials. (3) Radiation-induced ionic polymerizations show no dose-rate effect whereas radiation-induced free radical polymerizations are proportional to the square root of the radiation intensity. As allyl radical formation shows no dose-rate effect in this study, it provides additional evidence for an ionic process.

THIS report is a continuation of a study[1] that is concerned with the kinetics and mechanism of allyl-free radical formation in Marlex 50, a linear polyethylene. The purpose of this report is to provide additional evidence for the mechanism presented in the previous publication[1]. The mechanism is based on a sequence of reactions initiated by an alkyl ion whose charge delocalizes, migrates, and is captured by a vinyl or vinylene group, forming ions. The vinyl ion subsequently reacts with another vinyl group, forming a divinyl ion. The resultant divinyl and vinylene ions form allyl radicals following charge recombination.

It was assumed in the above reaction sequence that charge migration provided the means whereby reactivity was transferred from the alkyl group, where radiation interacted with the polyethylene chain, to the unsaturated groups where the allyl radicals were formed following charge recombination. An alternative mechanism for the transfer of reactivity would involve conversion of the alkyl ion to an alkyl radical, with subsequent migration of the radical to an unsaturated group where it would become an allyl radical.

More specifically, the purpose of this report is to provide evidence for a charge migration process in the mechanism for allyl radical formation in polyethylene. The evidence is provided by: (1) the intramolecular character of the migration process in allyl radical formation, (2) comparable G values for vinyl decay in polyethylene and for lower molecular weight 1-olefin (vinyl) type monomers, and (3) the absence of a dose-rate effect in vinyl decay.

*This work was supported by the United States Atomic Energy Commission.

The evidence is supported by the following observations. First, an ionic mechanism would involve a charge migration process which is intramolecular. A free radical mechanism, on the other hand, would involve migration processes that would not be restricted to an intramolecular process. To determine which process accounted best for the results in the present study, predicted relative rates from statistical models for intra- and inter-molecular processes were compared with experimental results. It was found that an intramolecular model and, hence, an ionic mechanism was favoured. Secondly, lower molecular weight 1-olefins undergo ionic polymerizations under radiation conditions. The similarity in the G values for vinyl decay in polyethylene and for the lower molecular weight olefins suggests that both types of materials react similarly. Thirdly, the yields for radiation-initiated free radical reactions depend on the square root of the radiation intensity whereas the yields for ionic reactions are dose-rate independent. As allyl radical formation in polyethylene is dose-rate independent[1], an ionic mechanism is favoured.

Early studies related to allyl radical formation emphasized radical migration processes[2–5]. More recently, however, the role of the ion in radiation chemistry has been more carefully assessed and ionic mechanisms are considered instrumental in a number of reactions initiated by radiation in saturated and unsaturated hydrocarbons. Reviews on this subject are available[6, 7]. In a recent publication[8] related to vinyl group decay in polyethylene, the authors also favoured an ionic mechanism.

RESULTS AND DISCUSSION

Intramolecular character of the ion capture process

Evidence for a charge migration process can be derived from a consideration of the mechanism (intramolecular or intermolecular) which prevails in the transfer of the reactivity site from the initially formed alkyl ion to the relatively stable allyl radical. Two statistical models for the transfer of reactivity—a model based on an ionic mechanism which would be intramolecular in character and a free radical mechanism which would not be restricted to an intramolecular migration process—are examined.

The model for the charge migration process assumes the reaction sequence presented in the previous publication[1] and summarized in the introduction of this paper. The free radical reaction sequence and mechanism are discussed by others[2–5]. Each mechanism provides a ratio for the relative capture probabilities of the vinyl and vinylene groups for the migrating charge or radical. These ratios are compared with the experimental values for the vinyl and vinylene reaction constants given in the previous publication[1].

The initial 3×10^{21} eV/g radiation dose period is considered. During this period, approximately 90 per cent of the vinyl groups decay and an equivalent number of vinylene groups are formed. As Marlex 50 polyethylene has, initially, about one vinyl group per molecule, each molecule will, therefore, average possession of one vinyl and one vinylene group during this radiation period. It is assumed that the vinylene groups will be formed at random positions along the polyethylene chain. It is also assumed that

the sites at which radiation interacts with the polyethylene molecule are randomly selected. Corrections are not made for the prevailing condition that exists initially when vinyl groups are in large excess and at the end of the above radiation period when vinylene groups are in large excess.

The probability that the delocalized charge will be captured by a vinyl or vinylene group will depend on two terms: a position probability term, i.e. the probability that the ion which is formed initially when radiation interacts with polyethylene will be formed between the vinyl and vinylene groups or outside these groups, and a capture probability term, i.e. the probability that the delocalized charge will be captured by one or other of these groups from each of the above positions.

The molecular structure of polyethylene that is assumed in this statistical model has the following form, $CH_2{=}CH(CH_2)_mCH{=}CH(CH_2)_nCH_3$ where m and n represent numbers of methylene groups. Assuming that the radiation will interact with the polyethylene molecule on either side of the vinylene group with equal probability, i.e. with an m designated methylene group, position 1, or an n designated methylene group, position 2, then the position probability, P, that the ion will be formed in position 1 or 2 can be represented as P_1 or P_2 or, in general, P_n. P_1 and P_2 will have values of 1/2.

The probability that the charge associated with the initial ion will, on delocalization, be captured by a vinyl or vinylene group will depend on the location of the charge. If in position 1, then the probability that the vinyl or vinylene group will capture the charge, P_1(Vi) or P_1(Vl), respectively, is assumed to be the same and will have a value of 1/2. If in position 2, then the charge will always encounter the vinylene group first as it migrates along the alkyl chain. Hence P_2(Vl) = 1 and P_2(Vi) = 0.

The overall probability that radiation energy interacting with a polyethylene molecule will manifest itself as a charge on a vinyl or vinylene group will be a product of the position and the capture probability terms. Thus,

$$P(\text{Vl}) = P_n\,[P_1(\text{Vl}) + P_2(\text{Vl})] = 3/4 \tag{1}$$

and

$$P(\text{Vi}) = P_n\,[P_1(\text{Vi}) + P_2(\text{Vi})] = 1/4 \tag{2}$$

The probability that the charge will occur on a vinylene rather than on a vinyl group will be the ratio of equations (1) and (2), or

$$P(\text{Vl})/P(\text{Vi}) = 3 \tag{3}$$

The above relationships can be used to predict the ratio of the reaction constants that are related to the competitive behaviour of vinyl and vinylene groups for the delocalized charge. To obtain this ratio, however, the value realized from equation (3) should be corrected for the experimental observation, noted in the previous publication[1], that the vinyl groups react in pairs. P(Vi), therefore, becomes 1/2 rather than 1/4, and P(Vl)/P(Vi) becomes 1·5 instead of 3.

Validity for this statistical model is obtained from the values for the experimentally determined reaction constants in allyl radical formation provided in the previous publication[1]. The reaction constants, k_{1R} and k_{2R}, represent charge capture probabilities for vinyl and vinylene groups, res-

pectively, which were evaluated from radical formation data. Their values are given in *Table 2* of the previous publication[1]. The validity for the statistical model is shown in terms of the ratio k_{2R}/k_{1R} which corresponds to $P(Vl)/P(Vi)$ and which has a value of 2·10. This value compares favourably with the calculated value of 1·5.

The corresponding reaction constant values that were obtained from vinyl decay data[1] also provide values for the same ratio which correlate well with the 1·5 value obtained from statistical considerations. These data must be corrected, however, because of the factor of two difference that exists between the radical formation and the vinyl decay reaction constants. The factor of two arises from the fact that a radical is formed for every vinyl group that is lost, i.e. charge capture occurs each time a radical is formed. For vinyl decay, however, each time charge capture occurs, two vinyl groups are involved in the decay process. Thus, the reaction constant k_{1Vi} associated with charge capture by vinyl groups and whose value is obtained from vinyl decay data must be doubled. The corresponding reaction constant for charge capture by vinylene groups, k_{2Vi}, is divided by two for comparable consideration because an approximate factor of two difference also exists here. The two sets of vinyl decay data in *Table 2* of the previous publication[1] provide k_{2Vi}/k_{1Vi} values of 1·88 and 2·32. These are, again, reasonably close to the calculated value of 1·5 and suggest that the statistical model is appropriate.

In contrast with the above mechanism for allyl radical formation, which is based on charge migration, is the possible mechanism that allyl radical formation takes place by a radical migration process. This mechanism has been discussed in detail[2–5].

It is assumed in the radical migration mechanism that hydrogen atoms and alkyl radicals, which are formed during the radiation process, extract allyl hydrogen atoms adjacent to the vinyl and vinylene groups, that the allyl hydrogens of both groups are equally reactive toward hydrogen-atom extracting reactants and that the reactions are intermolecular in character, in the absence of evidence for an exclusively intramolecular free radical migration reaction. As the reactant is not affected by the relative positions of the vinyl and vinylene groups, the probability that a reactant will encounter an allyl hydrogen adjacent to either unsaturated group will be proportional to its concentration. Over the 3×10^{21} eV/g dose range that the vinyl groups decay, an equivalent number of vinylene groups will appear. Thus, the probabilities for a vinyl or vinylene allyl hydrogen being extracted are equal and $P(Vl)/P(Vi)=1$.

As shown in the previous publication, vinyl groups react in pairs when allyl radicals are formed from this group. Therefore, vinyl groups would react twice as rapidly as vinylene groups and provide radicals twice as rapidly. If this additional factor is introduced in the determination of the probability ratio of one for comparison with the reaction constant ratios of k_{2R}/k_{1R} or k_{2Vi}/k_{1Vi}, a value of 0·5 is obtained. It is evident that the experimental values of 2·10, 1·88 and 2·32 for the ratios of the reaction constants correlate better with the result of the charge migration or ionic mechanism model for vinyl decay and allyl radical formation than with that for the radical migration mechanism.

Comparative olefin data

A second source of evidence for a charge migration process is found in a comparison between the G values for vinyl decay in polyethylene, $G(-\mathrm{Vi})$, and in lower molecular weight 1-olefins, $G(-\mathrm{M})$. The comparative values are sufficiently similar to suggest that polyethylene and the lower molecular weight 1-olefins undergo the same reactions during irradiation. This conclusion was derived from the following studies.

1-Hexene and 1-octene were irradiated with γ-rays and electrons[9], and an average value for $G(-\mathrm{M})$ of 15·3 was obtained. The γ-ray polymerization of 1-hexadecene was studied by others[10] who obtained a $G(-\mathrm{M})$ value of 16·4 for the liquid monomer and for solid monomer when some polymer was present.

The value for pure solid 1-hexadecene, 33·1, is not relevant to the present study in which a comparison with polyethylene is being made, as an amount of polymer which may be as small as seven per cent changes the $G(-\mathrm{M})$ value to 16·4. The value of 16·4 is more appropriate for the above comparison of G values because polymeric matrices would be involved in both cases. The seven per cent value cited above was obtained from an empirical linear plot of data provided by Collinson *et al.*[10]. Log $G(-\mathrm{M})$ was plotted against the ratio of polymer weight to weight of 1-hexadecene, and extrapolated to a $G(-\mathrm{M})$ value of 16·4.

The $G(-\mathrm{Vi})$ values for Marlex 50 polyethylene which were used for comparison with those for the above olefins were obtained from the decay constants for vinyl groups. One of these values is provided in the previous publication[1], where it is indicated that vinyl group decay can be represented as a second-order process. The initial rate, $G(-\mathrm{Vi})$, can therefore be obtained from the relationship

$$-\mathrm{d}[\mathrm{Vi}_0]/\mathrm{d}D = k[\mathrm{Vi}_0]^2 \tag{4}$$

where $[\mathrm{Vi}_0]$ is the initial vinyl group concentration, D is the dose and k is the decay constant. Four other sets of data which are available in the literature[8, 11–13] were also used to obtain values for k. The initial vinyl group concentrations which were used were those associated with each set of vinyl group data. An average $G(-\mathrm{Vi})$ value of $14{\cdot}6 \pm 2{\cdot}4$ was obtained. The large average deviation is a reflection of the wide variation in the reported initial concentrations, $0{\cdot}85 \times 10^{-4}$ to $1{\cdot}21 \times 10^{-4}$ moles/g, rather than the decay constants, $2{\cdot}21 \pm 0{\cdot}35 \times 10^{-17}$ to $2{\cdot}67 \pm 0{\cdot}25 \times 10^{-17}$ (mole eV)$^{-1}$.

In addition to the above value for $G(-\mathrm{Vi})$, two additional values are available in the second table of the previous publication[1]. These were obtained from a kinetic expression in which $G(-\mathrm{Vi})$ was evaluated from an ion yield, φ, rather than from initial rates. Values of 13·1 and 16·4 were obtained by this method.

Of particular interest to this study is the close proximity in the values for $G(-\mathrm{Vi})$ for polyethylene and $G(-\mathrm{M})$ for the lower molecular weight 1-olefins. The correlation suggests that the same reactions are involved in both systems. Since both Chang *et al.*[9] and Collinson *et al.*[10] found their results to be explicable only if an ionic mechanism was assumed, the

correlation in $G(-\text{Vi})$ and $G(-\text{M})$ suggests that an ionic mechanism is also operative in the vinyl group decay for polyethylene.

Dose-rate effect

A third experimental source for evidence which supports an ionic rather than a free radical mechanism is the dose-rate effect. This effect is absent in allyl radical formation for polyethylene, as seen in the values for the radical formation reaction constants (*Table 1*[1]), and therefore in vinyl group decay as well. The dose-rate criterion is based on free radical polymerization rate studies in the liquid state which are generally proportional to $I^{1/2}$ where I is the dose rate[14]. Unequivocal radiation-induced ionic polymerizations are, on the other hand, dose-rate independent[15]. The absence of a dose-rate effect in the previous study[1] over a 28-fold variation in dose rate provides, therefore, additional evidence for the proposed ionic mechanism.

CONCLUSION

The mechanism for radiation-induced allyl free radical formation in polyethylene involves an ionic rather than a free radical migration process in the transfer of reactivity from the alkyl ion site to the allyl radical site.

Discussions with D. K. Brice and G. P. Steck are gratefully acknowledged.

Reentry Studies 9326,
Sandia Corporation, Sandia Base,
Albuquerque, N.M., U.S.A.

(*Received March 1967*)

REFERENCES

[1] AUERBACH, I. *Polymer, Lond.* 1967, **8**, 63
[2] KORITSKII, A. T., MOLIN, IU. N., SHAMSHEV, V. N., BUBEN, N. IA. and VOEVODSKII, V. V. *Vysokomol. Soedineniya.* 1959, **1**, 1182
[3] CHARLESBY, A., LIBBY, D. and ORMEROD, M. G. *Proc. Roy. Soc. A,* 1961, **262**, 207
[4] DOLE, M. and CRACCO, F. *J. phys. Chem.* 1962, **66**, 193
[5] ORMEROD, M. G. *Polymer, Lond.* 1963, **4**, 451
[6] WILLIAMS, F. *Quart. Rev. chem. Soc., Lond.* 1963, **17**, 101
[7] KEVEN, L. and LIBBY, W. F. *Advances in Photochemistry,* Vol. II. Interscience: New York, 1964
[8] DOLE, M., FALLGATTER, M. B. and KATSUURA, K. *J. phys. Chem.* 1966, **70**, 62
[9] CHANG, P. C., YANG, N. C. and WAGNER, C. D. *J. Amer. chem. Soc.* 1959, **81**, 2060
[10] COLLINSON, E., DAINTON, F. S. and WALKER, D. C. *Trans. Faraday Soc.* 1961, **57**, 1732
[11] LAWTON, E. J., BALWIT, J. S. and POWELL, R. S. *J. Polym. Sci.* 1958, **32**, 257
[12] DOLE, M., MILNER, D. C. and WILLIAMS, T. F. *J. Amer. chem. Soc.* 1958. **80**, 1580
[13] CHARLESBY, A., GOULD, A. R. and LEDBURY, K. J. *Proc. Roy. Soc. A,* 1964, **277**, 348
[14] CHAPIRO, A. *Radiation Chemistry of Polymeric Systems,* Chaps. IV–VII, Interscience: New York, 1962
[15] PLESCH, P. H. and PINNER, S. H. *Chemistry of Cationic Polymerization,* Chap. 17. Macmillan: New York, 1963

Turbidimetry as a Tool for the Characterization of Molecular-weight Distributions

C. F. CORNET

This paper deals with the use of turbidimetric measurements as a rapid method to characterize molecular-weight distributions of polymers. An important limitation of the method, not previously reported, is discussed. It is concluded that turbidimetry gives rapid qualitative information only on the high-molecular-weight side of the distribution curve.

THE need for reliable and preferably simple and rapid methods to determine the molecular-weight distribution (MWD) of polymer samples is obvious. The literature mentions quite a number of procedures for this purpose, most of them based on the molecular-weight-dependent solubility of polymers. A good review was recently given by Schneider[1]. The majority of techniques in use are laborious and very time-consuming. However, turbidimetry, gel permeation chromatography and, for some routine measurements, ultracentrifugation are relatively simple and rapid methods. This paper only discusses some aspects of turbidimetry.

THEORETICAL DISCUSSION

Limitations of turbidimetry

When a polymer is slowly precipitated from a dilute solution, either by cooling down or by adding non-solvent, fractionation takes place[2–17]. The highest-molecular-weight fractions are precipitated first, followed by those of decreasing molecular weight. This holds for the precipitation of both amorphous and crystalline polymer phases. But when a crystalline phase is separated, the molecular weight dependence is very small and may be obscured by the influence of structural chain properties on crystallization. We will therefore only discuss separations into two amorphous phases.

Precipitation gives rise to a turbidity, which may be measured photoelectrically in a turbidimeter or nephelometer. Turbidimetry is a technique allowing the turbidity to be recorded as a function of temperature or amount of non-solvent. A turbidigram is a plot of turbidity against temperature or amount of non-solvent and may be considered very roughly equivalent to a MWD curve. It is, however, very difficult and sometimes even impossible to find the correct MWD curve from a turbidigram, for the following reasons.

(1) The relation between turbidity and amount of polymer precipitated is very complex, because the turbidity depends on the composition of precipitate and solution and on the time-dependent size of the precipitated

particles. The problem has been dealt with by several authors[2–5] and will not be discussed here. Some authors[5–7] assume that under carefully selected experimental conditions turbidity is sufficiently proportional to the amount of polymer precipitated to obtain a reliable solubility curve. An approximate solubility distribution plot can thus be found from the corresponding turbidigram.

(2) The precipitation conditions depend not only on molecular weight but also on the fractional concentration of precipitating species[2, 5, 8–11]. This makes it impossible to convert a solubility curve directly into a MWD curve and makes exact calibration with monodisperse samples illusory. Some authors have developed rather complicated procedures to try and solve this problem [2, 12–14]. According to Brice[12] it is sometimes impossible to obtain the correct MWD from the solubility distribution curve even if sophisticated calculation procedures are used. Other authors [5–7] simply neglect the fractional concentration dependence and take the total polymer concentration in solution into account. This procedure may easily lead to erroneous results.

(3) In addition, we have now found another disturbing phenomenon, which, as far as we know, has not been reported before. The conditions under which a polymer fraction precipitates depend not only on its molecular weight and fractional concentration, but also on the presence of already precipitated fractions of higher molecular weight. This was shown by measurements* on dilute solutions of two poly (α-methylstyrene) samples (PAMS) with a very narrow MWD and of a mixture of these samples and confirmed qualitatively by theoretical calculations, which will be discussed in the next section.

The above clearly shows that it is doubtful whether the turbidigram can yield the exact MWD; at best it could do so only after laborious and complicated calibration and computation. Consequently, turbidimetry completely loses its advantages over other techniques. A turbidigram can, however, supply qualitative information on the MWD, especially on the high-molecular-weight side, and is very useful to characterize roughly differences between the MWDs of homologous samples. Within this limited field of application turbidimetry has been used with more or less success by various workers (see e.g. refs. 2, 5–7 and 15–17).

Effect of precipitated polymer on precipitation conditions

The solubility of a monodisperse polymer fraction depends on its molecular weight and on the quality of the solvent. Experimental and theoretical work[10] has shown that at the verge of separation into two amorphous phases there is an approximately linear relationship between the logarithm of the volume fraction of polymer, φ, and the polymer–solvent interaction parameter, χ, as defined by Flory and Huggins (see e.g. ref. 8). The parameter χ varies approximately linearly with the reciprocal absolute temperature T^{-1}.

*See Experimental part.

The relations between polymer concentration at incipient turbidity and the corresponding solvent quality parameters are approximated by:

$$\chi - \tfrac{1}{2} = -K \log \varphi \tag{1}$$

and

$$T^{-1} - \theta^{-1} = -K^0 \log \varphi \tag{2}$$

where θ is the θ-temperature (see e.g. refs. 8 and 10) and K and K^0 are constants depending on the molecular weight of the polymer and on the system considered. Similar relations are often quoted in the literature (see e.g. refs. 2, 4, 9, 11, 13 and 17).

The precipitation of a strictly monodisperse polymer fraction can now be described with equations 1–2. The situation for a system with initial polymer volume fraction φ^0 is shown graphically in *Figures 1* (a) and *1*(b).

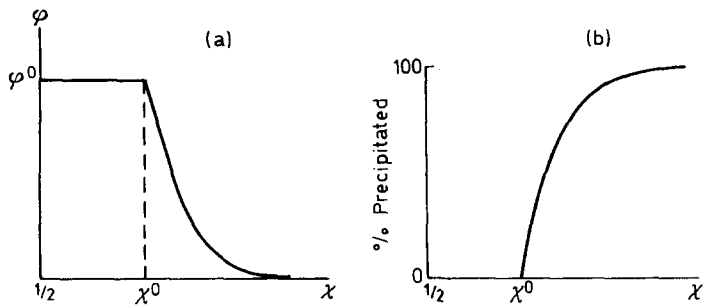

Figure 1(a)—φ versus χ; χ^0 corresponds to φ^0
Figure 1(b)—Percentage of polymer precipitated versus χ

Actual polymers are, however, never monodisperse and the precipitation behaviour is then more complicated. Many authors assume that the precipitation of a polymer fraction from a polydisperse sample is independent of the presence of other fractions and that the different fractions precipitate one after another. The precipitation curve is then divided into small parts which are considered to be the partial precipitation curves of the individual fractions. The value of the constants K or K^0 can then be found and so the molecular weight of each fraction calculated (see e.g. refs. 2 and 12–14).

However, our experiments on almost monodisperse PAMS samples revealed that the precipitation of the lowest-molecular-weight fraction is considerably influenced by the highest-molecular-weight fraction. In addition, it will be clear from *Figures 1*(a) and *1*(b) that fractions with closely neighbouring molecular weight can never precipitate separately. It seems therefore useful to try and calculate the precipitation curve of a polydisperse sample by means of an existing theory on polymer solubility. As the application of the simple Flory–Huggins theory in our previous work has given satisfactory results[10], we used it also for the above calculations. For the sake of simplicity we only considered a polymer–single-solvent system.

The chemical potentials of solvent, $\Delta\mu_s$, and polymer component i, $\Delta\mu_i$, in a polydisperse polymer–solvent system are given by[8]:

$$\Delta\mu_s = RT\left[\ln\varphi_s + 1 - \varphi_s - \sum_i\left(\frac{\varphi_i}{m_i}\right) + \chi\left\{\sum_i(\varphi_i)\right\}^2\right] \tag{3}$$

and

$$\Delta\mu_i = RT\left[\ln\varphi_i - (m_i - 1) + m_i\sum_i(\varphi_i) - m_i\sum_i\left(\frac{\varphi_i}{m_i}\right) + \chi m_i\varphi_s^2\right] \tag{4}$$

R is the gas constant; φ_s and φ_i are the volume fractions of solvent and polymer component i, respectively, and m_i is the ratio between the molecular volumes of component i and the solvent. In a two-phase equilibrium system thermodynamics demand that

$$\Delta\mu_s' = \Delta\mu_s'' \quad \text{and} \quad \Delta\mu_i' = \Delta\mu_i'' \tag{5}$$

A single prime refers to the dilute solution and a double prime to the precipitate. Combination of equations (3) and (4) with (5) gives:

$$\chi(P^2 - Q^2) = \ln[(1-Q)/(1-P)] - (P-Q) + \sum_i[(\varphi_i'' - \varphi_i')/m_i] \tag{6}$$

and

$$(1/m_i)\ln(\varphi_i''/\varphi_i') = 2\chi(P-Q) - \ln[(1-Q)/(1-P)] \tag{7}$$

if

$$P = \sum_i(\varphi_i'') = 1 - \varphi_s'' \quad \text{and} \quad Q = \sum_i(\varphi_i') = 1 - \varphi_s'$$

When employing turbidimetry, the polymer concentration in the dilute solution is always taken very low, whereas the concentration in the precipitate is much higher. We are therefore justified in neglecting Q as compared with P. After rearrangement we then find

$$(1/m_i)\ln(\varphi_i''/\varphi_i') = (1 - 2/P)\ln(1-P) - 2 + (2/P)\sum_i[(\varphi_i'' - \varphi_i')/m_i] \tag{8}$$

and

$$\chi = -(1/P^2)[P + \ln(1-P)] + (1/P^2)\sum_i[(\varphi_i'' - \varphi_i')/m_i] \tag{9}$$

A mass balance of a two-phase multicomponent polymer–solvent system shows that

$$V_0\varphi_i^0 = V_s\varphi_i' + V_p\varphi_i'' \tag{10}$$

and

$$V_0 R = V_s Q + V_p P \tag{11}$$

V_0, V_s and V_p are the volumes of the original solution, of the dilute phase and of the precipitate, respectively; φ_i^0 is the volume fraction of polymer component i in the original solution and $R = \sum_i \varphi_i^0$. If we assume volume additivity, so that $V_0 = V_s + V_p$, we find that

$$\varphi_i' = \varphi_i^0(P-Q)/\{P - R + (R-Q)(\varphi_i''/\varphi_i')\} \tag{12}$$

The precipitation curve of any polymer sample is given by the relation between Q and χ, which can in principle be found by numerical computations using equations (8), (9) and (12). As a very simple model for a

polydisperse polymer sample we used a mixture of two strictly monodisperse fractions. In order to allow comparison of the results of these calculations with those of the experiments with PAMS samples we took $\varphi_1^0 = \varphi_2^0 = 10^{-5}$; $m_1 = 10^4$ and $m_2 = 2 \times 10^3$ (equivalent to molecular weights of about 10^6 and 2×10^5, respectively).

The calculation procedure is as follows. An arbitrary value for P and an estimated value for $\sum_i [(\varphi_i'' - \varphi_i')/m_i]$ are inserted into equation (8). The values of φ_1''/φ_1' and φ_2''/φ_2' can now be found. Approximate values for φ_1' and φ_2' are derived from equation (12) after insertion of an estimated Q. A better estimation of $\sum_i [(\varphi_i'' - \varphi_i')/m_i]$ can now be used and the process is repeated until all variables are in agreement with each other. The calculations have also been carried out for the individual fractions, again with $\varphi^0 = 10^{-5}$. The results are shown in *Figure 2*.

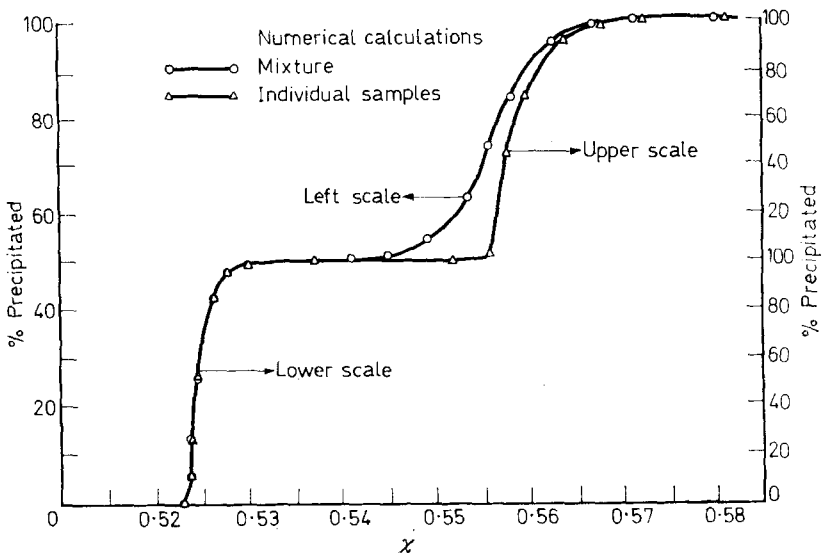

Figure 2—Relative amount of polymer precipitated versus polymer–solvent interaction parameter

It can be seen that the precipitation of the high-molecular-weight component in the mixture is not influenced by the presence of the low-molecular-weight component*, but the reverse is true.

EXPERIMENTAL

(a) *Apparatus*

The apparatus now in use is considerably more sophisticated than that described previously[10]. Whereas the old apparatus recorded the transmission of light through a cuvette, the new instrument measures a fixed proportion of the light scattered in a direction perpendicular to the incident

*This is in agreement with data of Klein and Patat[11].

beam. In this way sensitivity is much improved. In addition, the new apparatus measures the ratio between the amount of light scattered and the intensity of the incident beam via a ratio recording system, which leads to improved stability, A diagram is shown in *Figure 3*. The solution in the cuvette can be stirred and its temperature controlled to within 0·1 deg. C by means of an outside thermostatic bath in combination with a small heat exchanger in the cuvette.

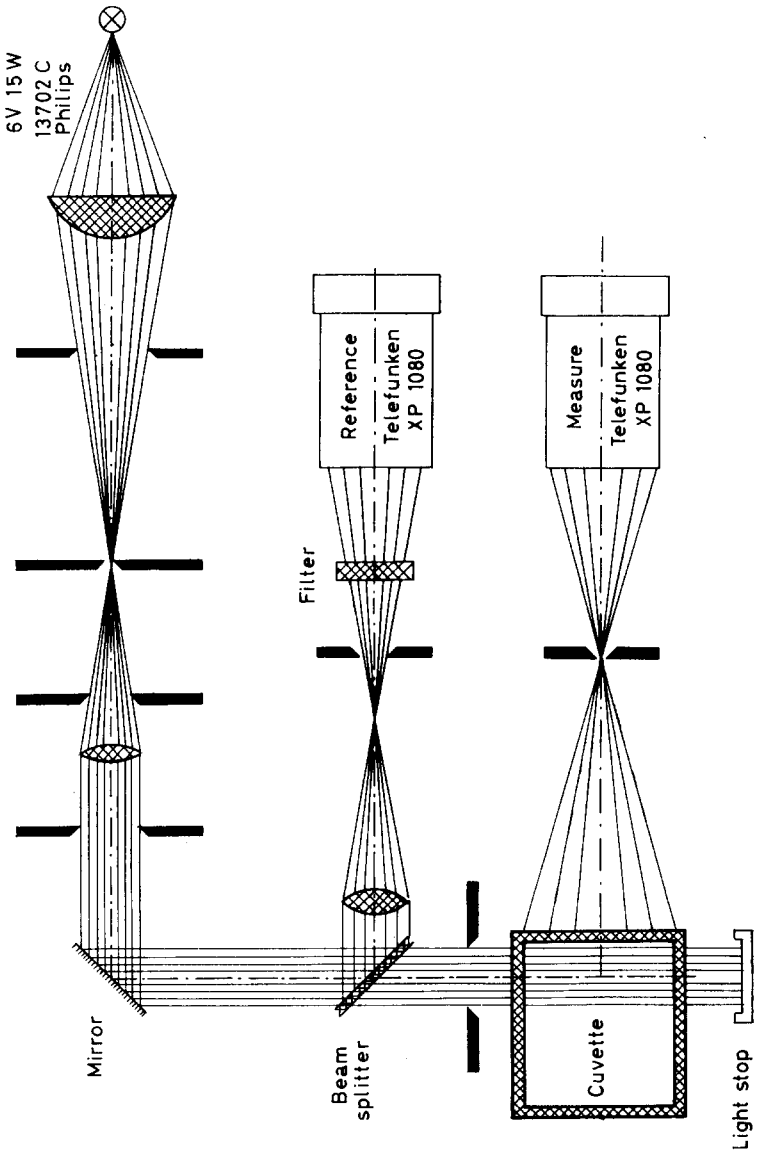

Figure 3—Turbidimeter system

(b) *Procedure*

A stirred dilute polymer solution is cooled down until the turbidity reaches an approximately constant level or until the precipitate begins to coagulate considerably. The rate of cooling is about 1 deg. C per minute. The output of the turbidimeter and the signal of a thermocouple placed in the solution are fed to an X/Y recorder (Moseley, 7030 AM), thus producing a turbidity/temperature plot. The turbidity is assumed to be proportional to the amount of polymer precipitated.

(c) *Measurements on poly (α-methylstyrene)*

We have used two PAMS samples, both prepared by anionic polymerization and purified by removal of the low-molecular-weight 'tail' by fractional precipitation. The molecular weights were approximately 10^6 (sample A) and 2×10^5 (sample B); the MWDs were very narrow.

A solution of sample A in methylcyclohexane with a polymer volume fraction of $1{\cdot}35 \times 10^{-5}$, a solution of sample B in the same solvent with a polymer volume fraction of $1{\cdot}40 \times 10^{-5}$ and a 1:1 mixture of these

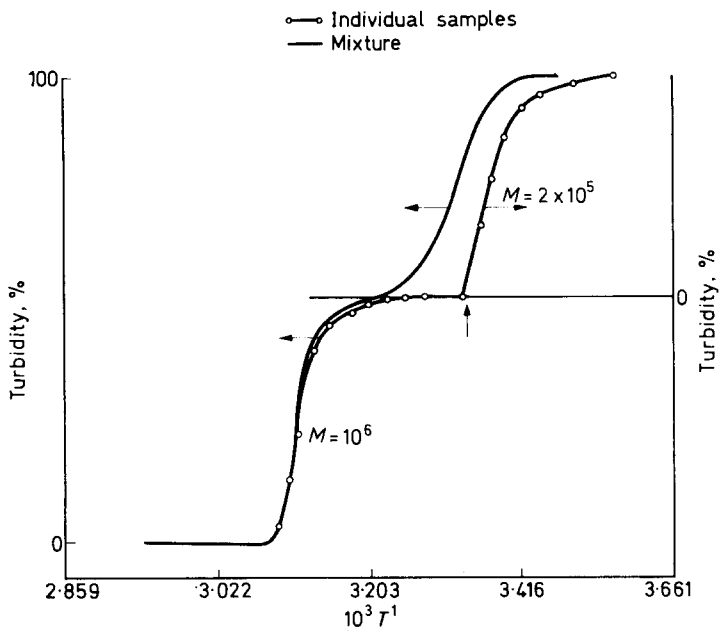

Figure 4—Percentage of total turbidity versus reciprocal absolute temperature

solutions were submitted to turbidimetric measurements. The turbidity, expressed as a percentage of the ultimate turbidity of the mixed system, was plotted against the corresponding temperature (see *Figure 4*).

CONCLUSIONS

We have shown experimentally and theoretically that turbidimetry is a simple method only when used to characterize the high-molecular-weight

side of the MWD. The interpretation of the low-molecular-weight side, if possible at all, would need very extensive computations, rendering the method cumbersome. It would therefore seem advisable to use turbidimetry only for the determination of θ-conditions[10] and, if other methods fail, for a rough characterization of MWDs of polymers.

Koninklijke/Shell-Laboratorium,
Amsterdam,
The Netherlands

(*Received April 1967*)

REFERENCES

[1] SCHNEIDER, N. S. *J. Polym. Sci. C*, 1965, **8**, 179
[2] GOOBERMAN, G. *J. Polym. Sci.* 1959, **40**, 469
[3] BEATTIE, W. H. *J. Polym. Sci. A*, 1965, **3**, 527
[4] RABEL, W. and ÜBERREITER, K. *Kolloidzschr. u. Z. Polym.* 1964, **198**, 1
[5] URWIN, J. R., MCKENZIE STEARNE, J., JORDAN, D. O. and MILLS, R. A. *Makromol. Chem.* 1964, **72**, 53
[6] GAMBLE, L. W., WIPKE, W. T. LANE, T. J. *appl. Polym. Sci.* 1965, **9**, 1503
[7] HARRISON, G. D. and PEAKER, F. W. *Soc. Chem. Ind. Monogr. No. 17*, 1963, 96
[8] FLORY, P. J. *Principles of Polymer Chemistry*, Cornell University Press: Ithaca, 1953
[9] PATAT, F. and KLEIN, J. *J. Polym. Sci. B*, 1965, **3**, 615
[10] CORNET, C. F. and VAN BALLEGOOIJEN, H. *Polymer, Lond.* 1966, **7**, 293
[11] GRUBER, U. and ELIAS, H. G. *Makromol. Chem.* 1964, **78**, 58
[12] BRICE, W. A. J. 'Molecular weight distribution curves obtained by turbidimetric titrations'. Lecture presented at the Faraday Society Informal Discussion on The Molecular Weight and Molecular Weight Distribution of High Polymers held on 30 March 1966, at Battersea College of Technology, London
[13] MOREY, D. R. and TAMBLYN, J. W. *J. appl. Phys.* 1945, **16**, 419
[14] CLAESSON, S. *J. Polym. Sci.* 1955, **16**, 193
[15] TANAKA, S., NAKAMURA, A. and MORIKAWA, H. *Makromol. Chem.* 1965, **85**, 164
[16] PRAVIKOVA, N. A., RYABOVA, L. G. and VYRSKII, Y. P. *Vysokomol. Soedineniya*, 1963, **5**, 1165
[17] HOWARD, G. J. *J. Polym. Sci. A*, 1963, **1**, 2667
[18] KLEIN, J. and PATAT, F. *Makromol. Chem.* 1966, **97**, 189

The Difference in Mechanical Properties of Fibres of Linear Polyesterurethanes, Prepared with Different Diamines

D. HEIKENS, A. MEIJERS and P. H. VON RETH

The initial modulus, the tensile strength and the elongation of linear soluble polyesterurethane fibres were shown to alternate with the number of carbon atoms of the built-in diamines.

AIM OF THE INVESTIGATION

THIS research was set up in order to examine the influence of possible physical crosslinks on the mechanical properties of chemically crosslinked polyurethane fibres. Therefore soluble fibres from linear polyesterurethanes were prepared, in which only physical crosslinks were present.

DESCRIPTION OF THE SAMPLES

Linear polyesterurethanes. Syntheses[1,2]

Chain formation was brought about in the following way. A linear polyester of adipic acid and ethyleneglycol of an average molecular weight of 2 000 (Desmopheen 2 000, Bayer) with alcoholic OH groups at the chain ends, was reacted with diphenylmethanediisocyanate (Desmodur 44, Bayer) in a molar ratio of 1 : 2 at 60°C.

An essentially linear macrodiisocyanate with urethane groups with an average molecular weight of about 2 500 was formed.

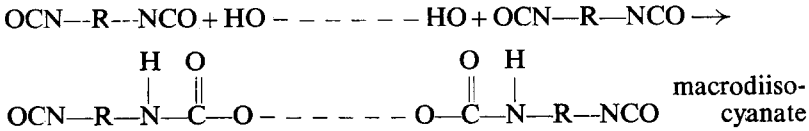

abbreviated as OCN———NCO

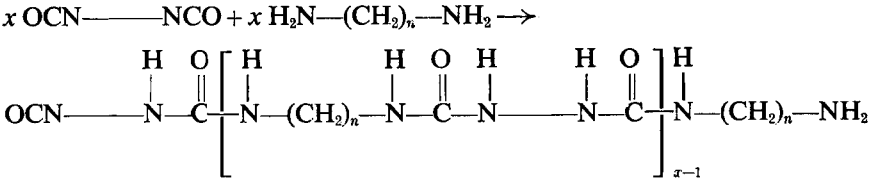

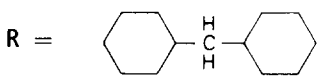

The macrodiisocyanate, dissolved in dimethylformamide (DMF) was reacted with a linear aliphatic *n*-diamine in a molar ratio of 1 : 1 to form longer linear macromolecules with urea groups. From this solution polyurethane fibres were made by wet-spinning into water at 20°C.

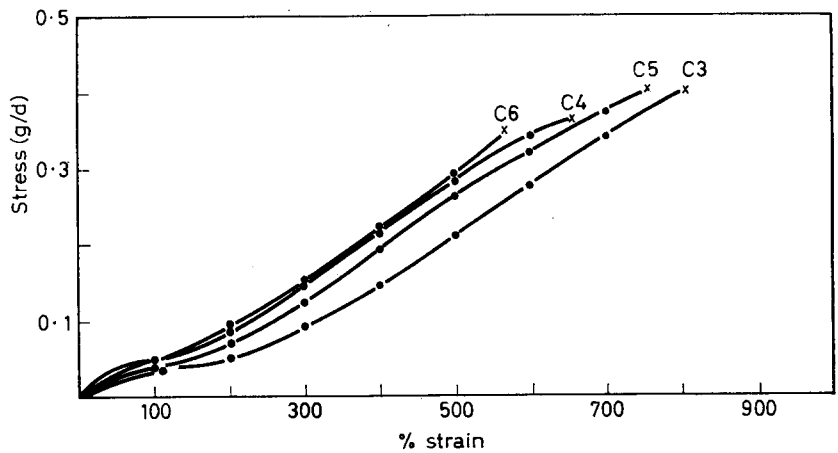

Figure 1(a)—Stress/strain curve of some linear polyesterurethane fibres (called C3, C4, C5, C6)

During preparation of the polymer and fibres the conditions were such that network formation by chemical crosslinks was avoided and fibres resulted, which were soluble in DMF. The fibres obtained were rubber-elastic and thus the molecules should be connected by physical crosslinks.

The intrinsic viscosity of our fibres, dissolved in DMF, was about 0·6.

Commercial fibres

Three types of commercial polyurethane fibres were taken for compari-

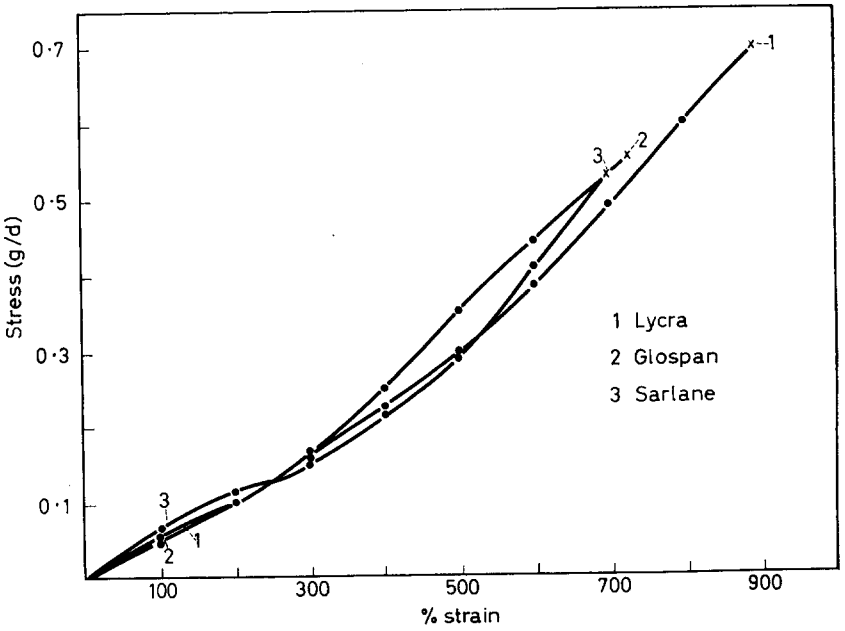

Figure 1(b)—Stress/strain curve of some commercial polyurethane fibres

son; two of them are not soluble in DMF and are supposed to contain chemical and physical crosslinks. These fibres are: Lycra® (type 124, Du Pont)[3–6], a chemical crosslinked polyetherurethane fibre; Glospan® (A.K.U.), a chemical crosslinked polyesterurethane fibre[7–8] and Sarlane® (U.C.B. Belgium), which is soluble in DMF.

MECHANICAL PROPERTIES AT ROOM TEMPERATURE (20°C)

Tensile strength, elongation at break and modulus were tested on an Instron Tensile Testing Machine (type TT-BM). All fibres were conditioned at 65 per cent relative humidity and a temperature of 20°C. The tensile strength, the elongation at break and modulus were measured on samples of length 5 cm at a straining rate of 200 per cent/min. For clearness of representation the results of only some of the fibres [*Figure 1*(a)] are given together with those of three commercial fibres [*Figure 1*(b)].

As *Figure 1*(b) shows, the commercial fibres have a higher tensile strength but about the same elongation at break. The difference may be caused by production techniques in industrial practice other than those used in our limited research, where optimal results were not aimed at.

Figures 2(a) and *2*(b) show that the tensile strength and the elongation at break oscillate with the number of carbon atoms in the diamines used

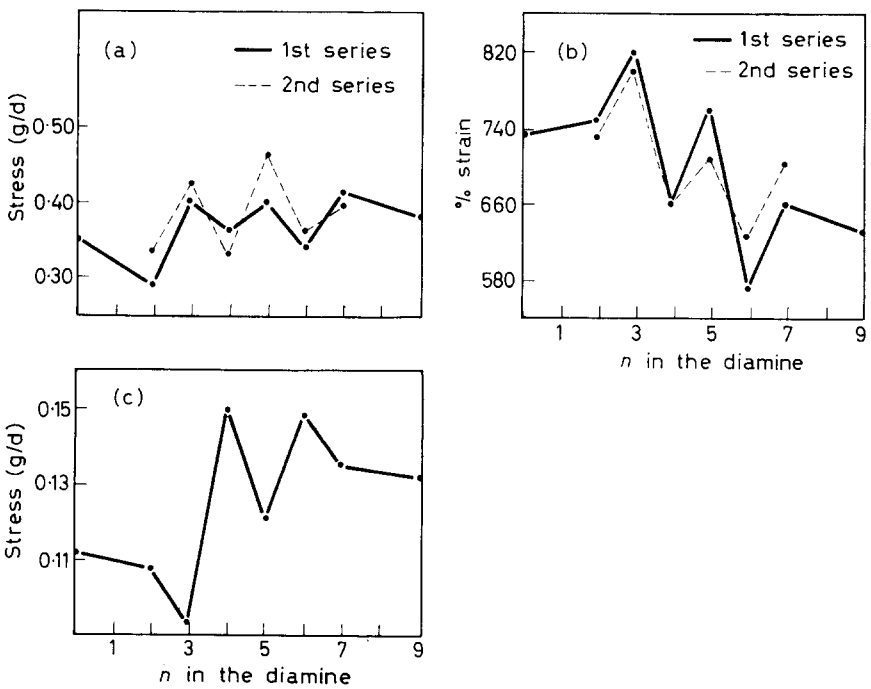

Figure 2(a)—Effect of number of carbon atoms in the diamine on the tensile strength
Figure 2(b)—Effect of number of carbon atoms in the diamine on the elongation at break
Figure 2(c)—Effect of number of carbon atoms in the diamine on the modulus (at 300 per cent)

for the preparation of the various fibres. The fibres with odd numbers of carbon atoms in the diamines have a higher tensile strength and elongation.

Figure 2(c) shows that the reverse is true for the modulus (stress at 300 per cent elongation), which is also oscillating. These unexpected results were confirmed by a second series of experiments in which fibres were spun from polymers from another, new batch. Though the values of the quantities measured were slightly different their dependence on the number of carbon atoms followed the same pattern. Part of the phenomena may be explained as follows. Rubberlike polymers have higher tensile strength if they crystallize at high elongation[9]. In a similar way it may be that intermolecular bonds are formed in our fibres; the strength of these may oscillate with the number of the carbon atoms of the diamines which form the hard blocks in the chains.

Research on this project will be continued.

Department of Chemical Technology,
Technological University,
Eindhoven, Netherlands

(*Received April 1967*)

REFERENCES

[1] RINKE, H. *Chimia*, 1962, **16**, 93
[2] BAYER, O. *Angew. Chemie*, 1947, **59**, 257
[3] BAMFORD, C. H. *J. Text. Inst.* 1965, **55**, No. 4, 84
[4] Du Pont de Nemours and Co. Inc. *U.S. Pat. No. 2 929 804*, 1955
[5] MEERWEIN, H., DELPH, D. and MARCHEL, H. *Angew. Chemie*, 1960, **72**, 927
[6] RINKE, H. *Agnew. Chemie* (*Internat. Edn*), 1962, **1**, 419
[7] Private communication.
[8] Globe Manufacturing Co.*Brit. Pat. No. 947 840*, 1964
[9] FLORY, P. J. *Principles of Polymer Chemistry*, p 482. Cornell University Press: Ithaca, 1957

On Crystallization Kinetics and Bulk Polymer Morphology II—Polypropylene*

IAN H. HILLIER

Crystallization kinetics of polypropylene, yielding non-integral values of the Avrami exponent, are analysed by a model which involves a density increase within the outline of the growing spherulites. The form of the rate law governing the density increase is examined and compared to that found by other workers.

THE crystallization kinetics of bulk polymers from the melt is traditionally described in terms of the growth of crystalline entities of definite geometric shape (i.e. rods, discs or spheres), having a constant density. This model leads to the well known Avrami equation[1],

$$\chi(a, t) = \chi(a, \infty)\,[1 - \exp(-Z_1 t^{n_1})] \qquad (1)$$

Here, $\chi(a, t)$ is the crystallinity of the sample at time t, $\chi(a, \infty)$ the limiting value of the crystallinity (at $t=\infty$), Z_1 a temperature dependent parameter determined by the nucleation and growth processes, and n_1 an integer depending both on the geometry of the crystalline entities and the nature of the primary nucleation process. For the particular case of growth of spherical entities, $n_1=3$ if growth is from predetermined nuclei, and 4 when nucleation is sporadic. However, the use of the Avrami equation to describe bulk crystallization kinetics has usually failed to provide correlation between bulk morphology and experimental crystallization isotherms[2]. Although the Avrami equation often provides a satisfactory fit to the data, the non-integral values of the Avrami exponent which usually result have no physical meaning. Even in those cases where an integral exponent is found, its value may not correlate with the shape of the crystalline entities in the bulk polymer. Thus, poly(ethylene oxide) yields[2,3] an exponent of 2, although spherulites are found in the bulk sample[3].

In view of these results, the validity of the two assumptions used to derive equation (1) (apart from the assumption of the random distribution of primary nuclei) must be examined. These assumptions are the constant density of the growing crystalline bodies, and their constant linear growth rate.

Measurements on microtomed sections of bulk crystallized polyethylene terephthalate[4] and polyhexamethylene adipamide[5] confirm a linear radial spherulite growth rate. Furthermore, microscope measurements on thin films have invariably led to a constant radial growth rate.

The morphological observations of several authors[6,7] provide substantial evidence that the deviation from the Avrami equation is due to an increase in density within the body of the spherulite. We have shown that a model based on this assumption in which the density increase is described by a first-order process is successful in fitting the crystallization kinetics of

*Part I is taken to be reference 2.

polymethylene and poly(ethylene oxide)[2]. Other workers have used a similar model to interpret the crystallization kinetics of polypropylene[6] and poly(propylene oxide)[8].

In this paper we extend our analysis to the discussion of the crystallization kinetics of polypropylene. This polymer is particularly suitable for the evaluation of such a model, for it is possible to compare the results obtained with the direct morphological observations of other workers[6,7].

In this work the form of the density increase is not restricted to be first order. An overall rate equation is derived in which this secondary crystallization is described by an Avrami equation with an exponent which can take on any value.

DERIVATION OF RATE EQUATION

In the model described here, spherulites grow with a constant radial rate from random centres in the supercooled melt. The volume fraction filled with spherulites, $\chi(a, t)/\chi(a, \infty)$, is then given by equation (1). Once a volume element is incorporated into the growing spherulite its crystallinity jumps from zero to $\chi(a, \infty)$. We now assume that a density increase occurs within the spherulite such that the crystallinity of a volume element, included in the spherulite at time θ, is increased by $\chi(s, t-\theta)$ at time t.

We have shown that the total crystallinity at time t $[\chi(c, t)]$ arising from these two consecutive processes is given as[2]

$$\chi(c, t)=\chi(a, t)-\int_0^t \frac{\chi(a, \theta)}{\chi(a, \infty)} \frac{\mathrm{d}}{\mathrm{d}\theta}[\chi(s, t-\theta)]\,\mathrm{d}\theta \tag{2}$$

The secondary process is now described by the Avrami equation

$$\chi(s, t-\theta)=\chi(s, \infty)[1-\exp\{-Z_2(t-\theta)^{n_2}\}] \tag{3}$$

Substitution of equations (1) and (3) into equation (2) yields

$$\chi(c, t)=\chi(a, \infty)[1-\exp\{-Z_1 t^{n_1}\}]$$
$$+\chi(s, \infty) Z_2 n_2 \int_0^t [1-\exp\{-Z_1\theta^{n_1}\}][(t-\theta)^{n_2-1}\exp\{-Z_2(t-\theta)^{n_2}\}]\,\mathrm{d}\theta \tag{4}$$

The overall rate equation (4) is now used to analyse some crystallization isotherms of polypropylene.

ANALYSIS OF CRYSTALLIZATION KINETICS OF POLYPROPYLENE

In a previous paper[9], we have reported dilatometric data for the crystallization kinetics of polypropylene. The sample used had a viscosity average degree of polymerization, $P_v=9{\cdot}8\times10^3$. Analysis of the data in terms of the conventional Avrami equation (1) yielded an exponent very near 2·5 over a wide temperature range. It was suggested that this value of the exponent may arise from the diffusion controlled growth of sporadically nucleated spherulites. However, direct microscope measurements on thin films of the polymer used in this work gave a constant radial spherulitic

growth rate[9]. In view of the morphological observations of other workers on samples of polypropylene, we now examine the possibility that the value of the Avrami exponent near 2·5 arises from two consecutive crystallization processes as discussed above. The dilatometric data are now analysed in terms of the overall rate equation (4) describing these two processes.

In general, the integral occurring in this expression cannot be evaluated analytically and was approximated by use of the 20-point Gauss formula. The values of the adjustable parameters in this expression which minimized the standard deviation between the experimental and theoretical dilatometric heights were determined by the use of a computer programme based upon the method of Rosenbrock[10].

A density increase has been found[6] within polypropylene spherulites by X-ray measurements, this density increase being best described by an Avrami equation with an exponent of 1·8. In view of these results our dilatometric data were first fitted to the convoluted rate equation (4) in which the primary crystallization was described by an Avrami process with $n_1=3$, and the secondary crystallization occurring within the spherulite by an Avrami process with $n=2$. We chose $n=2$ rather than the value[6] 1·8, as fractional Avrami exponents do not usually have any physical meaning.

There are thus three adjustable parameters, the rate constants Z_1 and Z_2 for the primary and secondary processes, and the ratio of the limiting crystallinities for these two processes. The results of such an analysis are shown in *Table 1*. Usually a standard deviation of less than one per cent is achieved showing that the dilatometric data can be very successfully described in terms of the convoluted rate equation (4).

Table 1. Fit of convoluted rate equation (4) to polypropylene isotherms. Secondary process with Avrami exponent of two

Temperature, °C	Z_1	Z_2	$[h(0)-h(\infty)]_a$, *cm*	*Total experimental contraction, cm*	σ, %
134·08	$1{\cdot}33\times10^{-4}$	$2{\cdot}87\times10^{-2}$	1·3	5·88	0·5
135·50	$7{\cdot}49\times10^{-5}$	$1{\cdot}18\times10^{-3}$	0·9	5·77	0·3
137·04	$1{\cdot}02\times10^{-4}$	$4{\cdot}23\times10^{-4}$	0·5	5·77	0·8
138·98	$1{\cdot}01\times10^{-5}$	$2{\cdot}17\times10^{-4}$	1·01	6·23	0·8
140·20	$1{\cdot}65\times10^{-6}$	$1{\cdot}05\times10^{-4}$	1·62	6·71	0·5
143·54	$5{\cdot}25\times10^{-8}$	$1{\cdot}56\times10^{-5}$	3·99	6·94	1·2
149·30	$1{\cdot}90\times10^{-9}$	$1{\cdot}19\times10^{-6}$	3·97	6·97	0·5

We have also fitted the data to our model in which the secondary crystallization is described by a first-order process. In all cases, a worse fit is achieved, the standard deviations being near two per cent in general. The contribution of the primary process to the total crystallinity is found to be dependent on the form of the secondary process.

For a first-order secondary process, the primary Avrami process contributes more than 60 per cent to the final crystallinity. This value is much reduced when the secondary process is described with an Avrami exponent

of two. In the latter model, which gives the best fit to the data, the Avrami process accounts for a greater fraction of the total crystallinity at the higher temperatures. This indicates that the spherulites formed at low supercoolings have an initial higher degree of crystal perfection than those formed at lower temperatures. A similar feature has been observed directly[6] from X-ray measurements. When the exponent of the secondary process was allowed to vary, the optimum value was found to be slightly less than two, with only slight improvements in the standard deviations shown in *Table 1*.

DISCUSSION

The analysis described here rationalizes the non-integral values of the Avrami exponent found for the bulk crystallization of polypropylene in terms of two consecutive processes, the growth of spherulites having a constant density at a constant radial rate, followed by a density increase within the spherulites which can be described by an Avrami equation with an exponent near two. Both of these processes receive support from morphological observations by other workers. In particular, the form of the secondary process that best fits our data agrees with that proposed by Hoshino *et al.*[6].

The precise nature of the secondary process is still unresolved. A number of processes leading to an increase in spherulite crystallinity can be envisaged. Interlamellar crystallization of low molecular weight and stereoirregular species has been proposed by Keith and Padden[7]. Other possible mechanisms include isothermal lamellae thickening and other relaxation processes leading to an increase in crystal perfection.

The examination of the crystallization kinetics of blends of known molecular weight distribution and stereoregularity in terms of the model used here will probably provide the needed clarification of the nature of the secondary process.

The calculations reported herein were performed on the Atlas Computer of Manchester University.

Chemistry Department,
University of Manchester,
Manchester, 13

(*Received April 1967*)

REFERENCES

[1] MANDELKERN, L. *Growth and Perfection of Crystals*, pp 467–497. Chapman and Hall: London, 1958
[2] HILLIER, I. H. *J. Polym. Sci. A*, 1965, **3**, 3067
[3] BANKS, W. and SHARPLES, A. *Makromol. Chem.* 1963, **59**, 233
[4] HARTLEY, F. D., LORD, F. W. and MORGAN, L. B. *Phil. Trans.* 1954, **247**, 23
[5] HARTLEY, F. D., LORD, F. W. and MORGAN, L. B. *Ric. sci.* 1955, **25**, 577
[6] HOSHINO, S., MEINECKE, E., POWERS, J., STEIN, R. S. and NEWMAN, S. *J. Polym. Sci. A*, 1965, **3**, 3041
[7] KEITH, H. D. and PADDEN, F. J. *J. appl. Phys.* 1964, **35**, 1270 and 1286
[8] AGGARWAL, S. L., MARKER, L., KOLLAR, W. L. and GEROCH, R. *J. Polym. Sci. A*, 1966, **2**, 715
[9] GORDON, M. and HILLIER, I. H. *Polymer, Lond.* 1965, **6**, 213
[10] ROSENBROCK, H. M. *Comput. Jnl*, 1960, **3**, 175

Morphology of Polypropylene Crystallized from the Melt

F. L. BINSBERGEN and B. G. M. DE LANGE

The lamellar build-up of polypropylene α-spherulites is different from the radiating lamellar structure of polyethylene and several other polymers. In the initial stage of crystallization quadrites are found, parallelogram-shaped aggregates of two sets of lamellae crossing at an angle of about 80°. The cross-hatched pattern persists during the growth of the spherulites, and explains their low birefringence. Crystallographically the cross-hatching is accounted for by an epitaxial fit of lamellae contacting along (010) faces. The dependence of birefringence on temperature of crystallization finds a qualitative explanation in the temperature dependence of epitaxial nucleation. The cross-hatched pattern suggests for polypropylene a deformation mechanism different from that of polyethylene and may account for the lower tendency to warpage of polypropylene.

AMONG the synthetic high polymers polyethylene is the one most studied with respect to the morphology of crystallization both from solution and from the melt. Depending on the base polymer, the concentration in solution and the rate of cooling, it crystallizes into single lamellae, dendrites, stacks of lamellae, sheaves, axialites or spherulites†. There is only a gradual transition from one morphological type to another[1]. Sheaves of lamellae have often been encountered as precursors of spherulitic crystallization and spherulites have been shown to consist of lamellae radiating from their centres. The polymer chain axis proved to be perpendicular or nearly perpendicular to the plane of the lamellae and hence to lie tangentially in the spherulites.

Many features of this morphology have been encountered in most other crystallizing polymers[2] and are therefore easily generalized. However, a deviating type has been found for polypropylene[3–5], whose birefringence was difficult to explain in terms of the morphology mentioned above.

CRYSTAL STRUCTURE AND BIREFRINGENCE OF POLYPROPYLENE

Polypropylene generally crystallizes from the unstrained melt for the greater part in the α-modification (m.pt 168°–174°C), while a few spherulites in the β-modification (m.pt 150°–154°C) are often present. Crystal structures have been proposed for both modifications: a monoclinic structure for the α-modification[6] ($a=6{\cdot}65$ Å, $b=20{\cdot}96$, $c=6{\cdot}50$, $\beta=99°20'$, four chains of three monomer units per cell), and a hexagonal structure for the β-modification[7a, b] ($a=6{\cdot}38$ Å or a multiple of this value, $c=6{\cdot}33$).

In both modifications the isotactic polypropylene chain has a threefold helix configuration, the succession of the methyl groups determining right- or left-handed conformation of the helix. A further distinction can be made

†Excellent reviews are found in ref. 1 and 2.

between helices with consecutive D- or L-configurations at the asymmetric carbon atoms, otherwise distinguished as 'up'-helices and 'down'-helices. This discrimination, however, has little influence on the envelope of the chain, the packing of the chains being the same if e.g. a right-hand 'up'-helix is replaced by a right-hand 'down'-helix[6].

Calculation of the optical anisotropy of a single isotactic polypropylene helix[8] from bond polarizabilities indicates a positive birefringence for the polymer chain. The birefringence, Δn, of an elongated object is called positive when the refractive index of light polarized parallel to the long axis of the object, n_p, is larger than that of light polarized perpendicular to the long axis, n_q

$$\Delta n = n_p - n_q \text{ (elongated object)}$$

Similarly, the birefringence of a spherulite is called positive when the refractive index for light polarized parallel to the radius of the spherulite, n_r, is larger than for tangentially polarized light, n_t

$$\Delta n = n_r - n_t \text{ (spherulite)}$$

The positive birefringence of the polypropylene helix is in agreement with that of stretched polypropylene fibres[8] and of nucleation lines observed when a sheared melt is cooled down[9].

On generalizing the rule—valid for polyethylene and several other polymers—that the polymer chain axis in a spherulite is oriented tangentially, one would expect the birefringence of polypropylene spherulites to be clearly negative. This only applies, however, for β-spherulites.

The birefringence of α-spherulites is low and often inhomogeneous, mainly weakly positive for spherulites grown at temperatures below 130°C and mainly weakly negative for those grown above 140°C[10]. This has not yet been accounted for[11]. Although the monoclinic arrangement of polymer chains in the α-modification would essentially change the uniaxial anisotropy of the single chain into a biaxial one, this fact can hardly account for the low birefringence observed.

DEVIATING MORPHOLOGY OF POLYPROPYLENE

Besides a radial fibrillar pattern tangential striations have also been found in polypropylene α-spherulites[4,5]. Recently, crystallization of polypropylene from dilute solutions[12,13], from moderately concentrated solutions[14,15], from very concentrated solutions[16] and from drying films cast from a solution[17] was reported in the course of our investigations. In these studies, parallelogram-like structures have been found having a cross-hatching parallel to the diagonals. Sauer *et al.* called these structures *quadrites*[12,13], a term we will use henceforth.

Quadrites crystallized from dilute or moderately concentrated solution were shown by electron microscopy to be networks of two parallel sets of lamellae, crossing each other at an angle of about 100° (or 80°) and with the planes of the lamellae perpendicular to the plane of the quadrite. Outgrowths were visible with the crystallographic *a* direction as the direction of growth, while the polymer chain axis was perpendicular to the plane of the lamellae. Microbeam X-ray analysis of quadrites[14] showed the *a* axis

and the *c* axis to be nearly superimposed on each other along the diagonals of the quadrites and the *b* axis to be perpendicular to the plane of the quadrite. A schematic representation is given in *Figure 1*.

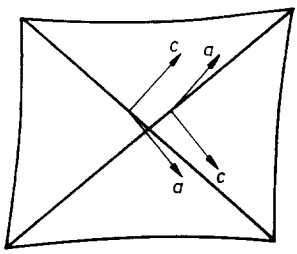

Figure 1—Crystallographic directions in a quadrite

The *c* axis was shown to be perpendicular and the *a* axis to be inclined about 10° to the long direction of the lamellae.

The purpose of this paper is to show the general occurrence of quadrites in initial stages of crystallization of polypropylene from the melt and of a cross-hatched pattern in both artificially nucleated and unnucleated polypropylene. A crystallographic explanation of the crossing of lamellae will be presented and the effect of this morphology on the birefringence of polypropylene α-spherulites and its dependence on temperature of crystallization will be discussed.

EXPERIMENTAL

(1) *Samples*

Several polypropylene samples were used both from pilot plant and from commercial production. Most of them were in the range of injection-moulding grades. All the samples were stabilized by adding 0·15 to 0·3 p.h.r.† of 'Ionox' 330 (reg. trademark of Shell Chemical Co.).

Nucleated samples were prepared by precipitating 0·25 to 3 p.h.r. of aluminium monohydroxy-di-*p-tert*-butylbenzoate [AlOH(ptbb)$_2$] on to polymer powder according to a method described earlier[18], filtering off, drying, milling the mixture on a two-roller mill at 180°C for 5 min and pressing a sheet at 270°C. In this way a very effective dispersion of the nucleating agent was obtained; no particles larger than 0·2 μm were found.

(2) *Optical microscopy*

Microscope preparations were made by pressing 5 mg of polymer powder or a 5 mg piece cut from a sheet between slide and cover glass at about 220°C to a film of 30 to 100 μm thickness. In order to relieve strains set up during moulding the specimen was kept at 250°C for 1 min. Subsequently it was crystallized at the desired temperature on a hot plate or on a Kofler hot-stage mounted in the microscope.

A Reichert Zetopan-Pol polarizing microscope was used, equipped with a de Sénarmont compensator (see Appendix). In a few cases, specimens were mounted in a Leitz Universal tilting stage fitted on to the rotating stage of the microscope, in order to observe the objects in the specimen in various directions.

†p.h.r.=parts per hundred parts of resin.

(3) *Electron microscopy*‡

Free surfaces for replication were obtained, either by:

(a) lifting the cover glass from crystallized microscope preparations after cooling to room temperature, or

(b) crystallizing without cover glass, under nitrogen, in a closed vessel hung in a thermostatically controlled bath.

Replicas were made by platinum/carbon-shadowing the polypropylene surface, backing with polyvinyl alcohol, dissolving the polypropylene at 150°C in decalin and subsequently dissolving the polyvinyl alcohol in water. The swelling of polypropylene in decalin sometimes caused fracture of the replicas, while often some polypropylene adhered to the replica. Therefore another method was used as well. Platinum-shadowing, backing with polyvinyl alcohol, pulling off the polyvinyl alcohol film to which the metal adhered, depositing the carbon and dissolving the polyvinyl alcohol in water[19].

Electron micrographs were taken by means of a Siemens Elmiskop I.

(4) *X-Ray diffraction*

Large spherulites were grown by crystallization of a microscope specimen at 150°C for a number of days. An X-ray flat-plate diagram was taken by using as a diaphragm a 0·2 mm pinhole mounted on to the polymer film. The selected area was part of a large spherulite, about 0·5 mm from its centre. Nickel-filtered copper-radiation was used from a Philips 25623/62 tube mounted on a PW 1010/25 generator.

OBSERVATIONS

(1) *Initial stage of crystallization*

(a) *Growth of a single spherulite*—Plain polypropylene was crystallized at 146°C, at which temperature very few spherulites were formed, growing to a large size, thus permitting unhurried observation of the growth of a single one. The initially growing elongated particles, observed as precursors of some of the spherulites, were positively birefringent. Close examination by means of the de Sénarmont compensator showed that the optical retardation in the elongated particle increased from the ends inwards (*Figure 2*).

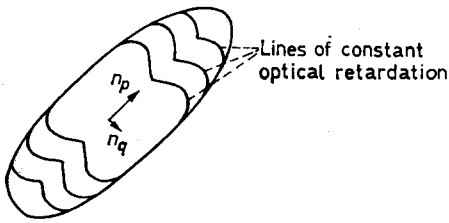

Figure 2—Elongated particle observed in the first stage of crystallization of polypropylene. Vectors indicate polarization directions for larger and smaller refractive indices

‡The electron-microscopical work was carried out by Mrs Raadsen and Mewe.

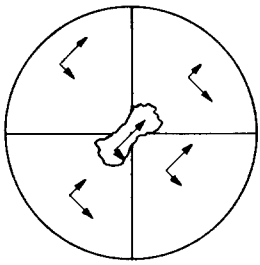

Figure 3—Birefringence pattern in a negative spherulite. Vectors indicate polarization directions for larger and smaller refractive indices

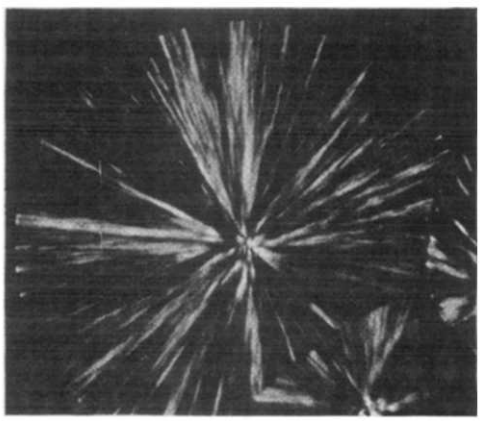

Figure 4—Polypropylene spherulites grown at 130°C (crossed polarizers; magnification ×260; reduced 2/3 on reproduction)

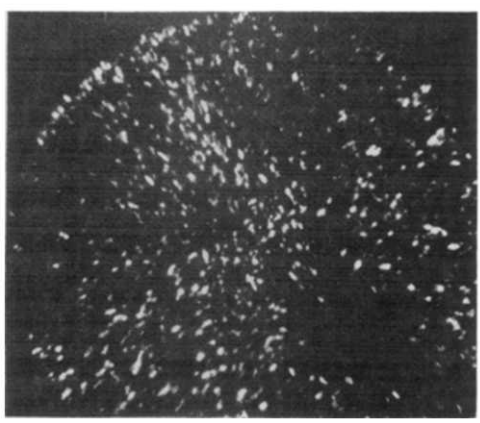

Figure 5—Polypropylene spherulites grown at 130°C and recrystallized at 136°C after incomplete melting at 169°C (crossed polarizers; magnification ×260; reduced 2/3 on reproduction)

The spherulite developing from this particle was negatively birefringent, except for its central part, which was still positively birefringent (*Figure 3*). Similarly, spherulites grown isothermally at a temperature where they acquire a mixed or positive birefringence often showed a central part having a much higher birefringence than the remainder of the spherulite.

(b) *Recrystallization after incomplete melting*—Large spherulites of polypropylene were grown at about 130°C. They were of the mixed bire-

fringent type[10] (*Figure 4*). After they had reached a certain size, the specimen was heated to such a temperature that the birefringence just disappeared. Then the specimen was cooled again to 136°C and kept at that temperature. An abundant nucleation resulted in the spot where the large spherulites had been. The initial stage of recrystallization included elongated particles, like those described under (1)(a), mainly with their long axis parallel to the radius of the original spherulite (*Figure 5*) and showing positive birefringence (*Figure 6*). After some time the spherulite seemed to have recrystallized, but now with strong, positive birefringence. Further outgrowth of the spherulite had the same appearance as before and was weakly, negatively birefringent.

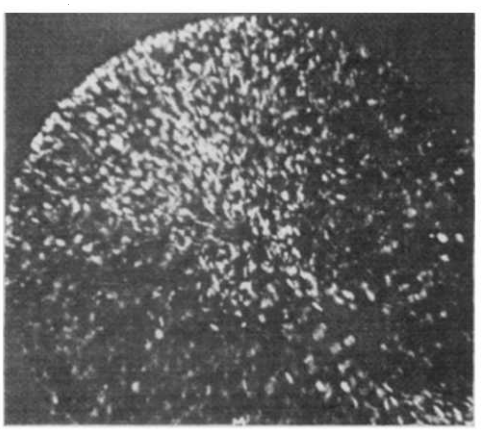

Figure 6—As *Figure 5* using a de Sénarmont compensator (polarizer W–E; λ/4-plate between preparation and analyser with fast axis W–E; analyser rotated 10° clockwise from N–S; magnification ×260; reduced 2/3 on reproduction

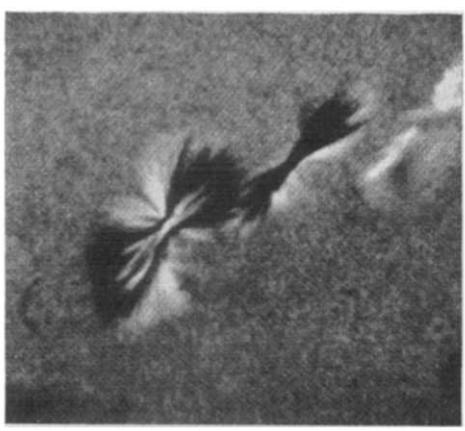

Figure 7—Negatively birefringent sheaves of polypropylene lamellae, crystallized at 160°C (polarizer N–S; λ/4-plate with fast axis N–S; analyser rotated 5° clockwise from W–E; magnification ×800; reduced 2/3 on reproduction)

(c) *Slow crystallization of polypropylene with a high content of nucleating agent*—Polypropylene containing 1 or 3 p.h.r. effectively dispersed $AlOH(ptbb)_2$ was crystallized isothermally for several hours at temperatures from 154° to 160°C, by which treatment 5 to 20 μm large bodies developed. Subsequently the specimen was quenched in liquid nitrogen;

this caused an extremely fine crystallization of the remainder of the polymer, which enabled the isothermally crystallized bodies to be clearly observed.

Crystallization at 160°C produced negatively birefringent sheaves of lamellae (*Figure 7*).

Crystallization at 154° to 156°C resulted, however, in parallelogram-type bodies, which we assume to be actually bulk-crystallized quadrites (*Figure 8*). These quadrites were weakly birefringent. Their diagonals intersected at an angle of about 100° and faint cross-hatching parallel to the diagonals was visible, especially when moving the particles through focus or by using phase contrast optics. The optical retardation, invariably very low, was largest at the loci of the diagonals, each of which showed negative birefringence. In addition to the weakly birefringent parallelograms, strongly, positively birefringent, elongated particles were found. After mounting the specimen in the tilting stage, these particles proved to be quadrites seen edge-on, having an appearance similar to that of the elongated particles mentioned under (1)(a). Rotation of a quadrite in its own plane while viewed edge-on did not visibly change its birefringence.

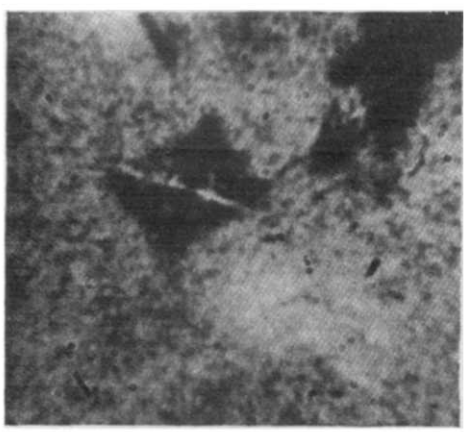

Figure 8—Quadrite crystallized at 155°C (polarizer N–S; λ/4-plate with fast axis N–S; analyser rotated 5° clockwise from W–E; magnification × 1 600; reduced 2/3 on reproduction)

Figure 9—Further stage of growth of quadrites crystallized at 155°C (polarizer N–S; λ/4-plate with fast axis N–S; analyser rotated 5° anticlockwise from W–E; magnification × 800; reduced 2/3 on reproduction)

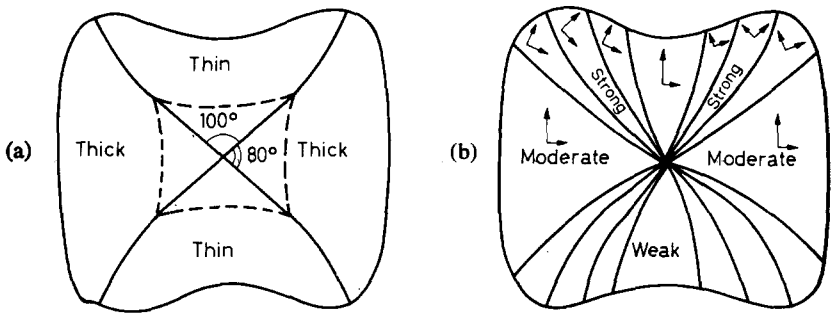

Figure 10(a)—Outgrowth of a quadrite; curvature of diagonals
Figure 10(b)—Birefringence pattern in quadrite slightly grown out with areas of strong, moderate and weak birefringence

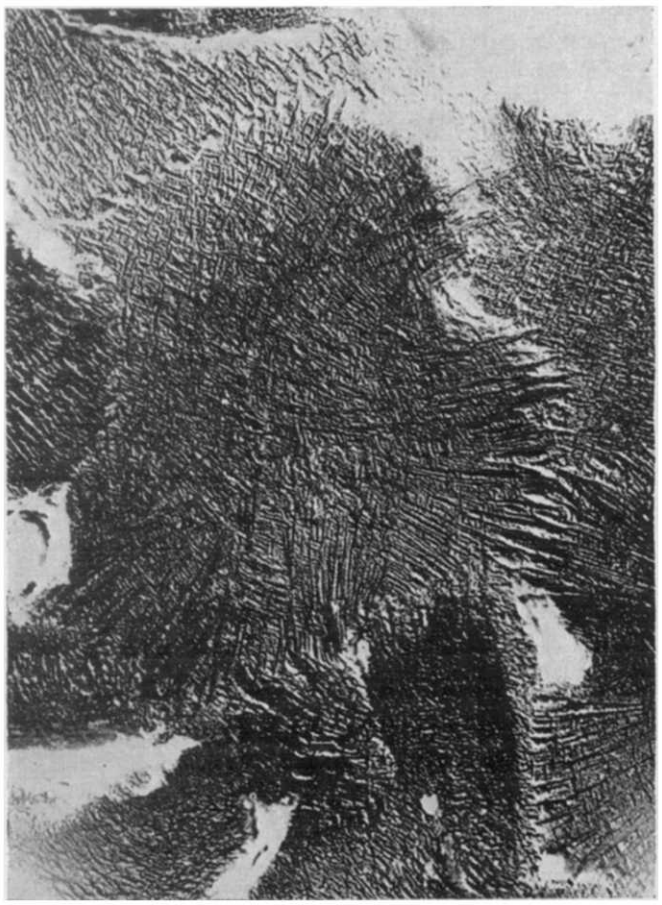

Figure 11—Quadrites in polypropylene nucleated by 0·5 p.h.r. AlOH-$(ptbb)_2$ and crystallized at 143°C with free surface (magnification × 25 000; reduced 2/3 on reproduction)

On further growth the quadrites increased in birefringence (*Figure 9*) and changed slightly in form. The diagonals tended to curve, as shown in *Figure 10*(a), and the quadrite thickened, except for its central part and the area enclosed by the curving diagonals (area of the 100° angle; see next paragraph), as indicated in *Figure 10*(a). This curvature of the lamellae was confirmed by the orientation of the birefringence as determined by means of the de Sénarmont compensator and by the extinction position between crossed polarizers without compensator [see *Figure 10*(b)].

(2) *Completed crystallization*

(a) *Polypropylene containing nucleating agent*—Polypropylene containing 0·25, 0·5 or 1 p.h.r. of $AlOH(ptbb)_2$ was crystallized at 137°C or 143°C. A grain size of 1 to 8 μm resulted. Electron micrographs show a cross-hatched pattern in the grains (*Figure 11*). The striations make an angle of

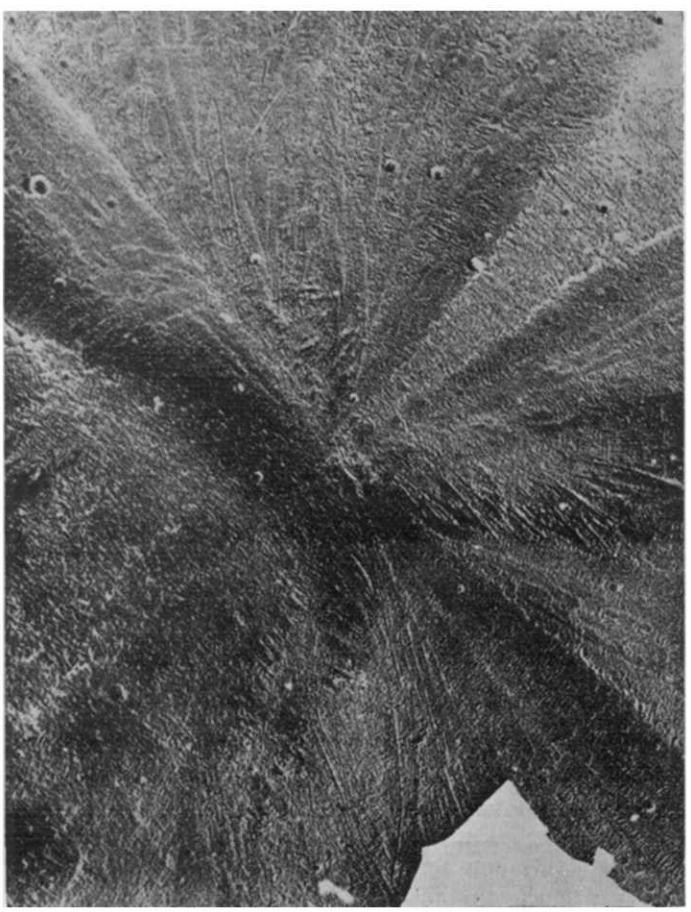

Figure 12—α-Spherulite crystallized at 140°C with free surface (magnification ×25 000; reduced 2/3 on reproduction)

about 100° (or 80°) with each other. The grains are very probably quadrites whose growth ended by impingement on each other.

The curvature around the 100° angle (as drawn in *Figure 10*) is clearly visible here. It is a general feature observed in nearly all our electron micrographs of quadrites.

(b) *Plain polypropylene*—α-Spherulites show a cross-hatched pattern[4] similar to that of quadrites but less pronounced. In spherulites crystallized at 140°C radial striations often predominate (*Figure 12*).

The X-ray flat-plate diagram of part of a spherulite grown at 150°C showed, in addition to strong (110) reflections in a radial direction and (130) reflections at about 45° of azimuth, also (110) and (130) reflections, but much weaker, in tangential directions (*Figure 13*).

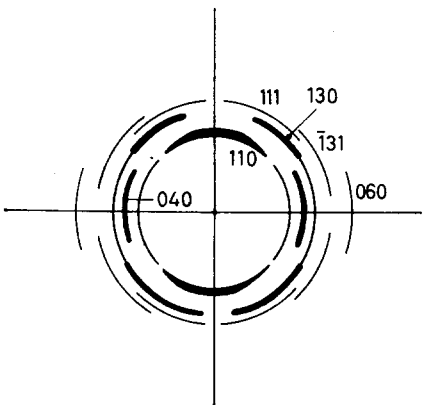

Figure 13—Flat-plate X-ray diagram of selected portion of α-spherulite, grown at 150°C (spherulite radius vertical)

(c) *Crystallization after orientation-induced nucleation*—Most lamellae growing from a nucleation line[9] were found perpendicular to this line, but even at a short distance from the axis of the nucleation line some cross-hatching was visible. Our electron micrographs are similar to one presented earlier by Geil (ref. 2, Fig. III-27). It is seen clearly that the crossing striations make a small angle with the nucleation line.

Shear-induced crystallization of polypropylene has been observed in the entrance of a melt rheometer capillary at a certain critical shear stress depending on the temperature (160° to 175°C), which gave rise to a considerable increase in apparent viscosity†. After quenching the capillary and pulling out the solidified polypropylene rod, X-ray diffraction of such a rod gave a fibre diagram.

However, an X-ray diagram of a rod quenched after application of a shear stress somewhat below the critical one showed *b*-axis orientation only, perpendicular to the direction of shear stress. Presumably, in this case most of the crystallization took place at quenching, not at 160°C, but started on induced nucleation lines.

†A. K. v.d. Vegt and P. P. A. Smit; 'Crystallization phenomena in flowing polymers'. Lecture to the Joint Plastics Conference (Society of Chemical Industry), London, 22 September 1966.

(3) *β-Spherulites*

Incorporation of a finely divided aluminium salt of 6-quinizarin sulphonic acid† caused spherulites grown at about 130° to 135°C to be mainly of the β-type, but without reducing their size. We have used this technique for the preparation of β-spherulites. Contrary to α-spherulites, the β-spherulites show the radial lamellar morphology (*Figure 14*) inherent in polyethylene and several other polymers, in accordance with their birefringence.

Figure 14—β-Spherulite crystallized at about 130°C between slides (magnification × 12 500; reduced 2/3 on reproduction)

DISCUSSION

The above observations show that the cross-hatched pattern found earlier in polypropylene crystallized from solution[12–16] is also a general phenomenon in crystallization from the melt, both in the initial stage of crystallization and in spherulites, as demonstrated by optical and electron microscopy and X-ray diffraction, except for crystallization at 160°C (or higher temperatures). We will now try to explain this phenomenon.

†Private communication: Dr A. K. v.d. Vegt, Kon./Shell Plastics Laboratory, Delft.

(1) *Epitaxial fit of crossing lamellae*

The lamellae crossing at 100° (or 80°) were assumed[13,15] not to penetrate each other, but to touch sideways along (010) planes. Khoury[15] proposed a model (his model II) in which he assumed epitaxial contact due to close similarity of *a* and *c* repeat distances. However, similarity of lattice parameters is a necessary but not a sufficient condition for epitaxy. There has to be some type of fit of the complete structures on to each other.

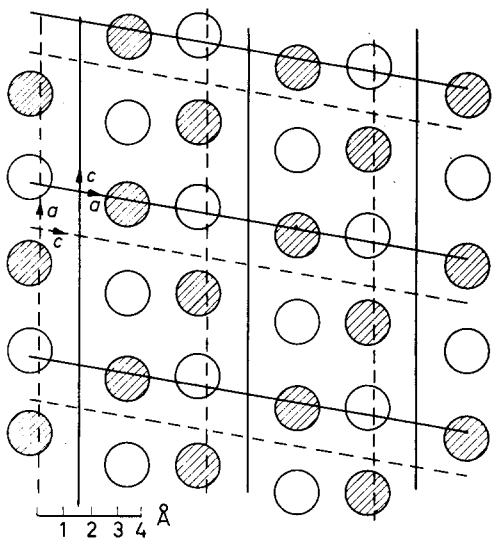

Figure 15—Crystallographic fit along (010) plane between adjacent layers of elementary cells (protruding methyl groups only; *b* axis perpendicular to plane of drawing). *a*—Normal fit: solid lines are lattice lines, solid circles are methyl groups below, and open circles methyl groups above, plane of drawing. *b*—Epitaxial fit. solid lines are lattice lines and solid circles are methyl groups of lamellae below plane of drawing, dashed lines and open circles are methyl groups of lamella above plane of drawing

It now appears that the elementary cells can thus be fitted in two ways:

(*a*) As pointed out in the second section of this paper, the packing of the polypropylene chains is primarily governed by the methyl groups. *Figure 15* is an illustration of the methyl groups of one elementary cell penetrating in the *b* direction between methyl groups of the next elementary cell. The methyl groups just below an *ac* plane are represented by solid circles, the ones just above by open circles and the lattice lines by solid lines, according to the crystal structure given by Natta and Corradini[6]. It is thus seen how the methyl groups of one layer of elementary cells fit in the holes between the methyl groups of an adjacent layer.

(*b*) Another fit is obtained by placing a layer of elementary cells with *c* axis (or *a* axis) parallel to the *a* axis (or *c* axis) of the substrate. This can be done in such a way that the holes between the methyl groups in the substrate (solid circles) are fitted by the methyl groups (open circles) of the superimposed layer of elementary cells (dashed lattice lines) in the same places as under (*a*) above.

Thus the (010) contact between crossing lamellae is actually a case of epitaxy with a fit of molecular subgroups. The misfit is about two per cent, i.e. the difference between the elementary *a* and *c* periods at room temperature. Close to the melting point misfit is probably somewhat larger, since the *a* period, which is already the larger one, is expected to expand more rapidly on heating than the *c* period.

(2) *Positions of the crystal lattice in an α-spherulite*

The *b* axis is invariably found to be perpendicular to the radius of the spherulite. This radius therefore lies in the *ac* plane, which is the same as the a^*c^* plane of the reciprocal lattice. The radius of the spherulite can be seen as the axis of rotation of the reciprocal lattice or as the 'fibre-axis', for which *Figure 13* is the 'fibre diagram'.

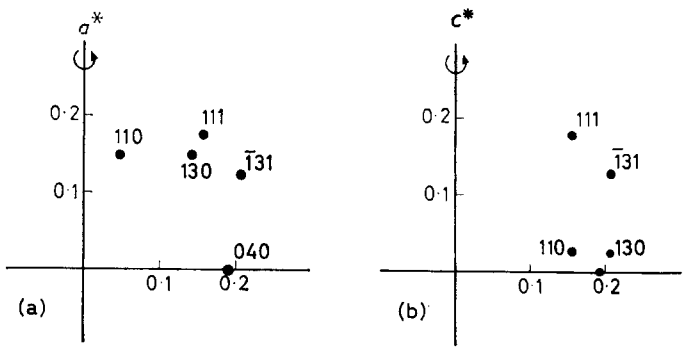

Figure 16—Positions of reflection of various lattice planes: (a), a^* axis is axis of rotation of reciprocal lattice; (b), c^* axis is axis of rotation of reciprocal lattice (units in $Å^{-1}$)

Let us assume the a^* axis to coincide with the spherulite radius for the set of radially oriented lamellae. By rotation of the reciprocal lattice around the a^* axis the lattice planes successively come into position of reflection, approximately when they go through a flat plane through the a^* axis (approximation of the Ewald sphere). The resulting positions of reflection are plotted in *Figure 16*(a). Comparison of *Figures 16*(a) and *13* then shows that the radius of the spherulite must actually make an angle of 5° to 10° with the a^* axis and one of 70° to 75° with the c^* axis. The angle of 20° to 25° between a^* axis and spherulite radius, as has been suggested earlier[11], would be difficult to reconcile with the positions of the (110) and ($\bar{1}$31) reflections. Also, tilting the specimen somewhat less than 10° produces the (200) reflection in that part of the X-ray diagram whose distance to the specimen becomes larger by the tilting.

When the radial lamellae have their a^* axes approximately along the radius of the spherulite, the tangential lamellae have the c^* axes in the same direction. *Figure 16*(b) is similar to *Figure 16*(a), but now with the c^* axis as axis of rotation of the reciprocal lattice. Comparison of *Figure 16*(b) with the position of the weak (110) and (130) reflections in a tangential direction suggests the presence of a relatively small amount of tangential lamellae. We assume that the relative amount of this material increases at decreasing crystallization temperature [see (4)]. At temperatures much below 150°C it was not possible, however, to obtain spherulites large enough for application of our micro X-ray diffraction technique.

(3) *Birefringence*

Owing to the mode of packing of the polymer chains in the monoclinic

lattice the principal refractive indices of the α-modification n_a, n_b and n_c belong to directions of polarization along the reciprocal a^* axis, the b axis and the c axis, respectively. Since the polymer chain is a threefold helix, n_a and n_b will differ only very slightly, but n_c is considerably different from the other two

$$n_c > n_a \approx n_b$$

By using this relation it is immediately seen that a quadrite seen edge-on is positively birefringent (*Figure 1*):

$$n_p = (n_a + n_c)/2 \tag{1}$$

$$n_q = n_b \tag{2}$$

Similarly, it may be shown that a quadrite seen flat is hardly birefringent. The diagonals show a weak, negative birefringence; presumably they are either thicker or have more parallelism of lamellae than the remainder of the quadrite.

In a spherulite the lamellae are oriented either radially or approximately tangentially. Let the fraction of the former be r and of the latter t; then $r+t=1$ (see *Figure 17*). The radial refractive index is then approximately

$$n_r = rn_a + tn_c \tag{3}$$

and the tangential one

$$n_t = r\,(n_b + n_c)/2 + t\,(n_a + n_b)/2\dagger \tag{4}$$

so that the birefringence is

$$\Delta n = n_a\,(r - t/2) - n_b\,(r+t)/2 - n_c\,(r/2 - t) \tag{5}$$

which for $n_a = n_b$ becomes

$$\Delta n = (n_c - n_a)\,(t - r/2) \tag{6}$$

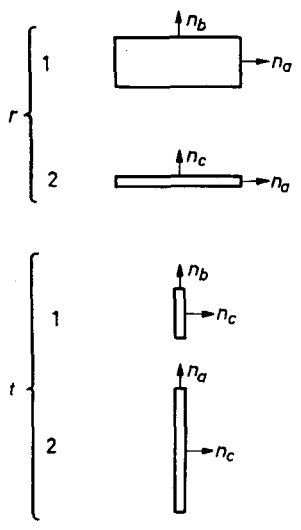

Figure 17—Possible combinations of principal refractive indices lying in the plane of observation and corresponding positions of the lamellae

†Instead of the arithmetic mean, the geometric mean of refractive indices should be taken according to averaging over an ellipsoid.

Although the absolute value of the birefringence will in fact be smaller, since most lamellae do not lie exactly radially or tangentially, an estimate of the relative amounts of radial and tangential lamellae may be obtained from the sign—or absence—of birefringence.

Since a nucleation line is clearly positively birefringent, most lamellae will in its immediate vicinity be oriented perpendicular to it. In spite of the strain in the specimen the further outgrowth shows the birefringence of spherulites crystallized at the same temperature†, which once more stresses the opinion that strain in a polymer melt may be very inhomogeneous[9].

Upon recrystallization after incomplete melting strongly positively birefringent particles are observed, oriented parallel to the radius of the original spherulite, and weakly birefringent particles. The former are a recrystallization of r_1 and t_1 lamellae (*Figure 17*) and the latter of r_2 and t_2 lamellae. The crystalline orientations in the original spherulite are well preserved in the orientations of the recrystallizing quadrites. From *Figure 17* it is also clear that no tangentially oriented quadrites arise.

(4) *Relative amounts of radial and tangential lamellae as functions of temperature of crystallization*

The fraction of tangential lamellae in mixed or non-birefringent spherulites is about a third, as deduced from equation (6). Spherulites crystallized below 130° have a higher fraction (up to a half) and those crystallized above 140° a lower fraction of tangential lamellae. So the fraction of tangential lamellae tends to be lower at smaller degrees of supercooling. Also, crystallization at 160°C did not produce quadrites but only sheaves of lamellae, and quadrites seem to have a more open structure when crystallized at a smaller degree of supercooling as seen in phase contrast microscopy and electron microscopy.

A thermodynamic explanation follows. The velocity of crystal growth in the b direction, v_b, is, according to simple nucleation theory, assumed to be governed by the activation free energy of secondary nucleation on the corresponding growth plane (010) (ref. 20)

$$\Delta G_b^* = 4b_0\sigma_a\sigma_e/\Delta\mu_v \tag{7}$$

in which ΔG^* is the activation free energy, $\Delta\mu_v$ the difference in bulk free energy per unit volume between liquid and solid, b_0 the thickness of one monolayer of molecules and σ_a and σ_e the interfacial free energies per unit area of the (100) or (001) interface between solid and liquid.

Similarly, the frequency of epitaxial deposit of a monolayer giving rise to growth of a crossing lamella is governed by the activation free energy of epitaxial nucleation‡ on the parent crystal

$$\Delta G_{be}^* = 4b_0\sigma_a\sigma_e/(\Delta\mu_v - \sigma_{be}/b_0) \tag{8}$$

in which σ_{be} is the specific interfacial free energy between lamellae packed epitaxially along a (010) plane as illustrated in *Figure 14*.

Now
$$\Delta\mu_v = \Delta S_v \cdot \Delta T \tag{9}$$

†Ref. 9, Fig. 2.
‡See for instance ref. 21.

ΔS_v being the entropy of melting per unit volume and ΔT the degree of supercooling. Similarly

$$\Delta\mu_v - \sigma_{be}/b_0 = \Delta S_v\,(\Delta T = \vartheta) \tag{10}$$

in which ϑ is the reduction in melting point of an epitaxially deposited monolayer

$$\vartheta = \sigma_{be}/\Delta S_v b_0 \tag{11}$$

Thus, the epitaxial nucleation of crossing lamellae is governed by an apparently lower degree of supercooling than is the normal growth in the *b* direction. At an increasing degree of supercooling the difference between ΔG^*_{be} and ΔG^*_b decreases, which gives rise to a higher relative frequency of nucleation of crossing lamellae and thus to a higher fraction of tangential lamellae in a spherulite. The exact fraction of tangential lamellae is difficult to calculate, since the unknown ratio between the velocities of crystal growth in the *a* and in the *b* direction plays an important role.

Equation (8) is only valid[21] as long as

$$\Delta\mu_v > 2\sigma_{be}/b_0 \tag{12}$$

and consequently

$$\Delta T > 2\vartheta \tag{13}$$

At a lower degree of supercooling the critical nucleus for epitaxial deposit is no longer a monolayer. In that case we assume that ΔG^*_{be} becomes so much larger than ΔG^*_b that no crossing lamellae will be observed.

Since above 160°C no quadrites are found, 2ϑ is estimated to be about 16°C or somewhat less. Incorporation of this value in equation (11) together with $\Delta S_v = 0{\cdot}11$ cal/cm³ 1 deg. C and $b_0 = 5{\cdot}24$ Å gives for σ_{be} an estimate of roughly 1·5 erg/cm².

(5) *Practical implications*

Since the microstructure of polypropylene is basically different from that of polyethylene, different deformation mechanisms will apply to these materials. This is illustrated by the fact that the strain optical coefficient of polypropylene is negative at small elongations, but positive at large ones. An initial deformation of the cross-hatched polypropylene structure, similar to that of a lozenge pulled at opposite corners, could give an explanation. At larger deformations, chains start to be pulled out of lamellae.

At equal moulding conditions polypropylene is less prone to warpage than polyethylene. This may be explained by the fact that as a result of stress-induced nucleation the polyethylene chains are oriented almost perfectly parallel to the direction of shear stress, while in polypropylene an appreciable fraction of the chains takes a different orientation due to the growth of crossing lamellae already in the immediate neighbourhood of the nucleation lines (see page 32).

CONCLUSIONS

1. In confirmation of findings by other authors, the sub-microscopic morphology of polypropylene is quite different from that of polyethylene

and several other polymers. Instead of lamellae growing nearly parallel, two sets of lamellae crossing at an angle of about 80° are found. This basic pattern applies both to the initial stage of growth and to α-spherulites, while β-spherulites consist solely of lamellae radiating from the centre of the spherulites.

2. The amount of cross-growth depends on the degree of supercooling, no cross-growth being found at 160°C and above and an increasing amount at increasing degrees of supercooling.

3. The cross-hatched morphology and its temperature dependence explain the variable and low birefringence of polypropylene α-spherulites.

4. After orientation-induced nucleation cross-growth is observed in the immediate vicinity of the nucleation lines, the effect of the orientation thus being reduced. This may explain why polypropylene is less prone to warpage than polyethylene.

Koninklijke/Shell-Laboratorium,
Amsterdam, The Netherlands

(Received April 1967)

APPENDIX

USE OF DE SÉNARMONT COMPENSATOR

A de Sénarmont compensator actually consists of a quarter-wave plate inserted between specimen and analyser, having its fast axis† parallel to the direction of polarization of the polarizer. The birefringent object is rotated 45° from its extinction position between crossed polarizers. Provided the optical path difference is less than half a wavelength, the sign of birefringence can be determined by slightly rotating the analyser (see table) and the value of the retardation by rotating the analyser to extinction, extinction angle φ, in degrees. Then the retardation is given in cycles by

$$r = \pm 2\varphi/360$$

or in wavelengths by

$$\Delta = \pm 2\varphi\lambda/360$$

Table 1. Determination of direction of fast axis of (weakly) birefringent object

Starting situation: ↓ *polarizer* *object* *fast axis quarter-wave plate* *analyser*	*I* *W–E* *in 45° position* *W–E* *N–S*	*II* *N–S* *in 45° position* *N–S* *W–E*

Analyser is slightly rotated ↓	object becomes ↓	direction of fast axis of object: *I*	*II*
anticlockwise	darker	SW–NE	NW–SE
	brighter	NW–SE	SW–NE
clockwise	darker	NW–SE	SW–NE
	brighter	SW–NE	NW–SE

†Fast axis = direction of polarization of lowest refractive index.

REFERENCES

[1] KELLER, A. *Polymer, Lond.* 1962, **3**, 393
[2] GEIL, P. H. *Polymer Single Crystals.* Interscience: New York, 1963
[3] KELLER, A. *Kolloidzschr.* 1959, **165**, 15
[4] BAILEY, G. W. *J. Polym. Sci.* 1962, **62**, 241
[5] Ref. 2, pp 211–220, pp 266–271
[6] NATTA, G. and CORRADINI, P. *Nuovo Cim.* Suppl. to Vol. 1960, **15**, 40
[7a] ADDINK, E. J. and BEINTEMA, J. *Polymer, Lond.* 1961, **2**, 185
[7b] TURNER JONES, A., AIZLEWOOD, J. M. and BECKETT, D. R. *Makromol. Chem.* 1964, **75**, 134
[8] KEEDY, D. A., POWERS, J. and STEIN, R. S. *J. appl. Phys.* 1960, **31**, 1911
[9] BINSBERGEN, F. L. *Nature, Lond.* 1966, **211**, 516
[10] PADDEN, F. J. and KEITH, H. D. *J. appl. Phys.* 1959, **30**, 1479
[11] KEITH, H. D., PADDEN, F. J., WALTER, N. M. and WICKOFF, H. W. *J. appl. Phys.* 1959, **30**, 1485
[12] SAUER, J. A., MORROW, D. R. and RICHARDSON, G. C. *J. appl. Phys.* 1965, **36**, 3017
[13] MORROW, D. R. *Dissertation.* Pennsylvania State University, 1965
[14] SELIKHOVA, V. I., ZUBOV, Y. A., MARKOVA, G. S. and KARGIN, V. A. *Vysokomol. Soedineniya,* 1965, **7**, 216; *transl.*: *Polymer Sci. U.S.S.R.* 1965, **7**, 232
[15] KHOURY, F. *J. Res. Nat. Bur. Stand.* 1966, **70A**, 29
[16] PADDEN, F. J. and KEITH, H. D. *J. appl. Phys.* 1966, **37**, 4013
[17] KARGIN, V. A. and GORINA, I. I. *Vysokomol. Soedineniya,* 1965, **7**, 220; transl.: *Polymer Sci. U.S.S.R.* 1965, **7**, 237
[18] *French Pat. No. 1366996* (to Shell Int. Research Mij).
[19] Ref. 2, pp 68 ff.
[20] VOLMER, M. *Kinetik der Phasenbildung.* Steinkopf: Leipzig, 1939
[21] LACMANN, R. *Z. Kristallogr.* 1961, **116**, 13

Notes and Communications

The Structure of Polycarbonate Spherulites

A STUDY of polycarbonate crystallization in thin films has revealed previously unreported phenomena. A new technique for breaking down film has been used. The preliminary findings are reported briefly and certain tentative conclusions concerning the structure of polycarbonate spherulites are put forward.

The material used in this study was Makrolon 3000/6521 (the polycarbonic ester of 2,2-bis(4-hydroxyphenol)-propane m.pt 222° to 230°C in the form of granules.

Solvent cast films were prepared by solvent evaporation on microscope cover glasses from 1·4 per cent chloroform solution. They were examined after standing in air for periods of between a few days and ten months. There was no detectable difference between observation at the two extremes of time so that it is unlikely that any of the phenomena observed were due to solvent retention. Melt cast films were prepared by melting and spreading the material on glass microscope slides at about 300°C and were then transferred directly to an annealing oven at 180°C for periods of between one and sixty hours. Some specimens were cooled and examined at regular intervals during the heating and others were heated for a predetermined time before examination and were not reheated. The intermittent cooling and reheating did not appear to affect the overall crystallization. Strain was introduced into the film by drawing the end of a microscope slide over the film just prior to transfer to the annealing oven. The films which could be stripped readily from the substrate when required were examined with a Beck polarizing microscope.

Spherulites in polycarbonate have been reported by several authors[1–4] and in the present work most of the types previously described have been observed.

Spherulites formed by heat treatment of melt cast film run through a distinct pattern of build up. The smallest resolvable particle which first appears is a roughly elliptical entity but light scatter makes the precise shape difficult to detect. This rapidly grows to a perfectly symmetrical dumb-bell shape (i.e. a rod with spherical swellings at each end) and no departure from this structure has been seen except where there has been an obvious interference with growth. Growth then commences roughly perpendicular to the dumb-bell between the swollen ends often at several different points. The spherulites appear to be fibrillar and built up of rope or ribbonlike entities, a general structure suggested by Keller[5–7]. Eventually the ends of the dumb-bell shaped particle fan out at an angle of about 90° filling two quadrants of a circle, the two remaining quadrants are filled by the growths perpendicular to the central portion. This picture is very similar to that reported by Schuur for gutta percha[8].

Occasionally the dumb-bell grows into a sheaf (as shown by Keller[7]) and proceeds to form a spherulite in the classical manner as summarized recently by Shubnikov[9].

The growth of spherulites is greatly influenced by stress. There appears to be a threshold stress below which spherulites are not formed and also an optimum stress for spherulite growth. The stress produced by crystallization and cooling in the solid state results in the majority of heat produced spherulites being cracked.

Spherulites formed in film cast by evaporation of chloroform solutions are always nearly perfect however small and show little obvious evidence of their build up from simpler units. However, study under polarized light with crossed polaroids and a first order tint plate show that the structure is similar to that produced by heat treatment in that two quadrants of the spherulite are joined through the centre by a narrow rod and the other two quadrants appear to arise by growth perpendicular to this. A dumb-bell structure can sometimes be seen in rapidly crystallized films. Solution grown spherulites appear to be much more regular and the rope or ribbon-like entities of which they are composed seem to be less branched and less tangled.

Heat treated spherulitic films can be etched with chloroform which first dissolves out the amorphous material between spherulites freeing them from the matrix. The spherulite itself is then dissolved piece by piece into its component parts, which ultimately appear as fan-like sections and small rods. The dissolution takes place along cracks and discontinuities in the spherulite. Relatively large fan-shaped portions finally break away at the centre.

If the corresponding solution cast spherulitic films are treated with chloroform they dissolve, both completely and rapidly, but a solution of chloroform in acetone will etch them satisfactorily. Solutions of between 60 and 80 per cent chloroform are suitable, the etching being fastest in solutions containing the most chloroform. 80 per cent chloroform solution appears to be critical since some film dissolves in it quickly and completely, whilst other portions of the same film are etched. Besides separating each spherulite from its neighbours the etching removes the centre of the spherulite before any other marked change is noticeable, *Figures 1* and *2*.

I suggest, therefore, that the centre of a spherulite is essentially amorphous. In formation from solution folded chain crystals grow on low energy folds of an amorphous particle or discontinuity; as soon as these crystals begin to grow they form into sheaves or dumb-bell shaped structures as has already been described. From solution the strains produced in crystallization are largely radial, so that the dumb-bells produce spherulites which consist largely of straight ribbons or rods of material radiating from the centre without much entanglement, branching or interlacing. When these dissolve they break up readily into rods of varying sizes mostly small compared to the size of the spherulite.

In heat treated material similar sheaves or dumb-bell shaped structures are probably formed at a discontinuity in the material which may be a partially oriented area or merely a void or a region of rapid stress change.

Figure 1—Solution cast polycarbonate film etched 15 min with 80 per cent chloroform–acetone. Polaroids parallel. Magnification about 750. Reduced 6/10 on reproduction

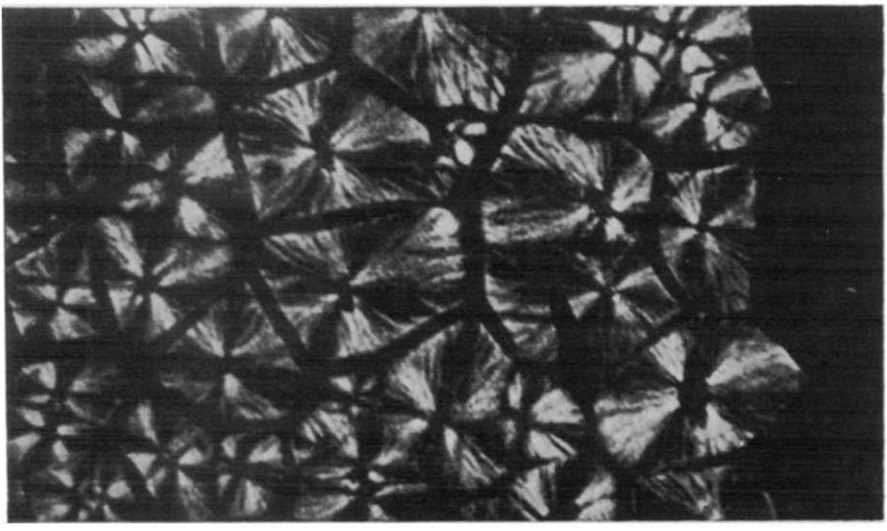

Figure 2—Solution cast polycarbonate film etched 15 min with 80 per cent chloroform–acetone. Polaroids crossed. Magnification about 750. Reduced 6/10 on reproduction

The spherulites grow in an environment of continuously varying stress and as a result consist of radiating rods or ribbons which suffer branching, entanglement and interlacing. The spherulite is not nearly as regular as it

appears consisting of a series of radially arranged overlapping fans of material loosely held together at the centre. The centre of this spherulite being a void or a particle of amorphous material not very closely associated with the rest of the structure, does not, when it dissolves, constitute a point for further attack by solvent.

The spherulite which is formed from solution, however, has a centre consisting of an amorphous particle surrounded by a random array of small crystallites embedded in amorphous material or with voids between them with the completely regular structure arising some distance from the centre. When attacked by solvent, therefore, both the amorphous material and the randomly arranged crystallites dissolve leaving a fairly large void in the structure. Little further change occurs unless the proportion of chloroform in the etching liquid is increased slightly when the spherulites often dissolve completely and rapidly from the centre towards the perimeter.

A detailed report of these investigations is being prepared for publication.

B. J. MACNULTY

Materials 1, Explosives Research and Development Establishment, Ministry of Technology, Waltham Abbey, Essex

(Received May 1967)

REFERENCES

[1] KAMPF, G. *Kolloidzschr.* 1960, **172**, 50
[2] KAMPF, G. *Kolloidzschr.* 1962, **185**, 6
[3] VON FALKAI, B. and RELLENSMANN, W. *Makromol. Chem.* 1964, **75**, 112
[4] VON FALKAI, B. and RELLENSMANN, W. *Makromol. Chem.* 1965, **88**, 38
[5] KELLER, A. *J. Polym. Sci.* 1955, **17**, 291
[6] KELLER, A. *J. Polym. Sci.* 1955, **17**, 351
[7] KELLER, A. and WARING, J. R. S. *J. Polym. Sci.* 1955, **17**, 447
[8] SCHUUR, G. *Commun. No. 276.* Rubber-Stichting: Delft, 1955
[9] SHUBNIKOV, A. V. *Soviet Phys. Crystallogr.* 1959, **2**, 578

Estimation of the Glass Transition of Polyethylene by Extrapolation of a Series of Polyethers

THERE has been much discussion about the glass transition of polyethylene[1(a)(b)]. The basic difficulty is the fact that this polymer is always highly crystalline and cannot be quenched to a glass; hence, the usual methods for measuring the transition temperature (dilatometry, calorimetry) do not give satisfactory results[2,3]. To be sure, definite transitions have been observed by dielectric and mechanical loss, but their assignment has been subject to some doubts. Thus, the well defined γ-transition at $-125°$ to $-130°$C has been ascribed to very limited segmented motion, and is not necessarily the main glass transition.

appears consisting of a series of radially arranged overlapping fans of material loosely held together at the centre. The centre of this spherulite being a void or a particle of amorphous material not very closely associated with the rest of the structure, does not, when it dissolves, constitute a point for further attack by solvent.

The spherulite which is formed from solution, however, has a centre consisting of an amorphous particle surrounded by a random array of small crystallites embedded in amorphous material or with voids between them with the completely regular structure arising some distance from the centre. When attacked by solvent, therefore, both the amorphous material and the randomly arranged crystallites dissolve leaving a fairly large void in the structure. Little further change occurs unless the proportion of chloroform in the etching liquid is increased slightly when the spherulites often dissolve completely and rapidly from the centre towards the perimeter.

A detailed report of these investigations is being prepared for publication.

B. J. MACNULTY

Materials 1, Explosives Research and Development Establishment, Ministry of Technology, Waltham Abbey, Essex

(Received May 1967)

REFERENCES

[1] KAMPF, G. *Kolloidzschr.* 1960, **172**, 50
[2] KAMPF, G. *Kolloidzschr.* 1962, **185**, 6
[3] VON FALKAI, B. and RELLENSMANN, W. *Makromol. Chem.* 1964, **75**, 112
[4] VON FALKAI, B. and RELLENSMANN, W. *Makromol. Chem.* 1965, **88**, 38
[5] KELLER, A. *J. Polym. Sci.* 1955, **17**, 291
[6] KELLER, A. *J. Polym. Sci.* 1955, **17**, 351
[7] KELLER, A. and WARING, J. R. S. *J. Polym. Sci.* 1955, **17**, 447
[8] SCHUUR, G. *Commun. No. 276.* Rubber-Stichting: Delft, 1955
[9] SHUBNIKOV, A. V. *Soviet Phys. Crystallogr.* 1959, **2**, 578

Estimation of the Glass Transition of Polyethylene by Extrapolation of a Series of Polyethers

THERE has been much discussion about the glass transition of polyethylene[1(a)(b)]. The basic difficulty is the fact that this polymer is always highly crystalline and cannot be quenched to a glass; hence, the usual methods for measuring the transition temperature (dilatometry, calorimetry) do not give satisfactory results[2,3]. To be sure, definite transitions have been observed by dielectric and mechanical loss, but their assignment has been subject to some doubts. Thus, the well defined γ-transition at $-125°$ to $-130°$C has been ascribed to very limited segmented motion, and is not necessarily the main glass transition.

In view of such difficulties some workers have resorted to the extrapolation of copolymer data, such as are afforded by the ethylene–vinyl acetate and ethylene–vinyl propionate systems[4]. Compositions containing less than 50 per cent ethylene are amorphous and have well defined glass transitions. However, the −25°C 'branching' transition causes complications for these materials[5], and the behaviour of the main transition in the 75 to 100 per cent ethylene compositions is always very difficult to determine.

A more promising approach is to measure transitions of a homologous series of polymers with increasing content of methylene groups. Grieveson[6] has presented data for several such series. The plot of glass transition temperature against weight fraction of methylene units gives straight lines that could be extrapolated to a value of about −165°C for pure polymethylene. As he points out, this treatment is equivalent to considering such series as random copolymers and using the Gordon–Taylor equation[7] with $k=1{\cdot}0$. In the data used by Grieveson the methylene content by weight did not exceed some 60 per cent, thus leaving a fairly long extrapolation to polymethylene.

We wish to show here that the well known polyether series —$(CH_2)_nO$— can also be treated in this manner. In this case a methylene content of nearly 80 per cent can be attained.

EXPERIMENTAL

Measurements were made by a mechanical loss method at about 1 c/s using a torsion pendulum. The glass transition was taken as the temperature at which the maximum in the loss modulus, G'', occurred.

n=1: Poly(oxymethylene)—A commercial sample of Celcon (Celanese Corp.) was used. In this case there are two peaks: the γ-transition at about −70°C and the β-transition at −10°C. The latter was taken as the glass transition in agreement with the recent work of Bohn[8] and Park[9]. According to Bohn, when a comonomer is added to poly(oxymethylene) the −10° transition increases in height and changes temperature position as expected for a glass transition, while the γ-peak at −70°C remains virtually unchanged.

n=2: Poly(ethylene oxide)—High molecular weight coagulant grade POLYOX (Union Carbide Chemicals Division) was used. This polymer is semi-crystalline. The limiting glass transition for very high molecular weights[10] is −53°C.

n=3: Poly(trimethylene oxide)—The sample was made in the laboratory and was not of very high molecular weight (intrinsic viscosity in benzene approximately 0·4). It had to be supported on a cellulose blotter to make mechanical loss measurements. The glass transition temperature was −68°C. This sample was partly amorphous when quenched, as the curve of the storage modulus, G', rose sharply (due to crystallization) after the transition was reached.

n=4: Poly(tetramethylene oxide)—The polymer was a laboratory sample of high molecular weight (intrinsic viscosity in benzene about 4·0). It could be made completely amorphous by quenching in liquid nitrogen. The transition occurred at −85°C and was clearly marked by a large peak in *G″*.

DISCUSSION

Transition temperatures are plotted in *Figure 1* for the four polyethers as

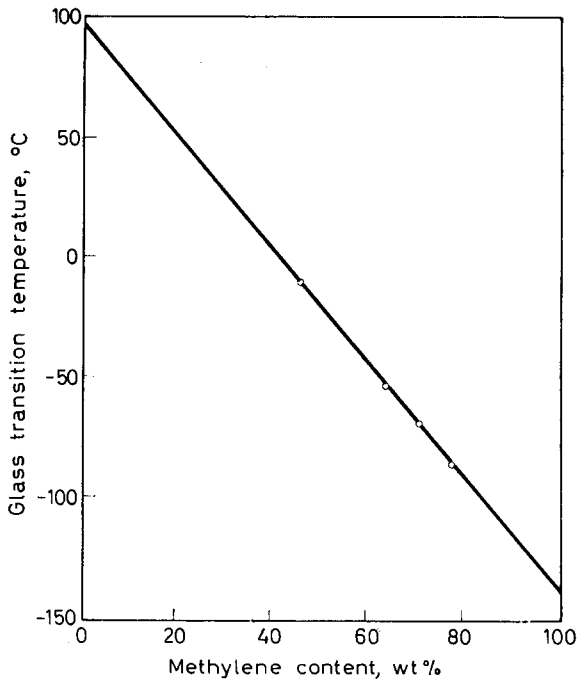

Figure 1 — Transition temperatures for four polyethers as a function of percentage content (by weight) of methylene

a function of methylene content on a weight basis. In so doing, we are essentially assuming that the main glass transition in this series is determined by a balance between the polar oxygen atom and the non-polar methylene groups of the repeat unit. It is apparent that the points for these polyethers fall on a rather good straight line, which can be extrapolated to about −135°C for (amorphous) polymethylene. This value coincides with the well known γ-transition of polyethylene. Indeed, in our view these transitions are to be regarded as being fundamentally the same. The difference between our −135°C and the −165°C value of Grieveson is in large part due to the different methods used. The mechanical loss experiment is 'faster' than dilatometry and consistently produces higher values for the transition temperature.

Although transition data were available previously for these polymers, the relationship shown in *Figure 1* was not evident for several reasons. Most important, the glass transition of poly(oxymethylene) was considered

to be $-70°C$, i.e. the γ-peak. For the pure, highly crystalline polymer this is the only apparent transition, and the β-peak is almost totally absent. The advent of less crystalline samples (Celcon contains small amounts of ethylene oxide which prevents complete crystallization) has shown the importance of the higher loss peak. Among others Bohn[8] has argued persuasively for identifying the β-peak as the main glass transition.

As for poly(trimethylene oxide) and poly(tetramethylene oxide), the results of Willbourn[11] show transitions of about $-50°C$ and $-55°C$. These high values are due in part to the use of frequencies of several hundred cycles per second and in part to the high crystallinity of the samples (as evidenced by low values of mechanical loss).

An interesting byproduct of the plot in *Figure 1* is the extrapolation to 100 per cent oxygen content. The hypothetical polymer of this composition should have a glass transition of about $+95°C$ among its other presumably highly interesting properties.

J. A. FAUCHER

Union Carbide Plastics Division,
Bound Brook, New Jersey

and J. V. KOLESKE

Union Carbide Chemicals Division,
South Charleston, West Virginia

(*Received May 1967*)

REFERENCES

[1(a)] BOYER, R. F. *Rubb. Chem. Technol.* 1963, **36**, 1341
[(b)] FAUCHER, J. A. and KOLESKE, J. V. *J. Polym. Sci.* 1962, **57**, 483
[2] QUINN, F. and MANDELKERN, L. *J. Amer. chem. Soc.* 1958, **80**, 3178
[3] DAINTON, F. S., EVANS, D. M., HOARE, F. E. and MELIA, T. P. *Polymer, Lond.* 1962, **3**, 277
[4] ILLERS, K. H. *Kolloidzschr.* 1963, **190**, 16
[5] REDING, F. P., FAUCHER, J. A. and WHITMAN, R. D. *J. Polym. Sci.* 1962, **57**, 483
[6] GRIEVESON, B. M. *Polymer, Lond.* 1960, **1**, 499
[7] GORDON, M. and TAYLOR, J. S. *J. appl. Chem.* 1952, **2**, 493
[8] BOHN, L. *Kolloidzschr.* 1965, **201**, 20
[9] PARK, I. K. *Bull. Amer. phys. Soc.* 1965, **11**, 213
[10] FAUCHER, J. A., KOLESKE, J. V., SANTEE JR, E. R., STRATTA, J. J. and WILSON, C. W. *J. appl. Phys.* 1966, **37**, 3962
[11] WILLBOURN, A. H. *Trans. Faraday Soc.* 1958, **54**, 717

Effect of Polarity on the Heats of Dilution of Polymethylmethacrylate Solutions

RECENTLY, Yamakawa *et al.*[1] have extended the thermodynamic treatment of high polymer solutions taking account of the effect of orientation of solvent molecules and polymer segments due to the polarity of one of the species or of both. Accordingly, the thermodynamic interaction parameter χ which characterizes the polymer–solvent pair is the sum of χ^* which comes from non-polar interactions and χ_p which comes from polar interactions.

to be $-70°C$, i.e. the γ-peak. For the pure, highly crystalline polymer this is the only apparent transition, and the β-peak is almost totally absent. The advent of less crystalline samples (Celcon contains small amounts of ethylene oxide which prevents complete crystallization) has shown the importance of the higher loss peak. Among others Bohn[8] has argued persuasively for identifying the β-peak as the main glass transition.

As for poly(trimethylene oxide) and poly(tetramethylene oxide), the results of Willbourn[11] show transitions of about $-50°C$ and $-55°C$. These high values are due in part to the use of frequencies of several hundred cycles per second and in part to the high crystallinity of the samples (as evidenced by low values of mechanical loss).

An interesting byproduct of the plot in *Figure 1* is the extrapolation to 100 per cent oxygen content. The hypothetical polymer of this composition should have a glass transition of about $+95°C$ among its other presumably highly interesting properties.

J. A. FAUCHER

Union Carbide Plastics Division,
Bound Brook, New Jersey

and J. V. KOLESKE

Union Carbide Chemicals Division,
South Charleston, West Virginia

(*Received May 1967*)

REFERENCES

[1(a)] BOYER, R. F. *Rubb. Chem. Technol.* 1963, **36**, 1341
[(b)] FAUCHER, J. A. and KOLESKE, J. V. *J. Polym. Sci.* 1962, **57**, 483
[2] QUINN, F. and MANDELKERN, L. *J. Amer. chem. Soc.* 1958, **80**, 3178
[3] DAINTON, F. S., EVANS, D. M., HOARE, F. E. and MELIA, T. P. *Polymer, Lond.* 1962, **3**, 277
[4] ILLERS, K. H. *Kolloidzschr.* 1963, **190**, 16
[5] REDING, F. P., FAUCHER, J. A. and WHITMAN, R. D. *J. Polym. Sci.* 1962, **57**, 483
[6] GRIEVESON, B. M. *Polymer, Lond.* 1960, **1**, 499
[7] GORDON, M. and TAYLOR, J. S. *J. appl. Chem.* 1952, **2**, 493
[8] BOHN, L. *Kolloidzschr.* 1965, **201**, 20
[9] PARK, I. K. *Bull. Amer. phys. Soc.* 1965, **11**, 213
[10] FAUCHER, J. A., KOLESKE, J. V., SANTEE JR, E. R., STRATTA, J. J. and WILSON, C. W. *J. appl. Phys.* 1966, **37**, 3962
[11] WILLBOURN, A. H. *Trans. Faraday Soc.* 1958, **54**, 717

Effect of Polarity on the Heats of Dilution of Polymethylmethacrylate Solutions

RECENTLY, Yamakawa *et al.*[1] have extended the thermodynamic treatment of high polymer solutions taking account of the effect of orientation of solvent molecules and polymer segments due to the polarity of one of the species or of both. Accordingly, the thermodynamic interaction parameter χ which characterizes the polymer–solvent pair is the sum of χ^* which comes from non-polar interactions and χ_p which comes from polar interactions.

Table 1. Heat of dilution data for PMMA solutions at 25°C

m_2 (g)	ϕ_2	ϕ'_2	$\Delta H_d \times 10^3$ (cal.)
Solvent: chlorobenzene			
1·341	$0{\cdot}147_7$	$0{\cdot}103_9$	$1{\cdot}94_9$
0·918	$0{\cdot}100_5$	$0{\cdot}079_1$	$1{\cdot}56_9$
0·920	$0{\cdot}100_5$	$0{\cdot}078_2$	$1{\cdot}05_6$
0·628	$0{\cdot}069_6$	$0{\cdot}054_1$	$2{\cdot}78_7$
0·616	$0{\cdot}069_6$	$0{\cdot}054_2$	$1{\cdot}80_6$
0·441	$0{\cdot}048_2$	$0{\cdot}038_0$	$1{\cdot}05_2$
0·307	$0{\cdot}033_7$	$0{\cdot}026_3$	$1{\cdot}23_6$
0·303	$0{\cdot}033_7$	$0{\cdot}026_2$	$0{\cdot}53_1$
0·214	$0{\cdot}023_4$	$0{\cdot}018_4$	$0{\cdot}74_2$
0·208	$0{\cdot}023_4$	$0{\cdot}018_0$	$1{\cdot}16_5$
Solvent: benzene			
1·290	$0{\cdot}139_5$	$0{\cdot}115_7$	$7{\cdot}19_5$
1·258	$0{\cdot}139_5$	$0{\cdot}110_6$	$10{\cdot}54_0$
0·854	$0{\cdot}095_3$	$0{\cdot}077_4$	$8{\cdot}44_5$
0·587	$0{\cdot}065_8$	$0{\cdot}052_6$	$7{\cdot}59_5$
0·579	$0{\cdot}065_8$	$0{\cdot}052_8$	$7{\cdot}82_5$
0·406	$0{\cdot}045_7$	$0{\cdot}036_6$	$6{\cdot}93_2$
0·404	$0{\cdot}045_7$	$0{\cdot}036_6$	$3{\cdot}29_5$
0·289	$0{\cdot}031_8$	$0{\cdot}025_4$	$3{\cdot}47_5$
0·283	$0{\cdot}031_8$	$0{\cdot}025_2$	$4{\cdot}10_7$
0·194	$0{\cdot}020_0$	$0{\cdot}017_4$	$2{\cdot}16_3$
0·192	$0{\cdot}020_0$	$0{\cdot}017_1$	$1{\cdot}83_4$
Solvent: *o*-dichlorobenzene			
1·395	$0{\cdot}153_9$	$0{\cdot}119_8$	$12{\cdot}63_9$
1·351	$0{\cdot}153_9$	$0{\cdot}121_0$	$14{\cdot}63_6$
0·974	$0{\cdot}105_7$	$0{\cdot}081_8$	$9{\cdot}49_0$
0·969	$0{\cdot}105_7$	$0{\cdot}083_0$	$9{\cdot}71_9$
0·680	$0{\cdot}073_4$	$0{\cdot}057_3$	$6{\cdot}05_3$
0·461	$0{\cdot}050_7$	$0{\cdot}040_0$	$4{\cdot}25_6$
0·450	$0{\cdot}050_7$	$0{\cdot}039_3$	$2{\cdot}70_1$
0·210	$0{\cdot}023_6$	$0{\cdot}018_5$	$0{\cdot}90_4$
0·136	$0{\cdot}015_2$	$0{\cdot}011_8$	$0{\cdot}27_8$
0·136	$0{\cdot}015_2$	$0{\cdot}011_9$	$-0{\cdot}06_5$

The parameter χ may be resolved into an entropy parameter and an enthalpy parameter. The enthalpy parameter, κ, is itself the sum of two parameters so that

$$\kappa = \kappa^* + \kappa_p$$

In connection with Yamakawa *et al.*'s theory, we may predict that:

(*a*) κ_p increases with increasing concentration when the dipole moment of the solvent (μ_1) is greater than that of the polymer (μ_2);

(*b*) $\kappa_p = 0$ when $\mu_1 = \mu_2$;

(*c*) κ_p decreases with increasing concentration when $\mu_1 < \mu_2$.

Corneliussen, Rice and Yamakawa[2] have tested the theory by determining χ for structurally similar polymers in a given solvent. In this work, we have used the theory to explain some results obtained on the heats of dilution of solutions of polymethylmethacrylate in benzene, chlorobenzene and *o*-dichlorobenzene.

The polymethylmethacrylate fraction used in this investigation came

from a commercial sample and the fractionation has been described elsewhere[3]. Its viscosity average molecular weight is 182 000 as determined in benzene and its average dipole moment[4] is 1·4 D. Its density[5] is 1·221 at 25°C. Reagent grade solvents were purified by distillation using a high efficiency column. The dipole moment of chlorobenzene[6] is 1·58 D and that of *o*-dichlorobenzene[6], 2·27 D. The heat of dilution measurements were carried out using a modified rocking Tian–Calvet microcalorimeter[7].

The calorimetric data are given in *Table 1* where m_2 is the mass of polymer and ΔH_d is the heat of dilution as measured. An apparent enthalpy parameter κ_a can be defined[8] by

$$\kappa_a = \Delta H_d V_1 / RT v_2 m_2 (\phi_2 - \phi_2') \tag{1}$$

where V_1 is the molar volume of solvent and v_2, the specific volume of polymer. ϕ_2 is the volume fraction of polymer before dilution and ϕ_2', after dilution. From equation (1), it is then possible to calculate κ_a for all three systems and *Figure 1* shows the variation of κ_a with the average

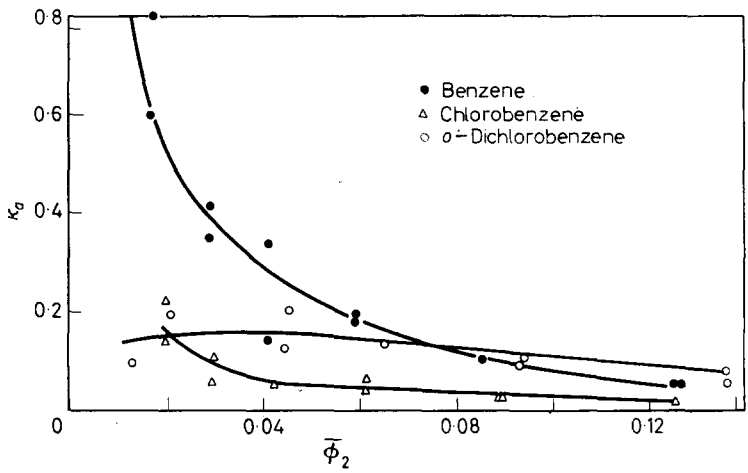

Figure 1—Variation of total enthalpy parameter with average volume fraction of polymethylmethacrylate in three different solvents at 25°C

volume fraction of polymer $\bar{\phi}_2$ $[=\frac{1}{2}(\phi_2 + \phi_2')]$. If one assumes that with PMMA and chlorobenzene $\mu_1 \approx \mu_2$, then $\chi_p = 0$ and also $\kappa_p = 0$; then $\kappa_a = \kappa^*$. The plot of κ_a versus $\bar{\phi}_2$ shows a slight increase with dilution at low concentration for chlorobenzene. If one assumes furthermore that κ^* is almost the same for the three solvents, one may conclude from *Figure 1* that κ_p decreases rapidly with increasing concentration with benzene as predicted by Yamakawa *et al.*'s theory since $\mu_2 > \mu_1$. For *o*-dichlorobenzene where $\mu_2 < \mu_1$, one sees that κ_p increases with concentration as predicted, when compared with chlorobenzene, since κ_a is almost independent of concentration and as $\kappa_p = \kappa_a - \kappa^*$. Thus, the effect of polarity change in solvent on κ_p seems to diminish rapidly as concentration increases. The theory predicts that χ_p varies less rapidly with concentration and one may

conclude that the entropy contribution to χ_p is more important than the enthalpy counterpart.

H. DAOUST
A. HADE

Department of Chemistry,
University of Montreal

(*Received June 1967*)

REFERENCES

[1] YAMAKAWA, H., RICE, S. A., CORNELIUSSEN, R. and KOTIN, L. *J. chem. Phys.* 1963, **38**, 1759
[2] CORNELIUSSEN, R., RICE, S. A. and YAMAKAWA, H. *J. chem. Phys.* 1963, **38**, 1768
[3] LÉONARD, J. and DAOUST, H. *Canad. J. Chem.* 1967, **45**, 409
[4] BRANDRUP, J. and IMMERGUT, E. H. *Polymer Handbook.* Interscience: New York, 1965
[5] FOX, T. G and LOSHAEK, S. *J. Polym. Sci.* 1955, **15**, 371
[6] MCCLELLAN, A. L. *Tables of Experimental Dipole Moments.* Freeman: San Francisco and London, 1963
[7] CALVET, E. and PRATT, H. *Microcalorimétrie. Applications physico-chimiques et biologiques.* Masson: Paris, 1956
[8] KABAYAMA, M. A. and DAOUST, H. *J. phys. Chem.* 1958, **62**, 1127

Proton Spin-Lattice Relaxation in Polyethylene Oxide

(*Comment on T. M. Connor's Note, this Journal 1966, 7, 426*)

IN THE calculation given in T. M. Connor's paper on the contribution of the rotating methyl groups to the total proton relaxation rate, spin diffusion is considered to be the relaxation limiting process and hence equation (1) is used

$$1/T_1 = 4\pi NbD \tag{1}$$

(See, for example, Abragam[1] p 382, where definitions of the symbols are also given.)

There are, however, two limiting cases, as shown by Rorschach[2] if spin diffusion plays an important role in nuclear spin relaxation: the 'diffusion limited' case, in which equation (1) applies, and the 'relaxation limited' case, in which the total relaxation is determined by the limited ability of the relaxation sinks—paramagnetic impurities, mobile molecules or atom-groups, as the case may be—to transport magnetization or Zeeman energy from the spin system to the lattice.

If the sinks are mobile groups of atoms, e.g. methyl groups, it is not possible to use Rorschach's criterion directly $\delta \ll 1$ or $\gg 1$ in order to distinguish between the two cases mentioned above. δ is defined by $\delta = \beta^2/2B^2$, where β is the pseudo-potential radius, introduced by de Gennes[3], and B is the barrier radius, introduced by Khutsishvili[4].

There is, however, another possibility to characterize the two cases, which may easily be applied to polyethylene oxide (PEO) and similar systems[5]. For the diffusion limited case, the nuclei that relax directly are 'practically

conclude that the entropy contribution to χ_p is more important than the enthalpy counterpart.

H. DAOUST
A. HADE

Department of Chemistry,
University of Montreal

(*Received June 1967*)

REFERENCES

[1] YAMAKAWA, H., RICE, S. A., CORNELIUSSEN, R. and KOTIN, L. *J. chem. Phys.* 1963, **38**, 1759
[2] CORNELIUSSEN, R., RICE, S. A. and YAMAKAWA, H. *J. chem. Phys.* 1963, **38**, 1768
[3] LÉONARD, J. and DAOUST, H. *Canad. J. Chem.* 1967, **45**, 409
[4] BRANDRUP, J. and IMMERGUT, E. H. *Polymer Handbook.* Interscience: New York, 1965
[5] FOX, T. G and LOSHAEK, S. *J. Polym. Sci.* 1955, **15**, 371
[6] MCCLELLAN, A. L. *Tables of Experimental Dipole Moments.* Freeman: San Francisco and London, 1963
[7] CALVET, E. and PRATT, H. *Microcalorimétrie. Applications physico-chimiques et biologiques.* Masson: Paris, 1956
[8] KABAYAMA, M. A. and DAOUST, H. *J. phys. Chem.* 1958, **62**, 1127

Proton Spin-Lattice Relaxation in Polyethylene Oxide

(*Comment on T. M. Connor's Note, this Journal 1966, 7, 426*)

IN THE calculation given in T. M. Connor's paper on the contribution of the rotating methyl groups to the total proton relaxation rate, spin diffusion is considered to be the relaxation limiting process and hence equation (1) is used

$$1/T_1 = 4\pi NbD \tag{1}$$

(See, for example, Abragam[1] p 382, where definitions of the symbols are also given.)

There are, however, two limiting cases, as shown by Rorschach[2] if spin diffusion plays an important role in nuclear spin relaxation: the 'diffusion limited' case, in which equation (1) applies, and the 'relaxation limited' case, in which the total relaxation is determined by the limited ability of the relaxation sinks—paramagnetic impurities, mobile molecules or atom-groups, as the case may be—to transport magnetization or Zeeman energy from the spin system to the lattice.

If the sinks are mobile groups of atoms, e.g. methyl groups, it is not possible to use Rorschach's criterion directly $\delta \ll 1$ or $\gg 1$ in order to distinguish between the two cases mentioned above. δ is defined by $\delta = \beta^2/2B^2$, where β is the pseudo-potential radius, introduced by de Gennes[3], and B is the barrier radius, introduced by Khutsishvili[4].

There is, however, another possibility to characterize the two cases, which may easily be applied to polyethylene oxide (PEO) and similar systems[5]. For the diffusion limited case, the nuclei that relax directly are 'practically

always' in thermal equilibrium with the lattice because of being in the neighbourhood of a paramagnetic impurity or participating in the fast motion of a mobile group of atoms. 'Practically always' here means most of the time which is needed to relax the total spin-magnetization of the specimen.

Those nuclei which relax indirectly do so as fast as is allowed by the limited transport of nuclear magnetization to the sinks via spin diffusion. The bottleneck is the diffusion. The ability of the sinks to relax nuclear magnetization is not fully exploited.

For the relaxation limited case, both types of nuclei (directly and indirectly relaxing) approach thermal equilibrium almost simultaneously. The bottleneck here is the relaxation, not the diffusion. The ability of the sinks to relax nuclear magnetization is fully exploited.

For the real relaxation process to occur, both steps—diffusion, and relaxation at the sinks—are necessary; they are coupled 'in series'. The slower step is the limiting one.

By using equation (1), T. M. Connor has shown that for the diffusion step

$$T_{1d} = \frac{1}{4\pi N}\left[\frac{g}{40}\gamma^4\hbar^2\left(\frac{\tau_c}{1+\omega_0^2\tau_c^2} + \frac{4\tau_c}{1+4\omega_0^2\tau_c^2}\right)\right]^{-1/4} D^{-3/4} \qquad (2)$$

which gives

$$T_{1d} = 8{\cdot}25 \times 10^{-3}\ \text{sec}$$

(the index d denotes diffusion) using the following numerical values: $N = L/M$; $L = 6{\cdot}02 \times 10^{23}$ molecules/mol; $M = 750$ g/mol; $\gamma = \gamma_{\text{proton}} = 2{\cdot}675 \times 10^4$ sec^{-1} Oe^{-1}; $\omega_0\tau_c = 0{\cdot}616$; $\omega_0 = 2\pi \times 30 \times 10^6$ sec^{-1}; $D = [\{\overline{\Delta\omega^2}\}^{1/2}/30]\, a^2$; $\{\overline{\Delta\omega^2}\}^{1/2} = 5 \times 2{\cdot}7 \times 10^4$ sec^{-4}; $a = 2{\cdot}5$ Å.

The relaxation step gives

$$\frac{1}{T_{1r}} = 2\frac{n_{CH3}}{n_H}\frac{2}{5}\frac{\gamma^4\hbar^2}{a'^6} I(I+1)\left[\frac{\tau_c}{1+\omega_0^2\tau_c^2} + \frac{4\tau_c}{1+4\omega_0^2\tau_c^2}\right] \qquad (3)$$

The index r denotes relaxation. The initial factor two is necessary because every proton in a methyl group interacts with *two* neighbouring protons. n_{CH3}/n_H is the ratio of the number of nuclei relaxing *directly* to the total number of relaxing nuclei, and for PEO of molecular weight 750, $n_{CH3}/n_H = 3/106$.

The remaining part of the above formula is the usual BPP formula (see ref. 1, p 300) which should be modified, it's true, because the methyl groups do not move in an isotropic random manner, as is assumed in the derivation of the BPP formula, but are restricted to rotations about one single axis. Using $a' = 1{\cdot}76$ Å as the distance between protons in the methyl group gives $T_{1r} = 1{\cdot}24$ sec.

Comparing T_{1d} and T_{1r}, we conclude that the relaxation process is much slower than the diffusion process, and is indeed the limiting one. Our numerical value compares favourably with Connor's experimental value which is near the T_1 minimum of about 0·9 sec.

It must be recalled that there are some other relaxation mechanisms parallel to that considered here, e.g. the *direct* relaxation of CH_2 protons by the rapid fluctuating magnetic fields produced by the rotating methyl groups. These other mechanisms will shorten T_1.

The above considerations show that our interpretation can explain Connor's experimental results quite well and, in fact, considerably improve his discrepancy between theory and experiment.

I am obliged to T. M. Connor for sending me a reprint of his paper and for a discussion of this comment before publication.

U. HAEBERLEN

I. Physikalisches Institut der Technischen Hochschule Stuttgart,
Weiderholdstrasse 13,
7 Stuttgart N, Germany

(*Received June 1967*)

REFERENCES

[1] ABRAGAM, A. *The Principles of Nuclear Magnetism*, Oxford, 1961
[2] RORSCHACH, H. E. *Physicas', Grav.* 1964, **30**, 38
[3] DE GENNES, P. G. *Physics Chem. Solids*, 1958, **7**, 345
[4] KHUTSISHVILI, G. R. *J. exp. theor. Phys., Moscow*, 1962, **42**, 1311
[5] HAEBERLEN, U. *Dissertation*, T. H. Stuttgart, 1967

Mechanical Degradation of Polystyrene in Solution

IN THE year 1930 Staudinger[1] observed degradation of dilute polystyrene solutions by hydrodynamic shear. Since that time the breaking of long-chain molecules mechanically and ultrasonically has been investigated extensively[2]. Among recent publications, that of Harrington and Zimm[3] should be mentioned. In their experiments reductions in specific viscosity of the order of 40 per cent were produced in solutions of polystyrene (degree of polymerization 10^5) passed five times through a capillary where the maximum shearing force was 10^{+6} sec^{-1}. In 1944 Frenkel[4] presented a theory of stability of linear molecules, according to which the hydrodynamic shear rate necessary to cause a rupture of a long-chain molecule is inversely proportional to the square of the number of segments in it. Thus sufficiently high molecular weight polymer could be degraded at relatively low rates of shear.

We have observed polymer degradation in a capillary viscometer using polystyrene for which the limiting viscosity number was about 1 400 ml/g with an estimated degree of polymerization $>10^5$. To eliminate the effects due to oxygen, the polystyrene solution in toluene was deaerated and sealed under vacuum. The viscometer was automatically rotated at intervals and a fixed volume was allowed to flow through the capillary. The solution contained 0·070 per cent of polymer. The rate of shear at the wall of the capillary of 0·80 mm diameter was 180 sec^{-1} at the beginning of the experiments. The flow time dropped from 550 sec to about 462 sec after

It must be recalled that there are some other relaxation mechanisms parallel to that considered here, e.g. the *direct* relaxation of CH_2 protons by the rapid fluctuating magnetic fields produced by the rotating methyl groups. These other mechanisms will shorten T_1.

The above considerations show that our interpretation can explain Connor's experimental results quite well and, in fact, considerably improve his discrepancy between theory and experiment.

I am obliged to T. M. Connor for sending me a reprint of his paper and for a discussion of this comment before publication.

U. HAEBERLEN

I. Physikalisches Institut der Technischen Hochschule Stuttgart,
Weiderholdstrasse 13,
7 Stuttgart N, Germany

(*Received June 1967*)

REFERENCES

[1] ABRAGAM, A. *The Principles of Nuclear Magnetism*, Oxford, 1961
[2] RORSCHACH, H. E. *Physicas', Grav.* 1964, **30**, 38
[3] DE GENNES, P. G. *Physics Chem. Solids*, 1958, **7**, 345
[4] KHUTSISHVILI, G. R. *J. exp. theor. Phys., Moscow*, 1962, **42**, 1311
[5] HAEBERLEN, U. *Dissertation*, T. H. Stuttgart, 1967

Mechanical Degradation of Polystyrene in Solution

IN THE year 1930 Staudinger[1] observed degradation of dilute polystyrene solutions by hydrodynamic shear. Since that time the breaking of long-chain molecules mechanically and ultrasonically has been investigated extensively[2]. Among recent publications, that of Harrington and Zimm[3] should be mentioned. In their experiments reductions in specific viscosity of the order of 40 per cent were produced in solutions of polystyrene (degree of polymerization 10^5) passed five times through a capillary where the maximum shearing force was 10^{+6} sec^{-1}. In 1944 Frenkel[4] presented a theory of stability of linear molecules, according to which the hydrodynamic shear rate necessary to cause a rupture of a long-chain molecule is inversely proportional to the square of the number of segments in it. Thus sufficiently high molecular weight polymer could be degraded at relatively low rates of shear.

We have observed polymer degradation in a capillary viscometer using polystyrene for which the limiting viscosity number was about 1 400 ml/g with an estimated degree of polymerization $>10^5$. To eliminate the effects due to oxygen, the polystyrene solution in toluene was deaerated and sealed under vacuum. The viscometer was automatically rotated at intervals and a fixed volume was allowed to flow through the capillary. The solution contained 0·070 per cent of polymer. The rate of shear at the wall of the capillary of 0·80 mm diameter was 180 sec^{-1} at the beginning of the experiments. The flow time dropped from 550 sec to about 462 sec after

28 220 passages as shown in *Figure 1* where flow times are plotted against the logarithm of the number of passages through the capillary. The time between the first and last passage is 250 days. Another viscometer with the same solution served as a control standard. It showed only the change corresponding to the number of passages which were necessary to determine the viscosity from time to time.

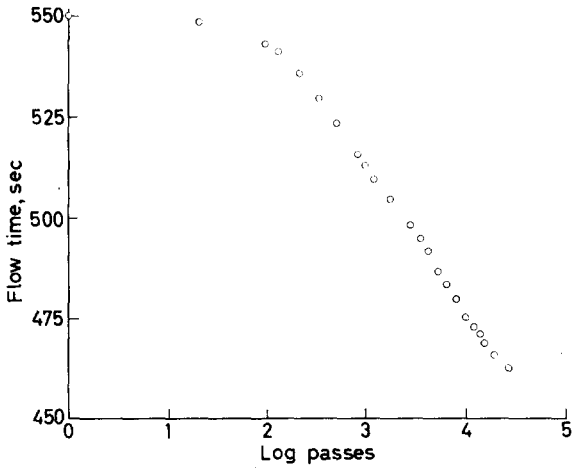

Figure 1—Flow time as a function of the logarithm of the number of passages through the capillary

The fact that each succeeding passage had less and less influence on the decrease in viscosity is a clear indication that as the size of the macromolecule is decreased it is less liable to be disrupted. This follows also from the calculations of Frenkel[4], according to which the disrupting force at a given rate of shear increases proportionally to the square of the number of monomer units in the molecule. As the rate of shear in a capillary viscometer varies from a maximum value at the wall to zero, and as the polymer is not of a homogeneous size, the actual behaviour is difficult to estimate. The polymer might also contain, to a very small extent, besides carbon–carbon links, some weaker links (peroxidic perhaps). Also the disruption may be due partly to the presence of tangled molecules.

The molecular weight distribution curve of the polymer used was not known. We hope to be able to perform the experiments with more homogeneous material.

D. E. MOORE

Department of Pharmacy,
University of Sydney,
Sydney, Australia

and A. G. PARTS

Department of Physical Chemistry,
University of Sydney

(*Received September 1967*)

REFERENCES

[1] STAUDINGER, H. *Ber. dtsch. chem. Ges.* 1930, **63**, 3152

[2] JELLINEK, H. H. G. *Degradation of Vinyl Polymers,* Chapter 4. Academic Press: New York, 1955

[3] HARRINGTON, R. E. and ZIMM, B. H. *J. phys. Chem.* 1965, **69**, 161

[4] FRENKEL, J. *Acta phys.-chim. U.R.S.S.* 1944, **19**, 51

The Effect of Casting Conditions on the Crystalline Forms of Nylon-6 Films

IT IS well known that Nylon-6 (polycaproamide) can exist in at least two well defined crystalline forms. These forms have been shown to be monoclinic and hexagonal (or psuedo-hexagonal) by X-ray diffraction techniques, and are usually described as α- and γ-respectively[1]. The α-form is the more stable up to about 150°C. Both crystalline forms can occur in samples of Nylon-6 yarn. Yarn which has been freshly spun from the polymer melt is amorphous and unoriented, but crystallizes to the γ-form on standing. Conversion to the α-form is encouraged by drawing or annealing.

During attempts to correlate the crystalline structure of Nylon-6 films with sample history, we have come to recognize the importance of standardizing the conditions under which the films are cast from solutions of polymer. We have examined the spectra of a series of films of Nylon-6 obtained by dissolving about 1 g of polymer in 10 ml of formic acid or orthochlorophenol at room temperature, and spreading about 0·5 ml of the resultant solution on to a variety of surfaces at controlled temperatures. After complete removal of the solvent by evaporation, the infra-red spectrum of such a film was obtained using a Unicam SP.200 spectrometer.

The two crystalline forms of Nylon-6 can be conveniently distinguished by relatively weak absorption bands in the region of 10 to 11 microns. The α-form absorbs at 960 cm^{-1} and 928 cm^{-1}, the γ-form at 977 cm^{-1}. In the course of his work on the polarized micro-infra-red spectroscopy of doubly oriented Nylon-6 specimens, Arimoto has assigned these absorption frequencies to —CONH in-plane vibrations[2]. It is largely on the basis of these 'diagnostic bands' that our conclusions have been drawn.

When a solution of Nylon-6 yarn in formic acid was spread on to a plane glass surface and the solvent evaporated, it was found that the α-crystalline form predominated in the resultant film. The presence of a weak 'shoulder' at about 980 cm^{-1} suggested that a small amount of γ-crystalline form might also have been present. When the same polymer solution was spread on to mercury, nickel foil, phenoplast, polycarbonate or polyester surfaces, films of similar composition were obtained. (The procedure was carried out at various temperatures between 20°C and 50°C for the glass surface, at 20°C for the mercury surface, and at 35°C for each of the others.) Upon spreading the same solution on to the (100) faces of either sodium chloride or potassium bromide at 35°C, however, the spectra indicated that the resultant films were largely in the γ-crystalline form. An examination of the spectra of a series of films cast from the same solution on to a sodium chloride surface at 30°, 35°, 40°, 45° and 50°C indicated that the propor-

REFERENCES

[1] STAUDINGER, H. *Ber. dtsch. chem. Ges.* 1930, **63**, 3152

[2] JELLINEK, H. H. G. *Degradation of Vinyl Polymers,* Chapter 4. Academic Press: New York, 1955

[3] HARRINGTON, R. E. and ZIMM, B. H. *J. phys. Chem.* 1965, **69**, 161

[4] FRENKEL, J. *Acta phys.-chim. U.R.S.S.* 1944, **19**, 51

The Effect of Casting Conditions on the Crystalline Forms of Nylon-6 Films

IT IS well known that Nylon-6 (polycaproamide) can exist in at least two well defined crystalline forms. These forms have been shown to be monoclinic and hexagonal (or psuedo-hexagonal) by X-ray diffraction techniques, and are usually described as α- and γ-respectively[1]. The α-form is the more stable up to about 150°C. Both crystalline forms can occur in samples of Nylon-6 yarn. Yarn which has been freshly spun from the polymer melt is amorphous and unoriented, but crystallizes to the γ-form on standing. Conversion to the α-form is encouraged by drawing or annealing.

During attempts to correlate the crystalline structure of Nylon-6 films with sample history, we have come to recognize the importance of standardizing the conditions under which the films are cast from solutions of polymer. We have examined the spectra of a series of films of Nylon-6 obtained by dissolving about 1 g of polymer in 10 ml of formic acid or orthochlorophenol at room temperature, and spreading about 0·5 ml of the resultant solution on to a variety of surfaces at controlled temperatures. After complete removal of the solvent by evaporation, the infra-red spectrum of such a film was obtained using a Unicam SP.200 spectrometer.

The two crystalline forms of Nylon-6 can be conveniently distinguished by relatively weak absorption bands in the region of 10 to 11 microns. The α-form absorbs at 960 cm^{-1} and 928 cm^{-1}, the γ-form at 977 cm^{-1}. In the course of his work on the polarized micro-infra-red spectroscopy of doubly oriented Nylon-6 specimens, Arimoto has assigned these absorption frequencies to —CONH in-plane vibrations[2]. It is largely on the basis of these 'diagnostic bands' that our conclusions have been drawn.

When a solution of Nylon-6 yarn in formic acid was spread on to a plane glass surface and the solvent evaporated, it was found that the α-crystalline form predominated in the resultant film. The presence of a weak 'shoulder' at about 980 cm^{-1} suggested that a small amount of γ-crystalline form might also have been present. When the same polymer solution was spread on to mercury, nickel foil, phenoplast, polycarbonate or polyester surfaces, films of similar composition were obtained. (The procedure was carried out at various temperatures between 20°C and 50°C for the glass surface, at 20°C for the mercury surface, and at 35°C for each of the others.) Upon spreading the same solution on to the (100) faces of either sodium chloride or potassium bromide at 35°C, however, the spectra indicated that the resultant films were largely in the γ-crystalline form. An examination of the spectra of a series of films cast from the same solution on to a sodium chloride surface at 30°, 35°, 40°, 45° and 50°C indicated that the propor-

tion of γ-form to α-form increased with increasing temperature of the casting surface.

Preliminary studies on the specific orientations of certain groups contained in the polymer film were made by obtaining spectra with the plane of the film at 90° and 45° to the direction of the infra-red beam. Using films in which the γ-crystalline form predominated, it was found that the absorbances of the —NH and —C═O stretching vibrations were on average slightly greater with the plane of the film at 45° than they were at 90° to the beam direction. This suggests that these polar groups tend to be oriented perpendicular to the plane of the film. It is therefore thought that a considerable interaction occurs between the substrate ions and the polar groups of the polymer in the formation of the γ-crystalline form.

The influence of alkali halide substrates on the orientation of crystal overgrowths has been reported by other workers[3–5]. For example, Fischer and Willems have observed epitaxial crystallization of polyamides cast from *m*-cresol solution on to (001) potassium chloride faces[4]. Nylon-6 in particular was found to crystallize in the α-form under these conditions.

Our work has shown that the solvent as well as the substrate can affect the deposition process. Thus, in contrast to our observations made on films prepared from solutions of polymer in formic acid, we have found that α-crystalline form always predominates in a film cast from a solution of Nylon-6 yarn in *o*-chlorophenol, irrespective of whether the casting surface is plane glass or sodium chloride at 37°C or 50°C. Hence the solvent in which the Nylon-6 is dissolved, as well as the surface on to which the films are cast, must influence the crystalline form produced.

All the above results refer to solutions made from stretched yarn, but were not significantly different for solutions prepared from unstretched yarn or the polymer chips from which the yarn had been melt-spun. It is clear therefore that the casting conditions (i.e. solvent, casting surface, temperature) and not the polymer history, govern the type of crystalline form produced. Under the experimental conditions employed the above results can be reduced to the statement that the γ-form was only produced to any significant extent in a film, when a formic acid solution of Nylon-6 was cast on to an alkali halide surface.

J. W. DODD,

Department of Chemistry and Metallurgy,
Lanchester College of Technology,
Coventry

P. HOLLIDAY

Acetate and Synthetic Fibres Laboratory,
Courtaulds Ltd,
Coventry

and B. E. PARKER

Department of Chemistry and Metallurgy,
Lanchester College of Technology,
Coventry

(*Received September 1967*)

REFERENCES
[1] BRADBURY, E. M., BROWN, L., ELLIOTT, A. and PARRY, D. A. D. *Polymer, Lond.* 1965, **6**, 465
[2] ARIMOTO, H. *J. Polym. Sci. A*, 1964, **2**, 2283
[3] VAN DER MERWE, J. H. *Disc. Faraday Soc.* 1949, **5**, 201
[4] FISCHER, E. W. and WILLEMS, J. *Makromol. Chem.* 1966, **99**, 85
[5] KOUTSKY, J. A., WALTON, A. G. and BAER, E. *J. Polym. Sci. A-2*, 1966, **4**, 611

A Note on Vapour Diffusion and Polymer Structure

Two aspects of the effect of polymer structure on the diffusion and solution of organic vapours in rubbery membranes are reported on briefly. The first is the effect of *cis–trans* isomerization in the polyisoprene chain in relation to the permeation of *n*-butane through natural rubber (NR), gutta percha (GP) and a *cis–trans* (2:3 mole ratio) polyisoprene (CTP). The second is the effect of changes in a side group to the main chain as in the permeation of propane through polydimethylsiloxane (DMS), a polyphenylmethylsiloxane (PMS) copolymer and poly-3,3,3-trifluoropropylmethylsiloxane (FMS). The polyisoprene membranes were supplied by the Natural Rubber Producers Research Association and were prepared from deproteinized gum by curing lightly with dicumyl peroxide. From swelling measurements in benzene the molecular weight between crosslinks was estimated as 7 400, 4 500 and 13 000 for NR, CTP and GP respectively. The silicone membranes were supplied by Midland Silicones Ltd and the Dow Corning Corporation and were lightly crosslinked with peroxides. The PMS sample was a copolymer of PhMeSiO and $(Me)_2SiO$ units and contained 7·5 mole per cent of PhMeSiO.

Permeation measurements were made at several temperatures with conventional apparatus to give the steady state permeability $\overline{P}$ and the time lag L[1,2]. The diffusion constant D was obtained from $D=l^2/6L$ where l is the membrane thickness, and the Henry's law solubility coefficient[1] σ from the relation $\overline{P}=D\sigma$. The results, along with those for the propane–natural rubber system of a previous investigation[3], are shown in *Table 1*. The relationships $D=D_0\exp(-E_D/RT)$ and $\sigma=\sigma_0\exp(-\Delta\overline{H}^0/RT)$ were obeyed with D_0 and σ_0 effectively independent of temperature over the range investigated. Values of E_D, D_0 and $\Delta\overline{H}^0$ are also given in *Table 1*. The errors in the $\overline{P}$ and D values were estimated to be approximately ± 2 per cent and ± 5 per cent respectively. The error in σ is correspondingly larger as it was obtained indirectly from the ratio $\overline{P}/D$.

Within the experimental error there is no significant difference in the diffusion and solution behaviour of *n*-butane in the three polyisoprenes. Values of the glass transition temperature T_g were also obtained for all six polymers using a Du Pont Differential Thermal Analyser and are given in *Table 2*. Saunders[4], from photoelastic measurements, suggested that the gutta percha chain compared with that of natural rubber is stiffer and less kinked, in keeping with its higher crystalline melting point. Although *cis–trans* isomerization in the polyisoprene chain has a marked effect on its

REFERENCES
[1] BRADBURY, E. M., BROWN, L., ELLIOTT, A. and PARRY, D. A. D. *Polymer, Lond.* 1965, **6**, 465
[2] ARIMOTO, H. *J. Polym. Sci. A*, 1964, **2**, 2283
[3] VAN DER MERWE, J. H. *Disc. Faraday Soc.* 1949, **5**, 201
[4] FISCHER, E. W. and WILLEMS, J. *Makromol. Chem.* 1966, **99**, 85
[5] KOUTSKY, J. A., WALTON, A. G. and BAER, E. *J. Polym. Sci. A-2*, 1966, **4**, 611

A Note on Vapour Diffusion and Polymer Structure

Two aspects of the effect of polymer structure on the diffusion and solution of organic vapours in rubbery membranes are reported on briefly. The first is the effect of *cis–trans* isomerization in the polyisoprene chain in relation to the permeation of *n*-butane through natural rubber (NR), gutta percha (GP) and a *cis–trans* (2:3 mole ratio) polyisoprene (CTP). The second is the effect of changes in a side group to the main chain as in the permeation of propane through polydimethylsiloxane (DMS), a polyphenylmethylsiloxane (PMS) copolymer and poly-3,3,3-trifluoropropylmethylsiloxane (FMS). The polyisoprene membranes were supplied by the Natural Rubber Producers Research Association and were prepared from deproteinized gum by curing lightly with dicumyl peroxide. From swelling measurements in benzene the molecular weight between crosslinks was estimated as 7 400, 4 500 and 13 000 for NR, CTP and GP respectively. The silicone membranes were supplied by Midland Silicones Ltd and the Dow Corning Corporation and were lightly crosslinked with peroxides. The PMS sample was a copolymer of PhMeSiO and $(Me)_2SiO$ units and contained 7·5 mole per cent of PhMeSiO.

Permeation measurements were made at several temperatures with conventional apparatus to give the steady state permeability $\overline{P}$ and the time lag L[1,2]. The diffusion constant D was obtained from $D=l^2/6L$ where l is the membrane thickness, and the Henry's law solubility coefficient[1] σ from the relation $\overline{P}=D\sigma$. The results, along with those for the propane–natural rubber system of a previous investigation[3], are shown in *Table 1*. The relationships $D=D_0\exp(-E_D/RT)$ and $\sigma=\sigma_0\exp(-\Delta\overline{H}^0/RT)$ were obeyed with D_0 and σ_0 effectively independent of temperature over the range investigated. Values of E_D, D_0 and $\Delta\overline{H}^0$ are also given in *Table 1*. The errors in the $\overline{P}$ and D values were estimated to be approximately ± 2 per cent and ± 5 per cent respectively. The error in σ is correspondingly larger as it was obtained indirectly from the ratio $\overline{P}/D$.

Within the experimental error there is no significant difference in the diffusion and solution behaviour of *n*-butane in the three polyisoprenes. Values of the glass transition temperature T_g were also obtained for all six polymers using a Du Pont Differential Thermal Analyser and are given in *Table 2*. Saunders[4], from photoelastic measurements, suggested that the gutta percha chain compared with that of natural rubber is stiffer and less kinked, in keeping with its higher crystalline melting point. Although *cis–trans* isomerization in the polyisoprene chain has a marked effect on its

Table 1. Values of D, $\overline{P}$ and σ

Vapour	°*K*	$D \times 10^6$ ($cm^2\ sec^{-1}$)			$\overline{P} \times 10^7 \left(\frac{cm^3\ s.t.p. \cdot cm}{cm^2 \cdot cm\ Hg \cdot sec}\right)$			$\sigma \times 10^2 \left(\frac{cm^3\ s.t.p.}{cm^3 \cdot cm\ Hg}\right)$		
n-C_4H_{10}		*NR*	*CTP*	*GP*	*NR*	*CTP*	*GP*	*NR*	*CTP*	*GP*
	323·2	0·60	0·65	0·62	0·94	0·87	0·91	15·7	13·4	14·7
	333·2	0·89	0·94	0·9	1·09	1·01	1·06	12·2	10·7	11·8
	343·2	1·3	1·3	1·3	1·25	1·17	1·21	9·7	8·7	9·2
	353·2	1·8	1·9	1·9	1·42	1·35	1·39	7·8	7·2	7·5
	363·2	2·6	—	2·6	1·60	—	1·57	6·3	—	6·0
C_3H_8		*NR*	*DMS*	*PMS*	*FMS*	*NR*	*DMS*	*PMS*	*FMS*	*NR*	*DMS*	*PMS*	*FMS*
	303·2	0·29	6·4	5·1	0·95	0·177	5·5	5·2	0·53	6·0	8·6	10·2	5·6
	313·2	0·50	7·6	6·3	1·28	0·264	5·3	5·2	0·64	5·3	7·0	8·3	5·0
	323·2	0·80	8·9	7·5	1·7	0·356	5·05	5·2	0·75	4·4	5·7	6·9	4·4
	333·2	1·26	10·4	8·8	2·2	0·473	4·9	5·2	0·87	3·8	4·7	5·8	4·0
	343·2	—	11·9	10·4	2·85	—	4·7	5·2	0·98	—	3·9	5·0	3·4

Table 2. Values of E, D_0 and $\overline{\Delta H^0}$

Vapour	*Polymer*	T_g (°C)	E_D ($kcal\ mole^{-1}$)	D_0 ($cm^2\ sec^{-1}$)	$\overline{\Delta H^0}$ ($kcal\ mole^{-1}$)
n-C_4H_{10}	*NR*	−66	8·5	0·34	−4·9
	CTP	−69	8·1	0·17	−5·3
	GP	−68	8·4	0·30	−5·2
C_3H_8	*DMS*	−120	3·2	0·0012	−3·9
	PMS	−118	3·5	0·002	−3·8
	FMS	−73	5·6	0·011	−2·6
	NR	−66	9·8	3·2	−3·3

crystallization behaviour it would appear that its effect on segmental mobility is much less pronounced.

The replacement of a methyl group in the Me_2SiO unit by the bulky 3,3,3-trifluoropropyl constituent decreases appreciably both the permeability and the diffusion coefficient and raises the glass transition temperature. The introduction of the fluoro substituent leads presumably to a stiffening of the main chain by increasing either the steric hindrance to segmental rotation or the interchain attractive forces. The higher activation energy for diffusion E_D and pre-exponential factor D_0 are therefore to be expected. On the other hand the transport properties of the PMS copolymer differ little from those of the pure polydimethylsiloxane. Polmanteer and Hunter[5] showed that for copolymer gum containing 7·5 mole per cent of PhMeSiO units T_g was raised several degrees but the effect on the crystallization temperature was much more striking. Again segmental motion is not affected to the same extent as crystallization behaviour by these structural changes.

The NR and FMS samples have approximately the same T_g but quite different D values. Also for polyisobutylene with a T_g around $-70°C$ the diffusion coefficient for propane at 35°C is several orders of magnitude[6] smaller ($D = 4{\cdot}8 \times 10^{-9}$ cm^2 sec^{-1}). It is clear that for these systems the diffusion coefficient cannot be expressed as a function of T_g only.

The high permeabilities and low activation energies for diffusion obtained with the silicone polymers have already been discussed[7]. A transition-state theory analysis of the D_0 values in *Table 2* would yield negative entropies of activation for diffusion for the silicones and positive entropies for the polyisoprenes. In this respect the silicones are liquid-like in their behaviour[8]. However, the fluorosilicones tend to normal elastomer behaviour with a higher value for E_D and a $\overline{P}$ which increases with temperature (cf. the temperature dependence of $\overline{P}$ for DMS and PMS in *Table 1*).

J.C.T. and J.B.A. are indebted to the Dunlop Rubber Company and N.A.T.O. respectively for scholarships. The authors are also grateful to the Natural Rubber Producers Research Association, Midland Silicones Ltd and Dow Corning Corporation for the preparation of samples.

J. B. ALEXOPOULOS,
J. A. BARRIE,
J. C. TYE
and M. FREDRICKSON

Physical Chemistry Department,
Imperial College of Science and Technology,
South Kensington, London, S.W.7

(*Received September 1967*)

REFERENCES

[1] DAYNES, H. *Proc. Roy. Soc. A*, 1920, **97**, 286
[2] BARRER, R. M. *Diffusion in and through Solids*, p 18. Cambridge University Press: London, 1951

[3] BARRIE, J. A., LEVINE, J. D., MICHAELS, A. S. and WONG, P. *Trans. Faraday Soc.* 1963, **59**, 869
[4] SAUNDERS, D. W. *Trans. Faraday Soc.* 1957, **53**, 860
[5] POLMANTEER, K. E. and HUNTER, M. J. *J. appl. Polym. Sci.* 1959, **1**, 3
[6] PRAGER, S. and LONG, F. A. *J. Amer. chem. Soc.* 1951, **73**, 4072
[7] BARRER, R. M., BARRIE, J. A. and RAMAN, K. *Polymer, Lond.* 1962, **3**, 595
[8] BARRER, R. M. and CHIO, H. T. *J. Polym. Sci. C*, 1965, **10**, 111

The Polymerization of Isobutyl Vinyl Ether by Diethylaluminium Chloride

WE have found that $AlEt_2Cl$ is completely inactive for the polymerization of isobutyl vinyl ether. This fact is inconsistent with the result reported by Natta[1], and adds an additional example to Kennedy's finding[2] concerning the cationic inactivity of $AlEt_2Cl$ for the polymerization of olefins and dienes.

$AlEt_2Cl$ requires a cocatalyst for both stereospecific and non-stereospecific polymerization of isobutyl vinyl ether. Oxygen is an effective cocatalyst for the high stereospecific, carbon dioxide–oxygen combination for the low stereospecific, and water for the non-stereospecific polymerization. The polymerization reactions catalysed by these catalyst systems proceed in an apparently homogeneous phase.

As a measure of stereospecificity we use the value of the index of stereospecificity (*I.S.*), which is defined as the percentage of the weight of methyl ethyl ketone (MEK) insoluble fraction against the total polymer yield (*Y*). Fractionation of the polymer was carried out by using 100 ml of MEK per 0·5 g of the total polymer at 30°C for 48 h. Polymerization was carried out at −78°C by using 15 ml of toluene, $7{\cdot}63 \times 10^{-3}$ mole of the monomer and $1{\cdot}526 \times 10^{-4}$ mole of $AlEt_2Cl$.

Oxygen is the most interesting cocatalyst because of its capacity for giving a high yield of isotactic polymer. The catalyst system was prepared by bubbling oxygen, dried by passage through a 150 cm column packed with phosphorus pentoxide, through the toluene solution of freshly distilled $AlEt_2Cl$ at −78°C at a flow rate of 100 ml/min. The polymerization was carried out by adding the monomer to the catalyst solution at −78°C and then leaving it to polymerize at −78°C for 24 h. By bubbling dry oxygen through the solution of $AlEt_2Cl$, the activity of $AlEt_2Cl$ rose sharply at first and then dropped gradually to a constant value. A maximum stereospecificity ($Y = 93{\cdot}4$ per cent; $I.S. = 86{\cdot}5$ per cent) was observed at between 20 and 40 sec of bubbling, and a nearly constant value ($Y = 61{\cdot}4$ per cent; $I.S. = 51{\cdot}6$ per cent) was obtained after 5 to 30 minutes bubbling. These results indicate clearly the cocatalytic activity of oxygen for stereospecific polymerization and the formation of at least two different kinds of active species, one for the medium stereospecific polymerization.

Monoethoxide Al(OEt)EtCl may be considered as a possible active species of the catalyst system: $AlEt_2Cl$–O_2, as the reaction between $AlEt_2Cl$ and oxygen is reported to give the monoethoxide ultimately[3]. Al(OEt)EtCl, prepared by an equimolar reaction of $AlEt_2Cl$ and ethanol[3], was purified by

[3] BARRIE, J. A., LEVINE, J. D., MICHAELS, A. S. and WONG, P. *Trans. Faraday Soc.* 1963, **59**, 869
[4] SAUNDERS, D. W. *Trans. Faraday Soc.* 1957, **53**, 860
[5] POLMANTEER, K. E. and HUNTER, M. J. *J. appl. Polym. Sci.* 1959, **1**, 3
[6] PRAGER, S. and LONG, F. A. *J. Amer. chem. Soc.* 1951, **73**, 4072
[7] BARRER, R. M., BARRIE, J. A. and RAMAN, K. *Polymer, Lond.* 1962, **3**, 595
[8] BARRER, R. M. and CHIO, H. T. *J. Polym. Sci. C*, 1965, **10**, 111

The Polymerization of Isobutyl Vinyl Ether by Diethylaluminium Chloride

WE have found that $AlEt_2Cl$ is completely inactive for the polymerization of isobutyl vinyl ether. This fact is inconsistent with the result reported by Natta[1], and adds an additional example to Kennedy's finding[2] concerning the cationic inactivity of $AlEt_2Cl$ for the polymerization of olefins and dienes.

$AlEt_2Cl$ requires a cocatalyst for both stereospecific and non-stereospecific polymerization of isobutyl vinyl ether. Oxygen is an effective cocatalyst for the high stereospecific, carbon dioxide–oxygen combination for the low stereospecific, and water for the non-stereospecific polymerization. The polymerization reactions catalysed by these catalyst systems proceed in an apparently homogeneous phase.

As a measure of stereospecificity we use the value of the index of stereospecificity (*I.S.*), which is defined as the percentage of the weight of methyl ethyl ketone (MEK) insoluble fraction against the total polymer yield (*Y*). Fractionation of the polymer was carried out by using 100 ml of MEK per 0·5 g of the total polymer at 30°C for 48 h. Polymerization was carried out at −78°C by using 15 ml of toluene, $7{\cdot}63 \times 10^{-3}$ mole of the monomer and $1{\cdot}526 \times 10^{-4}$ mole of $AlEt_2Cl$.

Oxygen is the most interesting cocatalyst because of its capacity for giving a high yield of isotactic polymer. The catalyst system was prepared by bubbling oxygen, dried by passage through a 150 cm column packed with phosphorus pentoxide, through the toluene solution of freshly distilled $AlEt_2Cl$ at −78°C at a flow rate of 100 ml/min. The polymerization was carried out by adding the monomer to the catalyst solution at −78°C and then leaving it to polymerize at −78°C for 24 h. By bubbling dry oxygen through the solution of $AlEt_2Cl$, the activity of $AlEt_2Cl$ rose sharply at first and then dropped gradually to a constant value. A maximum stereospecificity ($Y = 93{\cdot}4$ per cent; $I.S. = 86{\cdot}5$ per cent) was observed at between 20 and 40 sec of bubbling, and a nearly constant value ($Y = 61{\cdot}4$ per cent; $I.S. = 51{\cdot}6$ per cent) was obtained after 5 to 30 minutes bubbling. These results indicate clearly the cocatalytic activity of oxygen for stereospecific polymerization and the formation of at least two different kinds of active species, one for the medium stereospecific polymerization.

Monoethoxide Al(OEt)EtCl may be considered as a possible active species of the catalyst system: $AlEt_2Cl$–O_2, as the reaction between $AlEt_2Cl$ and oxygen is reported to give the monoethoxide ultimately[3]. Al(OEt)EtCl, prepared by an equimolar reaction of $AlEt_2Cl$ and ethanol[3], was purified by

distilling twice *in vacuo* (b.pt 35°C/10^{-3} torr) before use, and was used as a catalyst. Although this compound acted as a stereospecific catalyst ($Y = 98{\cdot}1$ per cent; $I.S. = 48{\cdot}1$ per cent), the stereospecificity was similar to that of the medium and was far inferior to that of the high stereospecific $AlEt_2Cl$–O_2 system. An optimum result ($Y = 87{\cdot}1$ per cent; $I.S. = 58{\cdot}3$ per cent) obtained by a mixed catalyst Al(OEt)EtCl–$AlEt_2Cl$ (molar ratio = 10 : 1) was similarly medium stereospecific. These results indicate that the medium stereospecific active species is probably Al(OEt)EtCl.

The results mentioned above strongly suggest that the high stereospecific active species of the catalyst system $AlEt_2Cl$–O_2 is an intermediate reaction product in the formation of Al(OEt)EtCl from $AlEt_2Cl$. Possible compounds are the oxygen complex $AlEt_2Cl{\cdot}O_2$ and the peroxide Al(OOEt)EtCl, but at this stage the nature of the high stereospecific active species cannot be specified.

The effect of carbon dioxide is rather peculiar. Dry carbon dioxide does not activate $AlEt_2Cl$ when bubbled through the solution at −78°C. A catalyst system $AlEt_2Cl$–CO_2–O_2 was prepared by bubbling dry carbon dioxide at room temperature for a short time, followed by dry oxygen at −78°C. Polymerization by this catalyst system has a higher rate and a far lower stereospecificity ($Y = ca.$ 100 per cent; $I.S. = ca.$ 20 per cent) than that by $AlEt_2Cl$–O_2. The former system polymerized the monomer completely in a few minutes, while the latter took several hours. These results suggest that in the former system the polymerization proceeds mainly by a free cationic mechanism and in the latter by a coordinated cationic mechanism.

The effect of water was examined by bubbling water-containing nitrogen through the solution of $AlEt_2Cl$. This system catalysed the non-stereospecific polymerization ($Y = 100$ per cent; $I.S. = 5{\cdot}5$ per cent).

HIROTAKA HIRATA

Department of Engineering Chemistry,
Faculty of Engineering, Osaka University,
Higashinoda, Osaka, Japan

HISAYA TANI

Department of Polymer Science,
Faculty of Science, Osaka University,
Toyonaka, Osaka, Japan

(*Received October 1967*)

REFERENCES

[1] NATTA, G., DALL'ASTA, G., MAZZANTI, G., GIANNINI, U. and CESCA, S. *Angew. Chem.* 1959, **71**, 205
[2] KENNEDY, J. P. *Polymer Preprint*, 1966, **7**, 485
[3] SCHERER, H. and SEYDEL, G. *Angew. Chem.* 1963, **75**, 846

A Cyclic Copolymer of Maleic Anhydride and Cyclododecatriene

A RECENT publication[1] has described the radical copolymerization of maleic

distilling twice *in vacuo* (b.pt 35°C/10^{-3} torr) before use, and was used as a catalyst. Although this compound acted as a stereospecific catalyst ($Y = 98{\cdot}1$ per cent; $I.S. = 48{\cdot}1$ per cent), the stereospecificity was similar to that of the medium and was far inferior to that of the high stereospecific $AlEt_2Cl$–O_2 system. An optimum result ($Y = 87{\cdot}1$ per cent; $I.S. = 58{\cdot}3$ per cent) obtained by a mixed catalyst Al(OEt)EtCl–$AlEt_2Cl$ (molar ratio = 10 : 1) was similarly medium stereospecific. These results indicate that the medium stereospecific active species is probably Al(OEt)EtCl.

The results mentioned above strongly suggest that the high stereospecific active species of the catalyst system $AlEt_2Cl$–O_2 is an intermediate reaction product in the formation of Al(OEt)EtCl from $AlEt_2Cl$. Possible compounds are the oxygen complex $AlEt_2Cl{\cdot}O_2$ and the peroxide Al(OOEt)EtCl, but at this stage the nature of the high stereospecific active species cannot be specified.

The effect of carbon dioxide is rather peculiar. Dry carbon dioxide does not activate $AlEt_2Cl$ when bubbled through the solution at −78°C. A catalyst system $AlEt_2Cl$–CO_2–O_2 was prepared by bubbling dry carbon dioxide at room temperature for a short time, followed by dry oxygen at −78°C. Polymerization by this catalyst system has a higher rate and a far lower stereospecificity ($Y = ca.$ 100 per cent; $I.S. = ca.$ 20 per cent) than that by $AlEt_2Cl$–O_2. The former system polymerized the monomer completely in a few minutes, while the latter took several hours. These results suggest that in the former system the polymerization proceeds mainly by a free cationic mechanism and in the latter by a coordinated cationic mechanism.

The effect of water was examined by bubbling water-containing nitrogen through the solution of $AlEt_2Cl$. This system catalysed the non-stereospecific polymerization ($Y = 100$ per cent; $I.S. = 5{\cdot}5$ per cent).

HIROTAKA HIRATA

Department of Engineering Chemistry,
Faculty of Engineering, Osaka University,
Higashinoda, Osaka, Japan

HISAYA TANI

Department of Polymer Science,
Faculty of Science, Osaka University,
Toyonaka, Osaka, Japan

(*Received October 1967*)

REFERENCES

[1] NATTA, G., DALL'ASTA, G., MAZZANTI, G., GIANNINI, U. and CESCA, S. *Angew. Chem.* 1959, **71**, 205
[2] KENNEDY, J. P. *Polymer Preprint*, 1966, **7**, 485
[3] SCHERER, H. and SEYDEL, G. *Angew. Chem.* 1963, **75**, 846

A Cyclic Copolymer of Maleic Anhydride and Cyclododecatriene

A RECENT publication[1] has described the radical copolymerization of maleic

anhydride and various bicyclic dienes to give low molecular weight polymers for which a fused ring structure (I) is proposed.

The analysis, however, did not show the ratio of anhydride to diene to be exactly 2 : 1.

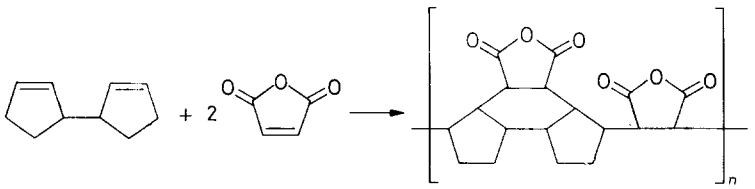

I

A previous paper[2] reported a similar copolymerization of maleic anhydride and *cis,cis*-1,5-cyclooctadiene to give a 1 : 1 copolymer of structure II:

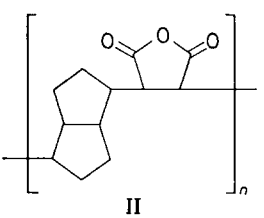

II

We now wish to report a copolymer of maleic anhydride with cyclododecatriene (either *cis, trans, trans* or *trans, trans, trans* isomer) for which we propose a cyclic structure.

All reactions were carried out using reagent grade, but not especially purified, materials, since it was observed that special purification and drying had no effect on the yield or quality of the product. Maleic anhydride was not hydrolysed under experimental conditions in wet solvents, and significant product hydrolysis only occurred when the isolation procedure was delayed. Reaction solutions were approximately ten per cent in total reagents and were maintained under an atmosphere of nitrogen throughout. Isolation of the polymer was by filtration if the reaction medium was a non-solvent or by precipitation with methanol. Purification was carried out by one or two precipitations from acetone or tetrahydrofuran using methanol.

Specific reaction conditions and analytical results are summarized in *Table 1*.

The polymers obtained were white powders with softening points above 300°C and having no crystallinity as shown by X-ray diffraction studies. They are soluble in acetone, tetrahydrofuran, dimethyl sulphoxide and dimethyl formamide and insoluble in dioxan, ether, benzene, xylene, chloroform and methanol. One sample, when pressed between aluminium plates at 140° to 170°C and 4 000 lb/in^2 for five minutes, gave a yellow but transparent button which was very brittle and shattered easily.

Table 1

Expt No.	Molar ratios of reagents			Solvent	React. time (h)	React. temp. (°C)
	cis, trans, trans-CDT	*MA*	*AZDN*‡			
1	1	1	0·1	Dioxan	5	70
2	1	1	0·1	Xylene	5	70
3	1	2	0·1	Xylene	5	70
4	2	1	0·1	Xylene	5	70
5	1	1	0·05	Xylene	5	70
6	1	1	0·05	Acetone	24	56
7	1	1	0·05	THF	6	65
8	1	1	0·05	Benzene	5	80
9	1	1	0·005	Benzene	5	80
10	1	1	—	Xylene	20	135
	trans, trans, trans-CDT					
11	1	1	1	Xylene	5	70

Expt No.	Yield* (%)	Mol. wt	Analyses†			
			C	H	O	N
1	24	$4·0 \times 10^3$	68·25	7·36	23·52	
			68·48	7·48	23·54	
2	43	4·4				
3	55	4·3	65·28	6·70	22·97	
			65·26	6·68	23·16	
4	32	2·7	70·18	7·28	21·14	1·1
			70·19	7·11	20·93	
5	27	2·0				
6	35	2·6				
7	42	—				
8	37	§				
9	10	§				
10	9	5·8				
11	43	5·0				

*Based on total weight of maleic anhydride, cyclododecatriene.
†Calc. for $C_{16}H_{20}O_3$ (1:1) C 73·81; H 7·75; O 18·44.
Calc. for $C_{20}H_{22}O_6$ (1:2) C 67·02; H 6·19; O 26·79.
‡Azobisisobutyronitrile.
§Molecular weights 8,9 shown to be identical by gel permeation chromatography.

The polymers showed no evidence of unsaturation either by infra-red or nuclear magnetic resonance spectroscopy.

The i.r. spectrum and all other properties of the polymer prepared from *trans, trans, trans*-1,5,9-cyclododecatriene were identical to those prepared from the *cis, trans, trans* isomer. The spectrum was also very similar to that of a sample of the *cis, cis*-1,5-cyclooctadiene, maleic anhydride copolymer prepared according to the published procedure[2].

On the basis of the above results, we propose the mechanism opposite for the radical copolymerization of maleic anhydride and cyclododecatriene.

Structure III indicates a regular alternating copolymer terminated by initiator fragments. The inclusion of two isobutyronitrile units per polymer molecule is justified on the grounds of elemental analysis and by the results of experiments 8 and 9, in which only the yield of polymer and not its molecular weight, is reduced by a ten per cent reduction in AZDN content.

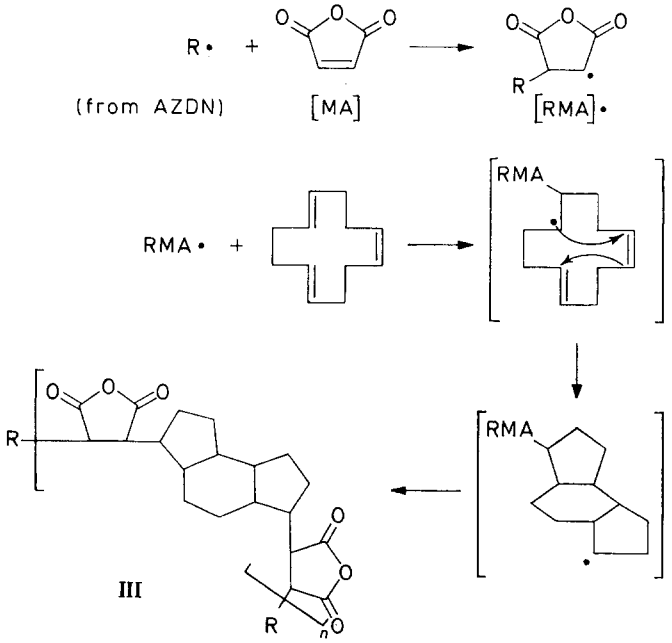

At higher temperatures, an initiator is unnecessary (expt 10), and the product should be a true copolymer containing only maleic anhydride and cyclododecatriene.

Analysis also indicates that the ratio of maleic anhydride to cyclododecatriene in the copolymer lies somewhere between one and two. Lang *et al.*[3], however, have reported that maleic anhydride may be homopolymerized by radical initiators under similar conditions, and so we conclude that extra maleic anhydride is included randomly along the chain to give the observed polymer composition.

E. W. DUCK,
J. M. LOCKE
and M. E. THOMAS

Research and Development Laboratories,
The International Synthetic Rubber Co. Ltd,
Southampton

(*Received October 1967*)

REFERENCES

[1] MEYERSON, K. and WANG, J. Y. C. *J. Polym. Sci. A-1*, 1967, **5**, 1845
[2] DOWBENKO, R. and CHANG, W. H. *J. Polym. Sci. B*, 1964, **2**, 469
[3] LANG, J. L., PAVELICH, W. A. and CLAREY, H. D. *J. Polym. Sci. A*, 1963, **1**, 1123

Model Polyethers IV—Vapour Pressures of Oligomers of Polytetramethylene Oxide

T. P. HOBIN

Vapour pressures of polytetramethylene oxide oligomers $H[(CH_2)_4O]_n(CH_2)_4H$, *where* $n=2$ *to* 4, *have been measured over the range* 80° *to* 200°C. *They are compared with those of* n-*paraffins and of polymethylene oxide oligomers and discussed in terms of cohesive energies and chain configurations.*

BOYD[1] obtained vapour pressure data for oligomers of polymethylene oxide (PMO) and used them to estimate the incremental molar cohesive energy per repeat group of the amorphous high polymer. The present work was undertaken in order to derive similarly the incremental molar cohesive energy per repeat group of amorphous polytetramethylene oxide (PTMO).

EXPERIMENTAL

(1) *Materials*

Model polytetramethylene oxides were prepared and purified as described in Parts I–III[2–4].

(2) *Apparatus*

A manometric apparatus was used, immersed in a silicone oil bath controlled to ±0·1 deg. C. Mercury cut-off valves were preferred to greased taps to avoid interaction between the vapour and the grease and to ensure freedom from leakage. The system could be pumped down to high vacuum at any time; volatile decomposition products, if formed at the higher temperatures, could have been removed prior to the measurement of the vapour pressure. No such problem was encountered over the periods of the experiments. The degassing facility was used to withdraw vapour during cooling cycles in order to prevent undesired condensation inside the apparatus—particularly on the meniscus of the mercury manometer, where it could have interfered with the manometric reading.

The system required at least five minutes to attain equilibrium following a degassing operation. Fuller details of the apparatus will be given elsewhere.

(3) *Results*

The results are set out in *Table 1* and illustrated in the form of a $\log P$ versus $10^3/T$ plot in *Figure 1*. Also shown in *Figure 1* are data, taken from the literature, for selected *n*-paraffins[5], for Boyd's PMO oligomers[1] and for di-*n*-butyl ether[5]. The latter, the monoether of the PTMO series, is reported to obey the relationship

$$\log P\,[\text{mm Hg}] = 8{\cdot}002 - 2106{\cdot}059/T\,[^\circ\text{K}]$$

over the range 50° to 150°C.

Table 1. Vapour pressures of polytetramethylene oxide oligomers.
$H[(CH_2)_4O]_n(CH_2)_4H$
Pressure P in mm Hg. Temperature T in °C.

$n=2$		$n=3$		$n=4$	
T	P	T	P	T	P
80	2·0	119	1·6	140	1·9
87	3·0	127	2·1	145	2·5
92	3·6	137	3·6	152	3·0
102	6·8	143	4·9	158	3·6
107	8·9	152	7·6	164	4·4
116	13·5	160	9·1	170	5·9
125	20·0	167	11·2	178	6·9
130	24·5	174	15·1	182	8·1
135	31·6	182	19·5	186	9·6
145	46·8	188	29·5	192	12·0
150	51·3			197	13·2
				203	17·4

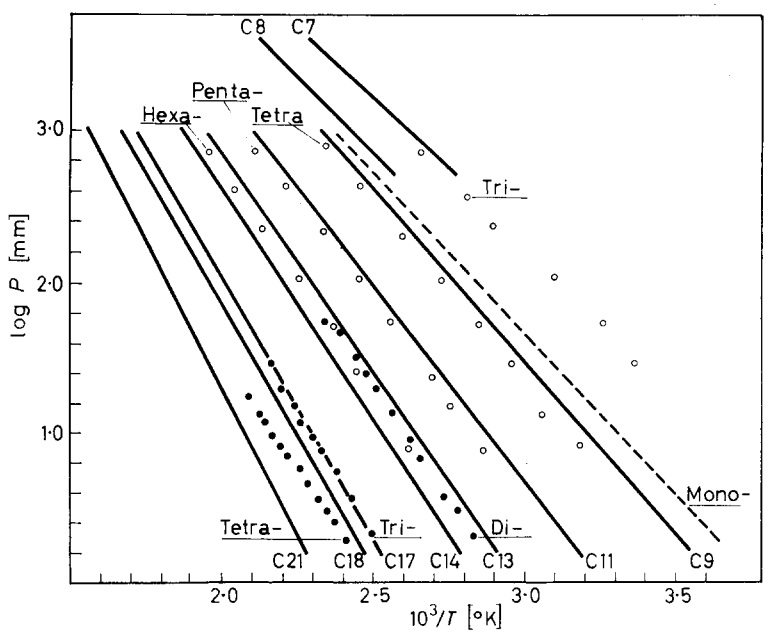

Figure 1—Pressure versus reciprocal temperature data. ● This work; ○ Boyd's data for PMO oligomers $HCH_2[OCH_2]_nH$. Full lines — *n*-Paraffins; Dashed line — di-*n*-butyl ether

The following features are evident from *Figure 1*.

(a) The *n*-paraffins form a regular family of curves.

(b) Boyd's PMO oligomers appear to fit in with the paraffin family; each lies very close to the curve for the *n*-paraffin with the same number of chain atoms.

(c) The mono-, di- and tri-ethers of the PTMO series also appear to fit in with the paraffin family. Their nearest neighbours in the paraffin series, however, have slightly fewer chain atoms.

(d) The tetra-ether of the PTMO series deviates from the family formed by the lower oligomers of the series. It exhibits a slight decrease in slope in comparison to the triether and is considerably displaced from the *n*-paraffin with the same number of chain atoms.

DISCUSSION

(1) *Comparison of PMO oligomers with the* n-*paraffins*

The close proximity in *Figure 1* of the PMO oligomers and their corresponding *n*-paraffins raises the question as to whether both series possess comparable average molar cohesive energies per chain atom. Boyd[1] by the use of a computer on his data, arrived at a value of 2·36 kcal for the incremental molar cohesive energy per —CH_2O— group of the liquid polymer at 25°C. He recognized that this value was very close to Billmeyer's[6] value of 2·34 kcal/mole of —CH_2CH_2— for the *n*-paraffins at 25°C. On this basis, wherever plots of $\log P$ versus $1/T$ for any two series of oligomers form a single regular family of curves, there would be justification for the estimation of the heats of vaporization of members of one series by comparison of their positions with those of members of the other series, provided the heats of vaporization of the members of the other series are known.

(2) *Comparison of PTMO oligomers with the* n-*paraffins and estimation of their cohesive energies*

Computation of vaporization energies from the present results by the method used by Boyd[1] would not be justifiable because of the shorter range of the present studies and the greater molecular weights of the PTMO oligomers, which reduce the differences in slopes, e.g. between diether and triether. However, comparison of the positions of the PTMO oligomers up to triether with those of the nearest paraffins suggests that they would have the same vaporization energies as the following hypothetical paraffins: monoether—$C_{8\cdot5}$, diether—$C_{13\cdot2}$, and triether—$C_{17\cdot2}$. The vaporization energies of these hypothetical paraffins can be obtained from a plot of vaporization energy at 25°C versus number of C atoms which, using the data of Bristow and Watson[7], is a smooth curve, almost linear. The results in kcal/mole at 25°C are: $C_{8\cdot5} = 10\cdot5$, $C_{13\cdot2} = 16\cdot0$ and $C_{17\cdot2} = 20\cdot5$. The corresponding cohesive energies obtained by subtraction of the expansion energy RT are 9·9, 15·4 and 19·9 kcal/mole respectively. Assignment of these values to the PTMO oligomers gives an average value of 5·0 kcal/mole of —$(CH_2)_4O$— as the estimated cohesive energy associated with the repeat group of liquid PTMO at 25°C.

(3) *Empirical calculation of the cohesive energy per mole of* $(CH_2)_4O$

By use of the empirical molar attraction constants (F) claimed by Small[8] to be constitutively additive, ΣF values can be calculated for PTMO oligomers at 25°C. The molar cohesive energies would then be given by the

quotient $(\Sigma F)^2/V_{25}$ where V_{25} refers to the molar volumes at 25°C. Molar volumes at 20°C can be calculated from densities[3] and these will differ from values at 25°C by only a fraction of one per cent. The estimated molar cohesive energies calculated from $(\Sigma F)^2/V_{20}$ are as follows:

Monoether: $(1296)^2/169 = 9{\cdot}94$ kcal

Diether: $(1898)^2/240 = 15{\cdot}1$ kcal

Triether: $(2500)^2/312 = 20{\cdot}0$ kcal

Tetraether: $(3102)^2/387 = 24{\cdot}9$ kcal

These are in good agreement with the experimental values estimated in the previous section. They give an average incremental cohesive energy per mole of $(CH_2)_4O$ of 4·93 kcal which compares favourably with the experimental estimate of 5·0 kcal

(4) *Cohesive energy density of polytetramethylene oxide*

The molar volumes of the PTMO oligomers are a linear function of the number of repeat groups and yield an average volume of 73·0 cm^3 per mole of $-(CH_2)_4O-$ in the liquid state at 20°C (equivalent to a polymer density of 0·986 g/cm^3 in the same state). The cohesive energy density of the liquid high polymer in the region of 25°C is therefore given by $5{\cdot}0 \times 10^3/73{\cdot}0 = 69$ cal/cm^3. This result is of the same order as that of polyethylene[1,9] but differs considerably from the value of 104 cal/cm^3 for polymethylene oxide[1].

(5) *General comparison of the cohesive energies of* n-*paraffins, PMO oligomers and PTMO oligomers*

Replacement of every fifth methylene group of a paraffin by an oxygen link gives rise to a small reduction in molar cohesive energy (*Figure 1*) but, because the —O— link is shorter than the $-CH_2-$ link, there is not a very significant difference in the cohesive energy densities of the corresponding high polymers. By analogy it might be expected that replacement of every second $-CH_2-$ by —O— to give a PMO oligomer would result in a substantial reduction in molar vaporization energy. In practice, however, there is scarcely any change. The probable explanation is that substitution of every *n*th $-CH_2-$ by —O— occurs in positions that are all on one side of the planar zig-zag of the paraffin chain when *n* is even but on alternate sides when *n* is odd. Hence there will be considerable differences in dipole moments. This is reflected in the high c.e.d. of PMO in comparison to that of PTMO. The dipole moments of these polymers and oligomers have been discussed[10].

(6) *The deviation shown by the PTMO tetraether*

The PTMO tetraether appears to have a slightly lower heat of vaporization than the triether. It is likely that its four —O— links render it more flexible than the corresponding paraffin with the result that the molecule, because it is longer than the triether, can adopt a configuration in the vapour state that involves significant intramolecular cohesion. The energy released by such cohesion would offset some of the energy required for vaporization.

The possibility of a reduction in vaporization energy in cases where intramolecular cohesion could occur in the perfect gas state has been discussed by Scatchard[11], who has quoted experimental evidence to show that increases in cohesive energies on ascending a homologous series have been found to be lower when calculated from vaporization energies than when calculated from polarizability data.

Rose[12] has shown that relatively large yields of a strain-free cyclic tetra-ether (16 chain atoms) can be obtained by polymerization of trimethylene oxide. This indicates that there is considerable flexibility in the tetra-ether of the polytrimethylene oxide series and also that in this series a chain length of 16 atoms is necessary before the ends can meet. Presumably in members of the same series with more than 16 atoms the ends could do more than meet—they could overlap and lie side by side with considerable intramolecular cohesion.

Explosives Research and Development Establishment,
Waltham Abbey, Essex

(*Received April 1967*)

REFERENCES

[1] BOYD, R. H. *J. Polym. Sci.* 1961, **50**, 133–141
[2] HOBIN, T. P. *Polymer, Lond.* 1965, **6**, 403–409
[3] HOBIN, T. P. and LOWSON, R. T. *Polymer, Lond.* 1966, **7**, 217
[4] HOBIN, T. P. *Polymer, Lond.* 1966, **7**, 223
[5] JORDAN, T. E. *Vapor Pressures of Organic Compounds.* Interscience: New York, 1954
[6] BILLMEYER, F. W. *J. appl. Phys.* 1957, **28**, 1114
[7] BRISTOW, G. M. and WATSON, W. F. *Trans. Faraday Soc.* 1958, **54**, 1733
[8] SMALL, P. A. *J. appl. Chem.* 1953, **3**, 71
[9] ALLEN, G., GEE, G. and WILSON, G. J. *Polymer, Lond.* 1960, **1**, 465
[10] FLORY, P. J. and MARK, J. E. *J. Amer. chem. Soc.* 1966, **88**, 3702–3707
MARK, J. E. *J. Amer. chem. Soc.* 1966, **88**, 3708–3711
[11] SCATCHARD, G. *Chem. Rev.* 1949, **44**, 24
[12] ROSE, J. B. *J. chem. Soc.* 1956, 542–555

Temperature Dependence of Surface Tension for Polytetrafluorethylene (Supercooled Liquid) Estimated from Contact Angles

HAROLD SCHONHORN

The surface tension of polytetrafluorethylene (supercooled liquid) as a function of temperature is estimated by using a modified Young–Fowkes equation and the experimental contact angle data of Brewis for the glycerol–polytetrafluorethylene system. The temperature coefficient of the surface tension is estimated to be −0·02 dyne/cm deg. From these data it is possible to predict the wettability of other liquids in contact with polytetrafluorethylene.

RECENTLY, investigators[1, 2] have measured the temperature dependence of the surface tension for several molten polymers employing a variety of conventional techniques. Certain polymers, notably polytetrafluorethylene, because of their high melting temperature, melt viscosity, and inherent degradation at elevated temperatures, are not amenable to convenient measurement by these techniques. However, knowledge of the surface tension for these polymers may be of considerable importance.

The utility of the surface tension of molten polymers in the area of adhesion has been stressed already[3]. Further, the surface tension obtained by conventional methods has proved useful in predicting the temperature dependence of the contact angle for polar liquids on both polyethylene[4] and polypropylene[5] by using a modified Fowkes[6] approach to interfacial phenomena.

The purpose of this note is to explore the possibility of estimating the surface tension of polytetrafluorethylene by using the data for the temperature dependence of the contact angle of a liquid on the solid polymer. Essentially, we are reversing the situation that we employed previously[4, 5]. The major source of error involved in this approach is the contact angle. If θ is close to 90°, a small error in the contact angle will result in a large error in the estimated value of the surface tension for the polymer. The recent data of Brewis[7] for the polytetrafluorethylene–glycerol system will serve as a basis for the following analysis.

It has been proposed[8] on the basis of the reported surface tensions for a variety of non-polar polymers[1, 2, 9] that at all temperatures below the melt

$$\gamma_{LV} = \gamma_C \tag{1}$$

where γ_{LV} is the surface tension of the supercooled molten polymer and γ_C is the critical surface tension of wetting.

Certainly, this assumption is not valid for many polar species, since the value of γ_C is dependent upon the nature of the wetting liquid. For example, the γ_C of water with respect to hydrocarbons is 21·8 dyne/cm, while γ_{LV} is 72·5 dyne/cm at 20°C. The non-spreading of water on gold[10]

is another example. For melt-crystallized non-polar polymers, as normally prepared for wettability studies, equation (1) is a good approximation.

When this proposal is incorporated into the Young–Fowkes equation[6] we obtain[4]

$$\cos\theta = 2\{[(\gamma_{LV})_p\gamma^d_{LV}]^{1/2}/\gamma_{LV}\} - 1 - (\pi_e/\gamma_{LV}) \quad (2)$$

where p refers to polymer, d refers to the dispersion contribution to the surface tension of the wetting liquid and π_e is the equilibrium spreading pressure.

For systems exhibiting high contact angles, spreading pressures can be ignored[6]. Consequently, equation (2) becomes

$$\cos\theta = 2\{[(\gamma_{LV})_p\gamma^d_{LV}]^{1/2}/\gamma_{LV}\} - 1 \quad (3)$$

For non-polar liquids $\gamma^d_{LV} = \gamma_{LV}$; for polar liquids $\gamma^d_{LV} \neq \gamma_{LV}$. We assumed further that $\gamma^d_{LV}/\gamma_{LV}$ is constant with temperature. Now equation (2) becomes

$$\cos\theta = 2k^{\frac{1}{2}}[(\gamma_{LV})_p/\gamma_{LV}]^{\frac{1}{2}} - 1 \quad (4)$$

where $k = [\gamma^d_{LV}/\gamma_{LV}]$.

Recent work of Sutula *et al.*[11] on the temperature dependence of the wettability of both non-polar and polar liquids on FEP Teflon has justified the above assumption. For each liquid, the rate of change of θ with temperature, $\Delta\theta/\Delta T$ was effectively constant, and small, from 25°C to 150°C or to the boiling point of the liquid. For the polar liquids, $\gamma^d_{LV}/\gamma_{LV}$ was nearly independent of temperature. Further, Sutula *et al.* found it unnecessary to consider spreading coefficients for the polar liquid–polymer systems but found it necessary to employ spreading coefficients to obtain agreement with the Fowkes model for the *n*-hydrocarbon–polymer systems. From equation (4) it is readily apparent that for low energy polymers $(\gamma_{LV})_p$ may be estimated by knowing the surface tension of the wetting liquid and the equilibrium advancing contact angle of that liquid on the melt crystallized polymer surface.

It is important to consider the polymer as being of the melt crystallized variety. Recently, Schonhorn and Ryan[12] have shown that the wettability of polyethylene single crystal aggregates is considerably different from that of melt crystallized polyethylene. The apparent surface density of the melt crystallized variety is similar if not equal to the amorphous density. This has been described recently by Roe[2] and by Lee, Muir and Lyman[13] who demonstrated that the Parachor concept is applicable to melt crystallized polymers. This is precisely why there is such remarkable agreement between γ_{LV} and γ_c. Although a polymer may exist in a range of densities, the surface region of the melt crystallized polymer is essentially amorphous. This may be understood from the theory of the crystallization of polymers[14]. There is apparently a syneresis occurring during crystallization resulting in an accumulation of non-crystallizable species at the liquid/air, or liquid/non-nucleating surface interface. These species assume an amorphous configuration. Since the contact angle measurement is de-

pendent solely upon the nature of the outermost layer, the surface of the polymer appears to be similar in density to that of the supercooled liquid.

Rearranging equation (4) we obtain

$$(\gamma_{LV})_p = \tfrac{1}{4}[1+\cos\theta]^2\,\gamma_{LV}/k \qquad (5)$$

The pertinent data for computing $(\gamma_{LV})_p$ are presented in *Table 1*. The contact angle data are those of Brewis[7] and of Zisman[15]. The surface tension data for glycerol were obtained from the *International Critical Tables*[16]. The estimated value of 37·0 erg/cm^2 for γ^d_{LV} from the data of Fowkes[6] yields a value of $k=0{\cdot}584$. The calculated values of $(\gamma_{LV})_p$ were obtained from equation (5).

Except for the higher contact angle at 90°C, the temperature coefficient of the $(\gamma_{LV})_p$ is approximately $-0{\cdot}02$ dyne/cm deg. Because θ is close to 90°, a small error in θ produces a rather large error in cos θ and consequently in $(\gamma_{LV})_p$. A better choice of test liquid would be one whose contact angle is in the vicinity of 45°. This choice was made by Johnson and Dettre in a recent study of the *n*-hexadecane–FEP Teflon system[17].

Table 1. Temperature dependence of the surface tension of polytetrafluorethylene (supercooled liquid) derived from contact angle measurements

T°C	θ degrees	cos θ	k	γ_{LV} dyne cm	$(\gamma_{LV})_p$ dyne cm
20	100±1*	−0·1737	0·584	63·4†	18·5±0·7
30	100±1	−0·1737		62·7	18·3±0·7
60	100±1	−0·1737		60·6	17·7±0·7
90	101±1	−0·1908		58·6†	16·4±0·7
110	100±1	−0·1737		57·2	16·7±0·7

*Zisman, ref 15.
†ICT, ref 16.

The γ_C at 20°C for polytetrafluorethylene is 18·5 dyne/cm[15]. This is what we have estimated $(\gamma_{LV})^{20}_p$ to be. Therefore, equation (1) is suited for polytetrafluorethylene. The insensitivity of θ to temperature for the glycerol–polytetrafluorethylene system is similar to earlier work with polyethylene[4] and polypropylene[5]. As pointed out previously[4], there is expected to be a temperature, possibly in the vicinity of the critical temperature of the wetting liquid, when $(\gamma_{LV})_p=\gamma_{LV}$ and $\theta=0$. Since glycerol is expected to have a lower critical temperature (T_c) than polytetrafluorethylene[18], a lowering of θ as the temperature increases is predicted.

Johnson and Dettre[17] have found θ to be relatively constant with increasing temperature for the hexadecane–FEP Teflon system. Sutula *et al.*[11] have shown that $\Delta\theta/\Delta T$ was negative and small for the homologous series of *n*-hydrocarbons, ranging from C_7 to C_{16}, on FEP Teflon. For *n*-hexadecane on FEP Teflon, $\Delta\theta/\Delta T$ was $-0{\cdot}05$ deg./deg. C. By employing spreading coefficients in conjunction with the Fowkes model, reasonably good agreement with the results of Johnson and Dettre[17] is obtained.

Although other wettability results[17, 11] were determined for FEP Teflon, the similarity between polytetrafluorethylene and FEP Teflon suggests that

their results are directly applicable to the wettability of polytetrafluorethylene.

Once the temperature dependence of the contact angle in conjunction with the Fowkes–Young equation has provided values for the temperature dependence of the surface tension of polytetrafluorethylene, the wettability of the polymer by other liquids is calculable.

The virtue of the contact angle approach is that it provides a relatively simple way of determining the temperature dependence of the surface tension for polymers that are not amenable to having their surface tensions measured by conventional techniques.

Bell Telephone Laboratories,
Murray Hill, N.J., U.S.A.

(*Received April 1967*)

REFERENCES

[1] SCHONHORN, H. and SHARPE, L. H. *J. Polym. Sci. A*, 1965, **3**, 569; *B*, 1965, **3**, 235
[2] ROE, R. J. *J. phys. Chem.* 1965, **69**, 2809
SAKAI, T. *Polymer, Lond.* 1965, **6**, 659
DETTRE, R. H. and JOHNSON JR, R. E. *J. Colloid & Interface Sci.* 1966, **21**, 367
[3] SHARPE, L. H. and SCHONHORN, H. *Advanc. Chem. Ser.* 1964, **43**, 189; SCHONHORN, H. and SHARPE, L. H. *J. Polym. Sci. B*, 1964, **2**, 719; *A*, 1965, **3**, 3087
[4] SCHONHORN, H. *Nature, Lond.* 1966, **210**, 896
[5] SCHONHORN, H. *J. phys. Chem.* 1966, **70**, 4086
[6] FOWKES, F. M. *ASTM Spec. Tech. Publ. No.* 360 (1964) p 20
[7] BREWIS, D. M. *Polym. Engng. Sci.* 1967, **7**, 17
[8] SCHONHORN, H. *J. phys. Chem.* 1965, **69**, 1084
[9] TARKOW, H. *J. Polym. Sci.* 1958, **27**, 35
MARIAN, J. E. *ASTM Spec. Tech. Publ. No. 340* (1963), p 122
SCHONHORN, H., RYAN, F. W. and SHARPE, L. H. *J. Polym. Sci. A*, 1966, **2**, 538
[10] WHITE, M. L. *J. phys. Chem.* 1964, **68**, 3083
[11] SUTULA, C. L., HAUTALA, R., DALLA BETTA, R. W. and MICHEL, L. A. Presented at Division of Colloid and Surface Chemistry at the 153rd American Chemical Society Meeting, Miami Beach, Florida, April 1967
[12] SCHONHORN, H. and RYAN, F. W. *J. phys. Chem.* 1966, **70**, 3811
[13] LEE, I. J., MUIR, W. M. and LYMAN, D. J. *J. phys. Chem*, 1965, **69**, 3220
[14] KEITH, H. D. and PADDEN, F. J. *J. Appl. Phys.* 1964, **35**, 1270, 1286
[15] ZISMAN, W. A. *Advanc. Chem. Ser.* 1964, **43**, 1
[16] *International Critical Tables of Numerical Data, Physics, Chemistry, and Technology*, Vol. IV. McGraw-Hill: New York, 1928
[17] JOHNSON JR, R. E. and DETTRE, R. H. *J. Colloid Sci.* 1965, **20**, 173
[18] FRISCH, H. L. and ROGERS JR, C. E. *J. Polym. Sci. C*, 1966, **12**, 297

Thermodynamics of Polymerization of Heterocyclic Compounds I—The Heat Capacity, Entropy and Enthalpy of Trioxan

G. A. CLEGG, T. P. MELIA and A. TYSON

An adiabatic, vacuum calorimeter has been used to measure the heat capacity of trioxan from 80°K to 310°K. An approximate extrapolation procedure has been used to estimate heat capacities below 80°K. Entropy and enthalpy values have been derived and are listed at ten degree intervals. Published vapour pressure data have been used to calculate the entropy of trioxan gas at one atmosphere pressure and 298·16°K. The value obtained 68·09±0·82 cal deg^{-1} mole^{-1} compares with that of 68·99±0·01 cal deg^{-1} mole^{-1} obtained by statistical methods. The entropy of polymerization of trioxan to crystalline polyoxymethylene, $\Delta S^0_{gc'}$, has been calculated as −37·2 cal deg^{-1} mole^{-1}.

AS PART of a general study of the thermodynamics of polymerization of heterocyclic compounds the heat capacities of various monomers and polymers have been measured over the temperature range 80° to 310°K. Heat capacities below 80°K can be evaluated using the Kelley, Parks and Huffman extrapolation procedure[1] and this enables an estimate to be made of the Third Law entropy.

The material studied in this work, trioxan, is a cyclic trimer of formaldehyde which readily undergoes cationic polymerization in solid[2] and liquid[3,4] phases and in solution[3–7] or suspension[3,4,6] to yield high molecular weight polyoxymethylenes.

The thermodynamic functions of trioxan gas at one atmosphere pressure over the temperature range 0° to 1 000°K have recently been calculated by Melia, Bailey and Tyson[8] using the methods of statistical thermodynamics. Vapour pressure data for the sublimation of trioxan are also available[9,10] so the results presented enable a comparison to be made between the statistical and Third Law entropies of trioxan.

EXPERIMENTAL

Calorimeter

The calorimeter used for the heat capacity measurements is of the adiabatic, vacuum type closely resembling that of Scott *et al.*[11]. Temperature measurements were made with a platinum resistance thermometer (R_0=25 ohms) calibrated by the National Physical Laboratory. The thermometer was housed in a re-entrant well in the base of the calorimeter. The calorimeter was close wound with 'Eureka' resistance wire which serves as the heater. Temperature rise and heat input were measured on a thermoelectric-free potentiometer of the Diesselhorst type, supplied by H. Tinsley and Co. Ltd. The top, bottom and sides of the adiabatic shield were manually maintained at the temperature of the calorimeter. The calorimeter was

calibrated in the range 80° to 320°K using thermochemically pure benzoic acid supplied by British Drug Houses Limited.

Heat capacity measurements

Because of its high vapour pressure trioxan was subjected to only 30 minutes degassing under vacuum prior to sealing in the calorimeter. A small quantity of helium gas, sufficient to give a pressure of 500 mm of mercury at room temperature, was sealed in the calorimeter and served to accelerate thermal equilibrium during the experiments. Heat capacity measurements were made over the temperature range 80° to 310°K, temperature increments being varied from 5 deg. to 13 deg. K. The magnitude of the temperature increment did not appear to affect the heat capacity value. Temperature equilibrium was reached about seven minutes after the end of a heating period over the whole temperature range.

Material

Laboratory Reagent grade trioxan supplied by British Drug Houses Limited was purified by sublimation from silver oxide using the method described by Jaacks and Kern[12].

RESULTS

Observed values of the heat capacity, calculated from the relationship

$$C=(C_s-C_c\pm E)/(M_s-M_c) \tag{1}$$

where C_s is the gross heat capacity of the calorimeter plus sample, C_c is the heat capacity of the empty calorimeter, M_s and M_c are the weights, respectively, of the calorimeter full and empty, and E is a small correction term for the different weights of grease, Wood's metal and copper capillary tube used in the two sets of measurements, are shown in *Table 1*. Smoothed values of the heat capacity, together with derived values of entropy and enthalpy, are shown in *Table 2*. The heat capacity data below 90°K were obtained using the Kelley, Parks and Huffman[1] procedure. Cyclohexane was chosen as the standard substance for this extrapolation. A cubic equation was fitted to the experimental data in the range 80° to 310°K by the method of least squares using a KDF9 English Electric computer. The equation obtained is

$$C=0{\cdot}2467+3{\cdot}754\times10^{-3}T-6{\cdot}192\times10^{-6}T^2+1{\cdot}602\times10^{-8}T^3 \text{ abs. J deg}^{-1}\text{g}^{-1} \tag{2}$$

Although maximum deviation of the experimental values from the smoothed curve is one per cent (one point), the vast majority lie within $\pm0{\cdot}2$ per cent of the smoothed curve values. Since trioxan sublimes readily at room temperature the heat capacity, C, should be converted to the quantity $C_{sat.}$ thus making allowance for the fact that C includes some heat of sublimation. This correction can be carried out by means of the equation[13]

$$C_{sat}=C-(T/M)\{d\,(V-Mv)/dT\}(dP/dT) \tag{3}$$

Table 1. Observed values of heat capacity for trioxan

Temperature (°K)	*C* (*abs. J deg*$^{-1}$ *g*$^{-1}$)	*Temperature* (°K)	*C* (*abs. J deg*$^{-1}$ *g*$^{-1}$)
RUN 1		RUN 3	
87·10	0·5355	203·36	0·8909
102·54	0·5854	209·37	0·9055
117·05	0·6276	215·25	0·9232
130·68	0·6694	221·01	0·9476
143·72	0·7094	226·87	0·9663
156·30	0·7406	233·00	0·9875
168·63	0·7798	239·15	1·013
180·61	0·8200	245·29	1·060
RUN 2		251·68	1·053
85·05	0·5298	258·40	1·081
95·12	0·5615	265·23	1·119
107·54	0·6017	272·52	1·129
121·77	0·6426	RUN 6	
134·93	0·6802	217·79	0·9216
147·27	0·7205	226·57	0·9877
171·05	0·7870	233·51	0·9848
182·35	0·8265	238·34	1·000
193·77	0·8559	242·04	1·020
204·86	0·8933	245·96	1·038
RUN 4		250·42	1·038
279·26	1·165	255·42	1·059
290·14	1·211	261·04	1·088
300·75	1·258	267·53	1·122
310·86	1·300	274·40	1·140
RUN 5			
281·53	1·168		
292·25	1·218		
303·00	1·252		
313·37	1·308		

where $C_{sat.}$ is the heat capacity of unit mass of trioxan in equilibrium with its own vapour, M is the mass of sample contained in the calorimeter, V is the total volume of the calorimeter, v is the specific volume of solid trioxan, T is the temperature in °K, and P is the vapour pressure. This correction has been applied to the smoothed values of the heat capacity shown in *Table 2*. The term dP/dT in equation (3) was evaluated from the relationship

$$\log P\,(\text{mm Hg}) = 10{\cdot}808 - 2894/T \qquad (4)$$

which was obtained from the vapour pressure data of Auerbach and Barschall[10].

DISCUSSION

The results obtained in the present investigation together with previously published[10] vapour pressure data for solid trioxan can be used to calculate the entropy of trioxan gas at one atmosphere pressure and 298·16°K. The results of this calculation are presented in *Table 3*. The value obtained for

Table 2. Smoothed values of heat capacity, entropy and enthalpy of trioxan

Temperature (°K)	$C_{sat.}$ (*abs. J deg*$^{-1}$*g*$^{-1}$)	$S^0_T - S^0_0$ (*abs. J deg*$^{-1}$*g*$^{-1}$)	$H^0_T - H^0_0$ (*abs. J g*$^{-1}$)
0	0	0	0
10	0·014	0·007	0·04
20	0·092	0·036	0·51
30	0·207	0·095	2·01
40	0·303	0·168	4·58
50	0·372	0·244	7·97
60	0·428	0·317	11·98
70	0·472	0·386	16·49
80	0·511	0·452	21·40
90	0·5459	0·514	26·68
100	0·5767	0·573	32·29
110	0·6065	0·629	38·20
120	0·6362	0·683	44·42
130	0·6658	0·735	50·93
140	0·6955	0·786	57·73
150	0·7252	0·835	64·84
160	0·7551	0·883	72·24
170	0·7854	0·929	79·94
180	0·8160	0·975	87·94
190	0·8471	1·020	96·26
200	0·8783	1·064	104·9
210	0·9112	1·108	113·8
220	0·9444	1·151	123·1
230	0·9784	1·193	132·7
240	1·013	1·236	142·7
250	1·050	1·278	153·0
260	1·087	1·320	163·6
270	1·125	1·361	174·7
273·16	1·138	1·373	178·2
280	1·165	1·404	186·2
290	1·205	1·445	198·0
298·16	1·237	1·477	208·0
300	1·246	1·487	210·3
310	1·289	1·528	223·0

Table 3. Entropy of trioxan gas at 1 atm pressure and 298·16°K calculated from heat capacity and vapour pressure data on the solid

Source of data	*Entropy contribution* (*cal deg. K*$^{-1}$ *mole*$^{-1}$)
$S^0_{90} - S^0_0$ (Kelley, Parks and Huffman extrapolation)	11·06 ± 0·55
$\int_{90}^{298\cdot16} C_{sat.}/T$	20·73 ± 0·06
$\Delta S_{298\cdot16}$ (sublimation)	44·39 ± 0·20
$\Delta S = R \ln 12\cdot7/760$	−8·09 ± 0·01
Entropy of gas at 298·16°K	68·09 ± 0·82

the entropy of trioxan gas, $68{\cdot}09 \pm 0{\cdot}82$ cal deg^{-1} mole^{-1}, is in reasonable agreement with that of $68{\cdot}99 \pm 0{\cdot}01$ cal deg^{-1} mole^{-1} calculated by Melia, Bailey and Tyson[8] using the methods of statistical thermodynamics.

The entropy change, ΔS^0_{gc}, associated with the polymerization of one mole of trioxan gas, at one atmosphere pressure and 298·16°K, to crystalline polyoxymethylene can be obtained by subtracting the entropy of the gaseous monomer from that of the crystalline polymer[14] (31·8 cal deg^{-1} mole^{-1}) at the same temperature. The value obtained is $-37{\cdot}2$ cal deg^{-1} mole^{-1}. A similar value ($-35{\cdot}9$ cal deg^{-1} mole^{-1}) has been found for the polymerization of cyclohexane to polyethylene[15,16].

G. A. Clegg and A. Tyson thank the University of Salford for the award of maintenance grants. We are also indebted to the Science Research Council for a grant in aid of this investigation.

Department of Chemistry and
Applied Chemistry,
University of Salford

(*Received April 1967*)

REFERENCES

[1] KELLEY, K. K., PARKS, G. S. and HUFFMAN, H. M. *J. phys. Chem.* 1929, **33,** 1802
[2] SACK, *H. Belg. Pat. No. 612 792* (1962)
[3] HUDGIN, D., SUMMIT, E. and BERARDINELLI, F. M. *U.S. Pat. No. 2 989 507* (1961)
[4] HUDGIN, D., SUMMIT, E. and BERARDINELLI, F. M. *U.S. Pat. No. 2 989 506* (1961)
[5] HUDGIN, D., SUMMIT, E. and BERARDINELLI, F. M. *U.S. Pat. No. 2 989 508* (1961)
[6] HUDGIN, D., SUMMIT, E. and BERARDINELLI, F. M. *U.S. Pat. No. 2 989 505* (1961)
[7] SCHNEIDER, A. K. *U.S. Pat. No. 2 795 571* (1961)
[8] MELIA, T. P., BAILEY, D. and TYSON, A. *J. appl. Chem.* 1967, **17,** 15
[9] FRANK, C. F., see WALKER, J. F. *Formaldehyde,* 3rd ed., p 193. Reinhold: New York, 1964
[10] AUERBACH, F. and BARSCHALL, H. *Studien über Formaldehyde—Die Festen Polymeren des Formaldehydes,* p 38. Springer: Berlin, 1907
[11] SCOTT, R. B., MEYERS, C. H., RANDS, R. D., BRICKWEDDE, F. D. and BEKKEDAHL, N. *J. Res. Nat. Bur. Stand.* 1945, **35,** 39
[12] JAACKS, V. and KERN, W. *Makromol. Chem.* 1962, **52,** 37
[13] HOGE, H. J. *J. Res. Nat. Bur. Stand.* 1946, **36,** 111
[14] DAINTON, F. S., EVANS, D. M., HOARE, F. E. and MELIA, T. P. *Polymer, Lond.* 1962, **3,** 263
[15] DAINTON, F. S., EVANS, D. M., HOARE, F. E. and MELIA, T. P. *Polymer, Lond.* 1962, **3,** 277
[16] DAINTON, F. S., DEVLIN, T. R. E. and SMALL, P. A. *Trans. Faraday Soc.* 1955, **51,** 1710

The Metal Salts-catalysed Autoxidation of Atactic Polypropylene in Solution I—Manganese Salts-catalysed Autoxidation

C. E. H. BAWN and SHAMIM A. CHAUDHRI*

The manganese-catalysed autoxidation of atactic polypropylene has been studied in the liquid phase. The maximum steady rate showed a variable dependence on the catalyst concentration. In the region where the rate varied with an approximate square root of the catalyst concentration, the maximum steady rate gave an order of 1·7 with respect to [RH], *the polymer concentration and of 1·0 with respect to* $p(O_2)$, *the partial pressure of oxygen above the solution. At higher catalyst concentrations the rate became almost independent of the amount of catalyst added to the system. In this region the maximum steady rate gave an order of two with respect to* [RH] *and of one with respect to* $p(O_2)$. *From studies with the β-naphthol-inhibited system, the reciprocal of the induction period was found to vary directly with* [RH] and $p(O_2)$, *and with an approximate square root of the catalyst concentration. An initiation mechanism and an overall mechanism have been put forward to explain the experimental results.*

SALTS of some metals of variable oxidation state are known to have a strong influence on the autoxidation of hydrocarbons. The various aspects of their influence on such systems have been discussed in the literature[1,2].

Although a fair amount of work has been done on the autoxidation of polypropylene under uncatalysed conditions[3–10], no systematic studies have been carried out in the presence of metal salts. The purpose of this paper is to report the kinetic behaviour of the manganese salts-catalysed autoxidation of atactic polypropylene in solution, and to explain the empirical results by extending the mechanism proposed earlier for the liquid-phase uncatalysed autoxidation of this polymer[11].

EXPERIMENTAL

The apparatus used and the other details have been given in an earlier work[11], which also reports the methods adopted for the purification of atactic polypropylene and the solvent, 1,2,4-trichlorobenzene.

Catalysts

(i) *Manganous stearate*—This compound was prepared by aqueous metathesis of sodium stearate with manganous chloride. The precipitate was separated by filtration and washed repeatedly with hot water to remove the excess manganous chloride. This was followed by several washings with alcohol and then with acetone. The sample was dried at 50° to 60° under vacuum and stored in a desiccator. As manganous stearate is not very soluble in trichlorobenzene at room temperature, the catalyst samples were

*Permanent address: Pakistan Atomic Energy Commission, Karachi.

weighed direct into the reaction vessel before pipetting in the polymer solution.

Manganese contents in the sample were determined by the sodium bismuthate method[12]. Actual analysis gave the average manganese content of 8·67 per cent which agrees fairly well with the calculated manganese content of 8·86 per cent on the basis of the formula, $(C_{17}H_{35}COO)Mn$, and fixes the purity of the sample at about 98 per cent.

(ii) *Manganic catalyst*—An attempt was made to prepare manganic stearate by oxidizing manganous stearate with *t*-butyl hydroperoxide in the presence of stearic acid. A mixture of equi-molecular quantities of the three constituents was heated on a water bath to slightly above 70° to melt the stearic acid. A dark brown product was formed from which excess stearic acid was removed through repeated washings with hot alcohol. The mixture was extracted with benzene and the catalyst precipitated by addition of an excess of alcohol to the filtrate. The sample was dried under vacuum at 60°C.

Analysis gave an average manganese content of more than twice the value expected on the basis of the formula, $(C_{17}H_{35}COO)_3Mn$, with 6·08 per cent manganese. Clearly then the sample used contained large amounts of manganous salts.

The catalyst was used as its solution in trichlorobenzene. Experimental results showed no change in catalytic activity of the sample even after its solutions had been stored for a very long period.

β-Naphthol

The B.D.H. sample was twice recrystallized from hot water. The pure sample gave white crystals. A suitable volume of its ether solution was pipetted into the reaction vessel and the solvent removed under vacuum.

Results

The rate of oxygen uptake was strongly influenced by the addition of manganese salts. When the catalyst was added in the higher valency state from the very start no induction period was observed and the maximum steady rate was reached soon after the shaking was started. A different behaviour resulted when the catalyst was added in the lower oxidation state. In the absence of an externally added hydroperoxide a long induction period was observed during which very little oxygen was absorbed. The maximum steady rate was reached only after an appreciable fraction of the manganese catalyst was converted to the higher oxidation state. This was also shown by the experiments in which a high concentration of partially oxidized manganous salt was used. The absorption of oxygen started from the very beginning but at a much lower rate than the maximum steady rate, which was reached only after some time. *Figure 1* shows the characteristic curves for the three cases.

The autoxidation of polypropylene was studied using either the Mn^{3+}-catalyst or Mn^{2+}-stearate with the addition of sufficient *t*-butyl hydroperoxide to convert it to the higher oxidation state. The maximum steady rates were reproducible to ± 3 per cent.

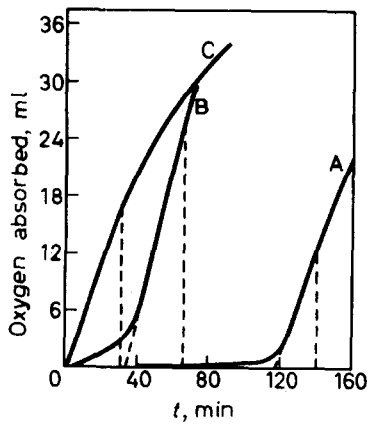

Figure 1—Volume of substrate 20 ml. Temperature 135°C. A: $[Mn^{2+}]$ $3{\cdot}45\times10^{-3}$ ml^{-1}, [RH] 1·10 ml^{-1} B: $[Mn^{2+}]$ $11{\cdot}65\times10^{-3}$ ml^{-1}, *t*-BHP added, [RH] 1·29 ml^{-1}. C: $[Mn^{3+}]$ $3{\cdot}78\times10^{-3}$ $mole^{-1}$, [RH] 1·10 ml^{-1}

Rate dependence on the catalyst concentration

The effect of the catalyst on the rate of oxygen uptake was studied over a wide range of concentration of both manganous stearate and the manganic catalyst. *Figure 2* shows the shape of the log rate versus log [Mn] curves.

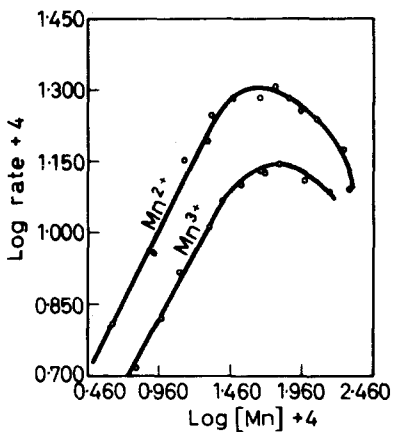

Figure 2—Variation of rate with catalyst concentration. Temperature 135°C. For Mn^{2+} [RH] 1·29 ml^{-1}, $p\ (O_2)_{partial}$ 657 mm Hg. For Mn^{3+} [RH] 1·10 ml^{-1}, $p\ (O_2)_{partial}$ 671 mm Hg

The initial part of each of the two curves is a straight line with a value of the slope equal to 0·59 for Mn^{2+}- and 0·55 for Mn^{3+}-catalysed systems. Thus, within the limits of experimental error, the rate is proportional to the square root of the catalyst concentration.

This relationship holds only up to about $2{\cdot}6\times10^{-3}$ $mole^{-1}$ of manganese, after which the rate starts falling off. At 4·5 to $5{\cdot}5\times10^{-3}$ $mole^{-1}$ of catalyst the rate apparently becomes independent of the catalyst as is commonly observed with the trace metal-catalysed oxidation of alkyl aromatic hydrocarbons. The subsequent fall-off in the rate at high catalyst concentration and high rate of oxidation is due to deactivation and precipitation of the catalyst, probably as a result of carboxylic acids formed. The kinetics of autoxidation of polypropylene have mainly been confined to two regions; first, where a square root relationship holds and secondly, in the region of

the maximum in the curve where the rate becomes independent of the catalyst concentration. These are respectively described as the low and the high catalyst concentration regions. It is relevant to mention that at the catalyst concentrations below $0{\cdot}5 \times 10^{-3}$ mole^{-1} the maximum steady rates, at 135° and above, were not very different from the corresponding values of the uncatalysed rates. All catalysed 'runs' were therefore carried out at the catalyst concentrations above this value.

Kinetics in the low catalyst concentration region

(i) *Rate dependence on polypropylene concentration*—At fixed catalyst concentration, oxygen pressure and temperature, the concentration of polypropylene was varied from 1·77 to 0·74 mole^{-1}. *Figure 3* shows the log

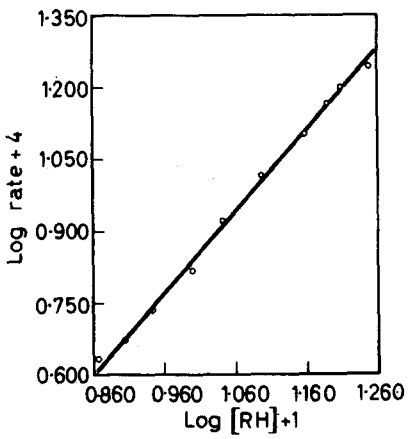

Figure 3—Dependence of rate on polypropylene concentration in the low catalyst concentration region. $[Mn^{3+}]$ $1{\cdot}26 \times 10^{-3}$ ml^{-1}, $p\,(O_2)_{\text{partial}}$ 680 mm Hg, temperature 135°C

rate versus log [RH] plot to be a straight line with a value of the slope equal to 1·7.

(ii) *Rate dependence on oxygen pressure*—The total oxygen pressure above the solution was varied from 557 to 760 mm Hg at constant concentrations of the catalyst and polypropylene at 135°. The rate showed a variation with the oxygen pressure and it was established that the rate was not diffusion-controlled and that a further increase in the shaking frequency or the surface area of the reaction vessel had no effect.

Figure 4 shows the plot of log rate against log partial pressure of oxygen above the solution. The straight line has a slope of 1·15. The catalysed rate is, therefore, directly proportional to the partial pressure of oxygen over the pressure range investigated.

(iii) *Variation of rate with temperature*—The reaction was studied over a temperature range of 125° to 145°C. The observed values of the rate were corrected for the change in vapour pressure of the solution with temperature. The Arrhenius plot is shown in *Figure 5*; it gives $E_{\text{overall}} = 21{\cdot}5$ kcal/mole.

Kinetics in the high catalyst concentration region

In this region, where $-\mathrm{d}\,(O_2)/\mathrm{d}t \propto [Mn]^0$, the effect of variation of

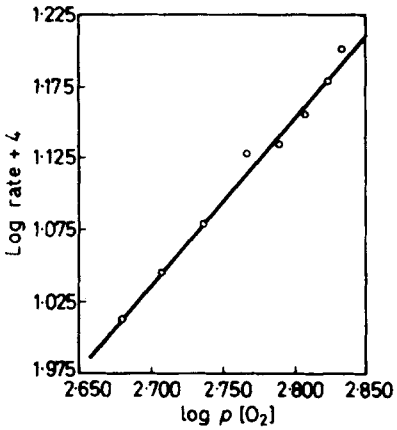

Figure 4—Dependence of rate on partial pressure of oxygen in low catalyst concentration region. $[Mn^{3+}]$ $1{\cdot}26\times10^{-3}$ ml^{-1}, [RH] 1·61 ml^{-1}, temperature 135°C

the polymer concentration and the oxygen pressure on the maximum steady rate were studied.

(i) *Rate dependence on* [RH]—The concentration of the polymer solution was varied from 1·72 to 0·86 $mole^{-1}$ at constant temperature, oxygen pressure and catalyst concentration. The plot of log rate versus log [RH], *Figure 6*, yields a straight line with a value of the slope equal to 2·07. In

Figure 5—Variation of maximum steady rate with temperature. $[Mn^{2+}]$ $1{\cdot}8\times10^{-3}$ ml^{-1}, [RH] 1·29 ml^{-1}, $p\ (O_2)_{\text{partial}}$ 700 mm Hg

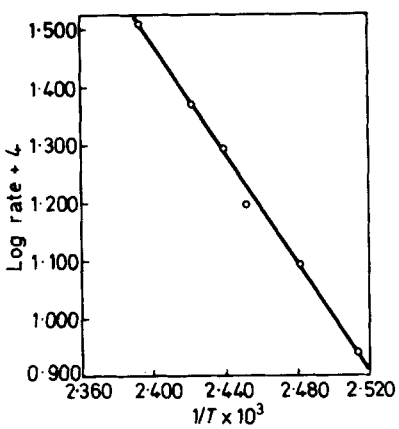

the high catalyst concentration region, therefore, the rate varies directly with the square of the polymer concentration.

(ii) *Rate dependence on oxygen pressure*—It was of particular interest to find out if the rate showed variation with the oxygen pressure in this region where the former becomes independent of the catalyst concentration. The oxygen pressure was varied over a suitable range and the corresponding maximum steady rates were measured. *Figure 7* shows the log rate versus $\log p\,(O_2)$ plot. The straight line so obtained has a slope of 0·9 which shows that even in the region of high catalyst concentration the rate is directly proportional to the partial pressure of oxygen above the solution.

β-Naphthol-inhibited system

The effect of the addition of β-naphthol to the Mn^{3+}-catalysed autoxidation of polypropylene was studied in detail to get information about the initiation step. The addition of β-naphthol produced an induction period

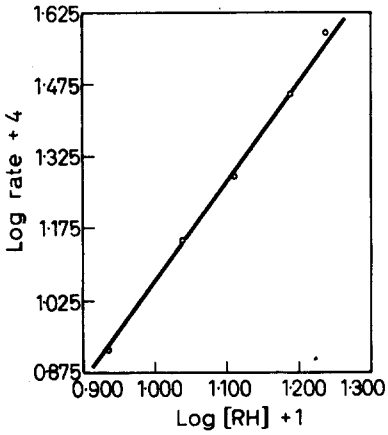

Figure 6—Dependence of rate on polypropylene concentration in the higher catalyst concentration region. $[Mn^{2+}]$ $4{\cdot}8 \times 10^{-3}$ ml^{-1}, $p\ (O_2)_{partial}$ 675 mm Hg, temperature 135°C

during which practically no oxygen was absorbed. The length of the induction period increased with increasing inhibitor concentration. The maximum steady rate reached after the end of the induction period did not seem to be affected by the amount of β-naphthol initially added to the system.

Figure 7—Dependence of rate on partial pressure of oxygen in high catalyst concentration region. [RH] 1·29 ml^{-1}, $[Mn^{2+}]$ $4{\cdot}65 \times 10^{-3}$ ml^{-1}, temperature 135°C

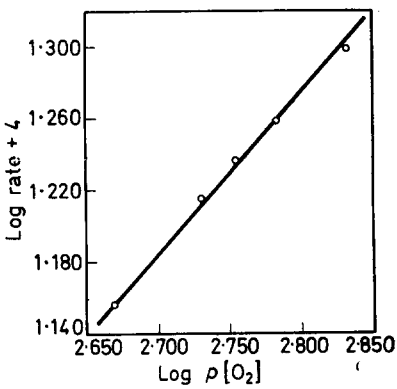

A series of experiments was carried out to establish exact relationships between the length of the induction period, t_I, and the other variables of the system. The results are represented graphically in *Figures 8* to *12*.

The plots of $\log 1/t_I$ against $\log [RH]$, $\log p\ (O_2)$, and $\log [Mn]$ are all straight lines with slopes equal to 1·1, 0·95 and 0·45 respectively. Thus

$$1/t_I \propto [RH], \quad \propto p\ (O_2) \quad \text{and} \quad \propto [Mn]^{1/2}$$

The overall energy of activation for this process comes out to be 22·5 kcal/mole.

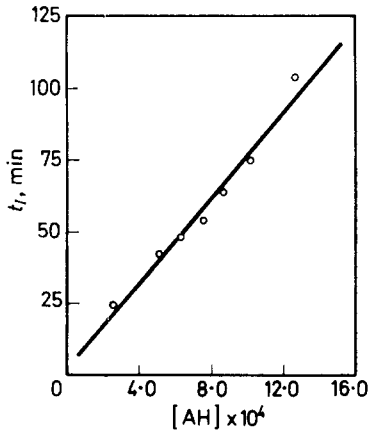

Figure 8—Variation of length of induction period with concentration of β-naphthol, [RH]. $[Mn^{3+}]$ $1{\cdot}26\times10^{-3}$ ml^{-1}, [RH] 1·36 ml^{-1}, $p\ (O_2)_{partial}$ 670 mm Hg, temperature 135°C

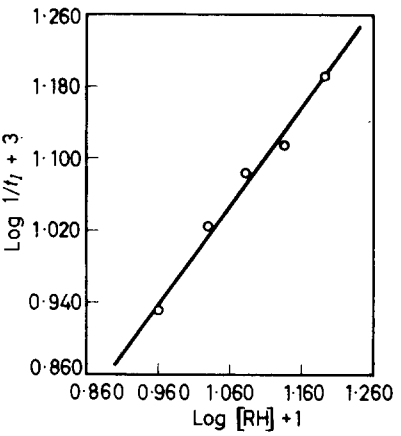

Figure 9—Dependence of induction period on polypropylene concentration. $[Mn^{3+}]$ $1{\cdot}26\times10^{-3}$ ml^{-1}, [AH] $1{\cdot}12\times10^{-3}$ ml^{-1}, $p\ (O_2)_{partial}$ 670 mm Hg, temperature 135° C

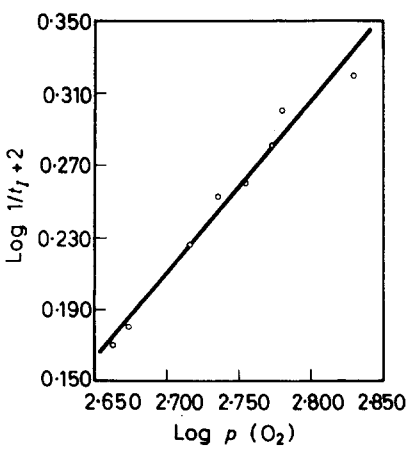

Figure 10—Dependence of induction period on partial pressure of oxygen. $[Mn^{3+}]$ $1{\cdot}26\times10^{-3}$ ml^{-1}, [RH] 1·36 ml^{-1}, [AH] $6{\cdot}3\times10^{-4}$ ml^{-1}, temperature 135°C

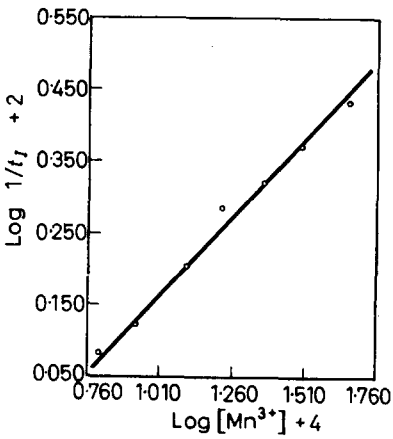

Figure 11—Dependence of induction period on catalyst concentration. [RH] 1·36 ml^{-1}, [AH] $8{\cdot}2\times10^{-4}$ ml^{-1}, p $(O_2)_{partial}$ 678 mm Hg, temperature 135°C

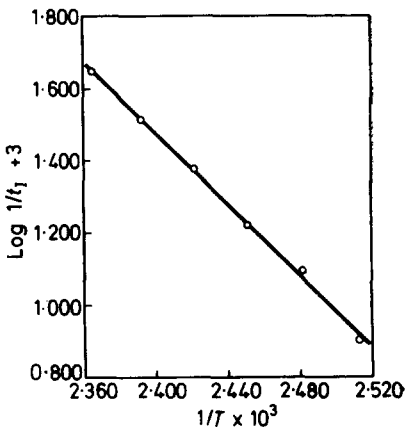

Figure 12—Variation of induction period with temperature. [Mn^{3+}] $1{\cdot}26\times10^{-3}$ ml^{-1}, [RH] 1·36 ml^{-1}, [AH] $8{\cdot}6\times10^{-4}$ ml^{-1}, p $(O_2)_{partial}$ 700 mm Hg

DISCUSSION

The catalysed system has some features in common with the uncatalysed one reported earlier[11]. The rate dependence on oxygen pressure is again an important characteristic, which the system shows under all the conditions studied. The dependence on polypropylene concentration is of the same order as in the uncatalysed autoxidation. It could be argued that basically a similar mechanism would also hold for the catalysed autoxidation of polypropylene. The major difference would lie in the way the catalyst could affect certain reactions in the proposed scheme, the most important of which would be the primary initiation reaction and the catalytic decomposition of the peroxide produced during autoxidation.

Initiation reaction

The investigation of the nature of the primary initiation reaction was complicated by the fact that the reciprocal of the induction period varied with $[catalyst]^{1/2}$. During the induction period an almost immeasurably small amount of oxygen was absorbed. The presence of a significant amount of peroxide can therefore be discounted. The only major source of free radicals, which consumed β-naphthol, would then be the primary initia-

tion step, or steps. There are two reasons for believing that β-naphthol is consumed only through its reaction with free radicals. First, the induction period remains directly proportional to the inhibitor concentration even at higher values of the latter. Secondly, the nature of the Arrhenius plot for $1/t_I$ suggests that there is no change in the mechanism of inhibitor consumption with an increase in temperature. The direct oxidation of β-naphthol is therefore negligible under these conditions. From the kinetics of the inhibited system it appears that the initiation process probably involves an interaction between the polymer, oxygen and the catalyst. The following points are of interest.

(a) With Mn^{3+}-catalyst the oxidation reaction starts almost immediately. Then Mn^{2+}-catalyst, on the other hand, produces a long induction period in the absence of an externally added hydroperoxide. This rules out the metal–oxygen complex of the type suggested by Uri[13] for a cobaltous system. That would require the metal to be in its lower oxidation state for it to function as an initiator.

(b) The induction period varies with oxygen pressure. This shows that the initiation process directly involves oxygen in the production of free radicals and that it cannot be a simple metal–hydrocarbon interaction of the type postulated by Erofeene and Soroko[14] for explaining the results of cumene autoxidation in the presence of manganese salts.

(c) The addition of Mn^{3+}-catalyst to the β-naphthol-inhibited system produces a drastic decrease in the length of the induction period. If it were assumed that the primary initiation process was the same as for the uncatalysed system and that the catalyst only decomposed the resultant peroxide to free radicals, the above experimental fact would be contradicted.

The following mechanism is put forward for the primary initiation process in the Mn^{3+}-catalysed autoxidation of polypropylene. A loosely bound complex between the hydrocarbon molecule and the metal catalyst is formed, which then reacts with a molecule of oxygen to produce free radicals.

$$Mn^{3} + RH \rightleftharpoons [Mn^{3+} \ldots\ldots RH]$$
$$[Mn^{3+} \ldots\ldots RH] + O_2 \longrightarrow Mn^{2+} + RO_2^{\bullet} + H^+$$

This is essentially equivalent to the decomposition of a hydroperoxide molecule by the manganic catalyst.

It is quite clear that this suggested mechanism should lead to

$$1/t_I \propto [RH]\,[O_2]\,[Cat] \qquad (1')$$

whereas the experimental results show

$$1/t_I \propto [RH]\,[O_2]\,[Cat]^{\frac{1}{2}} \qquad (2')$$

The probability of an effective primary initiation process not involving a catalyst molecule in this system has been ruled out for the reasons given above. Comparison of equations (1′) and (2′) suggests that with an increase in the catalyst concentration the number of free radicals which consume β-naphthol is much less than the expected total. The initiation process

produces manganese catalyst in the lower oxidation state, and as it is known to have a strong affinity for the oxidizing free radicals[2], it is very probable that such a reaction is taking place. The overall effect would be to decrease the order with respect to Mn^{3+}-catalyst to a value less than one. This suggestion will be made use of in the overall mechanism.

Overall mechanism

The following mechanism is put forward for the manganese-catalysed autoxidation of polypropylene.

$$\text{Initiation} = \phi = k_i\,[RH]\,[O_2]\,[Mn^{3+}] \tag{1}$$

which provides the system with free radicals.

$$R + O_2 \xrightarrow{k_2} RO_2 \tag{2}$$

$$RO_2 + RH \xrightarrow{k_3} RO_2R + H \quad \text{or} \quad ROOH + R\cdot \tag{3}$$

$$RO_2 + RH \xrightarrow{k_4} \text{Inactive products} \tag{4}$$

$$RO_2 + Cat \xrightarrow{k_4'} \text{Inactive products} \tag{4'}$$

$$RO_2R\,(ROOH) + Mn^{3+} \xrightarrow{k_5} RO_2 + Mn^{2+} + R^+ \tag{5}$$

$$RO_2R\,(ROOH) + Mn^{2+} \xrightarrow{k_5'} RO + Mn^{3+} + RO^- \tag{5'}$$

$$RO_2R\,(ROOH) + Cat \xrightarrow{k_6} \text{Inactive product} \tag{6}$$

$$RO \xrightarrow{k_7} R' + \text{volatile products} \tag{7}$$

$$R' + RH \xrightarrow{k_8} R'H + R \tag{8}$$

$$R' + O_2 \xrightarrow{k_9} \text{less active products} \tag{9}$$

Reaction (4') has been included to account for the deactivation of free radicals by the catalyst. No differentiation has been made as to the oxidation state of the catalyst molecule which undergoes this reaction.

As the catalyst is mainly present in the Mn^{3+} state and any Mn^{2+} formed would be rapidly converted to the higher oxidation state, it is assumed that

$$k_5\,[Mn^{3+}] = k_5\,[Cat] = k_5'\,[Mn^{2+}]$$

The following equations determine the stationary state conditions:

$$d\,[R]/dt = \phi - k_2\,[R]\,[O_2] + k_8\,[R']\,[RH] = 0 \tag{3''}$$

$$d\,[R']/dt = k_5\,[RO_2R]\,[Cat] - k_8\,[R']\,[RH] - k_9\,[R']\,[O_2] = 0 \tag{4''}$$

$$d\,[RO_2]/dt = k_2\,[R]\,[O_2] - (k_3 + k_4)\,[RO_2]\,[RH] - k_4'\,[RO_2]\,[Cat] + k_5\,[RO_2R]\,[Cat] = 0 \tag{5''}$$

and

$$d[RO_2R]/dt = k_3[RO_2][RH] - (2k_5 + k_6)[Cat][RO_2R] \qquad (6'')$$

Adding (3″) and (5″) and substituting the value of [R′] from (4″), then

$$[RO_2] = \frac{\phi}{(k_3 + k_4)[RH] + k_4'[Cat]} + \frac{k_5[Cat](2k_8[RH] + k_9[O_2])[RO_2R]}{\{(k_3 + k_4)[RH] + k_4'[Cat]\}(k_8[RH] + k_9[O_2])} \qquad (7'')$$

In equation (3) the initiation process has been assumed to provide the system with R· radicals. If it supplied RO_2· radicals instead of R· radicals, the addition of (3″) and (5″) would again lead to exactly the same expression as (7″).

Substituting the value of $[RO_2]$ from equation (7″) into equation (6″) and integrating we get

$$[RO_2R] = \frac{\dfrac{k_3[RH]\phi}{(k_3 + k_4)[RH] + k_4'[Cat]}(1 - e^{-At})}{\left[(2k_5 + k_6)\dfrac{k_3k_5[RH]}{(k_3 + k_4)[RH] + k_4'[Cat]}\dfrac{2k_8[RH] + k_9[O_2]}{k_8[RH] + k_9[O_2]}\right][Cat]} \qquad (8')$$

where A is the value of the denominator in this expression. Since $-d[O_2]/dt = k_5[Cat][RO_2R]$,

$$\{-d[O_2]/dt\}_{max.} = \frac{\dfrac{k_3[RH]\phi}{(k_3 + k_4)[RH] + k_4'[Cat]}\dfrac{k_5}{2k_5 + k_6}(1 - e^{-At_m})}{1 - \dfrac{k_3[RH]}{(k_3 + k_4)[RH] + k_4'[Cat]}\dfrac{k_5}{(2k_5 + k_6)}\dfrac{2k_8[RH] + k_9[O_2]}{k_8[RH] + k_9[O_2]}} \qquad (9'')$$

This expression, in general, is of the same form as that derived earlier for the uncatalysed autoxidation reaction[11]. The observed kinetics of the catalysed system will be derived from this expression.

Rate dependence on oxygen pressure

For the conditions of constant [RH], [Cat] and temperature, equation (9′) yields

$$\{-d[O_2]/dt\}_{max.} = \frac{\alpha - \phi}{(1 - \beta)\{(2K + [O_2])/(K + [O_2])\}} \qquad (10'')$$

where α, β and K are constants. Two cases may be considered: (i) At high $[O_2]$ values when

$$(1 - \beta)[O_2] \gg (1 - 2\beta)K$$

equation (10″) yields

$$-\{d[O_2]/dt\}_{max.} = \frac{\alpha K\phi}{(1 - \beta)[O_2]} + \frac{\alpha\phi}{(1 - \beta)} \qquad (11'')$$

which, on substitution of the value of ϕ, becomes

$$-\{d[O_2]/dt\}_{max.} = \alpha' + \beta'[O_2]$$
$$\alpha' + B''p(O_2) \qquad (12'')$$

(ii) At very low values of $[O_2]$ when

$$(1-2\beta)K \gg (1-\beta)[O_2]$$

$$-\{d[O_2]/dt\}_{max.} = \alpha_1'[O_2]$$

$$= \alpha_1'' p(O_2) \qquad (13'')$$

The rate of oxygen uptake in the catalysed system under all conditions shows a direct linear dependence on the partial pressure of oxygen above the solution. This is in agreement with the experimental results.

Rate dependence on the catalyst concentration

Rewriting equation (9″) for constant values of $[O_2]$, [RH] and temperature

$$-\{d[O_2]/dt\}_{max.} = \frac{C_1 k_3 k_5 [RH]\phi}{k_4'[Cat] + (1-C_2)(k_3+k_4)[RH]} \qquad (14'')$$

Two cases may be considered: (i) At very low values of the catalyst concentration the contribution by reaction (4′) can be considered negligible, so that

$$k_4'[Cat] \ll (1-C_2)(k_3+k_4)[RH]$$

Equation (14″) after substitution of the value of ϕ becomes

$$-\{d[O_2]/dt\}_{max.} = C_3[Cat] \qquad (15'')$$

(ii) At fairly high catalyst concentration when

$$k_4'[Cat] \gg (1-C_2)(k_3+k_4)[RH]$$

$$-\{d[O_2]/dt\}_{\infty} = C_4 \qquad (16'')$$

C_1, C_2, C_3 and C_4 are all constants and the subscript ∞ denotes the value of the rate in the high catalyst concentration region.

Equations (15″) and (16″) suggest that at very low catalyst concentrations the order with respect to [Cat] will be one, which eventually tends to zero at high catalyst concentrations. It was pointed out earlier that the steady rate of oxygen uptake with less than $0{\cdot}5 \times 10^{-3}$ mole^{-1} of manganese was almost identical with the uncatalysed steady rate, and therefore the catalyst concentrations used in these studies were always higher than this value. It is very probable, therefore, that the conditions for equation (15″) are never realized in this system. At intermediate concentrations of the catalyst the apparent order with respect to the catalyst will be between one and zero. The experimental results show that over the concentration range of $0{\cdot}5$ to $2{\cdot}6 \times 10^{-3}$ mole^{-1} of manganese, the value of this order is 0·5 to 0·6. The order continues to decrease over the concentration range of 2·6 to $4{\cdot}5 \times 10^{-3}$ mole^{-1} of manganese, after which the rate becomes independent of the catalyst concentration, as is shown by equation (16″). This mechanism, therefore, provides a satisfactory explanation for the observed kinetic behaviour.

Rate dependence on polypropylene concentration

(i) At low catalyst concentrations: rewriting the general equation (9″) for the condition that

$$k_4'[\text{Cat}] \ll (k_3 + k_4)[\text{RH}]$$

$$-\{\text{d}[\text{O}_2]/\text{d}t\}_{\text{max.}} = \frac{C_5\phi\,(k_8[\text{RH}] + k_9[\text{O}_2])}{k_9[\text{O}_2](1-\beta) + k_8[\text{RH}](1-2\beta)} \qquad (17'')$$

Applying the same conditions as in equation (11″) for high oxygen pressure, and substituting the value of ϕ, the above equation yields

$$-\{\text{d}[\text{O}_2]/\text{d}t\}_{\text{max.}} = C_5'[\text{RH}]^2 + C_6[\text{RH}] \qquad (18'')$$

This suggests that the apparent order with respect to [RH] would lie between one and two, the exact value depending upon the relative magnitude of the constants C_5' and C_6.

(ii) At high catalyst concentrations: the rate dependence on polypropylene concentration in the region where the former becomes independent of the catalyst concentration, can be derived from equations (14″) and (16″). Thus

$$-\{\text{d}[\text{O}_2]/\text{d}t\}_{\infty} = \frac{C_1k_3k_5[\text{RH}]\,\phi}{k_4'[\text{Cat}]} \qquad (19'')$$

which on substitution of the value of ϕ yields

$$-\{\text{d}[\text{O}_2]/\text{d}t\}_{\infty} = C_6'[\text{RH}]^2 \qquad (20'')$$

The rate of oxygen uptake in this region varies directly with the square of the polymer concentration. This agrees, too, with the experimental results.

Rate dependence on oxygen pressure in the high catalyst concentration region

It can be seen readily from equation (19″) that under the conditions of constant [RH], [Cat] and temperature,

$$-\{\text{d}[\text{O}_2]/\text{d}t\}_{\infty} = C_7[\text{O}_2]$$
$$= C_7'p(\text{O}_2) \qquad (21'')$$

is borne out very well by the experimental results in the high catalyst region.

One of us (S.A.C.) thanks the Commonwealth Scholarship Commission in the U.K. for a Scholarship and the Pakistan Atomic Energy Commission for leave of absence to undertake this work.

Department of Inorganic and Physical Chemistry,
University of Liverpool

(*Received May 1967*)

REFERENCES

[1] BAWN, C. E. H. *Disc. Faraday Soc.* 1953, **14,** 181
[2] DENISORE, E. T. and EMANUEL, N. M. *Russ. chem. Revs.* 1960, **29,** 645
[3] NOTLEY, N. T. *Trans. Faraday Soc.* 1964, **60,** 88
[4] STIVALA, S. S., REICH, L. and KELLEHER, P. *Makromol. Chem.* 1963, **59,** 28
[5] LUONGO, J. P. *J. appl. Polym. Sci.* 1960, **3,** 302
[6] MILLER, V. B., NEIMAN, M. B., PUDORE, V. S. and LAFER, L. I. *Polymer Sci., U.S.S.R.* 1961, **2,** 121
[7] MILLER, V. B., NEIMAN, M. B. and SHYLAPNIKOVA, YU. A. *Polymer Sci., U.S.S.R.* 1961, **2,** 129
[8] DUDROV, V. V. *Kinetics and Catalysis,* 1963, **4,** 185
[9] RYSAREV, D., BALABAN, L., SLAVIK, V. and RUZA, J. *Polymer Sci., U.S.S.R.* 1962, **3,** 855
[10] HANSEN, R. H. RUSSELL, C. A., DE BENEDICTIS, T., MARTIN, W. M. and PASCALE, J. V. *J. Polym. Sci.* 1964, **2,** 587
[11] BAWN, C. E. H. and CHAUDHRI, S. *Polymer, Lond.* 1968, **9,** in press
[12] VOGEL, A. I. *Quantitative Inorganic Chemistry,* p 287. Longmans Green: London, 1953
[13] URI, N. *Nature, Lond.* 1956, **177,** 1177
[14] EROFEERE, B. V. and SOROKO, T. I. *J. appl. Chem. U.S.S.R.* 1960, **33,** 900

Extended Range Elasto-osmometry

J. VAN DAM and W. PRINS

*Elasto-osmometry is based on the deswelling of swollen gels which occurs if the solvent around the gel is replaced by a solution of a polymer with a sufficiently high molecular weight to prevent penetration into the gel. An elasto-osmometer is described in which the change in retractive force at constant length due to the deswelling is measured. This change in force is proportional to the activity of the polymer solution outside the gel and thus inversely proportional to the number average molecular weight of the polymer. Deswelling equilibrium is attained in about 15 minutes. The balance-type construction allows measurements with a sensitive inductive force transducer on strips varying widely in modulus. With strips of poly(dimethylsiloxane) and poly(*cis*-isoprene) molecular weights of polystyrenes and poly(vinylacetates) up to 100 000 have been determined with an accuracy of about four per cent, in good agreement with the independently determined molecular weights.*

ELASTO-OSMOMETRY is based on the phenomenon that the elastic properties of a swollen gel submerged in a swelling agent are influenced by changing the activity of the swelling agent around the gel. This change in activity can be achieved by adding a solute to the surrounding swelling agent, with a sufficiently high molecular weight to prevent penetration into the gel. From the thermodynamic condition that the chemical potential of the solvent inside and outside the gel must be equal in equilibrium, it follows that addition of a solute leads to deswelling of the gel. As has been pointed out before[1-3] one of the simplest methods to trace this deswelling effect is to measure the increase in retractive force of a stretched gel strip at constant length. The relation between this change in force and concentration is easily shown to be[1]

$$(\partial f/\partial c)_{L,c=0} = BRT/\overline{M}_n \tag{1}$$

or in the integrated form

$$\Delta f = f - f_0 = (BRT/\overline{M}_n) \,.\, c \,.\, (1 + A_2 c + A_3 c^2 + \ldots\ldots) \tag{2}$$

where R is the gas constant, T the absolute temperature, $\overline{M}_n$ the number average molecular weight of the (polymeric) solute, f_0 the force when the strip is swollen in the pure solvent and B a proportionality constant, dependent on the material and dimensions of the gel strip and on the swelling agent, but independent of the nature of the solute; A_2, A_3,.. are virial coefficients.

The experimental arrangements can be made such that deswelling occurs within 15 minutes. Thus, in principle elasto-osmometry is equivalent to the recently developed fast membrane osmometers like Mechrolab's or Shell Stabin's. In a previous contribution from this laboratory[3] an elasto-osmometer has been described by which number average molecular weights

have been obtained up to 14 000 with an accuracy of ten per cent. The present paper deals with a description of and measurements with an at least tenfold more sensitive elasto-osmometer based on the same principle. The instrument also allows measurements on swollen strips varying widely in modulus.

DESCRIPTION OF THE APPARATUS AND OPERATING PROCEDURE

The first step in extending the molecular weight range of an elasto-osmometer is to use a more sensitive force indicator. In the instrument of Mieras and Prins[3] where the strip is connected directly to the strain gauge, this is not possible because sensitive force indicators have a small maximum load. This is important because, in order to avoid slack and other irreversible non-elastic behaviour, the strip has to be given a degree of elongation of five to ten per cent which for our strips of silicone rubber and poly(*cis*-isoprene) amounts to a force of from 10 to 40 g.

For this reason an elasto-osmometer has been designed in which the strip is connected to one end of a balance, whereas the force indicator is attached to the other arm of the balance (see *Figures 1* and *2*). By placing a counterweight on the same side as the force indicator the initial force due to the stretching can be compensated. A second advantage of the use of a

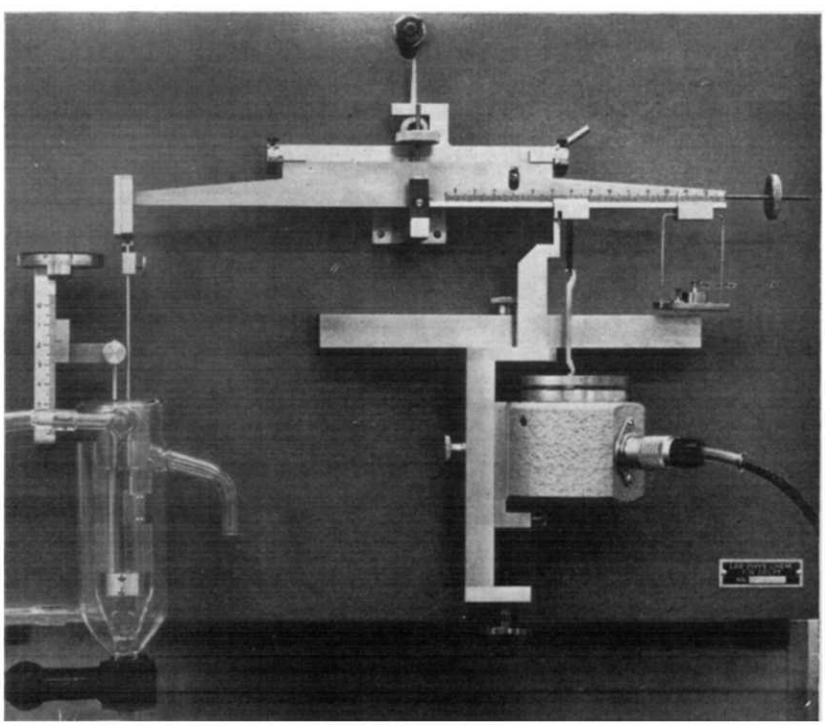

Figure 1—The improved elasto-osmometer. Swollen strip in measuring cell on left, force transducer on right

balance is that an additional amplification can be obtained by moving the point of attachment of the force indicator closer to the centre of the balance.

An inductive transducer (Type Q1/10-50, Hottinger, Darmstadt, Germany) serves as force indicator. This instrument gives a much smaller displacement than a strain gauge, viz. only 30 microns at a (maximum) load

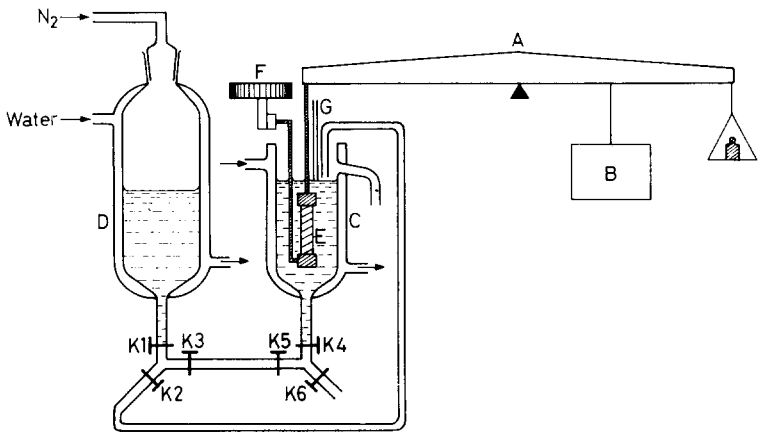

Figure 2—Schematic diagram of elasto-osmometer. A balance; B inductive force pick-up; C thermostatically controlled measuring cell; D thermostatically controlled solution vessel; E swollen polymer strip; F micrometer connected to lower clamp of strip; G adjustment device for constant immersion level; K1–6 metal housing stopcocks for introducing, replacing and draining polymer solutions

of 10 g. This is important because a small change in length of the strip as a result of the displacement of the transducer due to the increasing force may give a considerable decrease of that force. For a resistance strain gauge this can sometimes lead to a 20 per cent reduction in signal.

The output of the transducer is supplied to an amplifier (type KWS/II-50, Hottinger) connected to a 4 V recorder. It appears from a calibration of the transducer–balance combination by means of known weights that changes in force down to 1 mg are still measurable. A condition for attaining such a high sensitivity is that the instrument should be well isolated from mechanical vibrations. This was achieved in our case by mounting it on a heavy concrete pillar in the basement, set on its own foundation separate from the rest of the building.

The gel strip is held between two clamps of which the upper one is connected to the balance arm by means of an Invar rod. The lower clamp is attached to the baseplate of the balance, also by means of an Invar rod. A micrometer moves this lower clamp in order to adjust the length of the strip.

The strip, together with the clamps, is placed in a vessel with a volume of about 60 ml, thermostatically controlled with a water jacket. At the beginning of an experiment this vessel is filled with the pure solvent. After establishment of the equilibrium this solvent is replaced by a polymer

solution of known concentration from the storage vessel D (see *Figure 2*) by applying a small nitrogen pressure and operating the metal stopcocks K1, K3, K5 and K4. A check on this procedure showed that if one does not carry out the replacing process too fast, especially at the beginning, the concentration in the measuring-cell is exactly equal to that of the prepared polymer solution. A reasonable time for this process is ten minutes. Meanwhile the new swelling equilibrium begins to establish itself and is usually attained in 15 to 20 minutes. It is also possible to replace a concentrated solution by a more dilute (lighter) solution by operating stopcocks K1 and K2, whilst the original solution is drained by way of stopcocks K4 and K6.

In view of the buoyancy effect on the Invar rod of the upper clamp it is important to adjust the liquid level always to precisely the same height. This is achieved by first lowering the liquid level, after the replacement, to below the end of a narrow steel tube (G, *Figure 2*) and after that making it rise again slowly until the liquid surface touches the end of the tube. This adjustment is accurate within 0·2 mm, which corresponds to a buoyancy difference of about 0·5 mg. The buoyancy effects due to differences in density between the various polymer solutions are usually small. If necessary a correction for this effect can easily be calculated.

MEASUREMENTS WITH VARIOUS STRIPS AND POLYMERS

Figure 3 shows a series of measurements on anionically prepared polystyrene samples in toluene. The molecular weight distribution of these samples should be narrow. The gel strip of 2·5 cm length, 0·5 cm width and 0·02 cm thickness consisted of poly(dimethylsiloxane) crosslinked by γ-irradiation

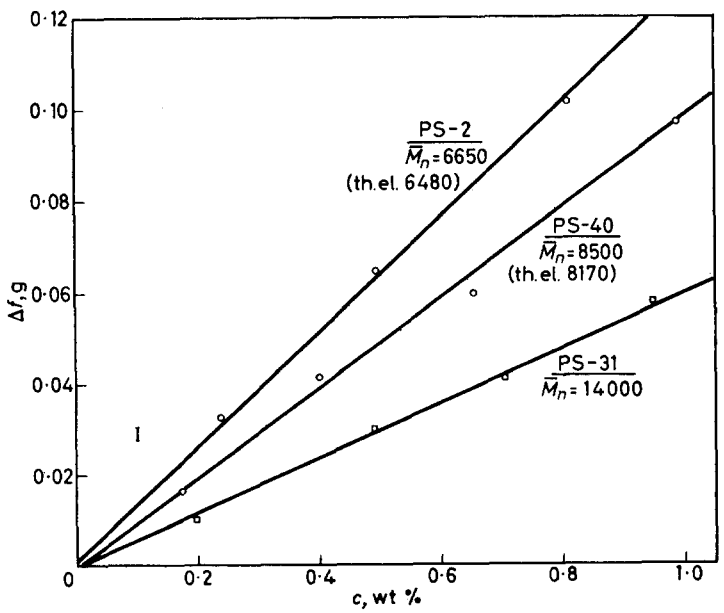

Figure 3—Elasto-osmometric data for polystyrene samples

(^{60}Co source, dose about 10 megarads). The degree of swelling was 6·3 and Young's modulus of the swollen strip was 5×10^5 dyne/cm^2.

Elasto-osmometry is not an absolute method unless one is able to calculate the constant B in equation (1). As a rule the physical properties of the gel strip required for calculating B, cannot be obtained with sufficient accuracy. Moreover, it is difficult to say which network theory applies to the particular gel under consideration. Therefore, it is easier and better to calibrate the strip for a particular solvent by means of a polymer of known molecular weight. The number average molecular weights of all polystyrenes have also been measured by thermoelectric vapour phase osmometry[4]. Consequently we could have used each of these samples as a calibration sample. We have chosen PS-31 of molecular weight 14 000 and thus calculated the constant B in equation (1). Now, as B is known, the molecular weights of the other polystyrenes follow from the slopes of the $\Delta f/c$ curves at infinite dilution. The close correspondence between the values obtained through the vapour phase method and the elasto-osmometric method shows that there is no penetration of the solute into the swollen strip.

In *Figure 4* two poly(vinylacetate) samples are given which have also been measured with a silicone rubber strip and toluene as a solvent. These samples were prepared by radical polymerization at 70°C of approximately

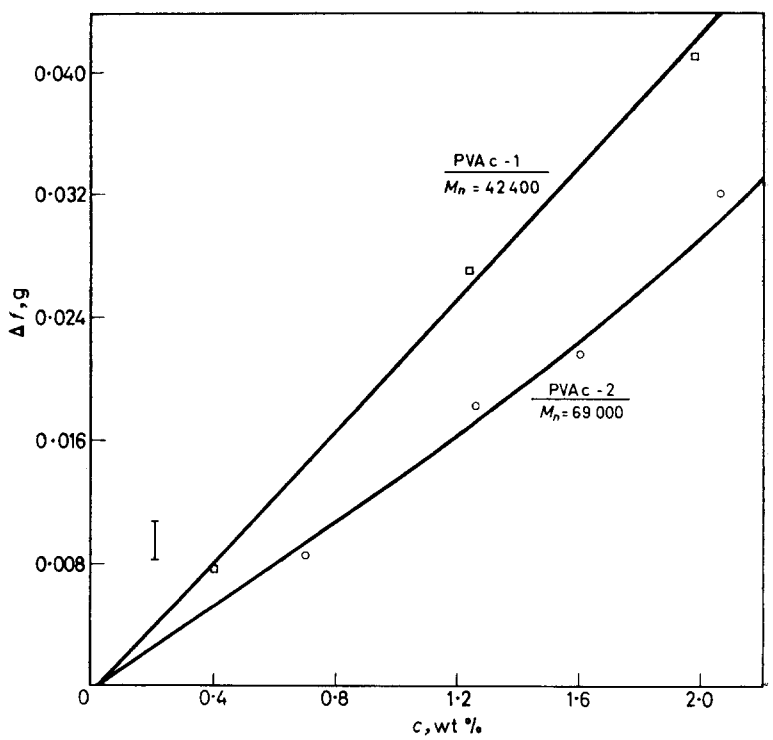

Figure 4—Elasto-osmometric data for poly(vinylacetate) samples using a swollen crosslinked poly(dimethylsiloxane) strip

40 per cent vinyl acetate solutions in benzene, using azobisisobutyronitrile as initiator. Triethyl amine was used as chain transfer agent to adjust the desired molecular weight. The conversion was kept below ten per cent. The molecular weights as determined by regular membrane-osmometry turned out to be 42 400 for PVAc-1 and 70 000 for PVAc-2.

If we use PVAc-1 as calibration sample and calculate the molecular weight of PVAc-2, we obtain a value of 69 000, in close agreement with the value obtained from regular osmometry.

With these measurements on poly(vinylacetate) a curious difficulty occurs. If we replace the pure solvent by the most diluted polymer solution, a normal deswelling takes place. If we then replace this polymer solution by a solution of higher concentration the measured force does not increase roughly proportionally as one would expect. Instead, there is almost no change in force. The only way to obtain usable results in this case is to condition the gel strip again in pure solvent, taking care that the polymer solution of higher concentration is not brought into the cell until after the swelling equilibrium is complete in pure solvent. The probable explanation of this effect is that the gel strip does not respond to the higher concentration because of clogging of its surface due to adsorbed polymer molecules. As a result diffusion of solvent molecules out of the strip is strongly hindered. This adsorption can be considerable in our case because both the dissolved polymer and the strip material are rather polar.

For this reason we have changed over from silicone rubber to the non-polar poly(*cis*-isoprene). The strips made of this rubber were also cross-linked by γ-irradiation (dose about 30 megarads); Young's modulus of the swollen strip was $1{\cdot}4 \times 10^6$ dyne/cm^2, and the degree of swelling in toluene 7·4. The poly(*cis*-isoprene) strips did indeed behave normally. The difficulties mentioned above did not occur. Some measurements with a poly(*cis*-isoprene) strip are given in *Figure 5*. Because the PVAc solutions are not ideal solutions at the rather high concentrations employed, $\Delta f/c$ has been plotted against c instead of Δf against c in order to make possible accurate extrapolation to infinite dilution.

The number average molecular weights of these samples were also determined by means of regular membrane-osmometry. These values and the elasto-osmotically measured $\overline{M}_n$ values are compared in *Table 1*.

Table 1

	$\overline{M}_n$ *membrane-osmometry*	$\overline{M}_n$ *elasto-osmometry*
PVAc-2	70 000	70 000
PVAc-3	88 300	97 200
PVAc-4	33 600	31 200
PVAc-5	23 700	22 000

In this series PVAc-2 has been used as a calibration sample in order to calculate the constant B [equation (2)]. The agreement between the two sets of molecular weight values is quite reasonable, considering that the accuracy in both methods is of the order of three to four per cent. Here

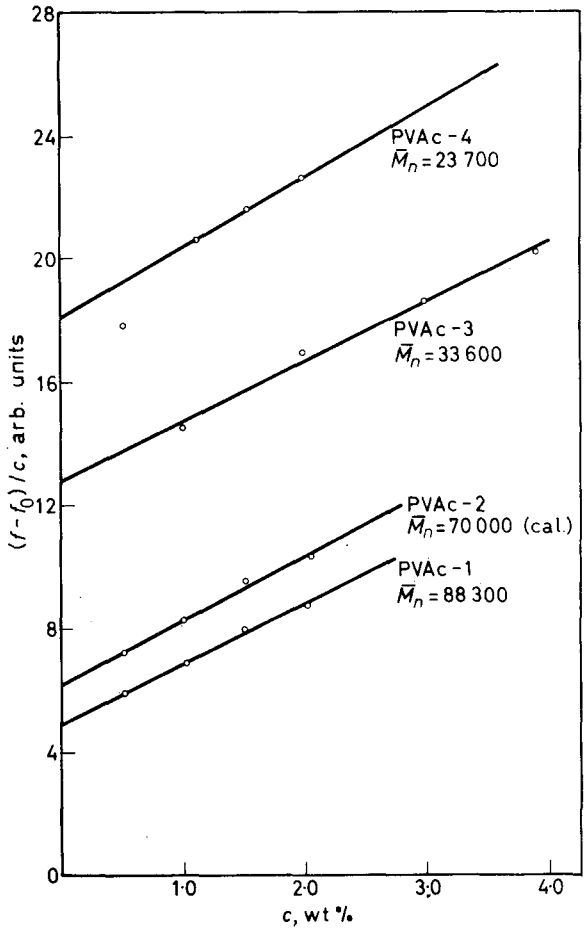

Figure 5—Elasto-osmometric data for poly(vinylacetate) samples using a swollen crosslinked poly (cis-isoprene) strip

again there appears to be no penetration of solute into the swollen strip. In this case the polymer has a fairly wide distribution ($\bar{M}_w/\bar{M}_n \simeq 2{\cdot}0$), so it is conceivable that the low molecular weight tail diffuses into the gel. This diffusion effect would, however, have to be identical in the elasto-osmometer and the regular membrane osmometer in order to give the observed agreement in $\bar{M}_n$ values. Although not impossible, this seems somewhat unlikely.

CONCLUSIONS

The measurements with an elasto-osmometer described in this paper show the possibility of determining number average molecular weights up to 100 000 with an accuracy of four per cent. This means that with the present strips the upper limit is about 200 000 with ten per cent accuracy.

NOTE ADDED IN PROOF

This range can be extended to at least 500 000 by using strips of poly (butadiene-co-acrylonitrile); further work with these and other strips is reported in the *Ph.D. Thesis* of one of us (J.v.D.)[5]. The effect of partially penetrating polydisperse polymer samples can be accounted for in a more reliable manner than in regular membrane-osmometry[5].

Physical Chemistry Laboratory,
Technische Hogeschool,
Delft, The Netherlands

(*Received May 1967*)

REFERENCES

[1] YAMADA, S., PRINS, W. and HERMANS, J. J. *J. Polym. Sci. A*, 1963, **1**, 2335
[2] HERMANS, J. J. 'Elasto-osmometry', in *New Methods in Polymer Chemistry*. Interscience: New York, 1963
[3] MIERAS, H. J. M. A. and PRINS, W. *Polymer, Lond.* 1964, **5**, 177
[4] VAN DAM, J. *Rec. Trav. chim. Pays-Bas*, 1964, **83**, 129
[5] VAN DAM, J. *Thesis*. Delft, 1967.

Block Copolymers Based on Polyalkylene Oxides and the Polyterephthalates of 2,2-Bis(4-hydroxyphenyl)Propane and Dimethylolcyclohexane

K. RICHES* and R. N. HAWARD

Alternating block copolymers of polyesters and polyethers have been prepared by end-tipping one of the base units with phosgene, followed by reaction with the second block. The method also provides a novel route for the preparation of high molecular weight polyethylene oxide. The yield stresses of the block polymers are dependent on block ratio and relatively insensitive to block size over the range investigated.

SEVERAL papers and patents have been published in recent years which describe the preparation and properties of linear segmented copolymers in which, in most cases, high and low softening segments alternate with varying regularity along the polymer chain[1–11]. The techniques that have been developed for the preparation of linear block copolymers, other than by anionic polymerization, generally fall into two classes.

The first class involves the pre-synthesis of one of the component blocks of the copolymer with functional end groups followed by the polymerization *in situ* of the components of the other block[1–6]. The second class involves the pre-synthesis of both of the component blocks either with terminal functional groups which are different but mutually reactive, in which case the product is a regularly alternating block copolymer[7–9], or both component blocks with the same terminal functional groups coupled, which results in a random distribution of blocks along the chain[10,11].

It has been shown previously that the melting point of a crystalline polyester decreases sharply with increasing concentration of another randomly copolymerized structural unit of lower melting point[9]. However, Coleman[1], Goldberg[2], Papava *et al.*[3,4] and Flory[9] have shown that, within reasonable limits, the crystalline melting points of block copolymers from similar starting materials vary little with composition.

In a segmented copolymer composed of high melting, highly crystalline 'rigid' blocks and low melting amorphous 'flexible' blocks, the crystallization of the former is enhanced by the chain or segmental mobility of the flexible units. The effect of this can, in fact, slightly raise the heat distortion temperature of the copolymer above that of the homopolymer of lower crystallinity[8].

In the present paper we describe the preparation and tensile properties of regularly alternating block copolymers of several polyalkylene oxides and the polyterephthalates of 2,2-bis(4-hydroxyphenyl)propane (Bisphenol A) and a mixture of 1,3- and 1,4-dimethylolcyclohexane (65 per cent 1,4).

*Present address: Shell Research Ltd, Woodstock Agricultural Research Centre, Sittingbourne, Kent.

The block copolymers have been prepared by a solution process at room temperature. It is believed that, under the present conditions, the loss of block homogeneity by ester exchange and thermal cleavage, which must occur to some extent in high temperature processes for the condensation of pre-synthesized blocks, has been reduced to a minimum. We were unable to obtain consistent results using the inter-phase condensation technique described by Merrill[7] for the preparation of polycarbonate block copolymers.

EXPERIMENTAL

To obtain block copolymers of high structural regularity both block species were pre-synthesized with terminal hydroxyl groups. The bischloroformate of one block species (usually the lower softening or more soluble component) was prepared and condensed with an equimolar concentration of the other hydroxyl terminated block in a suitable solvent at room temperature. In this manner block copolymers of polyalkylene oxides with poly (Bisphenol A terephthalate) and poly (dimethylolcyclohexane terephthalate) have been prepared.

As in more conventional ester condensation processes high polymer formation is generally favoured by an equimolar balance of the coreactants; an excess of either of the coreactants results in chain termination, the terminating group being common to the component in excess in the system. In view of the high molecular weight, high softening point and low solubility of some of the polyester blocks used in this work, end group analysis

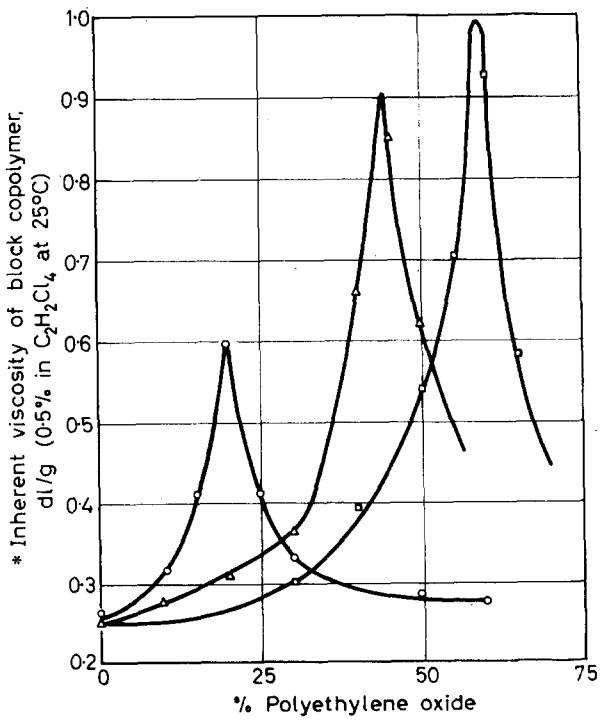

Figure 1—Influence of block ratio on molecular weight (shown by inherent viscosity) of poly (Bisphenol A terephthalate)–polyethylene oxide block copolymers. PEO ○ mol. wt 400, △ 1 000, □ 2 000. Inherent viscosity of poly (Bisphenol A terephthalate) 0·25 dl/g.

*Inherent viscosity $= \frac{1}{C} \ln \eta \text{ rel}$

was not always sufficiently accurate to enable predetermination of the optimum ratio of the coreacting species.

The results of a series of small-scale experiments designed to determine this ratio are illustrated in *Figure 1*, where the extreme sensitivity of the copolymer molecular weight to the ratio of the coreacting blocks is apparent.

Polyalkylene oxides

Polyethylene and polypropylene oxides were supplied by Shell Chemicals (U.K.) Limited, Carrington, Manchester. Polytetramethylene oxide was a sample of Teracol 30 supplied by E. I. DuPont de Nemours.

Bischloroformates

A 20 per cent to 30 per cent solution of the α–ω dihydroxy polyether in tetrachlorethane was added dropwise with stirring to a 5 M excess of phosgene in the same solvent cooled to $-10°C$ to $+5°C$. The temperature was maintained at or below $+5°C$ for two hours and then the mixture was allowed to warm to room temperature and left to stand for 24 hours. Excess phosgene was removed by passing a vigorous stream of dry nitrogen through the solution followed by the application of a vacuum. The bischloroformate was made up to a standard volume in tetrachlorethane.

Poly (Bisphenol A terephthalate)

Bisphenol A (0·2 mole) and terephthaloyl chloride (0·16 mole) were dissolved in 230 ml of dry benzene and the temperature raised slowly to that of reflux. A test sample removed after ten minutes gave no polymer on dilution with methanol. A repeat experiment containing 50 ml of dry pyridine produced a gelatinous precipitate shortly after mixing. Samples removed at 10, 20, 30 and 60 minute intervals and precipitated in methanol gave inherent viscosities of 0·145, 0·210, 0·289, 0·304 dl/g respectively (0·5 per cent solutions in tetrachlorethane). Larger batches of polyester of various molecular weights were prepared and the molecular weight controlled by varying the polymerization time.

Poly(dimethylolcyclohexane terephthalate)

Dimethylolcyclohexane (65 per cent, 1,4, 35 per cent, 1,3) (0·2 mole) and dimethylterephthalate (0·1 mole) were heated in the presence of two drops of tetraisopropyl titanate in a stream of nitrogen with vigorous stirring for two hours at 230°C. During this time most of the methanol formed in the ester exchange reaction had distilled from the system. The pressure was slowly reduced to 0·2 mm Hg at which point the glycol began to distil from the system. The reaction temperature was raised to 280°C and the polymerization continued until the required molecular weight was achieved.

The block condensation process

The polyalkylene oxide bischloroformate and polyester, both as ten per cent solutions in tetrachlorethane, were mixed in various ratios, and the combined weight of the reactants at each ratio was one gramme. Analytical reagent grade pyridine (2 ml) was added to this solution at room temperature and the mixture vigorously agitated. The solutions containing approxi-

mately equimolar concentrations of the coreacting blocks rapidly thickened and the reactions seemed complete after approximately 30 minutes. The solutions were left to stand for several hours then made up to 100 ml in tetrachlorethane. The inherent viscosities of the solutions were then determined assuming a one per cent concentration of polymer. Typical composition/inherent viscosity plots derived from these experiments are illustrated in *Figure 1*.

A further guide to the equivalence point was given by a pink colouration, probably due to a complex between the bischloroformate and pyridine, which increased in intensity with increasing concentration of bischloroformate after the equivalence point had been passed. No colouration developed before this point. Attempts to titrate a bischloroformate–pyridine solution with a solution of polyester until the disappearance of the red colouration only resulted in low molecular weight products.

Larger batches of material were prepared by scaling up the above method at the optimum block concentrations. The block copolymers were precipitated in aqueous methanol and washed repeatedly in a 'Waring blender' with aqueous methanol until free from pyridine. The product was dried under vacuum at 60°C.

At the peak of the composition/inherent viscosity curves shown in *Figure 1* there must be an equivalent number of end groups present in the two blocks. Therefore

$$W_A/W_B = MW_A/MW_B$$

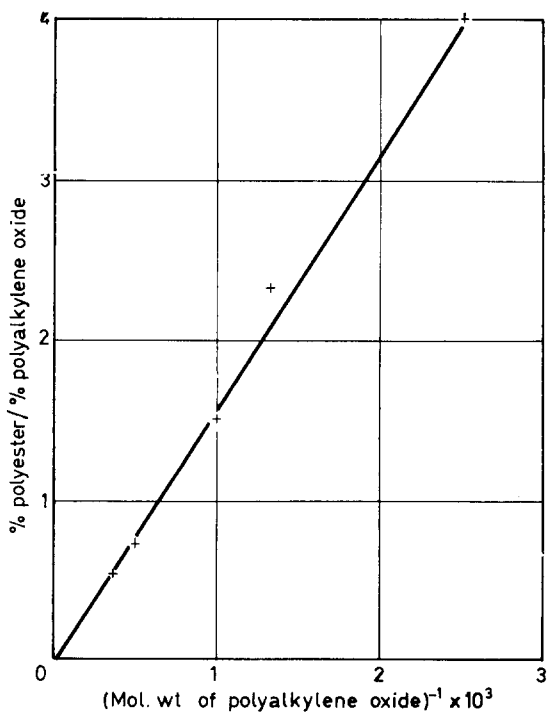

Figure 2—Plot of block weight ratio at maximum inherent viscosity against the reciprocal of the polyalkylene oxide block molecular weight

where W_A and W_B, MW_A and MW_B are the weights and (number average) molecular weights of the blocks A and B. *Figure 2* shows a plot of this relation for a Bisphenol A terephthalate–polyalkylene oxide block system. From the line obtained a molecular weight of 1 560 for the polyester may be derived. Obviously measurements of this type could be used to compare the molecular weights of difunctional polymers.

High molecular weight polyalkylene oxide

The block condensation process has been used to prepare polyethylene and polypropylene oxides of high molecular weight. Using two different polyethylene oxides (molecular weights 1 000 and 1 500) in equimolar proportions we were able to prepare a high molecular weight polyethylene oxide (inherent viscosity 1·27 dl/g). Experiments with linear polypropylene oxides were less successful, a difference which is believed to be due to the absence of complete difunctionality in the polypropylene oxides. This method also provides for the production of 'homopolymers' with a relatively precise location of carbonyl groups along the chain.

Preparation of test specimens

Films of the copolymers were cast from concentrated solutions in tetrachlorethane. Residual solvent was stripped under vacuum at 60°C. Instron tensile tests were carried out on 4 in. × 0·5 in. × 0·002 in. specimens with an elongation speed of 4 in./min.

RESULTS AND DISCUSSION

Film structure

X-Ray structural analysis of the solution-cast films of high molecular weight block polymer indicated that the polyester segments were more highly crystalline than would have been the case in the homopolymer, whereas the polyethylene oxide and polytetramethylene oxide segments appeared to be completely amorphous. Low molecular weight products, which were obtained when a large excess of polyethylene oxide bischloroformate (mol. wt 2 000) over polyester was used in the preparation, did show evidence of crystallinity in the ethylene oxide segments. Solution-cast films of such materials often developed large spherulitic formations. The work-up procedure of the polymer was such as to exclude the possibility of this being due to free polyethylene oxide. Since, on the extreme right of the viscosity/composition curves (*Figure 1*), one and three block copolymers will predominate, it appears that under the present experimental conditions, the polyethylene oxide segments can crystallize when one end of the chain is free, but crystallization is suppressed when both ends are bound in a multi-block copolymer.

The mechanical properties of cast films

One of the objects of this work was to observe the effect of varying the block length on the mechanical properties of the block polymers. For this purpose a series of blocks of poly(dimethylolcyclohexane terephthalate) were prepared and condensed with polyethylene oxide of the appropriate molecular weight to give products with a particular ethylene oxide content (*Table 1*). The stress/strain curves shown in *Figure 3* suggest that the

Table 1. Block copolymers of polyethylene oxide with poly(dimethylolcyclohexane terephthalate)

Polyester	*Polyethylene oxide*		*Block copolymer*				
*Mol. wt**	*Mol. wt*	% †	*I.V.‡* (*dl/g*)	*Stress* (*lbf/in²*)		*Elongation* (%)	
				Yield	*Ult.*	*Yield*	*Ult.*
1 600	400	20	0·62	3 750	B	36	B
1 400	600	30	0·62	2 650	2 580	30	166
2 340	1 000	30	1·00	2 580	2 890	16	370
3 500	1 500	30	0·61	2 830	2 470	10	270
600	400	40	—	1 690	1 620	36	251
1 500	1 000	40	0·75	1 740	2 320	36	447
2 250	1 500	40	0·69	1 522	1 620	10	441
470	400§ 1 000	55	—	600	B	38	B

*Polyester molecular weights are theoretical.
†Polyethylene oxide percentages are derived from viscosity/composition curves and are correct to within two per cent.
‡Inherent viscosities (I.V.) determined on 0·5 per cent solutions in tetrachlorethylene at 25°C.
§1:1 mixture of polyethylene oxide 400 and 1 000.
B Broke at yield.

block size, over the limited range studied, is a relatively minor factor in determining properties. The yield stress is determined primarily by the proportion of the two blocks present.

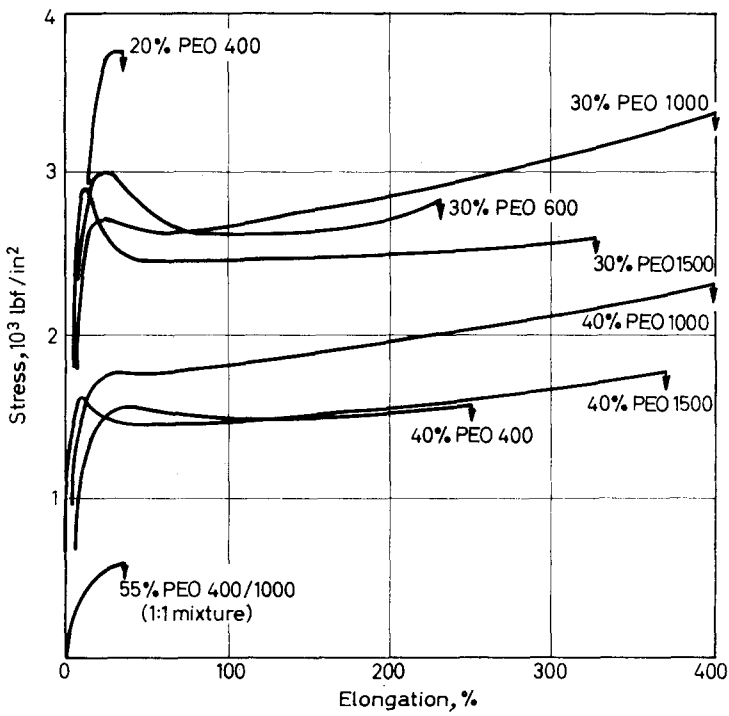

Figure 3—Effect of block size on tensile properties of block polymers. All polymers were poly (dimethylolcyclohexane terephthalate)–PEO block polymers

Table 2. Block copolymers of various polyalkylene oxides with poly(Bisphenol A terephthalate)

Polyester	*Polyalkylene oxide*			*Block copolymer*				
I.V. (*dl*/*g*)	*Type*	*Mol. wt*	%	*I.V.* (*dl*/*g*)	*Stress* (lbf/in²)		*Elongation* (%)	
					Yield	*Ult.*	*Yield*	*Ult.*
0·25	PPO	750	30·0	—	3 675	4 084	10	117
0·25	PEO	1 000	44·0	0·94	1 960	5 065	20	450
0·35	PEO	1 000	31·7	0·68	2 680	2 624	10	40
0·26	PPO	1 500	39·4	0·58	1 680	1 373	20	123
0·25	PEO	2 000	58·0	0·87	830	1 532	15	724
0·25	PTMO	2 700	65·3	1·04	6 600	3 709	60	753

PPO Polypropylene oxide. PEO Polyethylene oxide. PTMO Polytetramethylene oxide.
I.V. Inherent viscosity—(0·5 per cent in tetrachlorethane at 25°C).
Tensile values are the mean of at least four determinations.

Figure 4 and *Table 2* show the properties of the Bisphenol A terephthalate–polyalkylene oxide block system. The polymers show an interesting contrast to the previous system. Four of the polymers show a marked

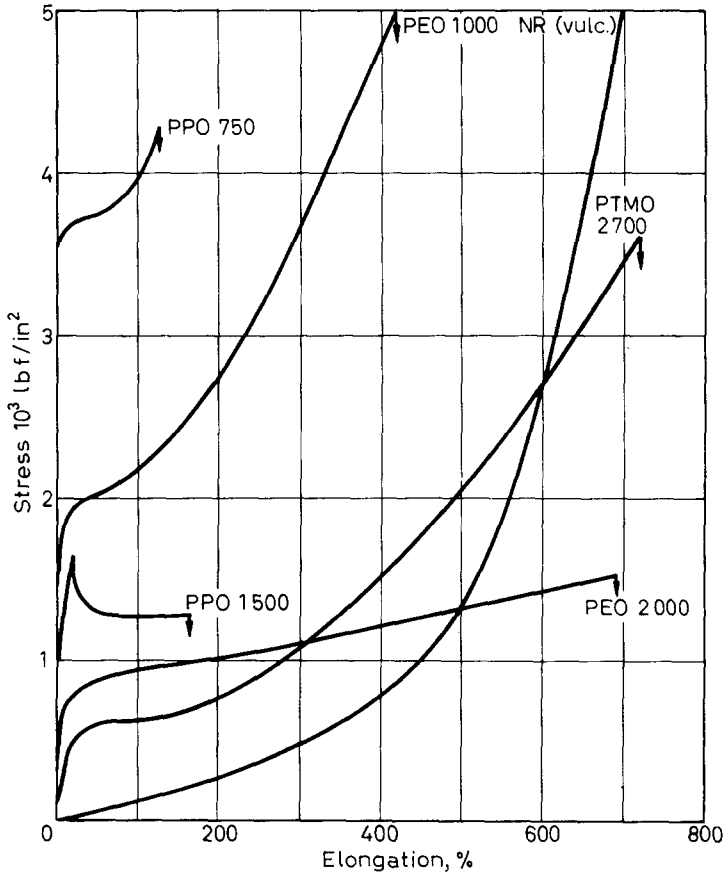

Figure 4—Tensile properties of poly (Bisphenol A terephthalate)–polyalkylene oxide block copolymers. PPO—polypropylene oxide, PEO—polyethylene oxide, PTMO—polytetramethylene oxide, NR—natural rubber

tendency for the stress to rise after yielding starts. The steepness of this rise and extension at which it occurs appear to be related to the molecular weight of the flexible polyalkylene oxide. This observation could be interpreted in terms of the theory of Krigbaum *et al.*[12] who have accounted for the elasticity of a semi-crystalline polymer (polyethylene) in terms of the extension of the amorphous chains between the crystalline units. On similar lines we might expect the elongation of our specimens to be related to the length of the extensible polymer chains between the crystalline blocks. With the Bisphenol A terephthalate blocks, both of the polymers containing low molecular weight polyalkylene oxide units show a tendency to develop a higher modulus as the elongation increases (work hardening). This trend is largely absent when the higher molecular weight ethylene oxide or propylene oxide blocks are used. However, this work hardening effect is also absent when the dimethylolcyclohexane polyester blocks are used (*Figure 3*). This difference in behaviour is correlated with the X-ray

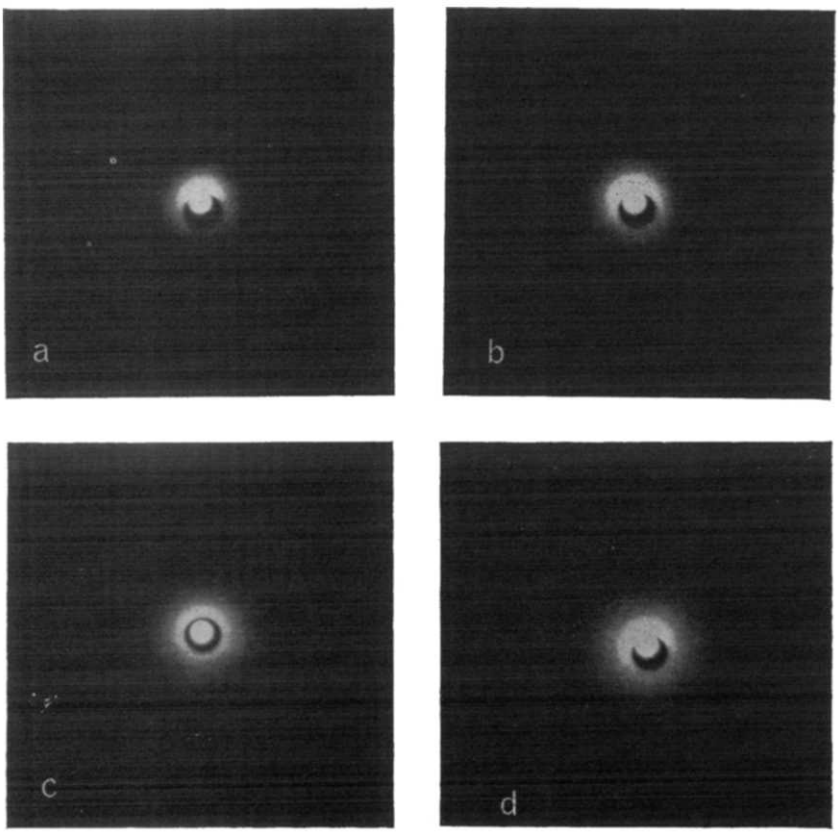

Figure 5—X-Ray diffraction photographs: (a) Bisphenol A terephthalate–polyethylene oxide 1 000. As cast; (b) Bisphenol A terephthalate–polyethylene oxide 1 000. Extended 300 per cent; (c) Dimethylolcyclohexane (30 per cent polyethylene oxide 1 000). As cast; (d) Bisphenol A terephthalate–polyethylene oxide 1 000. Extended 100 per cent

photographs (*Figure 5*) which showed that the Bisphenol A terephthalate blocks crystallized more strongly than those derived from dimethylolcyclohexane. In each case there was some evidence of orientation as elongation took place.

'Shell' Research Limited,
Carrington Plastics Laboratory,
Urmston, Manchester

(*Received May 1967*)

REFERENCES

[1] COLEMAN, D. *J. Polym. Sci.* 1954, **14**, 15
[2] GOLDBERG, E. P. *J. Polym. Sci.* 1964, **C4**, 707
[3] KORSHAK, V. V., VINOGRADOVA, S. V. and PAPAVA, G. SH. *Izvest. Akad. Nauk S.S.S.R.* (January 1964) No. 1
[4] PAPAVA, G. SH., VINOGRADOVA, S. V., KORSHAK, V. V. and TSISKARISHVILI, P. D. *Izvest. Akad. Nauk S.S.S.R.* (January 1964) No. 1. English translation p 128
[5] FRAZER, A. H. *U.S. Pat. No. 3 037 960* (1962)
[6] SCHAEFGEN, J. R. and SHIVERS, J. C. *U.S. Pat. No. 3 044 987* (1962)
[7] MERRILL, S. H. *J. Polym. Sci.* 1962, **55**, 343
[8] MERRILL, S. H. and PETRIE, S. E. *J. Polym. Sci. A*, 1965, **3**, 2189
[9] FLORY, P. J. *U.S. Pat. No. 2 691 006* (1954)
[10] IWAKURA, Y., TANEDA, Y. and UCHIDA, S. *J. appl. Polym. Sci.* 1961, **5**, 108
[11] GRIEVESON, B. M. *Polymer, Lond.* 1960, **1**, 499
[12] KRIGBAUM, W. R., ROE, R-J. and SMITH, K. J. *Polymer, Lond.* 1963, **5**, 533

Autoxidation of Atactic Polypropylene in Solution I—2, 2′-Azo-bis-isobutyronitrile-Initiated Autoxidation

C. E. H. BAWN and SHAMIM A. CHAUDHRI*

Kinetics of the liquid-phase autoxidation of atactic polypropylene, using azobisisobutyronitrile as initiator, have been determined. The order of reaction with respect to initiator concentration has been found to be 0·85, and that with respect to polymer concentration to be varying from 0·37 to 0·12 over the concentration range used. The overall values of the above orders have been shown to be influenced by the relative rates of the two steps in the chain mechanism. 'Geminate recombination' as an additional termination reaction of the free radicals provides a qualitative explanation for the variation of the rate with polymer concentration.

AUTOXIDATION of polypropylene has been studied by many workers[1–4] in solid phase by exposing thin films of the polymer to air or oxygen under a variety of experimental conditions, and following the progress of the reaction by measuring oxygen absorption, pressure changes, i.r. absorption in the carbonyl region, etc. Very few studies of autoxidation of polypropylene, however, have been carried out in the liquid phase and no detailed information on the overall kinetics is available beyond the initiation stage[5]. The aim of this paper is to report some kinetic aspects of the liquid-phase autoxidation of atactic polypropylene in which 2,2′-azo-bis-isobutyronitrile (AIBN) has been used as a source of free radicals to initiate oxidation chains. The subsequent papers in this series will deal with uncatalysed and metal salts-catalysed liquid-phase autoxidation of atactic polypropylene.

AIBN AS INITIATOR

AIBN has been used extensively as a source of free radicals in both polymerization and autoxidation reactions, due to its straightforward monomolecular decomposition in a number of solvents. Various methods have been employed to determine the kinetics of AIBN decomposition and these are reviewed critically by Van Hook and Tobolsky[6]. Later results, with styrene[7] and tetralin[8] as solvents, are also in close agreement with their reported values.

The AIBN-initiated autoxidations may be represented by the following steps:

Initiation:

$$A \xrightarrow{k_i} 2R^{\bullet} + N_2 \qquad (1)$$

Propagation:

$$R^{\bullet} + O_2 \xrightarrow{k_2} RO_2^{\bullet} \qquad (2)$$

*Permanent address: Pakistan Atomic Energy Commission.

$$RO_2^{\bullet} + RH \xrightarrow{k_3} RO_2H + R^{\bullet} \qquad (3)$$

Termination:

$$RO_2^{\bullet} + RO_2^{\bullet} \xrightarrow{k_6} \text{Inactive products} \qquad (6)$$

At oxygen pressures above 200 mm of mercury, termination by $R^{\bullet} + R^{\bullet}$ or $R^{\bullet} + RO_2^{\bullet}$ reaction is negligible compared to the effect of (6). Decomposition of RO_2H to give free radicals is also of less significance at the low temperatures usually employed in AIBN-initiated oxidations, and, therefore, reaction (1) is considered to be the only important initiation reaction in the scheme.

Assuming $k_2 [R^{\bullet}] [O_2] = k_3 [RH] [RO_2]$ for long kinetic chains, and making corrections for evolution of nitrogen ($k_i [A]$) and absorption of oxygen in the initiation step ($2ek_i [A]$), the overall rate of oxygen uptake can be represented by

$$-d [O_2]/dt = 2ek_i [A] + k_3 [RH] [RO_2] - k_i [A] \qquad (1')$$

where 'e' is the efficiency of initiation of free radicals. At stationary state conditions, the above equation becomes:

$$-d [O_2]/dt = (2e - 1) k_i [A] + k_3 (ek_i/k_6)^{\frac{1}{2}} [RH] [A]^{\frac{1}{2}} \qquad (2')$$

If the first term on the RHS can be neglected compared to the second, then the order of reaction with respect to AIBN will be 0·5 as has been experimentally found in autoxidation of many substances such as cumene[9,10], ethylbenzene[10], tetralin[8], etc.

EXPERIMENTAL

(A) *Measurement of oxygen uptake*

The course of the oxidation reaction was followed by measuring the volume of oxygen absorbed at constant pressure, generally atmospheric. The apparatus used was essentially the one described by Cooper and Melville[11] in which a slight decrease in pressure, due to absorption of oxygen on one side of a gas burette, is compensated by generation of gases on the other, through a relay-operated electrolytic cell.

The reaction vessel was thermostatically controlled in an oil bath, with temperature control of $\pm 0{\cdot}05$ deg. C and shaking speed regulated at more than 300 rev/min. The maximum rates of oxygen uptake were independent of shaking frequency in the above range.

A pre-weighed amount of AIBN was then rapidly introduced into the reaction vessel containing a known volume of the polymer solution, and shaking started immediately. The maximum steady rate which was maintained after the first few minutes was calculated from the amount of oxygen absorbed versus time plot.

All polymer concentrations are expressed as moles per litre, based on the monomer unit, and this corresponds to moles of tertiary hydrogen atoms on the polymeric chain.

(B) *Materials*

(1) *Atactic polypropylene*—An inhibitor-free polymer sample (I.C.I. Ltd) was refluxed with diethyl ether for two hours and insoluble residue removed by filtering through a glasswool plug. Polymer was precipitated by slowly adding the ether solution to methanol. The precipitated polymer was repeatedly washed with methanol and then dried under vacuum at room temperature, and was further purified by repeating the operations. It was finally purified by shaking the ether solution with activated aluminium oxide and reprecipitating with methanol. No difference in results was found between samples purified by this procedure and those in which ether solution was chromatographed over a column of aluminium oxide.

The purified polymer was dried under vacuum, at 40° to 50°C for an hour, and then at 90° to 100°C for half an hour. The i.r. spectrum of the polymer agreed with that of Luongo[12]. Solutions were made in trichlorobenzene under an atmosphere of carbon dioxode and used for oxidation studies.

(2) *1,2,4-Trichlorobenzene*—The B.D.H. sample was chromatographed over aluminium oxide and distilled at atmospheric pressure. The fraction distilling over at 210° to 212°C was collected and redistilled before use.

(3) *AIBN*—A commercial sample was recrystallized from ether, dried under vacuum and stored in a dark, cool place.

RESULTS

The kinetic order with respect to AIBN was found to be different from the expected value of 0·5 [equation (2)]. The results are shown in *Figure 1* and indicate that the order with respect to AIBN (A) was $0{\cdot}85 \pm 0{\cdot}03$. (It should be noted that $(-\mathrm{d}[O_2]/\mathrm{d}t)_{\text{observed}} = -\{(\mathrm{d}[O_2]/\mathrm{d}t) - (\mathrm{d}[N_2]/\mathrm{d}t)\}$. *Figure 2*(a) shows the variation of the rate with polymer concentration. The variable slope of the log/log curve [*Figure 2*(b)] indicates an order which ranges from 0·12 at higher to 0·37 at lower polymer concentrations.

The above results were so different from those observed with alkyl aromatic hydrocarbons or expected according to the theory of long chains that it was thought desirable to compare the oxidation of polypropylene in solution with the structurally similar hydrocarbon, 2,6,10,14-tetramethyl pentadecane (pristan)[18]

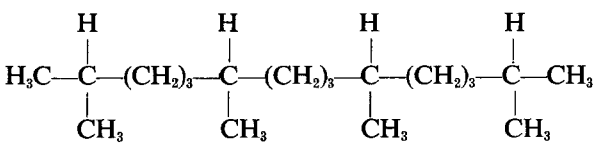

which like polypropylene has tertiary hydrogen atoms along the carbon backbone.

The results obtained for the AIBN-initiated oxidation of the pure hydrocarbon at 100°C are given in *Table 1*. The slope of the log (rate) versus log [AIBN] plot indicated a reaction order with respect to AIBN of 0·55. This observation, together with an alternative representation of the results discussed later in this section, shows that the oxidation of pristan conforms

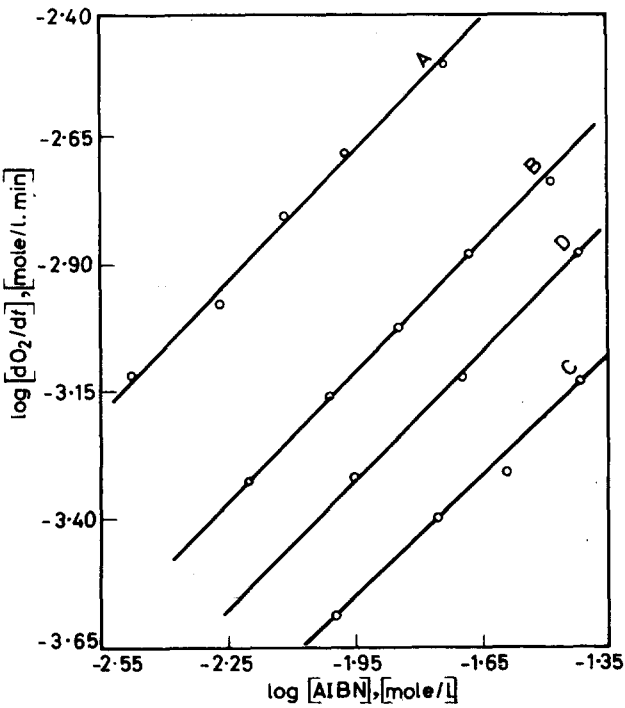

Figure 1—Rate dependence on AIBN concentration. Polymer concentration 1·51 mole litre^{-1}. A 100°C, B 90°C, C 80°C. D Polymer concentration 0·15 mole litre^{-1}, 90°C

to the theory for long chains and that it oxidizes in a similar manner to the paraffinic and alkylaromatic hydrocarbons.

In contrast the above results clearly indicate the inadequacy of equation (2′)—derived for long kinetic chains—in explaining the observed kinetics for the autoxidation of polypropylene solutions. In the present

Table 1. Temperature=100°C. [Pristan]=11·5 moles (tertiary hydrogen atom) litre^{-1}

[A]×10^3 mole litre^{-1}	7·56	12·30	17·55	26·30	36·40
Rate×10^4 mole l^{-1} mm^{-1}	8·26	11·22	14·15	17·78	21·20

work chain lengths, calculated from the overall rates of oxygen-uptake and rates of initiation at a known [AIBN], were three or less and it is therefore not justifiable to use the stationary state condition $k_2[R][O_2]=k_3[RO_2][RH]$. The probable reason for this difference in the behaviour of the polymer solution and other substrates such as cumene, ethylbenzene, etc., is perhaps related to the higher energy of activation of the propagation step (3) for paraffinic substrates with tertiary hydrogen[13,14] than for the alkyl aromatics[15,16] mentioned above.

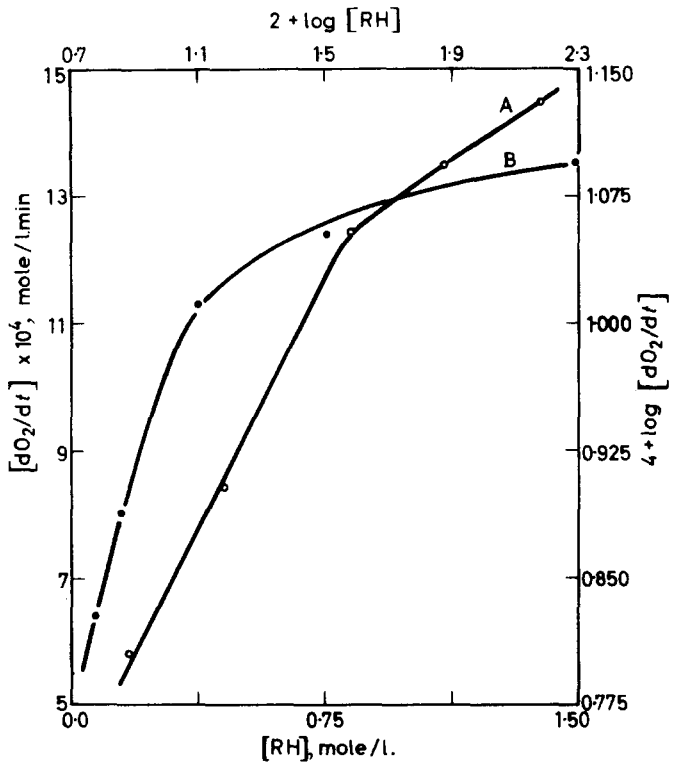

Figure 2—Rate dependence on polymer concentration, [RH]. [AIBN] $2{\cdot}07\times10^{-2}$ mole litre^{-1}. Temperature 90°C. A log/log plot; B linear plot

The rate of oxygen-uptake, without applying the assumption of reaction (2) equal to (3) can now be expressed as

$$-\mathrm{d}[O_2]/\mathrm{d}t=(2e-1)\,k_i\,[A]+k_2\,[R^\bullet]\,[O_2] \qquad (3')$$

which on substitution of the stationary state concentration of [R•] gives

$$-\mathrm{d}[O_2]/\mathrm{d}t=(4e-1)\,k_i\,[A]+k_3\left(\frac{ek_i}{k_6}\right)^{\frac{1}{2}}\,[A]^{\frac{1}{2}}\,[RH] \qquad (4')$$

The efficiency of chain initiation, e, in trichlorobenzene was determined using 2,5-di-*tert*-butyl-4-methylphenol as inhibitor, by the method described by Howard and Ingold[7], and was found to be 0·6 in good agreement with values in other solvents[17].

The first term on the RHS in equation (4′) is not only seven times larger than that of equation (2′) but also due to comparatively low k_3 [RH] values for polymer solution its importance relative to the second term must have increased considerably. In the extreme case when the second term becomes negligible compared to the first, the overall kinetics will be controlled by the first order decomposition of AIBN, i.e. $\mathrm{d}[O_2]/\mathrm{d}t \propto [A]$ and is independent of [RH].

In between the normal rate for long chains and the extreme behaviour the order of reaction with respect to AIBN will be expected to lie between a half and one, and that with respect to polymer, between one and zero.

Calculations using published values[14] of k_3 and k_6 for related hydrocarbons show that up to about 80 per cent of the total rate may be contributed by the first term. This would account qualitatively for the observed kinetic behaviour of the polymer solution since the preponderant influence of the second term would raise the order with respect to AIBN close to one and lower that with respect to polymer towards zero, as was in fact found experimentally.

According to equation (4′) the plot of $(-\mathrm{d}[O_2]/\mathrm{d}t)/[A]$ versus $1/[A]^{\frac{1}{2}}$ should be a straight line with intercept equal to $(4e-1)k_i$ and slope $k_3(k_i/k_6)^{\frac{1}{2}}[RH]$. Such plots are shown in *Figure 3* for three different temperatures.

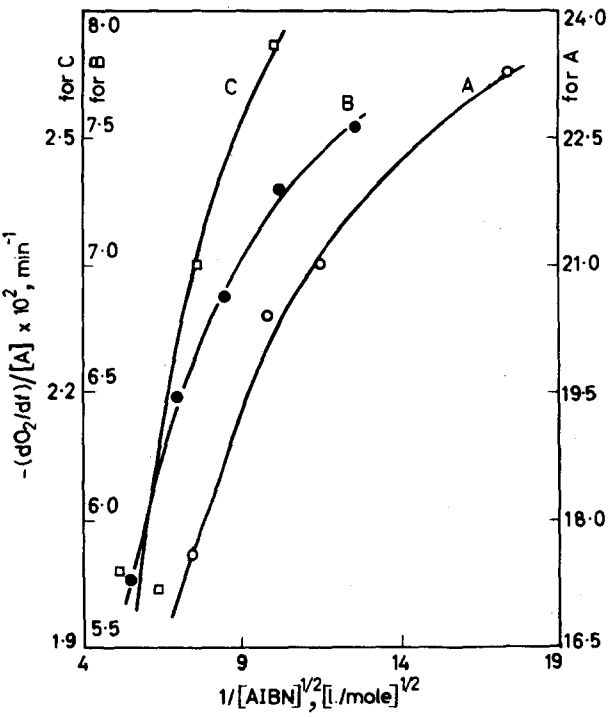

Figure 3—Polymer concentration 1·51 mole litre^{-1}. A 100°C, B 90°C, C 80°C

The agreement at the lowest temperature is reasonable. At 100°C the divergence is to be expected since the published data show that the half-life of AIBN at this temperature is 7·6 minutes and other factors discussed later, such as geminate recombination of the initially formed radical, provide an additional qualitative explanation of the observed results.

The corresponding results for pristan are shown in *Figure 4*(a). A plot of $(-\mathrm{d}[O_2]/\mathrm{d}t)/[A]$ versus $1/[A]^{\frac{1}{2}}$ is a straight line, with calculated value

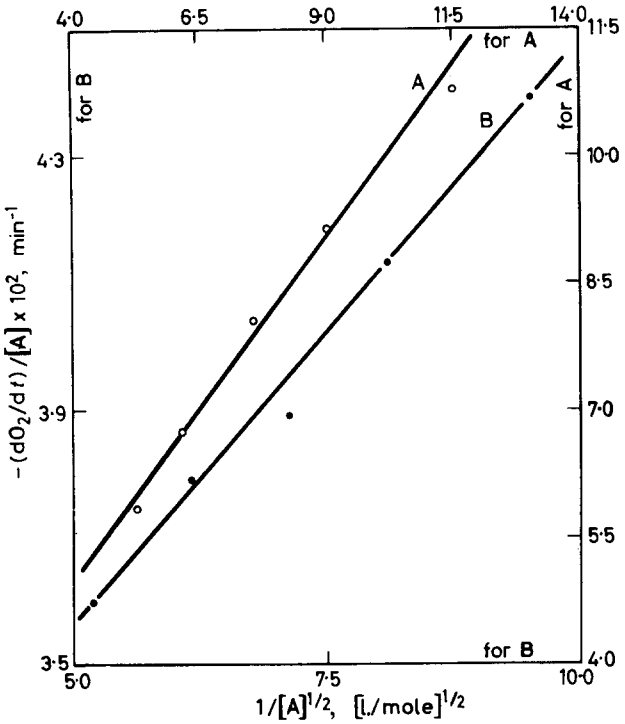

Figure 4—A Pristan at 100°C;
B Polymer solution [concentration 0·15 mole litre^{-1}] at 90°C

of the intercept equal to $1{\cdot}75 \times 10^{-2}$ min^{-1}, which is very close to the numerical value of $(2e-1)k_i$ at 100°C, namely $1{\cdot}82 \times 10^{-2}$ min^{-1}. This suggests that, in common with many other substrates, equation (2′) is applicable in this case, too. The choice between equations (2′) and (4′) here is influenced by the availability of a much higher concentration of attackable tertiary hydrogen in this substrate (about 11·5 moles litre^{-1}) and also independent measurements have shown that the chain length is now increased to about 100.

The results with pristan clearly show that in the autoxidation of low molecular weight liquid hydrocarbons there is no substantial kinetic difference in the behaviour of paraffinic or of alkylaromatic substrates; and that the different kinetics with polypropylene solutions might be in some ways dependent upon the transition from a low to a high molecular weight substrate.

*Figure 4*B shows the corresponding plot with a very dilute polymer solution which, in contrast to those with more concentrated ones (*Figure 3*), is a straight line.

DISCUSSION

Polymeric substances bring about considerable changes in the physical properties of the solvents in which they are dissolved. Differences in kinetic

behaviour of polypropylene solutions from that of pristan, a structurally related hydrocarbon, and those of other substrates, may possibly be the result of the changes in solution properties. Increase in viscosity among others is of much importance as it could affect the diffusion processes of free radicals and thus favour some special reactions not common in ordinary low molecular weight substrates.

As pointed out by Noyes[19] and by Allen and Patrick[20], recombination of a pair of radicals may occur when they are still in the same 'cage' where they are formed, or they may undergo secondary recombination after slight diffusion (geminate recombination) or may combine with radicals from other dissociations. The extent of geminate recombination will, obviously, be controlled by the rate of diffusion of the radicals, and the overall rate of production of free radicals in the system.

In polypropylene solutions at 80° to 100°C the copious production of pairs of radicals from the decomposition of AIBN occurs in a medium of comparatively high viscosity and this factor favours geminate recombination of free radicals as an additional termination step, concurrent with the usual bi-molecular termination of radicals. The inclusion of the further reaction to the above autoxidation scheme, viz.

$$2R^0 \longrightarrow \text{Inactive products} \qquad (7)$$

where R^0 is the concentration of free radicals undergoing geminate recombination, leads to a complex kinetic relationship. This is not reproduced since it is not possible to give quantitative significance to the terms involved but the inclusion of geminate recombination does explain qualitatively the observed decrease in order with respect to polymer concentration as the polymer concentration is increased. At low polymer concentration when geminate termination becomes less important the expressions derived can be reduced to equation (4').

One of us (S.A.C.) wishes to thank the Commonwealth Scholarship Commission in U.K. for a maintenance grant, and the Pakistan Atomic Energy Commission for granting leave of absence.

Department of Inorganic, Physical and Industrial Chemistry,
University of Liverpool

(*Received May 1967*)

REFERENCES

[1] MILLER, V. B., NEIMAN, M. B. and SHYLAPNIKOV, YU. A. *Polymer Sci., U.S.S.R.* 1961, **2**, 129
[2] RYSAVY, D., BALABAN, L., SLAVIK, V. and RUZA, J. *Polymer Sci., U.S.S.R.* 1962, **3**, 855
[3] STIVALA, S. S., REICH, L. and KELLEHER, P. *Makromol. Chem.* 1963, **59**, 28
[4] NOTLEY, N. T. *Trans. Faraday Soc.* 1964, **60**, 88
[5] DULOG, VON L., RADLMAN, E. and KERN, W. *Makromol. Chem.* 1963, **60**, 1
[6] VAN HOOK, J. P. and TOBOLSKY, A. V. *J. Amer. chem. Soc.* 1958, **80**, 779
[7] HOWARD, J. H. and INGOLD, K. U. *Canad. J. Chem.* 1962, **40**, 1851

[8] KAMIYA, Y., BEATON, S., LAFORTUNE, A. and INGOLD, K. U. *Canad. J. Chem.* 1963, **41**, 2020
[9] HOWARD, J. A. and INGOLD, K. U. *Nature, Lond.* 1962, **195**, 280
[10] KULITSKI, Z. I., TERMAN, L. M., TSEPALOV, V. F. and SHYLAPINTOKH, V.YA. *Bull. Acad. Sci., U.S.S.R.* [Div. Chem. Sci.], 1963, No. 2, 230
[11] COOPER, H. R. and MELVILLE, H. W. *J. chem. Soc.* **1951**, 1984
[12] LUONGO, J. P. *J. appl. Polym. Sci.* 1960, **3**, 302
[13] ARNDT, R. R., BARBOUR, J. B., ENGELS, E. J., HORN, D. H. S. and SUTTON, D. A. *J. chem. Soc.* **1959**, 3258
[14] BUCHACHENKO, A. L., KAGANSKAYA, K. YA., NEIMAN, M. B. and PETROV, A. A. *Kinetics and Catalysis*, 1961, **2**, 38
[15] MELVILLE, H. W. and RICHARDS, S. *J. chem. Soc.* **1954**, 944
[16] BAMFORD, C. H. and DEWAR, M. J. S. *Proc. Roy. Soc. A*, 1949, **198**, 252
[17] HAMMOND, G. H., SEN, J. N. and BOOZER, C. F. *J. Amer. chem. Soc.* 1955, **77**, 3244
[18] BAWN, C. E. H. and PARRY, A. Unpublished results
[19] NOYES, R. M. *J. Amer. chem. Soc.* 1955, **77**, 2042
[20] ALLEN, P. E. M. and PATRICK, C. R. *Nature, Lond.* 1961, **191**, 1194

Autoxidation of Atactic Polypropylene in Solution II—The Uncatalysed Oxidation

C. E. H. BAWN and SHAMIM A. CHAUDHRI*

The uncatalysed autoxidation of atactic polypropylene has been studied in the liquid phase. The maximum steady rate of oxygen uptake gave an order of 1·7 with respect to the polymer concentration and of unity with respect to the partial pressure of oxygen above the solution. In the autocatalytic region the instant rate varied directly with the square root of the amount of oxygen absorbed by the solution. The peroxide and hydroperoxide contents and the intrinsic viscosity of the polymer solutions have been determined at different extents of oxidation. A mechanism has been suggested and the empirical results have been explained on the basis of the derived kinetic expressions.

AUTOXIDATION of hydrocarbons of simple structures has been studied thoroughly and most of the aspects of the process are now well understood. The corresponding work with high molecular weight substances has largely been confined to the unsaturated materials, although the saturated polymeric substances have been receiving increasing attention during the last ten years or so[1–13]. The autoxidation of polypropylene[6–13], a comparatively newer member of the saturated polymers of commercial importance, has mostly been studied in the solid phase. No detailed kinetic studies have, however, been carried out on the autoxidation of polypropylene in solution beyond the initial stages[14]. In the previous paper results were reported for the free radical initiation oxidation of atactic polypropylene in trichlorobenzene solution. This paper reports a corresponding investigation of the uncatalysed oxidation. The experimental procedures used were as described previously (Part I).

RESULTS

Uncatalysed solutions of polypropylene oxidized with autocatalysis in the initial phases. The rate increased gradually and finally attained a steady value, which was maintained for a fairly long period. The length of the autocatalytic and the steady state periods was influenced by the temperature of the reaction and the polymer concentration. At higher temperatures the steady state was reached earlier. A similar behaviour was observed by increasing the polymer concentration. In general, at 135°C the steady rate was maintained from 2·5 to 7 per cent oxidation of the polymer, as based on moles of tertiary hydrogen atoms on the chain. *Figure 1* shows a typical curve for this system. The reaction has been studied in the steady rate and the autocatalytic regions separately.

*Permanent address: Pakistan Atomic Energy Commission, Karachi.

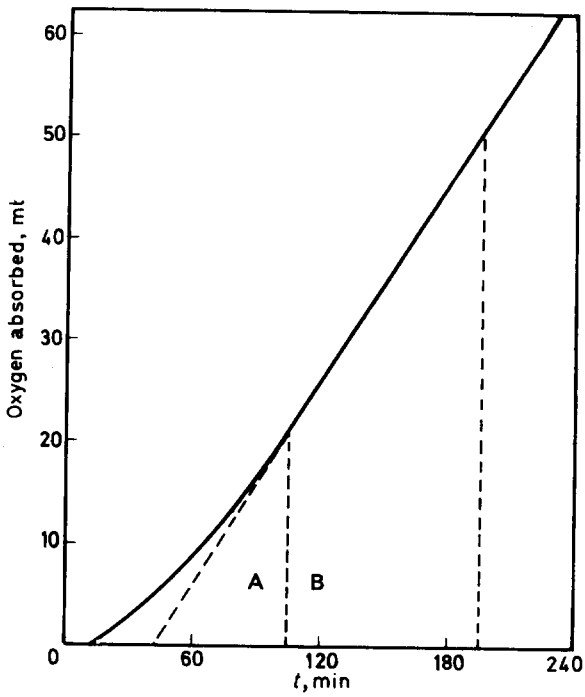

Figure 1—A. Autocatalytic region; B. Steady rate region. (i) 20 ml sample, [RH]=1·51 mole litre^{-1}; (ii) total oxygen pressure 755 mm Hg; (iii) temperature 135°C

STEADY RATE REGION

Experiments were carried out under different conditions of polymer concentration, temperature and oxygen pressure above the solution. The maximum steady state value of the rate, $-\mathrm{d}[O_2]/\mathrm{d}t$, was used as a characteristic for the given set of experimental conditions. The value of the steady rate was reproducible to better than ± 5 per cent.

(a) *Rate dependence on the polymer concentration,* [RH]

The concentration of polypropylene was varied from 0·75 to 1·82 mole litre^{-1} at 135°C. The average total pressure of oxygen in these 'runs' was 745 mm of mercury, and the maximum variation did not exceed one per cent of this value. *Figure 2* shows the plot of log (rate) against log [RH]. The slope of the straight line so obtained is 1·7 and thus.

$$-\mathrm{d}[O_2]/\mathrm{d}t \propto [RH]^{1.7}$$

(b) *Rate dependence on oxygen pressure*

At a fixed polypropylene concentration and a constant temperature, the total pressure of oxygen above the solution was varied from 548 to 781 mm of mercury. It was established in a series of 'runs' that variation of the

shaking frequency and surface area of the reaction vessel had no effect on the steady state rate in this system.

The correction for the vapour pressure of the polymer solution in tri-

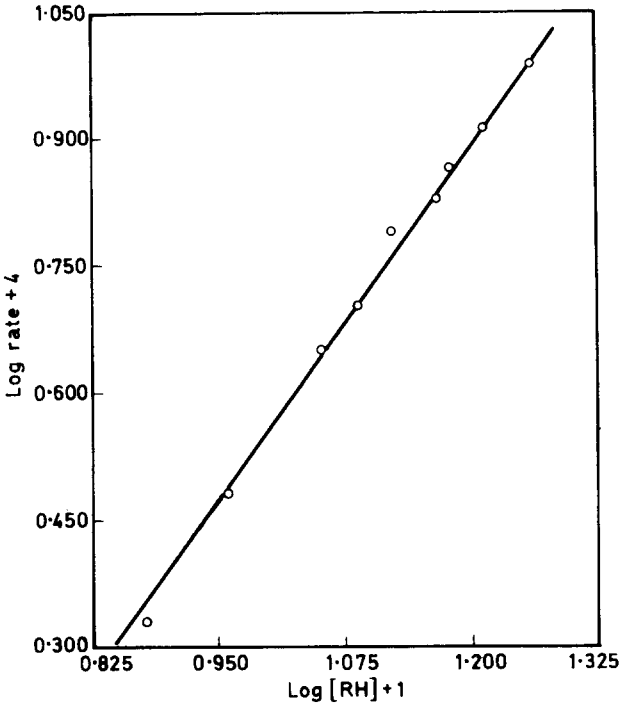

Figure 2—Dependence of rate on polypropylene concentration: (i) temperature 135°C; (ii) total oxygen pressure 745 mm Hg

chlorobenzene was applied using the following empirical equation, which was found to hold for zero to ten per cent polymer solutions[15]

$$\log (p)_{mm} = 7{\cdot}883 - 2441/T$$

where p is the value of the vapour pressure at temperature $T°$.

Figure 3 shows a plot of log (rate) versus log $p[O_2]$. The slope of the straight line is unity. A linear plot of the two variables is also shown in the same figure.

(c) *Variation of rate with temperature*

The rate of oxygen uptake, corrected for the change in the vapour pressure of the solution with temperature, was measured at temperatures from 125° to 144°C at a fixed polypropylene concentration. The Arrhenius plot (*Figure 4*) gives a value of the overall activation energy $E = 30{\cdot}3$ kcal/mole.

AUTOCATALYTIC REGION

The rate of oxygen uptake showed a steady increase during the initial stages

of the reaction. This region, where the autocatalysis is observed, is shown in *Figure 1*. The value of the rate at a given extent of oxidation was calculated by drawing tangents to the oxygen absorbed versus time curve at

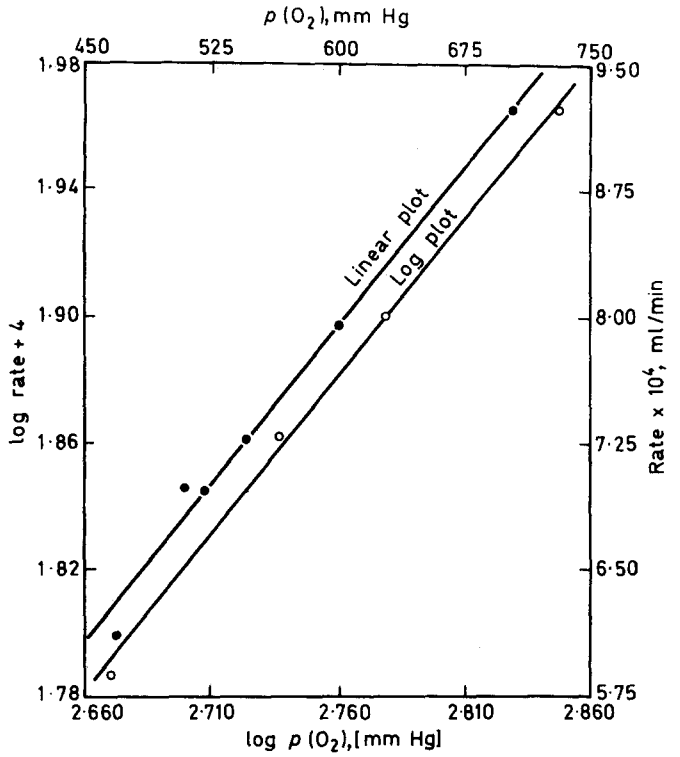

Figure 3—Dependence of rate on the partial pressure of oxygen above the solution: (i) [RH] 1·82 mole litre^{-1}; (ii) temperature 135°C

different points. The calculated values for a typical differential plot are listed in *Table 1*. The notation $[O_2]_{abs.}$ is used for the amount of oxygen

Table 1.

[RH] = 1·63 mole litre^{-1} Temperature 135°C

Time (min)	$\frac{[O_2] \times 10^2}{\text{mole litre}^{-1}}$	$\frac{[O_2]^{\frac{1}{2}} \times 10^2}{\text{mole litre}^{-1}}$	$\frac{\text{Rate} \times 10^4}{\text{mole litre}^{-1}\ \text{min}^{-1}}$
20	0·51	7·13	3·50
30	0·87	9·35	4·08
40	1·32	11·5	4·66
50	1·81	13·4	5·22
60	2·33	15·3	5·71
70	2·93	17·1	6·22
80	3·55	18·8	6·65
90	4·30	20·7	7·01
100	4·90	22·3	7·36
110	5·80	24·1	8·06

absorbed by the solution in clear distinction to $[O_2]_{diss.}$ which is used later for the concentration of oxygen in the solution. *Figure 5* shows the plots of rate against $[O_2]_{abs.}$, $[O_2]^{\frac{1}{2}}_{abs.}$ and time, t, and it is apparent from *Figure 5*

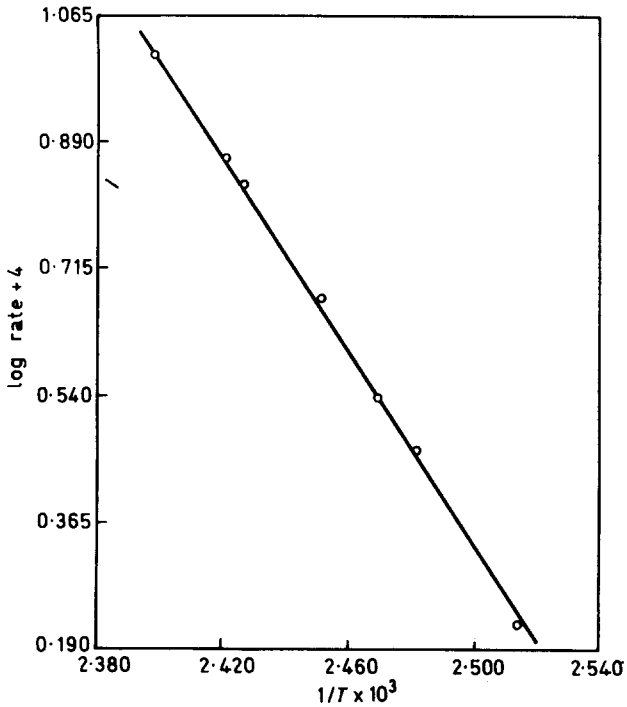

Figure 4—Variation of rate with temperature: (i) [RH] 1·13 mole litre^{-1}; (ii) $p\ (O_2)_{partial}$ 700 mm Hg

that whereas the plot of rate versus $[O_2]_{abs.}$ does not yield a straight line, that of rate versus $[O_2]^{\frac{1}{2}}_{abs.}$ is a fair straight line. A similar straight line is also given by the rate versus t plot. In the autocatalytic region, therefore,

$$-\mathrm{d}\,[O_2]_{abs.}/\mathrm{d}t = K_A\,[O_2]^{\frac{1}{2}}$$

The effect of the variables of the system on the value of the proportionality constant, K_A, was investigated in a series of 'runs'. The empirical results are summarized below.

$$K_A \propto [RH]^{1\cdot0}$$

$$\propto p\,[O_2]^{0\cdot7\rightarrow1\cdot2} \quad (p\,[O_2] = 702 \longrightarrow 469 \text{ mm Hg})$$

Another point of interest results from the fact that the straight line obtained by plotting rate versus $[O_2]^{\frac{1}{2}}_{abs.}$, produces a positive intercept on the rate axis at zero oxidation. This has been found to be a general behaviour of all the plots of this kind for this system, and the value of the

intercept always remains positive. The values of the intercept have been found to show a variation with the polymer concentration, oxygen pressure and temperature. The reproducibility of these values was, however, very

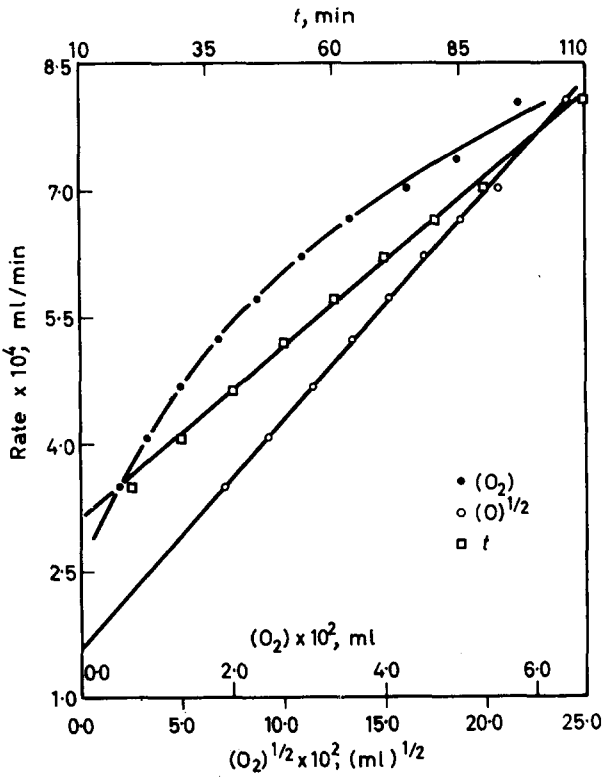

Figure 5—Rate at different extents of oxidation: (i) [RH] 1·63 mole litre^{-1}; (ii) temperature 135°C

poor and no attempt was made, therefore, to establish definite relationships between them.

Determination of active oxygen in the oxidized polymer

The amount of the total peroxidic oxygen, —O—O—, present as peroxide and hydroperoxide, and the amount of hydroperoxide alone, were determined by the methods reported by Beati *et al.*[16]. The peroxide present was calculated as a difference of the two values. Such determinations were carried out at different extents of polypropylene oxidation and the calculated results are given in *Table 2*.

It is seen that the peroxide appears in amounts comparable to those of the hydroperoxide from the very early stages of the reaction. With an increasing extent of oxidation the decrease in the hydroperoxide contents, expressed as a percentage of the total oxygen absorbed, is much larger than the corresponding decrease in peroxide contents. In the first 0·5 per cent oxidation of the polymer sample almost all the oxygen absorbed can be

accounted for by the total of the peroxide and hydroperoxide contents, whereas at ten per cent oxidation less than one third exists in this active form.

Table 2.

[RH]=1·82 mole litre^{-1} Oxidation temperature 135°C

% oxidation of the sample	Total oxygen absorbed $m.\ l^{-1}\times10^3$	Total active oxygen $m.\ l^{-1}\times10^3$	Hydroperoxide contents ROOH $m.\ l^{-1}\times10^3$	Peroxide contents ROOR $m.\ l^{-1}\times10^3$	ROOH as % of total oxygen absorbed	ROOR as % of total oxygen absorbed	Total active oxygen as % of oxygen absorbed
0·5	9·1	8·85	5·1	3·75	56·0	41·2	97·2
1·0	18·2	13·25	6·0	7·25	33·2	39·8	73·0
2·0	36·4	22·1	8·0	14·1	22·0	38·8	60·8
4·0	72·8	38·7	11·1	27·6	15·2	37·9	53·1
6·1	111·0	42·8	7·7	35·1	7·0	31·6	38·6
7·4	134·8	49·4	9·4	40·0	6·9	29·7	36·6
8·7	160·0	47·6	7·1	40·4	4·5	25·2	29·7

Viscosity measurements

The effect of oxidation on the molecular weight of polypropylene was investigated by determining the intrinsic viscosity, [η], of the polymer solutions at different extents of oxidation. A typical behaviour is shown graphically in *Figure 6*. The average molecular weight decreases rapidly during

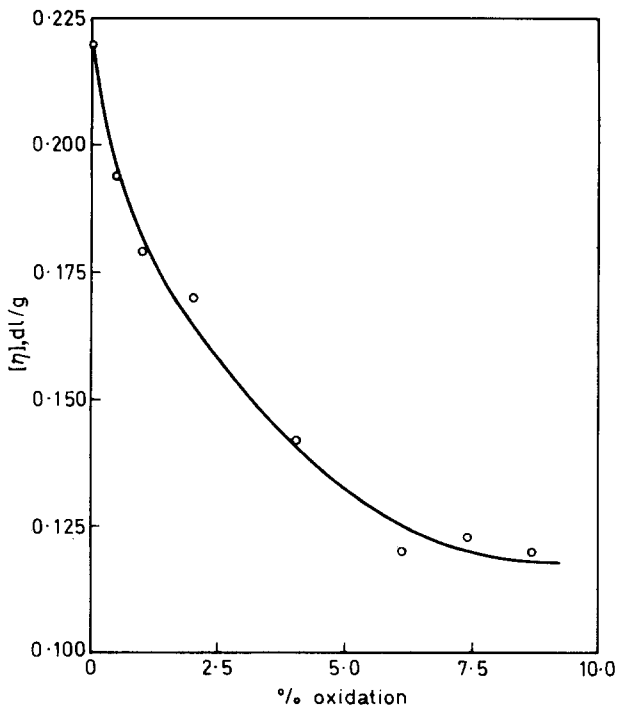

Figure 6—Effect of oxidation on molecular weight of polypropylene as evidenced by intrinsic viscosity

the first three to four per cent of oxidation, whereas at advanced states it attains a steady value. This may, probably, be due to the simultaneous processes of chain rupture and crosslinking balancing each other.

DISCUSSION

The kinetic studies with this system gave an order of 1·7 with respect to the polymer concentration and of unity with the partial pressure of oxygen above the solution. The most significant fact is that this dependence on oxygen does not result from the diffusion-controlled conditions and that there is no tendency of the rate towards an independence of oxygen pressure even up to the pressure values in the range of one atmosphere. These results are obviously not readily explained by the usual Bolland–Gee[17–19] mechanism for the autoxidation of hydrocarbons.

The autoxidation of polypropylene in solution shows the characteristics of a chain reaction and the propagation steps in the Bolland–Gee mechanism are accepted as the most probable ones for such systems. The nature of the initiation and termination processes, may, however, differ depending upon the experimental conditions. Termination by a bimolecular reaction of peroxy free radicals is the most effective one for primary and secondary peroxy radicals under conditions of high oxygen pressure[20]. The interaction of two tertiary peroxy radicals, however, does not follow a mechanism similar to that for primary and secondary peroxy radicals. Alkoxy radicals are produced first which may then undergo a variety of reactions, a considerable proportion of which are non-terminating in the strict sense[21].

It was suggested by Hinshelwood[22] that when a free radical, produced through a non-terminating disproportionation of another free radical, gives less reactive products than those from the parent one, the overall effect would be equivalent to a termination process. This concept was originally embodied in a mechanism put forward for explaining the gas phase autoxidation of saturated hydrocarbons[22,23]. In the autoxidation of polypropylene the peroxy radical produced in the propagation cycle is tertiary in nature. A considerable decrease in the average molecular weight of the polymer from the very early stages of the reaction, and the subsequent appearance of a whole range of oxygenated compounds, suggest a high degree of disproportionation of the intermediate free radical. As the course of low temperature oxidation (25° to 300°C) of hydrocarbons in the liquid and vapour phase is basically the same[24], a mechanism similar to the one proposed by Hinshelwood will be considered.

The exact nature of the primary initiation reaction (rate $=\phi$) has not been investigated separately, but evidence as to its nature will be adduced later.

$$\text{Initiation} \longrightarrow \text{R}\cdot \qquad \text{Rate} = \phi \tag{1}$$

$$\text{R}\cdot + \text{O}_2 \xrightarrow{k_2} \text{RO}_2\cdot \tag{2}$$

$$\text{RO}_2\cdot + \text{RH} \xrightarrow{k_3} \text{RO}_2\text{R} + \text{H}\cdot \text{ or } \text{ROOH} + \text{R}\cdot \tag{3}$$

$$\text{RO}_2\cdot + \text{RH} \xrightarrow{k_4} \text{Inactive products} \tag{4}$$

$$\text{RO}_2\text{R} \xrightarrow{k_5} 2\text{RO}\cdot \tag{5}$$

$$RO_2R \xrightarrow{k_6} \text{Inactive products} \tag{6}$$

$$RO\cdot \xrightarrow{k_7} R'\cdot + \text{products} \tag{7}$$

$$R'\cdot + RH \xrightarrow{k_8} R'H + R\cdot \tag{8}$$

$$R'\cdot + O_2 \xrightarrow{k_9} \text{Less active products} \tag{9}$$

Reaction (3) in the above scheme has been shown to produce either peroxide or hydroperoxide. Either product would lead to a similar kinetic expression as derived on the basis of the proposed scheme.

Under stationary state conditions:

$$d[R\cdot]/dt = \phi - k_2\,[R\cdot]\,[O_2] + k_8\,[R'\cdot]\,[RH] = 0 \tag{1'}$$

$$d[R'\cdot]/dt = 2k_5\,[RO_2R] - k_8\,[R'\cdot]\,[RH] - k_9\,[R'\cdot]\,[O_2] = 0 \tag{2'}$$

$$d[RO_2\cdot]/dt = k_2\,[R\cdot]\,[O_2] - (k_3 + k_4)\,[RH]\,[RO_2\cdot] = 0 \tag{3'}$$

$$d[RO_2R]/dt = k_3\,[RO_2\cdot]\,[RH] - (k_5 + k_6)\,[RO_2R] \tag{4'}$$

Adding equations (1') and (3') and substituting the value of $[R'\cdot]$ from equation (2'),

$$[RO_2\cdot] = \frac{\phi}{(k_3 + k_4)\,[RH]} + \frac{2k_5k_8\,[RO_2R]}{(k_3 + k_4)\,(k_8\,[RH] + k_9\,[O_2])} \tag{5'}$$

Substituting the value of $[RO_2\cdot]$ in equation (4') leads to

$$\frac{d[RO_2R]}{dt} + A\,[RO_2R] = \frac{k_3}{k_3 + k_4}\,\phi$$

where

$$A = (k_5 + k_6) - \frac{2k_3k_5k_8\,[RH]}{(k_3 + k_4)\,(k_8\,[RH] + k_9\,[O_2])}$$

This equation may be integrated to give

$$[RO_2R] = \frac{k_3\phi}{A\,(k_3 + k_4)}\,(1 - e^{-At}) \tag{6'}$$

The rate of oxygen absorption is therefore

$$-(d\,[O_2]_{abs.})/dt = k_2\,[R\cdot]\,[O_2] + k_9\,[R'\cdot]\,[O_2]$$
$$= 2k_5\,[RO_2R] + \phi \tag{7'}$$

and thus from (6')

$$-(d\,[O_2]_{abs.})/dt = \frac{2k_3k_5\phi}{A\,(k_3 + k_4)}\,(1 - e^{-At}) \tag{8'}$$

Since the amount absorbed on the primary initiation step must be extremely small ϕ may be neglected in comparison with the first term in (7'). This

expression may be developed to provide relationships between the rate and the variables of the system.

Rate dependence on oxygen pressure and polypropylene concentration

At constant temperature and concentration of the polymer, equation (8′) can be rewritten as

$$-(\mathrm{d}\,[O_2]_{abs.})/\mathrm{d}t = \frac{K_1 + (K_1/K_2)\,[O_2]_{diss.}}{(K_1 - K_2) + [O_2]_{diss.}} \times \phi\,(1 - e^{-At}) \qquad (9')$$

where

$$K_1 = (k_5 + k_6) - A$$

$$K_2 = (k_8/k_9)\,[RH]$$

The maximum steady rate of oxygen absorption is reached after a time, t_m, from the start of the reaction. At higher values of the oxygen pressure, polypropylene concentration and temperature the maximum rate is reached earlier than at the lower values of the above variables. The effect of increasing the oxygen pressure in the system, for example, would be to increase the value of A [denominator in equation (6′)] and to decrease that of t_m. The overall effect results in maintaining the value of $(1 - e^{-At_m})$ nearly constant, as has been checked by calculations of the values of A and t_m by graphical methods.

Equation (9′) may be further simplified by assuming that for the limiting rate $[O_2]_{diss.} \gg K_2 - K_1$ and thus

$$-(\mathrm{d}\,[O_2]_{abs.})/\mathrm{d}t = K_1\phi\ (1 - e^{-At_m}) + (K_1/K_2)\,[O_2]_{diss.}\,\phi\,(1 - e^{-At_m})/[O_2]_{diss.} \qquad (10')$$

ϕ, the primary initiation reaction, may be represented as

$$\phi = k_i\,[RH]^x\,[O_2]_{diss.}$$

where x may be one or two, depending upon whether $RH + O_2$ or $2RH + O_2$ is the primary initiation reaction.

Substitution in (10′) leads to

$$(\mathrm{d}\,[O_2]_{abs.}/\mathrm{d}t)_{max.} = \alpha + \beta\,[O_2]_{diss.} \qquad (11')$$

where α and β are constants.

Since Henry's law of the solubility of gases is generally applicable to hydrocarbon solution[11] the concentration of oxygen in the liquid phase is proportional to the pressure above the solution

$$-(\mathrm{d}\,[O_2]_{abs.}/\mathrm{d}t)_{max.} = \alpha + \beta' p_{O_2} \qquad (12')$$

It is evident from these equations that over the whole range of oxygen pressure above the solution, the rate would show a direct proportionality to the oxygen pressure. This agrees very well with the experimental results. A similar mechanism was used by Stivala *et al.*[7,25] to explain the rate dependence on oxygen pressure in the oxidation of thin films of isotactic polypropylene. This shows the general applicability of this mechanism irrespective of whether a substrate is in a gaseous, liquid or solid phase.

For the conditions of constant oxygen pressure and temperature, equation (10′) yields

$$-(\mathrm{d}[O_2]/\mathrm{d}t)_{\max.} = C(k_8/k_9)(1-e^{-At_m})k_i[RH]^{x+1} + C(1-e^{-At_m})k_i[O_2][RH]^x$$
$$= C_1[RH]^{x+1} + C_2[RH]^x \qquad (13')$$

where C, C_1 and C_2 are constants.

For $x=1$, the apparent order with respect to [RH] would be between two and one, as was in fact found experimentally. The value of the order will be maintained constant only over a restricted range of the polymer concentration, and will be determined by the relative magnitude of C_1 and C_2, the coefficients of the two terms.

Comparison of the derived and empirical expressions shows that the primary initiation reaction is first order with respect to the polymer concentration, that is

$$\phi \propto [RH][O_2] \qquad (14')$$

Autocatalytic region

In the early stages of the reaction when the rate is gradually building up, the value of At is relatively small, and introducing the simplifying assumption that $(1-e^{-At}) \sim At$, equation (8) becomes

$$-\mathrm{d}[O_2]_{\mathrm{abs.}}/\mathrm{d}t = \{2k_3k_5/(k_3+k_4)\}\,\phi \times t \qquad (15')$$

i.e.

$$-\mathrm{d}[O_2]_{\mathrm{abs.}}/\mathrm{d}t \propto t \qquad (16')$$

in agreement with experimental results (*Figure 5*). This result may be expressed in an alternative form by integrating equation (15') with the condition that $[O_2]=0$ at $t=0$, viz.

$$[O_2]_{\mathrm{abs.}} = \{k_3k_5/(k_3+k_4)\} \times \phi \times t^2 \qquad (17')$$

and combining equations (15') and (17') leads to

$$-\mathrm{d}[O_2]_{\mathrm{abs.}}/\mathrm{d}t = 2(\{k_3k_5/(k_3+k_4)\} \times \phi)^{\frac{1}{2}} \times [O_2]^{\frac{1}{2}}_{\mathrm{abs.}}$$
$$= K_A[O_2]^{\frac{1}{2}}_{\mathrm{abs.}} \qquad (18')$$

This relationship between the rate and the amount of oxygen absorbed during the autocatalytic stages of the reaction is a most outstanding characteristic of the system. The same result was reported by Kern *et al.*[14] in the initial stages of the autoxidation of atactic polypropylene. They explained this behaviour as a result of the initiation step consisting of a monomolecular decomposition of the hydroperoxide of atactic polypropylene. Their conclusion was based on a tacit assumption that this system obeyed the Bolland–Gee mechanism, although no detailed kinetic studies of the system were carried out to justify it. The present work has shown that the same relationship can be derived from a mechanism which, in addition to explaining the kinetic results at advanced stages of the reaction, is very different in nature from the Bolland mechanism.

The variation of K_A, the proportionality constant in equation (18'), with the polymer concentration and oxygen pressure, however, does not agree strictly with the empirical values. The divergence may very largely be due

to the difficulties of obtaining reliable data at very early stages of an uncatalysed autoxidation reaction.

The proposed scheme explains also the presence of a positive intercept on the rate axis for the rate versus $[O_2]^{\frac{1}{2}}$ plots. Equation (7′) shows that the value of the intercept would vary with ϕ, and therefore with [RH] and $p[O_2]$. Such behaviour was found experimentally, although due to poor reproducibility of the intercept values no definite relationship could be established.

The value of the overall energy of activation for the rate of oxygen uptake by atactic polypropylene in solution is found to be 30·3 kcal/mole. This is in the range of values reported for the solid phase oxidation of this polymer.

An interesting feature of the oxidation is the formation of the peroxide ROOR (*Table 2*) in comparable amounts to that of the hydroperoxide ROOH from the early stages of the reaction. Further the concentration of ROOR becomes higher than that of ROOH when the steady rate of oxygen uptake is attained. This observation is contrary to the widely accepted view that the solution phase oxidation of aliphatic hydrocarbons gives mostly hydroperoxides. This conclusion, however, is largely founded on studies with unsaturated hydrocarbons which give allylic hydroperoxides as major products. The formation of ROOR is variously postulated as arising from the termination reaction of the $RO_2\cdot$ radical intermediate, viz.

$$RO_2\cdot + RO_2\cdot \longrightarrow ROOR + O_2$$

$$2RO\cdot \longrightarrow ROOR$$

$$RO_2\cdot + R \longrightarrow ROOR\cdot$$

but reactions of this type are unlikely to account for the high yield of ROOR in the early stages of the oxidation. It seems that some major reaction other than hydrogen abstraction by the $RO_2\cdot$ radical is occurring and this may possibly be an isomerization reaction of the type

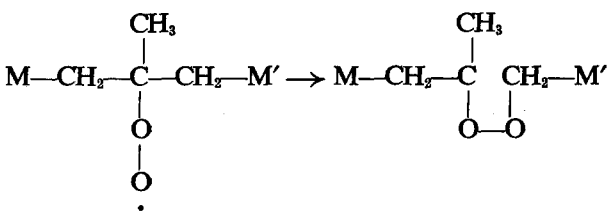

One of us (S.A.C.) thanks the Commonwealth Scholarship Commission in the U.K. for the scholarship, and the Pakistan Atomic Energy Commission for leave of absence during the tenure of this work.

Department of Inorganic, Physical and Industrial Chemistry,
University of Liverpool

(*Received May 1967*)

REFERENCES

[1] ACHHAMMER, B. G., REINEY, M. J., WALL, L. A. and REINHART, F. W. *J. Polym. Sci.* 1952, **8**, 555
[2] RUGG, F. H., SMITH, J. J. and BACON, R. C. *J. Polym. Sci.* 1954, **13**, 535
[3] GRASSIE, N. *The Chemistry of High Polymer Degradation Processes.* Butterworths: London, 1956
[4] BAUM, B. *J. appl. Polym. Sci.* 1959, **2**, 281
[5] NOTLEY, N. T. *Trans. Faraday Soc.* 1962, **58**, 66
[6] NOTLEY, N. T. *Trans. Faraday Soc.* 1964, **60**, 88
[7] STIVALA, S. S., REICH, L. and KELLEHER, P. *Makromol. Chem.* 1963, **59**, 28
[8] LUONGO, J. P. *J. appl. Polym. Sci.* 1960, **3**, 302
[9] MILLER, V. B., NEIMAN, M. B., PUDOV, V. S. and LAFER, L. I. *Polymer Sci., U.S.S.R.* 1961, **2**, 121
[10] MILLER, V. B., NEIMAN, M. B. and SHLYAPNIKOV, YU. A. *Polymer Sci., U.S.S.R.* 1961, **2**, 129
[11] DUDROV, V. V. *Kinetics and Catalysis,* 1963, **4**, 185
[12] RYSAVY, D., BALABAN, L., SLAVIK, V. and RUZA, J. *Polymer Sci., U.S.S.R.* 1962, **3**, 855
[13] HANSEN, R. H., RUSSELL, C. A., DE BENEDICTIS, T., MARTIN, W. M. and PASCALE, J. V. *J. Polym. Sci.* 1964, **2**, 587
[14] DULOG, L., RADLMANN, E. and KERN, W. *Makromol. Chem.* 1963, **60**, 1
[15] Unpublished measurements
[16] BEATI, E., SEVERINI, F. and CLERICI, G. *Makromol. Chem.* 1963, **61**, 104
[17] BOLLAND, J. L. *Quart. Rev. Chem. Soc., Lond.* 1949, **3**, 1
[18] BOLLAND, J. L. *Proc. Roy. Soc. A,* 1946, **186**, 218
[19] BOLLAND, J. L. and GEE, G. *Trans. Faraday Soc.* 1946, **42**, 236
[20] RUSSELL, G. A. *J. Amer. chem. Soc.* 1957, **79**, 3871
[21] BLANCHARD, H. S. *J. Amer. chem. Soc.* 1959, **81**, 4548
[22] CULLIS, C. F. and HINSHELWOOD, C. N. *Disc. Faraday Soc.* 1947, **2**, 117
[23] CULLIS, C. F. *Trans. Faraday Soc.* 1949, **45**, 709
[24] DE LA MARE, H. E. and VAUGHAN, W. E. *J. chem. Educ.* 1957, **34**, 64
[25] REICH, L. and STIVALA, S. S. *J. Polym. Sci. B,* 1965, **3**, 227

Differential Scanning Calorimetry of Epoxy Resins

R. A. FAVA

The techniques of differential scanning calorimetry applied to polymerization studies have been investigated using one epoxy resin system. Three methods, using the Perkin–Elmer DSC–1 isothermally or as a scanning calorimeter, of obtaining isothermal cure curves in terms of heat of reaction versus time are compared and the merits of each method when applied to fast and slow cure rates are given. In one of these methods where the residual heat of reaction of partly cured samples was measured, a glass transition temperature related to the resin softening point was revealed as a discontinuity in specific heat. The temperature of the glass transition increased on cure, to a limiting value at the isothermal cure temperature. Further reaction in these cases was shown to be extremely limited in the glassy state. This was made clear by scanning samples previously cured for extended periods of up to twelve weeks: the thermograms showed little change both in the position of the transition and the magnitude of the residual exotherm.

DIFFERENTIAL Scanning Calorimetry (DSC) gives a measure of the difference in the rates of heat absorption by a sample with respect to an inert reference as the temperature is raised at a constant rate. This contrasts with conventional differential thermal analysis in which the differential temperature caused by, but only indirectly related to, heat changes in the sample is monitored. Measurements of heats of reaction in a sample whose temperature is scanned should give useful information on the reaction kinetics if it is assumed that the heat of reaction is directly proportional to the extent of the reaction[1,2]. This is an assumption which is reasonable for simple reactions but not obviously valid for the complex crosslinking reactions which take place as an epoxy resin polymerizes.

DSC yields a thermogram of rate of heat absorption, dH/dt, as a function of temperature, T. Because a constant heating rate, dT/dt, is used, this rate of heat absorption is proportional to the specific heat of the sample. In the absence of chemical reaction, therefore, a second-order transition is shown as a discontinuity in the thermogram. Second-order transitions associated with the softening point in crosslinked networks have been investigated by Gordon *et al.*[3] by a dynamic mechanical method and the temperature of the transition is shown to increase with the extent of cure. If it approaches the cure temperature, further reaction must be controlled by diffusion processes in the glassy state.

Both of the above aspects of studying cure of epoxy resins by DSC will be described in this paper. No attempt will be made to analyse the results in terms of the possible mechanisms of polymerization. Only physical interpretations will be discussed.

EXPERIMENTAL AND RESULTS

1. *Apparatus*

The Perkin–Elmer DSC-1 was used. This instrument, which has been described in detail by the designers[4], accommodates a 30 mg sample in a

0·6 cm diameter, shallow aluminium pan. This is placed in the sample cell while the reference cell remains empty. Both cells are covered with domed aluminium covers and the whole assembly sealed beneath a stainless steel cover so that experiments can be performed in an inert atmosphere. The temperature may be scanned at rates increasing in factors of two from 0·5 deg. C/min to 64 deg. C/min or held isothermally at any desired temperature up to 500°C. The instrument monitors the differential rate of heat absorption or evolution by the sample with respect to the reference and yields a voltage output with a maximum nominal sensitivity of 2·5 mV per millicalorie/s. This sensitivity could be reduced sixteenfold in factors of two.

The thermograms were traced out on a millivolt recorder as a function of time and a second pen marked the programmed temperature on this time axis during a scan. Since the true sample temperature may differ from this programmed temperature, the apparatus was calibrated by scanning 99·9 per cent pure indium, tin and lead samples which have known melting points of 429°K, 505°K and 600°K respectively. Calibration at lower temperatures utilized the crystal transitions at 315°K and 398°K of ammonium nitrate (cf. ref. 4). The system was adjusted such that the true sample temperature did not depart from the programmed linearity by more than 1·5 deg. C over the entire temperature range. The sample temperature lagged behind the programmed temperature by an amount increasing with scan speed. This lag was determined and corrected for in the final thermogram. The true differential power output, dH/dt, was calibrated in terms of unit deflection on the millivolt recorder by scanning an indium sample (latent heat: 6·75 cal/g) and using the fact that the area enclosed between melting thermogram and the baseline on a time axis yielded the heat of fusion.

2. *Materials*

All experiments were performed on one epoxy resin system since the object was to examine the method rather than give detailed results on the kinetics of a number of epoxy resin systems. The system was an amine-catalysed epoxy–anhydride mixture comprising:

Dow DER 332/LC	
(Pure diglycidyl ether of bisphenol A)	100 parts
Hexahydrophthalic anhydride	80 parts
Tris-2,4,6-dimethylaminomethyl phenol	1 part

3. *Methods of producing isothermal cure curves*

From a practical point of view, the most useful information one can obtain on the cure of an epoxy resin is the set of isothermal cure curves, giving the extent of polymerization as a function of time at given temperatures. In terms of heat of reaction these curves have been obtained by DSC using three techniques:

(*a*) Isothermal operation
(*b*) Analysis of thermograms with different scan rates
(*c*) Scans on partly cured resins.

Each of these techniques will now be discussed in conjunction with the results they yield. In accordance with conventional practice in calorimetry, endotherms (positive differential power absorption) and specific heat increases will be represented by an increase in the ordinate from the baseline position.

(a) *Isothermal operation*—A sample was placed in the cell and the temperature increased manually as quickly as possible to the test temperature. A time record of the rate at which heat was generated in the sample by the exothermic curing reaction was made until the curve levelled off to a baseline indicating completion of the reaction. *Figure 1* shows a typical isotherm. The isothermal cure curve was obtained by stepwise integration of the thermogram as a function of time.

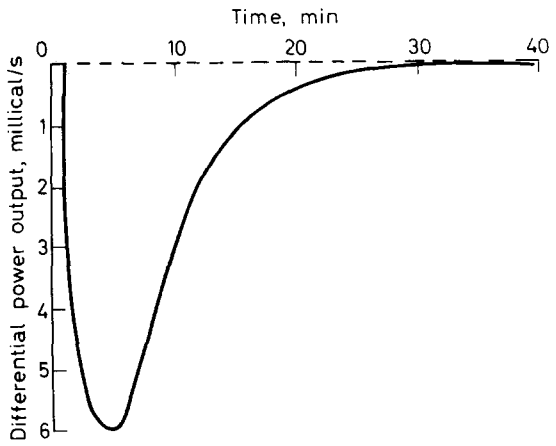

Figure 1—A typical isotherm. 42 mg sample cured at 400°K

An isothermal method has also been applied by Anderson[5] for reactions in solution using a large isothermal calorimeter. The method becomes unreliable for very fast cures because even with the miniature sample sizes used in the present investigation one or two minutes are needed for the sample and test cell to heat up to the desired temperature and the initial portion of the exotherm is partially obliterated by the heat absorbed as the sample warms up.

Weighed samples were cured by this method at temperatures from 360°K to 450°K and the isothermal cure curves deduced from these thermograms were used to compare with the other methods cited below. In order to render a comparison possible it was necessary to represent heats of reaction in reduced form; i.e. as a fraction, H/H_0, of the total, H_0. This was because the total heats of reaction varied with cure temperature in the manner shown in *Table 1* (a). The variance in H_0 from sample to sample was very much less than the systematic differences tabulated here.

Table 1. Apparent heats of reaction, H_0, as measured isothermally and from scans

(a) *Isotherms*		(b) *Scans*		
$T(°K)$	H_0 (*cal/g*)	*Scan rate (deg. C/min)*	H_0 (*cal/g*)	*Temperature at thermogram peak* (°K)
360	54			
380	68	0·5	61	379
390	65	1	83	390
400	81	2	93	401
420	87	4	93	415
430	86	8	88	425
435	80	16	68	441
440	76	32	60	455
445	62	64	51	468
450	64			

It is recognized that undercure may contribute to the low values at lower temperatures. In fact experiments to be discussed later have shown that subsequent scans on the samples cured at 360°K yielded a residual exotherm of about 5 cal/g. For the 380°K cure the residual exotherm was about 2 cal/g while it was less than 1 cal/g for all higher temperature cures. Thus, this only partially explains the large differences. It is also possible that the cure mechanism changes with temperature and is most efficient in the region of 420°K where H_0 is maximum. Such changes should be revealed as discrepancies between the three methods of constructing isothermal cure curves at present being discussed. The decrease of H_0 above 420°K was expected for reasons already discussed. The cure time was of the order of minutes so that the heat absorbed as the sample equilibrated at the cure temperature partially cancelled out the exotherm. This effect will also be revealed as a discrepancy between the methods.

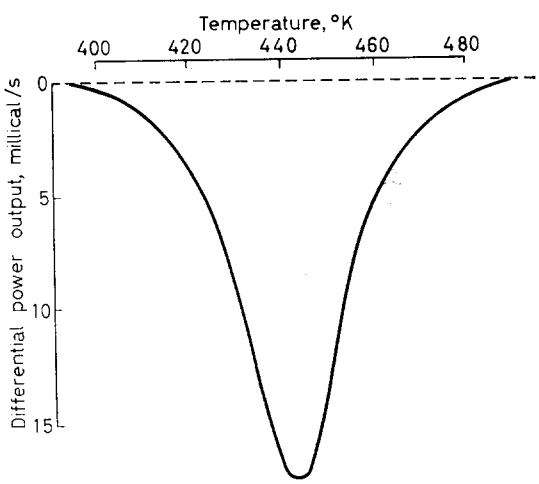

Figure 2—A typical scan. 28 mg uncured sample scanned at 16 deg.C/min

(b) *Analysis of thermograms with different scan rates*—Uncured samples were scanned at rates 0·5 deg. C/min to 64 deg. C/min yielding eight thermograms of rate of heat evolution versus temperature with the typical appearance shown in *Figure 2*. The total heats of reactions, measured from the areas enclosed by the thermograms on a time axis are depicted in *Table 1* (b) together with the temperatures at which the curves peaked. These variations in H_0 are consistent with a change in cure mechanism since they follow the same trend as those in *Table 1* (a). The shift in peak temperatures as scan rate was increased was caused by the time and temperature dependence of cure and forms the basis of this method for obtaining the isothermal cure curves. The method of doing this is illustrated in *Figure 3*.

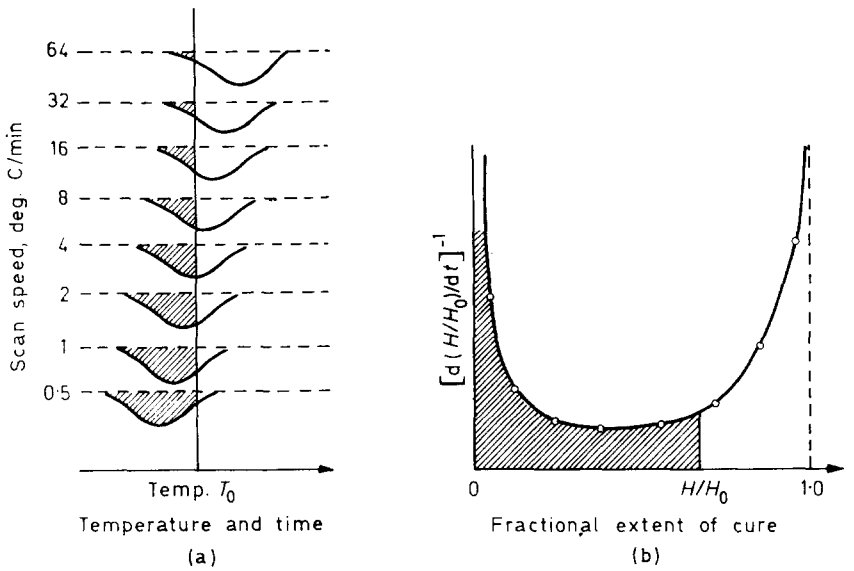

Figure 3—(a) Set of displaced thermograms; (b) Curve deduced from (a) and used to obtain isothermal cure curve at temperature T_0

Figure 3(a) shows schematically the set of displaced thermograms on a temperature axis. The time scale of the experiment varied from minutes at 64 deg. C/min to several hours at 0·5 deg. C/min and it was necessary to increase the sensitivity of the ordinate axis accordingly so that thermograms of similar sizes were retained. In order to construct an isothermal cure curve at temperature T_0, an ordinate at this temperature is drawn in each thermogram. Where it cuts the curve, the state of the resin is described by three parameters: temperature, T_0, heat generation rate (dH/dt) and heat of reaction per gramme of resin (H). The value of H is calculated from the areas, on a time axis, shaded in *Figure 3*(a) and the total heat of reaction H_0 is given by the area enclosed by the complete curve on a time axis. The eight isothermal states are plotted in reduced form as $[d(H/H_0)/dt]^{-1}$ versus H/H_0 as shown in *Figure 3*(b). The integral of the curve through these points

from zero to H/H_0, i.e. the shaded area, is equal to the time, t, to reach degree of cure H/H_0 at temperature T_0. Hence the isothermal cure curve of H/H_0 versus t can be plotted. This process can be repeated at any temperature but at temperatures lower than T_0 in *Figure 3*(a) the final part of the cure curve will be missing since even the sample producing the thermogram at 0·5 deg. C/min will not have reached an advanced state of cure.

In the experiments undertaken, the scans were analysed for those temperatures between 360°K and 450°K examined by the isothermal method (a). The complete set of cure curves derived by methods (a) and (b) is shown in *Figure 4* (a) to (j).

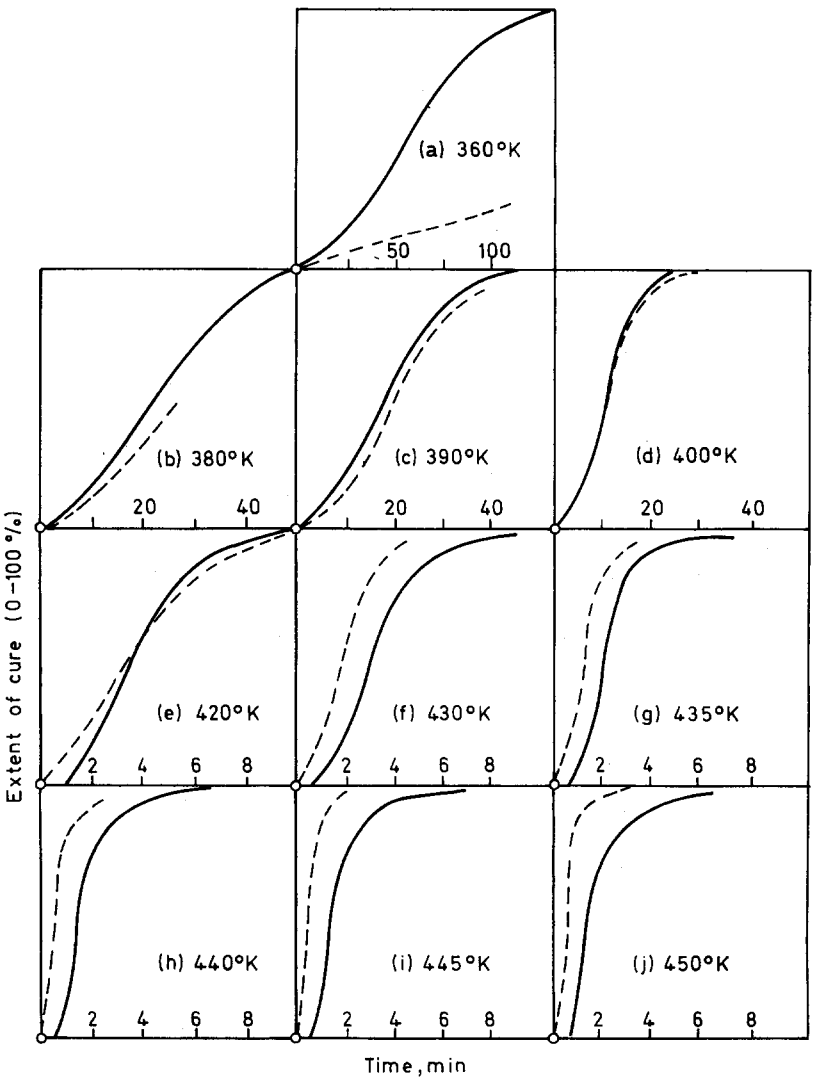

Figure 4 (a–j)—Comparison of cure curves at various temperatures obtained from isothermal method (a) (solid lines) and method (b)

These figures show differences between the two methods which change systematically with increasing temperature. At low temperatures where the reaction is proceeding slowly the isothermal method (a) gives reliable results while the scan method (b) provides insufficient data from which to construct a reliable curve. The two methods give results which agree at 400°K [*Figure 4*(d)]. Above this temperature, the isothermal method (a) gives unavoidable temperature lags due to the finite heating time of the sample and test cell so that the curve is shifted along the time axis by about one minute. Above 435°K [*Figure 4* (h) to (j)] the peak of the exotherm is clipped off by this heat-up time which distorts the shape of the cure curve. Thus the two methods are complementary. For fast cures the scan method (b) yields information on the state of cure for isothermal times of the order of one second which could not possibly be done by any direct isothermal method because of thermal lags.

(c) *Scans on partly cured resins*—Samples were cured isothermally in an oven for times ranging from zero to that previously estimated as being required for 'complete' cure. Each partly cured sample was then scanned in the calorimeter at a rate of 16 deg. C/min and the area enclosed by the thermogram on a time axis gave the residual heat of reaction $(H_0 - H)$ from which H could be derived. H_0 is the heat of reaction of an initially uncured sample.

This method becomes useful when the rate of heat evolution is too small for isothermal detection and is the usual way of investigating cure by differential thermal analysis, being applied, for instance, by Johnson *et al.*[6]. Because of the large number of samples needed for this method, cure only at 400°K was investigated. The result is compared with the isothermal method (a) in *Figure 5*, where the continuous curve is from the isothermal method. There appears to be good agreement in this case.

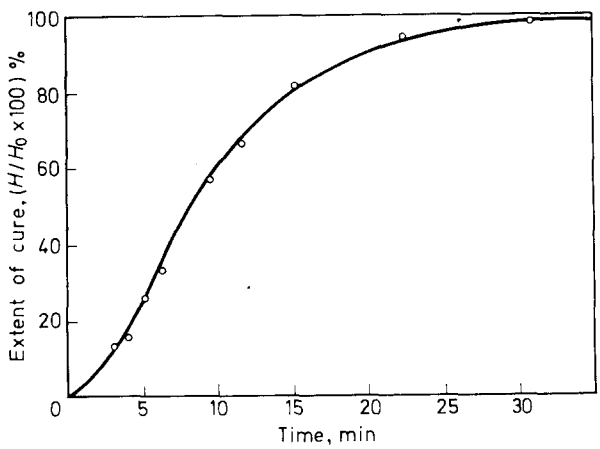

Figure 5—Comparison of cure curve at 400°K obtained from isothermal method (a) (solid line) and method (c) (open circles)

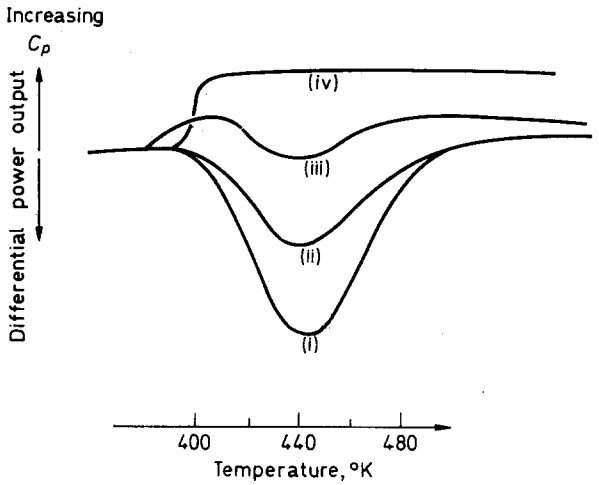

Figure 6—Scans on part-cured resins after (i) 10 min, (ii) 16 min, (iii) 22 min, and (iv) 60 min cure at 400°K

Some of the thermograms of partly cured samples are shown superimposed on a temperature axis in *Figure 6*. For cure times exceeding 16 minutes, an accurate assessment of the residual exotherm was hampered by the appearance of a second-order transition, identified as a positive step in specific heat on the 60 minute thermogram in *Figure 6*. It should be recalled at this stage that the ordinate axis is also proportional to specific heat changes when a constant heating rate is used. The actual step in specific heat amounted to about 0·1 cal/g.°C for this resin system. Experiments to investigate the transition more fully are described in the next section.

4. *Studies of glass transition*

Figure 7 shows superimposed thermograms of an initially partly-cured sample which was scanned five times from 300°K to 520°K. The first scan (a) shows the residual curing exotherm while subsequent scans (b) to (e) demonstrate that the second-order transition has shifted to higher temperatures as the resin became more and more cured. For these and all subsequent experiments to investigate the second-order transition, a heating rate of 8 deg. C/min was used.

There are indications in *Figure 7* that the position of the transition region could be used as a sensitive cure index during the later stages of cure where the DSC is not sensitive enough to detect any residual exotherm in the sample. Since the transition region embraces a temperature range of about 30 deg. C it is necessary to define a transition temperature. It will be shown that it is most meaningful to define this temperature at the low temperature end of the transition region. For practical purposes it is taken as the point of intersection of the extrapolated baseline at the low temperature end and the tangent to the curve at the inflection point.

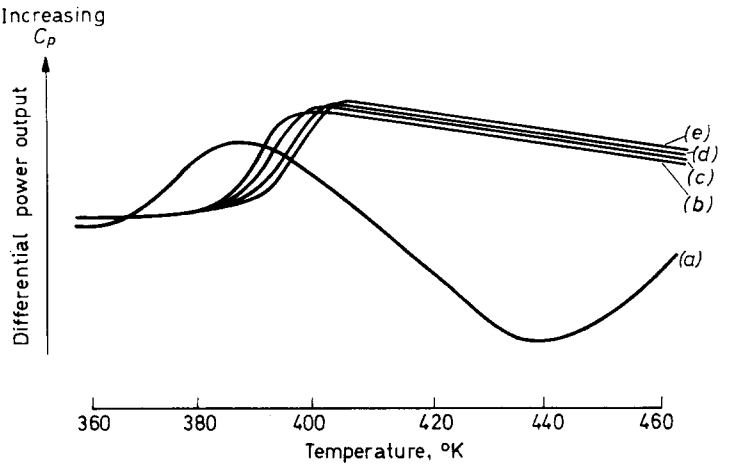

Figure 7—Repeated scans (a) to (e) on an initially part-cured resin

In order to demonstrate that this transition was in fact a glass transition, associated with the softening point, a series of epoxy resins was prepared with different softening points, by the addition of poly-azalaic poly-anhydride as a reactive diluent. The heat distortion temperatures, T_d, were measured by the ASTM *D 648-56* test and compared with the transition temperature, T_g, as measured by DSC. The results are plotted in *Figure 8*. The correla-

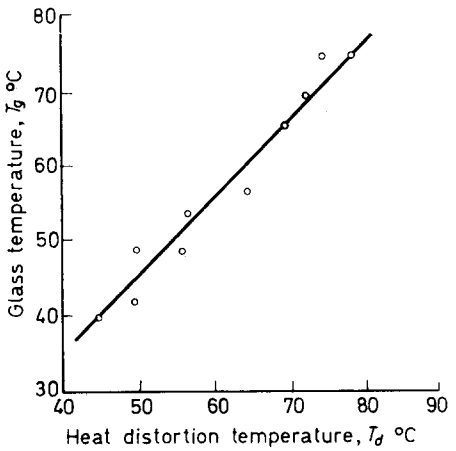

Figure 8—Comparison of DSC transition temperature (T_g) with heat distortion temperature (T_d)

tion is good, although exact quantitative agreement is not expected on account of the different definition of a transition temperature on the broad transition range and the different heating rates. T_d was defined as the temperature at which a standard bar of resin had deformed under load by a given amount as temperature was scanned at 50 deg. C/h.

The correlation in *Figure 8* immediately suggests that measuring T_g by DSC provides a convenient estimate of the heat distortion temperature, without resorting to the cumbersome ASTM test. The author has in fact been able to measure T_g of resins filled with glass fibre which could not be done by the ASTM test.

Figure 6 shows that for prolonged cures the temperature, T_g, of the glass transition for the resin system investigated approached 390°K to 400°K. It was of interest therefore to cure samples isothermally below 390°K in order to discover how the onset of the glassy state affected the speed of the curing reaction. Samples were accordingly cured in the DSC at temperatures ranging from 330°K to 440°K. The reaction exotherm was recorded during these isothermal cures until no further polymerization was detectable in terms of heat evolution. The cures were then terminated and each sample was scanned at 8 deg. C/min to observe any transition in the apparently cured material. The results are shown in *Figure 9*.

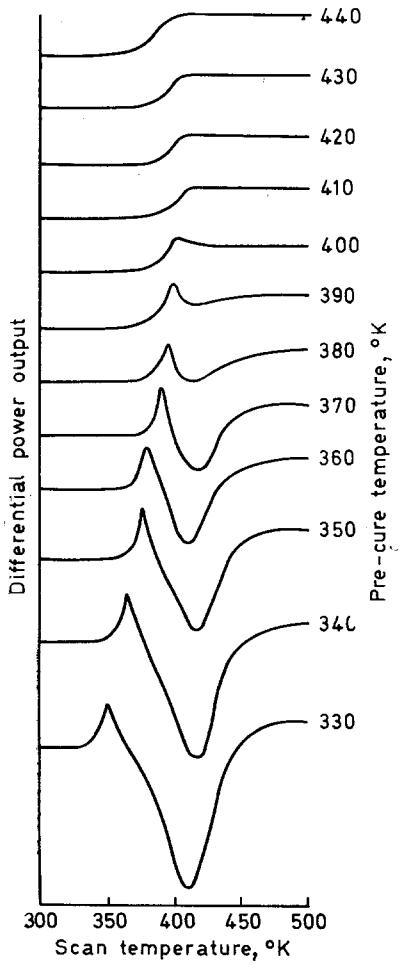

Figure 9—Scans on samples previously cured to apparent completion at temperatures 330°K to 440°K

For the 330°K cure, the subsequent scan reveals a residual exotherm of about 12 cal/g and this residual exotherm diminishes, as the pre-cure temperature increases, to vanish at 400°K. The figure further shows that the glass transition occurs at the cure temperature, indicating that as soon as the resin becomes glassy further reaction is very slight and not detectable with the present equipment by the isothermal method (a). It was possible, however, to use method (c) to investigate the cure rate in the glassy state. Samples were cured for extended periods at 360°K and subsequently scanned to note any changes in the position of the glass transition temperature and size of residual exotherm. The thermogram for 360°K in *Figure 9* was after four hours cure. *Figure 10*(a) shows the shapes of the thermograms

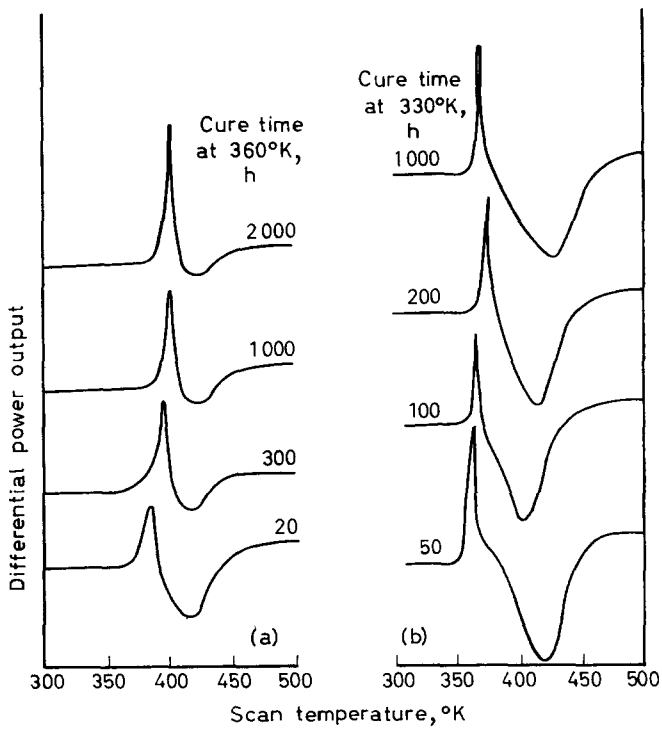

Figure 10—Scans on samples previously cured for extended periods at (a) 360°K, (b) 330°K

after cures at 360°K of up to 2 000 hours (three months). Only slight changes in the state of cure are detectable indicating that the glassy state provides a large barrier to continued polymerization. A similar series of curves for cure at 330°K for times up to 1 000 hours is shown in *Figure 10*(b). At 330°K the resin is in a more undercured state and the looser structure should allow faster polymerization in the glassy state. All thermograms are reduced in proportion to sample mass.

DISCUSSION

The foregoing results show that isothermal cure curves of epoxy resins can be obtained very simply by DSC without resorting to the rather dubious application of reaction kinetics to these complex reactions. It is, however, amazing that the Arrhenius equation, $(dH/dt)_{max.} = A \exp(U/RT)$, where A is a constant and U the activation energy, is obeyed exactly by the system studied. This is revealed in *Figure 11* which shows that a plot of

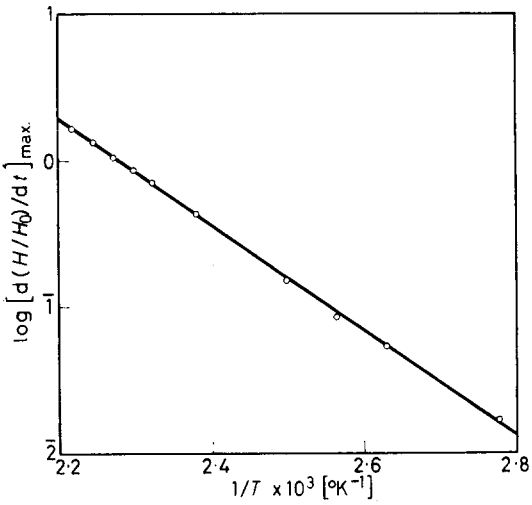

Figure 11—Arrhenius plot of the reaction rate variation with temperature

$\log [d(H/H_0)/dt]_{max.}$ versus $1/T$ is accurately linear, yielding an activation energy of 17·8 kcal/mol. Because a linear Arrhenius plot is obtained and because any disagreement between the three methods of investigating cure has been satisfactorily explained otherwise, it must be assumed that any change in the curing mechanism with curing temperature does not affect the overall reaction rate.

By analysing the thermograms of the resin cured at different scanning rates [method (b)], information has been indirectly obtained about the isothermal behaviour within seconds of applying a cure temperature. This information is difficult to obtain directly because of the finite heat-up time of the resin to the cure temperature. The difficulty cannot be avoided by using a smaller sample in the DSC because both heating effects and exotherm size are diminished proportionally. It may be argued that if the isothermal situation at zero time is impossible to achieve in practice it is of no interest. However, the interest would arise in the elucidation of kinetic processes which are treated theoretically on the assumption of such an ideal state. The principle of this method could be usefully applied, therefore, to any rate process provided that only the rate, and not the mechanism, changes with temperature.

The underlying molecular mechanisms leading to a glass transition in crosslinked resin systems have not been treated in detail but the glass transi-

tion in thermoplastics has been described in terms of a supercooled liquid state[7]. The liquid state is supposed to contain holes which are characterized by a molar volume and a molar excess energy over the 'no-hole' situation. Since production and disappearance of holes require an activation energy, below a certain temperature the hole equilibrium is frozen-in and the material becomes glass-like. The transition from liquid to glass is accompanied by a discontinuity of specific heat. The rate of approach to equilibrium is characterized by a relaxation time so that the temperature at which the transition occurs should depend on thermal history and heating rate.

Kwei[8] performed a systematic series of dynamic mechanical measurements on DER 332/LC epoxy cured with aliphatic amines. He found that the temperature of the transitions decreased with increasing aliphatic chain length and concluded that the viscoelastic absorption was directly related to motion in the CH_2 sequences between crosslinks. An extension of this interpretation of the 'hole' theory should be relevant to the resin system reported in this paper. The short chain sequences would tend to minimize relaxation effects. Thus it was discovered that the position of T_g was affected by heating rate but increased by only 5 deg. C as heating rate was increased from 2 deg. C/min to 64 deg. C/min. Furthermore, annealed epoxy resins showed the characteristic endothermic peak in thermograms as predicted by the 'hole' theory. A sample of cured resin was annealed by cooling it through T_g at a rate of 0·5 deg. C/min, and the thermogram of this is compared with that of a quenched sample in *Figure 12*. The endothermic peak

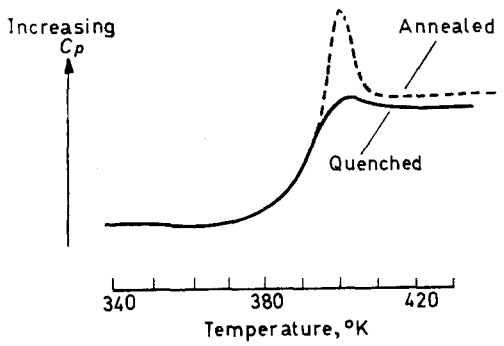

Figure 12—Effect of annealing on the glass transition of an epoxy resin

is due to the higher degree of order in the glassy state for the annealed sample. It is also very pronounced in the thermograms in *Figure 10* since the prolonged cure times, although unable to induce further polymerization, do result in a highly annealed state in the resin.

The experiments reported in this paper demonstrate the relationship between the glass transition and cure. *Figure 7* indicates that the transition moves to higher temperatures as cure proceeds and is a sensitive index beyond the state where all measurable heat of reaction has ceased. The increase in T_g at this stage of cure is probably associated more with rearrangement of the crosslinked network rather than with creating further crosslinks.

Figures 9 and *10* illustrate in a striking way that the onset of the glassy state presents a large barrier to the continuation of epoxy resin cure. One can define a glass transition, presumably, at all stages of cure and the temperature of the transition will increase steadily until it reaches the temperature of cure. Then no further reaction can take place. The subsequent scans in *Figure 9* show that the glass transition temperature has not increased beyond the cure temperature and that as soon as the temperature during scan exceeds the limiting glass transition temperature the residual cure can take place. Obviously, the lower the cure temperature, the greater is the residual exotherm. On this particular resin system, complete cure appears to correspond to a glass temperature near 400°K since scans on samples cured above this temperature show no further increase in the transition temperature and the residual exotherm diminishes to zero at 400°K. This exercise demonstrates the importance of curing a resin above its limiting glass transition temperature if optimum physical properties are to be desired.

The actual position of the glass temperature has hitherto been fairly arbitrarily assigned to various parts of the thermogram but the above results show that the temperature at the onset of the recorded transition has a meaningful interpretation. Below this temperature molecular motions become frozen-in and chemical reaction is very limited. For the resin system employed here, *Figure 10*(a) shows that chemical reaction becomes almost completely inhibited in the glassy state. After 2 000 hours (12 weeks) at 360°K, the transition has moved up about 20 deg. C and the residual exotherm has been reduced only slightly. A similar state of cure was achieved after only 1½ hours at 380°K.

CONCLUSIONS

A commercially available differential scanning calorimeter has been used in three different ways to produce isothermal cure curves for epoxy resins. One of these methods yielded indirectly information related to the curing reaction during the first seconds of an idealized isothermal experiment and has important applications in fundamental studies of rate processes. The isothermal method of obtaining cure curves is suitable if very little happens to the resin during the first few minutes at the cure temperature. Otherwise the exotherm is distorted by heating effects. This method is therefore suitable for cure times of the order of hours. If the cure proceeds for longer than about six hours, the exotherm is generally too slight to be detectable accurately by this apparatus. For these cases it is necessary to use the third method in which the residual exotherm of partially cured samples is detected by a scanning technique. The isothermal cure curves derived for one resin system by these three methods show good agreement. Any discrepancies could be explained in terms of the limitations stated above.

From the cure curves, the suitability of applying simple kinetic laws to the reaction has been considered. For the system examined, the Arrhenius equation appears to be applicable, yielding an activation energy of 17·8 kcal/mol.

A glass transition temperature, T_g, associated with the softening point of the resin, has been investigated by DSC. This temperature increased during cure and is therefore a sensitive index of effective cure. If T_g reached the cure temperature, however, further reaction in the glassy state was extremely limited and to a first approximation completely absent. This demonstrated the importance of curing a resin above its limiting T_g for optimum physical properties.

A glass transition temperature measurement on an epoxy resin using DSC is a simpler and more versatile alternative to the ASTM heat distortion test against which it can be calibrated.

Passfield Research Laboratories,
Joint Research Establishment of the
Inland Steel Container Company and
Metal Containers Ltd,
Passfield, Liphook, Hants.

(Received May 1967)

REFERENCES

[1] BORCHARDT, H. J. and DANIELS, F. *J. Amer. chem. Soc.* 1957, **79**, 41
[2] KISSINGER, H. E. *Analyt. Chem.* 1957, **29**, 1702
[3] GORDON, M. and SIMPSON, W. *Polymer, Lond.* 1961, **2**, 383
[4] WATSON, E. S., O'NEILL, M. J., JUSTIN, J. and BRENNER, N. *Analyt. Chem.* 1964, **36**, 1233
[5] ANDERSON, H. M. *J. Polym. Sci. A-1*, 1966, **4**, 783
[6] JOHNSON, G. B., HESS, P. H. and MIRON, R. R. *J. appl. Polym. Sci.* 1962, **6**, 519
[7] HIRAI, N. and EYRING, H. *J. Polym. Sci.* 1959, **37**, 51
[8] KWEI, T. K. *J. Polym. Sci. A-2*, 1966, **4**, 943

Viscosities of Dilute Solutions of Polyethylene Terephthalate

W. R. MOORE and D. SANDERSON

Intrinsic viscosities of solutions of fractions of polyethylene terephthalate in o-chlorphenol, dichloracetic acid, phenol–tetrachlorethane and trifluoracetic acid have been obtained at 25°, 35°, 45° and 55°C. The variation of [η] with solvent depends on both molecular weight and temperature. Temperature coefficients of [η] are large, being positive for trifluoracetic acid and negative in other cases. Values of K_M and a in the expression $[\eta]=K_M M^a$ are given and compared with those obtained by other workers. There is evidence for association of polymer in dichloracetic acid.

THE factors affecting dilute solution viscosities of polyethylene terephthalate do not seem to have been extensively studied. The polymer is soluble in only a few liquids at room temperature and most studies have involved *o*-chlorphenol or phenol–tetrachlorethane mixture as solvents. Viscosity/molecular weight relationships have been given for these[1–7] and for trifluoracetic acid[7]. These relationships were based on molecular weights determined by end-group[1,2,6], osmotic[3], infra-red absorption[4], cryoscopic[5] and light-scattering[7] methods, often using unfractionated samples. In some cases the data were related to viscosities determined at finite concentrations[2,4,5]. Some of the results have been used to estimate unperturbed dimensions[8,9]. The effects of variations in temperature on the intrinsic viscosity [η] and other parameters do not seem to have been systematically studied. Polyethylene terephthalate is a moderately stiff chain polar polymer and these properties may be reflected in variations of viscosity with solvent, molecular weight and temperature. This paper is concerned with dilute solution viscosities of polyethylene terephthalate fractions covering a number-average molecular weight range of 10 000 to 40 000 in four solvents at 25°, 35°, 45° and 55°C. The effects of variations in solvent, molecular weight and temperature on [η] and other parameters are considered.

EXPERIMENTAL

A commercial sample of polyethylene terephthalate was fractionated by the method of Moore and Sheldon[10] involving stepwise addition of hexane to a one per cent solution of polymer in *o*-chlorphenol. A first very small head fraction was discarded. Six further fractions were obtained, of which the first, constituting nearly half the total weight of the six, was refractionated to give four sub-fractions designated 1a, 1b, 1c and 1d. These, with fractions 2, 3 and 5, were used in further work, fractions 4 and 6 being too small. Some low molecular weight polymer, possibly containing cyclic oligomers, remained in solution after precipitation of fraction 6.

Number-average molecular weights of the fractions were obtained by end-group analysis using the method of Conix[1] in which both carboxyl and

hydroxyl end groups are estimated. Molecular weights were calculated by use of the formula[1]

$$\overline{M}_n = (2/B) - 200\,(B - A)/B \qquad (1)$$

where A and B represent the carboxyl content of the polymer respectively before and after conversion of hydroxyl end groups into carboxyl by succinic anhydride, the end groups being expressed as equivalents per gramme.

o-Chlorphenol, trifluoracetic acid, dichloracetic acid and a 40–60 by weight phenol–*s*-tetrachlorethane mixture were used as solvents. The latter is very nearly a 1 : 1 mixture by volume. The liquids were purified by appropriate methods, dried and fractionally distilled immediately prior to use.

Viscosities of the solvents and of solutions in the concentration range 0·25 to 1·0 g/dl at 20°C were measured at 25°, 35°, 45° and 55° using suspended level capillary viscometers in water baths controlled to ±0·025 deg. C at each temperature. Solutions were filtered before use. Intrinsic viscosities were obtained by extrapolation of linear plots of η_{sp}/c against concentration c, using the method of least squares. Concentrations were corrected for thermal expansion.

RESULTS

Table 1 gives number-average molecular weights of the fractions used with an estimated uncertainty of ±5 per cent for molecular weights less than

Table 1. Number-average molecular weights

Fraction	1a	1b	1c	1d	2	3	5
$\overline{M}_n \times 10^{-3}$	38	31	26	16·5	18	15·5	15

30 000. Molecular weights above 30 000 are subject to a somewhat greater uncertainty.

Figure 1 shows plots of η_{sp}/c versus c for the fractions of highest and lowest molecular weight used in each solvent at 25° and 55°, these being typical of results obtained with other fractions at other temperatures. Intrinsic viscosities for all the fractions at each temperature are given in *Table 2*. Values of k' in the equation

$$\eta_{sp}/c - [\eta] + k'[\eta]^2 c \qquad (2)$$

Table 2. Intrinsic viscosities

Solvent	*Temp. (°C)*	*1a*	*1b*	*1c*	*1d*	*2*	*3*	*5*
o-Chlorphenol	25	0·98	0·82	0·72	0·56	0·60	0·47	0·37
	35	0·94	0·78	0·70	0·54	0·58	0·46	0·36
	45	0·92	0·75	0·68	0·52	0·56	0·45	0·35
	55	0·90	0·73	0·66	0·50	0·54	0·44	0·35
Dichloracetic acid	25	—	0·86	0·79	0·67	0·78	0·66	0·58
	35	0·87	0·75	0·66	0·58	0·64	0·56	0·52
	45	0·85	0·73	0·65	0·56	0·62	0·53	0·50
	55	0·82	0·72	0·64	0·55	0·59	0·50	0·48
Trifluoracetic acid	25	1·22	1·07	0·97	0·82	0·90	0·72	0·66
	35	—	1·16	1·04	0·86	0·96	0·78	0·70
	45	—	1·25	1·08	0·90	1·02	0·81	0·74
	55	—	1·29	1·13	0·92	1·07	0·84	0·76
Phenol–tetrachlorethane	25	1·20	1·07	0·88	0·67	—	0·64	0·56
	35	1·18	1·04	0·87	0·67	—	0·64	0·56
	45	1·17	1·02	0·86	0·66	—	0·62	0·54
	55	1·09	0·98	0·80	0·62	—	0·62	0·51

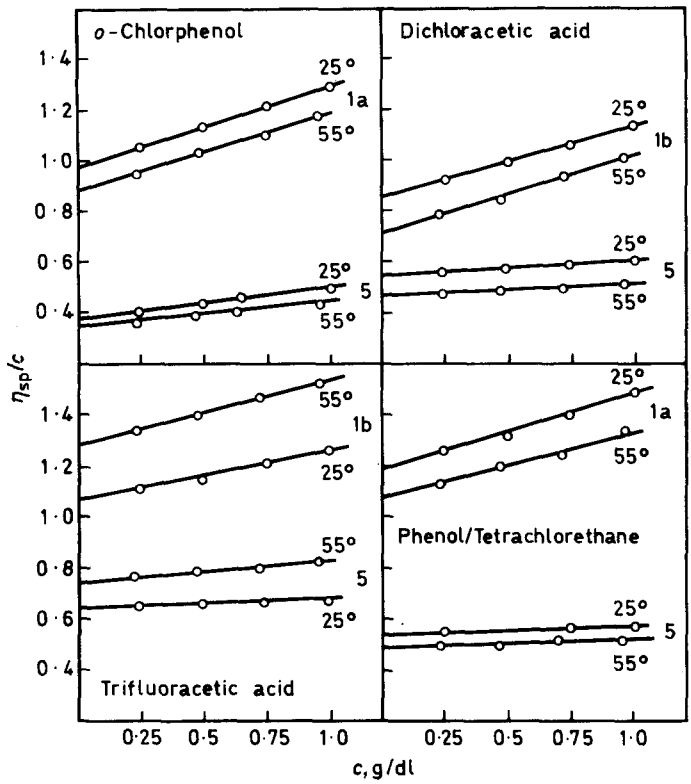

Figure 1—η_{sp}/c versus c plots for high and low molecular weight fractions at 25° and 55°

for fraction 1b in all the solvents at each temperature are given in *Table 3*. The slopes of the η_{sp}/c versus c plots for fractions 1c, 1d, 2, 3 and 5 were often too small to allow accurate evaluation of k'.

Flow times of solutions of fraction 1a in trifluoracetic acid at temperatures above 25° showed a fairly rapid decrease in successive determinations, implying degradation. This did not occur at 25° and seems to be restricted to this one fraction. Other fractions in trifluoracetic acid did not show this behaviour and there was no such evidence of degradation of any fraction in the other solvents at either of the four temperatures. Solutions in each solvent showed no significant change in viscosity during storage at room temperature. Viscosities of solutions of the same concentration of a given fraction in the same solvent but prepared at different times were in good agreement.

DISCUSSION

The variation of $[\eta]$ with solvent seems to depend on both molecular weight and temperature. At 25° the order, for higher molecular weight fractions, is trifluoracetic acid > phenol–tetrachlorethane > dichloracetic acid > *o*-chlorphenol but at lower molecular weights values for phenol–tetrachlorethane and dichloracetic acid are similar. At higher temperatures higher

molecular weight fractions give trifluoracetic acid > phenol–tetrachlorethane > *o*-chlorphenol > dichloracetic acid but at lower molecular weights values for dichloracetic acid exceed those for *o*-chlorphenol and are similar to those for phenol–tetrachlorethane. The ratios of values of $[\eta]$ for trifluoracetic acid and phenol–tetrachlorethane are similar to those of Wallach[7]. The values of k' in *Table 3* show little variation with temperature except

Table 3. Values of k' for fraction 1b

Solvent	25°	35°	45°	55°C
o-Chlorphenol	0·24	0·29	0·28	0·27
Dichloracetic acid	0·37	0·57	0·61	0·61
Trifluoracetic acid	0·19	0·14	0·14	0·18
Phenol–tetrachlorethane	0·08	0·07	0·04	0·09

for dichloracetic acid and do not vary with solvent in a manner inverse to that of $[\eta]$. Values of k' for *o*-chlorphenol, trifluoracetic acid and phenol–tetrachlorethane are small in contrast to higher values for dichloracetic acid which may be indicative of association of polymer in this solvent.

Differences in the variation of $[\eta]$ with solvent at different temperatures are at least partly a consequence of variations in temperature coefficients of $[\eta]$. *Figure 2* shows $[\eta]$ as a function of temperature for higher molecular

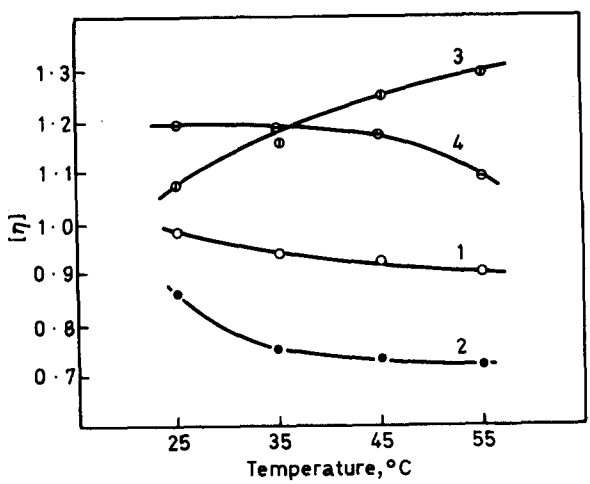

Figure 2—$[\eta]$ as a function of temperature for higher molecular weight fractions: 1. 1a in *o*-chlorphenol, 2. 1b in dichloracetic acid, 3. 1b in trifluoracetic acid, 4. 1a in phenol–tetrachlorethane

weight fractions in the solvents. Dichloracetic acid shows a marked decrease in $[\eta]$ between 25° and 35° while phenol–tetrachlorethane shows a greater decrease at higher temperatures. Temperature coefficients of $[\eta]$ for trifluoracetic acid are positive in contrast to those for the other solvents.

Average values of $d[\eta]/dT$, derived from the data shown in *Figure 2*, are given in *Table 4*. They are similar in magnitude to those for stiff chain

Table 4. Average values of $d[\eta]/dT$

Solvent	*Fraction*	$d[\eta]/dT \times 10^2$
o-Chlorphenol	1a	−0·27
Dichloracetic acid	1b	−0·47
Trifluoracetic acid	1b	−0·73
Phenol–tetrachlorethane	1a	−0·33

polar polymers such as cellulose derivatives[11,12] and considerably greater than those for flexible polar polymers of comparable molecular weight[13,14].

Figure 3 shows plots of $\log[\eta]$ against $\log \overline{M}_n$ for each solvent at the lowest and highest temperatures. Values of K_M and a in the expression

$$[\eta] = K_M M^a \tag{3}$$

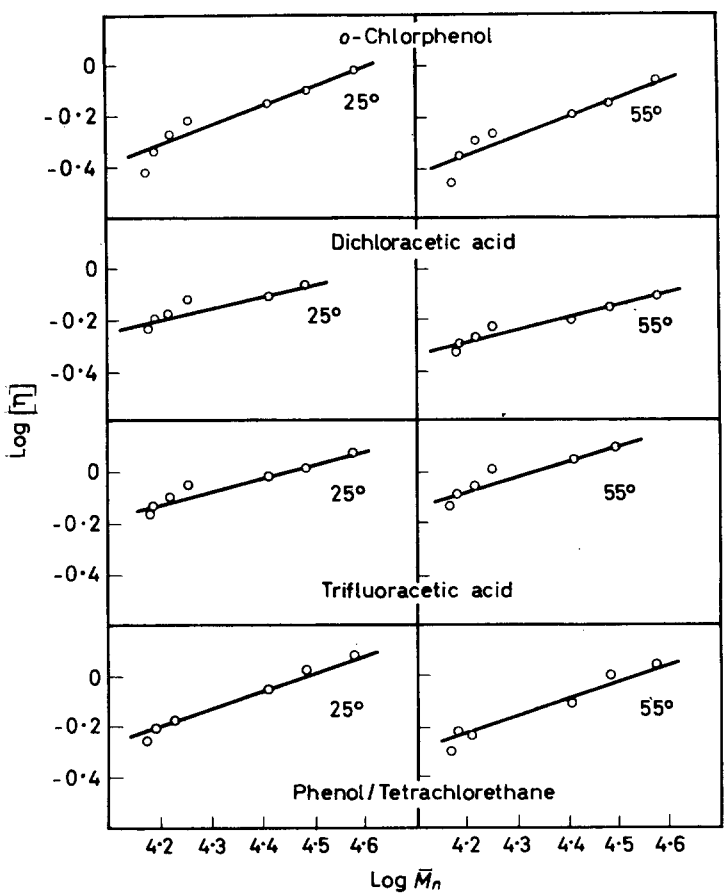

Figure 3—Log $[\eta]$ versus log $\overline{M}_n$ plots at 25° and 55°

at all four temperatures, obtained by the method of least squares, are given in *Table 5.*

Table 5. Values of K_M and a

	$K_M \times 10^4$				$a \pm 0.02$			
Solvent	*25°*	*35°*	*45°*	*55°*	*25°*	*35°*	*45°*	*55°*
o-Chlorphenol	1·9	2·1	2·3	2·6	0·81	0·80	0·78	0·77
Dichloracetic acid	67	49	40	33	0·47	0·49	0·50	0·52
Trifluoracetic acid	14	13	11	10·5	0·64	0·66	0·68	0·69
Phenol–tetrachlorethane	14	12·5	11	9	0·64	0·65	0·66	0·67

Values of K_M and a for *o*-chlorphenol at 25° are in good agreement with those of Ward[4] (3×10^{-4}, $0{\cdot}77 \pm 0{\cdot}09$) in spite of the scatter seen in *Figure 3.* They are in poor agreement with those of Marshall and Todd[3] whose results, however, show considerable scatter in a plot of $\log [\eta]$ against $\log \overline{M}_n$. Values of K_M and a for trifluoracetic acid are in reasonable agreement with those of Wallach[7] ($4{\cdot}33 \times 10^{-4}$, 0·68) who used weight-average molecular weights and measured $[\eta]$ at 30°. Values of the exponent a for phenol–tetrachlorethane are less than that of Wallach[7] at 30° (0·73) and much less than those of Griehl and Neue[2] at 20° (0·86) and of Conix[1] at 25° (0·82). Griehl and Neue measured inherent viscosities at $c = 0{\cdot}5$ g/dl and obtained values of $[\eta]$ from a one-point viscosity equation. Conix used unfractionated polymers. The low values of a and high values of K_M for dichloracetic acid and the rapid decrease in K_M with increasing temperature may be due to association of polymer which decreases with increase of temperature. Similar results have been obtained with polyvinyl acetate in toluene[13] and polymethyl methacrylate in *n*-amyl methyl ketone[14], both cases in which association of polymer is known to occur[15].

School of Polymer Science,
University of Bradford

(Received May 1967)

REFERENCES

[1] CONIX, A. *Makromol. Chem.* 1958, **26**, 226
[2] GRIEHL, W. and NEUE, S. *Faserforsch. u. Textiltechn.* 1954, **5**, 423
[3] MARSHALL, J. and TODD, A. *Trans. Faraday Soc.* 1953, **49**, 67
[4] WARD, I. M. *Nature, Lond.* 1957, **180**, 141
[5] TURSKA-KUSMIERZ, A. and SKWARSKI, T. *Prace Inst. wlók.* 1952, **2**, 49
[6] CHUL-YOUNG, C. *Polymer Letters,* 1964, **2**, 1069
[7] WALLACH, M. L. American Chemical Society *Polymer Preprints,* 1965, **6**, 860
[8] KRIGBAUM, W. R. *J. Polym. Sci.* 1958, **28**, 213
[9] KURATA, M. and STOCKMAYER, W. *Fortschr. Hochpolym. Forsch.* 1963, **3**, 196
[10] MOORE, W. R. and SHELDON, R. P. *J. Textile Inst.* 1959, **50**, T294
[11] MOORE, W. R. and BROWN, A. M. *J. Colloid Sci.* 1959, **14**, 343
[12] FLORY, P. J., SPURR, O. K. and CARPENTER, D. K. *J. Polym. Sci.* 1958, **27**, 231
[13] MOORE, W. R. and MURPHY, M. *J. Polym. Sci.* 1962, **56**, 519
[14] MOORE, W. R. and FORT, R. J. *J. Polym. Sci.* 1963, **A1**, 929
[15] MOORE, W. R. and MURPHY, M. Unpublished results

Semiconduction in Phenylene Polymers

D. D. ELEY and B. M. PACINI*

The semiconductive behaviour of compressed discs of polymers in the polyphenylene series has been examined. Some polymers showed a resistance increase with time to an equilibrium value, possibly due to space charge effects, but after allowance for this the conductivity was ohmic up to 500 V/cm or beyond. Thermoelectric power results pointed to electronic rather than ionic conduction, with positive holes as majority carriers, and in one case (polybenzone) a mobility of $3{\cdot}8\times10^{-4}$ cm²/V sec was established, in agreement with expectations from band theory for an intrinsic semiconductor. The polyaromatics gave relatively high energy-gap values which agree with values found for the monomers which have been associated with electron injection. This applies in the absence of bridging groups, and also for the bridging groups —CH_2— and —O—. Certain other bridging groups, in order of increasing effectiveness —AsO(OH)—, —AsPh—, —CO— *and* —NH— *gave polymers with energy-gaps lower than the monomer values. Presumably these groups allow the extension of conjugation between the monomers along the polymer chain, and result in intrinsic semiconduction. Hydrogen, oxygen and nitrogen have no effect, but boron trifluoride gas increases the conductivity of the polymers, supporting the positive hole concept.*

THERE have been several recent reviews of semiconduction in synthetic polymers[1,2]. The specific conductance σ follows the equation well-known for inorganic materials,

$$\sigma = \sigma_0 \exp(-\Delta\epsilon/2kT) \qquad (1)$$

where σ_0 is approximately independent of temperature, and $\Delta\epsilon$ is an activation energy. Frequently the conducting polymers are regarded as intrinsic semiconductors, and $\Delta\epsilon$ is equated to the 'energy gap' between valence band and conduction band.

The present paper presents measurements on terphenyl, quaterphenyl, and the range of polymers shown in *Figure 1* which embraces a varied range of aromatic and linking groups. Mainly, these polymers are thermally stable and infusible up to 300°C, so that measurements may be carried out at temperatures much higher than is possible for the monomers benzene, naphthalene and anthracene.

EXPERIMENTAL

Dark conductivity

The cell is shown in *Figure 2*. The polymers were pressed as discs of 13 mm diameter under a pressure of 10^4 kg cm^{-2}, with outgassing to remove air and moisture. The discs were mounted between thin platinum foil electrodes, and compressed by light spring pressure against the copper block shown. A copper–constantan thermocouple was inserted into the copper block to within 2 mm of the disc. While the cell itself was of Pyrex, by the use of silica supports and inserts for the leads it was found possible to ensure a 'blank' resistance for the cell, when evacuated to 10^{-6} torr, of

*Now at Research Department, I.C.I. Fibres Ltd, Pontypool.

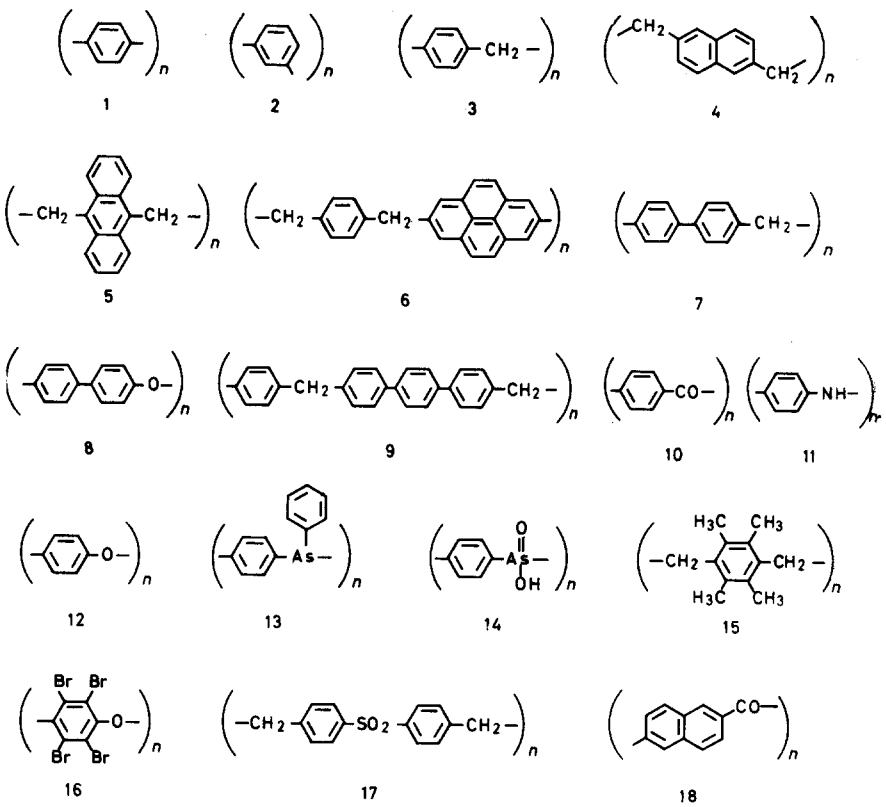

Figure 1—The polymeric structures

greater than 10^{16} ohms. The d.c. resistance of the cell was determined in the usual fashion by passing a current through the cell in series with a standard resistor, and comparing the potential drops across cell and resistor by an E.I.L. Type 33C Vibron electrometer, with a limiting value for measurement of 10^{16} ohms.

The cell was heated in a non-inductively wound electrically heated air bath, both bath and cell being screened by an earthed copper box. Two types of experiment were made:

(*a*) energy gap determinations were made by successive resistance measurements as the cell cooled at a rate of 0·33 deg. C min^{-1}, starting from temperatures quite frequently in excess of 200°C;

(*b*) temperature equilibrium measurements. In this case the cell was placed in a stirred oil bath contained in a Dewar vessel, which was electrically heated and maintained at a pre-set constant temperature by a platinum resistance thermometer and electronic controller. This technique was used in those cases where on switching on the applied voltage there was a measurably slow change in resistance with time until it reached a steady value. It was also used for thermoelectric power and Ohm's law investigations.

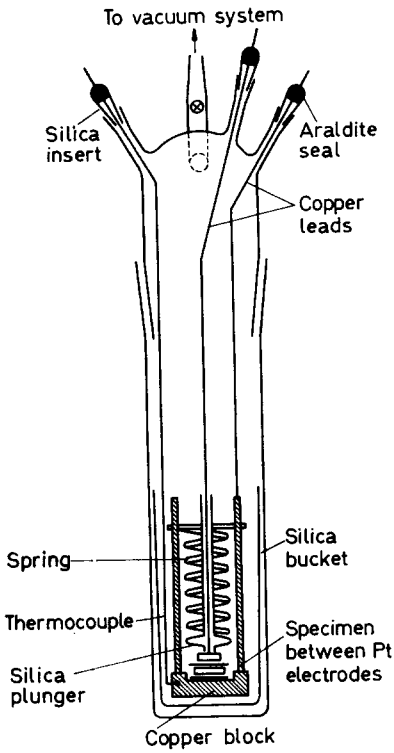

Figure 2—The measuring cell for dark conductivity

Thermoelectric power

The Seebeck Coefficient cell used is shown in *Figure 3.* The specimen disc was sandwiched between two polished, hollow, copper electrodes, each 1·5 in. in length, heated separately by silica-insulated wire coils of 1 ohm resistance, using 4 V accumulators in series with a 10 ohm resistor. These two heaters allowed a temperature difference of approximately 5 deg. C to be maintained between the electrodes, which were monitored by thermocouples passing through the electrodes and reaching to within 0·5 mm of the specimen. All leads and the cell were carefully screened. In practice measurements could only be carried out on specimens with room temperature resistivities of 10^{12} ohm cm or less, which limited the work to four out of the eighteen polymers.

Photoconduction

The cell was a surface cell, based on that of Chynoweth and Schneider[3]. Light from a medium pressure arc, after being passed through a liquid heat filter, was transmitted through an annular copper electrode on to the compressed disc, with its lower copper electrode resting on a copper block which was thermostatically controlled by circulating water. The cell was evacuated to 10^{-6} torr.

Electron spin resonance

The samples were examined in an *X*-band spectrometer, with a trans-

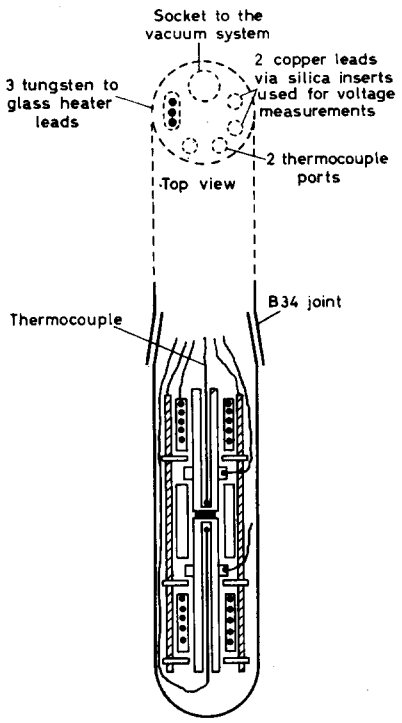

Figure 3—The Seebeck cell

mission cavity working in the H_{014} mode designed and constructed by Mr W. E. Porter of this Department.

The polymers

The amorphous powdered polymers, prepared according to published methods[4–6], were kindly supplied by Drs J. H. Golden and T. P. Hobin of the E.R.D.E., Ministry of Aviation, and by Dr W. W. Wright of the R.A.E., Farnborough. The microanalytical results, provided by these workers, are shown in *Table 1*, and the polymer numbers refer to *Figure 1*. The insolubility and infusibility make the polymers difficult to analyse, and analytical difficulties may be responsible for the discrepancies between observed and calculated data for polymers 1 and 13. The available evidence[6–11] suggests that the phenylene polymers are linear rigid structures with little or no crosslinking. Where molecular weights have been determined (usually by end group analysis) they have lain in the range 10^3 to $1{\cdot}3 \times 10^4$.

RESULTS AND DISCUSSION

Dark conductivity

Values of R, the resistance in ohms, were plotted against $1/T°K$, as

$$\log R = \log R_0 + \Delta\epsilon / 4{\cdot}606\, kT \qquad (2)$$

to give the 'energy gap' $\Delta\epsilon$ from the slope of the line. The resistance at

Table 1. Analytical data for the polymers

Polymer	Found C %	Found H %	Other elements %	Empirical formulae	Calculated C %	Calculated H %	Other elements %
1	66·0	4·3		$(C_6H_4)_n$	94·7	5·3	
2	89·2	5·55*		$(C_6H_4)_n$	94·7	5·3	
3	93·3	6·6		$(C_7H_6)_n$	93·3	6·7	
4	92·5	6·3	Br 1·6	$(C_{12}H_{10})_{81}Br_2$	92·3	6·4	Br 1·3
5	94·4	5·6		$(C_{16}H_{12})_n$	94·1	5·9	
6	93·2	4·6		$(C_{24}H_{16})_n$	94·7	5·3	
7	94·0	5·9		$(C_{13}H_{10})_n$	94·0	6·0	
8	80·4	4·2	Br 8·8	$(C_{12}H_8O)_n$	85·7	4·8	O 9·5
9	92·3	5·39		$(C_{26}H_{20})_n$	94·0	6·02	
10	79·8	3·9	O 16·2	$H(C_7H_4O)_{15}OH$	79·8	3·9	O 15·9
11	72·0	5·9	N 13·5	$(C_6H_5N)_n$	79·1	5·5	N 15·4
12	79·9	3·99		$(C_6H_4O)_n$	78·3	4·34	
13	34·2	2·77	As 25·7	$(C_{12}H_8As)_n$	63·4	3·5	As 33·0
14	41·6	3·51	As 36·4	$(C_6H_5O_2As)_n$	39·1	2·72	As 40·8
15	86·5	9·3	I 4·3	$(C_{12}H_{16})_{35}I_2$	86·1	9·6	I 4·3
16	20·1	0·67	Br 76·1	$(C_6Br_4O)_n$	17·7	—	Br 78·4
17	68·2	4·9	S 13·2	$(C_{14}H_{12}O_2S)_n$	68·85	4·92	S 13·1
18	84·0	3·9		$H(C_{11}H_6O)_9OH$	84·6	4·0	

*Microanalysis in our laboratory gave C 92·6, H 7·09.

300°K, R_{300} gives the specific resistivity ρ_{300}, knowing a the area and l the thickness of the disc, by

$$\rho_{300} = R_{300}ax/l \text{ ohm cm}$$

The volume fraction factor x is taken as 1·0 for these compressed discs. From $\sigma_{300} = 1/\rho_{300}$ ohm^{-1} cm^{-1} and $\Delta\epsilon$, substituting in equation (1) we calculate $\log \sigma_0$ ohm^{-1} cm^{-1}.

In general several reproducible straight line $\log R$ versus $1/T$ plots were obtained for each polymer. Examples are shown in *Figures 4*(a) and *4*(b) of these plots for a low $\Delta\epsilon$ polymer, No. 10, and a high $\Delta\epsilon$ polymer, No. 12. Gases such as hydrogen, oxygen and nitrogen had no appreciable effect. A gas atmosphere was necessary to prevent sublimation of polymer 12.

Electron spin resonance

Several of the polymers were examined at room temperature, and found to show a single line at a g value around the free spin value of 2·000. The line-width at half-height ΔH, and the number of free spin gram^{-1} (f.s.g.) are listed in *Table 2.*

Intrinsic conductivity and chemical structure

Because these polymers are insoluble, infusible and available in small quantities it is not possible to use extensive purification procedures. For polymer 11 there was sufficient material for a series of extractions with several solvents, but the electrical properties remained unchanged. Bearing in mind the difficulties of handling infusible powders, the analytical data usually correspond to a reasonable purity, and the view has been expressed

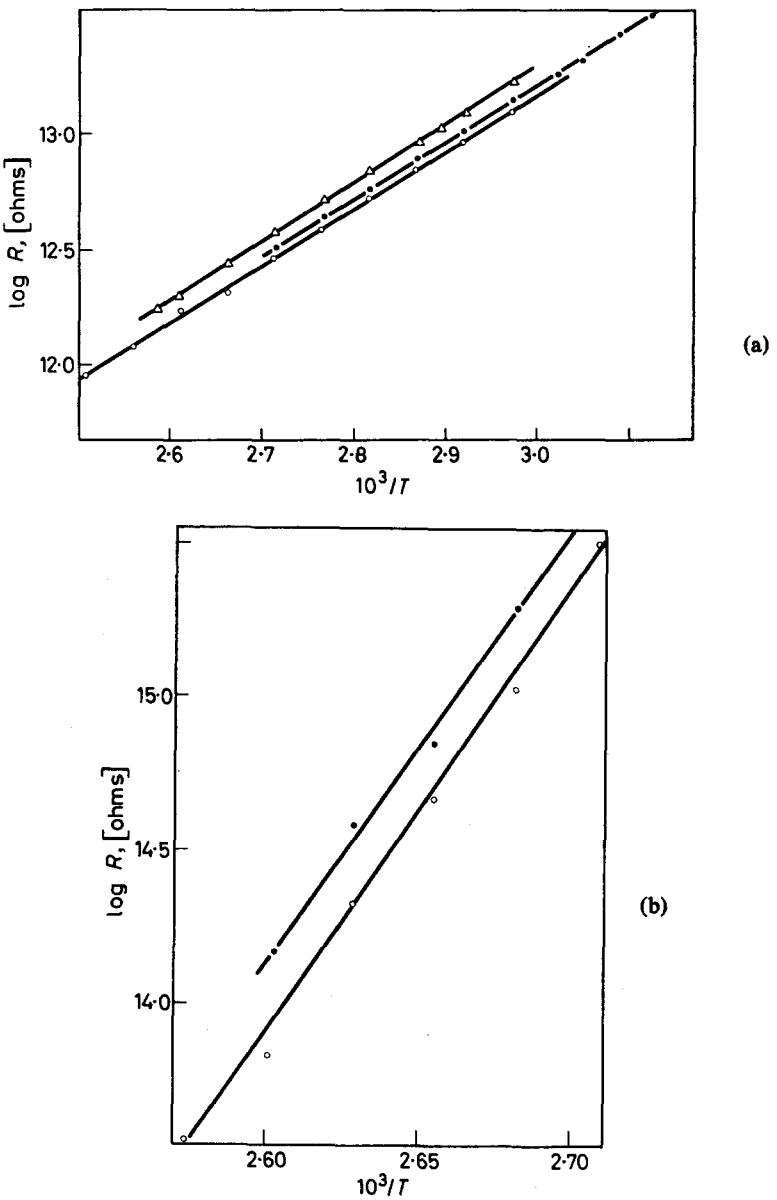

Figure 4—A log R versus $1/T°K$ plot for (a) polybenzone, No. 10, (b) polyphenyl ether, No. 12

that impurity effects play a relatively unimportant role in semiconduction in organic polymers[11, 13]. To make progress we shall assume the $\Delta\epsilon$ value is a true energy gap characteristic of the π-electrons in the polymer. We shall apply the potential-box theory[13, 14] in a modified form. This theory equates the energy gap to the energy required to raise a π-electron from the highest

filled $n/2$th to the lowest empty $(n/2+1)$th level in the molecule, where n is the number of conjugated π-electrons in the molecule. This excitation energy depends upon the value of n, and is lower for a linear or open path molecule, than for a ring or closed path molecule. The electrons so excited

Table 2. Dark conductivity and *e.s.t.* data

			Dark conductivity			*Electron spin resonance*	
No.	*Polymer colour*	$\Delta\epsilon$ *eV*	$\log \rho_{300}$ Ω *cm*	$\log \sigma_0$ Ω^{-1} *cm*$^{-1}$	*Temp. range °C*	*f.s.g.*	ΔH *gauss*
1	Yellow	3·38	20·7	5·1	280–180	—	—
2	Brown*	—	—	—	20–250	$6{\cdot}7\times10^{18}$	11·3
3	Yellow	3·6	22·0	8·7	181–80	$7{\cdot}6\times10^{17}$	13·1
4	Yellow	2·3	19·3	$\bar{1}{\cdot}0$	115–200	$7{\cdot}0\times10^{17}$	14·5
5	Ochre	1·67	15·3	$\bar{2}{\cdot}7$	50–100	$4{\cdot}4\times10^{16}$	9·9
6	Brown	2·3	20·7	$\bar{1}{\cdot}0$	120–200	—	—
7	Buff	2·61	21·6	0·3	144–200	—	—
8	Ochre	2·34	20·6	$\bar{1}{\cdot}0$	—	—	—
9	Ochre	3·6	22·5	7·7	150–180	—	—
10	Black	1·09	14·3	$\bar{5}{\cdot}0$	50–180	$2{\cdot}0\times10^{18}$	13·0
11	Black	0·92	10·5	$\bar{3}{\cdot}2$	50–100	$7{\cdot}6\times10^{18}$	7·2
12	Buff	6·0	25·5	24·9	97–115	$3{\cdot}0\times10^{16}$	3·8
13	White	1·72	17·4	$\bar{2}{\cdot}1$	140–200	10^{15}	—
14	Black	2·35	14·0	5·7	50–125	10^{15}	—
15	White	2·75	20·6	2·6	150–235	—	—
16	Grey	2·45	22·5	$\bar{3}{\cdot}8$	144–200	—	—
17	White	4·1	29·7	4·1	240–290	—	—
18	Black†	—	—	—	—	—	—
	(Terphenyl m.pt 213°C) Quaterphenyl m.pt 316°C	—	$>10^{16}\,\Omega$ at 400°K $>10^{16}\,\Omega$ at 500°K	—	—	—	—

*$\rho > 10^{14\cdot5}\Omega$ at 420°K.
†Part sublimed at 100°C.

in the $(n/2+1)$th level, and the holes in the $n/2$th level, are regarded as being able to tunnel with a certain probability through to neighbouring molecules under the influence of the potential gradient, and hence through the crystal, or in this case amorphous specimen. From the dimensions of the barrier and other parameters a mobility term may be determined[14].

To apply this treatment to the present polymers we shall regard n as the number of π-electrons in the monomer units, and thereafter discuss deviations from the expected $\Delta\epsilon$ values in terms of a conjugation or hyperconjugation passing across the bridging groups, —CH_2—, —C=O, etc. This effect was called eka-conjugation by Pohl[12]. We shall see that this method gives a rational account of many of the results, which in itself supports the basic idea of an essentially intrinsic semiconduction.

The free electron spins are probably to be associated with broken C—H and C—C bonds arising during preparation, perhaps by atmospheric oxidation. Clearly they cannot arise from thermal excitation of the π-electron structure as this would imply that a high $\Delta\epsilon$ value would be associated with a low f.s.g. and no such correlation is apparent over the range of different

polymers. The question of free spins in aromatic type molecules will be discussed elsewhere, and there is no evidence that it has any direct bearing on dark conduction in these polymers.

The graphs calculated for the potential-box model are shown in *Figure 5*. It should be pointed out that the $\Delta\epsilon$ values predicted for the closed-path

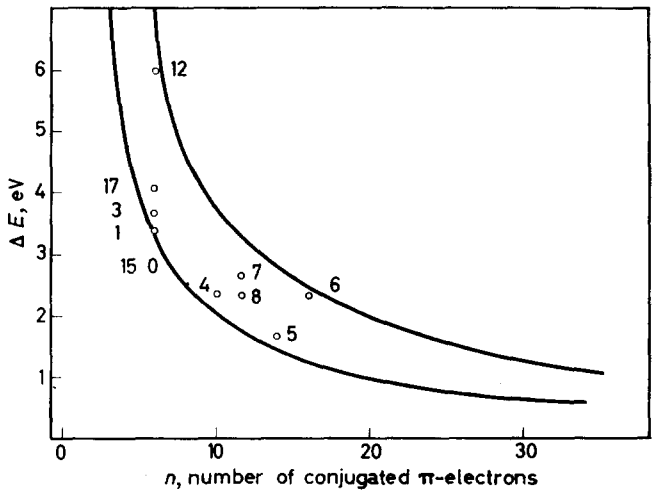

Figure 5—$\Delta\epsilon$ values for polymers with —O—, —CH_2—, and no bridging groups, compared with the free electron model

aromatic molecules given by the upper curve are anthracene ($n=14$) $\Delta\epsilon=2{\cdot}8$ eV, naphthalene ($n=10$) $\Delta\epsilon=3{\cdot}9$ eV, and benzene ($n=6$) $\Delta\epsilon=6{\cdot}5$ eV. In practice lower values are often observed for these molecules, or their derivatives, e.g. 1·7 eV ($n=14$), 2·7 eV ($n=10$) and 4·2 eV ($n=6$), and these values have been associated with a surface conductivity, since with single crystals the conduction is eliminated by a guard ring[16]. Taking a typical mobility value of $\mu=1$ cm^2 V^{-1} s^{-1}, and using the band theory equation $\sigma_{400}=4\exp(-\Delta\epsilon/2k\,400)$, then the maximum value of $\Delta\epsilon$ measurable at 400°K is 2·5 eV (corresponding to 10^{-15} ohm^{-1} cm^{-1})[16]. Recent evidence definitely favours high $\Delta\epsilon$ values, viz. 2·8 eV[17], and 4 eV[18] and 3·7 eV[19] for the energy gap in anthracene. In the present experiments guard rings were not used, and they can never eliminate surface conduction with compressed discs. The possible presence of surface conduction therefore remains an undetermined factor in these experiments.

Size of aromatic groups

With the exception of polymer 16, the methylene tetramethyl benzene polymer, the ten polymers with —CH_2— and —O— bridging groups lie between the two theoretical curves for the open and closed paths as shown in *Figure 6*. In this graph we take as n the value for the largest monomer, which is that with the lowest optical excitation energy, and treat diphenyl as completely conjugated with 12 π-electrons. However, five of these polymers lie near the lower limit, i.e. the curve for the open path. We are in-

clined to suggest that a surface conduction mechanism is operative for these latter five polymers. Polymer 10, the anthracene polymer, $\Delta\epsilon = 1{\cdot}67$ eV ($\log \sigma_0 = 2{\cdot}7$) gives values closely similar to those of anthracene powder, 1·65 eV (2·5)[20], single crystals 1·65 eV (0·3)[21] and 1·5 eV[22], and film 1·93 eV (2·3)[23], which fall into the class of low values attributed to surface conductivity. An alternative possibility is that some conjugation extends through the polymer across bridging CH_2 groups in the anthracene monomer.

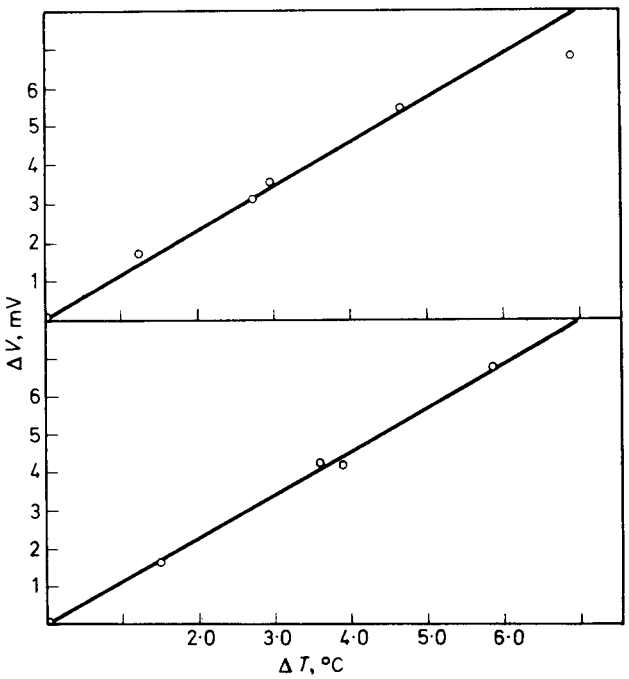

Figure 6—Seebeck voltage as a function of temperature difference ΔT, for average temperatures of 340·3° and 396·6°K. The polymer is polybenzimide, No. 11

We attribute conduction in polymer 6, the phenylene–pyrene copolymer, to pyrene, $n = 16$. Here again, the polymer results, $\Delta\epsilon = 2{\cdot}3$ eV ($\log \sigma_0 = \bar{1}{\cdot}1$) is fairly similar to results on the monomer, viz. evaporated films, 2·40 eV (3·0)[22] and single crystals 2·0 eV ($\bar{1}{\cdot}0$)[24].

With polymer 10 it is possible that hyperconjugation of the four methyl groups might raise n from 6 to 10.

The ether group would appear to 'insulate' neighbouring monomer groups, as in polymer 12, polyoxyphenylene, with $\Delta\epsilon = 6{\cdot}0$ eV, while —CH_2— bridges in polymer 3 allow a certain hyperconjugation since $\Delta\epsilon = 3{\cdot}6$ eV. In polyphenylene, No. 1, $\Delta\epsilon = 3{\cdot}38$ eV and presumably quinonoid forms allow resonance interaction along the whole chain. In this event we should expect $\Delta\epsilon$ to increase with chain length, and the polyphenylene measured had an average chain length of perhaps ten units. In support of

this view terphenyl and quaterphenyl showed immeasurably high resistivities at the highest possible temperatures, also *m*-polyphenylene, where extensive quinonoid resonance is impossible.

Polymers 10, 11, 13 and 14 allow a comparison of the effect of bridging groups, CO, NH, AsPh and AsO(OH) on the conjugation between phenylene groups as manifested in the lowering of $\Delta\epsilon$. The $\Delta\epsilon$ values are respectively 1·09, 0·92, 1·72 and 2·35 eV, as compared with polymer 10 with O as bridging group where $\Delta\epsilon = 6{\cdot}0$ eV. The possibilities for π-electron conjugation through these bridges clearly exist, and the effects on $\Delta\epsilon$ are quite marked. as also on the colour, all the polymers being black, indicative of easy excitation of the optical electron, except rather surprisingly polymer 13, with $\Delta\epsilon = 1{\cdot}72$ eV which is white. It is of interest that the possibilities of conjugation through C=O and NH groups have been considered in biological polymers, and the present results suggest the groups are certainly active in this respect.

Band theory for an intrinsic semiconductor gives, at room temperature, $\sigma_0 \simeq 4\mu$, where μ is the average mobility of the charge carriers, which may lie in the range 10^{-5} to 10^{3} $cm^2 V^{-1} s^{-1}$. Clearly in about half the polymers in *Table 2*, the σ_ps observed correspond to reasonable values of μ. Later on an accurate value of average mobility of $3{\cdot}8 \times 10^{-4}$ $cm^2 V^{-1} s^{-1}$ is determined for polybenzene imide No. 11. This compares very well with the value of $\sigma_0/4$. The most notable exception is polymer 12, with $\Delta\epsilon = 6{\cdot}0$ eV and $\log \sigma_0 = 24{\cdot}9$. Clearly no explanation can be forthcoming from band theory mobilities for such very high values of σ_0, which we now regard as arising from an electrode injection mechanism with a temperature-variable activation energy[25].

There does not appear to be any regular correlation between colour and conductivity, although if the latter were simply a matter of molecular excitation energy, the black polymers would have the lowest $\Delta\epsilon$. There are obvious exceptions in *Table 2*, such as polymer 13 which has a fairly low $\Delta\epsilon$ value, although it is white.

Electrode and polarization effects

A wide range of electrodes was tested; nickel, aluminium, copper, silver, platinum and graphite showed ohmic as opposed to rectifying behaviour. Generally, platinum electrodes were used in all the work described here. However, polarization phenomena, i.e. an increase in resistance with time to a steady value, following switching on of the applied voltage, as in *Figure 9*, was found for polymers 10, 12, 15 and 16. In polybenzone, No. 10, where the effect was most marked, true equilibrium values were only reached after 24 hours. For routine investigations, all resistance values were recorded 30 minutes after a change of voltage, partially to allow for polarization effects, and this technique gave good reproducibility in both temperature coefficient (*Figure 4*) and Ohm's law (*Figure 7*) experiments. We later note the very definite Seebeck coefficient evidence for electronic conductivity in polybenzone, so ionic effects cannot be invoked to explain the observed polarization. Also, the cell plus sample had a low capacity and therefore a short time constant. It seems possible that the effects in

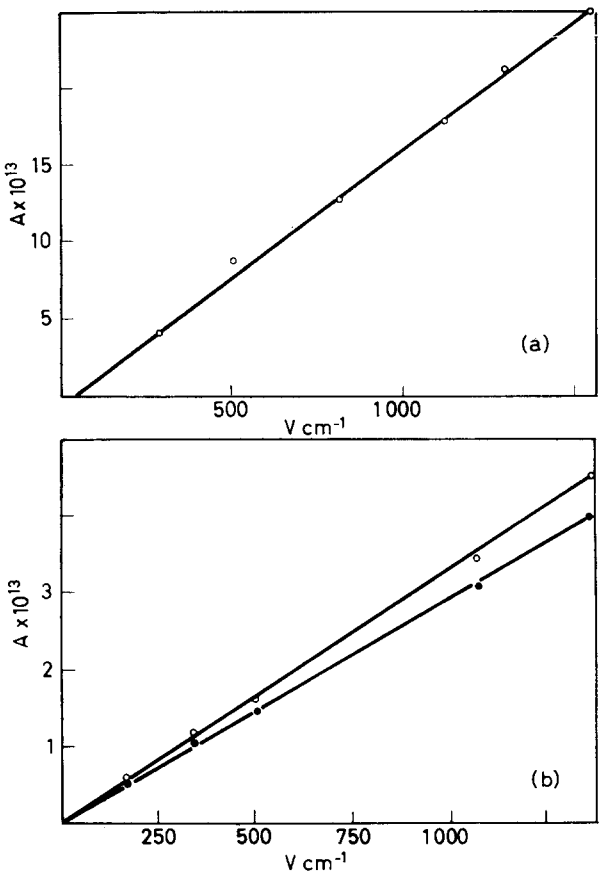

Figure 7—Ohmic plots for (a) a high energy gap polymer (polymer 12) at 110°C and (b) a low energy gap polymer (polymer 10) at 215°C. The effect of time on taking the current reading is shown

polymers 10 and 15 may arise from space-charge build-up occurring as a rate determining step in the specimen.

In polymer 16 there is the prospect of thermal breakage of C—Br bonds, and a conduction process involving halogen ions, similar to that postulated for phosphonitrilic chloride. Such ionic mechanisms usually give rise to time-dependent polarization effects[36].

Ohmic behaviour

Most of the polymers showed Ohm's law behaviour up to a well-defined voltage: the first deviations from a straight line relation between current (measured after 30 minutes, see above) and applied voltage are noted as follows: polymer 4, 600 V cm^{-1}, polymer 5, $>$ 1 000 V cm^{-1}, polymer 8, $>$ 2 500 V cm^{-1}, polymer 12, $>$ 1 500 V cm^{-1}, polymer 11, 2 500 V cm^{-1}, polymer 9, $>$ 500 V cm^{-1}, polymer 15, 1 000 V cm^{-1}. The inequality sign

indicates that no deviations were observed up to the highest voltage examined, which is that quoted. An example is shown in *Figure 7*. Departures from Ohm's law are probably to be associated with a barrier set up at the electrode/polymer interface.

Thermoelectric measurements

The measurements were restricted to the four polymers 5, 10, 11 and 14, and for these a positive value was found for the sign of the Seebeck coefficient Q, indicative of positive holes as the majority charge carrier. Only in the phenylene imide polymer, No. 11, was the resistance low enough to permit a determination of *accurate* values of Q. *Figure 6* shows that for four different average temperatures the Seebeck voltage ΔV was linear against the temperature gradient across the sample. Assuming band theory, ratio $c=\mu_e/\mu_h$ of mobilities of electron to hole is given by the equation[27]

$$\Delta V/\Delta T=Q=-[\{k(c-1)\}/\{e(c+1)\}]\,[\Delta\epsilon/2kT+2]\ V\ \text{deg}^{-1}$$

Combining this with the specific conductivity

$$\sigma=en(\mu_e+\mu_h)=en\mu_h(1+c)$$

it is possible to calculate values of μ_e and μ_h for a two-carrier process, calculating n from band theory with the assumption that the effective mass of both charge carriers is equated to the rest mass of the electron. The results for polymer 11 are shown in *Table 3*.

Table 3. Seebeck coefficients and mobilities for polymer 11

Mean temp. °K	$Q=\Delta V/\Delta T$ *mV deg*$^{-1}$	*Carrier conc.* *cm*$^{-3}$	c	$10^4\mu_h$ *cm*^{2} *V*$^{-1}$ *sec*$^{-1}$	$10^4\mu_e$ *cm*^{2} *V*$^{-1}$ *sec*$^{-1}$
293·3	1·23	2×10^{11}	0·28	5·78	1·62
340·3	1·19	$5{\cdot}1\times10^{12}$	0·14	3·11	0·44
356·6	1·19	1×10^{13}	0·12	4·34	0·52
396·6	1·12	5×10^{13}	0·12	4·00	0·44

Values of Q as high as those found here, 1 mV deg^{-1}, are only matched by those found for charge transfer complexes[28], and clearly indicate an electronic rather than an ionic conduction mechanism. The temperature coefficient $dQ/dT\simeq-1\ \mu$V deg^{-2}, which is identical with the value found for low resistance PAQR polymers[29].

Compaction pressure

Discs of polybenzone, No. 10, were compacted at pressures from 750 to 10^4 kg cm^{-2}. The results are shown in *Figure 8* and *Table 4*.

Table 4. Effect of compaction pressure on polybenzone discs

Compaction pressure (*kg cm*$^{-2}$)	log ρ_{300} (Ω *cm*)	$\Delta\epsilon$ (*eV*)	log σ_0 (Ω^{-1} *cm*$^{-1}$)	*Voltage gradient* (*V cm*$^{-1}$)
760	15·7	1·39	−4·0	387·5
1 540	15·7	1·30	−4·8	533
2 300	15·8	1·32	−4·8	548
10 000	16·0	1·32	−4·8	604

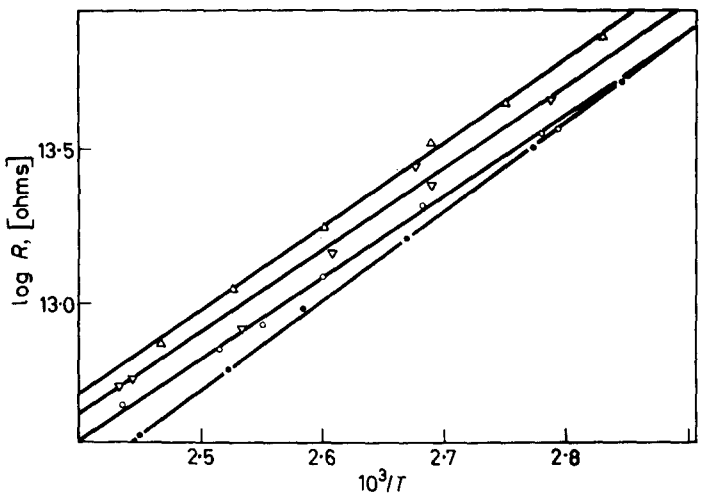

Figure 8—Effect of pressing discs of polybenzone, No. 10, at successively increasing pressures, from first, 750 kg cm^{-2} (●) through second (○), third (▽) to fourth compression at 10 000 kg cm^{-2} (△)

Clearly, compaction pressure has little effect on the results, in agreement with other workers. The sample of polybenzone used here was probably of lower molecular weight than the sample of *Table 2*, which explains the higher $\Delta\epsilon$ value observed. The $\Delta\epsilon$ for this specimen, however, is still much less than that found for polybenzyl, No. 3.

Effects of adsorbed gases

As shown in *Figures 4* (a) and (b), the gases hydrogen, oxygen and nitrogen were without any appreciable effect on the conductivity of a compressed

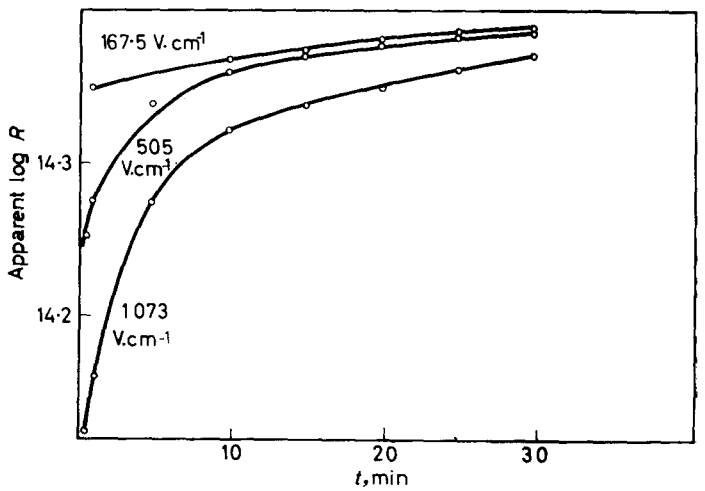

Figure 9—Increase in resistance with time for polybenzone, No. 10, for three applied voltages. All three curves tend to log R=14·46 after two hours

disc of polybenzone, No. 10, and polyphenyl ether, No. 12. However, boron trifluoride gas was absorbed to the extent of 6·8 wt % in five hours at room temperature by a disc of polybenzone. This ratio corresponds roughly to one BF_3 to ten CO groups in the polymer. During the adsorption process the resistance of the disc initially fell from 10^{14} to 10^{8} Ω, which supports positive hole conduction in this polymer, since boron trifluoride is an electron acceptor. On heating the disc to 100°C *in vacuo* and recooling, the original 10^{14} Ω was regained. Clearly, only strongly chemisorbed gases have any influence on conduction in this polymer.

Qualitative observations were carried out on polymers 1 and 11. Large and rapidly responding photocurrents, respectively 10^{-13} and 10^{-11} A, were found which provide further evidence for electron transport in phenylene polymers.

Chemistry Department,
University of Nottingham

(Received May 1967)

REFERENCES

[1] POHL, H. A. *Modern Aspects of the Vitreous State* (ed. J. M. MACKENZIE), Vol. II, p 72. Butterworths: London, 1962
[2] BERLIN, A. A. *J. Polym. Sci.* 1961, **55,** 621
[3] CHYNOWETH, A. G. and SCHNEIDER, W. G. *J. chem. Phys.* 1954, **22,** 1021
[4] GOLDEN, J. H. *J. chem. Soc.* **1961,** 1604 and 3741
[5] GOLDEN, J. H. *Soc. Chem. Industr. Monogr. No. 13,* p 231
[6] HOBIN, T. P. *Soc. Chem. Industr. Monogr. No. 13,* p 303
[7] GILLAM, A. E. and HEY, D. H. *J. chem. Soc.* **1939,** 1176
[8] GOLDFINGER, G. *J. Polym. Sci.* 1949, **4,** 93
[9] PICKETT, L. V. *J. Amer. chem. Soc.* 1936, **58,** 2299
[10] PAULING, L. and SHERMAN, J. *J. chem. Phys.* 1933, **1,** 679
[11] BROWN, C. J. and FARTHING, A. C. *J. chem. Soc.* **1953,** 3270
[12] POHL, H. A. *Electronic Aspects of Biochemistry* (ed. B. PULLMANN), p 121. (Ravello Conference 1963.) Academic Press: New York, 1964
[13] ELEY, D. D. and PARFITT, G. D. *Trans. Faraday Soc.* 1955, **51,** 1529
[14] ELEY, D. D. and WILLIS, M. R. *Electronic Conduction in Organic Compounds* (Duke University Conference, 1960) (ed. H. KALLMANN and M. SILVER), p 257. Interscience: New York, 1961
[15] POHL, H. A. and ENGLEHARDT, H. *J. phys. Chem.* 1962, **66,** 2085
[16] ELEY, D. D., FAWCETT, A. S. and WILLIS, M. R. *Nature, Lond.* 1963, **200,** 255
[17] NAKADA, I., ARIGA, K. and ICHIMIYA, A. *J. phys. Soc. Japan,* 1964, **19,** 1587
[18] CASTRO, G. and HORNIG, J. F. *J. chem. Phys.* 1965, **42,** 1459
[19] POPE, M. *Scientific American,* January 1967, 86
[20] ELEY, D. D., PARFITT, G. D., PERRY, M. J. and TAYSUM, D. H. *Trans. Faraday Soc.* 1953, **49,** 79
[21] METTE, H. and PICK, H. *Z. Phys.* 1953, **134,** 566
[22] RIEHL, N. *J. phys. Chem. U.S.S.R.* 1955, **29,** 959
[23] NORTHROP, D. C. and SIMPSON, O. *Proc. Roy. Soc. A,* 1956, **234,** 136
[24] INOKUCHI, H. *Bull. chem. Soc. Japan,* 1956, **29,** 131
[25] ELEY, D. D. 'Symposium on Electrical Conduction Properties of Polymers', *J. Polym. Sci. C,* 1967 (No. 17), 73
[26] ELEY, D. D. and WILLIS, M. R. *J. chem. Soc.* 1963, **289,** 1534
[27] JOHNSON, V. A. and LARK-HOROVITZ, K. *Phys. Rev.* 1953, **92** (2), 226
[28] LABES, M. M., SEHR, R. and BOSE, M. *J. chem. Phys.* 1960, **32,** 1570
[29] POHL, H. A. and ENGELHARDT, H. *J. chem. Phys.* 1962, **66,** 2085

Communication

Characterization of Unloaded Crosslinked Polyethylene

The state of cure of low density crosslinked polyethylene, measured by solvent extraction as a function of the peroxide level, was found to be dependent on the melt flow index. A simple and rapid flow test was found to be sensitive to the degree of crosslinking and applicable for quality-control purposes.

CROSSLINKED polyethylene is a rather new polymer with certain advantages compared with the conventional thermoplastic polyethylene. Controlled crosslinking of the latter with the aid of suitable peroxides results in a thermoset resin with improved resistance to heat, stress cracking and creep. Additional effort is called for in the field of characterization and quality control of crosslinked polyethylene.

The most important test for the end product is its state of cure, for which purpose several tests were developed[1–4]. The solvent-extraction method[1] is well known as an appropriate and significant test for determining the degree of crosslinking. Its only drawback is that it is too slow, so that it cannot be used for quality-control purposes; however, any proposed new method for the state of cure had better be evaluated on the basis of comparison with solvent extraction data. As mechanical properties at room temperature are not sensitive enough to the state of cure, the 'hot modulus' test, referring to temperature above the crystalline melting point, was proposed. The dependence of the hot modulus on percentage solvent-extraction is rather close, so that this parameter is a good criterion for the degree of cure[2]. In the present communication a simple and rapid flow measurement as a control mean for the state of cure is described.

EXPERIMENTAL

Three low-density polyethylenes with melt flow indices of 0·3, 2 and 7 g/10 min were tested. Each polyethylene was ground to powdery form and the powder was thoroughly mixed at room temperature with known amounts of Varox peroxide (50 per cent active). 30 g of this mixture was placed in the roller measuring head of a Brabender Plasticorder (model PL 3S), which was kept at 75°C during the feeding stage and then closed, after which mixing at 20 rev/min and hot-oil circulation were started. All experiments were carried out at a bath temperature of 190°C. The temperature of the sheared polymer and the torque were recorded as functions of time.

At the end of the experiment the crosslinked polymer was removed and re-ground, and the powder was analysed by two methods:

(a) Solvent extraction, using boiling toluene;
(b) Flow test. The Atkinson Nancarrow Rheometer (Tensometer Ltd, England) was fitted with a capillary (2·1 mm diameter, 25·4 mm long) and a temperature of 170°C was maintained. Plunger velocity (12·7 mm diameter) was 14·1 mm/min.

A sample of the ground crosslinked polyethylene was placed in the rheometer reservoir and tested after a residence time of five minutes. The equilibrium load required for forcing the material through the capillary under these conditions was measured.

At a constant bath temperature the maximum torque indicated on the Brabender plastogram decreased with increasing peroxide level. The same behaviour was obtained[5] when the peroxide concentration was kept constant and the bath temperature increased. The maximum torque is thus unsuitable as a criterion for crosslinking efficiency, since the torque increase due to crosslinking is opposed by a grinding process.

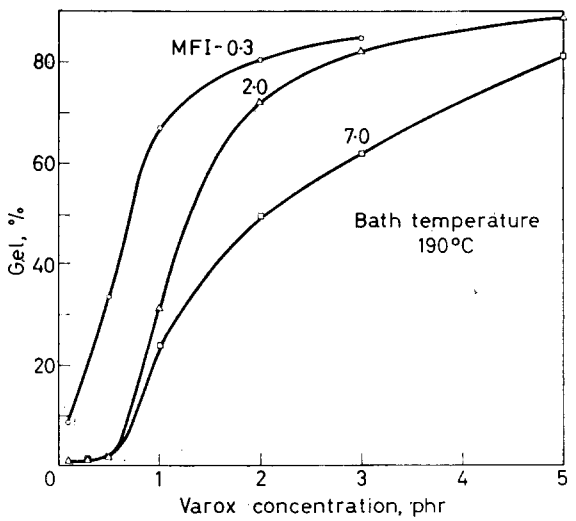

Figure 1—Dependence of gel content on Varox concentration for different low density polyethylene

The mixing time in the measuring head was chosen so as to ensure complete decomposition of the peroxide. The gel content of the samples from the measuring head as a function of the peroxide concentration is shown in *Figure 1* for the three polyethylenes. The gel content increases steeply with the peroxide concentration and for a given level is closely dependent on the melt flow index, or molecular weight. This is in agreement with the work of Carlson[4], who found that the Mooney scorch increased with the melt flow index; accordingly it was stated that resins with high melt index are safer to process, at the same peroxide level (weight basis), than those of low melt index.

If a constant peroxide concentration (p.h.r.) is kept while increasing the molecular weight, i.e. reducing the melt flow index, the number of peroxide molecules available per polyethylene molecule is increased, in other words, non-extractable molecules are formed faster with increasing molecular weight of the original thermoplastic polymer.

According to *Figure 1*, in order to obtain well-cured material[6] (60 to 70% gel content), about 1, 1·7 and 3·2 p.h.r. Varox are required for the polyethylenes with melt flow indices of 0·3, 2 and 7 respectively.

Since crosslinking results in higher resistance to flow, a test of the dependence of flow behaviour on the state of cure was of interest. Since the flow test is simple and rapid and calls for rather inexpensive equipment, sensitive dependence of flow resistance on the state of cure would provide a convenient means of quality control. In the course of the experiments it was found that too narrow capillaries and too high shear rates gave rise to unstable flow. Stable flow was obtained with the equipment described in the experimental part up to about 80 per cent gel content.

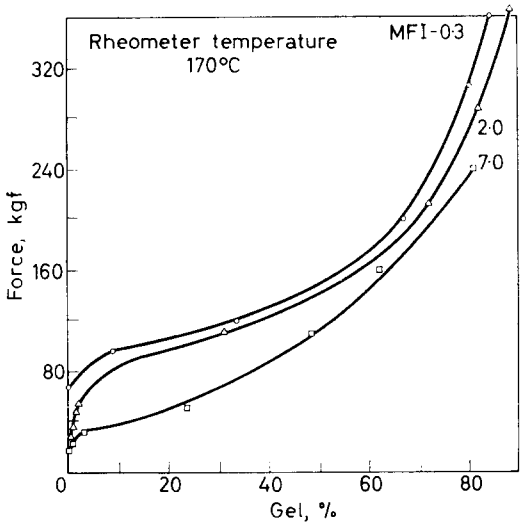

Figure 2—Dependence of extrusion force on gel content for different low density polyethylene

In *Figure 2* the dependence of the equilibrium force on the gel content is shown for the three polyethylenes tested. The equilibrium force appears to be a sensitive function of state of cure. This force is also a function of melt flow index, so that calibration curves are required for each polymer.

The curves shown in *Figure 2* cover the whole practical range of crosslinking degree and therefore can be used as a sensitive means of quality control. In order to prevent changes in the polymer during the flow test, a rheometer temperature of 170°C was chosen, namely 20 deg. C below the crosslinking temperature. In addition, the residence time in the rheometer is much shorter than the crosslinking time.

In conclusion the melt viscometer working under suitable conditions is a useful, sensitive and rapid tool for characterizing the state of cure of crosslinked unloaded low density polyethylenes.

JOSEPH MILTZ and MOSHE NARKIS

Department of Chemical Engineering,
Technion—Israel Institute of Technology,
Haifa, Israel

(Received October 1967)

REFERENCES

[1] 'Cure testing of vulcanized polyethylene', *Kabelitems No. 128*, Union Carbide, 1964
[2] MARTENS, S. C. 'Evaluating chemically crosslinked polyethylenes', *Twelfth Annual Symposium, Technical Progress in Communication Wires and Cables*, New Jersey, December 1963
[3] BOONSTRA, B. B. and JERMYN, T. E. *S.P.E. Jnl*, 1962, **18**, 315
[4] CARLSON, B. C. *Rubb. World*, 1960, **91**, 142
[5] NARKIS, M. and MILTZ, J. 'Brabender Plasticorder studies of the process of cross-linking polyethylene', *J. Appl. Polym. Sci.* In press
[6] BENNING, C. J., GREGORIAN, R. S., KIRK, C. C. and WERBER, F. X. *Mod. Plast.* 1966, **44** (4), 131

ANNOUNCEMENT

UNIVERSITY OF BRADFORD
SCHOOL OF POLYMER SCIENCE

A course on 'Time-dependent effects in polymeric systems' will be held on 10 and 11 May 1968.

Papers will include a general introduction, viscoelasticity, creep, dynamic properties of polymers, flow behaviour of polymer melts and the flow behaviour of PVC–plasticizer systems. Fee for the course is £5.0.0.

Further details and forms of application may be obtained from The Registrar, University of Bradford, Bradford, 7.

Annealing of Polyethylene Single Crystals

HIROSHI NAGAI and NAOHARU KAJIKAWA*

Annealing of polyethylene single crystals in a temperature range of between 90° and 110°C has been studied by electron microscopy. Under the conditions employed, single crystals exhibited various aspects of transformed morphology without appreciable changes in their long periods. Morphological transformation is described in terms of 'stage', which is tentatively defined as the extent of annealing by the characteristics developed in morphology. Selective transformation was observed in the {100} sectors of specimens crystallized in different ways. It was found that each sector begins its transformation at a temperature characteristic for that sector. Molecular tilt around the b-axis was observed below 110°C. Lamellar thickening was found at temperatures higher than 110°C, while the orientation of crystallographic axes became random in the temperature range of interest. On the other hand, morphological change took place at all temperatures depending on the annealing temperature and time.

CONSIDERABLE research[1] has been done on the annealing behaviour of polyethylene (PE) single crystals. During the annealing process, two mutually independent mechanisms were observed, one concerned with lamellar thickening along the chain axis[2] and the other with tilting of the molecular chain around the *b*-axis[3]. Many workers have attempted to elucidate lamellar thickening from the theoretical and experimental points of view.

Recently, Takayanagi and Nagatoshi[4] reported that PE single crystals thicken through two different mechanisms corresponding to different ranges of annealing temperature; one above 120° to 124°C and the other below this temperature range. Thickening above 124°C was explained by the theory of crystallization kinetics from the melt[5], while below 120°C the migrational motion of molecules along the chain axis[6] was proposed.

More recently, Mandelkern and Allou[7], working on DSC measurement, reported that the heat evolution observed is always preceded by a process of heat absorption, and concluded that it is not necessary to divide the temperature region into two parts, each part having a different mechanism.

Our principal objective is to describe the morphological transformation process under heat treatment and to obtain some information to elucidate the mechanisms of lamellar thickening and tilting of the molecular chains from the morphological point of view.

EXPERIMENTAL

Preparation of single crystals

Unless otherwise stated, a fractionated Marlex 6009 PE sample having a viscosity average molecular weight of 130 000 was used. Crystallization

*Present address: Department of Chemistry, Faculty of Science, Tokyo College of Science, Kagurasaka, Shinjuku-ku, Tokyo, Japan.

from dilute solution (0·05 per cent, w/v) was conducted as follows. The polymer sample was dissolved in boiling solvent and immersed in a silicone oil bath that had been thermostatically controlled at a given crystallization temperature (T_c).

Before preparation of the sample, the decrease in temperature to T_c of the boiling solutions in the bath was noted, and the time to first appearance of crystals was measured by the visual observation of turbidity. According to the results of these preliminary experiments, it is confirmed that the crystallization procedures used here are 'isothermal' unless the values of T_c are lower than 83°C. One of the results is shown in *Figure 1*.

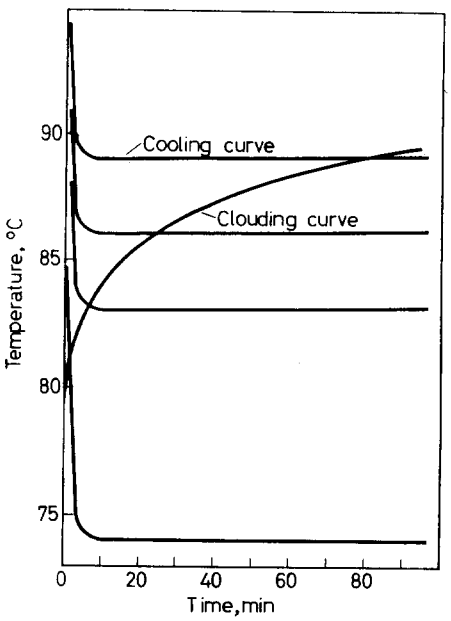

Figure 1—Identification of isothermal crystallization. Cooling curve represents the decrease in temperature of boiling xylene in a controlled oil bath at a given crystallization temperature (T_c). Clouding curve shows the waiting time for the first appearance of crystals from visual observation of turbidity. If the clouding curve crosses the cooling curve of a given T_c at plateau, the crystallization procedure is isothermal at that temperature

After the crystallization time (t_c) which affects the morphology and amount of imperfection in lamellar crystals[8], the suspension was gradually cooled to room temperature fo.· a night. The crystallization conditions used are summarized in *Table 1*.

Table 1. Conditions for the crystallization of single crystals

Sample	*Solvent*	*Concentration per cent w/v*	*Crystallization*	
			Temp. °C	*Time, min.*
Xy–87	Xylene	0·05	87	1000
Cl–86	Cl–ϕ	0·05	86	1000

A part of the crystal suspension was used to observe the morphological changes due to annealing, and the rest to evaluate thickening behaviour by means of small angle X-ray scattering.

Electron microscope observations

The crystal suspension was sprayed on to the collodion-coated meshes and allowed to dry in air or in a vacuum. Annealing was then carried out in the air bath which was controlled thermostatically to within ± 2 deg. C for a given annealing time (t_a). Single crystals on the meshes were subsequently shadowed with germanium at an angle of $\tan^{-1}(1/3)$. A Hitachi HU-10 electron microscope was used.

Small angle X-ray measurement

The crystals were filtered slowly to form oriented crystal mats in which the lamellae of the individual crystals lie essentially in the plane of the specimens. To evaluate the variation in fold period with annealing, X-ray small angle measurement was carried out at the annealing temperature (T_a) by a counter method using $2d\theta = n\lambda$.

RESULTS AND DISCUSSION

Morphology of as-crystallized single crystals

Single crystals crystallized in xylene at 87°C and in monochlorobenzene at 86°C, hereafter referred to as Xy-87 and Cl-86, respectively, are both found to exhibit truncated lozenges with hollow pyramidal form as shown in *Figures 2* and *3*. The scale bar included in illustrations in this paper

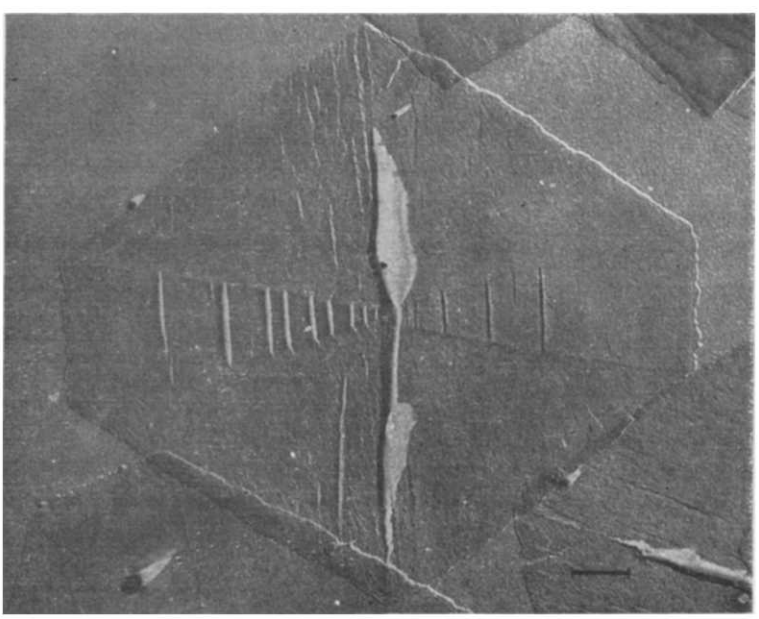

Figure 2—Sample of Xy–87 crystals (annealed at 93°C for 60 min) shows the representative crystalline morphology grown from xylene solution. The striations developed near the sector boundaries between the {110} sectors are only observed for annealed crystals

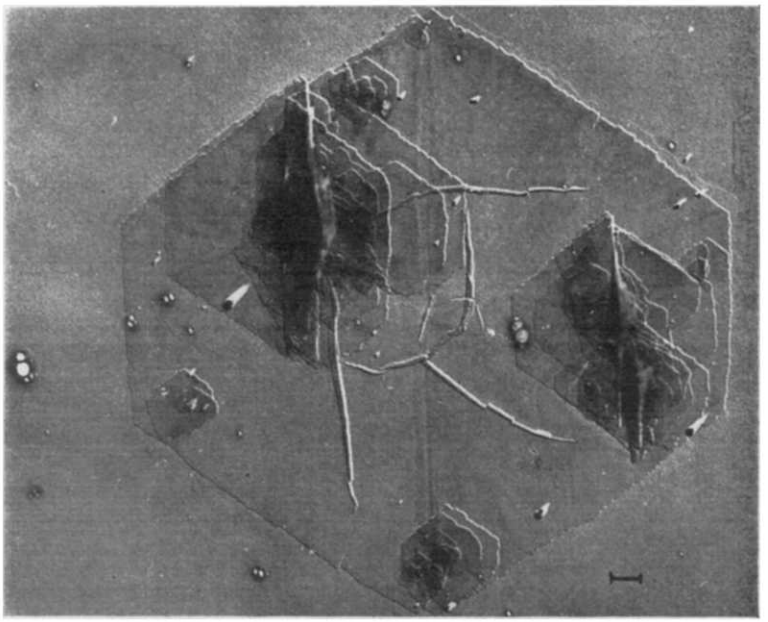

Figure 3—Sample of Cl-86 crystals (annealed at 93°C for 60 min). There are spiral growths near the apices and several ridges approximately parallel to the sector boundaries between the {110} sectors. The observations suggest that the {110} sectors failed to match each other at their boundaries

denotes one micron everywhere. The Xy-87 crystal is similar to those reported in the literature[9], but, by comparison, the Cl-86 crystal shows extensive truncation. Some characteristic features of these two crystals are summarized below.

(*1*) The index of the sector boundary between {110} and {100} fold domains depends[10] on T_c and the solvents. The angle between the sector boundary and the *a*-axis (on the projection of the horizontal plane) for Xy-87 is estimated to be about 13° (the calculated angle is 12° 31′) from which the index of the sector boundary can be deduced as ⟨130⟩. The corresponding value for Cl-86 leads to the index ⟨120⟩. Data are shown in *Table 2* and *Figure 4*, where the results for the single crystal grown from

Table 2. Index of sector boundary for truncated lozenges crystallized in different ways

Crystallization condition		*Angle**		
		Obsd	*Calc.*	*Index*
Xylene	87°C	13°	12°31′	<130>
Cl-ϕ	86°C	20°	18°26′	<120>
Octane	98°C	36–39°	33°40′	<110>

*Angle between sector boundary and the *a*-axis.

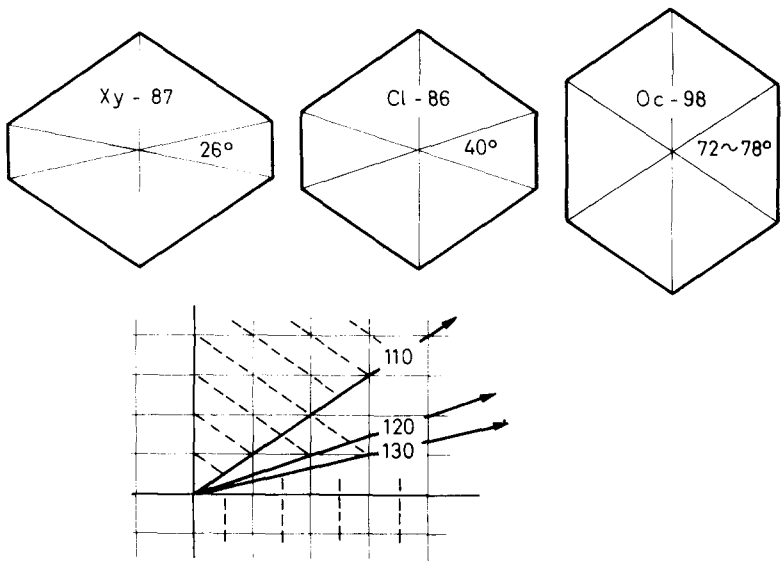

Figure 4—Characteristics of truncated lozenges crystallized in different ways. The number of folded ribbons in each sector is not the same for the truncated crystals except for those grown from octane solution

octane solution are included for reference. The numbers of folded ribbons in sectors of different indices are not equal in the truncated lozenges except for the crystals grown from octane solution. It is expected, therefore, that the regions near the sector boundaries have disordered structure.

(*2*) Ridges, approximately parallel to the sector boundaries between {110} fold domains and the spiral growths near the apex (see *Figure 3*), are frequently observed for Cl-86. The observations suggest that the {110} fold domains fail to match each other at their boundaries because of the non-planar nature of the crystals.

(*3*) During solvent evaporation, Xy-87 collapsed to form central pleats, regular ridges along the *b*-axis in the {100} sectors, and the striations parallel to the ⟨130⟩ or ⟨250⟩ directions in the {110} sectors, while only pleats were observed for Cl-86. Single crystals grown from xylene or octane solution generally show pleats approximately parallel to the *b*-axis. On the contrary, Cl-86 shows pleats having random orientation, as observed in *Figure 3*. The appearance of these pleats must depend on the modes of collapse. For Cl-86, the main factors affecting the appearance of pleats having random orientation must be the shape of the hollow pyramid, the location and size of daughter crystals on the terraces and the rate of solvent evaporation.

General trend of morphological transformation due to annealing

It is well known that the annealing of PE single crystals gives rise to lamellar thickening and the tilting of molecular chains, accompanied by many types of morphological transformations. Some of the foregoing

remarks[3, 6, 11–13] are summarized in *Table 3*. Although these remarks are of value in following the morphological changes due to annealing, complex causal relationships between factors and results make the information rather

Table 3. Remarks on morphological changes due to annealing

Preparation condition	*Annealing condition*	*Remarks on morphological transformation*	*Ref.*
Not given	Not given	The corrugations developed gradually in the *b*-axis direction. They give the impression of a sheared stack of cards	3
Not given	Near 130°C	The {100} sectors in the truncated lozenge melt, or are transformed at a lower temperature than the {110} sectors	13
Gradual cooling of dilute perchlorethylene solution	116°C for 30 min 120°C for 12 h 125°C for 30 min (on glass)	Many holes develop in the region of only a single lamella The smallest crystals underwent recrystallization while the larger ones did not The holes developed in lamellae are larger in regions where the crystal is more than one lamella thick	11
0·02 per cent xylene	120°C for 10 min 130°C for 10 min (on collodion)	A change in outline of crystals occurs with no apparent change in area before hole formation The (100) plane seems to be tilted to the film surface	6
0·1 per cent xylene at 85°C	125°C for 1h (on mylar)	The original linear edge is replaced by an irregular one The holes formed are oriented in a specific direction, and may have a crater-like structure The holes developed in the region where crystals overlapped are not only larger than those in the region consisting of only one lamella but their orientation seems to depend on an interaction between the two lamellae	12

fragmentary. It would be significant here to have a unified and quantitative interpretation of these phenomena. This is attempted by dividing the morphological aspects caused by annealing into five 'stages', in which the extents of changes in apparent characteristics are tentatively defined as follows:

Stage 1—This is defined as the state where the lattice disorder is produced without morphological transformation. One of the examples is shown in *Figure 5*, in which the unusual contrast observed on the terraces implies the lattice disorder produced. Additional evidence is obtained by the disturbance of the Moiré pattern observed in a dark field electron photomicrograph[14].

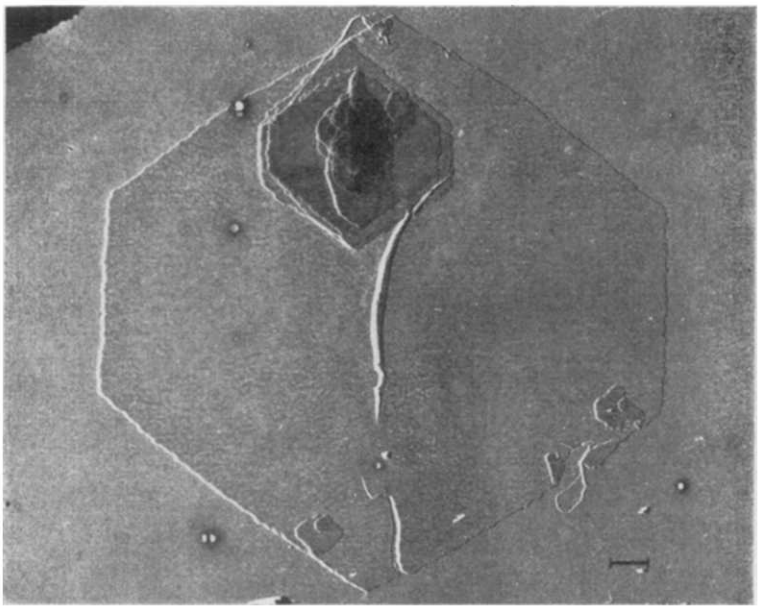

Figure 5—Sample of C1–86 crystals (annealed at 93°C for 60 min). Stage 1: the unusual contrast giving the impression of a pockmark reveals that the crystal lattice is considerably disordered without morphological change

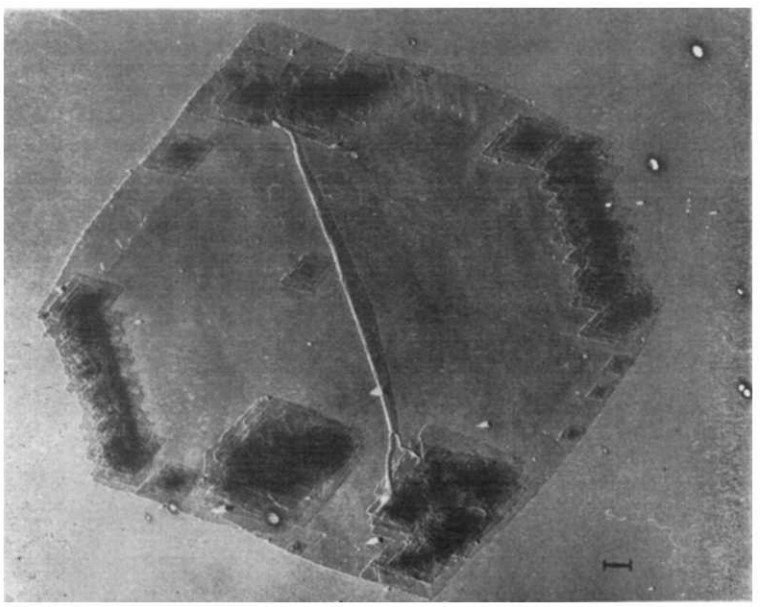

Figure 6—Sample of C1–86 crystals (annealed at 96°C for 10 min). Stage 2: the holes develop only at the thinner contour. Note that the holes develop in the overgrowths. They are observed only in the regions where overgrowths are overlapped by a thinner contour

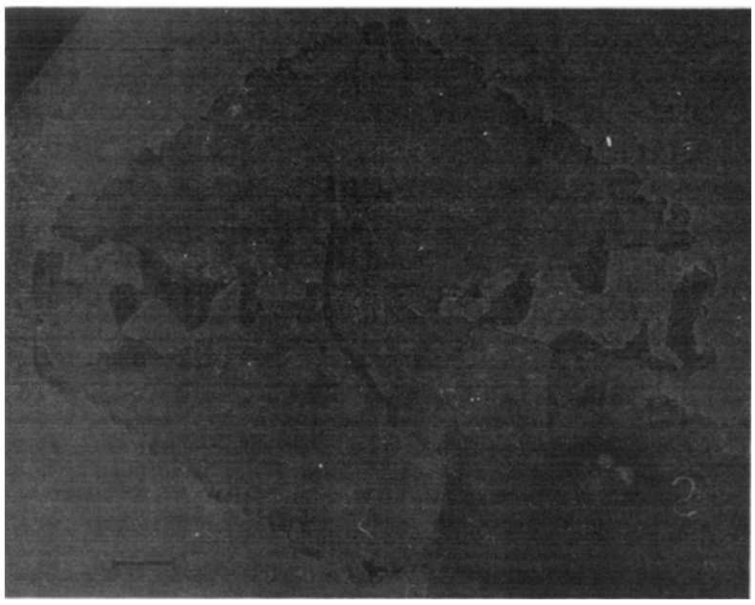

Figure 7—Sample of Xy–87 crystals (annealed at 105°C for 30 min). Stage 3: the {100} fold domains are selectively transformed. Rod-like substances remain behind. The holes that develop concentrate near the sector boundaries between the {110} sectors. The original linear edge is replaced by the thickened irregular one

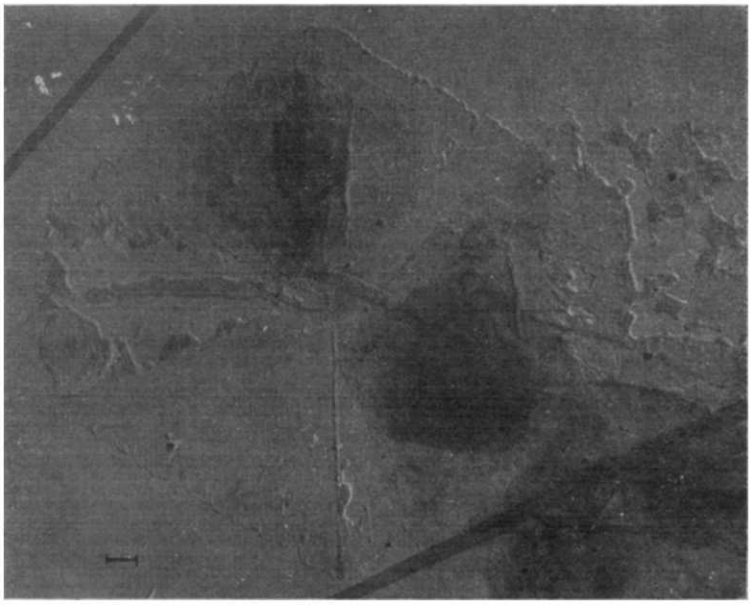

Figure 8—Sample of C1–86 crystals (annealed at 110°C for 20 min). Stage 3: the selective transformation of the {100} sector is one of the characteristic features observed for annealed PE single crystals. The evidence is also observed in the overgrowth

Stage 2—This is where the holes develop in the thinner contour (which grows during the cooling process of crystallization[15]), while there are no apparent changes in the thicker region (which grows during the isothermal crystallization process). The circumstances are clearly observed in *Figure 6*.

Stage 3—Typical examples are shown in *Figures 7* and *8*. The characteristic morphologies that develop at this stage are as follows. The contours (of the thicker terraces in general) are eroded to form irregular thickened edges that give the impression of a sheared stack of cards[3]. Further annealing reveals the distinct difference between the {110} and {100} sectors. The {100} sectors are selectively transformed as reported by Keller and Bassett[13]. The phenomenon is also observed in the daughter crystal as found in *Figure 8*. Small holes appear in the {110} sectors at this stage, and are similar to those reported by Geil[12]. The holes appear close together in the regions near the sector boundaries between the {110} sectors, and appear to be oriented along the ⟨310⟩ or ⟨520⟩ directions. It seems reasonable to correlate the occurrence of holes with the collapse of hollow pyramids because of their location.

Stage 4—This is defined as the intermediate stage between stages 3 and 5. One of the morphological characteristics observed at this stage is the coexistence of the transformed morphology and the unchanged parts of the

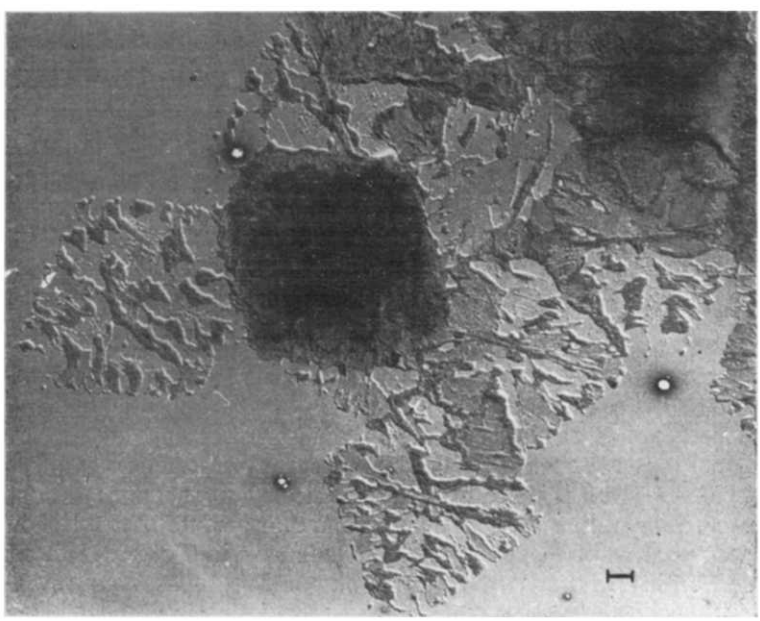

Figure 9—Sample of Xy–87 crystals (annealed at 105°C for 10 min). Stage 4: a morphological characteristic observed at this stage is the coexistence of the transformed morphology and the unchanged parts of the original terraces. The striations observed at the transformed region are oriented approximately parallel to the *b*-axis. Materials transformed resemble a sheared stack of tilted lamellae

original terraces. Progressive transformations are also observed at the holes and the contours eroded. A typical resultant is shown in *Figure 9*.

Stage 5—At this stage of morphological transformation, all crystals show aspects suggesting the occurrence of melt followed by recrystallization, as seen in *Figure 10*. The lamellae originally isolated are replaced by the

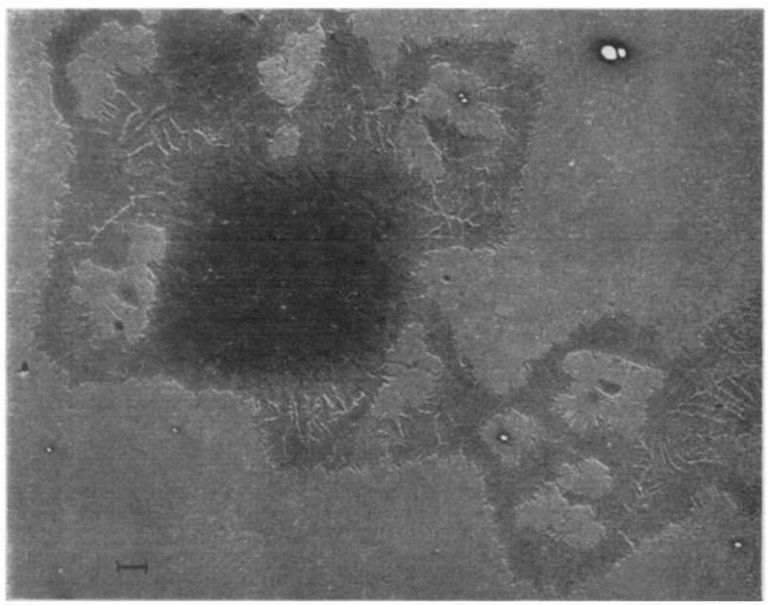

Figure 10—Sample of Xy–87 crystals (annealed at 110°C for 5 min). Stage 5: all of the materials are transformed to the new morphology, depending on annealing temperature and rate of temperature change. The morphological aspect of an isolated lamella is quite different from those observed at the regions consisting of overlapping lamellae

corrugated ones that give the impression of a sheared stack of cards, while the aggregates of single crystals and the regions where daughter crystals were originally located take on a two-dimensional spherulitic appearance in which the lamellae are twisted. The original terraces have disappeared.

In general, it is certain that morphological transformation is affected by many factors. Even if the crystals are subjected to the same history with respect to preparation and annealing conditions, none of them shows the same appearance of morphology. The summary in *Table 4* is a random selection from hundreds of electron photomicrographs, and reveals the relationship between morphological transformation and annealing conditions.

Effects of annealing on lamellar thickness

A decrease in long period has been observed[16] in the temperature range 95° to 125°C for specimens crystallized at 85° to 90°C in dilute xylene

Table 4. Relationship between 'stage' and annealing conditions

Annealing condition		*Cl-86*		*Xy-87*	
T_a(°C)	t_a(min)	*Dried in vacuum*	*Dried in air*	*Dried in vacuum*	*Dried in air*
90	30	1,2	1	1	1
90	120	1	1	1,2	–
93	60	1,2	1,2	2	1,2
93	150	1,2	1,2	1,2	1,2
96	10	2	2	1,2	1,2
96	120	2	1,2	–	–
100	10	1	1,2	–	–
100	30	1,2	1,2	1,2	–
105	10	1,2	1,2	5	2,3,4
105	30	1,2	1,2	1,2,3,4	1,2,3,4
105	120	1,2	1,2	4,5	3,4
110	5	2	2	5	4,5
110	20	2	3,4	5	4,5
110	60	4,5	5	5	5

solution, corresponding to crystals having a lamellar thickness of more than 120 Å. This reduction has been explained by assuming an increased molecular tilt within the crystal lamellae instead of a decrease in fold length. Additional evidence on the decrease in long period was found when long period was measured at room temperature immediately after the measurement at T_a. *Figure 11* shows an example[17]. As the specimens were crystallized at 60°C, the onset of lamellar thickening was found at about 90°C, which is considerably lower than those observed for Cl-86 and Xy-87. The

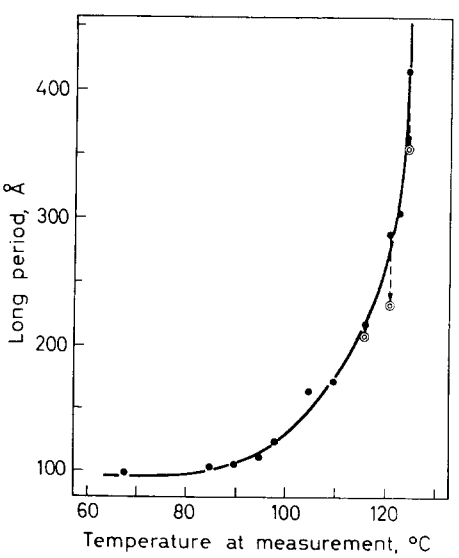

Figure 11—Dependence of X-ray long period on temperature. Long period measured at: (●) each annealing temperature; (○) room temperature. Arrows indicate decrease in long period on cooling the sample to room temperature

decrease in long period is only a few Ångström units for the specimens annealed at 115°C, but is greater for those annealed at higher temperatures. Under the annealing conditions employed here, however, such evidence was not found for specimens crystallized at 86°C and having a lamellar thickness of 133 Å.

The annealing temperature corresponding to the onset of increase in lamellar thickness is about 110°C[2,11,18]. The temperature, however, changes slightly with change of crystallization conditions and techniques to prepare the crystal mats for X-ray measurement. From our experiments it seems to be about 115°C or higher, as shown in *Table 5*. It is obvious that the long

Table 5. Effect of annealing conditions on long period

Annealing condition		*2θ*			*Long period* (Å)
T_a(°C)	t_a(min)	*Left*	*Right*	*Average*	
86	0	40′00″	39′30″	39′45″	133
90	60	40′00″	39′30″	39′45″	133
100	60	40′00″	39′30″	39′45″	133
100	1000	41′00″	38′00″	39′30″	134
110	60	40′00″	39′00″	39′30″	134
115	60	40′00″	38′00″	39′00″	136
115	120	39′30″	38′00″	38′45″	137
115	1200	39′30″	37′30″	38′30″	138
Room temp.		40′00″	39′00″	39′30″	134

period of annealed crystals estimated by the X-ray measurements does not reflect any local thickness of lamellae, even if corrections of the type suggested by Balta Calleja *et al.*[16] are made on the molecular tilt. The data shown in *Table 5* imply that the morphological transformations mentioned above are not accompanied by lamellar thickening, while the molecular chains are tilted, as described below.

Factors affecting morphological transformation

The factors affecting the morphological transformation due to annealing may be classified into two categories: those concerning the inherent properties of polymers, and those being governed by external conditions.

Factors concerning inherent properties of polymers—

(I) Molecular weight.

(II) Types and numbers of branches and their distribution in a chain.

Several factors such as molecular weight distribution and chain ends are also in this category. It is difficult to evaluate the effects of such factors at the present time, and so our remarks are confined to the influence of molecular weight and branching on annealing behaviour.

Factors governed by external conditions—

(III) Original crystalline morphology in a sense of including crystallization conditions, such as lamellar thickness; degree of truncation; and types of collapse and the resultant pleats and striations.

(IV) Annealing conditions, such as temperature T_a, time t_a, and rates of increasing or decreasing temperature.
(V) Interaction between overlapped lamellae.
(VI) Trapped solvent under the hollow pyramid.
(VII) Presence of impurities.

In general, it could be very difficult to decide which factor is predominant, because of the complicated aspects of the phenomenon. The following discussion is an attempt to interpret the effects of these factors one by one.

Factor I: molecular weight—The influence of molecular weight on the annealing behaviour was examined by using a sample of a low molecular weight fraction ($M_n = 8\,000$) extracted from Marlex 50 PE with boiling trichlorethylene. Single crystals were obtained from 0·05 per cent w/v trichlorethylene at 70°C.

One of the most interesting features observed is the interference fringes of equal inclination which appear as the dark strips running approximately parallel to the *b*-axis. A typical example is shown in *Figure 12*. The fringes

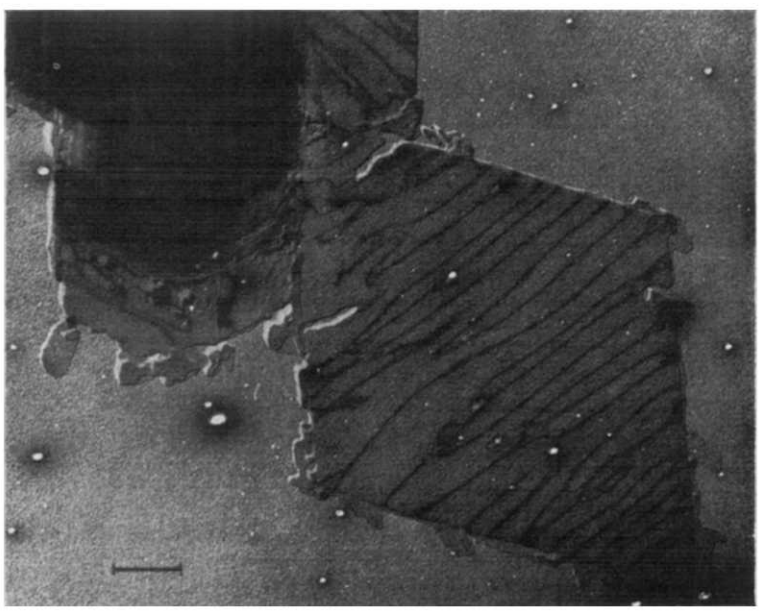

Figure 12—Sample of a low molecular weight fraction of Marlex 50, crystallized in 0·05 per cent w/v trichlorethylene at 70°C (annealed at 96°C). The interference fringes appear frequently in this species with the orientation approximately parallel to the *b*-axis. The thin layer of materials observed at the edge of the crystal results from the amoeba-like motion[6]

reveal that the crystal still maintains the perfection and orientation of as-crystallized structure. This feature is found only with low molecular weight polymers.

When originally isolated crystals were melted and recrystallized, they

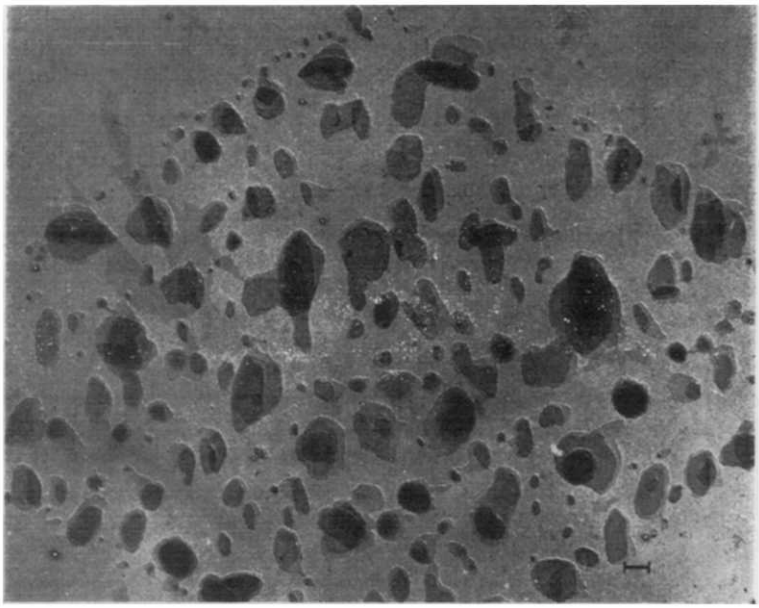

Figure 13—Sample and annealing condition as *Figure 12*. The single crystal melted and recrystallized to form 'islands' consisting of two or more layers. No single layer is observed

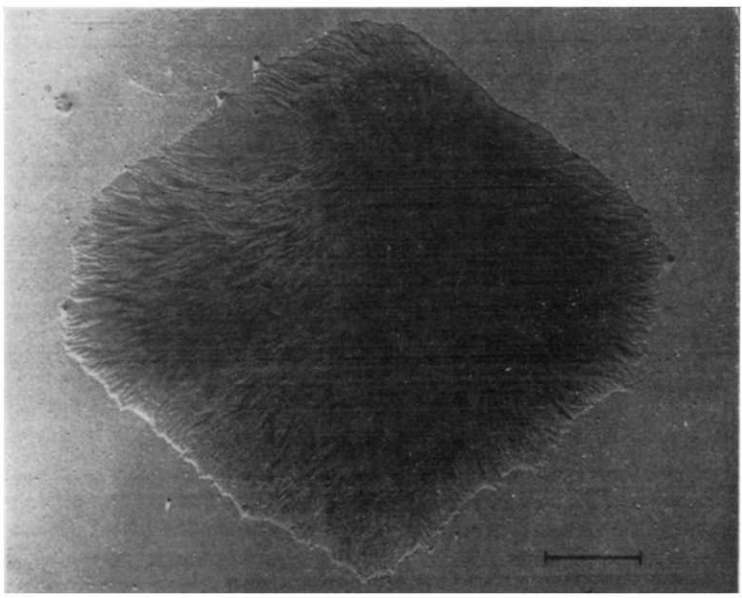

Figure 14—Sample of high density PE with 8·8 ethyl branches per 1 000 methylene chain units, crystallized in 0·05 per cent w/v xylene at 85°C (annealed at 115°C). Retaining the original hexagonal outline, the crystal assumes the structure in which the lamellae are twisted periodically as usually observed in a spherulite

formed aggregates of the 'islands' that are composed of two or more smooth layers as shown in *Figure 13*. The structure developed is quite different from that of high molecular weight components like those in *Figure 10*. The difference may depend upon the mobility of polymer molecules and the recrystallization conditions.

Factor II: branching—High density PE having an ethyl branch concentration of 8·8 per 1 000 chain carbon atoms is used to evaluate the influence of branching upon annealing behaviour. Crystallization was conducted at 85°C in 0·05 per cent w/v xylene. Crystals are truncated lozenges with many undefined overgrowths. When annealed at temperatures higher than their melting points, they transform to spherulitic structures that consist of many lamellae twisted periodically. An example is shown in *Figure 14*. Such a structure also develops in the regions of overlapped lamellae with linear high molecular weight species (see *Figure 10*).

Factor III: crystalline morphology—According to the kinetic theory of polymer crystallization[5], the melting temperature, T_m, is represented by the equation

$$T_m = T_m^0 (1 - 2\sigma_e/\Delta h_f l)$$

where T_m^0 is the equilibrium melting temperature, σ_e the fold surface free energy, Δh_f the heat of fusion and l the lamellar thickness. In the equation, $\sigma_e/\Delta h_f$ seems to be constant within experimental error when crystallization is conducted isothermally[8]. Under these conditions, lamellar thickness could be a main factor affecting T_m, and the contributions of σ_e and Δh_f to T_m might be negligible. The degree of truncation, on the other hand, depends largely on T_c; the higher T_c the more highly truncated the crystal. It is to be expected therefore that the highly truncated lozenges will have larger lamellar thickness and will be thermally more stable than the less truncated crystals. *Table 4* gives results that confirm the above considerations. At or below 100°C, Xy-87 and Cl-86 show little difference in morphology; however, the features characteristic to stage 3 were found at higher temperatures for highly truncated species.

Concomitant with the erosion of contours and the formation of holes in the {110} sectors, lamellar thickening or melting occurs significantly over the {100} sectors as shown in *Figures 7* and *8*. Materials transformed are accumulated at the sector boundaries and also at the contours to form thickened areas that give the impression of a sheared stack of cards[3]. It should be noted that the change is restricted in the {100} sectors[13] and is observed for both Xy-87 and Cl-86. Even though recent studies performed with DSC[7,19,20] did not reveal such a difference in the thermal stability of sectors, a transformation temperature which is characteristic to each sector must exist. The evidence shown in *Table 4* and *Figures 7* and *8* suggests that the difference in transformation temperature between the {100} and the {110} sectors is definite, but of only very few degrees. The existence of such a difference in annealing behaviour between sectors implies, in turn, that the fold structure of polymer chains is governed by the regularity peculiar to each sector.

Crystals with thinner edges show that the holes start to develop at the border between thin and thick terraces as shown in *Figure 15*. During

prolonged annealing time, a side of a hole, generally on the outer side of the crystal, is thickened to form elongated 'wall-like' terraces. The border must involve many disordered sites because the thinner edge always results from abrupt changes in crystallization conditions. Such sites could be responsible for the formation of holes.

Some defects that result from the collapse of the hollow pyramid also influence the morphological transformation due to annealing. An example is frequently observed at stage 3, where holes are densely located near the sector boundaries between the {110} sectors. In this region, striations approximately parallel to the *b*-axis are sometimes observed for the lightly annealed crystals (see *Figure 2*). The striations must result from the collapse of the hollow pyramid during annealing, because no striations of the same type have been found in as-crystallized samples. Therefore, the origin of hole formation must be related to the defects generated from the collapse of the hollow pyramid. The holes developed in the {110} sectors are oriented approximately parallel to ⟨310⟩ direction, which is essentially

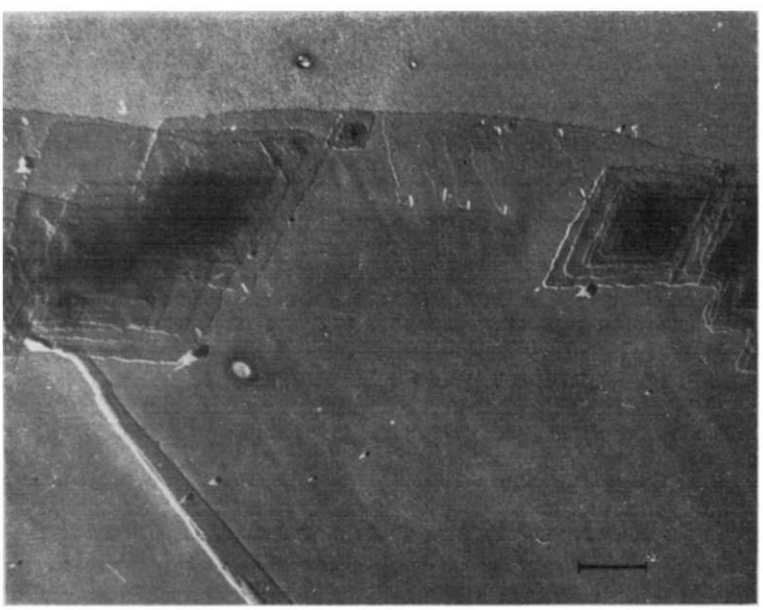

Figure 15—High magnification of a part of the crystal shown in *Figure 6*. The holes develop in the thinner contour and at the border between thin and thick terraces. A side of a hole, generally on the inner side of the crystal, is not thickened, while the outer is thickened to form the elongated wall-like terraces

perpendicular to the growth faces[12]. This also may be related to the collapse of the hollow pyramid.

Factor IV: annealing conditions—The annealing conditions considered here are temperature, time and rates of increasing and decreasing tempera-

ture. Of these factors the influences of the first two have been thoroughly studied by many workers, and are also inferred from the data shown in *Table 4*. The rate of temperature change is also expected to produce effects on the annealing behaviour, but these effects are only slight and are not clearly observed except at the morphological transformation at stage 5.

The characteristic features observed at stage 5 are as follows.

(*1*) The originally isolated crystals show various aspects of morphology. *Figure 10* shows one of the typical examples in which crystals have smooth terraces in some places and the regular stack of tilted lamellae in others. Large holes like 'inland seas' are developed in the vicinity of the {100} sectors. The appearance of these large holes reveals the morphological transformation as having passed through stage 3 at which the selective transformation in the {100} sectors occurs. Another example suggested by *Figure 9* is the skeleton-like structure in which the accumulated materials are located randomly to form a skeleton-like appearance. The structure always comprises a stack of tilted lamellae and no smooth terraces are observed.

(*2*) The aggregates of overlapped lamellae are replaced by the spherulitic structure with twisted lamellae under the same conditions. An example is observed in *Figure 10*. These various morphologies can be explained by taking into account the rates of increasing and decreasing temperature for melted and recrystallized crystals. When the rate of increase in temperature was too high for morphological changes to follow the successive stages, the resultant crystals exhibited the aspect corresponding to the final stage. When, on the contrary, the rate was low, they showed the characteristic features of the successive stages passed through. For example, large holes developed in the vicinity of the {100} sectors, suggesting the occurrence of the selective transformation of the {100} sectors at stage 3. Therefore, it can be concluded that the rates of increasing and decreasing temperature, as well as temperature and time of annealing, have large influences on morphological transformation. In other words, crystalline morphology depends on the kinetic factors such as mobility of polymer molecules in the melt.

Factor V: interaction between overlapping lamellae—For the region where two lamellae originally overlapped each other, Geil[12] has reported that the holes in the overlapped region are larger than those found in a single lamella. Another point is that the orientation of holes seems to depend on an interaction between the two lamellae. One of our examples is shown in *Figure 16*. It must be noted that the holes in the {110} sectors are oriented approximately normal to their corresponding growth face. Such orientation is also observed in *Figure 7*. As shown in *Figure 16*(b), the {100} sectors of the right-hand crystal (R) and the ($\bar{1}$00) sector of the left-hand one (L) are morphologically transformed, while a part of the (100) sector of the L is unchanged. Because of the selective transformation in the {100} sectors, it is suggested that the L lies uppermost. More holes develop in the overlapped region than in the region of a single lamella, and in the overlapped region they are roughly grouped into four from their orientation, as in the drawing. In region A, the orientation of the holes is

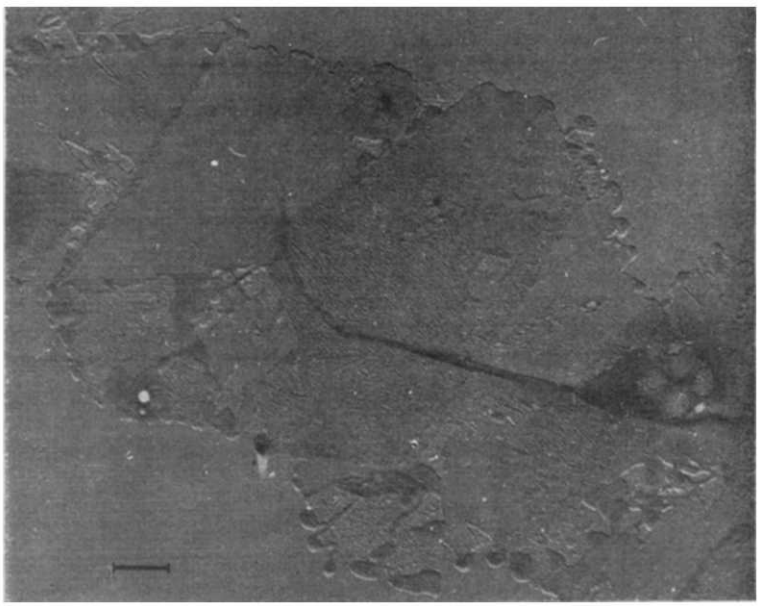

Figure 16(a)

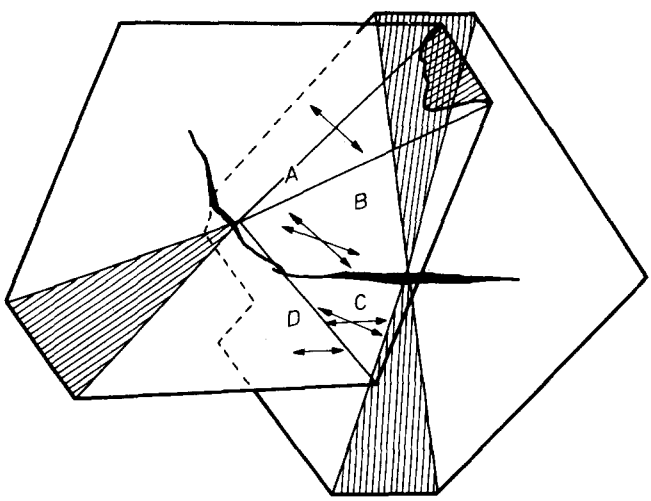

Figure 16(b)

Figure 16(a)—Sample of Xy–87 crystals (annealed at 105°C for 120 min). The holes seem to be oriented approximately perpendicular to the corresponding growth face. According to the oriented nature of the holes, the lamella in which the holes develop can be distinctively identified. The holes observed in region A [*Figure 16*(b)] must develop in the (110) sector of the right-hand crystal as shown by arrow. Some of them observed in region B, for example, must develop in the (110) sector of the right-hand crystal, while the remainder are in the ($1\bar{1}0$) sector of the left-hand crystal

approximately perpendicular to the (110) growth face of the R. In region B, the orientations are of two kinds, one perpendicular to the (110) growth face of the R and the other perpendicular to the $(1\bar{1}0)$ growth face of the L. In region C there are also two kinds, one perpendicular to the $(1\bar{1}0)$ growth face of the L and the other approximately parallel to the *b*-axis of the R or parallel to the $(\bar{1}\bar{1}0)$ growth face of the L. The last orientation of holes is also observed near the central pleats of the R in region B. Some of them located near the central pleat may have resulted from the collapse of the hollow pyramid, as described in the preceding section. The orientation of holes in region D is also directed parallel to the $(\bar{1}\bar{1}0)$ growth face of the L. At the present time it is not clear why the rest are oriented parallel to the growth face. It is concluded that the orientation of the holes in such cases seems to be characteristic of the sector in which they develop, and not to be affected by interaction between the two lamellae. Such a conclusion is not adequate at stage 5 because of the mixing of molecules in each layer to make a spherulitic structure.

The holes developed in the overgrowth reveal the transportation mechanism of heat. As shown in *Figure 15*, a part of the daughter crystal on the thinner edge of the basal lamella develops many little holes, while the remainder on the thicker lamella is not affected. In this case the morphological transformation seems to be influenced by the lamellar thickness of the deepest crystal and not by the total thickness of the crystals underneath.

Factor VI: trapped solvent—It has been reported[21] that single crystals with retained solvent develop a structure considerably different from those without solvents, because of the dissolution and recrystallization of polymers under the heat treatment. However, in our experiments where it was possible to compare the data for 'dried in vacuum' crystals with those for 'dried in air' crystals, there appeared to be only a slight difference between the two methods as is shown in *Table 4*. Under the drying conditions employed, only a small amount of solvent can remain under the hollow pyramid, so that the apparent morphological transformation due to trapped solvent must require large amounts of solvents.

On the other hand, measurements with a mass spectrometer[22] have revealed that for sedimented mats the retained solvent between lamellae could not be removed by prolonged pumping, even for several weeks. Therefore it must be extremely difficult to elucidate only the effect of trapped solvent on the annealing behaviour of crystals grown from solution and also to compare the annealing behaviour of isolated single crystals with that of sedimented mats.

Factor VII: existence of impurity—In this paper the impurity referred to is that visible under the electron microscope. One of the examples where the effect of impurity is clearly observed is shown in *Figure 17*. The crystal is annealed at 105°C for 30 minutes and exhibits, as a whole, the aspects characteristic of stage 2 except that relatively large holes developed around the dust (impurity). The holes are much larger than those observed in the inner parts of the crystals at stage 3 (see *Figure 7*) and have no character-

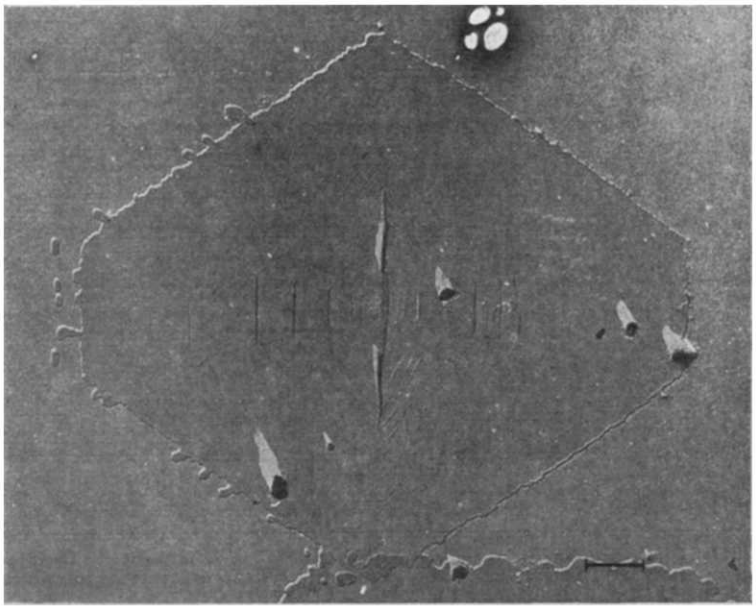

Figure 17—Sample of Xy–87 crystals (annealed at 105°C for 30 min). Morphological aspects show the characteristics of stage 2, and relatively large holes are observed around the impurities. It is deduced that the holes are formed because of the presence of impurities

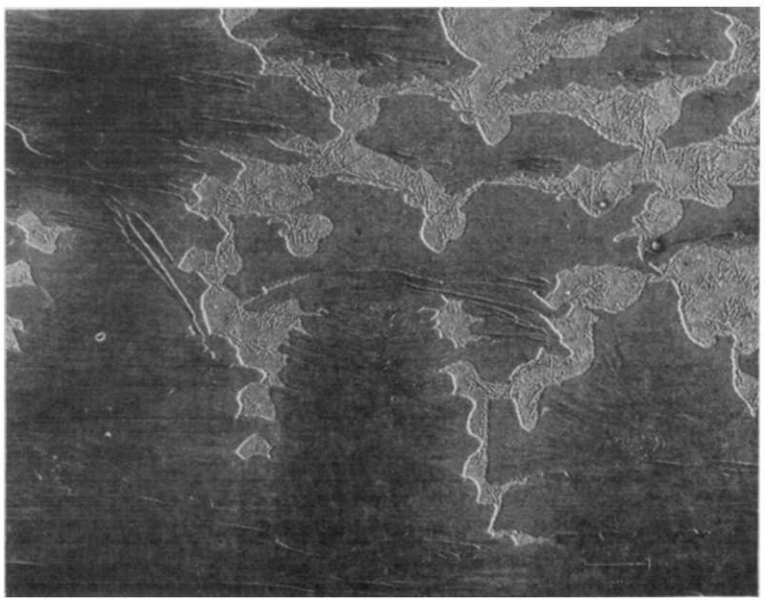

Figure 18—A single crystal of a sample of a high molecular weight fraction of Marlex 50, crystallized in 0·05 per cent w/v xylene at 83°C (annealed at 116°C) melted and recrystallized. The resultant morphology resembles a sheared stack of tilted lamellae. Some of the rod-like substances remain behind

istic orientation. From these descriptions it can be deduced that the holes are produced because the impurities were there.

Relationship between lamellar thickness and morphological transformation

The lamellar thickening of single crystals during annealing has been explained by two mechanisms, the sliding diffusion of chain molecules in a crystalline state[6], and the fractional melting of the crystals followed by recrystallization[23]. On the molecular motion during annealing, the first explanation assumes that the thickening may involve either the motion of point dislocations of the type suggested by Reneker[24] or the collective jumps of entire segments of straight chain sections between folds[25]. On the other hand, the second explanation assumes that the melting occurs in small localized regions and that the unmelted crystals serve as nuclei for re-crystallization.

In our study, the long period of annealed crystal mats estimated by the small angle X-ray scattering is not appreciably varied under the annealing conditions used for the morphological observation (see *Tables 4* and *5*). The long period starts to increase at temperatures higher than 115°C, where spherulitic structure is observed as shown in *Figure 18*.

Additional evidence to elucidate annealing behaviour was obtained from the electron diffraction pattern. As a result of the hollow pyramidal form, the truncated lozenges give in general strong (020), and weak (110) and

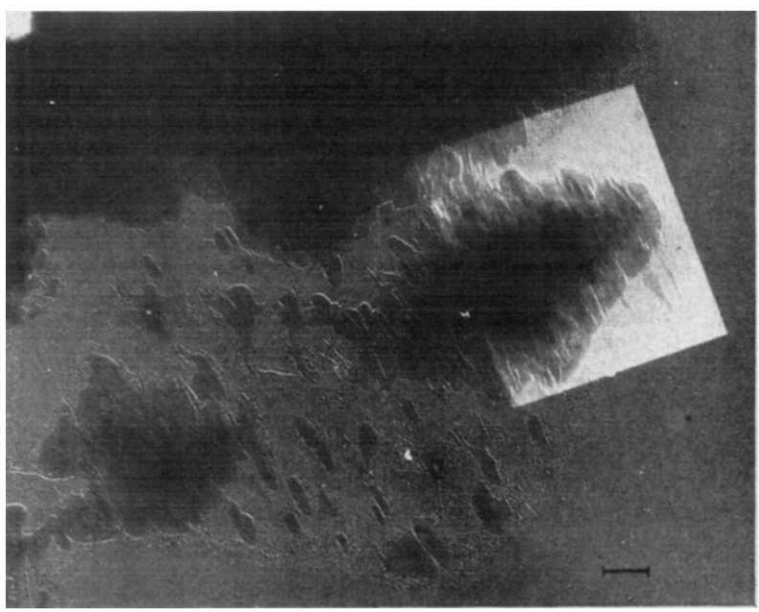

Figure 19(a)—Same sample as in *Figure 18* (but annealed at 111°C). Considerable transformation (stage 5) is observed. Nevertheless electron diffraction patterns [*Figure 19*(b)] reveal that the crystal is well oriented and tilted around the *b*-axis as a whole

(200) reflections. When annealing progressed further with respect to temperature and time, the intensity of the weak [especially (200)] reflections, decreased relatively to the strong reflection. An example is shown in *Figure 19*. This implies that the *a*- and *c*-axes rotated around the *b*-axis to an extent dependent on the annealing, while the latter was unchanged. The electron diffraction pattern shown in *Figure 19*(b) also reveals that the major part of the crystal is well oriented like as-crystallized single crystals; nevertheless the tilting around the *b*-axis and the transformation to a considerable extent (stage 5) are obviously present.

Electron diffraction patterns combined with the morphological and small angle X-ray studies offer some information towards the clarification of the

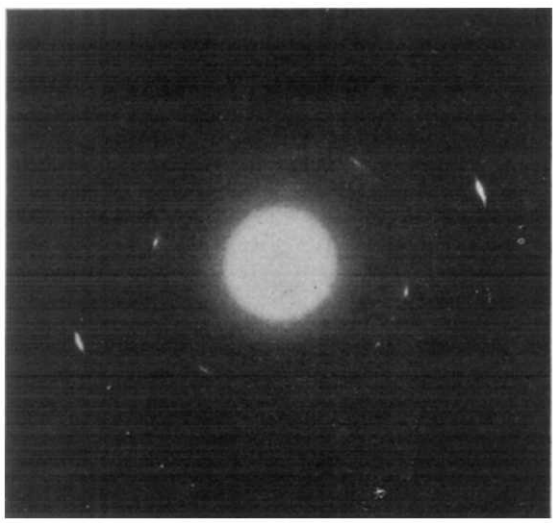

Figure 19(b)—Pattern from area marked in *Figure 19*(a)

annealing behaviour of polymer crystals. From the morphological point of view, the transformation could be interpreted as follows. At first, the apparent changes occur in the thinner lamellae and at the disordered sites that have been generated during the crystallization process or the collapse of the hollow pyramid. The change then proceeds successively to the surrounding areas. The materials changed in morphology are accumulated in the portions consisting originally of two or more lamellae and the borders between changed and unchanged structure (termed as 'transformation front'). In addition, small rod-like substances frequently remain behind. During these processes, the *a*- and *c*-axes rotate around the *b*-axis and the long period remains constant.

CONCLUSION

Annealing at 110°C or below causes morphological transformation accompanied by tilting of the molecular chain around the *b*-axis, while the long period estimated by the small angle X-ray scattering remains constant.

Above 110°C, single crystals assume a spherulitic structure. The structures developed have random orientation of crystallographic axes, in spite of the similar appearances of morphologies to those observed at stage 5. Then the lamellar thickening could be explained by the melting of the crystals followed by recrystallization.

The selective transformation observed in the {100} sectors at stage 3 indicates the existence of a characteristic temperature of transformation for each sector. It can also be deduced that the chain folding structure in truncated crystals is governed by the regularity peculiar to each sector.

We thank Dr K. Nakagawa for valuable discussions and criticism. The electron photomicrographs were taken by S. Shibata.

Electrical Communication Laboratory,
Nippon Telegraph and Telephone Public Corporation,
Tokai-mura, Nakagun,
Ibaraki-ken, Japan

(Received June 1967)

REFERENCES

[1] GEIL, P. H. *Polymer Single Crystals*, p 311. Interscience: New York, 1963
[2] FISCHER, E. W. and SCHMIDT, G. F. *Angew. Chem.* 1962, **74**, 551
[3] BASSETT, D. C. and KELLER, A. *J. Polym. Sci.* 1959, **40**, 565
[4] TAKAYANAGI, M. and NAGATOSHI, F. *Mem. Fac. Engng Kyushu Univ.* 1965, **24**, 33
[5] HOFFMAN, J. D. and LAURITZEN JR, J. I. *J. Res. nat. Bur. Stand. A*, 1961, **65**, 297
[6] HIRAI, N., YAMASHITA, Y., MITSUHATA, T. and TAMURA, Y. *Rep. Res. Lab. Surface Sci. Okayama Univ.* 1961, **2**, 1
[7] MANDELKERN, L. and ALLOU JR, A. L. *Polymer Letters*, 1966, **4**, 447
[8] NAGAI, H. and KAJIKAWA, N. *Rep. Progr. Polym. Phys. Japan*, 1966, **9**, 133
[9] BASSETT, D. C. and KELLER, A. *Phil. Mag.* 1961, **6**, 345
[10] KAWAI, T. and KELLER, A. *Phil. Mag.* 1965, **11**, 1165
[11] STATTON, W. O. and GEIL, P. H. *J. appl. Polym. Sci.* 1960, **3**, 357
[12] GEIL, P. H. *J. Polym. Sci. A*, 1964, **2**, 3835
[13] KELLER, A. and BASSETT, D. C. *J. R. microsc. Soc.* 1960, **79**, 243
[14] HOLLAND, V. F. *J. appl. Phys.* 1964, **35**, 3235
[15] BASSETT, D. C. and KELLER, A. *Phil. Mag.* 1962, **7**, 1553
[16] BALTÁ CALLEJÁ, F. J., BASSETT, D. C. and KELLER, A. *Polymer, Lond.* 1963, **4**, 269
[17] NAGAI, H., UETAKE, K., NAKAGAWA, K. and NISHIOKA, A. Paper presented at the Annual Meeting of the Society of Polymer Science, Kyoto, June 1964
[18] STATTON, W. O. *J. appl. Phys.* 1961, **32**, 2332
[19] PETERLIN, A. and MEINEL, G. in *Thermoanalysis of Fibers and Fiber-forming Polymers* (Appl. Polym. Symp. No. 2) (SCHWENKER JR, R. F.), p 85. Interscience: New York, 1966
[20] BAIR, H. E., SALOVEY, R. and HUSEBY, T. W. *Polymer, Lond.* 1967, **8**, 9
[21] GEIL, P. H. Reference (1) above, p 331
[22] SALOVEY, R. and BASSETT, D. C. *J. appl. Phys.* 1964, **35**, 3216
[23] KAWAI, T. *Kolloidzschr.* 1965, **201**, 104
[24] RENEKER, D. H. *J. Polym. Sci.* 1962, **59**, 539
[25] PETERLIN, A. *Polymer, Lond.* 1965, **6**, 25

Nuclear Magnetic Resonance and Optical Spectroscopic Studies of Poly L and Poly D Alanine

E. M. BRADBURY and H. W. E. RATTLE

Nuclear magnetic resonance spectroscopy is finding increasing application to studies of conformational changes in biological macromolecules and their synthetic analogues. It has been suggested that the resonance peaks due to backbone protons in helical polymers will be broadened by non-averaging of dipole–dipole interactions and that the areas of these resonance peaks will be a measure of the random coil content of the system. In agreement with others, we do not find this to be the case for poly L *and poly* D *alanine in trifluoracetic acid (TFA)–deuterochloroform ($CDCl_3$) solvent systems where the optical rotatory dispersion parameters indicate a helix content in excess of 50 per cent while the n.m.r. spectra for these solutions are still fully developed. It is suggested that the peak narrowing process operating in this system is rapid exchange between random coil and helical segments. Others suggest that, although the b_0 values for the TFA–$CDCl_3$ solvent systems indicate 54 per cent helix content, this o.r.d. parameter is an unreliable guide to helix content and that the polypeptide is helical; furthermore that they are observing for the first time a well developed n.m.r. spectrum for a polypeptide 'purported to be in a helical conformation'. These conclusions are not supported by the results obtained from studies of poly* L *and poly* D *alanine in dichloracetic acid (DCA)–TFA and DCA–$CDCl_3$ solvent systems. In these systems it is possible to obtain appreciably higher b_0 values (up to 458°) than was observed for the TFA–$CDCl_3$ solvent system and these increases in b_0 are accompanied by marked broadening and loss of area of the proton resonance peaks. It is suggested therefore that when the helix content is greater than 50 per cent the motions of helical segments become too slow for the peak narrowing process of exchange between helical and random coil forms to be effective. These observations support the earlier suggestions that in fully helical macromolecules the backbone protons resonance peaks will be broadened by non-averaging of dipole–dipole interactions.*

It is possible to correlate the shifts in the poly L *alanine resonance peaks with helix content and it has been suggested that the shifts are due to exchange of the protons between two chemical environments, i.e. the helical and random coil forms. Infra-red studies show, however, that there is a specific interaction between the carboxylic acid molecule and the* helical *form of poly alanine and we suggest that part of the shifts observed in the resonance peaks may result from magnetic anisotropy effects of the carboxyolic acid molecules complexed with hydrogen bonded amide groups in the helical form. In agreement with others it is suggested that the mode of interaction of the carboxylic acid molecules with poly alanine is a strong hydrogen bonding interaction and not protonation as has been suggested.*

NUCLEAR magnetic resonance (n.m.r.) spectroscopy is being increasingly applied to studies of macromolecules, both synthetic and natural, in solution. The basic principles of the method and its applications to studies of macromolecules have been described in several review articles[1-6]. From these studies it can be seen that the n.m.r. spectra of proteins and the changes in the spectra when the proteins undergo conformational changes are complex and in order to establish some criteria for the interpretation of such spectra n.m.r. spectroscopic investigations have been made of simple homopolypeptides in the region of their helix–coil transition.

There have been few earlier n.m.r. studies of polypeptides and these have not been very detailed. Bovey, Tiers and Filipovitch[7] have described spectra of poly-γ-benzyl-L-glutamate, while Goodman and Masuda[8] have used n.m.r. spectroscopy to follow the helix–coil transition of poly-γ-ethyl-L-glutamate in a trifluoracetic acid–trifluorethanol solvent system and from their study have suggested that the area of the resonance peak of the amide N—*H* is a measure of the proportion of the polypeptide in the random coil form. Marlborough, Orrell and Ryden[9] have made similar studies of poly-γ-benzyl-L-glutamate and have pointed out the importance of n.m.r. spectroscopy as a tool for the investigation of sidechain interactions.

More detailed n.m.r. studies of poly L alanine, poly DL alanine, and poly L leucine in trifluoracetic acid (TFA)–deuterochloroform ($CDCl_3$) solvents have recently been described by Glick *et al.*[10,11] who have shown that poly L alanine can undergo a partial coil–helix transition without any observable change in the areas of the different proton resonance peaks in the spectra of the polypeptides, indicating that the suggestion of Goodman and Masuda[8] does not have general application to the study of helix–coil transitions in polypeptides. They have concerned themselves more with shifts in the proton resonance peaks and have shown by comparing the shifts of the pure enantiomorph with those of the DL polymer in the same solvent system, that these shifts can be correlated with the conformational changes of the polypeptides during the helix–coil transition. It was also inferred from this study that fully helical polypeptides can give rise to well developed n.m..r. spectra with no loss in area of the proton resonance peaks and that the Moffitt optical rotary dispersion (o.r.d.) parameter b_0 is not a reliable index of either the maximum or minimum per cent helix; they further adduced evidence that the TFA–polypeptide interaction does not result in protonation of the polypeptide as had been previously postulated[12-15] and proposed instead that 'the principal acid–polymer interaction is hydrogen bonding without proton transfer'.

We have made similar studies of poly L, poly D and poly DL alanine in the TFA–$CDCl_3$ solvent system and have also made further studies of these polypeptides in TFA–dichloracetic acid (DCA) and DCA–$CDCl_3$ solvent systems. Six poly alanines of differing molecular weights have been studied in the above solvent systems over a range of temperature from 33°C to 120°C. Although there is a certain amount of agreement, not all of the conclusions drawn by Glick *et al.*[10] and by Stewart *et al.*[11] are supported by this study since the additional information obtained, including that from infra-red (i.r.) spectroscopic studies, leads in certain instances to different interpretations of the n.m.r. data.

EXPERIMENTAL

Nuclear magnetic resonance

The n.m.r. spectra were recorded on two Perkin–Elmer R10 60 Mc/s spectrometers, a Varian A60, and the Perkin–Elmer R14 100 Mc/s instrument. The solutions were allowed to equilibrate thoroughly at the operating temperature of 33·5°C before their spectra were recorded. Spectra of solutions at elevated temperatures were recorded on the Perkin–Elmer proto-

Table 1. Poly D alanine ($\eta_{sp}/c = 24 \cdot 5$) in TFA–DCA, DCA–$CDCl_3$ and TFA–$CDCl_3$ solvents

No.	Solvent	b_0	Positions (T)				
			NH	CH	CH_3	Solvent CH	Solvent OH
1	90%TFA–10%DCA	+	2·26	5·36	8·42	3·87	−1·38
2	70%TFA–30%DCA	168	2·22	5·41	8·41	3·85	−1·34
3	60%TFA–40%DCA	220	2·22	5·46	8·39	3·84	−1·32
4	50%TFA–50%DCA	275	2·2	5·49	8·39	3·84	−1·31
5	40%TFA–60%DCA	292	2·2	5·53	8·40	3·82	−1·35
6	20%TFA–80%DCA	306	2·2	5·55	8·40	3·81	−1·32
7	DCA	344	2·2	5·55	8·42	3·81	−1·33
8	60%DCA–40%$CDCl_3$	386	2·2	5·64	8·42	3·87	−1·38
9	30%DCA–70%$CDCl_3$	400	2·2	5·70	8·44	3·91	−1·26
10	20%DCA–80%$CDCl_3$	458	2·2	5·75	8·4		
11	90%TFA–10%$CDCl_3$	+121	2·20	5·39	8·39		−1·46
12	80%TFA–20%$CDCl_3$	+239	2·16	5·48	8·35		−1·40
13	70%TFA–30%$CDCl_3$	+279	2·13	5·51	8·36		−1·38
14	60%TFA–40%$CDCl_3$	+322	2·12	5·54	8·37		−1·38
15	40%TFA–60%$CDCl_3$	+325	2·12	5·60	8·39		−1·25
16	30%TFA–70%$CDCl_3$	+322	2·14	5·64	8·42		−1·19

No.	Widths (c/s)						Areas (arb. units)		
	NH	CH	CH_3	Solvent CH	Solvent OH	TMS	NH	CH	CH_3
1	13	19	14	0·80	1·05	0·80	1·59	1·42	4·32
2	18	19	15	0·75	0·86	0·76	1·63	1·55	4·60
3	25	20	17	0·79	0·99	0·71	1·59	1·57	4·42
4	33	21	18	0·72	0·90	0·71	1·32	1·44	4·10
5	40	24	20	0·75	0·96	0·80	1·17	1·35	3·86
6	45	30	24	0·76	0·90	0·70	0·72	1·01	2·70
7	39	35	32	0·85	1·00	0·75	0·31	0·42	1·52
8	53	33	27	0·76	0·95	0·70	0·37	0·53	1·78
9	54	32	28	0·90	1·20	0·79	0·34	0·53	1·76
10				0·85	1·90	0·9			
11	15·3	19·4	14·7		0·72	0·58	1·29	1·09	3·42
12	18·4	20·1	15·2		0·68	0·63	1·32	1·15	3·51
13	19·2	20·4	15·9		0·71	0·65	1·24	1·15	3·66
14	19·8	20·4	16·1		0·71	0·65	1·35	1·18	3·69
15	21·8	20·6	16·2		0·75	0·60	1·35	1·25	3·70
16	24·7	20·9	16·6		1·02	0·73	1·30	1·16	3·51

type variable temperature probe at Perkin–Elmer Ltd, Beaconsfield, Bucks., and also on the Varian A60 at the University of Southampton. Time averaged spectra were obtained using a Perkin–Elmer computer of average transients. For series where areas and half band linewidths were measured, all spectra were recorded under identical conditions using the same sample tube for all solutions. The performance of the spectrometer was monitored by recording the spectrum of a test solution between runs; no changes were observed in the test spectrum.

The n.m.r. line positions quoted (*Table 1*) are the average of three measurements relative to the reference signal of tetramethylsilane (TMS); linewidths of resonances are the arithmetic mean of ten measurements while areas were measured by cutting out and weighing ten peaks traced on to thick uniform tracing paper. Estimated random errors in linewidths and areas, calculated from the observed scatter in results, are less than five per cent.

Optical rotatory dispersion

The same solutions as were used for the n.m.r. measurements were also used for o.r.d. studies in 10 mm cells at 33·5°C in a photoelectric spectropolarimeter designed and constructed by Malcolm and Elliott[16]. The results were analysed according to the Moffitt and Yang[17] equation

$$[R_{\text{vac}}] = \frac{a_0\lambda_0^2}{\lambda^2-\lambda_0^2} + \frac{b_0\lambda_0^4}{(\lambda^2-\lambda_0^2)^2}$$

to give the parameters a_0 and b_0. The b_0 value was related to the helix content of the polypeptide through the usual scale of $b_0 = -630°$ for a fully helical L polymer ($+630°$ for a D polymer) to zero for a fully random polymer.

Infra-red

The i.r. spectra of solutions were recorded on a Grubb–Parsons Spectromaster using barium fluoride cells. Polarized i.r. spectra were recorded on an i.r. microspectrometer designed and constructed in this laboratory (Bradbury and Ford[18]), the films being mounted in a sealed micro-cell for exposure to DCA vapour.

Solvents and materials

Deuterochloroform (99 per cent) was obtained from Ciba Ltd, and trifluoracetic acid from Aldrich; these were used without further purification. Dichloracetic acid was obtained from Griffin and George and was redistilled before use. The polypeptides were synthesized by W. E. Hanby at the Courtaulds Research Laboratory, Maidenhead, before its closure in 1962. All solutions were made up to 0·5 residue molar strength, which corresponds approximately to a 3·5 per cent w/v solution, for the recording of single spectra, while the spectra of 0·05 residue molar solutions were accumulated using the computer of average transients. Six samples were studied and the intrinsic viscosities ($\eta_{sp.}/c$) quoted are those given by Hanby; they were measured in DCA.

RESULTS

The n.m.r. spectra of poly L alanine in TFA and 50%TFA–50% $CDCl_3$ have been published by Glick *et al.*[10] and show the resonance peaks characteristic of the three different proton systems of poly alanine. In these spectra the N—*H* resonance peak is a symmetrical doublet which persists throughout the range of TFA–$CDCl_3$ solvents in which the polymer is soluble. In our studies of poly alanine we have observed this symmetrical doublet form for only one sample, that of lowest molecular weight which was initiated for a 100 mer. We have also observed this doublet form for the N—*H* resonance peak in the n.m.r. spectra of other polypeptides in TFA; poly-β-benzyl-L-aspartate, poly-β-*n*-propyl-L-aspartate, poly-β-methyl-L-aspartate and poly-α-amino-*n*-butyric acid. All of these polypeptides were known to be of low molecular weight and we have associated the appearance of the splittings in the N—*H* resonance peak with low molecular weight polypeptides.

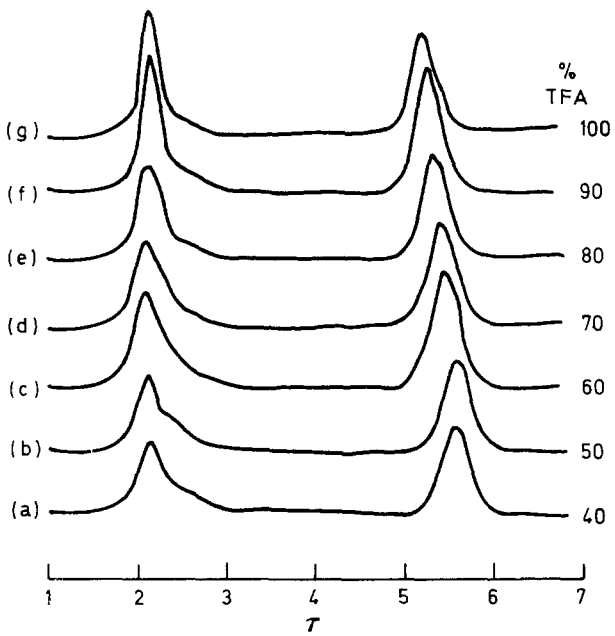

Figure 1—The n.m.r. spectrum of the amide and α-carbon protons of poly L alanine in TFA–$CDCl_3$ solutions

The shapes observed for the N—*H* and C—*H* resonance peaks of poly L alanine are shown in *Figure 1* where it can be seen that the N—*H* peak is asymmetrical. A narrow component predominates in the 100% TFA solution, but as the acid content is diminished a broad component gains area at the expense of the narrow component, the total area remaining constant over the range 100% TFA to 40% TFA–60% $CDCl_3$. To establish further the presence of a broad component in the N—*H* resonance peak a second

sample was examined, poly D alanine ($\eta_{sp.}/c=7{\cdot}73$) at concentrations of 0·35% w/v, a computer of average transients being employed to average out 32 spectra. The peaks obtained for this polymer are shown in *Figure 2*,

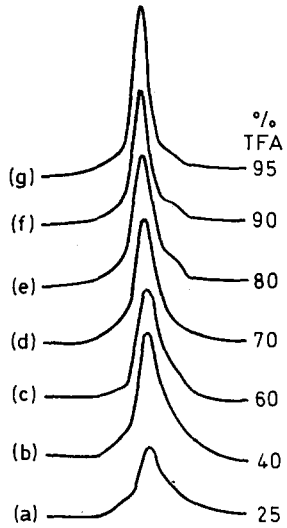

Figure 2—Amide proton resonance taken from time-averaged spectra of poly D alanine ($\eta_{sp.}/c=7{\cdot}73$ in DCA) in TFA–$CDCl_3$ solutions. 32 spectra were averaged

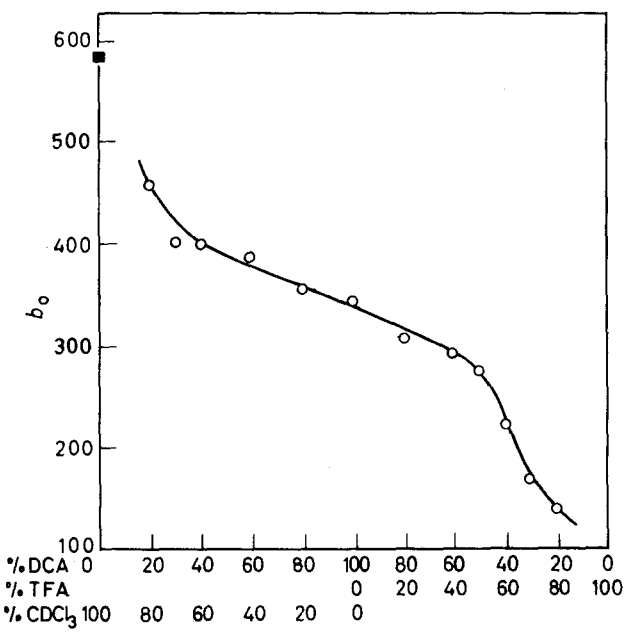

Figure 3—Optical titration curve of poly D alanine ($\eta_{sp.}/c=24{\cdot}5$) in $CDCl_3$–DCA–TFA. The point at 100 per cent $CDCl_3$ is taken from the Doty and Gratzer (1962) study of alanine block copolymers[20]

and the N—*H* resonance peak is observed to behave in a similar manner to that shown in *Figure 1*. To eliminate the possibility of artefacts the spectra were recorded on three other n.m.r. spectrometers; a second Perkin–Elmer R10 60 Mc/s instrument, the Varian A60 and the Perkin–Elmer R14 100 Mc/s instrument. The same behaviour was observed on these instruments and the same line-shape was observed in the 100 Mc/s spectra.

The optical titration curves (b_0 versus percentage acid content) of all the poly alanines agree with those published by Fasman[19], Hanlon and Klotz[13] and Stewart *et al.*[11]. The maximum b_0 values obtained for our poly alanines were between $\pm 320°$ and $\pm 340°$, the negative sign applying to poly L alanine. These b_0 values were obtained in a solvent system 30% TFA–70% $CDCl_3$; poly alanines were found not to give true solutions for solvent mixtures containing a smaller proportion of acid. The maximum b_0 values for the TFA–$CDCl_3$ solution were not, however, the highest values obtained for poly alanines in solution as can be seen from *Figure 3* where a b_0 value of $+458°$ was obtained for poly D alanine ($\eta_{sp.}/c = 24{\cdot}5$) in 20% DCA–80% $CDCl_3$. This curve is in accord with that published by Fasman[19], and

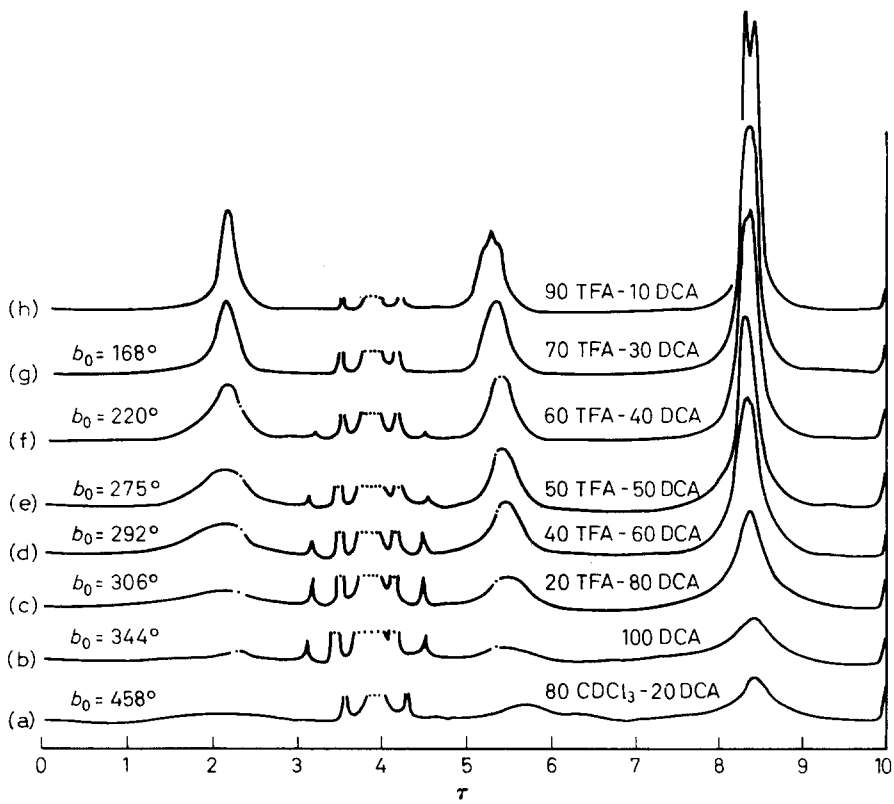

Figure 4—The n.m.r. spectra of poly D alanine ($\eta_{sp.}/c = 24{\cdot}5$ in DCA) in solvent systems of indicated percentage compositions. All spectra were run under identical conditions in the same sample tube

the b_0 value marked at zero per cent acid is taken from the Doty and Gratzer[30] study of block copolymers of alanine flanked by poly DL glutamic acid. The n.m.r. spectra of poly D alanine in this solvent system and in TFA–DCA are shown in *Figure 4* and these spectra show features which were not observed in the spectra of solutions in TFA–$CDCl_3$; the broadening and loss of area of all the resonance peaks in the spectra of the solutions of low acid content and high b_0 values should be noted. In order to check that the observed effects were not due to concentration or aggregation phenomena, time-averaged spectra were obtained of solutions of concentration (residue molar)/20, i.e. about 0·35% w/v. These spectra were identical to those obtained at the higher concentration, indicating that little or no aggregation was occurring. It is to be noted that for solutions which gave b_0 values up to 300°, i.e. comparable to the values obtained in TFA–$CDCl_3$ mixtures, the area of the resonance peaks remained constant, although broadening of the peaks occurred.

The positions, widths and areas of the proton resonance peaks of poly D alanine ($\eta_{sp.}/c=24{\cdot}5$), together with the positions and widths of the solvent proton resonances for the TFA–DCA and DCA–$CDCl_3$ solvent systems are given in *Table 1*, which also gives similar data for solutions in

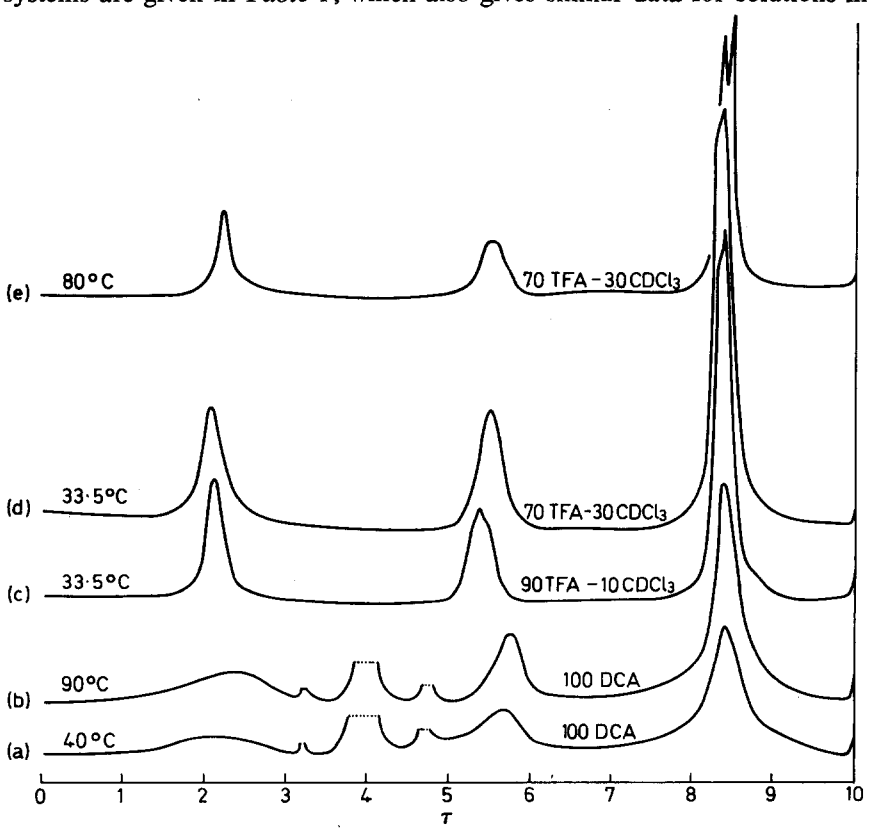

Figure 5—The n.m.r. spectra of poly D alanine ($\eta_{sp.}/c=24{\cdot}5$) showing the effects of varying temperature and solvent compositions

the TFA–$CDCl_3$ system. The chemical shifts measured for this last system are in close agreement with those given by Stewart *et al.*[11]. As can be seen from the table, a larger shift is observed for the α-carbon proton resonance peak with changing solvent composition. The position of this peak has similar values in solutions of similar b_0 values in both TFA–$CDCl_3$ and TFA–DCA solvent systems, and it is tempting to associate this shift with breakdown of the helix form of the polypeptide during the helix–coil transition. To pursue this point further, n.m.r. spectra of poly L and poly D alanine in TFA–$CDCl_3$ and DCA solutions were recorded at elevated temperatures. The solvent mixtures chosen in the TFA–$CDCl_3$ system were 40% TFA–60% $CDCl_3$ and 70% TFA–30% $CDCl_3$ which are points of inflection on the optical titration curve. Spectra were recorded at several temperatures up to 120°C; at temperatures above 100°C the solutions were observed to discolour and eventually turn black, and additional resonance peaks developed which remained on cooling the solutions. Above 100°C, therefore, degradation of the polypeptide was taking place. The changes observed in the n.m.r. spectra of the TFA–$CDCl_3$ solution on going from 33·5°C to 100°C were very small and the 33·5°C and 80°C spectra can be seen in *Figure 5*. Allowing for the expansion of the solution and the change in the Boltzmann distribution of the energy levels, there was little or no change in the areas of the resonance peaks and only a slight sharpening of the peaks at the higher temperature. With increasing temperature there were small shifts *upfield* in the positions of the N—H and C—H resonance peaks; the shift at 100°C being 5 c/s in each case. This is to be compared with the shift in the C—H peak of 15 c/s *downfield* on changing the composition of the $CDCl_3$–TFA solvent system; this spectrum is included in *Figure 5* for comparison. These results can be interpreted in two ways; either a large part of the shift in the C—H resonance peak is conformation sensitive and the shift upfield with increasing temperature is an indication of a temperature inverted helix–coil transition with increasing temperature, as has been observed for other polypeptides in mixed solvent systems (Doty and Yang[21], Schellman[22]), or a helix–coil transition does occur on heating the solution with small shifts upfield of the resonance peaks and the shift downfield on changing the solvent composition in the mixed solvent system is a solvent induced effect. To check these possibilities o.r.d. studies were made at elevated temperatures on the 70% TFA–30% $CDCl_3$, 40% TFA–60% $CDCl_3$ and DCA solutions. The maximum temperature to which the mixed TFA–$CDCl_3$ solvents could be raised in stoppered cells was 55°C and for the 70% TFA–30% $CDCl_3$ solution of poly D alanine the b_0 value was found to change from +306° at 20°C to +325° at 55°C while for the 40% TFA–60% $CDCl_3$ the change in b_0 was from +322° to +325° on going from 33·5°C to 55°C. There is little change in the b_0 values of poly D alanine in DCA (+312° at 25°C and +297° at 90°C) which indicates little change in the helix content. The peaks in the n.m.r. spectrum, however, are observed to gain in area and sharpen considerably. The behaviour of the DCA solutions is different to that of those in TFA–$CDCl_3$; time-averaged spectra of the DCA solution diluted ten times were run in order to check on the possibility of aggregation, and were found to give results identical to the original spectra.

In order to try to gain more specific information about solvent effects, measurements were made on the positions and widths of the peaks due to solvent and to TMS; the results are summarized in *Table 1*. Even in the systems for which the polypeptide peaks are very broad, it will be seen that the TMS peak is still very sharp, indicating that the broadening is not simply caused by increase in the macroscopic viscosity of the solution. The position of the C*H*Cl_2 peak of DCA in the systems containing that solvent follows a similar pattern to that of the polypeptide methyl proton peak, moving first downfield, then up. In general, the O—*H* peak of the solvent acid appears to move upfield as acidity is decreased, but in the TFA–DCA–$CDCl_3$ system the movement is not steady or continuous; probably the rapid changes in solvent composition have some bearing on this. In the solutions of low acid content the acid O—H resonance peak is observed to broaden to a greater extent than the C—H peak of DCA and the TMS reference peak. As shown in *Figure 6* the O—H peak of the acid

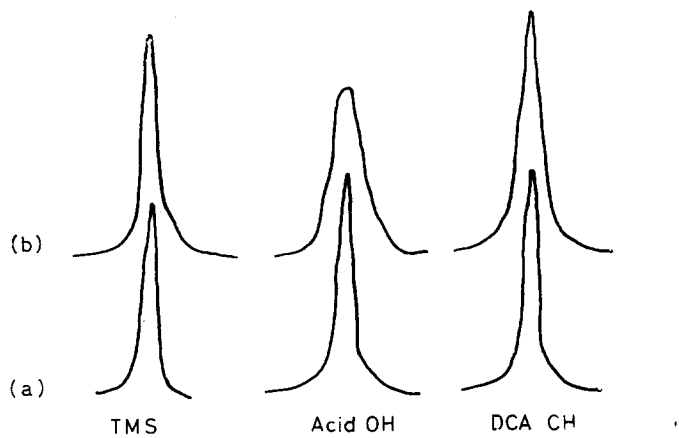

Figure 6—Comparison of TMS and DCA solvent peaks in (a) 90 per cent TFA–10 per cent DCA, and (b) 30 per cent DCA–70 per cent $CDCl_3$ solutions

broadens in the solution of highest b_0, indicating the possibility of a specific interaction between solvent and the helical form of the polymer similar to the type of interaction discussed by Jardetzky[3]. If the lifetime of such a complex were sufficient to cause the observed broadening of the O—*H* resonance, then for the purposes of optical spectroscopic measurements it should be long-lived and hence detectable by i.r. spectroscopy. The i.r. spectra of a solid film of poly L alanine and of solutions in 25% TFA–75% $CDCl_3$, 25% DCA–75% $CDCl_3$ and in TFA are shown in *Figure 7*. The frequencies of the amide I and II bands at 1 655 and 1 558 cm^{-1} are characteristic of the α-helix form of poly L alanine[23,24] as shown by the spectrum of the solid film. The peak at 1 615 cm^{-1} in the spectra of the solutions is unusual; it is just outside of the range of frequencies for the amide I band of hydrogenated polypeptides in the extended chain conformation and there is no corresponding amide II peak for the β-form which would be expected in the range 1 520 to 1 540 cm^{-1}. Further-

more, it is not the acid solvated coil frequency of the amide I since this peak appears at *ca.* 1 630 cm^{-1} in the TFA solution and is very much broader than the 1 615 cm^{-1} peak. In addition the 1 615 cm^{-1} peak is most prominent in the solutions of lowest acid content, i.e. highest helical content, which indicates that its origin resides in the interaction of DCA or TFA

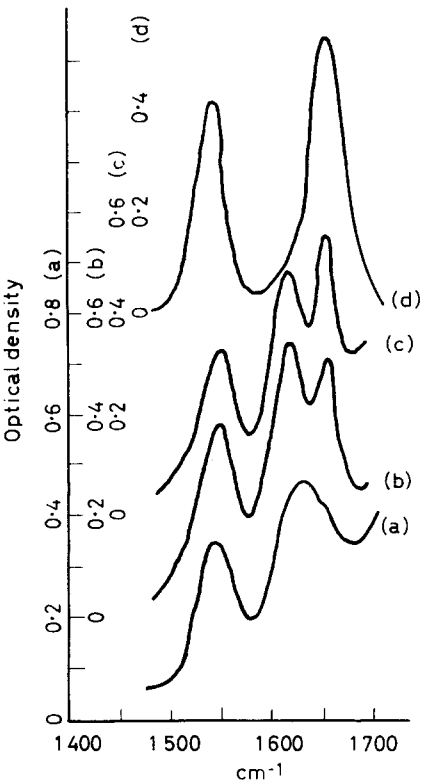

Figure 7—The i.r. spectra of 0·5 residue molar solutions in (a) TFA, (b) 25 per cent TFA–75 per cent $CDCl_3$, (c) 20 per cent DCA–80 per cent $CDCl_3$ and also (d) the solid film cast from solution (b)

with the helical form of poly alanine. It is of interest to note that in the i.r. spectrum of poly L alanine in pure TFA there is a shoulder at 1 655 cm^{-1} characteristic of the α-helix; this shoulder becomes more prominent and develops into a band as the acid content is reduced.

Further information on the nature of the interaction of carboxylic acids with poly alanine may be obtained from polarized i.r. spectroscopic studies of oriented films of the polypeptide. *Figure 8* shows the dichroic spectra of an oriented film of poly D alanine and the same portion of the same film exposed to DCA vapour in a sealed microcell. The main amide bands, amide A at $3\,280 \pm 15$ cm^{-1}, amide I at $1\,655 \pm 3$ cm^{-1} and amide II at $1\,547 + 3$ cm^{-1} are observed to weaken considerably on exposure of poly D alanine to DCA vapour, and new bands (other than DCA bands) appear at $3\,325 \pm 15$ cm^{-1} and at $1\,616 \pm 3$ cm^{-1}. Both these bands are dichroic indicating that their transition moments reside in the ordered polypeptide component. The marked reduction in the intensity of the amide bands and the appearance of new amide bands are an indication of a strong interaction between the amide group and the carboxylic acid molecules which leads

to a change in the normal modes of vibration of the amide groups in the polypeptide chain.

Another indication of specific interaction becomes apparent when trying

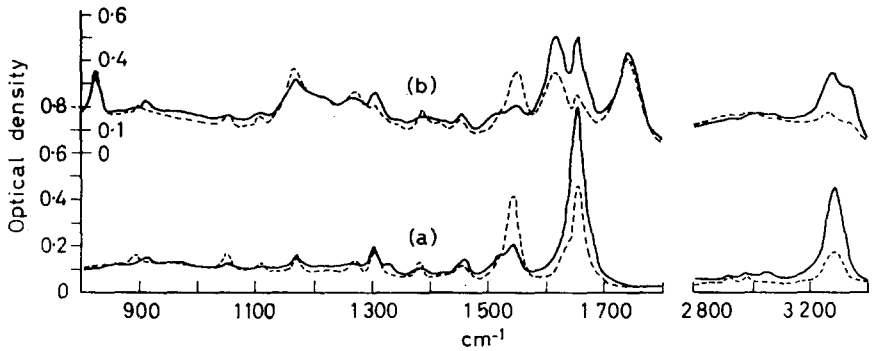

Figure 8—Polarized i.r. spectra of poly D alanine ($\eta_{sp.}/c=24{\cdot}5$): (a) film cast from DCA, (b) the same film exposed to DCA vapour.
——— *E*-vector parallel, - - - - *E*-vector perpendicular.

to dissolve poly alanine in solvents consisting of low concentrations of TFA mixed with chloroform. The resulting 'solution' is cloudy and after some hours separates into two clear layers. Upon examination of these layers by n.m.r. the upper, clear layer appears to consist of a solution of polymer in a fairly acid solvent, while the lower consists mostly of chloroform. As the temperature is raised, less TFA is needed to make the polymer dissolve; a true solution may be formed in 30% TFA–70% $CDCl_3$ at 33°C, but this will separate into two layers at room temperature.

DISCUSSION

We have been concerned with the application of n.m.r. spectroscopy to the study of conformational changes in poly alanine and the correlation of these results with those obtained from optical techniques.

It has been suggested for macromolecular systems that the proportion of the macromolecule in the random coil form can be determined from the area of the backbone proton resonance[25–27]. In particular, Goodman and Masuda[8] have suggested from n.m.r. studies of poly-γ-ethyl-L-glutamate that the area of the amide proton resonance is a measure of the random component in a helix–coil transition and that these changes are paralleled by changes in b_0 values from o.r.d. studies. In agreement with Stewart *et al.*[11] we find that these suggestions do not hold for poly alanine in the TFA–$CDCl_3$ solvent system. Over the range of solvent mixtures when the b_0 values change from *ca.* 100° to *ca.* 300° there was no measurable change in the areas of the peaks from all the proton systems in poly alanine. Similar observations were made for poly D alanine in the TFA–DCA solvent system at the high TFA content end of the range. From their studies on poly L alanine in TFA–$CDCl_3$ mixtures Stewart *et al.*[11] make the suggestion that no reliance can be placed on b_0 values as a measure of high helix contents and infer that although the maximum b_0 in the TFA–$CDCl_3$ solvent system indicates a helix content of 54 per cent the actual helix content is

in fact much higher. They further stress that an important aspect of their study is that for the first time well-developed resonance peaks 'due to protons attached to the backbone have been observed when the polypeptide is purported to be in the helical conformation'. Our observations do not support these conclusions because of the additional information in the DCA–TFA and DCA–$CDCl_3$ mixtures. We find that in these solvent systems as the acidity is reduced the b_0 values increase well beyond the values observed for the TFA–$CDCl_3$ system and these higher b_0 values are accompanied by marked broadening and loss of area of the resonance peaks as shown in *Figure 4*. From this it is suggested that the higher b_0 values and the observed changes in the n.m.r. spectra indicate that poly alanine is capable of assuming a higher helix content than the maximum value obtained for the TFA–$CDCl_3$ solvent system.

The appearance of single peaks of unchanged areas for all the proton resonances when optical techniques indicate 50 per cent helix content can be interpreted in three ways:

(*1*) That large conformational changes in the polypeptide are not reflected in the widths or areas of the peaks in the n.m.r. spectrum. This would appear unlikely in the face of results such as those of Marlborough, Orrell and Rydon[9].

(*2*) As the acidity of the solution is reduced, short fixed lengths of helix are formed which retain sufficient mobility to prevent their resonance lines broadening. However, it seems unlikely that such helical lengths would give resonances of identical widths and positions as those for the random coil form and this is borne out by the shift observed for the C—H resonance which has been attributed to the change of environment resulting from the helix–coil conformational change.

(*3*) This leads to the third interpretation that there is a dynamic equilibrium between the helix and coil forms as helical segments 'ripple' along the polypeptide chain. From the shift observed for the C—H resonance peak an approximate estimate of the lifetime of the proton in the helical conformation can be made and it is found to be less than 7×10^{-3} second in agreement with Stewart *et al.*[11]. It is also possible that such an exchange could proceed through an intermediate state, perhaps in association with solvent molecules as suggested by Glick, Mandelkern and Stewart[10]. It is reasonable to suggest that this process of exchange between helix and coil forms plays a large part in maintaining sharp resonance peaks in partially helical homopolypeptides. However, there must be a point during the coil–helix transition when the helical regions are sufficiently large that their thermal motions are too slow to average out the dipole–dipole interactions and that broadening and loss of area of the peaks occur. In this context we make the suggestion that this point is reached with poly alanine when the b_0 values are in excess of 300° in the TFA–DCA and DCA–$CDCl_3$ solvent systems. In the TFA–$CDCl_3$ system the minimum acid content in which the polypeptide is soluble at 33·5°C is 30% TFA–70% $CDCl_3$ and the b_0 value for this system is about 320°; thus it is possible that for this solvent system the helix content does not reach sufficiently high values to produce peak broadening and loss of area. Obviously there must be a high proportion of random coil material to allow the peak-narrowing process

of exchange between helical and non-helical regions to take place and there is no reason to suggest that the b_0 value of 320°, which on the conventional scale represents just over 50 per cent helix, is not a reasonable indication of helix content.

Discussing further the peak broadening processes, it can be seen from *Table 1* that, although the areas of the resonance peaks remain constant up to a b_0 value of *ca.* 300°, marked broadening of the N—*H* resonance peak appears before this point in the solvent systems containing DCA; in fact there is a steady broadening throughout the whole range of DCA content. This is a specific broadening since neither the C*H* nor the CH_3 proton peaks broaden appreciably until the solvent mixture is reached (20% TFA–80% DCA, $b_0 = 306°$) where there is also loss of area. Although there is a much smaller broadening of the N—*H* resonance peak in TFA–$CDCl_3$ as given by the width at half peak height, it can be seen in *Figures 1* and *2* that the N—*H* peak is asymmetrical and a broad component develops, as the TFA content is reduced, at the expense of the narrow component. It would appear that there is a specific interaction between the carboxylic acid and the amide N—*H* of poly alanine and it might be suggested that the differences observed in this broadening behaviour in the two solvent systems result from differences in the time of interaction of the polypeptide with the TFA and DCA acids.

The n.m.r. and o.r.d. studies at elevated temperatures are interesting from several points of view. First, they demonstrate that there is a temperature inverted helix–coil transition; that is, with increase of temperature up to 55°C for the TFA–$CDCl_3$ system and up to 90°C for the DCA solution there is either an increase of helix content or little change in helix content in the case of the DCA solution. The temperature inverted helix–coil effect has been observed previously for polypeptides in mixed solvents and there is a thermodynamic explanation[21,22]. Secondly, these studies also demonstrate the stability of the poly alanine α-helix in that the DCA solution can be heated to 100°C without any evidence of a breakdown in the helix while there is strong evidence to suggest that poly alanine degrades chemically at 120°C. Also, while there is little change in the n.m.r. spectra of TFA–$CDCl_3$ solutions with increasing temperature except for small shifts upfield in the positions of the N—*H* and C—*H* resonance peaks, there are marked changes in the n.m.r. spectra of the DCA solutions. Although increasing the temperature from 25°C to 90°C produces no change in the b_0 value, the peaks in the n.m.r. spectrum are observed to gain in area and sharpen. This indicates either that the interaction of DCA with poly alanine promotes association of the polypeptide molecules, though this is rendered unlikely by the observation that identical spectra are obtained for more dilute solutions, or that the interaction of DCA with poly alanine, is more effective than that of TFA in slowing down the exchange of helical and non-helical regions and this leads to peak broadening.

The broadening of the DCA O—*H* resonance peak suggested a specific interaction between the acid and the poly alanine and the nature of this interaction was studied further by i.r. spectroscopy. It has been suggested[12–14] that the interaction of strong carboxylic acids with *N*-methyl acetamide and polypeptides causes protonation of the carboxyl of the amide group.

However, whereas we have evidence from i.r. studies in the fundamental region of *N*-methyl acetamide in carboxylic acids to support this suggestion (Bradbury and Stephens, unpublished), the spectral changes observed for poly alanine are different from those observed for *N*-methyl acetamide and are not consistent with the suggestion that protonation of the carboxyl group occurs. The new bands which appear in the i.r. spectra of poly alanine exposed to DCA or TFA are most prominent in the solutions of low acid content, indicating that there is a specific interaction between the acid molecules and the helical component of poly alanine. The changes observed are evidence for a strong hydrogen bonding interaction between a hydrogen-bonded *pair* of amide groups in helical regions and a carboxylic acid molecule, the new bands arising from modified vibrations in the amide groups complexed with the carboxylic acid. This interpretation is supported by the very small shifts of the acid O—*H* peaks observed in the n.m.r. spectra of the solution (*Table 1*) and discussed in detail by Stewart *et al.*[11] who suggest a hydrogen bonding interaction with a single amide group.

It has been suggested[11] that the chemical shifts observed for the different poly L alanine proton resonance peaks with increasing acid content result from anisotropic shielding of protons which is different in the helical polymer from that in the random form and that the shifts are an indication of conformational change in the polypeptide. Our results agree with those of ref. 11 in that the shifts observed, particularly for the α-C*H* and the N*H* peaks, follow changes in b_0 values. However, the i.r. studies show that there is a specific interaction between the carboxylic acids and the *helical* form of poly alanine, and additional magnetic anisotropy effects may result from this interaction; shifts of the peaks observed during the helix–coil transition could reflect changes in the magnetic environment due to the breakdown of this complex as well as that of the helical form of the polypeptide. It is not possible from these studies to determine which would be the major effect; even if it were possible to obtain a helix–coil transition in a single solvent system, e.g. by varying the temperature, it would still not be possible to distinguish between these effects because they would change simultaneously. However, preliminary studies of helix–coil transitions in water-soluble homo- and hetero-polypeptides (Bradbury, Crane-Robinson and Rattle, unpublished observations) show a very much smaller shift in the α-C*H* resonance peak than that observed for poly alanine in the TFA–DCA–$CDCl_3$ solvent mixtures. This suggests that the specific interaction of the carboxylic acid molecule with the helical form of poly alanine is a possible cause of shifts observed over the helix–coil transition. Because this interaction is between the acid molecule and the helical form of the polymer, the shifts due to it would be expected to follow the breakdown of the helix, as is observed.

It is well known[19] that solutions of poly alanine in the highest acid content do not give zero b_0 values. In this study it was found that solutions of poly L alanine in TFA and poly D alanine in 90% TFA–10% $CDCl_3$ gave b_0 values of $-96°$ and $+121°$ respectively. It is of interest to know whether these b_0 values indicate a fully random polypeptide or whether there is a residual helix content even in TFA. Stewart *et al.*[11] have compared the shifts of the poly L alanine resonance peaks with those of poly DL alanine in the

same solvent systems and suggest that because the positions of the poly L alanine peaks converge on those of poly DL alanine in TFA that poly L alanine must be completely random in this solvent. However, although the positions of the α-C*H* peak and the methyl proton peak converge on the values obtained for poly DL alanine, there remains an experimentally significant difference for TFA solutions and it is not clear whether this difference might indicate a low residual helix content in poly L alanine in TFA. The i.r. spectra of poly alanine in TFA or in 90% TFA–10% $CDCl_3$ are interesting in that they show the presence of a weak shoulder at 1 651 cm^{-1} which increases in intensity as the acid content of the solution is reduced. This band is characteristic of the α-helix form of poly alanine and the presence of a weak shoulder in the spectrum of the pure TFA solution probably indicates a residual helical component in the TFA solution. Our studies therefore do not support the conclusions of Stewart *et al.*[11] that b_0 values are an unreliable guide for the measurement of high and low helix contents of polypeptides.

An essential point raised by these studies and by similar studies of polynucleotides[2,25] is the definition of order and disorder of macromolecules in solution. The widely used techniques of optical rotatory dispersion, circular dichroism and i.r. spectroscopy when applied to solutions measure ordered conformations which have a lifetime which is long compared with 10^{-12} to 10^{-14} second. Hence intermediate values of optical parameters can arise either from a dynamic equilibrium between helical and non-helical regions where exchange between these regions occurs at frequencies corresponding to thermal motions, as has been shown here for poly alanine and for polynucleotides[2,25] or from a static equilibrium between helical and non-helical regions where there is no exchange between these regions, as probably exists for macromolecules such as myoglobin, haemoglobin and lysozyme. It does not follow, however, that all proteins belong to the latter class and it is not impossible that for some proteins, particularly those of low molecular weight, the optical parameters measure the helical content of a dynamic equilibrium between helical and non-helical regions. Magnetic resonance techniques may be the only ones able to characterize such dynamic equilibria.

The authors are grateful to Dr C. Crane-Robinson and Mr L. G. M. Mariasy for their helpful suggestions and discussions of this work and to Mr R. M. Stephens for recording the i.r. spectra. Facilities for use of the variable-temperature probe were kindly provided by Perkin–Elmer Ltd, Beaconsfield, Bucks., and by the Department of Chemistry, University of Southampton on their Varian A60 spectrometer. Perkin–Elmer Ltd also allowed the authors to record spectra on their 100 Mc/s spectrometer.

Acknowledgement is also made to the Governors of the College for the award of a research assistantship to one of us (H.W.E.R.) and to the Science Research Council for research grants B/SR/399 and B/SR/2892.

Department of Physics,
College of Technology,
Portsmouth, Hants.

(Received May 1967)

REFERENCES

[1] JARDETZKY, O. and JARDETZKY, C. D. *Methods of Biochemical Analysis.* Vol. IX, p 235. Ed. D. GLICK, Interscience: New York, 1962
[2] JARDETZKY, O. *Biopolymers Symposia No. 1,* p 501. Interscience: New York, 1964
[3] JARDETZKY, O. *Adv. Chem. Phys.* 1964, **7,** 499
[4] KOWALSKY, A. and COHN, M. *Ann. Rev. Biochem.* 1964, **33,** 481
[5] KOWALSKY, A. *J. biol. Chem.* 1962, **237,** 1807
[6] BOVEY, F. A. and TIERS, G. V. D. *J. Amer. chem. Soc.* 1959, **81,** 2870
[7] BOVEY, F. A., TIERS, G. V. D. and FILIPOVICH, G. *J. Polym. Sci.* 1959, **38,** 73
[8] GOODMAN, M. and MASUDA, Y. *Biopolymers,* 1964, **2,** 107
[9] MARLBOROUGH, D. I., ORRELL, K. G. and RYDON, H. N. *Chem. Commun.* 1965, **1** (No. 21), 518
[10] GLICK, R. E., MANDELKERN, L. and STEWART, W. E. *Biochim. Biophys. Acta.* 1966, **120,** 302
[11] STEWART, W. E., MANDELKERN, L. and GLICK, R. E. *Biochemistry,* 1967, **6,** 143
[12] HANLON, S., RUSSO, S. F. and KLOTZ, I. M. *J. Amer. chem. Soc.* 1963, **85,** 2024
[13] HANLON, S. and KLOTZ, I. M. *Biochemistry,* 1965, **4,** 37
[14] HANLON, S. *Biochemistry,* 1966, **5,** 2049
[15] STAKE, M. J. and KLOTZ, I. M. *Biochemistry,* 1966, **5,** 1726
[16] MALCOLM, B. R. and ELLIOTT, A. *J. sci. Instrum.* 1957, **34,** 48
[17] MOFFITT, W. and YANG, J. T. *Proc. Nat. Acad. Sci., Wash.* 1956, **42,** 596
[18] BRADBURY, E. M. and FORD, M. A. *Applied Optics,* 1966, **5,** 235
[19] FASMAN, G. D. *Polyamino Acids, Polypeptides and Proteins,* p 221. Ed. M. STAHMANN. University of Wisconsin Press, 1962
[20] DOTY, P. and GRATZER, W. B. *Polyamino Acids, Polypeptides and Proteins,* p 111. Ed. M. STAHMANN. University of Wisconsin Press, 1962
[21] DOTY, P. and YANG, J. T. *J. Amer. chem. Soc.* 1956, **78,** 498
[22] SCHELLMAN, J. *J. phys. Chem.* 1958, **62,** 1485
[23] BAMFORD, C. H., ELLIOTT, A. and HANBY, W. E. *Synthetic Polypeptides.* Academic Press: New York, 1956
[24] ELLIOTT, A. *Proc. Roy. Soc. A,* 1954, **226,** 408
[25] MCTAGUE, J. P., ROSS, V. and GIBBS, J. H. *Biopolymers,* 1964, **2,** 163
[26] MCDONALD, C. C., PHILLIPS, W. D. and PENSWICK, J. *Biopolymers,* 1965, **3,** 609
[27] MCDONALD, C. C., PHILLIPS, W. D. and PENMAN, S. *Science,* 1964, **144,** 1234

Book Review

Progress in Nuclear Magnetic Resonance Spectroscopy Vols. 1 and 2

Edited by J. W. EMSLEY, J. FEENEY and L. H. SUTCLIFFE. 386 pp; 270 pp. 6 in. by 9 in.

Pergamon: Oxford, 1966, 1967. 115*s*, 90*s*

POLYMER scientists will be disappointed to read in the preface that the editors propose to limit this series of review volumes to the high resolution aspects of n.m.r. spectroscopy. The implication is that broad line measurements on polymers and the study of molecular mobility by pulsed techniques will not be covered. Although the simultaneous appearance of *two* review ventures in the same field is unfortunate, at least the Academic Press volumes *Advances in Magnetic Resonance* promise a wider coverage of n.m.r. spectroscopy.

The nine articles in the first two volumes of *Progress in Nuclear Magnetic Resonance Spectroscopy* are, each in their own way, of a commendably high standard. There are very few specific references to polymers but some of the reviews include relevant information.

Volume one has four chapters:

1. 'The Use of Modulation in Magnetic Resonance' by O. HOWARTH and R. E. RICHARDS.
2. 'High Resolution Nuclear Magnetic Double and Multiple Resonance' by R. A. HOFFMAN and S. FOREN.
3. 'Computer Techniques in the Analysis of n.m.r. Spectra' by J. D. SWALEN.
4. 'Studies of Phosphorus Compounds using the Magnetic Resonance Spectra of Nuclei other than ^{31}P' by G. MAVEL.

Chapters 2 and 3 are useful introductions for anyone wishing to specialize in the analysis of high resolution spectra. Chapter 4, distinguished by its gigantic bibliography, is of value only to workers with a direct interest in phosphorus compounds.

The five chapters of volume two are:

1. 'Chemical Shift Calculations' by D. E. O'REILLY.
2. 'High Resolution Nuclear Magnetic Resonance in Partially Oriented Molecules' by A. D. BUCKINGHAM and K. A. MCLAUCHALN.
3. 'Nuclear Magnetic Resonance of Paramagnetic Systems' by E. DE BOER and H. VAN WILLIGEN.
4. 'Calculation of Live Shapes by Density Matrix Methods' by RUTH M. LYNDEN-BELL.
5. 'The Cause and Calculation of Proton Chemical Shifts in Non-conjugated Organic Compounds' by R. F. ZURCHER.

Apart from the general interest in correlating chemical shifts with molecular structure discussed semi-quantitatively in Chapter 5, there are snippets of the various contributions of direct concern to the polymer scientist. Chapter 2 ends with a tantalising reference to a private communication to molecular orientation in a swollen crosslinked butadiene–styrene rubber, but no real information. The sections on chemical exchange and the influence of relaxation on line shapes in Chapter 4 will be useful to specialists.

These two volumes are valuable assets for polymer science libraries but only a few scientists will need to buy personal copies.

G. ALLEN

Communications

Comments on the Papers on 'Thermal Degradation of Vinyl Polymers' Parts I to III by Richards and Salter[1]

THESE interesting publications contain a number of inaccuracies. Also, the history of the degradation of polystyrene is not stated correctly. 'Weak links' in polystyrene were postulated as far back as 1944[2]. The kinetic chain length of five to six monomer units per radical chain end produced was reported in 1949[3]. The criticism of Atherton mentioned in the first paper by Richards and Salter does not refer to the U-tubes but to a vacuum spring balance[3]. This criticism is based on unsuccessful manipulation of this balance by Atherton at Cambridge in 1945. There was negligible sputtering for the temperature range employed in the degradation experiments on polystyrene[3]; sputtering only became appreciable for higher temperatures, where the loss of weight became very fast.

The assertion that styrene was not formed at about 280°C contradicts results obtained previously[2, 3]. The amounts of monomer were not large, but could be ascertained readily.

The calculations of Simha, Wall and Blatz[4], which are quoted repeatedly in the paper are only valid for the initial stages of degradation, where volume decrease is negligible or for degradation in inert solvents. Volume changes and concentration terms during degradation were not considered by these authors. Degradation processes formulated in terms of concentrations and treating in detail the influence of volume changes have been published[5]. Volume changes can be neglected in cases where only first order reactions are operative.

The equation in Part I, p 135 (bottom) for the rate of styrene production is not correct, if the assumption is made that each α•-monomer radical leads to one chain scission in polystyrene. In this case, the rate of chain scission is independent of the amount of polystyrene. One has for styrene production from one volume unit for a heterogeneous system

$$dm_1'/dt = k_d\,[\mathrm{R}] \text{ moles volume}^{-1} \text{ time}^{-1} \tag{1}$$

where [R] is the steady state radical concentration

$$[\mathrm{R}] = (2k_i/V_{m,\alpha}k_t)^{1/2} \tag{2}$$

Here $V_{m,\alpha}$ is the monomeric unit molar volume for poly-α-methylstyrene, which is a constant. The number of monomeric unit moles in a volume unit is a constant, i.e. $1/V_{m,\alpha}$, and the number of moles of main chain bonds in a volume unit is given by

$$(1/V_{m,\alpha})\,(\overline{DP}_{n,t} - 1)/(\overline{DP}_{n,t}) \tag{3}$$

where $\overline{DP}_{n,t}$ is the chain length, not including monomer, at time t. This factor is practically equal to one, except for very high degrees of degrada-

tion. Hence, the rate of monomer formation from one monomeric-unit mole is

$$dm_1''/dt = k_d (2k_i/V_{m,a}k_t)^{1/2} V_{m,a} \tag{4}$$

and from W_a/m_a monomeric unit moles

$$dm_1'''/dt = k_d (2k_i/k_t)^{1/2} V_{m,a}^{1/2} (W_{a,t}/m_a)$$

The styrene production in grammes per time for the whole system is then given by

$$\frac{dm_1}{dt} = \frac{dm_1''' m_s}{dt} = r_s^0 = k_d \left(\frac{2k_i}{k_t}\right)^{1/2} V_{m,a}^{1/2} \frac{W_{a,t}}{m_a} m_s \,(\mathrm{gt}^{-1}) \tag{5}$$

The notation is the same as in Richards and Salter's papers.

Equations (3), (4), (5), (7) and (8) in Part II are not the expressions for the monomer evolved from the whole system, but refer only to the monomer obtained from one volume unit. For monomer evolved from one volume unit, one has for ($k_c \longrightarrow 0$),

$$\frac{dm_1}{dt} = k_d \left(\frac{2k_i}{k_t}\right)^{1/2} \left(\frac{\overline{DP'}_{n,t} - 1}{\overline{DP}_{n,t}}\right)^{1/2} [\mathrm{X}]^{1/2} \frac{\text{moles}}{\text{volume} \times \text{time}} \tag{6}$$

The term containing the chain lengths is practically equal to one; [X] is the concentration of weak links. For the moles evolved from the whole system, one has

$$dm_{1,\text{total}}/dt = k_d (2k_i/k_t)^{1/2} [\mathrm{X}]^{1/2} V_t \text{ moles/time} \tag{7}$$

Here V_t is the volume of the whole polymer system at time t. $V_t = V_m (m_0 - m_{1,\text{total}})$, where V_m is again the monomeric unit molar volume and m_0 the monomeric unit moles in the polymer at time $t=0$; $m_{1,\text{total}}$ is the number of moles produced from the whole system at t. Hence,

$$dm_{1,\text{total}}/dt = k_d (2k_i/k_t)^{1/2} [\mathrm{X}]^{1/2} V_m (m_0 - m_{1,\text{total}}) \tag{8}$$

Equation (8), on integration, gives

$$\ln \frac{m_0}{m_0 - m_{1,\text{total}}} = 2k_d \left(\frac{[\mathrm{X}_0]}{k_i k_t}\right)^{1/2} V_m (1 - e^{-k_i t/2}) \tag{9}$$

or, as

$$[\mathrm{X}] = X/(m_0 - m_{1,\text{total}})$$

$$2\,[m_0^{1/2} - (m_0 - m_{1,\text{total}})^{1/2}] = 2k_d \left(\frac{X_0}{k_i k_t}\right)^{1/2} V_m (1 - e^{-k_i t/2}) \tag{10}$$

Similarly ($k_t \longrightarrow 0$),

$$\ln m_0/(m_0 - m_{1,\text{total}}) = (k_d V_m/k_c)\,[\mathrm{X}_0]\,(1 - e^{-k_i t}) \tag{11}$$

or

$$m_{1,\text{total}} = (k_d/k_c)\, X_0 (1 - e^{-k_i t}) \tag{12}$$

The LHS of equation (3) in Richards and Salter's paper (Part II) should read $\ln m_0/(m_0 - m_{1,\text{total}})$ and the RHS should be multiplied by V_m.

Lastly, a few remarks may be made about transfer during polystyrene degradation (Part III). Nakajima, Harmeda and Shimizu[6] have investigated isotactic polystyrene recently. They found no trace of weak links and the energy of activation agreed with that found previously for normal links in atactic polystyrene[3]. It is very unlikely that the mechanism of thermal degradation for iso- and a-tactic polystyrene, respectively, is different except for small numerical differences in the rate constants, energies of activation, etc. Hence, the work by these Japanese authors constitutes definitive proof that weak links are present in the atactic polymer; if the phenomenon were due to transfer, there is no reason why transfer should not also be operative in the isotactic polymer. It appears still likely that the nature of the weak links as found previously[3] is due to oxygenated groups.

H. H. G. JELLINEK

Department of Chemistry,
Clarkson College of Technology,
Potsdam, N.Y. 13676, U.S.A.

(Received November 1967)

REFERENCES

[1] RICHARDS, D. H. and SALTER, D. A. *Polymer, Lond.* 1967, **8**, 127, 139, 153
[2] JELLINEK, H. H. G. *Trans. Faraday Soc.* 1944, **40**, 1
[3] JELLINEK, H. H. G. *J. Polym. Sci.* 1949, **4**, 1; see also JELLINEK, H. H. G. *Trans. Faraday Soc.* 1948, **44**, 345; *J. Polym. Sci.* 1948, **3**, 850; 1949, **4**, 13; Chapter 13, *Monograph of Styrene, No. 115,* ACS (1952); *NBS Circular 525* (1952); *Degradation of Vinyl Polymers,* Academic Press: New York, 1955
[4] SIMHA, R., WALL, L. A. and BLATZ, P. J. *J. Polym. Sci.* 1950, **5**, 615; 1951, **64**, 39
[5] JELLINEK, H. H. G. *Encyclopedia of Polymer Science,* Vol. IV, p 740. Wiley: New York, 1966; see also BOYD, R. H. *J. chem. Phys.* 1959, **31**, 321 and BOYD, R. H. and TUNG-PO LIN, *Symposium on Mechanisms of Polymer Degradation,* ACS Meeting, Chicago, September 1964, *Polymer Preprints,* **5**, No. 2, p 317
[6] NAKAJIMA, A., HARMEDA, F. and SHIMIZU, T. *Makromol. Chem.* 1966, **90**, 229

Reply to Jellinek's Comments

WE READ with interest Jellinek's comments on the three papers we published in this Journal about a year ago and will deal with these observations in the order in which they are presented above.

Jellinek is mistaken in his belief that the introductory paragraph in Part I was meant to be an historical survey of the work on polystyrene degradation. This is a long and complicated subject and has been adequately covered by a number of books including Jellinek's own. Our few lines merely put the variety of viewpoints currently held, by reference to some of the more recent papers in the field. However, we readily acknowledge Jellinek's claim to have been the first to propose both the weak link theory and the short kinetic chain length in polystyrene.

The LHS of equation (3) in Richards and Salter's paper (Part II) should read $\ln m_0/(m_0 - m_{1,\text{total}})$ and the RHS should be multiplied by V_m.

Lastly, a few remarks may be made about transfer during polystyrene degradation (Part III). Nakajima, Harmeda and Shimizu[6] have investigated isotactic polystyrene recently. They found no trace of weak links and the energy of activation agreed with that found previously for normal links in atactic polystyrene[3]. It is very unlikely that the mechanism of thermal degradation for iso- and a-tactic polystyrene, respectively, is different except for small numerical differences in the rate constants, energies of activation, etc. Hence, the work by these Japanese authors constitutes definitive proof that weak links are present in the atactic polymer; if the phenomenon were due to transfer, there is no reason why transfer should not also be operative in the isotactic polymer. It appears still likely that the nature of the weak links as found previously[3] is due to oxygenated groups.

H. H. G. JELLINEK

Department of Chemistry,
Clarkson College of Technology,
Potsdam, N.Y. 13676, U.S.A.

(Received November 1967)

REFERENCES

[1] RICHARDS, D. H. and SALTER, D. A. *Polymer, Lond.* 1967, **8**, 127, 139, 153
[2] JELLINEK, H. H. G. *Trans. Faraday Soc.* 1944, **40**, 1
[3] JELLINEK, H. H. G. *J. Polym. Sci.* 1949, **4**, 1; see also JELLINEK, H. H. G. *Trans. Faraday Soc.* 1948, **44**, 345; *J. Polym. Sci.* 1948, **3**, 850; 1949, **4**, 13; Chapter 13, *Monograph of Styrene, No. 115,* ACS (1952); *NBS Circular 525* (1952); *Degradation of Vinyl Polymers,* Academic Press: New York, 1955
[4] SIMHA, R., WALL, L. A. and BLATZ, P. J. *J. Polym. Sci.* 1950, **5**, 615; 1951, **64**, 39
[5] JELLINEK, H. H. G. *Encyclopedia of Polymer Science,* Vol. IV, p 740. Wiley: New York, 1966; see also BOYD, R. H. *J. chem. Phys.* 1959, **31**, 321 and BOYD, R. H. and TUNG-PO LIN, *Symposium on Mechanisms of Polymer Degradation,* ACS Meeting, Chicago, September 1964, *Polymer Preprints,* **5**, No. 2, p 317
[6] NAKAJIMA, A., HARMEDA, F. and SHIMIZU, T. *Makromol. Chem.* 1966, **90**, 229

Reply to Jellinek's Comments

WE READ with interest Jellinek's comments on the three papers we published in this Journal about a year ago and will deal with these observations in the order in which they are presented above.

Jellinek is mistaken in his belief that the introductory paragraph in Part I was meant to be an historical survey of the work on polystyrene degradation. This is a long and complicated subject and has been adequately covered by a number of books including Jellinek's own. Our few lines merely put the variety of viewpoints currently held, by reference to some of the more recent papers in the field. However, we readily acknowledge Jellinek's claim to have been the first to propose both the weak link theory and the short kinetic chain length in polystyrene.

Our statement regarding Atherton's paper was rather badly phrased and was perhaps open to misinterpretation. Our initial experiments using U-tubes identical to those of Jellinek gave variable results which we ascribed to sputtering. This effect was minimized by introducing thin-walled glass bulbs to contain the polymer samples.

We think that Jellinek's comment on styrene evolution at 280°C is pedantic. Our remarks referred specifically to the time scales of our experiments and we are aware the exponential relationship between rate constant and temperature implies that a reaction observable at 330°C, say, would also proceed at 280°C but more slowly. Furthermore, in Part III we measured the amount of styrene evolved from thermally polymerized polystyrene at 284°C and commented that it was about twenty-five times that given by anionically synthesized polystyrene.

We have repeatedly quoted the paper of Simha, Wall and Blatz precisely because our systems, too, are concerned with the initial stages of degradation where the volume decrease is negligible (< 1 per cent polystyrene Part I and ≈ 5 per cent Part II), or for degradation in inert solvents (Parts II and III).

Jellinek's analysis of the kinetics of polystyrene degradation induced by α-methyl styrene monomer radicals [equations (1) to (5)] is not correct. This may be seen qualitatively as follows:

If each $\alpha\cdot$ monomer radical leads to one chain scission in polystyrene then the rate of chain scission is, of course, independent of the amount of polystyrene. However, the rate of termination of these polystyrene radicals, assuming a second order process, will depend on their concentration. Hence the radical lifetime, and so the rate of monomer evolution, will increase with dilution in the polystyrene melt. This dependence should be reflected in a term involving w_s, but this does not appear in his equation (5).

We are unable to follow the reasoning behind Jellinek's analysis and suspect that he has misunderstood the nature of the system we were studying. We therefore give our derivation of the disputed equation. For simplicity we use base mole units as previously rather than Jellinek's volume units.

Under conditions where the PMS radicals unzip completely, rate of formation of monomer radicals is twice the rate of scission of PMS

$$= 4k_i w_\alpha / m_\alpha \text{ moles/sec}$$

Then, rate of formation of PS radicals/base mole styrene

$$= 4w_\alpha m_s k_i / m_\alpha w_s$$

Under steady state conditions,

$$\text{rate of formation of radicals} = \text{rate of their termination}$$

$$4w_\alpha m_s k_i / m_\alpha w_s = 2k_t P\cdot^2$$

$$P\cdot = (2w_\alpha m_s k_i / w_s m_\alpha k_t)^{\frac{1}{2}}$$

rate of production of styrene in moles/sec per base mole styrene

$$= k_d P\cdot$$

$$= k_d (2w_\alpha m_s k_i / w_s m_\alpha k_t)^{\frac{1}{2}}$$

rate of production of styrene (g/sec) from sample (g)

$$r_s = k_d (2w_s w_a m_s k_i / m_a k_t)^{\frac{1}{2}}$$

We accept Jellinek's point regarding the rate equations in Part II. The symbol 'm' on the LHS of these equations should have been defined as the fraction of monomer evolved (m/m_0) rather than the amount. The calculations in this paper, however, have used this fractional relationship, and are therefore unaffected. Jellinek's equations (10) and (11) differ from ours in two respects, the RHS has the extra term V_m arising from the difference in units and a more complicated LHS. In both cases, when the LHS is expanded and a first approximation taken, it can be reduced to the m/m_0 obtained in our corrected equations. As the maximum volume change in our experiments is ≈ 5 per cent, the maximum error introduced into our calculations by having made this approximation is $< 0{\cdot}1$ per cent.

We cannot see the relevance of Jellinek's last paragraph in relation to chain transfer during degradation. There is considerable evidence that the concentration of weak links in the polymer is related to the temperature and other conditions of polymerization. We have found large differences in the low temperature breakdown of thermally polymerized (180°C) and anionically polymerized polystyrene (0°C) (Part III). In both these cases the polymerizations were conducted in high vacuum conditions so that it is extremely unlikely that weak links found in either material were due to oxygenated groups. The point at issue is, however, the prominence of chain transfer during degradation rather than the presence or absence of weak links. Whilst we accept that our Part III paper is not necessarily conclusive on chain transfer, we cannot accept that the excellent work of the Japanese authors provides definitive proof on this matter either.

D. H. RICHARDS
and D. A. SALTER

Explosives Research and Development Establishment,
Ministry of Technology,
Waltham Abbey, Essex

(Received January 1968)

Moulding Anisotropy in ABS Polymers as Revealed by Electron Microscopy

KOICHI KATO

The causes of delamination in thin-walled ABS injection-mouldings were investigated by light and electron microscopy of thin sections. Delamination occurs at some depth below the moulded surface, and is due to a layered structure in which the rubber particles are segregated according to size, obliquely deformed, and grouped along the flow lines in rows. This structure is set up during moulding when a certain shear rate is exceeded.

THE injection moulding of thermoplastics usually produces mouldings which are more or less anisotropic owing to the orientation of the polymer molecules[1, 2]. The degree of anisotropy depends on the chemical and physical properties of the polymer involved, the moulding conditions, the geometry of the mould used, etc. This type of anisotropy should be called molecular anisotropy.

ABS polymers are heterogeneous in nature, being composed of two different phases, viz. a finely dispersed rubber phase and a continuous resin phase. As a result of this structure, injection moulding can produce another type of anisotropy, which is caused by the orientation of the particulate phase along the flow lines. This phenomenon, which may be called phase anisotropy, is the main subject of the present paper.

The osmium tetroxide procedure for light and electron microscopy of ABS plastics was described in a previous paper[3], and was further applied to the study of electroplating of ABS mouldings, in combination with a surface replica technique[4]. The same sectioning procedure has now been used to reveal characteristic flow patterns in ABS injection mouldings. In the course of this work it has been found that the so-called delamination, an occasional trouble in the practice of ABS injection moulding, can be accounted for in terms of phase anisotropy due to the orientation of rubber particles.

EXPERIMENTAL

Test specimens were specially prepared in the form of a wash basin with a 2 mm wall thickness, under a set of conditions so severe as to result in typical delamination. They were found to peel readily into layers, just like mica. The resin used was Toyolac 100, a standard grade of ABS polymer made by Toyo Rayon Co.

OPTICAL MICROSCOPY

Figure 1 shows a photomicrograph of a section about three microns thick prepared from the side wall of the test specimen described above. The sectioning direction was set exactly parallel to the injection flow direction, and the thin section was positioned diagonally between the crossed polaroids of a polarizing microscope. If any birefringence is caused by the orientation of the polymer molecules, the corresponding area should appear

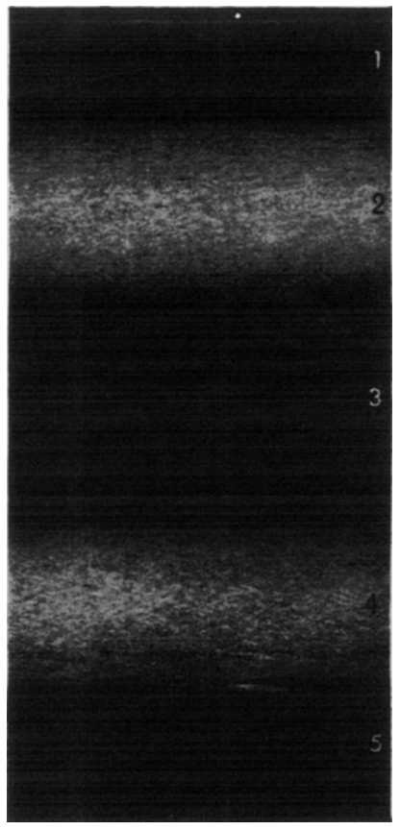

Figure 1—Photomicrograph of a thin section through an ABS injection-moulded piece under polarized light. Magnification × 50: reproduced without reduction. 1, Top surface layer: 2, Delaminating layer: 3, Central zone: 4, Delaminating layer: 5, Bottom surface layer

more or less bright against the dark background. Disregarding the top and bottom surface layers, which were in direct contact with the mould wall, the photomicrograph shows very bright zones on each side of the dark central zone. It has been ascertained that delamination takes place precisely in these most birefringent zones.

It should be noted that the birefringence observed here is of negative sign with respect to the flow direction, indicating that the oriented molecules are simply the copolymer of styrene and acrylonitrile, with its inherent negative birefringence.

Figure 2 shows a series of photomicrographs of thin sections prepared from the same specimen as shown in *Figure 1*. The pictures on the left were taken from sections cut along the injection flow direction, while those on the right were obtained from sections cut perpendicular to the flow direction. The numbers entered in *Figure 2* correspond to the numbers in *Figure 1*. Each section preparation was processed with osmium tetroxide vapour to differentiate the rubber phase in the light microscope[3]. Dark-stained rubber particles, though not individually resolved, show up general flow patterns that vary considerably with the depth in the moulding as well as with the direction of observation.

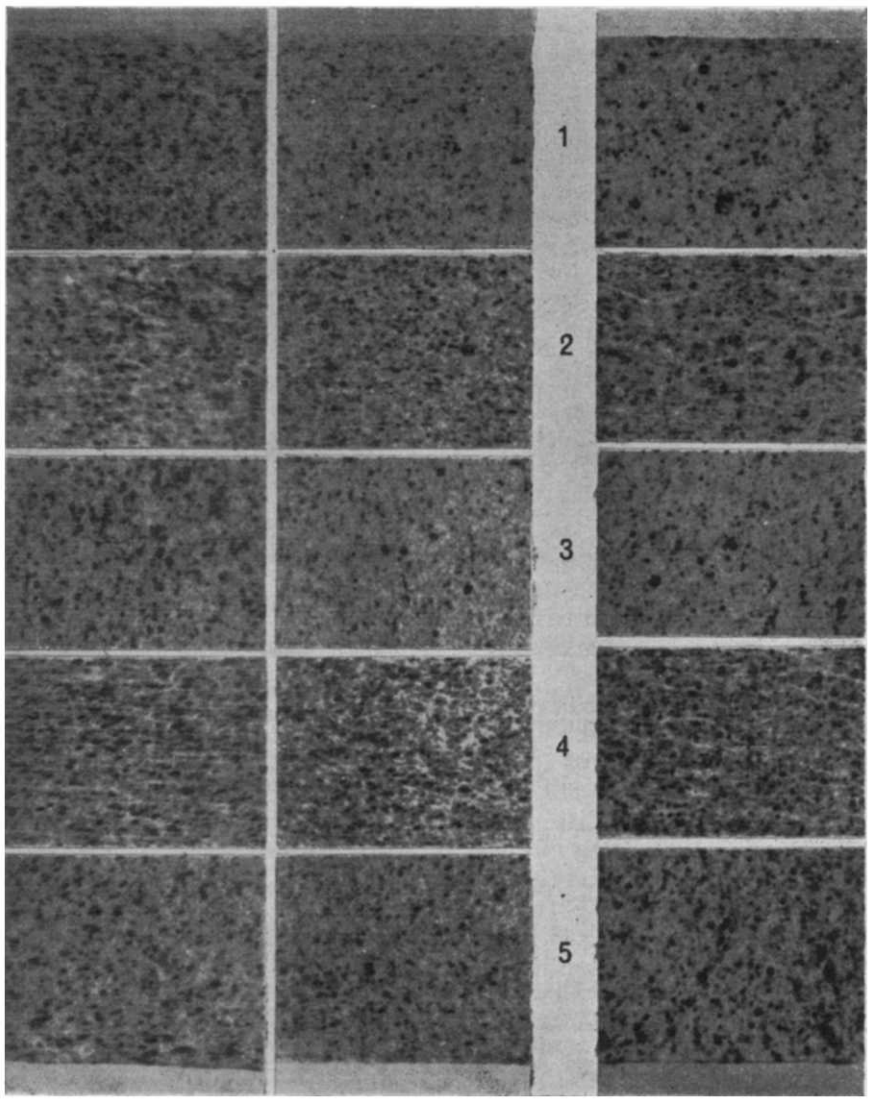

Figure 2 *Figure 3*

Figure 2—Photomicrographs of thin sections through an ABS injection-moulded piece with transmitted light. Osmium tetroxide vapour stained. Magnification × 550: reproduced without reduction

Figure 3—Photomicrographs of thin sections through an ABS injection-moulded piece after annealing. Magnification × 550: reproduced without reduction

The most noticeable pattern is localized in the delamination layers, and consists of a number of parallel bright lines with apparently aligned rubber particles. The true nature of this structure will be shown later by electron microscopy.

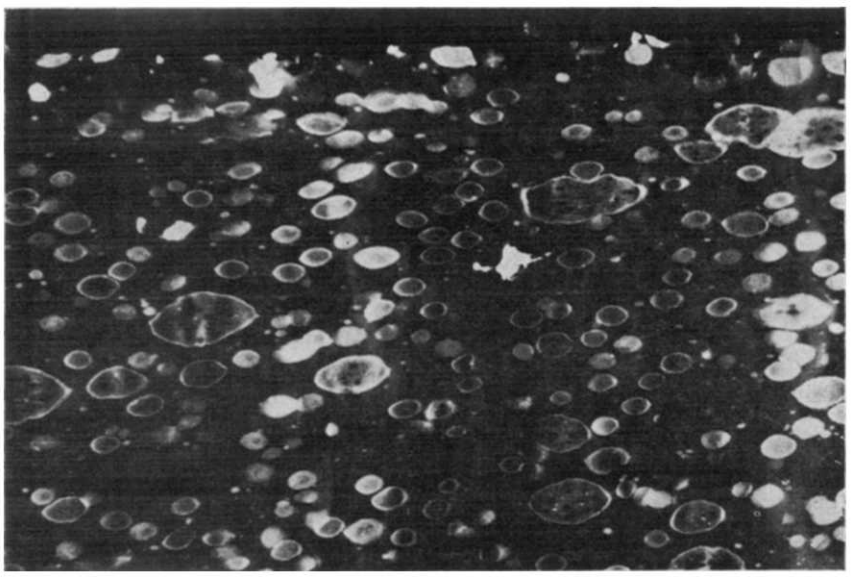

Figure 4—Ultrathin section (parallel) through surface layer of the same specimen as in *Figure 3*

Figure 3 illustrates the effect of annealing on the test specimen, although only sections cut along the flow direction are shown. Every rubber particle appears to have recovered from deformation, and the parallel lines in the delamination layers are also seen to be considerably disordered. In fact, after annealing the test specimens no longer exhibited any tendency to delaminate.

ELECTRON MICROSCOPY

Figures 4 to *10* are electron micrographs of ultrathin sections prepared by the osmium tetroxide procedure[3]. Each of these figures carries a one-micron scale bar. They are presented as negative prints, in which the osmium-stained rubber phase appears bright against the darker resin matrix. The ultrasectioning was carried out in a direction normal to the specimen surface (wash basin wall surface), either parallel or perpendicular to the flow direction. In all pictures showing parallel sections the injection flow direction runs horizontally from left to right.

A parallel section through the surface layer is shown in *Figure 4,* in which all the rubber particles are elongated parallel to the surface edge. This effect has already been discussed in relation to electro-plating in a previous paper[4]. Strictly speaking, the outermost edge layer should be distinguished from the underlying subsurface zone, because the former was formed in contact with the mould wall. Evidence for this distinction may be seen in *Figure 5*, which shows a perpendicular section through the surface layer. The outermost layer, appearing in the upper portion of the picture, contains seriously deformed rubber particles, whereas each particle

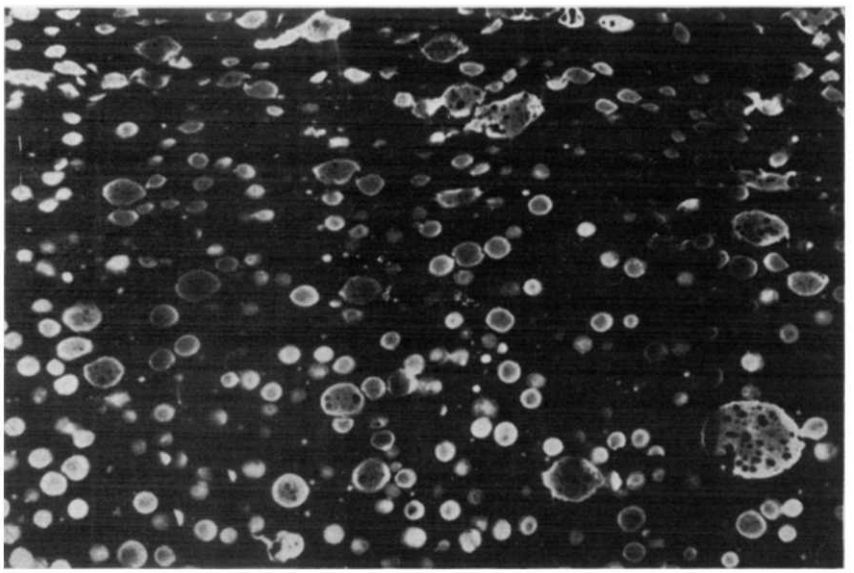

Figure 5—Ultrathin section (perpendicular) through surface layer

in the subsurface zone appears almost circular in shape as viewed from the flow direction.

A parallel section through the zone lying between the surface layer and the delamination layer is shown in *Figure 6*. The rubber particles, particularly the larger ones, are obliquely deformed and inclined to the flow

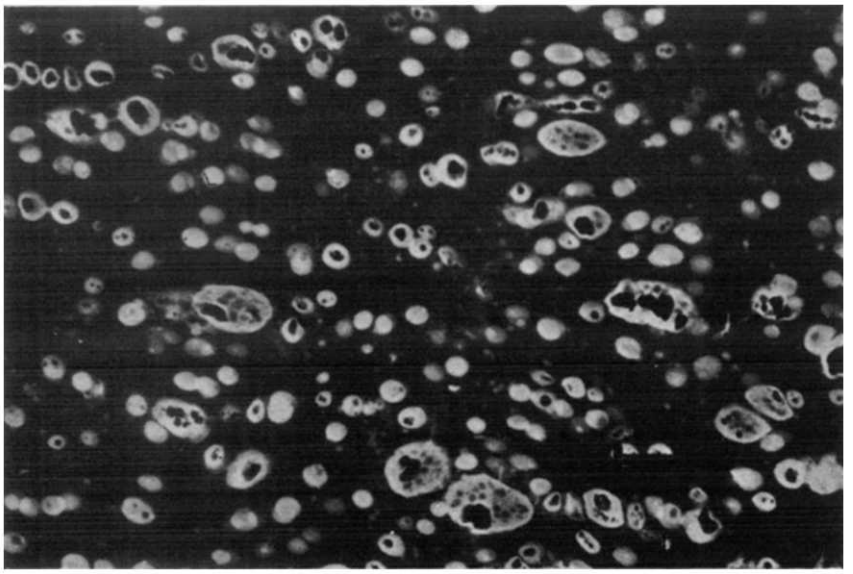

Figure 6—Ultrathin section (parallel) through the portion lying between surface layer and delamination layer

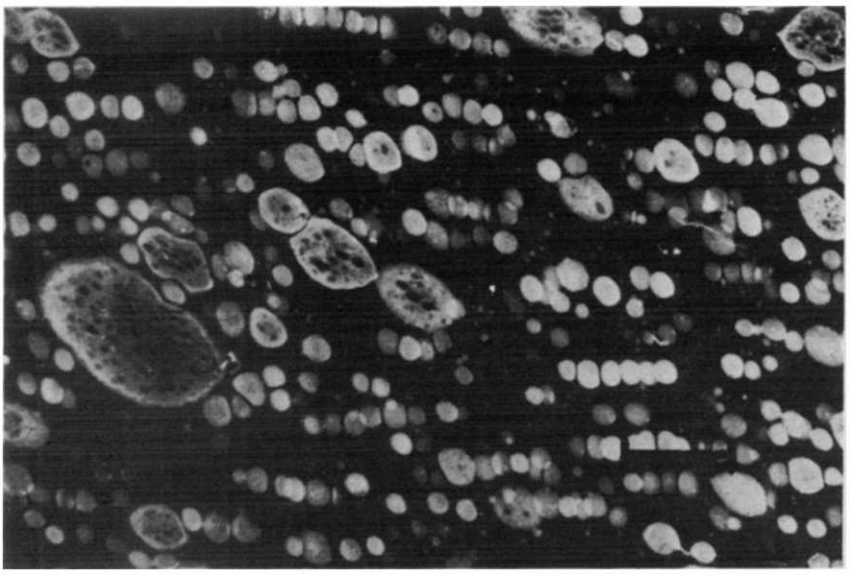

Figure 7—Ultrathin section (parallel) through delamination layer

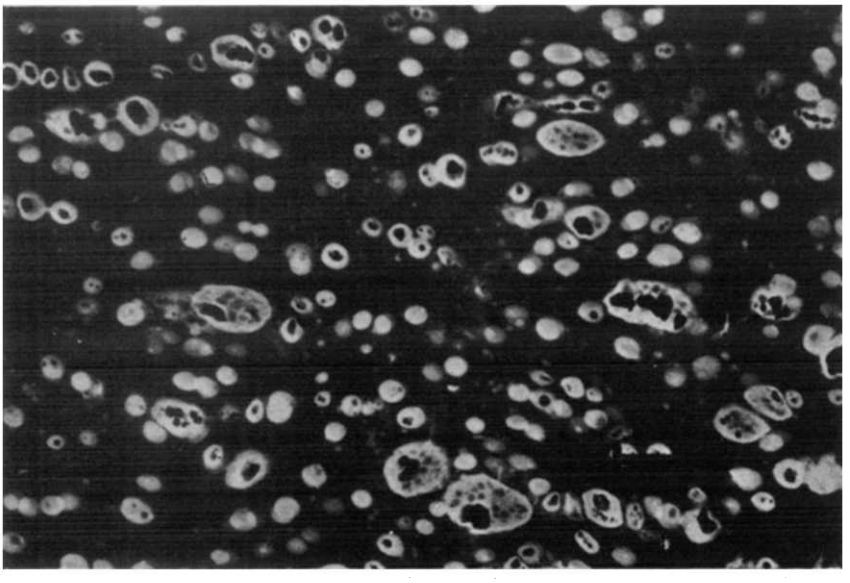

Figure 8—Ultrathin section (perpendicular) through delamination layer

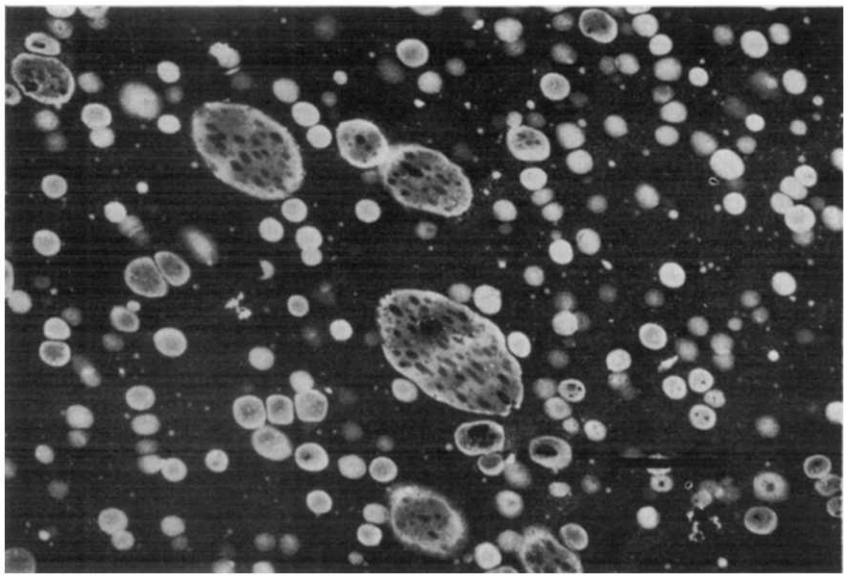

Figure 9—Ultrathin section (parallel) through the portion lying below delamination layer

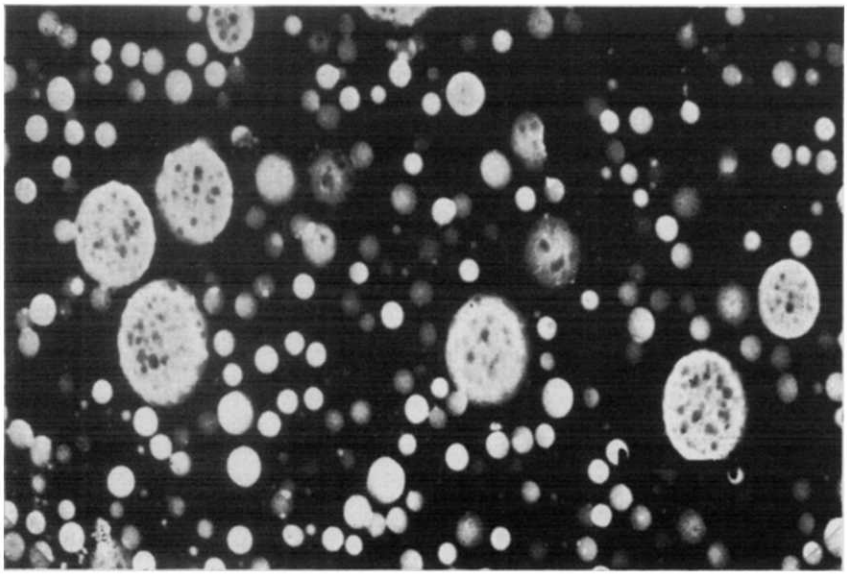

Figure 10—Ultrathin section (parallel) through central zone

direction, indicating a gradient of flow velocity during moulding.

A parallel section through the delamination layer is presented in *Figure 7*. It is clear that the rubber particles are not only segregated according to size, but are also arranged row by row along the flow lines. This row pattern appears to a lesser degree in *Figure 8*, which shows a perpendicular section through the same delamination layer. The parallel bright lines observed under the light microscope are obviously due to this planar alignment of rubber particles. *Figure 8* also reveals that some destructive changes occurred within each larger rubber particle.

A parallel section through the zone beneath the delamination layer is illustrated in *Figure 9*. The row structure has virtually disappeared, but the rubber particles are again inclined in the same manner as in *Figure 6*, and must therefore have been subjected to the same kind of flow velocity gradient.

A parallel section through the central zone is shown in *Figure 10*. There appears to be no flow pattern; on the contrary, every rubber particle is somewhat elongated in the direction normal to the injection flow. This observation suggests that moulding conditions in this zone are similar to those occurring in compression moulding.

CONCLUSIONS

Low power examination with the polarizing microscope (*Figure 1*) has indicated that molecular orientation reaches a maximum in the delamination layer. A light microscope application of the osmium tetroxide procedure (*Figure 2*) has suggested the presence in this layer of a peculiar structure which may be responsible for delamination. Styrene–acrylonitrile copolymer alone, however, does not peel readily, so that a simple orientation of the copolymer molecules cannot account for the observed delamination.

A feature to which the delamination is attributable has finally been revealed by electron microscopy. The rubber particles are found to be arranged in rows, forming a laminar structure along the injection flow direction. In order to produce such a structure it is necessary for the velocity gradient to exceed a certain limiting value, which should, in turn, vary with both polymer composition and moulding conditions.

In conclusion, it should be emphasized that phase anisotropy rather than molecular anisotropy may often be of practical importance in dealing with such polymer systems as ABS. It should also be pointed out that rubber particles as revealed by the electron microscope can be utilized as internal indicators for moulding flow patterns.

The author sincerely thanks K. Yoshimura, M. Nishimura and S. Horii for their skilful assistance throughout this study. He is indebted to Dr M. Inoue and associates for supplying test specimens.

Central Research Laboratories,
Toyo Rayon Company Ltd,
Otsu, Shiga-ken, Japan

(Received June 1967)

REFERENCES

[1] KESKKULA, H. and NORTON, JR., J. W. *J. appl. Polym. Sci.* 1959, **2**, 289
[2] KESKKULA, H., SIMPSON, G. M. and DICKEN, F. L. Private communication
[3] KATO, K. *Polym. Engng Sci.* 1967, **7**, 38
[4] KATO, K. *Polymer, Lond.* 1967, **8**, 33

Free Radical Polymerization of Unconjugated Dienes VI—Vinyl-trans-crotonate in Benzene at 60°C

LUIGI TROSSARELLI and MARINO GUAITA

*With the aim of checking the hypothesis that, in the free radical cyclopolymerization of unconjugated dienes, inter- and intra-molecular chain propagation reactions have to be slow to allow the formation of large fractions of cyclic structural units in the resulting polymers, the free radical polymerization at 60°C of vinyl-*trans*-crotonate in benzene solutions has been investigated. The experimental results agree with the above hypothesis and show that the crotonic and vinyl double bonds of the monomer are chiefly involved in the intermolecular and intramolecular chain propagation steps, respectively.*

IN A previous paper[1], on the basis of what has been reported in the literature about the free radical cyclopolymerization of symmetrical unconjugated dienes[2] and our own results on the free radical polymerization of some unsymmetrical unconjugated dienes[1, 3, 4], we were led to suggest that, since the ratio between cyclic and linear structural units depends on the competition between the intramolecular and intermolecular chain propagation steps, these reactions have to be slow enough to allow suitable orientation of the reacting groups in order to have the formation of a large fraction of cyclic structural units. This might occur when rather stable radicals and double bonds are involved in the process.

With the aim of checking the validity of such a hypothesis, we thought it of interest to investigate the free radical polymerization of some unsymmetrical unconjugated dienes in which one of the two double bonds gives rise to a highly reactive radical and the other is so unreactive that it does not homopolymerize but only copolymerizes when attacked by suitably reactive radicals. In this paper are presented and discussed the results obtained from a kinetic investigation on the free radical polymerization at 60°C in benzene solutions of vinyl-*trans*-crotonate which, as already reported by Arbuzova and Rostovskii[5], undergoes cyclopolymerization.

EXPERIMENTAL

Monomer

Vinyl-*trans*-crotonate was prepared according to Swern and Jordan[6] by transvinylation from *trans*-crotonic acid and vinylacetate. Its purity, as checked by gas chromatography, was found to be higher than 99·9 per cent.

Polymers

Polymerizations were carried out at 60°C in benzene solutions of different concentration, using α,α'-azobisisobutyronitrile (3×10^{-2} mole/l.) as a free radical initiator. Ampoules sealed under high vacuum were employed. The conversions to polymer were kept as low as convenient and did not exceed five per cent.

The polymers were purified from monomer and initiator by several precipitations in ethyl ether from benzene solutions. They were easily soluble in benzene, acetone, chloroform and bromoform and insoluble in aliphatic hydrocarbons and in ethyl ether. The softening point was found near 250°C. In *Figure 1* the infra-red spectrum (film from benzene) of a typical poly(vinyl-*trans*-crotonate) is reported.

Analysis of the polymers

The mole fraction of crotonic (f_{Cr}) and of vinyl (f_V) residual unsaturations in the polymers from vinyl-*trans*-crotonate were determined by infra-red spectroscopy (Beckman IR 9) in three per cent $CHBr_3$ solutions. The C—H out-of-plane bending vibrations at 970 cm^{-1} and at 950 cm^{-1} were taken respectively as analytical bands for crotonic and vinyl residual unsaturations. The calibration plots were obtained from ethyl-*trans*-crotonate and vinylacetate mixtures in $CHBr_3$, prepared in such a way as to give, in the range 900 to 1 000 cm^{-1}, bands of shape and absorbance similar to those of the polymers under investigation. The Lambert–Beer law was observed to be obeyed in the concentration range of interest.

RESULTS

In *Table 1* are collected, as obtained from the analysis of the polymers from the free radical polymerization at 60°C of vinyl-*trans*-crotonate in

Table 1. Mole fractions of structural units in the products of the free radical polymerization at 60°C of vinyl-*trans*-crotonate in benzene solutions. Initiator: AIBN (3×10^{-2} mole/l.)

Monomer concentration (mole/l.)	f_V	f_{Cr}	f_C
4·22	0·26	0·27	0·47
2·41	0·19	0·22	0·59
2·11	0·17	0·21	0·62
1·40	0·13	0·20	0·67
0·84	0·08	0·17	0·75
0·45	0·05	0·14	0·81
0·40	0·04	0·14	0·82
0·17	0·02	0·11	0·87

benzene solutions, the mole fractions of residual vinyl unsaturations (f_V) and the mole fractions of crotonic residual double bonds (f_{Cr}). The presence in the polymers of both crotonic and vinyl residual unsaturations leads to consideration of the following two linear structural units:

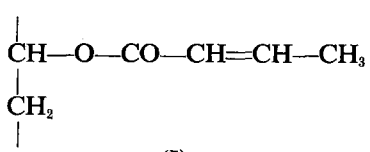

(I)

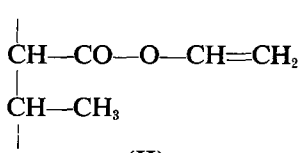

(II)

The fact that, for all the polymers investigated, $f_V + f_{Cr} < 1$, indicates, in agreement with Arbuzova and Rostovskii[5], the presence of lactone-type cyclic structural units. The infra-red spectra of the polymers (see *Figure 1*),

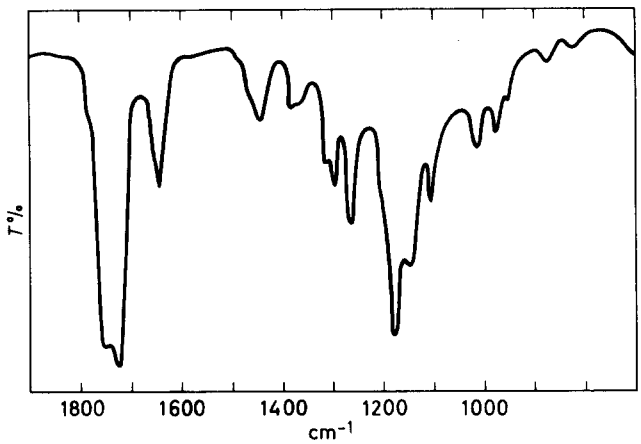

Figure 1—Infra-red spectrum of a typical product of the free radical polymerization at 60°C of vinyl-*trans*-crotonate in benzene solutions

in the region of carbonyl stretching, shows, besides an absorption band at 1 725 cm^{-1} and a shoulder at about 1 780 cm^{-1}, due to linear structural units I and II respectively, an absorption at 1 750 cm^{-1} most probably to be attributed to the carbonyl stretching of γ-lactone-type structural units, account being taken that the overlapping of the absorption of the α,β-unsaturated ester carbonyl stretching (1 725 cm^{-1}) might result in an apparent shift toward lower frequencies of the transmission minimum of the band of the γ-lactone carbonyl stretching. On the other hand, it must be considered that, in the free radical polymerization of vinyl-*trans*-crotonate, the most stable radicals which can be formed, namely radicals III and IV,

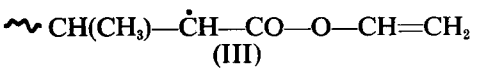

(III)

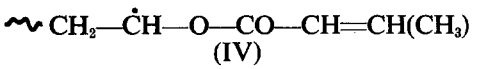

(IV)

should give rise, through the intramolecular chain propagation (cyclization) steps, exclusively to γ-lactone structural units V and VI:

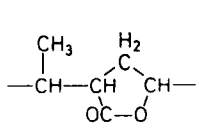

(V)

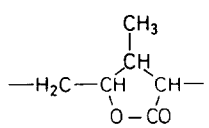

(VI)

The overall mole fractions $f_O = 1 - (f_V + f_{Cr})$ of cyclic structural units in the polymers from vinyl-*trans*-crotonate are collected in *Table 1*.

On the basis of what has already been shown[3, 7], the mole fractions of structural units are related to the monomer concentration [*M*] by

$$\frac{f_V + f_{Cr}}{f_C} = \frac{1}{r_{cV\cdot}} \frac{1 + f_V/f_{Cr}}{1 + f_{V*}/f_{Cr*}} [M] \tag{1}$$

and

$$\frac{f_V}{f_{Cr}} = \frac{r_{cV\cdot}}{r_{cCr\cdot}} \frac{f_{V*}}{f_{Cr*}} \tag{2}$$

where f_{Cr}, f_V, f_{V*} and f_{Cr*} are respectively the mole fractions of structural units I, II, V and VI, and $r_{cV\cdot}$ and $r_{cCr\cdot}$ are the cyclization ratios[3, 7] for radicals IV and III respectively. From equations (1) and (2) it is easy to derive

$$(f_C/f_{Cr})\,[M] = r_{cV\cdot} + r_{cCr\cdot}\,(f_V/f_{Cr}) \tag{3}$$

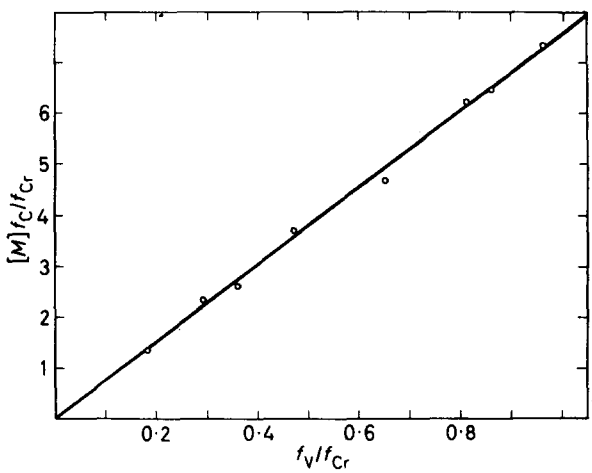

Figure 2—Plot of the experimental data of *Table 1* according to equation (3)

In *Figure 2* the experimental data of *Table 1* are plotted according to equation (3) and, by the method of the least squares, one obtains $r_{cV\cdot} = 0{\cdot}00\ldots$ mole/l. and $r_{cCr\cdot} = 7{\cdot}57$ mole/l. The value $r_{cV\cdot} = 0{\cdot}00\ldots$ obviously means that, within the limits of the experimental errors, in the free radical polymerization products of vinyl-*trans*-crotonate, cyclic structural units VI are absent, and f_C may be identified with f_{V*}.

DISCUSSION

The values of the cyclization ratios show the strong tendency of radicals III to undergo cyclization according to reaction (4) and the extremely low ability of radicals IV to give cyclic structural units through reaction (5). This agrees with our previous hypothesis[1] that cyclization takes place only

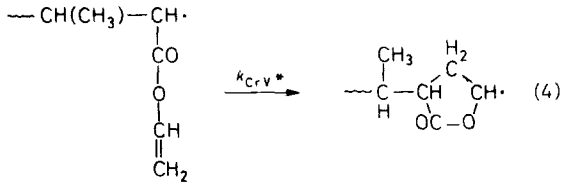

when the rates of the chain propagation reactions involved in the process are low enough to allow proper orientation of the reacting groups for ring

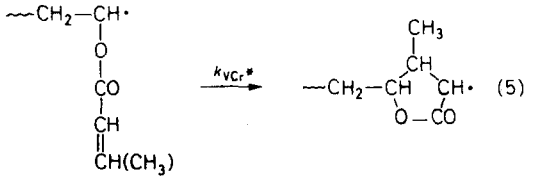

closure. In fact, radicals III can propagate the chain either through reaction (4) or through reactions (6) and (7). Reactions (4), (6) and (7), which involve the rather stable radicals III and two double bonds of low reacti-

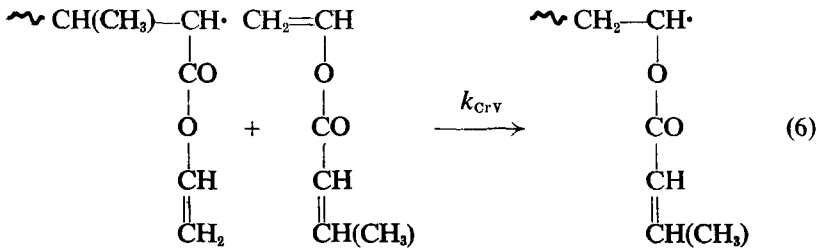

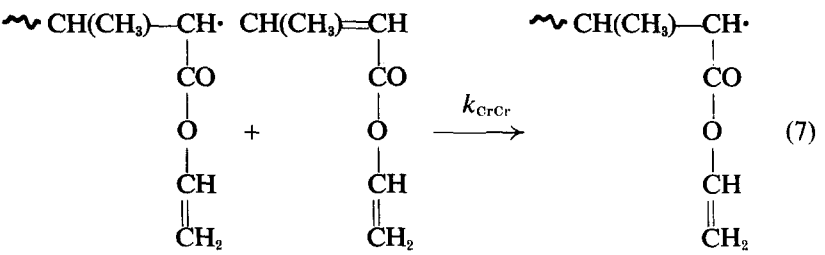

vity, should be slow. On the other hand, the highly unstable radicals IV should be so quickly consumed through reactions (8) and (9) that the

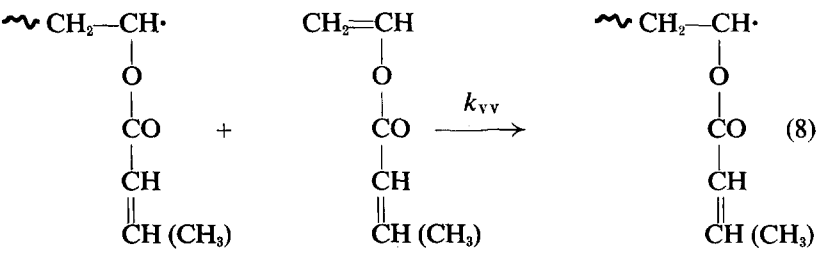

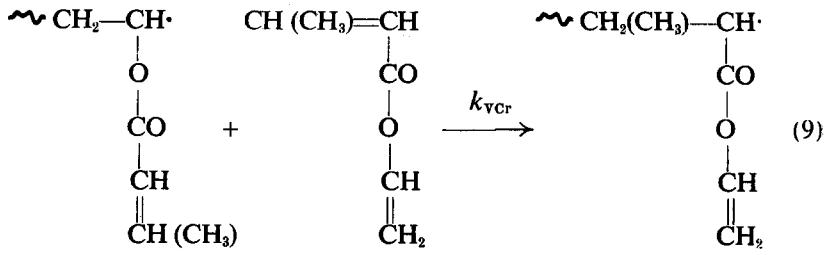

(9)

pendant crotonic double bonds cannot assume the proper orientation for cyclization.

According to our previous treatment of cyclopolymerization[3, 7], the mole fractions f_V and f_{Cr} of linear structural units II and I respectively are related to the monomer concentration by the relationship

$$f_V/f_{Cr} = \alpha\,\{[M]+\beta\}/\{[M]+\gamma\} \tag{10a}$$

where

$$\alpha = \frac{1+k_{CrCr}/k_{CrV}}{1+k_{VV}/k_{VCr}} \tag{10b}$$

$$\beta = \frac{k_{VCr_*}/k_{VCr}}{1+k_{Cr_*V}/k_{Cr_*Cr}} \tag{10c}$$

$$\gamma = \frac{k_{CrV_*}/k_{CrV}}{1+k_{V_*Cr}/k_{V_*V}} \tag{10d}$$

and k_{V_*V}, k_{V_*Cr}, k_{Cr_*V} and k_{Cr_*Cr} are respectively the rate constants of the intermolecular chain propagation reactions involving cycloradicals and monomer:

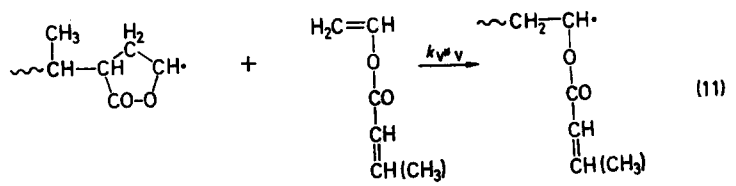

(11)

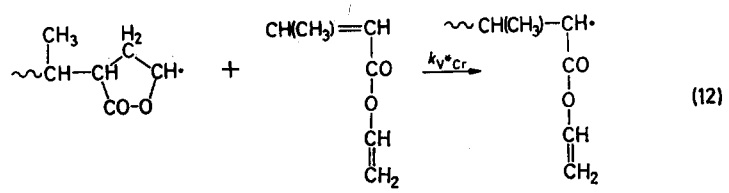

(12)

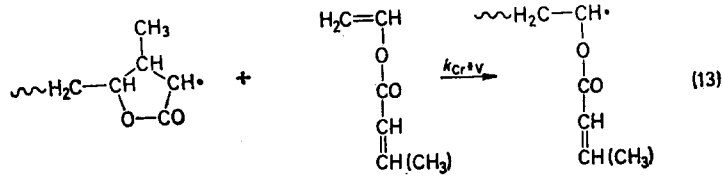

(13)

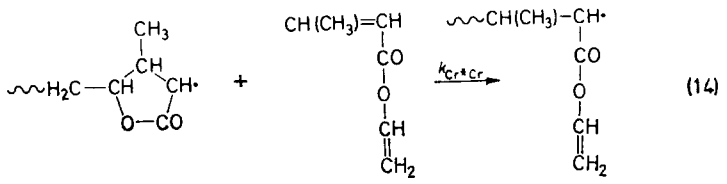

(14)

Since $r_{cV\cdot} = k_{VCr_*}/(k_{VV} + k_{VCr})$, it is easy to see that it must be $\beta \leqslant r_{cV\cdot}(1 + k_{VV}/k_{VCr})$. According to copolymerization data of crotonic derivatives and vinylacetate[8, 9], k_{VV}/k_{VCr} can be reasonably assumed less than unity and then the value of β is to be taken close to zero. As a consequence, equation (10a) may be rewritten to give

$$\frac{f_{Cr}}{f_V} = \frac{1}{\alpha} + \frac{\gamma}{\alpha}\frac{1}{[M]} \tag{15}$$

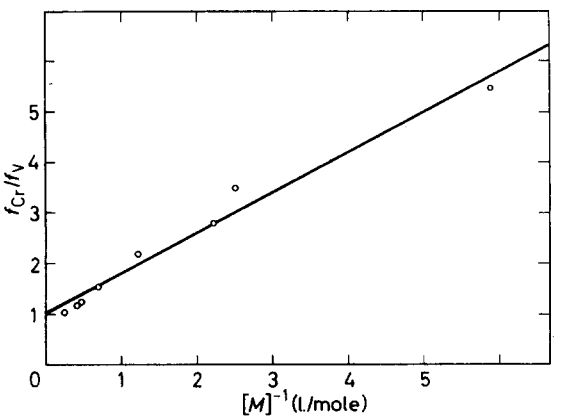

Figure 3—Plot of the experimental data of *Table 1* according to equation (15)

In *Figure 3* the data of *Table 1* are plotted according to equation (15). The experimental points fit well on a straight line and, by the least squares method, one obtains $\gamma = 0{\cdot}80$ mole/l. and $\alpha = 1{\cdot}00$. This value of α, according to our previous treatment of cyclopolymerization[3, 7], might well be compared with the value 0·76 calculated from equation (10b), taking $k_{VV}/k_{VCr} = 0{\cdot}33$ and $k_{CrCr}/k_{CrV} = 0{\cdot}01$ as though from the free radical copolymerization at 68°C of vinylacetate and *trans*-crotonic acid[8], account being taken of the difference in the temperatures of polymerization and of the role of the substituents in determining the reactivity of the monomers and of the radicals involved.

According to what has been shown already[3, 7], the ratio $(f_V + f_{Cr})/f_C$ between the overall mole fractions of linear and cyclic structural units is related to the monomer concentration by

$$\frac{f_V + f_{Cr}}{f_C} = \frac{a[M]^2 + b[M]}{[M] + c} \tag{16a}$$

where

$$a = \frac{k_{VV}k_{CrV} + k_{CrCr}k_{VCr} + 2k_{VCr}k_{CrV}}{k_{VCr^*}k_{CrV} + k_{CrV^*}k_{VCr}} \tag{16b}$$

$$b = \frac{k_{CrV^*}k_{V^*V}\dfrac{k_{VV} + k_{VCr}}{k_{V^*V} + k_{V^*Cr}} + k_{VCr^*}k_{Cr^*Cr}\dfrac{k_{CrV} + k_{CrCr}}{k_{Cr^*V} + k_{Cr^*Cr}}}{k_{VCr^*}k_{CrV} + k_{CrV^*}k_{VCr}} \tag{16c}$$

$$c = \frac{k_{VCr^*}k_{CrV^*}\left(\dfrac{k_{V^*V}}{k_{V^*V} + k_{V^*Cr}} + \dfrac{k_{Cr^*Cr}}{k_{Cr^*V} + k_{Cr^*Cr}}\right)}{k_{VCr^*}k_{CrV} + k_{CrV^*}k_{VCr}} \tag{16d}$$

The constants a, b and c in equation (16a) are related, as previously shown[3], to the cyclization ratios and to the constants α, β and γ in equation (10a) by:

$$\alpha(\beta - c)/(c - \gamma) = r_{cV\cdot}/r_{cCr\cdot} \tag{17a}$$

$$b/a = (\alpha\beta + \gamma)/(\alpha + 1) \tag{17b}$$

In the present case, since both β and $r_{cV\cdot}$ are in practice close to zero, it is easy to see from equation (17a) that c must also be close to zero, and then equation (16a) can be rewritten to give

$$(f_V + f_{Cr})/f_C = a[M] + b \tag{18}$$

Neglecting in equation (17b) $\alpha\beta$ with respect to γ, and introducing the numerical values of α and γ, one obtains $b/a = 0{\cdot}40$. From the experimental values of $[M]$, $f_V + f_{Cr}$ and f_C one calculates $a = 0{\cdot}25$ l./mole and $b = 0{\cdot}10$. *Figure 4* shows that the agreement between calculated and experimental data is quite satisfactory.

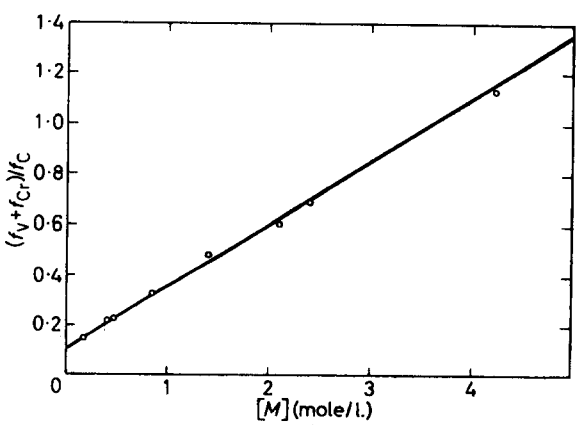

Figure 4—Plot of the experimental data of *Table 1* according to equation (18). Solid line as calculated taking $b/a = 0{\cdot}40$

The above discussion of the experimental results has been carried out simply by considering that $r_{cV\cdot} = 0{\cdot}00$ . . means $k_{VCr^*} \ll k_{VV} + k_{VCr}$, and

without any assumption about the value of the individual rate constants. Since, by definition[3, 7], r_{cV} represents the monomer concentration at which the ratio between the mole fractions, that is between the rates of formation, of structural units VI and I is unity, it is easy to see that, in the range of monomer concentrations usually employed, the rate of reaction (5) must be negligible with respect to the rates of reactions (8) and (9). Obviously, the experimental data of *Table 1* could also have been interpreted by taking $k_{VCr^*}=0$ and therefore $\beta=c=0$, by which equations (10a) and (16a) can be reduced to equations (15) and (18) respectively. The former interpretation seems, however, more correct because it does not imply taking as zero the rate constant of reaction (5), which would result in a γ-lactone ring as well as reaction (4). On the other hand, such an assumption would be inconsistent with copolymerization data[8, 9], which show that vinyl radicals easily attack the crotonic double bonds.

The above analysis of the experimental results indicates that, in the free radical polymerization at 60°C in benzene solutions of vinyl-*trans*-crotonate, the vinyl double bonds are chiefly involved in the intramolecular propagation of the chain and the crotonic double bonds are predominantly involved in the intermolecular chain propagation reactions. This makes the mechanism of polymerization of vinyl-*trans*-crotonate completely different from the one considered by other authors[10, 11] for the free radical polymerization of vinyl-*trans*-cinnamate. According to the latter mechanism, vinyl double bonds would be responsible for the intermolecular chain propagation, in contrast with copolymerization data[10, 11], whereas the cinnamic ones would only take part in the cyclization reactions. It is to be noted that the mechanism presented here is to be regarded as more reliable since it is derived from the application to the experimental data of general equations relating cyclopolymer composition to monomer concentration, taking into account all the reactions involved in the process, and it results in fairly good agreement with what is expected from copolymerization data.

The authors thank Prof. G. Saini for many helpful suggestions and valuable discussions.

Istituto di Chimica Analitica dell' Università e Centro Nazionale di Chimica delle Macromolecole del C.N.R., Sezione II, Turin, Italy

(*Received May 1967*)

REFERENCES

[1] TROSSARELLI, L., GUAITA, M. and PRIOLA, A. *Ric. Sci.* 1966, **36**, 993
[2] MERCIER, J. and SMETS, G. *J. Polym. Sci. A*, 1963, **1**, 1491
SMETS, G., HOUS, P. and DEVAL, N. *J. Polym. Sci. A*, 1964, **2**, 4825
GIBBS, W. E. *J. Polym. Sci. A*, 1964, **2**, 4815
SIMPSON, W. and HOLT, T. *Proc. Roy. Soc. A*, 1956, **238**, 154
[3] TROSSARELLI, L., GUAITA, M. and PRIOLA, A. *International Symposium on Macromolecular Chemistry (Prague) 1965*, preprint P.442; *J. Polym. Sci.* In press
[4] TROSSARELLI, L., GUAITA, M. and PRIOLA, A. *Ric. Sci.* 1965, **35(II-A)**, 429
TROSSARELLI, L., GUAITA, M. and PRIOLA, A. *Annal. Chim. (Roma)*, 1966, **56**, 1065
TROSSARELLI, L., GUAITA, M. and PRIOLA, A. *Makromol. Chem.* 1967, **100**, 147

[5] ARBUZOVA, I. A. and ROSTOVSKII, E. N. *J. Polym. Sci.* 1961, **52,** 325
[6] SWERN, D. and JORDAN, E. F. *Org. Synth.* 1950, **30,** 106
[7] TROSSARELLI, L., GUAITA, M. and PRIOLA, A. *Ric. Sci.* 1965, **35(II-A),** 379
[8] CHAPIN, E. C., HAM, G. E. and MILLS, C. L. *J. Polym. Sci.* 1949, **4,** 597
[9] USHAKOV, S. N. and TRUKHMANOVA, L. B. *Vysokomol. Soedineniya,* 1959, **1,** 1754
[10] VAN PAESSCHEN, G., JANSSEN, R. and HART, R. *Makromol. Chem.* 1960, **37,** 46
[11] ROOVERS, J. and SMETS, G. *Makromol. Chem.* 1963, **60,** 89

The Molecular Weight Distribution of Natural Rubber Latex

BARBARA WESTALL

Two samples of natural rubber latex have been fractionated by differential solvent extraction of polymer coated glass beads, and molecular weight distributions derived from the experimental data. The distributions are shown to be bimodal, with peaks at $M < 0{\cdot}25 \times 10^5$, *and at* $3{\cdot}25 \times 10^6 < M < 4{\cdot}50 \times 10^6$, *over a total molecular weight range of 72 000 to* $4{\cdot}50 \times 10^6$. *The initial fraction was variously estimated at* $46\,000 < M < 67\,000$ *after refractionation.*

A TECHNIQUE for the fractionation of natural rubber by means of solvent extraction has recently been established[1]. This shows whole crêpe rubber to possess a markedly skew and possibly bimodal molecular weight distribution with fractions ranging from $M = 0{\cdot}07 \times 10^6$ to $M = 2{\cdot}50 \times 10^6$. It was thought to be of interest to see whether the rubber hydrocarbon component of the latex from which crêpe rubber is prepared, displayed a similar distribution.

EXPERIMENTAL

Two samples of latex from an 'immature' tree (an illegitimate seedling derived from Clone No. RRIM 501), and a 'mature' tree (Clone No. RRIM 501), have been fractionated by the technique referred to above. The 'immature' latex was pricked from a five-year-old tree grown in this country. 3 g of the latex were freeze-dried within half an hour of collection, 200 ml of analytical reagent grade benzene added, and the mixture left for one week in the dark at room temperature. The resulting solution was filtered through lens tissue and a No. 1 porosity sintered glass filter before fractionation by the standard technique. The second sample was taken from trees in regular tapping in Malaya, centrifuged at 2 000 *g* to remove lutoid particles, stored in ice and despatched by air to this country. It was received within three days of dispatch, and stored at $-20°C$ for one week before treatment as above prior to fractionation. The standard technique with the following slight modifications was employed for the mature latex: (*i*) the latex coated glass beads were extracted with acetone for one hour on the fractionating column, and then dried under nitrogen for half an hour, before commencing solvent extraction; (*ii*) 80 ml of benzene–methanol solvent mixtures for extraction were prepared, instead of 50 ml; (*iii*) 300 g of glass beads were used instead of 200 g. The fractions were characterized by determination of intrinsic viscosity in toluene as outlined by Bristow and Westall[2] (2 ml suspended level dilution viscometers were used for the smaller fractions).

RESULTS

A summary of the fractionation data is given in *Table 1*. The amount of the acetone extract in the mature latex is of the same size (0·6 per cent) as the first fraction of the immature latex, which has a negligible intrinsic viscosity and the two extracts are thought to be comparable. The major

Table 1. Fractionation of natural rubber latex

% Benzene in extract	Immature latex w_i	n_i	$[\eta]$	$M_v \times 10^{-6}$	Mature latex w_i	n_i	$[\eta]_i$	$M_v \times 10^{-6}$
78·00	0·6	—	—	—	16·4	70·0	0·88	0·072
78·25	16·0	65·0	0·93	0·087	11·6	16·6	1·89	0·230
78·50	11·8	19·5	1·81	0·214	5·3	2·4	3·88	0·670
78·75	6·6	4·1	3·50	0·562	3·4	1·7	3·70	0·630
79·00	5·8	2·6	4·30	0·776	3·2	1·4	3·97	0·690
79·25	2·4	1·0	4·54	0·832	2·5	1·0	4·29	0·780
79·50	1·9	0·8	4·54	0·832	1·6	0·7	4·04	0·710
79·75	1·1	0·7	3·28	0·513	1·2	0·7	3·31	0·540
80·00	3·6	0·8	6·89	1·549	2·1	0·7	4·86	0·940
80·25	4·7	0·9	7·80	1·862	5·8	0·7	9·28	2·450
80·50	10·5	1·5	9·55	2·512	7·7	0·8	10·65	3·000
80·75	10·3	1·2	11·42	3·236	7·7	0·8	10·89	3·100
81·00	13·1	1·1	13·90	4·365	15·7	1·4	11·77	3·500
81·25	8·4	0·7	14·25	4·467	7·7	0·6	12·12	3·700
81·50	3·0	0·2	14·65	4·677	—	—	—	—
100·00	0·2	0·1	13·04	3·890	8·1	0·6	13·45	4·300

% Acetone extract	—	0·6
% Recovery	85·0	85·0
% Recovery*	94·6	94·6
Initial $[\eta]$	5·80	5·43
Initial $[\eta]$*	7·64	7·24
$\Sigma w_i [\eta]_i$	7·37	7·19
M_n experimental	—	414 000
M_n calculated	354 000	307 000
M_w experimental	—	$2{\cdot}220 \times 10^6$
M_w calculated	$2{\cdot}001 \times 10^6$	$1{\cdot}985 \times 10^6$

*Corrected values—see text.
w_i denotes % weight fraction
n_i denotes % number fraction.
$[\eta]$ denotes intrinsic viscosity.
M_v denotes viscosity average molecular weight.

part (*ca.* 10 per cent by weight of total dry weight of whole rubber) of the non rubber hydrocarbon portion of the latex is assumed to have dissolved in the methanol used in precipitating the rubber on to the column. The values of weight recovery of the fractions have been corrected for the presence of soluble non rubber material. The initial intrinsic viscosity of the latex in toluene has also been corrected according to the empirical observation of Freeman[3], who noted that for whole rubber latex, the intrinsic viscosity is approximately 75 per cent of the intrinsic viscosity of the rubber hydrocarbon, due to the presence in the latex of approximately ten per cent by weight of non rubber materials which depress the intrinsic viscosity. This observation has been confirmed in this laboratory. The molecular weights of the fractions were calculated from the viscosity data using the Carter–Scott–Magat relationship[4], and hence values of number average and weight average molecular weight were estimated since

$$M_n = \frac{\Sigma w_i}{\Sigma w_i/m_i}, \quad M_w = \frac{\Sigma w_i m_i}{\Sigma w_i}$$

Values of M_n and M_w for the sample of mature latex were determined by osmotic pressure and light scattering methods[2]. These agreed satisfactorily with those calculated.

Histograms showing the weight fraction molecular weight distribution for the two latices are given in *Figure 1*, together with the previously deter-

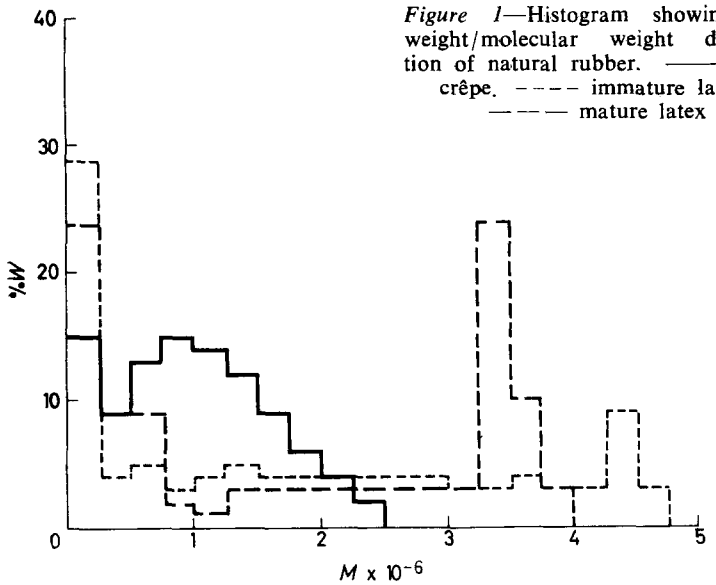

Figure 1—Histogram showing the weight/molecular weight distribution of natural rubber. ——— pale crêpe. - - - - immature latex. — — — mature latex

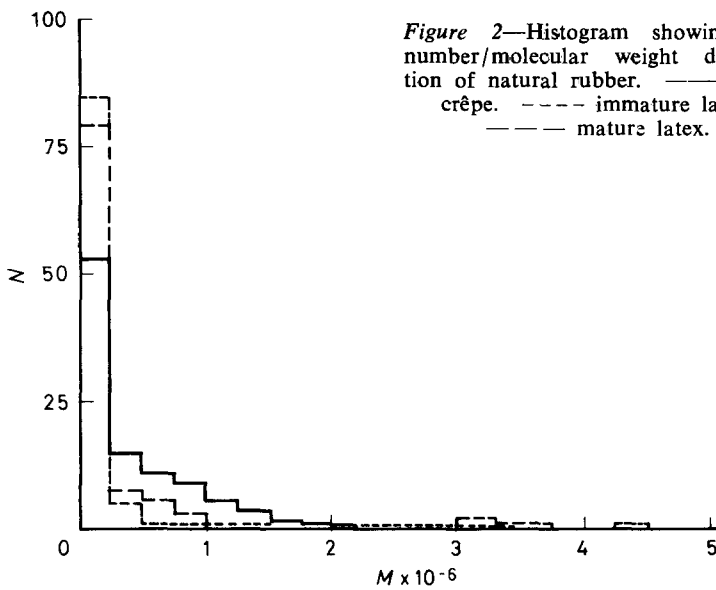

Figure 2—Histogram showing the number/molecular weight distribution of natural rubber. ——— pale crêpe. - - - - immature latex. — — — mature latex.

mined distribution for pale crêpe[1]. The range of molecular weights found for the latices (72 000 to $4{\cdot}50 \times 10^6$) is nearly twice as great as that found for crêpe (72 000 to $2{\cdot}00 \times 10^6$). The bimodal nature of the distributions is considerably more pronounced. Between 24 and 30 per cent by weight of both latices is of $M < 0{\cdot}25 \times 10^6$ as against approximately 15 per cent in the case of crêpe rubber. One most marked feature is the virtual replication of the molecular weight distributions of the two samples of latex

taken from trees grown in two different countries, and of different ages. This is most apparent in the first portion of the distribution (*Figure 2*). The agreement is less marked in the second portion in which there is a pronounced maximum at $3{\cdot}25 \times 10^6 < M < 3{\cdot}50 \times 10^6$ for the sample of mature latex, and at $4{\cdot}25 \times 10^6 < M < 4{\cdot}50 \times 10^6$ for the immature latex. The position of the first maximum for crêpe rubber is at the same range of molecular weight as for the latices. The position of the second maximum for crêpe rubber is $0{\cdot}75 \times 10^6 < M < 1{\cdot}25 \times 10^6$, from which it may be inferred that degradation of higher molecular weight material has taken place during its manufacture from latex.

The fractionation results, together with those obtained for pale crêpe, are also plotted on arithmetic probability paper in *Figures 3* and *4*. As previously mentioned[1] the points for pale crêpe fall on a straight line cutting the ordinate at 10 per cent, suggesting a positively skew Gaussian distribution. By contrast the Σw and Σn plots show three clearly defined straight lines, similar for both latices, but not identical, and possibly indicative of two distributions with an overlapping central area. The hypothetical lines for a normal Gaussian distribution of $M_w = 2{\cdot}6 \times 10^6$, and $M_n = 350\,000$ are shown for comparison.

In order to check homogeneity of the first fraction, refractionation of the initial fraction of mature latex was carried out (*Table 2*). Weight recovery was 76 per cent and $\Sigma w_i [\eta]_i$ had the anticipated value, i.e. no overall change in molecular weight had taken place during the refractionation. Two major fractions were obtained of $M_v = 59\,000$ and $M_v = 52\,000$ comprising 26·6 per cent, and 43·0 per cent of the recovered weight, respectively. As a check on the accuracy of the equation used to calculate M_v,

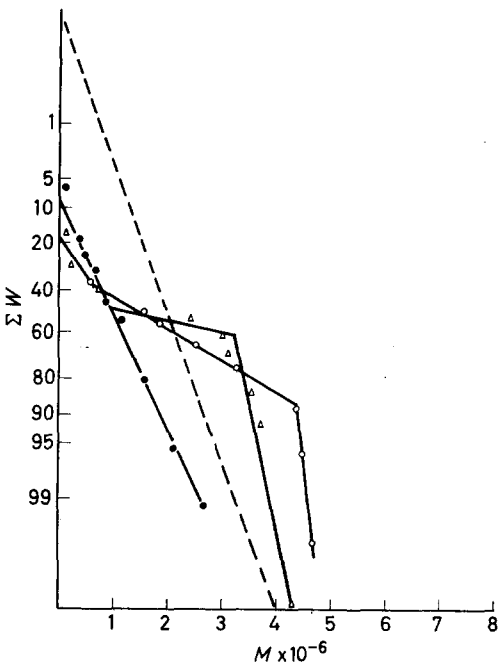

Figure 3—Arithmetic probability plot showing the weight/molecular weight distribution of natural rubber. ● pale crêpe. ○ immature latex. △ mature latex. ——— normal distribution for $M_w = 2 \times 10^6$

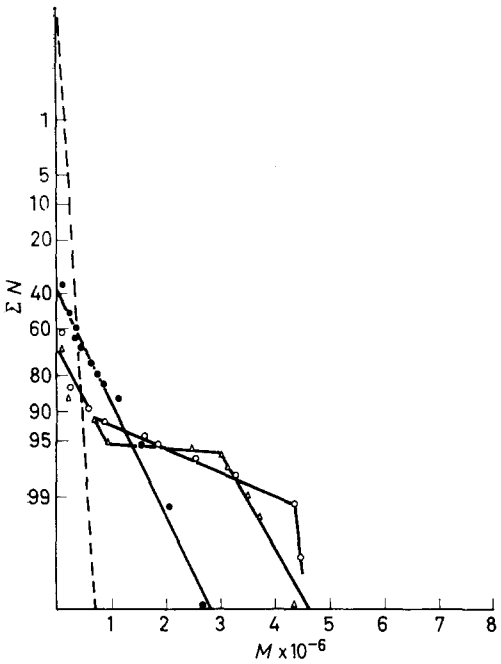

Figure 4—Arithmetic probability plot showing the number/molecular weight distributions of natural rubber. ● pale crêpe. ○ immature latex. △ mature latex. — — — normal distribution for $M_n = 350\,000$

Table 2. Refractionation of initial fraction mature latex. Fraction weight 0·0742 g. Intrinsic viscosity 0·73 dl g^{-1}, $M_v = 55\,000$. Weight recovery 75·8 per cent, $\Sigma w_i [\eta]_i = 0{\cdot}52$

% *Benzene*	w_i	$[\eta]_i$	M_v	M_n
*†	13·0	0·06	—	
*	26·6	0·78	59 000	
76·00	4·7	—		
76·25	43·0	0·70	52 000	67 000
76·50	5·1	—		
76·75	4·9	—		
77·00	2·1	—		
100·00	0·6			

Anticipated $\Sigma w_i [\eta]_i$ for 75·8 per cent recovery = 0·55.

*Fractions separated from filtrate after precipitation of solution on to beads, by differential freezing.
†Fraction brown coloured.

M_n was determined on the second of these fractions using a Mechrolab high speed osmometer with an *ultracella allerfeinst* membrane. The solvent was toluene, and operating temperature was 25°C ± 0·2°C (thermostatically controlled to ± 0·001°C). A value of 67 000 was obtained. This value is somewhat higher than M_v, but not appreciably so when it is considered that there may be an error of at least ± 10 per cent on these determinations.

For a further fractionation of Malayan latex, where the molecular weight of the first major fraction (after refractionation) was calculated to be 46 000 by the Carter–Scott–Magat equation, a determination of the intrinsic

viscosity of this fraction in a solvent, methyl *n*-propyl ketone, was made at 25°C. This temperature is somewhat higher than the θ temperature for the solvent as determined by Wagner and Flory[5], who obtained a value of 14·5°C, but the variation of intrinsic viscosity over this range of temperature is very slight. These workers showed that for fractions of natural rubber dissolved in methyl *n*-propyl ketone $[\eta]/M^{\frac{1}{2}}$ is a constant of value $1{\cdot}2 \times 10^{-3}$. Using this expression, M for the first latex fraction was again calculated to be 67 000.

DISCUSSION

It is noteworthy that all three distributions display initial fractions of approximately the same molecular weight, i.e. $M = 87\,000$, and $M = 72\,000$, in the case of the two latices, and at $M = 72\,000$ for the pale crêpe. It is suggested tentatively that this value of $M = 70\,000$ to 90 000 is in fact the molecular weight of a fundamental macromolecular unit formed from the precursors of natural rubber, i.e. the mevalonic acid and isopentyl pyrophosphate discussed by Archer *et al.*[6]. It is further suggested that these units link up, by an unspecified mechanism, to form polyisoprene of higher molecular weight possibly corresponding to the second maximum of the latex weight fraction distributions. This rubber may then degrade, as does the crêpe. This view is supported by a study of the values of the number fractions given in *Table 1* and *Figure 2* where slight but definite increases are again shown at $4{\cdot}25 \times 10^6 < M < 4{\cdot}50 \times 10^6$ for the immature latex and $3{\cdot}00 \times 10^6 < M < 3{\cdot}25 \times 10^6$ for the mature latex. For the crêpe, the number fraction at the first peak is 53 per cent as against 80 to 85 per cent for the latices.

Summing up, it has been shown by means of fractionation that natural rubber latex possesses an initially skew and markedly bimodal molecular weight distribution. The first fraction obtained by this technique is apparently homogeneous, with molecular weights estimated to be between 46 000 and 67 000. The presence of a fundamental sub-unit within this molecular weight range, from which natural rubber of higher molecular weight is built up, is postulated.

Thanks are due to Dr G. M. Bristow for advice in the above work, and to Miss F. H. E. Noble for assistance with the experimental work, which forms part of the research programme of the Natural Rubber Producers' Research Association.

The Natural Rubber Producers' Research Association,
48–56 Tewin Road,
Welwyn Garden City, Herts.

(*Received August 1967*)

REFERENCES

[1] BRISTOW, G. M. and WESTALL, B. *Polymer, Lond.* 1967, **8**, 609
[2] BRISTOW, G. M. and WESTALL, B. *J. appl. Polym. Sci.* 1965, **9**, 495
[3] FREEMAN, CH. I. *Chemistry and Physics of Rubber-like Substances.* Ed. BATEMAN, L. Maclaren: London, 1963
[4] CARTER, W. C., SCOTT, R. L. and MAGAT, M. *J. Amer. chem. Soc.* 1946, **68**, 1480
[5] WAGNER, H. L. and FLORY, P. J. *J. Amer. chem. Soc.* 1952, **74**, 195
[6] ARCHER, B. L. *et al. Nature, Lond.* 1961, **189**, 663

The Density of Polyethylene Single Crystals

D. A. BLACKADDER and P. A. LEWELL

One of the most controversial matters concerning regular single crystals of polyethylene is the true value of the density. The pyknometric and density gradient column techniques are reviewed critically and it is shown that excellent agreement between the two methods is possible if certain important precautions are observed. A value of 0·972 g/cm³ is advanced as the true density, and a well documented explanation is offered to explain the anomalous high values which can result from pyknometry.

TEN years since their discovery, the precise structural constitution of polyethylene single crystals remains a controversial matter[1]. Despite a great deal of morphological information and the certain knowledge that the polymer chains fold, there is still uncertainty as to the overall state of perfection of the crystals, commonly known as the degree of crystallinity. Apart from the possibility of voids within the crystal there is much discussion as to the nature of the large plane surfaces containing the folds. These folds may be sharp and regular forming a crystallographic plane, or they may be loose and irregular providing a kind of amorphous surface layer. Discussion of these possibilities has frequently involved the evidence of density determinations of the degree of crystallinity.

Since the interior of a crystal consists of parallel polymer chains in an ordered configuration, a crystallographic sub-cell can be defined and its density calculated by measuring the lattice parameters. The most recent determination by Kawai and Keller[2] gave a value of $0{\cdot}993 \pm 0{\cdot}002$ g/cm³ in agreement with earlier measurements by Charlesby and Callaghan[3] but significantly lower than the density of 1·000 g/cm³ resulting from work by Swan[4] and by Bunn[5]. Knowing the theoretical sub-cell density, many investigators have attempted to measure the density of single crystals, compare their values with the theoretical limit, and interpret the results in terms of a model of crystal structure.

Wunderlich and Kashdan[6] in 1961 measured the density of crystals prepared from 0·05 wt % solution, and their flotation technique gave a value of 0·965 g/cm³. Fischer and Lorenz[7], in a later density study, measured the density of single crystals by three volume displacement techniques. Their flotation measurements, which they judged to be the most reliable, gave 0·970 g/cm³ for crystals prepared from dilute solution at 70°C, and the density gradient column indicated a density of $0{\cdot}968 \pm 0{\cdot}002$ g/cm³ for the same crystals. A pyknometer was used to measure the density of crystals prepared from 1·0 wt % solution, but experimental errors limited the reliability of the results to $\pm 0{\cdot}01$ g/cm³. Nevertheless, the results were at least in harmony with those obtained by the other methods.

Prompted by this evidence for structurally imperfect polymer single crystals, Kawai and Keller[2] made an exhaustive study of density measurement techniques and reported their findings in 1963. They reasoned that pyknometry was least subject to consistent experimental errors. Improving

upon the original pyknometric technique of Fischer and Lorenz[7], they obtained four values for the density of crystals prepared from 1·0 wt % solution at 70°C: 1·003 ± 0·004, 0·998 ± 0·004, 1·003 ± 0·008, 0·993 ± 0·006 g/cm³. Careful measurements using a flotation technique yielded another series of high values: 0·993, 0·990, 0·990 and 0·995 g/cm³. Only the density gradient column gave lower values—around 0·97 g/cm³. In a later publication[8], the density gradient column was declared to be unsuitable for measurements on single crystals due to the existence of an interfacial free energy gradient in the column which affects particles of high specific surface area. The high density values were interpreted in terms of a 'perfectly crystalline' single crystal, with sharp folds and negligible internal defects. The fact that the average of the density determinations was slightly higher than the value which they had obtained via the crystallographic sub-cell was attributed to the fold planes being more dense than the interior of the crystal. When combined with other experimental evidence, the density determinations of the Bristol workers made a very strong case for the sharp folding theory of perfect crystals.

The conflict was by no means resolved, however. In the same year, Jackson, Flory and Chiang[9] used a seemingly reliable flotation technique to determine the densities of crystals formed from 0·1 wt % solution. For a crystallization temperature of 70°C they obtained a result of 0·970 g/cm³. Later, Peterlin and Meinel[10] also used a flotation technique and obtained a density of 0·975 g/cm³ for crystals prepared from 0·1 wt % solution at 80°C.

In 1966 Fischer and Hinrichsen[11] offered a convincing defence of the results they had obtained earlier using a density gradient column, and this development is particularly important in the light of recent investigations by Okada and Mandelkern[12]. They too measured the densities of single crystals by means of a density gradient column and estimated that their sample had a degree of crystallinity of 0·87. They then verified this value by infra-red (i.r.) measurements, exploiting the fact that certain i.r. bands characteristic of linear polyethylene distinguish between methylene groups in the crystalline and amorphous phases. Schonhorn and Ryan[13], also using a density gradient column, measured the density of single crystals prepared from 0·04 wt % solution when in suspension and when pressed into thin films. Identical densities of 0·972 g/cm³ were obtained, despite the widely differing specific surfaces of the samples.

By mid-1966 the situation had therefore become very complex indeed, with apparently reliable experimental evidence for both 'high' and 'low' densities. Reasoning that the discrepancy could arise from morphologically different samples having been used by the various investigators, Kawai *et al.*[14,15] repeated the pyknometric measurements in an attempt to detect density variations as a consequence of changes in the conditions of crystallization. Experiments were carried out over a wide range of molecular weights, crystallization temperatures and concentrations, using various solvents. Twenty two independent determinations yielded an average density value of 0·996 ± 0·005 g/cm³. No conclusive evidence was found to indicate that the density varied significantly with any of these parameters.

Noting that high densities seemed to arise only from pyknometric measurements, Martin and Passaglia[16] made an attempt to identify and reduce experimental errors inherent in this technique. In eight independent experiments, using crystals prepared from 0·75 wt % solution, they obtained densities ranging from 0·964 g/cm^3 to 0·989 g/cm^3. The weighted average result of 0·978 g/cm^3 was significantly lower than the crystallographic density, and was the first 'low' pyknometric density to be reported.

The present investigation was planned with a view to resolving the controversy. It was clear from the outset that the pyknometric technique should be employed because of its fundamental simplicity in providing an absolute value for the density. Other techniques appear to be much more susceptible to error, and in addition Martin and Passaglia had raised the possibility of single crystals forming within a range of densities. At the time, the accuracy of their work seemed to justify the assumption that the difference between their lowest and highest values was real. No previous study had revealed a spread in density values, and further investigation seemed desirable.

The morphology of the crystals used has been of fundamental concern in the present work. For reasons that will be discussed later, previous pyknometric work has been limited to crystals formed from relatively concentrated solutions (about 1 wt %) with the exception of part of Kawai's latest series of measurements[14,15], about which little experimental detail is available. Electron microscopy has revealed significant differences between the regular independent single crystals obtainable only from dilute solution and the more complicated aggregates resulting from crystallization in more concentrated solutions. It seemed at least possible that the splayed aggregates prepared from 1 wt % solutions were responsible for a range of permissible densities, as suggested by the results of Martin and Passaglia. It was therefore decided to begin the present series of experiments with a determination of the density of crystals obtained from 0·1 wt % solutions, using a refined pyknometric technique in the first instance.

EXPERIMENTAL

Materials

Polyethylene—Two samples supplied by ICI Ltd were used. Most of the experiments were carried out on commercial Rigidex 50, having a weight average molecular weight of 8×10^4 and an $\overline{M}_w/\overline{M}_n$ ratio of about five. The other sample was a special batch of Rigidex, reference number F2609. It had a weight average molecular weight of $10{\cdot}4 \times 10^4$ and its $\overline{M}_w/\overline{M}_n$ ratio was 8·5. The backbone chain had at most one side branch per thousand carbon atoms.

p-*Xylene*—99% *p*-xylene was supplied by ICI Ltd, with the other isomers as the major contaminants. Remarks concerning the stability and purification of this solvent appear elsewhere in the text.

Suspensions—Approximately 1·2 g of polyethylene were dissolved in enough *p*-xylene to make a 0·1 wt % solution. The solution was refluxed for two hours to ensure complete mixing of the low mobility polymer chains and crystallized for two hours at 75°C. Following the procedure of Blundell

and Keller[17] the suspension was slowly heated (10 deg. C/h) to 100°C where the temperature was maintained constant for 30 minutes. The clear solution was returned to the 75°C bath and allowed to crystallize for 16 hours. It was then cooled to room temperature and stored for several weeks prior to further treatment. The crystals grown by this method have been shown to be very well defined and of uniform size with a minimum of imperfections caused by crystal stacking.

Apparatus

Pyknometer—A special pyknometer was designed for this work and its appearance is shown in *Figure 1*. The pyknometer had a nominal volume

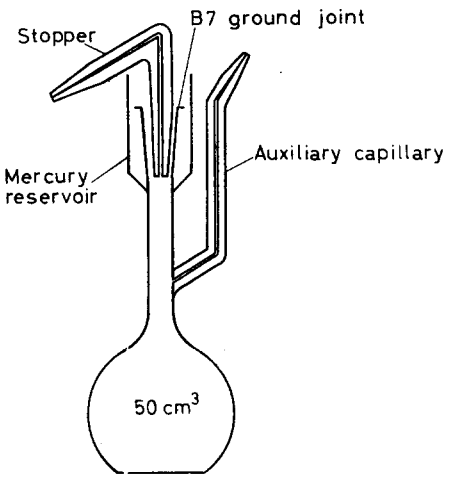

Figure 1—Pyknometer

of 50 ml and was made entirely of soda glass to facilitate the dissipation of static charges which accumulated on the vessel unavoidably during the filling process. If not eliminated through the use of soda glass such charges can lead to serious errors. In conventional pyknometers evaporation losses during weighing can also lead to experimental errors. Investigation has shown that most of the evaporation occurs through the ground glass joint between stopper and neck, rather than through the capillary in the stopper. Elimination of the glass joint, however, would greatly prolong the polymer drying time besides interfering with the filling operation. Consequently the glass joint was surrounded with a reservoir which could be filled with clean mercury to prevent evaporation. The reservoir also served to contain overflow during the initial stages of the drying operation. The stopper consisted of a 0·5 mm i.d. capillary, bent sharply to prevent expanding solvent from contaminating the mercury below, and drawn down to less than 0·1 mm i.d. at the tip. To facilitate the filling process another capillary was attached to the body of the pyknometer and also drawn down to less than 0·1 mm i.d. at the tip to minimize evaporation. Evaporation losses from the completely assembled pyknometer were negligible, amounting to less than 0·1 mg n

four hours when filled with solvent. Clean mercury could be weighed into the reservoir using a specially designed filling device to within an accuracy of $\pm 0{\cdot}1$ mg.

Density gradient column—A Tecam density gradient column, manufactured by Techne Ltd, was used, with *p*-xylene and carbon tetrachloride as the column liquids.

Procedures

Pyknometry—The density of single crystals in suspension form can be determined by pyknometry through use of the following equation

$$\rho = \rho_s / \{1 - (T - X)/(D - P)\}$$

where ρ denotes single crystal density, ρ_s is density of solvent, P is the weight of the empty pyknometer, D is the weight of the pyknometer together with polymer present in the suspension, T is the weight of the crystal suspension which the pyknometer can contain, and X denotes weight of pure solvent which the pyknometer can contain.

A primary requirement is an accurate value of ρ_s, so the density of *p*-xylene was determined several times at 25·00°C, using distilled water as the reference liquid and the special pyknometer shown in *Figure 1*. Care was taken to use *p*-xylene from the same batch as that used to prepare the crystal suspensions, and to subject it to the same thermal treatment as it would undergo in the preparation of a suspension. An average of several determinations gave $0{\cdot}8566 \pm 0{\cdot}0001$ g/cm^3.

The density, ρ, of single crystals in a suspension could then be determined as follows. The clean, empty pyknometer was weighed daily for a week prior to each density determination to obtain P. The pyknometer was then filled with pure solvent using a hypodermic needle and placed under vacuum to remove dissolved air. Again care was taken to use solvent identical in thermal history to that in the crystal suspension. The stopper was then inserted, the reservoir dried with rolled tissue, and clean mercury was carefully weighed in to prevent evaporation through the joint. The pyknometer was immersed in a water bath maintained at $25{\cdot}00° \pm 0{\cdot}01$°C and allowed to reach thermal equilibrium. The capillary tips were then dried and the vessel removed from the bath, dried and placed in the balance case for twenty minutes prior to weighing. This filling procedure was repeated at least eight times in every experiment, and care was taken to ensure complete removal of the mercury before each repetition of the topping-up operation. An average value of X was calculated together with the probable error based on the standard deviation. As a check, the supernatant liquid from a crystal suspension was also used to find X, the consistency of the results indicating that the two solvent samples were indeed identical.

The pyknometer was then dried and reweighed and filled to the bottom of the neck with crystal suspension. Realizing that the accuracy of the pyknometric technique is directly related to the amount of polymer used in a density determination, earlier investigators used crystal suspensions that had been prepared from 1·0 wt % solution and in so doing departed from those conditions under which single crystals are known to be well

defined. In this investigation, the problem was avoided by centrifuging batches of crystals formed from 0·1 wt % solutions into a concentrated suspension of about 2 wt %. The large flocs of crystals formed at 0·1 wt % settled readily at 3 000 rev/min. The resulting concentrated suspension of well defined single crystals flowed with difficulty, and the special pyknometer was designed to facilitate insertion of the suspension. To transfer the viscous suspension to the pyknometer, the stopper was removed and a narrow glass tube reaching to within 2 mm of the bottom of the pyknometer was mounted, using PTFE tape to make an airtight seal at the top. The other end of the tube was immersed in the suspension storage vessel. By applying gentle suction through the auxiliary capillary the suspension was drawn into the pyknometer with a minimum of air contact. The vessel was then placed under vacuum to remove any air bubbles that may have formed during the transfer operation. To avoid fouling of the capillaries as well as polymer losses during successive fillings it was essential that only clear solvent should be in the pyknometer neck. This was achieved by attaching a small reservoir to the tip of the auxiliary capillary and allowing the solvent to fill the neck very slowly. In this manner, the solvent was added gently enough to avoid disturbing the crystals in the pyknometer bulb. The stopper was then replaced, mercury added, and the pyknometer heated to 25·00°C and weighed as before. Topping up was repeated several times and an average value of T was calculated, together with a probable error.

Having found P, X and T, it only remained to find D, the weight of the pyknometer plus the weight of polymer present in the suspension. Crystallization of 1 g of polymer from 0·1 wt % solutions inevitably involves a large volume of solution. Reduction of this volume by centrifugation and decantation followed by transfer of the concentrated suspension into the pyknometer unavoidably leads to loss of polymer due to surface adhesion. Consequently, any attempt to determine the amount of material in the pyknometer by weighing the polymer prior to crystallization is futile. The suspension must be evaporated to dryness as the final step in the procedure and this was achieved as follows*. The stopper and mercury were first removed together with the clear solvent from the pyknometer neck. The pyknometer was placed in a vacuum oven at 80°C and the pressure reduced to obtain a vacuum of 25 inches of mercury. The suspension expanded into the mercury reservoir but no splashing occurred as the solvent evaporated. After several days, the suspension was merely moist so that a full vacuum could be employed. If the polymer was allowed to form a compact mass during drying, the rate of solvent escape was appreciably slower than if the polymer was frequently agitated. In the former case, it was found that a plot of sample weight versus reciprocal time yielded a straight line that could easily be extrapolated to zero to obtain the dried

*It seemed possible that solvent molecules could become trapped within the crystal lattice during crystallization, and remain firmly in place even after constant weight was reached in the vacuum oven. Clearly, such an effect would invalidate accurate density work and give abnormally low values. A series of experiments was therefore performed using vessels of known weight similar in geometry to the special pyknometer. The polymer was weighed at the outset, and dissolved and crystallized within the vessel. Constant weight was reached after about a week in the vacuum oven at 80°C. Calculation revealed that the dried polymer contained less than 0·1 wt % solvent, which is negligible in the context of these density measurements.

sample weight. In the latter case, constant weight was achieved after about five days at full vacuum.

Although pyknometry is essentially a reliable method of density determination, serious experimental errors may arise when it is applied to polymer single crystals. The calculation of the term $(T-X)$ involves the direct measurement of a small difference between two large numbers. This problem is unavoidably aggravated by the necessity of using solvents with a density close to unity and hence close to the crystal density. Further, the total amount of polymer used in making a density determination is of necessity rather small. In this investigation, the amount of polymer required for a reliable density measurement was considered to be at least 1·0 g. A typical value for the difference $(T-X)$ under these conditions was about 0·110 g. By repeated topping up of the pyknometer when filled with suspension and with solvent the probable random errors associated with T and X were calculated. A typical value was $\pm 0{\cdot}0012$ g. These errors were large enough to overshadow those from all other sources and hence determined the probable error in the final density value.

Following the manner of Kawai and Keller[2], the confidence limits placed on the final density value were obtained by calculating the density using the maximum and minimum values of $(T-X)$. These extreme values for $(T-X)$ were in turn calculated by using the upper limit of T and lower limit of X, and vice versa. This rather severe procedure yielded an uncertainty of $\pm 0{\cdot}002$ g/cm^3 for the final density value. This uncertainty is greater by a factor of ten than that inherent in more refined techniques such as the density gradient column used under ideal conditions. It is, however, a factor of ten *less* than the discrepancy in the literature between low and high values of the density of polyethylene single crystals. The present pyknometric results are therefore well qualified to resolve the controversy, especially since they are in harmony with results obtained by an alternative technique.

Density gradient column—The crystals were prepared as described above and the liquids used in the column were consistent with the recommendations of Ziabicki and Wasiak[18]. Kawai and Keller[8] had provided an analysis of the equilibrium of small particles in a density gradient column and claimed that there is an intrinsic error in the use of such a column to determine the density of crystals having a large specific surface area. Ziabicki and Wasiak considered further the equation obtained by Kawai and Keller and proposed the following relationship for the density discrepancy, $\Delta\rho$.

$$\Delta\rho = \rho - \rho_L = -\frac{f}{g}\left(\frac{\mathrm{d}\gamma_l}{\mathrm{d}\rho_l}\right)\left(\frac{\mathrm{d}\rho_l}{\mathrm{d}x}\right)$$

Here ρ is the true density of the solid, ρ_l is the density of liquid in the region surrounding the solid particle in the column, f is the specific surface area of the solid particle, x is the distance measured up the column, and γ_l denotes surface tension of the liquid/air interface.

Pearson[19] has shown that the original analysis of Kawai and Keller[8] is fundamentally unsound, but nevertheless the analysis serves to underline features of the density gradient column which, in the absence of adequate precautions, can lead to serious errors. For example, according to Ziabicki

and Wasiak, the maximum value of $d\gamma_L/d\rho_L$ is only 5·16 dyne cm²/g, compared to a value of 617 dyne cm²/g using ethanol and water. The latter pair of liquids should clearly be avoided.

In the present work efforts were made to reduce the enormously high specific surface associated with independent single crystals. By centrifuging 2 ml samples of the dilute suspensions into a concentrated form, physical stacking of the crystals was promoted. Several drops of the concentrated suspension were then placed in the density gradient column and allowed to settle for several days. The settling process was very slow since at any horizontal plane in the column the liquid in a drop of concentrated suspension had to equilibrate with the more dense liquid in the plane immediately below. In every case, however, the concentrated drops reached a steady position after about 100 hours.

The concentrated drops, containing crystal aggregates of reduced specific surface, settled at different rates, with the smallest drops usually settling fastest. This was to be expected as the rate of equilibration of the liquid in a drop will depend, among other things, on the overall specific surface of the drop. In every experiment the drops prepared from a given suspension came to rest in the same horizontal plane whatever their rate of settling.

For the system carbon tetrachloride–*p*-xylene, γ_L increases up the column making $\Delta\rho$ negative according to Ziabicki and Wasiak. Thus if samples of significant specific surface are placed in the density gradient column they should come to rest at a point in the column which is too low and where the liquid density is greater than the density of the solid. To test this prediction flocs of crystals were taken from the suspension used previously and placed in the column *without* centrifuging to promote stacking of the crystals. The flocs did indeed settle lower in the column giving apparent density values higher than that consistently obtained using the concentrated drops. In addition the flocs showed a very definite size classification with the smallest flocs settling deepest and thus showing the highest apparent densities. A spread of values from 0·972 to 0·987 g/cm³ was observed, the latter value being the upper limit of the column as established. It seems probable that equilibration of these loose uncompacted flocs was very slow and size dependent, making them quite unsuitable for accurate density determinations.

There is therefore a marked difference in behaviour between samples of high specific surface and those of low specific surface. It thus becomes apparent that the special precautions taken in this work are absolutely essential if the results are to be free of gross errors associated with the large specific surface area of individual crystals.

RESULTS AND DISCUSSION

Three independent determinations of the density of polyethylene single crystals were made by the pyknometric method described above and the following results were obtained, the units being g/cm³: $0{\cdot}971 \pm 0{\cdot}002$, $0{\cdot}972 \pm 0{\cdot}002$, $0{\cdot}972 \pm 0{\cdot}002$. The final value was obtained with the special sample of Rigidex but the density is no higher than that of the ordinary material.

The density gradient column results indicated a density of $0{\cdot}972 \pm 0{\cdot}001$ g/cm^3, and this excellent agreement lends support to the view that sources of error have been successfully removed from *both* procedures.

There remained, however, a worrying discrepancy between the present results and some previous pyknometric densities close to unity. The authenticity of such high values has been defended on the ground that X-ray crystallography leads to a perfect crystal density of between 0·99 and 1·00 g/cm^3; if, then, single crystals are perfect in the normal crystallographic sense they too would be expected to have this density.

An intensive investigation was made into possible causes of this discrepancy. In the paragraphs which follow several possibilities are discussed and all but one are rejected on the ground that they do not explain a discrepancy of the required magnitude. The acceptable explanation leads to the correct numerical value of the difference between the 'low' and 'high' pyknometric densities.

(*i*) It could be argued that the low density values obtained in the present investigation were due to a significant fraction of the polymer being in the less dense dissolved form when the critical weighings were carried out to determine T. If 0·01 g of polymer was dissolved in the 50 ml of solvent, the apparent density would be lower than the true value by 0·002 g/cm^3. If this were so, however, the supernatant liquid discarded after centrifuging would contain the same concentration of polymer and 0·24 g would be lost. The *total* loss of polymer from all sources is easily calculated from the weight of dried polymer in the pyknometer at the end of the measurements and the weight of polymer used to make up the initial suspension. This loss proved to be of the order of 0·2 g and most of this would be due to surface adhesion. It was concluded that dissolved polymer had no significant effect on the experimental results.

(*ii*) Observations revealed that the pyknometer reached thermal equilibrium in the bath about five times faster when filled with pure solvent than when filled with polymer suspension. Failure of the suspension-filled pyknometer to reach the bath temperature would result in high density values, and a large pyknometer would be particularly likely to fail in this respect. Thermocouples were placed inside a 100 ml pyknometer, believed to be the size used by the Bristol workers, and the temperature difference between the suspension and the bath was measured as a function of time. After one hour, the temperature difference was certainly less than 0·06 deg. C, the limiting sensitivity of the digital voltmeter used in the experiment. It would seem that reliable measurements can indeed be made with a pyknometer of 100 ml capacity.

(*iii*) Use of a pyknometer from which there is a finite rate of evaporation through a ground glass joint can lead to a consistent experimental error when the thermal properties of the suspension are markedly different from those of the pure solvent. When the contents of the pyknometer are at a given temperature approaching the bath temperature it is easily observed that the rate of expansion of pure solvent is significantly greater than the rate of expansion of a suspension. Apparent thermal equilibrium will be reached when the expansion rate is equal to the evaporation rate. This will

occur at a lower temperature when the pyknometer is filled with suspension than when it is filled with pure solvent. The magnitude of the temperature discrepancy will depend upon the evaporation rate. When used without the mercury seal the pyknometer shown in *Figure 1* gave a value of $(T-X)$ that was 7 mg higher than the value obtained using the seal, for the same sample of suspension containing 1 g of polymer. The density calculated from the former measurement was 0·008 g/cm^3 higher than the true value obtained from the latter measurement. The effect on the density would be much more serious if a smaller amount of polymer were present, or if the circumference of the ground glass stopper were greater. Nevertheless, the evaporation effect does not appear to be large enough to explain the discrepancy of about 0·025 g/cm^3 between previous pyknometric densities and the present values obtained with the special pyknometer.

(*iv*) It is quite conceivable that crystal morphology could have a significant effect on the density. As mentioned earlier, previous pyknometric investigators had been restricted to a range of crystallization concentrations where single crystals ceased to exist as independent entities and had become part of complex spraying aggregates. The end seemed to justify the means in this respect since it is generally agreed that imperfections caused by crystallization from concentrated solution would lower the density. The values obtained, being high, were not attacked on morphological grounds.

To check if crystals prepared from 1 wt % solution gave different density values, a series of experiments was conducted in which every effort was made to duplicate the technique established by Kawai and Keller[2]. A conventional 100 ml specific gravity bottle was used to measure the density of one per cent suspensions containing about 0·65 g of the ordinary Rigidex 50 polyethylene. To avoid the time-consuming drying stage the amount of polymer in the pyknometer was determined directly by weighing in the appropriate amount at the beginning. Refluxing for two hours and crystallization at 70°C for 16 hours were carried out *in situ* with a condenser fitted to the pyknometer itself. The pyknometer was maintained at room temperature for 24 hours prior to topping up with pure solvent and weighing. Between each pair of density determinations the pyknometer was filled with pure solvent and weighed to verify that the heat treatment had had no effect on the volume. The following values were obtained for the density of crystals prepared under these conditions: $0{\cdot}977 \pm 0{\cdot}004$, $0{\cdot}989 \pm 0{\cdot}004$, $0{\cdot}973 \pm 0{\cdot}004$, $0{\cdot}978 \pm 0{\cdot}004$, $0{\cdot}985 \pm 0{\cdot}004$, $0{\cdot}973 \pm 0{\cdot}004$ g/cm^3. The error limits were determined by the method described earlier, and consequently represent rather severe estimates of the probable error. The error was larger for this set of measurements since rather less polymer was used per determination. The values are consistently higher than those obtained for crystals prepared from 0·1 wt % solution, and display a scatter outside the range of experimental error. They are comparable with the densities reported by Martin and Passaglia[16], but are consistently lower than the values obtained by Kawai and Keller[2]. The evaporation effect described in (*iii*) probably contributes to the discrepancy but is not an adequate explanation.

It appeared, therefore, that pyknometric measurements based on crystals

prepared from 1 wt % solutions had a curious tendency to give high values (though not as high as unity) of very poor reproducibility. This effect is quite plain in the results of Martin and Passaglia[16]. It still seemed at least possible that the 'high' and 'low' densities had a morphological explanation. It could be argued that a unique molecular configuration is available to some polymer chains crystallizing from 1 wt % solution, such that the chains are more tightly packed than in the configuration resulting from crystallization in 0·1 wt % solution. If a random number of chains were involved in the unique configuration a spread of densities might be expected from one preparation to another. If such an explanation were correct, it is to be expected that the amount of the dense phase could perhaps be altered by heat treatment, with the result that some high densities would be lowered and some low densities increased. Experiments along these lines provided the clue to the whole problem.

After determining the density of crystals prepared from 1 wt % solution the suspensions were subjected to the heating cycle recommended by Blundell and Keller[17] and crystallized at 70°C for 16 hours. After cooling to room temperature the density was redetermined at intervals. The crystals were then destroyed by refluxing at 138°C for two hours, recrystallized, and the density redetermined. The densities obtained in a typical sequence are shown in *Table 1*. The whole experiment was repeated several times and

Table 1

Thermal history	*Density* (g/cm^3)
Refluxed for 2 h, crystallized for 16 h at 70°C, held at room temperature for 24 h	0·978 ± 0·004
Heated at 10 deg. C/h to 100°C, maintained at 100°C for 0·5 h, crystallized at 70°C for 16 h, held at room temperature for 2 h	0·981 ± 0·004
" " " " " 24 "	0·993 ± 0·004
" " " " " 28 "	0·995 ± 0·004
" " " " " 48 "	0·996 ± 0·004
Refluxed for 2 h, crystallized at 70°C for 16 h, held at room temperature for 2 h	0·996 ± 0·004
" " " " " 26 "	1·000 ± 0·004
" " " " " 48 "	1·000 ± 0·004
Refluxed for 2 h, crystallized at 70°C for 16 h, held at room temperature for 2 h	1·000 ± 0·004
" " " " " 48 "	1·004 ± 0·004

gave the following final values for the densities of the crystals: 1·009 ± 0·004, 0·990 ± 0·004, 1·006 ± 0·004, 0·989 ± 0·004 g/cm³.

Two effects were observed from the results of these experiments. Following recrystallization and cooling to room temperature, the density increased with time. Twenty four to forty eight hours were required before results could be obtained which were reproducible to within experimental error. Dr Keller[20] has experienced a similar increase in density with time over a longer time interval.

In every case the density exhibited a memory effect after heat treatment, even after dissolution and recrystallization. High densities were never reduced by heat treatment and low values were always increased. This result is not consistent with the notion of a random number of chains crystallizing in a unique configuration thereby giving rise to arbitrarily high densities. It would appear that there is not a morphological explanation of the 'high' density values.

The memory effect, however, gave rise to speculation that the liquid phase was somehow responsible, since the solid phase was completely dissolved by refluxing. To eliminate effects peculiar to the liquid phase, samples of the suspensions giving densities of 1·004 g/cm^3 and 0·989 g/cm^3 were concentrated and tested in the density gradient column. Consistent values of 0·972 ± 0·001 g/cm^3 resulted in both cases. Kawai and Keller[2] reported a similar experience and attributed the failure of the density gradient column to support the high pyknometric densities in terms of interfacial effects in the column. However, in view of the good agreement obtained in this laboratory between pyknometric and density gradient column measurements on crystals prepared from 0·1 wt % solution, it seemed altogether simpler to suppose that 0·972 g/cm^3 is indeed the true density of crystals prepared from 0·1 wt % and 1 wt % solutions, with a hitherto undetected random error being introduced during pyknometric measurements on crystals prepared at the higher concentration. Oxidation comes naturally to mind as a source of error, especially in view of the remarkable memory effect. Dr Keller has been thinking along these lines in connection with the polyethylene itself[20], but it seems unlikely that a polymer which succumbs only slowly to fuming nitric acid should oxidize significantly under the conditions of density measurements. Furthermore, any oxidation products would have to be associated with the liquid phase of the suspension in order to affect the pyknometric density but not the value obtained from the density gradient column. Under the circumstances, oxidation of the solvent seemed more probable, and experiment confirmed this as being the source of error.

The crystals were removed by centrifugation from the 1 wt % suspensions that had shown high density values, and the density of the remaining clear liquid was determined. In a typical case it was found that the liquid was 0·000118 g/cm^3 denser than a sample which had been taken through identical heat treatment in the absence of polymer. The amount of polymer in the clear liquid was estimated by evaporation to dryness at room temperature and found to be $2{\cdot}84 \times 10^{-4}$ g/cm^3. It is quite inconceivable that this amount of polymer could be responsible for even the small increase in solvent density noted above. It was therefore concluded that the solvent itself had become more dense during the preparation of the crystal suspension; this has the effect of increasing the difference term $(T - X)$ and results in erroneously high pyknometric densities of the suspended solid. Correcting for the change in solvent density lowered the pyknometric crystal density to 0·971 ± 0·004 g/cm^3, in good agreement with the density gradient column results for the same crystals. Very small changes in solvent density therefore affect the apparent crystal density by exactly the right amount to explain the discrepancies.

To confirm chemically that the increase in solvent density during heat treatment is due to oxidation, samples of *p*-xylene were tested as shown in *Table 2*. The products resulting from the oxidation of *p*-xylene are *p*-tolualdehyde and *p*-toluic acid, with densities of 1·02 and 1·05 g/cm³ respectively. These compounds may be successively eliminated by washing with

Table 2

p-Xylene sample history	*Density of p-xylene sample (g/cm³)*
Fresh from supplier	0·856653
Refluxed for several hours at atmospheric pressure	0·856697
Fresh sample washed with aqueous solutions of $NaHSO_3$ and $NaHCO_3$ to remove oxidation products	0·856621
Refluxed sample washed with aqueous solutions of $NaHSO_3$ and $NaHCO_3$	0·856619

aqueous solutions of sodium bisulphite and sodium bicarbonate. The chemical reactions involved are highly specific serving as a useful verification of the presence of carbonyl and carboxylic acid groups. The results in *Table 2* show clearly that the change in density of *p*-xylene during refluxing is due to oxidation. The fresh solvent itself contained traces of oxidation products. Although a smaller density change occurred while refluxing pure solvent than when polymer was present at a concentration of 1 wt % it should be noted that even a density change of 0·000196 g/cm³ shown to occur under the latter conditions requires only a very small amount of oxidation. A quantity of *p*-toluic acid equivalent to a final oxygen content of only 0·03 wt % would be quite sufficient and this amount is not susceptible to estimation by normal techniques of quantitative analysis.

It will be remembered that in the experiments with 0·1 wt % suspensions described earlier, solvent was removed from the top of suspensions and used to calculate X, the value agreeing with that obtained with solvent which had undergone the same thermal treatment in the absence of polymer. Evidently 0·1 wt % of polymer does not measurably increase the amount of oxidation above the level encountered in the absence of polymer. For 1 wt % of polymer this is not so, and it is no longer possible to obtain reliable values of X simply by using solvent which has undergone the same thermal treatment in the absence of polymer.

It remains to explain why oxidation is enhanced by the presence of 1 wt % of polymer during thermal treatment. It is known that many organic solvents oxidize in the presence of small amounts of catalysts. Now polyethylene samples may contain variable amounts of catalyst residues originating from the catalysts used in the manufacturing process. It is therefore understandable why sufficiently high concentrations of polymer could measurably enhance the amount of oxidation undergone by the solvent. Additionally it is possible that a minute amount of polymer is oxidized and that the hydroperoxides so released are responsible for the initiation of the oxidation of a relatively much larger amount of the solvent present

in excess. In this manner an undetectable amount of polymer oxidation could effect the observed amount of solvent oxidation. Quite possibly low molecular weight fractions of polymer may be particularly prone to catalyse solvent oxidation, partly because of a higher concentration of catalyst-bearing chain ends and partly because of a higher incidence of points of unsaturation where oxidation could be initiated.

Finally, it is to be expected that small differences in procedure, such as the time of refluxing, would introduce a scatter in the results for the apparent density, due to variable amounts of solvent oxidation having taken place. It is equally true that a very rigid and well standardized procedure could lead to consistent high density values.

CONCLUSIONS

(*i*) The true density of polyethylene crystals is about 0·972 g/cm^3. This value applies equally well to the very simple regular crystals prepared from 0·1 wt % solution by the Blundell and Keller method[17], and to the much more complicated species crystallized directly from 1 wt % solution.

(*ii*) Densities determined by pyknometry and by means of the density gradient column are in excellent agreement when adequate precautions are observed.

(*iii*) There is an explanation for the high density values of poor reproducibility which can result from pyknometry when the essential precautions are not observed. The oxidation of *p*-xylene to give products of higher density is the cause of the trouble. The extent of the oxidation can be correlated with the thermal history of the solvent and the polymer concentration during thermal treatment. The magnitude of the effect in 1 wt % polymer solutions is exactly right to explain the discrepancies between 'low' and 'high' density values for polyethylene crystals.

(*iv*) The density of 0·972 g/cm^3 for single crystals might appear strange in the light of observations by Okada and Mandelkern[21] and by Wunderlich and Kashdan[6] that carefully annealed samples of unfractionated bulk polymer may have higher densities, even as high as 0·981 g/cm^3. It will be shown in another paper[22], however, that it is at least possible on theoretical grounds for the amorphous phase to have an unusually high density at very high degrees of crystallinity. This intriguing possibility is being pursued at the experimental level.

Dr Keller read the manuscript of this paper and made a number of suggestions. One of us (P.A.L.) is indebted to the Athlone Fellowships for financial support.

Department of Chemical Engineering,
University of Cambridge

REFERENCES

[1] BLACKADDER, D. A. *J. macromol. Sci. (Revs)*, 1967, **C1** (2), 297
[2] KAWAI, T. and KELLER, A. *Phil. Mag.* 1963, **8**, 1203
[3] CHARLESBY, A. and CALLAGHAN, L. *Physics Chem. Solids*, 1958, **4**, 227
[4] SWAN, P. R. *J. Polym. Sci.* 1962, **56**, 403
[5] BUNN, C. W. *Trans. Faraday Soc.* 1939, **35**, 482

[6] WUNDERLICH, B. and KASHDAN, W. H. *J. Polym. Sci.* 1961, **50,** 71
[7] FISCHER, E. W. and LORENZ, R. *Kolloidzschr.* 1963, **189,** 97
[8] KAWAI, T. and KELLER, A. *Phil. Mag.* 1963, **8,** 1973
[9] JACKSON, J. B., FLORY, P. J. and CHIANG, R. *Trans. Faraday Soc.* 1963, **59,** 1906
[10] PETERLIN, A. and MEINEL, G. *Applied Polymer Symposia,* 1966, **No. 2,** 85
[11] FISCHER, E. W. and HINRICHSEN, G. *Polymer, Lond.* 1966, **7,** 195
[12] OKADA, T. and MANDELKERN, L. *J. Polym. Sci. B,* 1966, **4,** 1043
[13] SCHONHORN, H. and RYAN, F. W. *J. phys. Chem.* 1966, **70,** 3811
[14] KAWAI, T. *Reports on Progress in Polymer Physics in Japan,* 1966, **9,** 141
[15] GOTO, T., KAWAI, T. and MAEDA, H. *Reports on Progress in Polymer Physics in Japan,* 1966, **9,** 145
[16] MARTIN, G. M. and PASSAGLIA, E. *J. Res. Nat. Bur. Std A,* 1966, **70,** 221
[17] BLUNDELL, D. J. and KELLER, A. *J. Polym. Sci. B,* 1966, **4,** 481
[18] ZIABICKI, A. and WASIAK, A. *Kolloidzschr.* 1967, **215,** 158
[19] PEARSON, J. R. A. *Polymer, Lond.* 1968, **9,** 283
[20] KELLER, A. Private communication, PRIEST and KELLER—to be published
[21] OKADA, T. and MANDELKERN, L. *J. Polym. Sci. A-2,* 1967, **5,** 239
[22] BLACKADDER, D. A. and BOWDEN, P. B. To be published

*Structures of the Poly(diphenylene ether sulphones) obtained by Polysulphonylation**

M. E. A. CUDBY, R. G. FEASEY, S. GASKIN, MRS V. KENDALL and J. B. ROSE

A study of hydrogen chloride evolution versus time curves for polysulphonylations, conducted in the presence of excesses of sulphonyl chloride groups, shows that chain branching proceeds very much more slowly than chain extension, but that branching occurs to a greater extent in reaction (iii) than in reactions (i) and (ii). The proportion of linear repeat units, I and II, and branch point units, III, are estimated by analysis of the hydrogen chloride evolution curves, and/or by an n.m.r. technique involving spectrum accumulation. The results show that high polymers obtained from reaction (iii) contain the units I, II and III in the approximate percentage proportions 90 : 10 : 1·6 respectively, while the polymers from reactions (i) and (ii) consist essentially of unit I (ca. 99 per cent) and contain less than 0·7 per cent of the branch point units, III.

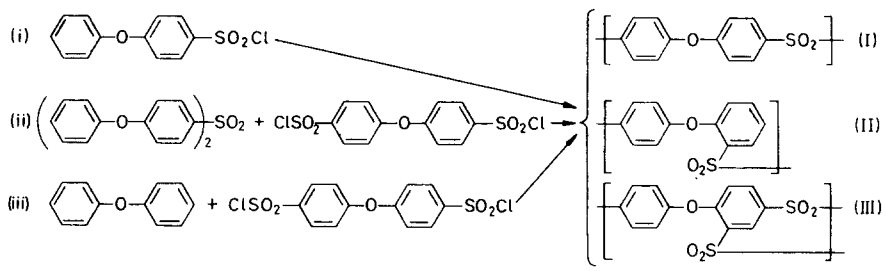

IN PREVIOUS papers[1, 2], we have presented n.m.r. data indicating that the structures of the poly(diphenylene ether sulphones) obtained by polycondensations involving diphenyl ether sulphonyl chlorides, either in the melt[1, 3] or in nitrobenzene solution[3], depend on the structures of the diphenyl ether derivatives employed, as indicated in relations (i) to (iii). Reasons for these structural variations have been discussed[1], together with

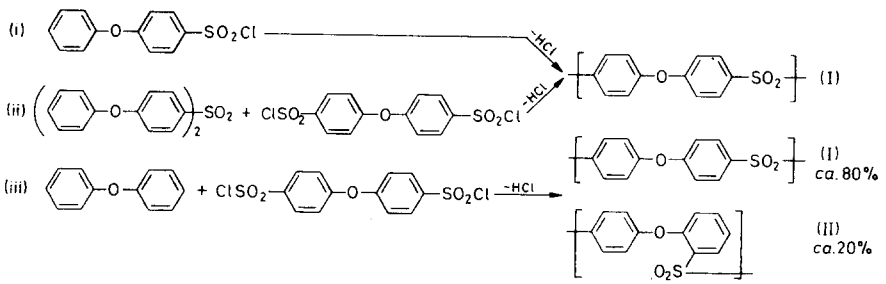

*Paper presented at 155th National Meeting of the American Chemical Society, San Francisco, April 1968.

the possibility that chain branching may occur by attack of sulphonyl chloride chain ends on either of the linear repeat units I or II[1, 2]. We have shown[1, 2] that reactions such as (iv) and (v) can occur in systems containing an excess of sulphonyl chloride over the amount required to monosulphonylate all of the phenoxyl groups present, and have obtained circumstantial evidence indicating that reaction (iv) proceeds faster than reaction (v). Phenoxyl groups will react much more rapidly with sulphonyl chloride

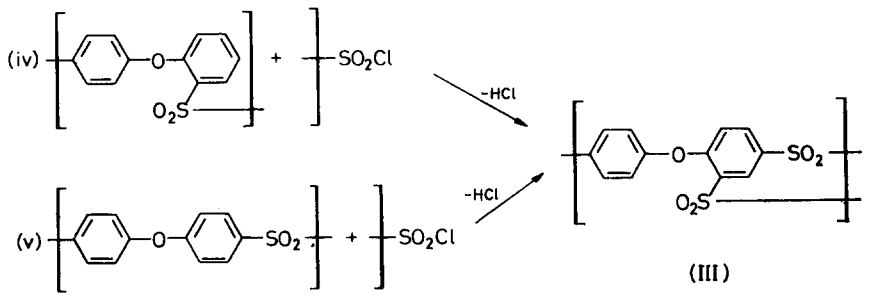

groups than will the sulphonyl phenoxyl groups comprising repeat units I or II, due to the deactivating effect of the $-SO_2-$ group[4]. Thus, the relative rates of reaction at comparable reactant concentrations will be (i), (ii) or (iii) $\gg$ (iv) $>$ (v), and, in systems containing equivalent quantities of sulphonyl chloride and phenoxyl groups, reactions (iv) and (v) should occur to a small extent only. However, hydrogen chloride evolution from systems containing an excess of sulphonyl chloride over phenoxyl groups proceeds beyond that expected from monosulphonylation of all the phenoxyl groups[2], so that, under these conditions, reactions (iv) and (v) become significant. A plot of hydrogen chloride evolution versus time for such systems should therefore be of the idealized form shown in *Figure 1*, and

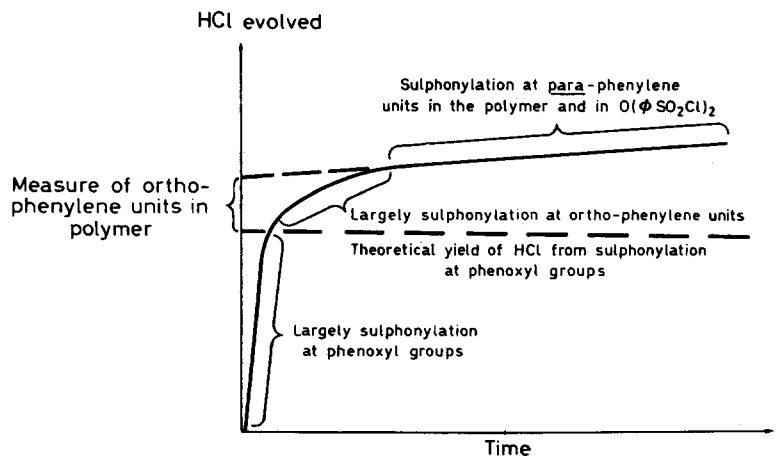

Figure 1—Theoretical plot of hydrogen chloride evolution versus time for a polysulphonylation in the presence of added diphenyl ether-4,4′-disulphonyl chloride

it appeared possible that data concerning the relative importance of these competing reactions, and therefore information about the structure of the polymers, might be obtained from an analysis of experimental hydrogen chloride evolution curves.

This paper records hydrogen chloride versus time measurements for reactions (i) and (iii) conducted in the presence of excess sulphonyl chloride, added in both cases as diphenyl ether disulphonyl chloride, and shows how the data obtained can be analysed to provide information concerning the structures of the polymers obtained from these reactions in the absence of excess sulphonyl chloride. We also report the use of an improved n.m.r.

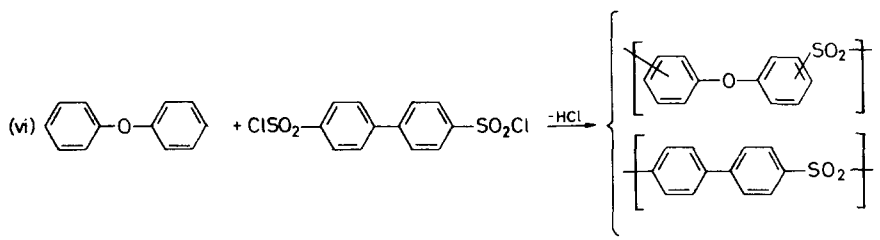

technique employing spectrum accumulation for the direct estimation of branched units, III, in the polymers from reactions (i) to (iii), and also the use of n.m.r. techniques to obtain structural information concerning the polymer from reaction (vi).

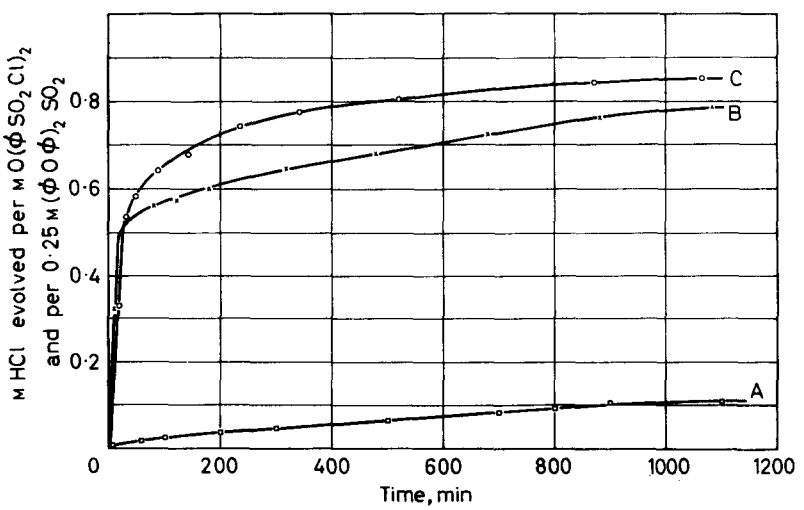

Figure 2—Hydrogen chloride evolution versus time plots for the reactions of diphenyl ether-4,4′-disulphonyl chloride alone and with 4,4′- and 2,4′-diphenoxydiphenyl sulphone. $[O(\phi SO_2Cl)_2]=0{\cdot}59$ м l^{-1}. $[FeCl_3]=0{\cdot}012$ м l^{-1}. Solvent: nitrobenzene. Temperature 120°C

Key		$[(\phi O\phi)_2SO_2]$ м l^{-1}
□	A	None present
×	B	0·16—4,4′-isomer
○	C	0·16—2,4′-isomer

RESULTS

Sulphonylations with model compounds

Curve A (*Figure 2*) is a plot of hydrogen chloride evolution versus time from a solution of diphenyl ether-4,4′-disulphonyl chloride (0·59 M l^{-1}) in nitrobenzene (17 ml) at 120°C to which ferric chloride (0·012 M l^{-1}) had been added at time zero. It is seen that hydrogen chloride evolution proceeds at an approximately constant slow rate from 100 to 900 minutes so that the conversion of disulphonyl chloride during 1 000 minutes is only about five per cent. The other two curves in *Figure 2* are plots of hydrogen chloride evolution versus time for the reactions between the disulphonyl chloride (0·59 M l^{-1}) and either 4,4′-diphenoxydiphenyl sulphone IV (0·16 M l^{-1}) (curve B) or 2,4′-diphenoxydiphenyl sulphone, V (0·16 M l^{-1}),

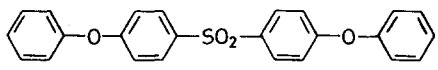

(IV)

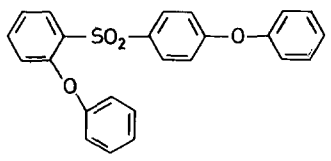

(V)

(curve C) under conditions comparable to those for curve A. Curves B and C both show three reasonably distinct phases of reaction:

(*a*) an initial phase of very fast reaction lasting some 50 minutes during which *ca.* 2 M hydrogen chloride per M diphenoxydiphenyl sulphone was evolved,

(*b*) an intermediate phase from 50 to, say, 500 minutes during which hydrogen chloride evolution occurs at a moderate rate, faster in the case of the reaction involving V than that involving IV,

(*c*) a final phase beyond 500 minutes during which hydrogen chloride evolution from both reactions occurs at approximately the same slow rate.

Polysulphonylations with a large excess of sulphonyl chloride

Plots D1–D4 (*Figure 3*) show hydrogen chloride evolution versus time from reactions between diphenyl ether-4,4′-disulphonyl chloride and various amounts of diphenyl ether conducted under the same experimental conditions as described for curve A (*Figure 2*). Plots E1–E4 (*Figure 4*) are for analogous experiments in which mixtures of the disulphonyl chloride with various amounts of diphenyl ether-4-sulphonyl chloride were employed. In both these series of experiments the addition of diphenyl ether or of the monosulphonyl chloride was delayed until the self-condensation reaction of the disulphonyl chloride had 'settled down' to a slow and approximately constant rate, the moment at which these additions were made being taken as the zero of time. For both sets of experiments the hydrogen chloride evolution is plotted as a percentage of that expected from monosulphonylation of all the phenoxyl groups (two per diphenyl ether molecule and one per molecule of monosulphonyl chloride) present. Averaged curves drawn between each set of plots are of the same general

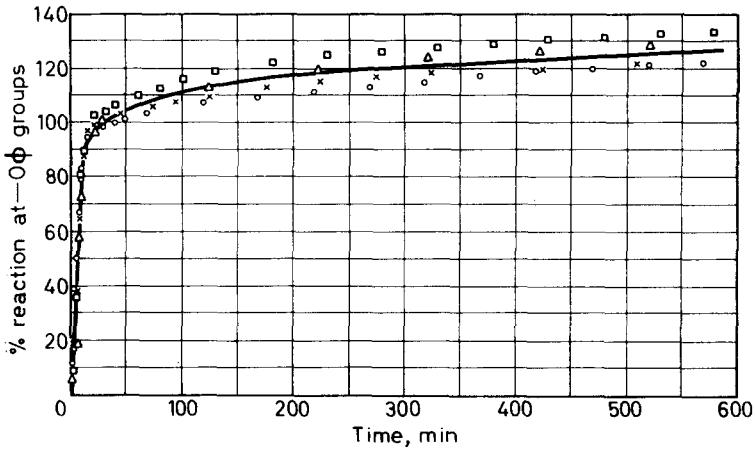

Figure 3—Hydrogen chloride evolution versus time plots for polycondensation of diphenyl ether-4,4′-disulphonyl chloride and diphenyl ether in the presence of large quantities of added disulphonyl chloride. $[O(\phi SO_2Cl)_2]=0{\cdot}59$ M l^{-1}. $[\phi_2O]=0{\cdot}15$ to $0{\cdot}31$ M l^{-1}. $[FeCl_3]=0{\cdot}012$ M l^{-1}. Solvent: nitrobenzene. Temperature 120°C

Key		—SO_2Cl groups per —Oϕ group
×	D1	1·93
○	D2	2·22
□	D3	3·58
△	D4	3·88

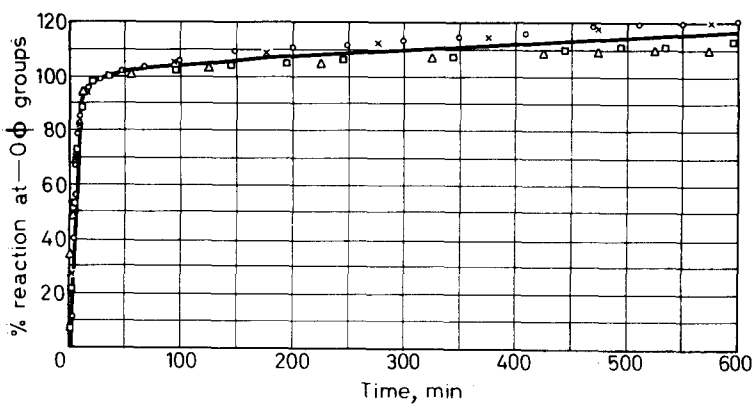

Figure 4—Hydrogen chloride evolution versus time plots for the polycondensation of diphenyl ether-4-sulphonyl chloride in the presence of large quantities of added diphenyl ether-4,4′-disulphonyl chloride. $[O(\phi SO_2Cl)_2]=0{\cdot}39$ M l^{-1}. $[\phi O\phi SO_2Cl]=0{\cdot}26$ to $2{\cdot}28$ M l^{-1}. Solvent: nitrobenzene. Temperature 120°C

Key		—SO_2Cl groups per —Oϕ group
△	E1	1·34
□	E2	1·98
×	E3	2·80
○	E4	3·96

shape as curves B and C, and are very similar in slope during the initial and final phases. During the intermediate phase (50 to 500 minutes), the rate of hydrogen chloride evolution in the D series is substantially faster than that in the E series so that the average percentage of hydrogen chloride evolution from the diphenyl ether–disulphonyl chloride system at 600 minutes (127) is greater than that from the diphenyl ether monosulphonyl chloride–disulphonyl chloride system (116).

Polysulphonylations with a small excess of sulphonyl chloride

Curves F1–F3 (*Figure 5*) and G1–G4 (*Figure 6*) show hydrogen chloride evolution, expressed as a percentage of that expected from monosulphonylation of all phenoxyl groups, versus time curves for reactions similar to the C and D series (*Figures 3* and *4*) except that the excess of sulphonyl chloride used did not exceed 15 M per cent of that required for monosulphonylation. Both systems show a fast initial hydrogen chloride evolution up to 100 per cent monosulphonylation. The diphenyl ether system, curves F (*Figure 5*), shows a subsequent fairly rapid reaction so that after *ca.* 400 minutes hydrogen chloride evolution has nearly stopped, due to almost complete reaction of sulphonyl chloride. The subsequent reaction beyond 100 per cent from the monosulphonyl chloride system, curves G (*Figure 6*), occurs more slowly and after *ca.* 400 minutes settles down to a steady rate for at least a further 500 minutes, and in contrast with the 'F' series of reactions,

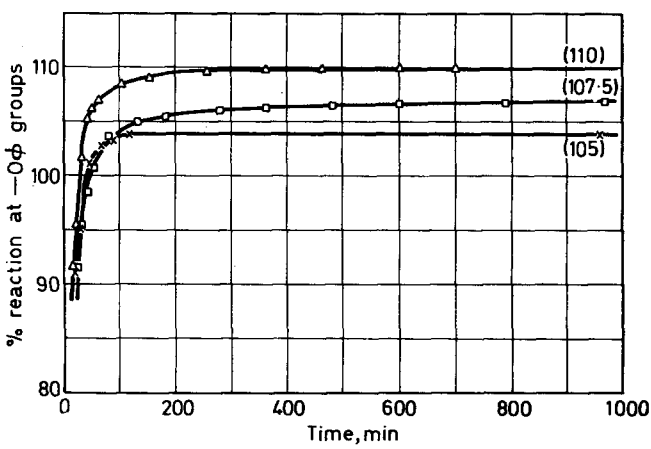

Figure 5—Hydrogen chloride evolution versus time plots for the polycondensation of diphenyl ether-4,4′-disulphonyl chloride and diphenyl ether in the presence of small quantities of added disulphonyl chloride. Numerals in parentheses indicate the theoretical values for complete reaction of $—SO_2Cl$ groups. $[\phi_2O]=0{\cdot}56$ M l^{-1}. $[FeCl_3]=0{\cdot}011$ M l^{-1}. Solvent: nitrobenzene. Temperature 120°C

Key		$[O(\phi SO_2Cl)_2]$ M l^{-1}
×	F1	0·584
□	F2	0·597
△	F3	0·611

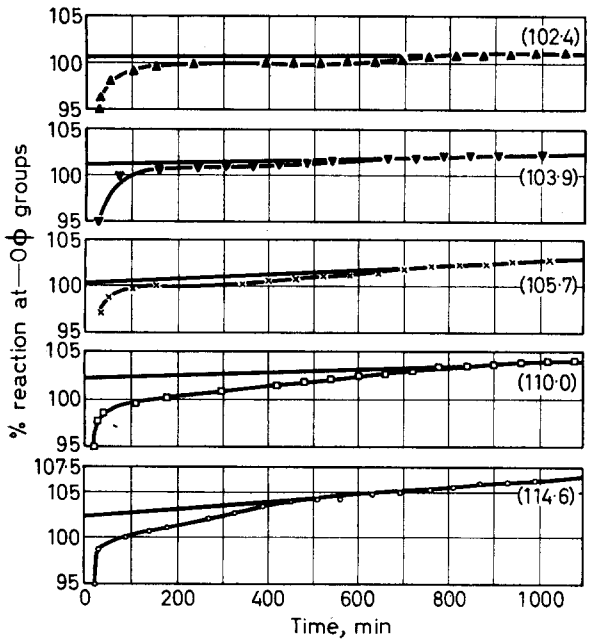

Figure 6—Hydrogen chloride evolution versus time plots for the polycondensation of diphenyl ether-4-sulphonyl chloride in the presence of small quantities of added diphenyl ether-4-4′disulphonyl chloride. Numerals in parentheses indicate the theoretical values for complete reaction at $—SO_2Cl$ groups. $[\phi O\phi SO_2Cl]=1{\cdot}25$ M l^{-1}. $[FeCl_3]=0{\cdot}013$ M l^{-1}. Solvent: nitrobenzene. Temperature 120°C

Key		$[O(\phi SO_2Cl)_2]$ M l^{-1}
▲	G1	0·0153
▼	G2	0·0241
×	G3	0·0355
□	G4	0·0625
○	G5	0·0913

a significant proportion of sulphonyl chloride in the 'G' series remains unreacted after 1 000 minutes.

Accumulated n.m.r. spectra

Figure 7 shows a portion of the accumulated n.m.r. spectrum[6] (64 scans) of polymer (H 1; R.V.* 0·55) prepared by reaction (iii) recorded in dimethyl sulphoxide solution. The resonance at 1·40 τ is assigned to the

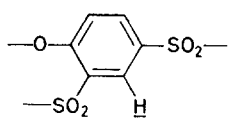

(VI)

*Reduced viscosity of a ten per cent solution in dimethyl formamide at 25°C.

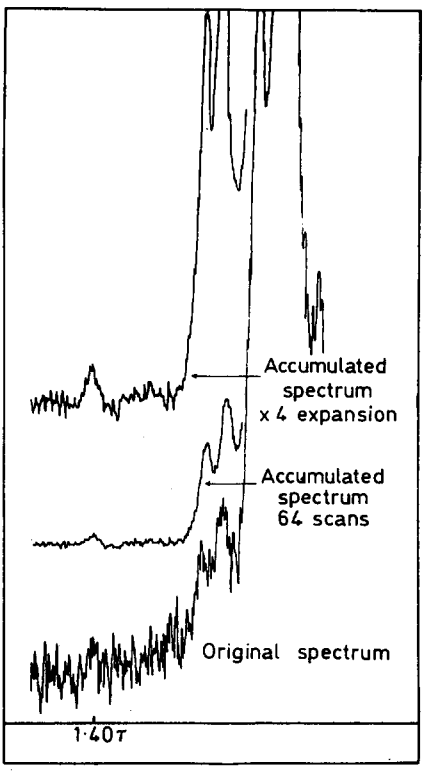

Figure 7—Portion of accumulated n.m.r. spectrum (64 scans) of polymer H 1

proton indicated in structure VI by analogy with the assignment[8] of the resonance at 1·23 τ observed in the spectrum of a branched oligomer, recorded in deuterochloroform solution. The difference in chemical shift of protons in the same chemical environment is attributed to solvent effects.

The areas of the band at 1·40 τ and of the small doublet at 1·85 τ were measured. The complete spectrum of the polymer was recorded without accumulation and the area of the 1·85 τ resonance related to that of the remaining resonance areas. From these measurements it was calculated that polymer H 1 contains 1·7 units of structure VI per hundred polymer repeat units.

Successive dilutions of the polymer H 1 with polymer prepared from the potassium salt of 4-hydroxy-4′-chlorodiphenyl sulphone in the melt[7] enabled a detection limit to be set of 0·4 unit of structure VI per hundred polymer repeat units, on examination of accumulated spectra after 350 scans.

Other polymers prepared by reaction (iii) were examined under conditions of identical amplification, field homogeneity and accumulation, and the proportions of units of structure VI present in these polymers measured by direct comparison of band areas at 1·4 τ with the band area at 1·40 τ obtained from polymer H 1. The results obtained are shown in *Table 1*.

Polymer prepared by reaction (ii) in the melt (I, R.V. 0·49) was subjected to 350 scans for spectral accumulation in order to observe a reson-

Table 1. Proportions of branch units in polymers prepared by reaction (iii)

Polymer	*R.V.*	*Branch units, VI, per 100 repeat units*
H 1	0·55	1·7
H 2	0·56	1·6
H 3	0·40	1·3
H 4	0·11	0·7

ance at 1·4 τ. By comparison with H 4 and a diluted sample of H 1, this polymer was found to contain between 0·4 and 0·7 unit of structure VI per 100 repeat units.

Polymer prepared by reaction (i) (J, R.V. 0·47) was similarly subjected to 350 scans but no resonance was observed around 1·4 τ. It is therefore deduced that polymer J contains fewer than 0·4 unit of structure V per 100 repeat units.

Polymer prepared by reaction (vi) (K, R.V. 0·29) was examined similarly to polymer H 1. A resonance was observed in accumulated spectra at 1·4 τ which corresponds to 1·5 units of structure V per 100 diphenyl sulphonyl and diphenyl ether sulphonyl units. The complete spectrum (non-accumulated) of polymer K is shown in *Figure 8*. The large block of resonances at *ca.* 2·1 τ are attributed to the protons of *p,p'*-diphenyl sulphonyl units, VI, and the protons ortho to the sulphone group in *p,p'*-diphenyl ether sulphonyl units, I; the doublet at 2·80 τ is assigned to the protons ortho to

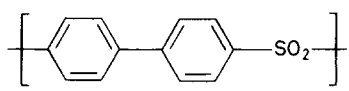

(VII)

the ether group in *p,p'*-diphenyl ether sulphonyl units. Further resonances are observed at 1·81 τ, 2·3 to 2·5 τ and 3·12 τ which cannot arise from para-phenylene links. The n.m.r. spectrum of the *p,o*-diphenyl ether sulphonyl unit, VIII, has been discussed previously[1] and the resonances at 3·12 τ and 2·3 to 2·5 τ may well arise from protons H_A and protons H_B, H_C and H_D

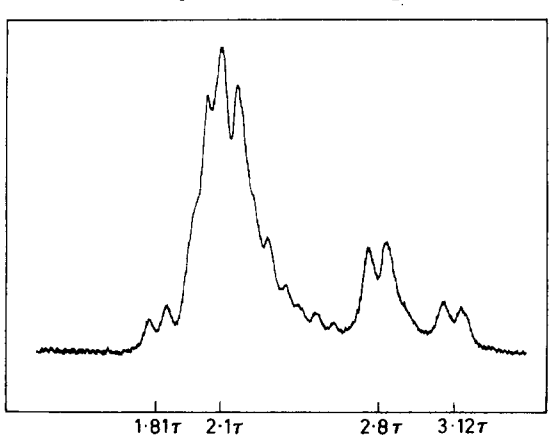

Figure 8—N.m.r. spectrum of polymer K

respectively in such a unit; the proton H_E is expected to occur 'to low field' and may well be that observed at 1·81 τ.

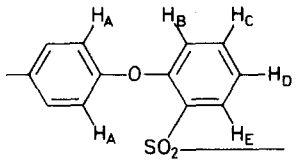

(VIII)

DISCUSSION

Interpretation of the hydrogen chloride evolution curves

The data obtained for sulphonylation of the model compounds IV and V with diphenyl ether-4,4′-disulphonyl chloride (curves B and C in *Figure 2*) show qualitatively the relative importance of the branching processes, (iv) and (v), which may occur in competition with chain extension via reactions (i) to (iii) during the polycondensations under consideration. Thus, it is clear from both curves that monosulphonylation to give sulphonyl phenoxyl units I or II is very much faster than the subsequent reaction of these units

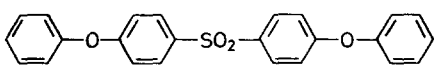

(IV)

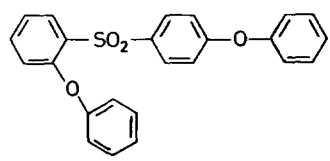

(V)

to form products containing disulphonyl phenoxyl units, III. Further reaction beyond that required for monosulphonylation proceeds faster during the intermediate phase from 50 to 500 minutes with compound V than with IV, indicating that *o*-sulphonyl phenoxyl groups, II, are more reactive than their para-isomers, I. However, after some 500 minutes the reaction rate for compound V drops back to about that of compound IV suggesting that by this time most of the *o*-sulphonyl phenoxyl groups have been consumed, and evolution of hydrogen chloride now comes from the reaction between sulphonyl chloride and *p*-sulphonyl phenoxyl groups. The rate of hydrogen chloride evolution during this final phase is comparable to that from the self condensation of diphenyl ether disulphonyl chloride, curve A, as would be expected since this (latter) reaction also involves sulphonylation of phenoxyl groups deactivated by *p*-sulphonyl substituents.

The above picture of relative reactivities towards sulphonylation provides a sound basis for interpreting the hydrogen chloride evolution curves obtained for reactions (i) (systems E and G) and (iii) (systems D and F) conducted in the presence of excess sulphonyl chloride. Considering first the experiments in which sulphonyl chloride was present in large excess, it is seen that during the intermediate phase hydrogen chloride evolution from System D (*Figure 3*), is substantially greater than that from System E

(*Figure 4*). This difference is analogous to that found between the sulphonylation reactions of the model compounds V and IV (curves C and B in *Figure 2*), and arises from analogous structural differences between the substrates for sulphonylation during the intermediate phase of these reactions. Thus, whereas the product formed during the initial phase in system E consists essentially of the all para structure I, the first product in system D contains a substantial proportion of *o*-sulphonyl phenoxyl units, II, and as with the model compound V, it is the presence of these units which leads to the relatively rapid production of hydrogen chloride via reaction (iv) from system D as compared with E during the intermediate phase. The slopes of the initial sections (0 to 50 min) of curves D and E are similar to one another and to those of curves B and C, showing that monosuphonylation occurs at comparable rates in all four systems; the slopes of the final sections (beyond 500 min) of curves B to E are also comparable, as, by this time, hydrogen chloride evolution comes only from sulphonylation of *p*-sulphonylphenoxyl groups (reaction v).

This difference in reactivity during the intermediate phase is emphasized by the series of experiments in which reactions (i) and (iii) were carried out in the presence of small excesses of sulphonyl chloride (systems G and F respectively). Under these conditions, the excess of sulphonyl chloride was not sufficient to sulphonylate all of the *o*-sulphonyl phenoxyl groups formed during the first phase in systems F and as is seen from curves F 1–3 (*Figure 5*), hydrogen chloride evolution was complete during the first 500 minutes and virtually equivalent to all the sulphonyl chloride employed. However, in systems G 1–5 (*Figure 6*) the excess of sulphonyl chloride was greater than that required to sulphonylate the small proportion of *o*-sulphonyl phenoxyl groups formed during the initial phase, so that hydrogen chloride evolution from the sulphonylation of *p*-sulphonyl phenoxyl groups continued steadily even after reaction times exceeding 1 000 minutes.

Derivation of structural information from the hydrogen chloride evolution curves

The slopes of the final sections of curves D and E are approximately the same, so that the vertical distance between these parallel lines represents the additional hydrogen chloride evolution from systems D as compared with E due to the reaction of the different proportions of *o*-sulphonyl phenoxyl groups formed in these systems during the initial phase. Reaction of these groups is complete by the end of the intermediate phase, so that this additional hydrogen chloride evolution measures the difference between the proportions of *o*-sulphonyl phenoxyl groups formed in these systems during the initial phase, and reference to the curves shows that if x per cent of the phenoxyl groups present at the start in system E are monosulphonylated at the ortho-position then the corresponding percentage in system D is $(x+10)$ per cent. There is no reason to believe that the orientation of monosulphonylation during the initial phase of systems E and D will be different from that during the polycondensations reactions (i) and (iii), so that the percentage of ortho-substituted repeat units in the polymers obtained is x and $(x+10)$ respectively.

Some measure of the percentage, x, of *o*-sulphonyl phenoxyl repeat units, II, in the polymers obtained from reaction (i) can be obtained from the hydrogen chloride evolution curves, G 1–5, for reaction (i) performed in the presence of small amounts of diphenyl ether disulphonyl chloride. The final sections of these curves, representing reaction of sulphonyl chloride with *p*-sulphonyl phenoxyl groups, are linear, and if it is assumed that the extrapolations of these lines back to the time zero represents this reaction during both the initial and the intermediate phases, then the intercept on the hydrogen chloride axis gives the amount arising from sulphonylation of all phenoxyl and *o*-sulphonyl phenoxyl groups. Thus, subtraction of 100 from this intercept gives the percentage of *o*-sulphonyl phenoxyl groups formed. The data so obtained are given in *Table 2*, and indicate that self condensation of the monosulphonyl chloride, reaction (i), gives polymers containing 1 ± 1 per cent of *o*-sulphonyl phenoxyl repeat units, II, and hence that the condensation of diphenyl ether with its 4,4′-disulphonyl chloride, reaction (iii), gives polymers containing 11 per cent of these units.

Table 2. Extrapolation of hydrogen chloride evolution from reaction (v) to time zero

Reaction	[*disulphonyl chloride*] M l^{-1}	*Intercept of* HCl *axis*	% *II*
G 1	0·0153	100·8	0·8
2	0·0241	101·1	1·1
3	0·0355	100·3	0·3
4	0·0625	102·2	2·2
5	0·0913	102·2	2·2

The above extrapolation technique is strictly valid only if reaction (v) proceeds at approximately constant speed through all three phases of reactions G 1–5. However, the concentration of sulphonyl chloride during the final phase is only 0·1 to 0·01 of that at the start of the reaction, while the concentration of *p*-sulphonyl phenoxyl groups increases during the reaction, by a factor of about two. Thus, although the orders of reaction with respect to these two reactants are not known, it is most unlikely that reaction (v) proceeds more slowly during the initial and intermediate phases than it does during the final phase of these reactions, so that the extrapolation technique gives an upper estimate of the extent to which reaction (iv) occurs.

The n.m.r. spectra of the polymers from reactions (i) and (ii) are very similar[1,2] so that the polymer from reaction (ii) must contain a very low proportion of *o*-sulphonyl phenoxyl units, II, similar to that (about one per cent) contained by the polymer from reaction (i).

The curves G 1–5 can also be used to obtain an estimate of the extent to which branching occurs during reaction (i). Thus, by the time that the hydrogen chloride evolution curve has become linear, all reaction other than sulphonylation of *p*-sulphonyl phenoxyl groups, I, has ceased. The total hydrogen chloride evolution at this time is that due to complete monosulphonylation of phenoxyl groups plus the further reactions of sulphonyl

phenoxyl groups (I or II) to give disulphonyl phenoxyl branch points, III. Therefore, the percentage hydrogen chloride evolution at this point, less 100 per cent due to monosulphonylation of phenoxyl groups, measures the amount of branching that has occurred during the time required for complete monosulphonylation of phenoxyl groups. Data obtained in this way are given in *Table 3*. As expected, the extent to which branching occurs decreases as the amount of added disulphonyl chloride is reduced, and although no precise relationship can be discerned, it is clear that in the absence of added disulphonyl chloride the polymer from reaction (i) contains less than one branch unit III for 100 polymer repeat units I or II.

Table 3. Percentage branching in reactions G 1–5

Reaction	[*added disulphonyl chloride*] M l^{-1}	HCl *evolution**	$\frac{III}{I+II}$ * $\times 100$
G 1	0·0153	100·9	0·9
2	0·0241	100·9	1·9
3	0·0355	102·1	2·1
4	0·0625	103·6	3·6
5	0·0913	104·2	4·2

*At the time when the curve becomes linear.

N.m.r. investigation of polymers

The n.m.r. investigation of polymers using the spectrum accumulation technique provides a direct means of measuring branching by reactions (iv) and (v) during polysulphonylation. The results of these measurements are summarized in *Table 4*.

The extents to which the polymers are branched clearly depend upon their molecular weight and upon the reactants from which the polymers are prepared. The H series of polymers (*Table 4*) shows that the extent of branching increases with increasing molecular weight. This is because reactions (iv) and (v) compete increasingly more effectively for sulphonyl chloride groups as chain extension proceeds and as phenoxyl groups are consumed. In polymers of high molecular weight, the dependence of branching on the reactants employed, and therefore on the proportion of *o*-sulphonyl phenoxyl units, II, in the polymers formed, is consistent with the evidence obtained from the hydrogen chloride evolution versus time plots. Thus, polymers from reaction (iii) contain a relatively high proportion of branches since this reaction yields polymer containing a significant proportion of *o*-sulphonyl phenoxyl units which are sulyphonylated (reaction v) comparatively readily to give branches. However, polymers from reactions (i) and (ii) contain only very small proportions of *o*-sulphonyl phenoxyl units and are correspondingly substantially linear since sulphonylation of *p*-sulphonyl phenoxyl units (reaction iv) is very slow. The hydrogen chloride evolution experiment G 1–5 indicated that the polymer from reaction (i) contains less than one per cent of branches and this is consistent with the more accurate estimate, $< 0{\cdot}4$ per cent, obtained by the n.m.r. technique. The n.m.r. spectrum of the polymer from reaction (vi) shows the presence of a significant proportion of *o*-sulphonyl phenoxyl units, II, and, as would be expected, this polymer is branched to a considerable extent.

Taken together, the n.m.r. and hydrogen chloride evolution data show that the high polymers obtained from reaction (iii) contain units, I, II and III in the approximate proportions 90 : 10 : 1·6 per cent respectively, whereas the polymers from reactions (i) and (ii) consist essentially of unit I and contain less than 0·7 per cent of branch point units, III.

Table 4. Determination of branching by n.m.r.

Polymer	*Preparative reaction*	*R.V.*	*Branches (IV) per 100 repeat units*
H 1	(iii)	0·55	1·7
H 2	(iii)	0·56	1·6
H 3	(iii)	0·40	1·3
H 4	(iii)	0·11	0·7
I	(ii) melt	0·49	0·4–0·7
J	(i)	0·47	< 0·4
K	(vi)	0·29	1·5*

* per 100 $\dashv\phi\text{—}\phi\text{—}SO_2\vdash$ and $\dashv\phi O\phi SO_2\vdash$ units.

EXPERIMENTAL

Materials

Nitrobenzene—Nitrobenzene (B.D.H. Laboratory Reagent) was stood over phosphorus pentoxide for several days and then distilled, under dry nitrogen, at 84°C/17 mm into a dry receiver.

Nitrogen—Nitrogen was passed through a drying tower (20 in. × 1 in. diameter) containing phosphorus pentoxide, supported upon vermiculite, and then into the apparatus through copper tubing. The nitrogen contained <5 p.p.m. v/v water on entry into the apparatus.

Ferric chloride catalyst solution—Ferric chloride (Hopkin and Williams Reagent) was sublimed in an atmosphere of chlorine and then weighed into a dry flask. Dry nitrobenzene was then added to give a clear red solution containing 1 mM ferric chloride in 10·0 ml (1·62 per cent w/v).

Diphenyl ether—Diphenyl ether (Hopkin and Williams Reagent) was distilled through a vacuum-jacketed column (13 in.), packed with glass helices. The fore-run was discarded (about ten per cent of the total volume) and the fraction boiling at 126°C/13 mm was collected in a dry receiver.

Diphenyl ether-4-sulphonyl chloride—Diphenyl ether-4-sulphonyl chloride was prepared by the method described previously[2] and had m.pt 45° to 47°C (Suter[5] reports m.pt 45° to 46°C).

When polymerized (see later) in stirred nitrobenzene (15 ml) solution at 120°C under dry nitrogen for 22 hours, catalysed by ferric chloride (0·2 mM), this material (5·376 g; 0·02 M) yielded 100 per cent of the theoretical quantity of hydrogen chloride and polymer of reduced viscosity 0·81 (1% w/v solution in dimethyl formamide at 25°C).

Diphenyl ether-4,4′-disulphonyl chloride—Diphenyl ether-4,4′-disul-

phonyl chloride was prepared by the method described previously[2] and had m.pt 131·5° to 133°C (Suter[5] reports m.pt 128° to 129°C).

When copolymerized (see later) in stirred nitrobenzene (15 ml) solution at 120°C under dry nitrogen for 22 hours, catalysed by ferric chloride (0·2 mM), this material (3·672 g, 0·01 M) and diphenyl ether (1·702 g, 0·01 M) yielded 100 per cent of the theoretical quantity of hydrogen chloride and polymer of reduced viscosity 1·07 (1% w/v solution in dimethyl formamide at 25°C).

Diphenyl-4,4′-disulphonyl chloride—Diphenyl-4,4′-disulphonyl chloride was prepared by a method exactly analogous to that used to prepare diphenyl ether-4,4′-disulphonyl chloride and had m.pt 214° to 215°C (Suter[5] reports m.pt 203°C).

Preparation of 4,4′-diphenoxydiphenyl sulphone (IV)

A mixture of an aqueous solution of potassium hydroxide (495 g; 3·8 M KOH), phenol (376·4 g; 4·0 M), dimethyl sulphoxide (1 600 ml) and benzene (450 ml) was refluxed for 16 h under nitrogen until water evolution (removed with a Dean and Stark apparatus) had practically ceased (water evolution 355 ml; theoretical 352 ml).

The reaction mixture was cooled to room temperature, 4,4′-dichlorodiphenyl sulphone (344·6 g; 1·2 M) added, and the mixture refluxed at 130° to 133°C for 6 h under nitrogen (some benzene distilled out). While still warm, the reaction mixture was poured into a vigorously stirred mixture of methanol (1 l.) and water (1·2 l.), The precipitate was collected, washed with the same volume of the above solvent mixture, stirred with methanol (2 l.), washed with further methanol, and dried to a white crystalline solid (461·4 g; 95·6 per cent yield), m.pt 142·5° to 143°C. This material was recrystallized from isopropanol to yield white crystals, m.pt 143° to 143·5°C.

Found: C 71·6, H 4·6, S 7·7 per cent. $C_{24}H_{18}O_4S$ requires: C 71·6, H 4·5, S 8·0 per cent.

The n.m.r. and infra-red spectra of the product were consistent with the required structure.

Preparation of 2,4′-diphenoxy-diphenyl sulphone (V)

Phenol (3·952 g; 0·042 M), concentrated potassium hydroxide solution (5·19 g; 0·042 M), sulpholan (300 ml) and xylene (*ca.* 20 ml) were placed in a 250 ml RBF fitted with a stirrer, nitrogen inlet, Dean and Stark head and thermometer. The reaction mixture was heated and water was completely azeotropically distilled from the flask during 1½ h. The light brown reaction mixture was allowed to cool slightly and crude 2,4′-dichlorodiphenyl sulphone (containing *ca.* 6 per cent of the 2,2′-isomer) (5·752 g; 0·02 M) was washed in with a little xylene.

The temperature of the reaction mixture was allowed to rise to 240°C, and xylene distilled from the flask. The reaction mixture was stirred at 240°C for 4 h and then allowed to cool. The resulting brown liquid was poured into ice–water (*ca.* 1 l.) and the dark oil which precipitated crystal-

lized on standing. The crystalline precipitate was collected at the pump, washed thoroughly with water and dried. The resulting light brown solid (7·0 g) was recrystallized from isopropanol to yield white needles (3·0 g, 35 per cent), m.pt 123°C.

Found: C 72·3, H 4·8, O 15·9, S 7·8 per cent. $C_{24}H_{18}O_4S$ requires: C 71·6, H 4·5, O 15·9, S 8·0 per cent.

The n.m.r. spectrum of the product was consistent with the required structure.

Kinetic runs—apparatus and procedure

The reaction vessel consisted of a 100 ml conical flask, fitted with a mechanical stirrer passing through an oil-sealed gland, a dry nitrogen inlet reaching almost to the surface of the reaction mixture, an injection port fitted with a rubber diaphragm and a reflux condenser; the conical flask was immersed in a thermostatically controlled (±1 deg. C) oil bath. Nitrogen from the bench supply was passed through a Speedivac constant pressure valve, a needle valve, the drying tower and then at a constant rate, into the reaction vessel.

During a kinetic run, hydrogen chloride evolved from the reaction mixture was swept out of the reaction vessel, through the reflux condenser, to a two-way tap via glass tubing. When the evolution of hydrogen chloride from the reaction mixture was fast, the tap was set to lead the gas stream to the base of a beaker containing stirred water (*ca.* 400 ml), through a dip-leg, perforated at its lower end. The gases thus rose through *ca.* 5 in. of stirred water as a stream of small bubbles. The aqueous scrubber solution was periodically titrated with standard sodium hydroxide solution (0·100 N) using phenol red indicator. When the evolution of the hydrogen chloride from the reaction mixture became slow, the tap was set to lead the gas stream to the base of a beaker containing stirred buffer solution [400 ml water containing sodium citrate (0·004 M) and ammonium citrate (0·004 M)], through a perforated dip-leg. The electrodes of an E.I.L. Model 23 A direct reading pH meter, which was connected in turn to a pen recorder, were immersed in the buffer solution. The pen recorder response was directly proportional to the quantity of hydrogen chloride absorbed by the buffer solution, up to 10^{-3} M hydrogen chloride absorbed. Before each run, the unit was calibrated by the addition of standard hydrochloric acid (10 ml; 0·100 N) to the buffer solution in 0·5 ml portions from a burette.

In the course of a run, monomers and nitrobenzene (usually 15 ml) were introduced into the reaction vessel (dried overnight in an air oven at 110°C) and the resulting solution was stirred under a stream of dry nitrogen for a half to one hour so that it attained the temperature of the surrounding oil bath, and air and water vapour, let into the apparatus during charging, were swept out. The ferric chloride catalyst solution was then injected into the reaction vessel and a clock was started. Any initial, fast evolution of hydrogen chloride was followed by manual titration and subsequent slow evolution by means of the pH meter–pen recorder unit.

Individual hydrogen chloride evolved/time parameters were obtained by manual titration, but the data obtained from the pH meter–pen recorder unit were in the form of a continuous plot of hydrogen chloride evolved

versus time. The graphs reproduced in this paper were obtained using individual parameters measured directly from the continuous plots.

Polymer preparation and work-up

Poly(diphenylene ether sulphones) were prepared as previously described[2,3]. Polymers H1 to 4 were prepared[2] from diphenyl ether and its 4,4′-disulphonyl chloride in nitrobenzene solution at 120°C.

Polymer I was prepared[8] from 4,4′-diphenoxy diphenyl sulphone and diphenyl ether-4,4′-disulphonyl chloride by a melt-powder technique.

Polymer J was prepared[2] from diphenyl ether-4-sulphonyl chloride in nitrobenzene solution at 120°C.

Polymer K was prepared[2] from diphenyl ether and diphenyl-4,4′-disulphonyl chloride in nitrobenzene solution at 140°C.

All polymers were re-dissolved in nitrobenzene and then the nitrobenzene solution was washed (four times) with five per cent hydrochloric acid and with water (twice). The nitrobenzene solution was then dripped into a large volume of stirred methanol and the polymer, which precipitated, was collected, washed thoroughly with hot methanol and then dried *in vacuo*.

N.m.r. spectra

The spectra of all polysulphones quoted were obtained with a Varian HA 100 MHZ spectrometer operated in the H.A. mode. The accumulated spectra of these materials were obtained using a Japan Electron Optics Laboratory RA I. spectrum accumulator. All samples and standards were dissolved in dimethyl sulphoxide to give a 3·6% w/v concentration. The H.A. mode field/frequency lock was achieved using the resonance at 7·5τ due to the solvent. Each sample was subjected to 64 scans of the region 1·0 to 2·0τ and the resulting accumulated spectrum amplified four times by the RA I. The spectra were obtained under identical r.f. power and amplification conditions.

The authors thank the Misses S. M. Bowman and N. C. Walker for assistance in producing the manuscript of this paper and Mr A. Bunn for experimental assistance.

Imperial Chemical Industries Ltd,
Plastics Division,
Welwyn Garden City, Herts.

(Received December 1967)

REFERENCES

[1] CUDBY, M. E. A., FEASEY, R. G., JENNINGS, B. E., JONES, M. E. B. and ROSE, J. B. *Polymer, Lond.* 1965, **6**, 589
[2] CUDBY, M. E. A., FEASEY, R. G., GASKIN, S., JONES, M. E. B. and ROSE, J. B. Paper presented at the I.U.P.A.C. Symposium on Macromolecular Chemistry, Brussels 1967; to be published in *J. Polym. Sci.*
[3] JENNINGS, B. E., JONES, M. E. B. and ROSE, J. B. *J. Polym. Sci. C*, 1967, No. 16, 715
[4] DE LA MARE, P. B. D. and RIDD, J. H. *Aromatic Substitution*, p 81. Butterworths: London, 1959
[5] SUTER, C. M. *The Organic Chemistry of Sulphur*, p 485. Wiley: New York, 1944
[6] ALLEN, L. C. and JOHNSON, L. F. *J. Amer. chem. Soc.* 1963, **85**, 2668
[7] *French Pat. No. 1 495 132* (1966)
[8] *Brit. Pat. No. 1 016 245* (1966)

Notes and Communications

On the Gradient Column Method for Measuring Densities

AN EARLIER communication by Kawai and Keller[1] (henceforth K & K) purported 'to point out that the density gradient method for measuring densities is fundamentally unsound and can give grossly erroneous results where the specific surface of the particles to be measured is large . . . .'; their argument is based upon a statement, attributed to Dr C. R. Burch, that, where 'in the column of liquid of varying composition there is a gradient of interfacial free energy with respect to a solid object placed in it, this gradient of energy, by definition, represents a force . . . . . which adds, with the appropriate sign, to that due to gravity'. This statement, and certainly the deductions based on it by K & K, are themselves, I believe, fundamentally unsound.

The simple equation

$$\nabla F = \mathbf{f} \tag{1}$$

where F is an energy and $\mathbf{f}$ the concomitant force can only be useful in a subsequent mechanical (whether dynamical or statical) argument if the energy concerned can be separated from other terms in the total energy of the system under examination.

Clearly the gravitational force, which can be considered as the gradient of the gravitational potential, and is the result of long-range forces (i.e. caused almost entirely by matter outside the density column) can be treated independently of other forces. In the language of mechanics it is a conservative body force. Even so, it is essential when considering the mechanics of the column to include the gravitational forces on the liquid also, as is evidenced in the use of the Archimedean gravitational force $(\rho_{\text{solid}} - \rho_{\text{liquid}})\,\mathbf{g}$ in K & K's equation (2).

On the other hand the interfacial energy T is the result of short-range forces and cannot be isolated from other forms of energy, such as thermal energy, once forces of the form (1) above are postulated. We may expect it to give rise to internal forces: any net mechanical force on the solid must be balanced, according to Newtonian mechanics, by an opposite force acting on the matter responsible for the energy gradient, which in this case is the immediately neighbouring fluid. The approximations inherent in the concept of a *surface* energy means that we may regard this as a contact force at the interface between fluid and solid. K & K seem completely to have neglected this question of the balance of forces, and have merely substituted an apparent body force on the solid *alone*.

A proper resolution of the problem will not be attempted here, for we must expect it to be more complex than supposed by earlier authors. Because of the existence of the density gradient in the fluid (and consequent mass fluxes), for example, we are faced with a problem in irreversible thermodynamics, and so familiar arguments, like (1) above, from equilibrium thermodynamics, cannot be applied directly. Indeed they may prove to be totally incorrect. In any position of equilibrium, it will almost certainly

be true that the distribution of fluid density (i.e. fluid composition) in the neighbourhood of the suspended solid particle will *not* be the same as it would have been in the absence of the particle. This circumstance alone would dispose of K & K's argument.

There are grounds for believing that, if a situation of equilibrium (i.e. quasi-static equilibrium) can be achieved with a particle suspended motionless in a density gradient, then the effects of surface energy variations are likely to be much smaller than those predicted by K & K. To see this consider a control volume, large compared with the particle and containing it, whose surface is nowhere close to the particle, lying wholly within the fluid of the density column. Compare the mechanical equilibrium of the control volume with and without the particle present (this is the argument implicitly employed in any consideration of density columns). We may assume that the fluid around the control volume exerts precisely the same surface forces on the control volume in both cases. Therefore the total weight of the material within the control volume will be the same in both cases. Therefore the density of the particle will be correctly predicted except in so far as it causes changes in the *density* of neighbouring fluid. These we believe to be small; it is worth noting that these density discrepancies can be due both to the presence of the interface alone (i.e. to the effect of an interface between solid and liquid of *constant* bulk properties), and to the additional presence of a gradient in liquid properties.

This matter was brought to my notice by D. A. Blackadder and P. A. Lewell of this Department, who have recently[2] carried out detailed experiments showing that the density column method may indeed give reliable results, and that earlier discrepancies between it and other methods can be attributed to errors in the other (pyknometric) methods.

J. R. A. PEARSON

Department of Chemical Engineering,
Pembroke Street, Cambridge

(Received November 1967)

REFERENCES

[1] KAWAI, T. and KELLER, A. *Phil. Mag.* 1963, **8**, 1993
[2] BLACKADDER D. A. and LEWELL, P. A. *Polymer, Lond.* 1968, **9**, 249

Analytical Gel Permeation Chromatography used for Preparative Fractionation of Polymers for Degradation Studies

WHEN micropyrolysis–gas–liquid–chromatography is used to study the kinetics of high polymer degradation, the samples used in individual pyrolyses may be as small[1] as 10^{-8}g. Moreover, it may be necessary to use such small samples in order to eliminate anomalous dependence of rate on sample size[2]. The elucidation of the mechanisms of the reactions may require the measurement of specific rates for a series of fractions, in order that the dependence of rate on molecular weight may be assessed[3].

Gel permeation chromatography (GPC)[4] may be used to provide a very rapid and convenient fractionation of soluble polymers, and the weights of

be true that the distribution of fluid density (i.e. fluid composition) in the neighbourhood of the suspended solid particle will *not* be the same as it would have been in the absence of the particle. This circumstance alone would dispose of K & K's argument.

There are grounds for believing that, if a situation of equilibrium (i.e. quasi-static equilibrium) can be achieved with a particle suspended motionless in a density gradient, then the effects of surface energy variations are likely to be much smaller than those predicted by K & K. To see this consider a control volume, large compared with the particle and containing it, whose surface is nowhere close to the particle, lying wholly within the fluid of the density column. Compare the mechanical equilibrium of the control volume with and without the particle present (this is the argument implicitly employed in any consideration of density columns). We may assume that the fluid around the control volume exerts precisely the same surface forces on the control volume in both cases. Therefore the total weight of the material within the control volume will be the same in both cases. Therefore the density of the particle will be correctly predicted except in so far as it causes changes in the *density* of neighbouring fluid. These we believe to be small; it is worth noting that these density discrepancies can be due both to the presence of the interface alone (i.e. to the effect of an interface between solid and liquid of *constant* bulk properties), and to the additional presence of a gradient in liquid properties.

This matter was brought to my notice by D. A. Blackadder and P. A. Lewell of this Department, who have recently[2] carried out detailed experiments showing that the density column method may indeed give reliable results, and that earlier discrepancies between it and other methods can be attributed to errors in the other (pyknometric) methods.

J. R. A. PEARSON

Department of Chemical Engineering,
Pembroke Street, Cambridge

(Received November 1967)

REFERENCES

[1] KAWAI, T. and KELLER, A. *Phil. Mag.* 1963, **8**, 1993
[2] BLACKADDER D. A. and LEWELL, P. A. *Polymer, Lond.* 1968, **9**, 249

Analytical Gel Permeation Chromatography used for Preparative Fractionation of Polymers for Degradation Studies

WHEN micropyrolysis–gas–liquid–chromatography is used to study the kinetics of high polymer degradation, the samples used in individual pyrolyses may be as small[1] as 10^{-8}g. Moreover, it may be necessary to use such small samples in order to eliminate anomalous dependence of rate on sample size[2]. The elucidation of the mechanisms of the reactions may require the measurement of specific rates for a series of fractions, in order that the dependence of rate on molecular weight may be assessed[3].

Gel permeation chromatography (GPC)[4] may be used to provide a very rapid and convenient fractionation of soluble polymers, and the weights of

virtually all the fractions obtained are sufficient for many repeat degradation experiments by the above technique. In GPC, the heterodisperse polymer is eluted through a suitably-packed column[5], and the weight concentration of polymer in the effluent is monitored and continuously displayed on a chart recorder. From the trace obtained, the molecular weight distribution, number average molecular weight, and weight average molecular weight may be assessed.

In the present work, a Waters Associates Analytical GPC apparatus has been used. The solvent was tetrahydrofuran; its rate of flow was 1 cm^3/min. The polymer sample fractionated was polymethylmethacrylate ($\overline{M}_n = 53\,000$, $\overline{M}_w = 99\,000$) which had been synthesized in the presence of lauryl mercaptan, a transfer agent. 12 mg of polymer in 5 cm^3 solvent was injected into the head of the column, and a series of fractions was collected in consecutive 5 cm^3 samples of the effluent. The dead volume between the monitor (a refractometer cell) and the effluent syphon was 2 cm^3, and this must be taken into account when relating the effluent samples collected to the appropriate regions of the recorder trace. The weights of the fractions are listed in *Table 1*. These weights were calculated in the following way. The chromatogram was divided vertically into a number of sections of equal width corresponding to the volumes of solution containing the fractions; the weight of material in each fraction could then be calculated using the fractional area of each section. The total weight of the fractions in *Table 1* is about 85 per cent of the injected weight. The remaining material was not collected; it was present in the very high or very low molecular weight extremes of the chromatogram.

Table 1

Fraction No.	*Weight (mg)*	$\overline{M}_n$	*Specific reaction rate* (sec^{-1})
1	2·54	297 000	0·0074
2	3·13	160 000	0·0074
3	2·65	97 000	0·0074
4	1·39	57 000	0·0079
5	0·48	33 000	0·0095
6	0·11	18 600	0·0150
7	0·01	10 700	0·0250

The molecular weights of the fractions were calculated from the chromatogram as follows. Each section corresponding to a fraction was subdivided into a number, r, of rectangles of equal width so as to form a histogram. In this way the continuous distribution was converted to a discrete one. The molecular weight, M_i, of the species in each rectangle was determined from a standard calibration plot of straight chain length against elution volume. The number average molecular weight of each fraction was then found from $\overline{M}_n = (\text{total area of section}) / \sum^{r} (\text{area of rectangle } i/M_i)$. It was found that a five-rectangle histogram was adequate; i.e. results obtained in this way were indistinguishable within experimental error from those obtained using seven- or nine-rectangle histograms. The number average molecular weight of each fraction is shown in *Table 1*. Using the

weight average molecular weight of each fraction (also determined from the histogram), the dispersity of each fraction was calculated, and found to be within the range 1·02 to 1·04. Such values may well be optimistic since it is known that each molecular species contributes not a vertical line, but a peak, to the chromatogram. (Re-injected fractions, obtained from GPC, have recently been reported[6] to have a dispersity of 1·2 to 1·3).

Table 1 also shows kinetic data obtained by degrading the fractions using micropyrolysis–gas–liquid–chromatography. In order to ensure that the sizes of the samples for degradation did not exceed 10^{-8}g, the volume of solution of each fraction deposited was chosen according to its concentration. The specific reaction rates for monomer evolution were measured at 340°C; each rate quoted is the average of six determinations. The standard deviation never exceeded 15 per cent. Similar studies have been performed at a number of temperatures, and the results used to interpret the change in pyrolysis mechanism with temperature. This will be presented in a forthcoming publication[7].

Although fractionation involving the injection of samples of ten times the present size has recently been described (*vide* the Ana-Prep GPC technique[8]), the important conclusion from the present work is that the scale of conventional analytical GPC is more than adequate for degradation studies involving micropyrolysis–gas–liquid–chromatography. The particular advantage of this fractionation technique is its speed and convenience; the more time-consuming gradient-elution method is perhaps preferable for large-scale work[9].

The authors wish to express their thanks to Dr F. W. Peaker, Mr K. E. Brierley-Jones, and Mr C. R. Tweedale for their cooperation in the use of the GPC technique.

G. BAGBY
R. S. LEHRLE,
and J. C. ROBB

Chemistry Department,
University of Birmingham,

(*Received December 1967*)

REFERENCES

[1] BARLOW, A., LEHRLE, R. S., ROBB, J. C. and SUNDERLAND, D. *Polymer, Lond.* 1967, **8**, 523
[2] BARLOW, A. LEHRLE, R. S. and ROBB, J. C. *Makromol. Chem.* 1962, **54**, 230
[3] BARLOW, A., LEHRLE, R. S., ROBB, J. C. and SUNDERLAND, D. *Polymer, Lond.* 1967, **8**, 537
[4] MOORE, J. C. *J. Polym. Sci. A*, 1964, **2**, 835
[5] TWEEDALE, C. R. and PEAKER, F. W. *Nature, Lond.* 1967, **216**, 75
[6] PEAKER, F. W. and PATEL, J. M. Proceedings of the Fourth International Seminar on GPC at Miami Beach, 1967 (Waters Associates, Framingham, Massachusetts)
[7] BAGBY, G., LEHRLE, R. S. and ROBB, J. C. To be published.
[8] BOMBAUGH, K. J., DARK, W. A. and KING, R. N. Proceedings of the Fourth International Seminar on GPC at Miami Beach, 1967 (Waters Associates, Framingham, Massachusetts)
[9] BRIERLEY-JONES, K. E., PATEL, J. M. and PEAKER, F. W. Proceedings of the Third International Seminar on GPC at Geneva, 1966 (Waters Associates, Framingham, Massachusetts)

Racemization of Isotactic Polymethylmethacrylate by Ultra-violet and Gamma Irradiations

IT HAS been shown recently that electron irradiation of isotactic polymethylmethacrylate (PMMA) results in partial racemization of the polymer[1]. The present work was undertaken in order to compare the efficiency of ultra-violet and gamma irradiations in that process.

EXPERIMENTAL

Isotactic PMMA was obtained by butyl-lithium-initiated polymerization in toluene at 0°C. For the ultra-violet irradiations, thin films were prepared by slow evaporation, in flat rectangular Pyrex dishes (5 cm × 10 cm), of benzene solutions containing 0·175 g polymer. Their thickness was calculated to be about 29 microns. After outgasing at 80°C they were irradiated under vacuum in a quartz tube with a Philips TUV 15 W lamp. The absorption of light at 2 537 Å was calculated to be about 6·3 per cent by the relation[2] $I = I_0\ e^{-kL}$ where L is the thickness of the film in cm and $k = 19\ cm^{-1}$. The intensity of the light was measured by the ferri-oxalate actinometer[3]: it was 9×10^{-8} E $min^{-1}\ cm^{-2}$ on the film. Isotactic PMMA was irradiated as a powder with gamma rays in carefully outgased Pyrex bulbs.

The tacticity of the samples before and after irradiation was determined from the n.m.r. spectra recorded on a Varian A-60 spectrometer in deuterated chloroform at room temperature.

The infra-red spectra were recorded on a Perkin–Elmer Model 237 spectrometer from films cast on potassium bromide pellets after dissolution of the irradiated samples in benzene.

Changes in the i.r. spectra were in agreement with the calibration curve established by Baumann *et al.*[4].

RESULTS AND DISCUSSION

The racemization yields were calculated from the decrease of the number of meso pairs (dd or ll). The amount of these (M) was determined from the relative areas of the peaks attributed by Bovey and Tiers[5] to isotactic (I), heterotactic (H) and syndiotactic (S) triads according to the relation $M = I + \frac{1}{2}H$. The results are summarized in *Table 1*.

Table 1. Racemization of isotactic PMMA (Initial polymer: 89 per cent meso pairs)

Type of irradiation	*Dose (eV/g)*	*Meso pairs* %	*Racemization* %
Gamma	$2{\cdot}50 \times 10^{22}$	77	13·5
Gamma	$4{\cdot}99 \times 10^{22}$	67	24
Ultra-violet	$2{\cdot}52 \times 10^{22}$	82	7·9
Ultra-violet	$2{\cdot}38 \times 10^{23}$	77	13·5

The results of our gamma irradiations are in agreement with those obtained by E. V. Thompson for electron irradiation[1]. It can be seen that the same amount of racemization requires the dissipation of less energy by gamma than by ultra-violet irradiation.

The same phenomena were observed for main chain scission: one rupture produced by gamma irradiation required the dissipation[6] of 55 eV whereas one rupture produced by the 2 537 Å radiation is accompanied by the dissipation[7] of 125 eV.

On the other hand, side chain scission, as evidenced by the formation of volatile products, is easier under ultra-violet[7] than gamma[8] irradiation. It may thus be concluded that racemization is associated with main chain scission rather than with side chain breaking.

We are very grateful to Professor L. de Brouckère and to Professor A. Charlesby for their interest in this work.

C. DAVID
A. VERHASSELT
and G. GEUSKENS

Service de Chimie Générale II,
Faculté des Sciences,
Université Libre de Bruxelles,
Belgium.

(*Received January 1968*)

REFERENCES

[1] THOMPSON, E. V. *Polymer Letters*, 1965, **3**, 675
[2] SHULTZ, A. R. *J. phys. Chem.* 1961, **65**, 967
[3] HATCHARD, C. G. and PARKER, C. A. *Proc. Roy. Soc. A*, 1956, **235**, 518
[4] BAUMANN, U., SCHREIBER, H. and TESSMAR, K. *Makromol. Chem.* 1959, **36**, 81
[5] BOVEY, F. A. and TIERS, G. V. D. *J. Polym. Sci.* 1960, **44**, 173
[6] CHAPIRO, A. *Radiation Chemistry of Polymeric Systems.* Interscience: New York, 1962
[7] FOX, R. B., ISAACS, L. G. and STOKES, S. *J. Polym. Sci.* 1963, **A1**, 1079
[8] TODD, A. *J. Polym. Sci.* 1960, **47**, 223

ANNOUNCEMENT

Polymer Meeting Point 2

This will take place at the University of Essex on Friday 24 May. The subject will be Biopolymers, and lectures by Professor D. CHAPMAN (Unilevers and Sheffield University), and Professor JULIAN H. GIBBS (Brown University, R.I., U.S.A.) will be included. Details from: Professor M. GORDON, University of Essex, Wivenhoe Park, Colchester, Essex (Tel.: Colchester 5141, dialling code OCO 6).

Dielectric Relaxation and Other Properties of Syndiotactic and Isotactic Poly(methyl methacrylate)

S. HAVRILIAK, JR

The dielectric properties of s-PMMA and i-PMMA have been determined over a wide range of temperature and frequency. The complex plane method was used to represent the data. For s-PMMA in the glass phase the single relaxation process observed could be represented as a circular arc. Above the glass temperature, two dispersions were observed and each could be represented by a circular arc. For i-PMMA only one relaxation process was observed above the glass temperature. This process could be represented by a skewed circular arc whose parameters are similar to those of many other polymers. Below the glass temperature a relaxation process is observed; however, evidence is considered to show that it is the same process as the one above the glass temperature but one that disappears with decreasing temperature. The magnitude of the effective dipole moment for each process in s-PMMA and i-PMMA is treated from the point of view of Kirkwood. The necessary structural details are obtained from infra-red measurements previously reported. The variation of the effective moment with temperature is treated as a variable segment length of a polymer chain whose assumed structure is consistent with the infra-red evidence. The dielectric β-process in s-PMMA is shown to be equivalent to the mechanical β-process in the same polymer. X-Ray evidence is considered to show that the decrease in the glass temperature with increased bulkiness of the side chain is indeed due to an increase in the chain–chain separation.

THE polymers, syndiotactic and isotactic poly(methyl methacrylate) hereafter referred to as s-PMMA and i-PMMA, respectively, comprise an interesting pair of polymers for dielectric study. Although these materials have been studied previously, there are several important questions that remain to be answered. For example, Mikahelov and Borisova[1] remarked that the decomposition of the relaxation data for i-PMMA into two components was somewhat arbitrary. On the other hand, in a paper by the author[2], it was shown that the relaxation behaviour of i-PMMA could be represented by a single relaxation function, implying that a single relaxation process exists. In the polymer s-PMMA there are two relaxation mechanisms, a behaviour which is in marked contrast to that of i-PMMA. The significance of these observations needs to be more fully explored.

A second reason for re-investigating the relaxation behaviour of PMMA is that for a number of other methacrylates[3] the normalized relaxation data could not be superimposed on to a master curve. For these systems the complex plane α parameter which is a measure of the breadth of the relaxation process appears to vary with temperature. It is important to ascertain the extent to which α can account for the lack of superimposability of the data because this parameter is related to the distribution of relaxation times. The dependence of the distribution of relaxation times on temperature is relevant to a basic understanding of polymers. This concept is basic to the procedure usually referred to as the Time-Temperature-Superposition Principle.

A third reason for re-investigating the dielectric properties of PMMA is based on the conclusion reached from an infra-red study[4] of s-PMMA. In that study, direct evidence on the conformational structure of the ester side chain relative to the plane of the backbone carbon atoms was obtained. This information is relevant to dielectric behaviour because the side chain contains the dipole moment. The conformation of the side chain was found to be in a plane that is perpendicular to the plane of the main chain. The plane of the side chain was found to be mobile above the glass temperature but frozen in place below the glass temperature. Enough structural information was obtained from that study to compute the effective dipole moment, based on Kirkwood's equilibrium correlation model. The third object of this work is to interpret the α and β dispersions of PMMA in terms of Kirkwood's equilibrium correlation theory and what is known about local three-dimensional structure.

Lastly, for many polymers a correlation was found to exist between the dielectric and mechanical dispersions. The fourth object of this work is to investigate to what extent this dielectric and mechanical β-dispersion of PMMA are equivalent processes.

EXPERIMENTAL PROCEDURE

Dielectric measurements

The dielectric measurements were made in the usual way[5] using the General Radio two-terminal sample holder together with the General Radio type 716-C capacitance bridge assembly. The two-terminal sample holder was placed inside a well insulated and regulated oven. The connections to the bridge and external substitution capacitor were made using General Radio's air line. The air line was modified by replacing the plastic separators by those machined from a ceramic material. The complex dielectric constant was measured isothermally from 30 c/s to 150 kc/s, always at the same set of frequencies (i.e. 3·1, 5·0, 7·0, 10, 15, 22, all multiplied by 10^1, 10^2, 10^3 and 10^4 c/s).

Torsion pendulum measurements

The torsion pendulum used in this work is of conventional design[6]. Briefly, the apparatus consists of two clamps in a constant temperature environment with the specimen, in the form of a rectangular slab of uniform thickness, mounted vertically between them in such a manner that its lower end is held fixed and its upper end is free to rotate about its longitudinal axis. The upper end of the specimen, i.e. the end nearest the vertical weights, is twisted by hand and then released by an electromagnetic device so that the system swings or oscillates at its natural frequency. Connected to the oscillating end with the inertial weights is a rotary differential transformer whose output is displayed on an oscilloscope. The trace is recorded photographically from which all calculations are made in the usual way.

X-Ray measurements

The X-ray measurements were made photographically with a G.E. XRDl instrument. Nickel filtered copper radiation from a 40 kV, 15 mA source was used. The broad diffraction maxima were measured visually.

Multiple readings were averaged and values thus determined. The specimen to film distance was carefully calculated from a sodium chloride pattern. Location of the maximum values obtained from direct scans on the diffractometer (geiger-counter) scans or microdensitometer scans of the photographs were in good agreement with the visual average values.

Polymer samples

The samples of s-PMMA from which the dielectric specimen was made were prepared[7] by polymerizing pure methyl methacrylate (MMA) monomer in liquid ammonia at $-88°C$ using the oxidation products of sodium as an initiator. The intrinsic viscosity in chloroform at 25°C indicated the viscosity average molecular weight to be $1{\cdot}93 \times 10^6$. The number average ($\overline{M}_n$) molecular weight from osmometric measurements was found to be $0{\cdot}138 \times 10^6$. The infra-red characteristics (J value)[8] indicated that the polymer sample was very highly syndiotactic. An n.m.r. study of the sample in chloroform indicated that at least 92 per cent of the monomer repeat triads[9] were syndiotactic; the remaining triads were distributed among heterotactic and isotactic sequences. Solvent swelling with 4-heptanone crystallized the sample indicating the sequence of syndiotactic units to be very long.

The sample of i-PMMA from which the dielectric specimen was made was prepared[8] by polymerizing the MMA monomer in Esso octane under a helium blanket at 0°C using phenyl magnesium bromide as an initiator. The resulting polymer was washed up in the conventional way and freeze dried. The intrinsic viscosity in chloroform at 25°C indicated the viscosity average molecular weight ($\overline{M}_v$) to be $5{\cdot}5 \times 10^5$. The number average molecular weight ($\overline{M}_n$) from osmometric measurements was found to be $0{\cdot}44 \times 10^5$. The infra-red characteristics (J value) indicated that the polymer sample was very highly isotactic. An n.m.r. study of the sample in chloroform indicated that at least 90 per cent of the monomer repeat triads were isotactic. The remaining triads were distributed among heterotactic and isotactic sequences.

Dielectric specimens were prepared from the samples of s-PMMA and i-PMMA by compression moulding the powders using a circular mould in a Carver press. The diameter of the specimens was 1·5 in. and the thickness was 0·10 in. The resulting discs were of optical quality. Chromium electrodes were sputtered on to the specimens in a way that is similar to the preparation of surface replicas that are used in electron microscopy. We believe this procedure to be superior to the one where a film is cast from a solvent and electrodes painted on using silver paint. It has been our experience that solvent is never removed regardless of drying conditions. Any retained solvent is likely to lead to spurious results.

The sample of i-PMMA chosen for this study is not the most isotactic version of PMMA prepared in these laboratories. The most isotactic polymers undergo crystallization at elevated temperatures, a phenomenon which would make the representation and interpretation of the data exceedingly difficult. A sample with low isotacticity would be contaminated with sequences of heterotactic and syndiotactic units which would also make the representation and interpretation exceedingly difficult. The sample

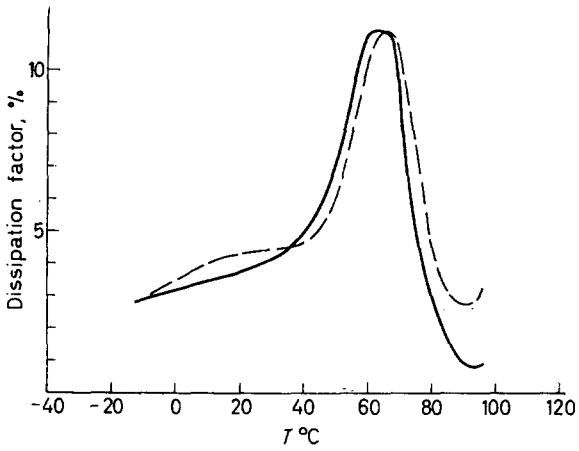

Figure 1.—The dissipation factor as a percentage determined at 60 c/s is plotted against temperature in degrees centigrade for two i-PMMAs of different tacticities. The solid line represents the behaviour of the polymer used throughout this work while the dashed line represents the behaviour of a polymer with a lower (about 85 per cent) isotacticity

of i-PMMA chosen for this study is believed to represent the best compromise between these two difficulties. The sample chosen does not undergo any crystallization at elevated temperatures. On the other hand a plot of the dissipation factor versus temperature does not exhibit the small low temperature loss maximum found in the work of Mikahelov and Borisova[1]. In *Figure 1* a plot of the dissipation factor for the two i-PMMAs is given. The solid line represents the behaviour of the one used in this work while the dashed line represents the behaviour of another i-PMMA of lower tacticity (about 85 per cent). The polymer with the lower tacticity exhibits a small loss maximum similar to the one observed by Mikahelov and Borisova[1]. We conclude therefore that the low temperature loss peak originates from syndiotactic and heterotactic units and is therefore considered to be spurious to the present work.

A limited number of measurements were made on other acrylic type polymers. The details for preparation of the following polymers have been given elsewhere[13]: the poly acrylates of secbutyl, isobutyl, isopropyl, phenyl, benzyl, neopentyl, 2-phenylethyl, 2,4-dichlorophenyl, chlorophenyl; the poly methacrylates of secbutyl, isopropyl, phenyl, benzyl, neopentyl, 2-phenylethyl. The poly acrylates of methyl, ethyl, propyl, butyl hexyl, butyl, cyclohexyl, 2-ethylhexyl, isobornyl, menthyl and stearyl as well as the poly methacrylates of ethyl, propyl, butyl, hexyl, cyclohexyl, isobornyl, menthyl, stearyl were prepared by similar techniques and supplied to the author by the same group of people. The monomers were either commercial products of the Rohm and Haas Co. or were prepared in its Research Laboratories. In all cases the monomers were purified either by distillation or by crystallization. The monomers were polymerized in solution (such as methyl propionate) using a Benzoin-UV initiator system and brought to about 25 per cent completion at 44·1 °C. The polymers were isolated using conventional techniques. The number average molecular weights for all the polymers were in the range of 2 to 20×10^5. These polymers are believed not to be tactic ones because of the method of initiation.

EXPERIMENTAL RESULTS

s-PMMA

In the complex plane method of representing dielectric relaxation data, the real part of the complex dielectric constant is plotted against its imaginary counterpart for each frequency of measurement at the same temperature. In general the shapes of the experimental quantities in the complex plane are neither of the simple shapes that have been observed and described by Cole and co-workers[10] for simple molecules. Rather the locus appears to be the combined behaviour of a circular arc at low frequencies and a straight line (skewed semicircular behaviour) at high frequencies. An empirical relaxation function[2] has been proposed to represent the relaxation behaviour of twenty polymers. The parameters of this equation which takes the form

$$(\epsilon^*(\omega)-\epsilon_\infty)/(\epsilon_0-\epsilon_\infty)=[1+(i\,\omega\,\tau_0)^{(1-\alpha)}]^{-\beta} \qquad (1)$$

are readily determined graphically; the exact procedure has been described elsewhere[11]. This procedure will be used here to represent the data after first demonstrating its reliability.

Over the entire temperature and frequency range of the experiments a relaxation process was found to exist. At a temperature of 105·1°C the dispersion was centred in the available frequency range [see *Figure 2*(a)]. This relaxation process is usually referred to as the β process†. At this temperature the shape of the relaxation process appears to be a circular arc. The complex plane parameters are readily determined and together with equation (1) can be used to calculate the complex dielectric constant which can then be compared with the experimental values. In *Figure 2*(a) the agreement between calculated and experimental results is good so that this method of representation is reliable approximately within experimental error. This method of data representation is readily extended to the other temperatures lower than 105°C. The parameters are given in *Table 1*.

At temperatures above 120°C significant deviations from circular arc behaviour are observed [see *Figure 2*(b)]. These deviations can be represented in terms of another relaxation process by assuming the complex dielectric constant to be additive from the two mechanisms that contribute at each frequency of measurement, i.e.

$$\epsilon_T^*(\omega)=\epsilon_\beta^*(\omega)+\epsilon_\alpha^*(\omega)+\epsilon_\infty$$

where the subscripts refer to the observed (T), α process (α), β process (β), and the infinite (∞) dielectric constants. A complex plane plot of the deviations in *Figure 2*(b) is given in *Figure 2*(c). The locus is a circular arc and is usually referred to as the α process. The parameters of this arc are determined in the usual way and the calculated $\epsilon_\alpha^*(\omega)$ [represented by □ in *Figure 2*(c)] are in fair agreement with the experimental ones [represented

†The Greek letters α and β have been widely used to denote the two relaxation processes that exist in polymers. Equally widespread is the use of α and β as the complex plane parameters. No difficulty will be encountered because the letters are adjectives and will always be used with the appropriate nouns, e.g. α process, β parameter.

Table 1. Complex plane parameters for β-dispersion in s-PMMA

$T°C$	ϵ_1	ϵ_∞	M_v	$2\pi\tau_0$	$1-\alpha$	β	g†
37·8	4·60	2·40	—	$3{\cdot}50\times10^{-2}$	0·256	1·0	—
45·5	4·53	2·45	83·00	$1{\cdot}54\times10^{-2}$	0·311	1·0	—
57·3	4·62	2·46	84·58	$6{\cdot}90\times10^{-3}$	0·324	1·0	0·41
59·0	4·53	2·50	84·60	$5{\cdot}88\times10^{-3}$	0·333	1·0	—
65·5	4·49	2·55	84·71	$3{\cdot}23\times10^{-3}$	0·350	1·0	—
71·9	4·52	2·49	84·84	$1{\cdot}73\times10^{-3}$	0·372	1·0	0·41
77·0	4·50	2·57	84·92	$1{\cdot}33\times10^{-3}$	0·383	1·0	—
82·2	4·50	2·52	85·01	$7{\cdot}30\times10^{-4}$	0·414	1·0	0·41
86·7	4·48	2·55	85·10	$5{\cdot}88\times10^{-4}$	0·396	1·0	—
92·6	4·51	2·52	85·21	$3{\cdot}52\times10^{-4}$	0·436	1·0	0·42
105·1	4·51	2·57	85·43	$1{\cdot}72\times10^{-4}$	0·474	1·0	0·43
116·7	4·56	2·59	85·66	$8{\cdot}67\times10^{-5}$	0·493	1·0	0·46
127·7	4·49	2·52	86·11	$4{\cdot}58\times10^{-5}$	0·502	1·0	0·47
133·6	4·10	2·26	86·42	$3{\cdot}03\times10^{-5}$	0·488	1·0	0·45
137·5	4·13	2·30	86·63	$2{\cdot}50\times10^{-5}$	0·512	1·0	0·46
139·8	4·21	2·31	86·75	$2{\cdot}00\times10^{-5}$	0·515	1·0	0·48
144·2	4·20	2·29	86·98	$1{\cdot}63\times10^{-5}$	0·516	1·0	0·49
150·2	4·18	2·21	87·30	$8{\cdot}70\times10^{-6}$	0·530	1·0	0·49
154·0			87·50				
156·8			87·64				
163·8			88·01				

† g calculation based on assuming $\mu_0=1{\cdot}8$ D.U.

by ■ in *Figure 2*(c)]. The results of a similar calculation performed on the dispersion data at 150·2°C are given in *Figure 2*(d) where it can be seen that the locus is a circular arc. The dispersion parameters for a number of other temperatures are given in *Table 2*.

Table 2. Complex plane parameters for α dispersion in s-PMMA

$T°C$	ϵ_1	ϵ_0	α	β	$2\pi\tau_0$
127·7	4·490	4·775	0·0557	1·0	2×10^{-1}
133·6	4·110	4·350	0·500	1·0	1×10^{-1}
137·5	4·126	4·386	0·500	1·0	$3{\cdot}2\times10^{-2}$
139·8	4·205	4·465	0·556	1·0	$2{\cdot}0\times10^{-2}$
144·2	4·198	4·458	0·500	1·0	$1{\cdot}4\times10^{-2}$
150·2	4·167	4·420	0·500	1·0	5×10^{-3}
154·0					3×10^{-3}
156·8					3×10^{-4}

An Arrhenius rate plot of the α and β relaxation times is a straight line that can be represented by

$$\log 2\pi\tau_0=(18{\cdot}7/2{\cdot}3\,RT)-14{\cdot}57 \tag{3a}$$

for the β process and by

$$\log 2\pi\tau_0=(68{\cdot}0/2{\cdot}3\,RT)-37{\cdot}55 \tag{3b}$$

for the α process. The variation of the molar volume ($V_0=84$ cm^3) with temperature can be represented by

$$V_T=V_0[1+2{\cdot}0\times10^{-4}(T_g-T)] \tag{4a}$$

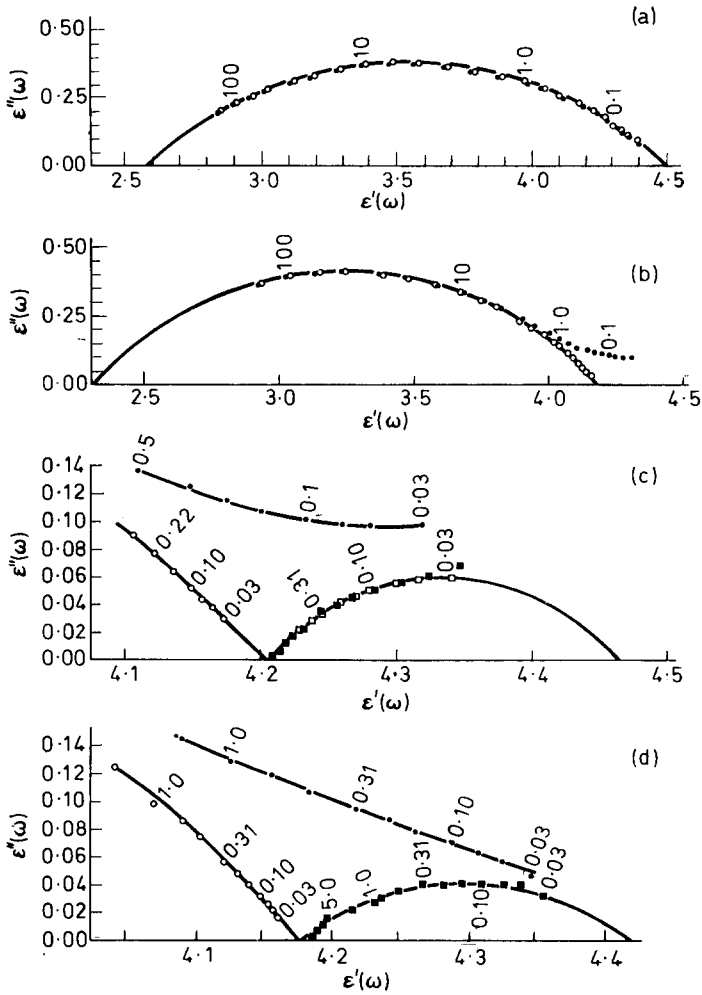

Figure 2—(a) Complex plane plot of s-PMMA at 105·1°C. Numerals alongside points are frequencies in kc/s. Filled circles represent experimental quantities while open circles represent quantities obtained from the circular arc parameters and equation (1). (b) Complex plane plot of s-PMMA at 139·8°C. (c) Complex plane plot of s-PMMA at 139·8°C in the low frequency region where the deviations between observed and calculated values are greatest. Black squares represent values obtained from equations (2) and (2a). Open squares represent quantities obtained from circular arc calculations and the necessary parameters given in *Table 2*. (d) Complex plane plot of s-PMMA at 150·2°C in the same low frequency region

below the glass temperature ($T_g = 120°C$) while above the glass temperature the specific volume is given by

$$V_T = V_0 [1 + 5{\cdot}7 \times 10^{-4} (T - T_g)] \tag{4b}$$

The calculated values for V_0, together with the experimental values for

ϵ_0 and ϵ_∞ were used to calculate the effective moment at some temperatures from Kirkwood's equation, viz.

$$g\mu_0^2 = (\epsilon_0 - \epsilon_\infty)\frac{(2\epsilon_0 + \epsilon_\infty)}{3\,\epsilon_0}\left(\frac{\epsilon_\infty + 2}{3}\right)^2\left(\frac{3\,kTV}{4\,\pi N}\right) \tag{5}$$

These values are given in *Table 1*.

i-PMMA

The breadth of the dispersion for i-PMMA (α process) in a complex plane makes it impossible to determine all of the dispersion parameters at a single temperature, see filled circles in *Figures 3*(a)–(c). However, the techniques outlined in Appendix B of ref. 12 are readily adapted to the present system in the following way. The relaxation data are readily extrapolated (linearly) at temperatures below 72°C to obtain ψ_L and ϵ_∞. At temperatures above 72°C the relaxation data are readily extrapolated (along a circular arc) to obtain ϵ_0.

The temperature dependences of these parameters are then determined and extrapolated to the temperatures where they are not known. The parameters $(1-\alpha)$, β and τ_0 are readily determined at any temperature once ψ, ϵ_∞ and ϵ_0 are known. The dispersion parameters were determined for the three temperatures in *Figure 3* and together with equation (1) were used to calculate the complex dielectric constant. The calculated values of the complex dielectric constant (open circles in *Figure 3*) agree quite well with the experimental values (filled circles in *Figure 3*). Usually small adjustments (no more than 5 per cent) had to be made to some of the parameters to obtain the agreement shown in *Figure 3*. The dispersion parameters for i-PMMA using this method of representation are given in *Table 3*. The

Table 3.—Complex plane parameters for α dispersion in i-PMMA

T°C	φ_L	α	β	$\epsilon_0-\epsilon_\infty$	ϵ_∞	$\tau_0\times10^3$ (sec)	Mol. vol. (cm³/100g)	g
151·0				2·91	(2·34)		87·3	0·67
143·6				2·72	(2·35)		86·9	0·63
127·6				2·88	(2·36)		86·1	0·61
114·6				2·97	(2·37)		85·5	0·60
112·9				3·12	(2·38)		85·4	0·62
101·4				3·39	(2.39)	0·020	84·8	0·64
90·1	(22·4)	0·355	0·385	3·71	(2·40)	0·120	84·2	0·67
77·4	(18·3)	0·364	0·320	4·05	(2·41)	1·95	83·6	0·69
72·6	16·8	0·428	0·327	4·19	2·42	10·0	83·4	0·69
63·0	15·0	0·495	0·320	4·46	2·43	85·0	82·9	0·70
57·5	13·1			4·61	2·43		82·6	0·70
44·5	10·9				2·45		82·2	
37·3	9·3				2·45		82·1	
21·8	6·64				2·46		81·9	
7·6	5·5				2·46		81·7	
−13·0	4·8				2·46		81·5	

Numerals in parentheses are extrapolations.
gs were calculated assuming μ_0 to be 1·8 D.U.

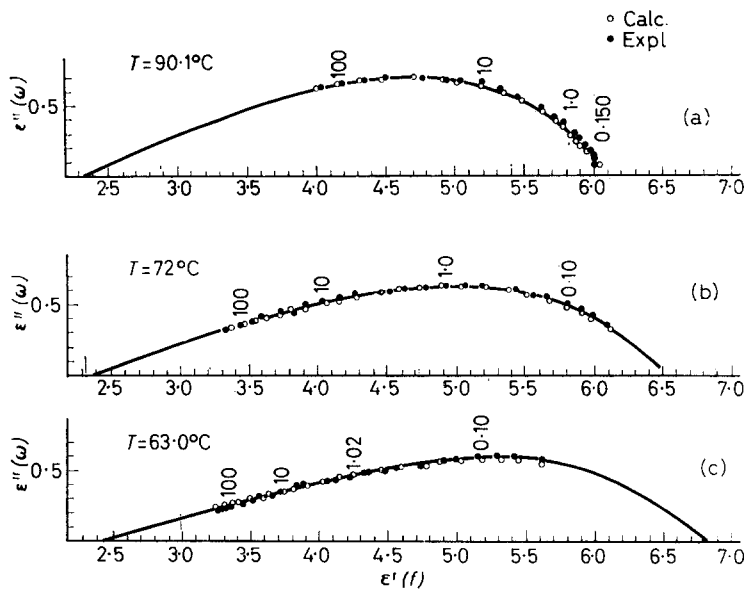

Figure 3.—Complex plane plot of i-PMMA. (a) at 90·1°C; (b) at 72°C and (c) 60·3°C. In all cases, filled circles are experimental quantities while the open circles represent calculated quantities. Numerals alongside points represent frequency in kc/s

most important point in the treatment of these relaxation data is that they can be represented by a single relaxation function.

At temperatures below the glass transition region (53°C) the high frequency tail of the α process persists, *Figure 4*. The main change is that ψ_L continually decreases with decreasing temperature. At temperatures considerably below the glass temperature (-13°C) the tail was still present.

An Arrhenius rate plot of the relaxation time for the α process is a straight line that can be represented by

$$\log \tau_0 = (55{\cdot}0/2{\cdot}303\,RT) - 38{\cdot}00 \tag{6}$$

The variation of the molar volume (V_0=cm^3) with temperature below the glass temperature (T_g=52° to 53°C) can be represented by

$$V_T = V_0\,[1 + 0{\cdot}72 \times 10^{-4}\,(T_g - T)] \tag{7a}$$

while above the glass temperature the expression is

$$V_T = V_0\,[1 + 4{\cdot}8 \times 10^{-4}\,(T - T_g)] \tag{7b}$$

The refractive index measured at room temperature is $n=1{\cdot}47$. The square of this quantity after some allowance (five to seven per cent) is

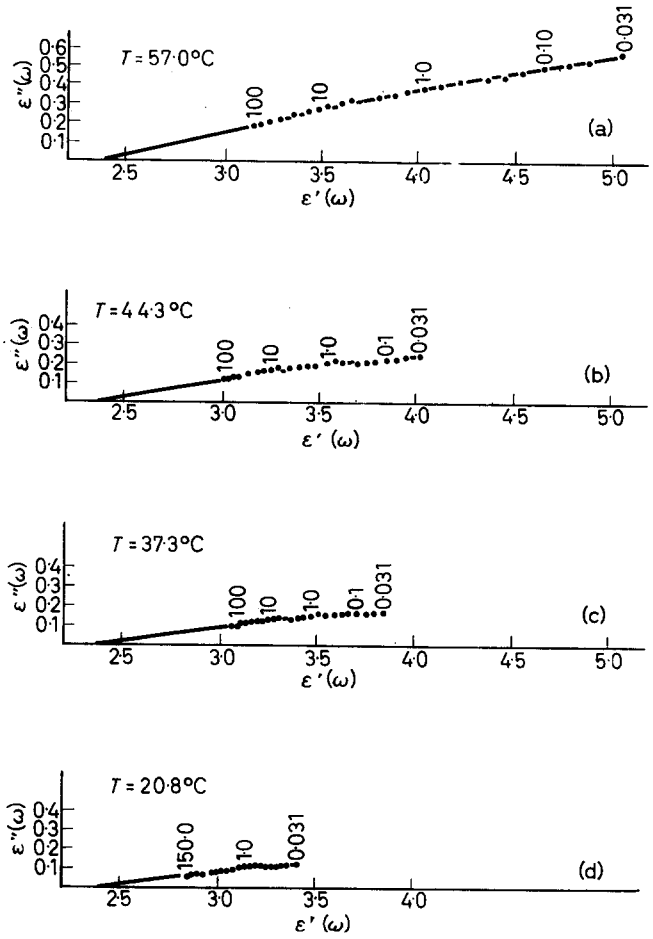

Figure 4—Complex plane plot for i-PMMA at (a) 57·0°C; (b) 44·3°; (c) 37·3° and (d) 20·8°. Numerals next to circles represent frequency in kc/s

made for the contribution due to atomic polarization agrees quite well with ϵ_∞. This agreement is an excellent, independent verification of the high frequency linear extrapolation procedures used to determine ϵ_0. The parameters ϵ_0, ϵ_∞ and V_t together with Kirkwood's equation (5) can be used to calculate the effective dipole moments $g\mu_0^2$ which are listed in *Table 1.*

Mikahelov and Borisova[1] also studied i-PMMA and attempted to represent the data as the sum of two processes, a procedure similar to the one used to represent the deviations which occurred in s-PMMA. In *Figure 5,* the dispersion behaviour of i-PMMA is represented as the filled circles. The low frequency portion of the data is readily fitted to a circular arc.

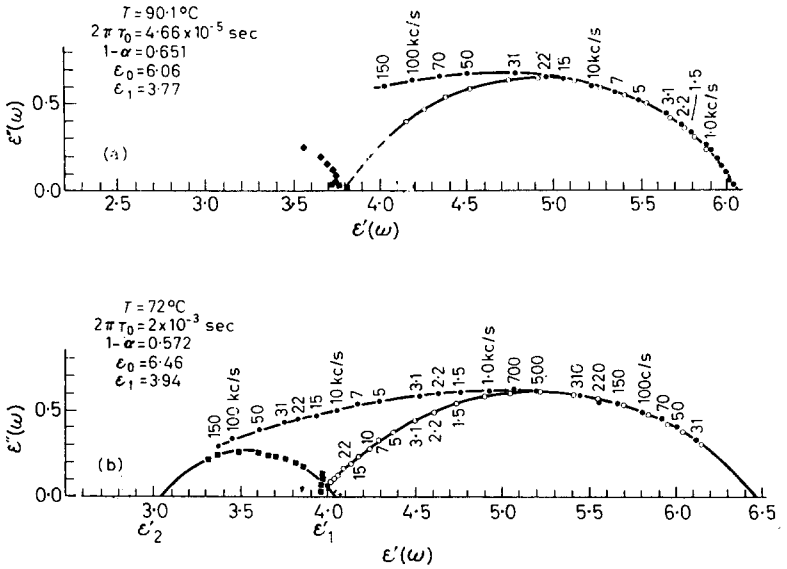

Figure 5—Complex plane plot of i-PMMA (a) at 90·1°C and (b) at 72°C. Filled circles are experimental, open circles calculated. Black squares represent the difference between calculated and observed values

The circular arc parameters are determined, the complex dielectric constant is calculated (○s in *Figure 5*) and subtracted from the observed values (■s in *Figure 5*) for each frequency of measurement. The parameters obtained in this method of representation are similar to those of Mikahelov and Borisova[1]. The major difficulty in representing data in this way is that a separate loss maximum was never observed. An unsymmetrical relaxation process does not prove the existence of two mechanisms. For example[2] the α relaxation mechanisms of poly(bisphenol carbonate) as well as that of other polymers are as unsymmetrical as the one for i-PMMA. Another difficulty is that the relaxation data at temperatures below 63°C can be extrapolated to obtain ϵ_∞. The agreement between the extrapolated value of ϵ_∞ and the one from refractive index measurements is good. This means that any high frequency dispersion, if it exists, would have to be exceedingly small. In addition to these difficulties, eight parameters are needed to represent the relaxation data when two processes are assumed while only five parameters are needed when the skewed arc method is used. For these reasons, then, we shall interpret the response of i-PMMA to the electric field as a single relaxation mechanism which exists above and below the glass transition temperature.

Torsion pendulum data

The complex compliance was measured solely for s-PMMA at essentially constant frequency (viz. 2·5 to 3·0 c/s) from −40°C to +120°C. The variation of the log decrement as a function of reciprocal absolute tempera-

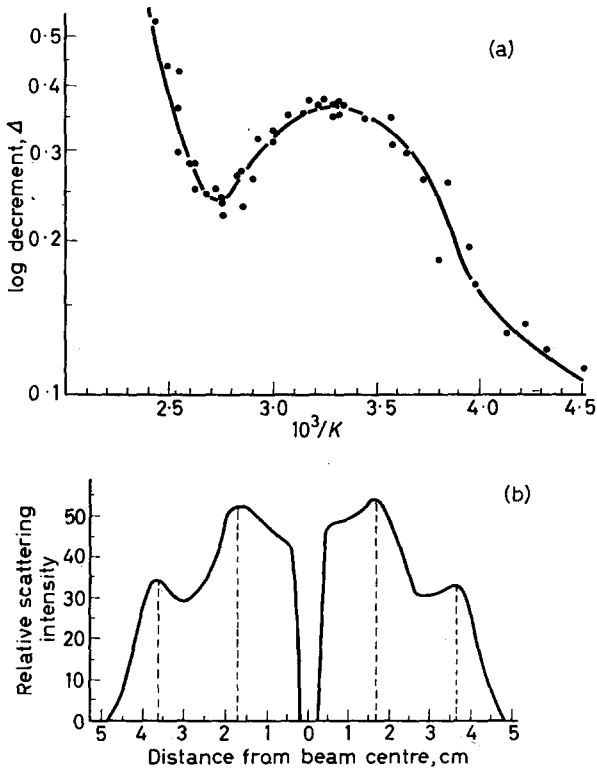

Figure 6—(a) The log decrement for s-PMMA versus reciprocal absolute temperature. (b) The relative scattering intensity versus distance from beam centre for a typical acrylic polymer, poly(ethyl methacrylate). Operating parameters are: magnification 2 to 1; radiation, copper K_α with a 40 kV source at 15 mA using nickel filtered radiation with a film to specimen distance of 10 cm

ture is given in *Figure 6*(a). At a temperature of approximately 30°C a maximum in the log decrement is observed. This maximum is usually referred to as the β process. At temperatures below 30°C this quantity decreases uniformly while at temperatures above 30°C there is first a decrease and then an increase in the decrement. The increase in the log decrement with temperatures above 60°C is referred to as the α relaxation process.

X-Ray results

Klug and Alexander[12] have discussed the diffraction characteristics of a number of typical polymers. They pointed out that these non-crystalline maxima denote the frequent occurrence of particular interatomic distances in a largely disordered substance. They considered the case of a large number of interatomic vectors of magnitude R and found that a strong maximum in the pattern at an angle 2θ is equal to 1·25 times that of the

d spacing calculated from the Bragg equation. For most polymers studied in this work two such scattering maxima are observed [for a typical microdensitometer tracing see *Figure 6*(b)]. The innermost peak is nearly always the strongest and it is due principally to interatomic vectors between adjacent chains. Consequently, these scattering maxima can be interpreted in terms of an approximate value for interchain separations. The second, weaker peak is not so easily interpreted but is included in *Table 4* for the sake of completeness. Also listed in this table are glass temperatures obtained from dilatometric measurements[13].

Table 4. Non-crystalline X-ray scattering maxima and glass transition temperatures for various poly acrylates and methacrylates

Polymer	*-acrylate*			*-methacrylate*		
	d_1(Å)	d_2(Å)	T_g°C	d_1(Å)	d_2(Å)	T_g°C
Group I—poly(*n*-alkyl acrylates and methacrylates)						
poly(methyl-	9·3	5·2	8	9·1	—	120
poly(ethyl-	10·8	5·5	−22	9·6	9·6	65
poly(propyl	13·0	5·6	−44	—	—	—
poly(butyl-	16·1	5·7	−54	16·1	6·4	19
poly(hexyl-	—	—	—	17·6	6·2	−5
Group II—poly(isomers of butyl acrylate and methacrylate)						
poly(*n*-butyl-	16·1	5·7	−54	16·1	6·4	19
poly(isobutyl-	14·8	6·1	—	15·1	6·5	48
poly(secbutyl-	12·9	6·0	−20	12·8	6·7	60
poly(*t*-butyl-	12·0	6·4	31	12·5	7·1	107
Group III—miscellaneous polymers						
poly(isopropyl-	11·5	5·9	−5	11·5	6·6	78
poly(phenyl-	14·9	6·1	55	14·5	6·6	110
poly(cyclohexyl-	14·4	6·1	15·0	14·3	6·5	66
poly(benzyl-	15·3	5·9	6·0	15·9	6·4	54
poly(2-ethyl hexyl-	17·9	5·9	—	16·6	6·3	—
poly(*i*-bornyl-	17·9	7·4	95·0	15·8	7·6	110
poly(ethyl-α-ethyl-	11·0	5·1	27·0	—	—	—
poly(neopentyl-	15·0	6·4	22·0	—	—	—
poly(*n*-hexyl	—	—	—	17·6	6·2	−5
poly(menthol-	—	—	—	17·8	6·7	—
poly(stearyl-	—	—	—	37·8	18·8	38
poly(2-phenylethyl-	17·0	7·5	−3	15·2	6·3	26

DISCUSSION

Dynamic behaviour

From an examination of the literature on the dielectric relaxation data of polymers it becomes apparent that five parameters are needed to represent any such process. These would be the instantaneous (ϵ_∞), equilibrium (ϵ_0), response time (τ_0), width ($1-\alpha$) and skewness (β) parameters. For this reason, any method that yields the above information is desirable while any method that places a restriction on these parameters, such as temperature independence, becomes less desirable depending on the validity of the assumption.

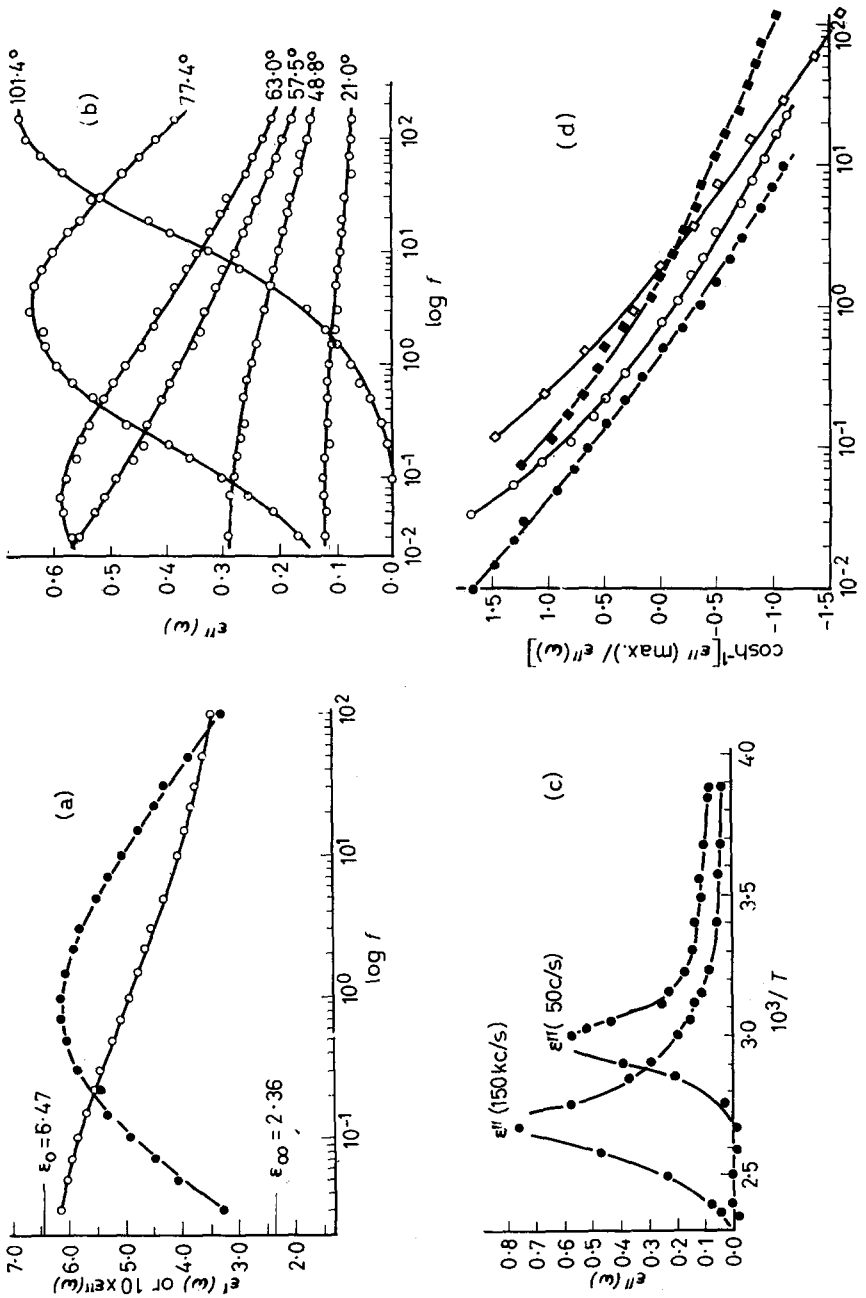

Figure 7—(a) Real and imaginary parts of the complex dielectric constants versus log frequency for i-PMMA at 72°C. (b) Dielectric loss versus log frequency for i-PMMA at the marked temperatures. (c) Dielectric loss versus reciprocal absolute temperature. (d) Fuoss–Kirkwood plot for various polymers. Filled circles represent s-PMMA at 105·1°C, filled squares represent i-PMMA at 72°C, open circles represent poly(isobutyl methacrylate) at 102·8°C and open squares represent the polycarbonate of bisphenol at 164·9°C

There are a number of methods that have been used to represent dispersion data of polymers that we attempted to use to represent the relaxation data of s- and i-PMMA and failed for the following reasons. The simplest of these methods is to plot the real or the imaginary part against the

logarithm of the frequency [see *Figure 7*(a)]. It is obvious that this method falls short of the goals outlined in the previous paragraph. Another related method which also fails is a 3-dimensional plot of $\epsilon''(\omega)$–log f–T or $\epsilon'(\omega)$–log f–T. A third often used technique is based on the superposition integral[14] which leads to

$$\epsilon_0 - \epsilon_\infty = (2/\pi) \int_0^\infty \{\epsilon''(\omega)/\omega\}\, d\omega \tag{8}$$

However, inspection of the $\epsilon''(\omega)$–log ω curves such as those in *Figure 7*(b) for i-PMMA leads to the conclusion that it is not possible to perform the necessary extrapolations in order to obtain the numerical integrations. Attempts to use the methods described by Read and Williams[15] also failed because the various assumptions, such as the independence of shape with temperature, were not applicable to these polymers. Attempts to apply the Fuoss–Kirkwood[16] method which assumes the loss to take the form

$$\epsilon''(\omega) = \epsilon''(\text{max.})\ \text{sech}\ [\alpha_t \log \omega_n/\omega] \tag{9}$$

failed because the appropriate plot was not linear, see *Figure 7*(d). The linear behaviour observed for s-PMMA is consistent with the circular arc representation (i.e. $\beta = 1$) as was pointed out by Böttcher[17].

Of the methods of data representation discussed so far, perhaps the most powerful and certainly the most common technique for representing dispersion data is the one referred to as the Time Temperature Superposition Method (TTSM). This method does not place any restrictions on the behaviour of $\epsilon_0 - \epsilon_\infty$. Furthermore, this method does not assume any particular shape for the relaxation process. The chief features of this method are that the distribution of relaxation times as well as the temperature behaviour of the average time are determined with relative ease. This method is not free from any assumptions although these may be expressed in several ways. Perhaps the simplest one is to state that the shape of the normalized complex dielectric constant in an $\epsilon'(\omega)/\log \omega$ or $\epsilon''(\omega)/\log \omega$ plane must be independent of temperature. In terms of the complex plane method, this means that both $(1-\alpha)$ and β must be independent of temperature, which was not observed for either s-PMMA or i-PMMA.

A second, more fundamental formulation of the assumption basic to the TTSM has already been given[11]. This formulation assumes only cause and effect, linearity, superposition and the concept of a distribution of relaxation times and leads to the following expression[14]

$$\epsilon_n^*(\omega) = \frac{\epsilon^*(\omega) - \epsilon_\infty}{\epsilon_0 - \epsilon_\infty} = \int_{-\infty}^{+\infty} F(\tau/\tau_0) \left(\frac{1}{1 + i\,\omega\,\tau_0}\right) d \ln (\tau/\tau_0) \tag{10}$$

In this equation, $F(\tau/\tau_0)$ is a function of relaxation time only and is referred to as the distribution of relaxation times. We see from this equation that since $F(\tau/\tau_0)$ must be a single valued function of τ/τ_0, then for a given value of τ/τ_0, $\epsilon_n^*(\omega)$ is completely and uniquely specified. If $F(\tau/\tau_0)$ is independent of temperature while τ_0 depends on temperature then a whole range of $\epsilon_n^*(\omega)$ will be obtained. Finally, a complex plane plot of the data

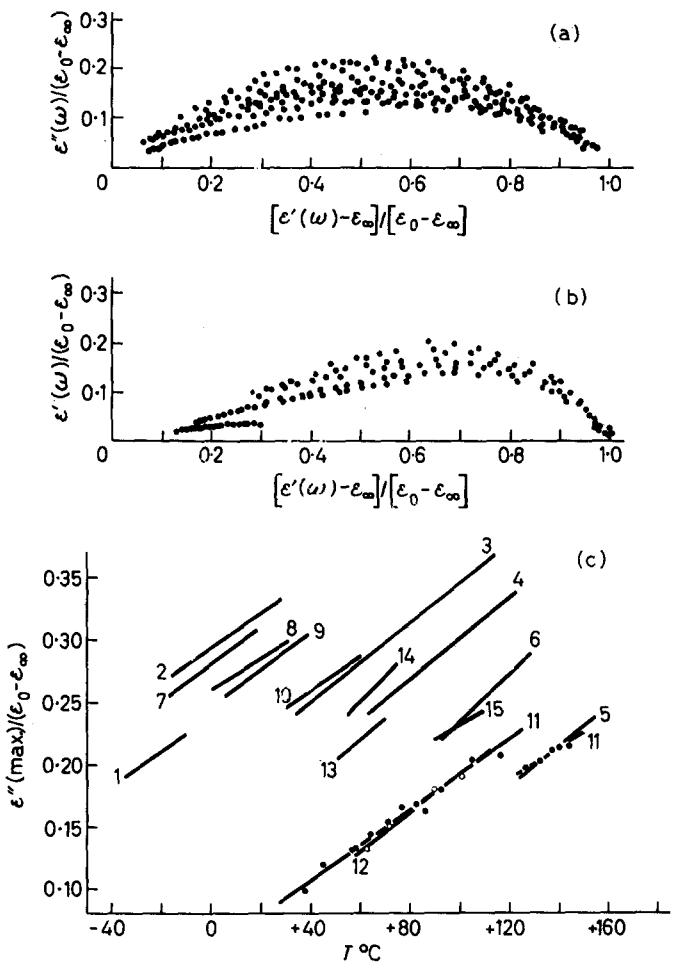

Figure 8—Normalized dielectric relaxation data of (a) s-PMMA. (b) i-PMMA. (c) Normalized loss maximum versus temperature (°C). Numerals beside curves denote: 1. poly(chloroprene), 2. poly(vinyl octanoate), 3. poly(nonyl methacrylate), 4. poly(butyl methacrylate), 5. poly(cyclohexyl methacrylate), 6. poly(*i*-butyl methacrylate), 7. poly(vinyl decanoate), 8. poly(vinyl laurate), 9. poly(*n*-octyl methacrylate), 10. poly(*n*-hexyl methacrylate), 11. i-PMMA, 12. s-PMMA, 13. poly(vinyl chloroacetate) $\rho^*(\omega)$ data, 14. poly(vinyl acetate) $\rho^*(\omega)$ data, 15. poly(vinyl acetal)

obtained from several temperatures should fall on a single line. It is of importance to note the difference between this method of testing the TTSM and the one that is customarily used. In the latter procedure the data are first operated upon for normalization and then shifted on to an unknown curve. Any changes in the shape of the curve with temperature can be compensated for by an over or under shifting of the data. In the proposed method the normalized data either form a single curve or they do not.

There is no possibility of under or over shifting the data to compensate for changes in the shape of $\epsilon_n^*(\omega)$ with temperature. In *Figure 8*(a) we have made such a complex plane plot of $\epsilon_n^*(\omega)$ for s-PMMA and in *Figure 8*(b) a plot for i-PMMA. For both polymers the data do not fall on a single locus, rather they form a wide band which nearly fills half the area in the complex plane.

A third method for formulating the assumption which is basic to the TTSM is to state that the distribution of relaxation times must be independent of temperature. A single point on the distribution function is readily determined from the approximate methods that exist to compute that function from more complete data. Ferry *et al.*[18] have shown that the distribution function is related to the shape of the $\epsilon''(\omega)/\log \omega$ curve by means of the following equation.

$$F(\tau = 1/\omega) = B\,\epsilon''(\omega)\,[1 - |\,\mathrm{d}\,\{\log \epsilon''(\omega)\}/\mathrm{d}\,\{\log \omega\}\,|\,] \qquad (11)$$

Evaluating the equation at the loss maximum leads to the most probable time as

$$F(\tau = 1/\omega) = B\,\epsilon''(\mathrm{max.}) \qquad (11a)$$

In words, a temperature plot of the normalized loss maximum with temperature is related to the temperature dependence of the most probable relaxation time. Such a plot is made in *Figure 8*(c) not only for s-PMMA and i-PMMA but also for thirteen other polymers. Except for poly(vinyl acetate) and poly(vinyl chloroacetate) the temperature dependence of the reduced loss maximum is the same. An interpretation of this anomalous behaviour for the acetates in terms of Scaife's remarks has already been given[11]. The temperature dependence of these reduced loss maxima cannot be maintained throughout the entire temperature region because of the following restrictions. At some low temperature, the loss must either become zero or its temperature dependence approaches zero because systems with losses less than zero are physically impossible (except for generators). At the other extreme of temperature the losses must either become 0·5 or the temperature dependence must change so that the losses approach this value. This limit comes about because the narrowest dispersion that has yet been observed is the Debye process in which the reduced loss maximum reaches a maximum value of one-half.

The question of whether or not a normalization scheme can be constructed to take into account the changes of dispersion shape with temperature is important to the understanding of polymers because of the widespread use of the TTSM. For this purpose, the loss data of s-PMMA are particularly useful because the process is a symmetrical one so that computations are somewhat simpler than those for the skewed arc case. The normalized loss ($\epsilon_n''(\omega)$) was determined by dividing the losses at each frequency by the appropriate value of $\epsilon_0 - \epsilon_\infty$ for that temperature. A plot of $\epsilon_n''(\omega)$ against log ω is given in *Figure 9*(a) where it can be seen that not only does the normalized loss maximum increase but the loss curve becomes narrower with increasing temperature.

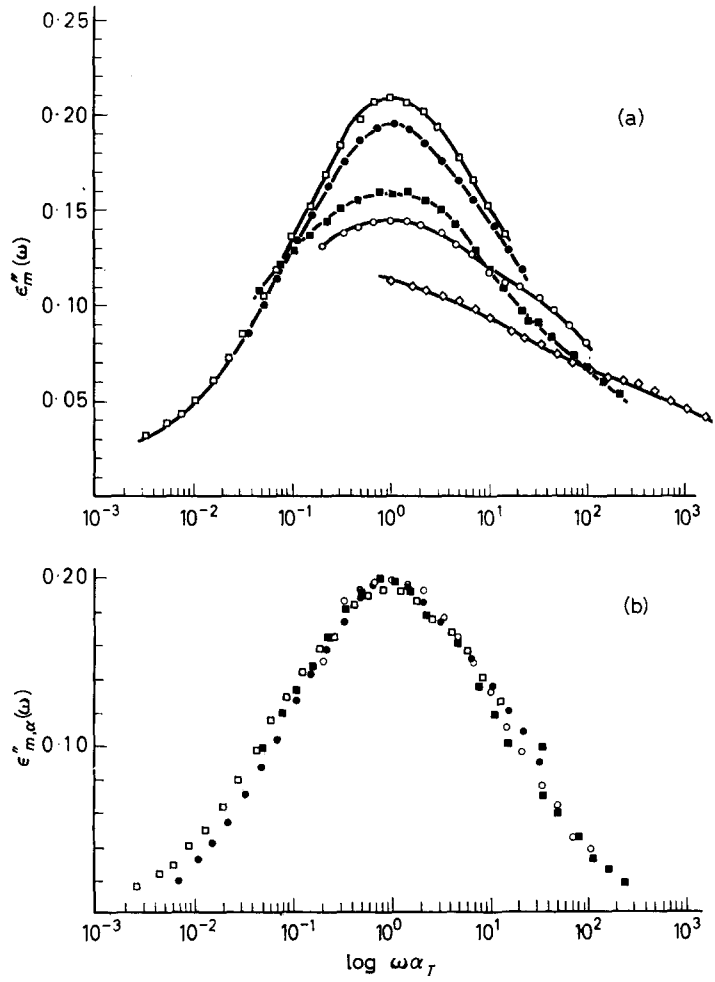

Figure 9—(a) Normalized loss versus log ωa_T. (b) Normalized loss according to equation 13 versus log ωa_T. In both plots, the temperatures are as follows: open squares 116°C; filled circles 105°C; filled squares 71·4°C; open circles 57·3°C; and filled diamonds 37·8°C

The variation of the normalized loss maximum with temperature can be interpreted in terms of the variation of α with temperature. The loss becomes a maximum for the case $\beta = 1$ when $\omega \tau_0 = 1$; this leads to

$$\frac{\epsilon''(\omega \tau_0 = 1)}{\epsilon_0 - \epsilon_\infty} = \frac{\cos \alpha \pi/2}{2 + 2 \sin \alpha \pi/2} \tag{12}$$

A plot of the LHS of equation (12) calculated from the RHS as a function of α is given in *Figure 10* along with the experimental values of these quantities. The agreement between the experimental quantities represented

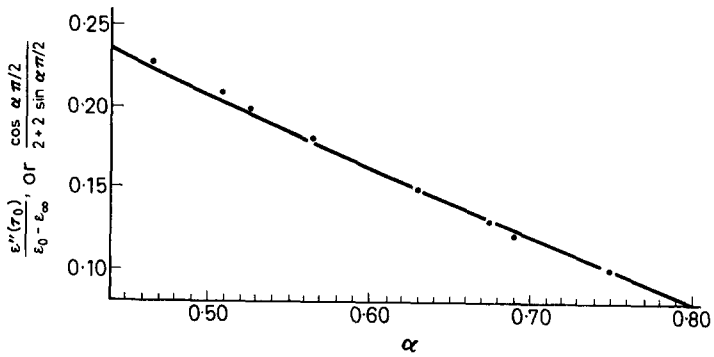

Figure 10—Normalized loss maximum (filled circles) or the RHS of equation (12) (solid line) versus experimental values of α

by filled circles in *Figure 10* and the calculated quantities represented by the line proves that the variation of the loss maximum is due to the variation of $(1-\alpha)$ with temperature.

To analyse the variation of the width of the loss curve in terms of a change in α is not a simple matter. Perhaps the most straightforward way of examining this problem is to investigate the functional dependence of $\epsilon''(\omega)$ on the parameters that influence $\epsilon''(\omega)$ as described in the introduction of this section. This generalized functional dependence leads to

$$\epsilon''(\omega) = \epsilon''(\alpha, \beta, \epsilon_0, \epsilon_\infty, \tau_0)$$

where the parameters α, β, etc. have their more general meaning, i.e. width, skewness, etc. The quantity $\epsilon_n''(\omega)$ has already been normalized so that it is no longer a function of ϵ_0 and ϵ_∞. In addition, we are considering the case of a symmetrical dispersion so that $\epsilon_n''(\omega)$ is not a function of β. Therefore,

$$\epsilon_n''(\omega) = \epsilon_n''(\alpha, \tau_0)$$

In other words, if $\epsilon_n''(\omega)$ could be adjusted for the experimental value of α_T at the experimental temperature T and then readjusted for the value of α_R at the reference temperature T_R, then the experimental values of $\epsilon_n''(\omega)$ would be normalized with respect to α. This computation was performed on some of the data, $\epsilon''(\omega)$ in *Figure 9*(a), by the following expression

$$\epsilon_{n\alpha}''(\omega) = \epsilon_n''(\omega)[\epsilon''(\alpha_R, \omega)/\epsilon''(\alpha_T, \omega)]_\alpha \qquad (13)$$

where $\epsilon''(\alpha_R, \omega)$ is the calculated value of ϵ'' at frequency ω and α_R and $\epsilon''(\alpha_T, \omega)$ is the calculated value of ϵ'' at frequency ω and α_T. The results of this calculation are given in *Figure 9*(b) after the data were shifted along the frequency axis. The experimental quantities are now superimposed so that the changes in shape are due to changes in α. Unfortunately the term $[\ \ldots\ ]_\alpha$ is not independent of frequency or temperature so that a

simple procedure cannot be devised. It is necessary to have some analytical function first to represent the data and then to correct them for shape changes with temperature. These features nullify any advantage of the TTSM.

Of the ways that exist for representing dispersion data, the most compact and accurate way described so far is the complex plane method. From this method, all the information necessary for defining the relaxation process is readily obtained. The single assumption concerning the shape of the relaxation process, i.e. equation (1), is readily verified by direct determination of the parameters followed by a comparison of the calculated $\epsilon^*(\omega)$ with the observed ones. So far equation (1) has represented the dispersion data of twenty three polymers as the complex dielectric constant. In addition, the relaxation data of nearly that number of polymers in the form of the complex polarization can be so represented which means that Scaife's[11] remarks can be evaluated quantitatively. Another advantage for this method of representation is that when mechanical dispersion data are suitably normalized they can be represented by the same function. This technique can lead to an unprecedented view on the nature of the internal reaction field used in dielectric theory because no external electrical field has been applied. Perhaps the most significant potential for this method of analysis or data representation is that the assumptions inherent to the TTSM can be investigated, a fact which seems to be constantly overlooked. Based on the observations recorded in *Figure 8*(c) it is probably better to represent dielectric data as a series function of some sort so that the variation of dispersion shape with temperature can be determined than to assume the shape to be independent of temperature.

Equilibrium structure

The relaxation behaviour of non-crystalline polymers has received considerable attention in the past. The α and β dispersions of conventionally initiated PMMA as well as those for the higher alkyl methacrylates[19] have also received considerable attention. The usual interpretation of the β-dispersion is to consider it as a hindered rotation of the side chain relative to the main chain or polymer backbone. Although there is much evidence to support this assignment, another interpretation which is in terms of recent observations and Kirkwood's equilibrium theory will be put forth. Kirkwood's equilibrium theory relates the relative positions of the dipole moments of neighbouring molecules with the central dipole moment in a cavity to the equilibrium dielectric constant. In order to apply Kirkwood's theory to polymeric dispersions, then, it is necessary to know the relative positions of the polar groups along the main or polymer chains. For the two polymers under consideration, the dipole moments are located in the planes of the ester groups.

In a previous paper[4], the general nature of esters was considered in detail. Briefly, esters were found to be associated with high heats of formation which can be attributed to resonance structures, i.e. a modified boat or chain conformation. The boat form was found to predominate because of evidence obtained from dipole moment, electron diffraction,

vapour phase infra-red absorption spectra and microwave measurements. Trace quantities of the chain form were postulated in the formates to account for the acoustical relaxation process, and to explain a small shoulder on the main absorption peak. For these reasons the ester will be assumed to be planar, the heavy atoms in a boat form with no internal arrangements possible.

Although X-ray structural information is not available for non-crystalline s-PMMA, some structural features of that molecule were deduced from infra-red measurements[20]. First of all, the backbone carbon atoms were found to form a planar zig-zag. In addition, the ester groups are perpendicular to the chain because the absorption peaks of this group were found to be σ (perpendicularly) polarized. There are two positions for the dipole moment of each ester group to be in; either pointing up (u) or pointing down (d). Each dipole moment can then be found in either one of six conformations relative to its two neighbours. These are ddd, ddu, udu, uuu, uud and dud. Spectroscopically, not all of these units are different. Each pair ddd-uuu, ddu-uud and udu-dud is expected to lead to similar interactions, hence to similar group splittings. On the other hand, the dipole moments of these triads are quite different particularly when two adjacent triads are coupled together. By combining these triads, a segment of a polymer molecule can be constructed with a dipole moment consistent with experimental values. Although this technique will not lead to any unique structure for the polymer molecule, many side chain conformations will be ruled out.

The thermal experiments described in ref. 20 are very important to the understanding of the β dispersion in s-PMMA. Both the relative intensities of the ester oxygen absorption peaks and the integrated intensities of these peaks were determined to be independent of temperature below the glass temperature. These quantities did vary above the glass temperature. Furthermore, high temperature ratios could be obtained at room temperature by quenching the specimen from high to room temperature. These observations were interpreted in terms of discrete rotational conformations of the ester side chain relative to the backbone to cause the original splittings. However, these conformations were not accessible ones at temperatures below the glass temperature. In other words, ester side chain rotation could take place above the glass temperature but not below it.

Some structural information[21] exists for i-PMMA in the crystalline phase. This molecule was found to crystallize into a 5_2 helix with little or no change in the density. We shall assume that the backbone form in the non-crystalline phase is the same helical structure. Infra-red dichroisms[22] indicate that not all of the ester oxygen absorption peaks are perpendicular to the main chain: one peak is parallel to the main chain. Unpublished results of experiments on i-PMMA similar to those in ref. 20 indicate that the ester groups are undergoing rearrangements above the glass temperature. No information was obtained below the glass temperature.

The relaxation behaviour of s-PMMA clearly indicates that a relaxation mechanism which contains the major component of the dipole moment exists below the glass temperature. Above the glass temperature a second

VECTOR DIAGRAM OF THE DIPOLE MOMENTS

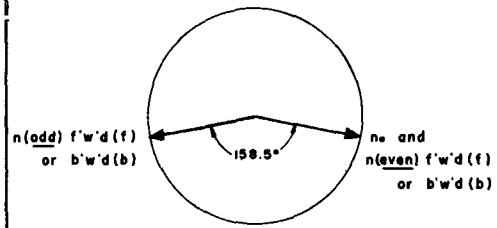

ℓ	Shorthand Conformation	$\bar{g}_\ell$
1	n_0	1.000
2	$n_b(n_1)$	0.070
3	$(n_2)n_f$	0.426
4	$n_b(n_3)$	0.140
5	$(n_4)n_f$	0.368
6	$n_b(n_5)$	0.210
7	$(n_6)n_f$	0.382
8	$n_b(n_7)$	0.280
9	$(n_8)n_f$	0.422
10	$n_b(n_9)$	0.350
11	$(n_{10})n_f$	0.472
12	$n_b(n_{11})$	0.420
13	$(n_{12})n_f$	0.521
14	$n_b(n_{13})$	0.490

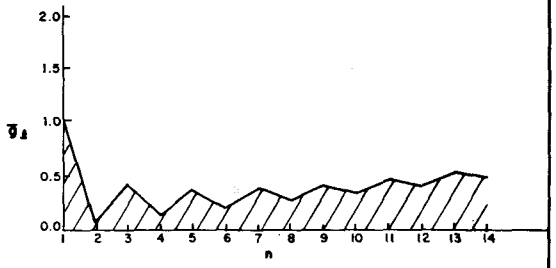

VECTOR DIAGRAM OF THE DIPOLE MOMENTS

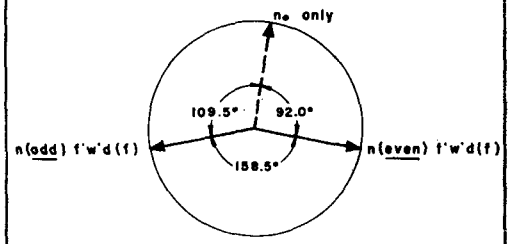

ℓ	Shorthand Conformation	$\bar{g}_\ell$
1	n_0	1.000
2	$(n_1)n_2$	0.666
3	$(n_2)n_3$	0.134
4	$(n_3)n_4$	0.218
5	$(n_4)n_5$	0.016
6	$(n_5)n_6$	0.116
7	$(n_6)n_7$	0.006
8	$(n_7)n_8$	0.099
9	$(n_8)n_9$	0.032
10	$(n_9)n_{10}$	0.018
11	$(n_{10})n_{11}$	0.073
12	$(n_{11})n_{12}$	0.153
13	$(n_{12})n_{13}$	0.124
14	$(n_{13})n_{14}$	0.198
15	$(n_{14})n_{15}$	0.179

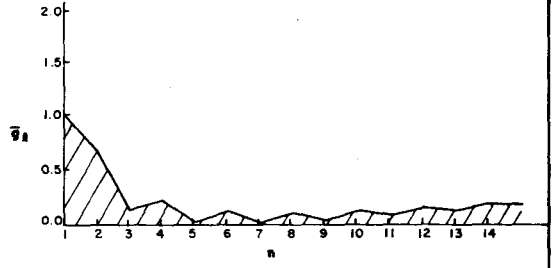

VECTOR DIAGRAM OF THE DIPOLE MOMENTS

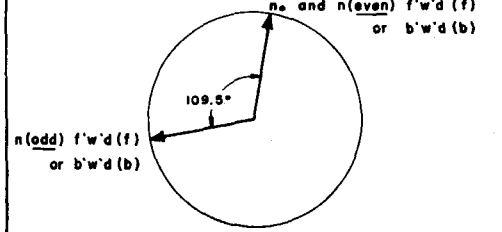

ℓ	Shorthand Conformation	$\bar{g}_\ell$
1	n_0	1.000
2	$n_b(n_1)$	0.666
3	$(n_2)n_f$	1.221
4	$n_b(n_3)$	1.332
5	$(n_4)n_f$	1.798
6	$n_b(n_5)$	1.998
7	$(n_6)n_f$	2.426
8	$n_b(n_7)$	2.664
9	$(n_8)n_f$	3.071
10	$n_b(n_9)$	3.330
11	$(n_{10})n_f$	3.723
12	$n_b(n_{11})$	3.996
13	$(n_{12})n_f$	
14	$n_b(n_{13})$	
15	$(n_{14})n_f$	

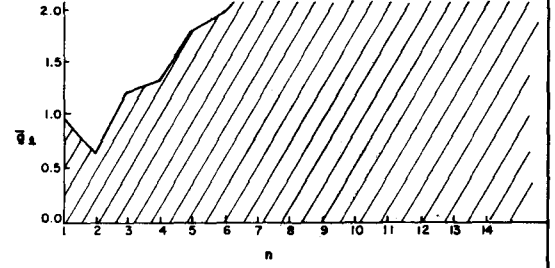

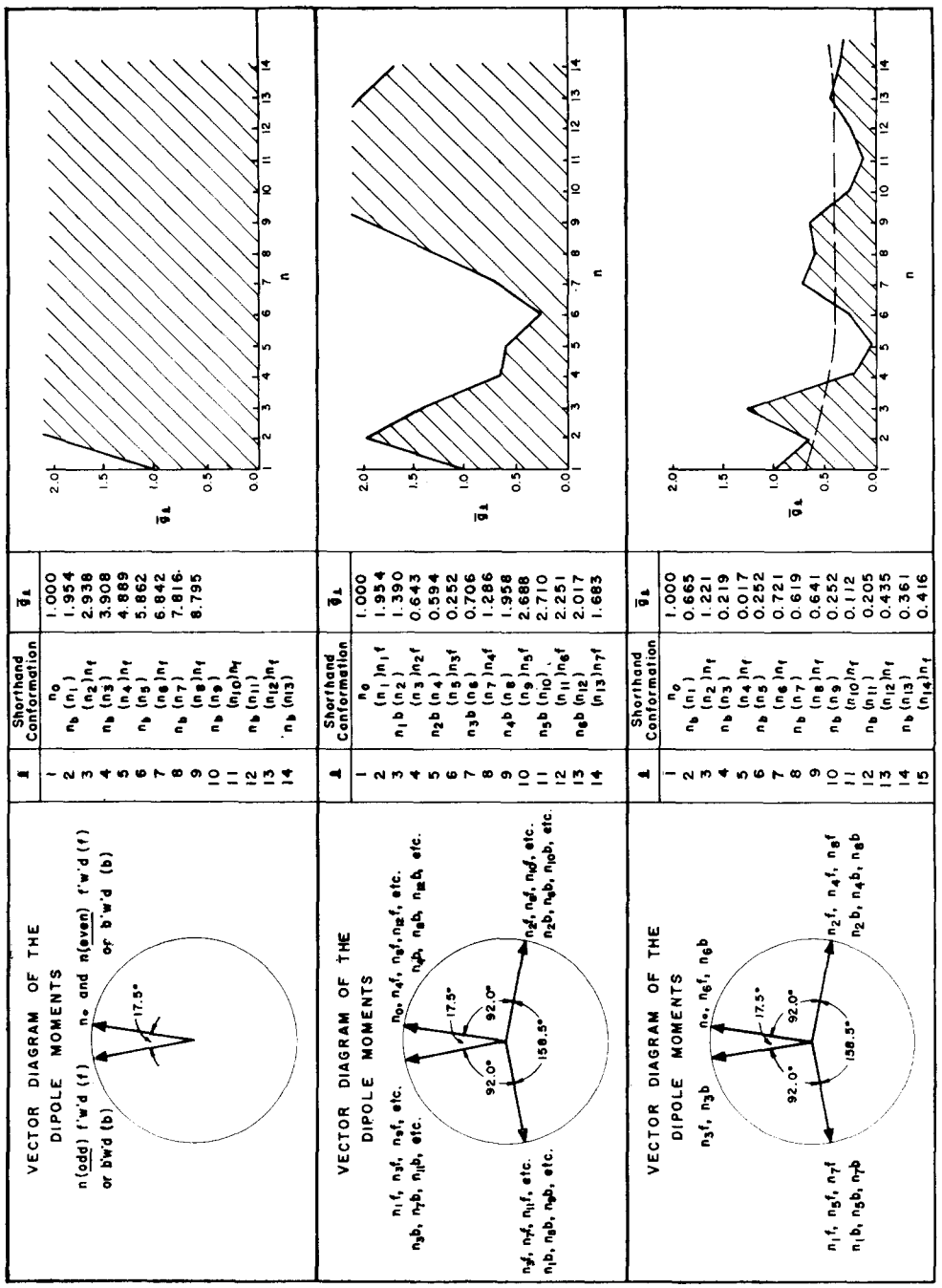

#	Shorthand Conformation	$\bar{g}_L$
1	n_0	1.000
2	$n_b\ (n_1)$	1.954
3	$(n_2)n_f$	2.938
4	$n_b\ (n_3)$	3.908
5	$(n_4)n_f$	4.889
6	$n_b\ (n_5)$	5.862
7	$(n_6)n_f$	6.842
8	$n_b\ (n_7)$	7.816
9	$(n_8)n_f$	8.795
10	$n_b\ (n_9)$	
11	$(n_{10})n_f$	
12	$n_b\ (n_{11})$	
13	$(n_{12})n_f$	
14	$n_b\ (n_{13})$	

#	Shorthand Conformation	$\bar{g}_L$
1	n_0	1.000
2	$(n_1)n_1f$	1.954
3	$n_1b\ (n_2)$	1.390
4	$(n_3)n_2f$	0.643
5	$n_2b\ (n_4)$	0.594
6	$(n_5)n_3f$	0.252
7	$n_3b\ (n_6)$	0.706
8	$(n_7)n_4f$	1.286
9	$n_4b\ (n_8)$	1.958
10	$(n_9)n_5f$	2.688
11	$n_5b\ (n_{10})$	2.710
12	$(n_{11})n_6f$	2.251
13	$n_6b\ (n_{12})$	2.017
14	$(n_{13})n_7f$	1.683

#	Shorthand Conformation	$\bar{g}_L$
1	n_0	1.000
2	$n_b\ (n_1)$	0.665
3	$(n_2)n_f$	1.221
4	$n_b\ (n_3)$	0.219
5	$(n_4)n_f$	0.017
6	$n_b\ (n_5)$	0.252
7	$(n_6)n_f$	0.721
8	$n_b\ (n_7)$	0.619
9	$(n_8)n_f$	0.641
10	$n_b\ (n_9)$	0.252
11	$(n_{10})n_f$	0.112
12	$n_b\ (n_{11})$	0.205
13	$(n_{12})n_f$	0.435
14	$n_b\ (n_{13})$	0.361
15	$(n_{14})n_f$	0.416

Figure 11—Trial structures for s-PMMA used to calculate effective moment according to Kirkwood's scheme. The arrows represent the direction of the dipole moments when the polymer chain is viewed end on (see text)

mechanism was found but one whose moment was small. On the other hand, the relaxation behaviour of i-PMMA above the glass temperature could be represented as a single process and one that contains the major component of the dipole moment. In addition, the parameters of this process are similar[2] to many other α processes. The relaxation process below the glass temperature appears to be the same one observed above this temperature but one that is disappearing rapidly with temperature. The change in $\epsilon_0 - \epsilon_\infty$ below the glass temperature is not known. The parameter ψ_L changes abruptly so that either $(1-\alpha)$ or β or both must decrease rapidly with decreasing temperature.

The structural details of the two polymers are quite different. In s-PMMA all of the ester groups are perpendicular to the main chain so that the component of the dipole moment parallel to the main chain is small or perhaps even zero. Therefore, the β orientation process in s-PMMA can be thought of as an orientation about an axis parallel to the main chain axis. In a similar way the dispersion(s) in i-PMMA can be so represented. In helical structures one would expect considerable cancellation of the dipole moments that are perpendicular to the main chain. Therefore, the effective moment, $\epsilon_0 \cdot \epsilon_\infty$ associated with an orientation about the chain axis would either be small or zero. On the other hand, the dipole moments in the direction of the main chain need not cancel, hence they could add and result in a large value of $\epsilon_0 \cdot \epsilon_\infty$ for the orientation process about an axis perpendicular to the main chain.

Kirkwood trial structures

The interpretation of the α and β dispersions given in the previous section can be put into a quantitative form in the following way. An end view of the structure of the s-PMMA polymer chain that is consistent with the infra-red evidence given in *Figure 11*. From this block diagram a vector diagram can be constructed. The function of this vector diagram is to picture the relative positions of the dipole moments when the polymer chain is viewed end on, as shown in *Figure 11*. Kirkwood has related the equilibrium dielectric constant to the product of the dipole moment in a cavity with the moment of the structure in that cavity. We shall extend Kirkwood's model to the polymer structure in a way that is similar to Cole's[23] work on alcohols. In a polymer segment containing n monomer units the g value for each dipole moment will be different, depending on its location within the segment. Therefore, it is convenient to define a mean value $\bar{g}_l$ given by

$$\bar{g}_l = \frac{1}{l} \sum_i g_{ii} \tag{14}$$

In this expression, the subscript l refers to the segment length while the summation index i represents the ith dipole inside the segment. From Kirkwood's equilibrium theory g_{ii} is given by

$$g_{ii} = \sum_y \frac{\mu_i \cdot \bar{\mu}_y}{\mu^2} = 1 + \sum_{y \neq 1,\, \neq i}^{l} \frac{\mu_i \cdot \mu_y}{\mu_i^2} \cos(i, y) = 1 + \sum_{y \neq 1,\, \neq i}^{l} \cos(i, y) \tag{15}$$

because

$$|\mu_i| = |\mu_y|$$

In this expression (i, y) is the angle between the ith and yth dipole moments. In the previous cases the value of (i, y) was calculated from statistical considerations. In the present case (i, y) will be calculated from specific molecular models. If we combine these two sums we have

$$\bar{g}_l = \frac{1}{l} \sum_i \left| 1 + \sum_{y \neq 1, \neq i}^{l} \cos(y, i) \right| \tag{16}$$

which in expanded notation becomes

$$\bar{g}_l = \frac{1}{l} \times \left| \begin{array}{ccccccc|c} & +\cos(2,1) & +\cos(3,1) & +\ldots\ldots & +\cos(l-1,1) & + & \cos(l,1) & + \\ 1+\cos(1,2) & + & +\cos(3,2) & +\ldots\ldots & +\cos(l-1,2) & + & \cos(l,2) & + \\ 1+\cos(1,3) & +\cos(2,3) & + & +\ldots\ldots & +\cos(l-1,3) & + & \cos(l,3) & + \\ \hline 1+\cos(1,l-1) & +\cos(2,l-1) & +\cos(3,l-1) & +\ldots\ldots & +\cos(l-1,l-1) & + & \cos(l,l-1) & + \\ +\cos(1,l) & +\cos(2,l) & +\cos(3,l) & +\ldots\ldots & +\cos(l-1,l) & & 1 & \end{array} \right| \tag{17}$$

In other words, the doubly expanded sum can be represented by the sum of all the elements of four arrays an $(l-1)\times(l-1)$ array, an $(l-1)$ column array, an $(l-1)$ row array and a unit array. The elements in the $(l-1)\times(l-1)$ array can be contracted to the following form

$$\begin{aligned} |(l-1)\times(l-1)| &= \sum_{i=1}^{l-1} \{1 + \cos(1, i') + \cos(2, i) + \ldots + \cos(l-1, i)\} \\ &= \sum_{i=1}^{l-1} \{1 + \sum_{y \neq 1, \neq i}^{l-1} \cos(y, i)\} \sum_{i=1}^{l-1} g_i, \quad (l-1) = (l-1)\,\bar{g}_{l-1} \end{aligned} \tag{18}$$

It can also be shown that the $l-1$ column array is equal to the $l-1$ row array so that

$$\sum_{i=1}^{l-1} \cos(i, l) = \sum_{i=1}^{l-1} \cos(l, 1) \tag{19}$$

Substituting these equations into equation (16) we have

$$\bar{g}_l = \frac{1}{l} \{(l-1)\,\bar{g}_l - 1 + 1 + 2 \sum_{i=1}^{l-1} \cos(l, i)\} \tag{20}$$

which is a useful recursion formula relating to $\bar{g}_l$ to $\bar{g}_{l-1}$. In this expression $\sum_{i=1}^{l-1} \cos(l, 2)$ represents the sum of cosines of the element i which were not present in the $l-1$ segment with all of the remaining $l-1$ elements in that segment. With these equations the quantity $\bar{g}_l$ can be calculated for a variety of assumed segmental structures.

VECTOR DIAGRAM OF THE DIPOLE MOMENTS

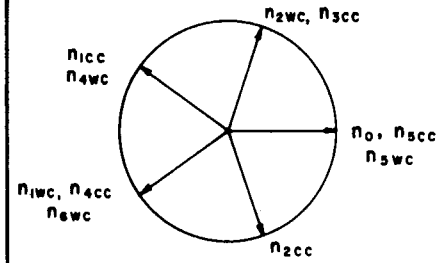

λ	Shorthand Conformation	$\bar{g}_\lambda$
1	(n_0)	1.000
2	n_{1cc} (n_1)	0.192
3	$(n_2)n_{1wc}$	0.129
4	n_{2cc} (n_3)	0.251
5	$(n_4)n_{2cc}$	0.000
6	n_{3cc} (n_5)	0.000
7	$(n_6)n_{3wc}$	0.054
8	n_{4cc} (n_7)	0.048
9	$(n_8)n_{4wc}$	0.100
10	n_{5cc} (n_9)	0.000
11	$(n_{10})n_{5wc}$	0.091

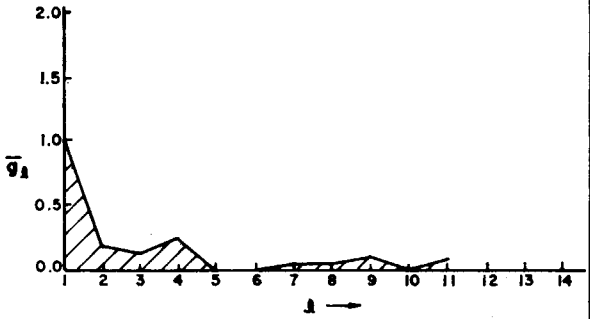

VECTOR DIAGRAM OF THE DIPOLE MOMENTS

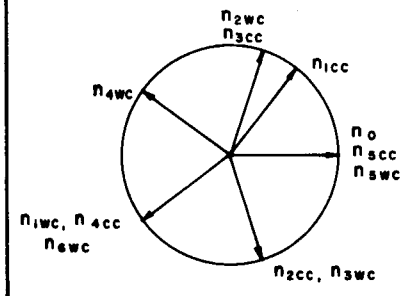

λ	Shorthand Conformation	$\bar{g}_\lambda$
1	(n_0)	1.000
2	n_{1cc} (n_1)	1.620
3	$(n_2)n_{1wc}$	0.230
4	n_{2cc} (n_3)	0.450
5	$(n_4)n_{2wc}$	0.420
6	n_{3cc} (n_5)	0.680
7	$(n_6)n_{3wc}$	0.590
8	n_{4cc} (n_7)	0.450
9	$(n_8)n_{4wc}$	0.250
10	n_{5cc} (n_9)	0.250
11	$(n_{10})n_{5wc}$	0.410
12	n_{6cc} (n_{11})	0.210

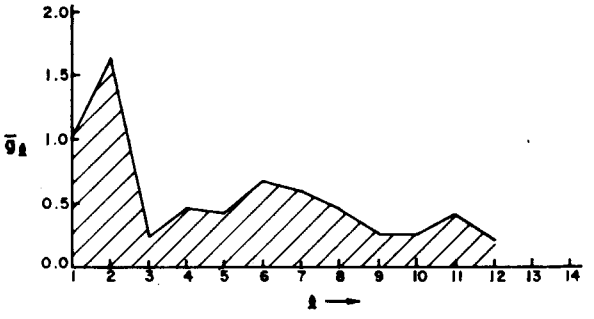

VECTOR DIAGRAM OF THE DIPOLE MOMENTS

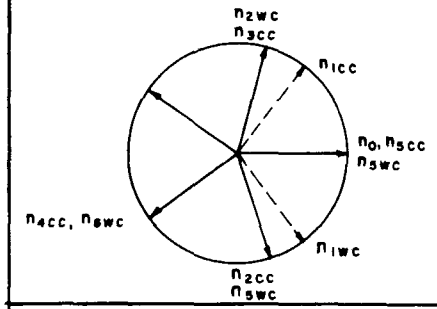

ℓ	Shorthand Conformation	$\bar{g}_\ell$
1	(n_0)	1.000
2	$n_{1cc}\,(n_1)$	1.620
3	$(n_2)n_{1wc}$	1.650
4	$n_{2cc}\,(n_3)$	1.700
5	$(n_4)n_{2wc}$	1.520
6	$n_{3cc}\,(n_5)$	1.730
7	$(n_6)n_{3wc}$	1.640
8	$n_{4cc}\,(n_7)$	0.950
9	$(n_8)n_{4wc}$	0.410
10	$n_{5cc}\,(n_9)$	0.840
11	$(n_{10})n_{5wc}$	1.370
12	$n_{6cc}\,(n_{11})$	1.090
13	$(n_{12})n_{6wc}$	0.800

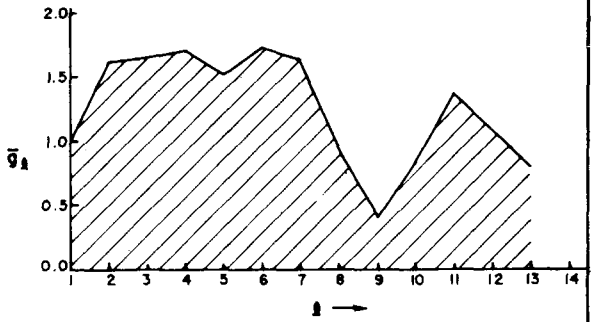

VECTOR DIAGRAM OF THE DIPOLE MOMENTS

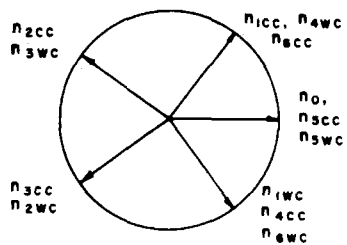

ℓ	Shorthand Conformation	$\bar{g}_\ell$
1	(n_0)	1.000
2	$n_{1cc}\,(n_1)$	1.616
3	$(n_2)n_{1wc}$	1.160
4	$n_{2cc}\,(n_3)$	0.918
5	$(n_4)n_{2wc}$	0.350
6	$n_{3cc}\,(n_5)$	0.304
7	$(n_6)n_{3wc}$	0.628
8	$n_{4cc}\,(n_7)$	0.612
9	$(n_8)n_{4wc}$	0.414
10	$n_{5cc}\,(n_9)$	0.515
11	$(n_{10})n_{5wc}$	0.781
12	$n_{6cc}\,(n_{11})$	1.040
13	$(n_{12})n_{6wc}$	1.220

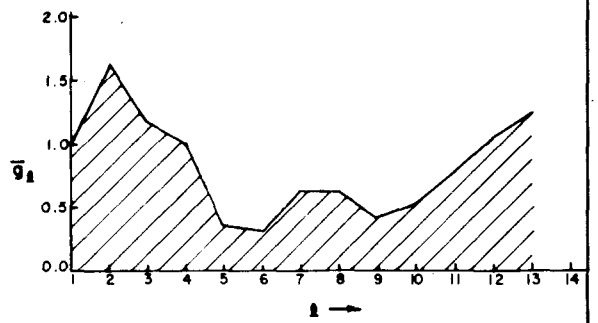

Figure 12—Trial structures for i-PMMA used to calculate effective moment according to Kirkwood's scheme. The arrows represent the direction of the dipole moments when the polymer chain is viewed end on (see text)

Equilibrium behaviour of s-PMMA

The first model chosen for calculation will be given in some detail while the results for other models will be summarized below in graphical form. In this first model all of the dipole moments are pointing down, i.e.

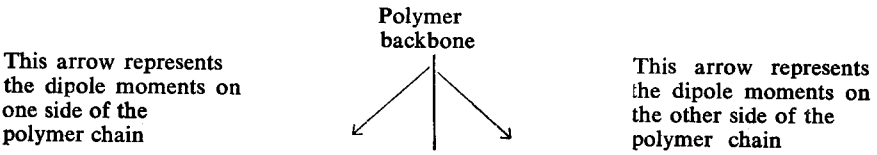

The angle between the dipole moment and the plane of the backbone carbon atoms is taken to be 79·3°. The effective moment for a segment containing a single dipole moment referred to as n_0 is 1·0, see *Figure 11*(a). The average effective moment of a longer segment [now referred to as n_b (n_1)] when a second dipole group is added according to the scheme is 0·070. The average effective moment of a still longer segment [now referred to as (n_2) n_t] when a third dipole group is added according to the scheme is 0·426. In this way, the effective moment of the segment can be built to include 15 monomer units, see *Figure 12*(a). At a segment length of 11 to 13 units the effective moment is calculated nearly to equal the experimental value. Although this model for ester side chain conformation does represent the equilibrium behaviour there are two shortcomings. The first is that all of the units are of the ddd type so that the infra-red splitting cannot be accounted for. Secondly, the model does not account for the temperature dependence of g (which increases with temperature) because the calculated $\bar{g}_i$ increases with segment length. The expected behaviour is for the segment length to decrease with temperature.

A second scheme for calculating the effective moment is to keep the central (n_0) dipole moment pointing up with the remaining moments pointing down, see *Figure 11*(b). The variation of the effective moment with segment length is a minimum at a length of five to seven units. The effective moments of segments with two monomer units are in agreement with the experimental values. Segments with more than three monomer units would exhibit the incorrect temperature dependence for the effective moment.

A third scheme for calculating the effective moment is to keep all of the moments pointing down on one side of the chain and pointing up on the other side of the chain. The effective moment of such a conformation increases without limit and for this reason is unacceptable, see *Figure 11*(c).

A fourth scheme for calculating the effective moment is to keep all of the moments pointing up on both sides of the chain. The effective moment of such a conformation increases without limit and for this reason is unacceptable, see *Figure 11*(d).

A fifth scheme for calculating the effective moment is to alternate the dipole moments between up and down positions on one side of the chain and repeat the process for the other side. These chain halves are meshed in such a way as to read uu dd uu dd . . . etc. in the forward direction and udd uu dd . . . etc. in the backward direction. As in the previous

cases, the effective moments increase drastically with segment length, see *Figure 11*(e).

The last scheme to be considered for s-PMMA is a variation of the one in the previous paragraph. Starting from the central dipole on the LHS of the chain and going in either direction the sequences are udd udd. On the other side of the chain the forward and reverse sequences are dudd udd. The average effective moment of such a segment is slightly erratic. The dashed line in *Figure 11*(f) serves to smooth out those peaks because one would expect a distribution of segment lengths. The effective moment of a segment nine to eleven units long is in agreement with the experimental ones. Furthermore, the changes in effective moment that were observed experimentally can now be interpreted in terms of decreasing segment size with increasing temperature. For the present model the segmental length would change from about ten units at room temperature to about 4 units at temperatures near 150°C. In addition, a segment eleven units long would have three udd arrangements, three ddu arrangements and three dud arrangements. The polar interaction associated with the udd arrangements should be the same as those in the ddu placements and both of these should be different from the interactions in the dud trials. Therefore, there are two different arrangements that could lead to two different interactions that would lead to two different sets of infra-red absorption peaks. For the present model, these are in ratio of 2 : 1 which is in good agreement with the integrated intensity ratios determined for the two pairs of peaks to be 2 : 1 and 1·4 : 1.

Equilibrium behaviour of i-PMMA

The isotactic polymer can be treated in the same way as the syndiotactic polymer except that helical structures are assumed for the backbone carbon atoms. There are two ways in which the dipole moments can be arranged and still be consistent with the σ dichroisms observed for three of the four infra-red absorption peaks. These are either in the direction of the helical pitch (forward) or in the opposite direction (backward). In *Figure 12*(a) a vector diagram is given for a helical polymer chain with all of the ester groups attached to the polymer chain in exactly the same way. In segments where all of the moments are either in the forward or backward directions the results are the same. The effective moment of such a structure quickly drops from a value of unity (segment length = 1) to 0 for a segment length of five units and remains low thereafter because of helical symmetry. The orientation of this segment about any of its axes would not lead to any significant value of the polarization and hence would result in either a low or perhaps zero value for the dielectric constant.

Not all of the ester groups are in the plane which is perpendicular to the chain direction. Some of the groups are parallel to this direction. If every fifth dipole moment in *Figure 12*(a) is turned parallel to the main chain direction then not only is the dipole moment which is perpendicular to the main chain small but a net dipole moment is achieved in the parallel direction. The dipole moment parallel to the main chain direction is, however, not significant enough to account for the experimental values. The

dipole moment in the parallel direction may be increased by the following scheme. The dipole moments that are perpendicular to the main chain direction can be rotated from 10° to 30° in the forward direction and still exhibit σ dichroisms in the infra-red. In this way the effective moment perpendicular to the main chain is not changed while the effective moment parallel to the main chain direction can vary from 0·2 to 0·7 depending on the extent of rotation into the main chain direction. If this segment is constrained to move only about two axes then the orientation about the chain axis (β process) would lead to a small or perhaps zero value for the dielectric constant. On the other hand, the orientation (α process) about the axis perpendicular to the main chain direction would lead to those values observed experimentally. In addition to representing the dielectric behaviour, this model for the segment can qualitatively account for the splittings of the ester oxygen absorption bands observed in the infra-red. In this segment there are three kinds of triads: $\sigma\pi\sigma$, $\pi\sigma\sigma$ and $\sigma\sigma\sigma$ ones where σ and π represent the perpendicular and parallel arrangements, respectively. These different triads would lead to different neighbouring interactions and hence to different splittings of the main ester oxygen peak.

Although the above segment represents the dielectric behaviour, there are a number of other arrangements that are worth mentioning. The second scheme for building up the segment length of the polymer chain is based on placing the dipole moment which is next to the centre one in the backward direction and all of the remaining ones in the forward direction. The variation of the effective moment of such a structure [*Figure 12*(b)] with segment length is similar to the behaviour of the structure in *Figure 12*(a) except that the segment must be longer to compensate for the original asymmetry incorporated in the segment. Another variation of the segment structure in *Figure 12*(a) is to place the two dipole moments next to the centre one in the backward direction and place the remaining ones in the forward direction. The variation of the effective moment with segment length [see *Figure 12*(c)] is even more exaggerated than the previous one studied. Another scheme for building up the segment length is to place the first and fifth units (clockwise and counter clockwise) in the forward direction and the intervening units pointing in the backward direction. The variation of the effective moment with segment length is given in *Figure 12*(d). In addition to these schemes several others were tried. For example, the variation of the effective moment with segment length for a looser helical structure (an 11_4 helix, where 11 monomer units make 4 turns) was tried with essentially similar results to the 5_2 helix except that the periodicity was longer.

In summarizing these two sections of the discussion, several features of the proposed mechanism need to be emphasized. First, the interpretation of two dispersions in terms of an orientation of unsymmetrical segments, each with its own relaxation time has been used[24] for representing dispersion behaviour for small unsymmetrical molecules. For this interpretation, the difference between the high and low frequency limiting values of the dielectric constant is to be interpreted in terms of the effective moment associated with a particular degree of freedom. With s-PMMA there are two such mechanisms each to be associated with a particular degree of

freedom of the polymer chain. With i-PMMA there is only one; if the second one exists it must be quite small. The absence of this second dispersion is not to be construed as a freezing out of a particular movement of a polymer chain but rather that the effective moment in one direction is zero. Similarly, the increased magnitude of the α dispersion in i-PMMA when compared to s-PMMA is not to be attributed to a more flexible backbone structure but rather to a greater effective moment in the main chain backbone structure but rather to a greater effective moment in the chain direction. Chain flexibility is more properly associated with the kinetics of the relaxation mechanism and not with equilibrium structure. The proposed mechanism is consistent with the infra-red dichroisms of these polymers.

Secondly, interpretations of dielectric dispersions in terms of three-dimensional details of local structure are quite common for small molecules. This procedure seems to be seldom, if ever, used for interpreting dielectric behaviour. This absence is presumably due to the lack of structural details. In the case of acrylics, the dipole moment lies in the plane of the ester group. The ester group is a very strong absorbing group in the infra-red region so that it is possible to use this characteristic to determine some details of three-dimensional structure. To the best of our knowledge this almost obvious fact has never been used for interpreting dielectric behaviour.

Finally, of the many methacrylates whose dielectric behaviour has been reported in the literature only s-PMMA and its ethyl analogue (PEMA) have β dispersions. In all other methacrylates, the major component of the dielectric constant is associated with the α process. All of the α processes studied so far are unsymmetrical while the β processes are all symmetrical. In terms of the present interpretation, a twisting of the polymer chain can take place anywhere along the chain. The overall shape of such chains is nearly cylindrical, so that one would expect the local structure to be the close packing of cylinders. In this environment there can be six equivalent positions which are separated by symmetrical potential energy barriers. Symmetrical potential energy barriers would lead to a symmetrical time dependent correlation function. The α process, on the other hand, is taken to be an orientation about the axis perpendicular to the main chain. Any such movement would require a hole or a vacancy which would lead to an unsymmetrical potential energy barrier which in turn leads to an unsymmetrical time dependent correlation function. Symmetrical or unsymmetrical time dependent correlation functions lead to symmetrical or unsymmetrical dispersions.

Dielectric and mechanical β dispersions

In a previous study[11], a method for comparing the dielectric and mechanical α dispersions was described. A normalization procedure was derived to take into account certain effects which have been expounded upon by Scaife[11]. When the data have been so normalized the dielectric and mechanical dispersions were found to be equivalent. This equivalence was observed only in the time parameters (α, β, τ_0) and not in the equilibrium (ϵ_0) or in the instantaneous (ϵ_∞) parameters. This normalization procedure was found to modify significantly the shape of the relaxation curve when the

ratio of the equilibrium to instantaneous parameters ($\epsilon_0/\epsilon_\infty$ or J_0/J_∞) is of the order of ten thousand. On the other hand, when this ratio is in the range of two or three, the shape of the relaxation curve is not affected. The ratio of $\epsilon_0/\epsilon_\infty$ or of J_0/J_∞ for the β process in s-PMMA is not expected to exceed five. Therefore, there is some basis to expect a meaningful comparison when the complex compliance is compared with the complex dielectric constant for the β process in s-PMMA.

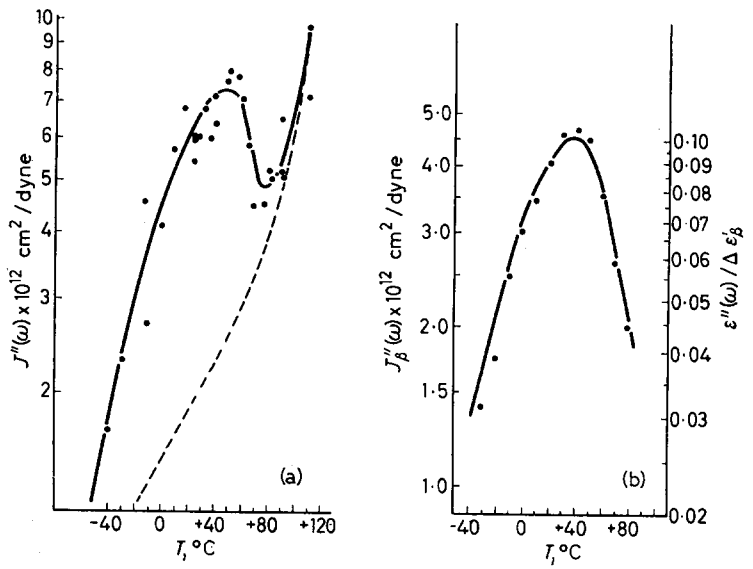

Figure 13—(a) Imaginary part of complex compliance versus temperature (°C). (b) The filled circles represent the smooth values obtained by subtracting the contribution of the α process from the experimental value to yield the β process. The solid line represents the middle term in equation (21)

The complex compliance is readily calculated from the logarithm of the decrement and the geometry of the specimen for the natural frequency of oscillation. A plot of the imaginary part of the complex compliance with temperature is given in *Figure 13*(a). At any temperature, over the range of measurement, there was a significant contribution from the α process to the β one. However, it is possible to assume a behaviour for the α process [dashed line in *Figure 13*(a)] and subtract it from the total contribution to obtain the β process [filled circles in *Figure 13*(b)].

To test for the equivalence of the dielectric and mechanical mechanisms we proceed as follows. The dielectric β process can be represented at any temperature for any frequency by the circular arc function

$$\frac{\epsilon''(\omega)}{\epsilon_0-\epsilon_\infty}=\frac{\cos(\alpha\pi/2)}{2\{\cosh[(1-\alpha)\ln\omega\tau_0]+\sin(\alpha\pi/2)\}}\stackrel{?}{=}\frac{J''(\omega)}{J_0-J_\infty} \tag{21}$$

and the appropriate value of $1-\alpha$ and τ_0. The question can be rephrased to ask whether or not the imaginary part of the complex compliance can

be written in the same form, in words the RHS of equation (21). If $J_0 - J_\infty$ were known then $J''(\omega)$ could be calculated because everything on the LHS is known. However, $J_0 - J_\infty$ is not known so that an alternative procedure must be devised. The quantity $\epsilon_0 - \epsilon_\infty$ is nearly independent of temperature so that it may be reasonable to assume $J_0 - J_\infty$ to be independent of temperature. The centre terms of equation (21) can be computed from the known dielectric parameters α and τ_0 at the experimental frequency (ω) for the mechanical dispersion over the temperature range of $-40°C$ to $80°C$. A logarithmic plot of the centre term is made and shifted up or down until superposition is achieved. The results of such a procedure are given in *Figure 13*(b) where the agreement between the two processes is seen to be quite good. The quantity $J_0 - J_\infty$ determined by this procedure was found to be $4{\cdot}46 \times 10^{-11}$ cm^2/dyne.

Other measurements

The nature of the glass transition region has received considerable attention in the past. A critical review of the subject in relation to the evidence discussed in the previous sections is beyond the scope of this work. On the other hand, there are two relevant correlations that should be mentioned. Perhaps the most important one is the observation reported on by Dyvick, Bartoe and Steck[25]. In that work they measured the 60 c/s dielectric, dilatometric and Vicat properties of a number of acrylic polymers and copolymers. They found a correlation to exist between the temperature at which the 60 c/s dielectric loss became a maximum (T_a) with the glass temperature (T_g) and with the Vicat temperature (T_v). In *Figure 14* we have reproduced such a plot not only for their polymers but for a number of others not yet reported. As can be seen from that figure the correlation of T_a with T_g or T_v is good and exists for a number of polymers whose glass temperatures span nearly two hundred degrees.

There are several important features that need to be mentioned concerning this first correlation. Any discussion concerning T_g determined dilatometrically needs to include properties that were obtained below T_g. The nature of this glass phase is necessarily obscure because of certain time or supercooling effects that have been observed near this region[26]. These observations place very serious limitations on any thermodynamic discussion of this transition region if the discussion includes a knowledge of the glass phase. On the other hand, T_a is determined entirely above the glass transition region where these supercooling or time effects are absent. Therefore, there are no serious questions concerning the thermodynamic equilibrium of this phase. The correlations observed between T_g and T_a imply that a knowledge of T_g is possible from a knowledge of the temperature region above T_g.

The correlation observed between T_g and T_a means that the discussion of T_g can be recast into the following terms. What are the factors that control the temperature at which T_a determined at 60c/s becomes a maximum? From a dielectric point of view, this correlation amounts to a discussion of the factors that control the temperature dependence of the relaxation time. There are two parameters which describe the temperature

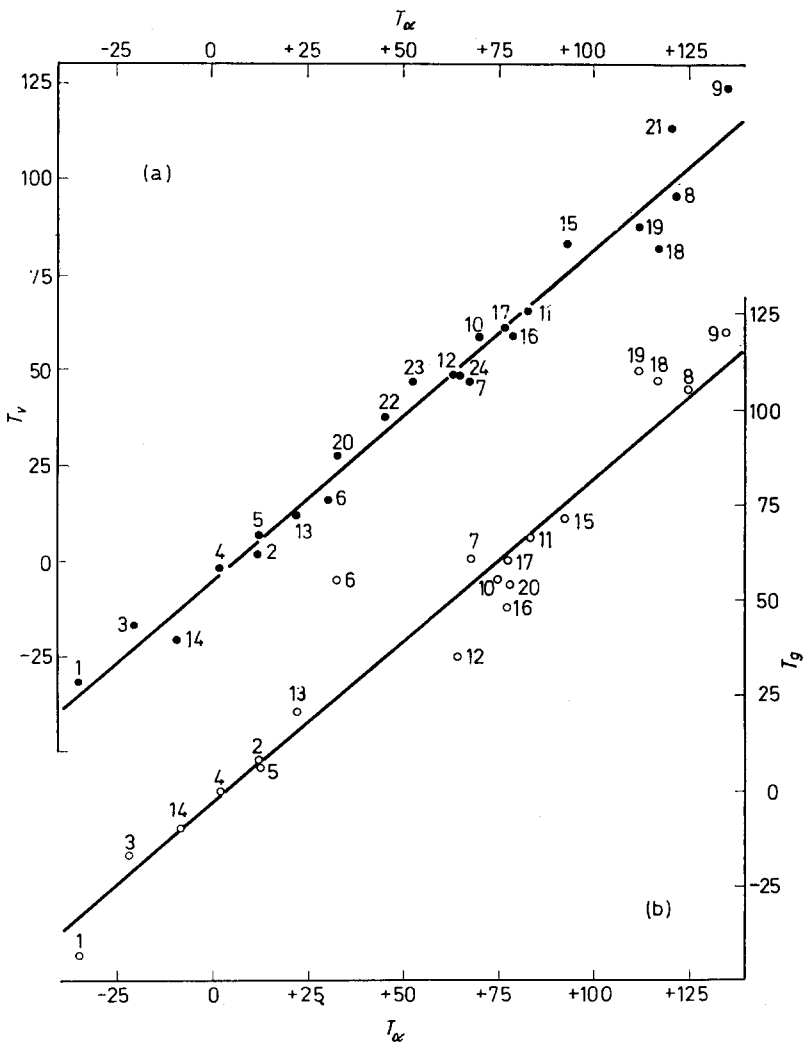

Figure 14—The Vicat (●, T_v in °C) and the glass (○, T_g in °C) temperatures versus the temperature at which the 60 c/s loss (T_α in °C) becomes a maximum. Numerals next to marked points refer to the following polymers: 1. poly(*n*-propyl acrylate), 2. poly(methyl acrylate), 3. poly(ethyl acrylate), 4. poly(*i*-propyl acrylate), 5. poly(benzyl acrylate), 6. poly(phenyl acrylate), 7. poly(2,4-dichlorophenyl acrylate), 8. conventionally initiated poly(methyl methacrylate), 9. s-PMMA, 10. i-PMMA, 11. poly(ethyl methacrylate), 12. poly(*n*-propyl methacrylate), 13. poly(*n*-butyl methacrylate), 14. poly(*n*-hexyl methacrylate), 15. poly(*i*-propyl methacrylate), 16. poly(*i*-butyl methacrylate), 17. poly(secbutyl methacrylate), 18. poly(tertbutyl methacrylate), 19. poly(phenyl methacrylate), 20. poly(benzyl methacrylate), 21. poly(cyclohexyl methacrylate), 22. poly(phenoxyethyl methacrylate), 23. poly(2,2′,2″-trichloroethyl acrylate), 24. poly(chlorophenyl acrylate)

dependence of the relaxation time: the energy of activation $\Delta H(T)$ and the entropy of activation $\Delta S(T)$. These quantities are written in a form to indicate that they may be temperature dependent. The temperature dependences of these properties would come about because there may be changes in the structure of the system. An Arrhenius rate plot using either relaxation times or shift factors is often curved. This curvature implies a temperature dependent activation energy.

The second correlation to be discussed which is relevant to the nature of the glass transition region is based on the data in *Table 4*. The acrylates and methacrylates in Group I exhibit a dependence of their T_g on the average chain separation. In other words, as the chain separation increases the glass temperature decreases. The polymers in Group II exhibit the same dependence. The polymers in Group III are considerably more complex but there is in some cases the same dependence.

The author would like to express his appreciation to Mr J. A. Shetter who made all the dielectric measurements, to Mr J. Scott who made all of the mechanical measurements, to Dr H. S. Yanai who provided all the X-ray data and finally to N. Steck who made the T_a, T_g and T_v data available.

Rohm and Haas Co.,
Research Laboratories,
Bristol, Pa, U.S.A.

(*Received July 1967*)

REFERENCES

[1] MIKAHELOV, G. P. and BORISOVA, T. I. *Vysokomol. Soedineniyà*, 1966, **2**, 619
[2] HAVRILIAK, S. and NEGAMI, S. *J. Polym. Sci. Part C*, 1966, No. 14, 99
[3] STRELLA, S. and ZAND, R. *J. Polym. Sci.* 1957, **25**, 97
[4] HAVRILIAK, S. and ROMAN, N. *Polymer, Lond.* 1966, **7**, 387
[5] *Instruction Manual* for the Type 1610-B Capacitance Measuring Assembly from The General Radio Company, West Concord, Mass., U.S.A.
[6] FERRY, J. D. *Viscoelastic Properties of Polymers.* Wiley: New York, 1961
[7] GOODE, W. E., SNYDER, W. H. and FETTES, R. C. *J. Polym. Sci.* 1960, **42**, 367
[8] GOODE, W. E., OWENS, F. H., FELLMANN, R. P., SNYDER, W. H. and MOORE, J. E. *J. Polym. Sci.* 1960, **56**, 317
[9] BOVEY, F. A. and TIERS, G. V. D. *J. Polym. Sci.* 1960, **44**, 173
[10] COLE, K. S. and COLE, R. H. *J. chem. Phys.* 1941, **9**, 341
COLE, R. H. *J. chem. Phys.* 1955, **23**, 403
[11] HAVRILIAK, S. and NEGAMI, S. *Polymer, Lond.* 1967, **8**, 161
[12] KLUG, H. P. and ALEXANDER, L. E. *X-Ray Diffraction Procedures for Polycrystalline and Amorphous Materials.* Wiley: New York, 1954
[13] KRAUS, S., GORMLEY, J. J., ROMAN, N., SHETTER, J. A. and WATANABE, W. H. *J. Polym. Sci. A*, 1965, **3**, 3573
[14] FRÖHLICH, H. *Theory of Dielectrics.* Clarendon Press: Oxford, 1958
[15] READ, B. E. and WILLIAMS, G. *Trans. Faraday Soc.* 1961, **57**, 1979
[16] FUOSS, R. M. and KIRKWOOD, J. G. *J. Amer. chem. Soc.* 1941, **63**, 385
[17] BOTTCHER, C. J. F. *Theory of Electric Polarization.* Elsevier: New York, 1952
[18] WILLIONS, M. L. and FERRY, J. D. *J. Polym. Sci.* 1953, **11**, 459
[19] ISHIDA, Y. and YAMAFUJI, K. *Kolloidzschr.* 1961, **177**, 98
[20] HAVRILIAK, S. and ROMAN, N. *Polymer, Lond.* 1966, **7**, 387
[21] STROUPE, J. D. and HUGHES, R. E. *J. Amer. chem. Soc.* 1958, **80**, 2341

[22] NAGAI, H., WATANABE, H. and MISHIOKA, A. *J. Polym. Sci.* 1962, **62,** 595
[23] DANNHAUSER, W. and COLE, R. H. *J. chem. Phys.* 1955, **23,** 1768
[24] SMYTH, C. P. *Dielectric Behavior and Structure.* McGraw-Hill: New York, 1955
[25] DYVIK, G. K., BARTOE, W. F. and STECK, N. S. *SPE Trans.* 1964, **4** (No. 2), 1
[26] SAITO, S. and NAKAJIMA, T. *J. appl. Polym. Sci.* 1959, **11,** 93

Structural Investigations on Polyethylenes and Ethylene–Propylene Copolymers by Reaction Gas Chromatography and X-Ray Diffraction

L. MICHAJLOV, P. ZUGENMAIER and H.-J. CANTOW

Dedicated to Prof. Dr A. Peterlin on the occasion of his 60th birthday.

Experimental results obtained from reaction gas chromatography investigations on polyethylene and ethylene–propylene copolymers are discussed with regard to the polymer microstructure. With a series of ethylene–propylene copolymers ranging between plastomers and elastomers it is shown that it is possible to correlate the mass distribution of the chain fragments with the blockiness of the polymer chains. The conclusions drawn from the reaction gas chromatography studies concerning the block structure of some copolymers are supported independently by X-ray diffraction and DTA measurements. The quantitative evaluation of the iso-alkanes and the straight chain fragments resulting from low density-, Ziegler- and Phillips-type polyethylene enables one to differentiate between them. The most frequent short branches in the polyethylene samples analysed are ethyl and butyl. The detection and the quantitative evaluation of longer chain fragments (up to C_{50}) enables one to get more information about the microstructure of the polymers studied. The experimental technique is discussed and some illustrative examples are given.

THE thermal fragmentation method coupled with gas chromatography has so far been applied essentially to the identification of polymers, for studying their thermal stability, the mechanism of chain scission reactions and for determining the overall composition of copolymeric systems.

The potentiality of the method for studying polymer microstructure on a quantitative basis still remains almost unexploited. The need for rigorous control of the experimental conditions, the great variety of pyrolysis and gas chromatographic apparatus and thereby the difficulties of comparing the results obtained in different laboratories are the most probable discouraging factors—they prevent wide application of the method under discussion for quantitative studies on polymer microstructure.

Despite these difficulties recent publications[1–5] show that thermal degradation, especially if coupled with gas chromatographic separation of scission products, may be successfully used for study of comonomer distribution in copolymers.

Recent studies have clearly demonstrated[6] that the pyrograms of olefinic copolymers depend on the blockiness.

The pyrolysis gas chromatographic method may deliver additional information concerning the microstructure of copolymers besides the usual methods used today for determining sequence length distribution, i.e. n.m.r., i.r. and u.v. spectroscopy. Whereas the spectroscopic methods yield only the averaged effect of the different structural units, pyrolysis gas chromato-

graphy separates the scission products of the polymeric chain. Their identification may be achieved by appropriate methods.

The problem, however, seems to be to what extent intrasequential bond scissions can be reduced in favour of intersequential ones by an appropriate choice of pyrolysis conditions.

In this work we sought information on the structure of polyethylene and ethylene–propylene copolymers by determining the distribution of chain fragments according to their carbon numbers as a function of the blockiness in terms of the crystallinity of the polymer samples.

EXPERIMENTAL

Apparatus and procedure

Flash pyrolysis coupled with in-line hydrogenation and gas chromatographic separation of the pyrolysis products was used.

The chromatographic analyses were carried out with a Varian Aerograph dual column, dual FID gas chromatograph with matrix temperature programmer, type Moduline 1522 B. For the quantitative evaluation of the peak areas a Perkin–Elmer printing digital integrator type D 24 with automatic baseline correction was used. Registration of the detector signals was obtained with a Westronics recorder with 1 mV full scale deflection.

The pyrolyser is a platinum–rhodium dish-type filament (Hewlett-Packard Co.), calibrated in our laboratory for temperature against amperage for the carrier gas conditions applied here. It was attached through an adaptor to the injection block inlet of the gas chromatograph. The power supply to the filament is controlled by a variable transformer fed by constant voltage. The pyrolysis time is governed automatically. The carrier gas preheated to 280°C enters the pyrolyser so allowing fragments with relatively high molecular weight to enter the column. The sample, usually 0·2 mg, is first inserted into a capillary quartz tube sealed at one end and then put into a sample holder. In this way catalytic effects due to contact between metal filament and sample are eliminated, the pyrolysis temperature being more uniform and the reproducibility greatly improved.

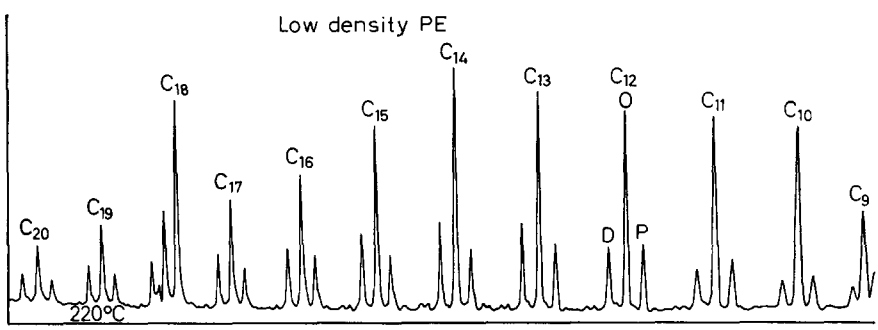

Figure 1—Pyrogram of a low-density polyethylene, density 0·918. Experimental conditions: pyrolysis temperature 820°C; column 50 m×0·01 in. o.d. coated with polyphenylether OS 128; carrier gas nitrogen, flow rate 1·2 ml/min; split ratio 1/30; temperature programme 50° to 220°C at 3 deg. C/min; attenuation 1; P denotes paraffin; O, olefin; D, diolefin

As is well known, polyolefins degrade and give rise to a great number of saturated and unsaturated cracking products, whose identification and quantitative evaluation is extremely difficult.

Figure 1 shows a pyrogram of a low density (high pressure type) polyethylene (PE). The homologous members of the *n*-paraffins, α-olefins and α,ω-diolefins are well resolved. Between the straight chain fragments there are many more or less saturated iso-compounds.

Less complicated pyrograms are obtained by direct hydrogenation of the pyrolysis products using hydrogen as carrier gas and a hydrogenation catalyst.

For this purpose the injection block (4 in. $\times \frac{1}{8}$ in. i.d. stainless steel tube) of the gas chromatograph is filled with the catalyst, consisting of one per cent palladium on glass micro-beads (Degussa, Hanau) as support. The temperature of the catalyst is maintained constant at 280°C. The pyrolysis products pass over the hydrogenation catalyst immediately after their formation and are then fed directly to the column.

Figure 2 is a 'hydrogenated' pyrogram of the low density PE discussed above. Experimental conditions are summarized in *Table 1*. Under these conditions the range of detectable fragments is up to C_{36}.

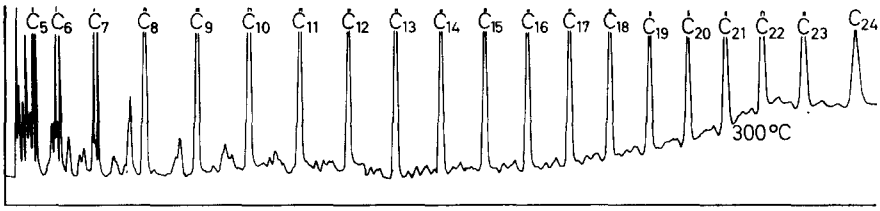

Figure 2—Pyrogram of a low-density polyethylene; sample weight 0·366 mg; without automatic baseline correction

Table 1. Reaction gas chromatography experimental conditions

Pyrolysis	
Sample weight*, mg	~ 0·2
Temperature, °C	680
Time, sec	20
Hydrogenation	
Catalyst	1% Pd on glass beads 100/120 mesh
Temperature, °C	280
Gas chromatography	
Inj. block, °C	280
Column*	3 m × ⅛ in. i.d. packed with 10% Apiezon L
Temperature programme	40°–300°C at 4 deg. C/min
Carrier gas*, ml/min	20 H_2
Detector oven, °C	340
Detector	Dual FID
Air, ml/min	350
Nitrogen, ml/min	20
Attenuation*	10

*Unless otherwise stated.

Peak identification

The *n*-alkane peaks and some of the iso-alkane peaks were identified in three ways:

(1) by comparing the retention times with those of model substances, and

(2) by synchronous injection of model substances. To do this we used an integrated injection pyrolysis hydrogenation unit, shown in *Figure 3*. The inlet attached to the one end of the micro-reactor allows simultaneous injection of test substances.

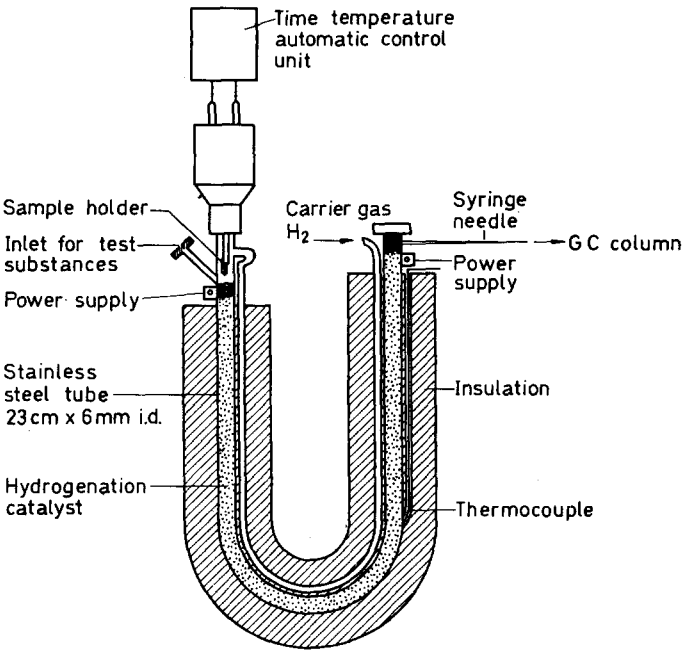

Figure 3—Integrated injection pyrolysis hydrogenation unit

(3) by preparative isolation of fragments and identification by attenuated total reflection (ATR) in the i.r. region.

Other methods—such as mass spectroscopy and n.m.r.—will also be applied for this purpose.

RESULTS AND DISCUSSION

Polyethylenes

Branching in ethylene polymers has been studied mainly by i.r.[7-15]. Valuable information has also been gained from electron irradiation studies[16,17]. Broad line n.m.r. has been proposed for analytical use in the study of branching in polyethylenes[18].

It is generally accepted that short side chains in the free radical polymer are mainly ethyl and butyl, branches such as propyl, pentyl or longer being infrequent.

The work of Tirpark[12] and of Elston[19] provided evidence that high pressure polyethylene contains branched branches such as 1-ethyl pentyl, 2-ethyl hexyl, 3-ethyl heptyl, etc.

The integrated pyrolysis gas chromatographic method, especially when combined

with hydrogenation, seems to be a powerful tool for the study of structural differences in various polyethylenes[20]. van Schooten and Evenhuis[6] have recently published quantitative data on the iso-alkanes, yielded after pyrolysis of high- and low-pressure polyethylene. They detected fragments with carbon number up to C_{13}.

Extending the range of detectable fragments, we were able to get more details about the distribution of fragments from ethylene polymers and consequently of the structure of the polymeric chains themselves.

In the following the pyrograms of three commercial types of polyethylenes*, prepared by free radical, Ziegler and Phillips processes, will be discussed. They are shown in *Figures 2, 4* and *5* respectively.

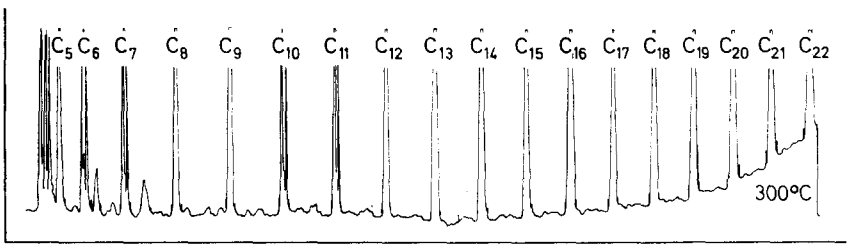

Figure 4—Pyrogram of a Ziegler polyethylene, density 0·943. Sample weight 0·365 mg; without automatic baseline correction

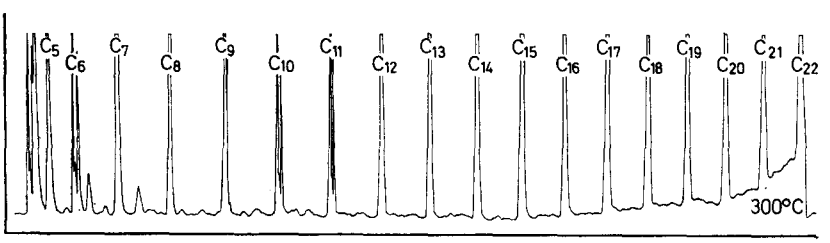

Figure 5—Pyrogram of a Phillips polyethylene, density 0·951. Sample weight 0·360 mg; without automatic baseline correction

In order to make the iso-alkane peaks more distinctive, we used somewhat increased sample sizes. For the same reason, no automatic baseline correction was applied.

As can be seen, the pyrograms contain a series of equidistant large peaks, each one representing a homologous straight chain alkane. The small peaks situated ahead of the large ones correspond to the branched alkanes with the same carbon number as the next *n*-alkane. The temperature programme ends at the C_{21} peak. From here on an isothermal period follows.

A comparison of the pyrograms of low density and Ziegler-type PE indicates an obvious difference in the amount of iso-alkanes, the low density polymer yielding more branched isomers than the high density one. It is

*The following PE samples were analysed:
1. Low density PE—Lupolen KR 1258 and KR 1257 (BASF),
2. High density PE (Ziegler)—Vestolen (CWH), and
3. High density PE (Phillips)—Lupolen 5261 (BASF).

evident that very similar branched fragments are formed, the differences being mainly in the relative concentrations of the individual components.

On comparing the pyrograms of the two high density polymers a very small difference in the amount of iso-alkanes is evident.

Some indication of the yield of branched isomers in the i-C_5 to i-C_{25} range may be obtained by summarizing the percentage of peak area of the particular components:

Low density PE	—	10·6 per cent iso-alkanes
Ziegler PE	—	4·2 per cent iso-alkanes
Phillips PE	—	3·9 per cent iso-alkanes

The assignment of the main iso-alkane peaks in the i-C_4 to i-C_9 range is as follows:

i-C_4	i-C_5	2MC*$_5$	2,4-MC$_5$	2,4MC$_6$	2MC$_8$	5MC$_9$
		3MC$_5$	2MC$_6$	(MC$_1$C$_6$)	(3EC$_7$)	2MC$_9$
			3MC$_6$	2MC$_7$	3MC$_8$	3MC$_9$
				(3EC$_6$)	4MC$_8$	(3EC$_8$)
				3MC$_7$	(4EC$_7$)	4MC$_9$
				4MC$_7$		(4EC$_8$)

*M denotes methyl, E ethyl. For example 2MC$_5$ means 2-methyl pentane, 3 EC$_6$ means 3-ethyl hexane, etc.

The reproducibility of the iso-alkane peaks is illustrated by the two pyrograms shown in *Figure 6*. Generally, the reproducibility of the normalized peak areas was in the region of two per cent relative. About 20 runs were made from each sample.

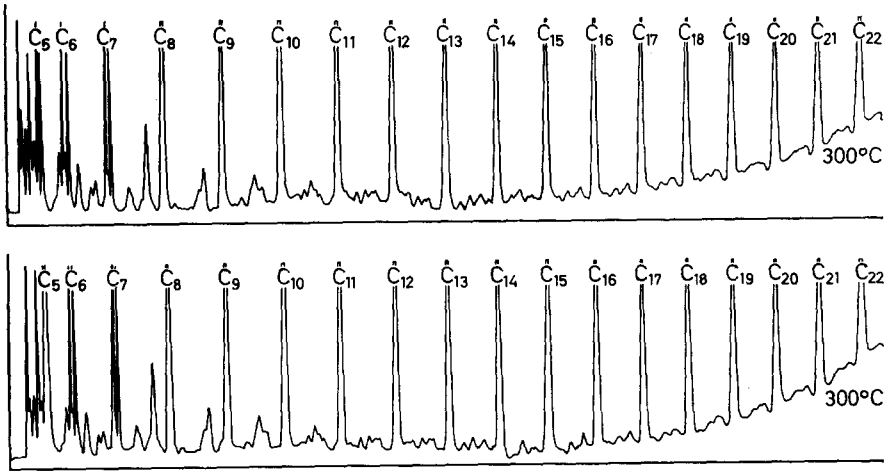

Figure 6—Pyrograms of a low-density polyethylene

On plotting the percentage peak area of each homologous member against carbon number we get a clear indication of the distribution of the

fragments from the low- and high-density PE. This is demonstrated in *Figure 7*.

It is evident that the concentrations of *n*-C_3, *n*-C_4 and *n*-C_5 are higher for the low density polymer, whereas the high density polymer by comparison shows higher percentages of fragments with carbon number ten or above. This fact may be interpreted in terms of the splitting-off of pendant side groups with 3, 4 and 5 carbon atoms and a higher frequency of tertiary carbon atoms in the polymer backbone of low density PE. Thus,

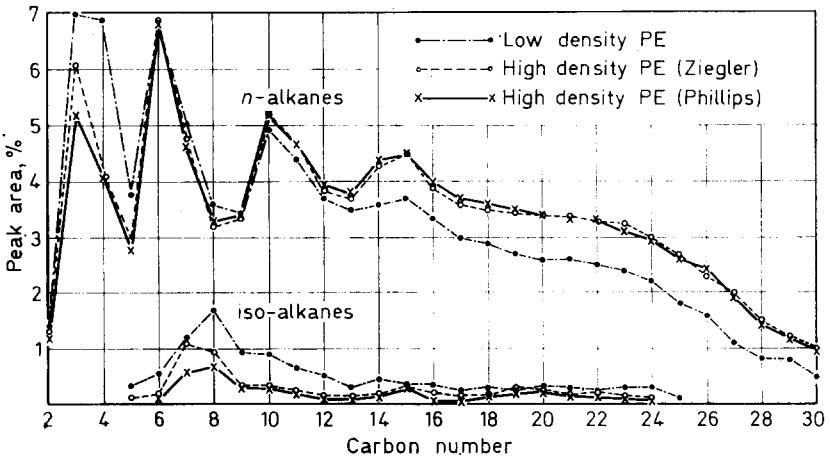

Figure 7—Distribution of pyrolysis fragments of low-density, Ziegler and Phillips polyethylene. Iso-alkanes with the same carbon number are given as the sum

low density polymers yield more iso-alkanes than the high density ones. Strong support for the above interpretations was obtained from pyrograms of an ethylene–hexene-1 copolymer. On pyrolysis this polymer yields an increased amount of *n*-butane stemming from the butyl side groups.

For the estimation of structural differences the relative distribution between normal and iso-fragments is not the only criterion. The mass distribution of the straight chain scission products up to long chain lengths is also significant. If one uses a silicone gum rubber column and temperature programme up to 330°C, followed by an isothermal period, fragments up to C_{50} can be detected. To realize this it is very important to minimize the dead space between pyrolyser and column inlet.

Figure 8 shows such pyrograms from low- and high-density PE.

Whereas the *n*-C_3, *n*-C_6 and *n*-C_{15} maxima (*Figure 7*) are almost irrelevant for differentiation between the different polyethylene samples, differences arise at higher carbon numbers (see *Figure 8*). Low density PE shows a maximum at *n*-C_{18}–*n*-C_{19} and Ziegler PE at *n*-C_{22}–*n*-C_{23} and *n*-C_{30}–*n*-C_{32}.

In the present state of our research we are unable to present an unequivocal interpretation concerning the particular peak maxima. The positions of these maxima seem almost independent of the pyrolysis temperature. The only change is in the mass distribution of chain fragments; this is

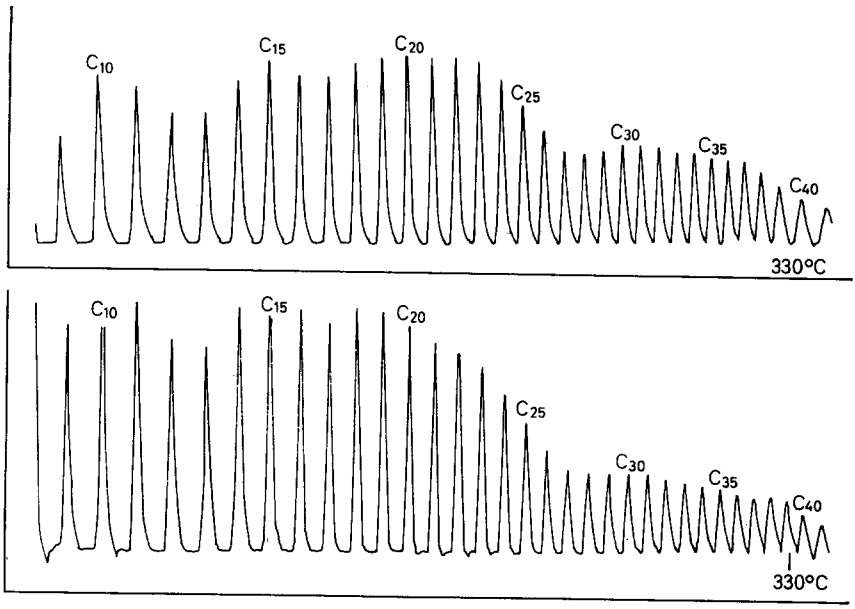

Figure 8—Pyrograms of a Ziegler (above) and a low-density polyethylene (below). Experimental conditions: column 2 m×⅛ in.; temperature programme 40° to 330°C at 6 deg. C/min; automatic baseline correction

demonstrated by the three runs made at different pyrolysis temperatures, as seen in *Figure 9*. 680°C, however, seems to be the best pyrolysis temperature for polyethylene and ethylene copolymers because pyrolysis is instantanous and complete. Higher temperatures favour the formation of more short-chain fragments, thus diminishing the interpretability of the pyrograms in terms of polymer chain architecture.

The distribution of iso-alkanes may be interpreted too. A significant difference between the low- and high-density polyethylenes is observed in the *i*-C_5–*i*-C_{16} range, as demonstrated in *Figure 7*. Both types of polymers seem to differ more in the concentration than in the nature of the branches. This is still more apparent for the two high-density samples. On considering the structure and yield of identified iso-alkanes from high-pressure polyethylene it may be concluded that ethyl and butyl branches predominate, but longer branches are also present to some extent.

Ethylene–propylene copolymers

For the study of comonomer distribution in ethylene–propylene copolymers, i.r. spectroscopy has been mostly used[21,22]. Nencini *et al.*[23] applied a pyrolysis–mass spectrometry method for blockiness determination in E–P copolymers, based on the quantitative evaluation of *n*-butane and *n*-pentane in the mixture of volatile pyrolysis products.

Changes in the composition of volatile pyrolysis products from block and random E–P copolymers were observed by Voigt[5] and by Groten[4].

Using high resolution n.m.r. spectroscopy for compositional analysis of E–P copolymers, Porter[24] came to the conclusion that n.m.r. analyses for

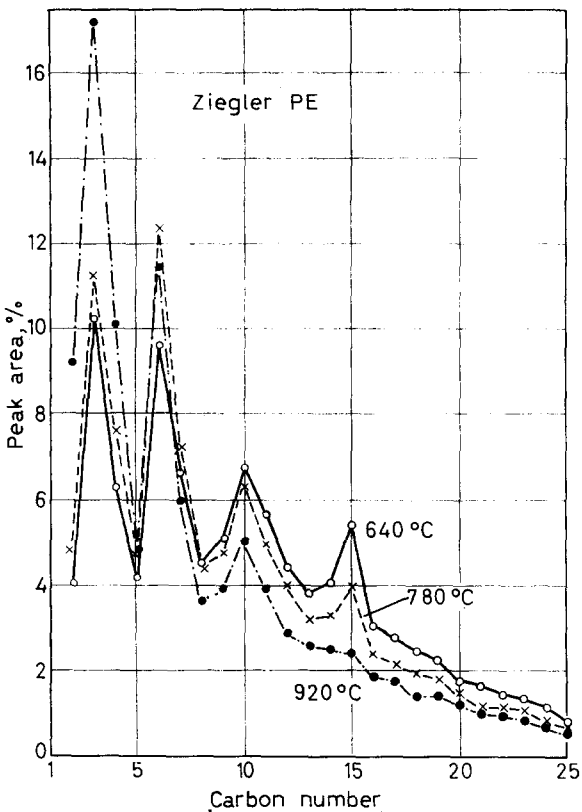

Figure 9—Mass distribution of straight chain fragments of Ziegler polyethylene, obtained at different pyrolysis temperatures

block and total ethylene content may provide a measure of randomness in these polymers.

As is well known from copolymerization kinetics, a copolymer is not characterized fully by its overall composition and chemical heterogeneity alone. Depending on the process of polymer formation, the average sequence lengths may vary even at constant average composition.

We tried to determine the 'blockiness' of E–P copolymers by the reaction gas chromatography method, as discussed above.

In what follows we discuss first the differences in fragmentation of a random copolymer and a physical mixture (polyblend) of polyethylene and polypropylene. For comparison the pyrograms of an isotactic, highly crystalline polypropylene and a Ziegler polyethylene are shown in *Figure 10*. The most frequent fragments from polypropylene, corresponding to the monomer, dimer, trimer etc. are propane (I), 2-methyl pentane (II), 2,4-dimethyl heptane (III) and the respective higher segments (IV–IX). In the pyrogram of Ziegler polyethylene the C numbers of the straight chain fragments are plotted.

The upper pyrogram in *Figure 11* represents the fragmentation of the 1 : 1 physical mixture of polyethylene and polypropylene. Superposition of the polypropylene fragments (I–IX) with the polyethylene fragments (C_5–C_{24}) is clearly recognizable.

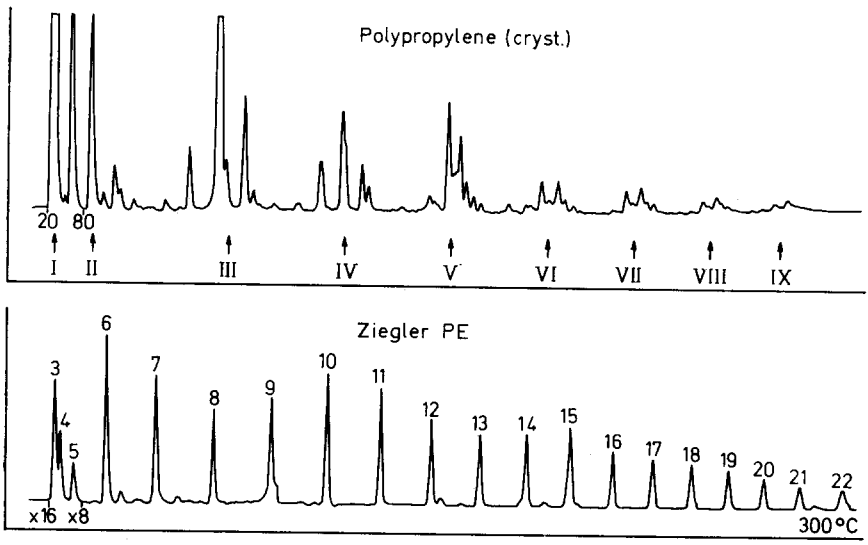

Figure 10—Pyrograms of a polypropylene and a Ziegler polyethylene

The lower pyrogram in *Figure* 11 finally demonstrates the fragmentation of the random copolymer with 50 mol per cent propylene. It is obvious that the concentration of the longer ethylene segments is drastically diminished, especially beyond C_{12}. From the propylene sequences only the monomer, dimer and trimer are still present in higher concentration, but fragments arising from heterosequences appear (indicated by ringed numerals with arrows). The peak marked with ringed and arrowed 7 corresponds to 2-MC_6 and 3-MC_6, the two compounds representing E–E–P and E–P–E sequences respectively. Similarly, 8 represents the 2-MC_7 and 3-MC_7 stem from C–E–E–P and E–E–P–C sequences. Finally, at 9, the 2-MC_8 and 3-MC_8 stem from E–E–E–P and E–P–E–E sequences is shown.

The reflection of the relatively short sequences of both ethylene and propylene is evident.

Reaction gas chomatography can not only elucidate structural differences concerning the arrangement of the chemical sequences. Sequences of different configurational composition may be detected too, as shown in *Figure 12* by the pyrograms of a highly crystalline-isotactic, and an amorphous-atactic, polypropylene, respectively.

In general atactic polypropylene yields a greater variety of fragments because of its content of syndio- and hetero-tactic sequences. The respective positions of the more characteristic peaks for the two samples are marked with arrows above the base line. Significant effects are clearly visible for fragments ranging up to the nonamer.

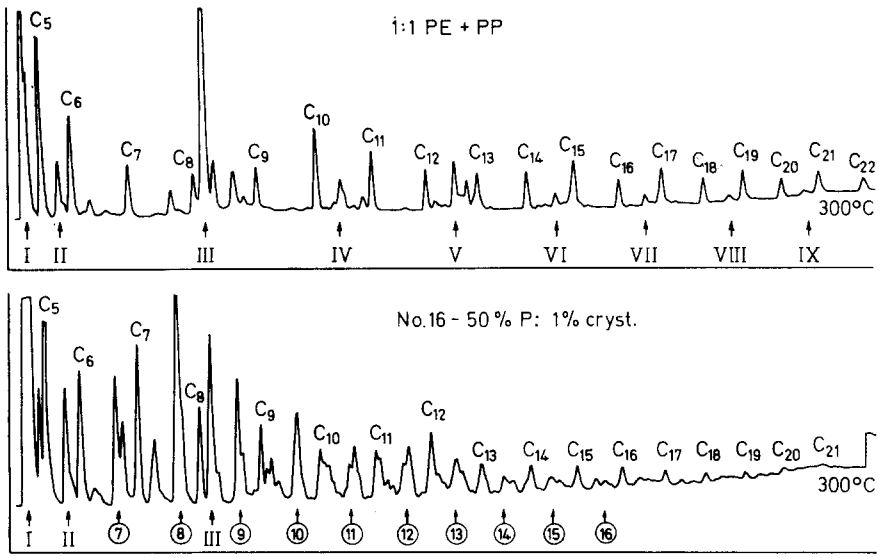

Figure 11—Pyrograms of a 1:1 physical mixture of polyethylene and polypropylene, and a random E–P copolymer with 50 mol % propylene

The reaction gas chromatography method, however, is able to discover substantially smaller structural differences such as those between a polyblend and a random E–P copolymer of the same overall composition. We have pyrolysed a great number of samples over a broad range of composition and crystallinity. The data are presented in *Table 2*. Some of these samples, which allow most distinctive conclusions, are discussed here.

First we compare the two samples 5 and 6, of identical overall composition, 23 and 24 mol per cent propylene, respectively. The mechanical

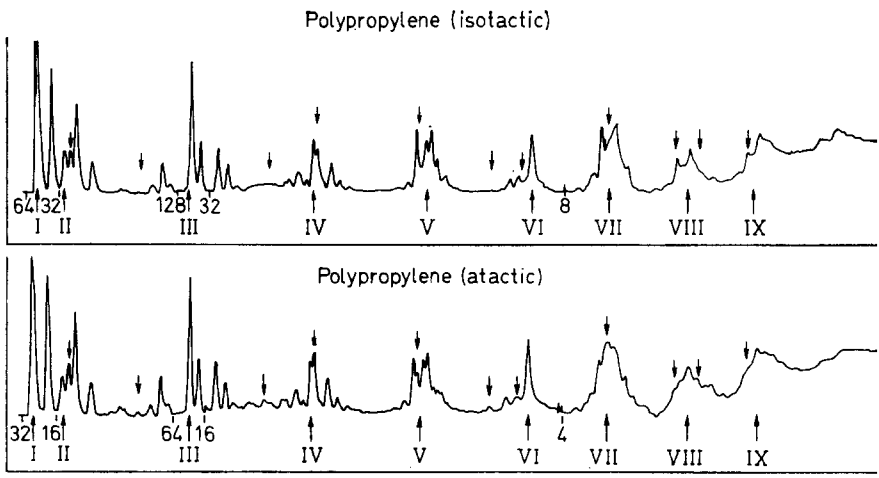

Figure 12—Pyrograms of isotactic and atactic polypropylene; pyrolysis temperature 580° C; temperature programme 40° to 310°C

Table 2. Pyrolysed ethylene–propylene copolymers

Sample No.	*Mol. % P, infra-red*[25]	*X-Ray crystallinity %*	*Sample No.*	*Mol. % P, infra-red*[25]	*X-Ray crystallinity %*
1	0·1	64	12	38	<1
2	0·2	61	13	41	0
3	1·3	57	14	43	10
4	18	41	15	50	5
5	23	4	16	50	<1
6	24	30	17	52*	0
7	30*	5	18	60*	0
8	33	<1	19	60*	0
9	34	14	20	64*	0
10	37	14	21	73*	0
11	38*	0			

*Denotes n.m.r. data. Both methods for determining the overall composition, i.e. i.r. and n.m.r., may not be free from systematic errors in analysing samples of different blockiness or of different tacticity in the propylene blocks. So, high resolution n.m.r. measurements show that part of the methylene resonance is situated in the methyl resonance region for isotactic polypropylene, giving rise to too high a propylene content in some copolymer samples. We generally preferred to use the i.r. data.

properties of these copolymers range between those of plastomers and elastomers. *Figure 13* gives their pyrograms.

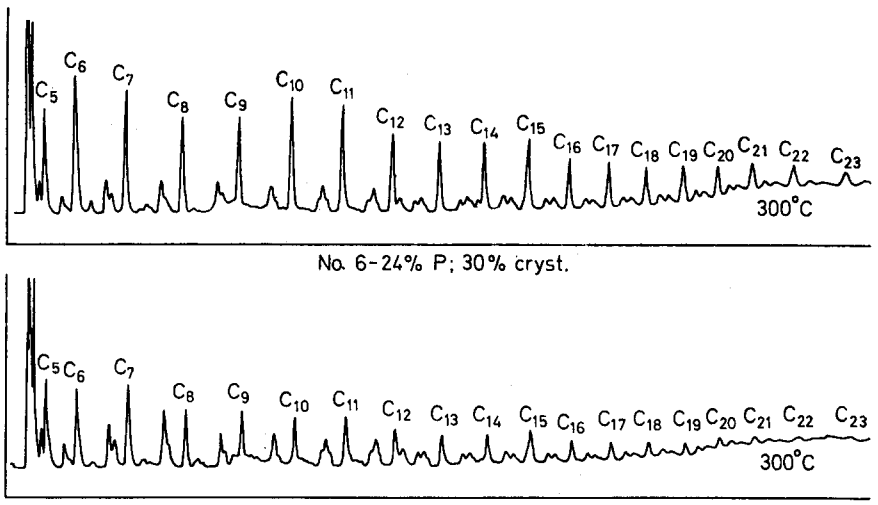

Figure 13—Pyrograms of ethylene–propylene copolymers; samples 5 and 6

There is a remarkable difference in the amount of iso-alkanes in the C_5–C_{15} region, the sample with four per cent crystallinity yielding more branched chain fragments than the one with 30 per cent crystallinity. A plot of the peak area against carbon number of the fragments obtained from the two samples is shown in *Figure 14*. Straight chain- and iso-products are plotted separately here.

The sample having more pronounced block structure yields more crystallizable straight chain hydrocarbons, starting at *n*-C_9. By contrast, the yield of iso-alkanes is lower, with a nearly constant distribution.

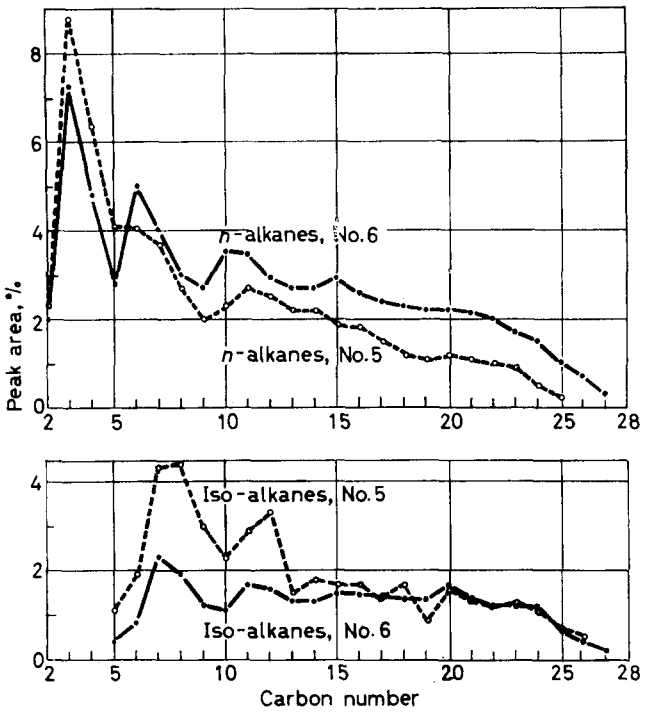

Figure 14—Distribution of the fragments from samples 5 and 6

The pronounced difference in the content of crystallizable ethylene blocks in these samples is confirmed by the X-ray diffractograms*, shown in *Figure 15.*

The higher crystallinity of the more blocky sample is evident. The 110- and 200-reflexes of the polyethylene, shifted with respect to their angular position and broadened, are clearly recognizable.

The spectrum of the more random copolymer, yielding a crystallinity of four per cent only exhibits solely a weak 110-reflex.

Analogous conclusions may be drawn from DTA measurements, which will be reported in a later paper.

Two other sample pairs, representing typical elastomers, are discussed next. These samples (Nos. 10 and 12) exhibit identical overall composition. Comparing their pyrograms in *Figure 16,* the more pronounced block structure of sample 10 is obvious.

The plot of the fragment distribution in *Figure 17* demonstrates the higher amount of longer crystallizeable ethylene sequences in sample 10 and the higher concentration of short hetero-sequences in sample 12. The respective X-ray patterns in *Figure 18* reflect these crystallinity differences. The random copolymer (8)† appears to be more or less amorphous, having

*Evaluation of the X-ray diffractograms is discussed briefly in the Appendix of this paper.
†This sample is of similar overall composition and microstructure as the sample 12 used for pyrolysis It has been used for X-ray measurement because of lack of a sufficient quantity of sample 12. For the same reason sample 12 in *Figure 20* is substituted for sample 13.

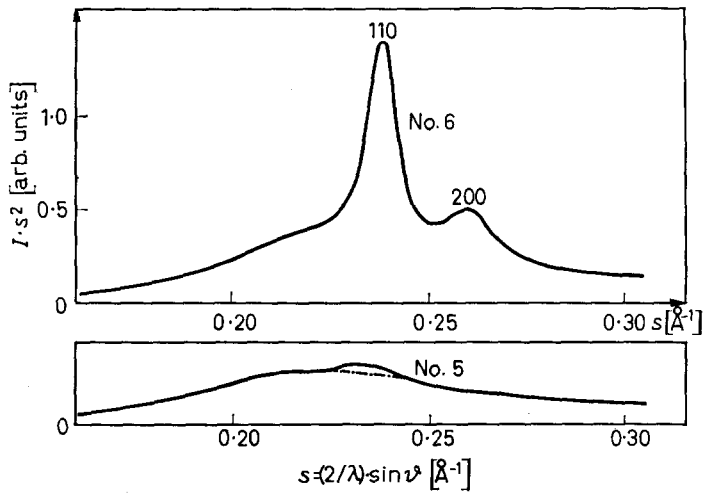

Figure 15—X-Ray diffractograms of ethylene–propylene copolymers; samples 5 and 6

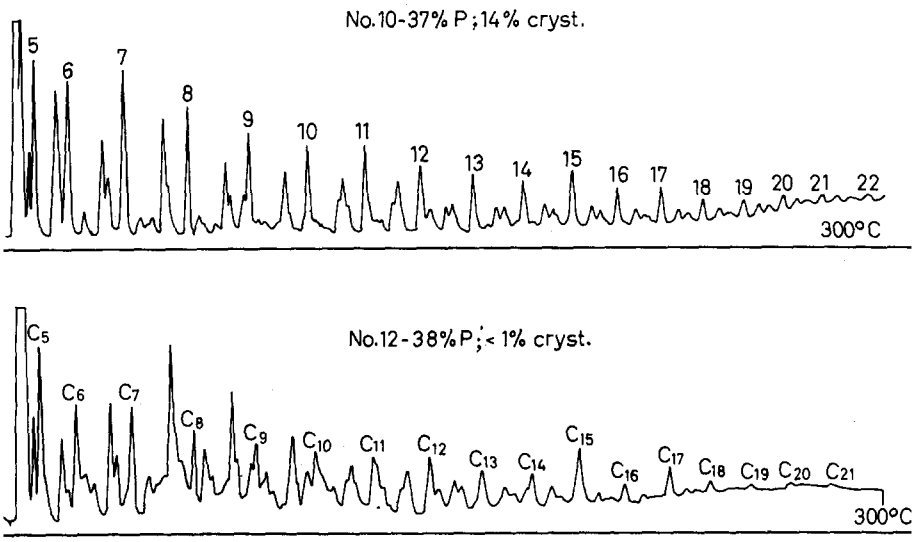

Figure 16—Pyrograms of ethylene–propylene copolymers; samples 10 and 12

less than one per cent crystallinity; the more blocky one exhibits the broadened 110- and 200-reflexes, having 14 per cent crystallinity.

With the last example to be discussed we will demonstrate that the reaction gas chromatography method facilitates structural differentation even in the amorphous region. *Figure 19* give the pyrograms of two E–P rubbers, the one (sample 12) discussed above and a second one (sample 8, 33 mol % P). Both samples are nearly amorphous, with less than one per cent crystallinity. The pyrograms and even more clearly the plot in

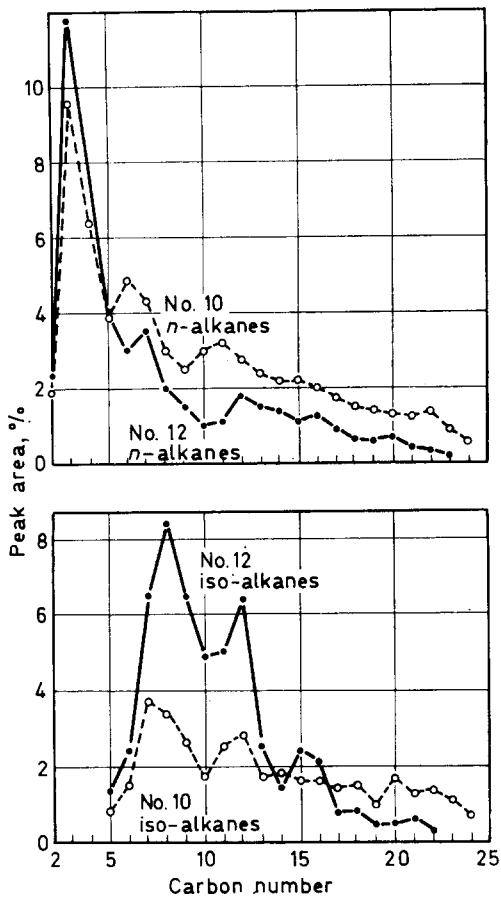

Figure 17—Distribution of the fragments from samples 10 and 12

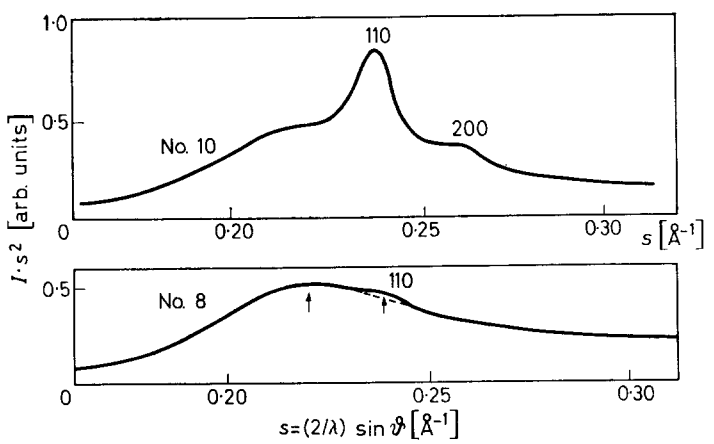

Figure 18—X-Ray diffractograms of ethylene–propylene copolymers; samples 10 and 8

Figure 20 demonstrate the difference in the content of longer ethylenic sequences.

Although the more blocky sample 8 exhibits a substantial amount (in the 20 per cent region), of potentially crystallizable sequences higher than C_{10}, practically no crystallization occurs. The randomness of their distribution may well be the reason why the crystal nuclei cannot be built up.

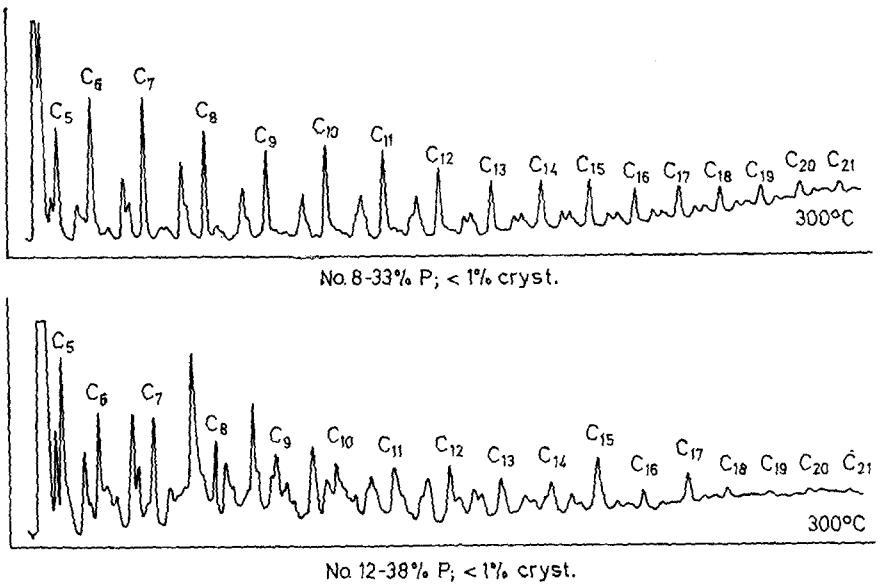

Figure 19—Pyrograms of ethylene–propylene copolymers; samples 8 and 12

Figure 21 gives the corresponding X-ray patterns, both exhibiting a nearly vanishing crystalline 110-reflex. Significant is the shift in the position of the maximum of the amorphous halo. This seems to be consistent with the differences in the 'amorphous' blockiness. Since the average van der Waals distance between the chains of the more blocky sample is less than that of the more random one, the angular position of the halo is shifted towards a higher angle as a consequence.

Finally we state, but definitely do not claim, that the distributions of the pyrolysis fragments must be identical with the sequence length distribution in the analysed copolymers. The tendency of both distributions to become identical increases with decreasing average block length. In every case, however, the pyrolysis distributions are reproducible and significant.

We are preparing now E–P copolymers under kinetically defined conditions, i.e. with the theoretically forseeable sequence length distribution. Pyrolytic investigation of them will help us to find a quantitative correlation between sequence and fragment distributions.

Further results (to be published soon) have been obtained since preparation of the manuscript by pyrolysing a series of ethylene–propylene copolymers prepared under kinetically controlled conditions. These results suggest that, for a wide range of copolymer composition, the distribution of the straight chain fragments is almost identical with the actual sequence

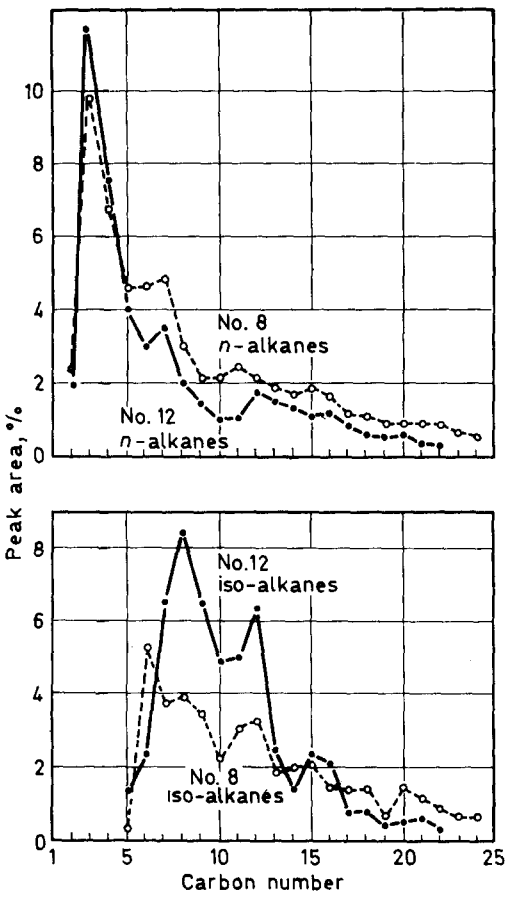

Figure 20—Distribution of the fragments from samples 8 and 12

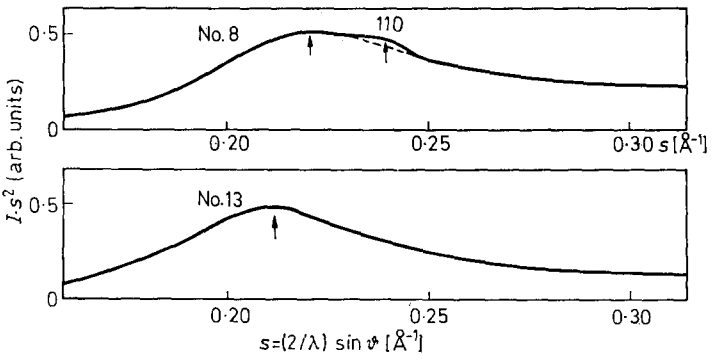

Figure 21—X-Ray diffractograms of ethylene–propylene copolymers; samples 8 and 13

length distribution of the ethylene units, as calculated on the base of the kinetic theory. The best fit has been observed in samples with relatively short sequences of the comonomeric units. A satisfactory correlation between the theoretical and the experimental values of the propylene sequence length distribution has been found in samples with nearly equimolar composition. We hope to obtain further information on the sequence length distribution and its heterogeneity by analysing labelled ethylene–propylene copolymers with the aid of appropriate analytical methods.

Thanks are due to the Deutsche Forschungsgemeinschaft and to the Fond der Chemischen Industrie for financial support for two of us. The authors thank Drs Ring, von Bassewitz, Böhm-Gössl and Frenzel from the Chemische Werke Hüls AG, Marl, for the supply of samples and compositional data, also Dr Gerrens from BASF, Ludwigshafen, Dr Kraus from Phillips Petroleum Co., Bartlesville, and Dr Groten from Esso Research, Zaventem, Bruxelles, for supply of samples. In addition the authors are grateful to Dipl.-Phys. Gronsky for n.m.r. analyses and to Mrs Groner for technical assistance.

Institut für Makromolekulare Chemie,
Lehrstuhl für physikalische Chemie der Makromolekularen Substanzen,
Universität Freiburg, Germany.

(*Received December 1967*)

APPENDIX

All measurements for the determination of crystallinity have been carried out using a Philips goniometer with Röntgen copper K_α-radiation (36 kV/20 mA). To make it monochromatic, a pulse-height discrimination technique combined with a nickel filter was used. The interval from $2\vartheta = 14°$ to 28°

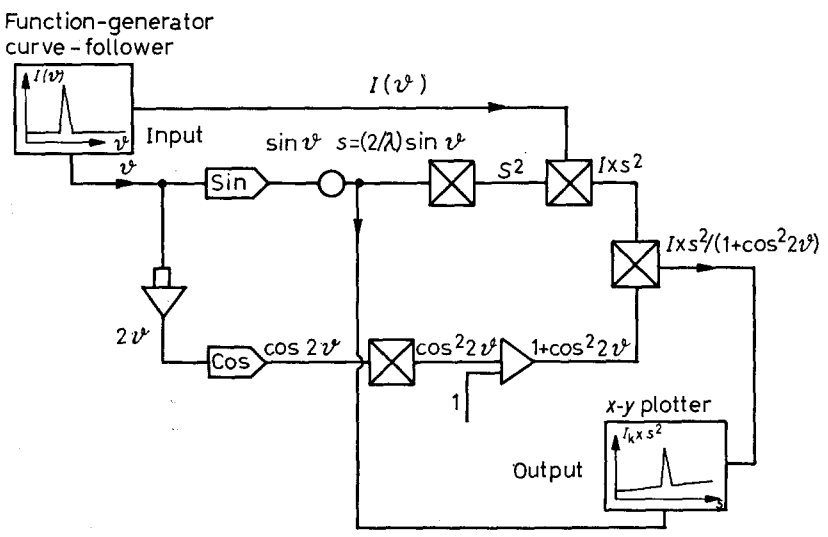

Figure 22—Block diagram of circuit for the analogue computer

was measured in steps of 0·05° counting the impulses for 40 seconds. The intensity distribution thus obtained was corrected for polarized radiation (division by $1+\cos^2 2\vartheta$ where ϑ is the angle of reflection) and multiplied by $s^2=(2/\lambda)^2\sin^2\vartheta$ ($\lambda=1{\cdot}54178$ Å, Cu K_α wavelength). In the X-ray diagrams shown above $I\times s^2$ is plotted versus s according to Ruland[26]. All these operations were carried out with an analogue computer. *Figure 22* gives the block diagram.

The experimental error in determining the angle of reflex-maxima is $2\vartheta=\pm 0{\cdot}1°$. The degree of crystallinity α has been evaluated according to Ruland[26] and Kilian[27].

$$\alpha=\int_{s_0}^{s_p} I_{cr}s^2\,\mathrm{d}s \Big/ \int_{s_0}^{s_p} Is^2\,\mathrm{d}s$$

Here I_{cr} is that part of the coherent scattering which is concentrated into the diffraction peaks, and I is the total coherent scattering of the substance.

$$s_0=0{\cdot}15\leqslant s\leqslant 0{\cdot}30=s_p$$

Result:

Sample No.	5	6	8	10	13
α	0·04	0·30	$<0{\cdot}01$	0·14	0·00

REFERENCES

[1] SHIBASAKI, Y. and KAMBE, H. *Chem. High Polymers (Japan)*, 1964, **21**, 71
[2] SHIBASAKI, Y. *Chem. High Polymers (Japan)*, 1964, **21**, 125
[3] BOMBAUGH, K. J., COOK, C. E. and CLAMPITT, B. H. *Analyt. Chem.* 1963, **35**, 1834
[4] GROTEN, B. *Analyt. Chem.* 1964, **36**, 1206
[5] VOIGT, J. *Kunststoffe*, 1964, **54**, 2
[6] VAN SCHOOTEN, J. and EVENHUIS, J. K. *Polymer, Lond.* 1965, **6**, 561
[7] WILLBOURN, A. H. *J. Polym. Sci.* 1959, **34**, 569
[8] BRYANT, W. M. D. and VOTER, R. C. *J. Amer. chem. Soc.* 1953, **75**, 6113
[9] CERNIA, E., MANCINI, C. and MONTAUDO, G. *J. Polym. Sci. B*, 1963, **1**, 371
[10] MAGROUPOV, M. A. and SLOVOCHOTOVA, N. A. *Dokl. Akad. Nauk S.S.S.R.* 1962, **146**, 826
[11] TIRPARK, G. A. *J. Polym. Sci. B*, 1965, **3**, 371
[12] TIRPARK, G. A. *J. Polym. Sci. B*, 1966, **4**, 111
[13] SHIRAYAMA, K., OKADA, T. and KITA, S. I. *J. Polym. Sci. A*, 1965, **3**, 907
[14] SIBILIA, J. P. and PATERSON, A. R. *J. Polym. Sci. C*, 1965, **8**, 41
[15] MACHI, S. J. *J. Polym. Sci. A*, 1966, **4**, 283
[16] BOYLE, D. A., SIMPSON, W. and WALDRON, J. D. *Polymer, Lond.* 1961, **2**, 323
[17] HARLEN, F., SIMPSON, W., WADDINGTON, F. B. and WALDRON, J. D. *J. Polym. Sci.* 1955, **18**, 589
[18] PETERLIN, A., KRASOVA, F., PIRKMAJER, F. and LEVSTEK, J. *Makromol. Chem.* 1960, **37**, 231
[19] ELSTON, C. T. *J. Polym. Sci. B*, 1964, **2**, 1053
[20] KOLB, B., KEMNER, G., KAISER, K. H., CIEPLINSKI, E. W. and ETTRE, L. S. *Z. anal. Chem.* 1965, **2**, 302
[21] BUCCI, G. and SIMONAZZI, T. *J. Polym. Sci. C*, 1964, **7**, 203
[22] CIAMPELLI, F. and VALVASSORI, A. *J. Polym. Sci. C*, 1967, **16**, 377
[23] NENCINI, G., GIULIANI, G. and SALVATORI, T. *J. Polym. Sci. B*, 1965, **3**, 483
[24] PORTER, R. S. *J. Polym. Sci. A-1*, 1966, **4**, 189
[25] GÖSSL, TH. *Makromol. Chem.* 1960, **42**, 1
[26] RULAND, W. *Acta cryst., Camb.* 1961, **14**, 1180
[27] KILIAN, H. G. *Kolloidzschr. u. Z. Polym.* 1962, **183**, 1

Book Review

The Stereochemistry of Macromolecules, Vol. I

Edited by A. D. KETLEY. Edward Arnold: London, 1968. 412 pp. 6¼ in. by 9¼ in. 175*s*

THIS book is the first of three volumes on this subject and is concerned exclusively with stereoregular polymers produced by Ziegler–Natta catalysts. The work is divided into six chapters each written by a separate author. The first three chapters are concerned with the general features of Ziegler–Natta catalysts and their role in producing homopolymers of the α-olefins. In the second half an account is given of copolymerization of α-olefins, the polymerization of dienes and the manufacture and commercial application of stereoregular polymers derived from α-olefins.

Despite the fact that it is now more than twelve years since the early publications of Natta, which demonstrated the wide applicability of Ziegler catalysts, the subject is still highly empirical. So much so in fact that writers on this subject find it difficult to present something more than a collection of recipes, whose formulation appears to be more a matter of art than science. It is the opinion of two of the contributors to this book (D. O. JORDON and D. F. HOEG) that fundamental disagreement exists on some of the most elementary features of the action of Ziegler–Natta catalysts. If a consensus of opinion does exist among these writers it is that the process requires only a transition metal with the appropriate ligands and the propagating species is anionic in character rather than cationic or free-radical. COSSEE'S explanation is the most favoured of the monometallic mechanisms but is recognized by many to suffer from serious defects. For example, the process is described as involving a transition from a relatively stable penta-coordinate state to an unstable hexa-coordinate state. This is contrary to experience, the compounds of Ti, V and Cr are almost exclusively hexa-coordinate whereas penta-coordinate compounds are rare indeed; we would therefore expect the latter to be the last stable.

The book is well written but some of the references quoted are a little old. For example D. F. HOEG does not mention the recent independent publications of Schindler, Vesely and Natta which appear to indicate that the order with respect to monomer is greater than unity. The cost of the book means that only libraries will buy it.

D. G. H. BALLARD

The Addition Stage in the Melamine–Formaldehyde Reaction: Computer Fittings to the Non-random Model

J. W. ALDERSLEY*, M. GORDON†, A. HALLIWELL and T. WILSON‡

The addition stage in the reaction between melamine and formaldehyde consists of the conversion of melamine into nine different methylol melamines (some of them isomers), ranging from mono- to hexa-methylol melamine. The kinetics and equilibria of this reaction are re-investigated in detail. The reaction is followed by titration of free formaldehyde as a function of time. The results agree with a simple model, as attested by comparison with computer integrations of eleven simultaneous differential equations derived from the model. This postulates that the rates of addition to, or removal from, a given nitrogen of a molecule of formaldehyde depend (a) on whether the nitrogen in question carries an additional methylol (local substitution effect) and (b) on the total number of methylols carried by the whole melamine nucleus (general substitution effect). The local substitution effect previously deduced is almost quantitatively confirmed, but the general effect is found to be so weak as to be negligible. Discussion of the kinetic results in terms of molecular mechanisms serves mostly to underline the degree of caution required.

THIS work continues a general attack[1,2] on the problems posed by the mechanism of the reaction between melamine and formaldehyde. This reaction forms the basis of resinification used on a large scale in industrial materials. The reaction can be split into an addition stage between melamine (I) and formaldehyde to form a mixture of nine methylol melamines, and a subsequent condensation stage. Parameters to describe the equilibrium and the kinetics of the addition stage have previously been measured by a combination of radio tracer techniques with chromatographic separation of equilibrium mixtures of methylol melamines[1], by analytical determinations of the amount of formaldehyde remaining at equilibrium[2], and by comparison of kinetic measurements with a first approximation treatment of the rate equation. It was pointed out[2] that more precise kinetic work could be based on computer integrations of the rate equations, and these are now presented.

THEORY

Two structurally different substitution effects were introduced earlier[1,2], a local effect confined to a single amino group and a general effect over the three amino groups of a given melamine nucleus (I). The latter effect was earlier found to be of marginal significance, and the present work shows that it makes at most a negligible contribution. Both effects represent small deviations from randomness of addition when expressed in terms of free energy increments (< 400 cal/mole). We continue, therefore, to postulate

*Present address: Ciba (A.R.L.) Ltd, Duxford, Cambridge.
†Present address: University of Essex, Wivenhoe Park, Colchester, Essex.
‡Present address: Birkbys Ltd., Liversedge.

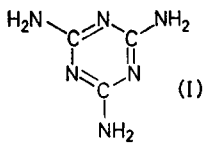
(I)

the linear form of these effects, which has the advantage that only one parameter needs to be fitted in connection with each of them.

Thus the postulated linear general effect is described by the equation

$$\Delta G_r = \Delta G^* + r\,\Delta G_g \tag{1}$$

Here $r\,\Delta G_g$ is the free-energy contribution, due to the general effect, in adding a methylol group to MF_r ($r=0, 1, \ldots 5$), i.e. a melamine already bearing r methylols. ΔG_r is the overall standard free energy change in this step, and ΔG^* is the value of this quantity in the absence of previous substitution ($r=0$), or its value for any r value if the reaction is postulated to be random ($\Delta G_g=0$).

In the presence of the local effect, equation (1) is generalized as follows

$$\Delta G_r = \Delta G^* + r\,\Delta G_g + \Delta G_l \tag{2}$$

for addition of a methylol to a nitrogen atom already bearing one methylol and belonging to a melamine already bearing a **total** of r methylols. Here ΔG_l is the increment in the standard free energy due to the local effect. If ΔG_g or ΔG_l is negative, the corresponding effect will be called positive (and vice versa). A positive substitution effect favours the production of highly substituted structures. For the random reaction $\Delta G_g=\Delta G_l=0$. N_g and N_l (previously denoted by x and y) are defined in terms of ΔG_g and ΔG_l:

$$N_g = \exp -(\Delta G_g/2RT) \tag{3}$$

$$N_l = \exp -(\Delta G_l/RT) \tag{4}$$

For the random reaction $N_g=N_l=1$. It has been shown that the equilibrium number fraction n_{ij} of melamine nuclei bearing i methylols on secondary, and j methylols on tertiary nitrogens, is given by

$$n_{ij} = \mathcal{N}\ C_{ij}\, N_g^{(i+j)^2}\, N_l^{j/2}\, q^{(i+j)}\,(1-q)^{6-i-j} \tag{5}$$

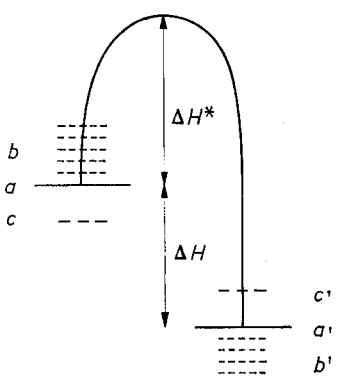

Figure 1—Schematic energy levels for addition of formaldehyde to melamine: *a* melamine level; *a'* monomethylol melamine level; ΔH^* activation energy; ΔH heat of reaction for formation of monomethylol melamine; *b* possible general substitution effect due to prior addition of from one to five formaldehyde molecules on the addition reaction; *b'* on its reverse reaction. Similarly, *c* and *c'* denote the observed local substitution effect, on which the general effect would be superposed [cf. equation (2)]

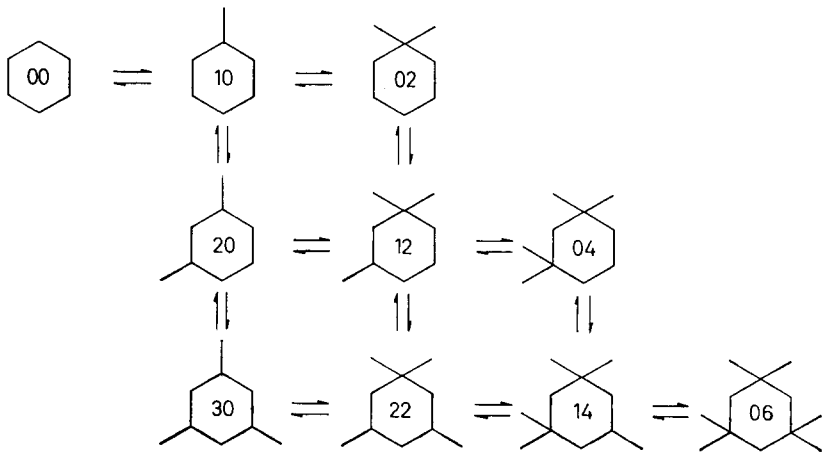

Figure 2—Scheme of all possible methylolation and demethylolation reactions, starting with melamine (top left) and ending with the formation of hexamethylol melamine (bottom right)

Here $\mathcal{N}$ is the normalizer, and q a conversion parameter determining the mean degree $\Sigma n_{ij}\ (i+j)$ of substitution at equilibrium. The basis of relating kinetic to equilibrium substitution effects is the conventional one (***Figure 1***) of splitting the standard free energy increments ΔG_g and ΔG_l **equally** between the activation free energies of the forward and backward reactions. This is found to be successful here.

This treatment implies that the forward rate constant, k_1, for adding a formaldehyde molecule to a melamine nucleus already bearing r methylols, will be multiplied by N_g^r, and further multiplied by $N_l^{1/2}$ if the addition occurs at a secondary amino group. The constant of the corresponding back reaction, k_2, will be multiplied respectively by N_g^{-r} and $N_l^{-1/2}$ [cf. equations (6) to (16)]. The scheme of the different reactions which can occur is shown in *Figure 2*. Accordingly, the following eleven kinetic rate equations together with stoichiometric conditions apply:

$$dC_{00}/dt = k_2C_{10} - 6k_1C_{00}F \tag{6}$$

$$dC_{10}/dt = 6k_1C_{00}F + 2k_2C_{20}N_{ij}^{-1} + 2k_2C_{02}N_{ij}^{-1}N_{il}^{-1/2} - k_2C_{10} - 4k_1C_{10}FN_{ij} - k_1C_{10}FN_gN_l^{1/2} \tag{7}$$

$$dC_{20}/dt = 4k_1C_{10}FN_{ij} + 3k_2C_{30}N_g^{-2} + 2k_2C_{12}N_g^{-2}N_l^{-1/2} - 2k_2C_{20}N_{ij}^{-1} - 2k_1C_{20}FN_{ij}^2 - 2k_1C_{20}FN^2N_l^{1/2} \tag{8}$$

$$dC_{30}/dt = 2k_1C_{20}FN_g^2 + 2k_2C_{22}N_g^{-2}N_l^{-1/2} - 3k_2C_{30}N_g^{-2} - 3k_1C_{30}FN_{il}^3N_l^{1/2} \tag{9}$$

$$dC_{02}/dt = k_1C_{10}FN_gN_l^{1/2} + k_2C_{12}N_{ij}^{-2} - 2k_2C_{02}N_{ij}^{-1}N_l^{-1/2} - 4k_1C_{02}FN_{il}^2 \tag{10}$$

$$dC_{12}/dt = 2k_1C_{20}FN_g^2N_l^{1/2-} + 4k_1C_{02}FN_g^2 + 2k_2C_{22}N_g^{-3} + 4k_2 C_{04}N_g^{-3}N_l^{-1/2} - 2k_2C_{12}N_g^{-2}N_l^{-1/2} - k_2C_{12}N_g^{-2} - 2k_1 C_{12}FN_g^3 - k_1C_{12}FN_g^3N_l^{1/2} \quad (11)$$

$$dC_{22}/dt = 3k_1C_{30}FN_g^3N_l^{1/2} + 2k_1C_{12}FN_g^3 + 4k_2C_{14}N_g^{-4}N_l^{-1/2} - 2k_2 C_{22}N_g^{-3}N_l^{-1/2} - 2k_2C_{22}N_g^{-3} - 2k_1C_{22}FN_g^4N_l^{1/2} \quad (12)$$

$$dC_{04}/dt = k_1C_{13}FN_g^3N_l^{1/2} + k_2C_{14}N_g^{-4} - 4k_2C_{04}N_g^{-3}N_l^{-1/2} - 2k_1C_{04}FN_g^4 \quad (13)$$

$$dC_{14}/dt = 2k_1C_{22}FN_g^4N_l^{1/2} + 2k_1C_{04}FN_g^4 + 6k_2C_{06}N_g^{-5}N_l^{-1/2} - 4k_2C_{14}N_g^{-4}N_l^{-1/2} - k_2C_{14}N_g^{-4} - k_1C_{14}FN_g^5N_l^{1/2} \quad (14)$$

$$dC_{06}/dt = k_1C_{14}FN_g^5N_l^{1/2} - 6k_2C_{06}N_g^{-5}N_l^{-1/2} \quad (15)$$

$$dF/dt = k_2[C_{10} + 2C_{20}N_g^{-1} + 2C_{02}N_g^{-1}N_l^{-1/2} + 3C_{30}N_g^{-2} + 2C_{12} N_g^{-2}N_l^{-1/2} + 2C_{22}N_g^{-3}N_l^{-1/2} + C_{12}N_g^{-2} + 2C_{22}N_g^{-3} + 4C_{04}N_g^{-3} N_l^{-1/2} + 4C_{14}N_g^{-4}N_l^{-1/2} + C_{14}N_g^{-4} + 6C_{06}N_g^{-5}N_l^{-1/2}] - k_1F[6C_{00} + 4C_{10}N_g + C_{10}N_gN_l^{1/2} + 2C_{20}N_g^2 + 2C_{20}N_g^2 N_l^{1/2} + 3C_{30}N_g^3N_l^{1/2} + 4C_{02}N_g^2 + 2C_{12}N_g^3 + C_{12}N_g^3N_l^{1/2} + 2C_{22}N_g^4N_l^{1/2} + 2C_{04}N_g^4 + C_{14}N_g^5N_l^{1/2}] \quad (16)$$

Equation (16) can be replaced by a stoichiometric equation in integrated form

$$F = F_0 - [\sum_{i=0}^{i=3} \sum_{j/2=0}^{j/2=3} (i+j)C_{ij}];\ 0 \leqslant 2i+j \leqslant 6 \quad (17)$$

The initial conditions are:

$$t = 0;\ C_{00} = 0{\cdot}055 \text{ mole/litre},\ F = F_0 = 0{\cdot}055R \text{ mole/litre} \quad (18)$$

and

$$C_{10} = C_{20} = C_{30} = C_{02} = C_{12} = C_{22} = C_{04} = C_{14} = C_{06} = 0 \quad (19)$$

Equation (6) shows that k_1 is the (forward) rate constant of forming monomethylol melamine from melamine and formaldehyde (with units l. mole^{-1} h^{-1}), and k_2 the (backward) rate constant for splitting monomethylol melamine (with units h^{-1}). F is the formaldehyde concentration in mole/l. and C_{00} the concentration of unsubstituted melamine in mole/l.; their initial ratio is

$$R = F(0)/C_{00}(0) \quad (20)$$

Throughout this work C_{00} was chosen to be 0·055 mole/l.

EXPERIMENTAL

Materials

The melamine was the British Oxygen Co. grade S (purity $> 0{\cdot}997$), while supplies of analytical reagent grade formaldehyde solution were obtained from British Drug Houses Ltd and from Hopkins and Williams Ltd. The pH was measured on a Pye Universal pH meter.

Reaction procedure

Aqueous melamine (0·055 mole/l.) was mixed with aqueous formaldehyde to produce ratios R of their concentrations in the range from 0·25 to 15. The total volume of solution was *ca.* 450 ml; the pH of the melamine solution was adjusted to 9·5 at 45°C before mixing with the formaldehyde, using either sodium carbonate or sodium hydroxide solution. The reaction was carried out in a closed glass vessel at 45·00° ± 0·05°C with mechanical stirring. The formaldehyde concentration was titrated intermittently using a modification[2] of the iodine/sulphite method of de Jong and de Jonge[3]. The bulk formaldehyde solution was standardized by this method and also by using hydrogen peroxide, with good agreement. No change of the titre occurred over three months; the presence of some methanol in analytical reagent grade formaldehyde (added as a stabilizer) is known not to affect the addition reaction with melamine in dilute solution. The iodine solution was standardized with sodium thiosulphate during each kinetic run. To minimize effects due to losses of small amounts of formaldehyde during sampling, the equilibrium data were collected separately from the kinetic runs. Strict control of pH (to ± 0·05) was necessary for kinetic experiments, but not for determinations of equilibrium. Equilibrium was generally attained within experimental error after nine hours, but the results quoted were determined after eighteen hours. This provides a safety margin against variations in rate due to changes in pH. At high concentrations of initial formaldehyde ($R \geqslant 5$), the control of pH proved difficult and sufficiently reliable data were not obtained for kinetic analysis. For each chosen value in the range $0{\cdot}25 \leqslant R \leqslant 5$, two runs were performed, and duplicate samples were titrated at several times in the range $0 \leqslant t \leqslant 7$ h. A rough notion of the prevailing pH is obtained from the colour when phenolphthalein is added to the cooled sample during the titration of the formaldehyde, but the pH was checked at least two hours after the beginning of each run.

Measurements of the equilibrium constant

For each value of F_e, the value of the equilibrium constant K was calculated first on the assumption of the classical random model, using the equation[2]

$$[(6/R) - 1 + F_e/F_0] - K\,(1/F_e - 1/F_0) = 0 \tag{21}$$

A plot of K against R should of course give a **horizontal** line if the random model applied exactly. It is seen in *Figure 3* that, instead, a curve is obtained. Inasmuch as the deviations from the random reaction are expected to vanish asymptotically at low R, a value of the real K can be obtained by extrapolation to $R = 0$. This follows because, asymptotically, nuclei with more than one methylol substituent can be neglected, and equation (1) shows that

$$\Delta G_0 = \Delta G^* \tag{22}$$

with a similar relation for the corresponding equilibrium constants. The following quantitative argument shows that for the range of measurements here presented, the extrapolated value of K should be reliable within experimental error. The monotonic increase of K with R in *Figure 3* signifies

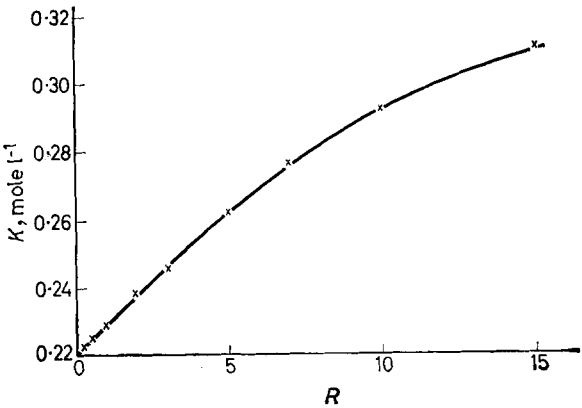

Figure 3—Plot of the equilibrium constant K against the ratio R of initial formaldehyde to melamine concentrations. (Curve: optimum fit of equation (21), using $K=0{\cdot}2209$ mole l^{-1}; $N_g=1{\cdot}00$; $N_l=0{\cdot}60_7$

that there is increasing deactivation with successive substitution of melamine nuclei with methylol groups. This agrees with previous findings using different techniques. The curve shown in *Figure 3* is about the optimum fit to the experimental points plotted. The curve was obtained from equation (21) with values of F_e calculated using the parameters: $K=0{\cdot}2209$ mole l^{-1}, $N_g=1{\cdot}00$; $N_l=0{\cdot}60_7$. More detailed information is given in *Table 1*.

Table 1. Comparison of theoretical and experimental values of F_e, the equilibrium concentration of formaldehyde (mole litre$^{-1}\times 10^2$)

R	n	F_e (exp.) (*this work*)	F_e (exp.) (*previous work*[2])	$\sigma\times 10^4$	(a)	(b)	(c)
0·25	4	0·563	—	0·410	0·5628	0·5636	0·5648
0·50	4	1·148	1·18	0·255	1·149	1·150	1·152
1	8	2·39	2·47	0·310	2·390	2·390	2·392
2	4	5·15	—	1·30	5·145	5·141	5·141
3	4	8·23	8·12*	1·50	8·246	8·239	8·236
5	4	15·33	15·65	4·74	15·35	15·34	15·34
7	16	23·41	24·40	9·20	23·39	23·38	23·39
10	12	36·66	37·90	10·5	36·65	36·66	36·67
15	12	60·66	61·51	24·8	60·66	60·68	60·70

n denotes number of experimental points.
σ is the standard deviation of these points about their mean
* In this experiment $R=2{\cdot}91_6$.

The parameters used in the three sets of calculations together with the coefficient of variation calculated from the experimental results appear

Table 2. Optimum values of the three parameters K, N_g and N_l and the coefficient of variation σ

	K (mole/l.)	N_g	N_l	σ
(a)	0·2208	1·00	0·607	0·110
(b)	0·2216	1·011	0·548	0·100
(c)	0·2226	1·02	0·504	0·136

in *Table 2*. The coefficients of variation in *Table 2* were calculated from the formula

$$\sigma = 100\left[\left\{\sum_{n}\left[\{F_e\,(\text{exp.}) - F_e\,(\text{theor.})\}/(F_0 - F_e)\right]^2\right\}\frac{1}{n}\right]^{1/2} \qquad (23)$$

where $n=9$, the number of values of R used. The series of F_e (theor.) was calculated using various values of the parameters N_g, N_l and K, in order to locate the absolute minimum of σ. Three families of contour lines in the vicinity of the absolute minimum are plotted in *Figure 4*. Here σ is plotted against $N_l^{1/2}$; in each family N_g is constant and K varies as a parameter. More detailed computer explorations for the simpler case $N_g=1$ (absence of general substitution effect) were undertaken, since it is apparent from *Figure 4* that the absolute minimum of σ (optimum fit) lies so close to $N_g=1{\cdot}00$ as to render the assumption of a general substitution effect somewhat doubtful. The required test for sensitivity of K to errors is obtained for the random reaction by differentiating equation (21).

$$\partial K/\partial F_e = 6/R\,(1 - F_e/F_0)^2 - 1 \simeq \Delta K/\Delta F_e \qquad (24)$$

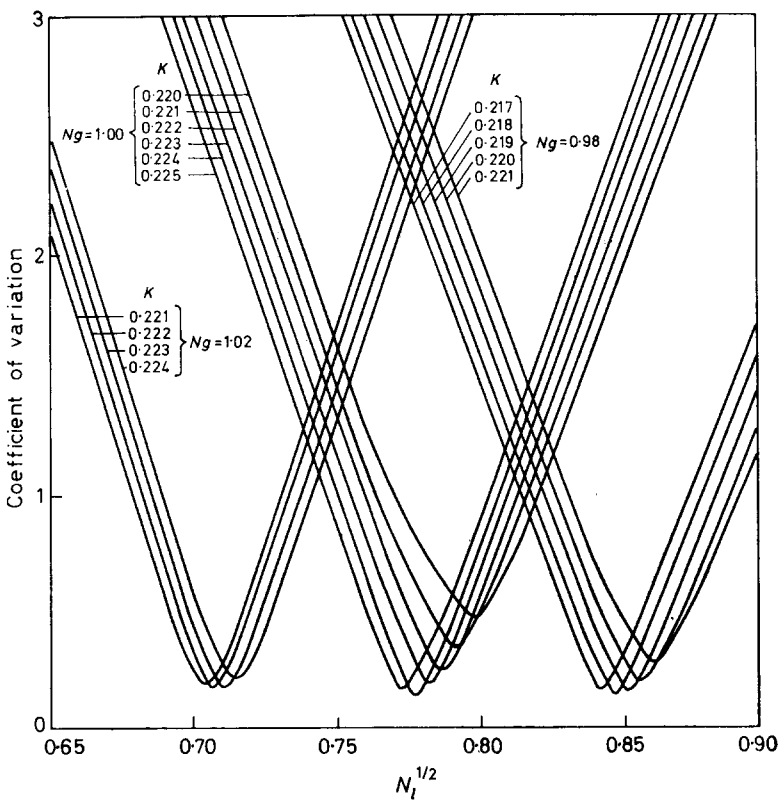

Figure 4—The behaviour of the coefficient of variation [equation (23)] as a function of K, N_g and N_l

From the computed results and equation (24) small changes in ΔK caused by small relative changes in ΔF_e and $\Delta(F_0 - F_e)$ were calculated (*Table 3*).

Table 3. Values of ΔK (mole/l. $\times 10^4$) when (a) $\Delta F_e/F_e = 0{\cdot}001$ and (b) $\Delta(F_0 - F_e)/(F_0 - F_e) = 0{\cdot}001$. The first value in each set is that calculated for the random reaction from equation (23) using the experimental data. The second value is found from the theoretical calculations, using the parameters $K = 0{\cdot}2208$ (mole/l.), $N_g = 1$ and $N_l = 0{\cdot}607$

R	a (1)	a (2)	b (1)	b (2)
0·25	3·82	3·75	5·51	5·41
1	4·25	4·19	5·53	5·45
5	7·86	7·21	6·24	5·72
15	28·56	22·47	10·28	8 09

The table shows that K is relatively insensitive to changes in F_e at low values of R and this means the value of K, obtained by graphical extrapolation, should be a good approximation. This value of $K = 0{\cdot}221 \pm 0{\cdot}001$ (mole/l.) obtained by extrapolation (*Figure 3*) so as to eliminate effects due to N_g and N_l, agrees excellently with the independent computer optimization (*Table 2*) of all three parameters together over the whole range of concentration ratios R.

Measurements of kinetic parameters

Computer calculations were performed to optimize the fit of the four rate curves together (*Figures 5* to *8*), i.e. for mole ratios $R = 1, 2, 3, 5$ for initial formaldehyde to melamine, to the set of differential equations (6) to (16) through adjustment of the parameters K (equilibrium constant), N_g (general substitution effect parameter), N_l (localized substitution effect parameter)

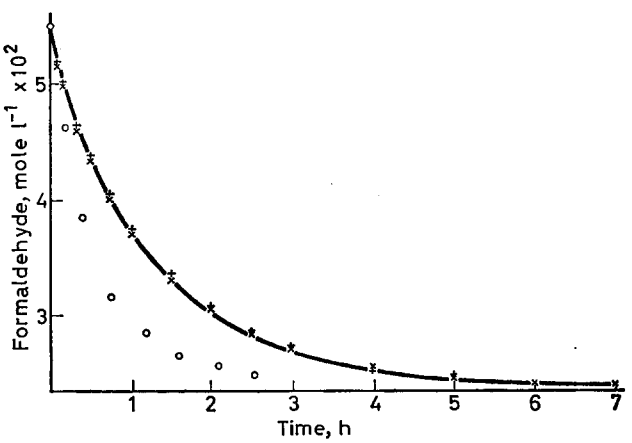

Figure 5—Kinetic rate curve (calculated) with experimental points + and × from two runs; ● experimental points of ref. 2, $R = 1$

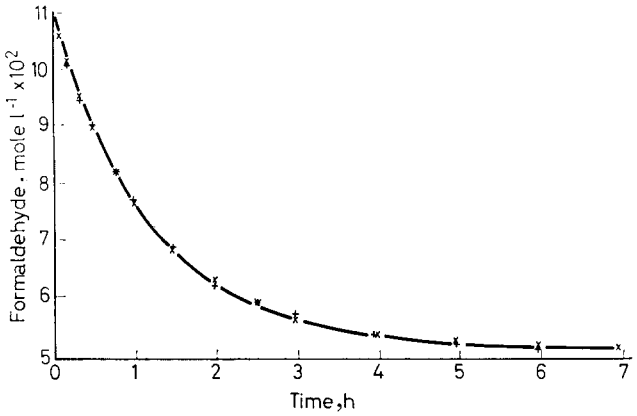

Figure 6—Kinetic rate curve (calculated) with experimental points + and × from two runs. $R=2$

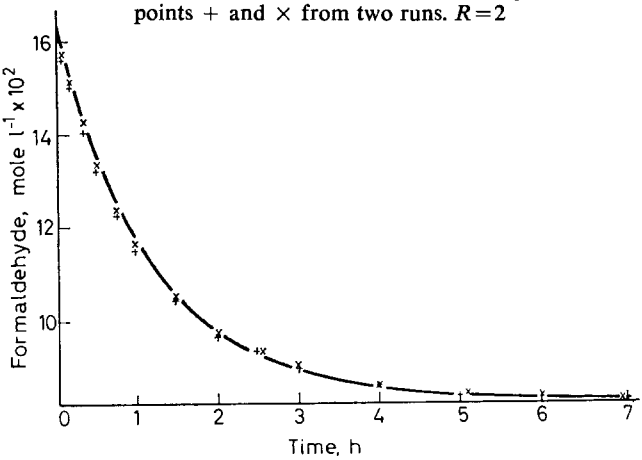

Figure 7—Kinetic rate curve (calculated) with experimental points + and × from two runs. $R=3$

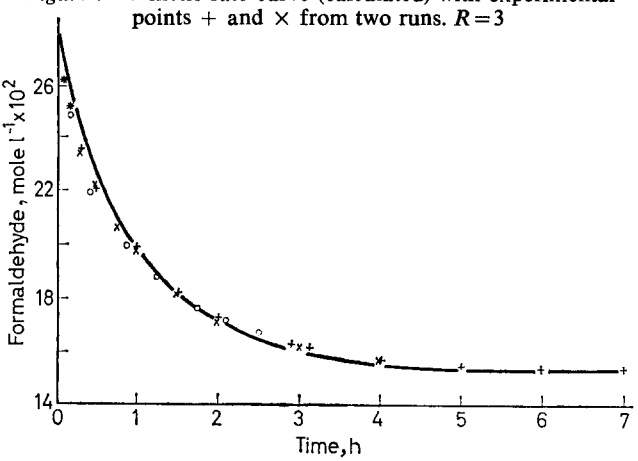

Figure 8—Kinetic rate curves (calculated) with experimental points + and × from two runs. ⊙ experimental points of ref. 2, $R=5$

and, last but most important, the forward rate constant k_1. Indeed, as regards K, N_g and N_l, it was sufficient to test the following two sets of values (see *Table 2*):

Set I $K=0{\cdot}2208$ (mole/l.) $N_g=1{\cdot}00$, $N_l=0{\cdot}607$
Set II $K=0{\cdot}2216$ (mole/l.) $N_g=1{\cdot}011$, $N_l=0{\cdot}548$

which were suggested by the analysis of equilibrium data alone (see *Table 1*) since the agreement achieved with these values cannot be expected to be significantly bettered. The criterion of goodness of fit adopted was again the coefficient of variation here calculated for 23 points from each rate curve (i.e. the deviation of the calculated value from a point read from the smoothed experimental curve). Optimum values of k_1 were found for each run separately, and also for the combined set of four runs. The results are shown in *Tables 4* and *5*. *Figures 5* to *8* show the actual experimental points

Table 4. Optimum values of the rate constants k_1 and k_2 using the parameters of set I

R	Optimum k_1 (l mole^{-1} h^{-1})	k_2 (h^{-1})	σ
1	1·426	0·3149	0·563
2	1·438	0·3175	0·457
3	1·442	0·3184	0·483
5	1·412	0·3118	0·789
Combined	1·430	0·3157	0·613

Table 5. Optimum values of the rate constants k_1 and k_2 using the parameters of set II

R	Optimum k_1 (l mole^{-1} h^{-1})	k_2 (h^{-1})	σ
1	1·426	0·3160	0·555
2	1·436	0·3182	0·471
3	1·440	0·3191	0·499
5	1·410	0·3125	0·805
Combined	1·428	0·3164	0·623

(as distinct from smoothed values) against the four rate curves calculated from the differential equations with **one** optimum set of parameters, viz. set I above plus $k_1=1{\cdot}430$ 1. mole^{-1} h^{-1}. The coefficients of variation (*Table* 6)

Table 6. Coefficients of variation σ of duplicate kinetic runs

R	1	2	3	5
σ	1·12; 1·53:	1·11*; 0·91:	2·35; 1·30:	2·11; 2·31
pH	$9{\cdot}5_0$; $9{\cdot}5_0$:	$9{\cdot}5_2$; $9{\cdot}4_9$:	$9{\cdot}5_5$; $9{\cdot}5_3$:	$9{\cdot}5_4$; $9{\cdot}5_5$
Time of pH measurements (h)	3·5; 4·25:	2·5; 3·5:	3·0; 3·0:	2·0; 5·0

*The pH in this run was adjusted with sodium carbonate solution, and in the remainder with sodium hydroxide solution.

calculated from equation (25) are of the order of one to three per cent of the total consumption of formaldehyde, which is acceptable in view of the limits imposed by the attainable experimental accuracy. If the experimental scatter is eliminated by graphical smoothing, the coefficient of variation from the calculated results is reduced to 0·6 per cent (last entry in *Table 4*), and this represents the final irreducible deviation of the experiments from the theory. The formula used was

$$\sigma = 100 \left[\{\Sigma[\{F(\text{exp.}) - F(\text{theor.})\} / F(F_0 - F_e)]^2\} \frac{1}{n} \right]^{1/2} \qquad (25)$$

where $n = 23$, the number of points taken from each curve.

Figures 5 to *8* show, in addition to the experimental results of the present work, the results of the previous investigation by Gordon, Halliwell and Wilson[2]. These are in good absolute agreement for *Figure 8*, but there is considerable deviation in *Figure 5*. (This is probably due to the abnormally high value of k_1 for $R = 1$, in the previous work, possibly due to pH variations, as shown in *Table 8* of ref. 2.)

DISCUSSION

Because of the complexity of resin chemistry involving formaldehyde, quantitative interpretations of mechanism of reactions in this field are difficult. In urea–formaldehyde, progress has depended largely on the successful isolation of various early intermediates, and literature values of kinetic and thermodynamic parameters have been analysed[4] in terms similar to the present work on melamine–formaldehyde. In the latter system, derivatives are unstable in solution, but have at least been separated by paper chromatography[1,5]. The problem here is to separate the competing reaction steps as far as possible by choice of reaction conditions, to test the experimental reproducibility of all measurements, and of all parameters, by using independent methods of evaluating them.

The fact that the addition reaction can be separated almost quantitatively from the subsequent condensation stage[2] is well confirmed by the sharpness with which the kinetic curves level off (*Figures 5* to *8*). The experimental reproducibility is satisfactory, as is shown by comparing the data of Gordon, Halliwell and Wilson[2] with present measurements in *Table 1* and *Figures 5* to *8*. Some of these measurements were carried out in two different laboratories with different batches of reagents.

It is necessary to compare the present measurements of the parameters K, N_g and N_l with earlier, somewhat less precise measurements. The present values of the equilibrium constant (at 45°C, pH = 9·5), namely (a) $K = 0{\cdot}221 \pm 0{\cdot}001$ mole $l.^{-1}$ by extrapolation (*Figure 3*) or (b) 0·2216 mole $l.^{-1}$ for the optimum fit (*Table 2*) of the three parameters to the same data without extrapolation, or (c) 0·2208 mole $l.^{-1}$ for the optimum fit (*Table 2*) of the two-parameter model to the same data (putting $N_g = 1$), lie close to the average of two estimates obtained previously from less extensive data[2] on the random model (viz. 0·237 mole $l.^{-1}$). The parameters N_g and N_l, previously[1,2] called x and y, require some amendment in the light of the present work. It was stated earlier that the general substitution effect was

slight and positive, i.e. there was a progressive increase in reactivity for further addition of methylols to a given nucleus of melamine for each methylol already carried by the nucleus (up to the total possible number of six methylols). This was expressed by N_g being slightly larger than unity; the value of $N_g = 1{\cdot}125$ was adopted for fitting the radioactive tracer data on the chromatographic distribution of the nine possible methylol melamines, but no confidence limits could be suggested for this particular small deviation from randomness. The optimum fit in the present work gives (*Table 2*) $N_g = 1{\cdot}011$; clearly this reduces the effect so much further, that it is more sensible, as well as simpler, to fit the data assuming the general effect to be absent ($N_g = 1$). In fitting any data, the two values of N_g and N_l are correlated (*Table 2*) so that a change in the value of one can to some extent be compensated by changing the other. The reduction in the general positive effect (N_g from 1·125 to unity) must be expected to lead to an increase in the optimum value of N_l, and this is observed. Thus N_l was previously deduced to lie in the range $0{\cdot}4 < N_l < 0{\cdot}6$ but is found, with the greater precision in the present work, to be $0{\cdot}61 \pm 0{\cdot}03$ (*Table 2*) for the model in the absence of the general effect ($N_g = 1$). According to equation (4)

$$N_l = \exp -(\Delta G_l / RT) \tag{4}$$

This represents a reduction in affinity for formaldehyde addition of 310 ± 30 cal mole^{-1} to a (R—N·CH_2OH)—H group when compared to a (R—N·H)—H group.

Mechanistic interpretation

Since the addition reaction is base-catalysed, we follow the views of Okano and Ogata[6] that a pre-equilibrium exists, in which a proton is lost from an NHR_1R_2 to produce an anion $^-NR_1R_2$, which then reacts with formaldehyde. The addition product then acquires a proton from the medium, thus neutralizing the anion (see also Ugelstad and de Jonge[7] for the addition of formaldehyde to amides). In support of the formation of an anion, we may mention the formation of potassium salts of melamine in liquid ammonia[8].

The general substitution effect

Our data on the general substitution effect could in principle be compared with ionization constants of NH_2 groups as a function of methylol substitution upon other nitrogens in the same molecule. Such comparison would relate only to the contribution of the pre-equilibrium constant to the overall reaction, and might be completely invalidated by concurrent general substitution effects on the collision between the nitrogen anion and formaldehyde. The further difficulty arises that the observed general substitution effect is so small as to be of marginal significance (see above); if there is any at all, it seems to be in the positive sense. In fact, average ionization constants of methylolated melamine are available[9,10], but these implicitly refer to mixtures of varying average methylolation. Moreover, they concern the equilibrium in which the nitrogen acts as a base by gaining a proton.

We might speculate that there exists a close correlation between the

substitution effects for equilibria in which nitrogens act as bases and acids respectively, in the sense that a weaker acid would be a stronger base. Accepting at its face value experiment 410B in Table 1 of ref. 9, a mixture of methylol melamines with an average of two methylols per melamine nucleus has an overall ionization constant (nitrogen acting as base) about an eighth of that of melamine. This alone makes it clear that the substitution effect must be substantially of the general variety (as distinct from local deactivation of a given nitrogen by a methylol carried by itself). This follows, because the majority of nuclei in the mixture will have one **unsubstituted** amino group, which, in the absence of a general deactivation around the nucleus would make a contribution to the apparent dissociation constant equal to $\frac{1}{3}$ ($> \frac{1}{8}$) of that of unsubstituted melamine. The general decrease in basicity of melamine with increasing methylolation, attested by this and other results in the Table I quoted[9], and which obeys the expected linear logarithmic plot (Fig. 4 of ref. 9) would lead to an expectation of a linear increase in acidity. This does signify, with all the reservations already made, that a positive general substitution could be due to variations in the ionization constant of the pre-equilibrium.

In urea, it is known that the general substitution effect is negative, but this is possibly due to intramolecular hydrogen bonding of the type

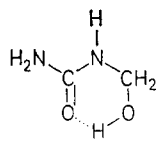

as postulated by Becher[11]. This kind of bonding is structurally impossible in melamine.

Many discussions can be found in the literature concerning the detailed mechanisms of condensation reactions between amines and formaldehyde, including speculations about the nature of reactive intermediates. The present attempt at a mechanistic interpretation, even though it is based on satisfactory verification of a quantitative model, serves only to underline the degree of caution required.

The authors wish to thank the directors of Formica Limited for permission to publish this work. One of us (J.W.A.) thanks the Science Research Council for a maintenance grant for the period during which this work was carried out.

University of Strathclyde, Department of Pure and Applied Chemistry, Thomas Graham Building, Cathedral Street, Glasgow, C.1.
Formica Research Division, Lower Cookham Road, Maidenhead, Berks.

(*Received June 1967*)

REFERENCES

[1] GORDON, M., HALLIWELL, A. and WILSON, T. *The Chemistry of Polymerization Processes, S.C.I. Monogr. No. 20*, pp 187–198. Society of Chemical Industry: London, 1966

[2] GORDON, M., HALLIWELL, A. and WILSON, T. *J. appl. Polym. Sci.* 1966, **10,** 1153
[3] DE JONG, J. I. and DE JONGE, J. *Rec. Trav. chim. Pays-Bas,* 1952, **71,** 890
[4] ALDERSLEY, J. W. and GORDON, M. To be published
[5] KOEDA, K. *J. chem. Soc. Japan* (Pure Chem. Sect.) 1954, **75,** 571
[6] OKANA, M. and OGATA, Y. *J. Amer. chem. Soc.* 1952, **74,** 5728
[7] UGELSTAD, J. and DE JONGE, J. *Rec. Trav. chim. Pays-Bas,* 1957, **76,** 919
[8] FRANKLIN, E. C. *J. Amer. chem. Soc.* 1922, **44,** 504
[9] DIXON, J. K., WOODBERRY, N. T. and COSTA, G. V. *J. Amer. chem. Soc.* 1947, **69,** 599
[10] DUDLEY, J. R. *J. Amer. chem. Soc.* 1951, **73,** 3007
[11] BECHER, H. J. *Chem. Ber.* 1956, **89,** 1951

Differential Thermal Analysis of Polyethylene in Tetrachlorethylene I—Morphological Effects on Solution Temperatures

J. L. KOENIG and A. J. CARRANO

The dissolution of polyethylene in tetrachlorethylene has been studied as a function of concentration, heating and cooling rates and different morphological structures. The solution behaviour of single crystals is compared to stirrer, melt, and high-pressure crystallized samples. Differences in fold period and crystallite size produce large changes in the solution behaviour. Annealing in solution at slow heating rates produces a multiplicity of dissolution exotherms. High heating rates cause superheating with extended chain crystals having the greatest tendency to superheat.

INITIAL investigations made by Blackadder and Schleinitz[1] indicate the feasibility of using differential thermal analysis (DTA) to study dilute polymer solutions and crystal suspensions. Using a linear polyethylene for their studies, they examined annealing and thermal history effects. The effect of concentration up to two per cent by weight on the solution temperature of the suspension was also investigated by DTA.

It is our purpose to report DTA studies of polyethylene single crystals suspended in tetrachlorethylene. This work complements the studies of Blackadder and Schleinitz[1] by extending the range of polyethylenes, heating rates, and morphologies. In addition, we wish to report a method of adapting a commercially available instrument to studies of this kind. The instrument allows the measurement of the kinetics of crystallization as well as the solution temperatures of the solute solutions. These crystallization measurements are useful in understanding differences in the solution behaviour.

EXPERIMENTAL

Apparatus

DTA serves a twofold function in this study. First, it is a method of observation, recording thermal transitions and giving peak temperatures, shapes, heights, and areas. Secondly, it is used to impart a thermal history to a polymer through the programme mode of the instrument, e.g. quenching to varying degrees by cooling, or annealing by imposing the isothermal or hold mode or using slow heating rates.

The Differential Thermal Analyzer (E. I. Du Pont de Nemours and Co.) is described in detail elsewhere[2].

Sample preparation

Commercial Marlex 6050 was the polyethylene used most extensively in this work. It is a linear polymer (containing 0·0 CH_3/1 000C) having a

weight average molecular weight of 80 000 and a number average molecular weight of 8 200. Crystalline suspensions of polyethylene were prepared by dissolving Marlex pellets in 3 l. of boiling tetrachlorethylene in a 5 l. round bottom flask (0·1% wt concentration). After 40 minutes the solution was cooled to room temperature on standing. Alathon 71 X-N pellets (containing 1·7 CH_3/1 000C) and Alathon 10 pellets (containing 22 CH_3/1 000C) were treated likewise to obtain their crystalline suspensions.

Stirrer crystallized polyethylene was prepared from Marlex 6050 as above, except that stirring was introduced with a glass stirrer (1 500 rev/min) with a Teflon fin at its end.

Concentration was varied by solvent extraction after the crystals floated to the upper regions of the separatory vessel. To obtain the 3·3% wt suspension, solvent evaporation by vacuum drying was employed in conjunction with extraction.

Three isothermally grown suspensions were prepared at 66·0°C, 71·5°C, and 73·0°C by obtaining boiling 0·1% wt concentrated solutions in the burette, and then allowing slow streams of the solutions (10 ml/min) to trickle into a crystallization chamber. The crystallization chamber was submerged in an accurately controlled ($\pm$0·2 deg. C) oil bath. A fourth isothermal suspension was prepared in this manner at 80·0°C at a 0·05% wt concentration.

An extended chain melt crystallized polyethylene sample was obtained from Mr A. Christiansen at Case Institute of Technology. The sample was Marlex 6050, crystallized at 5 000 atmospheres. Crystallization occurred as the crystallization bomb temperature decreased from 240°C to 230°C in a period of one hour and 40 minutes.

EXPERIMENTAL TECHNIQUE

For good thermal data, theory requires conduction as the mechanism of heat transfer. Only DTA of very concentrated polymer–diluent systems have been reported, where a homogeneous paste could be made from the components[3]. In the dilute concentration range, convection enters into the heat dissipation process and it has been usually assumed that lack of homogeneity would yield irreproducible results. It has been suggested that stirring can produce a homogeneous sample. Our studies of stirring indicated that only extremely high stirring rates would give a uniform thermal environment and these high rates introduced appreciable shear which was unacceptable.

Blackadder and Schleinitz[1] used single crystal suspensions in xylene which eventually settled to the bottom of the solution cell. Below 0·75 wt% polymer concentration, two phases existed—an upper solvent region and a lower suspended crystal region which formed an effectively continuous solid phase of very high porosity. At higher concentrations, the crystals apparently occupied the entire volume of the cell and gave good results.

In the present work, tetrachlorethylene is of greater density than the suspended crystals, an upper suspended phase exists at low concentrations. The result, however, is the same. Convective forces are introduced, and at higher heating rates, which apparently increase convection, detection of

solution becomes impossible. At higher concentrations (above 0·45% wt) noticeable settling of the crystals could be avoided by agitating the suspension in the sample cell. During the time of a single DTA run (ten minutes) no settling was observed. At 1·0% wt the suspensions appeared to remain in a homogeneous phase indefinitely.

Maximum sensitivity was obtained by having the thermocouple in direct contact with the solution components. This is accomplished by using the standard chromel–alumel thermocouples for the DTA, and cementing a ceramic sleeve to the ceramic insulation on the thermocouple wires immediately behind the junction point. The ceramic sleeve permits a fairly tight fit in the cell which minimizes thermocouple movement and allows location of the thermocouple in the centre of the cell. Having positioned the thermocouple in the suspension, a cement 'cap' (General Electric's RTV) is placed at the open end of the sample cell in order to ensure the stability of the thermocouple positioning, as well as to protect against evaporation of solvent or capillary creep out of the cell. The temperature of the sample is recorded on the abscissa of the thermograms to be presented.

Glass beads were used as the reference material in almost all instances. Pure solvent and silicone oil were found to give no better results when employed as reference materials. This is due to the change in thermal diffusivity which results from the dissolution process occurring in the sample cell. No reference material can adequately match the properties of the

Figure 1—Electron micrograph of slow cooled crystallized polyethylene (Marlex 6050)

sample before and after dissolution[1]. The resulting shifts in baseline for the samples investigated in this work have not been reproduced in order to focus attention better on the endo- and exo-therms themselves.

RESULTS AND DISCUSSION

Effect of concentration on the solution and recrystallization temperatures

The solution temperatures reported as peak temperatures of suspensions of Marlex 6050 single crystals (*Figure 1*) are shown in *Table 1*. Within the concentration range of 0·1 to 1·0% wt there appears to be no dependence of the initial solution temperatures on concentration, in agreement with previous workers[1]. The two heating rates (10 deg. C/min and 20 deg. C/min) gave a constant solution temperature of 84·1° ±0·6°C (*Figure 2*).

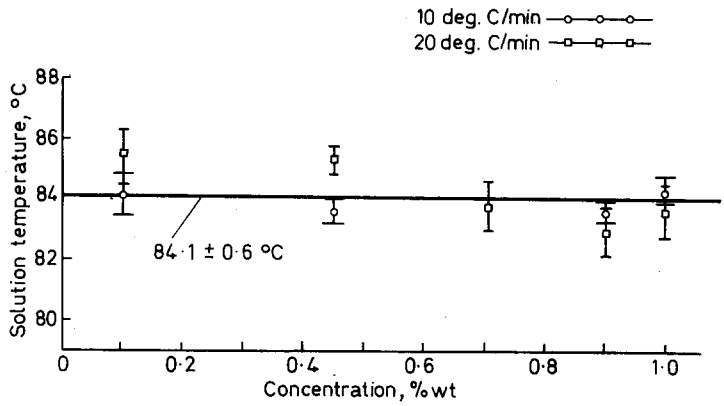

Figure 2—Solution temperature as a function of concentration

The 20 deg. C/min data showed more scatter than the 10 deg. C/min data. The standard deviation for the 20 deg. C/min data is 0·8 deg. C as compared to 0·4 deg. C for the 10 deg. C/min data. At 3·30% wt concentration, there is a 5 deg. C increase in the solution temperature over the values for the dilute range which indicates agreement with the general predicted behaviour of polymer–diluent systems.

Table 1. Effect of concentration on solution and recrystallization

Heating rate (deg. C/min)	*Concentration (% wt)*	*Solution temperature (°C)*	*Crystallization temperature (°C)*
10	0·10	84·2 ± 0·7	—
	0·45	83·6 ± 0·4	68·8 ± 0·5
	0·90	83·7 ± 0·3	70·0 ± 0·5
	1·00	84·6 ± 0·4	70·5 ± 0·7
	3·30	87·0 ± 0·5	75·0 ± 0·5
20	0·10	85·4 ± 0·9	68·3 ± 0·9
	0·45	85·3 ± 0·5	68·9 ± 0·7
	0·71	83·8 ± 0·8	68·8 ± 0·8
	0·90	83·0 ± 0·8	69·7 ± 0·8
	3·30	87·0 ± 0·5	75·0 ± 0·5

The recrystallization temperatures obtained by cooling the solutions in the DTA cell also appear in *Table 1*. The recrystallization temperatures appear to increase slightly with increasing concentration in the 0·1 to 1·0% wt range. At 3·3% wt concentration this increase is clearly evident. No recrystallization temperature could be reproducibly determined at 0·1% wt.

In dilute polymer solutions, crystallization studies have shown that the crystal growth rate at a given temperature increases with increasing concentration of the polymer[4]. Lancely and Sharples[5] postulate that the effect of concentration on the growth rate probably arises because an increase in concentration at constant temperature results in an increase in relative

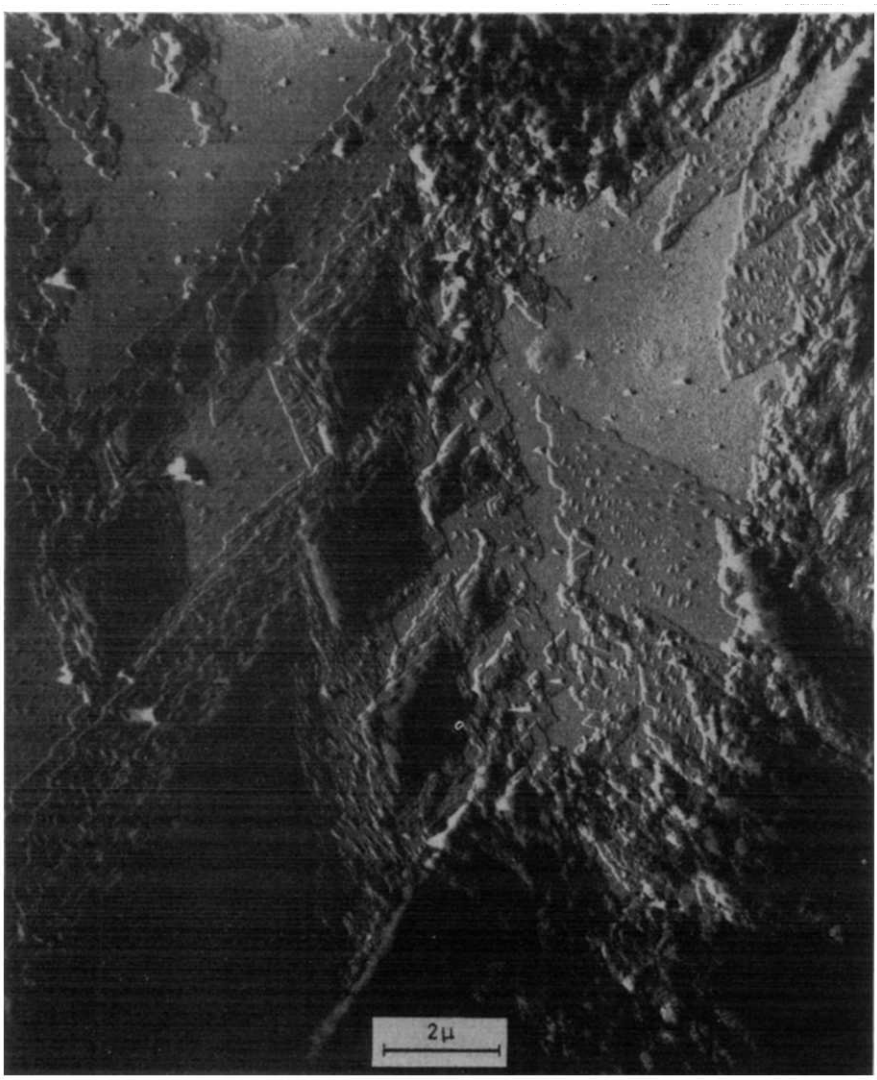

Figure 3—Electron micrograph of polyethylene crystallized in the DTA cell

degree of supercooling. Thus, the higher concentrations being subjected to the same cooling rate as the lower concentrations reach the same effective degree of supercooling at higher temperatures.

Samples crystallized in the DTA cell (*Figure 3*) are dendritic and of less perfection than the original preparation. The subsequent solution thermograms (*Table 2*) of the material crystallized in the cell show an increase in solution temperature with concentration (middle peak). Additional peaks are also observed indicating a multiplicity of dissolving species.

Effect of heating rate on the solution behaviour

In measuring the melting or solution temperature for a polymer or polymer–solvent system by DTA, one must consider the simultaneous and competitive kinetics of superheating, reorganization, and/or solution followed by recrystallization on the thermograms.

Table 2. Effect of concentration on solution following recrystallization in the DTA solution cell

Concentration (g/cm^3)	*Heating rate* (*deg. C/min*)	*Prior recrystallization temp.* (°C)	*Solution temp. (2nd cycle)*		
			Low (°C)	*Middle* (°C)	*High* (°C)
0·10	10	—	77·8 ± 0·8	81·1 ± 0·5	85·5 ± 0·6
0·45		68·8 ± 0·5	78·1 ± 0·3	81·4 ± 0·5	86·1 ± 0·2
0·90		70·0 ± 0	—	82·2 ± 0·3	86·7 ± 0·3
1·00		70·5 ± 0·7	—	82·8 ± 0·3	87·1 ± 0·3
0·10	20	—	78·5 ± 0·6	81·2 ± 0·4	84·1 ± 0·6
0·45		68·3 ± 0·9	78·3 ± 0·6	83·2 ± 0·5	
0·71		68·9 ± 0·7	—	82·4 ± 0·5	85·2 ± 0·5
0·90		68·8 ± 0·8	—	81·7 ± 0·8	—
1·00		69·7 ± 0·8	—	82·9 ± 0·4	—

Superheating occurs when the forces maintaining crystalline order are disrupted at a rate slower than the thermal forces of an imposed heating rate. Superheating shifts the melting or solution temperature to higher temperatures than would be attained under equilibrium conditions. Fibrillar or extended chain crystals have been shown to be particularly susceptible to this phenomenon[3,6]. In general, the larger and more perfect the crystals the greater is the tendency for superheating. Slow heating rates are required to minimize superheating. However, slower heating rates may produce a higher temperature of solution and melting due to material modified by heat effects (increase of crystalline perfection and/or fold period) rather than the delay of the melting or solution of the as-prepared material. The ideal situation is when the applied heating rate produces negligible superheating or alteration of the material subjected to the dynamic heating process. Wunderlich[7] refers to such a situation as the 'zero entropy production' path. Heating rates faster or slower than that producing the 'zero entropy production' path lead to superheating or 'annealing' respectively.

Crystal suspensions heated at 10 deg. C/min and 20 deg. C/min gave nearly identical endotherms (*Figure 4*) for the 0·1 to 3·3% wt concentration range (*Table 1*). Suspensions of crystals at 1·0% wt were investigated

using faster (40 deg. C/min) and slower (3 deg. C/min) heating rates. At 40 deg. C/min the solution endotherm gave a peak temperature of 84·0° ±0·7°C. This value agrees with those obtained at 10 and 20 deg. C/min. At a heating rate of three degrees per minute peak splitting was observed for the 1·0% wt suspension. The single peak observed for the three higher heating rates was still present, but there were two additional peaks, one above and one below the main endotherm (*Figure 4*).

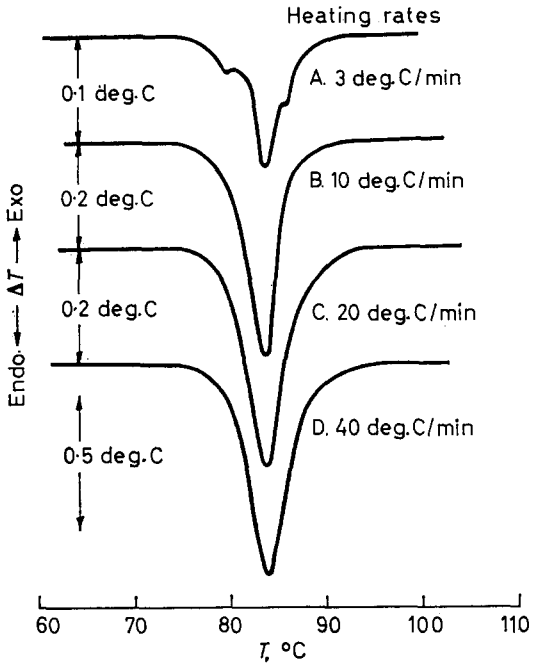

Figure 4—Effect of heating rate on the solution of slow cooled crystallized polyethylene (Marlex 6050)

The absence of the low temperature solution peak for the higher heating rates is attributed to superheating. At the higher heating rates, the material giving rise to this peak is superheated so it coincides with the main solution peak. The high temperature solution peak in the slowly heated sample is the result of 'annealing' a portion of the sample. The centre or main peak represents the solution of crystals following a 'zero entropy production' path.

An observation of similar superheatability behaviour was made on dissolving a crystalline suspension of a low molecular weight fraction of polyethylene (Celanese A50–500) at 0·5% wt. The solution behaviour at 3, 10, 20 and 40 deg. C/min is shown in *Figure 5*. The 10 deg. C/min and 20 deg. C/min heating rates produce identical thermograms; but at 40 deg. C/min superheating has occurred, selectively shifting the lower solution peak to a higher temperature, while having no influence on the higher peak. At 3 deg. C/min the higher peak was again unchanged. The shifting of the lower peak to a yet lower temperature indicates once more the superheat-

ability of the material responsible for this lower endotherm. A 5 deg. C increase in this solution peak is obtained upon increasing the heating rate from 3 to 40 deg. C/min.

In view of the earlier observations that extended chain or more perfect crystals are susceptible to superheating, it is surprising to see the superheatable fraction of a preparation dissolving on the low side of the main

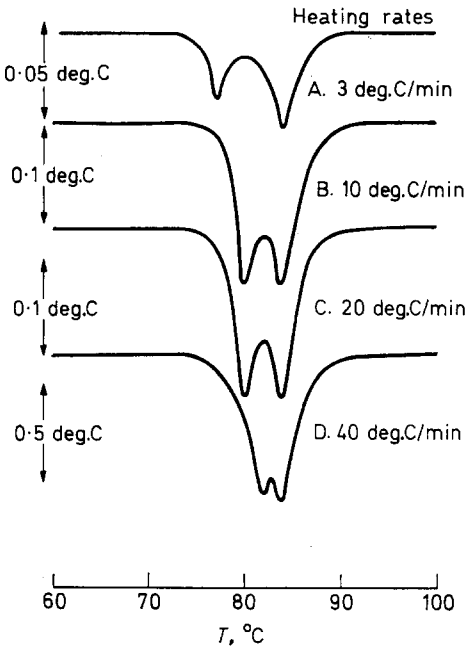

Figure 5—Effect of heating rate on solution of low molecular weight polyethylene

solution peak. One would expect to find the superheatable material dissolving on the high side of the solution peak at higher heating rates, and moving closer or eventually coinciding with the main solution peak as the heating rate is decreased. This low temperature peak exhibiting superheatability may be due to the presence of low molecular weight crystals with imperfections. The low molecular weight material may form extended chain structures giving rise to the superheatability of the peaks described here. Also, imperfections in such crystals could account for the low temperatures of dissolution. In both instances where the low peak was superheatable, low molecular weight polyethylene was present. The slow cooled crystals (Marlex 6050) have a molecular weight distribution which conceivably fractionates during crystallization[8].

Effect of crystallization temperature on the solution behaviour

Crystals grown isothermally from a given solvent have fold periods depending on the temperature of crystallization[9]. The relationship between

the fold period or crystal thickness and its solution temperature, T_s, is given in a classical treatment by Hoffman and Weeks[10]

$$T_s = T_s^0(1 - 2\sigma_e/\Delta h_f L)$$

where T_s^0 denotes solution temperature of an infinitely thick crystal in the same solvent, σ_e is the end surface free energy, Δh_f is the latent heat of fusion and L is the fold period.

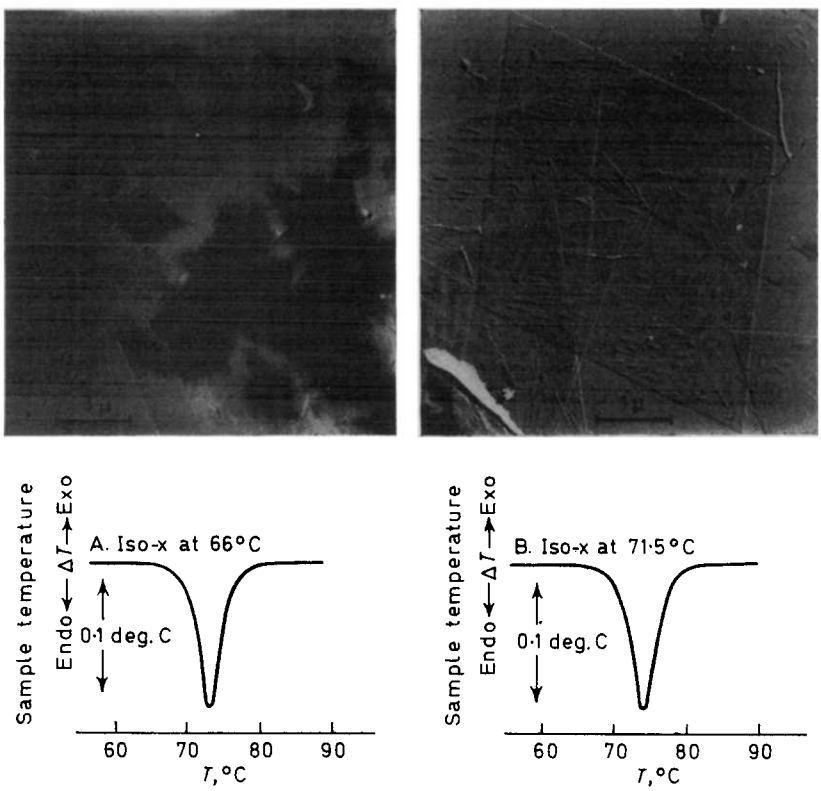

Figure 6—Electron micrographs and solution thermograms for isothermally crystallized polyethylene

The electron micrographs and solution thermograms for the isothermally prepared suspensions are shown in *Figures 6* and *7*. From the thermograms one observes that increasing the crystallization temperature produces crystals which undergo solution at progressively higher temperatures (*Table 3*). Plotting the solution temperatures versus the isothermal crystal-

Table 3. Solution temperatures for isothermally crystallized polyethylene

T_x (°C)	66·0	71·5	73·0	80·0
T_s (°C)	81·0	82·5	82·8	86·7

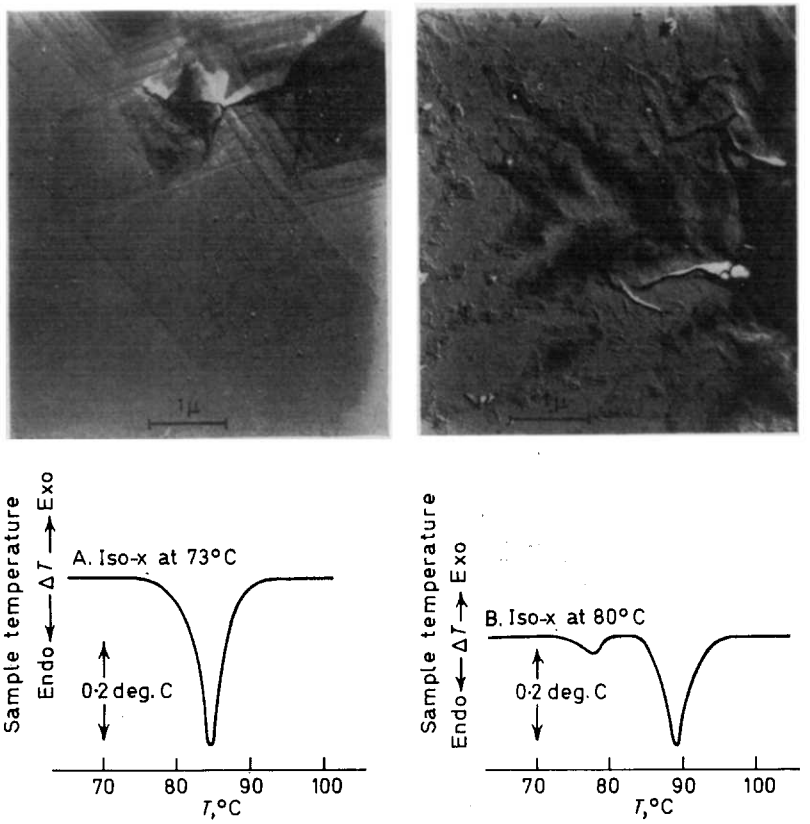

Figure 7—Electron micrographs and solution thermograms for crystallized polyethylene

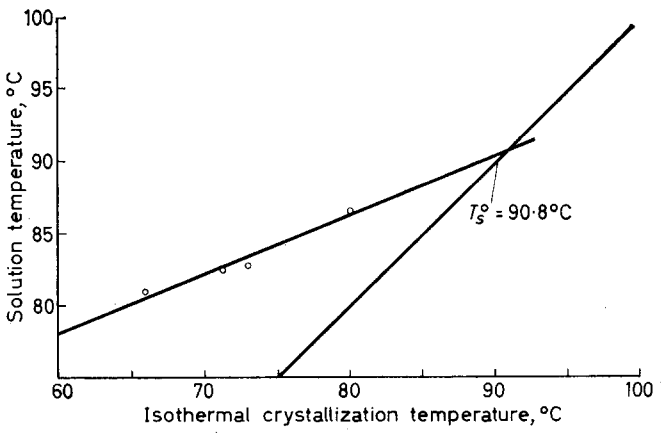

Figure 8—Solution temperature as a function of crystallization temperatures for polyethylene in tetrachlorethylene

lization temperatures of the samples produces a linear curve. The intersection of this curve with the line, $T_s = T_c$ (crystallization temperature), gives the value 90·8°C for T_s^0 in tetrachlorethylene (*Figure 8*). Holland[11] using this same approach found a value of 106°C for T_s^0 in xylene. Similarly, Blackadder and Schleinitz[1] found values of 93·1°C, 97·6°C and 108·1°C in decalin, *p*-xylene, and *n*-dodecane, respectively. The difference in these T_s^0 values is due to the difference in solvents. The surface free energies of the various crystalline preparations appear in *Table 4* along with the values

Table 4. Thermodynamic solution temperatures of polyethylene in different solvents

Solvent	Δh_f ($erg/cm^3 \times 10^9$)	T_x (°C)	T_s^0 (°K)	T_s (°K)	L ($cm \times 10^6$)	σ_e (erg/cm^2)
p-Xylene[1]	2·8	85	370·0	365·8	1·18	19
n-Dodecane[1]	2·8	100	380·8	378·7	1·44	11
Decalin[1]	2·8	80	366·0	361·2	1·14	22
Xylene[11]	2·5	80	379·0	363·0	1·20	57
Tetrachlorethylene	2·7	*	363·8	357·1	1·20	37·5

*Slow cooled crystallized polyethylene was used for this determination. The crystallization was assumed to take place isothermally in view of the slow cooling rate and the single solution endotherm obtained by DTA.

of the parameters necessary for their determination. Estimates of values for σ reported in the literature range from 20 to 180 erg/cm^2. The very low values given by Blackadder and Schleinitz (*Table 4*) may be in error. Their determinations of solution temperatures were made in their DTA solution cell using a heating rate of 2·35 deg. C/min. It is quite possible this slow heating rate produced annealing effects which led to decreasing the slopes of the T_s versus T_c plots thus producing low T_s^0 values. In the present work it was found that a heating rate of 20 deg. C/min was necessary to avoid annealing effects in the isothermally grown crystals in tetrachlorethylene. At slow heating rates, the samples crystallized at low temperatures exhibited the greater tendency to reorganize.

A small solution peak appears at 78°C in the thermogram of the crystals grown at 80°C (*Figure 7*), while no corresponding low temperature solution endotherms appear in any of the other thermograms. At the three lower crystallization temperatures, all of the detectable polymer had crystallized during the isothermal conditions. However, at 80°C a perceptible amount of polymer remains in solution, and appears to crystallize at lower temperatures as this preparation is cooled to room temperature. This portion, crystallized at lower temperatures, is responsible for the 78°C endotherm. The electron micrographs bear out this interpretation. Small crystallites can be seen as overgrowths on the 80°C sample, while such structures are absent from the lower temperature preparations.

The morphological habits for the 0·1% wt suspensions are very similar in appearance, while their solution behaviour is not. The solution behaviour depends primarily not on the morphological habit but on the fold period produced by crystallization conditions.

Different cooling rates cause crystallization to occur at different temperatures. *Figure 9* gives the crystallization thermograms for 1·0% wt suspen-

sions subjected to 3, 10 and 20 deg. C/min cooling rates. The crystallization temperature decreases from 73°C at three degrees per minute to 70°C for ten degrees per minute to 67°C for twenty degrees per minute. The

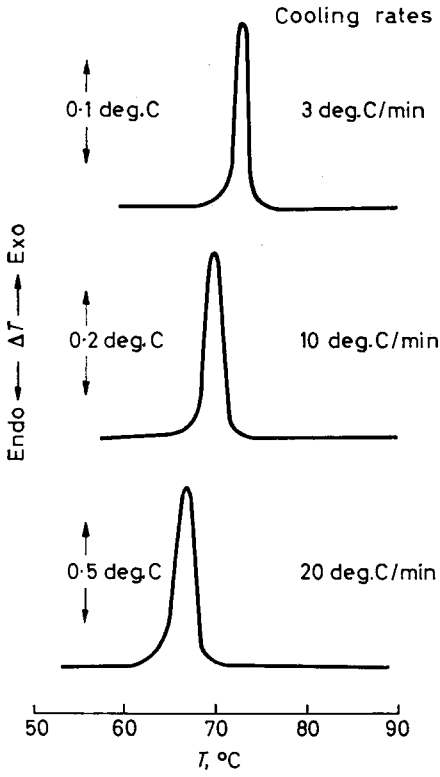

Figure 9—Effect of cooling rate on crystallization temperature

solution temperatures are 84°C, 83°C and 81·5°C, respectively, reflecting the descending order of the crystallization temperatures.

Effect of morphology on the solution behaviour

Morphology is a broad term. Included in this term are such features as: fold period, density or relative amorphous to crystalline content, crystallite size, dispersion of crystallites, structural appearance (hedrites, dendrites, etc.), or any other features which characterize the larger than molecular level of ordering in polymers. Molecular weight, solute concentration, crystallization conditions, annealing and stirring during crystallization from solution modify the morphological features.

It is well known that polyethylene will crystallize from dilute solution in the form of single crystals provided the experimental temperature of crystallization is such that the system parameters, molecular weight and concentration, affecting morphology are non-deleterious to such a habit. Agitation and rapidity of dilution (time required to attain the desired isothermal condition of crystallization) are the other experimental parameters, which

together with temperature and the system parameters determine the habit of crystallization[4].

When crystallization conditions were maintained constant except that stirring was introduced, the effect was drastically to change the morphological habit. The electron micrograph of stirrer crystallized material appears in *Figure 6*. Comparison of *Figure 10* with *Figure 1* for the non-stirred system shows very little resemblance. However, the subsequent solution thermograms for stirred and non-stirred preparations are nearly

Figure 10—Electron micrograph of smaller vessel slow cooled crystallized polyethylene (Marlex 6050)

identical. The stirrer crystallized thermogram exhibits a solution peak which is 0·5 to 1·0 deg. C higher than that for the unstirred crystals. This is due to crystallization occurring at a slightly higher temperature in the stirrer crystallized preparation than in the non-stirred preparation and/or external sample preparations.

Material adhering to the stirrer dissolved at a higher (87°C) temperature than that in suspension. The macroscopic size of the fibres of this material (*Figure 10*) probably has this effect on the solution behaviour, since drying these fibres and melting them in the DTA apparatus produced an endothermic peak at 130°C—the same melting temperature as filtered unstirred preparations (*Figure 11*). Also the return to baseline after the endothermic peaks are completed in both thermograms shows differing behaviour. The stirrer crystallized material has a melting tail while the non-stirred crystals exhibit a very sharp return to baseline. The tail of the stirrer crystallized material has been attributed by other investigators[12,6] to extended chain structures.

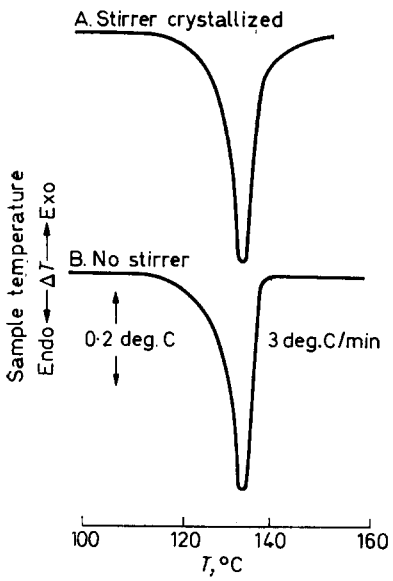

Figure 11—Melting thermograms of stirrer crystallized and slow cooled crystallized polyethylene

The morphological feature of extended chain melt crystallized polyethylene was investigated in an attempt to correlate the solution behaviour of such material to solution grown crystals. A razor blade was used to make very thin shavings of this high pressure melt crystallized polyethylene. These shavings were then dispersed in tetrachlorethylene and run in the DTA solution cell to obtain the solution thermogram of *Figure 12(A)*.

The high value of 110°C for the solution temperature of this sample we suggest is the result of three factors: (1) the relatively greater stability of melt crystallized polyethylene as compared with solution crystallized polyethylene; (2) the extended chain structure of the high pressure sample; and (3) the effect of external sample dimension. The work of Jackson, Flory

and Chiang[13] shows the greater stability of melt crystallized polyethylene over solution crystallized polyethylene by comparing the solution behaviour of both species. The greater stability of the melt crystallized material became more evident with increasing dilution. The increased melting or solution temperature associated with extended chain structures has been observed by several investigators[3, 12, 14]. Also isothermal crystallization shows that increasing fold periods (approaching extended chains) results in higher solu-

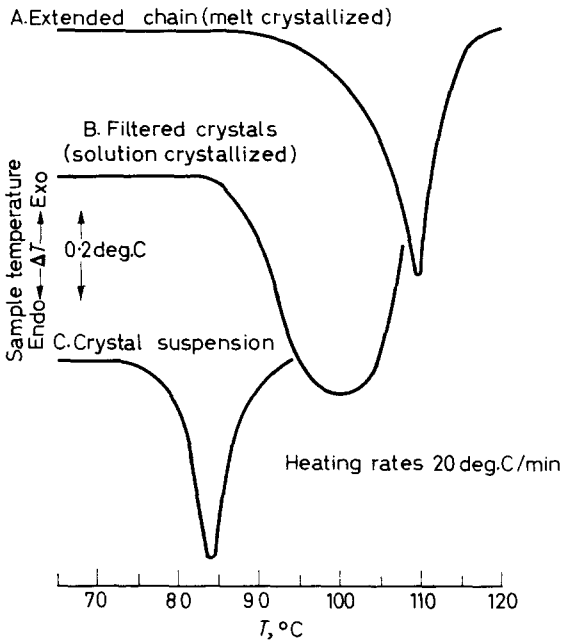

Figure 12—Effect of external sample dimensions on solution behaviour

tion temperatures. The effect of external sample dimensions is to increase the solution temperatures by permitting superheating to take place. *Figures 12(B)* and *(C)* show endotherms of crystals from the same preparation. The effect of filtering and re-suspending the crystals was to introduce external or large sample dimensions with the result of a 16 deg. C increase in solution temperature.

Shavings of as received Marlex 6050 pellets were prepared and run in the DTA solution cell in the same manner as for the extended chain melt crystallized polyethylene. The solution temperature at both 10 and 20 deg. C/min for this melt crystallized sample was found to be 97°C.

CONCLUSIONS

Differential Thermal Analysis exhibits a sensitivity to thermal transitions in dilute solution. The solution temperatures of the same crystal suspension at different concentrations are the same, indicating the enthalpy of mixing

as an undetectable small quantity[1]. But concentration affects the crystallization temperatures, and crystals prepared from solution of various concentrations have differing stabilities; these crystals have solution temperatures which are affected by the concentration of the precipitating solution and hence different enthalpies of fusion.

The rate of heating affects solution behaviour by causing superheating at faster rates and annealing at slower rates. Annealing studies indicate two different mechanisms for crystallite perfection: (1) Reorganization occurs at hold temperatures below the solution temperatures of the investigated samples, and (2) solution is followed by recrystallization when the hold condition coincides with any part of or is beyond the solution temperature of the sample. This behaviour is similar to studies performed with filtered crystals grown in xylene[13].

The solution of melt crystallized material occurs at higher temperatures than solution grown crystals. Part of the difference in solution temperature may be the larger particle size in melt crystallized samples. The differences in the solution temperatures increase with dilution. Jackson, Flory and Chiang have attributed such behaviour to the metastable nature of solution grown crystals[13]. The 13 deg. C difference in solution temperatures for the extended chain (high pressure melt crystallized) polyethylene and the Marlex pellets (atmospheric pressure melt crystallized) indicate differences in fold period or stability also produces a different solution temperature.

The authors thank the National Science Foundation for their support of this work.

Division of Polymer Science,
Case Western Reserve University,
Cleveland, Ohio 44106

(Received June 1967)

REFERENCES

[1] BLACKADDER, D. A. and SCHLEINITZ, H. M. *Polymer, Lond.* 1966, **7**, 603
[2] E. I. Du Pont de Nemours and Co., Inc., Du Pont 900 Thermal Analyzer Instruction Manual, Wilmington, Delaware
[3] KÊ, B. *J. Polym. Sci.* 1961, **50**, 79
[4] HOLLAND, V. F. and LINDENMEYER, P. H. *J. Polym. Sci.* 1962, **57**, 589
[5] LANCELY, H. A. and SHARPLES, A. *Makromol. Chem.* 1966, **94**, 30
[6] HUSEBY, T. W. and BAIR, H. E. To be published
[7] WUNDERLICH, B. *Polymer, Lond.* 1964, **5**, 611
[8] KELLER, A. and KAWAI, T. *Polymer Letters*, 1964, **2**, 333
[9] BASSETT, D. C. and KELLER, A. *Phil. Mag.* 1962, **7**, 1553
[10] HOFFMANN, J. D. and WEEKS, J. J. *J. Res. Nat. Bur. Stand. A*, (Physics and Chemistry), 1962, **66** (1), 13
[11] HOLLAND, V. F. *J. appl. Phys.* 1964, **35** (1), 59
[12] WUNDERLICH, B., CORMIER, C. M., KELLER, A. and MACHIN, M. J. To be published
[13] BAIR, H. E., SALOVEY, R. and HUSEBY, T. W. *Polymer, Lond.* 1967, **8**, 9
[14] HELLMUTH, E. and WUNDERLICH, B. *J. appl. Phys.* 1965, **36** (No. 10), 3039

Crystallization Phenomena in Polymers V—The Helical Theory of the Morphology of Crystalline Polymers

L. B. MORGAN and P. G. STERN*

The fundamental problem of the physics of crystalline polymers is to relate the polymerization conditions, through fabrication methods and the resulting morphology, to the physical properties. There is a very considerable literature with many conflicting interpretations. Most controversy centres around the morphology and the mechanism whereby the long chain molecules arrange themselves while crystallizing into the hypothetical models proposed to explain the properties of the fabricated samples.

Current hypotheses based on crystallites and chain folding have limited interpretative value as they can only be applied to narrow facets of the overall problem and are known to be unsatisfactory because of this lack of general applicability.

The basic facts of our knowledge of the mechanism and kinetics of crystallization from molten polymer are outlined and the most probable effect of orienting and relaxing the resulting semi-crystalline helical structure considered. This leads to morphologies which unify the interpretation of the data obtained by the many disciplines that have been brought to bear in this field.

THE nature of the morphology of crystalline polymers has been the subject of much speculation and research for the last 40 years. Hermann, Gerngröss and Abitz[1,2] concluded from their wide angle X-ray investigations on gelatin and natural rubber that the broadenings of the X-ray reflections were caused by the presence of very small crystals or crystallites. The size of these can be calculated using the Scherrer equation relating the broadening of the reflections to the dimensions of the crystal. This view is still prevalent but not now generally accepted.

Morgan[3] was of the opinion, based on the results of investigations carried out at the I.C.I. laboratories at Blackley on the mechanism and kinetics of crystallization of polymers from polymer melts[4–7] and on the results of the complementary morphological studies[8–15], that thisview of a unit of structure consisting of small crystals having dimensions of the order 50 to 500 Å was wrong. It was postulated that the structural unit was a long coiled acicular crystal or fibril which was imperfect and strained as a result of the mechanism by which it was formed from the polymer melt.

It has long been known[16,17] that when acicular crystals grow under conditions of high supersaturation and high viscosity, coiled or twisted crystals are formed, often arranged as radiating fibrils in spherulitic array. Crystallization from polymer melts at relatively high degrees of super-cooling provides such conditions.

The reason for the twisting or coiling is that the crystallizing medium at the growing crystal face will be pulled into terrace steps approximately at

*Present address: Spruance Research Laboratory, E. I. du Pont de Nemours & Co., Inc., P.O. Box 1477, Richmond, Virginia 23212, U.S.A.

right angles to the direction of growth of the crystal, and this will result in orientations being imposed on the viscous crystallizing medium immediately ahead of the growing face[18].

The extent of twisting or coiling will depend on the rate of growth of the crystal, the height of the terrace step and the relaxation time of the oriented crystallizing medium.

Usually with the polymers and under the conditions of crystallization in which we are interested, electron and optical microscopy and wide angle X-rays show that the crystals are tightly coiled.

The regions between these imperfect crystalline units of structure consist of amorphous polymer. By amorphous polymer we mean here short segments of polymer chains that are under constrictions imposed by the participation of the remainder of the molecules in neighbouring crystalline regions. They are therefore unable to be in a completely random state as weak structural relationships exist between the segments of polymer chain. In other words it is a region consisting of tie molecular chain segments connecting the crystalline units of structure together. As the term 'amorphous region' in crystalline polymers has varying connotations depending on methods used for measuring the crystalline/amorphous ratio, we will henceforth refer to this locality of tie molecules as the boundary–amorphous region. There will, of course, be tie molecules not only between the individual coiled crystals but also between neighbouring coils in the same crystal and in the central core of the coil.

Similarly, the term 'crystalline region' must be defined. It does not have the precise lattice dimensions of the crystallites of the fringed micelle theory of structure; it is disordered because there are many displaced polymer chains. The manner in which it is disordered depends on the detailed mechanism whereby the polymer chains attempt to move into crystalline array and occluding misplaced chains during the crystallization process, and also the disturbance to the so formed structure caused by further fabrication factors such as orientation during the drawing operation or subsequent annealing. There are different degrees of order geometrically disposed in crystalline polymers having varying orientations and polymer chain associations and merging continuously into each other.

On drawing the isotropic polymer in foil or filament form, these coiled acicular crystals will orient themselves in the direction of draw and either simultaneously or at a later stage of the drawing operation, depending on the polymer and the conditions of draw, extend themselves into twisted crystals separated by sections of polymer chains in the defined boundary–amorphous arrangement also oriented and elongated in the direction of draw.

Although this coiled or twisted crystal concept explained most of the experimental observations that had been made in this field, it was found necessary by Morgan[3, 18] to postulate coiled parallel bundles of acicular crystals or fibrils, to interpret certain features of the low angle X-ray reflections, notably the discrete quadrantal reflections and the elongated meridional smears, on the basis that the coiled assembly of fibrils formed a grating reflecting into the quadrants, and also to explain the increase in the long period on relaxing drawn polymers.

Meibohm and Smith[19] had reported that a comparison of the low angle X-ray diffractions and the orientation as indicated by wide angle X-ray diffraction showed no good correlation between the orientations of the polymer regions responsible for the two classes of diffraction. This coiled assembly of fibrils or rope structure would therefore have to be supplemented by some other element of structure and this has not been forthcoming in the many investigations that have been undertaken since it was first proposed in 1954. A more important objection to the coiled rope-like associations of these fibrils is that no acceptable mechanism can be advanced for the fibrils associating in this way, either in the primary or secondary crystallization processes that occur during the formation of the fibrils of crystalline polymer from the melt or during subsequent treatments.

The objective therefore is to ascertain why the most probable morphology based on crystallization mechanism and generally supported by microscopic observations, i.e. one involving a coiled imperfect crystalline fibrillar unit of structure, will on drawing, annealing, and relaxing naturally move into structural arrangements conforming with X-ray diffractions at all angles and is a reasonable basis for interpreting polymer properties and how and why they vary with the fabrication conditions.

An ancillary necessity, in view of the conflicting literature on this topic, is to place in their correct perspective the relevance of observations made on polymers fabricated under unique conditions, as thoughts on these have been generalized and interpolated unduly into the theorizing on the nature of the morphology of normally fabricated polymers.

Much relevant data are available in the literature, but it has been deemed desirable to supplement this by experimental work on optical transforms to demonstrate that the morphologies do explain the general features of the low angle X-ray scatterings and by elaborative wide angle X-ray measurements on the effect of the drawing operation on the induced morphological details. The latter is mentioned briefly in the section on orientation and will be the subject of a further communication by P. G. Stern.

MORPHOLOGY OF ISOTROPIC CRYSTALLINE POLYMERS

Our considerations are limited to polymers crystallized from the melt under the normal conditions of technical interest and certainly without the influence of surfaces such as would be pertaining if the crystallization occurred in thin films, say between tightly pressed glass microscope slides, or very slow crystallizations at temperatures just below the melting point.

Under isothermal conditions the primary crystallization process has been kinetically analysed and supplemented by visual inspection. This suggested that, for polyethylene terephthalate[6] and polyhexamethylene adipamide[7] and later for other polymers, e.g. polypropylene[20], the resulting structure would be based on long coiled fibrillar crystals. The mechanistic evidence for the resulting structure is not as conclusive for some other polymers such as polyethylene, where secondary crystallizations vitiate the simple kinetic analysis.

Whether these fibrils are single crystals or arranged in spherulitic families the X-ray reflections will be the same, namely from an isotropic disposition of coiled imperfect crystals.

The discrete wide angle X-ray reflections from the imperfect crystalline region will give the usual powder diagram with broadening of the rings caused by the imperfections and the small lateral dimensions of the fibrils. There is also the usual amorphous halo.

Information on the low angle X-ray diffractions of unoriented crystalline polymers is scant, probably because the discontinuous reflections develop on drawing and become more intense on relaxing. This is dealt with later. Meibohm and Smith[19], however, have reported that an unoriented crystallized polyethylene terephthalate gives a ring indicating a periodicity of 87 Å, and Statton[21] has reported similarly on polyhexamethylene sebacamide. In both cases the differences in the electron density between the amorphous and crystalline regions had to be augmented by annealing to be detectable by the techniques used. Isotropic polyethylene also shows this low angle X-ray ring (e.g. Kasai and Kakudo[22]). This is dealt with in more detail later with the drawing operation.

The tangential disposition of the polymer chains in the radiating fibrils of spherulites has now been established by birefringence and microbeam X-ray measurements[11, 23, 24]. The electron microscope investigations of Kassenbeck[25] confirm this. The fibrils in his samples are of the order of 100 Å wide and show striations along their length separated by about the same distance. He concluded that the polymer molecules are at an angle of about 70° with the axis of the fibrils.

If care is taken in the choice of crystallization conditions in very thin films, polymers can be induced to crystallize by chain folding to give lamellar crystals[26]. This is irrelevant here as we are dealing with the normal crystallization conditions encountered in technological processes for the fabrication of polymers.

Under normal conditions of polymer crystallization from the melt, optical and electron microscopy, X-ray measurements and mechanistic considerations supported by kinetical analysis indicate that usually the basic unit of structure is a long acicular imperfect crystal or fibril with the chain molecules disposed approximately tangential to the fibril axis. This structure is schematically represented in *Figure* 1. There will be small regions of boundary–

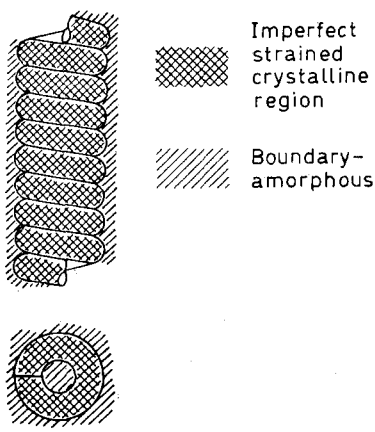

Figure 1—Coiled fibril unit of structure

amorphous between the coils and also trapped in the central core of the coiling crystal.

As branching of fibrils also occurs during crystallization due to secondary nucleation on the side of already formed fibrils[3], there will also be junction points resulting in branching, most obviously so when spherulites are formed. This is of secondary importance at this stage of the development of the thesis.

ORIENTATION

(*a*) *Mechanism*

When this isotropic arrangement of acicular crystalline units in a boundary-amorphous matrix is deformed by an extensive force, flow of the molecules will first occur in the boundary–amorphous regions between the fibrils where the interchain associations are at a minimum. These segments of chains will elongate in the direction of draw, and as they are integrated with the crystalline fibril units they also will orient in the same direction.

The movements will be accommodated by forcible release of polymer chain segments as required from the crystal surfaces, and, as the fibrils are initially at all orientations, it is to be expected that the movements will also be accompanied by releases in stress in some localities which could result in segments of polymer chains crystallizing into adjoining crystal surfaces. The helical acicular crystal structure will remain.

At some stage of the drawing operation, depending on the state of the boundary–amorphous and the intermolecular attractions in the coiled crystalline fibril, there will be superimposed the act of extending the coiled crystalline fibril. We therefore have two main movements in the drawing operation, namely the orientation of the helical crystal and its extension. The stage of the forcible elongation of the structure where extension of the helix starts will depend on the chemical nature and morphology and the conditions of drawing. Secondary movements will be further orientation of the polymer segments in the boundary–amorphous matrix accompanied by release of segments from the peripheral localities of the orienting acicular crystals into this phase.

When a tightly-wound helix is forcibly extended, the elements of structure nearest the central axis of the coiled fibril will be subjected to a much greater stress and strain in the direction of elongation than those at the perimeter because it follows from the geometry of the arrangement that a linear element of structure along the inside surface of the coil will have a shorter length than that of a similar element of structure on the outside surface.

Extension of this helical arrangement depicted in *Figure 1* will not only involve separation of the coiling cylinder and release of segments of polymer chains from the crystalline coiling cylinder into the boundary–amorphous between the coils. The boundary–amorphous region in the central core of the coil will orient in the direction of drawing and this will crystallize into a cylindrical imperfect crystal supplemented by the elements of structure from the inside surface of the original crystalline coil. This act of orientation and crystallization in the region of the central axis will rigidify the structure before the longer length of peripheral elements of structure is fully uncoiled.

It will be seen from this that the resulting structure will have a screw-like

configuration of the form shown in *Figure 2* the central core of the screw being highly oriented in the direction of draw and the external thread structure randomized perhaps more than in its initial condition.

A drawn fibre will therefore be made up of units having three *gradually intermerging* basic structures, viz: A, an imperfect crystalline cylinder oriented

Figure 2—Model of the crystalline unit in an oriented structure

in the direction of the fibre axis with the polymer molecules mainly in the same direction; B, a less crystalline region with the polymer molecules helically wound around A; and C the boundary-amorphous region, separating the individual screw structures described in A and B, and consisting of the polymer chains oriented in the direction of draw.

This is schematically represented in *Figure 3*.

The polymer segments in the boundary–amorphous region will join or release from the vicinal crystal units depending on the circumstances of their

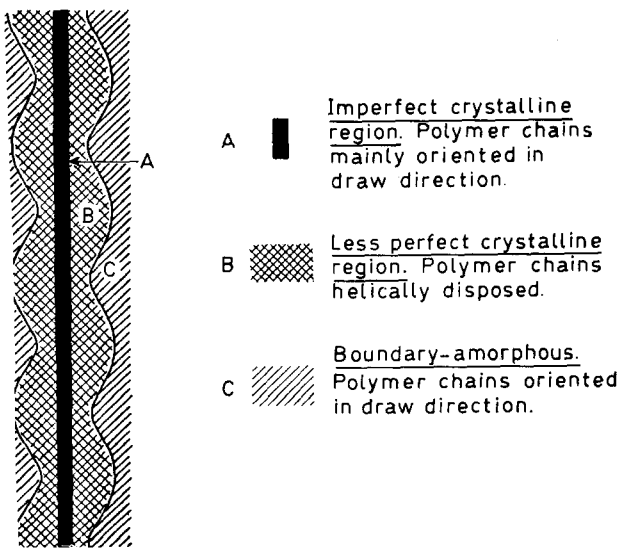

Figure 3—Oriented unit of extended coiled crystal. Schematic representation. Regions A, B and C merge continuously into each other

individual stresses or degree of relaxation occurring during the drawing operation. Therefore, depending on how the polymer has been drawn and relaxed, there will be a tendency for neighbouring fibrils to adjust their positions so that the threads of one fibril fit into the grooves of a neighbour. This will give the low angle X-ray four-point diagram.

Arnett, Meibohm and Smith[27] first reported this discrete quadrantal reflection in polyhexamethylene sebacamide. Meibohm and Smith[19] elaborated, and with the samples of this polymer fabricated for their measurements they showed that the drawn filaments gave a meridional smear but relaxation resulted in separation into the four-point discrete quadrantal reflections. This is explicable in a movement during relaxation of the coiled screw-like parallel crystalline units into the more comfortable configuration that will reflect into the quadrants. These configurations are schematically illustrated in *Figures 4* and *5*. They also observed that oriented polyethylene invariably gave this four-point reflection, which means that the structure here is more amenable to adjustment and was termed by them 'self-relaxing'.

This relaxation process will be discussed in more detail later.

(*b*) *Low angle X-ray diffractions and light diffraction from optical analogues*

Correct interpretation of the low angle X-ray reflections is the keystone of the problem. The equatorial continuous and discrete reflections from oriented fibres are due to a morphology involving cylinders of varying diameters and distribution of diameter size oriented in the direction of draw cognisance being taken of striated voids being formed under some conditions of fabrication. This has been briefly reviewed by Morgan[18], and the effect of voids on the reflections has been adequately dealt with by Hermans and Weidinger[28].

It is the meridional and quadrantal discontinuous reflections that have proved troublesome to interpret either in the details of the changes in their locations or on structures which can be achieved by mechanistic consideration of what it is possible for polymer molecules to do while moving under the influence of the imposed method of fabrication.

When Hess and Kiessig[29] reported the discrete meridional smears indicating periodicity in structure in the fibre axis direction explanations were sought in terms of an alternating crystallite and amorphous structure. This type of morphology has satisfied neither mechanistic considerations for its achievement nor the peculiarities of the changes in the form of the reflections with either fabrication method or subsequent treatment. The separation of the meridional layer line into discrete quadrantal reflections[27] indicated a more complex structure. The rope model[3] and Statton's model of alternating crystallites and amorphous regions[30, 31] have the difficulty of mechanistic attainment and lack of applicability to data on X-ray scattering during drawing and on relaxation.

With what is now the almost generally accepted view that the crystallization process from the melt involves chain folding[32] and the paracrystalline definition of an imperfect crystal[33, 34], many variants of polymer chain arrangements have been proposed which postulate models that largely disregard the polymer chain movements necessary for their formation and

do not adequately explain the changes in the low angle reflections and all the data available from other disciplines. For example, in recent papers by Dismore and Statton[35] and Predicki and Statton[36] it has been stated that a chain folded arrangement of the polymer chains in a paracrystal, if the distortions in the crystalline structure caused by the chain folds are suitably spaced, can give the required meridional and quadrantal reflections. Difficulties, however, are encountered in the use of this arrangement of the molecules in explaining the many other features presented by the overall problem.

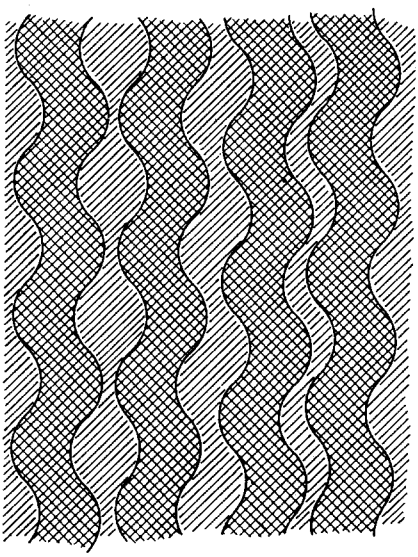

Figure 4—Schematic representation of assembly of oriented coiled units not adjusted by relaxation

It is now demonstrated by the use of optical diffraction methods that the helical structure schematically represented in *Figures 4* and *5* which have been arrived at without resort to the low angle X-ray observations will explain their peculiarities and why the reflections change in the way reported during the drawing operation.

As a result of a discusson by one of us (L.B.M.) at the Shirley Institute with Dr K. C. Ellis and Dr J. O. Warwicker in 1962, optical transforms of helical arrangements representing structures to be expected in fibres were made by the Shirley Institute in 1962 and are shown in *Figure 6*. These demonstrate that the low angle X-ray reflections could be probably explained on this basis. Subsequent preliminary measurements by Taylor[37] confirmed this.

Elaborating on the principles described by Taylor and Lipson[38], a further investigation has been undertaken. The optical diffractometer, described by Hughes and Taylor[39] and illustrated in *Figure 7* was employed. A high intensity monochromatic filtered beam from a mercury-vapour lamp is focused on the pinhole at the focus of the collimating lens, L_1, giving parallel light between the lenses L_1 and L_2. A mask representing the structure under investigation is interposed between L_1 and L_2 and the Fourier trans-

form observed through a microscope or recorded on a panchromatic microfile film. Electron density distributions in the investigated structures are simulated in masks by two-dimensional clear and opaque regions distributed on photographic plates, exposed X-ray films or etched copper plates. The simplest way of preparing masks is by mechanically punching holes in an

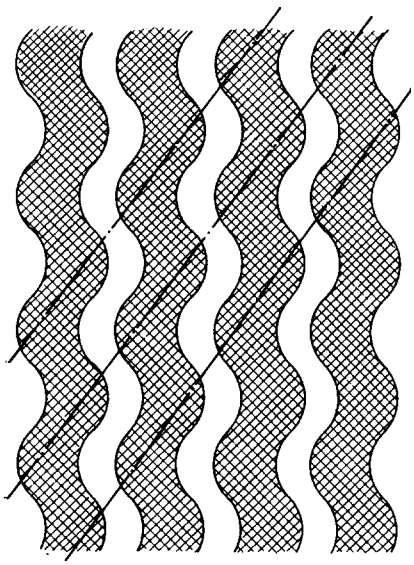

Figure 5—Schematic representation of assembly of oriented coiled units adjusted by relaxation

opaque card, but this is tedious when a large number of holes is required to represent complex structures. Another method is to photograph drawings of trial structures and use the resulting negatives as masks. It is necessary here to immerse the negatives in cedarwood oil and sandwich between optical flats. Alternatively, a representation of the structure is made by

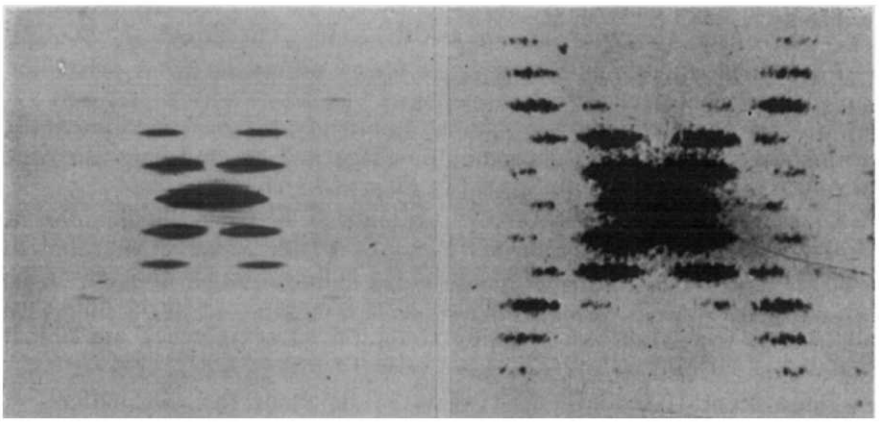

Figure 6—Typical optical transforms from oriented helices. [Dr K. C. Ellis and Dr J. O. Warwicker (1962). See text]

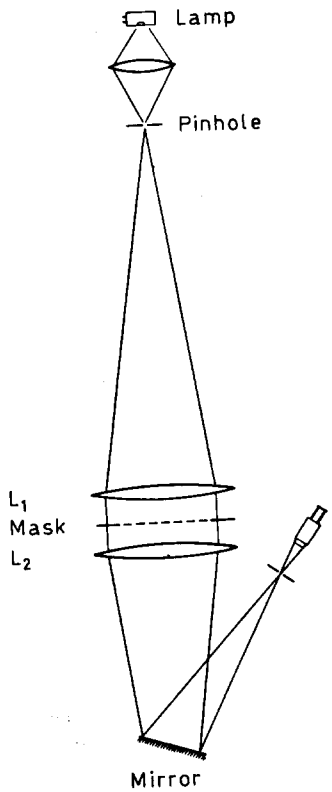

Figure 7—Optical components of the diffractometer

placing black dots on white paper, photographing and transferring the design via a contact print on to a thin copper foil by an etching process[40].

Figure 8 shows masks and Fourier transforms for oriented and unoriented springs by using the cedarwood oil and the etching technique[41].

For the interpretation of low angle X-ray diffraction from crystalline polymers we must consider morphologies based on *Figures 1, 2* and *12*. These units of structure in, for example, an oriented polymer, can present the forms shown in *Figure 9* depending on shape and tilt and they can pack together as schematically illustrated in *Figures 4* and *5*.

Other masks prepared to study relationships between distributions of structure and their optical Fourier transforms (*Figure 10* and others) showed that the arcs in the diffraction patterns are indeed a direct measure of the degree of orientation between the molecular arrangement and the fibre axis, and streak diffraction is caused by structural elements which are shifted parallel to each other.

Diffraction masks have been made to represent the distributions of coils ranging from the unoriented undrawn state to the fully oriented, and their Fourier transforms observed to satisfy the small angle X-ray diffraction patterns reported in the literature.

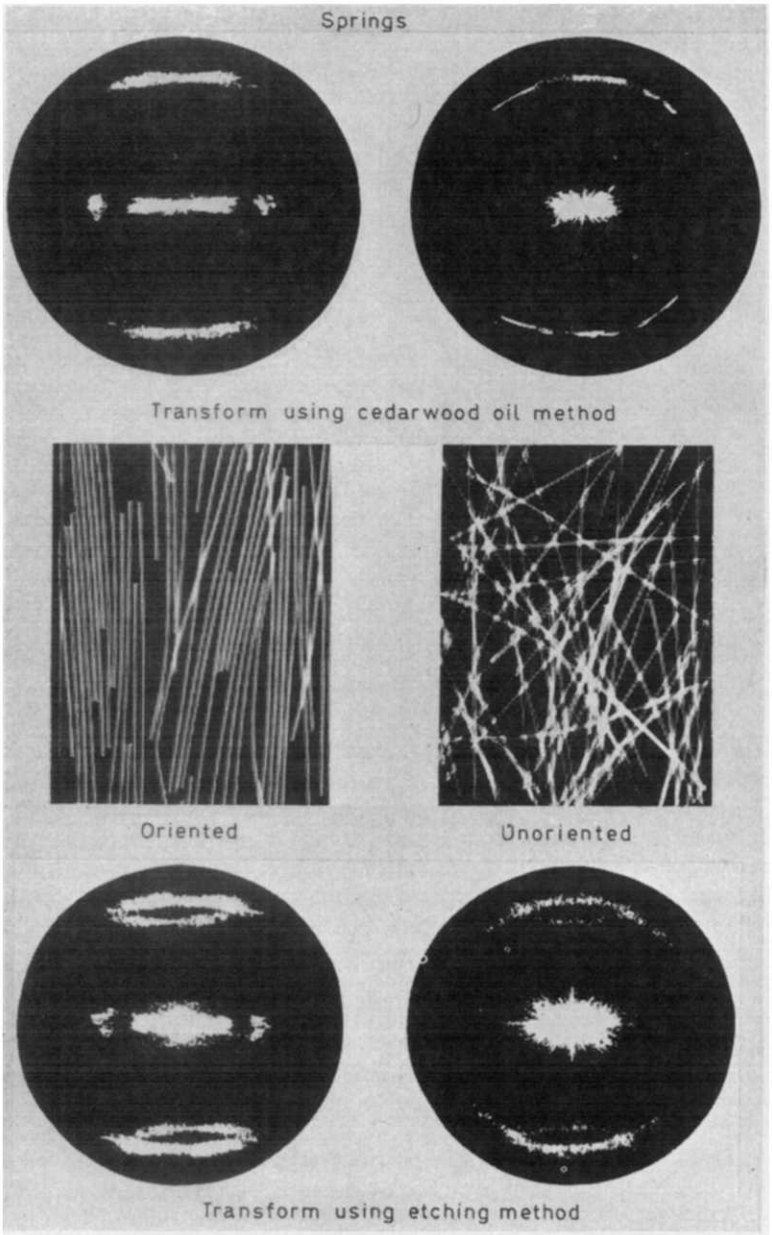

Figure 8—Various masks and Fourier transforms

We now have for the first time a satisfactory model based on reasonable mechanistic surmise for its attainment and supported by optical transform analogues to explain the changes in low angle X-ray diffractions that occur during the drawing operation.

There are many contributions in the literature on the effect of drawing and annealing on the details of the low angle X-ray scatterings, and most

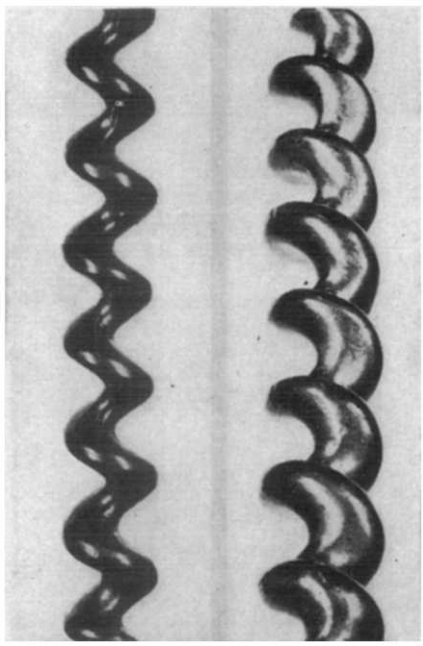

Figure 9—Units of ordered structure illustrated here and having higher electron densities, when suitably packed and oriented explain the low angle X-ray diffractions

of the features have been regarded as inexplicable when using the morphologies arrived at by various combinations of the 'crystallite' structure, chain folding and the refinements imposed by the paracrystalline state definition of the imperfect crystalline structure being dealt with here. An example is an article on polyethylene by Bonart[42].

These are readily explained on the helical morphology arrived at on the mechanistic premise.

To exemplify we will consider the most recent investigation namely that of Kasai and Kakudo[22] on polyethylene. This gives the most detailed description of the movement of the low angle scatterings during the orienting operation so far reported.

A 3 mm cylindrical rod of the polymer was forcibly extended at 10°C. Under these conditions of draw a neck is formed. Measurements were made on a 0·3 mm section cut from the centre of the rod from the undrawn portion through the neck to the drawn polymer. Some of these diffractions are shown in *Figure 11*.

The isotropic unoriented structure above the neck gives the circular halo [*Figure 11*(a)] to be expected from a collection of randomly disposed helices,

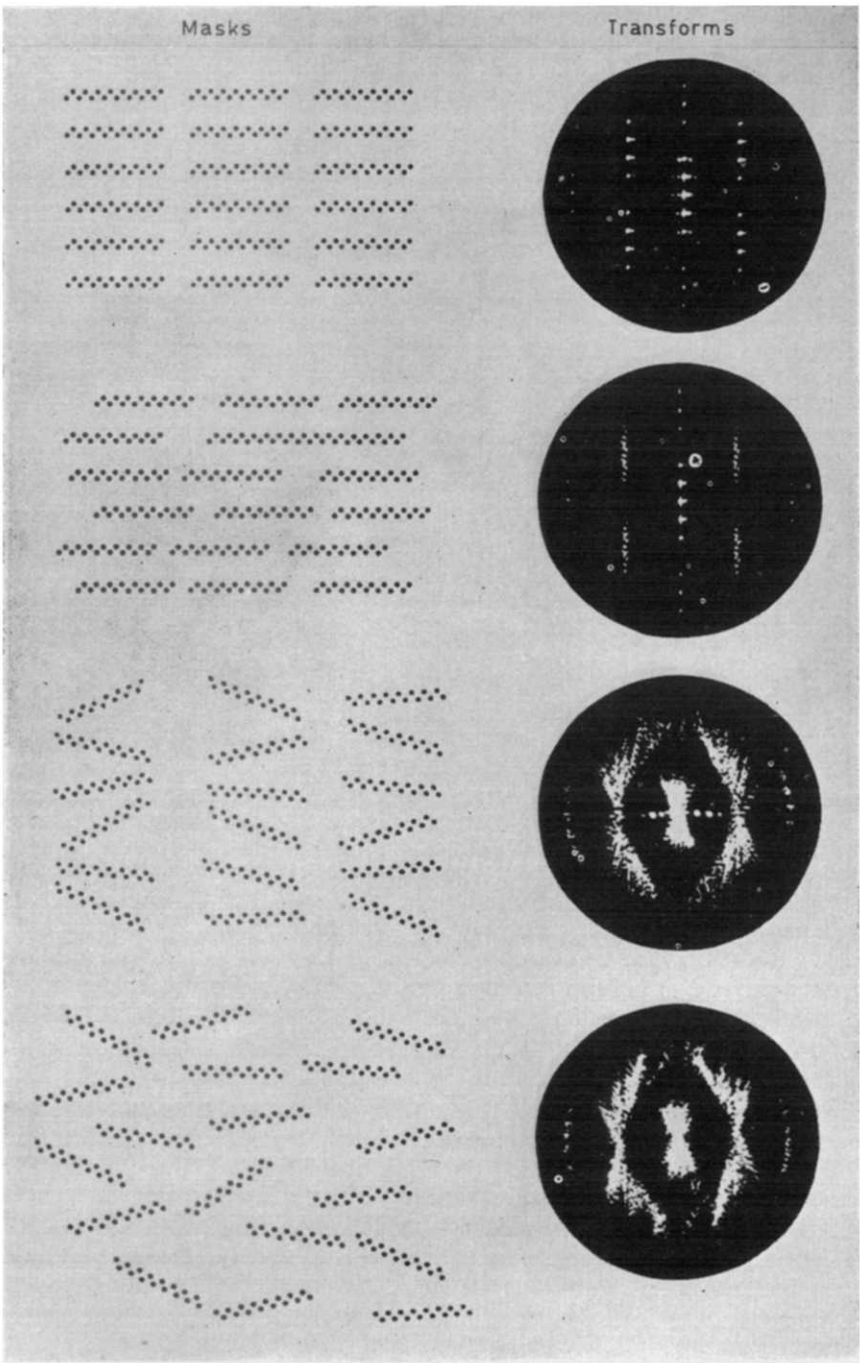

Figure 10—Punched masks and their transforms

i.e. from a randomly disposed collection of units having the structure shown in *Figure 1*. The Bragg distance will be along the helix and approximately that of the diameter of the basic coiling cylindrical crystal with the small distance of boundary–amorphous region between the coils. The first effect of orienting the structure is to transform the circle to an ellipse [*Figure 11*(b)]. This oval pattern had been previously observed by Hendus[43] and was also seen in low angle X-ray reflections from a polyurethane bristle by Zahn and Winter[44]. The explanation is that the helices having their axes in

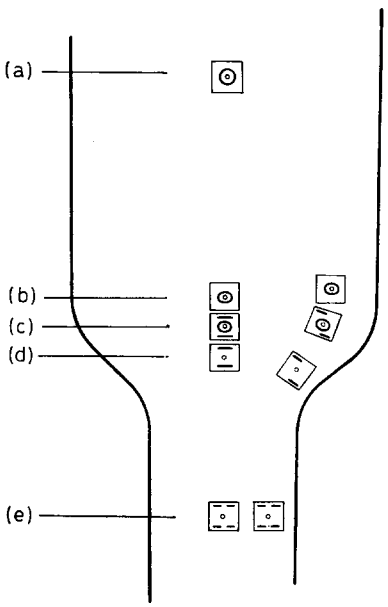

Figure 11—Low angle X-ray discrete diffractions at various stages of the orientation of polyethylene (Kasai and Kakudo[22])

the direction of draw will commence extending first, the amorphous between the coils being supplemented by release from the vicinal crystalline regions. The periodicity along these helices will therefore increase and the meridional reflection will contract towards the equator. In other words, diffraction is from a mixture of units of structure shown in *Figures 1* and *12*, the partially drawn units depicted in *Figure 12* being preferentially oriented in the direction of drawing.

Further drawing results in the appearance of the meridional smears extending into the quadrants and a simultaneous weakening and final disappearance of the elliptical halo. It is to be noted too that the new meridional smears are further removed from the equator than the elliptical diffraction on the meridian, and therefore the diffracting structure now has a smaller dimensional grating than the partially extended helix. This is because the more fully extended helices are diffracting collectively as the threads and grooves of adjoining units of crystal structure are moving into juxtaposition, and the diffraction will again be recording approximately the diameter of the basic coiling cylinder plus the small boundary–amorphous region separating, in this case, neighbouring crystals (see *Figure 4*).

At the outside edge of the necking filament the helices will not only be

subjected to a vertical distending force but also to a lateral displacement, which will result in the structural units being skew. This will diffract to give the displaced horizontal meridional smears moving into the quadrants as observed by the Japanese investigators.

On full extension, the grooves and threads align more perfectly, as can be seen in *Figure 5* (referred to as 'self-relaxing' by Meibohm and Smith[19]), and the four-point diagram of *Figure 11*(e) is obtained.

This explanation of the peculiarities of low angle X-ray diffraction can be demonstrated by the optical transform techniques described above.

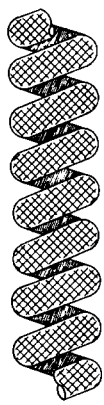

Figure 12—Partially drawn coiled fibril unit of structure

(c) *Wide angle X-ray diffraction*

The first point to note is that the model does not demand correlation of wide and low angle X-ray observations on orientation as the diffractions are from different parts of the unit of structure. The strongest wide angle X-ray scatterings will be from the first orienting and more perfectly crystalline core of the screw (region A in *Figure 3*) whereas the low angle X-ray scatterings are based on the total screw macrostructure and the dispositions of neighbouring threads and grooves (*Figures 4* and *5*).

As has been pointed out, the details of the polymer chain movements during the drawing operation are very dependent on the conditions of draw such as the temperature and rate of draw, and also the initial condition of the isotropic undrawn specimen. For example, if polyethylene is drawn slowly under the conditions described by Keller[9], the polymer chains tilt (monitored by wide angle X-ray) and are inclined to the direction of draw. With polyamides the chains can align themselves almost perpendicularly to the drawing direction during the early stages of the drawing performance[12]. These observations are best interpreted on the basis of orientation of the coiled helical crystals (*Figure 1*) with little disturbance of their internal structure during the initial stages of the drawing operation. Further drawing results in the extension of the helix to give the screw configuration with orientation of the unit cell with the *c* axis, i.e. the polymer chain direction, parallel to the direction of draw.

The interpretation of the wide angle X-ray diffractions during the drawing operation and resulting in the extension of the tightly coiled helix into the

screw-like unit of structure is of importance, particularly if we take into account the details of the discrete reflections, the amorphous halo and the simultaneous changes in the density of the polymer.

The wide angle X-ray reflections from crystalline polymers are not as sharp as those usually obtained from crystalline substances. This was attributed to the broadenings caused by the small dimensions of the individual polymer crystals in the structure, and has been the main basis of the 'crystallite' or fringed micelle theory of the morphology of crystalline polymers. Morgan[3, 18] considered this view to be incorrect as the broadening could also be caused by strain imperfections in the larger unit of crystalline structure required by mechanistic consideration of the crystallization process.

More recent investigations[45–58] indicate that both effects contribute to the broadening as might be expected with strained crystalline units having small lateral dimensions. Calculations of 'crystallite' sizes from these broadenings are therefore highly suspect, and definitions of structure based on values for the 'crystalline, amorphous' ratios are regarded as inadequate.

State of order or chain arrangements and associations in a crystalline polymer vary in a continuous manner as we traverse its structure. The term 'state of order' applied to a minute locality of the structure must be defined by distance between the chains, directional configuration of the chains and the amount and degree of regularity of the interaction forces between the chains due to van de Waals, dipole and hydrogen bonding.

Integration of chain separation defines the density (specific gravity), and integration of directional configuration and regularity of chain interaction defines the wide angle discrete reflections.

It is known that the discrete wide angle X-ray reflections vary not only in their breadths but also in the location of their peaks[49–52]. The variations are due to fabrication details, not only the extent of orientation but also any subsequent annealing or relaxation treatment. This means that the portion of the structure responsible for the wide angle reflections (i.e. region A of *Figure 3*) is varying in unit cell dimensions and density.

Experimental work has therefore been undertaken on the effect of draw ratio on the wide angle X-ray reflections normal and parallel to the draw direction, and the density of polyethylene, polypropylene and polyethylene terephthalate and the 'crystalline, amorphous ratios' calculated by the traditional methods[53, 54].

The details of this work are the subject of a pending publication by P. G. Stern. It shows conclusively that the interpretation of wide angle X-ray reflections and how they change on orientation cannot be explained on a two-phase system of a perfect crystalline state in a matrix of amorphous polymer.

RELAXATION

When oriented crystalline polymers are relaxed by heat treatment or in liquids which have a plasticizing action, the long period increases and the corresponding diffraction pattern increases in intensity. The increase in the long period occurs not only when the length of the oriented specimen is held constant, but also when it is left free to contract. This effect has

almost invariably been observed with oriented crystalline polymers. For example, the effect in polyamides has been described and theoretically considered[19, 29, 35, 55, 56].

The unexpected feature was the increase in long period, particularly where the length of the specimen was reduced and Morgan[3] on the basis that the unit of crystalline structure was a long fibril suggested that it might be due to the moving apart of the fibrils in a rope-strand model. The wide angle X-ray reflections, however, as pointed out previously, do not show the concomitant degree of disorientation to support this. The most recent suggestion is that of Dismore and Statton[35] which involves the refolding of the polymer molecules in a paracrystal. There are mechanistic objections to both the formation of a paracrystal of folded polymer molecules and the process of refolding of polymer molecules in a crystalline state. Furthermore, the proposed molecular arrangements are not suitable for explaining any of the other features of crystalline polymer properties.

The extended coiled strained crystal model with the crystals separated by boundary–amorphous regions consisting of extended sections of polymer molecules oriented in the fibre axis direction explains these observations in a more rational manner.

Let us first consider the consequences of subjecting the crystalline portion of the structure schematically represented in *Figure 3* to relaxing conditions. The structure has a central cylindrical core oriented in the direction of draw. It is surrounded by helical planes of decreasing crystal perfection the further they are from the axis, until at the screw surface of threads and grooves the crystallinity and helical disposition of chain molecules merge into relative disorder of the boundary–amorphous region of tie segments of polymer.

Relaxing by heat or plasticizers will result in the crystalline core (region A of *Figure 3*) tending towards greater crystal perfection. The immediate surrounding helical and somewhat less crystalline element of structure will also tend towards greater crystallinity and will also adjust itself as far as possible to conform with the oriented crystalline core. This direction of movement and rearrangement of the polymer chain molecules in the helical crystal will persist, but with decreasing magnitude as we move away from the axis of the structure. The overall result will be a structural rearrangement in the crystalline portion of the structure (regions A and B of *Figure 3*) tending towards greater crystallinity and a larger helical angle. Thus the wide angle X-ray reflections which register from region A will be expected to show very little difference in crystalline orientation and the diffractions will be sharper. The low angle X-ray diffractions which register from regions A and B will show an increase in the long period, and with the increase in electron density of the crystalline A and B phases of the structure there will be an increase in the intensity of the diffraction.

In the intervening matrix of the boundary–amorphous regions between these crystals, that is the continuous phase of the structure, the extended segments of chains will endeavour to contract to a more random configuration, and will also disengage sections of the polymer molecules from the adjacent regions of intermediate order in the region B thread and grooves of the screw-like crystals. Thus the continuous boundary–amorphous phase in the relaxing structure will contract in the fibre axis direction.

Although the fibre contracts, unless under imposed external constraint, the overall effect to be expected therefore will be the reported general features of the X-ray observations, viz. an increase in the intensity of the low angle X-ray diffractions; an increase in the long period, an increase in crystallinity as judged by wide angle X-ray diffraction, and little disorientation of the crystalline portion as judged by wide angle X-ray measurements.

Some elaboration is required on the last. Dismore and Statton[35] found that when their polyhexamethylene adipamide fibres relaxed there was little indication of crystal disorientation, although they observed the usual increase in long period and amount of crystallinity. The amount of disorientation as shown by wide angle X-ray measurements will depend on the initial structure of the drawn crystalline polymer and the relaxation factors, but the important general feature is that there is no relation between the low angle and wide angle X-ray assessment of orientation. Disorientation as judged by wide angle X-ray measurements could be caused by portions of region B, particularly near A, becoming more crystalline and therefore scattering the wide angle X-rays more strongly while still retaining some of their helical disposition.

The increase in the long period on relaxing is only one facet of the low angle X-ray scattering. When Porod[57] reviewed this field he said 'Considerable difficulties are encountered in interpreting dependence of long periods on pretreatment, annealing, elongation or swelling. Not only is the location of the reflection changed but also its distinctness, intensity and length of layer line; in the four-point diagrams the angle between the intensity maximum and the meridian is shifted. As a rule they take place irreversibly. Also a layer pattern can be converted into a four-point diagram'.

All these changes can be explained rationally by using the helical model and monitored by using optical transforms.

Thus the splitting of the meridional smear shown by Meibohm and Smith's[19] polyhexamethylene sebacamide sample into a four-point diagram on relaxing in water at 100°C is due to adjustment of the morphology from that represented by *Figure 4* to that of *Figure 5*. The shortening of the layer line in both polyhexamethylene sebacamide and polyhexamethylene adipamide and which accompanies the increase in the long period on relaxing with seven per cent phenol in water at 75°C will be due to an increase in the helical angle in a morphology of the type depicted in *Figure 4*.

Zahn and Winter's[44] low and wide angle X-ray examination of the changes induced in the polyurethane monofilaments obtained from 1,6-hexamethylene diisocyanate and 1,4-butylene glycol (Perlon L and Perlon U) after treatments in air, water and aqueous phenol at different temperatures is another of the many studies in this field which exemplifies the requirement for reconsideration in the light of the approach to the problem described in this communication. The accessibility of water, which lubricates hydrogen bonds in the boundary-amorphous, and phenol, which in addition has a solvating action on the crystalline regions, induces polymer chain movements in Regions A, B and C of *Figure 3* that can be anticipated.

These structural movements also explain the change of the other properties on relaxation or heat conditioning of oriented crystalline polymers.

For example, from n.m.r. measurements, Dismore and Statton[35] showed

that annealing polyhexamethylene adipamide caused a much earlier onset of fluid-like mobility and produced a greater amount of it, and they interpret this n.m.r. fraction in terms of increased defect mobility in their paracrystal model. As annealing an imperfect crystal would tend towards increasing its perfection, defect mobility might be expected to decrease. The relaxation of the boundary–amorphous phase, as described above, gives the natural explanation. A similar result has been obtained on polyethylene by Peterlin and Olf[58]. Their n.m.r. measurements, taken in conjunction with sorption of tetrachlorethylene after annealing at different temperatures, showed that the non-crystalline regions relaxed to a state typical of undrawn polyethylene. There is no disorientation of the crystalline regions and there is a simultaneous shrinkage in the length of the sample. Their explanation given in terms of crystallites with tie molecules would lead to a reduction in the long period, which is the opposite to what is observed from the low angle X-ray measurements. As Hyndman and Origlio[59] concluded from their observations on polyethylene and polypropylene fibres: 'Interpretation of n.m.r. spectra from polymers in terms of a simple two phase system must be applied with caution as areas of intermediate order contribute significantly to the observed line-shapes'.

The nature of the structure of crystalline oriented polymers and the way it might alter during the drawing and relaxing processes has been sought by other approaches.

The lack of agreement among various crystallinity and accessibility measurements on cellulosic fibres led Marchessault and Howsman[60] to advance their 'lateral order' concept. They proposed a definition of the order function more in keeping with infra-red evidence, showing that celluloses differ in distribition of H-bond strength, rather than in the actual number of H-bonds involved.

The 'lateral order' distribution of nylon 6 has recently been evaluated by Koshima and Tagawa[61] by deuteration and infra-red measurements. Polymer samples treated in various ways were placed in contact with D_2O vapour at various temperatures from 25° to 150°C, and the N-D to C-H intensity ratio in the three to four micron region calculated. The data obtained gave accessibility of the sample to D_2O at various temperatures, and the differential of the temperature/accessibility curve gives the 'lateral order' distribution. These show that amorphous and intermediate order (partially crystalline) regions decrease and higher order (more crystalline) regions increase on dry heat setting. On steam setting, however, both amorphous and crystalline regions increase at the expense of the region of intermediate order. This behaviour is reflected in the data given by Koshima and Kakishita[62] on the effect of heat setting in the diffusion of dyestuff molecules into nylon 6 fibres. This requirement of three kinds of order to explain properties and structure relationships has most recently been emphasized by Sakuma and Rebenfeld[63]. They have measured the changes in nylon 6·6 fibre taking place on orienting to various extents and after relaxing by treatment with aqueous phenol of various concentrations. For example, the density and moisture regain data are consistent with the view expressed by Kanetsuna[64] that relaxation by phenol treatment tended to increase the

amount of highly ordered crystalline and the amorphous portion of the structure at the expense of the intermediate part.

The model, which explains the X-ray observations (*Figure 3*), not only has the required three types of ordered regions but also has the polymer molecules disposed in these regions in such situations in relation to each other that they will naturally move under annealing and relaxing conditions in directions to forecast these effects. If we consider the schematic representation of the model shown in *Figure 3* and, bearing in mind that the regions A, B and C are not distinct but merge into each other in a continuous manner, the effects observed are to be expected.

During the annealing process there is a requirement that the molecules enter crystalline portion A from the intermediate region B, and as the mobility of the polymer chain segments in the boundary–amorphous region C increases, it not only results in a disorientation of polymer chains in this region but also in a release of chains from the intermediate region B. The direction of movement of the polymer chain segments will depend on the relaxing or annealing conditions. If, for example, the conditions include the presence of plasticizing molecules that can only gain access into the structure in region C, then movement into this portion of the structure is favoured; this is the likely explanation of Koshima and Tagawa's[61] observations on the differences between dry heat and steam setting and Kanetsuna's[64] on relaxation by phenol treatment.

DISCUSSION

The elementary mechanistic consideration of how polymer molecules will move from the molten condition to a more ordered semi-crystalline state leads to a coiled fibrillar unit of structure. Orientation and relaxing should therefore result in the type of morphology outlined here. As it is one which gives a satisfactory explanation of the experimental observations, it should also serve best for interpretation of the mechanical properties of the finally fabricated sample.

This aspect will be dealt with in a later communication, but it is appropriate to mention briefly the changes in the X-ray diffractions on stressing oriented fibres.

Zahn and Winter[44] showed that when a filament of an oriented polyurethane was extended, there was a reversible extension in the long period but the long period extension was greater than the extension of the filament. Beresford and Bevan[56] repeated these measurements on polyhexamethylene adipamide and obtained similar results, from which it was concluded that there was some unspecified higher modulus portion of the structure not associated with that giving the long period but which controlled the observed extension of the fibre. The explanation is that on extension the resulting orientation will cause region B to tend to crystallize into region A (see *Figure 3*) and this will result in an increase in the long period disproportionate to the fibre extension. The fibre they used gave the four-point diagram in the unstressed state. That is, it had the structure schematically represented in *Figure 5*. On stressing, as the coiled units will be to some extent branched, the structure will be disturbed to the more disordered arrangement of *Figure*

4. This explains the observed movement of the low angle X-ray reflections from the four-point diagram to the meridional smears.

Stress/strain relationships, creep and stress relaxation can be interpreted with greater facility and credence by using the morphology described here rather than the ones proposed based on the fringed micelle and chain folding.

The case for a chain folding mechanism of crystallization from the molten condition and a chain folded morphology of the resulting crystalline polymer has been presented several times (e.g. Geil[32], Keller[65] and Hoffman[66]).

The fact that in very dilute solutions polymers can only crystallize by chain folding, and if carefully selected conditions are chosen such as in thin films or with lower molecular weight polymers or at temperatures near the melting point, chain folding can be induced in crystallizing polymers in the molten state, has led to the present prevalent view that this is the normal mechanism of polymer chain re-arrangement during crystallization. This is erroneous. There are mechanistic objections to chain folding occurring under normal conditions of polymer fabrication and it has proved to be of limited value in interpretation.

If we consider a small element of crystallizable structure in a polymer melt there will be several times more chances of the forward interaction of inter-chain association occurring between different molecules than with an individual polymer molecule associating with itself. Thus on the build up to nucleation and crystallization propagation, this mechanistic requirement would apparently rule out the chain folding mechanism of growth in molten polymer.

However, it has been shown to occur in very thin films with low molecular weight polymers, and at temperatures of crystallization just below the melting point. It is therefore essential to understand how this occurs by re-examination of the crystallization mechanism from molten polymer. Consideration must be given to the reverse reaction step of dissociation.

An association such as, for example, a hydrogen bond formed between two adjacent polymer molecules remote from the ends of the chains will be subjected to thermal agitation influences from local thermal vibrations and also from the superimposed, more distant required conformation of the four lengths of polymer chains of the two polymer molecules involved. On the other hand, an association involving interaction in the same polymer molecule near the end of the chain will only have distant disturbances from one length of the polymer molecule. Although its chances of formation are much less it will be more stable.

Thus in the mechanistic build up to a critical size nucleus there will be two competing paths, one by the rapid tumbling together of associations between different molecules favoured by juxtaposition in the melt, and the second by the slower selective but more stable associations in the same molecule near the ends. The latter therefore can become dominant if the number of ends is increased by using lower molecular weight polymers, the selection of slower conditions of nucleation and propagation by crystallizing at temperatures close to the melting point and confining the crystallizing medium to very thin films (usually about 60 000 Å or less) thereby increasing peripheral surface localities where the effects of remote melt thermal agitations

are much reduced. These are the selected crystallization environments and conditions that have been chosen to demonstrate that chain folding into single crystals can be achieved in molten polymer.

Generalization from these observations made under narrow selected crystallization conditions to conclude that this is the sole mechanism of polymer crystallization under all circumstances could be regarded as unwarranted.

However, a further type of observation which in many quarters is regarded as indicative that this view is correct is the isolation from polyethylene[67, 68] and polypropylene[69] of single crystals by etching out the amorphous regions by oxidation over prolonged periods with nitric acid. There is chain scission and reduction in the polymer molecular weight. As the employment of chemical scissors in a partially crystalline structure will create and mobilize new chain ends desiring to crystallize, chain folding will occur and it could be argued that the progressive eroding into the amorphous and strained crystal structure by the hot acid would result in a re-arrangement to give a chain folded lamella crystal structure bearing no relationship to the original.

Takesue *et al.*[70] have repeated this work on undrawn and drawn polypropylene monofilaments. With the undrawn fibres similar results to those of Hock were obtained but even after more prolonged oxidative treatment the drawn fibres gave fibrils having the *c* axis parallel to the fibril axis, and in some cases there was evidence also of distortion of the polymer chain along the *c* axis. This is to be expected from the structure of oriented polymers as depicted in *Figure 3*. The nitric acid will first attack the boundary–amorphous region C and then progressively erode the threads and grooves of region B.

Fischer and Schmidt's[71] statement that there is no explanation available for a process designated 'periodic crystallization' which could lead to the formation of 'crystallites' is in agreement with our reiterated views. We therefore are limited on our present knowledge to consideration of the two mechanistic paths, namely that involving growth in the chain direct on leading to coiled fibrillar structures and that by sideways accretion which involves chain folding. Either can occur depending on the conditions under which the crystallization takes place.

As pointed out[18] sideways accretion with chain folding is to be expected in dilute solutions of polymers, and subsequent observations have shown that it can occur in melts under restricted conditions. In more concentrated polymer solutions and under delicately balanced melt conditions an initial folded chain initiation leading to the flat lozenge single crystal can be followed by a secondary nucleation in the partially participating chains protruding from the flat surfaces of the lozenge, thereby giving rise to the stacked flat crystals numerously exemplified and illustrated[32]. These structures all grow by chain folding sideways accretion and result in stacked lamellae of chain folded crystals attached to each other by interpenetrating chains. If, however, during the crystallization the concentration of protruding chains and vicinal amorphous polymer becomes large, crystal growth will switch to the normal growth in the chain direction and lead to the formation of coiled fibrils. The electron micrographs shown by Anderson[72] illustrate this effect of single

crystal growth by sideways accretion changing into growth in the chain direction and forming a twisted crystal.

CONCLUSION

A consideration of the mechanism whereby polymer molecule chains crystallize under most conditions from the melt suggests that they will form closely coiled fibrillar imperfect crystals in a matrix of not so ordered interconnecting segments of polymer chains. Forcible extension and relaxation will mechanistically result in a morphology having a crystalline screw as the configurational unit of structure, with the degree of crystallinity and order decreasing from the central axis of the screw through the screw threads to the interconnecting amorphous matrix. The polymer chain orientation in the screw axis direction will vary from the near perpendicular at the centre of the screw to a widening helical disposition of the molecules at the periphery. The orientation in the interconnecting segments of polymer chains in the boundary–amorphous matrix will vary according to the mode of frabrication.

This derived model explains the many puzzling features of the low and wide angle X-ray scatterings and how they vary in detail with fabrication. conditions. It is also a suitable model for rational interpretation of other fundamental properties and mechanical behaviour of crystalline polymers.

Imperial Chemical Industries Ltd.,
Dyestuffs Division,
Blackley, Manchester.

(*Received May 1967*)

REFERENCES

[1]HERMANN, K., GERNGRÖSS, O. and ABITZ, W. *Z. phys. Chem.* 1930, **B10,** 371
[2]HERMANN, K. and GERNGRÖSS, O. *Kautschuk*, 1932, **8,** 181
[3]MORGAN, L. B. *J. appl. Chem.* 1954, **4,** 160
[4]KELLER, A., LESTER, G. R. and MORGAN, L. B. *Phil. Trans.* 1954, **A247,** 1
[5]MORGAN, L. B. *Phil. Trans.* 1954, **A247,** 13
[6]HARTLEY, F. D., LORD, F. W. and MORGAN, L. B. *Phil. Trans.* 1954, **A247,** 23
[7]HARTLEY, F. D., LORD, F. W. and MORGAN, L. B. *Atti del Symp. Intern. Macromol. Chem., Milano-Turino, Ric. sci. (Suppl.),* 1955, **25,** 577
[8]KELLER, A. *J. Polym. Sci.* 1953, **11,** 567
[9]KELLER, A. *J. Polym. Sci.* 1955, **15,** 31
[10]KELLER, A. *J. Polym. Sci.* 1955, **17,** 291
[11]KELLER, A. *J. Polym. Sci.* 1955, **17,** 351
[12]KELLER, A. *J. Polym. Sci.* 1956, **21,** 363
[13]KELLER, A. and SANDEMAN, I. *J. Polym. Sci.* 1955, **15,** 133
[14]KELLER, A. and WARING, J. R. S. *J. Polym. Sci.* 1955, **17,** 447
[15]COOPER, A. C., KELLER, A. and WARING, J. R. S. *J. Polym. Sci.* 1953, **11,** 215
[16]MORSE, H. W., WARREN, C. H. and DONNAY, J. D. H. *Amer. J. Sci.* 1932, **23,** 421
[17]MORSE, H. W. and DONNAY, J. D. H. *Amer. Min.* 1936, **21,** 391
[18]MORGAN, L. B. *Progress in High Polymers*—1, Editors ROBB, J. C. and PEAKER, F. W. pp 233–277, Heywood: London, 1961
[19]MEIBOHM, E. P. H. and SMITH, A. F. *J. Polym. Sci.* 1951, **7,** 449
[20]VON FALKAI, B. *Makromol. Chem.* 1960, **41,** 86
[21]STATTON, W. O. *Newer Methods of Polymer Characterization*, Editors: BACON, KE, pp 238–239, Interscience: New York, 1964
[22]KASAI, N. and KAKUDO, M. *J. Polym. Sci.* 1964, **2A,** 1955
[23]BUNN, C. W. and ALCOCK, T. C. *Trans. Faraday Soc.* 1945, **41,** 317

[24]HERBST, M. *Z. Elektrochem.* 1950, **54**, 318
[25]KASSENBECK, P. *Melliand Textilber.* 1958, **39**, 55
[26]MAGILL, J. H. and HARRIS, P. H. *Polymer, Lond.* 1962, **3**, 252
[27]ARNETT, L. M., MEIBOHM, E. P. H. and SMITH, A. F. *J. Polym. Sci.* 1950, **5**, 738
[28]HERMANS, P. H. and WEIDINGER, A. *Makromol, Chem.* 1960, **39**, 67
[29]HESS, K. and KEISSIG, H. *Z. phys. Chem.* 1944, **193**, 196
[30]STATTON, W. O. and GODDARD, G. M. *J. appl. Phys.* 1957, **28**, 1111
[31]STATTON, W. O. *J. Polym. Sci.* 1959, **41**, 143
[32]GEIL, P. H. *Polymer Single Crystals*, Interscience: New York, 1963
[33]HOSEMANN, R. *Polymer, Lond.* 1962, **3**, 349
[34]HOSEMANN, R. and BAGCHI, S. N. *Direct Analysis of Diffraction by Matter*, North-Holland: Amsterdam, 1962
[35]DISMORE, P. F. and STATTON, W. O. *J. Polym. Sci.* Part C, 1966, No. 13, 133
[36]PREDICKI, P. and STATTON, W. O. *Conference on Small Angle X-ray Scattering*, Syracuse June, 1965. Gordon and Breach: New York
[37]TAYLOR, C. A. *Eur. Polym. J.* 1966, **2**, 279
[38]TAYLOR, C. A. and LIPSON, H. *Optical Transforms. Their Preparation and Application to X-ray Diffraction Problems*, Bell: London, 1964
[39]HUGHES, W. and TAYLOR, C. A. *J. sci. Instrum.* 1953, **30**, 105
[40]EISLER, P. *The Technology of Printed Circuits*, Heywood: London, 1959
[41]STERN, P. G., TAYLOR, C. A. and YEADON, E. C. *Conference of the X-ray Analyses Group*, British Institute of Physics and the Physical Society, University of Edinburgh, 8–9 April 1965
[42]BONART, R. *Kolloidzschr.* 1964, **194**, 97
[43]HENDUS, H. *Kolloidzschr.* 1959, **165**, 32
[44]ZAHN, H. and WINTER, V. *Kolloidzschr.* 1952, **128**, 142
[45]KATAYAMA, J. *J. phys. Soc. Japan*, 1961, **16**, 462
[46]THIELKE, H. G. and BILLMEYER, F. W. *J. Polym. Sci.* 1964, **A2**, 2947
[47]BONART, R., HOSEMANN, R. and MCCULLOUGH, R. L. *Polymer, Lond.* 1963, **4**, 199
[48]BUCHANAN, D. R. and MILLER, R. L. *J. appl. Phys.* 1966, **37**, 4003
[49]MILLER, R. L. and NEILSON, L. E. *J. Polym. Sci.* 1960, **44**, 391
[50]SEGERMAN, E. and STERN, P. G. *Nature, Lond.* 1966, **210**, 1258
[51]HERMANS, P. H. and WEIDINGER, A. *Makromol. Chem.* 1961, **44**, 24
[52]KRIMM, S. and TOBOLSKY, A. V. *J. Polym. Sci.* 1951, **7**, 56
[53]HERMANS, P. H. and WEIDINGER, A. *J. appl. Phys.* 1948, **19**, 491
[54]GOPPEL, J. M. qnd ARLMANN, I. J. *Appl. sci. Res.* 1949, **A1**, 468
[55]FANKUCHEN, J. and MARK, H. *J. appl. Phys.* 1944, **15**, 364
[56]BERESFORD, D. R. and BEVAN, H. *Polymer, Lond.* 1964, **5**, 247
[57]POROD, G. *Fortschr. HochpolymForsch.* 1961, **2**, 363
[58]PETERLIN, A. and OLF, H. G. *J. Polym. Sci.* 1966, Part A2, **4**, 587
[59]HYNDMAN, D. and ORIGLIO, G. F. *J. Polym. Sci.* 1959, **39**, 559
[60]MARCHESSAULT, R. H. and HOWSMAN, J. A. *Text. Res. (J.)*, 1957, **27**, 30
[61]KOSHIMA, A. and TAGAWA, T. *J. appl. Polym. Sci.* 1965, **9**, 117
[62]KOSHIMA, A. and KAKISHITA, T. *J. appl. Polym. Sci.* 1965, **9**, 91
[63]SAKUMA, Y. and REBENFELD, L. *J. appl. Polym. Sci.* 1966, **10**, 637
[64]KANETSUNA, H. J. *J. Soc. Text. Cellul. Ind. Japan*, 1962, **18**, 784 and 792
[65]KELLER, A. *Kolloidzschr.* 1964, **197**, 98
[66]HOFFMAN, J. D. *S.P.E. Trans.* 1964, **4**, 315
[67]PALMER, R. P. and COBBOLD, A. J. *Makromol. Chem.* 1964, **74**, 174
[68]KELLER, A. and SAWADA, S. *Makromol. Chem.* 1964, **74**, 190
[69]HOCK, C. W. *J. Polym. Sci., Pt A2*, 1966, **4**, 227
[70]TAKESUE, M., YOSHIHARA, T., ARITO, Z. and YAMADA, N. *Reports on Progress in Polymer Physics, Japan*, Vol. 9, p. 231, Kobyasi Institute of Physical Research: Tokyo, 1966
[71]FISCHER, E. W. and SCHMIDT, G. F. *Angew. Chem.* (Int. Edn. Engl.), 1962, **1**, 488
[72]ANDERSON, F. R. *J. Polym. Sci., Pt B*, 1965, **3**, 723

Book Reviews

Polymer Systems: Deformation and Flow

R. E. WETTON and R. W. WHORLOW (Editors). Macmillan: London, 1968. 6 in. by 9¼ in. $x+338$ pp. 70*s*.

THIS book is a printed version of the lectures given at the Annual Conference of the British Society of Rheology held at Loughborough during September 1966. It contains 25 papers (not 29 as stated on the jacket flap) on a wide range of rheological subjects concerning bulk polymers and solutions. It contains a subject index.

The breadth of the subject matter covered makes it difficult to discern the general themes and it might have been helpful if some of the contributions made to the discussions at the meeting could have been included because these often serve to emphasize common ground and interconnections between seemingly dissimilar papers. The inclusion of a short abstract with each paper might also have been useful since, despite its attractive book format, this is mainly a collection of research papers such as one might find in an international specialist journal and most readers will wish to use it as such.

The opening paper, by I. M. WARD, gives a very ordered and valuable review of the rheological properties of solid polymers with particular emphasis on the effects of anisotropy and partial crystallinity. It reveals that although a great deal is now firmly established regarding the physics of the rheological properties little headway has yet been made in relating these to molecular structure and motions. There are four further contributions which deal with the relations between crystallinity and mechanical properties.

Almost one-half of the papers at the Conference was devoted to the viscoelasticity of liquid polymers and concentrated solutions, especially the study of these in cone and plate rheogoniometers. The latter topic was considered from the theoretical as well as from the practical angle. This significant collection of information certainly makes the book essential reading for all scientists and technologists who are concerned with non-Newtonian flow.

Other papers are devoted to equilibrium elasticity and viscoelasticity of amorphous polymers, the flow properties of dilute solutions and to less readily characterized materials such as wood and filled elastomers. The book should certainly find a place in the polymer physics or chemistry section of every well-stocked library.

P. MEARES

Fracture in Polymers

E. H. ANDREWS. Oliver and Boyd: Edinburgh, 1968. 5½ in. by 8½ in. 208 pp. 63*s*.

THE study of fracture processes in polymers has developed rapidly during the last ten years and many new theories and experiments have been described. In this book, Professor ANDREWS sets out to summarize the current state of our knowledge in some 200 pages which are based on a series of lectures given at Cranfield.

The approach adopted is commendably concise and practical. Professor ANDREWS is interested in how his materials do behave rather than in how somebody's equation

says they should. Thus, his graphs are well adorned with experimental points and where these are occasionally omitted the reader can generally assume that it is only for convenience. In addition, he summarizes the existing theories of polymer fracture, both for rubbers and for rigid polymers. Here again, due attention is given to experimental work. On these lines, the book covers a great area of knowledge in a relatively small space.

The book contains six chapters. In the first chapter the structure and deformation properties of polymers are shortly described. The next two chapters, which broadly describe fracture phenomena, are concerned with summarizing experimental results. Next, the initiation and propagation of fractures are described and interpreted, largely in terms of the 'Griffiths' theories for crack propagation in rigid materials and through the various viscolastic hysteresis theories with rubbers. Finally, there is an illustrated discussion of fracture surfaces.

Any reader of this book soon realizes that the fracture of polymers is a field of bewildering variety. Many unreconciled theories compete to explain the observed phenomena. In these circumstances, any active worker in the field, such as the reviewer, will have his differences with some of the points of view expressed. For example, the proposal to relate yield stress to free volume generated by hydrostatic tension (page 57) has always seemed untenable in the face of the known level of yield stress values in compression. The writer would also have included the work of MARSH on the yield stress interpretation of the fracture of glass as this has a fundamental bearing on crack propagation theories generally. These, however, are points of interpretation. They would represent just one more point of view among the many which are currently proposed and which are properly summarized in this book. Also, Professor ANDREWS has commendably and particularly decided to tell the reader about those things which have actually been observed.

The book is very suitable for students taking university courses in material science.

R. N. HAWARD

Book Reviews

Polymer Systems: Deformation and Flow

R. E. WETTON and R. W. WHORLOW (Editors). Macmillan: London, 1968. 6 in. by 9¼ in. $x+338$ pp. 70*s*.

THIS book is a printed version of the lectures given at the Annual Conference of the British Society of Rheology held at Loughborough during September 1966. It contains 25 papers (not 29 as stated on the jacket flap) on a wide range of rheological subjects concerning bulk polymers and solutions. It contains a subject index.

The breadth of the subject matter covered makes it difficult to discern the general themes and it might have been helpful if some of the contributions made to the discussions at the meeting could have been included because these often serve to emphasize common ground and interconnections between seemingly dissimilar papers. The inclusion of a short abstract with each paper might also have been useful since, despite its attractive book format, this is mainly a collection of research papers such as one might find in an international specialist journal and most readers will wish to use it as such.

The opening paper, by I. M. WARD, gives a very ordered and valuable review of the rheological properties of solid polymers with particular emphasis on the effects of anisotropy and partial crystallinity. It reveals that although a great deal is now firmly established regarding the physics of the rheological properties little headway has yet been made in relating these to molecular structure and motions. There are four further contributions which deal with the relations between crystallinity and mechanical properties.

Almost one-half of the papers at the Conference was devoted to the viscoelasticity of liquid polymers and concentrated solutions, especially the study of these in cone and plate rheogoniometers. The latter topic was considered from the theoretical as well as from the practical angle. This significant collection of information certainly makes the book essential reading for all scientists and technologists who are concerned with non-Newtonian flow.

Other papers are devoted to equilibrium elasticity and viscoelasticity of amorphous polymers, the flow properties of dilute solutions and to less readily characterized materials such as wood and filled elastomers. The book should certainly find a place in the polymer physics or chemistry section of every well-stocked library.

P. MEARES

Fracture in Polymers

E. H. ANDREWS. Oliver and Boyd: Edinburgh, 1968. 5½ in. by 8½ in. 208 pp. 63*s*.

THE study of fracture processes in polymers has developed rapidly during the last ten years and many new theories and experiments have been described. In this book, Professor ANDREWS sets out to summarize the current state of our knowledge in some 200 pages which are based on a series of lectures given at Cranfield.

The approach adopted is commendably concise and practical. Professor ANDREWS is interested in how his materials do behave rather than in how somebody's equation

Differential Thermal Analysis of Polyethylene in Tetrachlorethylene II—Structural Effects on Solution and Crystallization Temperatures

J. L. KOENIG and A. J. CARRANO

A commercially available differential thermal analyser has been adapted for studying the dilute solution behaviour of polyethylene in tetrachlorethylene. Crystal suspensions were made from polyethylenes of different chain structure and molecular weight. Molecular weight studies showed differences in morphological habits and solution temperatures for molecular weight fractions crystallized by slow cooling. Increased chain branching led to solution occurring over a broader and lower temperature range.

POLYETHYLENE has received considerable study by differential thermal analysis (DTA) techniques[1-8]. Since polyethylenes crystallize readily, the high degree of crystallinity makes polyethylene amenable to DTA studies of melting. The melting thermograms give valuable information for understanding the properties and structure of polyethylene. In this paper, the effects of structural variations in polyethylene on the solution behaviour in tetrachlorethylene as measured by DTA will be examined.

The melting behaviour of polyethylene depends on several factors. The crystallite size and degree of crystallinity are influenced by the thermal history. Hence, the melting thermogram will reflect differences in the crystals produced during the crystallization process. Higher melting points are measured for the samples which were crystallized at the slower cooling rates[9].

Crystals from branched polyethylenes show that the crystalline perfection decreases with increasing number of pendant groups[2]. The melting endotherms for methyl and ethyl branched polyethylenes show that the greater the amount of branching, the larger was the melting point shift for both pendant groups. The nature, amount, and distribution of branches affect the melting temperature, with the greater number of short chain branches producing lower and broader melting ranges[10]. The effects of branching on the solution behaviour of single crystals are examined in this work.

EXPERIMENTAL

The Differential Thermal Analyzer (E. I. Du Pont de Nemours and Co.) is described in detail elsewhere[11,12].

Briefly, the sample holder consists of a cylindrical aluminium block with a central cavity for a cartridge heater. The sample and reference cells are located symmetrically around the cartridge heater. The thermocouples are imbedded directly in the sample and reference materials.

The sample and reference cells are cylindrical open glass tubes, measuring 1 in. in length and 4 mm in diameter. The cell assembly is covered by a glass bell jar seated on a neoprene O-ring to permit a controlled atmosphere.

The temperature differential (ΔT) signal is fed to a d.c. preamplifier and is recorded against sample temperature (T) on a modified Moseley X–Y recorder. Provisions exist for varying sensitivity and zero shift for both the ΔT and T scales. A baseline slope compensator can be used to match electronically the thermal masses of the reference and sample. The programmer permits controlled heating and cooling rates, and hold or isothermal modes.

Three molecular weight fractions (11 000, 80 000, 121 000 molecular weights) of relatively unbranched Celanese A60-500 were used in studying molecular weight effects. A tenth of one per cent by weight suspensions were obtained by dissolving the required amounts of polyethylene in 100 ml of boiling tetrachlorethylene in 250 ml vessels. After 30 minutes crystallization occurred as the vessels cooled to room temperature on standing.

RESULTS AND DISCUSSION

Effect of molecular weight on solution behaviour

The three molecular weight fractions used for this work were crystallized from smaller vessels than the Marlex 6050 slow cooled preparations discussed in the previous paper[13] because of the smaller amounts of available samples. The smaller vessels were responsible for crystallization occurring at lower temperatures as the solutions cooled faster to room temperature on standing. This would be seen by observing the solution behaviour of a Marlex 6050 'control' suspension grown at these conditions. The solution temperature of this preparation is some 2 deg. C lower than the slowly crystallized samples. Furthermore, the greater irregularity in morphological habit (*Figure 1*) than for the large vessel preparation indicates a greater deviation from equilibrium conditions. The fractions apparently (cf. Part I) crystallized at higher temperatures in the direction of increasing molecular weight. The solution temperatures (*Table 1*) can be seen to increase with increasing molecular weight.

Table 1. Effect of molecular weight on solution and recrystallization

Mol. wt fraction	*Solution temp. (°C)*	*Recrystallization temp. (cooling rate 10 deg. C/min)*
11 000	79·0	64·5
80 000	80·0	65·0
121 000	82·0	65·0
Control	82·0	65·0

After solution in the DTA cell had occurred, the solutions were cooled at a rate of 10 deg. C/min, and the recrystallization temperatures (*Table 1*) recorded. The constant value for the recrystallization temperatures for all the fractions shown is a result of the combination of cooling rate and concentration difference. The concentrations were less than 0·5% wt polyethylene, and since the crystallization rate at any given temperature decreases with a decrease in concentration[14], the faster DTA cooling rate depressed

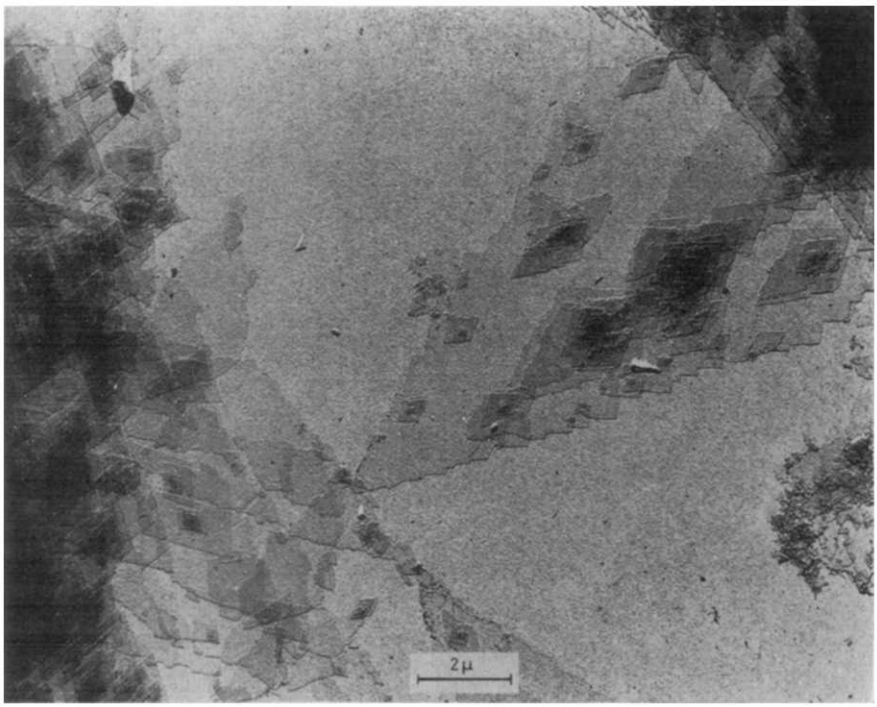

Figure 1—Electron micrograph of smaller vessel slow cooled crystallized polyethylene (Marlex 6050)

the crystallization temperatures and compressed the range over which the fractions crystallized. The 0·5 deg. C lowering of the crystallization temperature for the lowest fraction is within the experimental error.

The electron micrographs for the three fractions appear in *Figures 2, 3* and *4*. The morphological habits appear to be sensitive to molecular weight. The higher the molecular weight the more dendritic and fragmentary the crystals. Such observations have been made by other investigators[15]. Bassett and Keller[16] suggest that the crystal habit offers a rough means of distinguishing between samples of differing molecular weight.

Figure 5 gives the solution thermograms for these samples at heating rates of 10 and 20 deg. C/min. We suggest the endotherm recorded at the higher temperature for each fraction is apparently due to annealing in suspension. At slower heating rates a greater degree of annealing would be expected to occur and is observed. The 10 deg. C/min heating rate may produce the greater amount of annealed material as evidenced by the more fully developed higher temperature endotherms. The lowest molecular weight fraction is subjected to the greatest degree of reorganization during the heating process. At the 10 deg. C/min heating rate, all the samples show some annealing. At 20 deg. C/min there is noticeably less annealing, although the lowest fraction appears capable of reorganizing to a large extent.

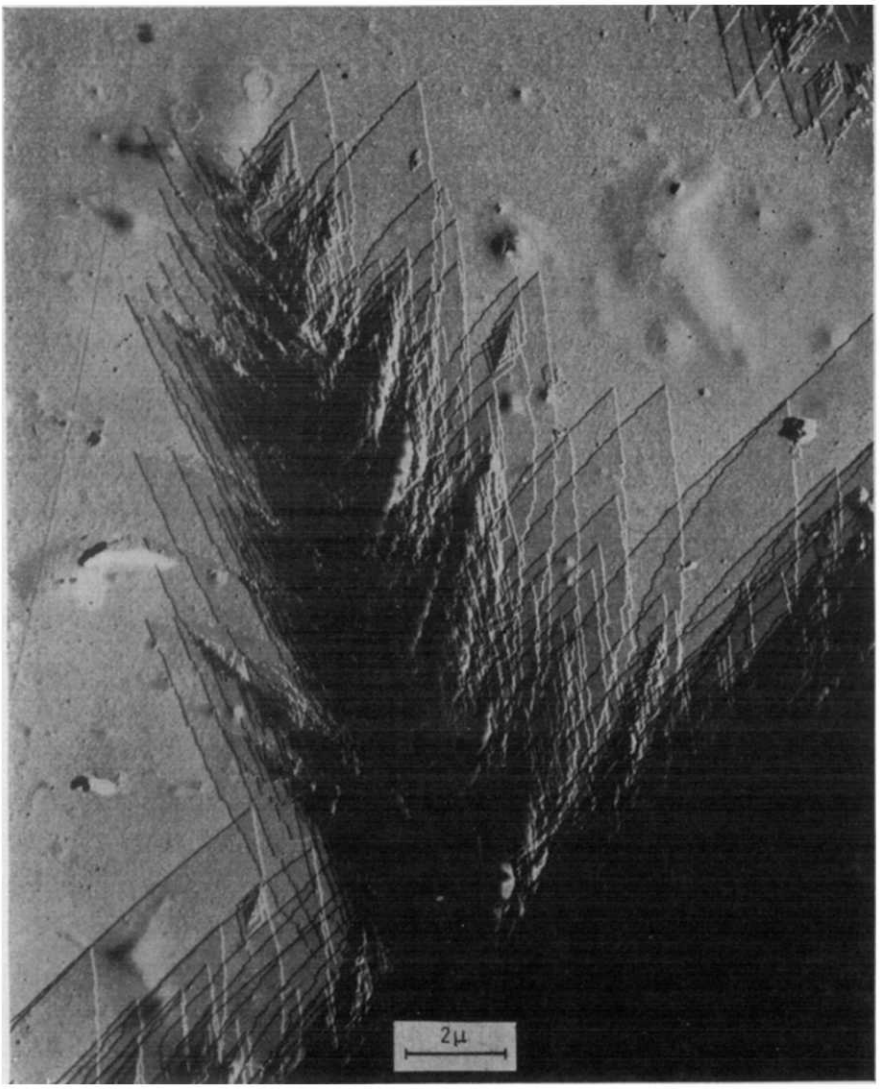

Figure 2—Electron micrograph of polyethylene crystals of molecular weight 11 000

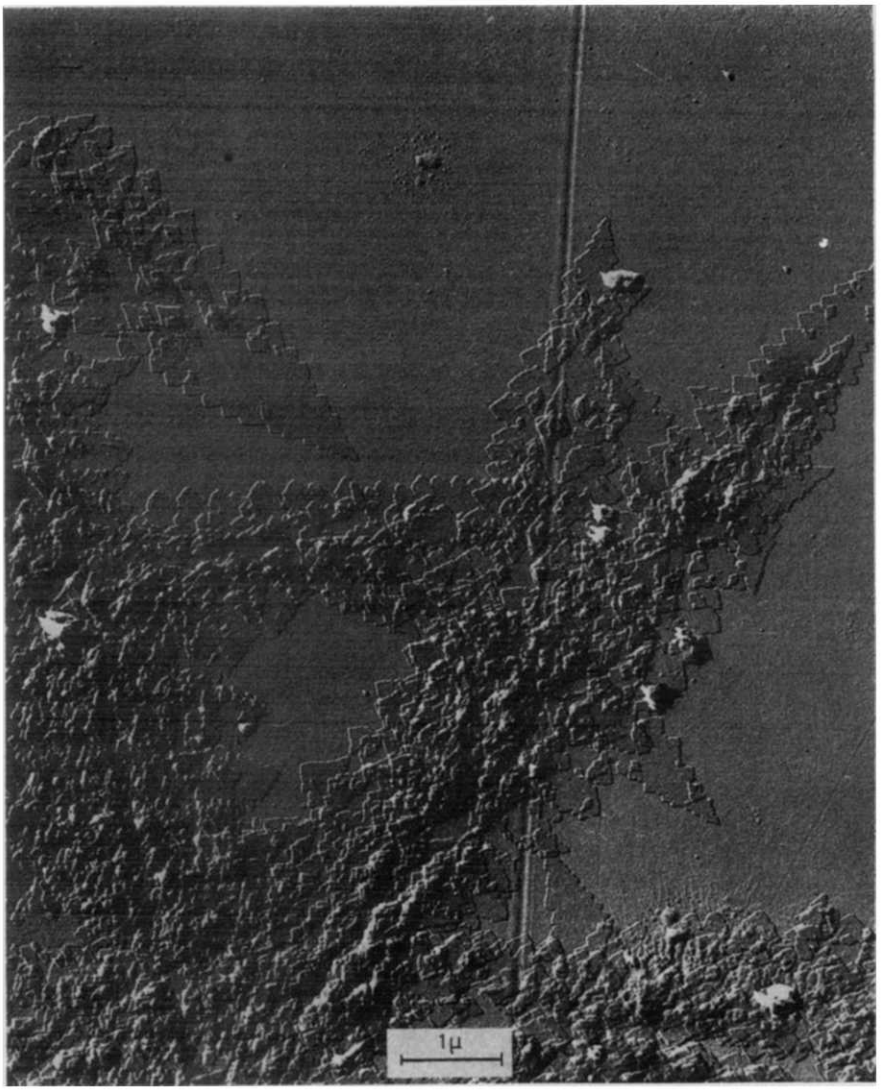

Figure 3—Electron micrograph of polyethylene crystals of molecular weight '80 000

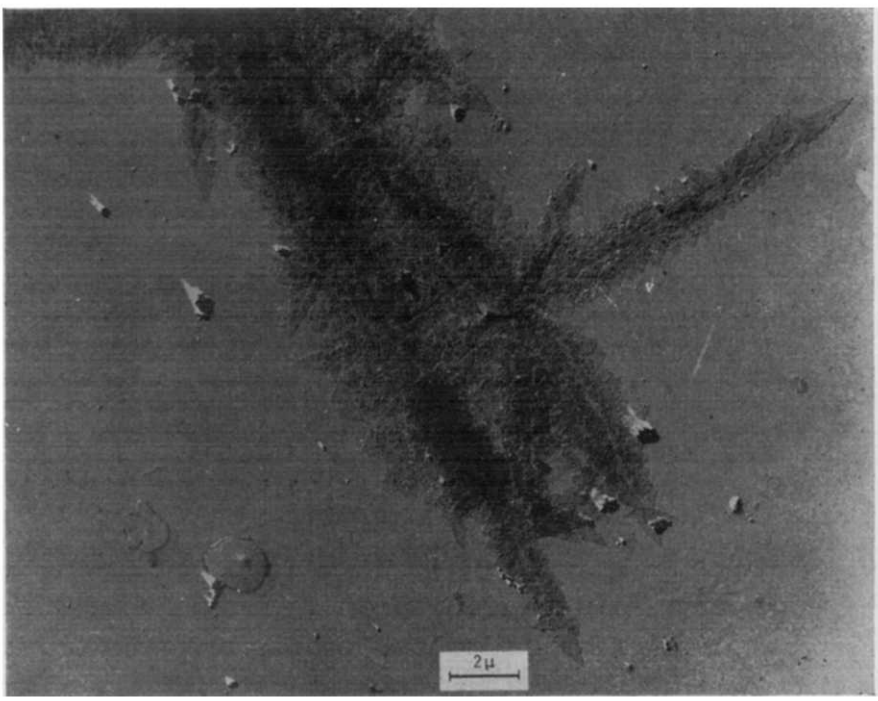

Figure 4—Electron micrograph of polyethylene crystals of molecular weight 121 000

Effect of branching on solution temperatures

There are two basic processes used in producing polyethylene—high pressure and low pressure. The high pressure branched polyethylene contains 8–40 CH_3 branches per 1 000 carbons compared to less than 5 CH_3 per 1 000 carbons for the low pressure linear species. Both types will crystallize from dilute solution in platelet form. However, the branched material has been shown to give smaller, less perfect crystals owing to the short chain branches[10].

Three different polyethylenes were investigated with the DTA solution cell: a linear polyethylene (Philips Marlex 6050), a slightly branched polyethylene (Du Pont Alathon 71 X-N) and a highly branched polyethylene (Du Pont Alathon 10).

The solution behaviour of Alathon 71 X-N (*Figure 6*) grown under identical conditions as Marlex 6050 (slow cooled-large volume vessel), was compared to Marlex. At a heating rate of 20 deg. C/min, the solution endotherms were identical for the Alathon 71 X-N and the Marlex 6050 suspensions. At 10 deg. C/min the Alathon 71 X-N endotherm exhibited a low temperature shoulder which had no counterpart in the Marlex 6050 endotherm. Upon recrystallization from a 1·0% wt solution at a cooling rate of 10 deg. C/min, recrystallization occurred at 66°–67°C for Alathon 71 X-N, about 3 deg. C lower than the recrystallization for the Marlex 6050.

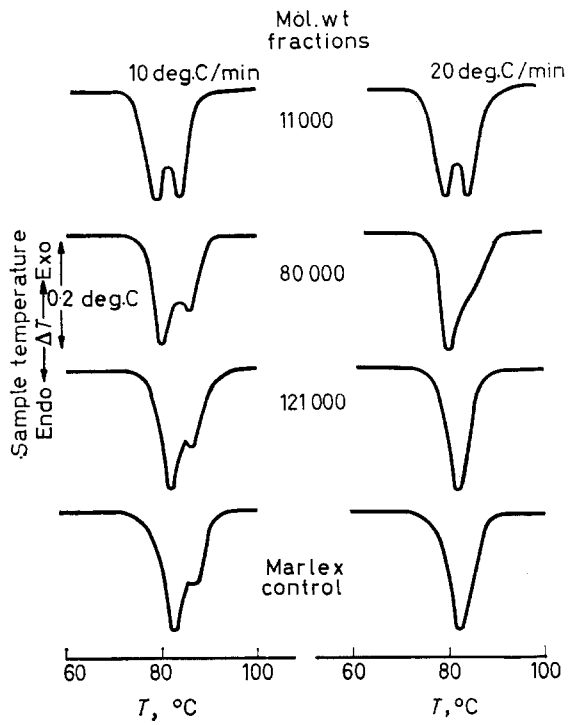

Figure 5—Solution thermograms of fractionated polyethylenes

This reduction in crystallization temperature may be due to the small (but apparently not negligible) amount of branching in Alathon 71 X-N.

When the linear and slightly branched polyethylene were quenched from solutions at 110 deg. C to room temperature, the subsequent solutions at heating rates of 10, 20 and 40 deg. C/min exhibited different behaviour. All six thermograms show two endothermic peaks (*Figure 7*) and, for both polyethylenes, decreasing the heating rate caused a decrease in area for the low dissolution endotherm. This low temperature peak we suggest represents the solution of the quenched material. The higher peaks may result from solution of material which undergoes reorganization during heating. The slower the heating rate, the greater would be the amount of reorganization. *Figure 7* shows that the Alathon 71 X-N crystals reorganize faster than the Marlex 6050 crystals.

When the chain branching is increased beyond the small amount of Alathon 71 X-N, solution crystallized Alathon 10 exhibits a much broader and lower solution endotherm (*Figure 8*). The increased branching also has produced a smaller yield of crystals. A significant amount of branched material remained dissolved. No good electron micrographs were obtained since the undissolved branched material deposited on the microscope slides as an amorphous layer after solvent evaporation and obscured the crystallites.

Effect of annealing on solution behaviour

Annealed polyethylene crystals have increased fold period producing an increase in melting point or solution temperature[16]. The increase in the fold

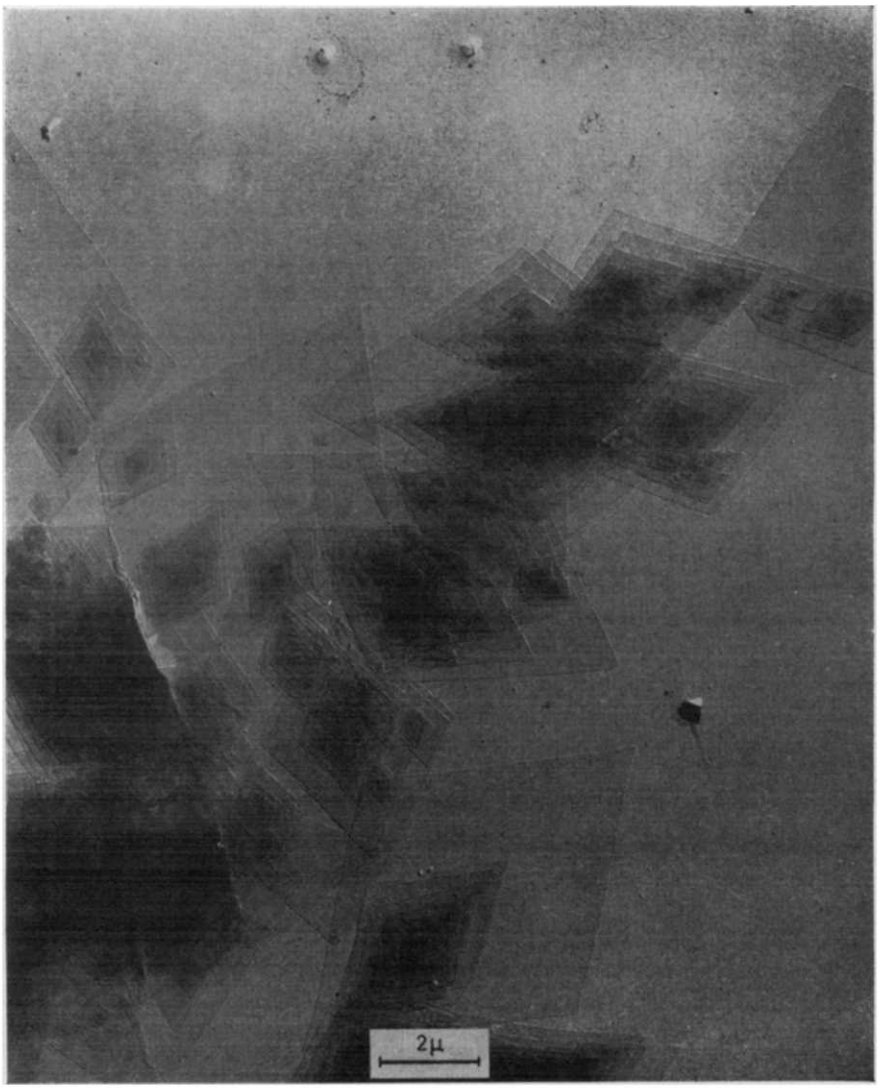

Figure 6—Electron micrograph of slow cooled crystallized polyethylene (Alathon 71 X-N)

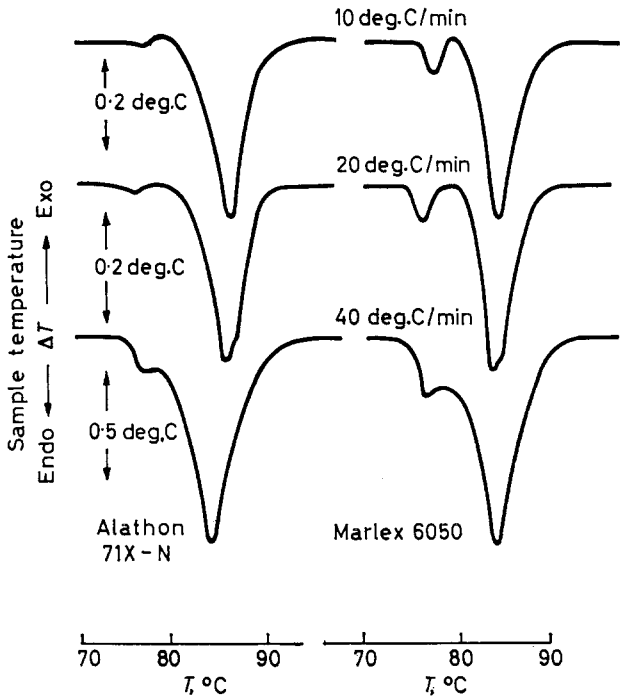

Figure 7—Solution behaviour of quenched samples of slightly branched and linear polyethylenes

period may involve a reorganization, and/or a melting or solution followed by recrystallization. In order to be more explicit in describing the results obtained in crystal suspensions, annealing will be taken to mean reorganization. That is, when a sample in suspension is held at a temperature below the solution point, annealing by reorganization will be invoked as the mechanism for crystalline perfection. When the 'hold' (annealing) temperature coincides with any part of, or is above, the solution range of the sample the process will be referred to as solution and recrystallization.

Single crystal suspensions (1·0% wt) were used to study 'annealing' behaviour in solution. *Figures 9*B and C are the resulting solution thermograms after the suspension had been heated to 80°C and 88°C respectively in the DTA cell, held there for 15 minutes, and cooled to room temperature.

A comparison of *Figures 9*B and C with *9*A shows considerable change in the annealed samples. When the hold temperature is below the solution temperature of the suspension (80°C) the modification in the solution behaviour is evident at two points. First, the initial departure of the baseline during dissolution is shifted to the hold temperature and the new slope is much more abrupt. Secondly, a new shoulder or inflection occurs on the high side of the dissolution peak of the annealed samples.

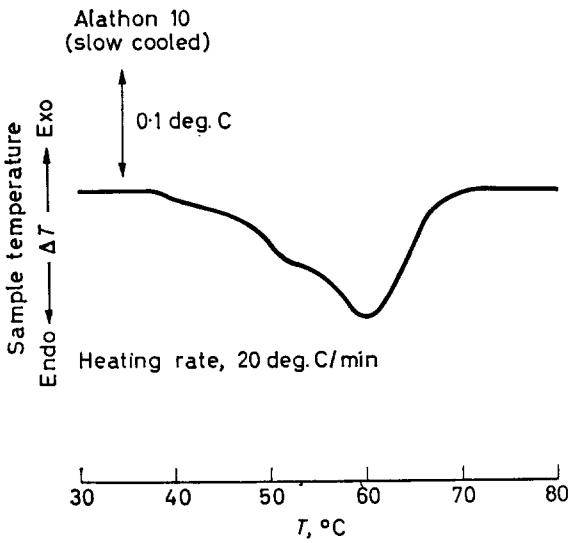

Figure 8—Solution behaviour of highly branched polyethylene

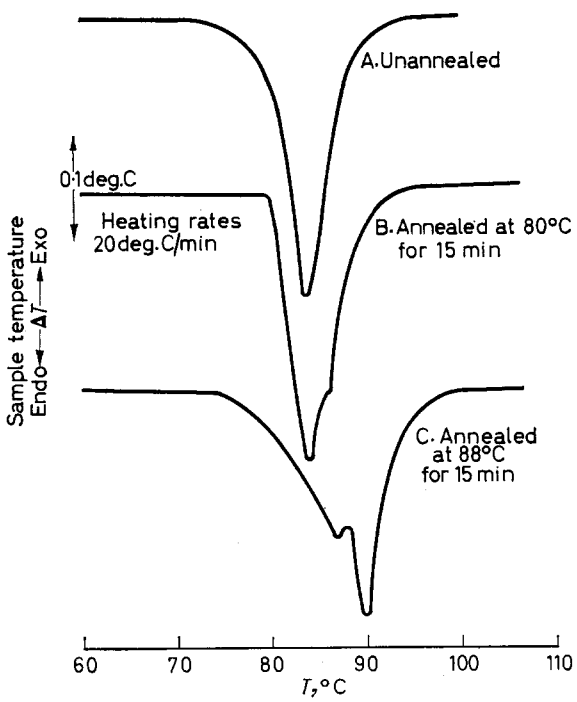

Figure 9—Effect of annealing temperature on solution behaviour of slow cooled crystallized polyethylene (Marlex 6050)

The sharpness of the onset of the solution in *Figure* 9B results from elimination by recrystallization of the lower dissolving portions of the sample. When the sample was cooled to room temperature, prior to the solution run, no crystallization was detected. Thus, the material responsible for this lower portion of the solution endotherm had recrystallized to a more stable form during the hold condition. The high temperature shoulder may also be due to annealed material from the material associated with the main solution peak.

After holding the single crystal suspension for 15 minutes at 88°C (*Figure* 9C), the original solution endotherm is not evident. Furthermore, two separate peaks at elevated temperatures have been produced. At the 88°C hold temperature nearly complete solution of the initial suspension occurs. Upon cooling to room temperature prior to the solution run, a small crystallization peak was detected at 80°C. The material crystallizing at this temperature redissolved at 87°C. The 90°C solution peak is due to the polymer which recrystallized during the isothermal hold condition at 88°C.

CONCLUSIONS

At slow cooling rates, polyethylene fractions crystallize from solution at temperatures which increase with increasing molecular weight. Similar observations by Keller and Kawai[17] show that during isothermal crystallization of unfractionated polyethylene the high molecular weight portion of the polymer crystallizes first.

Linear and slightly branched polyethylenes show very similar solution behaviour. The differences between the solution behaviour of these types of polyethylenes may be influenced more by the molecular weight differences than by the small differences in number of pendant groups. The highly branched polyethylene shows a lower and broader solution thermogram.

The authors thank the National Science Foundation for their support of this work.

Division of Polymer Science,
Case Western Reserve University,
Cleveland, Ohio 44106

(Received June 1967)

REFERENCES

[1] WUNDERLICH, B. and KASHDAN, W. H. *J. Polym. Sci.* 1961, **50**, 71
[2] KÊ, B. *J. Polym. Sci.* 1962, **61**, 47
[3] HELLMUTH, E. and WUNDERLICH, B. *J. appl. Phys.* 1965, **36** (No. 10), 3039
[4] WUNDERLICH, B., SULLIVAN, P., ARAKAWA, T., DICYAN, A. B. and FLOOD, J. F. *J. Polym. Sci.* 1963, **A1**, 3581
[5] WUNDERLICH, B., CORMIER, C. M., KELLER, A. and MACHIN, M. J. To be published
[6] KÊ, B. *J. Polym. Sci.* 1961, **50**, 79
[7] BLACKADDER, D. A. and SCHLIENITZ, H. M. *Polymer, Lond.* 1966, **7**, 603
[8] WUNDERLICH, B. and ARAKAWA, T. *J. Polym. Sci.* 1964, **A2**, 3697
[9] KÊ, B. *J. Polym. Sci.* 1963, **A1**, 1453
[10] BRANDRUP, J. and IMMERGUT, E. H. (Eds.) *Polymer Handbook*. Interscience: New York, 1966

[11] WENDLANDT, W. W. *Thermal Methods of Analysis.* Interscience: New York, 1964
[12] E. I. Du Pont de Nemours and Co., Inc., Du Pont 900 Thermal Analyzer Instruction Manual, Wilmington, Delaware
[13] KOENIG, J. L. and CARRANO, A. *J. Polymer, Lond.* 1968, **9**, 359
[14] LANCELY, H. A. and SHARPLES, A. *Makromol. Chem.* 1966, **94**, 30
[15] WUNDERLICH, B., JAMES, E. A. and SHU, T. W. To be published
[16] BASSETT, D. C. and KELLER, A. *Phil. Mag.* 1962, **7**, 1553
[17] KELLER, A. and KAWAI, T. *Polymer Letters,* 1964, **2**, 333

Intramolecular Transformations of Polyisoprene Chains in the Process of Sulphur Vulcanization

I. A. TUTORSKY, L. A. SHUMANOV and B. A. DOGADKIN

The change of cis *double bond content during vulcanization of natural and synthetic polyisoprenes has been studied[1]. This process has been compared with the formation of crosslinks, the change of polysulphide sulphur content and zinc sulphide content. The diminution of double bonds coincides with the reverse part of the curve characterizing the change of number of crosslinks and is caused mainly by intramolecular cyclic sulphide formation. The symbacity of the decrease* cis *double bond content and accumulation of polysulphide sulphur reaction products testifies to the formation of intramolecular cyclic sulphides due to polysulphide sulphur reactions with double bonds. Both in the presence of activators and without them, two double bonds that have participated in the reaction fall on each sulphur atom bonded intramolecularly. Thus, cyclic sulphides are formed by the reactions of polysulphide sulphur with double bonds and not with α-methylene groups and have the same structure as the model system of dihydromircene-sulphur. The kinetic study of crosslink formation and of polysulphide sulphur has been made in addition to the latter's further change into cyclic sulphides and zinc sulphide. Experimental values of the main structural parameters of vulcanizates are in fair accord with the theoretical relationship obtained. The tensile strength of vulcanizates falls sharply in the range of decrease of* cis *double bond content by 10 to 15 per cent for natural and 5 to 10 per cent for synthetic polyisoprenes. Irregularity of structure of chain segments due to intramolecular cyclic sulphide formation seems to be one of the factors leading to reversion of vulcanization.*

DURING sulphur vulcanization of polyisoprene some intramolecular-type reactions take place which lead to the microstructure change of chain segments in the vulcanizate. Because of the appearance of a new band at 965 cm^{-1} in the infra-red spectra of vulcanizates it was supposed[1] that the change of microstructure is connected with the formation of cyclic sulphides, conjugated double bonds and double bond migration with disubstituted structure formation. The investigation of the structure of sulphides formed by heating sulphur with low molecular model substances (dihydromircene) has led some English scientists[2] to conclude that, among the three mentioned intramolecular processes, the formation of cyclic sulphides prevails owing to the destruction of previously formed crosslinks. Because of the difference in reactivity of double bonds in low and high molecular substances[3], the transfer of the results obtained with model systems to real vulcanization conditions should be made with great care. The microstructure change of vulcanizate segments was observed as a high sulphur percentage (4 to 15 per cent), as at ordinary sulphur contents the 965 cm^{-1} band is of low intensity.

Literature data available at present enable only a qualitative assumption to be made about the mechanism of reactions resulting in the change of the microstructure of polymer segments.

This work is aimed at the establishment of a relationship between the

change of microstructure of polymer segments and other processes taking place during vulcanization, such as sulphur addition and crosslinking.

An attempt was made to study the influence of microstructure change on the tensile strength of vulcanizate.

METHODS AND MATERIALS

Pale crêpe natural rubber (NR) that had not been specially purified and synthetic *cis*-1,4-polyisoprene SKI-3 containing stearic acid, neozone D and diphenylphenylenediamine were used. Mixtures were prepared on laboratory mills and vulcanized in the press at a temperature and pressure of 140° to 142°C and 2 150 lb/in^2, respectively. At certain stages of vulcanization some parameters such as the content of bonded and polysulphide sulphur, zinc sulphide, degree of crosslinking and the change of microstructure of polymer segments were measured. Bonded sulphur was determined by the Schöniger method of burning an acetone-extracted vulcanizate sample on platinum contact in oxygen. Evolved sulphur dioxide is absorbed by hydrogen peroxide and SO_4^{2-} ions are titrated with barium nitrate[4]. The amount of zinc sulphide was determined from the difference between sulphur content in the vulcanizate before and after hydrochloric acid treatment. The content of polysulphide sulphur was determined from the difference of sulphur content in the vulcanizate treated with hydrochloric acid and lithium aluminium hydride ($LiAlH_4$) ether solution. The degree of crosslinking was calculated from the swelling maximum in *m*-xylene by using a correction factor for free chain ends and initial chain entanglement[5].

The change of microstructure of the vulcanizate chain segments was determined by infra-red spectroscopy. Because of the low intensity of the 965 cm^{-1} band, which appears during vulcanization, and the difficulties of the quantitative measurements, the 840 cm^{-1} band was used to evaluate the microstructure change; this band corresponds to the deformation vibration of the C—H bond in the structure

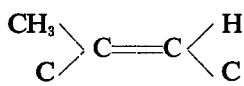

The measurements were made by the method of relative densities. The 1 378 cm^{-1} band (CH_3— group) was used as in internal standard, the intensity of which was kept constant.

The test-pieces were prepared by pressing the compound in the mould having a calibrated aluminium foil layer of $\approx$ 15 μ thickness. Spectra were obtained on an IR – 10 spectrometer.

To determine the absolute content of *cis* double bonds in the vulcanizate, the calibration relationship was obtained between the number of *cis* double bonds remaining in the vulcanizate after treatment with a known amount of perbenzoic acid and the number of double bonds determined spectroscopically (*Figure 1*). The mean-square error was $\pm$1·2 per cent.

KINETICS OF DIFFERENT PROCESSES PROCEEDING DURING VULCANIZATION

The decrease in content of *cis* double bond during vulcanization is an

overall process. A theoretically possible contribution to this may be made by crosslinking reactions at the double bonds, *cis-trans* isomerism, the transfer of double bonds and the formation of cyclic sulphides. When heating vulcanizates at 140°C for 300 min no bands appear at 1 100 to 1 150 cm^{-1}, 1 330 cm^{-1}, 1 385 cm^{-1} or 2 965 cm^{-1} which would be characteristic for *trans* trisubstituted double bonds. Consequently, *cis-trans* isomerism does not contribute much to the total process, this fact being in accord with the literature data[1].

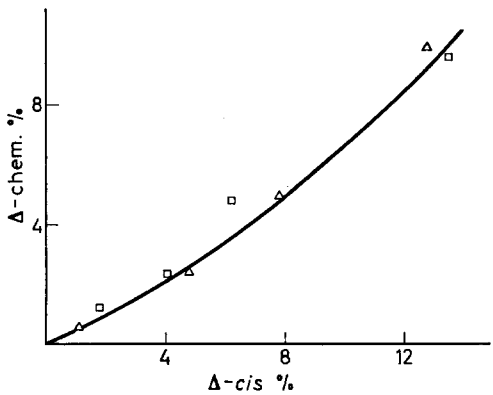

Figure 1—Calibration dependence between spectral (Δ-*cis*) and chemical (Δ-chem.) change of *cis* double bond content

Figure 2 shows the kinetics of crosslinked formation (curve 1) and the decrease of *cis* double bond content (curve 2) during vulcanization of the compound containing 2·6 parts by weight of sulphur and 2·5 parts of santocure per 100 parts of natural rubber. In the initial stage of vulcanization (first ten minutes) intensive crosslinking was observed and the diminution of double bonds was extremely insignificant. Even if it is assumed that all crosslinks are formed through reaction at the double bonds, the share of *cis* double bonds that participated in crosslinking reactions will be only 0·5 per cent. As the transfer of double bonds takes place as a process accompanying crosslinking, its contribution to the overall process of *cis* double bond content decrease is not high.

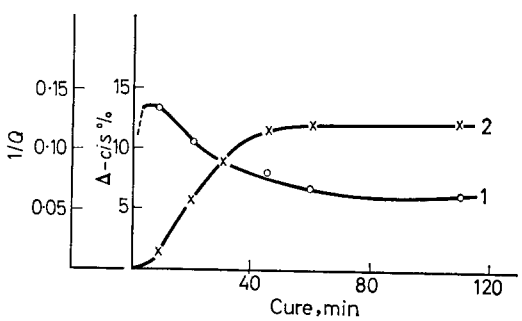

Figure 2—Kinetics of *cis* double bond content decrease (curve 2) and formation of crosslinks (curve 1). Compound formulation (parts by weight): natural rubber—100; sulphur—2·6; santocure—2·5

The diminution rate of *cis* double bonds is at its greatest for a 10-minute period starting 20 minutes after the beginning of the process. The content of crosslinks then drops.

For compounds of similar composition the decrease of polysulphide sulphur content coincides with the decrease of crosslink content[6]. Thus, the main process which results in the decrease of *cis* double bonds content is the formation of cyclic sulphides.

To determine the structure of the cyclic sulphides formed, it is interesting to compare the amount of intramolecular bonded sulphur with the diminution of double bonds. As seen from *Table 1*, both in the presence of

Table 1. Structural characteristics of vulcanizates

Composition by weight; parts per 100 parts rubber	*Sulphur as zinc sulphide (atoms per 100 iso-pentene groups)*	*No. of chemical cross-links (per 100 iso-pentene groups)*	*Sulphur in chemical cross-links† (atoms per 100 iso-pentene groups)*	*Sulphur in cyclic mono-sulphide groups (S′) (atoms per 100 iso-pentene groups)*	Δ-*Chem.* %	Δ-*Chem.* S′
NR (100), sulphur (1·1) santocure (3)	—	0·006	0·12	2·24	3·8	1·7
NR (100), sulphur (1·0) santocure (3)	—	0·089	0·18	3·88	6·9	1·78
NR (100), sulphur (3·1) santocure (3)	—	0·156	0·31	6·24	9·1	1·46
NR (100), sulphur (4·2) santocure (3)	—	0·258	0·52	8·48	16·0	1·89
NR (100), sulphur (1·2) DPhG (2·5)	—	0·005	0·01	2·54	4·0	1·57
NR (100), sulphur (2·0) DPhG (2·5)	—	0·055	0·11	4·14	7·1	1·72
NR (100), sulphur (3·0) DPhG (2·5)	—	0·16	0·32	6·03	10·0	1·67
NR (100), sulphur (4·3) DPhG (2·5)	—	0·36	0·72	8·43	15·9	1·89
SKI-3 (100), sulphur (3·5) santocure (1) ZnO(5), stearic acid (2)	2·21	1·33	2·66	2·48	4·6	1·86
SKI-3 (100), sulphur (4·4) santocure (1) ZnO(5), stearic acid (2)	3·3	1·62	3·24	2·81	5·5	1·96
SKI-3 (100), sulphur (3·5) Captax (2) ZnO(5), stearic acid (2)	2·47	0·97	1·94	3·04	6·0	1·97

†All crosslinks were considered as disulphide links.

activators and without them, two double bonds that have participated in the reaction fall on each intramolecular bonded sulphur atom. In cyclic sulphides formed by heating dihydromircene, two reactive double bonds also fall on each sulphur atom.

Therefore, the decrease of *cis* double bond content in the vulcanization of polyisoprene is mainly the result of cyclic sulphide formation, the structure of the latter being similar to that of heterocycles produced by the

reaction of dihydromircene with sulphur. Cyclic sulphides are formed by the reaction of polysulphide sulphur with polymer double bonds, as the formation of heterocycles through the sulphur atom bound with the hydrogen atom in the α-position to the double bond would cause one double bond to disappear.

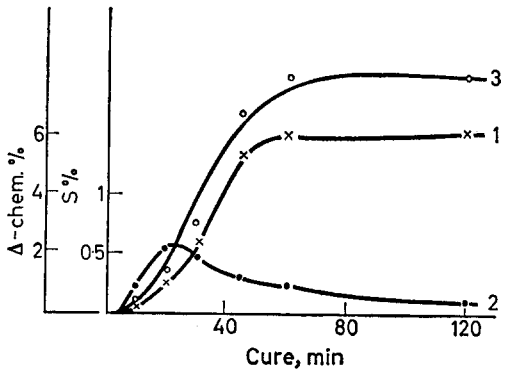

Figure 3—Kinetics of *cis* double bond content decrease (curve 1) and change of polysulphide sulphur content (curve 2). Curve 3 is the graphical integration of reaction products of polysulphide sulphur. Compound formulation (parts by weight): SKI-3—100; S—4; Captax—2; ZnO—5; stearic acid—2

Figure 3 shows the kinetics of the decrease of *cis* double bond content (curve 1) and the change in the amount of polysulphide sulphur (curve 2). Curve 3, which shows the rate of formation of polysulphide sulphur double bond reaction products, was obtained by graphical integration of curve 2. On the same scale this curve coincides with that of the decrease of *cis* double bond content. Consequently, in the general scheme of the process the stage of polysulphide bond formation must precede the formation of cyclic sulphides, which results in the decrease of *cis* double bond content.

For the mixtures containing activators it may be assumed that zinc sulphide is obtained by the reaction of Zn^{2+} with polysulphide bonds. The general scheme of reactions taking place during vulcanization is as follows.

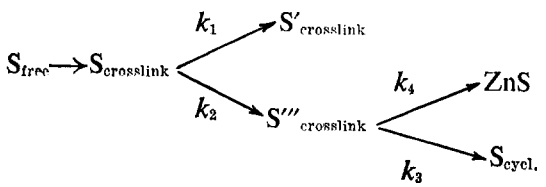

Sulphur combines with rubber to form crosslinks ($S_{crosslink}$). During vulcanization some bonds ($S''_{crosslink}$) change, which results in the formation of zinc sulphide and cyclic sulphides (S_{cycl}). In the process of sulphur addition, sulphur accumulates in crosslinks; this sulphur is incapable of transforming to ZnS and cyclic sulphides.

EFFECT OF MICROSTRUCTURE CHANGE ON TENSILE STRENGTH

The effect of change of microstructure of vulcanizate chain segments on the tensile properties is illustrated by the dependence of tensile strength

of natural and synthetic polyisoprene rubber vulcanizates on the change of *cis* double bond content (*Figure 4*). The vulcanizates had the same network density, which was obtained by changing the concentration of vulcanizing

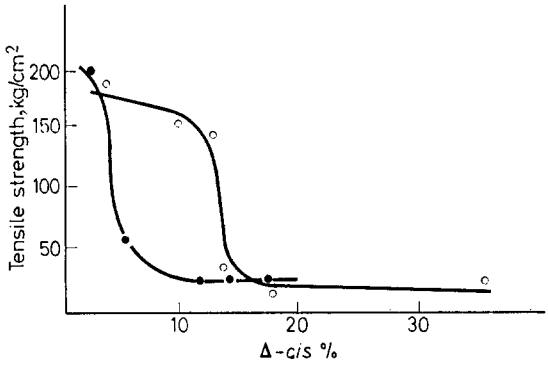

Figure 4—Tensile strength change versus the decrease of *cis* double bond content (Captax as an accelerator)

groups and vulcanization time. The decrease of *cis* double bond content results in a sharp drop of tensile strength in the range of $\Delta - cis$ by as much as 10 to 15 per cent for natural and 5 to 10 per cent for synthetic polyisoprenes. This difference is accounted for by the fact that the original synthetic type of polyisoprene already contained 7 to 8 per cent of irregular structure. Therefore, the formation of cyclic intramolecular structures during vulcanization results in the same effect of strength decrease that is observed in the case of irregularity of the structure caused by *cis-trans* isomerism under the action of sulphur dioxide[7].

The Lomonosov Institute of Fine Chemical Technology,
M. Pirogovskaya Street No. 1,
Moscow G-435,
U.S.S.R.

(*Received June 1967*)

REFERENCES

[1] SHIPMAN, J. J. and GOLUB, M. A. *J. Polym. Sci.* 1962, **58,** 1063
[2] BATEMAN, L., GLAZEBROOK, R. W. and MOORE, C. G. *J. chem. Soc.* **1958, 2846**
[3] TUTORSKY, I. A., NOVIKOV, S. V. and DOGADKIN, B. A. *Uspekhi Khimii, Mosk.* 1966, **35,** 191
[4] CHELISHCHEVA, G. A., CHEBYSHEVA, G. M. and SHCHERBACHEV, G. P. *Kauch. Rezina,* 1961, **No. 2,** 33
[5] MULLINS, L. *J. appl. Polym. Sci.* 1959, **2,** 1
[6] SCHEELE, W. and TSCHEKAS, A. *Kautsch. u. Gummi,* 1954, **18,** WT 501
[7] CUNNEEN, J. I. and HIGGINS, G. M. C. '*Cis-trans* isomerism in natural polyisoprenes', in *The Chemistry and Physics of Rubberlike Substances,* p. 36. (Ed. BATEMAN, L.) MacLaren: London, 1963

Electron Microscope Studies on the Etching of ABS Mouldings for Electroplating

KOICHI KATO

A method is described for preparing ultrathin sections through etched ABS surfaces. A layer of resinous black ink is used to identify and protect the surface during sectioning, and the specimen is treated with osmium tetroxide, which stains both the rubbery phase in the ABS and the ink layer. Electron micrographs show that the rubber particles are etched preferentially, but that some particles are etched more readily than others. This difference may be connected with differences in the structure of the surrounding matrix.

AN electron microscope study on ABS mouldings for electroplating was described in a previous paper[1]. In that work a PVA replica technique was used to examine surface etch patterns produced by the preparatory process for ABS metal-plating, and it was shown that the chemical etchant (chromic–sulphuric acid mixture) selectively attacks the rubber particles, leaving the resin matrix relatively unaffected. As a result of this differential effect, a large number of minute etch cavities are formed in the surface of ABS mouldings. It has been suggested that a surface etch structure of this kind might well account for the high adhesive strengths observed in metal-plated ABS[2].

In that earlier investigation[1] the osmium tetroxide procedure for ultra-sectioning ABS plastics[3] was used to reveal moulding flow patterns in the surface layer of the ABS, and the relationship between the moulding conditions and peel strength was discussed on the basis of the relevant electron micrographs.

The present work was carried out with the aim of revealing surface etch patterns not by replication, but in profile by means of a sectioning technique. However, in order to examine surface topography in profile, it is necessary to preserve the original specimen surface under study, as one edge of each thin section. Ultrathin sections for electron microscopy are usually as small as half a millimetre square, and the etched edge must be distinguishable in some way from the other three edges. Moreover, as the etching proceeds the surface roughness will increase, with deeper and deeper cavities, and unless suitable measures are taken, it will be difficult to preserve the surface details intact during sectioning.

It has been found that a felt-tipped pen charged with an oily black ink is useful in overcoming these difficulties. The ink is smeared on to the surface to be examined before trimming the moulding for sectioning, and the black stain identifies this surface throughout the subsequent procedures. As the ink penetrates accurately into every cavity, etch patterns can be observed in profile by light microscopy, as exemplified in *Figure 1*. It is however, in electron microscopy that this smear method proves its true merits.

Test specimens were moulded in the form of 3 mm thick plaques from two types of commercial ABS resin (types A and B). They were processed by a standard plating procedure, in which the degree of etching was controlled by varying the etching period at 65°C in an acid mixture of specific gravity 1·64.

All sectioning was carried out in the direction normal to the etched surface. For light microscopy, sections about 3 μ thick were mounted in K_2HgI_4–glycerol[4] and examined in transmitted light. For electron microscopy the osmium tetroxide procedure[3] was applied, and ultrathin sections about 350 Å thick were cut by means of an LKB ultramicrotome.

The photomicrographs shown in *Figure 1* (a, b and c) demonstrate that the smeared ink layer not only identifies the section edge originating from the etched surface, but also reveals etch pattern profiles to some degree.

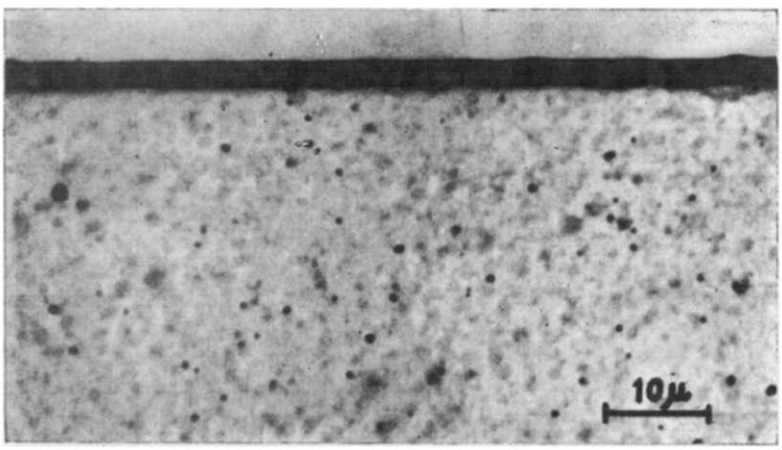

(a)

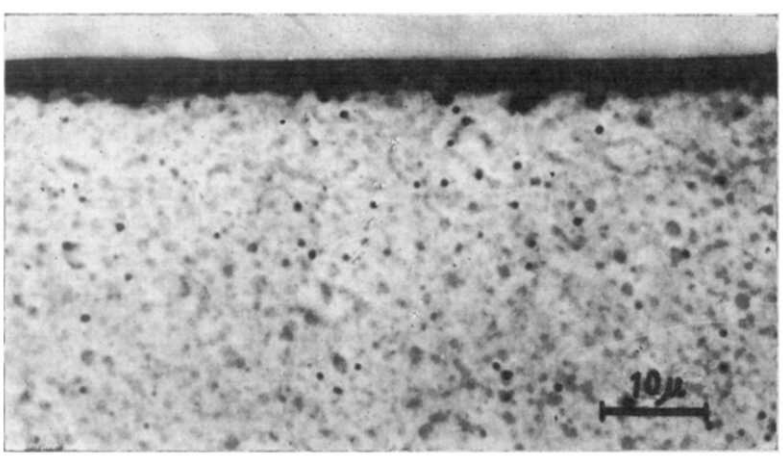

(b)

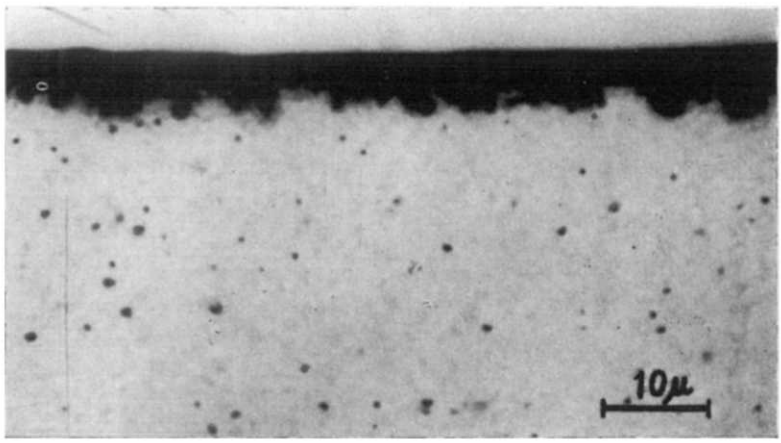

(c)

Figure 1—Thin sections through ABS specimens moulded from type B resin. The wide dark band in the upper part of each picture is the smeared ink layer, while the tiny dark spots are pigment particles: (a) untreated, (b) etched for 10 min, and (c) etched for 45 min

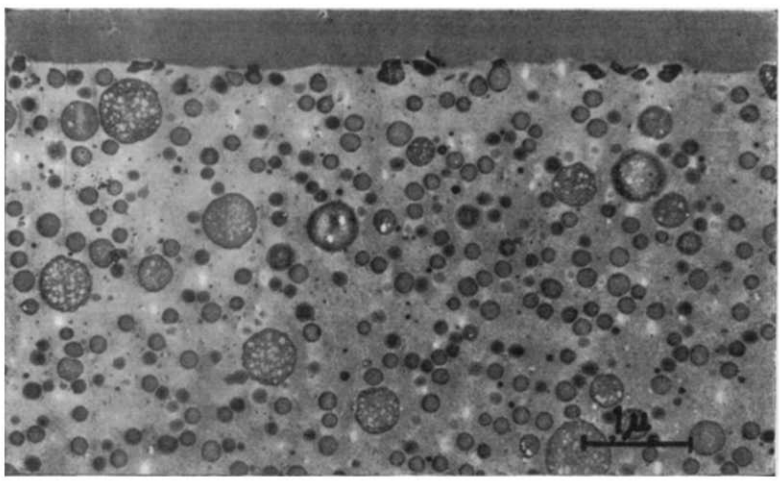

Figure 2—Ultrathin section through untreated surface of type A resin. The grey portion at the top (throughout from *Figure 2* to *Figure 7*) represents the smeared ink layer

The ABS resin shown here (type B) is seen to contain some pigment particles.

During the fixing and staining of the ABS resin block by osmium tetroxide, the ink layer smeared on to the specimen surface is also stained, probably due to the shellac material that it contains. Whatever the mechanism, the ink layer becomes very electron-dense, with the result that it

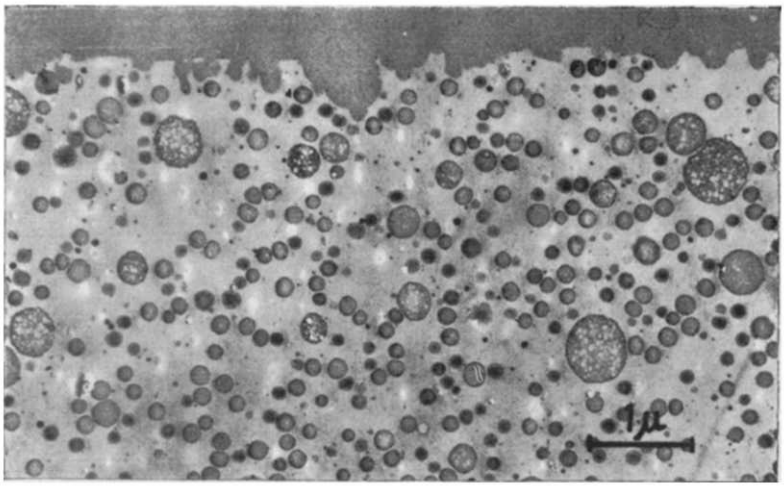

Figure 3—Ultrathin section through surface of type A resin after etching for 10 min

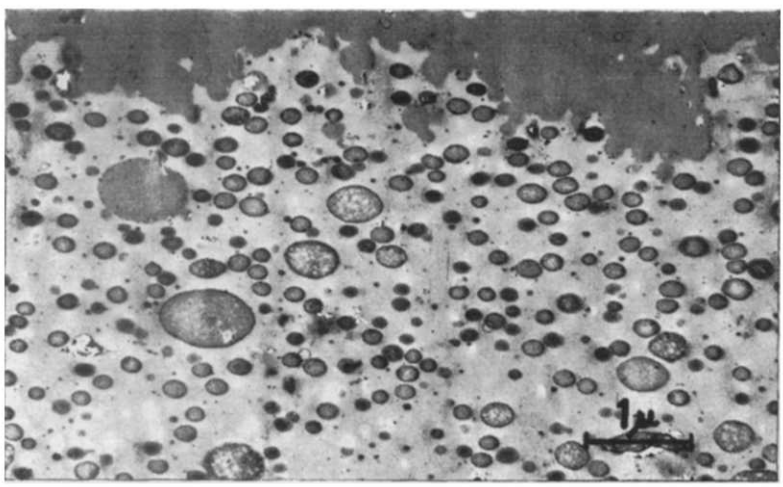

Figure 4—Ultrathin section through surface of type A resin after etching for 45 min

gives an excellent contouring effect against the section edge in question. In addition, it should be emphasized that the ink forms a continuous film over the whole surface, including the deepest cavities, thus protecting the surface irregularities from collapse during the sectioning operation.

The electron micrographs shown in *Figures 2, 3* and *4* are of ultrathin sections cut from type A resin specimens which had been etch-processed for 0, 10 and 45 min, respectively. The rubber particles in this resin have a wide distribution of diameters. It is evident from *Figure 3* that the rubber

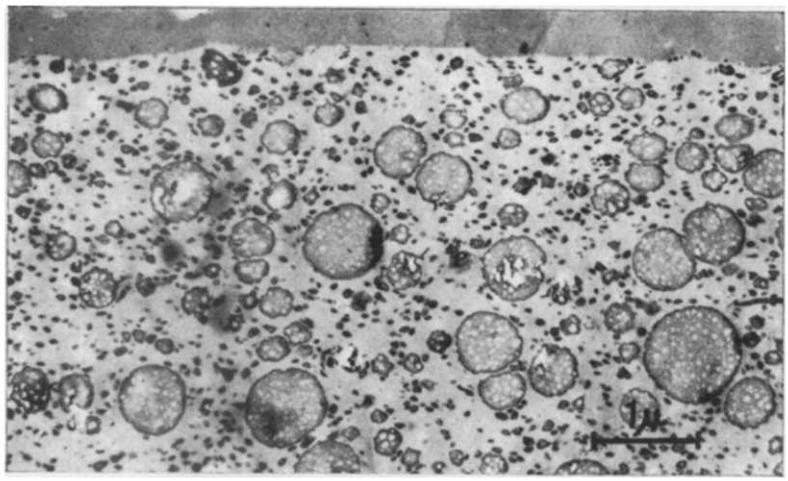

Figure 5—Ultrathin section through surface of type B, unetched resin

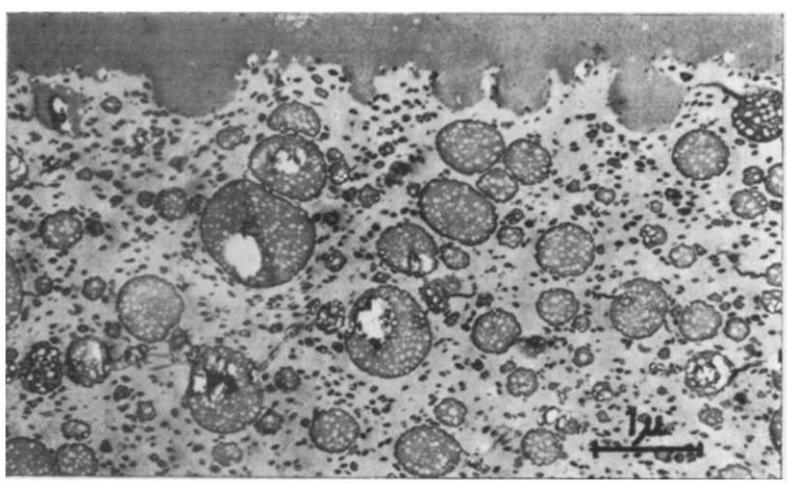

Figure 6—Ultrathin section through surface of type B resin after etching for 10 min

particles located in the surface are preferentially attacked and dissolved away to leave a large number of minute, 'dove-tailed'[2] hollow cavities. In *Figure 4* are shown several holes that appear to be occluded in the resin matrix, but as they are filled with ink, they must have been connected with the free surface by some form of channel.

The electron micrographs shown in *Figures 5, 6* and *7* were obtained from type B resin specimens that had been processed similarly to those described above. This type of resin is seen to contain rubber particles with a very wide range of diameters, and appears to be more readily etched than type A resin (compare *Figure 7* with *Figure 4*). It should be pointed out

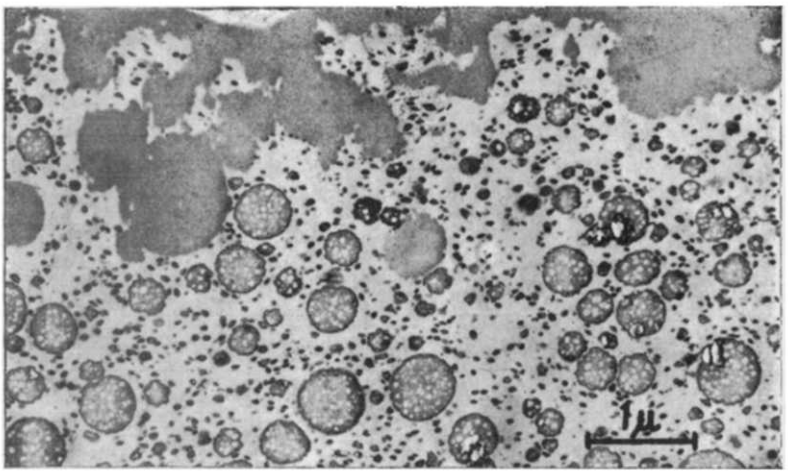

Figure 7—Ultrathin section through surface of type B resin after etching for 45 min

that only the larger rubber particles were attacked by the etchant, while the smaller ones in the immediate neighbourhood were left quite untouched. To understand this observation, a further study should be made of the structures in the copolymer phase surrounding the rubber-particle phase.

Zahn and Wiebusch[5] studied the electroplating of ABS plastics and showed a schematic diagram for the etching process on ABS mouldings. In its general features this picture is in good agreement with the results presented in the present paper. The chemical etching agent preferentially attacks the rubber particles and proceeds gradually from the surface into the interior, producing a complex etch pattern consisting of submicroscopic holes and canals. In fact, the particular suitability of ABS for electroplating can in general terms be attributed to these etching characteristics[2]. It appears, however, that more detailed structures should be taken into consideration in order to gain a better understanding of the etching and plating characteristics of ABS resins.

The author wishes to express his sincere thanks to Messrs K. Yoshimura, M. Nishimura, S. Horii and M. Yoshikawa for their skilful assistance throughout this study. He is also indebted to Dr O. Fukumoto and his staff for supplying suitable test specimens and for helpful discussions.

Central Research Laboratories,
Toyo Rayon Company, Ltd,
Otsu, Shiga-ken, Japan

(Received July 1967)

REFERENCES

[1] KATO, K. *Polymer, Lond.* 1967, **8**, 33
[2] Anon. *Rubb. Plastics Age*, 1966, **47**, 1204
[3] KATO, K. *Polym. Engng Sci.* 1967, **7**, 38
[4] TRAYLOR, P. A. *Analyt. Chem.* 1961, **33**, 1629
[5] ZAHN, E. and WIEBUSCH, K. *Kunststoffe*, 1966, **56**, 773

Fine Structures and Physical Properties of Styrene–Butadiene Block Copolymers

MASATO MATSUO, TAKU UENO, HIROSHI HORINO, SAYURI CHUJYO and HARUMI ASAI

Styrene–butadiene block copolymers appear to form heterogeneous two-phase systems, individual polybutadiene chains being dispersed in the polystyrene matrix. The physical properties are reported for a number of different kinds synthesized by the 'living polymer' technique. All samples approximated to the molecular weight $M_n = 1{\cdot}55 \times 10^5$.

BLOCK copolymers appear to show different properties from those of their component homopolymers and random copolymers. Block copolymers composed of rubber and plastic sequences are of special interest because of their contrasting properties. It thus seems important to know the effects of block chain length and types of sequence arrangements on the physical properties.

In the present study, several types of styrene(ST)–butadiene(BD) block copolymers representing SB, SBS, BSB, and SBSB* and some SBSs with varying BD sequence length have been synthesized. Variations of their physical properties were then investigated and fine structures in the solid state observed under the electron microscope.

While this study was in progress, similar findings were reported by Hendus, Illers and Ropte[1], who studied some physical properties of SBS block copolymers of varying sequence length. They also observed fine structures under the electron microscope.

BLOCK COPOLYMERIZATION

ST–BD block copolymers were synthesized by the 'living polymer' technique using *n*-butyl lithium catalyst in benzene at room temperature. The polymer was isolated from solution by pouring into methanol. It was then redissolved in benzene, and freeze dried.

First, four types of block copolymers of a given ST/BD mole ratio with varying sequence arrangements were prepared by changing the order of monomer addition. Whenever the same block sequences appeared twice in one block chain, they represented the same chain length.

Next, ST/BD mole ratios in SBS were changed from 80/20 to 40/60, and the samples expressed as SBS-1 to -5 as shown in *Table 2*.

All the samples used in the present study were prepared so as to attain the attempted molecular weight of $M_n = 1{\cdot}55 \times 10^5$.

For a comparison, an ionic copolymer (IC) was synthesized by polymerizing a mixture of the two monomers and a random copolymer (RC) synthesized by an emulsion method.

*S and B denote styrene and butadiene sequences, respectively.

CHARACTERIZATION

High resolution n.m.r. spectra of the block copolymers in a seven per cent carbon tetrachloride solution were observed at 60 Mc/s with tetramethylsilane (TMS) as a standard (*Figure 1*). Each one of the four peaks is

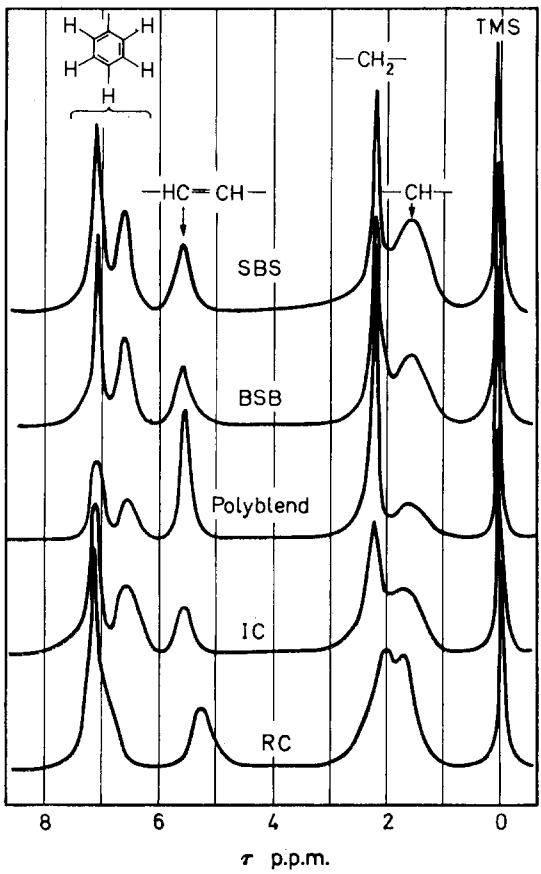

Figure 1—High resolution n.m.r. spectra of the ST–BD block copolymers, the blend of PS and PBD, and ST–BD random copolymer. (Hitachi, Model H-60)

assigned to the chemical shift of the protons of methyne (1·5 p.p.m.), methylene (2·1 p.p.m.), carbon–carbon double bond (5·4 p.p.m.) and phenyl (7·0 p.p.m.), respectively. The peak at 6·5 p.p.m. is the one separated from that of phenyl and has been assigned to the ortho-proton of PS of ten monomer units or more[2]. Spectra of SBS, BSB and IC are similar to that of a polystyrene–polybutadiene blend (Polyblend), but different from that of RC, indicating the presence of block chain sequences.

The relative height of the peak of methylene compared with that of methyne is larger in SBS and BSB than in the random copolymer. That of IC lies between them, suggesting that random copolymerization possibly occurred in a portion of the block chains.

A sharp single peak in the Schlieren pattern may indicate the absence of short chains from the three block copolymers. The molecular weights

(M_n) measured by the osmotic pressure method for the three block copolymers are greater than the expected values (*Table 1*). These facts indicate the probable partial loss of catalyst activity at the start of the polymerization.

Chemical compositions are determined by elementary analysis. ST contents were found to be somewhat higher than expected (*Table 1*).

Table 1. Characterizations of the samples

Samples	*ST/BD mole ratios (charged)*	*Molecular weights (Osmotic pressure)*	*ST/BD mole ratios (elementary analysis)*
SBS	60/40	$27{\cdot}9\times10^4$	64·1/35·9
BSB	60/40	28·6	67·4/32·6
IC	60/40	28·4	62·0/38·0
Commercial HI-PS	Styron 475 (Asahi Dow Co. Ltd)		
Polyblend	Blend of mono-dispersed polystyrene and *cis*-1,4-polybutadiene		

PHYSICAL PROPERTIES

Because of the limited amount of samples available, measurements were made for only one specimen.

Dynamic mechanical properties

Temperature dependences of the dynamic modulus (E') and the dynamic loss (E'') were measured by a direct-reading dynamic viscoelastometer

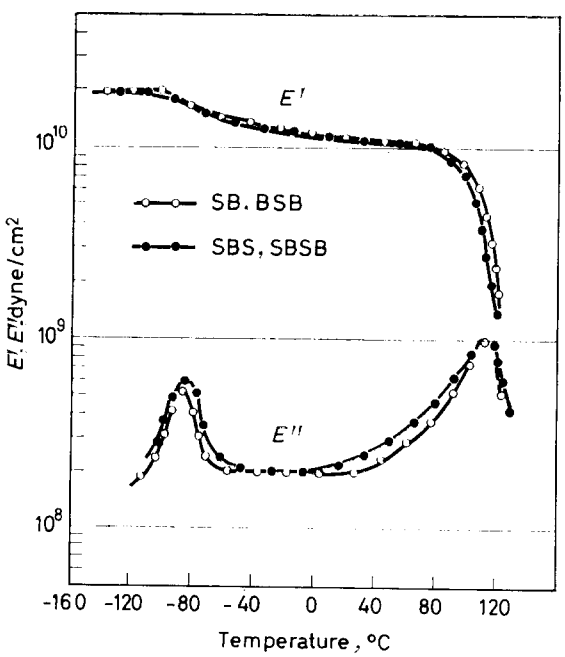

Figure 2 — Temperature dependences of dynamic modulus (E') and dynamic loss (E'') for the four types of ST–BD block copolymers. Measured frequency 110 c/s

'VIBRON DDV-II' (Toyo Measuring Instrument Co. Ltd) based on the principle developed by Takayanagi[5].

Despite the changes in sequence arrangements, each sample showed two E'' peaks at $-80°$ and 110°C, corresponding to that of pure polybutadiene (PBD) and polystyrene (PS), respectively (*Figure 2*). Thus a heterogeneous two-phase system is probably present in these block copolymers as observed in ABS polymer and high-impact polystyrene (HI-PS). The E'' value begins to increase at around 0°C in SBS and SBSB, which is slightly lower than that of SB and BSB.

In the ionic copolymer, however, the low temperature peak shifted up to -60°C and high temperature peak down to 95°C, suggesting the occurrence of random copolymerization in a portion of the block chains (*Figure 3*).

In SBS with various BD sequence lengths, the heights of the E'' peaks of the components varied in accordance with the changes in the ST/BD mole ratio, as expected (*Figure 3*).

Stress/strain behaviour

Stress/strain behaviour was observed by using a tensile tester (Shikoh

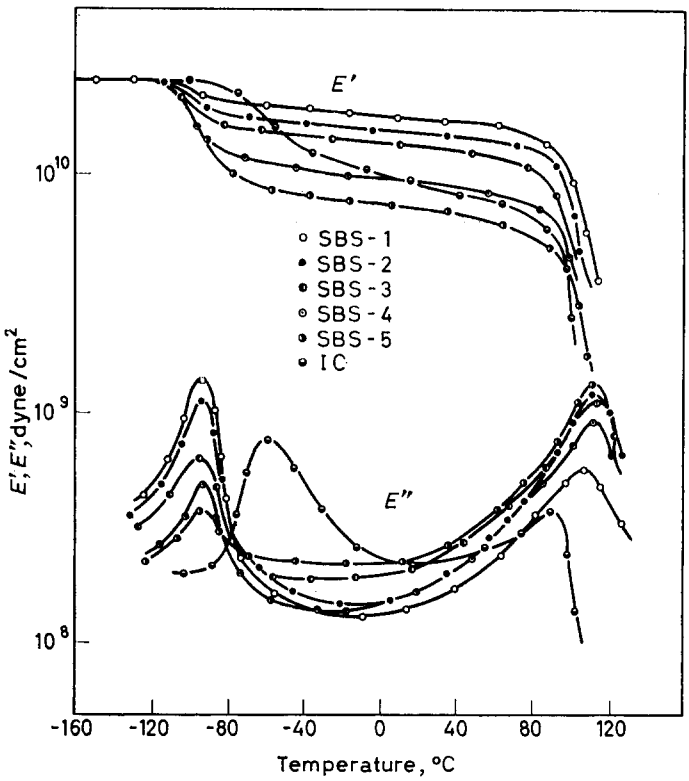

Figure 3—Temperature dependences of dynamic modulus (E') and dynamic loss (E'') for the SBS type block copolymers with varying BD sequence length and IC. Measured frequency 110 c/s

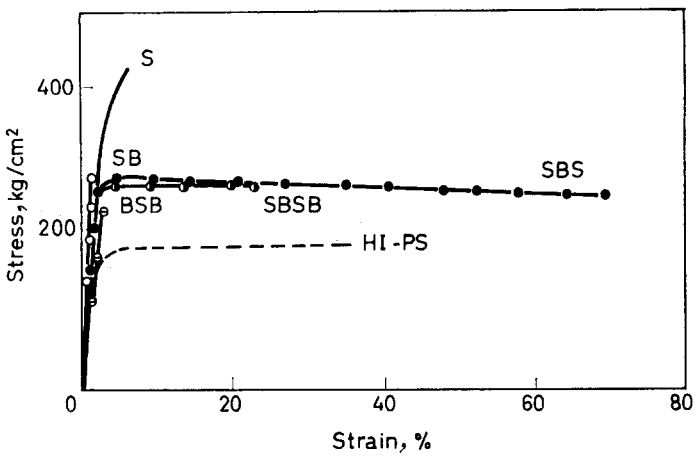

Figure 4—Stress/strain relationships for the four types of ST–BD block copolymers

Communication Industry Co. Ltd), at a strain rate of 0·5/min, at 25°C, under 65 per cent relative humidity.

The stress/strain behaviour is markedly affected by changes in the sequence arrangements (*Figure 4*). SBS and SBSB are extremely tough, as evidenced by their high elongation at break. It should be noted that SB and BSB are brittle in spite of the inclusion of the rubber component.

In SBS, the elongation at break increases and yield stress decreases with increasing BD sequence length as shown in *Figure 5*. Only SBS-4 showed unusually small elongation at break for ambiguous reason. The results of elongation at break are summarized in *Table 2*.

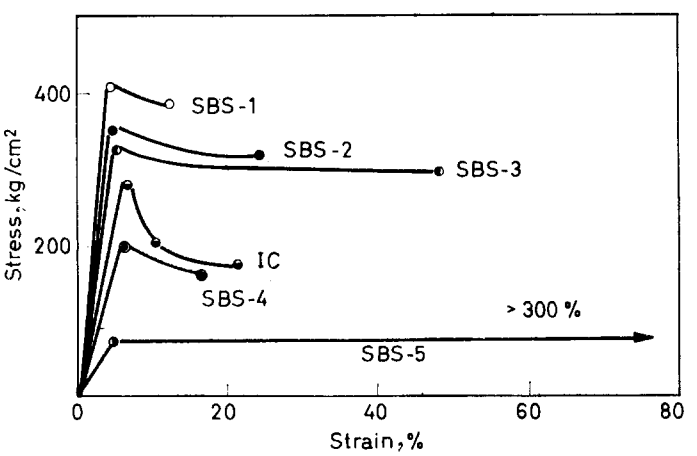

Figure 5—Stress/strain relationships for the SBS type block copolymers with varying BD sequence length

Optical properties

All the 1 mm thick plates of block copolymers appeared colourless and transparent, except that of SB, which was slightly translucent. Light transmittances of SBS, however, were smaller than that of pure PS and decreased with increase of BD sequence length (*Figure 6*). The results are summarized in *Table 2.*

Table 2. Properties of ST–BD block copolymers

Samples	*ST/BD mole ratios (charged)*	*Elongn at break*	*Light transmittance‡*	*Impact strength*	*Heat distort. temperature§*
		%	%		°C
S	100/0	7	90	2·1*	97
SB	60/40	2	62	2·5*	83
SBS	60/40	70	71	4·4*	67
BSB	60/40	2	51	2·4*	78
SBSB	60/40	23	70	3·1*	55
SBS–1	80/20	12	75	0·5†	100
SBS–2	70/30	25	81	0·4†	87
SBS–3	60/40	49	72	0·8†	66
SBS–4	50/50	17	68	>2·9†	54
SBS–5	40/60	>300	66	>2·9†	5
IC	60/40	22	57	1·6†	82
Commercial HI-PS	—	30	0	7·0*	75
Polyblend	60/40	2	0	0·5†	—

*Charpy impact strength (kg cm/cm²).
†Dynstatt impact value (kg cm).
‡Average values of the light transmittances of 1 mm thick plates measured at the wavelengths of 400, 500, 600 and 700 mμ.
§Clash and Berg method (JIS K-6745).

Refractive indices changed according to the BD content as with the ST–BD random copolymers (*Figure 7*).

Stress relaxation measurements

Stress relaxation behaviour was measured using SBS, BSB, IC and for a comparison, mono-dispersed PS as well as Polyblend by means of an Instron type tensile tester (Shimadzu Autograph IM–100) as shown in *Figure 8*. Because of shrinkage and brittle fracture, measurements using BSB were not successful.

Differences are noted in the longer time (box) region rather than in the shorter time (wedge) region. Curves for Polyblend show unusually short relaxation times as compared with its component PS, indicating the plasticizing effect of PBD.

The relaxation times of block copolymers are longer than that of Polyblend, in spite of BD sequences being included in them.

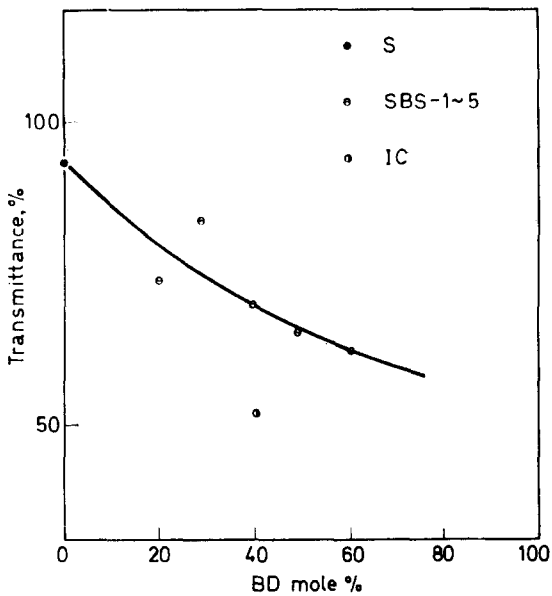

Figure 6—Light transmittances of 1 mm thick plates of ST–BD block coplymers versus BD mole per cent. Average values of the light transmittances measured at the wavelengths of 400, 500, 600 and 700 mμ

Other physical properties

Impact strength values of the block copolymers are summarized in *Table 2*. SBS showed the highest value among four types of block copolymers, as for stress/strain behaviour, but did not exceed the value of commercial HI–PS.

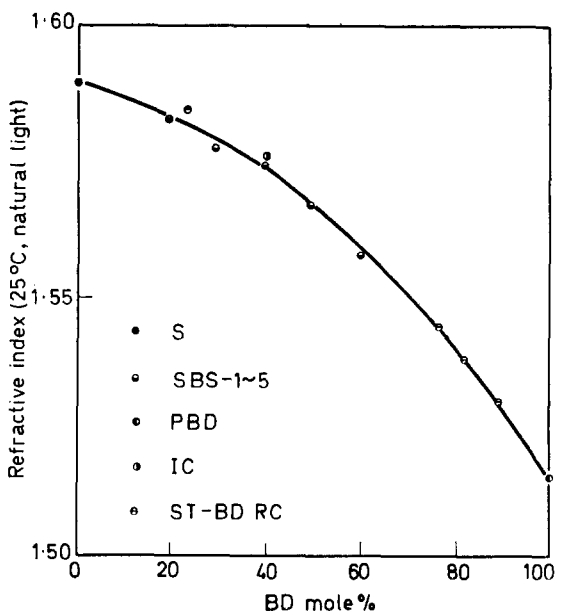

Figure 7—Refractive indices of SBS type block copolymers and ST–BD random copolymers versus BD mole per cent

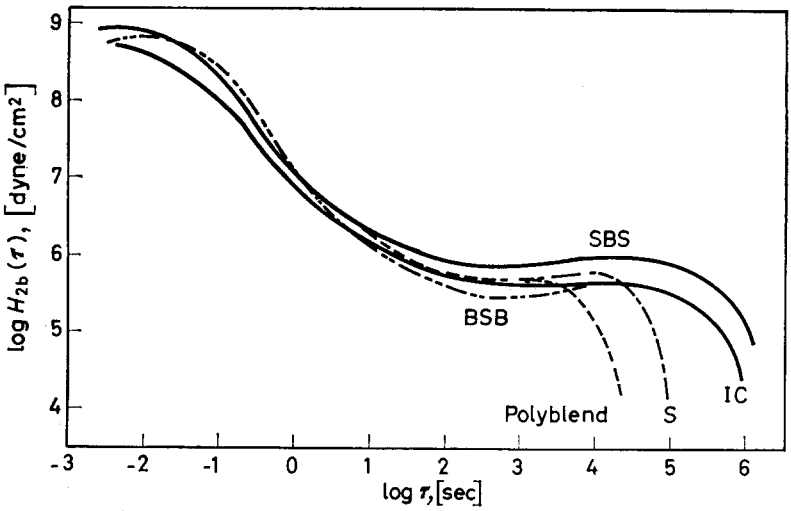

Figure 8—Stress relaxation spectra of the ST–BD block copolymers as compared with the blend of PC and PBD, and its component PS

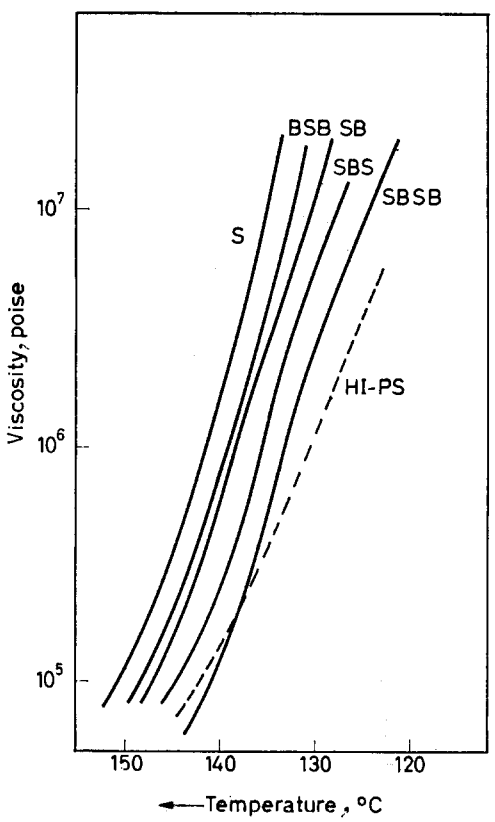

Figure 9—Flow curves of ST–BD block copolymers as compared with commercial HI–PS and PS

Heat distortion temperatures (HDT) were determined according to JIS K–6745 using the Clash and Berg method. Each value is smaller than that of pure PS and decreases with increasing BD ratio in SBS as shown in *Table 2*. An increase in BD sequence length in SBS thus causes an increase in impact strength and a decrease in heat distortion temperature.

The flow properties observed for block copolymers by a constant stress capillary rheometer (Koka Flow Tester developed in Japan) indicate easy processability, as the curves lie between that of PS and HI–PS (*Figure 9*).

ELECTRON MICROSCOPIC OBSERVATION

It is known that two-phase systems consisting of immiscible components of different refractive indices give an opaque sheet. The ST–BD block copolymers used here, however, gave a sheet of complete transparency or translucency, despite the presence of two-phase systems. Light transmittances exceed 50 per cent for all samples, a very high value compared with those of Polyblend and commercial HI–PS (*Table 2*). It may, therefore, be assumed that BD sequences in block copolymers coil and form islands in an extension of the PS matrix and that the dimensions of the islands are small enough so as not to scatter visible light.

The fine structures of the block copolymers were observed under the electron microscope by using the osmium tetroxide staining and hardening procedure developed by Kato[3]. An electron micrograph of an ultrathin section of compression-moulded sheet of SBS (ST/BD mole ratio 60/40) is shown in *Figure 10*. It is clear that almost spherical PBD particles (stained black) are dispersed evenly in the PS matrix. The dimension of the particles

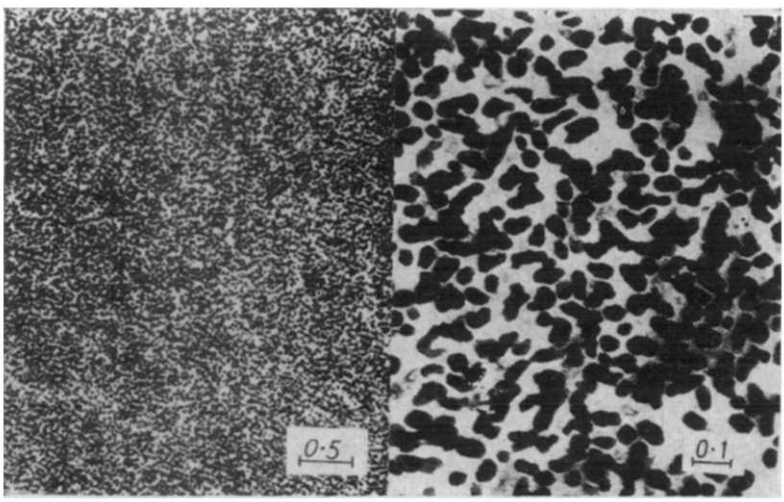

Figure 10—Electron micrograph of an ultrathin section of a compression-moulded sheet of SBS type block copolymer, showing spherical shapes of BD sequences. (ST/BD mole ratio=60/40)

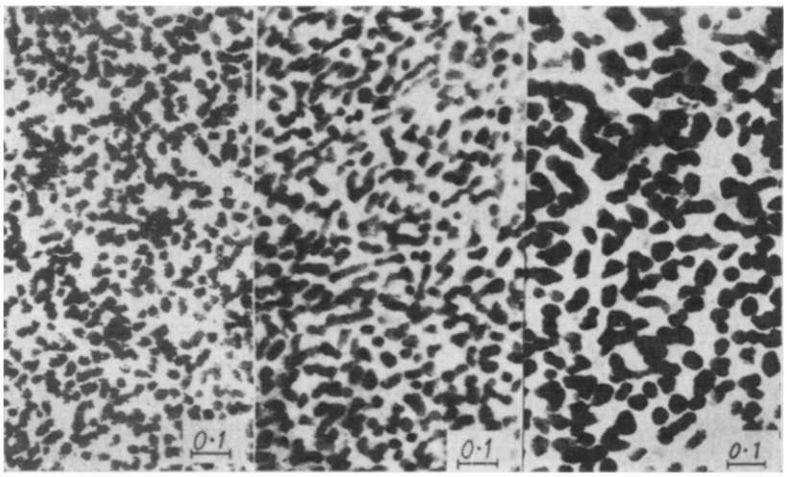

Figure 11—Electron micrographs of ultrathin sections of compression-moulded sheet of SBS type block copolymers. Effect of BD sequence length under a given total molecular weight. ST/BD mole ratios; left=80/20, middle=70/30, right=60/40

seemed to vary from 300 to 350 Å, although they are not always separated from each other. Dimensions of the particles decrease with decreasing BD sequence length in SBS block copolymers as shown in *Figure 11*.

SB and BSB, on the other hand, showed very different configurations of BD sequences as can be seen in *Figures 12* and *13*. PBD chains do not give spherical shapes, rather, they are linked together to form irregularly shaped rod-like structures in a compression-moulded sheet.

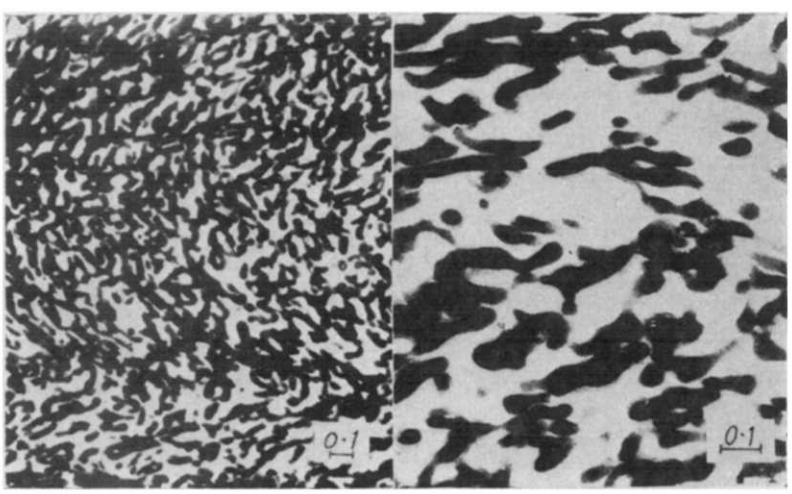

Figure 12—Electron micrograph of an ultrathin section of compression-moulded sheet of SB type block copolymer, showing irregular shaped rod-like structures. (ST/BD mole ratio=60/40)

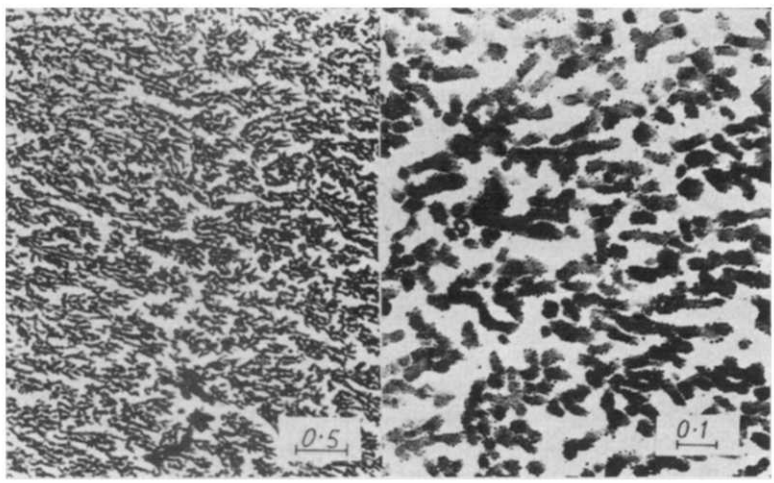

Figure 13—Electron micrograph of an ultrathin section of compression-moulded sheet of BSB type block copolymer, showing irregular shaped branched rod-like structures. (ST/BD mole ratio=60/40)

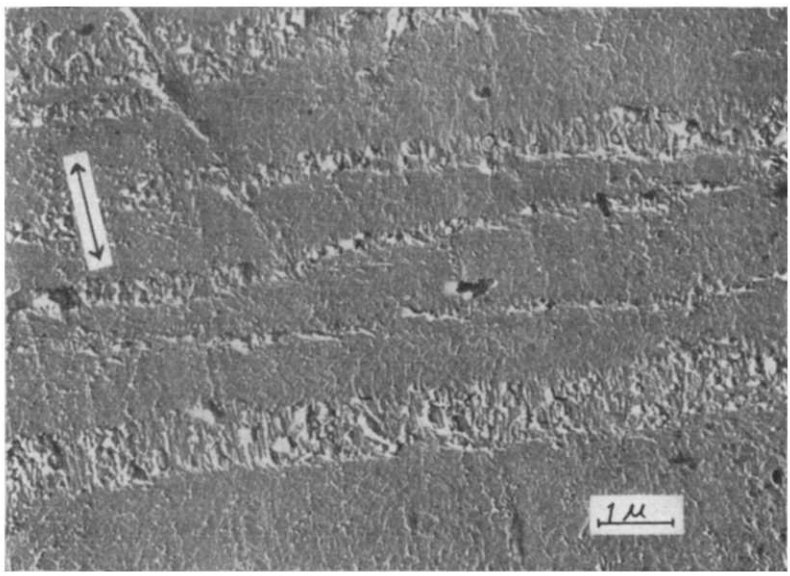

Figure 14—Electron micrograph of stress-whitened surface of compression-moulded sheet of SBS type block copolymer (ST/BD mole ratio=60/40), showing crazes about one micron in width. Arrow indicates direction of the applied stress. (Methylcellulose/carbon two-step replica)

DISCUSSION

The most striking results obtained in this study are the marked differences in mechanical properties with the change of block chain arrangements;

SB and BSB were as brittle as pure PS, whereas SBS and SBSB are tough. The last two were superior to the others in their sheet transparencies. These results may be attributed to their differences in block chain configuration in the solid state as observed in the electron micrograph.

These block copolymers generally show crazing (or whitening) under tensile stress, as observed in ABS polymers and HI–PS[4] (*Figure 14*).

In SB and BSB, however, the amount of crazing occurring before a crack start is extremely small, in contrast to SBS and SBSB. The brittleness of SB and BSB remains as yet to be investigated by a method based on the possibility that the extension of crazing is interrupted by the start of true cracking.

CONCLUSION

ST–BD block copolymers appear to form heterogeneous two-phase systems, individual PBD chains being dispersed in the PS matrix (this state is reversed as the BD content increases). Striking differences are noted in tensile and impact behaviours among the four types of block chain arrangements, although the differences are small in dynamic mechanical properties.

An increase in BD chain length in SBS of a given molecular weight results in an increase in impact strength and in elongation at break, and a decrease in yield stress, in heat distortion temperature, in sheet transparency, and refractive index.

PBD chain configurations in the solid state were observed under the electron microscope. The dimensions of PBD chain configurations appeared to vary between about 200 and 350 Å depending on the PBD chain length in SBS block copolymers. Such fine dispersions of BD sequences probably contribute to their excellent transparency.

Marked differences in the state of PBD chain configuration in a compression-moulded sheet among SB, SBS and BSB were also observed. It is proposed that the differences in their block chain configurations may explain the differences in their mechanical properties.

We thank Mr S. Izawa, Miss S. Sagae and Miss C. Nozaki for their experimental work.

The Japanese Geon Co. Ltd,
Central Research Laboratory,
Yako 1–2–1,
Kawasaki, Kanagawa-Ken, Japan

(*Received August 1967*)

REFERENCES

[1] HENDUS, H., ILLERS, K. H. and ROPTE, E. *Kolloidzschr.* 1967, **216–217,** 110
[2] BOVEY, F. A., TIRES, G. V. D. and FILLIPOVICH, G. *J. Polym. Sci.* 1955, **38,** 73
[3] KATO, K. *Polymer Letters,* 1966, **4,** 35
[4] MATSUO, M. *Polymer, Lond.* 1966, **7,** 421
[5] TAKAYANAGI, M. *Mem. Fac. Engng, Kyushu Univ.* 1963, **23,** 41

Reinforcement of Silicone Elastomer by Fine Particles

D. BAKER, A. CHARLESBY and J. MORRIS

The elastic modulus of silicone elastomers is greatly enhanced by the presence of fine particles (fillers). Exposure to high energy radiation offers a convenient method of introducing crosslinks in a quantitative manner. It is found that for a wide range of filler particles there is little linking between polymer and filler. The increase in modulus is proportional to dose (i.e. crosslink density) and to filler concentration, and is usually independent of the nature of the filler surface. However, it is inversely proportional to filler diameter. It is concluded that the increase is due primarily to physical interference of the filler particles with elastic deformation of the network.

THE incorporation of certain finely divided solid particles can greatly improve the mechanical properties of elastomers. The elastic modulus and the tensile strength are two of the parameters that can be profoundly influenced by such fillers. This enhancement in mechanical properties is described by the general term reinforcement.

When the elastic modulus of a filled elastomer is considered, three distinct mechanisms of reinforcement may be considered: (*i*) extra crosslinks, which are due to strong (chemical) filler–elastomer bonds; (*ii*) physical–mechanical interference of the filler particles with the stress distribution and deformation of elastomer molecules; (*iii*) filler–filler interactions which give rise to coherent filler networks.

The reinforcement observed with natural and other carbon backboned rubbers filled with carbon black has been frequently attributed to process (*i*) at high elongations, and process (*iii*) at very low elongations. The presence of extra crosslinks has been demonstrated[1] by the formation of 'bound rubber' (the insolubilization of the gum caused by the incorporation of filler in the absence of curing agents). Good correlation has been observed between the ability of a filler to form 'bound rubber' and its reinforcing properties. Reinforcement of other properties such as tear resistance, where stress diversion appears to be the dominant factor, is also said to depend on strong filler–elastomer bonds[2].

Filler–filler interactions have been investigated by electron microscopy[3], and by electrical conductivity experiments[4]. The low extension hysteresis demonstrated by dynamic testing techniques also shows the effects of a deformable filler network[5].

The highest degrees of reinforcement have been observed in silicone rubber compounded with silica fillers. Comparatively little work has been done on these systems, and the presence of a pre-cure ('bound rubber') reaction has tended to confuse the issue.

To determine the extent to which 'bound rubber' is responsible for reinforcement, it is necessary to determine separately the degree of crosslinking introduced in the curing process. With conventional chemical curing processes, the presence of fillers may interfere with the cure. This is most apparent with silicone rubbers, which cannot be cured by conventional peroxide catalysts if they have been compounded with carbon-black fillers.

The problem can be greatly simplified if ionizing radiation is used as the crosslinking (curing) agent. Very precise degrees of crosslinking can be introduced, and any type of filler can be incorporated. A further advantage is that filler–polymer reactions can be studied by means of model compounds. The G values for radiation-induced reaction in polymers are substantially independent of molecular weight[6]; the use of low molecular weight model compounds is therefore justified, and the difficulties associated with analysing gelled material can be avoided.

In the present work the study of reinforcement has been restricted to silicone rubbers. The choice of polydimethyl siloxane was governed by a number of relevant features. Silicone rubbers can be reinforced to a very high degree by the incorporation of fillers. Unlike natural rubber, silicone rubbers are not subject to strain-induced crystallization, so the additional complication of auto-reinforcement is avoided. The radiation chemistry of polydimethyl siloxanes is well established, and the wide range of molecular weights commercially available facilitates the use of model compounds. The lack of unsaturation also simplifies the chemistry of the system.

The extent to which filler–polymer bond formation occurs has been determined by solubility measurements with high molecular weight gum and with model compounds. The mechanical properties investigated were the ultimate tensile strength, elongation at break, high extension modulus and extension set of radiation cured silicone rubbers and these parameters were determined at various levels of crosslinking. A wide range of fillers was investigated at different concentrations.

EXPERIMENTAL

Materials

The polydimethyl siloxanes used were obtained from Midland Silicones Ltd. For the model studies, fluids from the M.S.200 range were used. These were the 10^2 cS and 10^5 cS fluids with molecular weights of $5{\cdot}4 \times 10^3$ and 107×10^3, respectively. The gum used was M.S.2211, with a molecular weight of 5×10^5. The fluids are not exact models for the gum as, due to the manufacturing process, the gum contains terminal hydroxyl groups. These are known to undergo condensation reactions with hydrated fillers. In this work a crosslinked gum is referred to as a rubber.

Fillers

All the fillers used were spherical with the exception of tioxide, which has rhomboidal crystals. The carbon blacks and tioxide were donated by W. R. Greef & Co. Ltd and the PMMA and Silbarex by I.C.I. Ltd. The conventional silicas (pyrogenetic) and their surface-treated counterparts

were bought from Bush Beach and Segner Bailey Ltd. *Table 1* shows the range and basic properties of the fillers used. The surface treated silicas were commercial fillers with the surface hydroxyl groups esterified so that reaction with the terminal hydroxyls on silicone gums was avoided.

Table 1. Basic properties of the fillers

Trade name	*Particle diameter (Å)*	*Composition*	*Comments*
Aerosil 2491	120	SiO_2	Apparent density 0·05 g cm $^{-3}$
E.P.154	120	SiO_2 surface treated	
Aerosil F.K.3	150	SiO_2	
E.P.93	150	SiO_2 surface treated	
Philblack E	170	S.A.F.	Reinforcing for natural rubber
Philblack 0	250	H.A.F.	Reinforcing for natural rubber
Philblack 55	250	E.P.F.	Surface oxidized, non-reinforcing
Philblack G	550	G.P.F.	Reinforcing
P.33	1 500	M.T.	Reinforcing
Tioxide	1 200	TiO_2 major dimensions	
PMMA I	1 000	Emulsion polymerized polymethyl methacrylate	
Silbarex	10 000	Co-precipitated $BaSO_4$-SiO_2	

Preparation of samples

The fillers were ultrasonically mixed with the model fluids. The samples were degassed by pumping for 16 hours at 10^{-4} mm of mercury in double glass tubes.

The gums were compounded with fillers on a Pascall triple-roll mill. The mixes were then pressed hydraulically in a template between polycarbonate film to give smooth sheets, and the pressed gums were then taped between polypropylene sheets for support during the irradiation.

Irradiation

The irradiation facility consists of 20 rads of ^{60}Co arranged in the form of an open cylinder[7]. Dosimetry was based on the Fricke (ferrous sulphate) dosimeter[8] as a standard.

The samples were irradiated at positions around the gamma source so as to receive the required dose in a convenient time (a preliminary experiment had established the dose-rate independence of the silicone crosslinking reaction).

Solubility determination

After irradiation, the degree of crosslinking was determined from solvent fraction measurements made by Soxhlet extraction for 100 hours with boiling xylene.

Physical testing

Tensile properties were determined on standard (*BS903*) dumb-bell test pieces (two cut from each sheet), using a Hounsfield automatic recording

rubber tester. For a properly cured rubber, previous experiments had shown the tensile properties to be substantially independent of the rate of stress over the range 0·4 to 20 inches/min and a fixed speed of 20 inches/min was used.

Extension set was determined six months after the samples had been extended to break.

RESULTS

Model compounds

To evaluate solubility data in its most useful form, the following relationship[9] was used.

$$S+\sqrt{S}=p_0/q_0+1/q_0ur$$

where S is the soluble fraction, p_0 is the density of chain scission per unit dose, q_0 is the density of crosslinking per unit dose, u is the initial degree of polymerization (assumed to be initially random) and r is the radiation dose.

When the results for filled 100 cS fluid are plotted as $(S+\sqrt{S})$ against $1/r$ curves, the intercept gives the ratio p_0/q_0. Previous work showed that this ratio decreased by 50 per cent with Aerosil present[10]. The effect of fillers at concentrations of 30 parts/100 for the carbon blacks E, G and O, together with previous results for FK3 and EP93 is shown in *Figure 1*.

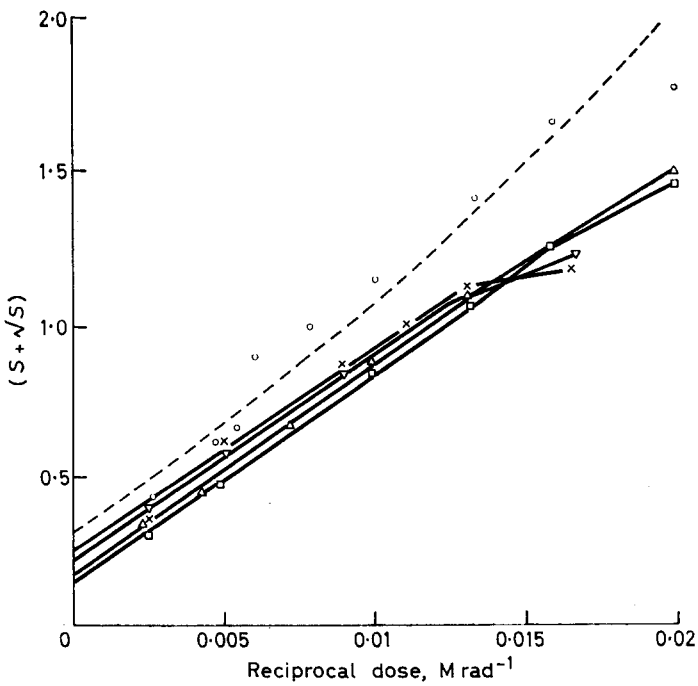

Figure 1—Soxhlet extraction of 100 cS silicone fluid loaded with reinforcing fillers (30 parts/100). (- - - -), unfilled fluid; (□), FK3; (△), EP93; (○), Philblack E; (▽), Philblack 0; (×), Philblack G

In the curves, the effect of filler is to lower the dose at which gel formation first occurs; this corresponds to the formation of bound rubber. The slopes are nearly identical in all specimens, indicating that q_0u is constant; this may be due to constant values of q_0 and u, or an increase of q_0, together with a corresponding decrease of u (due to a small degree of degradation during ultrasonic dispersion). The intercept (for $1/r=0$) is smaller for the filled mixtures, possibly due in part to a small increase in q_0. A decreased scission rate, caused by the reaction of filler with the end-groups at broken chains, seems less likely. The major conclusion from these measurements is that there is no drastic increase in the number of cross-links, resulting from the presence of filler particles. This confirms our earlier data showing that the G value for attachment of Aerosil particles to silicone molecules was comparable to the G value for crosslinks.

Some evidence of pre-cure attachment was shown by a higher molecular weight (10^5cS) fluid by using a gravimetric technique. Aerosil (FK3), showed a seven per cent increase in weight after standing in excess 10^5cS fluid for seven days.

Solubility of gum mixes

Similar $(S+\sqrt{S})$ versus $1/r$ plots were drawn for fillers compounded with the high molecular weight gum. At the highest concentration of 80 parts/100, treated Aerosil EP93 showed a reduction in $p_0/q_0\,(r\longrightarrow\infty)$ whereas Philblack E actually caused an increase in p_0/q_0, implying a protection effect (*Figure 2*).

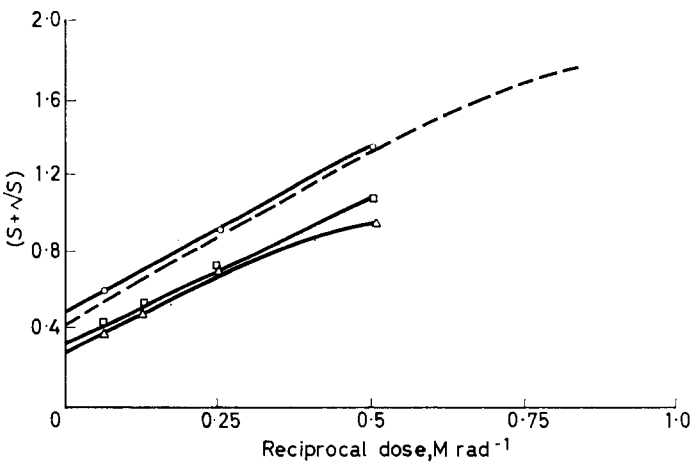

Figure 2—Soxhlet extraction of silicone gum loaded with reinforcing fillers (80 parts/100). (- - -), unfilled gum; (□), FK3; (△), EP93; (○), Philblack E

An important feature of the $(S+\sqrt{S})$ curves for models and gums is the very small dependence of the slope $(1/q_0u)$ on the presence of fillers. This may be attributed to a decrease in u caused by the degradation induced by the milling process counteracting the increase in q_0.

The radiation independent crosslinking (the 'pre-cure' or 'bound rubber' effect) is best illustrated by solvent fraction against dose curves. *Figure 3* compares the behaviour of FK3, EP93 and Philblack E.

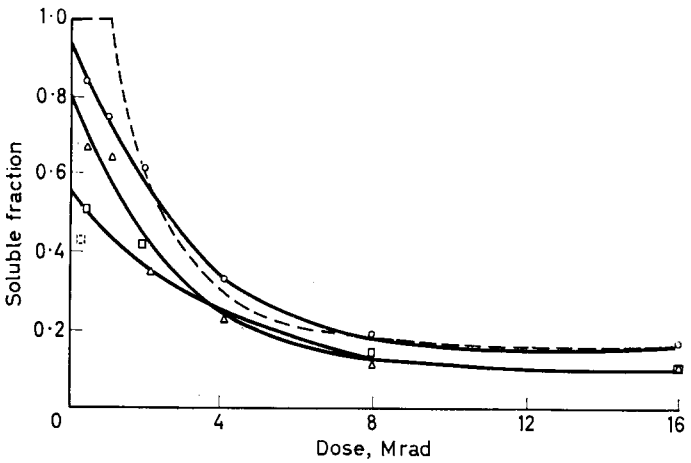

Figure 3—Soxhlet extraction of silicone gum loaded with reinforcing fillers (80 parts/100). (- - -), Unfilled gum; (□), FK3; (△), EP93; (○), Philblack E

Untreated Aerosil FK3 displays the highest degree of 'pre-cure' (defined as the horizontal shift required for coincidence with the curve for unfilled gum at low doses), the amount being equivalent to 2·5 Mrad; with Philblack E the pre-cure equivalent is approximately 1·2 Mrad.

Degrees of crosslinking have been determined by many workers from swelling ratio measurements. This was found to be impracticable with the present system due to non-reproducibility.

Mechanical properties of rubber

It has previously been established that, for most specimens, the limiting tensile properties are independent of rate of stress over the available range. An exception to this was shown by Philblack E at high loading and low doses. This may be attributed to an incomplete network, and is confirmed by the large positive extension-set shown in *Table 2* in contrast to the small negative values with silica fillers. The solubility data also confirm that the network is incomplete.

Tensile strength

As the tensile strength of materials is likely to be flaw dependent[11] a series of measurements with unfilled gum was performed so as to relate the ultimate tensile strength to the volume and surface area of the test specimens. The results in *Table 3* compare the tensile strength with the product of the cross-sectional area (A) and the cross-sectional perimeter

(P) of the test pieces. A surprising degree of agreement is obtained. For good (reinforcing) filler mixtures the variation with specimen dimensions is very small.

The tensile strength is greatly increased by the incorporation of fillers. The effects of FK3, EP93 and Philblack E have been reported previously.

Table 2. Dependence of extension set on dose

Filler	*Concentration (parts/100)*	*Extension set (%) Dose (Mrad)*		
		4	8	16
Pure gum	—	−10 −16	−10 −12	−11
Aerosil	40	− 4 − 5	− 4·5	− 4 − 5
FK 3	80	− 4 − 5	− 3·5 − 4·5	− 2 − 4
EP 93	40	− 1 − 2	0 − 2	− 6 −10
	80	− 3 − 7	− 1 − 4	− 2 − 8
Philblack E	40	+ 24	+10 +20	− 5
	80	+190	+60 +75	+25

Table 4 shows the dependence of tensile strength on dose and filler concentration for the other fillers investigated. The highest degree of reinforcement is shown by the smallest fillers, which also exhibit the most pronounced tensile maxima for dose and filler concentration. The largest particles showed very little dose dependence, and up to a filler concentration of 80 parts/100 the concentration dependence is roughly linear.

Elongation at break

A simple theory[12] proposes that for firmly bound fillers, the maximum elongation should be proportional to $(1-\phi_f^{\frac{1}{3}})$ where ϕ_f is the volume fraction of filler. For non-attached fillers, the elongation should be proportional[12] to $(1-\phi_f^{\frac{2}{3}})$. *Figure 4* compares selected results with the theoretical curves. At low doses (4 Mrads), when the rubber is not fully cured, reasonable agreement is obtained with the small fillers, but with the large fillers the relationship is only obeyed at low loadings; at high loadings the elonga-

Table 3. Dependence of tensile strength of unfilled silicone rubber on specimen size (radiation dose 16 Mrad)

Specimen thickness (in.)	*Tensile strength*			
	¼ in. wide specimen		*½ in. wide specimen*	
	lb/in²	*A × P (× 512)*	*lb/in²*	*A × P (× 256)*
1/16	3	5	12	9
1/8	12	12	17	20
3/16	20	21	34	33

tion is very much greater than predicted. At higher doses (16 Mrad corresponding to a full cure) the elongation depends very little on filler.

Elastic modulus

Ultimate tensile properties tend to lack reproducibility, and a more meaningful assessment of reinforcement can be gained from the elastic modulus for which good theoretical treatment is available. As rubbers seldom obey Hooke's law, the elastic modulus is not a true constant, but depends on the extension at which the modulus is determined. Many workers select the modulus at 300 per cent elongation as being representa-

Table 4. Tensile strength (lb/in²) of filled silicone rubbers ($\frac{1}{8}$in. thick, $\frac{1}{4}$in. wide)

Filler	*Dose Mrad* \ *Filler conc. (parts/100)*	20	40	60	80
Carbon black P33	4	23	28	47	88
	8	25	46	78	117
	16	30	51	70	119
Tioxide	4	38	69	91	117
	8	44	115	—	231
	16	34	98	—	223
PMMA I	4	—	101	91	112
	8	—	130	126	175
	16	—	122	162	187
Silbarex	4	178	269	338	216
	8	122	322	635	531
	16	91	184	687	755
Philblack G	4	139	94	41	22
	8	256	397	366	188
	16	240	506	477	478
Philblack 0	4	181	156	63	137
	8	253	562	406	278
	16	203	672	619	481
Philblack 55	4	67	175	190	108
	8	121	464	561	574
	16	49	356	692	724
EP 154	4	370	630	235	445
	8	510	565	1030	795
	16	370	896	1030	870
	Parts/100	10	20	30	40
Aerosil 2491	4	185	256	453	253
	8	205	356	888	465
	16	178	634	794	947

Values for unfilled silicone rubbers are far smaller and depend on specimen dimensions—see *Table 3.*

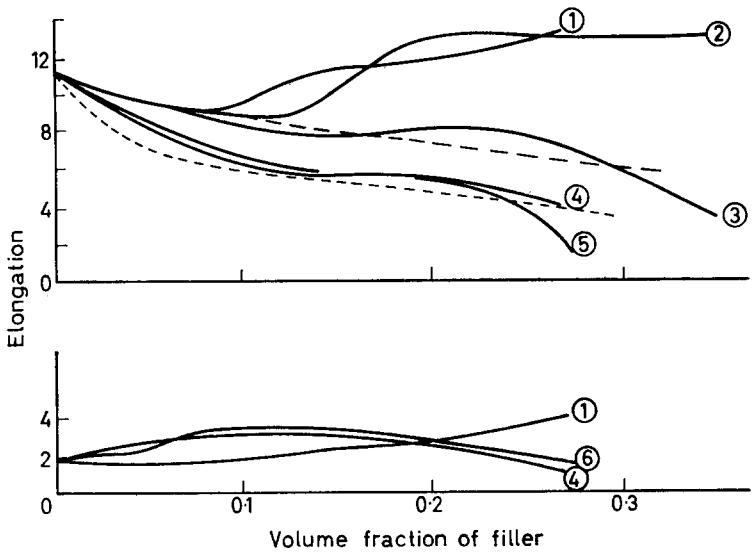

Figure 4—Dependence of elongation on filler concentration. (– – –), $(1-\phi^{2/3})$; (- - -), $(1-\phi^{1/3})$; ①, Tioxide; ②, P.33; ③, Philblack E; ④, EP 154; ⑤, FK3; ⑥, EP 93. Upper: Mrads; Lower: 16 Mrads

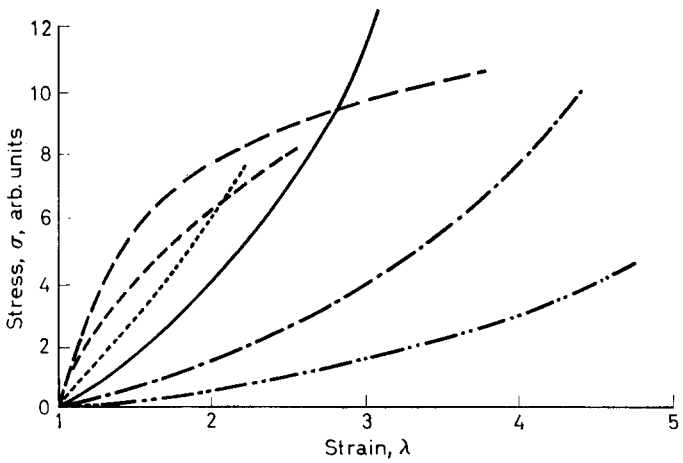

Figure 5—Extension characteristics of rubbers (variation of stress with strain). (— — —), EPR rubber[15]; (– – –), Philblack G (80 parts/100 parts of silicone gum); (- - -), Theoretical $C_2=0$; (———), FK3 (20 parts/100 parts silicone gum), 16 Mrads; (- — - —), FK3 (20 parts/100 parts silicone gum), 8 Mrads; (- - — - - —), FK3 (20 parts/100 parts silicone gum), 4 Mrads

tive of the materials. In the present work the modulus at a lower extension (150 per cent when possible) was also determined. The shapes of the stress/strain curves exhibited by 95 per cent of the silicone rubbers studied in the present work were different in character from those seen in natural rubber. *Figure 5* shows representative curves for silicone rubbers, and for a natural rubber curve following a typical Mooney–Rivlin relationship of

$$\sigma/(\lambda - 1/\lambda^2) = 2C_1 + 2C_2/\lambda$$

The majority of results in the present work correspond to a value of C_2 which is zero or negative.

Both the 150 and 300 per cent moduli were found to be proportional to the irradiation dose (plus a small constant dose equivalent to pre-cure). Reasonable agreement was found between the levels of 'pre-cure' dose extrapolated from the modulus against dose curves and those obtained from solubility measurements. With unfilled gum, the experimental modulus is comparable with that predicted by a simplified form[13] of the theory of rubber elasticity ($E = gp\,RT/M_c$ with $g \sim 3$).

For any filler the increase in modulus per unit dose was found to be proportional to filler concentration. This enables a specific modulus $\Delta E/rc$ to be defined for each filler. The specific moduli were found to be inversely proportional to the diameter of the filler particles. This relationship is shown in *Figure 6*. It can be seen that, with few exceptions, the reinforcing power of a filler is independent of the nature of the filler, and depends solely on the particle size. The two major deviations from this simple relationship represent the two fillers that do not exhibit negative C_2 values.

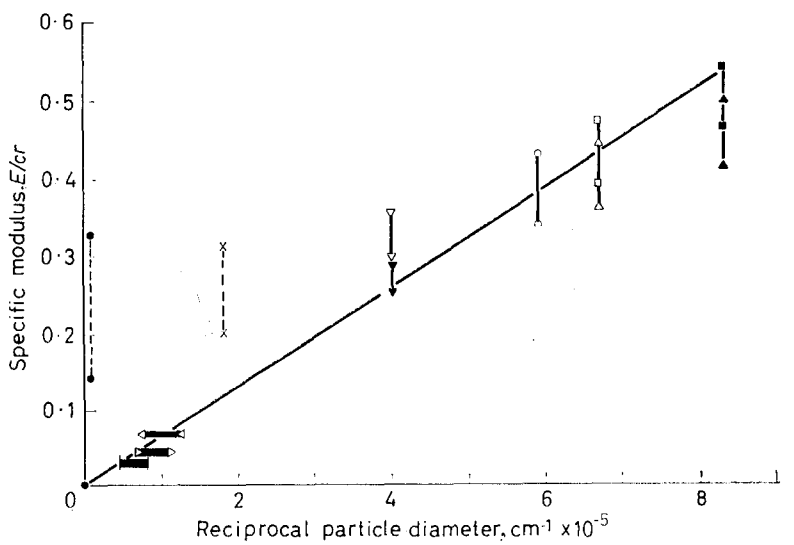

Figure 6—Dependence of specific modulus on particle size. (■) A2491; (▲), EP154; (□), FK3; (△), EP93; (○), Philblack E; (▽), Philblack 0; (▼), Philblack 55; (×), Philblack G; (●), Silbarex; (◁), PMMA I; (▷), Tioxide; (|), P.33

DISCUSSION

During the initial mixing process, some attachment between filler and gum takes place even in the absence of radiation. This pre-cure reaction (evidenced by both solubility and modulus) is particularly noticeable with untreated Aerosil as the filler. Radiation causes an increased density of crosslinks, proportional to dose, but this density is only slightly affected by filler type or surface or concentration; for several carbon-black fillers there may be even a small reduction at high filler concentration. The reinforcement cannot therefore be ascribed to extra crosslinks.

The ultimate tensile strengths of the rubbers studied in this work show less marked dose-dependences than would be expected from Bueche's theory[14]. The unfilled gum has very poor tensile properties and these have been shown to be due mainly to surface flaws. The poorly bonded fillers like Philblack E give rise to similar increases in tensile strength to those produced by the strongly bonded silica fillers.

The agreement between the elongation at break of the low dose rubber and the simple Nielson theory is somewhat surprising. At these low levels of crosslinking, end effects, which were ignored in the theoretical derivation, would be expected to play an important part. At high doses the unfilled rubber breaks at surface flaws at elongations well below those theoretically possible. The tear resistance introduced by the incorporation of filler can therefore cause an increase in elongation at low concentrations. This will be in competition with the decrease in elongation predicted by simple theory, and the rather flat dependence observed will result.

The atypical stress/strain relationships observed with the majority of the filled silicone rubbers are somewhat similar to the curves obtained with solvent-swollen rubbers[15]. It seems likely that the highly mobile silicone chains possess a certain degree of self lubrication. The two exceptions (particularly the very large Silbarex particles) may well result from a residual filler–filler interaction, and are somewhat reminiscent of the behaviour of Teflon-powder filled silicone. The remaining fillers, covering a very wide range of types and chemical compositions, show remarkable similarities in the reinforcement they produce. The specific modulus, defined as $\Delta E/cr$, has been shown to be dependent primarily on the size of the filler particles. The degree of attachment of the fillers to the polymers appears to be of little importance, as can be seen most readily in *Figure 6* (compare A2491 and EP154; FK3 and EP93). (The 'pre-cure' effect is of importance as regards ease of working prior to final cure, but is unaffected by radiation, and its effect on the modulus is negligible.) Although filler–filler interactions exist, e.g. the carbon-black filled rubbers have appreciable electrical conductivities, filler–filler networks are only of importance at very low elongations.

The simplest theory that does not require strong bonding to produce reinforcement is that expressed by the Guth–Gold Einstein equation[16]

$$E/E_0 = 1 + 2{\cdot}5\,\phi + 14{\cdot}1\,\phi^2$$

where ϕ is the volume fraction of filler. With Aerosil at 80 parts/100, $\phi = 0{\cdot}28$, and $E/E_0 = 3$, as against an observed ratio of about 50. The expression is still inadequate if ϕ is increased due to bound rubber.

The good reinforcing fillers have particle diameters which are of comparable size to the mesh dimensions in the polymer network. It is therefore proposed that in the present system the reinforcement is due to geometrical interference of filler particles situated inside the network 'holes' with the deformation of the network chains. When the particles exceed the hole size the restriction on the deformation will be much less.

When the molecular chains are placed under tension, the areas of contact with filler particles serve as temporary crosslinks; however, the tensile strength is almost unaffected by this process, as a strongly stressed chain can move over the surface of the filler particle. The major cause of the increase in tensile strength resulting from the incorporation of fillers can be ascribed to stress diversion so that the direction of a sharp tear no longer lies at right angles to the applied stress.

CONCLUSION

When finely divided spherical fillers are incorporated in radiation-cured silicone rubbers, the considerable increase in elastic modulus is found to be proportional to crosslink density, inversely proportional to filler size, and independent of the nature of the filler. In particular, surface treatment has little effect. It is therefore concluded that the type of reinforcement is primarily physical in character.

Physics Department,
Royal Military College of Science,
Shrivenham, Wilts.

(*Received August 1967*)

REFERENCES

[1] WATSON, W. F. *Proceedings of the Third Rubber Technology Conference*, p 86 (1954)
[2] ANDREWS, E. H. and WALSH, A. *J. Polym. Sci.* 1958, **331**, 39
[3] LADD, W. A. and WIEGAND, W. B. *Rubb. Age*, 1945, **57**, 299
[4] HARRIS, J. O. and WISE, R. W. *Reinforcement of Elastometers* (ed. Kraus, G.), p 268. Interscience: New York, 1965
[5] PAYNE, A. R. *Reinforcement of Elastometers* (ed. Kraus, G.), p 69. Interscience: New York, 1965
[6] CHARLESBY, A. *Proc. Roy. Soc. A*, 1959, **230**, 120
[7] MORRIS, J. and PENHALE, L. G. *Nucl. Eng.* 1965, 469
[8] FRICKE, H. and MORSE, S. *Phil. Mag.* 1929, **7**, 129
[9] CHARLESBY, A. and PINNER, S. H. *Proc. Roy. Soc. A*, 1959, **265**, 367
[10] MORRIS, J. and CHARLESBY, A. *IUPAC Polymer Symposium, Prague*, 1965
[11] THOMAS, A. G. *J. Polym. Sci.* 1955, **18**, 177
[12] NIELSEN, L. E. *J. appl. Polym. Sci.* 1966, **10**, 97
[13] TRELOAR, L. R. G. *The Physics of Rubber Elasticity*, Chap. 8. Oxford University Press: London, 1958
[14] BUECHE, F. *J. Polym. Sci.* 1958, **33**, 259
[15] BUECHE, F. *Reinforcement of Elastometers* (ed. Kraus G.). Interscience: New York, 1965
[16] GUTH, E. and GOLD, C. *Phys. Rev.* 1938, **52**, 322

The Elastic Modulus of an Amorphous Glassy Polymer

P. B. BOWDEN

Amorphous polymers in their glassy state have elastic moduli a few times 10^{10} dyne cm^{-2}, and these low values have been attributed to the weak intermolecular van der Waals polarization forces holding the material together. It is suggested that because of the imperfect chain packing in amorphous polymers, intermolecular forces, which fall off rapidly with increasing molecular separation, may not be sufficiently large to account for the observed moduli. An alternative explanation for the stiffness of these materials is that elongation of the randomly kinked chains making up the polymer can take place by rotation about selected carbon–carbon bonds in the chain backbone, and it is this rotation against intramolecular steric hindrance forces that controls the modulus. This mechanism is estimated to give rise to a modulus of approximately 6×10^{10} dyne cm^{-2}.

WHEN a glassy polymer is stretched elastically work is done against the forces holding the material together. These forces come from different sources and can be roughly divided into three groups. To pull neighbouring chains apart, work has to be done against the intermolecular forces holding chains together. For non-polar molecules these are primarily van der Waals polarization forces. To elongate individual chains work has to be done to bend and stretch the bonds between the carbon atoms making up the chain backbone. If the chains are randomly kinked as they are in an amorphous polymer, then they can be elongated if rotation takes place about certain bonds in the chain backbone in which case work has to be done against the steric hindrance to rotation. The overall elastic modulus of the structure will be determined by a combination of these various effects. This discussion is limited to glassy polymers at low temperatures where thermal activation provides no aid to deformation.

INTERMOLECULAR FORCES

For non-polar molecules there is an attractive interaction energy due to mutually induced dipoles in the two molecules, and at small separations there is also a repulsive interaction energy which increases rapidly as the molecules approach each other. The interatomic potential can be represented by a relationship of the form

$$\phi = A\,a^{-n} - B\,a^{-m}$$

where A, B, m and n are constants and a is the molecular separation. It has been shown[1] that, for non-polar molecules, $m=6$. The constant n for large molecules has a value[2] around 15.

By using a potential of this type it is possible to derive an expression for the elastic modulus of the material as a function of the intermolecular distance. The modulus is given approximately by the relation

$$Y \simeq (1/a)\,(\mathrm{d}^2\phi/\mathrm{d}a^2)$$

For two molecules at the equilibrium separation the interaction energy will be a minimum and $d\phi/da = 0$.

For a material whose elastic modulus and equilibrium molecular separation are known it is possible to use the three relations above to find numerical values for the constants A and B and then to use these values to predict how the modulus will vary with separation.

To apply this treatment to a polymer it is necessary first to consider a case where the modulus is due almost entirely to intermolecular forces. If a polyethylene crystal is stretched in a direction perpendicular to its c axis, then it is unlikely that the individual molecular chains are being very much distorted. The main effect will be to increase the interchain separation.

The transverse modulus of a polyethylene crystal has been estimated[3] to be $3{\cdot}55 \times 10^{10}$ dyne cm^{-2}. This is a value similar to that obtained for other van der Waals solids such as solid argon[4] and is close to values quoted for polymers when the modulus is attributed to van der Waals forces[5,6]. The equilibrium separation of nearest-neighbour chains in a polyethylene crystal is 4·46 Å.

Assuming a potential with $m = 6$ and $n = 15$ and substituting the above values gives values for A and B, respectively, of $1{\cdot}281 \times 10^{-124}$ erg cm^{15} and $4{\cdot}59 \times 10^{-58}$ erg cm^{6}. In *Figure 1*, values of the modulus obtained on this basis are plotted against percentage strain, and it is seen that the modulus falls to

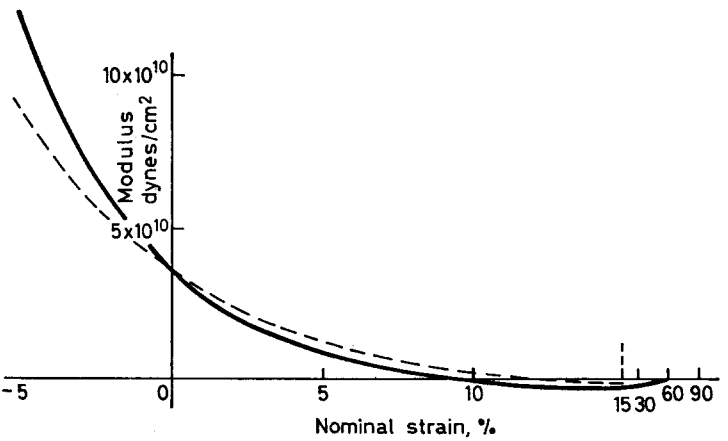

Figure 1—The continuous curve is a plot of the elastic modulus of a polyethylene crystal in a direction perpendicular to its c axis as a function of strain, obtained by fitting a 6:15 intermolecular potential to the equilibrium modulus and equilibrium chain separation. The dashed curve is for a 6:9 potential

zero and becomes slightly negative for strains greater than 9·5 per cent. This behaviour is not very sensitive to the particular intermolecular potential chosen, and a similar plot is shown for which $n = 9$.

In an amorphous polymer close packing is impossible because of the

tangled nature of the structure. The magnitude of the expansion of amorphous material with respect to crystalline can be estimated from the known change in specific volume. The specific volume of a polyethylene crystal at 23°C is estimated[7] from lattice parameter measurements to be 1·000 $cm^3\ g^{-1}$. The specific volume of amorphous polyethylene at 23°C, obtained by extrapolation of data on long chain paraffins[8], is 1·172 $cm^3\ g^{-1}$. These values indicate a volume expansion of 17·2 per cent. As the increase in volume has to be accounted for by increasing the intermolecular spacing with no increase in chain length the mean increase in intermolecular distance will be half this, or 8·6 per cent.

The modulus of the bulk amorphous material due to intermolecular forces will depend on the detailed distribution of intermolecular spacings, about which very little is known. Regions of close packing will have a high local modulus, and regions of open packing a small or negative modulus. The overall modulus will be some kind of average value. Whatever its exact value it is likely to be considerably less than that obtained for close packed chains.

It is true that there will need to be only a few regions where the 'strain' is of the order of 100 per cent (a molecular diameter) to account for the volume increase so that a relatively large number of chains may be at close to their equilibrium separation with a consequent high local modulus, but it is also true that deformation will take place preferentially in regions of low modulus away from these close packed regions leading to a lower overall modulus.

The observed elastic moduli of amorphous polymers in their glassy state are generally of the order of 4×10^{10} dyne cm^{-2}, and on the above treatment it seems improbable that values as high as this can be attributed to van der Waals bonding alone. If this is so, some other deformation mechanism must control the modulus.

The above discussion has been in terms of numerical values for polyethylene, but the same general arguments might be expected to apply to other polymers with non-polar molecules where the interchain forces have essentially a van der Waals origin.

INTRAMOLECULAR FORCES—BENDING AND STRETCHING OF BONDS

An individual polymer molecule can be elongated if carbon–carbon bonds in the chain backbone are bent so as to open up the interbond angles, and if individual bonds are stretched along their length. The modulus of a polymer crystal in the direction of its *c* axis, where bond bending and stretching will be the only mechanism of deformation, has been estimated theoretically by several authors (for example, ref. 9) to be in the region of 10^{12} dyne cm^{-2} and this value agrees well with experimental estimates[3]. Molecules therefore show a strong resistance to elongation and this is reflected in the high moduli of oriented polymers. However, in an amorphous polymeric material where the molecular chains are randomly kinked it is not necessary to deform covalent bonds elastically in order to extend the molecule, as extension can take place if rotation about carbon–carbon

bonds in the chain backbone is permitted. Bond bending and stretching is therefore not likely to contribute very much to the overall modulus.

INTRAMOLECULAR FORCES—BOND ROTATION

A randomly kinked polymer molecule can be extended if rotation is permitted about carbon–carbon bonds in the chain backbone. Rotation about such a bond is never completely free. In simple terms, the energy barrier to rotation is due to steric hindrance between substituted groups on adjacent carbon atoms, but this is not the whole picture as there is a finite barrier even if the substituted groups are too small to interfere with each other, and other effects are almost certainly involved[10]. The height of the energy barrier does not depend very critically on the size or nature of the substituted groups provided these are non-polar, and for a large number of simple molecules containing a carbon–carbon bond the barrier is approximately[10,11] 0·14 eV (3·2 kcal mole^{-1}). For molecules with threefold symmetry about the carbon–carbon bond the variation of the energy of the system with angle of rotation can be fitted approximately by a $\sin^2$ function with a period of 120° corresponding to rotation from one staggered position to the next.

Analysis of a polymer molecule is complicated because of the large number of possible conformations available. The energy of a polyethylene chain has been evaluated as a function of the angle of bond rotation when all bonds in the chain are rotated by the same amount from the *trans* position; i.e. the chain is arranged in a regular helix[12]. For rotations of up to $\pm 10°$ from the *trans* position this function is fitted quite well by a $\sin^2$ function with a barrier height of 0·14 eV.

It is possible to make an estimate of the modulus that would be expected for a polymeric material if hindered bond rotation is the controlling

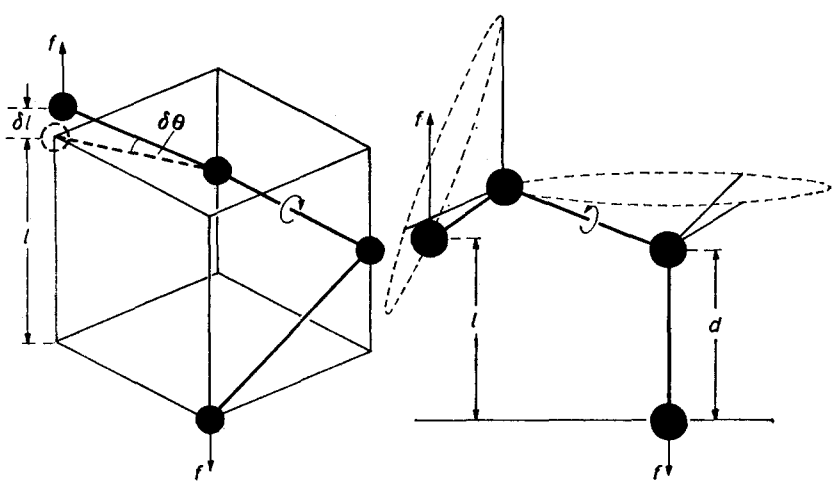

Figure 2—(a) Simple idealized model for a 'deforming unit': (b) more realistic 'deforming unit'. The interbond angles are set equal to 110°

mechanism. *Figure 2* shows two idealized models for 'deforming units'. In both of them elongation of a segment of chain containing three bonds can take place by rotation about one of the bonds. In elastic deformation the strains are small and there will be relatively little interference between neighbouring chains so that the material can be considered to be made up of isolated non-interfering 'deforming units'.

For the simpler idealized unit in *Figure 2*(a), the work done by the force f when the unit is extended by Δl and the bond is rotated through $\Delta\theta$ is

$$\Delta E = f\,\Delta l \simeq fl\,\Delta\theta$$

$$\text{Hence } f \simeq (1/l)\,(\mathrm{d}E/\mathrm{d}\theta)$$

The stress acting on a block of material made up of such units will be f/A where A (approximately equal to l^2) is the cross-sectional area of one unit. The modulus is the differential of stress with respect to strain. As the strain, $\Delta l/l$, is approximately equal to $\Delta\theta$, the modulus, Y, is expressed by

$$Y = \mathrm{d}(f/A)/\mathrm{d}\theta = (1/l^3)\,(\mathrm{d}^2E/\mathrm{d}\theta^2)$$

The variation in bond energy with the angle of rotation can be written

$$E = P\sin^2\psi$$

where P is the height of the energy barrier, and $\psi = \frac{3}{2}\theta$ as E must be zero when θ reaches 120°.

$$\text{Then} \qquad \frac{\mathrm{d}^2E}{\mathrm{d}\theta^2} = \frac{9}{4}\,\frac{\mathrm{d}^2E}{\mathrm{d}\psi^2} = \frac{9}{2}\,P(2\cos^2\psi - 1)$$

$$\text{Hence} \qquad Y = \frac{9P}{2l^3}(2\cos^2\psi - 1) \simeq \frac{4{\cdot}5P}{l^3} \text{ for small } \psi$$

Substituting $P = 0{\cdot}14$ eV and $l = 4$ Å gives a value for the modulus of $1{\cdot}6 \times 10^{10}$ dyne cm^{-2}.

If a more precise calculation is carried out for the unit in *Figure 2*(b) the result obtained is

$$Y = 8{\cdot}38P/Ad$$

where A is the effective cross-sectional area taken up by the unit and d is the bond length. The effective length of the unit in the direction of extension has been taken as the distance l shown in the figure. For polyethylene the parameter A is unlikely to have a value of less than 18·3 Å^2, which is for close packing in a crystal. To account for the observed increase in specific volume of amorphous polyethylene, A should be set equal to 21·4 Å^2. The bond length d is 1·54 Å. If P is taken as 0·14 eV these values predict a modulus of $5{\cdot}7 \times 10^{10}$ dyne cm^{-2}. This difference between the two models is to be expected because the second more realistic 'deforming unit' is less favourably oriented for extension. The calculated modulus of $5{\cdot}7 \times 10^{10}$ dyne cm^{-2} is of the same order as the observed moduli of amorphous glassy polymers which are in the region of 4×10^{10} dyne cm^{-2}.

DISCUSSION

The above considerations lead to an overall picture of the forces holding together an amorphous glassy non-polar polymeric material. Intermolecular van der Waals forces hold individual chains together to a certain extent, but they do not appear to be strong enough to account for the observed stiffness of the material. Individual chains can be extended by bending and stretching covalent bonds in the chain backbone, but generally this will not be necessary as extension can take place by rotation about selected bonds. A randomly kinked polymer chain being extended by bond rotation without the aid of thermal activation is surprisingly stiff and if this alone is the mechanism of deformation the predicted modulus is only slightly higher than that observed if the height of the energy barrier to rotation is taken as 0·14 eV. Low intermolecular forces are not capable of reducing this value appreciably because, however weakly the chains are held together, deformation cannot take place without extending chains. Bond bending and stretching will lower the modulus slightly by making the chains a little easier to stretch, but will not lead to a large reduction as the bonds are relatively stiff.

It is a generally observed phenomenon that amorphous glassy polymers become softer (their elastic moduli are reduced) when they are deformed elastically to large strains. It should be noted that this strain-softening in the elastic region is consistent with the idea that the resistance to deformation comes largely from the resistance to bond rotation. Interchain van der Waals forces will not lead to a softening of the material with strain unless there is an increase in interchain separation and an increase in volume, which is not observed. However, as bonds in the material are rotated the force necessary to rotate them further will drop and will become negative as they pass through their eclipsed positions.

I am grateful to St John's College, Cambridge, for the award of a Research Fellowship, during the tenure of which this work was carried out.

Department of Metallurgy,
University of Cambridge,
Pembroke Street, Cambridge

(*Received September 1967*)

REFERENCES

[1] LONDON, F. *Z. Phys.* 1930, **63**, 245
[2] MOELWYN-HUGHES, E. A. *Physical Chemistry*, Pergamon: Oxford, 1964
[3] SAKURADA, I., ITO, T. and NAKAMAE, K. *J. Polym. Sci. C*, 1966, **15**, 75
[4] BARKER, J. R. and DOBBS, E. R. *Phil. Mag.* 1955, **46**, 1069
[5] MARK, H. *High Polymers*, Vol. 5, p 990. Ed. Ott, E. 1943
[6] VINCENT, P. I. *Physics of Plastics*, ed. RITCHIE, P. D. Plastics Institute: London, 1965
[7] SWAN, P. R. *J. Polym. Sci.* 1962, **56**, 403
[8] RICHARDSON, M. J., FLORY, P. J. and JACKSON, J. B. *Polymer, Lond.* 1963, **4**, 221
[9] LYONS, W. J. *J. appl. Phys.* 1958, **29**, 1429
[10] ELIEL, E. L., ALLINGER, N. L., ANGYAL, S. J. and MORRISON, G. A. *Conformational Analysis*, Interscience: New York, 1965
[11] BAWN, C. E. H. *Trans. Plast. Inst., Lond.* 1967, **35**, 337
[12] SCOTT, R. A. and SCHERAGA, H. A. *J. chem. Phys.* 1966, **44**, 3054

Dynamic Mechanical Properties of Hybrids based on Atactic Polypropylene, Polystyrene and Polymethylmethacrylate

ANDREJ ROMANOV

Dynamic mechanical characteristics of hybrid copolymers based on atactic polypropylene–polystyrene and atactic polypropylene–polymethylmethacrylate have been investigated by the method of torsional vibration at ca. 1 *Hz. Atactic poly(propylene-block-styrene) and atactic poly(propylene-block-methylmethacrylate) have been prepared mechanochemically, atactic poly(propylene-grafted-styrene) from a solution by means of benzoyl peroxide. From the dynamic mechanical point of view all types behave as two-phase systems retaining the* T_G *of the parent homopolymers.*

MOST papers interpreting mechanical properties of polymers on the basis of their structure refer to homopolymers. Considerable knowledge has also been accumulated about statistical copolymers so that it is possible to estimate approximately their T_G if the T_Gs of the respective homopolymers are known, or to estimate from the amorphous copolymers the T_G of the crystalline polymers, whose dilatometric curves do not show a clear break. Estimates are based on empirical and semi-empirical relations. They are not founded on precise knowledge of the ways in which molecules can be put together, of interaction forces, energy barriers, moments of segments of molecular particles etc. Therefore these characteristics are also not known for hybrids, grafted and block copolymers.

From the chemical point of view grafted and block copolymers occupy a rather transitional position between statistical copolymers and homopolymer mixtures. If segments of their components form from the thermodynamic point of view one phase then hybrids will behave in a way similar to statistical copolymers. However, such cases are very rare[1]. Usually segments of hybrids form different phases and during dynamic mechanical tests display discrete transitional regions the positions of which on the temperature axis coincide with the positions of the respective homopolymers. However, there are known deviations which are attributed to the structural arrangement of components in the hybrid, the length and number of lateral branches or blocks, history of the sample, etc.[2]. Therefore experiment is indispensable for the characterization of every new hybrid.

The purpose of this paper is to study different types of block and grafted copolymers consisting of atactic polypropylene (aPP) and polystyrene (PS) composed of similar weights of similar components. In addition, we have examined block copolymers consisting of aPP and polymethylmethacrylate (PMMA), of a mixture of the former and the latter, and some mixtures of hybrids with parent homopolymers.

EXPERIMENTAL PART

Preparation of hybrid copolymers

Hybrids of the block type were prepared mechanochemically on a laboratory masticator[3]. The initial aPP had a molecular weight M_v of 3×10^5, and styrene or methyl methacrylate was added to the plasticizer in the form of cold vapours on an inert carrier. The method of preparation and characterization of the poly(propylene-block-styrene) hybrid has been reported[4,5]. Also involved was the complex aPP–PS–aPP type having a molecular weight of $4{\cdot}6 \times 10^5$ and a 35 per cent content of the PS component. Hybrids with a higher content of the PS component were obtained by prolonging the mechanochemical process. Atactic poly(propylene-block-methylmethacrylate) of molecular weight $2{\cdot}38 \times 10^5$ and with a 37 per cent PMMA content was prepared analogously with the difference that the initial polymer was cooled to -5°C and the reserve methylmethacrylate was kept at a temperature of 10°C.

The grafted type with 1 to 3 PS branches was prepared in a solution of aPP in styrene at 90°C using benzoyl peroxide as catalyst. The initial aPP used for this purpose had a molecular weight M_v of $1{\cdot}75 \times 10^5$. This molecular weight corresponded approximately to values of the polypropylene segment in the block type hybrid. The method of preparation and characterization of the grafted type has been described[6].

Isolation of hybrid copolymers

Hybrids were isolated from the parent homopolymers by selective extraction with ethyl acetate and heptane.

Pressing of foils

Foils for dynamic mechanical tests were prepared by mould pressing between highly polished aluminium sheets at temperatures of 100° to 110°C.

Torsional tests

Dynamic mechanical tests were carried out on a torsion pendulum[7] at *ca.* 1 Hz within the temperature range from -50° up to about 110°C. This type of torsion pendulum works by means of a suspended metal spring. The combined system, consisting of metal spring and sample, is described by the kinetic equation

$$I\ddot{\phi} + D_k^*\phi = 0$$

where ϕ is the torsion angle, I the moment of inertia and D_k^* the restoring moment of arrangement. Solution of the equation and deduction of the resulting relations can be found in ref. 7.

Results and discussion

Figure 1 shows the slope of G' and λ plotted against temperature with atactic poly(propylene-block-styrene) containing 0·35 and 0·60 weight fractions of the PS component. The first damping-maximum at -5°C corresponds to polypropylene, the other at 107°C to the PS component. Both

values agree well with literature data for the homopolymer components[8,9].

We have also investigated influences producing an increase in the share of the PS component. The increase in the share of the PS component owing to prolongation of the reaction time of the mechanochemical process causes failure of the previous structure. Precise information about the character of these structural changes is not available but on the basis of theoretical

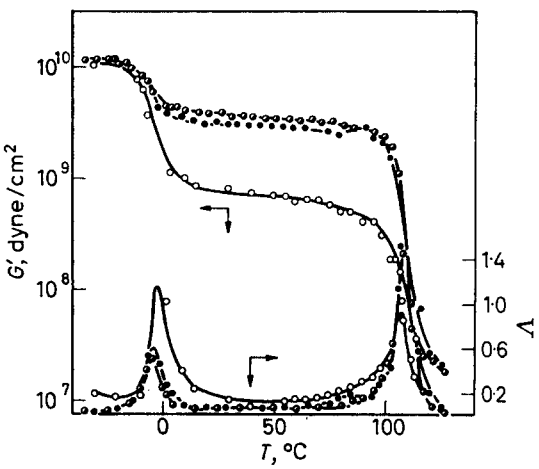

Figure 1 — Temperature dependence of G' and log decrement λ of the copolymer atactic poly(propylene-block-styrene). Content of the PS component shown by ○ 35 per cent, ● 60 per cent, and ◕ 65 per cent. The Λ for the last sample is practically identical with the plot for the sample containing 60 per cent of PS

knowledge from mechanochemistry we can expect growth of more complex structures than A–B–A (which we have identified during the first stages of reaction) and also an increase of grafted structures as a consequence of transfer reactions. As follows from *Figure 1*, this supposed change of structure has no effect on the position of the damping-maximum. We are entitled to this assumption by results obtained with the grafted type (*Figure 2*) whose position of the damping-maximum on the temperature axis is practically identical with those of the previous types. A more striking difference can, however, be observed regarding the plot of G' values, which together with the grafted type during the whole temperature interval, are lower than those of block type. Besides the lower content of the PS component (by about 13 per cent), the more extensive destruction of the polypropylene component during the process of grafting may play a part. In this way we can also explain the termination of the experiment before final attainment of the second damping-maximum corresponding to the PS component as a result of breaking the sample under the 5 g load (which belongs to the methodology of the experiment).

From the above it can be inferred that there is no difference between these two types (block and grafted) regarding the position of the damping-maximum on the temperature axis. This statement is not surprising, not least because both types are very similar regarding the content and distribution of the PS component. Differences could probably be expected, however, when there is a great number of lateral branches. Numerous lateral branches can

reduce interchain barriers of segment rotation so causing a shift of the damping-maximum to lower temperatures[2]. Recently there was published a paper by Waichira Tsuji *et al.*[10], who obtained similar results regarding the positions of the damping-maximum of isotactic polypropylene grafted with styrene. It is remarkable that they were able by sample history to shift the damping-maximum of the PS component on the temperature axis by about 10 deg. C. They explained this by limited mobility of the PS branch under the influence of PP crystallites. We have not observed anything similar with our samples which were amorphous.

Figure 2 (curves ●) is a plot of Λ and G' of an aPP and PS mixture. It can be seen that the trend of the curve does not differ characteristically from hybrid copolymers. Differences in modulus G' values are connected with a different content of the PS component.

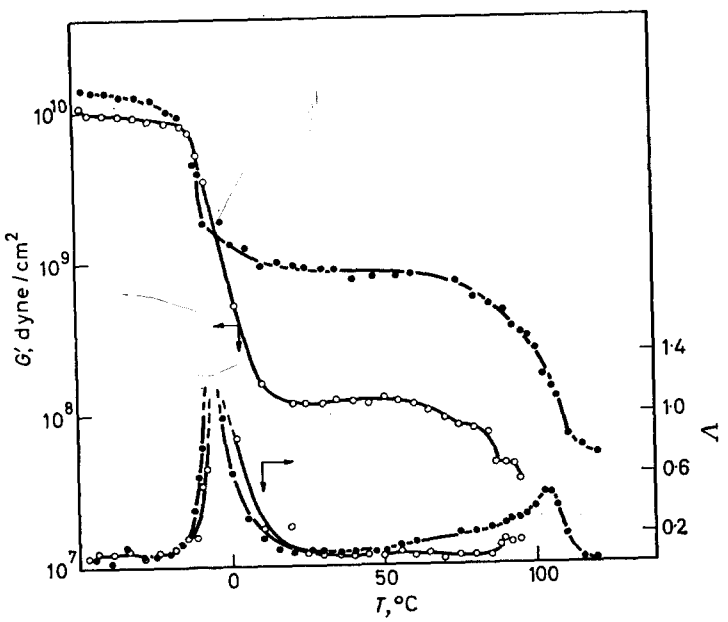

Figure 2—Temperature dependence of G' and log decrement Λ of the copolymer atactic poly(propylene-grafted-styrene) (○) and of the mixture of atactic polypropylene with styrene. (●) Content of PS component in grafted type 27 per cent, in mixture 50 per cent

Agreement between the mixture and the hybrids is explained by the fact that in the hybrids, provided there is sufficient length of component chains, the influence of their mutual chemical bonds on changes of the interaction régime and of energy barriers is practically negligible in comparison with the mixture. Sufficient length of chains enables them to penetrate similar ones by forming aggregates, the mobility of whose segments is practically the same as in the respective homopolymer.

Results relatively comparable with those of the block copolymer based on aPP-S were obtained with the block copolymer based on aPP-MMA

with 37 per cent of PMMA (*Figure 3*). However, some deviations were recorded especially regarding the behaviour of the PMMA component. Since PMMA had been the subject of many investigations deviations could be easily detected. With PMMA two damping-maxima are known[11] namely in the neighbourhood of 100° and 20°C, while damping at 20°C is attributed to movements of the lateral methoxy-carbonyl group. In the block copolymer considered the course of the damping-maximum at 100°C belonging to the PMMA component is indistinct and is absent from the 20°C region.

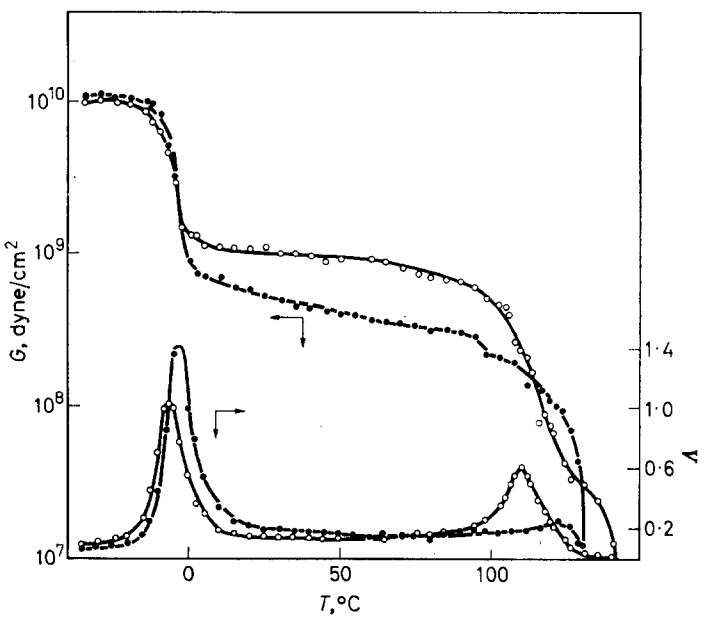

Figure 3—Temperature dependence of G' and of Λ of atactic poly(propylene-block-methylmethacrylate) (●) of 37 per cent MMA content and of the mixture of this copolymer with poly(propylene-block-styrene) (○) in the weight ratio 1 : 1

This should be attributed above all to the history of the sample which is marked by a kind of isolation from the parent homopolymers and by the thermal régime of pressing. In the last stage of separation the sample was extracted with *n*-heptane, this being a good solvent for the PP component only. Since an attempt was made to prepare foils at the lowest possible temperature (100° to 110°C), PMMA segments in contradistinction to aPP segments could not develop sufficiently during pressing. Consequently PMMA behaves more or less as a filler.

Curves (●) on *Figure 3* represent a mixture of the block copolymer based on aPP-PS and aPP-PMMA, weight ratio 1: 1. The occurrence of only two damping-maxima can be explained by the previous history of the

sample and by the proximity of positions of T_G of PS and PMMA as a result of which both T_G merge.

Polymer Institute of the Slovak Academy of Sciences, Bratislava, Czechoslovakia

(*Received October 1967*)

REFERENCES

[1] BEEVERS, R. B. and WHITE, F. T. *Trans. Faraday Soc.* 1960, **56**, 1529
[2] BACCAREDDA, M., BUTTA, E. and ROSINI, V. F., Dynamic Properties of some Graft Copolymers. *International Symposium of Macromolecular Chemistry*. I.U.P.A.C.; Paris, 1963
[3] WATSON, W. F. and WILSON, D. *J. sci. Instrum.* 1954, **31**, 3, 98
[4] ROMANOV, A., MAGARIK, S. J. and LAZÁR, M. *Vysokomol. soedineniya.*, Kratkije soobscenija, T IX B, 1967, **4**, 292
[5] ROMANOV, A. and LATH, D. *Chemické zvesti*, 1967, **21**, 255
[6] PAVLINEC, J., LAZÁR, M. and MANÁSEK, Z. *J. Polym. Sci. C*, 1967, **16**, 1113
[7] ILLERS, K. H. and BREUER, H. *Kolloidzschr.*, 1961, **176** (2), 110–119
[8] BECK, D. L., HILTZ, A. A. and KNOX, J. R. *S.P.E. Trans.* October 1963, 279
[9] NIELSEN, L. E. *Mechanical Properties of Polymers*, pp 16, 24. Reinhold: New York, 1962
[10] WAICHIRO TSUJI and HYON-DUG CHU. *J. Soc. Fiber Sci. Technol., Japan*, April 1967, **23** (4), 145–151
[11] TURLEY, S. G. and HENKO KESKKULA. *J. Polym. Sci. C*, 1966, No. 14, 69–87

On the Structure of Polypropylene Fibres

P. G. STERN and E. SEGERMAN*

Conventional wide angle X-ray diffraction and density techniques are used to measure the validity of a two phase model for the structure of polypropylene fibres. Percentage crystallinity studies showed that the crystallinity of polypropylene fibres when measured by the X-ray method as a function of increasing draw ratio remained constant, while the crystallinity of the same samples measured by the density method increased from 49 per cent (D.R.=3·0) to 77 per cent (D.R.=7·0). These data and a measured shift in the equatorial diffraction peaks strongly suggest the existence of intermediate states of order, and a paracrystalline model for the structure of polypropylene fibres is proposed.

VARIOUS methods have been used for the estimation of percentage crystallinity in high polymers, and it has become increasingly apparent that these measure different things and therefore do not always give the same result[1]. All current methods assume implicitly a two phase model of crystallites embedded in an amorphous matrix, in which the two phases contribute independently to the property under examination. Two examples of careful comparative studies may be cited:

(1) W. O. Statton[1] has used density, X-ray, and infra-red techniques to measure the crystallinity of five unoriented samples of polyethylene, and has found that the three methods agree, the range of crystallinity being 43 ± 2 to 77 ± 1 per cent.

(2) Farrow and Ward[2] have used density, infra-red and X-ray methods to study the changes in crystallinity when polyethylene terephthalate fibres were drawn and then heat set. The three sets of results were completely at variance, both in absolute level, and in that only the infra-red showed any change of crystallinity with draw ratio.

In this paper we have used density and X-ray methods to study the effect of draw ratio on the crystallinity of polypropylene fibres.

EXPERIMENTAL

X-Ray method

The methods for determining the degree of crystallinity by means of X-ray diffraction were developed by Hermans and Weidinger[3], and Goppel and Arlmann[4]. The general procedure is based on the law of conservation of intensity which states that the amount of intensity is determined by the integral over the volume for the square of the electron density, equation (1).

$$\int I_{(s)}\, dV_s = \int \rho^2(r)\, dV_r \qquad (1)$$

The mean electron density is roughly the same for the amorphous and crystalline phases of a given polymer, and it is possible to distinguish between them on the assumption that the intensity for the 'crystalline' scattering is concentrated in the sharp reflections and for the 'amorphous' in the diffuse halo and background.

*Present address: Unilever Research Laboratory, Port Sunlight, Cheshire.

The method is to try to separate and then measure, on one diffraction scan, the integrated intensities from the 'crystalline' and 'amorphous' phases. The integration is carried out over the whole range $2\theta=0°$ to 180°, where θ is the Bragg angle. The degree of crystallinity, calculated as a percentage, is given by

$$\text{D.C.} = 100\, A_c/(A_a + A_c) \qquad (2)$$

where A_a and A_c are respectively the amorphous and crystalline integrated intensities after corrections for the Debye–Waller, atomic scattering, and Lorentz polarization factors (see *Figure 1*). Orientation effects in the X-ray photograph are eliminated by mechanical fibre-randomization methods suggested by Hermans and Weidinger[3]. The procedure described above assumes that the increase in intensity in the sharp diffraction maxima accompanying crystal growth was originally in the amorphous halo. Conversely, if one has such a background on the X-ray diagram, it means that the diffraction peaks transferred some of their intensity quantitatively to it. One can then introduce an artificial Debye factor and give the lost intensity from the background back to the reflections to eliminate the effects of the distortions[5].

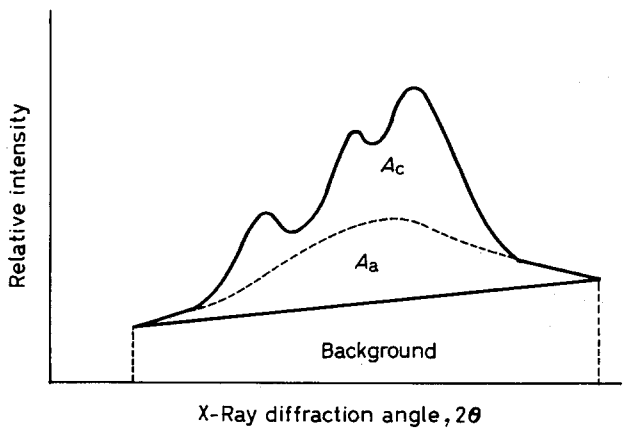

Figure 1—Typical microdensitometer scan of a fibre X-ray diffraction photograph used for calculating the percentage crystallinity. A_a='amorphous' contribution. A_c='crystalline' contribution

Density method

The density method for measuring the percentage crystallinity assumes that the density of the 'amorphous' material is always that measured on some sample supposed to be completely amorphous, and the density of the crystalline material is always that calculated from the crystal structure if it is known. A density gradient column[6] is used to measure the actual density of the sample, and a linear interpolation between the completely amorphous and completely crystalline densities leads to the percentage crystallinity of the sample.

Two conditions must be met for both the X-ray and density methods of calculating percentage crystallinity to be valid; (1) polymers must consist of a two phase system—crystallites embedded in an amorphous matrix, and (2) the properties of each phase must remain unaltered in the various admixtures found.

RESULTS AND DISCUSSION

Percentage crystallinity studies on polypropylene fibres as a function of increasing draw ratios showed that the unoriented halo ('amorphous' halo) does not change with drawing, which in turn illustrates the noncrystallizability of this phase. It is evident from the radial intensity scans of X-ray precession photographs (see *Figures 2* and *3*) scanned on a Joyce–Lobl

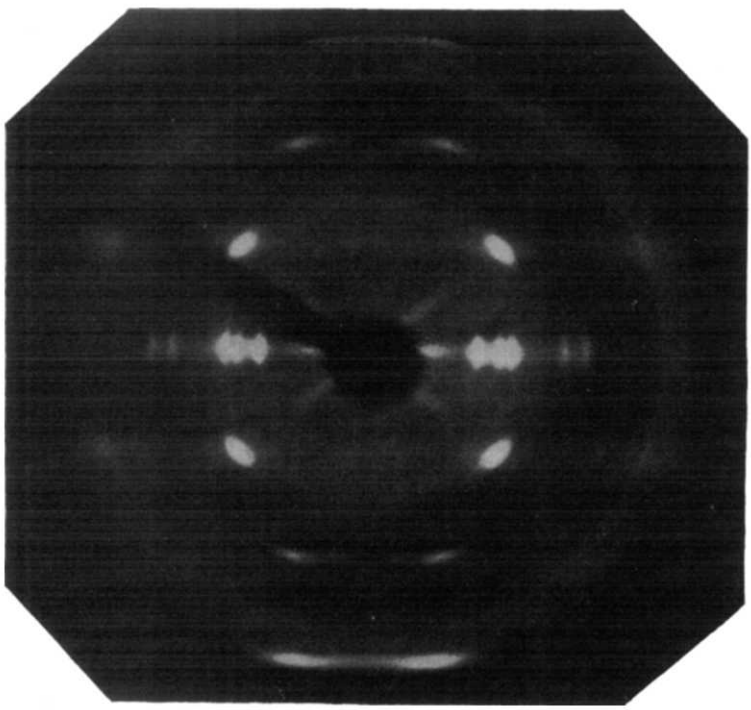

Figure 2—Precession X-ray diffraction photograph of an oriented polypropylene fibre. Fibre axis is vertical

microdensitometer, that the only change in the diffraction patterns, as a function of draw ratio of the fibres, is a redistribution of intensity above the 'amorphous' background. The shape of the 'amorphous' halo for various degrees of order in the sample was easily obtained by scanning the intensity distributions radially at several positions other than the equator.

The broad crystalline peaks in the diffraction scans for low draw ratios, could not be fitted with symmetrically broadened crystalline peaks, and a

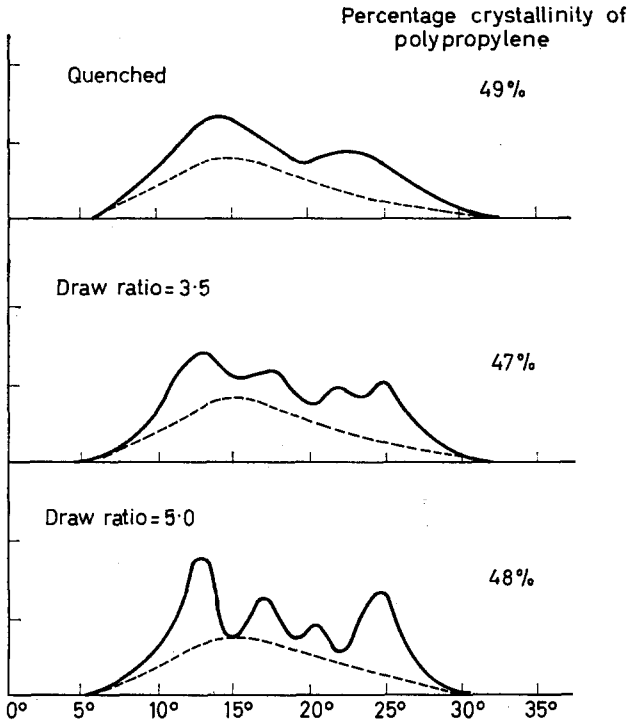

Figure 3—Microdensitometer scans of polypropylene X-ray diffraction photographs for different fibre draw ratios

substantial shift in their positions was recorded. This continuous shift indicates a change in the unit cell parameters which is experimental evidence that an intermediate state of order exists in polypropylene fibres[7]. Hermans and Weidinger[8] suggest a similar situation in polyethylene, and Krimm and Tobolsky[9] also report a change in the unit cell dimensions of polyethylene with drawing.

Percentage crystallinity measurements of polypropylene fibres obtained by the X-ray and density methods which were described earlier are compared in *Table 1*.

Table 1. Pin-and-plate drawn polypropylene fibres

Sample draw ratio	*Density* (g/cm^3)	*Crystallinity* (%)	
		Density	*X-ray*
3·0	0·902	49	49
3·5	0·902	49	48
4·0	0·904	51	47
4·5	0·905	52	49
5·0	0·909	58	47
5·5	0·912	53	48
6·0	0·913	64	47
6·5	0·920	75	47
7·0	0·922	77	48

It is important to observe from these results that the crystallinity measured by the X-ray method for pin-and-plate drawn fibres is constant within experimental error, while crystallinity measured by the density method increases as a function of draw ratio (see *Table 1* and *Figure 4*). These results confirm the existence of at least two relatively independent phases in polypropylene fibres. One of these phases is in an intermediate state of order similar to Hosemann's paracrystal[10, 11], and the other consists of randomly placed coiled polypropylene molecules and is described in greater detail in the forthcoming discussion. The drawing process increases the order in the paracrystalline regions which in turn sharpens the diffraction peaks in *Figure 3* but does not affect the amorphous halo. Consequently, the percentage crystallinity as measured by the X-ray method remains unchanged when the fibre is drawn, while when it is calculated by the density technique it increases substantially since there is an increase in the density of the paracrystalline regions.

From the previous discussion we see that since the general methods used to measure percentage crystallinity in fibres assume a system of crystallites embedded in an amorphous matrix, the existence of an intermediate state renders any single measurement of this degree of crystallinity invalid. Percentage crystallinity measurements on nylon 6.10 fibres also posed similar problems to those encountered in polypropylene which strongly suggests the existence of an intermediate state of order in this polymer[12, 13]. Supporting evidence for the two structural phases proposed in this paper is obtained by direct observation of the wide angle X-ray diffraction patterns (see *Figure 2*). The X-ray precession photographs were taken on a Hilger and Watts Microfocus X-ray generator and nickel filtered Cu Kα radiation was used throughout the experiments. The Microfocus generator provides a brilliant fine spot focus, and exposure times, normal with conventional equipment, are greatly reduced. The main characteristics of the diffraction patterns are; (1) the broadening and progressive weakening of the three-dimensional diffraction spots (isolated intensity spots), (2) the background diffuse scattering, (3) the 'amorphous' halo, and (4) the streak diffraction which is characterized by continuous intensity streaks along the layer lines. The sharp equatorial spots are evidence of a high degree of lateral order and orientation about the fibre axis. The streak diffraction along the layer lines, on the other hand, occurs if the regions of three-dimensional order are slightly disturbed by irregular displacements of the chains from their regular positions. These hypotheses were confirmed by optical diffraction studies which were described elsewhere[12, 13]. The four very intense quadrantal diffraction spots in *Figure 4* are due to the helical configuration of the polypropylene molecules which are arranged in regions of intermediate order (paracrystalline state). It is also important to observe on the X-ray photograph that the diameter of the circle on which the four intense quadrantal spots lie is greater than the diameter of the 'amorphous' halo, and it also passes on the periphery of the equatorial spots. A direct interpretation of these results would indicate that the molecular packing in the 'amorphous' phase (causing the halo) is closer than that in the ordered regions. Since this is an unlikely situation, the 'amorphous' halo must be caused by a

phase separate from the one producing three-dimensional diffraction. The disordered phase is visualized as consisting of individual coiled polypropylene molecules placed in all orientations throughout the structure. The helical molecules in the paracrystalline regions pack in an alternating sequence, and consequently the average distance between diffracting planes is somewhat shorter than the distance in the individual coiled molecules. This causes the

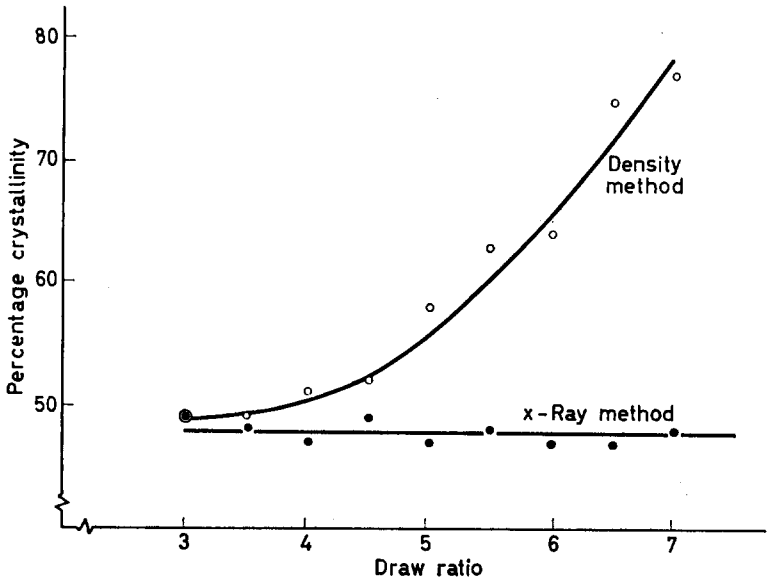

Figure 4—Graph of percentage crystallinity versus draw ratio for pin-and-plate drawn polypropylene fibres

four intense quadrantal diffraction spots, which are in reciprocal space, to lie on a circle with a larger diameter than the 'amorphous' halo.

It has been shown that percentage crystallinity studies based on a two phase model of crystallites embedded in an amorphous matrix can lead to completely erroneous results. Differences in crystallinity measurements by X-ray and density techniques for polypropylene fibres in this paper led to a proposal of a new model which is also primarily based on two structural phases; (1) random individual coiled polypropylene molecules or very small bundles of molecules placed in all orientations, and (2) interlinked units of intermediate order (paracrystalline) which at high draw ratios approach the crystalline structure proposed by Natta and Corradini[14]. This newly derived model explains the many puzzling features of the wide angle X-ray diffraction patterns outlined in this paper and how they vary in detail with fabrication conditions.

E. I. du Pont de Nemours & Co., Inc.,
Spruance Research Laboratory,
Richmond, Va, U.S.A.

(Received October 1967)

REFERENCES

[1]STATTON, W. O. *J. Polym. Sci. C*, 1967, **18**, 33
[2]FARROW, G. and WARD, I. M. *Polymer, Lond.* 1960, **1**, 330
[3]HERMANS, P. H. and WEIDINGER, A. *J. appl. Phys.* 1948, **19**, 491
[4]GOPPEL, J. M. and ARLMANN, I, J. *Appl. Sci. Res., A*, 1949, **1**, 462
[5]RULAND, W. *Acta cryst., Camb.* 1961, **14**, 1180
[6]PELSMAEKER, J. and AMELINCKX, S. *Rev. sci. Instrum.* 1961, **32**, 828
[7]STERN, P. G. and SEGERMAN, E. *Nature, Lond.* 1966, **210**, 1258
[8]HERMANS, P. H. and WEIDINGER, A. *Makromol. Chem.* 1961, **44**, 24
[9]KRIMM, S. and TOBOLSKY, A. W. *J. Polym. Sci.* 1951, **7**, 1956
[10]HOSEMANN, R. *Z. Phys.* 1950, **128**, 1, 465
HOSEMANN, R. *Kolloidzschr.* 1950, **119**, 129
HOSEMANN, R. *Acta Cryst., Camb.* 1950, **4**, 520
HOSEMANN, R. *Polymer, Lond.* 1962, **3**, 349
[11]HOSEMANN, R. and BAGCHI, S. N. *Direct Analysis of Diffraction by Matter*, North Holland: Amsterdam, 1962
[12]STERN, P. G. *Kolloidzschr. u. Z. Polym.* 1967, **215**, 140
[13]MORGAN, L. B. and STERN, P. G. (1967) *Polymer, Lond.* 1968, **9**, 375
[14]NATTA, G. and CORRADINI, P. *Nuovo Cim.* 1960, Suppl. to **15**, 40

The Thermal Degradation of Polyfluoral and Methods of Stabilization

W. K. BUSFIELD

The rates of thermal degradation of polymers of fluoral are reported. Both the thermal stability and the mechanism of degradation vary markedly according to the method of polymer preparation. In general the thermal stability is poor, one sample decomposing in 15 minutes at 120°C. Methods of stabilizing the polymer are described. After stabilization one sample did not degrade below 330°C.

POLYMERS of fluoral (trifluoroacetaldehyde) with varying degrees of thermal stability have been described in the literature. Husted and Ahlbrecht[1] produced polymers which they claim did not depolymerize below 380°C. On the other hand other workers have described polyfluoral samples as readily decomposable[2]. Such variations could be due to any combination of a number of causes such as the nature of polymer end groups, the average degree of polymerization, the polymer crystallinity or the presence of initiator residues trapped in the solid polymer. This paper describes the measurement of the rates of thermal degradation and techniques for improving the thermal stability of polyfluoral prepared by a variety of methods. Discussion of the mechanism of the degradation reactions is limited by the lack of molecular weight data.

EXPERIMENTAL

Polymer preparations

Fluoral was prepared and purified as previously described[3].

The polymers were prepared in evacuated ampoules by the methods detailed in *Table 1*. All the polymerizations were essentially complete except for sample F where, even after 18 months, there was only about 80 per cent conversion to polymer.

Infra-red spectra, recorded by internal reflection on the solid samples, showed that all the polymers had the polyacetal structure similar to those previously described[4].

Samples B and N′ were quite stable in air. Samples F, N, H and L all had a slight odour of fluoral and when kept in bottles, which were not quite sealed, fine crystals of the hemi hydrate[5] could be seen to grow from the polymer surface over a period of weeks. The crystals were very hygroscopic and disappeared on opening the bottle lid presumably due to the formation of fluoral hydrate.

All samples were pumped for at least eight hours at room temperature prior to degradation experiments.

Degradation experiments

(a) *Isothermal*—Polymer samples, cut into small pieces and usually weighing between 20 and 50 mg, were placed in a Pyrex bulb connected to

Table 1. Preparation details of the polyfluoral samples

Sample	*N**	*B*	*H*	*L*	*F*
Initiator	azo-bis-iso-butyronitrile	benzoyl peroxide	sulphuric acid	butyl lithium	None
Concentration (per cent with respect to monomer)	0·75	0·7	1·0	1·5	—
Solvent	None	Hexane	None	None	None
Monomer concentration (M)		9			
Time	2 h	7 h	1 month	2 sec	18 month
Temperature (°C)	—20	45	22	—78	22
Notes	Irradiated with medium pressure Hg lamp				Polymerization incomplete
Polymer nature	Homogeneous transparent elastomer	Heterogeneous white powder	Homo-geneous transparent brittle solid	White† elastomer	Heterogeneous translucent solid

*Polyfluoral N′ was made by a similar method to sample N but was kept in the evacuated ampoule 18 months at room temperature before opening a few days prior to degradation experiments.
†Discoloured in the region of the catalyst.

a glass spiral pressure gauge (sensitivity 1·40 cm of mercury per 1·00 cm of scale) and to the vacuum line via a silicone greased tap. The spiral gauge, connecting tubing and tap were heated electrically to about 130°C. Degradation experiments were started by immersing the bulb in an oil bath at the required temperature and followed by recording the pressures of the volatile products formed. The apparatus was calibrated using known weights of dichlorobenzene in order that pressures, at any given temperature, could be converted directly into moles of gas formed. The reaction volume was about 24 ml. Trial experiments showed that the reaction bulb took 45 sec to reach the bath temperature. It was estimated from actual degradation experiments that the polymer sample took from one to two minutes to reach a temperature close to the bath temperature (there would be a temperature profile across the polymer sample due to its low thermal conductivity and the endothermicity of the reaction taking place).

(b) *Temperature programmed*—5 to 15 mg samples of the polymer were heated in a nitrogen carrier gas stream in a Perkin–Elmer differential scanning calorimeter. The concentration of the product gases in the effluent carrier gas stream was recorded continuously by means of a katharometer as the sample temperature was increased at the rate of 8 deg. C per

minute. If the product is a pure gas (as in this case, see later) the pen records the relative rate of volatilization of the sample as its temperature is raised.

This method was used for investigating the thermal stability of the stabilized samples in the range 400° to 700°K.

Product gas analysis

The gaseous products of the degradations were analysed by gas chromatography and by infra-red spectroscopy. In the isothermal experiments, samples were taken directly from the reaction bulb. In the samples investigated on the differential scanning calorimeter separate degradation experiments were carried out in which the samples were completely degraded at 380°C and the gaseous products analysed. The major gaseous product from the degradation of all the samples investigated was fluoral. Only the degradation of a stabilized sample of polyfluoral L produced any other detectable gaseous products. Although unidentified, its concentration determined by the method of gas chromatographic peak heights was about 0·5 per cent.

RESULTS AND DISCUSSION

The thermal stability of the polymer samples at 120°C is represented by conversion/time graphs in *Figure 1*. As expected from earlier reports there is a marked variation in stability according to the method of preparation.

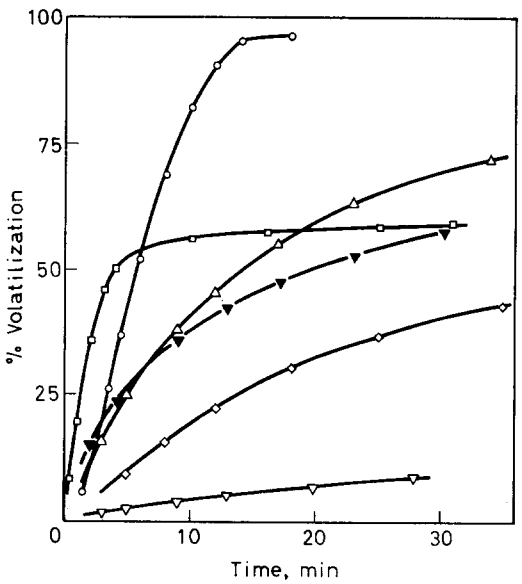

Figure 1—The production of volatile material in the thermal degradation of polyfluoral. At 120°C: ○ sample N; ▽ sample B; △ sample H; □ sample L; ◇ sample F. At 180°C: ▼ sample B

The large yield of monomer from the degradations indicates a large zip length, little transfer and consequently first order kinetics[6]. The rate conversion graphs shown in *Figure 2* show that samples L, F and B decay approximately by first order kinetics over limited ranges, whilst sample N

has an order of about one half between 25 and 95 per cent conversion and sample H decays by second order kinetics. Each case is discussed separately below.

Polyfluoral N

A fourfold increase of the initial weight of polymer in the reaction vessel had little effect on the rate of the reaction expressed as percentage conversion per minute as shown in *Figure 3*. Since this involved a fourfold increase in the monomer pressure during the reaction the polymerization reaction is of little significance under these conditions. This behaviour is

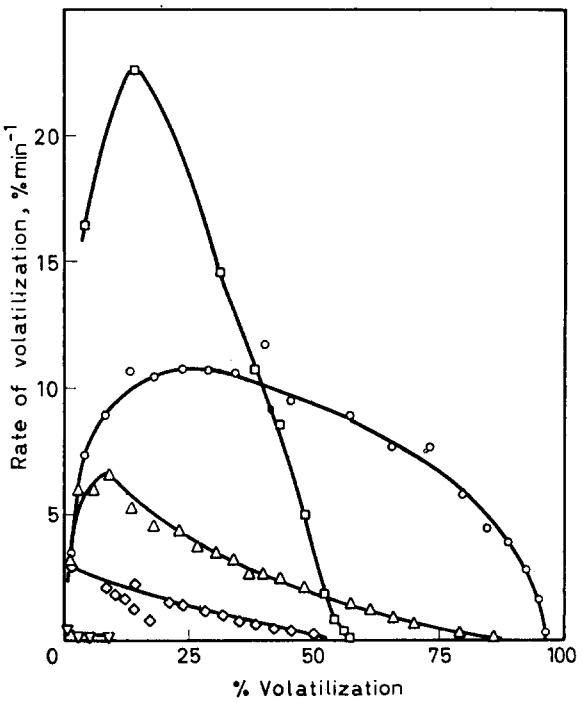

Figure 2—Rate of thermal degradation of polyfluoral as a function of extent of volatilization at 120°C. ○ sample N; ▽ sample B; △ sample H; □ sample L; ◇ sample F

quite unlike that of the formaldehyde system in which Iwasa and Imoto[7] found that the rate of depolymerization, R_d, depends upon the monomer pressure, p, according to the following (modified) expression at constant temperature

$$R_d \propto \frac{(1-x)^{0.8}}{x^{0.5}} p^{0.5} (1 - p/p_e)^{1.6}$$

where x is the conversion and p_e is the equilibrium pressure at that temperature.

At 120°C and after an initial induction period, which is only partially

caused by thermal lag effects in the system, the reaction proceeds smoothly to a conversion in excess of 95 per cent. There was always a small solid residue left which possessed a high degree of thermal stability. The rate versus conversion curves in *Figure 4* show that the rate is a maximum at about 25 per cent conversion. Thereafter the reaction follows approximately half order kinetics. According to the calculations of Wall and Flynn[6] this behaviour is expected for degradations involving a fair amount of transfer. This is compatible with the formation of thermally stable residues but not with the large monomer yield.

As the degradation temperature is reduced the rate versus conversion curves, see *Figure 4*, become shallower although the rate still passes through a maximum at about 25 per cent conversion. In the later stages the reaction order decreases with the temperature and is fairly close to zero at 90°C. It seems likely that the mechanism of the zero order reaction at lower temperatures is a slow monomer unzipping reaction from the polymer molecule ends, possibly by a molecular mechanism, causing a steady decrease in the degree of polymerization but not in the number of molecules as the reaction proceeds. Thus the rate, which is proportional to the number of active ends present, is independent of conversion giving zero order. At higher temperatures there is increasing competition with higher order reactions.

Sample history has a marked effect on the rate of degradation. The degradation experiments on sample N previously described were carried out within a few weeks of its preparation. The degradation of sample N′, however, was carried out 18 months after its preparation during which time it was kept in a sealed evacuated ampoule at room temperature. The degradation curve, see *Figure 3*, shows that the thermal stability is greatly improved by this treatment. On the other hand, the rate of degradation of sample N after six months in a sample bottle (apparently not quite airtight) in the presence of air was slightly enhanced, see *Figure 3*.

It seems likely that both these effects are caused by molecular weight changes occurring during storage. In the sealed ampoule no degradation to monomer occurs because the sample is always in contact with the equilibrium pressure of monomer. The molecular weight is probably increasing by some form of slow reaction involving end groups of neighbouring molecules thus improving its thermal stability. When in the presence of moist air, monomeric fluoral is converted to the fluoral hemi hydrate crystals mentioned in the experimental section. Consequently, the monomer equilibrium pressure is not maintained and the polymer slowly degrades with a resultant decrease in molecular weight and thermal stability.

The infra-red spectrum of sample N gave no indication of the nature of the end groups. A sample at room temperature in the presence of fluoral gas at a pressure of 30 cm of mercury increased in weight at the rate of 0·5 per cent per minute by absorption of monomer. This fact together with knowledge of the relative thermal instability indicates that at least one end group per molecule is moderately active. On the assumption that these were hydroxyl groups attempts were made to stabilize the polymer by esterification.

Both the methods used for stabilizing polyformaldehyde[8] and poly-

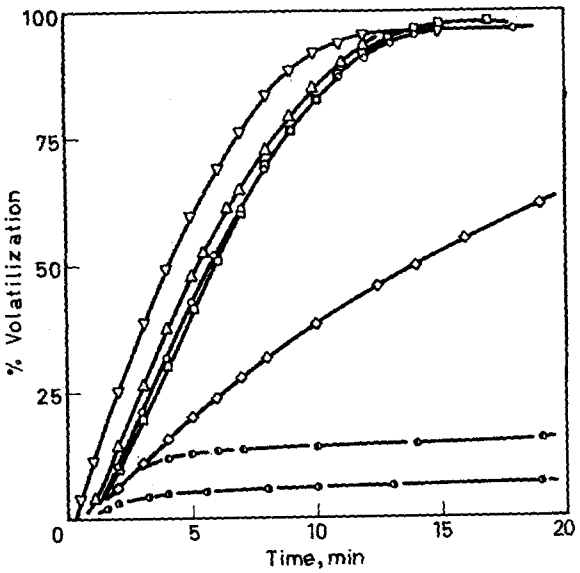

Figure 3—The production of volatile material in the thermal degradation of polyfluoral N and N′. At 120°C: □ 115·1 mg sample N; △ 53·2 mg sample N; ○ 29·1 mg sample N; ▽ sample N after 6 months in air (see text); ◇ sample N′ (see text).. At 180°C: ◑ sample N after treatment with $(CH_3CO)_2O$ in $HCCl_3$. ◐ sample N after treatment with $CH_3(CH_2)_{10}COCl$ in $HCCl_3$ and pyridine

chloral[9] caused complete degradation. Successful stabilization was achieved by refluxing a mixture of the polymer and excess acetic anhydride in chloroform, for at least 15 hours. Partial degradation occurred simultaneously, usually to the extent of about 30 per cent. Addition of pyridine greatly increased the rate of stabilization but also the extent of degradation. No evidence of acetylation could be derived from infra-red spectra but evidence of stabilization was derived from degradation experiments. A typical conversion/time curve with the sample at 180°C is shown in *Figure 3*.

Temperature programmed thermal degradation of the stabilized sample is represented by the curve of the relative rate of volatilization versus temperature in *Figure 5*. There was no solid residue indicating that the volatilization was complete. The rate passes through two maxima at 260°C and 345°C showing that two independent degradation reactions are occurring.

Sample N was also stabilized using lauroyl chloride in place of acetic anhydride in an attempt to estimate the degree of polymerization by a C, H analysis of the resultant stabilized polymer according to the method of Rosen *et al.*[9]. The presence of pyridine was necessary for this stabilization and 54 per cent of the polymer degraded during the reaction. The conversion/time curve at 180°C, see *Figure 3*, shows that this sample was slightly less thermally stable than the acetylated sample. The H and F

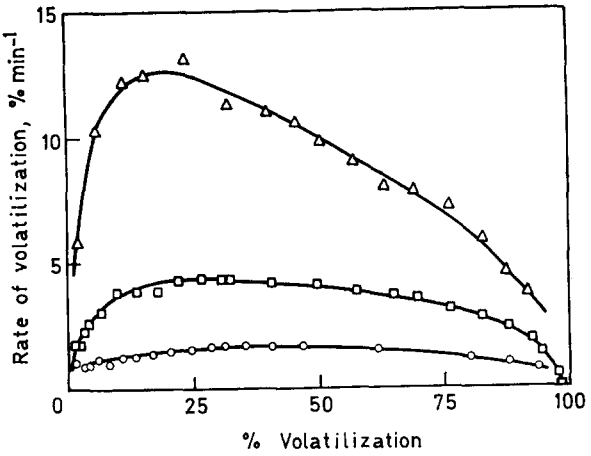

Figure 4—Rate of thermal degradation of polyfluoral N as a function of extent of volatilization at: △ 120°C; □ 106°C; ○ 90°C

analyses from three independent analytical laboratories were incompatible. The carbon analyses assuming the polymer end groups were $CH_3(CH_2)_{10}CO$— and $(CH_3)_2C(CN)$— gave a degree of polymerization of 66 ± 18. The extent of the possible decrease in degree of polymerization during stabilization is unknown.

Polyfluoral B

Polymer produced by benzoyl peroxide initiation was quite different to polyfluoral N in both appearance and thermal stability. The thermal stability curves in *Figure 1* show that polyfluoral B decomposes more slowly at 180°C than polyfluoral N at 120°C. Apparently sample B has more stable end groups.

Few experiments were carried out with sample B because of its heterogeneity and the consequent difficulty of selecting typical samples.

Polyfluoral H

Some X-ray diffraction photographs showed that sample H was extremely crystalline with lattice spacings identical to those of sample CM described in an earlier publication[4]. It is interesting to note that grinding the sample caused a significant decrease in the crystallinity. Evidently the crystalline regions break down when subjected to mechanical shock.

The degradation of sample H at 120°C is represented in *Figures 1* and *2*. The initial induction period is shorter than that of sample N under similar conditions and is probably due entirely to thermal lag effects. In direct contrast to the behaviour of sample N the remainder of the degradation obeyed second order kinetics fairly closely. When the reaction was stopped after 87 per cent conversion the residue was a discoloured elastomer quite different from the initial brittle polymer. Discolouration was presumably due to the presence of the original initiator sulphuric acid.

The fact that a high yield of monomer is produced in the degradation, and that sample H can be end group stabilized (see later) indicate end initiation followed by a monomer unzipping process for the degradation mechanism. With a large zip length first order kinetics would be expected. Thus some additional factor or factors cause a steady decrease in rate as the reaction proceeds. Further speculation is meaningless without molecular weight data.

There is a very weak broad absorption band centred at 3 200 cm^{-1} in the polymer infra-red spectrum indicating OH end groups. Stabilization with acetic anhydride was achieved by the same method as described for sample N. The product was a fine powder of unknown yield with a thermal stability similar to that of stabilized sample N. An X-ray diffraction photograph showed that, although the crystallinity was lower than that of the original sample, the diffraction lines were in the same position. Thus stabilization has little effect on the lattice structure. The infra-red spectrum (transmission through a potassium bromide disc) showed no absorption in the 3 200 cm^{-1} region and a small sharp peak at 1 825 cm^{-1}. This is significantly removed from corresponding absorption peaks reported for esterified polyformaldehyde[10] and polychoral[9] (1 760 cm^{-1}) but is still considered to indicate successful esterification.

A temperature programmed degradation in the higher temperature range is shown in *Figure 5*. A small black residue (about one per cent) remained after the degradation indicating approximately complete volatilization. As

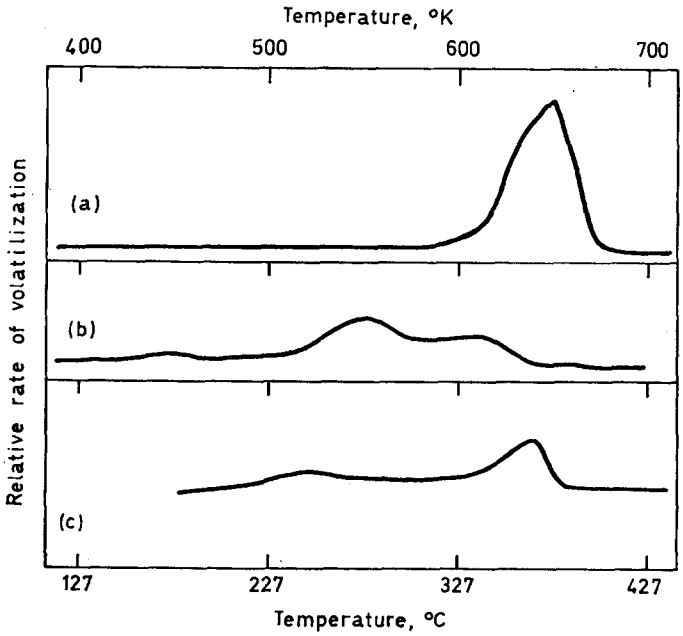

Figure 5—Relative rate of thermal degradation of stabilized polyfluoral samples as a function of increasing temperature at the rate of 8 deg. K min^{-1}. (a) polyfluoral L; (b) polyfluoral N; (c) polyfluoral H

with sample N two maxima, centred at 240°C and 370°C, occur indicating two independent degradation mechanisms. Approximately 70 per cent decomposes in the upper temperature region.

Stabilization with lauroyl chloride was achieved by refluxing in chloroform for 70 hours in the absence of pyridine. Microanalysis for C gave a degree of polymerization of 131 ± 3 assuming that both end groups are $CH_3(CH_2)_{10}CO—$.

Polyfluoral L

Polymer made by butyl lithium initiation was the least stable of all the samples and smelled very strongly of fluoral at room temperature. Degradation experiments were carried out after pumping for 50 hours at room temperature. The thermal stability curves, represented in *Figures 1* and *2*, show that, although some of the polymer is unstable, about 42 per cent has high thermal stability. Even at 180°C only a further five per cent (of the original) decomposed in 48 minutes. Thus either the original sample is composed of two fractions or a secondary reaction during degradation produces polymer with stable end groups possibly, for example, by combination.

Decomposition of the unstable fraction was so rapid that isothermal conditions were not attained before it was almost complete. No conclusion regarding the mechanism can therefore be made.

An infra-red spectrum gave no indication of the nature of the polymer end groups but thermal stabilization with acetic anhydride was achieved by the same method as used for sample N. Only eleven per cent was lost during the reaction. Thus 80 per cent of the originally unstable fraction was stabilized showing that, although it was thermally less stable than sample N, it was more amenable to stabilization.

In the temperature programmed degradation of the stabilized sample the rate of volatilization passes through only one maximum at 380°C. This sample had the highest thermal stability of the series. At the end of the experiment there was a small black residue (approximately one per cent) showing that volatilization was essentially complete.

Polyfluoral F

Few experiments were carried out with sample F because of its heterogeneity and the consequent difficulty of selecting typical samples. Thermal stability curves are shown in *Figures 1* and *2*. In general it was more stable than all samples except polyfluoral B and decomposed approximately according to first order kinetics. End initiation followed by a complete unzipping process is the probable mechanism.

The author is grateful to Dr J. Iball for providing the X-ray diffraction photographs, and to Dr J. R. McCallum for stimulating discussion.

Department of Chemistry,
University of Dundee,
Scotland.

(*Received October 1967*)

REFERENCES

[1] HUSTED, D. R. and AHLBRECHT, A. H. *Brit. Pat. No. 719 877* (1954)
[2] BROWN, F. and MUSGRAVE, W. K. R. *J. chem. Soc.* 1952, 5049
SHECHTER, H. and CONRAD, F. *J. Amer. chem. Soc.* 1950, **74,** 5422
[3] BUSFIELD, W. K. *Polymer, Lond.* 1966, **7,** 541
[4] BUSFIELD, W. K. and WHALLEY, E. *Canad. J. Chem.* 1965, **43,** 2289
[5] MCGREER, D. E., STEWART, R. and MOCOK, M. M. *Canad. J. Chem.* 1963, **41,** 1024
[6] WALL, L. A. and FLYNN, J. H. *Rubber Chem. Technol.* 1962, **35,** 1157
[7] IWASA, Y. and IMOTO, T. *J. chem. Soc. Japan, Pure Chem. Sect.* 1963, **84,** 31
[8] E. I. du Pont de Nemours and Co. *Brit. Pat. No. 770 717* (1957)
[9] ROSEN, I., HUDGIN, D. E., STURM, C. L., MCCAIN, G. H. and WILHJELM, R. M. *J. Polym. Sci. A,* 1965, **3,** 1535
[10] KOCH, T. A. and LINDVIG, P. E. *J. appl. Polym. Sci.* 1959, **1,** 164

Absorption Spectrum of Gamma-irradiated Poly(methylmethacrylate) within the Range 245 to 450mμ

R. J. FLEMING*

The absorption spectrum of poly(methylmethacrylate) irradiated with γ-rays at room and liquid nitrogen temperatures has been studied within the range 245 to 450 mμ. The materials used varied considerably in nature and concentration of initiator and chain-transfer agent additives. Most of the samples irradiated at liquid nitrogen temperature showed peak absorption wavelengths very close to those noted after room-temperature irradiation; a minority group showed shorter peak wavelengths, which shifted to the room-temperature values when subsequently warmed to room temperature. A marked dependence of spectral behaviour on both initiator and chain-transfer agent content was noted, indicating that most of the absorbing species originate in the additives; on the other hand, an absorption peak around 252 mμ was found in several samples independent of their additive content, and also independent of the temperature of irradiation. As a strong absorption peaking close to this wavelength was observed in radiation polymerized poly(methylmethacrylate), it is postulated that the species giving rise to this particular absorption is formed on methylmethacrylate monomer residue in the polymer. Evidence is presented to show that the absorbing species are not radicals. It is possible that they are ionic in nature, probably cations. It is postulated that the absorbing species formed on the monomer residue is a carbanion —$\dot{\dot{C}}$HCH=CH— *which, with appropriate electron pairing, would not give rise to an e.s.r. signal. Of the materials polymerized with the help of additives, those containing fairly large concentrations of mercaptan compounds as chain-transfer agents showed a slowly decaying absorption peaking around 252 mμ at liquid nitrogen temperature and 255 mμ at room temperature; the species giving rise to this absorption is to be distinguished from that formed on monomer residue. Materials containing benzoyl peroxide initiator showed peak absorption values around 280 and 290 mμ, independent of temperature.*

THE use of poly(methylmethacrylate) (PMMA) as a radiation dosimetry material has been extensively investigated during the past decade (Boag, Dolphin and Rotblat[1], Brownell, Stratton and Pinter[2], Orton[3]). Studies of a more academic nature have also been carried out by Kinell[4], Goodeve[5], and Melville[6]. Considerable variation in the nature and concentration of plasticizer added to the basic methylmethacrylate monomer before polymerization (producing commercial Perspex, Plexiglas, Lucite, etc.) is reported. More recently, Orton[7] has published the results of a study of the effect of varying amounts of benzoyl peroxide (BP) (added as a polymerization initiator) and residual monomer content on the absorption spectrum of Perspex irradiated at room temperature (RT) with 15 MeV electrons. This paper reports corresponding results for a wider range of additives, and for radiation (using γ-rays) at both liquid nitrogen temperature (LNT) and RT. General con-

*Present address: Department of Physics, Monash University, Clayton, Victoria, Australia.

clusions on the nature and origin of the species responsible for the changes in absorption following irradiation are drawn, but no attempt at a precise identification is made except for one particular species.

EXPERIMENTAL

(a) *Materials*

The samples used were in the form of transparent sheets, typical dimensions being 25 mm × 15 mm × 0·5 mm; each sample was cut from a larger sheet produced by pressing the appropriate polymer powder at a temperature of 180°C and a pressure of 20 000 lb/in.^{2}. Radiation polymerized PMMA was obtained by thoroughly washing methylmethacrylate monomer liquid in ten per cent caustic soda solution and in distilled water, drying with sodium sulphite, re-distilling under reduced pressure, and γ-irradiating at a pressure of 10^{-6} torr.

(b) *Irradiation procedure*

The samples were irradiated up to doses of about 15 Mrad, using a ^{60}Co γ-source having a maximum dose-rate of 1·75 Mrad/h. Irradiations were performed in a vessel evacuated to a pressure of 10^{-3} torr, the sample being positioned between a massive copper sample-holder and a lighter clamping plate. The sample-holder and clamping plate were cooled to about 77°K by pouring liquid nitrogen into a thin-walled stainless steel tube brased into a recess machined on the top of the sample-holder.

Spectral measurements

The absorption spectra measurements were carried out on the samples in position in the irradiation vessel, using a Unicam SP800 spectrophotometer, into which the irradiation vessel could be fitted and accurately positioned.

Table 1

Group No.	*Sample No.*	*Initiator in monomer, per cent w/w*	*Chain-transfer agent in monomer, per cent w/w*	*Polymerization temperature, °C*
1	1	0·01 azo-bis butyronitrile (ADIB)	—	120
	2	0·04 ADIB	—	110
	3	0·05 ADIB	—	70
	4	0·05 ADIB	0·1 Lauryl mercaptan (LM)	70
	5	0·05 ADIB	0·25 LM	70
	6	0·05 ADIB	0·45 LM	70
	7	0·05 ADIB	0·70 LM	70
	8	0·05 ADIB	1·1 LM	70
	9	0·2 ADIB	0·2 LM	80
2	10	0·5 Lauryl peroxide (LP)	0·2 LM	80
	11	0·5 LP	0·5 Tertiary dodecyl mercaptan	80
	12	0·5 LP	0·15 Primary octyl mercaptan	80
3	13	0·5 Benzoyl peroxide (BP)	—	100
	14	1·0 BP	—	100
4	15	Gamma-radiation polymerized (see text)		

Thus only a few minutes elapsed between the removal of a sample from the radiation source and the determination of its absorption spectrum. As it was not possible to place an identical radiation vessel in the reference beam of the spectrophotometer, the irradiated samples were measured against air and the absorption changes following radiation calculated by reference to the zero dose spectrum.

RESULTS

Details of the fifteen materials on which measurements were made are given in *Table 1*. The quoted concentrations of initiator and chain-transfer agent are those added (by weight) to the monomer before polymerization, and therefore do not necessarily accurately represent the concentrations of these materials in the irradiated samples.

Figures 1(a) to *4*(a) show, respectively, typical absorption spectra for one material from each of the four groups in *Table 1*, at zero, intermediate, and total accumulated doses absorbed at RT. The zero dose plot is that with the lowest absorbance values, and the difference spectrum at total dose is shown for each sample as a broken curve. In practice, the spectra near the short wavelength cut-off limit were obtained by inserting an $A=1$ absorber in the

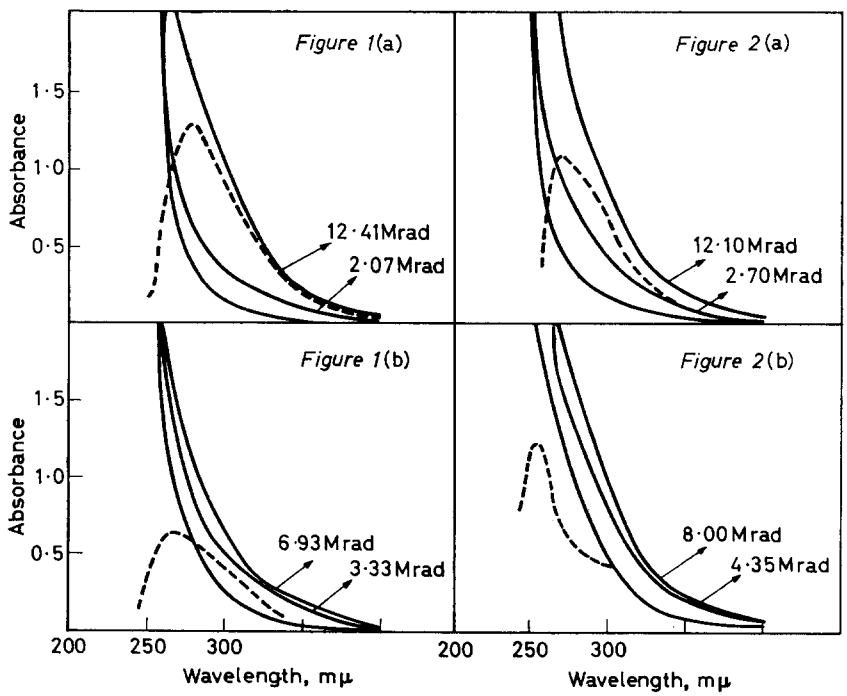

Figures 1(a) and *2*(a)—Typical absorption spectra, groups 1 and 2, at zero, intermediate, and total doses, absorbed at RT. The difference spectrum at total dose is shown as the broken curve

Figures 1(b) and *2*(b)—As for *Figures 1*(a) and *2*(a), doses absorbed at LNT

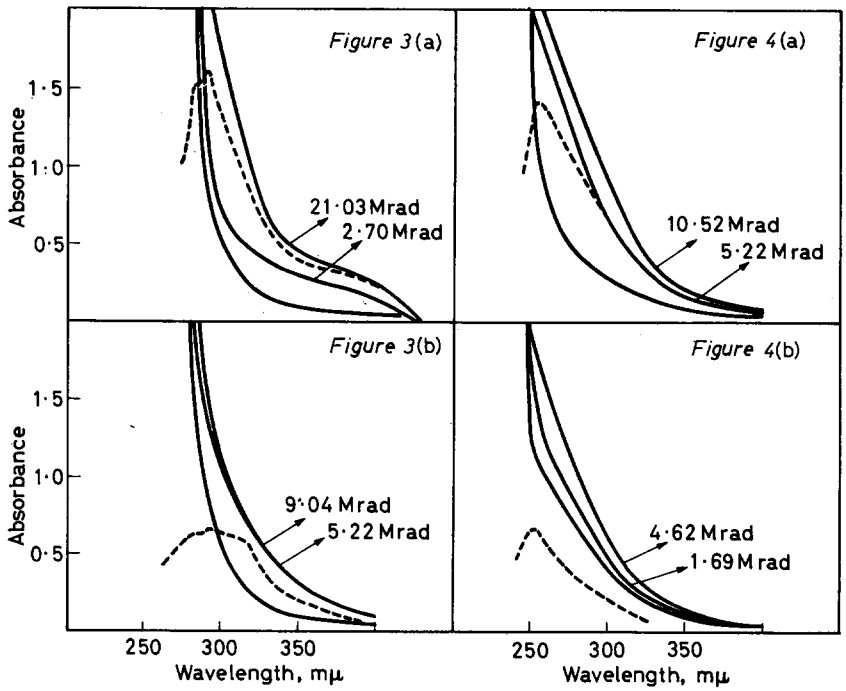

Figures 3(a) and *4*(a)—As for *Figures 1*(a) and *2*(a), groups 3 and 4
Figures 3(b) and *4*(b)—As for *Figures 1*(a) and *2*(a), groups 3 and 4, doses absorbed at LNT

reference beam, and re-plotting from $A = 1$ until the light transmitted through the sample was indistinguishable from the scattered light background. This lower wavelength limit occurred at about 245 mμ for all samples except those containing benzoyl peroxide additive, for which the corresponding value was 275 mμ. Conventionally, the absorbance A is defined by

$$A = \log (I_0/I)$$

where I_0 is the intensity of the incident light and I is the intensity of the transmitted light.

In *Tables 2*(a) to *5*(a), detailed information on the absorbance increase ΔA observed at peak wavelengths at total dose, and decay of these radiation-induced absorption peaks with time, is presented. These data refer to RT irradiation. The absorbance changes have been normalized to a constant sample thickness of 0·5 mm, assuming Lambert's law to be valid for materials produced as described above. Similar data for irradiation near 77°K are shown in *Figures 1* to *4*(b) and *Tables 2* to *5*(b). When sufficient dose had been absorbed at LNT the samples were allowed to warm up to RT, usually overnight, *in vacuo*. The rate of decay of the radiation-induced absorption was subsequently investigated by recording the decayed spectra at RT and at LNT. By recording at both temperatures, additional information on the temperature stability and nature of the absorbing species was

Table 2(a)

Sample No.	*Total dose (Mrad)*	*Peak wavelength (mμ)* — *Absorbance increase ΔA*	*Decay time (h)*	*Subsequent peak wavelength (mμ)* — *Absorbance increase ΔA*	*Remarks*
1	12·85	278/1·15, 289/1·19	45	280/1·08, 290/1·17	The 280 mμ peak was not observed at doses lower than about 5 Mrad
2	12·41	280/1·29	25	280/1·10	
3	17·06	278/1·30	25	278/1·23	
4	16·30	270/1·61	32	268/1·32	An additional peak around 253 mμ was observed at lower doses
5	12·39	265/1·39	24	265/1·16	As for sample 4, peak wavelength 251 mμ
6	17·31	263/1·63	24	263/0·72	As for sample 4, peak wavelength 253 mμ. A tendency for the main peak wavelength to move towards shorter wavelengths with increasing dose was noticed, e.g. 267/0·50 after 2·88 Mrad
7	12·57	256/1·25	25	255/1·11	
8	12·02	255/1·15	30	255/0·90	An absorption shoulder around 270 mμ was observed at lower doses, e.g. 270/0·38 after 2·50 Mrad
9	12·8	277/1·33	30	278/1·23	

Table 2(b)

Sample No.	*Total dose (Mrad)*	*Peak wavelength (mμ)* — *Absorbance increase ΔA*	*Decay time (h)*	*Subsequent measurement at LNT*	*Subsequent measurement at RT*	*Remarks*
1	6·03	262/0·65	16	280/0·32	280/0·32	
2	6·93	265/0·65	16	280/0·58	280/0·61	
3	9·29	261/0·80	15	280/0·47	277/0·54	An additional shoulder was observed at LNT at 282, 280 and 275 mμ after doses of 2·44, 4·74, and 6·48 Mrad respectively, but was indistinguishable at 9·29 Mrad
4	10·34	257/1·05	16	268/0·76	268/0·76	
5	7·14	251/1·08	16	248/1·00 267/0·67 (Shoulder)	253/0·75 267/0·65	An additional shoulder was observed as follows: 268/0·34 after 3·22 Mrad, 278/0·55 after 5·40 Mrad. This shoulder vanished at higher doses

Table 2(b)—continued

Sample No.	*Total dose (Mrad)*	*Peak wavelength (mμ) / Absorbance increase ΔA*	*Decay time (h)*	*Subsequent measurement at LNT*	*Subsequent measurement at RT*	*Remarks*
6	8·68	251/1·35	22	251/0·90	251/1·02	A plateau in the spectrum was observed at LNT as follows: (290-274)/0·45 after 2·00 Mrad; (290-270)/0·86 after 4·09 Mrad; (282-270)/1·07 after 6·16 Mrad; (282-274)/1·39 after 8·68 Mrad. This plateau disappeared on warming to RT
7	9·43	252/1·18	24	251/1·07	250/1·20	A subsidiary peak was noted as follows: 286/0·36 after 2·38 Mrad; 282/0·56 after 4·29 Mrad. This peak then flattened out to a plateau: (282-267)/0·65 after 6·40 Mrad; (282-274)/0·72 after 9·43 Mrad and disappeared on warming to RT
8	9·32	253/1·42	17	255/1·00	252/1·11	A plateau similar to that recorded in sample 7 was observed: (290-274)/0·37 after 2·32 Mrad; (290 - 274)/0·70 after 4·76 Mrad. At higher doses a point of inflection was noted moving towards shorter wavelengths as the dose increased
9	8·19	268/0·75	15	280/0·44	279/0·41	

Table 3(a)

Sample No.	*Total dose (Mrad)*	*Peak wavelength (mμ) / Absorbance increase ΔA*	*Decay time (h)*	*Subsequent peak wavelength (mμ) / Absorbance increase ΔA*	*Remarks*
10	12·5	275/1·52	25	275/1·41	
11	12·1	267/1·08	51	264/0·97	
12	12·0	273/1·25	27	275/0·65	The peak wavelength moved towards longer wavelengths as the dose increased, e.g. 269/0·77 after 5·1 Mrad

Table 4(a) [Columns as in *Table 3*(a)]

13	21·03	281/1·49 290/1·60	26	280/1·33 (Shoulder) 289/1·44	An additional peak was resolved around 281 mμ at lower doses, but was indistinguishable above about 12 Mrad, e.g. 281/0·64 after 11·25 Mrad and of much the same strength as the main peak at lower doses
14	19·81	290/1·62	27	289/1·45	

Table 5(a) [Columns as in *Table 3*(a)]

15	10·52	254/1·41	24	253/1·32	

Table 3(b)

Sample No.	*Total dose (Mrad)*	*Peak wavelength (mμ) / Absorbance increase ΔA*	*Decay time (h)*	*Subsequent measurement at LNT*	*Subsequent measurement at RT*	*Remarks*
10	9·00	265/0·93	16	269/0·59	270/0·56	The peak wavelength shifted to higher wavelengths as the dose increased, e.g. 257/0·31 after 1·74 Mrad 263/0·78 after 6·96 Mrad
11	8·00	252/1·23	16	251/1·05	251/1·03	
12	8·91	256/1·08	15	267/0·66 275/0·62	267/0·65 (250/0·63??)	

Table 4(b) [Columns as in *Table 3*(b)]

13	9·04	282/0·63 (Shoulder) 292/0·65 316/0·58 (Shoulder)	18	280/0·48 (Shoulder) 289/0·50	279/0·41 288/0·44
14	9·55	283/0·60 295/0·59 (Shoulder) 312/0·60	70	284/0·45 295/0·42	284/0·50 292/0·51

Table 5(b) [Columns as in *Table 3*(b)]

15	4·62	252/0·67	17	250/0·56 270/0·52 (Shoulder)	252/0·66 270/0·54 (Shoulder)

Table 6

Sample No.	*Time elapsed since cessation of dose (days)*	*Peak wavelength (mμ) / Absorbance increase ΔA*
1	54	280/0·73
		285/0·76
4	91	253/0·67
6	98	254/1·12
9	114	279/0·40
11	119	255/0·77
12	118	257/0·62
13	115	280/0·64
		288/0·76
15	87	253/1·33

obtained. Finally, it was thought advisable to measure the decay of the enhanced absorption of a few RT irradiated samples some considerable time after cessation of the dose. These results are presented in *Table 6*.

DISCUSSION

A common characteristic of all the un-irradiated samples, including those polymerized by radiation, is seen to be a marked increase in absorption at wavelengths below about 300 mμ. Although the increase is greater in materials containing BP, it is doubtful if it can be attributed entirely to the presence of BP initiator, as stated by Orton[7]. A more probable explanation is that the increase consists of the long wavelength side of the C=O group absorption profile [which vacuum u.v. studies (FYDELOR, P. J. Unpublished work) on thin films of PMMA have shown to peak at around 213 mμ] on which is superimposed the absorption of any additive present. Admittedly the relative contribution of BP to the total absorption is considerably greater than that of the other additives present in the samples now under consideration. On irradiation, an overall increase in absorption (due to the production of species whose absorption profiles partly overlap that of the C=O group) is observed, moving the u.v. cut-off to longer wavelengths.

RT irradiation

Group 1—A marked dependence of spectral changes following irradiation on both initiator and chain-transfer agent will be seen in *Tables 2*(a) to *5*(a). The azo-bis-butyronitrile (ADIB) initiator molecules are probably the origin of a radiation-induced, fairly stable absorption centred around 280 mμ in samples 1–3, as no corresponding absorption was observed in radiation-polymerized PMMA containing no additives. The addition of increasing amounts of lauryl mercaptan (LM) to a constant concentration of ADIB in the monomer before polymerization causes a steady movement of the peak absorption wavelength towards lower values, as shown by samples 4–8. On comparison of the results for samples 8 and 9, corresponding to a marked increase in ADIB and a marked decrease in LM concentrations, one finds a reversion of the peak absorption wavelength to a value very close to the original 280 mμ observed in samples 1–3. If the formation of an ADIB–LM

complex is ruled out, the above result suggests a two-part absorption, of which one component due to ADIB is centred around 280 mμ, and the other, due to LM, around 255 mμ. Although one might, in that case, reasonably expect to find a two-peak spectrum following irradiation, the uncertainty in the final concentrations of ADIB and LM in the polymer (which are almost certainly not the same as those added to the monomer) precludes a reliable mathematical analysis as a means of reaching a firm decision on this point. However, the references to absorptions around 255 mμ noted in the remarks column for some Group 1 samples at lower doses tend to support this analysis. The decay data for these samples suggest that the ADIB and LM species decay at similar rates. An alternative explanation of the absorption peaks at 280 (and 290) mμ proposed by Orton[7] is that they originate on methylmethacrylate monomer residue in the polymer. Although the same peak wavelengths (within experimental error) were observed in BP initiated samples (see Group 3), this explanation is rejected because a different peak wavelength was observed in radiation polymerized PMMA, which one would expect to contain a small concentration of monomer residue, and also because the wavelength reversion discussed above is considered as irrefutable evidence in favour of the first explanation. Further, if the MMA residue explanation was correct, one might reasonably expect to observe similar behaviour in Groups 1 and 3 following irradiation at LNT. This was not so, as is discussed below.

Group 2—The results for samples 10–12 again show that both initiator and chain-transfer agent content influence the peak absorption wavelengths, probably involving the same mechanisms as discussed for Group 1. Evidence in support of this suggestion is the correlation between mercaptan chain-transfer agent concentration and movement of the peak absorption wavelengths towards lower values; in general, the greater the mercaptan concentration, the further does the peak wavelength move downwards. Admittedly, the peak wavelength order for samples 10 and 12 is opposed to this generalization, but as the determination of the peak is subject to an error of at least ±1 mμ, the discrepancy is not considered serious in view of the relatively small difference in the probable mercaptan concentrations in these two samples.

Group 3—Absorption peaks around 290 mμ appear in both samples of this group, and an additional peak at 280 mμ in sample 13 only. As discussed under the Group 1 heading, these peaks could be assigned to species originating in MMA monomer residue, but this assignment is rejected in favour of a BP source for the reasons already presented. Hence the present results are in some disagreement with those of Orton[7] who calculated absorption peaks at 300, 315 and 360 mμ for BP-initiated PMMA samples of twice the thickness irradiated at RT. There is, however, some evidence in the present work for the production of an unstable peak at 315 mμ following irradiation at LNT (see later discussion); it may be that the thickness of the present samples was not sufficient to show up a peak at 360 mμ.

Group 4—A single absorption centred around 254 mμ was observed in sample 15, rather stronger than those noted at other wavelengths in the three preceding groups. In anticipation of a tentative identification of a majority of the absorbing species produced by irradiation of PMMA both at RT and LNT as ions (to be proposed below), this peak is assigned to the carbanion —$\ddot{C}$HCH=CH—. Bodily and Dole[8] expect this group to show a maximum absorption around 251 mμ, and if it is in fact present in the radiation polymerized PMMA, it probably originates in monomer residue.

To obtain further evidence on the nature of the absorbing species, in particular to eliminate the possibility of identifying them as radicals, further irradiations of one sample from each group were carried out at RT in air. The same peak wavelengths (within experimental error) occurred, and the absorbance values were similar to those obtained by irradiating *in vacuo*. The data presented in *Table 6*, showing the absorption values for samples irradiated *in vacuo*, and subsequently allowed to stand in air for periods of about three months, provide further evidence that the absorbing species are not radicals. It would be expected that the diffusion of oxygen into PMMA samples some 0·5 mm thick would be sufficiently fast[9] either to prevent the formation of radicals in any detectable concentration in samples irradiated in air, or completely to scavenge, within a few hours, radicals formed in samples irradiated *in vacuo*. Finally this conclusion was confirmed by the absence of e.s.r. signals from the samples listed in *Table 6*. This absence does not necessarily conflict with the above identification of a carbanion formed on monomer residue, as, if the two spins are correctly paired, then the species would not undergo resonance.

It is tentatively postulated that the species giving rise to the other observed absorptions are of an ionic nature, because it is generally accepted that the reaction rate of oxygen with ions in amorphous solids such as we are presently concerned with is not very great. Reasoning along the same lines a more precise identification could probably be made of the species as cations.

LNT irradiation

Group 1—Samples 1–3 exhibit absorptions of roughly equal magnitude (allowing for the larger dose given to sample 3) at much the same peak wavelengths. On warming the sample to RT and standing overnight the peak wavelengths all move to 280 mμ, although the rate of fall-off in absorbance is unexpectedly less for sample 2 than for samples 1 and 3. It is interesting to note that this is the peak wavelength obtained for RT irradiation. Two explanations of this result can be proposed. The first explanation is that the same absorbing species is formed independently of whether the samples are irradiated at RT or LNT, and the wavelength shift is merely a temperature effect; the second is that different species are formed depending on the temperature of irradiation, and, on warming to RT, the species formed on irradiation at LNT is converted into that formed on irradiation at RT.

The first explanation was ruled out by irradiating a test sample at RT, cooling to LNT, and noting that the lower peak wavelength did not appear.

Samples 4–9 show interesting behaviour on comparison with the RT results for the same materials. The presence of LM as chain-transfer agent again moves the peak wavelengths towards lower values, but the lower limit around 253 mμ (cf. 255 mμ for RT irradiation) is reached at much lower LM concentrations. Note also the wavelength stability of the peaks produced in samples 5–8 on warming to RT, and the movement of the peak in sample 9 in the same direction and to the same value as that observed for samples 1–3. It is clear that the relative concentrations of ADIB and LM have the same significance in both LNT and RT irradiations. Presumably the same absorbing species is produced in LM independently of whether it is irradiated at LNT or RT, and hence its peak wavelength is relatively temperature-independent. It is necessary to postulate at LNT an enhanced absorbance of the LM species compared with the ADIB species so as to account for the attainment of a peak short wavelength limit at lower LM concentration. The similarity of this limit (252 mμ) and the peak wavelength observed in radiation polymerized PMMA irradiated at either LNT or RT is considered fortuitous, in view of the considerable strength of the absorbance found in that material and the careful purification of the monomer before polymerization.

Group 2—The relative wavelength stability observed in samples 10–12 with respect to warming to RT is seen to be closely related to the concentration of mercaptan compounds present as chain-transfer agents, as has already been noted in Group 1. This correlation depends of course on the assumption that increasing mercaptan concentration in the monomer before polymerization is maintained in the polymer. Note also the attainment of the same short peak wavelength limit (252 mμ) as observed in Group 1 for sample 11 of this group. It is significant that, in the light of the assumption just mentioned, sample 11 contains the highest concentration of mercaptan chain-transfer agent. No explanation is offered for the appearance of an absorbance peak at 250 mμ in sample 12 when observed at RT some 15 hours after cessation of dose at LNT.

Group 3—Peak or 'shoulder' absorptions occurring at about 280 and 290 mμ observed in samples 13 and 14 are fairly stable with respect to warming to RT, and are almost certainly identical with those observed at RT. An additional shoulder around 316 mμ on the absorption profile, which disappears on warming to RT can probably be identified with the peak absorption noted by Orton[7] after irradiating BP initiated PMMA at RT. The results obtained from sample 14, while showing behaviour that is, in general, similar to that of sample 13, differ surprisingly in respect of change in absorbance when the spectrum is traced at LNT and then at RT. For both peaks sample 13 shows a decrease, sample 14 an increase. However, it may be concluded that stable absorption species (probably only one) having peak wavelengths at 280 and 290 mμ are produced in BP initiated PMMA when γ-irradiated either at LNT or RT. An additional species, absorbing maximally around 316 mμ, which is destroyed on warming to RT is produced following irradiation at LNT.

It should be noted that in the present work the overall absorption of the BP initiated materials following irradiation was much greater than that of

the other samples on which measurements were made, the short wavelength limit of the spectra being about 275 mμ. This applied also to RT irradiation. Hence it was not possible to investigate the possible existence in these two samples of the absorption having a peak wavelength around 250 mμ noted in some of the other materials.

Group 4—The same peak wavelength as observed for RT irradiation was found in sample 15, and was stable with respect to warming to RT.

CONCLUSIONS

The increased u.v. absorption of PMMA following γ-irradiation is closely dependent on the nature and concentration of initiator and chain-transfer agent additives included in the monomer before polymerization. For radiation polymerized PMMA, it is likely that the increased absorption originates in monomer residue in the polymer. This absorption may also be present in PMMA samples, which contain initiator and chain-transfer agent additives, but is probably masked by other absorptions due to these additives.

The absorbing species are almost certainly not radicals; in materials polymerized with the help of additives they are probably cations. In radiation polymerized PMMA the absorbing species could be carbanions —$\ddot{\text{C}}$HCH=CH— formed on monomer residue following irradiation. The peak wavelengths associated with the proposed cation absorbing species are approximately 252 and 255 mμ at LNT and RT respectively for the mercaptan compounds, 280 and 290 mμ for those originating in BP, and 252 mμ for the carbanion, independent of temperature in the latter two cases. For PMMA samples containing only ADIB additive, the peak wavelengths are 280 mμ at RT, and 262 mμ at LNT.

The author thanks Professor A. Charlesby and Mr P. J. Fydelor of Physics Department, Royal Military College of Science, for suggesting that this work be undertaken, and for much advice and encouragement during its progress. He also thanks M. King and Miss S. Moore for experimental assistance.

Physics Department,
Royal Military College of Science,
Shrivenham, Swindon, Wilts.

(Received October 1967)

REFERENCES

[1] BOAG, J. W., DOLPHIN, G. W. and ROTBLAT, J. *Radiat. Res.* 1958, **9**, 589
[2] BROWNELL, G. L., STRATTON, K. and PINTER, J. L. *Physics Med. Biol.* 1963, **8**, 265
[3] ORTON, C. G. *Ph.D. Thesis.* University of London, 1965
[4] KINELL, P. O. *Ark. Kemi*, 1959, **14**, 353
[5] GOODEVE, J. W. *Trans. Faraday Soc.* 1938, **34**, 1239
[6] MELVILLE, H. W. *Proc. Roy. Soc. A*, 1937, **163**, 511
[7] ORTON, C. G. *Physics Med. Biol.* 1966, **11**, 377
[8] BODILY, D. M. and DOLE, M. *J. chem. Phys.* 1966, **45**, 1428
[9] MICHEL, R. E., CHAPMAN, F. W. and MAO, T. J. *J. chem. Phys.* 1966, **45**, 4604

Thermodynamics of Polymerization of Heterocyclic Compounds II— The Heat Capacity, Entropy, Enthalpy and Free Energy of Polytetrahydrofuran

G. A. CLEGG, D. R. GEE, T. P. MELIA and A. TYSON

An adiabatic, vacuum calorimeter and a differential scanning calorimeter have been used to measure the heat capacity of a 69 per cent crystalline sample of polytetrahydrofuran from 80° to 360°K. An estimate has been made of heat capacity values below 80°K. Entropy, enthalpy and free energy values have been derived and are listed at 10 deg. intervals for the 69 per cent crystalline polymer. The glass transition temperature, melting point and heat of fusion were found to be 185°, 314° ± 1°K, and 2·959 ± 0·016 kcal. mole^{-1}. The temperature dependence of the excess entropy of amorphous polytetrahydrofuran, relative to the 100 per cent crystalline sample, has been calculated and is shown to be in good agreement with theoretical predictions. The increase in heat capacity of the amorphous polymer at the glass transition temperature, 2·7 cal. deg^{-1} mole bead^{-1}, is in agreement with that expected on the basis of the hole theory of melting. The entropy of polymerization, ΔS_{1c}, has been calculated as $-14{\cdot}8 \pm 1{\cdot}0$ cal. deg^{-1} mole^{-1}, whereas that obtained from equilibrium polymerization data is $-9{\cdot}8 \pm 2{\cdot}0$ cal. deg^{-1} mole^{-1}. Evidence in favour of the former value is presented. A value of $-5{\cdot}3 \pm 0{\cdot}4$ kcal. mole^{-1} has been derived for ΔH_{1c}.

AS PART of a general study of the thermodynamics of polymerization of heterocyclic compounds the heat capacities of various monomers[1] and polymers have been measured over the temperature range 80° to 310°K. Heat capacities below 80°K can be evaluated using the Kelley, Parks and Huffmann extrapolation procedure[2] and this enables an estimate to be made of the Third Law entropy.

The material studied in this work, polytetrahydrofuran, is a 69 per cent crystalline polymer of narrow molecular weight distribution[3,4].

Recently Ivin and Leonard[5] have used equilibrium data for the polymerization of liquid tetrahydrofuran to amorphous polymer to calculate the entropy of polymerization, ΔS_{1c}. Since the entropy of liquid tetrahydrofuran is readily calculable from previously published data[6,7] the results obtained in this work enable a comparison to be made between the Second and Third Law values of ΔS_{1c}.

EXPERIMENTAL

Preparation[3,4] and properties of polytetrahydrofuran

Laboratory chemical grade tetrahydrofuran (ex May and Baker) was dried over calcium hydride, refluxed with sodium wire and finally distilled from sodium wire under dry nitrogen. 3 g of antimony pentachloride was added to 72 g of the purified tetrahydrofuran under dry nitrogen and the

mixture left at 0°C for 48 hours. The sticky product was dissolved in benzene and the polymer precipitated by pouring this solution into a rapidly stirred methanol–water mixture (three parts methanol to one part water). The supernatant liquor was removed by decantation and the product dried *in vacuo* at room temperature. The dry polymer was redissolved in benzene and sufficient methanol added to precipitate 30 g of polymer. The supernatant liquor was again removed by decantation and the polymer dried *in vacuo* at 40°C. The polymer melt was allowed to solidify over a period of two days.

Dilatometric measurements on this material gave a melting point of 315°K and a specific volume of 0·9493 $cm^3\ g^{-1}$. A crystallinity of 69 per cent was estimated from the specific volume using the values 1·0191 (this work) and 0·9174 $cm^3\ g^{-1}$ for the specific volume of amorphous and 100 per cent crystalline[8] polytetrahydrofuran, respectively. The volume coefficient of expansion of the amorphous polymer at 25°C is $6{\cdot}94 \times 10^{-4}\ cm^3\ g^{-1}\ °K^{-1}$. Gel permeation chromatography analysis on the sample by Dr F. W. Peaker of the University of Birmingham yielded the values $\overline{M}_w = 17\,200$ and $\overline{M}_n = 12\,200$. There was no evidence for either a low or high molecular weight tail.

Calorimetry

Two calorimeters were employed. A precision, adiabatic, vacuum calorimeter, which has been described previously[9], and a Perkin–Elmer differential scanning calorimeter[10].

Heat capacity measurements

The weight of sample used in the heat capacity measurements carried out in the precision, adiabatic, vacuum calorimeter was 21·746 g. Before sealing the calorimeter the sample was degassed for 24 hours to remove air and moisture. A small quantity of helium gas, sufficient to give a pressure of 500 mm Hg at room temperature, was sealed in the calorimeter and served to accelerate thermal equilibrium during the experiments. Heat capacity measurements were made over the range 80° to 330°K, temperature increments being varied from 1 deg. to 15 deg. K.

The differential scanning calorimeter was calibrated over the temperature range 180° to 360°K with Al_2O_3. The method described by Wunderlich[11] was employed. Two weights, 33·50 and 131·40 mg of Al_2O_3, were used. Using Ginnings and Furukawa's[12] values on the heat capacity of Al_2O_3, which are believed to be accurate to ±0·2 per cent, a calibration curve was established. The calibration was checked using the standard N.B.S. broad molecular weight distribution, atactic polystyrene (N.B.S. No. 706) for which precise heat capacity data are available[13]. The overall precision of the measurements is better than ±2 per cent. The weights of polystyrene and polytetrahydrofuran used varied between 25 and 35 mg. Heating rates of 8 deg. per minute were employed.

Reliability of the heat capacity measurements

The reliability of the heat capacity measurements with polymers such

as the polytetrahydrofuran sample used in this work is difficult to evaluate because of the non-reproducibility of the physical state from experiment to experiment. The heat capacity measurements made previously in the adiabatic, vacuum calorimeter with normal materials[9] are believed to be accurate to $\pm 0{\cdot}2$ per cent. Because temperature drifts were observed over most of the temperature range the heat capacity values obtained show some scatter (especially in the glass transition and melting regions) since they are dependent upon how long temperature equilibrium is awaited and the thermal treatment to which the sample was subjected. In the regions where temperature drifts occurred the procedure adopted was to follow the drifts until they were less than 10^{-3} deg. K min^{-1}. In the glass transition (170° to 210°K) and melting (280° to 315°K) regions much larger drifts, of the order of 5×10^{-3} deg. K min^{-1}, were tolerated. It is emphasized that any decision on how long the temperature drifts are followed is of necessity arbitrary since the experience of other workers[14] has shown they may persist for days and even months, especially in the region of the glass transition temperature. However, Dainton *et al.* in their studies of hydrocarbon polymers[15] and Beaumont *et al.*[16] in their studies of oxygen-containing polymers have argued that the virtual neglect of drifts does not influence the broad conclusions.

Heat of fusion measurements

The heat of fusion measurements were carried out in both the adiabatic, vacuum calorimeter and the differential scanning calorimeter.

In the determinations carried out in the adiabatic, vacuum calorimeter the energy required to heat the calorimeter and its contents from a temperature below the melting point to a temperature above it was measured. The initial temperature was chosen so as to be below the pre-melting region of the polytetrahydrofuran sample. The heat of fusion was then obtained by substitution of the measured quantities in the equation

$$\Delta H^*_f = \Delta Q_1 - \Delta Q_2 - \Delta Q_3 \qquad (1)$$

where ΔH^*_f is the heat of fusion of the mass of sample contained in the calorimeter, ΔQ_1 is the total energy supplied to the calorimeter during the experiment, ΔQ_2 is the energy required to heat the calorimeter and its solid contents from the initial temperature to the melting point, and ΔQ_3 is the energy required to heat the calorimeter plus its liquid contents from the melting point to the final temperature. In computing ΔQ_2 the heat capacity data for the calorimeter plus solid contents were extrapolated from below the pre-melting region to the melting point. In this way the heat of premelting is included in the value obtained for the heat of fusion and errors due to premelting are avoided.

In determinations carried out in the differential scanning calorimeter sample weights of 3 to 6 mg were used and scanning rates of 2 deg. and 8 deg. K min^{-1} were employed. Calibration of the power input into the sample was performed by measurements of the heat of fusion of indium, benzene and benzoic acid. The literature values of the heat of fusion of these substances are respectively $6{\cdot}8$[17], $30{\cdot}2$[18] and $35{\cdot}2$[19] cal.g^{-1}. The overall precision of the measurements was again found to be better than ± 2 per cent.

RESULTS

The observed values of the heat capacity are plotted against temperature in *Figures 1* and *2*. Graphically smoothed values of the heat capacity together with derived values of entropy, enthalpy and free energy are shown in *Table 1*. The heat capacity data below 80°K were obtained using the Kelley, Parks and Huffmann extrapolation procedure[2]. Polyoxymethylene, for

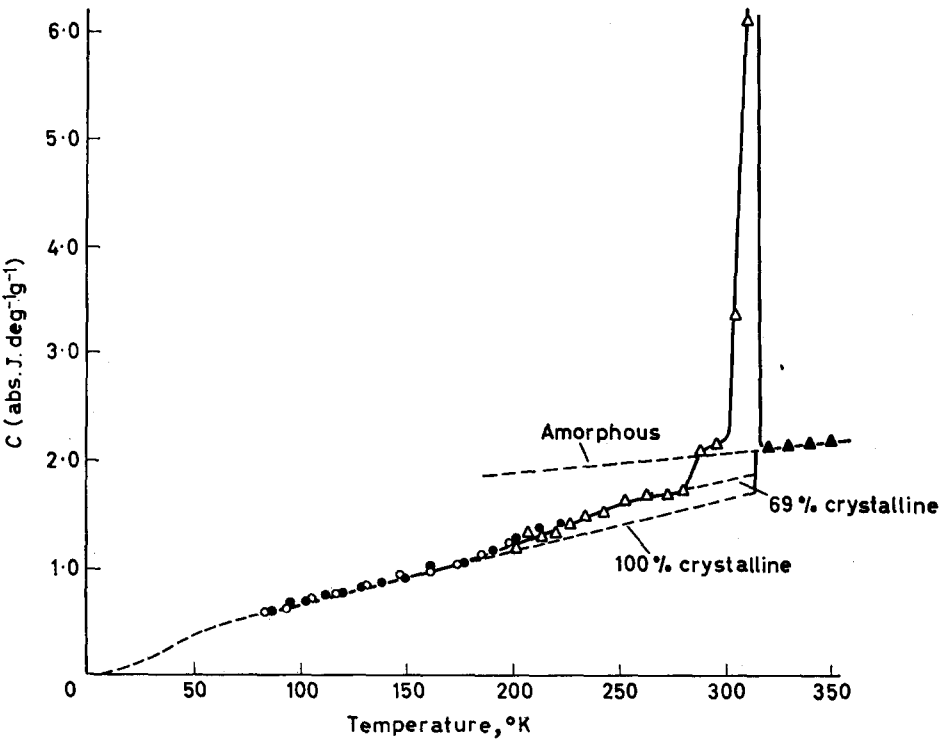

Figure 1—Observed heat capacities of 69 per cent crystalline polytetrahydrofuran, ○ run 1, △ run 2, ● run 8, ▲ run 10

which heat capacity data are available[15] down to 20°K, was chosen as the standard substance for this extrapolation. In the range 180° to 260°K the heat capacity data of run 2 were smoothed. The smoothed heat capacity values of polytetrahydrofuran between 260° and 314°K were obtained by a linear extrapolation of the heat capacity versus temperature plot. The broken lines in *Figure 1* represent extrapolated heat capacity values for the sample under investigation and estimated values for the amorphous and 100 per cent crystalline forms, respectively.

Inspection of *Figures 1* and *2* reveals the occurrence of two transitions in polytetrahydrofuran. The first, which can be recognized by the change in slope of the heat capacity versus temperature curve at about 185°K, probably corresponds to the glass transition for this material. The second, which occurs at 315° ±1°K, is the melting transition.

Table 1. Smoothed values of the heat capacity, entropy, enthalpy and free energy for polytetrahydrofuran (69% crystalline)

Temperature (°K)	C (*abs. J. deg*$^{-1}$ *g*$^{-1}$)	$S_T^0 - S_0^0$ (*abs. J. deg*$^{-1}$ *g*$^{-1}$)	$H_T^0 - H_0^0$ (*abs. J. g*$^{-1}$)	$-(G_T^0 - G_0^0)$ (*abs. J. g*$^{-1}$)
0	0	0	0	0
20	0·079	0·028	0·41	0·15
40	0·270	0·144	3·97	1·77
60	0·425	0·283	10·97	6·03
80	0·551	0·424	20·77	13·11
90	0·611	0·492	26·60	17·69
100	0·670	0·559	33·00	22·94
110	0·721	0·626	39·96	28·86
120	0·774	0·691	47·43	35·44
130	0·828	0·755	55·44	42·66
140	0·876	0·818	63·97	50·52
150	0·920	0·880	72·95	59·00
160	0·965	0·940	82·38	68·09
170	1·011	1·000	92·27	77·79
180	1·080	1·060	102·7	88·08
190	1·165	1·121	114·0	98·99
200	1·228	1·182	125·9	110·5
210	1·290	1·243	138·5	122·6
220	1·363	1·305	151·8	135·3
230	1·437	1·367	165·8	148·7
240	1·512	1·430	180·5	162·7
250	1·589	1·494	196·1	177·3
260	1·647	1·557	212·3	192·5
	EXTRAPOLATED DATA FOR THE SOLID			
270	1·709	1·620	229·1	208·3
273·16	1·721	1·639	234·2	213·5
280	1·725	1·682	246·3	224·7
290	1·778	1·743	263·8	241·7
298·16	1·797	1·792	278·4	255·9
300	1·815	1·804	281·7	259·5
310	1·868	1·864	300·1	277·7
314	1·888	1·888	307·6	285·2
		LIQUID		
314	2·107	2·266	426·1	285·4
320	2·118	2·306	438·8	299·1
330	2·137	2·371	460·1	322·3
340	2·156	2·435	481·6	346·6
350	2·175	2·498	503·3	371·0
360	2·194	2·560	525·1	396·5

Values of the calorimetric heat of fusion of polytetrahydrofuran obtained from adiabatic and differential scanning calorimetry are shown in *Table 2.*

DISCUSSION

Inspection of *Figures 1* and *2* reveals the pronounced dependence of the heat capacity (and hence the related thermodynamic functions entropy, enthalpy and free energy) on the thermal history and crystallinity of the polymer specimen employed in the investigation. Thus, values quoted for the thermodynamic functions refer to a particular polymer sample subjected

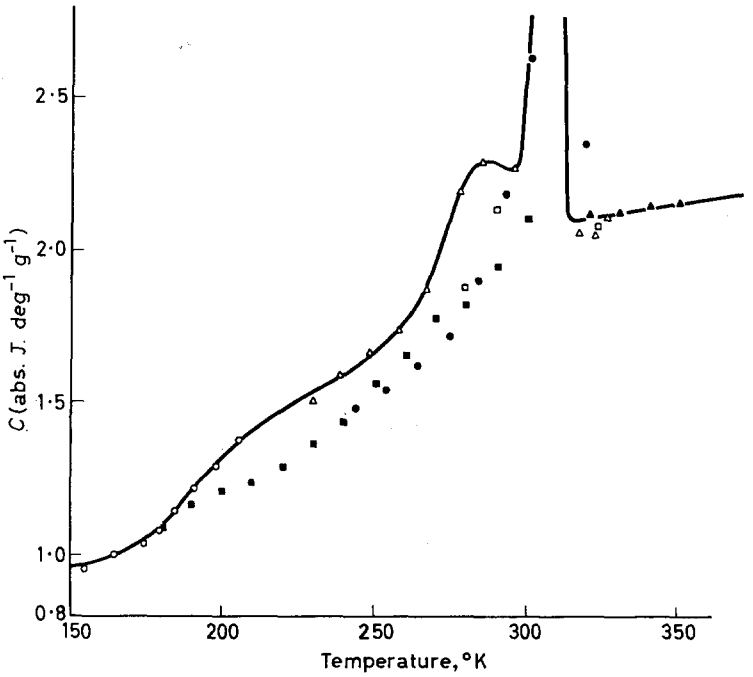

Figure 2—Observed heat capacities of semi-crystalline polytetrahydrofuran in the glass transition and melting regions showing the dependence of heat capacity on the thermal history of the sample. □ run 3, ○ run 4, △ run 5, ● run 6, ■ run 9, ▲ run 10

to a particular thermal treatment. This is an intolerable situation and an attempt has been made to overcome it as follows. In most cases an accurate representation of the heat capacity of a completely amorphous polymer (C_a) above the glass transition temperature can be obtained by a linear extrapolation of heat capacity data for the liquid polymer[20]. Similarly, an accurate representation of the heat capacity of a 100 per cent crystalline polymer (C_c) between the glass transition and melting temperatures can be

Table 2. Values of ΔH_f^* and V_c for polytetrahydrofuran samples subjected to different thermal treatments

Run No.	ΔH_f^* (*abs. J. g*$^{-1}$)	V_c
3	112·4±0·4	0·655
5	98·9±0·4	0·576
6	118·5±0·5	0·690‡
7	119·1±0·5	0·694
11	118·9±2·0	0·692
12	117·1±2·0	0·682
13	65·1±1·3	0·379

‡ Obtained from volume dilatometric measurements.

obtained by a linear extrapolation of heat capacity data for the solid polymer below the glass transition temperature[20]. The relevant equations for polytetrahydrofuran are:

$$C_a = 1{\cdot}510 + 1{\cdot}90 \times 10^{-3}\, T \text{ abs. J. deg}^{-1}\text{ g}^{-1} \tag{2}$$

and

$$C_c = 0{\cdot}168 + 4{\cdot}96 \times 10^{-3}\, T \text{ abs. J. deg}^{-1}\text{ g}^{-1} \tag{3}$$

The extrapolated values of the heat capacity for completely amorphous and 100 per cent crystalline polytetrahydrofuran are shown as broken lines in *Figure 1*.

The glass transition (185°K) and melting (314° ± 1°K) temperatures of polytetrahydrofuran observed in this work are consistent with those of 187°K and 315°K[21], respectively, quoted in the literature.

For semi-crystalline polymers, calorimetric measurements do not yield the true heat of fusion, ΔH_f, but only ΔH_f^*, the two quantities being related by the expression[1]

$$\Delta H_f = \Delta H_f^* / V_c \tag{4}$$

where V_c is the volume fraction of crystallinity. In estimating ΔH_f for polytetrahydrofuran the results obtained in run 6 were employed. The reasonable assumption was made that the sample used in run 6 and that on which the volume dilatometric measurements were made, which were subjected to similar thermal treatments, have the same volume fraction of crystallinity, namely 0·69. After making allowance for pre-melting the value obtained for ΔH_f^* is 118·5 ± 0·5 abs. J. g^{-1} The value obtained for ΔH_f is 171·7 ± 0·9 abs. J. g^{-1}. The values obtained for ΔH_f^* in runs 3, 5, 6 (stepwise heating), 7, 11, 12 and 13 (continuous heating), together with the volume fraction of crystallinity of the samples studied, calculated from equation (4), are presented in *Table 2*. Good agreement is observed between the ΔH_f^* values of runs 6, 7, 11 and 12, in which the samples studied were subjected to essentially the same thermal treatment above 300°K. However, the ΔH_f^* values observed in runs 3, 5 and 13, in which the samples underwent different thermal treatments above 300°K, are considerably smaller. This indicates that the thermal history of the polytetrahydrofuran sample above 300°K is critical in relation to the thermodynamic properties.

The excess entropy, ΔS_e, and excess enthalpy, ΔH_e, of a supercooled liquid polymer relative to the 100 per cent crystalline sample may be obtained from the expressions:

$$\Delta S_e = \Delta S_f - \int_T^{T_m} \frac{C_a}{T}\,dT + \int_T^{T_m} \frac{C_c}{T}\,dT \tag{5}$$

and

$$\Delta H_e = \Delta H_f - \int_T^{T_m} C_a\,dT + \int_T^{T_m} C_c\,dT \tag{6}$$

respectively. According to Gibbs and Di Marzio[22] a temperature, T_2, exists below the experimentally observed glass transition temperature at which the supercooled amorphous polymer, if it could be produced, would have

negligibly greater entropy than the crystal. Current approaches to the problem[23,24] suggest values around 50°K and 1·3 for $T_g - T_2$ and T_g/T_2, respectively. This theory can be tested by calculating ΔS_e as a function of temperature. The results of such a calculation for polytetrahydrofuran are presented in *Figure 3*. The values obtained for T_2, $T_g - T_2$ and T_g/T_2, 140°K, 45°K and 1·32, respectively, are in good agreement with theoretical predictions. The value of ΔS_e at the glass transition temperature, 4·1 cal. deg^{-1} mole^{-1}, is consistent with the values found for a variety of glass-forming materials[25].

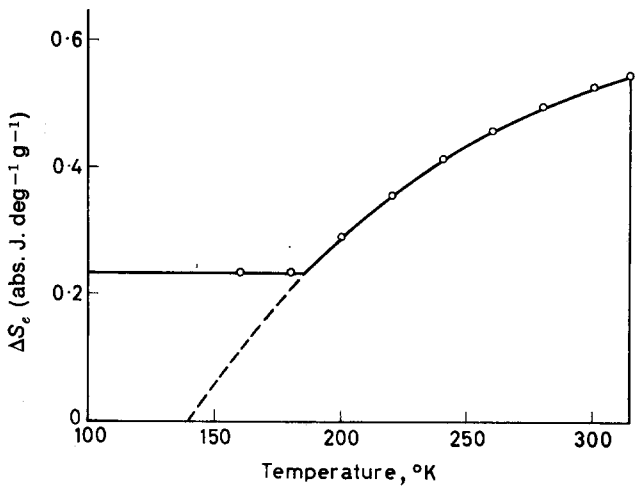

Figure 3—Excess entropy versus temperature plot for amorphous polytetrahydrofuran relative to the 100 per cent crystalline sample

The excess enthalpy versus temperature plot is shown in *Figure 4*. Zero enthalpy difference between the crystal and supercooled liquid polymer occurs at 80°K. Since this temperature is below T_2 it follows that if a supercooled polymer with entropy equal to that of the crystal were obtained the crystal would still represent the more stable phase because of the positive excess enthalpy term.

According to the Hirai-Eyring hole theory of the liquid state[26], at temperatures below the glass transition temperature the hole equilibrium is frozen and the number of holes remains constant as the temperature is lowered. Above the glass transition temperature the number of holes incorporated in the polymer structure increases with temperature and this causes the rise in heat capacity at this point.

Wunderlich[27] has compared the rise in heat capacity for a number of glass-forming substances at the glass transition temperature. For the purpose of this comparison he defined the simplest molecular unit whose movement may change the 'hole equilibrium' as a bead. For polymers a bead is generally regarded as a simple chain unit such as —CH_2— or —O—. Wunderlich found that the rise in heat capacity at the glass transition

temperature was equal to $2{\cdot}7 \pm 0{\cdot}5$ cal. deg^{-1} mole bead^{-1}. This value is in agreement with that of 2·97 cal. deg^{-1} mole bead^{-1} which he calculated from the hole theory. The increase in heat capacity ($C_a - C_c$) at the glass transition temperature for polytetrahydrofuran is 2·7 cal. deg^{-1} mole bead^{-1}, in agreement with the findings of Wunderlich[27].

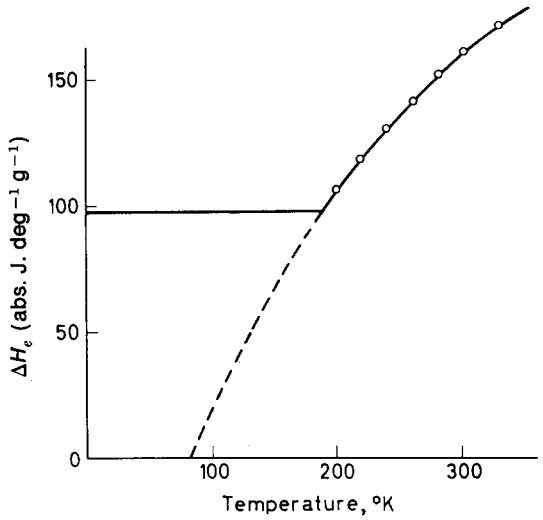

Figure 4—Excess enthalpy versus temperature plot for amorphous polytetrahydrofuran relative to the 100 per cent crystalline sample

The entropy changes associated with the transformation of gaseous (one atmosphere pressure and 298·16°K) and liquid (176 mm Hg pressure and 298·16°K) tetrahydrofuran to crystalline and amorphous polymer, respectively, are presented in *Table 3*. The value used for the entropy of liquid tetrahydrofuran in these calculations was obtained from McCullough's value[6] for the entropy of gaseous tetrahydrofuran and the vapour pressure data of Kobe, Ravica and Vohra[7].

Table 3. Entropies of polymerization of tetrahydrofuran at 298·16°K

State of monomer	*State of polymer*	*Monomer entropy (cal. deg^{-1} mole^{-1})*	*Polymer entropy (cal. deg^{-1} mole^{-1})*	*Entropy of polymerization (cal. deg^{-1} mole^{-1})*
Gas (1 atm)	crystalline	$72{\cdot}1 \pm 0{\cdot}4$	$29{\cdot}8 \pm 0{\cdot}3$	$-42{\cdot}3 \pm 0{\cdot}7$
(1 atm)	amorphous	$72{\cdot}1 \pm 0{\cdot}4$	$38{\cdot}8 \pm 0{\cdot}5$*	$-33{\cdot}3 \pm 0{\cdot}9$
Liquid				
(176 mm Hg)	crystalline	$53{\cdot}6 \pm 0{\cdot}5$	$29{\cdot}8 \pm 0{\cdot}3$	$-23{\cdot}8 \pm 0{\cdot}8$
(176 mm Hg)	amorphous	$53{\cdot}6 \pm 0{\cdot}5$	$38{\cdot}8 \pm 0{\cdot}5$*	$-14{\cdot}8 \pm 1{\cdot}0$

*Corrected for residual entropy effects.

The entropy change, ΔS^0_{gc}, associated with the polymerization of one mole of gaseous tetrahydrofuran at one atmosphere pressure and 298·16°K to crystalline polytetrahydrofuran ($-42{\cdot}3 \pm 0{\cdot}7$ cal. deg^{-1} mole^{-1}) is similar to those found for other related polymers, e.g. polyoxymethylene[15] ($-41{\cdot}4$ cal.

deg^{-1} mole^{-1}); polyethylene oxide[16] ($-41{\cdot}5$ cal. deg^{-1} mole^{-1}); polyethylene[28] ($-41{\cdot}5$ cal. deg^{-1} mole^{-1}).

There is a discrepancy between the value of ΔS_{lc} obtained in this work ($-14{\cdot}8 \pm 1{\cdot}0$ cal. deg^{-1} mole^{-1}) and that obtained by Ivin and Leonard[5] ($-9{\cdot}8 \pm 2{\cdot}0$ cal. deg^{-1} mole^{-1}) from equilibrium polymerization data.

In an attempt to decide which of the two values of ΔS_{lc} is correct a number of semi-empirical methods have been used to estimate this quantity. These are discussed below.

For the replacement of CH_2 by O, Small[29] has compared the entropies of ten ethers, esters, aldehydes and ketones, for which reliable data exist, with those of the parent hydrocarbon. He finds that, in general, the entropy of the parent hydrocarbon exceeds that of the corresponding oxygen-containing compound by approximately 1 cal. deg^{-1} mole^{-1}. If we regard polyethylene as the parent hydrocarbon from which polytetrahydrofuran [repeat unit —$(CH_2)_4$—O—] is derived, and use the value 7·4 cal. deg^{-1} per CH_2 unit for the entropy of amorphous polyethylene at 298·16°K[30], a value of 36 cal. deg^{-1} mole^{-1} is obtained for the entropy of amorphous polytetrahydrofuran at 298·16°K. This value is closer to the calorimetric ($38{\cdot}8 \pm 0{\cdot}5$ cal. deg^{-1} mole^{-1}) than the equilibrium polymerization value ($43{\cdot}8 \pm 2{\cdot}7$ cal. deg^{-1} mole^{-1}).

Dainton and Ivin[30] have analysed entropies of polymerization in terms of the component entropy changes translational (S^0_{tr}), internal (S^0_{ir}) and external (S^0_{er}) rotational, and vibrational (S^0_v). For simple monomers these quantities may be calculated from standard formulae[31]. For polymers it is found that $S^0_v + S^0_{ir} \gg S^0_{tr} + S^0_{er}$ regardless of molecular shape, therefore $S^0_{tr} + S^0_{er}$ may be neglected. It follows that the entropy of polymerization, ΔS_{lc}, of tetrahydrofuran may be obtained from the expression

$$\Delta S_{lc} = (S^0_v + S^0_{ir})_p - S_{lm} - \Delta S_v \qquad (7)$$

where $(S^0_v + S^0_{ir})_p$ represents the sum of the vibrational and internal rotational entropies of polytetrahydrofuran at 298·16°K, S_{lm} is the entropy of the liquid monomer at 176 mm Hg and 298·16°K, and ΔS_v is the entropy of vaporization of amorphous polytetrahydrofuran at 298·16°K. For polyethylene $(S^0_v + S^0_{ir}) = 9{\cdot}2$ cal. deg^{-1} per CH_2 unit[30] and $\Delta S_v = 1{\cdot}6$ cal. deg^{-1} per CH_2 unit[15]. Assuming similar values hold for polytetrahydrofuran, namely, $(S^0_v + S^0_{ir})_p = 46$ cal. deg^{-1} mole^{-1} and $\Delta S_v = 8$ cal. deg^{-1} mole^{-1}, we obtained $\Delta S_{lc} = 46 - 53{\cdot}6 - 8 = 15{\cdot}6$ cal. deg^{-1} mole^{-1}, again in good agreement with the calorimetric value.

The above considerations lead us to the conclusion that the value obtained for ΔS_{lc} in this work is essentially correct.

A ceiling temperature, T_c, of about 358°K appears well established for polytetrahydrofuran[21]. Substituting for T_c and ΔS_{lc} in the expression[30]

$$\Delta H_{lc} = T_c \Delta S_{lc} \qquad (8)$$

we obtain $\Delta H_{lc} = -5{\cdot}3 \pm 0{\cdot}4$ kcal. mole^{-1} for the polymerization of liquid tetrahydrofuran at 176 mm Hg pressure and 298·16°K. This compares with the value $\Delta H_{lc} = -6{\cdot}1 \pm 1{\cdot}0$ kcal. mole^{-1} obtained from heat of combustion data for the monomer[32] and polymer[33].

G. A. Clegg and A. Tyson thank the University of Salford for the award of maintenance grants. We are also indebted to the Science Research Council for a grant in aid of this investigation. We should like to express our appreciation to Mr J. M. Evans for help in the preparation of polytetrahydrofuran, and to Dr F. W. Peaker of the University of Birmingham who carried out the GPC analysis on the sample.

Department of Chemistry and Applied Chemistry,
University of Salford,
Salford 5, Lancashire

(*Received November 1967*)

REFERENCES

[1] CLEGG, G. A., MELIA, T. P. and TYSON, A. *Polymer, Lond.* 1968, **9**, 75
[2] KELLEY, K. K., PARKS, G. S. and HUFFMANN, H. M. *J. phys. Chem.* 1929, **33**, 1802
[3] MAKLETSOVA, N. V., EPEL'BAUM, I. V., ROZENBERG, B. A. and LYUDVIG, Y. B. *Vysokomol. Soedineniya*, 1965, **7** (1), 70; *Polymer Science U.S.S.R.* 1965, **7** (1), 73
[4] ROZENBERG, B. A., CHEKHUTA, O. M., LYUDVIG, E. B., GANTMAKHER, A. R. and MEDVEDEV, S. S. *Vysokomol. Soedineniya*, 1964, **6** (11), 2030; *Polymer Science U.S.S.R.* 1964, **6** (11), 2248
[5] IVIN, K. J. and LEONARD, J. *Polymer, Lond.* 1965, **6**, 621
[6] MCCULLOUGH, J. P. *Proc. Amer. Petrol. Inst.* 1963, **43** (Section III), 274. Also private communication
[7] KOBE, K. A., RAVICA, A. E. and VOHRA, S. P. *Chem. Engng Data Ser.* 1959, **1**, 50
[8] TRICK, G. S. and RYAN, J. M. *J. Polym. Sci.* 1967, **18C**, 93
[9] MELIA, T. P. and TYSON, A. *Makromol. Chem.* 1967, **109**, 87
[10] O'NEILL, M. J. *Analyt. Chem.* 1964, **36**, 1238
O'NEILL, M. J., JUSTIN, J. and BRENNER, N. *Analyt. Chem.* 1964, **36**, 1233
[11] WUNDERLICH, B. *J. phys. Chem.* 1965, **69**, 2078
[12] GINNINGS, D. C. and FURUKAWA, G. J. *J. Amer. chem. Soc.* 1953, **75**, 522
[13] KARASZ, F. E., BAIR, H. E. and O'REILLY, J. M. *J. phys. Chem.* 1965, **69**, 2657
[14] KAUZMANN, W. *Chem. Rev.* 1948, **43**, 319
[15] DAINTON, F. S., EVANS, D. M., HOARE, F. E. and MELIA, T. P. *Polymer, Lond.* 1962, **3**, 263
[16] BEAUMONT, R. H., CLEGG, B., GEE, G., HERBERT, J. B. M., MARKS, D. J., ROBERTS, R. C. and SIMS, D. *Polymer, Lond.* 1966, **7**, 401
[17] ROSSINI, F. D. 'Selected values of chemical thermodynamic properties'. *Circ. U.S. Nat. Bur. Stand. No. 500*, 1962
[18] OLIVER, G. D., EATON, M. and HUFFMANN, H. M. *J. Amer. chem. Soc.* 1948, **70**, 1503
[19] FURUKAWA, G. T., MCCOSKEY, R. E. and KING, G. J. *J. Res. Nat. Bur. Stand.* 1951, **47**, 256
[20] KARASZ, F. E., BAIR, H. E. and O'REILLY, J. M. Private communication
[21] DREYFUSS, P. and DREYFUSS, M. P. *Advanc. Polym. Sci.* 1967, **4**, 528
[22] GIBBS, J. H. and DI MARZIO, E. A. *J. chem. Phys.* 1958, **28**, 373
[23] KARASZ, F. E., BAIR, H. E. and O'REILLY, M. J. *Polymer, Lond.* 1967, **8**, 547
[24] ADAMS, G. and GIBBS, J. H. *J. chem. Phys.* 1965, **43**, 139
[25] BESTUL, A. B. and CHANG, S. S. *J. chem. Phys.* 1964, **40**, 3731
[26] HIRAI, N. and EYRING, H. *J. Polym. Sci.* 1959, **37**, 51
[27] WUNDERLICH, B. *J. phys. Chem.* 1960, **64**, 1052
[28] DAINTON, F. S., EVANS, D. M., HOARE, F. E. and MELIA, T. P. *Polymer, Lond.* 1962, **3**, 277
[29] SMALL, P. A. *Trans. Faraday Soc.* 1955, **51**, 1717
[30] DAINTON, F. S. and IVIN, K. J. *Quart. Rev. chem. Soc., Lond.* 1958, **12**, 61
[31] ROSSINI, F. D. *Chemical Thermodynamics.* Wiley: New York, 1950
[32] GREEN, J. H. S. *Quart. Rev. chem. Soc., Lond.* 1961, **15**, 125
[33] SIMS, D. *J. chem. Soc.* 1964, **162**, 864

The Characterization of Polymers by a Viscometric Method

A. POWELL

In work published previously, the viscosity of a polymer or polymer solution has been expressed in terms of the polymer molecular weight distribution and a new parameter x which is characteristic of the species of polymer.

In the present work, a method is presented for the determination of parameter x for a particular species of polymer using only viscosity data in continuous shearing. Knowing x, the ratio M_n/M_w can then be obtained for a polymer. (M_n is the number average molecular weight, and M_w is the weight average molecular weight.) The method is applied to polydimethylsiloxanes, for which a value of 1·11 is obtained for parameter x.

IN A previous publication [POWELL, A. *Polymer, Lond.* 1966, **7**, 91], the viscosity of a polymer or polymer solution is expressed in terms of the ratio M_n/M_w (where M_n and M_w are the number average and weight average molecular weights for the polymer), and in terms of a new parameter x which is characteristic of the species of polymer used.

In the present work a method is described for the determination of parameter x and hence the ratio M_n/M_w, using two polymers of the same type but with different molecular weight distributions. The method is applied to the characterization of polydimethylsiloxanes, making use of viscosity data obtained in continuous shear experiments.

THEORETICAL

In work previously published by the author, the Maxwell model is modified to take account of the distribution of relaxation times. A new parameter F is introduced which is characteristic of the molecular size distribution, and is given by

$$F=(M_n/M_w)^x \tag{1}$$

where x is a constant which is characteristic of the particular species of molecule. Also

$$M_n=B/A \qquad \text{and} \qquad M_w=C/B$$

$$\text{where} \qquad A=\Sigma n_i; \quad B=\Sigma n_i M_i; \quad C=\Sigma n_i M_i^2$$

and n_i is the number of molecules within the distribution which have a molecular weight M_i.

For a liquid containing only molecules of one species, such as a polymer melt, it has been shown that the viscosity of the liquid when subjected to continuous shear is a function of parameter F and is given by equation (2).

$$\eta_D=\eta_0/\{1+(D\gamma)^{2F}\} \tag{2}$$

where η_D and η_0 are the viscosities of the liquid at rates of continuous shear D and zero respectively; γ is the representative relaxation time for the liquid during continuous shearing.

For two polymers, p and q, each having the same structure (that is, the same value for parameter x), but with different molecular size distributions characterized by parameters F_p and F_q, respectively, equation (1) takes the forms:

$$\log (B_p/A_p) - \log (C_p/B_p) = (1/x) \log F_p \tag{3}$$

$$\log (B_q/A_q) - \log (C_q/B_q) = (1/x) \log F_q \tag{4}$$

where subscripts p and q refer to polymers p and q, respectively.

For a blend of polymers p and q, containing αg of polymer p per g of q, which is characterized by parameter F_α, equation (1) gives

$$\log \frac{B_p + B_q}{A_p + A_q} - \log \frac{C_p + C_q}{B_p + B_q} = \left(\frac{1}{x}\right) \log F_\alpha \tag{5}$$

From equations (3), (4) and (5), the following relationships are obtained:

$$-\log ac = (1/x) \log (F_p/F_q) \tag{6}$$

$$-\log \frac{(1+\alpha a)(1+\alpha c)}{(1+\alpha)^2} = \left(\frac{1}{x}\right) \log \frac{F_\alpha}{F_q} \tag{7}$$

where $a = (M_n)_q/(M_n)_p$ (8) and $c = (M_w)_p/(M_w)_q$ (9)

For blends for which $\alpha = 1$ and $\alpha = 2$, characterized by parameters F_1 and F_2, respectively, equations (6) and (7) give:

$$-\log ac/\{-\log (1+a)(1+c)/4\} = \log (F_p/F_q)/\log (F_1/F_q) \tag{10}$$

$$-\log ac/\{-\log (1+2a)(1+2c)/9\} = \log (F_p/F_q)/\log (F_2/F_q) \tag{11}$$

where equation (10) refers to the blend $\alpha = 1$, and equation (11) to the blend $\alpha = 2$.

EXPERIMENTAL

Viscosity measurements have been carried out under continuous shear, at 25°C, using samples of polydimethylsiloxanes.

In each test carried out, measurements were made on two polydimethylsiloxanes, p and q, and on two blends of compositions 50 per cent p, 50 per cent q by weight (namely, $\alpha = 1$) and 66·6 per cent p, 33·3 per cent q by weight (namely, $\alpha = 2$). Two tests were carried out, A and B, and in each case polymer q was a DC200 silicone of zero shear viscosity 500 000cS at 25°C. Polymer p was a different polydimethylsiloxane in each test (p_A for test A and p_B for test B). The results obtained for tests A and B are given in *Figures 1* and *2*, respectively; in *Figure 1*, $\log \{(\eta_0/\eta_D) - 1\}$ is plotted against $\log D$ for polymers p_A and q, and for each of the two blends 50 per cent p_A, 50 per cent q and 66·6 per cent p_A, 33·3 per cent q by weight. Similarly in *Figure 2* $\log \{(\eta_0/\eta_D) - 1\}$ is plotted against $\log D$ for polymers p_B and q, and for each of the blends 50 per cent p_B, 50 per cent q and 66·6 per cent q, 33·3 per cent q by weight.

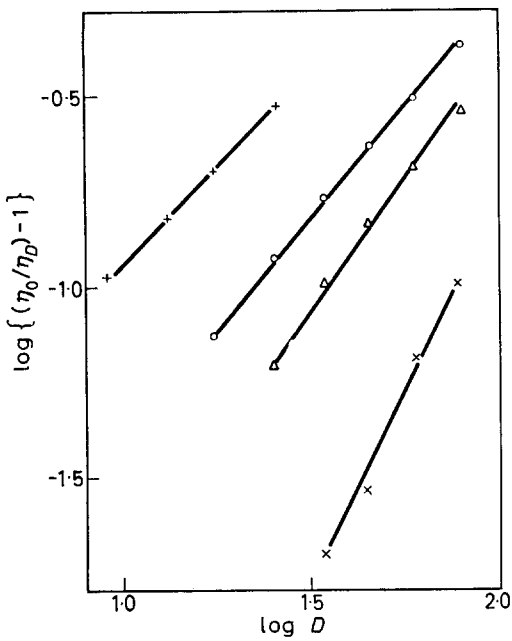

Figure 1—The dependence of $\log\{(\eta_0/\eta_D)-1\}$ on $\log D$ for + polymer q (a DC 200 silicone of zero shear viscosity 500 000 cS at 25°C; × polymer p_A (sample of polydimethylsiloxane used only in test A); ○ blend 50 per cent p_A/50 per cent q by weight; △ blend 66·6 per cent p_A/33·3 per cent q by weight

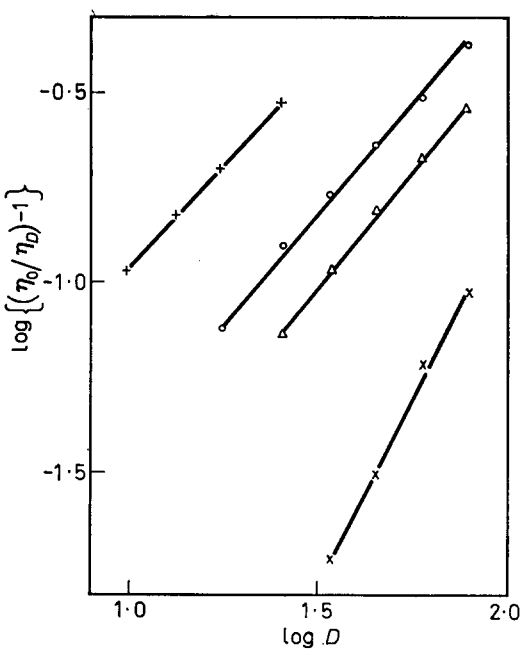

Figure 2—The dependence of $\log\{(\eta_0/\eta_D)-1\}$ on $\log D$ for + polymer q (a DC 200 silicone of zero shear viscosity 500 000 cS at 25°C; × polymer p_B (sample of polydimethylsiloxane used only in test B); ○ blend 50 per cent p_B/50 per cent q by weight; △ blend 66·6 per cent p_B/33·3 per cent q by weight

RESULTS AND CONCLUSIONS

In *Figures 1* and *2*, the plots of $\log\{(\eta_0/\eta_D)-1\}$ versus $\log D$ are straight lines, as predicted by equation (2). Values for parameters F_p, F_q, F_1 and F_2, obtained by applying equation (2) to the straight line plots in *Figures 1* and *2*, are given in *Table 1*. For each of the tests carried out, the values of F_p, F_q, F_1 and F_2 were used in equations (10) and (11) to determine the parameters a and c. [Equations (10) and (11) were solved using an iterative procedure.] For each test, three values of parameter x were then determined using equations (6) and (7). Using an average value for x, the value of ratio M_n/M_w was then determined from equation (1) for the polymers p_A and p_B used in tests A and B and polymer q.

Table 1. Results for polydimethylsiloxanes

	Sample	*F*		*x*	$\frac{Mn^*}{Mw}$
Test A	polymer p_A	0·990	$a = 1{\cdot}600$	1·09	0·99
	polymer q	0·532			0·56
	blend 50 per cent p_A/50 per cent q by weight	0·610	$c = 0{\cdot}350$	1·00	
	blend 66·6 per cent p_A/33·3 per cent q by weight	0·700		1·18	
Test B	polymer p_B	0·967	$a = 1{\cdot}704$	1·18	0·97
	polymer q	0·532			0 56
	blend 50 per cent p_B/50 per cent q by weight	0·580	$c = 0{\cdot}354$	1·00	
	blend 66·6 per cent p_B/33·3 per cent q by weight	0·660		1·21	

*Ratio (M_n/M_w) is calculated using an average value of 1·11 for parameter x.

Table 1 shows that the value of parameter c is approximately the same for each test. This, together with equation (9), and the knowledge that polymer q is the same for each test, indicates that polymers p_A and p_B have approximately the same value for M_w; this conclusion is in agreement with the fact that the polymers p_A and p_B used in the tests each have a zero shear viscosity in the region of 60 000 cS at 25 °C.

The data presented in *Table 1* give an average value of 1·11 (accuracy ±0·11) for parameter x for the polydimethylsiloxanes. In agreement with this, previously reported values of F and of M_n/M_w for other samples of polydimethylsiloxanes[1] give an independent value for x of approximately unity. The observed accuracy of ±0·11 in the value of x produces an accuracy of ±0·04 in the value of 0·56 for (M_n/M_w) calculated for polymer q.

Work is now in progress on the fractionation of polymers in order to investigate further the dependence of parameter F on the molecular weight distribution.

John Dalton College of Technology,
Chester Street, Manchester

(*Received October 1967*)

The Glass Transition Temperature of trans-*Polychloroprene*

R. NAGAO

The low temperature behaviour of trans-*polychloroprene (Neoprenes GRT and AC) above −196°C was observed by the broad-line proton magnetic resonance method. The glass transition temperature was indicated to be −40°C from the volume/temperature relationship and from the values of activation energy calculated using the maximum peak-to-peak line width. It is observed from the second moment values that a small-scale molecular motion sets in at about −90°C in the heating process.*

MANY investigations have been carried out on *trans*-polychloroprene, usually from the practical standpoint. At present, we have only few data related to the physical properties of unblended and unvulcanized *trans*-polychloroprene. The case is analogous to that of the glass transition of the polymer. Hitherto, various temperatures[1–3] between −50° and −17°C have been cited as the glass transition point. These values were derived mainly from the mechanical properties. The glass transition point was indicated to be −40°C in this experiment by dilatometry and the broad-line proton magnetic resonance method. The temperature corresponding to the inflection point of the line width/temperature curve of *trans*-polychloroprene is about 20 deg. higher than the glass transition point. In other polymers with a chlorine side group and in hydrocarbon polymers[4], the inflection point of the line width/temperature curve and the bending point of the volume/temperature curve almost coincide.

EXPERIMENTAL

The *trans*-polychloroprenes, $-(CH_2-CH=CCl-CH_2)_n-$, used in these experiments are the GRT, AC, WRT and AD Neoprenes, prepared by E. I. du Pont de Nemours and Co. It was found by organic micro analysis that Neoprene GRT was 0·9 per cent combined sulphur (by weight), while Neoprenes AC, WRT and AD contained no sulphur. The fundamental physical properties of Neoprenes GRT and AC are shown in *Table 1*. Neoprenes WRT and AD show properties similar to those of GRT and AD respectively.

Table 1. Physical properties of Neoprenes GRT and AC

Property	*GRT*	*AC*	*Property*	*GRT*	*AC*
Melting point*, °C	30	55	Characteristic		
Crystallization point*, °C	—	17	times of crystal-		
Degree of crystallinity*			lization* at 0°C,		
at 20°C, wt %	9·8	28	min		
Content of *trans*-1,4			Initiation	1 300	4
bond†, mole %	80	91·5	Half advance	3 600	12
			Equilibrium	*ca.* 2×10^5	*ca.* 3×10^4

*Estimated from dilatometric measurements.
†Estimated from melting point using Flory's equation[5].

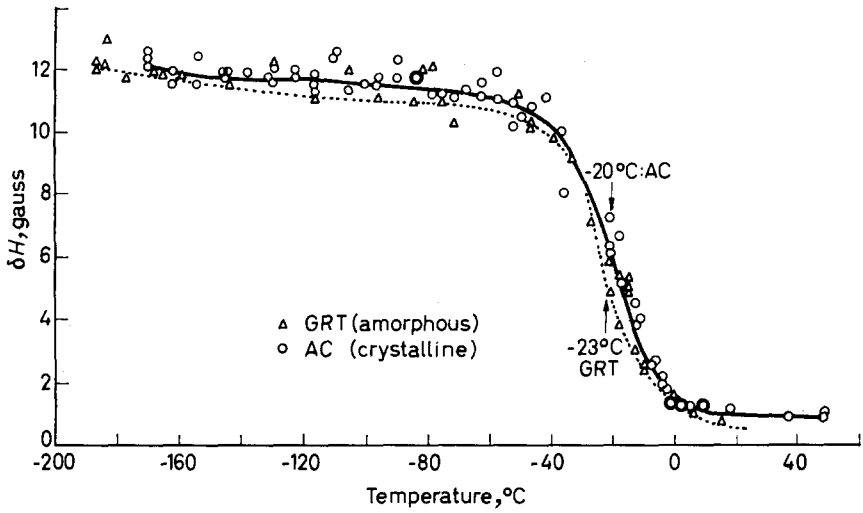

Figure 1—Line width/temperature curves of Neoprenes GRT and AC

The broad-line nuclear magnetic resonance spectrometer employed to observe the molecular motion was constructed by the Japan Electron Co. Ltd; the proton magnetic resonance absorption spectra were measured with the oscillation frequency of 30 Mc/s.

The measurements were carried out at the temperature-variation rate of five minutes per degree.

RESULTS AND DISCUSSION

Figures 1 and *2* show the maximum peak-to-peak line width, δH, and the mean second moment, $\langle \Delta H^2 \rangle$, respectively, plotted against temperature for Neoprenes GRT and AC. The correlation frequency/temperature relationships, calculated on the basis of the line width/temperature curve by Gutowsky's equation[6], of Neoprenes GRT and AC are shown in *Figure 3*.

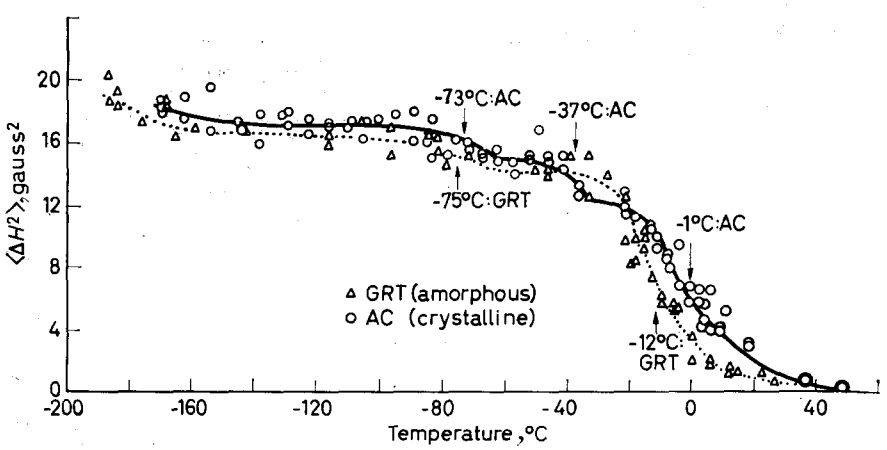

Figure 2—Second moment/temperature curves of Neoprenes GRT and AC

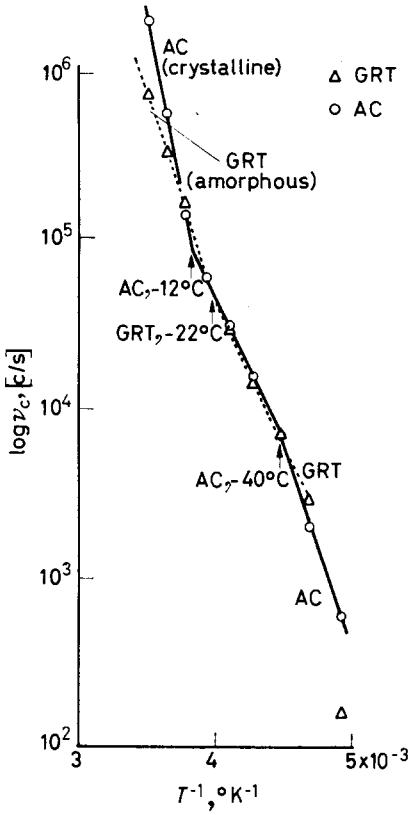

Figure 3—The correlation frequency/temperature relationships for Neoprenes GRT and AC

The temperatures of the inflection points of the line width/temperature or the second moment/temperature curve, $T(\delta H)$ or $T(\langle \Delta H^2 \rangle)$ respectively, and the activation energies, E_a, calculated from the tangents of the correlation frequency/temperature curves are tabulated in *Table 2*, where the $T(V)$

Table 2. Characteristic temperatures (T) and activation energies (E_a) of Neoprenes GRT and AC

Property	*GRT (amorphous)*	*AC (crystalline)*
$T(\delta H)$, °C	−23°	−20°
$T(\langle \Delta H^2 \rangle)$, °C	−75°, −12°	−73°, −37°, −1°
$T(V)$, °C	−40°	—
E_a, kcal/mole	—	7·62(−70° to −40°C)
	7·88(−60° to −22°C)	7·88(−40° to −12°C)
	12·00(−22° to −20°C)	20·80(−12° to 20°C)

is the temperature of the bending point of the volume/temperature curve composed of two straight lines between −80° and 30°C. The bending point of the volume/temperature curve is generally accepted as a glass transition point. The $T(V)$ value lies in the temperature region with activation energy of *ca.* 8 kcal/mole. The E_a value corresponds to an activation energy being

Table 3. Activation energies (E_a) and characteristic temperatures (T) of various polymers

Polymer	E_a *kcal/mole*	*Temperature range*, °C	$T(V)$ °C	$T(\delta H)$ °C
Polyvinyl chloride: Zeon 103EP	11	45 to 104	76	72
Chlorinated *trans*-polybutadiene: —(CH_2—CHCl—CHCl—CH_2)$_n$—	9·2	51 to 85	70	67
Polyethylene: Marlex 50	3·5	−58 to −10	−40	−47
Ethylene propylene copolymer (EP)[4]	5·2	−63 to −37		−38[4]
	8·8	−37 to −10	−31[4]	
cis-Polybutadiene (CB-4)[4]	3·4	−136 to −86	−95[4]	−95[4]
Polybutadiene (BD)[4]	6·3	−105 to −91	−100[4]	
	4·7	−91 to −62		−90[4]
Polybutadiene (BE)[4]	6·4	−77 to −55	−58[4]	−69[4]
trans-Polybutadiene (TB-2)[4]	5·3	−76 to −53	−58[4]	−65[4]
cis-Polyisoprene (CI)[4]	11·9	−53 to −45	−50[4]	−46[4]
Polyisoprene (IE)[4]	3·9	−51 to −16	−48[4]	−42[4]
trans-Polyisoprene (98 mole% *trans*-1,4 bond)	4·1	−100 to −57	−58	
	7·9	−57 to −40		−53

required for the micro-brownian chain motion of the amorphous part. The relationship between the activation energy and the $T(V)$ and $T(\delta H)$ values of the other polymers having a chlorine side group and hydrocarbon polymers are listed in *Table 3*. In these polymers the difference between the $T(V)$ and $T(\delta H)$ values of each polymer is small and nowhere more than eleven degrees. The difference between the corresponding values for the *trans*-polychloroprenes is approximately 20 degrees.

It is known from the second moment/temperature curves in *Figure 2* that a small-scale molecular motion sets in at about −90°C prior to the glass transition in the heating process.

CONCLUSIONS

The glass transition temperature of the unblended and unvulcanized *trans*-polychloroprene was taken to be −40°C.

In the heating process a small-scale molecular motion sets in at *ca.* = 90°C.

The temperature corresponding to the inflection point of the line width/temperature curve of *trans*-polychloroprene is about 20 degrees higher than the glass transition point, unlike other polymers with a chlorine side group and some hydrocarbon polymers in which the temperature differences are not so large as those found for *trans*-polychloroprene.

Department of Chemistry,
Tokyo Science University,
Shinjuku, Tokyo, Japan.

(*Received October 1967*)

REFERENCES

[1] WILEY, R. H., BRANER, G. M. and BENNETT, A. R. *J. Polym. Sci.* 1950, **5**, 609
[2] KING, G. E. *Industr. Engng Chem. (Industr.)*, 1943, **35**, 949
[3] YIN, T. P. and PARISER, R. *J. appl. Polym. Sci.* 1963, **7**, 667
[4] TAKEDA, M., TANAKA, K. and NAGAO, R. *J. Polym. Sci.* 1962, **57**, 517
[5] FLORY, P. J. *J. chem. Phys.* 1949, **17**, 223
[6] GUTOWSKY, H. S. and MEYER, L. H. *J. chem. Phys.* 1953, **21**, 2122

Evidence for Ionic Processes in Irradiated Polymers. Crosslinking of 4-Polyvinylpyridine at Low Temperature

C. DAVID, A. VERHASSELT and G. GEUSKENS

The influence of various additives on the crosslinking of 4-polyvinylpyridine has been studied. Only strong electron acceptors increase gel formation at 77°K and have an influence on the e.s.r. spectra of the irradiated polymer. These results demonstrate the occurrence of ionic processes.

Two main types of mechanism are proposed for polymer crosslinking by radiation; the most generally admitted involves recombination of radicals, the other assumes ion–molecule reactions. Formation of ionic states is clearly demonstrated in some liquid phase polymerization[1] and in irradiated organic glasses or polycrystalline solids at low temperature[2]. Ionic intermediates have been postulated in other reactions[3].

This work shows evidence for ionic processes in the crosslinking of poly-4-vinylpyridine (4-PVP) at low temperature using additives such as iodine, carbon tetrachloride, tribromomethane, tetracyanoethylene (TCNE) and sulphur dioxide that have been shown to be strong electron acceptors in organic glasses[4]. They markedly increase crosslinking in contrast to other additives such as amines, chloromethane, mercaptans or β-picoline. The radiation chemistry of 4-PVP at room temperature has been studied recently[5]. $G_{\text{crosslinking}}$ is 0·3 and the ratio of chain degradation to chain crosslinking is equal to zero.

EXPERIMENTAL

The polymer is prepared from twice distilled monomer using AIBN as initiator at 70°C. Conversion is limited to 20 per cent by pouring polymer and residual monomer into ether. 4-PVP is then dissolved in *t*-butanol and precipitated as a fine powder with heptane. Intrinsic viscosity of the polymer measured at 25°C in ethanol is 2·7 dl. g^{-1}. Molecular weight was calculated to be 854 000 by the relation[6]

$$[\eta] = 25 \times 10^{-5} M_v^{0.68}$$

This powder is introduced into irradiation bulbs and outgassed at 80°C under vacuum. Additive is then introduced according to its volatility; its amount is determined by weight or by pressure measurement in a known volume. The bulbs are sealed under vacuum and kept for 48 hours at 90°C to allow diffusion and homogeneous distribution of the additive in the polymer. Irradiations are performed with a ^{60}Co source; dose rate is estab-

lished by Fricke dosimetry as 0·6 Mr. h^{-1}. After irradiation volatile additives are pumped under vacuum and the soluble fraction of the polymer is extracted with methanol in a Soxhlet apparatus; quantitative analysis is carried out by absorption spectrophotometry at 2 565 Å ($\epsilon_{2\,565\,\text{Å}}$ in methanol = 1·634 l. cm. $mole^{-1}$). The e.s.r. spectrometer and measurement technique for irradiated samples at low temperature have been described previously[7].

RESULTS AND DISCUSSION

Post-irradiation effects in pure polymer were first studied by varying time of storage at liquid nitrogen temperature from 18 hours to 33 days and time of heating to room temperature from a few minutes to five hours. Some samples were annealed at 100°C. The results of all these experiments were not significantly different.

Table 1. Solubility of 4-PVP containing various additives irradiated at 77°K (Dose: 10·5 Mr)

Additive	*Mole %*	*Solubility %*	*Relative electron acceptor efficiency**
—	—	97	—
CCl_4	1	23	20
SO_2	1	12	23
$CHBr_3$	1	10	20
I_2	2	13	37
TCNE	1·5	50	—
CH_3Cl	1	100	0
C_6H_5SH	1	100	—
NH_3	3	100	—
Butylamine	1	98	—
β-Picoline	1	99	—
CH_3OH	2	93	0

*As determined in competitive reactions with naphthalene for the formation of anions in organic glasses[4].

The effect of various additives on gel fraction at constant irradiation dose is summarized in *Table 1*. A gelling dose of 10 Mr for the polymer irradiated without additive yields[8]

$$G_{cl} = \frac{0{\cdot}48 \times 10^6}{r_{gel} \times M_w} = 0{\cdot}056 \text{ at } 77°\text{K}$$

The various additives used in this work have been thoroughly studied in other reactions.

Mercaptans have a protecting effect in systems undergoing free radical reactions while amines and ammonia inhibit cationic processes. Iodine, carbon tetrachloride, tribromomethane and TCNE have in common their high electron affinity. With the exception of TCNE, these latter compounds were used by Hamill in competitive reactions with naphthalene for the formation of anions in organic glasses; they have all been shown to be strong electron acceptors[4].

Table 1 indicates that among the various additives used, only those possessing a high electron affinity increase crosslinking yield in 4-PVP. Crosslinking index (number of crosslinked units per weight average molecule) increases from one to about four if one assumes a random molecular weight distribution for the polymer[8]. Such a large effect cannot be explained by an enhancement in the free radical production due to the presence of the additives, free radical yield as measured at room temperature being very different for iodine, tribromomethane, carbon tetrachloride, sulphur dioxide and TCNE[9,10]. Increased crosslinking efficiency must be attributed to the electron attaching power of the additives. It seems likely, by analogy with pyridine, that the electrons to be captured are produced by ionization of the non-bonding pair on the nitrogen atom giving cation radical I

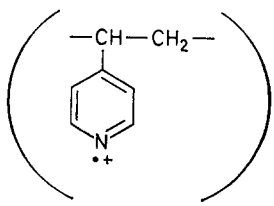

(I)

This conclusion arises from the comparative study by e.s.r. of 4-PVP and pyridine irradiated at low temperature. Both spectra consist of a triplet with 30 gauss hyperfine splitting which is superimposed on a singlet in the case

Figure 1—The e.s.r. spectrum recorded at 77°K of 4-PVP irradiated at 77°K. Dose 16 Mr

of the polymer (*Figure 1*). The triplet of pyridine was recently identified as due to the cation radical

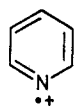

(II)

by analysis of pyridine and pyridine-d_5 spectra[7]. Assignment of the triplet component of 4-PVP to radical I seems thus straightforward*. When irradiation is carried out in the presence of iodine†, sulphur dioxide and tribromomethane, triplet relative importance considerably increases (*Figures 2* and *3*) giving further strong support to our interpretation. TCNE and carbon tetrachloride used as additives respectively give rise to the spectrum of the TCNE anion and to an asymmetric spectrum difficult to analyse.

Figure 2—The e.s.r. spectrum recorded at 77°K of 4-PVP irradiated at 77°K+5 wt % $CHBr_3$

No enlargement in the triplet component is observed with the other additives. This triplet irreversibly decays at the same temperature as the corresponding triplet in pyridine, i.e. at about −80°C.

*Formerly this spectrum had been wrongly assigned to a radical formed by addition of a H atom to a carbon atom of the pyridine ring[8].

†K. Tsuji *et al.* have recently reported (*J. chem. Phys.* 1967, **46** 2808) that irradiation of pyridine at −196°C in the presence of 1·7 mole per cent iodine brings about an increase in the *G* value for radical II from 0·5 to 13 as measured by e.s.r.

Cation I obviously takes an essential part in the crosslinking process since additives, which sensitize network formation, also increase its amount in the irradiated sample.

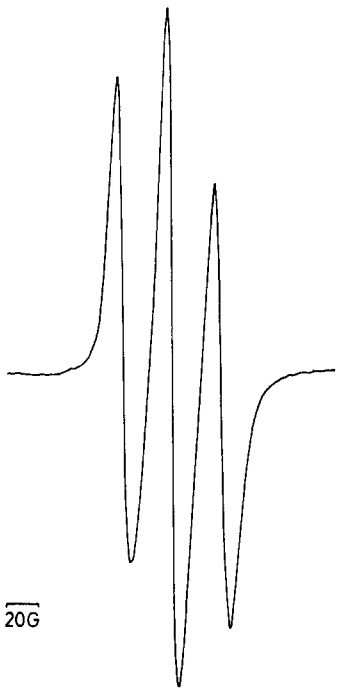

Figure 3—The e.s.r. spectrum recorded at 77°K of 4-PVP irradiated at 77°K + 4·8 wt % I_2

Network formation in 4-PVP can be assigned to an ionic reaction or to free radical recombination, if cation I is a precursor of these radicals.

The first hypothesis, however, seems the most probable because there is no post-irradiation effect, usual in the case of a radical mechanism[11]. Crosslinks would thus be formed at low temperature since the triplet attributed to cation I disappears at −80°C.

We are very grateful to Professor de Brouckère and Professor Charlesby for their interest in this work and helpful discussion. We also thank Dr Jung of Union Carbide European Research Associates, Brussels, for kindly recording the e.s.r. spectra.

Service de Chimie Générale II,
Faculté des Sciences,
Université Libre de Bruxelles

(*Received October 1967*)

REFERENCES

[1] COLLINSON, E., DAINTON, F. S. and GILLIS, H. A. *J. phys. Chem.* 1959, **63**, 909
BUSLER, W. R., MARTIN, D. H. and WILLIAMS, F. *Disc. Faraday Soc.* 1963, **36**, 103
[2] SHIDA, T. and HAMILL, W. H. *J. Amer. chem. Soc.* 1966, **88**, 5376

[3] DOLE, M. 'Mechanism of chemical effects in irradiated polymers' in *Crystalline Olefin Polymers*, Part I. (R. A. RAFF and K. W. DOAK, Editors). Interscience: New York, 1965
[4] GUARINO, J. P., RONAYNE, M. R. and HAMILL, W. H. *Radiat. Res.* 1962, **17**, 379
[5] DAVID, C., VERHASSELT, A. and GEUSKENS, G. International Symposium on Macromolecular Chemistry, Prague 1965, Preprint 261
[6] BERKOWITZ, J. B., YAMIN, M. and FUOSS, R. M. *J. Polym. Sci.* 1958, **28**, 69
[7] DAVID, C., GEUSKENS, G., VERHASSELT, A., JUNG, P. and OTH, J. F. M. *Molec. Phys.* 1966, **11**, 257
[8] CHARLESBY, A. *Atomic Radiation and Polymers.* Pergamon: Oxford, 1960
[9] HAÏSSINSKY, M. and MAGAT, M. *Constantes sélectionnées—Rendements radiolytiques.* Pergamon: Oxford, 1961
[10] ROTHSCHILD, W. G. *J. Amer. chem. Soc.* 1964, **86**, 1307
[11] ORMEROD, M. G. *Adv. nucl. Sci. Technol.* 1964, **2**, 107 and references therein

Isomorphism in Aliphatic Copolyesters

G. J. HOWARD and S. KNUTTON

Two series of aliphatic copolyesters have been prepared by ester interchange from four homopolymers. Melting points, densities, X-ray diffractograms and heats of fusion have been measured. Although the melting point/composition relation is of the eutectic type, usually attributed to systems in which only one type of monomer residue crystallizes, all other measurements show that a high and apparently constant level of crystallinity persists throughout the composition range. It is concluded that extensive cocrystallization takes place and that alignment of ester groups is not a requirement for efficient crystal packing.

CONSIDER a set of random copolymers composed of various proportions of A and B residues; consider further that the corresponding homopolymers (poly A and poly B) are crystallizable. If, because of geometrical or polarity considerations, B units are unable to enter the crystal lattice of A sequences (and vice versa), copolymerization of relatively small proportions of the foreign unit will, relative to the homopolymer, markedly reduce the crystallinity, lower the melting point, broaden the melting range and bring about other concomitant changes in physical properties. On the other hand, if B units are able to pack into the A lattice with little distortion these changes in crystallinity and related properties will not occur to any appreciable extent. This latter situation is that usually described as isomorphous replacement, although it should be noted that Tranter[1] has criticized the use of this term.

Most experimental studies of copolymer series of the type described above have been of the dependence of melting point on composition. Usually, melting point/composition curves show a pronounced minimum (eutectic type). However, systems have been reported in which there is no depression of the melting temperature below that of the homopolymers and in which the melting point/composition curve is linear[2] or nearly so[3-5]. It has become usual to identify only those copolymer series which exhibit melting point/composition curves having no minimum as systems in which either unit is tolerated in a common crystal lattice. By supplementing softening point data with crystallographic studies, Tranter[1] has shown that this criterion is unsound and that several series of copolyamides show cocrystallization whilst having melting point/composition curves of the eutectic type. In these copolymers the repeating units were of similar length and Tranter[1] considers this similarity as a prime requirement for isomorphous replacement.

In the studies on copolyesters reported here, the repeat lengths (ester–ester distance of extended chain) of the structural units are in the (approximate) ratio 3 : 2.

EXPERIMENTAL

Materials

Four homopolyesters, polyhexamethylene adipate (6G6), polyhexamethylene sebacate (6G10), polydecamethylene adipate (10G6) and polydeca-

methylene sebacate (10G10) were prepared by reaction of the appropriate diol and diacid chloride in diglyme solution following the method of Wright[6] Two series of copolymers (6G10–10G6) and (10G10–6G6) were prepared by ester interchange of the requisite quantities of the homopolyesters. Appropriate amounts of homopolymers were mixed in benzene solution, two or three small crystals of *p*-toluene sulphonic acid added, the solution frozen and the solvent removed by vacuum sublimation. Ester interchange to form a random copolymer was carried out at 135°C under vacuum for 120 to 135 min.

Molecular weights of three of the homopolyesters were determined from their intrinsic viscosities using literature values[7-9] for the constants of the Mark–Houwink equation.

Table 1. Molecular weights of homopolyesters

Polyester	$[\eta]$ (*dl/g*)	$\overline{M}_v$
6G6	0·361 chloroform, 25°C	13 500
10G6	0·246 chlorobenzene, 25°C	9 020
6G10	0·264 benzene, 20°C	6 360

As the randomization reaction was carried out under continuous vacuum, further polycondensation will have taken place and the copolyesters will have higher molecular weights than the homopolymers; it is assumed that the copolymers have melting points substantially independent of molecular weight.

Melting points

Optical melting points were measured on a microscope hot stage. The sample, held between cover slips, was first melted on the stage, cooled to some 8 deg. C below the initially observed melting point to permit slow crystallization to occur and then remelted at a heating rate of *ca.* 0·5 deg. C min^{-1}. The melting point was taken as the temperature of the disappearance of birefringence. The melting points of another set of copolymers are also quoted; the copolymers were prepared and their melting points measured by Wright[6]; in this case the heating rate was *ca.* 0·2 deg. C min^{-1}. All the polyesters show a spherulitic structure in the solid state.

Melting points are also recorded from observations using the Perkin–Elmer scanning calorimeter (DSC-1). Heating rates of 16 deg. C min^{-1} and 8 deg. C min^{-1} were employed and the maximum of the melting endotherm was taken as the polymer melting point; the reproducibility is not better than ± 1 deg. C and the values are *ca.* 5 to 7 deg. C higher than the optical melting points. The vertical lines on the curves of *Figure 1* join the extreme values recorded. Both series of ester copolymers yield the usual eutectic curves. Observed homopolyester melting points are close to literature values[10,11]; these, however, sometimes spread over a range of *ca.* 10 deg. C.

X-Ray diffraction

Powder photographs were made of the diffraction of 1·54 Å radiation: diameters of the Debye–Scherrer rings were measured to 0·5 mm and lattice

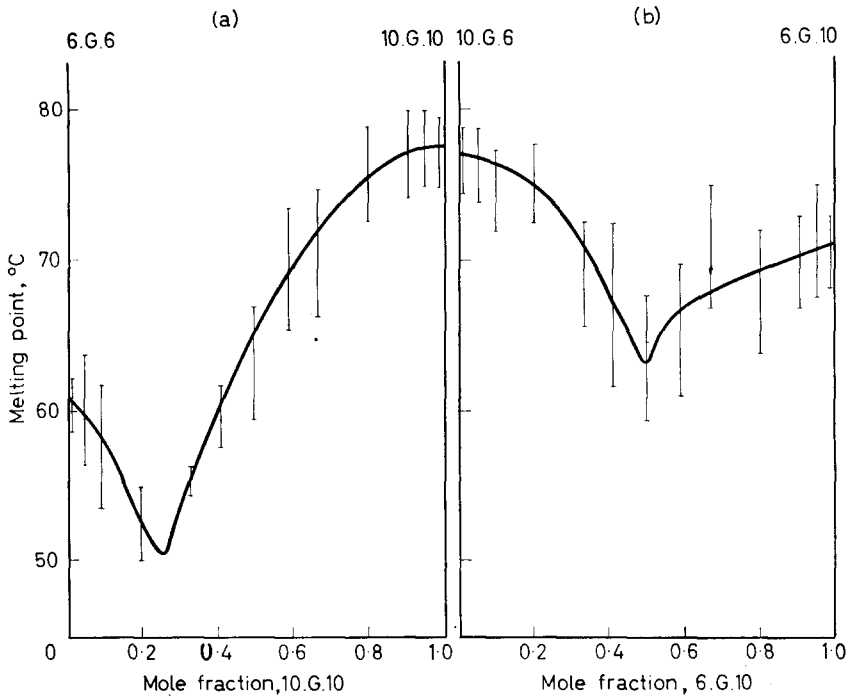

Figure 1—Melting point/composition curves for copolyesters: (a) copolymers of hexamethylene adipate and decamethylene sebacate; (b) copolymers of decamethylene adipate and hexamethylene sebacate

spacings calculated. Most spacings appear common to all copolymers of a series (*Figure 2*). The spacings for the homopolymers 10G6 and 10G10 agree closely with those found in the fibre diagram by Fuller and Frosch[12].

In the 6G6–10G10 series, the copolymers having more than *ca.* 30 per cent of decamethylene sebacate units (that is, compositions lying to one side of the melting point minimum) show two new outer rings. However, 6G6 homopolymer has a similar lattice spacing and as, in all cases, the diffraction rings are faint, their absence at low hexamethylene adipate contents cannot be regarded as established.

Densities

Polymer densities were measured by flotation in aqueous potassium bromide solutions. The densities agree closely with the values calculated by assuming volume additivity on mixing.

Heats of fusion

Heats of fusion of known weights of the polyesters were determined from the area under the melting peak trace on the differential scanning calorimeter record: a heating rate of 8 deg. C min^{-1} was used and the instrument calibrated by carrying out similar measurements on samples of zone-refined

benzoic acid and naphthalene, making use of the literature[13] values for their latent heats of fusion. The results recorded in *Tables 2* and *3* are means of duplicate determinations, the average deviation from the mean being about two per cent.

Table 2. Heats of fusion of (6G6–10G10) copolymers

Mole fraction 10G10 units	*Heat of fusion cal/g polymer*	*Mole fraction 10G10 units*	*Heat of fusion cal/g polymer*
0·000	21·6	0·588	34·2
0·048	29·8	0·667	35·9
0·091	29·9	0·800	40·0
0·200	29·3	0·909	40·6
0·333	22·9	0·953	40·8
0·500	34·8	1·000	36·0

Table 3. Heats of fusion of (10G6–6G10) copolymers

Mole fraction 6G10 units	*Heat of fusion cal/g polymer*	*Mole fraction 6G10 units*	*Heat of fusion cal/g polymer*
0·000	34·4	0·588	37·2
0·048	39·1	0·667	36·7
0·091	38·6	0·800	37·6
0·200	34·0	0·909	38·1
0·333	36·5	0·952	38·8
0·412	37·1	1·000	33·7
0·500	37·1		

DISCUSSION

Discussion of the observed properties of these aliphatic copolyesters is in terms of the mutual participation of both monomer residues in a common crystal lattice and it is assumed that the copolymers have a random sequence structure. Judging from the known rate of polyester re-equilibration via ester interchange[14], the conditions used should have ensured randomization of the structural units. This was confirmed for the first series prepared by Wright[6], who found that the copolyester formed from equimolar proportions of decamethylene adipate and hexamethylene sebacate units melted at 59·0°C whilst that containing equal numbers of decamethylene sebacate and hexamethylene adipate units melted at 59·3°C: the two polymers should have identical structures if randomization of units is complete. A separate test was also performed by preparing a random copolymer having equimolar proportions of decamethylene sebacate and decamethylene adipate by reaction of the requisite mixture of the diacid chlorides with decamethylene glycol: this product melted at 68°C whilst the corresponding copolymer made by the re-equilibration method melted at 69°C.

All the evidence accumulated suggests that the level of crystallinity exhibited by the homopolymers is maintained throughout the range of copolymer compositions. This evidence will be summarized briefly. First, all copolyesters have a spherulitic structure in the solid phase, indicative of long-range order. Secondly, the melting range is similar for all samples: the temperature range of melting was judged from the differential thermal

analysis traces and was taken to be the temperature interval between the beginning and the peak of the melting endotherm. Observed values of this interval vary between 10 deg. C and 20 deg. C; the deviations from the

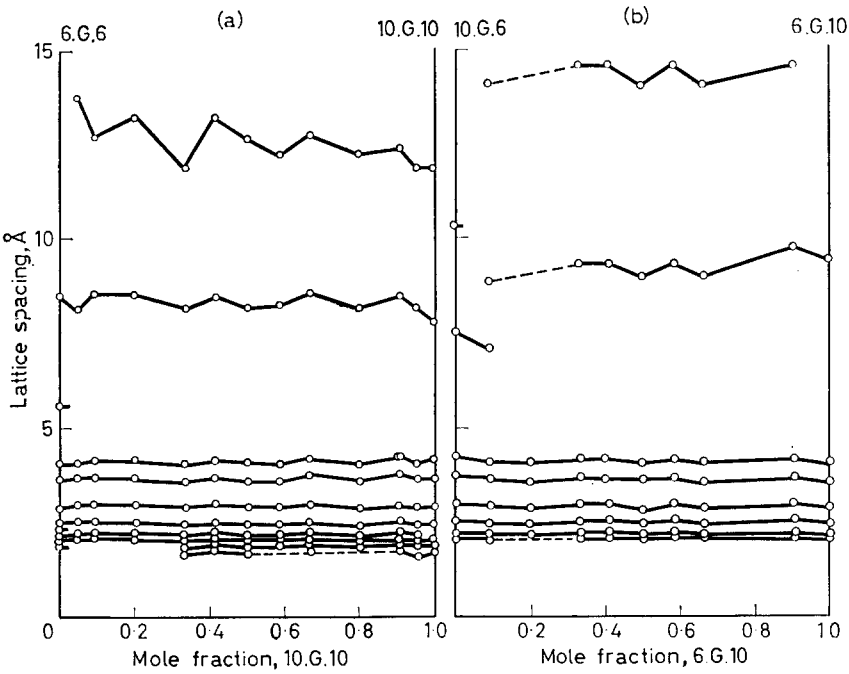

Figure 2—Variation of lattice spacings with copolyester composition: (a) copolymers of hexamethylene adipate and decamethylene sebacate; (b) copolymers of decamethylene adipate and hexamethylene sebacate

mean of 14·5 deg. C are random. These observations stand in marked contrast to the expected behaviour of copolymers in which one of the monomeric residues is excluded from the crystal lattice; for such copolymers the crystallinity gradually diminishes over a wide temperature interval in the fusion process, which becomes progressively more diffuse with increasing content of non-crystallizable units[15].

X-Ray diffraction photographs show clearly that, even at the eutectic point, the copolymers exhibit reflections similar in number and intensity to those of their parent homopolymers; density measurements indicate no marked packing defects in the solid. Finally, the measured latent heats of fusion are much the same for all copolymers. Actually they are rather higher than the values for the homopolymers; this may be because of the different thermal history of the two types of polymer.

The degree of crystallinity may be taken to be the ratio between the measured heat of fusion and the calculated value for the fully crystalline polymer. Of published values of ΔH_f of homopolyesters, those obtained by

application of the copolymer melting-point equation[16] are disregarded, leaving the values appearing in *Table 4*.

Table 4. Heats of fusion (ΔH_f) of polyester crystallites

Polymer	ΔH_f (*cal/g crystal*)	*Method*
poly 10G10	36·0	Diluents[17]
„	39·7	Calculation[18]
poly 10G6	35·9	Diluents[19]
„	37·5	Chain length[17]
„	38·4	Calculation[18]

The above values, combined with the experimental data from *Tables 2* and *3*, predict crystallinities of *ca.* 95 per cent for polydecamethylene sebacate and 92 per cent for polydecamethylene adipate. These crystallinity values are unexpectedly high. Although care must be taken when using high resolution DTA techniques for calorimetry[20], the calibration constant used in this work appears substantially correct. For instance, the measured values for the heats of fusion of silver nitrate (13·6 cal/g) and potassium nitrate (21·3 cal/g) are in reasonable accord to reported[13] values of 16·2 and 22·7 cal/g respectively. Furthermore, polyethylene oxides of $\bar{M}_n = 4\,700$ are found to have heats of fusion (cal/g polymer) from 40·6 to 44·2, depending on the thermal history of the sample; a high molecular weight polyethylene oxide (Polyox 205) has a rather lower value of 37·2 (cal/g polymer). These values are in close agreement with the direct calorimetric measurements reported by Beaumont *et al.*[21].

Calculation of degrees of crystallinity from the density measurements lead to much lower values than those obtained from DTA. Values for the liquid densities and coefficients of expansion for the two homopolymers considered above are given by Flory[22], whilst the crystalline densities may be computed from the crystallographic data of Fuller and Frosch[12]. Crystallinities so calculated are *ca.* 30 per cent but this estimate cannot be considered reliable because of the uncertain extrapolation used in obtaining the amorphous density. We are unable to advance adequate explanations for the great discrepancy between the results obtained by the two methods, and the true crystallinities remain in doubt. In addition to the two series of copolyesters reported here, four other series may be derived from the four homopolyesters considered. Wright[6] has reported the melting point/composition curves for these series all of which show eutectic-type behaviour: no other studies were made on these copolymers except to note that spherulites were formed throughout the composition range. By comparing the melting point/composition curves for all six series it is seen that the melting point depression is not independent of the nature of the foreign unit whereas such independence is required by the Flory equation[16]. The occurrence of cocrystallization precludes the calculation of heats of fusion of polyesters from the copolymer melting point data.

Evans, Mighton and Flory[17] reported abnormally small melting point depressions in several series of aliphatic copolyesters and considered that this was the result of partial cocrystallization. Fuller[23] had presented crystal-

lographic evidence of mixed crystal formation in the copolymer comprised of equimolar proportions of 2G10, 2G11 and 2G12 units; the melting point, however, was not reported. Insertion of bulky chain repeating units will reduce the ease of cocrystallization in polyesters: thus copolymers of ethylene terephthalate (2GT) and tetramethylene terephthalate (4GT) exhibit a eutectic melting point/composition curve but are crystalline at all compositions whereas (2GT–3GT) and (2GT–16GT) copolymers are amorphous in the middle of the composition range[24].

CONCLUSIONS

The present study substantiates earlier evidence of cocrystallization in aliphatic copolyesters. Alignment of ester groups in polar layers is not a requirement of the crystal structure and the extended chain packing characteristic of the homopolyesters is maintained in the copolymers by the polymethylene interactions. The resulting crystallites are less perfect than those in the homopolymers and bring about a drop in the melting temperature.

In agreement with Tranter[1], it is clear that considerable cocrystallization of comonomer units can occur whilst retaining the eutectic type of melting point/composition curve; unlike the copolyamide studies[1], identity of repeat length is not a requirement for cocrystallization in aliphatic polyesters.

We are indebted to Dr L. C. Spark for assistance in making the X-Ray examinations and to Mrs D. D. Clark for additional differential scanning calorimetric measurements. Experimental work by S.K. was carried out as a research project in partial fulfilment of the requirements for the B.Sc. degree in Polymer Technology.

Department of Polymer and Fibre Science,
University of Manchester Institute
of Science and Technology

(*Received November 1967*)

REFERENCES

[1] TRANTER, T. C. *J. Polym. Sci.* 1964, **A2**, 4289
[2] EDGAR, O. B. and HILL, R. *J. Polym. Sci.* 1952, **8**, 1
[3] LEVINE, M. and TEMIN, S. C. *J. Polym. Sci.* 1961, **49**, 241
[4] YU, A. J. and EVANS, R. D. *J. Amer. chem. Soc.* 1959, **81**, 5361
[5] NATTA, G. *Makromol. Chem.* 1960, **35**, 94
[6] WRIGHT, P. V. *M.Sc. Thesis*, University of Manchester, 1964
[7] CHANG, P. S., ZAVAGLIA, E. A. and BILLMEYER, F. W. *J. Paint Technol.* 1965, **37**, 235
[8] FLORY, P. J. and STICKLING, J. *J. Amer. chem. Soc.* 1940, **62**, 3032
[9] BATZER, H. *Makromol. Chem.* 1953, **10**, 13
[10] KORSHAK, V. V. and VINOGRADOVA, S. V. *Polyesters*, p 31. Pergamon: Oxford, 1965
[11] *Polymer Handbook*, edited BRANDRUP, J. and IMMERGUT, E. H. Interscience: New York, 1966
[12] FULLER, C. S. and FROSCH, C. J. *J. Amer. chem. Soc.* 1939, **61**, 2575
[13] *Landolt–Börnstein Physikalisch–Chemische Tabellen*, Vol. II, part 4. Springer: Berlin, 1961
[14] FLORY, P. J. *J. Amer. chem. Soc.* 1942, **64**, 2205
[15] MANDELKERN, L. *Crystallization of Polymers*, p 80. McGraw-Hill: New York, 1964

[16] FLORY, P. J. *Principles of Polymer Chemistry*, p 570. Cornell University Press: Ithaca, 1953
[17] EVANS, R. D., MIGHTON, H. R. and FLORY, P. J. *J. Amer. chem. Soc.* 1950, **72**, 2018
[18] KIRSHENBAUM, I. *J. Polym. Sci.* 1965, **A3**, 1869
[19] MANDELKERN, L., GARRETT, R. R. and FLORY, P. J. *J. Amer. chem. Soc.* 1952, **74**, 3949
[20] HOLDEN, H. W. *J. Polym. Sci.* 1964, **C6**, 53
[21] BEAUMONT, R. H., CLEGG, B., GEE, G., HERBERT, J. B. M., MARKS, D. J., ROBERTS, R. C. and SIMS, D. *Polymer, Lond.* 1966, **7**, 401
[22] FLORY, P. J. *J. Amer. chem. Soc.* 1940, **62**, 1057
[23] FULLER, C. S. *J. Amer. chem. Soc.* 1948, **70**, 421
[24] SCHULKEN, R. M., BOY, R. E. and COX, R. H. *J. Polym. Sci.* 1964, **C6**, 17

The Effect of Non-solvent on Association in Polyacrylonitrile Solutions

R. B. BEEVERS

In earlier papers the kinetic aspects of the association of polyacrylonitrile molecules in dimethylformamide have been determined viscometrically using benzene as non-solvent. Results are now reported for a number of other non-solvents and for acetone plus water mixtures of varying composition. Kinetic measurements are used to define the aggregation point P as the volume per cent of non-solvent required to produce a rate constant of 1×10^{-6} sec^{-1}. It is then found that there is a simple relationship with the solubility parameter δ of the non-solvent given by $100/P = (0{\cdot}80 \pm 0{\cdot}07)\,\delta - (3{\cdot}3 \pm 1{\cdot}5)$.

IT HAS been shown[1,2] that solutions of polyacrylonitrile in *N,N'*-dimethylformamide become associated on addition of a non-solvent. Association is observed to occur over a relatively narrow range of non-solvent concentrations which is in the region of 35 per cent by volume for benzene. The rate of association determined viscometrically at constant temperature was found to depend markedly on the non-solvent concentration and to a much less extent on the polymer concentration. For the polyacrylonitrile sample used ($M_n = 76 \times 10^3$) the boundary between microgel and macrogel formation occurred at a polymer concentration of approximately 1·0 g dl^{-1}. In general the logarithm of the viscosity number of the polymer solution was found to depend linearly on the time elapsed from the addition of non-solvent and allowed a rate constant k_1 to be evaluated.

In the work so far reported the general kinetic features of the association of polyacrylonitrile in dimethylformamide solution have been investigated using benzene only as non-solvent. It is now pertinent to consider the part played by the non-solvent in the association. Unpublished work by Climie[3] has shown that the concentration of non-solvent required to produce association, or the aggregation point according to Climie and White[4], is greatly affected by the choice of non-solvent. No explanation has been advanced to account for these observations. There is no correlation with the dielectric constant of the non-solvent which might be anticipated in view of the nature of the association process[2].

This is of course also a problem of considerable technological importance in its application to the wet spinning of acrylic fibres. Many aspects of the spinning process for these fibres have been examined in detail by Takahashi[5], Kambara[6] and Okamura[7]. More pertinently it has been shown that the tensile properties of the acrylic fibre can be correlated with the aggregation point of the non-solvent used in the spinning bath[8]. In the work to be reported here the number of variables has been restricted by maintaining temperature and the initial polymer concentration constant and directly examining the effect of change of non-solvent. Attention has been confined to the association process[1]. Use has been made of kinetic viscosity measurements to achieve a more satisfactory method of characterizing non-solvent

behaviour and so dispense with the somewhat arbitrary definition of an aggregation point adopted by Climie and White[4].

EXPERIMENTAL

Materials

Measurements were continued with polyacrylonitrile (W12), details of which have already been given[1]. *N,N'*-dimethylformamide was used after careful drying and distillation at room temperature. Non-solvents used were of analytical reagent grade and used directly. All concentrations make allowance for dilution by non-solvent of the stock solutions of 0·500 g dl^{-1} in dimethylformamide.

Viscometry

Viscosities were determined at 25·00° ± 0·01 °C in suspended level dilution viscometers (Polymer Consultants Ltd). The procedure for determining the time dependence of the viscosity number was unchanged and as described earlier[1]. Briefly the method involves addition of a determined amount of non-solvent to the polymer solution in the viscometer. This takes a relatively short time at the commencement of the experiment. Subsequently the solution viscosity is determined after the lapse of known periods of time up to about 8×10^4 sec. Values of t_0 were determined directly prior to each experiment. Viscometric errors were minimized by restricting kinetic measurements to values of k_1 between 10^{-6} and 10^{-4} sec^{-1}. The time of flow in the viscometer was always sufficiently long and kinetic energy corrections were not applied.

Analysis of data

The detailed analysis given previously[2] was not applied and the small amount of curvative observed has been neglected. The change in the solution viscosity number with time was found to be satisfactorily given by

$$\ln (\Phi/\Phi_0) = -k_1 t \tag{1}$$

where $\Phi = \eta_{sp}/c$ at time t and $\Phi_1 = \Phi_0$ when $t = 0$, c being the polymer concentration in g dl^{-1} corrected for addition of non-solvent and k_1 the rate constant for the association reaction[1]. Error in k_1 is approximately $\pm 3 \times 10^{-7}$ sec^{-1}. Plots of ln k_1 showed a linear dependence on the volume fraction non-solvent and the equations to fit the data were obtained by least square analysis. They were used to derive the volume per cent of non-solvent P for which k_1 had a value of 1×10^{-6} sec^{-1}. The slope of the line a was also retained as a useful characterizing parameter.

Calculation of solubility parameters for the non-solvents

Bristow and Watson[9] have made careful calculations of the solubility parameter for a large number of solvents utilized in the swelling of rubber vulcanizates from the equation

$$\delta^2 = (\Delta H - \mathbf{R}T)/V_1 \tag{2}$$

where ΔH is the heat of vaporization at temperature T and V_1 the molar volume. Values of ΔH were obtained from vapour pressure measurements

and the gas imperfection factor applied. Less accurate data are sufficient for the present work and values of ΔH at 25°C were calculated from the Hildebrand equation

$$\Delta H_{25} = 23{\cdot}7\, T_b + 0{\cdot}020\, T_b^2 - 2950 \qquad (3)$$

where T_b is the boiling point. The tables of Timmermans[10] were used to give T_b and to calculate values of the molar volume at 25°C. The adjustment of $+1{\cdot}4$ $(\text{cal/cm}^3)^{\frac{1}{2}}$ for alcohols and $+0{\cdot}5$ $(\text{cal/cm}^3)^{\frac{1}{2}}$ for ketones suggested by Burrell[11] have not been applied to the values of δ calculated from equation (2).

Calculation of solubility parameters for mixed non-solvents

Association measurements have also been carried out in acetone plus water mixtures. As the values of δ are likely to be much less reliable three methods of calculation have been followed.

(i) *From boiling point measurements*—Values of T_b were obtained by linear interpolation of the boiling point measurements of Taylor which are given by Timmermans[12] after the values had first been calculated for a pressure of 760 mm Hg. Calculation of ΔH_{25} then followed from equation (3). Molar volumes were calculated at 25°C from the weight average molecular weight and the experimentally determined density. These latter values were obtained from Timmermans[12] there being good agreement between the data of Griffiths; Sandonnini and Gerosa; and Jacobson. The solubility parameter was then calculated from equation (2).

(ii) *From the equation of Burrell*—A simple mixture rule has been used by Burrell[11] with some success in studies of the solubility of various resins in mixed non-solvents. The solubility parameter δ_{mix} was obtained from

$$\delta_{mix} = (x_1 V_1 \delta_1 + x_2 V_2 \delta_2)/(x_1 V_1 + x_2 V_2) \qquad (4)$$

where x, V and δ are the respective mole fractions, molar volumes and solubility parameters for the two constituents. In evaluating δ_{mix} use has been made of values for δ_1 and δ_2 calculated from equation (2).

(iii) *From surface tension data*—Burrell[11] has reported satisfactory calculation of solubility parameters from surface tension data using the equation

$$\delta = 4{\cdot}1\, (\gamma / V_1^{1/3})^{0{\cdot}43} \qquad (5)$$

where γ is the surface tension in dyne/cm. Examination of this relationship for the solvents listed by Bristow and Watson[9] together with interpolated values of γ at 25°C taken from Timmermans[10] shows that δ is given quite satisfactorily by

$$\delta = (1{\cdot}65 \pm 0{\cdot}31)\, (\gamma / V_1^{1/3}) \qquad (6)$$

the effect of the term $V_1^{1/3}$ being small. For interest δ has been evaluated for various acetone plus water mixtures using the measurements of Teitelbaum, Ganelina and Gortalova reported by Timmermans[12]. The results are only reliable to about 12 per cent.

RESULTS AND DISCUSSION

The dependence of viscosity on non-solvent concentration

As a prelude to the kinetic measurements changes in η_{sp}/c were observed with progressive increase in the non-solvent concentration as described previously for benzene[1]. These curves showed the same multiple hysteresis effects observed earlier and are given for a selection of the non-solvents used in *Figure 1*. The approximate centre of the time-dependent region is

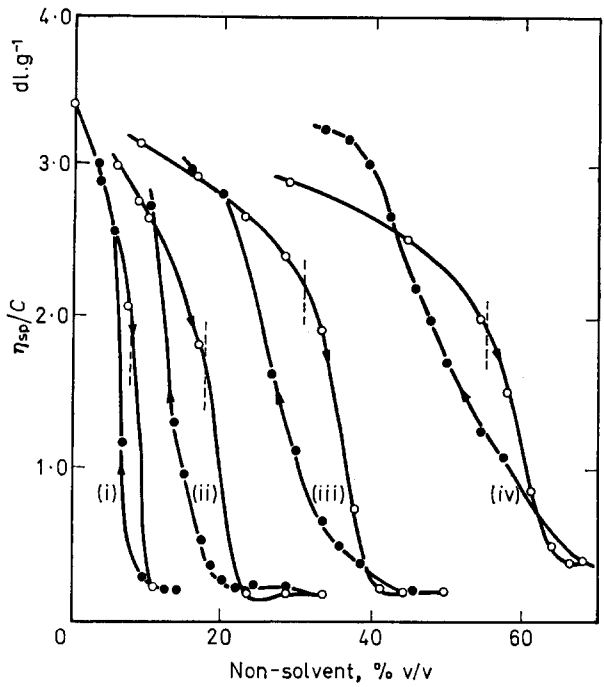

Figure 1—Changes observed in η_{sp}/c for solutions of polyacrylonitrile in dimethylformamide on the volume per cent of added non-solvent at 25°C. (i) water, (ii) ethylene glycol, (iii) toluene, (iv) acetone. ----- indicates the centre of the time-dependent region

indicated by the broken line. The width of the hysteresis loop is sufficiently wide to consider the association and dissociation reactions independently and so permit evaluation of the kinetic data from equation (1). The results for water may well be marginal in this respect and repay separate examination.

Association rate constants for a single non-solvent

Kinetic measurements for viscosity number were carried out for several non-solvents in the concentration range indicated by the broken lines in *Figure 1*. After the initial measurements the volume concentration of non-solvent was reduced so that the rate constants k_1 as determined from equation (1) were in the range 10^{-4} to 10^{-6} sec^{-1}. Values of k_1 are given in

Table 1. Dependence of the observed rate constant k_1 on the volume per cent non-solvent determined at 25°C

Non-solvent %	$10^6 k_1$ sec^{-1}	*Non-solvent* %	$10^6 k_1$ sec^{-1}	*Non-solvent* %	$10^6 k_1$ sec^{-1}	*Non-solvent* %	$10^6 k_1$ sec^{-1}
toluene		benzyl alcohol		methanol		isopropanol	
29·0	0·7	21·0	3·6	17·0	0·9	18·0	6·4
30·0	5·5	23·0	26·3	17·5	6·1	19·0	8·5
32·0	16·3	24·0	80·6	18·0	21·2	20·0	43·9
33·0	32·7	25·0	104	19·0	85·2	21·0	56·3
35·0	148			20·0	320	22·0	175
				21·0	517		
acetone		*n*-butanol		*n*-propanol		ethylene glycol	
50·0	7·5	18·0	2·2	17·0	4·7	14·0	3·8
54·0	33·9	19·0	8·4	18·0	7·6	15·0	4·2
55·0	59·7	21·0	31·1	19·0	22·5	16·0	10·2
58·0	273	23·0	165	20·0	31·6	17·0	25·0
				21·0	65·1	18·0	169

Table 1. Apart from adjustments to the amount of non-solvent the rate curves for the various non-solvents were qualitatively similar except for acetone where there was a noticeable increase in curvature. Once a few results had been obtained it was relatively easy to locate the relatively narrow time-dependent viscosity region with the first kinetic runs using a new non-solvent. Plots of ln k_1 showed a linear dependence on volume per cent non-solvent as shown for some of the data in *Figure 2*. The results for benzene obtained previously[1] are also shown and indicated by the broken line. The figure emphasizes the essential similarity of the association in the

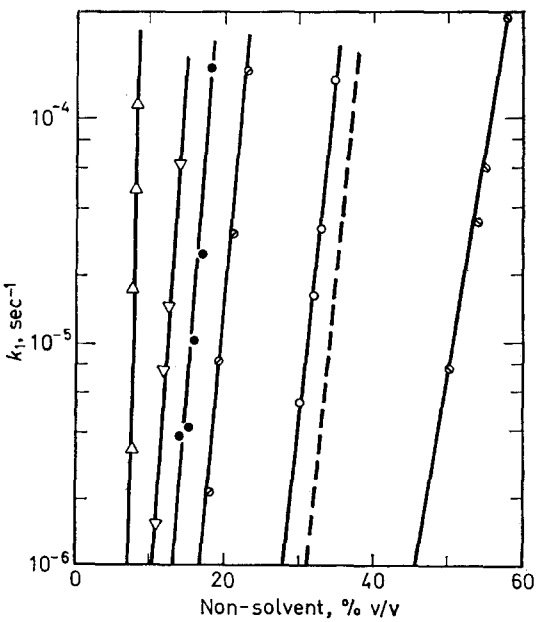

Figure 2—The effect of non-solvent on the rate of association at 25°C. △ water; ▽ 50:50 acetone plus water mixture; ● ethylene glycol; ⊘ *n*-butanol; ○ toluene; ⊘ acetone. ---- position of curve for benzene from ref. 1

polyacrylonitrile solutions brought about by the various non-solvents examined. Since the non-solvents have been chosen from various chemical types and with various hydrogen bonding capacity, as judged from the tables of Burrell[11], it is more than probable that these results give the general pattern in respect of association in polyacrylonitrile solutions.

Attention must be drawn to the neglect of the concentration dependence of k_1. A brief examination of this aspect of association has already been given[1]. Although it is expedient to make use of stock polymer solutions of constant concentration it is to be noted that dilutions are made here to give a much wider range of final polymer concentrations than when the non-solvent was restricted to benzene. The error involved is not easy to estimate since it has been observed that the concentration dependence of k_1 is not constant and may change sign when using benzene as the non-solvent[1]. Rough calculation places the error between 3 and 15 per cent.

The nature of the results shown in *Figure 2* makes it possible to consider

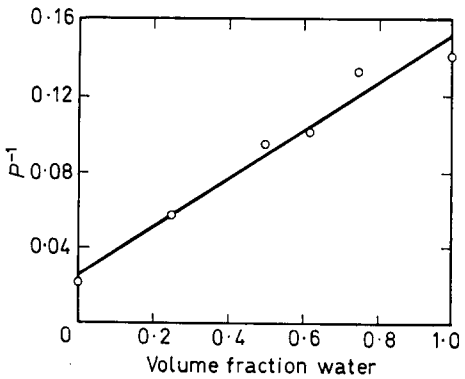

Figure 3—Dependence of P^{-1} on the volume fraction of water in the acetone plus water mixtures used to cause association at 25°C

an improved definition of an aggregation point. It is now clearly more practicable, though still arbitrary, to take the intersection on the abscissae corresponding to $k_1 = 1 \times 10^{-6}$ sec^{-1} as the volume per cent of non-solvent P which may be used to characterize the particular non-solvent. Climie and White[4] have defined the aggregation point as, 'lying between two points, namely the highest concentrations of non-solvent at which viscosity and turbidity are not time-dependent and the lowest concentrations at which they are time-dependent'. Although this is basically a kinetic definition it is rather difficult to apply in practice. The data from plots as shown in *Figure 2* have been evaluated in terms of P and the dependence of ln k_1 on the volume per cent non-solvent, a.

Rate constants for association using mixed non-solvents

In order to give more latitude to the investigation of association in polyacrylonitrile solutions a limited investigation was made of the behaviour of the system when the non-solvent was also a mixture. From *Figure 2* water and acetone were chosen since these two liquids are (i) both miscible in all proportions and with dimethylformamide, (ii) have extreme values of P as

defined above. Further interest in the use of water as one of the components stems from its use in spinning baths for acrylic fibres[5].

Association was found to be similar to that observed when using a single non-solvent. A plot showing the dependence of ln k_1 on non-solvent concentration is also included in *Figure 2* for comparison. Rate constants for the range of water plus acetone mixtures and for water only as non-solvent are given in *Table 2*. The associative properties of the water plus

Table 2. Dependence of the rate constant on the volume per cent non-solvent for various acetone plus water mixtures at 25°C

H_2O *vol. %*	*Non-solvent* %	$10^6 k_1$ sec^{-1}	H_2O *vol. %*	*Non-solvent* %	$10^6 k_1$ sec^{-1}
25	20·0	9·0	75	7·0	0·7
	21·0	14·4		8·0	1·8
	23·0	75·5		8·5	18·2
	25·0	358		9·0	75·6
50	11·0	1·6	100	7·6	3·4
	12·0	7·7		7·8	17·1
	13·0	14·1		8·0	48·8
	14·0	62·5		8·5	116
62	11·0	7·8			
	12·0	53·6			
	13·0	283			

acetone mixtures are readily predictable and show a linear dependence between the volume fraction of water and the reciprocal of the aggregation point as in *Figure 3*.

Influence of the solubility parameter on the association

The uniformity of the plots in *Figure 2* and the results obtained with water plus acetone mixtures make it necessary to forget the intrinsic chemical nature of the non-solvent, i.e. aromatic hydrocarbon or ketone, and consider a more basic interaction. In the previous papers evidence has been assembled to show that the addition of non-solvent affects the interactions between the solvent and polymer, not to the extent of bringing about precipitation, but sufficient to allow the polymer molecules to associate together to form a microgel. The nature of these intermolecular bonds is probably dipolar operating through the CN groups. It is reasonable to consider that as in the case of swelling[9] the formation of these bonds will be affected by the polymer–liquid interaction parameter χ. From a refinement of the Flory lattice treatment Huggins[13] has derived the approximate expression

$$\chi = \beta + (V_1/\mathbf{R}T)\,(\delta_a - \delta_b)^2 \tag{7}$$

where

$$\beta = (1/z)\,(1 - 1/m) \tag{8}$$

z being the lattice coordination number, m the chain length of the polymer and δ_a and δ_b the solubility parameter of the liquid and polymer respectively. For polyacrylonitrile a value of $\delta_b = 15{\cdot}4$ $(cal/cm^3)^{\frac{1}{2}}$ is often cited[11,14] but this may be unreliable and could well be lower. Calculation of the solubility parameter for dimethylformamide from equations (2) and (3)

gives $\delta_a = 11{\cdot}9$ (cal/cm^3)$^{\frac{1}{2}}$. The addition of non-solvent will vary the value of δ_a and χ will have a minimum value when $\delta_a \cong \delta_b$. In these polyacrylonitrile solutions association will be brought about more rapidly, that is the value of P will be lower, in mixed liquids of high δ_a. It would therefore appear reasonable to expect a relationship between δ the solubility parameter of the non-solvent component of the liquid mixture and the reciprocal value of *P*.

(1) *Single non-solvent*—The derived data from *Table 1* giving values of *P* and the slope of the plots in *Figure 2* together with calculated values of *a* for the various non-solvents used is given in *Table 3*. *Figure 4* shows a

Table 3. Derived parameters for various non-solvents at 25°C.
B, Burrell ref. 11; BW, Bristow and Watson ref. 9

Non-solvent	*P*	*a*	δ (*cal/cm*^{3})$^{\frac{1}{2}}$		
	%		*Calc.*	*B*	*BW*
toluene	28·7	0·36	8·92	8·9	8·91
benzene	31·1	0·34	9·05	9·2	9·15
acetone	45·8	0·20	9·32	10·0	9·71
n-butanol	16·8	0·36	9·77	11·4	
isopropanol	16·0	0·37	9·81	11·5	
n-propanol	14·7	0·29	10·3	11·9	
benzyl alcohol	19·4	0·38	10·9		
methanol	16·5	0·68	12·9	14·5	
ethylene glycol	13·1	0·41	14·7	14·2	

plot of these data using the values of δ calculated from boiling point data and includes results obtained with water. This demonstrates a linear relationship between δ and $1/P$ given by

$$100/P = (0{\cdot}80 \pm 0{\cdot}07)\,\delta - (3{\cdot}3 \pm 1{\cdot}5) \qquad (9)$$

Calculated values of δ are reasonably close to those of Bristow and Watson[9] and also to those given by Burrell[11] when allowance has been made for the corrections applied by him. The three non-solvents, *n*-butanol, iso-

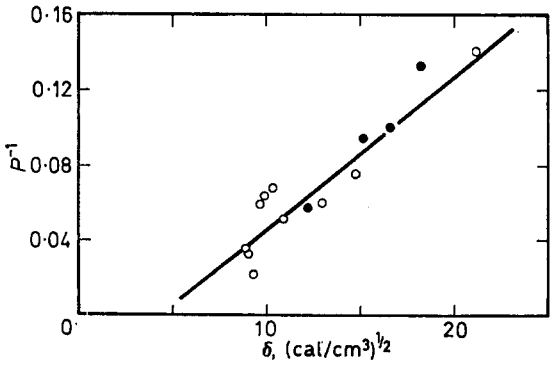

Figure 4—The dependence of P^{-1} on the solubility parameter of the non-solvent. ○ single non-solvents; ● acetone plus water mixtures

propanol and *n*-propanol fit more satisfactorily to the curve if Burrell's correction is applied but this would have the opposite effect for ethylene glycol and benzyl alcohol. The result for acetone falls below the curve and in view of previous remarks may be of doubtful value. *Figure 4* shows that considerable reliance is placed on the result for water. The solubility parameters for the majority of non-solvents fall between 7 and 10 $(cal/cm^3)^{\frac{1}{2}}$ with the alcohols extending the range to about 16 $(cal/cm^3)^{\frac{1}{2}}$. It is tacitly assumed that the higher values of δ for the alcohols and the very high value for water compensate for the well known colligative properties of these liquids. In order to strengthen the results shown in *Figure 4* measurements were carried out using mixed non-solvents of acetone plus water.

(ii) *Mixed non-solvents*—The corresponding data obtained from *Table 2* are given in *Table 4* with various calculated values of δ. When plotted in *Figure 4* as closed circles taking values of δ obtained from equation (4) these results strengthen the evidence for a linear dependence as given by equation (9). Values of the slope a show a regularity which is not so clear from the corresponding values in *Table 3*. The apparently low value of 0·20 for acetone fits in well with these results, and places more confidence in the results for this non-solvent.

Table 4. Derived parameters for non-solvent mixtures of acetone and water

Acetone % *v/v*	*P* %	*a*	$\delta\ (cal/cm^3)^{\frac{1}{2}}$		
			eqn (2)	*eqn (4)*	*eqn (6)*
0	7·10	1·57	21·2	—	—
25	7·47	1·15	16·0	18·2	22
38	9·85	0·79	14·4	16·7	19
50	10·5	0·51	13·2	15·2	16
75	17·3	0·33	11·2	12·3	12

The dependence of the slope a on P as given in *Tables 3* and *4* indicates that the curves given in *Figure 2* must yield a finite value of the rate constant in the absence of non-solvent. Examination of the data reveals, as far as can be judged over a long extrapolation, that the rate constant plots diverge from a common value of k_1 having a value between 10^{-15} and 10^{-12} sec^{-1}. Solutions of polyacrylonitrile in dimethylformamide are therefore unstable and should show association and possibly precipitation when stored over long periods[15].

The concept of solubility parameter is not easy to understand and especially in polymer plus liquid interactions. Small[16] has achieved some success in the calculation of δ from group molar attraction constants which have been derived in a similar manner to molar refractivities. Bristow and Watson[9], however, find that values of δ derived from swelling and viscosity measurements show a significant difference of about ten per cent, and demonstrate that the value of δ can only serve as a useful guide to polymer plus liquid interactions. The result given by *Figure 4* clearly underlines the significance of δ to the association in polyacrylonitrile solutions in dimethylformamide and shows that the onset of association can be readily controlled by adjustment of the value of δ using mixed liquids.

Acknowledgement is made to Miss F. Sutcliffe and Mrs. L. Hartley for experimental assistance and to Mr B. Armitage for some preliminary measurements.

University of Bradford,
Bradford 7

(*Received November 1967*)

REFERENCES

[1] BEEVERS, R. B. *Polymer, Lond.* 1967, **8**, 419
[2] BEEVERS, R. B. *Polymer, Lond.* 1967, **8**, 463
[3] CLIMIE, I. E. Unpublished results, 1960
[4] CLIMIE, I. E. and WHITE, E. F. T. *J. Polym. Sci.* 1960, **47**, 149
[5] TAKAHASHI, M. *Sen-i Gakkaishi,* 1961, **18**, 655
[6] KAMBARA, S., KATAYAMA, S. and KITAGAWA, H. *Kobunshi Kagaku,* 1951, **8**, 543
[7] OKAMURA, S. and YAMASHITA, T. *J. Soc. Textile Cell. Ind. (Japan),* 1950, **6**, 505
[8] BEEVERS, R. B. *J. appl. Polym. Sci.* 1965, **9**, 1499
[9] BRISTOW, G. M. and WATSON, W. F. *Trans. Faraday Soc.* 1958, **54**, 1731, 1742
[10] TIMMERMANS, J. *Physico-chemical Constants of Pure Organic Compounds.* Elsevier: New York, 1950
[11] BURRELL, H. *Interchem. Rev.* 1955, **14**, 3, 31
[12] TIMMERMANS, J. *The Physico-chemical Constants of Binary Systems in Concentrated Solutions,* Vol. 4. Interscience: New York, 1960
[13] HUGGINS, M. L. *J. chem. Phys.* 1941, **9**, 440
[14] WALKER, E. E. *J. appl. Chem.* 1952, **2**, 470
[15] Acknowledgement is made to the referees for drawing attention to the existence of a finite rate constant in the absence of non-solvent and the consequences of this in terms of the stability of the original polymer solution.
[16] SMALL, P. A. *J. appl. Chem.* 1953, **3**, 71

Fractionation of Low Molecular Weight Polymers by Dialysis

P. I. BREWER

The application of dialysis in non-aqueous solvents using rubber membranes to the fractionation of polymers has been investigated. It was found that provided the bulk of the polymer had a molecular weight of less than 10 000 it could be separated into fractions of differing molecular weight. Very little fractionation of the components with a molecular weight of greater than 10 000 was obtained. The molecular weights of the fractions must be determined by conventional methods. The method is simple to carry out but the fractionation efficiency is not high.

DIALYSIS has been used extensively for the separation of water soluble polymers of biochemical interest. Craig and Konigsberg[1] showed that it was possible to alter the porosity of cellulose membranes and they used these modified membranes to fractionate polymers in aqueous solution.

Few papers have been published dealing with the fractionation of polymers in non-aqueous solution by dialysis. Green, Hookway and Vaughan[2] fractionated polystyrene in toluene solution using methoxymethylnylon membranes. An apparatus for the continuous fractionation of polymers by dialysis has been described by Vink[3]. Using commercially available cellulose membranes of graded porosity he was able to fractionate 1 to 2 g of various high molecular weight polymers.

Brintzinger and Gotze[4] used rubber membranes to separate hydrophilic and colloidal substances from organophilic substances. Boldingh, van Beers and de Jongh[5] found that they could separate phospholipids from other lipids using a finger cut from a rubber glove; phospholipids form micelles in non-polar solvents and did not permeate through the rubber. Surgeons' finger-cots were used by Hill and Munsell[6] for the separation of various petroleum products into high and low molecular weight fractions. Rubber balloons were used for the same purpose by Jenkins and Humphreys[7]. They showed that useful separations of petroleum additives could be obtained by altering the time of dialysis. Reviews of methods of separation based on dialysis have been published by Carr[8] and by Craig[9].

Surgeons' finger-cots made of natural rubber were used for the work described in this paper. When used with solvents that swell the rubber, they are more permeable to the solvent than are cellulose membranes. Their shape enables a simple glass Soxhlet type of extractor to be used. It was found possible to modify the porosity of the rubber and to use these modified membranes to fractionate low molecular weight polymers.

EXPERIMENTAL

The apparatus used was a modified Soxhlet extractor fitted with a water jacket. The inner diameter of the extractor was 5 cm and the position of

the liquid return tube was such as to give a height of liquid in the extractor of about 9 cm. This liquid return tube extended to within about 1 cm of the bottom of the extractor; where it passed through the water jacket its diameter was increased to prevent syphoning. The finger-cot was held in position by means of a tube about 8 mm internal diameter and 60 cm long passing through the condenser. A B19 socket was fused to the bottom of the tube: The finger-cots found to be most suitable for this work were obtained from Louis Gilder & Co., 44 Bedford Row, London W.C.1 (catalogue number 818-large). They were stored under nitrogen before use. After being rinsed several times with the solvent a finger-cot was fastened to the B19 socket on the holder by means of glass tape. It was essential that the tape was wound sufficiently tight to give a leak-free seal as appreciable osmotic pressures sometimes developed. The holder was held in position by means of a spring clip resting on top of the condenser. The position of the holder in the clip was adjusted so that the rubber was just covered by liquid in the extractor. The temperature of dialysis could be modified by passing cold water through the jacket or by using the jacket as an air-bath. In the former case, the temperature varied between 15° and 20°C. When used as an air-bath, the temperature depended on the boiling point of the solvent; with *n*-heptane it varied between 60° and 70°C.

About 5 g of sample dissolved in 25 ml of solvent was passed down the holder into the finger-cot. The 500 ml flask containing the solvent was then heated at such a rate that solvent circulated through the apparatus. After a certain time, usually 24 hours, the polymers in the flask and finger-cot were recovered by evaporating the solvent under nitrogen on a water-bath and then heating under vacuum.

Boiling under reflux in pyridine was found to increase the porosity of the rubber. Usually finger-cots of two different porosities were prepared by boiling for $7\frac{1}{2}$ and 15 h. This treatment weakened the finger-cots and it was necessary to handle them with care; after preparation they were stored under *n*-heptane until required. The porosity of the finger-cots was decreased by immersing them for eight minutes in a five per cent sulphur chloride solution in *n*-heptane, and then storing in the same solvent. After this treatment the finger-cots became rather brittle and care was necessary when attaching them to the support.

The molecular weight distributions of the original polymer and fractions were determined by means of a Waters' gel permeation chromatograph (GPC). It was assumed that there was no change in refractive index of the polymer with molecular weight. The instrument was calibrated by means of polystyrenes with narrow molecular weight distributions and known molecular weights. The molecular weights of the distributions were expressed in terms of extended chain length in Ångström units.

Number average molecular weights were determined by means of the Mechrolab vapour pressure osmometer (VPO) using toluene as solvent at a temperature of 65°C. The instrument was calibrated with zone-refined benzil. The corrected molecular weights were obtained by extrapolating the reciprocals of the apparent molecular weights to zero concentration. The repeatability of a determination was about ± 5 per cent.

The low molecular weight polymers with narrow distributions which were used to investigate the properties of the rubber membranes are listed in *Table 1*.

Table 1. Substances used to investigate the properties of rubber membranes

Substances	*Number average molecular weight by VPO*
Polypropylene glycols	
PPG 4 000	$3{\cdot}7\times10^3$
PPG 3 000	$2{\cdot}9\times10^3$
PPG 2 000	$2{\cdot}1\times10^3$
PPG 1 000	$9{\cdot}9\times10^2$
PPG 425	$4{\cdot}3\times10^2$
PPG 150	$1{\cdot}7\times10^2$
Polybutadiene	$6{\cdot}8\times10^3$
Polybutadiene	$9{\cdot}9\times10^3$

RESULTS

Variation of the amount dialysed with time

If it is assumed that the concentration of the solute in the liquid surrounding the finger-cot is zero it can be shown that the equation connecting

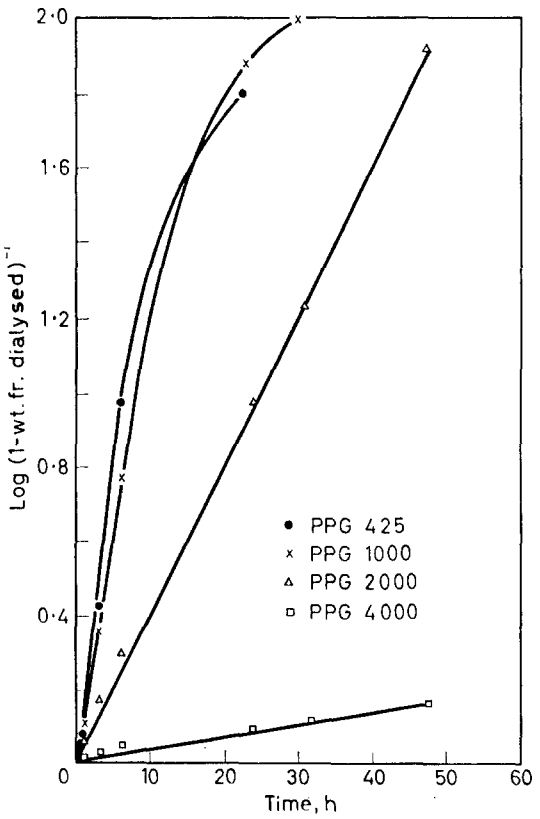

Figure 1—Variation of log $(1-\text{wt fr. dialysed})^{-1}$ with time for polypropylene glycols in *n*-heptane at 60° to 70°C

the amount of substance dialysed with time is

$$\ln (1 - \text{wt fr. dialysed in time } t)^{-1} = P\,At/lV \qquad (1)$$

where A denotes area of membrane, l is thickness of membrane, V is volume of liquid in finger-cot, t is time of dialysis, and P is the permeability coefficient of the substance. Thus a plot of log (1 – wt fr. dialysed)$^{-1}$ in time t against time for a particular substance should give a straight line; such plots for some polypropylene glycols are shown in *Figure 1*. Deviations from linearity are probably due to experimental inaccuracy and also to the fact that the polyglycols have a small but significant spread in molecular weight.

Variation of the permeability coefficient with composition of solute

In a previous paper[10] dealing with the chromatographic separation of substances on a column packed with small particles of rubber, it was shown that molecular size rather than chemical composition was the important factor in determining the elution volume of a substance. As the mechanism of separation involved in this chromatographic technique is similar to that involved in dialysis it is likely that molecular size rather than chemical composition is also the important factor in dialysis.

Variation of the amount dialysed with the initial weight of substance

The effect of the amount of substance taken on the amount dialysed in a given time was not investigated. Usually the initial weight was 5 g which was dissolved in about 25 ml of the solvent. In some instances the weight of sample taken was governed by the osmotic pressure that developed during dialysis. If this was sufficient to burst the finger-cot, the experiment was repeated using a smaller sample.

Variation of the permeability coefficient with the composition of the solvent

It would be expected that the more the solvent swelled the rubber the greater would be the permeability of the rubber. This is supported by the data given in *Table 2* which shows the amount of PPG 4 000 dialysed in 24 hours at 15° to 20°C, using various solvents. The solvent viscosity has also been included in the table; as the permeability coefficient decreases the viscosity increases.

Table 2. Effect of composition of solvent on the dialysis of PPG 4 000

Solvent	*Volume fraction of solvent in the swollen rubber*	*Viscosity at 20°C cP*	*Weight fraction dialysed in 24 h*
Methyl ethyl ketone	0·34	0·48	0·08
n-Heptane	0·66	0·41	0·12
Toluene	0·80	0·59	0·17

A variety of organic solvents can be used with rubber membranes. In the work on polymer fractionation described in this paper *n*-heptane was used. Aromatic solvents tended to make the rubber rather weak and if an appreciable osmotic pressure developed the finger-cots often burst.

Effect of temperature on the permeability coefficient

The effect of temperature on dialysis is shown in *Figure 2*. Increasing the temperature from 15°–20°C to 60°–70°C was equivalent to decreasing the dialysis time by a factor of about two or three.

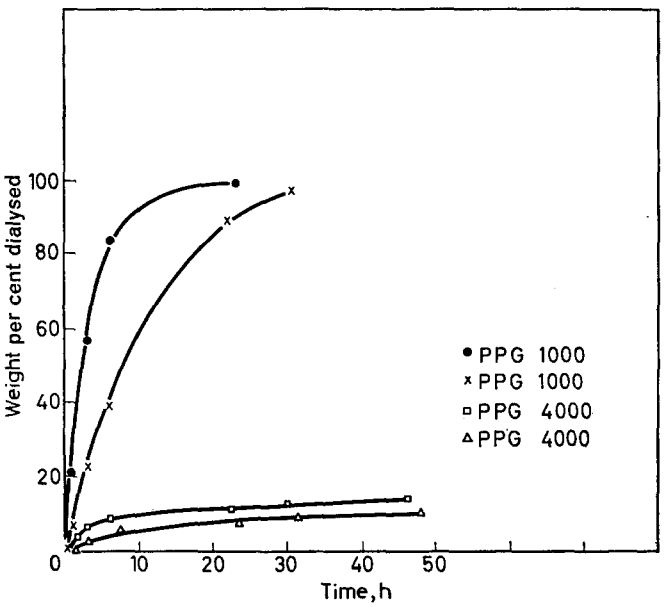

Figure 2—Effect of temperature on the dialysis of polypropylene glycols. ● 60°–70°C, solvent *n*-heptane, ×15°–20°C, solvent *n*-heptane, □ 60°–70°C, solvent methyl ethyl ketone, △ 15°–20°C, solvent methyl ethyl ketone

Variation of the permeability coefficient with molecular weight

The relations between the amount dialysed in 24 h and the molecular weight for finger-cots of different porosities are shown in *Figure 3*.

The variation of the permeability coefficient with molecular weight, M, can be written in the form

$$P \propto M^{a} \qquad (2)$$

When a membrane is absent, the permeability coefficient becomes equal to the diffusion coefficient and the exponent a has the value of about $-0{\cdot}5$ for low molecular weight compounds[11], and about $-0{\cdot}5$ to $-0{\cdot}6$ for polymers[12]. The value of a decreases in the presence of a membrane; Kuhn and Schultz[13] found values of a between $-2{\cdot}4$ and $-2{\cdot}9$ for the permeation of polymethylmethacrylate fractions dissolved in butanone through cellulose membranes.

It will be seen from equation (1) that log (1 − wt fr. dialysed in 24 h)$^{-1}$ is proportional to the permeability coefficient so that a plot of log [log (1 − wt fr. dialysed in 24 h)$^{-1}$] against log M can be used to obtain the value of a.

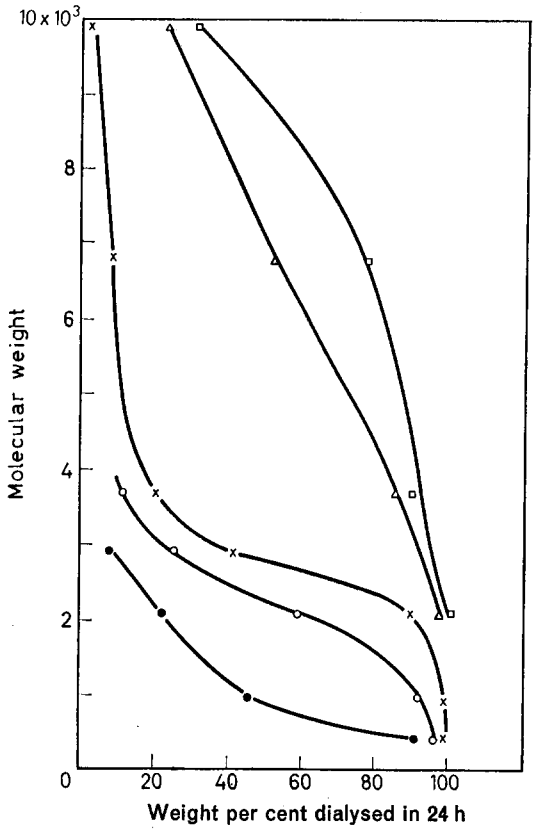

Figure 3 — Variation of amount dialysed in 24 h with molecular weight using *n*-heptane as solvent: ● 15°–20°C, finger-cot treated with S_2Cl_2; ○ 15°–20°C, finger-cot untreated; × 60°–70°C, finger-cot untreated; △ 60°–70°C, finger-cot treated with pyridine 7½ h; □ 60°–70°C, finger-cot treated with pyridine 15 h

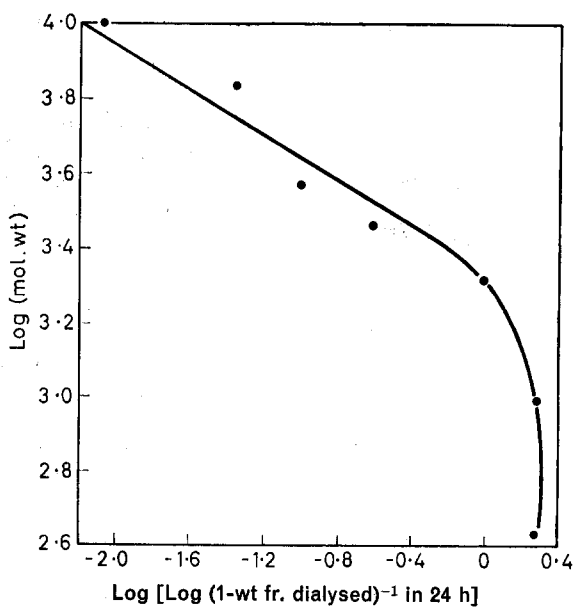

Figure 4—Variation of log [log (1—wt fr. dialysed in 24 h)$^{-1}$] with log (mol. wt) using untreated finger-cots with *n*-heptane at 60°–70°C

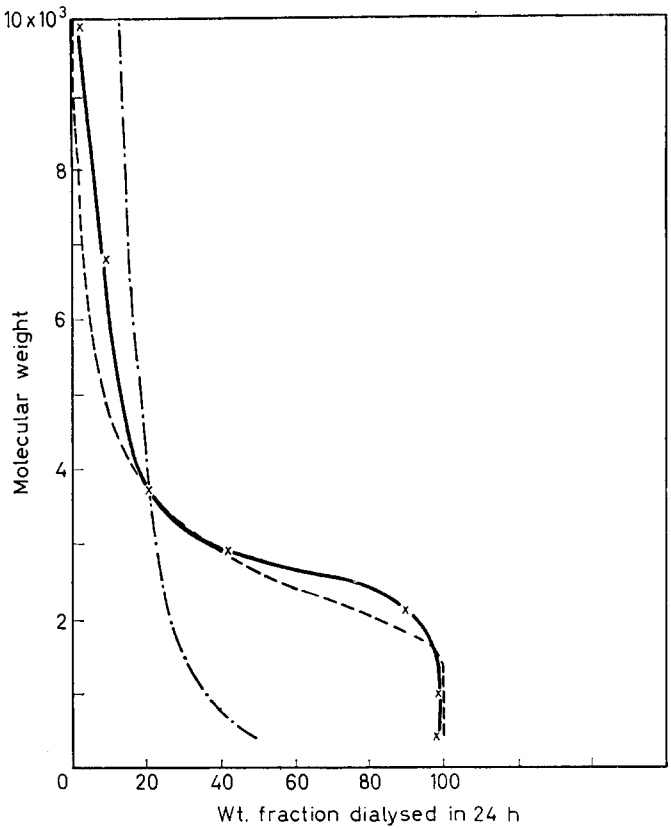

Figure 5—Variation of amount dialysed with mol. wt using untreated finger-cots with *n*-heptane as solvent at 60°–70°C. Full line: experimental curve. Dashed line:, calculated from $P \propto M^{-3\cdot4}$. Chain dotted line: calculated from $P \propto M^{-0\cdot5}$

It will be seen from *Figure 4* that as the molecular weight increases a decreases. It reaches an approximately constant value of $-3{\cdot}4$ above a molecular weight of about 3 000. The curves showing the relation between the amount dialysed in 24 h and molecular weight calculated by substituting $P \propto M^{-3\cdot4}$ and $P \propto M^{-0\cdot5}$ in equation (1) are shown in *Figure 5*.

The experimental curve is also plotted on this figure. The two calculated curves have been made to coincide with the experimental curve at a molecular weight of 3 700. The curve calculated from $P \propto M^{-3\cdot4}$ is in reasonable agreement with the experimental curve. The relation $P \propto M^{-0\cdot5}$ would be applicable in the absence of a membrane or in the presence of a very porous membrane such as a sintered glass thimble. The degree of separation obtained under these conditions would be poor.

Applications

Two samples of polyisobutene and a sample of a styrene–butadiene copolymer were then fractionated by dialysis. In each case the following

Wt of sample taken = 10·0 g

Solvent: *n*-heptane
Membrane: finger-cot, crosslinked sulphur chloride
Conditions: 15° to 20° C, 24h

Dialysate
Fraction 1

Residue
Solvent: *n*-heptane
Membrane: finger-cot
Conditions: 15° to 20° C, 24h

Dialysate
Fraction 2

Residue
Sotvent: *n*-heptane
Membrane: finger-cot
Conditions: 60° to 70° C, 24h

Dialysate
Fraction 3

Residue
Solvent: *n*-heptane
Membrane: finger-cot, 7½ h boiling pyridine
Conditions: 60° to 70° C, 24h

Dialysate
Fraction 4

Residue
Fraction 5

Figure 6—Fractionation of polyisobutene A

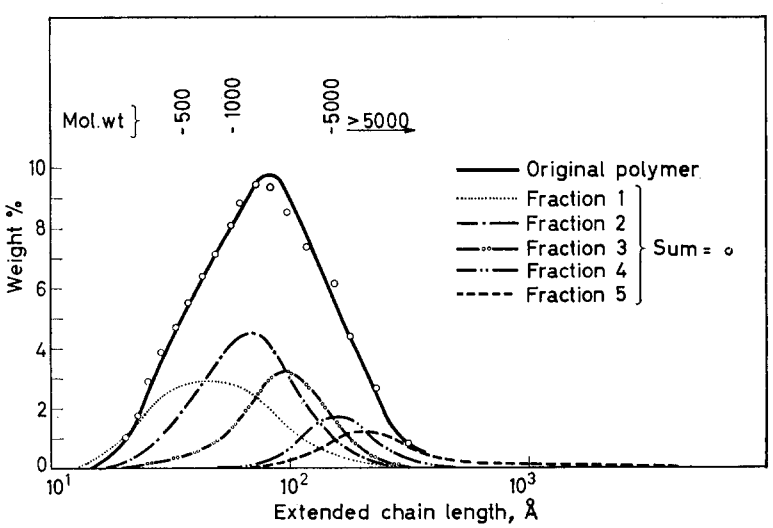

Figure 7—GPC elution curves of polyisobutene fractions from polyisobutene A

data are given:
1. The fractionation scheme.
2. The GPC elution curves of the original polymer and the fractions.

Table 3. Results of fractionation of polyisobutene A

Fraction	*Wt %* (*normalized*)	$\overline{M}_n$ *VPO*	$\overline{M}_w/\overline{M}_n$ *GPC*
1	31·8	600	1·3
2	36·5	920	1·2
3	20·3	1 250	1·2
4	6·7	3 700	1·1
5	4·7	5 800	1·2
Original sample		911	1·4

Loss during fractionation, one per cent.
Number average molecular weight calculated from fractionation data, 894.

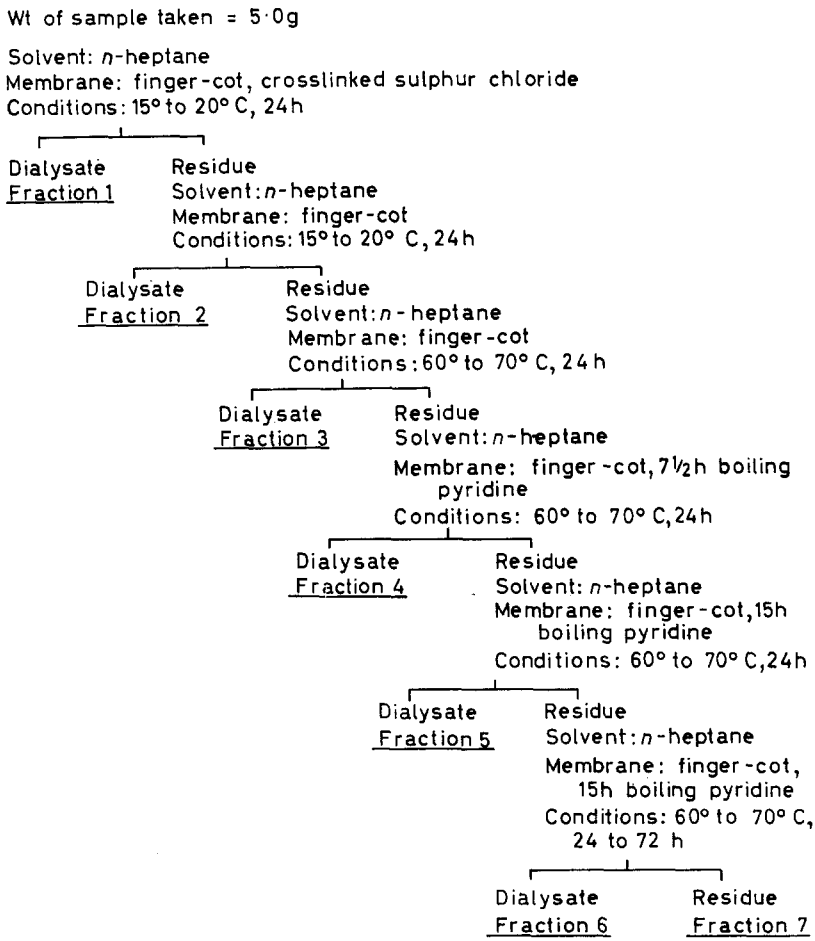

Figure 8—Fractionation of polyisobutene B

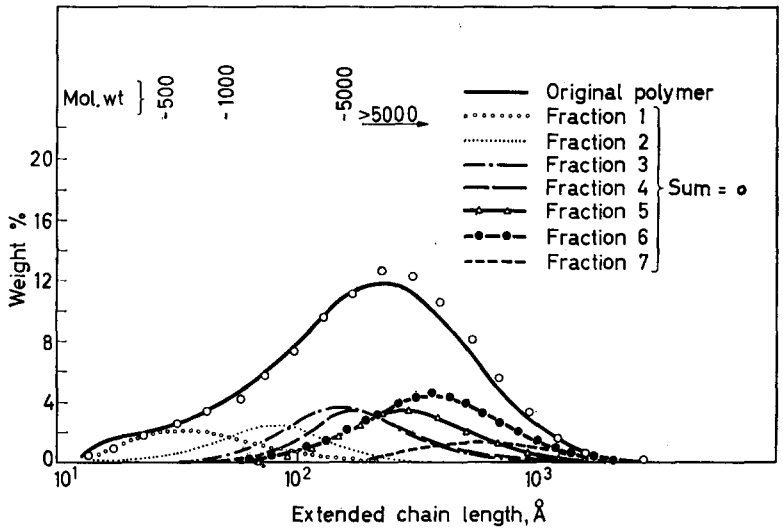

Figure 9—GPC elution curves of polyisobutene fractions from polyisobutene B

Table 4. Results of fractionation of polyisobutene B

Fraction	*Wt %* (*normalized*)	$\overline{M}_n$ *VPO*	$\overline{M}_w/\overline{M}_n$ *GPC*
1	9·5	680	1·3
2	10·4	1 400	1·3
3	18·6	3 700	1·4
4	13·7	5 000	1·4
5	17·5	8 300	1·4
6	24·3	9 900	1·4
7	6·1	11 900	1·3
Original sample		3 100	2·6

Loss during fractionation, 0·2 per cent.
Number average molecular weight calculated from the fractionation data, 2 900.

3. The number average molecular weights of the original polymers and fractions determined by means of the vapour pressure osmometer.
4. The number average molecular weight of the original polymer, calculated from the number average molecular weights of the fractions.
5. The loss incurred during the fractionation.

DISCUSSION

Although the apparatus used in this work was convenient for polymer fractionation it was not very satisfactory for measuring the effect of various parameters on dialysis. The temperature control was poor and the liquid in the finger-cot was not stirred. It was also found that the thickness of the rubber varied considerably in individual finger-cots. Samples containing a large proportion of high molecular weight material often generated high osmotic pressures that caused finger-cots to expand and sometimes burst.

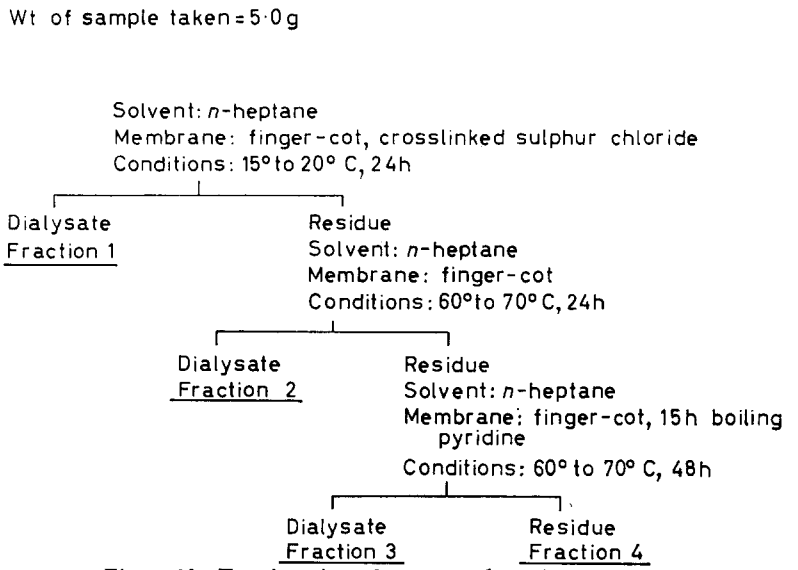

Figure 10—Fractionation of a styrene–butadiene copolymer

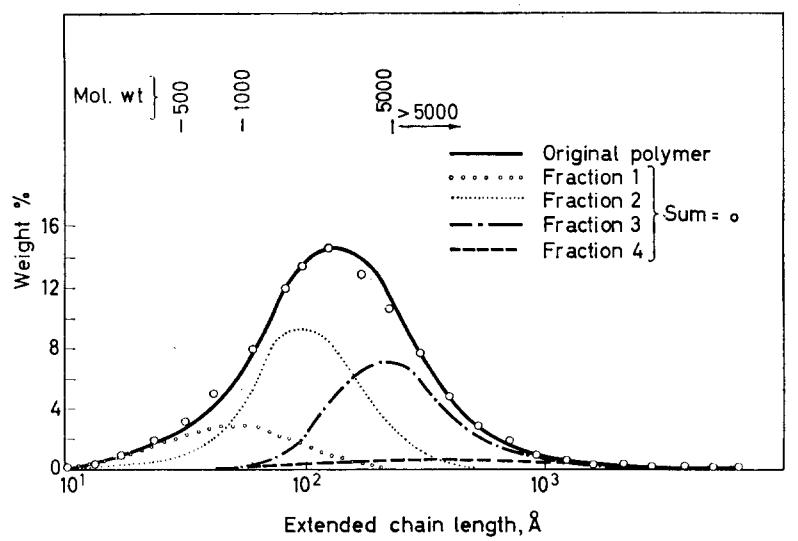

Figure 11—GPC elution curves of fractions from a styrene-butadiene copolymer

Several methods were tried to increase the porosity of the rubber. These included heating to different temperatures and also immersing in various liquids followed by solidification of the liquid by cooling. It was eventually found that the most effective method was to immerse the finger-cots in boiling pyridine for varying periods. This treatment could be continued for about 15 h: after this time the finger-cots became too weak to handle.

The fractionation scheme used for a particular polymer depended on the number of fractions required and on the molecular weight distribution

Table 5. Results of fractionation of a styrene–butadiene copolymer

Fraction	*Wt %* (*normalized*)	$\overline{M}_n$ *VPO*	$\overline{M}_w/\overline{M}_n$ *GPC*
1	15·5	746	1·4
2	44·1	1 900	1·3
3	36·0	4 020	1·5
4	4·3	5 000	2·4
Original sample		1 830	2·1

Loss during fractionation, 4·4 per cent.
Number average molecular weight calculated from fractionation data, 2 300.

of the polymer. It was usually found to be convenient to keep the dialysis time constant and to vary the temperature or the porosity of the membrane. As the pore size of the rubber was not uniform the molecular weight of the fractions depended on the molecular weight distribution of the original polymer. It was therefore not possible to calculate the molecular weights of the fractions from the conditions of dialysis.

In the examples given the average value of M_w/M_n for the fractions varied from 1·1 to 2·4 depending on the breadth of the distribution of the original polymer. The highest molecular weight fraction that permeated through the most porous rubber finger-cot was obtained from polyisobutene B. This had a number average molecular weight of 9 900. Thus, the method is only applicable to low molecular weight polymers. It is also useful for separating the low molecular weight components of a high molecular weight polymer before commencing fractionation by other methods.

The author wishes to thank Mr P. O'Connor for technical assistance in some phases of the work.

Esso Research Centre,
Abingdon, Berkshire

(*Received November 1967*)

REFERENCES

[1] CRAIG, L. C. and KONIGSBERG, J. *J. phys. Chem.* 1961, **65,** 166
[2] GREEN, J. H. S., HOOKWAY, H. T. and VAUGHAN, M. F. *Chem. & Ind.* **1958,** 862
[3] VINK, H. *Arkiv Kemi,* 1962, **19,** 531
[4] BRINTZINGER, H. and GOTZE, M. *Chem. Ber.* 1948, **81,** 293
[5] BOLDINGH, J., VAN BEERS, G. J. and DE JONGH, H. *Essential Fatty Acids,* edited by H. M. SINCLAIR. Butterworths: London, 1958
[6] HILL, M. W. and MUNSELL, M. W. Preprint, Division of Petroleum Chemistry, 138th American Chemical Society Meeting, September 1960
[7] JENKINS, G. I. and HUMPHREYS, C. M. A. *J. Inst. Petrol.* 1965, **51,** 1
[8] CARR, C. W. *Physical Methods in Chemical Analysis,* Vol. IV, edited by W. G. BERL. Academic Press: New York, 1961
[9] CRAIG, L. C. *Science,* 1964, **144,** 1093
[10] BREWER, P. I. *Polymer, Lond.* 1965, **6,** 603
[11] DAVSON, H. and DANIELLI, J. F. *Permeability of Natural Membranes.* Cambridge University Press: London, 1952
[12] ENDE, H. A. *Polymer Handbook,* edited by J. BRANDRUP and E. H. IMMERGUT. Interscience: New York, 1965
[13] KUHN, W. H. and SCHULZ, G. V. *Makromol. Chem.* 1961, **50,** 52

Book Reviews

Practical Toxicology of Plastics

R. LEFAUVE. English edition edited by P. P. HOPF. Iliffe: London. 580 pp. 135*s*

THIS book was originally published in Paris (1964). The present edition opens with a treatment of the chemistry of high polymers and the toxicology of the macromolecules. Evidence concerning the non-toxic nature of high polymers is carefully assembled according to the mode of entry into the human body.

A second part deals with industrial toxicology and the dermatoses and gathers together many conclusions about health and safety. The chemical, physical and pharmacological properties of the principal monomers and the main materials used for condensation processes are set out clearly with extensive references to the literature. The dermatoses are surveyed in two sections, one dealing with occupational conditions and the other with effects due to contact with finished articles: irritant and sensitizing actions are distinguished and risks attributable to different categories of ingredients—plasticizers, catalysts, emulsifiers, etc., are separated. Safety is considered both in relation to operations in large factories and in smaller conversion workshops. A good section on protection for the individual worker is followed by an account of inflammability of plastics and fire-proofing. An appendix summarizes a great deal of information on toxic gases, vapours, toxic dusts, smokes and fogs.

The third part of the book is concerned with medical and surgical plastics and with macromolecular compounds suitable for injection into the human body. The review of the different substances that can be used as substitutes for human plasma includes naturally-occurring substances like dextran as well as synthetic compounds. Quotations are made from the British Pharmaceutical *Codex* concerning ligatures and sutures and there are relevant excerpts from the French *Codex* (1949).

The fourth section deals with food toxicology, firstly with monomers and additives and secondly with plastics in the food industry. The account of monomers gathers together facts on 13 important types of ingredient and the information about plasticizers and stabilizers is very well presented. Anti-oxidants, surface-active compounds and some catalysts are listed and described. The use of plastics in the food industry raises many problems of migration from container or wrapping material to food. Equally important in the use of plastics as packaging materials is the special part they play in respect of regulating permeability to gases, water, vapour, organic vapours and odours and prolonging the shelf life of foods.

A wide range of possible constituents is necessary for the realization of sophisticated technological goals although many flexible wrappings need not be in immediate contact with the food. Finished products usually contain small residues of manufacturing additives, catalysts, decomposition products and machining additives. The book goes into a diversity of cases and the problem of solubility is discussed in detail.

Appendices (120 pages) summarize legislation in different countries and the American situation is dealt with faithfully. There is evidence that although the whole world is enormously indebted to the U.S.A. for pioneer work on food packaging control, there is some disarray through over-regulation. No country has yet solved the problems of legislative control. As soon as a risk becomes indubitable it is likely to be abolished and legislation should aim at the discovery of hazard as much as the enforcement of regulation.

This book is an excellent and notably timely compilation.

R. A. MORTON

Film Forming Compositions

Volume I, Part 1

Edited by R. R. MYERS and J. S. LONG. Arnold: London, 1967. 6 in. by 9 in. 564 pp. 315*s*

A *Treatise on Coatings* is planned in twelve volumes; the first volume on *Film Forming Compositions* will appear in three parts of which Part 1 only is reviewed here. The whole work is intended to replace that edited by MATIELLO and well-known to all coating technologists. It is not clear how many parts subsequent volumes will appear in nor what their arrangement will be. However, at 15 guineas per part the complete work will clearly cost at least 210 guineas!

The thirteen chapters of Part 1 cover acrylic emulsions, acrylic resins, alkyd resins, asphalt coatings, chlorinated rubber, driers, epoxy resins, hydrocarbon resins, hydrocarbon solvents, natural resins, polyethers and polyesters, urethane coatings and vehicle manufacturing equipment. It is an odd selection, in view of the title of Part 1; in addition I would have thought it better to have grouped like topics together, for example emulsion polymers of all types, so that a common introduction to the scientific background etc. would have sufficed.

As it is, the scientific background to the technology is woefully thin or completely lacking throughout Part 1. To give examples, there is no mention of the kinetics of emulsion polymerization, nor even a reference to the pioneering work of HARKINS and SMITH and EWART in this field. The chapter on driers virtually omits any reference to the mechanism(s) of formation of an insoluble film by autoxidative crosslinking from an unsaturated resin or to modern theories of the role of transition metals as oxidation catalysts. The chapter on alkyds is grossly misleading in my view; thus on page 72, it is said that 'the main function of the dibasic acid appears to be one of linking polyol units into a linear structure' and the diagrams at the bottom of page 75 repeat this suggestion. Gelation as a property of such resins is mentioned, of course, but nowhere is it brought out that the essential properties of alkyd resins depend on the fact that they are highly branched and not linear structures. There are no references to the works of P. J. FLORY and W. H. STOCKMEYER in this field.

There is a great deal of sound technological information in Part 1 but most of it is already available in manufacturers' literature and it tends to have a bias towards individual suppliers. Moreover, the balance of the work is disturbing. For example, the chapters on acrylic emulsions, alkyd resins and driers occupy 34, 26 and 11 pages respectively, whereas chlorinated rubber gets 78 pages; this hardly reflects the relative importance of the topics to the coating industry. It would appear that the editors have failed to give their authors clear instructions as to the plan of the total work so that detailed paint formulations appear in the otherwise sound chapter on chlorinated rubber whereas on other topics illustrative formulae only are included leaving the detail on paints to later volumes.

Finally, who is this work aimed at? As always in a highly technological subject, the latest developments and ideas are protected by commercial secrecy. An expert in any one of the fields covered by these thirteen chapters would be disappointed by the contents of that chapter; it stops short of revealing anything new to him and cannot be regarded as a balanced and critical review of the state of the subject. A newcomer to the field would find most of the chapters useful as a first introduction to a subject, but the limited reference lists would not guide him to the more stimulating and fundamental works in the field. It is doubtful whether he could undertake even a limited programme of development work on the basis of the information presented. The title of a *Treatise on Coatings* is not justified on the evidence of Part 1, but final judgement will have to await publication of the complete work.

J. P. WILTSHIRE

Carbonium Ions. An Introduction

D. BETHAL and V. GOLD. Academic Press: New York and London, 1967.
6¼ in. by 9¼ in. *xii*+387 pp. 95*s* or $16·00

THE subject matter of this book, carbonium ions, now covers such a vast area of pure and applied chemistry that a text-book unifying the subject has been needed for some time. It is evident that a summary of the topic in 305 pages must of necessity be very selective and reflect the personal interests of the writers. The authors of this book have set out to discuss carbonium ions in a manner rather different to books which are currently available. To this end they have collected together a large mass of material on the theory of carbonium ions and have chosen to emphasize this aspect. They have curtailed discussion of topics such as cationic polymerization, Friedel–Crafts reactions or rearrangement reactions of importance in the petrochemical industry which are covered in detail in other books and, presumably in the interests of brevity, have economized on diagrams and the more detailed explanations, which would have been helpful in making the reading of the book less arduous. The result is that though the cover sheet says 'the treatment is elementary' it is in fact a book which is more suitable for teachers and researchers in carbonium ion chemistry, than for undergraduates.

The Chapter headings are: 1, Introduction; 2, Experimental Techniques for the Detection and Study of Carbonium Ions; 3, Sources of Carbonium Ions; 4, Formation of Carbonium Ions: Quantitative Aspects; 5, Factors Governing the Stability of Carbonium Ions; 6, Reactions of Carbonium Ions; 7, Bridged Carbonium Ions; 8, Related Species.

The book finishes with an appendix containing a collection of reviews for additional reading corresponding to each chapter, which should be very useful.

This book, which has references as recent as 1967, is a useful addition to the literature. Scientists with an active interest in this subject will wish to read it.

N. B. GRAHAM

Anelastic and Dielectric Effects in Polymeric Solids

N. G. MCCRUM, B. E. READ and G. WILLIAMS. Wiley: New York and London, 1967.
6¼ in. by 9½ in. *xv*+617 pp. 160*s*

THIS book contains an extremely comprehensive account of the present state of knowledge on the mechanical and dielectric relaxation behaviour of polymers. There is a good balance between seven chapters concerned with a survey of theoretical developments and experimental methods, and a further seven chapters which provide a detailed review of the experimental data on various classes of polymers.

The introductory chapters provide an interesting survey of the relevant structural background and give a condensed but very readable account of the various molecular theories of relaxation. The chapters on dynamic mechanical and dielectric test methods contain a selection of these methods to illustrate the principles involved.

The discussion of experimental data in the following chapters, which form the major part of the book, is very detailed but in no way unmanageable to the reader. The authors have succeeded in maintaining the thread of their argument without exhibiting undue preference for one worker's views rather than another's. The reader will find these chapters the most valuable; they represent an extremely useful contribution in themselves to research in this particular area.

In conclusion this is an accurate and very well presented account of an area in polymer physics, which because of its firm theoretical base (in phenomenological terms) can be readily documented. A notable omission is the lack of direct reference to nuclear magnetic resonance techniques (although specific results are quoted) which have also played an integral part in our understanding. The book is highly recommended and the reviewer only regrets that its price will probably mean that it will remain as a reference book rather than for individual use.

I. M. WARD

Dissolving Pulps

Lectures presented at the International Symposium on Dissolving Pulps. Helsinki 24–27 May 1966

Butterworths: London, 1967. 6 in. by 9¼ in. *vi*+279–568 pp. of *Pure and Applied Chemistry*, Volume 14, 1967. 80*s*

THE Symposium was propitiously timed to provide a forum for reviewing the progress of development of high wet modulus (HWM) rayon and cellulose acetate. Additionally, the aim was to identify specific pulp properties as criteria of the usefulness of pulps in HWM rayon and cellulose acetate production.

Eighteen papers were concerned with HWM rayons and nine with cellulose acetate. Ten of the first group dealt with fibre-structure and physical properties, with some duplication in parts; five papers specifically discussed the inter-relationship of wood-pulp properties and fibre properties, and there could usefully have been more contributions here. A better balance was achieved in the acetate section, where four papers out of five were concerned with the influence of wood-pulp properties on the acetylation process and properties of the product.

Of particular value were two papers by Finnish workers on the use of sulphite pulps for HWM fibres, demonstrating that cold alkali-refined prehydrolysis kraft pulps are not essential. An interesting paper by CROON on pulp-resin gave added support. The overall conclusion was that, given a reasonable initial pulp viscosity, it was possible to use low alpha cellulose wood-pulp from the sulphite process for HWM fibre production, this being facilitated if the organic extractives and inorganic impurities were kept to a low level.

In the acetate section, interesting papers from Finland dealt with reasons for discolouration, either during acetylation or during pulp manufacture, and the importance of keto groups and *p*H were stressed.

GENEVRAY and ROBIN discussed the characteristics of cellulose relevant to continuous acetylation.

The Symposium was excellently organized and the Proceedings will be very useful to anyone associated with dissolving pulp manufacture or usage. Additional value would probably have accrued if some details could have been included of the questions raised after the lectures, and the ensuing discussions.

E. MYTUM

ANNOUNCEMENT

BUHL INTERNATIONAL CONFERENCE

'Polymers in the Engineering Curriculum' will be the subject of the Third Buhl International Conference on Materials to be held at Carnegie-Mellon University on 28 and 29 October 1968. Prominent scientists and engineers will (a) summarize the background science useful to engineers dealing with polymer materials, (b) present examples of engineering problems that arise in the fabrication and use of polymeric materials and (c) discuss the place of polymers in the curriculum of the engineering student whether or not he is specializing in polymers.

A brochure containing the programme and other details may be obtained by writing to Mr RICHARD B. BARNHART, Conference Manager, Warner Hall 111, Carnegie-Mellon University, Pittsburgh, Pa 15213, U.S.A.

The Finite Chain Segment Model of a Linear Polymer and the Molecular Weight Dependence of Intrinsic Viscosity

G. B. THURSTON

A relation between intrinsic viscosity and molecular weight is given for dilute solutions of flexible linear polymers. This is developed on the basis of the Gaussian chain model as composed of N *segments, where* N *is held to be a finite number and is considered to be proportional to the molecular weight. The effects of internal hydrodynamic interaction are described by a segmental factor* h* *which is independent of* N. *It is found that the intrinsic viscosity is proportional to the product of the square root of the molecular weight and a function of both* N *and* h*. *This function is evaluated for a range of* N *from 1 to* 10^5 *and for a range of* h* *from the free draining condition to the solvent immobilized condition. For a nearly free draining condition the intrinsic viscosity is directly proportional to molecular weight to the first power over a wide range. For increased hydrodynamic interaction effect the simple power relation becomes applicable over a narrower range and in the extreme interaction condition becomes proportional to the molecular weight to the 0·5 power.*

THE molecular weight dependence of the intrinsic viscosity in steady flow of dilute solutions of flexible linear polymer molecules has received considerable attention in measurement, determination of empirical relationships, and in the theory of chain molecules[1,2]. The relation between the chain dimensions and the molecular weight dependence of intrinsic viscosity has also been studied recently[3–5]. These studies indicate that the intrinsic viscosity is often proportional to the molecular weight to a power between 0·5 and 1, but in some ranges of molecular weight, this simple dependence is not found.

The theory for the intrinsic viscosity has been carried through by several investigators for the Gaussian chain model having flexible joints[6,7] and also for the chain with internal viscosity[8]. The influence of hydrodynamic interaction has been shown to affect the power relation between intrinsic viscosity and molecular weight[6]. The effect of internal viscosity is to bring about a gradient dependence to the intrinsic viscosity[8]. However, at small gradients, the results can be reduced to those for the model without internal viscosity. In these works, the number of elements in the chain model is usually taken to be very large and numerical factors are evaluated as the number of elements becomes infinite. However, recent work on the frequency dependence of optical birefringence in oscillatory flow of dilute polymer solutions[9] has shown the need for consideration of the theoretical model as it is composed of a finite number of elements. In the work herein, the influence of so restricting the number of elements is determined as it affects the relationship between intrinsic viscosity and molecular weight. A complete range of hydrodynamic interaction is also considered.

THEORY

A molecule of the linear polymeric material of molecular weight M is modelled by a linear sequence of N submolecular units, or segments. The end to end distance for each of these segments is l and each segment is of mass m_s, given by

$$m_s = M/(N_a N) \tag{1}$$

where N_a is Avogadro's number. The segments possess the properties described by Kuhn[10] and contain a sufficient number of monomers that the spatial orientation of the end points obeys the Gaussian probability function and each segment possesses springlike qualities. With this model, the form of the results for the intrinsic viscosity are essentially the same for the several published treatments[6-8]. While the analyses differ in the manner of inclusion of solvent interaction and excluded volume effects[11], the recent results of Pyun and Fixman[12] are specifically used in this work.

The theory gives the intrinsic viscosity in the form

$$[\eta] = \lim_{c \to 0} \frac{(\eta - \eta_s)}{\eta_s c}$$

$$= \frac{N_a kT}{M\eta_s} \sum_{p=1}^{N} \tau_p \tag{2}$$

where η is the solution viscosity, η_s is the solvent viscosity, c is the solute concentration, k is Boltzmann's constant, T is the Kelvin temperature, and τ_p are a set of characteristic relaxation times. All of the units are taken to be in the c.g.s. system. The times τ_p are given by

$$\tau_p = l^2 f/6kT\lambda_p \tag{3}$$

where f is the segmental friction factor for the hydrodynamic resistance to motion of the segment in the solvent and the λ_p are a set of eigenvalues, the magnitudes of which are dependent upon the hydrodynamic interaction conditions and the number of segments N. In the determination of the λ_p used herein[12], the solvent interaction and excluded volume effects do not appear explicitly, but are reflected in the segment length, l, the value of which is dependent upon a segment expansion coefficient.

The conditions of hydrodynamic interaction between segments is described by a factor h^* which is

$$h^* = h/N^{1/2}$$

$$= f/(12\pi^3)^{1/2}\,\eta_s l \tag{4}$$

where h is the more often used interaction factor. The h^* has the advantage of being independent of N, and if a hydrodynamic radius a_h is given to the segment such that f is equal to $(6\pi\eta_s a_h)$, then h^* is very nearly equal to the ratio of the hydrodynamic radius to the segment length (a_h/l). The free draining condition is characterized by $h^* = 0$ and the non-free draining interaction effects increase with h^*.

The intrinsic viscosity (2) may also be written in terms of the root mean square of the end to end distance for the molecule, L, where

$$L = N^{1/2} l \tag{5}$$

Then (2) becomes

$$[\eta] = \phi L^3 / M \tag{6}$$

where ϕ is a function of N and h^* and is

$$\phi\,(N, h^*) = (\pi^{3/2} N_a / 3^{1/2})\,(h^* / N^{3/2}) \sum_{p=1}^{N} 1/\lambda_p \tag{7}$$

Using (1), the intrinsic viscosity (6) may also be written to show the molecular weight dependence better and the dependence on the number of segments,

$$\begin{aligned}[\eta] &= \phi\,[l^3/(N_a m_s)^{3/2}]\, M^{1/2} \\ &= \phi\,[l^3/(N_a m_s)]\, N^{1/2}\end{aligned} \tag{8}$$

It is seen from (8) that if ϕ were independent of molecular weight, then the intrinsic viscosity would have the power dependence on M of $1/2$ which is usually ascribed to the theta solvent condition.

In order to examine the dependence of ϕ on molecular weight and hydrodynamic interaction, the function $\phi\,(N, h^*)$ of (7) has been computed for a wide range of parameters. The eigenvalues used are given by a modification of the results of Pyun and Fixman[12], as

$$\lambda_p \simeq \frac{\pi^2}{N^2}\left\{\frac{4N^2}{\pi^2}\,\sin^2\left(\frac{p\pi}{2N}\right) + \frac{4h^* N^{1/2}}{\pi^2}\,[I_1(p) + I_2(p)]\right\} \tag{9}$$

where the $I_1\,(p)$ and $I_2\,(p)$ are as defined by the referenced authors. This relation is developed by assuming N large and p small and, for cases other than for $h^* = 0$, is not precise. For p large, the sum $[I_1(p) + I_2(p)]$ can be approximated by $[p^{1/2}\pi\,(p\pi/2 - 1/4)]$.

Figure 1 shows the function $\phi\,(N, h^*)$ plotted versus N on logarithmic scales and with h^* as parameter. The range of N is from 1 to 10^5 while the range of h^* is from 0·0001 to 10. The function ϕ is zero for the totally free-draining case of $h^* = 0$. It is seen that the dependence of ϕ on the N, and hence the molecular weight, is variable. For the nearly free-draining condition of h^* small, ϕ is proportional to $N^{1/2}$ for a wide range of N. As N becomes very large and h^* becomes large, leading to greater internal hydrodynamic interaction, ϕ approaches a constant value. The upper limit for ϕ in these calculations is approximately $2{\cdot}645 \times 10^{23}$ (c.g.s. units) while Pyun and Fixman[12] give a value of $2{\cdot}680 \times 10^{23}$ for an infinite h and N.

In the figure it is seen that over limited ranges of N, the function may be approximated by a straight line on the logarithmic plot. Such a straight line would be

$$\phi = aN^b \tag{10}$$

where $b \leqslant 0{\cdot}5$. In such a case, the intrinsic viscosity would be given from (8) as

$$\begin{aligned}[\eta] &= a\,[l^3/(N_a m_s)^{(3/2+b)}]\, M^{(1/2+b)} \\ &= a\,[l^3/(N_a m_s)]\, N^{(1/2+b)}\end{aligned} \tag{11}$$

This relation shows the type of power dependence on molecular weight that is often found.

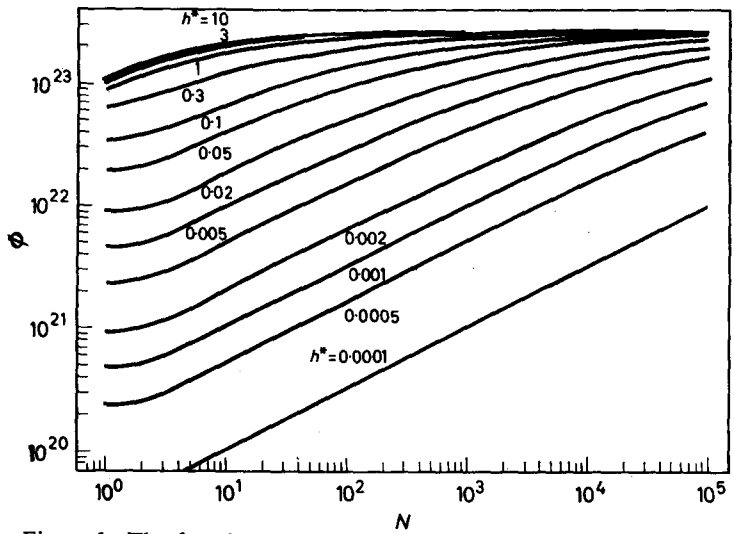

Figure 1—The function ϕ (N, h^*) of equation (7) versus number of segments N. The segmental hydrodynamic interaction factor h^* is specified.

DISCUSSION

The form of the presentation of the function ϕ (N, h^*) in *Figure 1* is such that a direct comparison against experimental data may be made by plotting $[\eta]/M^{1/2}$ versus M on the same logarithmic scales as used for ϕ versus N. Should the data and theory be in agreement, the shapes of the curves will be identical. By comparison of the numerical values of the ordinates and the abscissae they should differ by $\log [l^3/(N_a m_s)^{3/2}]$ and by $\log [1/(N_a m_s)]$ respectively according to (8) and (1). Thus, in principle, the numerical values of m_s and l may be determined.

From the dependence of ϕ on N, and hence on M, as shown in the figure, it is seen that for h^* small (nearly free-draining condition), the $[\eta] \sim M^1$ over a broad range of M. As h^* increases, the power becomes less than unity and the range of a simple power relation becomes more restrictive. Finally, as h^* is large and N is large, the power in the molecular weight dependence becomes 0·5. These results are in qualitative agreement with other analyses which emphasize solvent immobility[13].

The molecular weight range represented in *Figure 1* by the range of N depends upon the number of monomers per segment and the constitution of the monomer. If the molecular weight is sufficiently large that the molecule contains several segments, then it might be expected that a further increase in molecular weight would simply increase the number of segments without materially changing the number of monomers per segment, thus leaving l and m_s essentially unchanged. However, if M is reduced sufficiently, the effective number of monomers could perhaps begin to change and the basic concept of the model as being a Gaussian chain must

eventually become untenable. As the Gaussian chain is the basis for the model, then in effect the solvent must be a theta solvent. However, the solvent may be a determining factor in the constitution of the segment as well as the segment length.

The author wishes to thank Mr David Bowling for his assistance in programming the numerical calculations. This work was supported by the U.S. Army Research Office, Durham.

Physics Department,
Oklahoma State University,
Stillwater, Oklahoma 74074

(*Received February 1967*)

REFERENCES

[1] FLORY, P. J. *Principles of Polymer Chemistry,* see sect. 3 of Chap. XIV. Cornell University Press: Ithaca, New York, 1953
[2] MORAWETZ, H. *Macromolecules in Solution,* see sect. C.2 of Chap. VI (High Polymers, Vol. 21). Interscience: New York, 1963
[3] COWIE, J. M. G. *Polymer, Lond.* 1966, **7,** 487
[4] BAUMANN, H. *J. Polym. Sci. B,* 1965, **3,** 1069
[5] STOCKMAYER, W. H. and FIXMAN, M. *J. Polym. Sci. C,* 1963, **1,** 137
[6] KIRKWOOD, J. G. and RISEMAN, J. *J. chem. Phys.* 1948, **16,** 565
[7] ZIMM, B. H. *J. chem. Phys.* 1956, **24,** 269
[8] CERF, R. *J. Phys. Radium,* 1958, **19,** 122
[9] THURSTON, G. B. and SCHRAG, J. L. *J. chem. Phys.* 1966, **45,** 3373
[10] KUHN, W. *Kolloidzschr.* 1934, **68,** 2
[11] TSCHOEGL, N. W. *J. chem. Phys.* 1963, **39,** 149; 1964, **40,** 473
[12] PYUN, C. W. and FIXMAN, M. *J. chem. Phys.* 1965, **42,** 3838
[13] DEBYE, P. and BUECHE, A. M. *J. chem. Phys.* 1948, **16,** 573

Shear Rate Effects in Determination of Viscosity Average Molecular Weight of Poly(but-1-ene sulphone)

J. R. BROWN and J. H. O'DONNELL

Viscosity measurements on solutions of polydisperse poly(but-1-ene sulphone) with Ubbelohde-type suspended level viscometers over the range of shear rates and stresses showed that marked shear dependence occurred at shear rates below 400 sec^{-1} (shear stresses below 2 dyne cm^{-2}) for polymers with $\overline{M}_v \approx 700\,000$. Polymers with $\overline{M}_v$ below about 250 000 did not show any shear dependence and identical viscosities were obtained with a variety of straight and spiral capillary viscometers. The shear dependence showed a parabolic variation with concentration with a maximum at 5 g l^{-1}. Plots of η_{sp}/c against concentration for different shear stresses were curved in the shear dependent region and linear at higher shear stresses, but they could all be extrapolated to approximately the same intrinsic viscosity at zero concentration, provided that measurements at sufficiently low concentrations were included. However, linear extrapolations of viscosity measurements made at moderate concentrations in the shear dependent region could result in large errors in $\overline{M}_v$.

VISCOSITY measurements of dilute solutions provide an empirical, but extremely convenient, method of determining the molecular weight of a polymer. Two factors affecting the viscosity must be considered—concentration dependence and shear dependence. These will vary with the polymer, solvent, temperature, molecular weight average and molecular weight distribution.

Allowance is made for non-ideal solution behaviour by extrapolation of the viscosity measurements to zero concentrations. However, polymer solutions are non-Newtonian fluids and therefore measurements of solution viscosities should be made at a series of shear rates or stresses and extrapolated to zero shear. A number of measurements of the shear dependence of polymer solution viscosities have been reported, but these have mainly been at shear rates greater than those used in conventional viscometers. Also, despite numerous attempts, no satisfactory theoretical understanding of shear dependence in polymer solutions has been developed.

We have examined the shear dependence of solutions of poly(but-1-ene sulphone) at the shear rates and stresses occurring in a standard Ubbelohde viscometer and below and have observed marked shear dependence, which could produce serious errors in determinations of $\overline{M}_v$ by the usual linear extrapolations.

EXPERIMENTAL

Poly(but-1-ene sulphone) was prepared by u.v. illumination of 1:1 w/w liquid mixtures of butene-1 and sulphur dioxide at −80°C. The polymer was dissolved in acetone and precipitated in methanol several times and then dried in a vacuum oven at 25°C.

Viscosity measurements were made in a water bath at $30{\cdot}00 \pm 0{\cdot}02$°C using a variety of Ubbelohde-type suspended level viscometers with straight and spiral capillaries. The details of these are given in *Figure 1* and *Table 1*. Corrections for end effects (maximum 0·01 per cent) and kinetic energy terms (maximum 0·02 per cent) were negligible in all the spiral capillary viscometers.

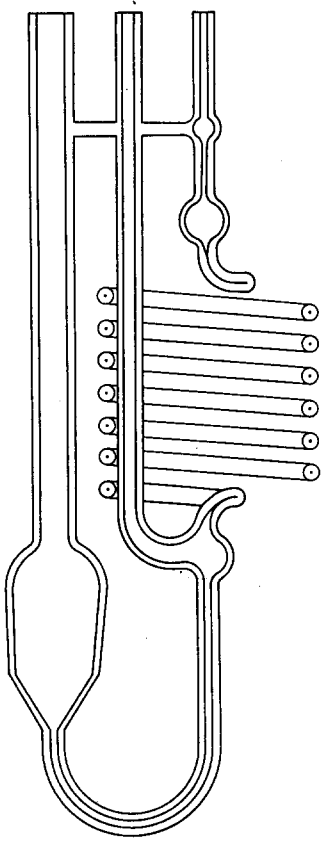

Figure 1—Spiral capillary viscometer

Solutions were prepared by agitation of weighed polymer with dried and distilled acetone on a shaker for two hours in a flask wrapped in aluminium foil to exclude light. No degradation was observed in the solution during shaking, on standing or during passage through the viscometer capillary tubes.

RESULTS AND DISCUSSION

Comparison of spiral and vertical capillary viscometers

Ubbelohde suspended level viscometers are widely used to measure the viscosities of dilute polymer solutions[1] in order to determine $\overline{M}_v$. The effect of high shear rates has been examined by application of external pressure[2]. To obtain low shear rates a short capillary and/or a narrow bore capillary can be used, but either method increases errors due to end effects, kinetic

energy terms, boundary layers and dust. A range of shear rates can be covered by using a series of bulbs in the viscometer, but this is only suitable for a narrow range[3].

Spiral capillaries have been used to increase the flow times and hence improve the accuracy of measurements on low molecular weight polymers. This also reduces the shear rate as well as the errors due to kinetic energy and end effects and by a judicious selection of capillary lengths and spiral

Table 1. Viscometer details

Viscometer	*Capillary length, l (cm)*	*Capillary diam., d (mm)*	*Mean hydrostatic head, h (cm)*	*Shear stress F(dyne cm^{-2})*	*Solvent shear rate, G (sec^{-1})*	*Solvent flow time, t (sec)*
V_1	152·4	0·40	6·5	0·31	51	3 640·2
V_2	152·4	0·40	12·5	0·63	122	1 468·6
V_3	152·4	0·40	22·5	1·13	267	669·3
V_4	100	0·65	15·5	1·92	418	94·4
V_5*	12·2	0·40	14·2	8·89	1 880	85·0

*Straight capillary.

pitches a series of viscometers can be constructed to cover any desired shear rate range without introducing significant errors. However, there is some uncertainty whether the equations of fluid flow developed for straight, vertical capillary tubes are applicable to spiral capillaries. We have measured the relative flow times of solutions of monodisperse polystyrene ($\overline{M}_w = 97\,200$) and of poly(but-1-ene sulphone) ($\overline{M}_w \approx 100\,000$) in all our viscometers and found no significant differences. Therefore, we conclude that spiral capillary viscometers are satisfactory for measuring polymer viscosities and that the measurements are directly comparable with those obtained with straight, vertical capillary tubes. Further, there is negligible shear dependence for these polymers at the above molecular weights.

Shear dependence of high molecular weight polymer

The shear rate varies over the cross section of the capillary, being maximum at the boundary layer and zero at the centre, and the average value is given[4] by

$$\overline{G} = 8V/3\pi r^3 t \qquad (1)$$

where V is the liquid volume flowing through the capillary in time t and r is the radius of the capillary. This is correct for Newtonian fluids, but is only the 'apparent' shear rate for non-Newtonian fluids. It varies with the viscosity (hence concentration) of the solution and therefore the shear stress, which is the same for all solutions in a particular viscometer, provided the driving pressure remains constant, is usually considered a more appropriate parameter. The shear stress at the wall of the capillary is given[5] by

$$F = rp/2l \qquad (2)$$

where p is the applied pressure (in our work $\rho g\bar{h}$, where ρ is the solvent

density, g is the acceleration due to gravity and $\bar{h}$ is the mean hydrostatic head) and l is the length of the capillary. This expression is correct for Newtonian and non-Newtonian fluids.

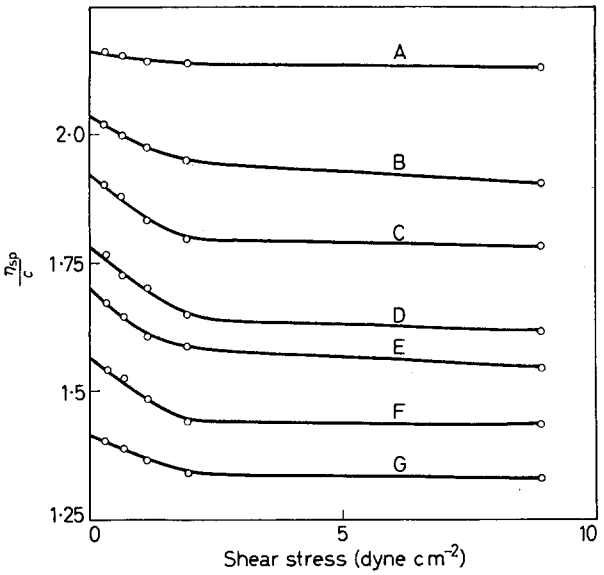

Figure 2—Variation of reduced specific viscosity (η_{sp}/c, c=g/100 ml) with shear stress (F). Concentration: A—10·0 gl^{-1}; B—7·692 gl^{-1}; C—5·882 gl^{-1}; D—4·166 gl^{-1}; E—3·333 gl^{-1}; F—2·020 gl^{-1}; G—1·010 gl^{-1}

The variation of η_{sp}/c with shear stress for poly(but-1-ene sulphone) ($\overline{M}_v \approx 700\,000$) is shown in *Figure 2**. Marked shear dependence occurs at shear stresses below 2 dyne cm^{-2}) which is much lower than the shear stress (9 dyne cm^{-2}) in a conventional Ubbelohde viscometer.

These results can be compared with those of other workers on different polymers. In particular Tuijnman and Hermans[6] found shear dependence in a fraction of poly(vinyl acetate)—$\overline{M}_v = 880\,000$—at shear stresses below 1·6 dyne cm^{-2}, causing a rise in η_{sp}/c with decreasing shear stress. Also they observed that the η_{sp}/c values reached another plateau region at very low shear stresses. However, they used very dilute solutions (one tenth of our concentrations). Van Oene and Cragg[7] found the intrinsic viscosity of a fraction of polystyrene of molecular weight 1×10^7 is markedly shear dependent even at low shear stresses. Fox, Fox and Flory[8] examined the shear dependence of dilute solutions of poly(isobutene) in various solvents at shear rates from several hundred to several thousand sec^{-1}. They found that log η_{sp} decreased with increasing shear rate according to a linear relationship which was independent of concentration. Their work was all at higher shear rates than the shear dependent region observed in the present

*The value of $\overline{M}_v$ was obtained from the intrinsic viscosity using the values of K and a in the Mark-Houwink equation obtained by Ivin, Ende and Meyerhoff[12] for poly(hex-1-ene sulphone) in the same solvent.

work. No shear dependence was observed in aqueous solutions of a dextran fraction ($\overline{M}_w = 9 \times 10^6$) by Van Oene and Cragg[2].

A measure of the shear dependence can be obtained from the slope of the approximately linear section of the η_{sp}/c versus shear stress plot for

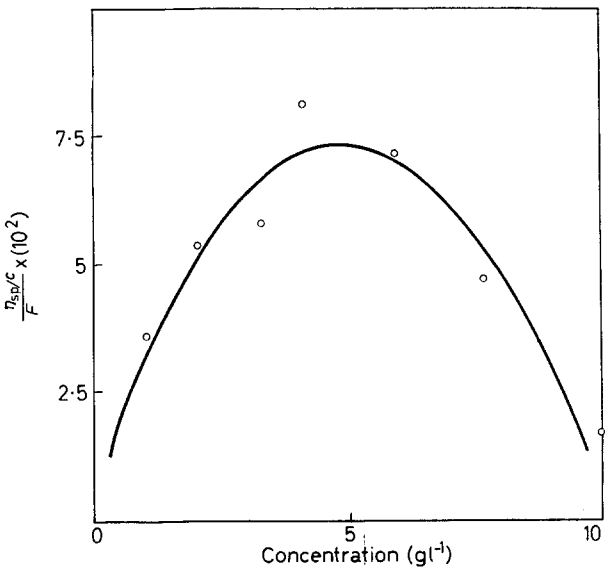

Figure 3—Variation of shear dependence with concentration

each concentration. There is clearly a parabolic relationship between shear dependence and concentration in our system as shown in *Figure 3*. The shear dependence approaches zero at $c = 0$ and 10 gl^{-1} and is a maximum at $c = 5$ gl^{-1}.

Intrinsic viscosities for various shear stresses

The conventional plots of η_{sp}/c versus c are shown in *Figure 4* for various shear stresses. First, it can be seen that the measurements in the approximately shear independent region (shear stresses of 2 to 9 dyne cm^{-2}) give a linear extrapolation. Secondly, the values obtained by extrapolation to zero shear stress give a curved relationship and can be extrapolated to about the same intrinsic viscosity. Thirdly, measurements in the shear dependent region lie between these two lines and can be extrapolated to about the same value as for the intrinsic viscosity. The intrinsic viscosity may decrease with increase in shear stress, but the effect can only be quite small.

Tuijnman and Hermans[6] found that for polyvinyl acetate ($\overline{M}_v = 880\,000$) in toluene at concentrations below 1 gl^{-1} plots of η_{sp}/c versus c gave increasingly curved extrapolations to zero concentration for shear stresses above 0·4 dyne cm^{-2} resulting in values of the intrinsic viscosity as much as 60 per cent less than that obtained from zero shear rate values. Passaglia, Yang and Wegemer[9] found that the intrinsic viscosity of polystyrene

($\overline{M}_w = 282 \times 10^6$) was reduced by 50 per cent at high shear rates, but their shear stress range was 10 to 1 000 dyne cm^{-2}, in excess of our work. Similarly Kawahara *et al.*[10] observed that the intrinsic viscosity of polystyrene decreased as the shear stress was increased from 8 to 40 dyne cm^{-2}, but they did not investigate the effect of lower shear stresses. They observed

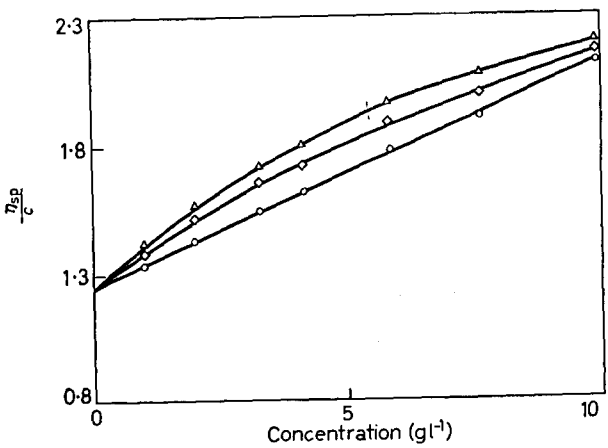

Figure 4—Variation of reduced specific viscosity (η_{sp}/c, c=g/100 ml) with concentration for measurements at different shear stresses (F). (○)—8·9 dyne cm^{-2}; (◇)—0·63 dyne cm^{-2}; (△)—extrapolated values at zero shear stress

no effect for molecular weights below $1{\cdot}3 \times 10^6$. Nowakowski and Meyerhoff[11] found that the intrinsic viscosities of cellulose nitrate ($M = 1\text{–}2 \times 10^6$) and of poly(methyl methacrylate) ($M = 16 \times 10^6$) were reduced by one half when the shear rate was increased from 15 to 30 000 sec^{-1}.

We therefore conclude that shear dependence may occur in dilute polymer solutions in the shear stress range above 10 dyne cm^{-2} and also at lower shear stresses. The shear dependence is influenced by the nature of the polymer, the solvent (it is known to increase with the goodness of the solvent), the temperature, the molecular weight of the polymer (it becomes progressively more serious above $\overline{M}_v$ of about 150 000), the molecular weight distribution and the concentration of the solution. The observations reported in this paper may result from the polydispersity of the sample (gel permeation chromatography indicated an approximately normal distribution). The effect on the extrapolated intrinsic viscosity depends on the above factors and particularly on the concentration range in which measurements are made. However, it is apparent that shear dependence should be taken into account for high molecular weight polymers in deriving $[\eta]/M$ relationships and in determining $\overline{M}_v$. Otherwise, errors of up to 100 per cent in $\overline{M}_v$ can result. Nevertheless, satisfactory results may be obtained with conventional Ubbelohde viscometers if the shear stress is in a shear independent region for the solutions being examined as in the case of poly(but-1-ene sulphone).

We wish to thank the Australian Atomic Energy Commission for supporting this work and Mr P. Vanderlinde for careful construction of the viscometers. J. R. B. is grateful to the University of Queensland for a demonstratorship.

Chemistry Department,
University of Queensland,
Brisbane, Australia

(*Received December 1967*)

REFERENCES

[1] PINNER, S. H. *A Practical Course in Polymer Chemistry*. Pergamon: London, 1961
[2] VAN OENE, H. and CRAGG, L. H. *J. Polym. Sci.* 1962, **57**, 175
[3] SCHURZ, J. and IMMERGUT, E. H. *J. Polym. Sci.* 1952, **9**, 279
[4] ONYON, P. F. in *Techniques of Polymer Characterization*, p 184. Edited by P. W. ALLEN. Butterworths: London, 1959
[5] MILLER, M. L. *The Structure of Polymers.* Reinhold: New York, 1966
[6] TUIJNMAN, C. A. F. and HERMANS, J. J. *J. Polym. Sci.* 1957, **25**, 385
[7] VAN OENE, H. and CRAGG, L. H. *Canad. J. Chem.* 1961, **39**, 203
[8] FOX, T. G., FOX, J. C. and FLORY, P. J. *J. Amer. chem. Soc.* 1951, **73**, 1901
[9] PASSAGLIA, E., YANG, J. T. and WEGEMER, N. J. *J. Polym. Sci.* 1960, **47**, 333
[10] KAWAHARA, K., UEDA, M., OKA, Y. and KUROIWA, T. *J. Polym. Sci.* 1958, **31**, 245
[11] NOWAKOWSKI, B. and MEYERHOFF, G. *Rheol. Acta*, 1964, **3**, 233
[12] IVIN, K. J., ENDE, H. A. and MEYERHOFF, G. *Polymer, Lond.* 1962, **3**, 129

The Unperturbed Dimensions of Poly-(2,6-dimethyl-1,4-phenylene oxide) and Poly(2,6-diphenyl-1,4-phenylene oxide)

P. J. AKERS, GEOFFREY ALLEN and M. J. BETHELL

Dilute solution properties are reported for poly(2,6-dimethyl-phenylene oxide) and for poly(2,6-diphenyl-phenylene oxide) at 25°C and 90°C in non-ideal solvents. Both polymers crystallize from solution and consequently no theta conditions could be found. Both polymer chains appear to be tightly coiled in solution. The conformational ratios determined from unperturbed chain dimensions, estimated by Stockmayer–Fixman and Kurata–Stockmayer extrapolation procedures in good solvents, lie in the range 1·0 to 1·2. The temperature dependences of chain dimensions also may be small. These results are consistent with a symmetrical potential function for internal rotation about the C—O *bond in which both minima have the same energy.*

HIGH molecular weight poly(phenylene oxides) can be prepared with a regular *para* structure by methods which have been reviewed[1] recently. Various polymers with a number of substituents in the aromatic rings have been synthesized and all products have good thermal stabilities and high glass transition temperatures. The latter property together with the high melt viscosities observed is characteristic of rigid, 'dynamically' stiff chains.

In this paper we describe the dilute solution properties of poly(2,6-dimethyl-1,4-phenylene oxide), **PMPO**, and poly(2,6-diphenyl-1,4-phenylene oxide), **PPPO**. The 'equilibrium' flexibilities of the polymer chains are evaluated in terms of the conformational ratio, σ, which is the ratio of the root-mean-square unperturbed end-to-end distance $\langle r_0^2 \rangle$ of a polymer chain to the r.-m.-s. value $\langle r_{0f}^2 \rangle$ for a corresponding Gaussian chain having completely free rotation about bonds connected by a fixed valence angle (θ), i.e.

$$\sigma^2 = \langle r_0^2 \rangle / \langle r_{0f}^2 \rangle \tag{1}$$

$$\langle r_{0f}^2 \rangle = nl^2 (1 - \cos\theta)/(1 + \cos\theta) \tag{1a}$$

where n is the average number, and l the length of the links in each chain.

EXPERIMENTAL

Capillary viscometry—Viscosities were measured with a modified Desreaux–Bischoff viscometer[2,3], having a low shear stress (2–3 g cm^{-1} sec^{-2}); extrapolation methods of Huggins[4] and of Kraemer[5] were used to evaluate intrinsic viscosities.

Light scattering—A Sofica light-scattering photometer was used and all measurements were made at $\lambda = 5\,461$Å with a mercury arc. The instru-

ment was calibrated with pure benzene and the angular alignment was checked with a dilute solution of fluorescein in slightly alkaline ethanol. The scattered intensity at different angles in the range 30° to 150° showed variations less than one per cent after the usual $\sin\theta$ correction for the change in scattering volume observed at angle θ. Solutions were clarified by ultracentrifugation for at least three hours at 30 000 g in a Spinco model-L ultracentrifuge. The dust-free solvent required for washing cells and pipettes was prepared from analytical reagent grade material by filtration under pressure through 100 nm millipore filters.

Results were analysed by the double extrapolation method due to Zimm[6].

Differential refractometry—Refractive index increments, necessary to determine absolute values of $\langle M \rangle_w$ from light scattering data, were determined with a Brice–Phoenix differential refractometer which was calibrated with aqueous sucrose solutions.

Gel permeation chromatography—Gel permeation chromatographs were measured on a commercial Waters instrument fitted with four columns (3×10^6, 10^5, 10^4, 10^3Å) packed with polystyrene gel. Toluene was the solvent for PMPO and chloroform for PPPO.

UNPERTERBED DIMENSIONS OF PMPO

Fractionation—Two samples of PMPO, with intrinsic viscosities in benzene at 25°C of 0·56 and 0·80 dl g^{-1} respectively, were fractionated[19] by successive precipitation from stirred dioxan solutions. Initial concentrations of polymer were 0·4 per cent by weight and precipitation began at ~65°C. About ten fractions were collected after thermostatic control of the solution for at least 24 hours at intervals of approximately 3 to 4 deg. C. Despite the fact that liquid–crystal phase separation occurred, the fractionation was reasonably efficient. GPC analysis showed that the ratio M_w/M_n for each fraction was in the range 1·3 to 1·7 compared with more than two for the whole polymer.

An attempt was made to fractionate a whole polymer of higher molecular weight, $[\eta]^{25°C} = 1{\cdot}3$ dl g^{-1}, but severe degradation made the resulting fractions valueless.

Intrinsic viscosity/molecular weight relations—Light scattering measurements were made in toluene, xylene and chloroform solutions respectively at 25°C. For these solvents the refractive index increments are:

	toluene	xylene	chloroform
dn/dc at 25°C	0·1153	0·1136	0·169 cm^3 g^{-1}

Solution viscosities were measured at 25°C in carbon tetrachloride and benzene (*Table 1*). During the course of these measurements results were published for solutions respectively in toluene, chloroform and chlorobenzene[14].

Table 1. Light scattering, viscometry and GPC data of PMPO fractions

Fraction	$\langle M\rangle_w \times 10^{-3}$	$\langle M\rangle_w / \langle M\rangle_n$	$[\eta]$, *dl* g^{-1}, 25°C	
			Benzene	*Carbon tetrachloride*
DC1	164	1·65	1·00	0·84
DA1	130	1·72	0·87	0·72
DC3	111	1·65	0·79	—
DA3	106	1·62	0·78	0·655
DA4	85	1·56	0·66	0·585
DA5	70	1·63	0·57	0·50
DA6	46	1·44	0·44	—
DA7	39·7	1·35	0·37	—

From the log/log plot of $[\eta]$ against molecular weight the following relations have been established:

$$[\eta]^{25°C}_{\text{benzene}} = 2{\cdot}60 \times 10^{-4} \langle M\rangle_v^{0{\cdot}69} \tag{2}$$

$$[\eta]^{25°C}_{CCl_4} = 7{\cdot}55 \times 10^{-4} \langle M\rangle_v^{0{\cdot}585} \tag{3}$$

Second virial coefficients—Large second virial coefficients were observed from the light scattering studies on all PMPO–solvent systems. In dioxan solution, even at temperatures close to that at which phase separation occurs, A_2 does not fall to zero. The phenomenon is indicative of liquid–crystal rather than liquid–liquid phase separation and crystallization from solution has been confirmed by X-ray diffraction studies.

Table 2 gives examples of the magnitudes of A_2 in a variety of solvents. In toluene, A^2 shows an unusually strong dependence on $\langle M\rangle_w$

$$A^2 = 0{\cdot}13 \langle M\rangle_w^{-0{\cdot}41} \tag{4}$$

For most polymer–solvent systems the exponent lies in the range $-0{\cdot}2$ to $-0{\cdot}3$.

Table 2. Second virial coefficients for PMPO fractions in various solvents

$\langle M\rangle_w \times 10^{-3}$	*T*°C	*Solvent*	$A_2 \times 10^4$ *mole* cm^3 g^{-2}
111	25	Toluene	9·4
130	25	Benzene	11·1
106	25	Xylene	8·8
130	25	Chloroform	14·1
85	65	Dioxan	2·0

Unperturbed dimensions—Due to the tendency of PMPO to crystallize readily from solution it was not possible to perform measurements under theta conditions. However, an estimate of the unperturbed dimensions was obtained from the intrinsic viscosity/molecular weight relations established in non-ideal solvents.

There are several graphical procedures available for such an evaluation and, of these, the methods due to Stockmayer and Fixman[7], and Kurata and Stockmayer[8], were selected as being the most reliable

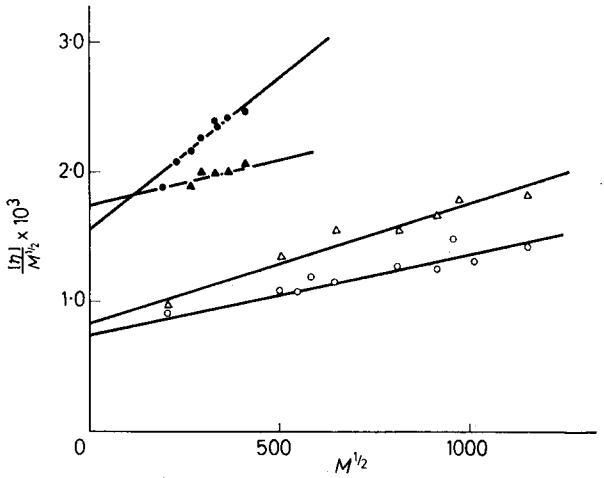

Figure 1—Stockmayer–Fixman plots at 25°C for PMPO in benzene (●) and carbon tetrachloride (▲) and PPPO in toluene (○) and chlorobenzene (△)

(*Figures 1* and *2*). The former method uses the closed Fixman[9] expression (which relates the expansion factor, α, to the excluded volume parameter Z) to derive the equation

$$[\eta]\, M^{-\frac{1}{2}} = K_\theta + 0{\cdot}50\Phi_0 B M^{\frac{1}{2}} \tag{5}$$

where the terms have their usual meaning. The relation of Kurata and Stockmayer as formulated from the solution theory of Kurata, Stockmayer and Roig[10] is

$$[\eta]^{2/3} M^{-1/3} = K_\theta^{2/3} + 0{\cdot}363\Phi_0 B\,[g\,(\alpha_\eta) M^{2/3}[\eta]^{-1/3}] \tag{6}$$

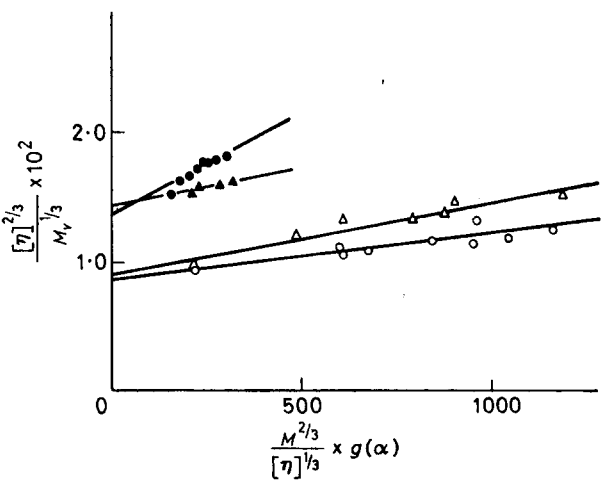

Figure 2—Kurata–Stockmayer plots at 25°C for PMPO in benzene (●) and carbon tetrachloride (▲), PPPO in toluene (○) and chlorobenzene (△)

An initial estimate of K_θ is obtained by assuming $g(\alpha_\eta)$ to be unity; $g(\alpha_\eta)$ is then determined from the relations:

$$g(\alpha_\eta) = 8\alpha_\eta^3(3\alpha_\eta^2 + 1)^{-3/2} \tag{7}$$

$$\alpha_\eta = ([\eta]/[\eta]_\theta)^{1/3} \tag{8}$$

The data are then replotted to obtain an accurate value of K_θ.

Both methods give approximately the same result for K_θ, as shown below:

	$10^3 K_\theta$ at 25°C	
Solvent	S–F	K–S
benzene	1·54	1·60
carbon tetrachloride	1·75	1·70

K_θ is related to the unperturbed dimensions by the equation

$$K_\theta = \Phi_0(\langle r_0^2/M\rangle)^{3/2} = \Phi_0 A^3 \tag{9}$$

the theoretical value of Φ_0 being $2{\cdot}87 \times 10^{21}$. In practice, however, combination of light scattering and viscometry measurements under theta conditions yields a lower value due to the heterogeneity of the samples. The experimental average is found[11] to be about $2{\cdot}5 \times 10^{21}$. Fortunately a correction for polydispersity can be made[12, 13] by using the relation

$$K_\theta = \Phi_0 A^3 \langle M^{\frac{1}{2}}\rangle_w / \langle M\rangle_w^{\frac{1}{2}} \tag{10}$$

We have determined the ratio $\langle M^{\frac{1}{2}}\rangle_w / \langle M\rangle_w^{\frac{1}{2}}$ for each fraction from the GPC distributions; the values ranged from 0·92 to 0·96. An average value of 0·94 was used in equations (9) and (10) to give the following dimensions of the unperturbed chain:

benzene	$A = 0{\cdot}84$Å
carbon tetrachloride	$A = 0{\cdot}86$Å

The values of K_θ determined above agree quite well with those reported in a preliminary note by Barrales-Rienda and Pepper[14] who used the same extrapolation techniques. The Mark–Houwink constants together with the values of K_θ (after correction for polydispersity) from both investigations are:

Solvent	$K \times 10^4$	a	$K_\theta \times 10^3$
benzene	2·60	0·69	1·67
toluene*	2·85	0·68	1·64
chlorobenzene*	3·78	0·66	1·67
chloroform*	4·83	0·64	1·73
carbon tetrachloride	7·55	0·585	1·83

(* ref. 14.)

The constant K shows the increase expected as a decreases. The plot of K versus a is a smooth curve and an empirical extrapolation to $a = 0{\cdot}5$ gives a value of $K_\theta = 1{\cdot}65 \times 10^{-3}$.

Temperature dependence of the unperturbed dimensions

The temperature coefficient, TC, of $\langle r_0^2 \rangle$ as expressed by

$$TC = \mathrm{d} \ln \langle r_0^2 \rangle / \mathrm{d}T \tag{11}$$

has been evaluated by application of the S–F and K–S extrapolations at 25°C and 90°C in chlorobenzene. Since this method is subject to errors due to the uncertainty in the extrapolations, the following precautions have been taken to ensure that a pure thermal effect is observed.

(a) Identical polymer fractions were used at each temperature to eliminate molecular weight errors.

(b) The variation of the kinetic energy correction with temperature for the viscometer was taken into account. It amounted to 0·7 per cent for the solvent used.

(c) A thermodynamically 'good' solvent was chosen, to minimize the possibility of specific solvent effects.

(d) The extrapolations were performed using the method of least squares to systematize errors in evaluating the intercepts.

The molecular weights of these fractions were determined from the intrinsic viscosity in chlorobenzene at 25°C using the relation[14]

$$[\eta] = 3{\cdot}78 \times 10^{-4} \langle M \rangle_v^{0{\cdot}66} \tag{12}$$

The intrinsic viscosities at 25°C and 90°C are given in *Table 3*. The intrinsic viscosity/molecular weight relation at 90°C was found to be

$$[\eta] = 5{\cdot}14 \times 10^{-4} \langle M \rangle_v^{0{\cdot}63} \tag{13}$$

Applying the S–F and K–S methods to these results the following values of K_θ and TC have been calculated:

	$K_\theta \times 10^3$		
Method	25°	90°C	$TC \times 10^3$
S–F	$1{\cdot}69_0$	$1{\cdot}65_0$	−0·2
K–S	$1{\cdot}67_6$	$1{\cdot}68_9$	0·1

Table 3. Viscosity data of PMPO fractions in chlorobenzene at 25°C and 90°C

	$[\eta]$ *dl* g^{-1}		
Fraction	*25°C*	*90°C*	$\langle M \rangle_v \times 10^{-3}$
DD2	1·10	1·005	176
3	1·00	0·93	151
4	0·925	0·89	135
5	0·79	0·718	105
DC5	0·705	0·687	89
6	0·54	0·525	59
7	0·365	0·356	33·1

THE UNPERTURBED DIMENSIONS OF PPPO

PPPO crystallizes readily from solution. Consequently an efficient fractionation could not be achieved either by precipitation from a binary solution on cooling or by addition of a non-solvent. Therefore the solution pro-

perties of ten unfractionated samples of PPPO were studied as supplied by A.K.U. and corrections for polydispersity were made.

GPC analysis of the samples showed that the molecular weight distributions were monotonic with $\langle M\rangle_w/\langle M\rangle_n$ ranging from 1·4 to 2·3. The experimentally determined distributions were fitted to the Schulz–Zimm equation[15, 16] in the form

$$W(M)=[y^{(h+1)}/(h+1)]\,M^h \exp(-yM) \tag{14}$$

where $W(M)$ is the weight fraction of molecules with molecular weight M in the sample. Parameters y and h are related to the molecular weight averages:

$$y=\frac{h}{\langle M\rangle_n}=\frac{h+1}{\langle M\rangle_w}=\frac{h+2}{\langle M\rangle_z}=\text{etc.} \tag{15}$$

A summary of the results obtained for the ten samples is given in *Table 3*.

Intrinsic viscosity/molecular weight relations—Light scattering studies were made in toluene solution at 25°C; the refractive index increment was 0·185 cm^3g^{-1}.

Solution viscosities were measured at 25°C in toluene and in chlorobenzene. The results are included in *Table 4*. An initial value of the Mark–Houwink

Table 4. Light scattering, viscometry and GPC data of PPPO samples

				Toluene 25°C		*Cl-benzene 25°*		*Cl-benzene 90°C*	
	$\langle M\rangle_w\times10^{-3}$	$\langle M\rangle_w/\langle M\rangle_h$	h	$[\eta]$	$\langle M\rangle_v\times10^{-3}$	$[\eta]$	$\langle M\rangle_v\times10^{-3}$	$[\eta]$	$\langle M\rangle_v\times10^{-3}$
PPPO/1	43·8	1·42	2·38	0·183	40·3	0·197	41·7	0·196	41·2
2	327	2·07	0·94	0·59	298	—	—	—	—
3	360	1·95	1·05	0·69	333	—	—	—	—
4	445	1·62	1·61	0·74	411	1·00	415	0·90	413
5	265	1·91	1·11	0·54	245	0·67	247	0·625	246
6	710	2·09	0·92	1·04	648	1·24	655	1·22	652
7	900	2·05	0·95	1·14	825	1·48	833	1·37	830
8	1,120	2·27	0·79	1·33	1,019	—	—	—	—
9	1,000	2·20	0·83	1·42	910	1·73	919	1·675	915
10	1,445	2·20	0·83	1·65	1,315	2·10	1,328	1·98	1,323

constant a was calculated from a plot of log $[\eta]$ against log $\langle M\rangle_w$. Values of $\langle M\rangle_v$ were then computed from the Schultz–Zimm relation

$$\frac{\langle M\rangle_w}{\langle M\rangle_v}=\left[\frac{\Gamma(h+a+1)}{(h+1)^a\Gamma(h+1)}\right] \tag{16}$$

and successive approximations allowed more accurate values of the Mark–Houwink constants to be determined.

The intrinsic viscosity/molecular weight relations determined by this procedure are:

$$[\eta]^{25°C}_{\text{toluene}}=214\times10^{-4}\langle M\rangle_v^{0.635} \tag{17}$$

$$[\eta]^{25°C}_{\text{Cl-benzene}}=1{\cdot}39\times10^{-4}\langle M\rangle_v^{0.68} \tag{18}$$

Second virial coefficients—As for PMPO the second virial coefficients measured in toluene solutions were large and showed an unusually strong dependence on $\langle M\rangle_w$.

$$A_2=5{\cdot}2\times10^{-2}\langle M\rangle_w^{-0.44} \tag{19}$$

Unperturbed dimensions—No θ-solvent was available within the temperature range of the Sofica light-scattering instrument. Estimates of unperturbed dimensions were made from the results obtained in toluene and chlorobenzene solutions using the S–F and K–S equations.

The values of K_θ differed by ten per cent for the two sets of data.

	10^3K_θ at 25°C	
Solvent	*S–F*	*K–S*
toluene	0·75	0·76
chlorobenzene	0·87	0·86

Using these values of K_θ, the unperturbed dimensions of the PPPO chain calculated from equation (9) are:

Toluene	$A = 0{\cdot}64$Å
Chlorobenzene	$A = 0{\cdot}68$Å

The temperature dependence of the unperturbed dimensions

To evaluate TC the intrinsic viscosities of seven of the unfractionated samples were measured at 25°C and 90°C in chlorobenzene, the following relations being established:

$$[\eta]_{25°C} = 1{\cdot}39 \times 10^{-4} \langle M \rangle_v^{0{\cdot}68} \tag{20}$$

$$[\eta]_{90°C} = 1{\cdot}55 \times 10^{-4} \langle M \rangle_v^{0{\cdot}67} \tag{21}$$

As well as the precautions applied with PMPO, the variation of $\langle M_v \rangle$ with temperature has also been allowed for.

	$K_\theta \times 10^3$		
Method	*25°C*	*90°C*	$TC \times 10^3$ *deg*$^{-1}$
S–F	$0{\cdot}86_8$	$0{\cdot}86_3$	−0·1
K–S	$0{\cdot}86_4$	$0{\cdot}85_3$	−0·1

DISCUSSION

Only indirect estimates could be obtained of the unperturbed dimensions of the two poly(phenylene oxides) because crystallization from solution always intervened before theta conditions were attained. However, the S–F and K–S extrapolation procedures allowed $\langle r_0^2 \rangle$ to be determined and the results from several different solvents gave a consistent set of values for the 2,6-dimethyl derivative. These results suggest that the average value of $(\langle r_0^2 \rangle / M)^{\frac{1}{2}}$ should be reliable to better ± 10 per cent.

Assuming the bond lengths and bond angles in poly(phenylene oxides) to be the same as the values found in diphenyl ethers, the segment length l in equation (1a) is 5·41Å. The calculated values of A_f, defined by

$$A_f = (\langle r_0^2 \rangle / M)^{\frac{1}{2}}$$

and the conformational ratios σ are then:

PMPO $A_f = 0{\cdot}855$Å; $\sigma = 1{\cdot}0$

PPPO $A_f = 0{\cdot}595$Å; $\sigma = 1{\cdot}1$

Values of σ close to unity imply that the poly(phenylene oxide) chains are tightly coiled in solution. The results also suggest (i) that the potential function $V(\phi)$ for internal rotation about the —C—O— bonds is symmetrical with no energy differences between isomers, and (ii) that short-range steric interactions are negligible between nearest neighbour segments. In keeping with (i) is the indirect observation that the unperturbed dimensions of PMPO and PPPO are independent of temperature within experimental error. Unfortunately an accurate measurement of $d \ln \langle r_0^2 \rangle / dT$ is difficult to obtain. Even if a range of θ-solvents had been available, the polar nature of the poly(phenylene oxide) backbone might have raised doubts about the possible influence of specific solvent effects. Measurement of $d \ln [\eta]/dT$ in an athermal solvent was not possible because a suitable solvent was not available. The corresponding measurement for low molecular weight polymer fractions in good solvents was not used because the assumption that α is unity under these circumstances is, as yet, of uncertain validity. Consequently only the one method was available to us, again of uncertain reliability. In the event the temperature dependence of dimensions proved too small to be determined with satisfactory precision. The conclusion that the dependence is small must be considered to be tentative.

Inspection of molecular models suggests that $V(\phi)$ should have twofold symmetry with minima at $\phi = 90°$ and 270° ($\phi = 0°$ being arbitrarily taken as the *trans* conformation) and since these two conformations are mirror images for 2,6 disubstituted phenylene oxide they must have identical energies. The infra-red spectra of 2,6 disubstituted anisoles[17] are consistent with this twofold barrier model in which the barrier height $V_0 = 3{\cdot}5$ kcal mole^{-1} in the gas phase and $V_0 = 6$ kcal mole^{-1} in the liquid state.

Short-range steric interactions between near-neighbour segments usually cause a significant increase in $\langle r_0^2 \rangle$ relative to $\langle r_{0f}^2 \rangle$. For example in poly(alkalene oxides) $\sigma = 1{\cdot}6$ and this is considered to be a reasonably low value. Such interactions, however, are likely to be strongly dependent on the segment length 'l'. In poly(phenylene oxides) etc. the effective value of l is large (5·4Å) and this must play an important role in relieving steric interactions, thus contributing to the abnormally low values of σ observed for the two poly(phenylene oxides) studied in this work.

The authors are extremely grateful for gifts of polymer samples by A.K.U. and G.E. (U.S.A.) They also wish to thank Dr C. Price and Mr F. D. Hartley for helpful discussions and Dr Allen Schultz for a preview of his work on similar polymers.

Department of Chemistry,
The University,
Manchester 13

(*Received February 1968*)

REFERENCES

[1] HAY, A. S. *Fortschr. Hochpolym.-Forsch.* 1967, **4**, 496
[2] DESREUX, V. and BISCHOFF, J. *Bull. Soc. Chim. Belg.* 1950, **59**, 93
[3] KAUFMAN, H. S. and SOLOMAN, E. *Industr. Engng Chem. (Industr.)*, 1953, **45**, 1779
[4] HUGGINS, M. L. *J. Amer. chem. Soc.* 1942, **64**, 2716
[5] KRAEMER, E. O. *Industr. Engng Chem. (Industr.)*, 1938, **30**, 1200
[6] ZIMM, B. *J. chem. Phys.* 1948, **16**, 1099
[7] STOCKMAYER, W. H. and FIXMAN, M. *J. Polym. Sci.* 1963, **1**, 137
[8] KURATA, M. and STOCKMAYER, W. H. *Fortschr. Hochpolym.-Forsch.* 1963, **3**, 196
[9] FIXMAN, M. *J. chem. Phys.* 1962, **36**, 3123
[10] KURATA, M., STOCKMAYER, W. H. and ROIG, A. *J. chem. Phys.* 1960, **33**, 151
[11] MCINTYRE, D., WIMS, A., WILLIAMS, L. C. and MANDELKERN, L. *J. phys. Chem.* 1962, **66**, 1932
[12] NEWMAN, S., KRIGBAUM, W. R., LANGIER, C. and FLORY, P. J. *J. Polym. Sci.* 1954, **14**, 451
[13] ALLEN, G., BOOTH, C. and PRICE, C. *Polymer, Lond.* 1967, **8**, 391
[14] BARRALES-RIENDA, J. M. and PEPPER, D. C. *J. Polym. Sci. B*, 1966, **4**, 939
[15] SCHULZ, G. V. *Z. phys. Chem. B*, 1935, **30**, 379
[16] ZIMM, B. *J. chem. Phys.* 1948, **16**, 1093
[17] FEWSTER, S. Unpublished results
[18] ALLEN, G., BOOTH, C. and PRICE, C. *Polymer, Lond.* 1967, **8**, 414
[19] BETHELL, M. *M.Sc. thesis.* University of Manchester, 1968

Notes and Communications

Cautionary Note on Extrapolation Methods for Determining Unperturbed Coil Dimensions

DURING the course of some light scattering experiments on polyisobutene (PIB) fractions, covering a 15-fold range of molecular weight, in cyclohexane it became necessary to try and estimate the unperturbed dimensions of these polymer fractions. A graph of log $\langle S^2\rangle_z$ versus log $\langle M\rangle_w$ is shown in *Figure 1*, and the $\langle S^2\rangle/\langle M\rangle$ relationship derived from this is $\langle S^2\rangle_z = 0{\cdot}046\,\langle M\rangle_w^{1{\cdot}16}$.

For other purposes, measurements were carried out on six of the PIB fractions at a number of temperatures (the number ranging from five to eight) in two different solvents and so it was possible to analyse the results for errors. The mean fractional error in $\langle M\rangle$ was found to be 0·031. The error in $\langle S^2\rangle$ must be at least as great and we would suggest that it is more likely to be about twice as great although we cannot estimate it from our data.

In order to estimate the unperturbed dimensions, the extrapolation methods of Kurata and Stockmayer[1] (*K–S*) and of Ptitsyn[2] were tried. The plots of

$$\frac{\langle S^2\rangle_z}{\langle M\rangle_w} \text{ versus } \frac{\langle M\rangle_w}{\langle S^2\rangle_z^{\frac{1}{2}}} \text{ and } \frac{\langle S^2\rangle_z}{\langle M\rangle_w} \text{ versus } \langle M\rangle_w^{1/3}$$

(the latter is equivalent to Ptitsyn's plot of $R^2/(DP)$ versus $(DP)^{\frac{1}{2}}$, where DP is the degree of polymerization) were both curved over the whole range. Over no range did the curves appear linear and at low values of M they tended towards the origin (*Figure 2*), especially if extra values were taken from the line of *Figure 1*. This behaviour made it impossible to carry out any linear extrapolation to find $\{\langle S^2\rangle/\langle M\rangle\}_0$ and caused us to examine the theory behind the extrapolation methods.

Both methods rely on the use of a closed expression for the expansion factor $\alpha^2 = \langle S^2\rangle/\langle S^2\rangle_0$ of the form $\alpha^n - \alpha^m = KM^{\frac{1}{2}}$, ($n=3$, $m=1$, in *K–S*, $n=3$, $m=0$ in Ptitsyn). However, it is now generally accepted[3–8] and can be seen from *Figure 1*, that for a linear polymer in solution $\langle S^2\rangle = kM^{1+\epsilon}$ where ϵ varies from 0, in a θ-solvent, to 0·25 or thereabouts, and is 0·16 in the case of PIB in cyclohexane.

In the light of this we can reconsider the nature of the extrapolation plots. The initial *K–S* plot amounts to a graph of kM^{ϵ} versus $M^{(1-\epsilon)/2} \times k^{-\frac{1}{2}}$ and will, in general, be a curve passing through the origin. This is precisely what we observe for PIB.

For any extrapolation of any part of the PIB curve, estimation of $g(\alpha) = \{8\alpha^3/(3\alpha^2+1)^{3/2}\}$ from the intercept gives values ranging from about 1 up to 1·4 as M covers its whole range. Use of these values to adjust the curve only serves to increase the curvature and does not improve the chances of extrapolation.

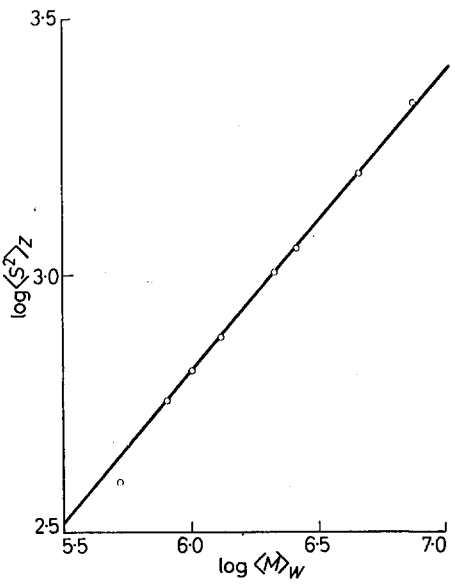

Figure 1

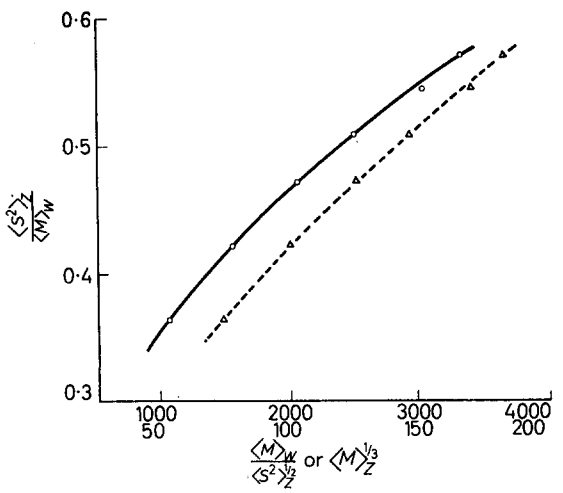

Figure 2—Abscissa scales: ○ upper, △ lower

Similar considerations apply to the Ptitsyn plots of $\langle S^2\rangle/DP$ versus $DP^{\frac{1}{2}}$. This is the same as $\langle S^2\rangle/\langle M\rangle$ versus $M^{\frac{1}{2}}$ (*see Figure 2*) and, since $\langle S^2\rangle = kM^{1+\epsilon}$, it can be reduced to kM^{ϵ} versus $M^{\frac{1}{2}}$ which will in general be curved and will pass through the origin.

It is clear from the quantities plotted in the two methods that straight lines will only be obtained if $\epsilon = \frac{1}{3}$, which also happens to be the value which makes the two expressions consistent with one another.

An inconsistency in the methods therefore arises when the approximate closed form for α is used when $\epsilon \neq \frac{1}{3}$ in spite of the fact that the form for $\langle S^2\rangle$ is quite well established both practically and theoretically. This inconsistency gives rise to curved plots if a wide range of molecular weights

is examined; and if the experiments only cover a small range and the plots appear linear, the intercept on the $\langle S^2\rangle/\langle M\rangle$ axis will depend on the particular range of molecular weights covered.

It would thus seem that the extrapolation methods discussed above will not, in general, work and indeed it is noticeable that many of the plots of the K–S or Ptitsyn types in the literature are in fact rather poor straight lines.

However, it may be that in some cases meaningful extrapolations can be made and for some systems the methods appear to work reasonably well[9]. In all cases when $\epsilon = 0$ the analyses obviously become meaningful but unnecessary.

A. J. HYDE and A. G. TANNER

Department of Pure and Applied Chemistry,
Strathclyde University,
Glasgow, C.1.

(*Received December 1967*)

REFERENCES

[1] KURATA, M. and STOCKMAYER, W. H. *Fortschr. Hochpolym. Forsch.* 1963, **3**, 196
[2] PTITSYN, O. B. *Vysokomol. Soedineniya,* 1961, **3**, 1673
[3] EDWARDS, S. F. *Proc. phys. Soc.* 1965, **85**, 613
[4] FISHER, M. E. and HILEY, B. J. *J. chem. Phys.* 1961, **34**, 1253
[5] FISHER, M. E. and SYKES, M. F. *Phys. Rev.* 1959, **114**, 45
[6] DOMB, C., GILLIS, J. and WILMERS, G. *Proc. phys. Soc.* 1965, **85**, 685
[7] SCHULTZ, A. R. *J. Amer. chem. Soc.* 1954, **76**, 3422
[8] HYDE, A. J. *Polymer, Lond.* 1966, **7**, 459
[9] ALLEN, G. Personal communication

Second Virial Coefficients in Ternary Systems

IN A recent study[1] of preferential adsorption in solvent (1), non-solvent (2), polystyrene (3) systems, values of the second virial coefficient (A_2) were obtained and compared with three theoretical treatments, which attempt to formulate the molecular weight dependence[2–4] of A_2. It was concluded that, under the experimental conditions used, the approach which best described the behaviour of the second virial coefficient was that of Casassa and Markovitz[3], where the general equation describing the molecular weight dependence of A_2 is

$$A_2 = \psi_1 (1 - \theta/T)(\bar{v}^2/V_1) \times F(X) \tag{1}$$

and the function $F(X)$, as given by Casassa and Markovitz, has the form

$$F(X) = (1/1{\cdot}093X)[1 - \exp(-1{\cdot}093X)] \tag{2}$$

in which X is defined as

$$X = 4C_m\psi_1 (1 - \theta/T) M^{\frac{1}{2}} \times \alpha^{-3} \tag{3}$$

Here ψ_1 is the entropy of mixing parameter, $\bar{v}$ the partial specific volume of the polymer, V_1 the molar volume of solvent, T and θ the temperature and

is examined; and if the experiments only cover a small range and the plots appear linear, the intercept on the $\langle S^2\rangle/\langle M\rangle$ axis will depend on the particular range of molecular weights covered.

It would thus seem that the extrapolation methods discussed above will not, in general, work and indeed it is noticeable that many of the plots of the K–S or Ptitsyn types in the literature are in fact rather poor straight lines.

However, it may be that in some cases meaningful extrapolations can be made and for some systems the methods appear to work reasonably well[9]. In all cases when $\epsilon = 0$ the analyses obviously become meaningful but unnecessary.

A. J. HYDE and A. G. TANNER

Department of Pure and Applied Chemistry,
Strathclyde University,
Glasgow, C.1.

(*Received December 1967*)

REFERENCES

[1] KURATA, M. and STOCKMAYER, W. H. *Fortschr. Hochpolym. Forsch.* 1963, **3**, 196
[2] PTITSYN, O. B. *Vysokomol. Soedineniya,* 1961, **3**, 1673
[3] EDWARDS, S. F. *Proc. phys. Soc.* 1965, **85**, 613
[4] FISHER, M. E. and HILEY, B. J. *J. chem. Phys.* 1961, **34**, 1253
[5] FISHER, M. E. and SYKES, M. F. *Phys. Rev.* 1959, **114**, 45
[6] DOMB, C., GILLIS, J. and WILMERS, G. *Proc. phys. Soc.* 1965, **85**, 685
[7] SCHULTZ, A. R. *J. Amer. chem. Soc.* 1954, **76**, 3422
[8] HYDE, A. J. *Polymer, Lond.* 1966, **7**, 459
[9] ALLEN, G. Personal communication

Second Virial Coefficients in Ternary Systems

IN A recent study[1] of preferential adsorption in solvent (1), non-solvent (2), polystyrene (3) systems, values of the second virial coefficient (A_2) were obtained and compared with three theoretical treatments, which attempt to formulate the molecular weight dependence[2–4] of A_2. It was concluded that, under the experimental conditions used, the approach which best described the behaviour of the second virial coefficient was that of Casassa and Markovitz[3], where the general equation describing the molecular weight dependence of A_2 is

$$A_2 = \psi_1 (1 - \theta/T)(\bar{v}^2/V_1) \times F(X) \tag{1}$$

and the function $F(X)$, as given by Casassa and Markovitz, has the form

$$F(X) = (1/1{\cdot}093X)[1 - \exp(-1{\cdot}093X)] \tag{2}$$

in which X is defined as

$$X = 4C_m\psi_1 (1 - \theta/T) M^{\frac{1}{2}} \times \alpha^{-3} \tag{3}$$

Here ψ_1 is the entropy of mixing parameter, $\bar{v}$ the partial specific volume of the polymer, V_1 the molar volume of solvent, T and θ the temperature and

Flory temperature respectively, α the expansion factor and C_m is the constant in the Flory–Fox solution theory.

Since publication of this work, Yamakawa[5] has shown that the value of A_2 measured in such ternary systems will in fact be dependent on the amount of preferential adsorption encountered and that, as a result, the experimental values of A_2 will only be apparent values. He has suggested that when the amount of precipitant (2) in the system is low, the effect can be corrected for by using

$$A_2 = (M^{app.}/M) \times A_2^{app.} \tag{4}$$

where $A_2^{app.}$ and $M^{app.}$ are the apparent or experimentally obtainable values of the second virial coefficient and molecular weight respectively, measured in a ternary system exhibiting preferential adsorption, while A_2 and M are the corresponding values in the absence of any such adsorption. By applying equation (4) to the data in ref. 1 (assuming that the correction is valid at higher concentrations of precipitant), new values of A_2 can be obtained and typical results are shown for the system benzene–heptane–polystyrene in *Table 1*. The weight average molecular weight of the polystyrene sample[1] was $2{\cdot}2 \times 10^6$.

Table 1. Experimental ($A_2^{app.}$) and corrected (A_2), second virial coefficients for the system benzene–heptane–polystyrene

ϕ_1*	$A_2^{app.} \times 10^4$ $cm^3 g^{-2}$ *mole*	$A_2 \times 10^4$ $cm^3 g^{-2}$ *mole*	$\langle \bar{S}^2 \rangle^{\frac{1}{2}} \times 10^{-8}$ *cm*
1·00	3·06	3·06	798
0·95	3·01	3·52	794
0·90	2·42	2·92	780
0·80	2·02	2·71	770
0·70	1·57	2·26	735
0·60	1·34	1·90	642
0·49	0·48	0·62	553
0·45	0·21	0·26	479
0·44	0·00	0·00	447

*ϕ_1 is the volume fraction of benzene in the mixture.

In *Figure 1*, where theory and experiment are compared, it can be seen that coincidence of A_2 with the Casassa–Markovitz equation (curve 1) is no longer apparent and it is obvious that the refined approach proposed by Casassa[4] (curve 2) is now more representative of the data. In this latter theory a new expansion factor α_2 was introduced by Casassa where

$$\alpha_2^5 - \alpha_2^3 = 1{\cdot}601\,(\alpha^5 - \alpha^3) \tag{5}$$

and

$$X = 1{\cdot}507\,(\alpha_2^2 - 1) \tag{6}$$

but, as was observed previously, A_2 at high values of ϕ_1 still deviates from the theoretical curve and only approaches the predicted value as the solvent power of the system deteriorates.

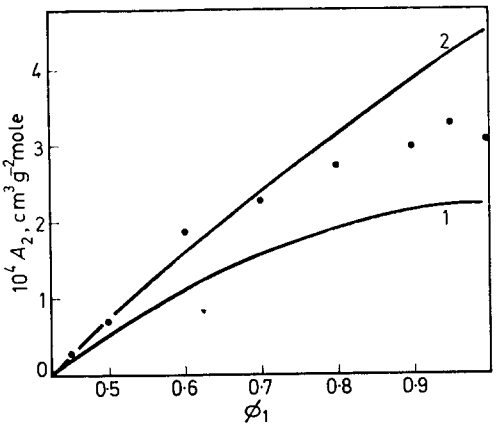

Figure 1—Variation of the corrected second virial coefficient A_2 with ϕ_1. Theoretical curves are calculated from Casassa and Markovitz—curve 1 and Casassa —curve 2

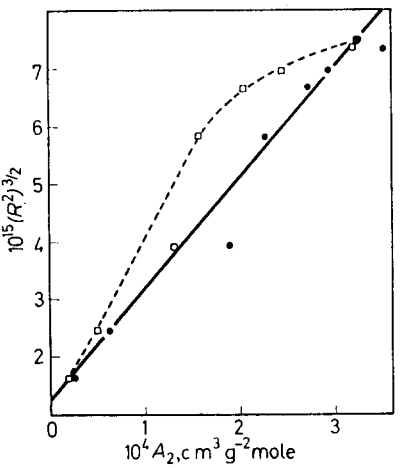

Figure 2—Dependence of $(\overline{R^2})^{3/2}$ on A_2 where the uncorrected experimental A_2 is □ and the corrected A_2 is ●

A further consequence of this correction to A_2 can be seen on examination of the variation of the polymer coil size with A_2. Krigbaum[6] proposed a semi-empirical relationship

$$(\overline{R^2})^{3/2} = (\overline{R_0^2})^{3/2} + 3\,(134/105)\,(3/2\pi)^{3/2}\,A_2 M^2/N_A \qquad (7)$$

where $(\overline{R^2})^{\frac{1}{2}}$ and $(\overline{R_0^2})^{\frac{1}{2}}$ are the perturbed and unperturbed root mean square end to end distances of the polymer chain and N_A is Avogadro's number. The equation predicts a linear dependence of $(\overline{R^2})^{3/2}$ on A_2 at constant M and the validity of equation (7) can be tested readily for the present system as shown in *Figure 2*. When $A_2^{app.}$ is used a curve is obtained, but replacement of $A_2^{app.}$ by the corrected A_2 produces a linear relationship as predicted by equation (7). Extrapolation to zero A_2 gives $(\overline{R_0^2})^{3/2} \simeq 1{\cdot}24 \times 10^{-15}$ cm^3 or $(\overline{S_0^2})^{\frac{1}{2}} = 438A$, in reasonably good agreement with the experimental value. Similar treatment of the other two systems originally reported[1] produces the same trends.

One must conclude from this that the proposed correction in A_2 is

necessary for ternary systems in which there is preferential adsorption of one component by another, and that the Casassa theory is at present the most successful in predicting the value of A_2 when solvent–polymer interaction is not too strong.

J. M. G. COWIE

Department of Chemistry,
University of Essex,
Wivenhoe Park,
Colchester, Essex.

(Received April 1968)

REFERENCES

[1] COWIE, J. M. G. and BYWATER, S. *J. macromol. Chem.* 1966, **1**, 581
[2] FLORY, P. J. and KRIGBAUM, W. R. *J. chem. Phys.* 1950, **18**, 1086
[3] CASASSA, E. F. and MARKOVITZ, H. *J. chem. Phys.* 1958, **29**, 493
[4] CASASSA, E. F. *J. chem. Phys.* 1959, **31**, 800
[5] YAMAKAWA, H. *J. chem. Phys.* 1967, **46**, 973
[6] KRIGBAUM, W. R. *J. Polym. Sci.* 1955, **18**, 315

The Free Radical Copolymerization of N-*Vinyl Carbazole*

N-VINYL carbazole is an interesting monomer for copolymerization studies since it is a powerful charge transfer donor capable of forming complexes with electrophilic species. Indeed in the presence of charge transfer acceptors the free radical polymerization of *N*-vinyl carbazole becomes converted to a cationic process[1]. Such a reaction immediately casts doubt[1] as to whether *N*-vinyl carbazole can copolymerize with weakly electron-accepting comonomers (such as acrylates and methacrylates) by a truly free radical process. However, an analysis[2] of the products of such polymerizations showed that this could be achieved in solution in tetrahydrofuran at 30°C. We report here the reactivity ratios for a series of free radical copolymerizations involving *N*-vinyl carbazole.

All copolymerizations were carried out at 30°C with appropriate amounts of both monomers (total monomer concentration 3·0 moles/litre) and either azo-bis(isobutyronitrile) (10^{-2} moles/litre) or ditertiary butyl peroxide (10^{-2} moles/litre) dissolved in tetrahydrofuran. The polymerizations were continued until conversion of the more reactive monomer reached five to ten per cent, which was usually less than one per cent conversion of the total monomer. Copolymer compositions were determined using elemental analysis. Spectroscopic analysis of the copolymers proved unreliable since the extinction of the carbazole group (the most prominent spectral feature in the u.v. spectrum) was a function of copolymer composition. Copolymer compositions were determined from duplicate runs at four initial monomer feed compositions. The reactivity ratios, r_1 and r_2, and the uncertainties in these values, δr_1 and δr_2, are listed in *Table 1*, where monomer 1 is always *N*-vinyl carbazole.

necessary for ternary systems in which there is preferential adsorption of one component by another, and that the Casassa theory is at present the most successful in predicting the value of A_2 when solvent–polymer interaction is not too strong.

J. M. G. COWIE

Department of Chemistry,
University of Essex,
Wivenhoe Park,
Colchester, Essex.

(Received April 1968)

REFERENCES

[1] COWIE, J. M. G. and BYWATER, S. *J. macromol. Chem.* 1966, **1**, 581
[2] FLORY, P. J. and KRIGBAUM, W. R. *J. chem. Phys.* 1950, **18**, 1086
[3] CASASSA, E. F. and MARKOVITZ, H. *J. chem. Phys.* 1958, **29**, 493
[4] CASASSA, E. F. *J. chem. Phys.* 1959, **31**, 800
[5] YAMAKAWA, H. *J. chem. Phys.* 1967, **46**, 973
[6] KRIGBAUM, W. R. *J. Polym. Sci.* 1955, **18**, 315

The Free Radical Copolymerization of N-*Vinyl Carbazole*

N-VINYL carbazole is an interesting monomer for copolymerization studies since it is a powerful charge transfer donor capable of forming complexes with electrophilic species. Indeed in the presence of charge transfer acceptors the free radical polymerization of *N*-vinyl carbazole becomes converted to a cationic process[1]. Such a reaction immediately casts doubt[1] as to whether *N*-vinyl carbazole can copolymerize with weakly electron-accepting comonomers (such as acrylates and methacrylates) by a truly free radical process. However, an analysis[2] of the products of such polymerizations showed that this could be achieved in solution in tetrahydrofuran at 30°C. We report here the reactivity ratios for a series of free radical copolymerizations involving *N*-vinyl carbazole.

All copolymerizations were carried out at 30°C with appropriate amounts of both monomers (total monomer concentration 3·0 moles/litre) and either azo-bis(isobutyronitrile) (10^{-2} moles/litre) or ditertiary butyl peroxide (10^{-2} moles/litre) dissolved in tetrahydrofuran. The polymerizations were continued until conversion of the more reactive monomer reached five to ten per cent, which was usually less than one per cent conversion of the total monomer. Copolymer compositions were determined using elemental analysis. Spectroscopic analysis of the copolymers proved unreliable since the extinction of the carbazole group (the most prominent spectral feature in the u.v. spectrum) was a function of copolymer composition. Copolymer compositions were determined from duplicate runs at four initial monomer feed compositions. The reactivity ratios, r_1 and r_2, and the uncertainties in these values, δr_1 and δr_2, are listed in *Table 1*, where monomer 1 is always *N*-vinyl carbazole.

Table 1. Copolymerization reactivity ratios

Monomer 2	r_1	δr_1	r_2	δr_2	$r_1 r_2$
Cyanoacetylene	0·075	0·005	0·030	0·005	0·002
Acrylonitrile	0·04	0·02	0·28	0·02	0·012
Methyl acrylate	0·11	0·02	0·43	0·02	0·05
p-Chlorostyrene	0·023	0·003	7·0	0·2	0·16
Methyl methacrylate	0·07	0·01	2·7	0·1	0·19
Vinyl acetate	3·9	0·2	0·13	0·03	0·51

It can be seen from the decrease in the product $r_1 r_2$ that the tendency to alternation in the copolymers increases in the series vinyl acetate to cyanoacetylene, as does the general electrophilicity of the comonomer. Although the most strongly electron-accepting comonomers show the strongest tendency towards the formation of alternating copolymers, the reactivity ratios obtained with acrylonitrile, methyl acrylate, methyl methacrylate and vinyl acetate all fit into conventional copolymerization theory. For example, they yield self-consistent Q, e values[3,4] of $+0{\cdot}43 \pm 0{\cdot}05$ and $-1{\cdot}03 \pm 0{\cdot}1$ respectively. There are no literature values at 30°C, though estimates at temperatures above 65°C give for Q, 0·33[5], 0·30[6], 0·41[4], and for e $-1{\cdot}60$[5], $-1{\cdot}20$[6] and $-1{\cdot}40$[4]. Because of the increasing probability of charge transfer initiation at the higher temperatures, it is felt that the values at 30°C are the most reliable.

Using the values of Q and e, values for cyanoacetylene were determined as $Q = +0{\cdot}163$, $e = +1{\cdot}43$.

The authors wish to acknowledge the use of facilities at the Donnan Laboratories, University of Liverpool, where this work was carried out.

A. M. NORTH and
K. E. WHITELOCK*

Department of Pure and Applied Chemistry,
University of Strathclyde,
Glasgow, C.1.

(*Received April 1968*)

REFERENCES

[1] ELLINGER, L. P. *Polymer, Lond.* 1965, **6**, 549
[2] LEDWITH, A., NORTH, A. M. and WHITELOCK, K. E. *European Polymer J.* 1968, **4**, 133
[3] ALFREY, J. and PRICE, C. C. *J. Polym. Sci.* 1947, **2**, 101
[4] HAM, G. E. *Encycl. Polymer Sci. and Technol.* 1967, **4**, 219
[5] SCHWAN, T. C. and PRICE, C. C. *J. Polym. Sci.* 1954, **40**, 457
[6] HART, R. *Makromol. Chem.* 1961, **47**, 143

*Present address: Pilkington Bros., Lathom, Lancs.

Polypropylene Oxide. Rotating Frame Proton Spin–Lattice Relaxation Measurements

MEASUREMENTS of nuclear spin–lattice relaxation times and broad line nuclear resonance spectra are familiar and much exploited techniques for investigating the molecular motions, phase changes and morphology of

Table 1. Copolymerization reactivity ratios

Monomer 2	r_1	δr_1	r_2	δr_2	$r_1 r_2$
Cyanoacetylene	0·075	0·005	0·030	0·005	0·002
Acrylonitrile	0·04	0·02	0·28	0·02	0·012
Methyl acrylate	0·11	0·02	0·43	0·02	0·05
p-Chlorostyrene	0·023	0·003	7·0	0·2	0·16
Methyl methacrylate	0·07	0·01	2·7	0·1	0·19
Vinyl acetate	3·9	0·2	0·13	0·03	0·51

It can be seen from the decrease in the product $r_1 r_2$ that the tendency to alternation in the copolymers increases in the series vinyl acetate to cyanoacetylene, as does the general electrophilicity of the comonomer. Although the most strongly electron-accepting comonomers show the strongest tendency towards the formation of alternating copolymers, the reactivity ratios obtained with acrylonitrile, methyl acrylate, methyl methacrylate and vinyl acetate all fit into conventional copolymerization theory. For example, they yield self-consistent Q, e values[3,4] of $+0{\cdot}43 \pm 0{\cdot}05$ and $-1{\cdot}03 \pm 0{\cdot}1$ respectively. There are no literature values at 30°C, though estimates at temperatures above 65°C give for Q, 0·33[5], 0·30[6], 0·41[4], and for e $-1{\cdot}60$[5], $-1{\cdot}20$[6] and $-1{\cdot}40$[4]. Because of the increasing probability of charge transfer initiation at the higher temperatures, it is felt that the values at 30°C are the most reliable.

Using the values of Q and e, values for cyanoacetylene were determined as $Q = +0{\cdot}163$, $e = +1{\cdot}43$.

The authors wish to acknowledge the use of facilities at the Donnan Laboratories, University of Liverpool, where this work was carried out.

A. M. NORTH and
K. E. WHITELOCK*

Department of Pure and Applied Chemistry,
University of Strathclyde,
Glasgow, C.1.

(*Received April 1968*)

REFERENCES

[1] ELLINGER, L. P. *Polymer, Lond.* 1965, **6**, 549
[2] LEDWITH, A., NORTH, A. M. and WHITELOCK, K. E. *European Polymer J.* 1968, **4**, 133
[3] ALFREY, J. and PRICE, C. C. *J. Polym. Sci.* 1947, **2**, 101
[4] HAM, G. E. *Encycl. Polymer Sci. and Technol.* 1967, **4**, 219
[5] SCHWAN, T. C. and PRICE, C. C. *J. Polym. Sci.* 1954, **40**, 457
[6] HART, R. *Makromol. Chem.* 1961, **47**, 143

*Present address: Pilkington Bros., Lathom, Lancs.

Polypropylene Oxide. Rotating Frame Proton Spin–Lattice Relaxation Measurements

MEASUREMENTS of nuclear spin–lattice relaxation times and broad line nuclear resonance spectra are familiar and much exploited techniques for investigating the molecular motions, phase changes and morphology of

polymeric materials. Within the last few years, however, a related method has become available[1] for studying polymer motions[2,3] which is the measurement of relaxation times in the rotating frame. The spin–lattice relaxation time, T_1 is a measure of the rate at which the macroscopic magnetization of the sample, which at equilibrium is aligned parallel to the direction of the polarizing field H_0, returns to this direction if the equilibrium is perturbed. In the rotating frame experiment, however, the magnetization is aligned by a suitable method parallel to an applied radiofrequency (r.f.) field, H_1, and its subsequent rate of decay along this axis is measured. The resulting time constant, $T_{1\rho}$, is the relaxation time in the rotating frame. Since $H_0 \gg H_1$ this method through variation of H_1 (and the resonance condition $\omega_1 = \gamma H_1$) makes possible relaxation measurements at a number of different frequencies, ω_1, and to some extent removes one of the disadvantages of conventional T_1 measurements (as compared for instance with dielectric relaxation measurements), i.e. that the measurement frequency is usually fixed in the MHz region. This results because straightforward measurements at lower frequencies are rendered impracticable through sensitivity considerations, whereas the rotating frame technique retains the sensitivity appropriate to measurements at a high frequency. The H_1 field is applied in resonant pulses and the height of the induction decay which follows the pulse is measured, this being proportional to the magnetization remaining along the H_1 direction. $T_{1\rho}$ is thus determined by measuring the height of the induction decay as a function of pulse length.

This method has been used to study polypropylene oxide (PPO) of molecular weight 4000, for which, along with a number of other PPOs, T_1 data have already been obtained at a frequency of 30 MHz. In this case the alignment of the magnetization along the 30 MHz r.f. field ('spin-locking') was achieved by the $\pi/2$ pulse–$\pi/2$ phase shift method[5]. The magnitude of the H_1 field was 4·3 gauss or 18·3 kHz in frequency units. To within experimental error the magnetization always decayed exponentially and was described in terms of a single time constant, in contrast to a number of other polymers, particularly those of a highly crystalline nature such as polyethylene[3] or polyethylene oxide[6].

The results obtained are shown in *Figure 1* where $T_{1\rho}$ is plotted as a function of reciprocal temperature along with the previous T_1 measurements for comparison. The $T_{1\rho}$ curve shows two minima which are displaced to lower temperatures as compared with those in the T_1 measurements. The high temperature minimum (235°K) may be assigned[4] to the motion setting in at the glass transition temperature whilst that at low temperature (95°K) is assigned to the CH_3 side group reorientational motion. The corresponding temperatures for the T_1 measurements are 261·5°K and 138°K respectively. Motional correlation times, τ_c, may be calculated at the positions of the minima. If $\tau_c \ll T_{2RL}$, where T_{2RL} is the spin–spin relaxation time characteristic of the rigid lattice, a modifiction of the BPP theory to the rotating frame[7] is appropriate which gives,

$$(1/T_{1\rho}) = A\,(\tau_c/\{1+4\omega_e^2\tau_c^2\}) \qquad (1)$$

where A is a constant related to $\langle \Delta H^2 \rangle$, the second moment of the resonance

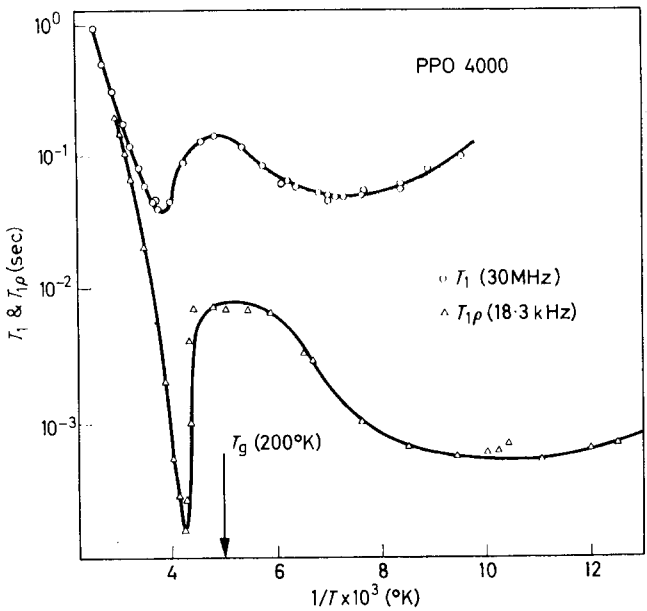

Figure 1—$T_{1\rho}$ and T_1 as a function of temperature for PPO 4000

line and $\omega_e = \gamma (H_1^2 + H_L^2)^{\frac{1}{2}}$ is the effective frequency in the rotating frame. H_L is the local field due to dipolar interaction and is defined[1] by $H_L^2 = \frac{1}{3}\langle \Delta H^2 \rangle$. At a minimum therefore $\omega_e \tau_c = 0{\cdot}5$, which compares with the relation $\omega_0 \tau_c = 0{\cdot}616$ which is appropriate to T_1 data. At the high temperature minimum H_L is small and may be neglected, but at the low temperature minimum $H_L \sim 3$ gauss. The motional frequencies, ν_c, derived from the high temperature minima ($\nu_c = 1/2\pi\tau_c$) and the reorientational frequencies[8] ($\nu_r = 1/3\pi\tau_c$) derived from the low temperature results are shown in *Figure 2*. Also shown is a point derived from neutron scattering experiments on a high molecular weight PPO which resulted in a peak identified with the CH_3 torsional mode[9] at 240 ± 10 cm^{-1} which corresponds to a barrier to rotation of 3·5 kcal mole^{-1}. Assuming a thermally activated process with an Eyring pre-exponential factor results in a frequency at room temperature of $\sim 10^{11}$ Hz. Since T_1 measurements on the same high molecular weight sample[4] showed that there was little molecular weight dependence of T_1 for samples with OH end-groups, it seems justifiable to include this point for comparison.

In fact, at the low temperature minimum the condition $\tau_c \ll T_{2RL}$ does not apply, τ_c and T_{2RL} being of comparable magnitude. This represents the region which lies between the BPP theory ($\tau_c \ll T_{2RL}$) and the strong collision Slichter–Ailion theory ($\tau_c > T_{2RL}$). However, since a minimum is observed it seems reasonable to suppose that a spectral density function of the type $\tau_c/(1 + 4\omega_e^2 \tau_c)$ may be used to derive a value of τ_c. The relative magnitudes of $T_{1\rho}$s measured in the BPP and Slichter–Ailion limits[1] are given by

$$T_{1\rho}\,(\mathrm{BPP})/T_{1\rho}\ (\mathrm{SA}) = H_1^2/(H_1^2 + H_L^2) \qquad (2)$$

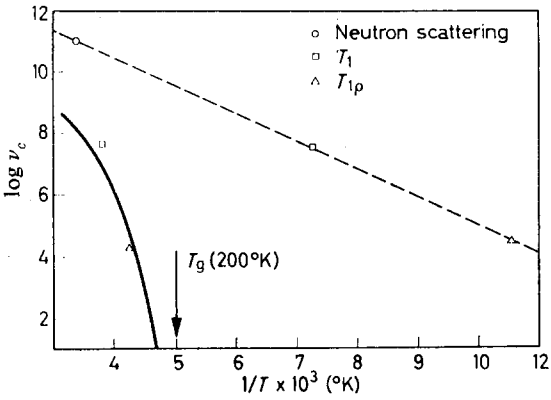

Figure 2—Correlation frequencies as a function of temperature for PPO 4000. The solid line is calculated from equation (3)

Previous comparisons of relative magnitudes of T_1 and $T_{1\rho}$ at CH_3 motional minima for polymethyl methacrylates indicated that the experimental ratios were smaller than those calculated on the basis of BPP theory for T_1 and $T_{1\rho}$. Part of this discrepancy is undoubtedly due to the fact that the $T_{1\rho}$ results are appropriate to the intermediate region where $\tau_c \sim T_{2RL}$, which from equation (2) is seen to reduce the expected value of the $T_1/T_{1\rho}$ ratio.

One may calculate activation energies for the processes concerned from the temperature dependence of the minimum positions. Since the correlation frequencies are derived in this way and do not depend on the detailed form of the relaxation theory, the activation energies obtained may be expected to be more realistic than those resulting from fixed frequency T_1 measurements alone. For the high temperature motion the mean activation energy is 34 kcal mole^{-1}. The frequency obtained from the $T_{1\rho}$ measurement correlated reasonably well with dielectric and mechanical measurements[4, 10, 11] of the same process which were fitted[10] by means of an expression of the form

$$\nu_c = a \exp\left[-b/(T - T_\infty)\right] \tag{3}$$

where $\log a = 11{\cdot}4$, $b = 893°K$ and $T_\infty = 174°K$. This expression is plotted in *Figure 2*. (For the sake of clarity the actual dielectric and mechanical measurements are not shown in *Figure 2*, see ref. 10.) In fact there is a small difference of 10 deg. C between the positions of the high temperature minimum for PPO 4000 and the similar minima which occur at higher temperatures for high molecular weight PPOs. This accounts for some part of the small discrepancy between T_1 measurements and the dielectric data, since equation (3) was used to fit data on a high molecular weight PPO. The apparent glass transition temperature, T_g, derived from the dielectric and mechanical data is ~200°K which is the same[12] as that obtained from dilatometric measurements. This value differs considerably from a dynamic determination of T_g by mechanical loss measurements[13] at 1–3 Hz which gave $T_g = 213°K$. Whilst some difference between these two values is to be expected, this mechanical transition does not correlate well with the data illustrated in ref. 10, the point falling well below the curve of $\log \nu_c$ against $1/T$. However, both T_g measurements and the

measurements of T_1 and $T_{1\rho}$ are consistent with the conclusion that T_g is independent of molecular weight for PPOs with OH end-groups. The lowest temperature at which evidence of the glass transition motion is seen in the T_1 and $T_{1\rho}$ results is $\sim$180°K which lies between the values of T_g and T_∞.

The activation energy for the CH_3 reorientational motion derived from the T_1 and $T_{1\rho}$ data is 4·2 kcal mole^{-1} which is similar to the barrier value derived from the neutron scattering data (3·5 kcal mole^{-1}) and much larger than the value of 1·7 kcal mole^{-1} previously obtained by fitting[4, 14] T_1 minimum data. It also agrees well with a value derived by interpolation from Stejskal and Gutowsky's calculations[8] of the effect of tunnelling on the CH_3 reorientational frequency. There is no evidence from the data in *Figure 2*, however, of the fall in apparent activation energy which would be expected from the results of these calculations if tunnelling was important at low temperatures.

Thanks are due to Dr P. Brier for providing neutron scattering data prior to publication. This work forms part of the research programme of the National Physical Laboratory.

T. M. CONNOR and A. HARTLAND

Molecular Science Division,
National Physical Laboratory,
Teddington, Middlesex.

(Received May 1968)

REFERENCES

[1] (a) SLICHTER, C. P. and AILION, D. *Phys. Rev.* 1964, **135,** A 1099
(b) AILION, D. and SLICHTER, C. P. *Phys. Rev.* 1965, **137,** A 235
[2] MCCALL, D. W. and DOUGLASS, D. C. *Appl. Phys. Letters,* 1965, **7,** 12
[3] CONNOR, T. M. and HARTLAND, A. *Physics Letters,* 1966, **23,** 662
[4] CONNOR, T M., BLEARS, D. J. and ALLEN, G. *Trans. Faraday Soc.* 1965, **61,** 1097
[5] HARTMANN, S. R. and HAHN, E. L. *Phys. Rev.* 1962, **128,** 2046
[6] CONNOR, T. M. and HARTLAND, A. To be published
[7] JONES, G. P. *Phys. Rev.* 1966, **140,** 332
[8] STEJSKAL, E. O. and GUTOWSKY, H. S. *J. chem. Phys.* 1958, **28,** 388
[9] BRIER, P. Private communication
[10] WILLIAMS, G. *Trans. Faraday Soc.* 1965, **61,** 1564
[11] BAUR, M. E. and STOCKMAYER, W. H. *J. chem. Phys.* 1965, **43,** 4319
[12] ALLEN, G., JONES, M. N., MARKS, D. J. and TAYLOR, W. D. *Polymer, Lond.* 1964, **5,** 547
[13] FAUCHER, J. A. *Polymer Letters,* 1965, **3,** 143
[14] CONNOR, T. M. and BLEARS, D. J. *Polymer, Lond.* 1965, **6,** 385

Free-radical Template Polymerization

THE polymerization of monomer molecules in organized arrays, for example molecules adsorbed on templates as in biopolymerization, provides a possible method of synthesizing copolymers of predetermined composition and structure. These materials are of potential importance both industrially and academically, yet comparatively little attention has been

measurements of T_1 and $T_{1\rho}$ are consistent with the conclusion that T_g is independent of molecular weight for PPOs with OH end-groups. The lowest temperature at which evidence of the glass transition motion is seen in the T_1 and $T_{1\rho}$ results is $\sim$180°K which lies between the values of T_g and T_∞.

The activation energy for the CH_3 reorientational motion derived from the T_1 and $T_{1\rho}$ data is 4·2 kcal mole^{-1} which is similar to the barrier value derived from the neutron scattering data (3·5 kcal mole^{-1}) and much larger than the value of 1·7 kcal mole^{-1} previously obtained by fitting[4, 14] T_1 minimum data. It also agrees well with a value derived by interpolation from Stejskal and Gutowsky's calculations[8] of the effect of tunnelling on the CH_3 reorientational frequency. There is no evidence from the data in *Figure 2*, however, of the fall in apparent activation energy which would be expected from the results of these calculations if tunnelling was important at low temperatures.

Thanks are due to Dr P. Brier for providing neutron scattering data prior to publication. This work forms part of the research programme of the National Physical Laboratory.

T. M. CONNOR and A. HARTLAND

Molecular Science Division,
National Physical Laboratory,
Teddington, Middlesex.

(Received May 1968)

REFERENCES

[1] (a) SLICHTER, C. P. and AILION, D. *Phys. Rev.* 1964, **135,** A 1099
(b) AILION, D. and SLICHTER, C. P. *Phys. Rev.* 1965, **137,** A 235
[2] MCCALL, D. W. and DOUGLASS, D. C. *Appl. Phys. Letters,* 1965, **7,** 12
[3] CONNOR, T. M. and HARTLAND, A. *Physics Letters,* 1966, **23,** 662
[4] CONNOR, T M., BLEARS, D. J. and ALLEN, G. *Trans. Faraday Soc.* 1965, **61,** 1097
[5] HARTMANN, S. R. and HAHN, E. L. *Phys. Rev.* 1962, **128,** 2046
[6] CONNOR, T. M. and HARTLAND, A. To be published
[7] JONES, G. P. *Phys. Rev.* 1966, **140,** 332
[8] STEJSKAL, E. O. and GUTOWSKY, H. S. *J. chem. Phys.* 1958, **28,** 388
[9] BRIER, P. Private communication
[10] WILLIAMS, G. *Trans. Faraday Soc.* 1965, **61,** 1564
[11] BAUR, M. E. and STOCKMAYER, W. H. *J. chem. Phys.* 1965, **43,** 4319
[12] ALLEN, G., JONES, M. N., MARKS, D. J. and TAYLOR, W. D. *Polymer, Lond.* 1964, **5,** 547
[13] FAUCHER, J. A. *Polymer Letters,* 1965, **3,** 143
[14] CONNOR, T. M. and BLEARS, D. J. *Polymer, Lond.* 1965, **6,** 385

Free-radical Template Polymerization

THE polymerization of monomer molecules in organized arrays, for example molecules adsorbed on templates as in biopolymerization, provides a possible method of synthesizing copolymers of predetermined composition and structure. These materials are of potential importance both industrially and academically, yet comparatively little attention has been

paid to template polymerization, no doubt partly because of the difficulty of finding suitable systems with conventional monomers.

Ballard and Bamford[1] established the existence of a template effect (or 'chain effect') in the polymerization of *N*-carboxy α-amino acid anhydrides (NCAs) in the presence of polysarcosine. In these systems adsorption of the NCA molecules on to polysarcosine chains[1-3] leads to a rapid polymerization, showing unusual kinetic features. Bamford, Block and Imanishi[4] showed that when a mixture of two different NCAs is polymerized in this manner, polymers with block-like character are formed if only one species of NCA is adsorbed on to the polysarcosine chain. Some degree of control of copolymer structure by template action is therefore possible in these reactions. Kargin and his colleagues[5] have investigated the specific polymerization by an ionic reaction of vinyl pyridinium salts on macromolecular matrices of polystyrene sulphonic acid and Kämmerer and Ozaki[6] have described the preparation of stereoregular and molecularly uniform acrylic acid oligomers on a matrix consisting of a polynuclear phenolic derivative. In this latter case the monomer was held to the matrix by covalent bonds so that the matrix exercised a very precise control over the reaction.

As far as we know there are no reports in the literature of free-radical template reaction analogous to the chain-effect polymerization of NCAs. For the past two years we have been studying such a process, viz. the free-radical polymerization of acrylic acid adsorbed on a template of the basic polymer polyethylenimine, and in this communication we present an outline of the kinetic results.

Polyethylenimine of degree of polymerization 275 was used and the solvent was a mixture of acetone and water, 2/1 (v/v). The systems were always homogeneous. *Figure 1* shows the initial rate of photopolymerization of acrylic acid (M) at 25°C as a function of the total base-molar concentration of polyethenimine $[T]_0$. The initial concentration of acrylic acid was constant at 0·1 ml^{-1}; with this low concentration no significant rate of polymerization is observed in the absence of polyethylenimine under the conditions described. However, the maximum initial rate, which occurs when $[T]_0/[M]_0 = 1$ approximately, ($[M]_0$ = initial concentration of monomer), is high, corresponding to about 30 per cent polymerization per minute. The shape of the curve in *Figure 1* is that expected for a template polymerization. At the lower values of $[T]_0$ the template is effectively saturated with monomer, and in this region the rate increases with increasing $[T]_0$. Eventually, however, as $[T]_0$ increases, a point is reached when there is not sufficient monomer in the system to maintain saturation of the template, and further increase in $[T]_0$ then leads to a reduction in rate of polymerization, since the continuity of the adsorbed monomer is interrupted. Other types of free-radical initiation give essentially similar results; we have examined thermal initiation by azo-bis-isobutyronitrile (3×10^{-3} ml^{-1}) at 60°C and photoinitiation by the $Mn_2(CO)_{10}$–$CHCl_3$ system[7] ($[Mn_2(CO)_{10}] = [CHCl_3] = 10^{-3} ml^{-1}$; $\lambda = 4\,358$ Å) at 25°C. When polyethylenimine was replaced by tetraethylene pentamine no template effect was observed at 25°C, the rate of polymerization remaining very low.

Before accepting a template mechanism we must ascertain whether

changes in $[T]_0$ can affect the rate of polymerization by any other mechanism. Both the viscosity and the *p*H of the reaction mixture are dependent on $[T]_0$, and these properties could influence the rate of polymerization of acrylic acid. However, the viscosity is almost proportional to $[T]_0$

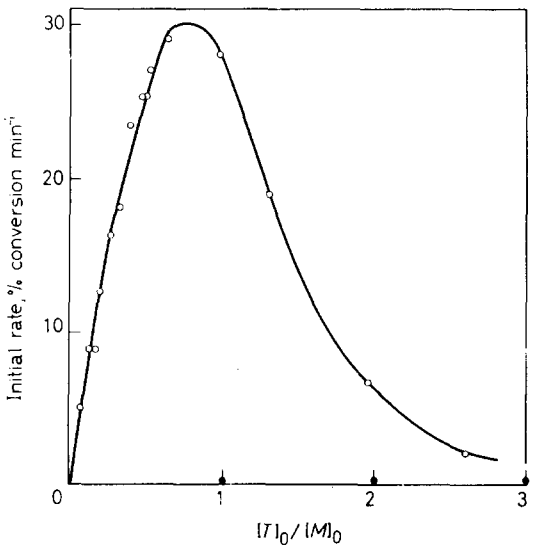

Figure 1—○ Dependence of initial rate of polymerization on base molar concentration of polyethylenimine $[T]_0$ at 25°C. ● Reaction in the presence of tetraethylene pentamine. ($[T]_0=0$). Acrylic acid concentration $[M]_0=0{\cdot}1$ ml^{-1}. Azo-bis-isobutyronitrile (6×10^{-3} ml^{-1}) as photosensitizer; λ in range 3 650–3 663 Å

over the range studied, so that if the rate increases arise from diffusion control of the termination reaction the rate should increase monotonically with $[T]_0$, which is clearly not so. Katchalsky and Bauer[8] showed that in the polymerization of methacrylic acid in aqueous media the rate decreases with increasing *p*H up to a value of six, at which point it is practically zero. In our case (*Figure 1*) the rate increases as the *p*H increases up to a value of five. Further, when the *p*H is controlled by sodium hydroxide in the absence of polyethylenimine no similar increase in the rate of polymerization (which remains effectively zero) is observed. Finally, the contribution of Michael addition of polyethylenimine to acrylic acid to the overall reaction must be assessed. At 25°C the observed rate of reaction in the absence of a free-radical initiator is negligible, showing that Michael addition does not contribute significantly. At 60°C when $[T]_0/[M]_0 > 2$ the rate of polymerization is low, and the Michael reaction accounts for most of the observed rate. The rate of Michael addition is proportional to $[T]_0$; for $[T]_0/[M] \leqslant 1$ it makes only a small contribution to the observed rate.

Confirmatory evidence for the template nature of the polymerization is provided by the observation that the addition of a non-polymerizable acid may

produce a large decrease in the rate of polymerization. *Table 1* illustrates this effect for addition of α-hydroxyisobutyric acid HBA. The latter is not a retarder of conventional free-radical polymerization; its behaviour in the present system arises from its competition with the monomer for the template sites. Clearly in the experiments referred to in *Table 1* the monomer is largely displaced by the stronger HBA. (The values of K_a for HBA and acrylic acid are $9{\cdot}2 \times 10^{-5}$ (18°C) and $5{\cdot}7 \times 10^{-5}$ (25°C), respectively.)

Table 1. Effect of α-hydroxyisobutyric acid (HBA) on initial rate of reaction. $[T]_0/[M]_0 = 0{\cdot}39$; $[M]_0 = 0{\cdot}1$ ml^{-1}; 25°C. Initiation as in *Figure 1*

$[HBA]/[M]_0$	0	1	2
Initial rate, % conversion per min	27	0·5	<0·1

We have developed the following expression for this type of template polymerization.

$$R_p = C \exp(-\alpha Z^\beta / kT)[X] \qquad (1)$$

Here R_p is the rate of polymerization, k, T are the Boltzmann constant and absolute temperature, respectively, [X] is the concentration of adsorbed monomer and $Z = [T]/[X]$, where $[T]$ is the concentration of free template sites. In equation (1) α, β are constants, and C is a function expressing the total free-radical concentration on the template molecules which is almost constant under the conditions of our experiments. The exponential term in equation (1) represents the important effects on the rate arising from interruptions in monomer sequences along the templates. The equilibrium constant for the adsorption of acrylic acid on polyethylenimine has been determined, hence [X] may be calculated. In *Figure 1* the curve shown is the theoretical one obtained from equation (1) with appropriate values of the parameters; it agrees well with the experimental observations.

We hope to extend this work to other free-radical template processes and to explore their suitability for synthetic purposes.

C. H. BAMFORD and Z. SHIIKI

Department of Inorganic, Physical and Industrial Chemistry,
The University of Liverpool,
Donnan Laboratories, Liverpool, 7.

(*Received May 1968*)

REFERENCES

[1] BALLARD, D. G. H. and BAMFORD, C. H. *Proc. Roy. Soc. A*, 1954, **223**, 495
[2] BAMFORD, C. H. and PRICE, R. C. *Trans. Faraday Soc.* 1965, **61**, 2208
[3] BALLARD, D. G. H. *Biopolymers*, 1964, **2**, 463
[4] BAMFORD, C. H., BLOCK, H. and IMANISHI, Y. *Biopolymers*, 1966, **4**, 1067
[5] KABANOV, V. A., ALIEV, K. V., KARGINA, O. V., PATRIKEEVA, T. I. and KARGIN, V. A. International Symposium on Macromolecular Chemistry, Prague, 1965. See also: KARGIN, V. A., KABANOV, V. A., ALIEV, K. V. and ROZVOLORSKY, E. F. *Dokl. Akad. Nauk S.S.S.R.*, 1965, **161**, 1131; KARGIN, V. A., KABANOV, V. A. and KARGINA, O. V. International Symposium on Macromolecular Chemistry, Brussels-Louvain (1967)
[6] KÄMMERER, H. and OZAKI, SH. *Makromol. Chem.* 1966, **91**, 1
[7] BAMFORD, C. H., CROWE, P. A. and WAYNE, R. P. *Proc. Roy. Soc. A*, 1965, **284**, 455
[8] KATCHALSKY, A. and BAUER, G. *Trans. Faraday Soc.* 1951, **47**, 1360

Dimensions of Poly(2,6-diphenyl-1,4-phenylene oxide) in Concentrated Solutions

IN A preceding publication Akers, Allen and Bethell[1] determined the unperturbed dimensions of poly(2,6-dimethyl-1,4-phenylene oxide) and poly(2,6-diphenyl-1,4-phenylene oxide), PPPO, from the dilute solution properties of these compounds. In addition, the temperature dependence of these chain dimensions was studied.

We wish to establish that their results on PPPO are in good agreement with our results, obtained from the examination of concentrated solutions.

It is well known that in a plot of the logarithm of the viscosity versus the logarithm of the concentration a breakpoint occurs at the so-called critical concentration[2,3]. Above the critical concentration the line is practically straight, below the critical concentration it is curved. Onogi, Kobayashi, Kojima and Taniguchi[2] conclude from their experiments that at the critical concentration a limiting case exists, where spheres of chain molecules are fully packed throughout the solution without any spaces between them and that the molecules will be in the unperturbed state. Consequently, they can evaluate the unperturbed dimensions. Their method has been refined by Cornet[3]. He assumes that at the critical concentration the total segment density of Gaussian coils becomes uniform throughout the solution. In addition, he assumes the centres of gravity of the coils to be arranged like an array of randomly packed spheres. The particle density of such a random array indicates a structure somewhere between a face-centred and a body-centred cubic lattice. Under these assumptions the following equation for the root-mean-square of the unperturbed end-to-end distance can be derived.

$$\langle r_0^2 \rangle^{\frac{1}{2}} = K \left(\frac{M_w}{C_{cr}} \right)^{1/3} \text{ cm} \qquad (1)$$

where the constant K has a value of $2{\cdot}84 \times 10^{-8}$ mole$^{1/3}$. C_{cr} is the critical polymer concentration in g/ml.

Our viscosity measurements were performed at various values of the shearing stress, using a Rotovisco (Gebrüder Haake, W. Germany). All flow curves indicated Newtonian behaviour up to a shearing stress of at least 800 dyne/cm^2. The zero-shear viscosity could be obtained with an accuracy of one per cent.

An example of a double logarithmic viscosity/concentration plot is given in *Figure 1*. From such plots the critical concentration can easily be determined with an accuracy of six per cent. The influence of this inaccuracy on the error in the unperturbed dimensions reduces to two per cent.

The characteristics of the PPPO samples are given in *Table 1*. *Table 2* gives the values of the unperturbed dimensions obtained in various solvents and at various temperatures. The unperturbed dimensions are nearly equal to the free-rotating dimensions, which, according to our calculations, using a segment length of 5·50Å and a bond angle of 120°, calculated from the crystalline structure of poly(phenylene oxide)[4], amount to 610×10^{-11} cm. These results also indicate that there is no, or at most a very small, dependence of the chain dimensions on the temperature.

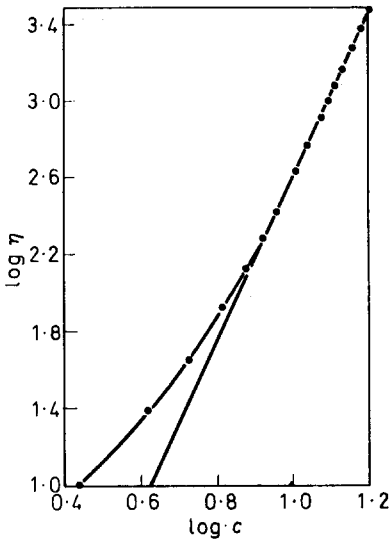

Figure 1—Solution viscosity of PPPO in chloroform at 25°C versus concentration in per cent by weight

Table 1. Characteristics of the PPPO samples

Method	$M_n \times 10^{-3}$		$M_w \times 10^{-3}$		$M_z \times 10^{-3}$		$\langle R^2_G \rangle_z^{\frac{1}{2}}$		$A_2 \times 10^4$	
Sample	I	II	I	II	I	II	I	II	I	II
GPC	203	252	592	507	1·172	967				
LS ($CHCl_3$)			611	550			338		2·42	
LS (CH_2Cl_2)			601				336		2·65	

Table 2. Values of the reduced unperturbed end-to-end distance obtained in various solvents and at various temperatures

Sample	*Temp.* °C	*Solvent*	C_{cr} wt-%	ρ_{cr} g/ml	$\langle r_0^2 \rangle / M_w)^{\frac{1}{2}} \times 10^{11}$ cm
I	20°	chloroform	8·7	1·452	617
I	25°	chloroform	8·7	1·445	620
I	40°	chloroform	8·7	1·421	622
I	25°	methylene chloride	8·9	1·311	634
I	25°	*n*-methylpyrrolidone	11·6	1·049	625
I	80°	*n*-methylpyrrolidone	11·8	1·000	631
II	25°	chloroform	9·4	1·444	617

Central Research Institute, AKU,
(Algemene Kunstzijde Unie N.V.),
and affiliated Companies,
Arnhem, The Netherlands.

A. OPSCHOOR

(Received May 1968)

REFERENCES

[1] AKERS. P. J., ALLEN, G. and BETHELL, M. J. *Polymer, Lond.* 1968, **9**, 575
[2] ONOGI, S., KOBAYASHI, T., KOJIMA, Y. and TANIGUCHI, Y. *J. appl. Polym. Sci.* 1963, **7**, 847
[3] CORNET, C. F. *Polymer, Lond.* 1965, **6**, 373
[4] VAN DORT, H. M., HOEFS, C. A. M., MAGRÉ, E. P., SCHÖPF, A. J. and YNTEMA, K. *European Polymer J.* In press

A Comment on the Crystal Moduli of Nylon 6 and Nylon 66

ON THE basis of chemical structure nylon 6 and nylon 66 might be expected to exhibit similar physical properties. However, in several instances nylon 6 and nylon 66 have been shown to differ in their behaviour, e.g. nylon 6 melts 50 deg. C below the melting point of nylon 66, which implies differences in intermolecular and intramolecular (chain flexibility) forces. The purpose of this note is to point out another area in which the properties of these two polymers appear to differ, namely, in the magnitude of their crystal moduli. The crystal modulus is primarily a measure of intramolecular forces.

The crystal modulus in the chain direction for nylon 66 has been calculated as $1{\cdot}96 \times 10^{12}$ dyne/cm^2 by Treloar[1], who used the assumption that the modulus could be calculated in terms of the primary valence forces in a single chain. The crystal modulus of α form nylon 6, in which the chains are fully extended[2], should be close to the value found for nylon 66.

The crystal modulus of nylon 6 in the chain direction has been measured by Sakurada, Ito and Nakamae[3] by a dead load method. It was found that for the α form the crystal modulus was $2{\cdot}45 \times 10^{11}$ dyne/cm^2 whilst that of the γ form was $2{\cdot}06 \times 10^{11}$ dyne/cm^2. The low modulus value is understandable for the γ form since the molecules adopt a contracted conformation. It is not understood why the extended α form chains should give such a low modulus.

Measurements of the crystal modulus of nylon 66 have not yet been reported in the literature but the work of Beresford and Bevan[4] provides the necessary information for carrying out the modulus calculation. These authors measured the change in fibre identity period from the change in spacing of the (015) plane, as a function of applied load, for a drawn nylon 66 yarn and they tabulated the change in fibre identity period with applied stress (g/den). A graph of stress (dyne/cm^2) versus crystal strain has been plotted from their data. The conversion from g/den to dyne/cm^2 was made with the assumption that the sample density was 1·14 g/cm^3. Fortunately the density of nylon 66 is relatively constant and the value assumed can only be in error by a few per cent at most. The graph of stress versus crystal strain is shown in *Figure 1*. A straight line fitted the data and the slope of

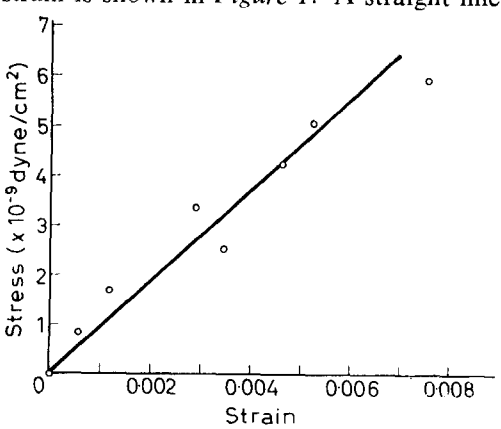

Figure 1—Applied stress versus crystal strain for nylon 66 from data of Beresford and Bevan[4]

the line gave a value of $9{\cdot}3 \times 10^{11}$ dyne/cm^2 for the crystal modulus in the chain direction. This value is rather low compared to the calculated value but it is certainly closer in agreement with the theoretical value than is the value found for nylon 6. One objection to the experiment of Beresford and Bevan is that the measurements were made under ambient conditions. Correction for this to zero relative humidity would change the modulus value by a small amount. A second objection is that measurements were made on the (015) plane the normal to which lies some 15° from the chain direction. It would be more satisfactory to use the (1,3,14) plane the normal to which lies within a degree or two of the chain direction. The (1,3,14) diffraction peak occurs near 77°(2θ) where θ is the Bragg angle, and the (1,3,14) reflection is more intense than the (015) reflection.

The results presented indicate that the crystal modulus in the chain direction of nylon 66 is three to four times higher than the corresponding value in α form nylon 6. Further work is required to resolve this discrepancy.

J. H. DUMBLETON and D. R. BUCHANAN

Chemstrand Research Center, Inc.,
Box 731, Durham, N.C.

(Received June 1968)

REFERENCES

[1] TRELOAR, L. R. G. *Polymer, Lond.* 1960, **1**, 95
[2] HOLMES, D. R., BUNN, C. W. and SMITH, D. J. *J. Polym. Sci.* 1955, **17**, 159
[3] SAKURADA, I., ITO, T. and NAKAMAE, K. *J. Polym. Sci.* 1966, No. 15C, 75
[4] BERESFORD, D. R. and BEVAN, H. *Polymer, Lond.* 1964, **4**, 247

Contribution of the Methylene Group to the Glass Transition Temperatures of Polymers

IN A recent paper[1], Faucher and Koleske discussed the glass transition temperatures (T_Gs) of a series of four polyethers. A plot of T_G against weight per cent methylene content was shown to be linear, and the plot could be extrapolated to a T_G of about -135°C for amorphous polymethylene. It is of interest to examine these data in terms of a T_G–structure relationship[2,3] which discriminates between the contributions to T_G of groups in different environments, and weights these contributions more simply, in terms of their mole fractions.

By treating a wide range of homopolymers as ideal copolymers in which the 'monomer' units are the structural groups of the homopolymer repeating unit, it was found[2,3] that the following equation could be used with considerable accuracy to relate T_G to structure

$$T_G = \sum_i n_i T_i / \sum_i n_i \qquad (1)$$

In this equation, n_i is the number of groups of the ith type in the repeating unit and T_i is an invariant additive temperature parameter associated with the ith group. A structural group, in general, is considered to be the smallest polymer segment capable of independent torsional oscillation with respect

the line gave a value of $9{\cdot}3 \times 10^{11}$ dyne/cm^2 for the crystal modulus in the chain direction. This value is rather low compared to the calculated value but it is certainly closer in agreement with the theoretical value than is the value found for nylon 6. One objection to the experiment of Beresford and Bevan is that the measurements were made under ambient conditions. Correction for this to zero relative humidity would change the modulus value by a small amount. A second objection is that measurements were made on the (015) plane the normal to which lies some 15° from the chain direction. It would be more satisfactory to use the (1,3,14) plane the normal to which lies within a degree or two of the chain direction. The (1,3,14) diffraction peak occurs near 77°(2θ) where θ is the Bragg angle, and the (1,3,14) reflection is more intense than the (015) reflection.

The results presented indicate that the crystal modulus in the chain direction of nylon 66 is three to four times higher than the corresponding value in α form nylon 6. Further work is required to resolve this discrepancy.

J. H. DUMBLETON and D. R. BUCHANAN

Chemstrand Research Center, Inc.,
Box 731, Durham, N.C.

(Received June 1968)

REFERENCES

[1] TRELOAR, L. R. G. *Polymer, Lond.* 1960, **1**, 95
[2] HOLMES, D. R., BUNN, C. W. and SMITH, D. J. *J. Polym. Sci.* 1955, **17**, 159
[3] SAKURADA, I., ITO, T. and NAKAMAE, K. *J. Polym. Sci.* 1966, No. 15C, 75
[4] BERESFORD, D. R. and BEVAN, H. *Polymer, Lond.* 1964, **4**, 247

Contribution of the Methylene Group to the Glass Transition Temperatures of Polymers

IN A recent paper[1], Faucher and Koleske discussed the glass transition temperatures (T_Gs) of a series of four polyethers. A plot of T_G against weight per cent methylene content was shown to be linear, and the plot could be extrapolated to a T_G of about -135°C for amorphous polymethylene. It is of interest to examine these data in terms of a T_G–structure relationship[2,3] which discriminates between the contributions to T_G of groups in different environments, and weights these contributions more simply, in terms of their mole fractions.

By treating a wide range of homopolymers as ideal copolymers in which the 'monomer' units are the structural groups of the homopolymer repeating unit, it was found[2,3] that the following equation could be used with considerable accuracy to relate T_G to structure

$$T_G = \sum_i n_i T_i / \sum_i n_i \qquad (1)$$

In this equation, n_i is the number of groups of the ith type in the repeating unit and T_i is an invariant additive temperature parameter associated with the ith group. A structural group, in general, is considered to be the smallest polymer segment capable of independent torsional oscillation with respect

to its nearest neighbours. For the relationship to hold for a wide variety of polymers it is essential that the neighbours of any particular group be invariable and groups are classified in this way.

The series of polyethers being considered, excluding the first member, comprises two types of methylene groups, $—CH_2\{CH_2\}O—$ and $—CH_2\{CH_2\}CH_2—$, and one type of ether group, $—CH_2\{O\}CH_2—$. These may be denoted A, B and C, respectively, and the first member of the series, polyoxymethylene, contains another group $—O\{CH_2\}O—$, denoted D.

The structure $\dagger CH_2\{CH_2\}_nCH_2—O\ddagger_x$ may now be written as $\dagger A\{B\}_nA—C\ddagger_x$, where the letters identify groups. Equation (1) then gives

$$(n+3)\,T_G=(2T_A+T_C)+nT_B \tag{2}$$

where $(2T_A+T_C)$ is a constant. A plot of $(n+3)\,T_G$ against n for the three polymers using the T_Gs from ref. 1 is given in *Figure 1*. The plot is linear and the least squares slope is 140·0°K, which is T_B, for the methylene group with methylene neighbours. This agrees well with Faucher and Koleske's extrapolated T_G for polymethylene of 138°K.

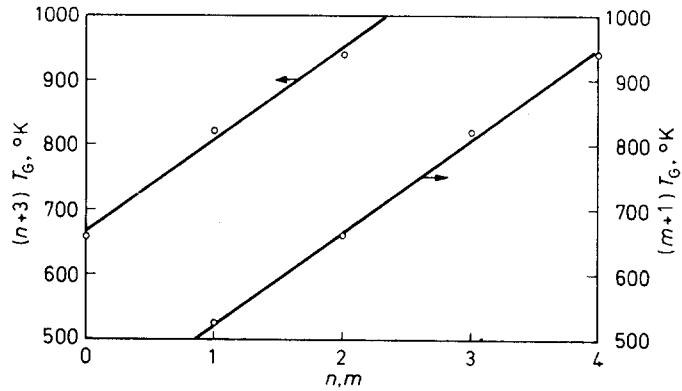

Figure 1—Plots of equations (2) and (3) for the polyethers

If all the methylene groups are considered to be equivalent so that $T_A=T_B=T_D=T_{B'}$, the T_G of polyoxymethylene can be included and we have for $\dagger\{CH_2\}_mO\ddagger_x$

$$(m+1)T_G=T_C+mT_{B'} \tag{3}$$

The plot of $(m+1)T_G$ against m is also shown in *Figure 1* and the relationship is seen to be a good fit to the data. The least squares slope of the plot, $T_{B'}$, is 140·2°K, which is not significantly different from T_B.

The weight fractional equivalent of equation (1), which describes Faucher and Koleske's plot, is

$$T_G=wT_{B'}+(1-w)T_C \tag{4}$$

where w is the weight fraction of methylene groups. Equation (4) may be rewritten as

$$T_G=w(T_{B'}-T_C)+T_C \tag{5}$$

and $w = 14m/(14m + 16)$, since the weights of CH_2 and O are 14 and 16, respectively.

Now, since $w = (14/16)\, m/[(14/16)\, m + 1]$, and $14/16 \simeq 1$, $w \simeq m/(m + 1)$ and equation (5) gives

$$(m + 1)\, T_G \simeq T_G + mT_B,$$

which is equation (3).

It is clear that, from the present data, it is not possible to determine whether T_G/structure relationships are best expressed on a weight, or a mole fractional, basis. It would be interesting to study a similar series of polymers of structure $\{x—y\}$ where the molecular weights of x and y are quite different, such as the polymethylene sulphides.

J. M. BARTON and W. A. LEE

Materials Department,
Royal Aircraft Establishment,
Ministry of Technology,
Farnborough, Hants.

(*Received July 1968*)

REFERENCES

[1] FAUCHER, J. A. and KOLESKE, J. V. *Polymer, Lond.* 1968, **9**, 44
[2] LEE, W. A. and O'MAHONY, D. Ministry of Technology, Royal Aircraft Establishment. *Tech. Rep. No. 66292* (1966)
[3] BARTON, J. M., LEE, W. A. and O'MAHONY, D. Ministry of Technology, Royal Aircraft Establishment. *Tech. Rep. No. 67298* (1967)

The Metal Salts Catalysed Autoxidation of Atactic Polypropylene in Solution II—Behaviour of Co, Ni, Fe *and* Cu *Salts as Catalysts*

IN A previous paper[1] we reported a detailed kinetic study of the autoxidation of atactic polypropylene in 1,2,4-trichlorobenzene solution catalysed by manganese salts. It is of interest to compare the efficiency of salts of other metal catalysts with that of manganese and this note reports results observed with Co, Ni, Fe and Cu salts in the same solvent.

COMPARISON OF THE CATALYTIC BEHAVIOUR OF DIFFERENT METALS

The salts of the different metals were studied for their effect on the autoxidation rate under identical conditions. The same polymer solution was used throughout and the initial concentration of each catalyst was also kept constant. With catalysts in the lower oxidation state, usually one drop of

and $w = 14m/(14m + 16)$, since the weights of CH_2 and O are 14 and 16, respectively.

Now, since $w = (14/16)\, m/[(14/16)\, m + 1]$, and $14/16 \simeq 1$, $w \simeq m/(m + 1)$ and equation (5) gives

$$(m + 1)\, T_G \simeq T_G + mT_B,$$

which is equation (3).

It is clear that, from the present data, it is not possible to determine whether T_G/structure relationships are best expressed on a weight, or a mole fractional, basis. It would be interesting to study a similar series of polymers of structure $\{x—y\}$ where the molecular weights of x and y are quite different, such as the polymethylene sulphides.

J. M. BARTON and W. A. LEE

Materials Department,
Royal Aircraft Establishment,
Ministry of Technology,
Farnborough, Hants.

(*Received July 1968*)

REFERENCES

[1] FAUCHER, J. A. and KOLESKE, J. V. *Polymer, Lond.* 1968, **9**, 44
[2] LEE, W. A. and O'MAHONY, D. Ministry of Technology, Royal Aircraft Establishment. *Tech. Rep. No. 66292* (1966)
[3] BARTON, J. M., LEE, W. A. and O'MAHONY, D. Ministry of Technology, Royal Aircraft Establishment. *Tech. Rep. No. 67298* (1967)

The Metal Salts Catalysed Autoxidation of Atactic Polypropylene in Solution II—Behaviour of Co, Ni, Fe *and* Cu *Salts as Catalysts*

IN A previous paper[1] we reported a detailed kinetic study of the autoxidation of atactic polypropylene in 1,2,4-trichlorobenzene solution catalysed by manganese salts. It is of interest to compare the efficiency of salts of other metal catalysts with that of manganese and this note reports results observed with Co, Ni, Fe and Cu salts in the same solvent.

COMPARISON OF THE CATALYTIC BEHAVIOUR OF DIFFERENT METALS

The salts of the different metals were studied for their effect on the autoxidation rate under identical conditions. The same polymer solution was used throughout and the initial concentration of each catalyst was also kept constant. With catalysts in the lower oxidation state, usually one drop of

t-butyl hydroperoxide was added to oxidize them to the higher oxidation state before the reaction was started. This also eliminated the induction period. The characteristic curves with various catalysts are shown in *Figure 1*, and the pertinent data are given below, *Table 1*.

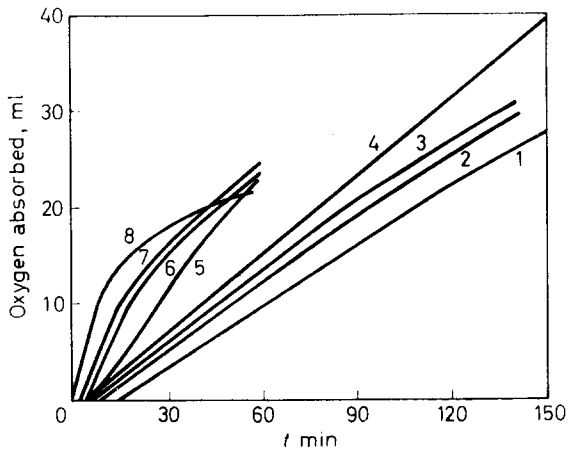

Figure 1

On the basis of their behaviour the catalysts fall into two distinct groups; the first consisting of the salts of cobalt and nickel, and the second of the salts of iron, manganese and copper. The general shape of the curve for the catalysts in the first group shows a steady region, which continues for a fairly long period before starting to curve off. The values of the steady

Table 1. [RH] = 1·63 mol l^{-1} [catalyst] = $1{\cdot}2 \times 10^{-3}$ mol l^{-1} Temperature 135°C

Curve No.	*Catalyst*	*Max. rate* $\times 10^4$ *Mol* l^{-1} min^{-1}	*Duration of steady state (% oxidation of polymer)*	*Efficiency relative to that of* Mn^{2+}
1.	Co^{2+}-(2-ethyl)-hexanoate	4·7	0·0–2·6	0·27
2.	Co^{2+}-(2, 2′dimethyl)-valerate	5·2	0·0–2·3	0·30
3.	Ni^{2+}-stearate	5·5	0·0–2·5	0·31
4.	Ni^{2+}-stearate	6·0	0·0–6·5	0·34
5.	Fe-naphthenate	10·5	0·6–1·8	0·60
6.	Mn^{3+}-catalyst	15·8	0·0–1·2	0·90
7.	Mn^{2+}-stearate	17·6	0·0–1·2	1·00
8.	Cu^{2+}-valerate	29·7	0·0–1·0	1·65

rate reached are very much lower than those obtained with the catalysts in the second group. With the iron, manganese and copper catalysts much higher initial rates are obtained which start slowing down after about 1–1·2 per cent oxidation of the polymer has been completed. Iron naphthenate, however, behaves differently in that the steady state is not reached till after about 0·6 per cent oxidation of the polymer. The duration of the

steady state, however, is almost the same, i.e. equivalent to 1·2 per cent oxidation of the polymer. No hydroperoxide was added in this case and this might explain the onset of steady state after a certain time lag. The curve for the copper catalyst shows a high initial rate after which it starts falling off much more abruptly than those for the other two catalysts in the same group. The relative efficiency of each catalyst with respect to manganese stearate is listed in the last column.

These results are not in accord with the general behaviour usually observed in other autoxidation systems. Cobalt is frequently found to be the most effective catalyst for the autoxidation reaction, followed by manganese, copper and other metal salts[2, 3]. The reason for this reversal of behaviour in the autoxidation of polypropylene in trichlorobenzene is not clear and might possibly be ascribed to the medium having some influence on the catalytic behaviour of the metal salts. In order to elucidate the causes of these differences several cobalt salts were investigated.

Co-2-*ethylhexanoate* (Co-2 EH)

This catalyst was very soluble in trichlorobenzene and gave a deep blue solution at relatively high concentrations. A drop of *t*-butylhydroperoxide was usually added to the system to oxidize Co^{2+} to Co^{3+}, as evidenced by the appearance of green colour.

At a cobalt concentration of $3{\cdot}75 \times 10^{-3}$ mol l^{-1} the rate of oxygen uptake by a 1·32 mol l^{-1} solution of the polymer was measured at 135°C. The maximum rate reached had the value of $1{\cdot}8 \times 10^{-4}$ mol l^{-1} min^{-1}, which when compared to the uncatalysed rate of $6{\cdot}2 \times 10^{-4}$ mol l^{-1} min^{-1} under similar experimental conditions, is unaccountably low.

At higher cobalt concentrations, however, a quick initial absorption rate was followed by a rapid slowing down. The same polymer solution absorbed oxygen at a rate of $9{\cdot}8 \times 10^{-4}$ mol l^{-1} min^{-1} when the cobalt concentration was raised to $1{\cdot}64 \times 10^{-2}$ mol l^{-1}. The steady rate was maintained till about $3{\cdot}6 \times 10^{-2}$ mol of oxygen per litre had been absorbed. For equal concentrations of cobalt no such initial high rate was shown when cobalt salts like stearate, and 2,2′-dimethyl valerate, were used.

The addition of 2-ethylhexanoic acid to the Co-2EH-catalysed autoxidation of polypropylene generally resulted in higher rates, but no steady state was maintained at any stage of the reaction. An addition of $6{\cdot}5 \times 10^{-2}$ mol l^{-1} of 2-ethylhexanoic acid to $1{\cdot}64 \times 10^{-2}$ mol l^{-1} of Co-2EH gave an average rate 10 to 15 per cent higher than the maximum steady rate reached in the absence of the acid.

Cobalt stearate

An addition of $1{\cdot}7 \times 10^{-2}$ mol l^{-1} of cobalt stearate to a 1·3 mol l^{-1} solution of polymer at 135°C did not increase the rate of oxygen uptake to a value higher than the uncatalysed one.

The effect of the addition of stearic acid on the rate of oxidation in the presence of cobalt stearate was investigated over a wide range of the acid concentration. It was expected that if the deactivation of the catalyst occurred by its conversion to insoluble cobalt salts the presence of an excess of stearic acid would prolong the period of the steady state. The rates

were, in fact, found to increase when stearic acid was added, and the steady state rate was maintained for a longer period than usual. However, this increase in the rate showed no sign of reaching saturation point even when the stearic acid concentration was 110 times the concentration of cobalt stearate. The plot of log rate versus log [st. acid] was linear and of slope 0·6, which shows that the rate varies directly with an approximate square root of the stearic acid concentration. The nature of the straight line obtained does not indicate any tendency of the rate to approach an independence of the acid concentration.

This could be explained by the fact that stearic acid itself was rapidly oxidized at an appreciable rate under the experimental conditions. This was confirmed by carrying out a separate series of 'runs' in which only cobalt stearate and stearic acid were oxidized in trichlorobenzene. Over the stearic acid concentration of 4·7 to 70×10^{-2} mol l^{-1} the rate of oxygen uptake varied with an order of 0·85 with respect to the concentration of the acid. Due to this complication this system was not subjected to a more detailed kinetic investigation.

Cobalt bromide–stearic acid system

This combination of an insoluble cobalt salt and stearic acid was also tested for its catalytic effect on the autoxidation rate. Generally the oxygen absorption started at a fairly high rate which did not show any steady state. Comparison of the results for this system with those in which cobalt stearate–stearic acid was used as a catalyst, shows that for equal polymer and stearic acid concentrations the rate has a much higher value with cobalt bromide than with the cobalt stearate catalysed autoxidation. The results in *Table 2* show it very clearly.

Table 2. Polymer concentration = 1·3 mol l^{-1} [st. acid] = $5{\cdot}8 \times 10^{-2}$ mol l^{-1}

[*Catalyst*] *mol* l^{-1}	*Initial rate* *mol* l^{-1} *min*$^{-1}$
Cobalt stearate $1{\cdot}56 \times 10^{-2}$	$15{\cdot}4 \times 10^{-4}$
Cobalt bromide $0{\cdot}84 \times 10^{-2}$	$24{\cdot}5 \times 10^{-4}$

It is seen that, although the concentration of cobalt bromide is almost one half of the concentration of cobalt stearate, the initial rate is about 60 per cent higher than the one obtained with cobalt stearate. This, however, may not seem very unexpected if one considers the possibility of catalysis by hydrogen bromide, which must be produced in this cobalt bromide–stearic acid system.

My thanks are due to the Commonwealth Scholarship Commission in the U.K. for financial support and the Pakistan Atomic Energy Commission for leave of absence.

SHAMIM A. CHAUDHRI*

Department of Inorganic, Physical and Industrial Chemistry, University of Liverpool

(Received May 1968)

*Present address: Pakistan Atomic Energy Commission, Karachi.

REFERENCES

[1] BAWN, C. E. H. and CHAUDHRI, S. A. *Polymer, Lond.* 1968, **9**, 81
[2] DENISOV, E. T. and EMANUEL, N. M. *Russ. chem. Revs.* 1960, **29**, 645
[3] CHALK, A. J. and SMITH, J. F. *Trans. Faraday Soc.* 1957, **53**, 1214

ANNOUNCEMENT

THE PHYSICS OF NON-CRYSTALLINE SOLIDS III

IT IS planned to hold a Conference on the above subject on 14 to 18 September 1970 in the University of Sheffield. Earlier conferences in this series took place at Alfred University, U.S.A., in 1958 and at Delft, The Netherlands, in 1964.

Sessions are expected to deal with: (1) Structure of inorganic and polymeric glasses, (2) Viscosity temperature relationships for supercooled liquids and glasses, (3) Relaxation and transformation range phenomena, (4) Mechanical properties of glassy materials. Members of the Conference Organizing Committee include Professors R. W. Douglas, G. Allen, J. Lamb, N. March and D. W. Saunders, B. Ellis is Secretary. Details are available on application to the Secretary, Department of Glass Technology, University of Sheffield, Northumberland Road, Sheffield, S 10 2TZ.

The Diffusion and Solution of Gases in Highly Crosslinked Copolymers

R. M. BARRER, J. A. BARRIE and P. S.-L. WONG*

A study has been made of the diffusion and solution of helium, hydrogen, neon, argon, krypton, oxygen, nitrogen, methane and carbon dioxide in a series of highly crosslinked copolymer membranes in the temperature range 40° to 80°C. The membranes were prepared by copolymerizing mixtures of tetraethyleneglycoldimethacrylate (TEGDM) and ethylacrylate (EA) containing 100, 80, 60, 40 and 20 mole per cent of TEGDM. Diffusion and solubility coefficients were obtained by several different methods. Some anomalies were found and are discussed in terms of the polymer microstructure. The diffusion and permeability coefficients of gases larger than neon decreased by almost an order of magnitude as the mole percentage of TEGDM was increased from 20 to 100. The solubility coefficient was little affected. The diffusion coefficients were analysed in terms of the transition state and activated zone theories of diffusion and several correlations of the diffusion and solubility coefficients with other physical parameters were examined. Separation factors for several gas pairs at 60°C were calculated and examined along with similar data for other systems. In general it appears that high permeation rates are gained at the expense of permselectivity.

THE transport of gases in polymers is affected amongst other factors by changes in the microstructure of the polymer. For example, crosslinking of a rubbery material reduces the flexibility of the polymer chains and eventually for sufficiently high degrees of crosslinking a hard often brittle material is obtained. The diffusion and sorption of gases and vapours in polymer systems with relatively small numbers of crosslinks has been investigated several times[1-8]. Highly crosslinked materials have not been investigated to the same extent although the greater selectivity of these materials in gas permeation has been pointed out[1]. It was therefore of interest to study the effect of crosslinking on gas permeation in more detail, in particular for a system in which the degree of crosslinking can be varied. For this purpose the copolymer system of ethylacrylate (EA) and tetraethyleneglycoldimethacrylate (TEGDM) was selected. The composition can be varied from 0 to 100 per cent of the crosslinking agent, TEGDM, and is accompanied by marked changes in the flexibility of the network.

EXPERIMENTAL

Gases

Helium, neon, argon, krypton, hydrogen, nitrogen, oxygen and carbon dioxide were supplied by the British Oxygen Co. and methane of 99·98 per cent purity by the National Physical Laboratory, England. The gases required no further purification.

Membranes

The EA and TEGDM monomers were supplied by Koch Light Ltd and the

*Present address: Department of Chemical Engineering, Massachusetts Institute of Technology, Cambridge, Mass., U.S.A.

Aldrich Chemical Co., respectively. About 0·2 per cent of hydroquinone inhibitor was removed from the EA by alkali extraction. The TEGDM contained 0·02 per cent of hydroquinone and was not purified further. Mixtures were prepared at room temperature and their densities determined. One per cent of benzoyl peroxide was added and polymerization allowed to proceed between glass plates under a sun lamp at approximately 75°C for about 30 hours. A few cylindrical specimens were prepared by polymerizing the mixture in a Teflon tube sealed at both ends. The samples were then evacuated at 80°C under high vacuum for several days and their densities determined. For no samples were X-ray diffraction patterns found, indicating that all were amorphous.

A uniform distribution of crosslinks requires the reactivity of vinyl groups in both monomers to be approximately equal. Kinetic data for this copolymerization system were not available and the existence of some degree of heterogeneity in the distribution of crosslinks on a microscopic scale cannot be ruled out. Following Loshaek and Fox[9] and Tobolsky *et al.*[10] the crosslinking efficiency was calculated from the volume contraction of the mixture on polymerization. It is assumed that all of the EA had reacted and that all the TEGDM had reacted at least once. Details of the samples used in the permeation and solubility measurements are given in *Table 1*. The low values of M_c, the molecular weight between crosslinks, indicate the high degree of crosslinking attained. The quantity C' in *Table 1* is the number of moles of TEGDM units crosslinked per cm^3 of polymer.

Table 1. Copolymer samples

Sample	*TEGDM, %*	*Thickness or diameter, mm*	*Density, g cm^{-3}*	M_c	$c' \times 10^3$
Permeation					
A1 (Film)	100	0·306 ± 1%	1·245	350	3·58
B (Film)	80	0·468 ± 1%	1·231	430	2·88
C1 (Film)	60	0·271 ± 2%	1·229	460	2·69
C2 (Film)	60	0·509 ± 2%	1·224	480	2·55
D (Film)	40	0·263 ± 3%	1·217	520	2·36
E (Film)	20	0·416 ± 2%	1·192	750	1·60
Desorption and solubility					
A2 (Cylinder)	100	1·6	1·235	390	3·18
A3 (Film)	100	0·51	1·240	371	3·34
C3 (Film)	60	0·49	1·227	460	2·66

Glass transition temperatures T_g of approximately 2°, 65° and 79°C for the 20, 40 and 60 per cent TEGDM samples respectively were determined with a Du Pont differential thermal analyser. For the 80 per cent and the 100 per cent TEGDM no easily defined transition was detected. Tobolsky *et al.*[10] showed that the shear modulus of these copolymers increased quite sharply as the temperature was lowered through the region of T_g. However, for the 70 to 100 per cent TEGDM copolymers the transition was more gradual and for the 100 per cent sample was spread over a wide range of temperature.

Apparatus

The permeation apparatus was similar to that used in earlier investigations[2]. However, the more brittle of the membranes tended to fracture on mounting in the conventional steel diffusion cell and accordingly glass cells of the type shown in *Figure 1* were used for all samples. The membrane was attached to the annular ground-glass surface of the cell with Araldite adhesive. A layer of Araldite was built up on the other face of the membrane as shown in *Figure 1* so that the area for diffusion was the same for both faces.

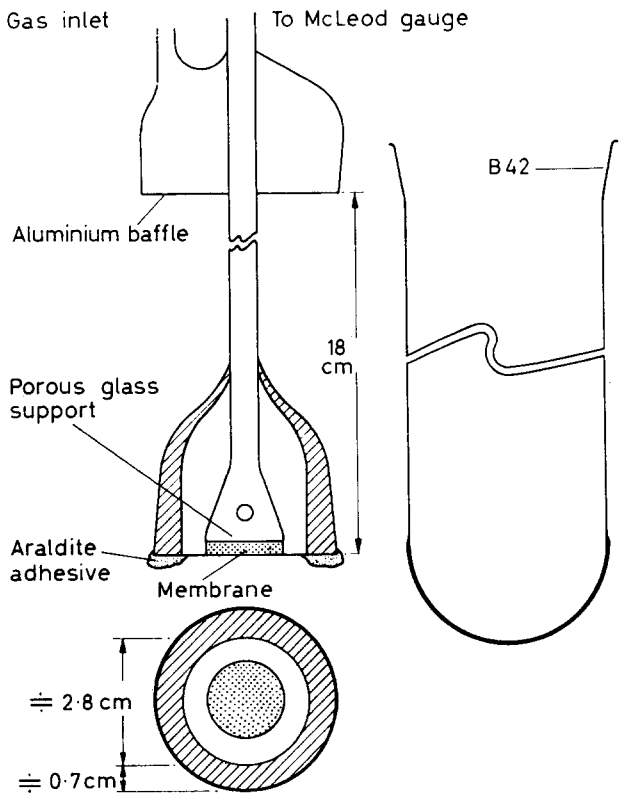

Figure 1—Glass diffusion cell

The procedure adopted for the measurement of both static solubilities and desorption kinetics has been described elsewhere[11–13].

Methods of analysis

Diffusion coefficients were evaluated by four different methods. The steady state coefficient D_s was obtained from the relation

$$P = D_s \sigma_s \tag{1}$$

where P is the steady state permeability coefficient (cm^3 at s.t.p. per second per cm Hg passing through 1 cm^3 and σ_s is the directly measured solubility

(cm³ at s.t.p. per cm Hg in 1 cm³). From the measurement of the time lag L, the coefficient D_L was obtained from the expression

$$D_L = l^2/6L \tag{2}$$

where l is the thickness of the membrane.

The transient state of permeation for relatively small times can be represented by the equation[14]

$$\ln\left(t^{\frac{1}{2}}\cdot\frac{dp_2}{dt}\right) = \ln\left[\frac{2A}{V}\,\sigma\,p_1\left(\frac{D_E}{\pi}\right)^{\frac{1}{2}}\right] - \frac{l^2}{4D_E t} \tag{3}$$

where A and l are respectively the area and thickness of the membrane and V is the volume of the system on the low pressure side of the membrane. The pressures on the membrane faces are p_1 and p_2 with $p_1 \gg p_2$. When the LHS of equation (3) is plotted against $1/t$, the coefficient D_E is obtained from the slope $l^2/4D_E$. The solubility coefficient σ may be determined from the intercept but often the error in this measurement is quite large.

For the later stages of desorption from a plane sheet[15]

$$\ln(p_{t+\Delta t} - p_t) = \ln K_1 - \pi^2 D_d t/l^2 \tag{4}$$

and from a cylinder of diameter a

$$\ln(p_{t+\Delta t} - p_t) = \ln K_2 - 5{\cdot}78\, D_d t/a^2 \tag{5}$$

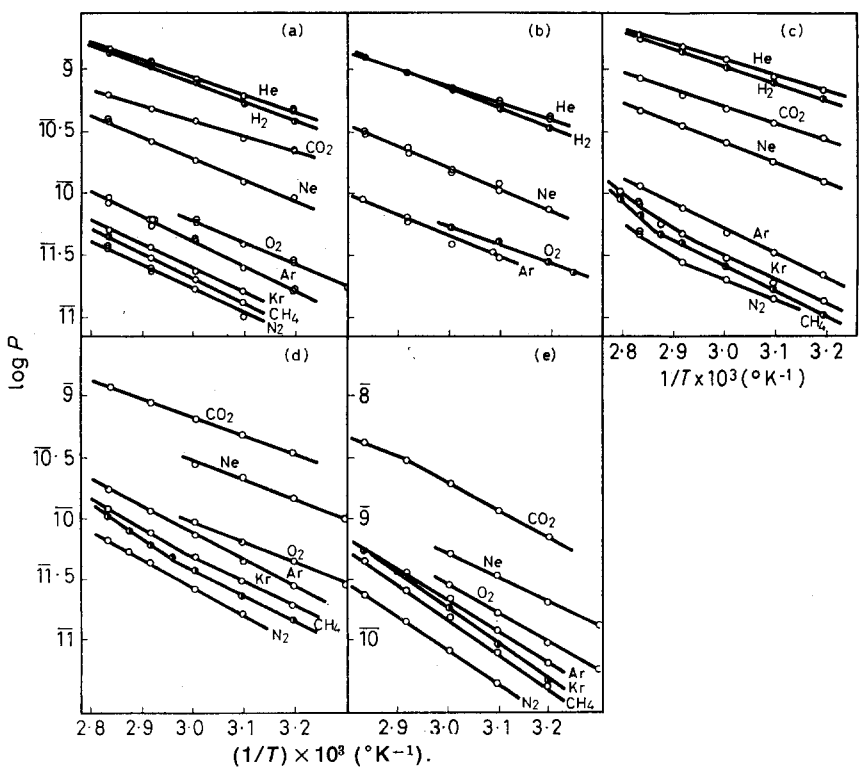

Figure 2—Temperature dependence of the permeability coefficient. (a) 100, (b) 80, (c) 60, (d) 40 and (e) 20 mole per cent TEGDM samples

where $p_{t+\Delta t}$ is the pressure at some time Δt after time t. The coefficient D_d is determined from the slopes of these linear equations.

For a homogeneous membrane in which the diffusion process is Fickian then $D_s = D_L = D_E = D_d$ and $\sigma_s = \sigma_E$.

RESULTS

The values of P, D_s, D_L, D_d, σ_s and σ_L where $\sigma_L = P/D_L$ are given in *Figures 2* to *5*. The coefficient D_E was obtained only for carbon dioxide in the 20 mole per cent TEGDM copolymer as the permeation rate in the transient state for the other gas–polymer systems was too small to be measured accurately. D_E and D_L are in good agreement (*Table 2*).

Table 2. Comparison of D_L and D_E for carbon dioxide in 20 per cent TEGDM copolymer

$t°C$	$D_L \times 10^7$ ($cm^2\ sec^{-1}$)	$D_E \times 10^7$ ($cm^2\ sec^{-1}$)
80	4·2	4·0
70	2·5	2·6
60	1·5	1·3
50	0·9	0·9
40	0·45	0·41

Measurements of static solubilities and of desorption kinetics were made for hydrogen (sample A2), neon, argon and carbon dioxide (sample A3) on

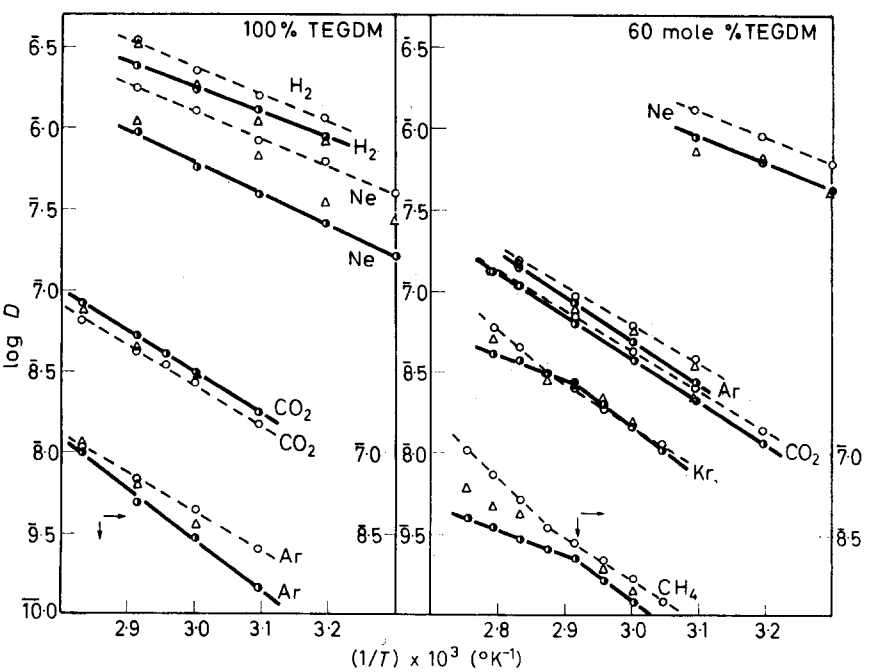

Figure 3—Temperature dependence of D_s, D_L and D_d in the 100 and 60 mole per cent TEGDM samples. ○, D_s; ◑, D_L; △, D_d

the 100 per cent TEGDM polymer and for neon, argon, carbon dioxide, krypton and methane on the 60 per cent TEGDM copolymer (sample C3). With helium it was not possible to measure static solubilities accurately as the gas diffused into the Pyrex glass walls of the apparatus[16]. D_s, D_L and D_E are compared in *Figure 3*. In *Figures 2, 4* and *5* Arrhenius plots of P, D_L, σ_{iL} and σ_s are shown for the systems investigated. Except for a few systems, in particular for the larger gases krypton and methane in the 60 and 40 per cent TEGDM samples, normal linear plots were obtained.

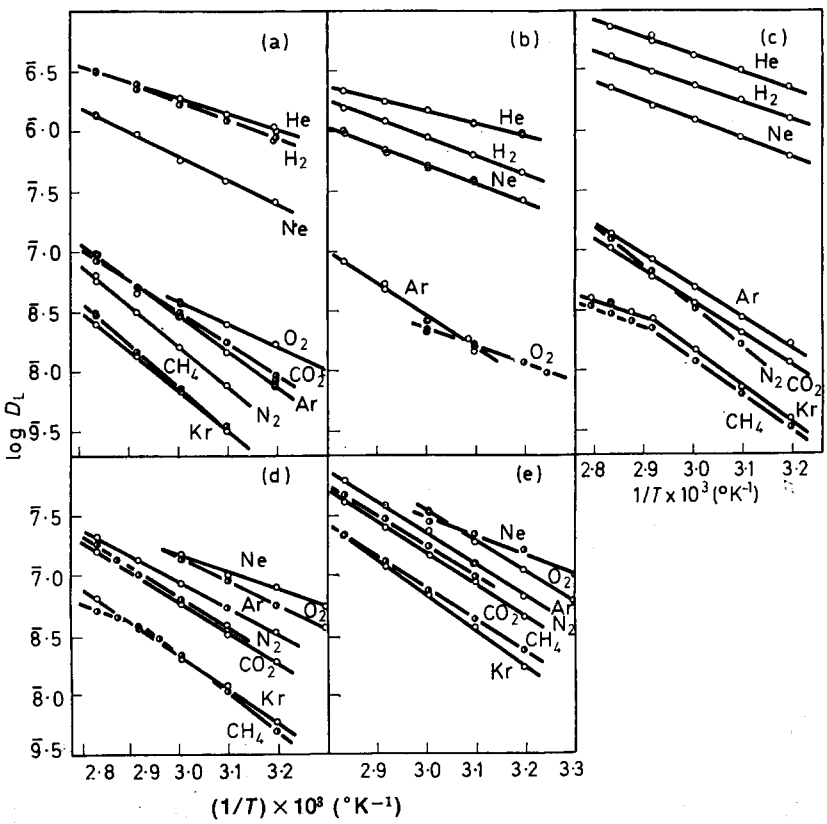

Figure 4—Temperature dependence D_L. (a) 100, (b) 80, (c) 60, (d) 40 and (e) 20 mole per cent TEGDM samples

For most but not all of the systems $D_s > D_d > D_L$. However, in the measurement of $D_s = P/\sigma_s$, different samples were used in the permeation and the solubility experiments and some difference in the density and degree of crosslinking was unavoidable. Therefore such factors could account for much of the difference between D_s and D_L. This difference was largest for neon but the solubility of this gas in the samples was very low and therefore more prone to error. The existence of voids or molecular-sized gaps in glassy polymers has been postulated to explain certain features of vapour transport in these systems[17]. The diffusion medium is then heterogeneous and the possibility of real differences between D_s and D_L arises.

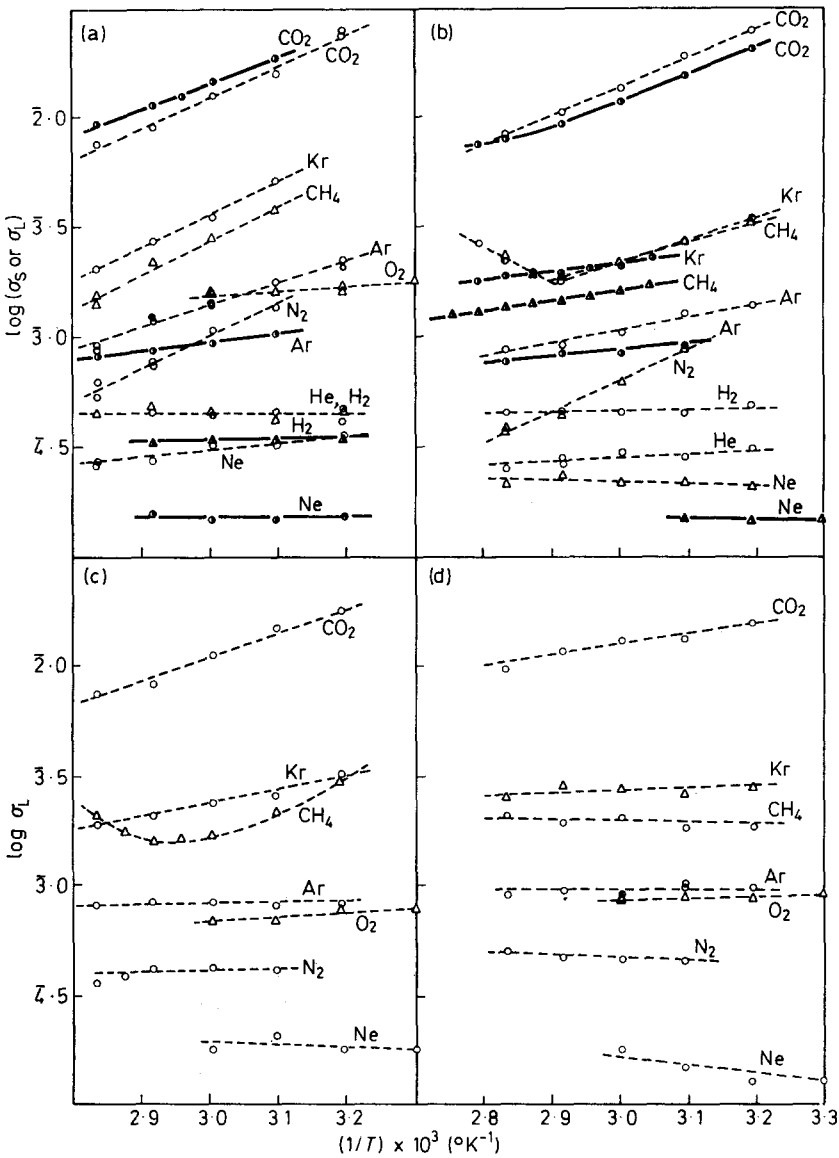

Figure 5—Temperature dependence of σ_L and σ_s. (a) 100, (b) 60, (c) 40 and (d) 20 mole per cent TEGDM samples. ○ and △ represent σ_L; ◑ and ◭ represent σ_s

The changes in the slopes of the Arrhenius plots for some of the krypton and methane systems are similar to those observed for gas diffusion in the glass transition region[18]. It has been suggested that in this region the polymer is a mixture of two phases, namely a glasslike phase and a liquid or rubbery phase. On cooling through this region the glassy phase grows at

the expense of the rubbery phase. The medium is again heterogeneous and D_s and D_L are necessarily average quantities which may or may not be the same. In addition the temperature coefficient of the volume fraction of any one phase will be reflected in that of the diffusion coefficient and will lead to an anomalous activation energy for diffusion. No anomaly is observed in the plots of $\log \sigma_s$ versus $1/T$, which would suggest that anomalies in the corresponding plots for D_L and σ_L may be a result of treating an essentially heterogeneous membrane as homogeneous.

Isotherms obtained from direct solubility measurements all obeyed Henry's law, even for carbon dioxide, the most condensable of the gases. σ_s and σ_L are compared for solution in the 100 and 60 per cent TEGDM samples in *Figures* 5(a) and (b).

DISCUSSION

Solubility coefficients

In *Table 3* smoothed values of σ_s and σ_L at 60°C are given. When $\log \sigma$ is plotted against the Lennard–Jones interaction parameter, ϵ/k, the curve over most of the range approximates (*Figure 6*) to a straight line. Defining

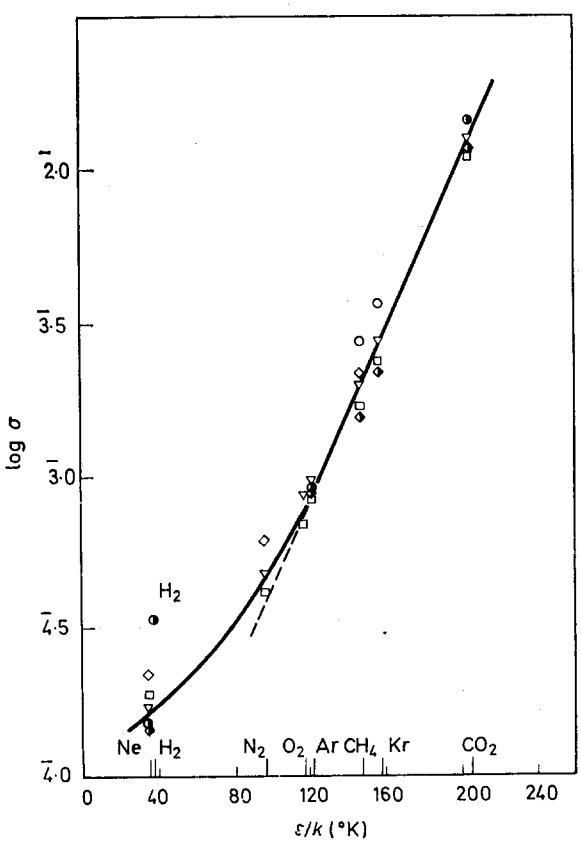

Figure 6—Log σ versus ϵ/k at 60°C. ○, 100; ◇, 60; □, 40 and ▽, 20 mole per cent TEGDM. samples. Half shaded points are σ_s data

σ^* as the solubility in cm^3 at s.t.p. per cm^3 per atm the equation of the straight line becomes

$$\log \sigma^* = -2{\cdot}88 + 0{\cdot}0139\, \epsilon/k \qquad (6)$$

Relations similar to equation (6) have been reported elsewhere[19,20].

Table 3. Smoothed values of σ_L and σ_s at 60°C. $\sigma \times 10^4$ in cm^3 at s.t.p. per cm^3 of polymer at 1 cm Hg pressure. Figures in brackets are σ_s

Gas	*Per cent TEGDM*			
	100	60	40	20
H_2	4·5 (3·35)	4·6	—	—
Ne	3·0 (1·50)	2·2 (1·48)	1·9	1·7
Ar	13·8 (9·30)	10·6 (8·60)	8·3	9·4
Kr	36·0	21·6 (21·6)	23·7	26·9
N_2	10·2	6·2	4·1	4·7
O_2	15·3	—	6·8	8·6
CH_4	27·4	21·8 (15·4)	16·7	19·8
CO_2	125 (143)	136 (118)	110	124

Equation (6) is best satisfied by the larger gas molecules, the smaller tending to lie off the line. This may be explained if for the larger molecules solution by mixing (substitutional solution) occurs but for the smaller one 'interstitial' solution can also occur in microvoids of molecular size in the polymer. Crosslinking does not influence the values of σ (or σ^*) very much, except that σ for the 100 per cent TEGDM has relatively high values. This again can be attributed to a larger number of microvoids in this sample.

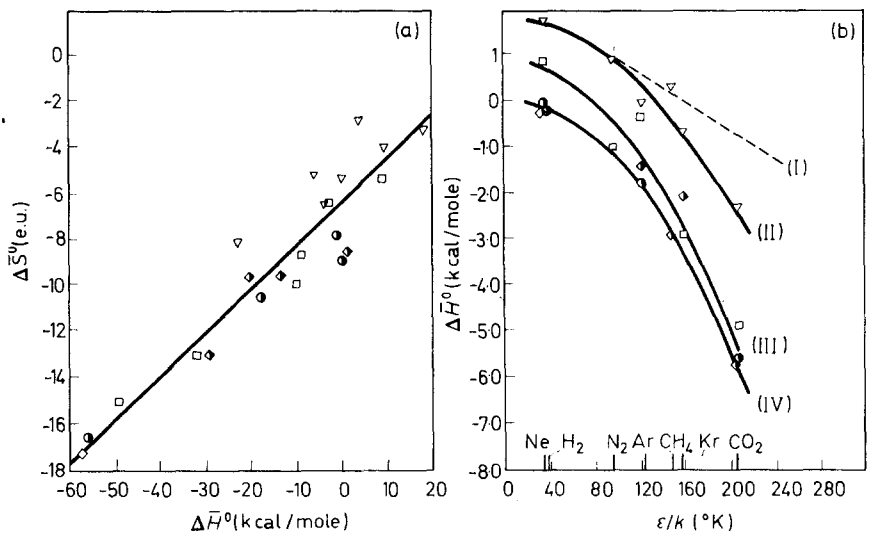

Figure 7—(a) $\Delta\bar{S}^0$ versus $\Delta\bar{H}^0$. ◑, 100; ◆, 60; □, 40 and ▽, 20 mole per cent TEGDM samples. (b) ΔH^0 versus ϵ/k. Symbols as for (a). Curve (I) is obtained from equation (9); curves (II), (III) and (IV) are 20, 40 and 100–60 mole per cent TEGDM samples respectively

The partial molar free energy, entropy and heat of solution were obtained from σ^* using the relations:

$$\left.\begin{aligned} \Delta\bar{G}^0 &= -RT \ln \sigma^* \\ \Delta\bar{S}^0 &= R\ln \sigma^* + RT\, \partial \ln \sigma^*/\partial T \\ \Delta\bar{H}^0 &= RT^2\, \partial \ln \sigma^*/\partial T \end{aligned}\right\} \quad (7)$$

Values of $\Delta\bar{S}^0$ and $\Delta\bar{H}^0$ are given in *Table 4*. A linear relation exists between $\Delta\bar{S}^0$ and $\Delta\bar{H}^0$ [*Figure 7*(a)] for which the equation is

$$\Delta\bar{S}^0 = -6{\cdot}33 + 0{\cdot}0019\, \Delta\bar{H}^0 \quad (8)$$

Table 4. $\Delta\bar{H}^0$ (cal mole^{-1}) and $\Delta\bar{S}^0$ (cal mole^{-1} deg^{-1}) at 60°C. Figures in brackets are caclulated from σ_s and the remainder from σ_L

Gas	*mole per cent TEGDM*	$\Delta\bar{H}^0$	$\Delta\bar{S}^0$
H_2	100	0 (−1500)	$-7{\cdot}8_1$
Ne	100	1300 (0)	$-8{\cdot}8_9$
	60	100 (150)	$-8{\cdot}5_0$
	40	890	$-5{\cdot}3_0$
	20	1800	$-3{\cdot}2_0$
Ar	100	−4600 (−1780)	−10·6
	60	−2800 (−1390)	$-9{\cdot}6_1$
	40	−330	$-6{\cdot}4_9$
	20	0	$-5{\cdot}2_5$
Kr	60	−4700 (−2040)	$-9{\cdot}7_3$
	40	−2900	−12·0
	20	−640	$-5{\cdot}1_0$
O_2	40	−910	$-8{\cdot}6_0$
	20	−360	$-6{\cdot}5_0$
N_2	40	−1000	$-9{\cdot}9_0$
	20	910	$-3{\cdot}9_0$
CH_4	60	−2900	−13·0
	20	330	$-2{\cdot}7_6$
CO_2	100	−6600 (−5600)	−16·3
	60	−6000 (−5700)	−17·3
	40	−4900	−15·1
	20	−2300	$-8{\cdot}1_0$

Similar relations have been found for gases dissolving in non-polar liquids[21], silicone rubber[22] and natural rubber[4] with slopes of 0·0011, 0·0016 and 0·0019, respectively.

The values of $\Delta\bar{H}^0$ calculated from σ_s are normally less negative than those from σ_L, but errors in the latter are relatively large. In *Figure 7*(b) $\Delta\bar{H}^0$ is plotted against ϵ/k; in all cases curves are obtained in which the curvature is greatest for the smallest molecules. For gases dissolving in elastomers, Michaels and Bixler[19] deduced the linear relation

$$\Delta\bar{H}^0 = -15{\cdot}6\epsilon/k + 1{\cdot}99\mu T \quad (9)$$

where μ is the Flory–Huggins interaction parameter. The slope of this line is shown as the dashed curve. With the more glassy polymers $\Delta\bar{H}^0$ may, however, consist of a fraction, x, associated with substitutional mixing and of a fraction, $(1-x)$, associated with occupation of microvoids:

$$\Delta\bar{H}^0 = \Delta H_c + x\Delta\bar{H}_m + (1-x)\,\Delta\bar{H}_s \tag{10}$$

In equation (10), ΔH_c is the molar heat of condensation, $\Delta\bar{H}_m$ is the partial molar heat of mixing, and $\Delta\bar{H}_s$ that of sorption into microvoids. If ϵ_{gg}, ϵ_{pp} and ϵ_{gp} are the interaction energies of a gas–gas, a polymer–polymer and a gas–polymer contact then approximately:

$$\left.\begin{aligned} \Delta H_c &= \tfrac{1}{2}Z_1\epsilon_{gg} - RT \\ \Delta\bar{H}_m &= \tfrac{1}{2}Z_1\epsilon_{gg} + Z_2\epsilon_{pp} - Z\epsilon_{gp} \\ \Delta\bar{H}_s &= \tfrac{1}{2}Z_1\epsilon_{gg} - Z\epsilon_{gp} \end{aligned}\right\} \tag{11}$$

so that

$$\Delta\bar{H}^0 = xZ_2\epsilon_{pp} - Z\epsilon_{gp} - RT \tag{12}$$

In these equations, Z_1 is the coordination number in condensed sorbate, Z_2 is the number of bonds between polymer segments broken in making a hole and Z the number of gas–polymer contacts formed when a gas molecule is inserted in this newly created hole or in a pre-existing microvoid assumed to be of the same dimensions. If $\epsilon_{gp} \sim (\epsilon_{gg}\epsilon_{pp})^{\frac{1}{2}}$ then for any one polymer and a series of gases equation (12) takes the form

$$\Delta\bar{H}^0 = Ax - B\epsilon_{gg}^{\frac{1}{2}} - RT \tag{13}$$

where A and B are constants. Since, however, x should be a function of ϵ_{gg}, no simple correlation between $\Delta\bar{H}^0$ and ϵ_{gg} is expected when equation (13) is valid.

If dissolved gases are freely rotating, and solution occurs only by mixing ($x=1$), the isotherm is[23]

$$\frac{v_1}{p\,(1-2v_2/Z)^{Z/2}} = \frac{1}{RT}\left(\frac{kT}{2\pi m}\right)^{3/2}\frac{1}{\bar{\nu}^3}\exp\left(\frac{-\Delta\bar{H}^0 + \frac{1}{2}RT}{RT}\right) \tag{14}$$

where v_1 and v_2 (~ 1) are the volume fractions of sorbed gas of molecular mass m and of polymer in equilibrium at the gas phase pressure p. $\bar{\nu}$ is the mean vibration frequency of dissolved gas relative to its environment of polymer segments. By using the data of *Tables 3* and *4*, values of $\bar{\nu}$ for the gases in the 100 and the 20 per cent TEGDM polymers have been calculated from equation (14) and are given in *Table 5*. These values are for infra-red frequencies which, in the 100 per cent TEGDM polymer, are somewhat larger than in the 20 per cent polymer. Equation (14) may, however, be less applicable in view of what has been said about microvoids. The frequencies in *Table 5* are quite comparable with similar frequencies calculated for gases in elastomers[22,23]. They are the mean oscillation frequencies that may be involved in the diffusion of gases in polymers.

Table 5. Values of $\bar{v} \times 10^{-12}$ (sec^{-1})

Gas	100 *per cent TEGDM*			20 *per cent TEGDM*		
	$v_1 \times 10^5$	$Z=4$	$Z=6$	$v_1 \times 10^5$	$Z=4$	$Z=6$
H_2	3·28	3·2	4·0	—	—	—
Ne	0·85	1·6	2·0	0·96	0·60	0·79
Ar	9·00	1·2	1·6	9·10	0·50	0·63
Kr	—	—	—	31·6	0·32	0·40
N_2	—	—	—	5·50	0·40	0·55
O_2	—	—	—	8·20	0·63	0·79
CH_4	—	—	—	26·0	0·40	0·50
CO_2	194	2·5	3·4	168	0·50	0·66

Diffusion coefficients

The coefficient D_L was obtained at several temperatures for helium, neon, argon, krypton, hydrogen, oxygen, nitrogen and carbon dioxide. The behaviour of oxygen, particularly in the 80 and 100 per cent TEGDM membranes, was anomalous. The time lag was abnormally long and became shorter on repeating the experiment while the permeability remained the same at any one temperature. Eventually identical time lags were obtained

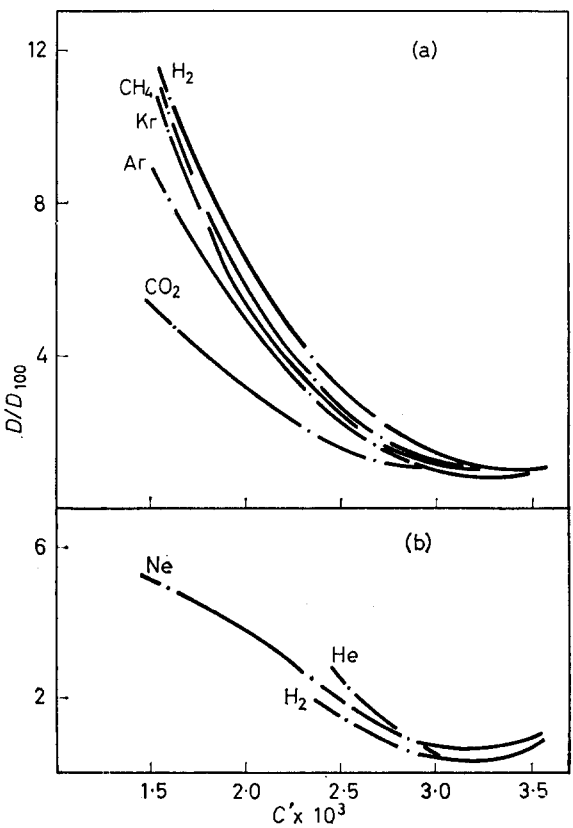

Figure 8—D/D_{100} versus crosslink density

for successive experiments after which the diffusion behaviour appeared to be normal at that temperature. When the temperature was raised the anomalous behaviour was observed again but on a reduced scale and disappeared after the experiment was repeated a few times. It appears that these highly crosslinked samples contained centres reactive to oxygen. The chemical reaction, the rate of which fell towards zero at longer times, would affect the time lag but not the steady state permeability. Checks with argon and carbon dioxide before and after oxygen permeation showed no difference in the permeation behaviour of these gases indicating that structural changes resulting from oxygenation did not have a significant effect on the diffusion process. In permeation measurements on a given sample oxygen was always used last in any series of gases.

In *Figure 8* the decrease in D/D_{100} with crosslink density is shown. D_{100} is the coefficient D_L for the 100 per cent TEGDM polymer. The decrease in D is greater for the larger gases, and for the smaller gases there is a shallow minimum.

In *Table 6* are given values of D_0 and E_D in the relation $D_L = D_0 \exp(-E_D/RT)$ for the range 40° to 80°C. As for most gas–polymer systems there is a tendency for the activation energy to increase with the size of the penetrant. E_D was then plotted against d^n where d is the collision diameter of the gas molecule estimated from gas viscosity data[24]. Several values of the exponent n were tried with $d^{2\cdot5}$ giving the most nearly linear plot. The values of E_D although large are not uncommonly so for plastic media and similar values were obtained for the rare gases in polyvinylacetate above its glass transition temperature[18]. The values for oxygen appear rather low compared with say nitrogen but because of the oxygenation of the sample must be regarded as somewhat suspect.

According to the transition-state treatment of diffusion

$$D = (kT/h)\lambda^2 \exp(\Delta S^*/R) \exp(-\Delta H^*/RT) \qquad (15)$$

where λ is the jump distance in a unit diffusion process and ΔH^*, ΔS^* are respectively the enthalpy and entropy of activation. Assuming a value for λ, for example $\lambda^2 = 10^{-15}$ cm^2, then ΔS^*, ΔH^* and ΔG^* $(= \Delta H^* - T\Delta S^*)$ are calculated (*Table 6*) using the values of D_0 and E_D. Except for helium and oxygen, positive values of ΔS^* are again obtained in common with crosslinked natural rubber[2] and most other polymer systems[22]. These are sometimes in excess of the whole (negative) entropy of solution showing that the polymer takes part in the activated diffusion step. For the smaller gas molecules E_D is relatively small and hence from equation (16) negative values of ΔS^* are quite reasonable. There is a linear relation[25] between ΔS^* and E_D/T, or $\Delta H^*/T$. Such a relation arises if the variation in ΔG^* among gas–polymer systems is considerably less than the variation of either ΔH^* or $T\Delta S^*$. Except for oxygen the data of *Table 6* were well represented by the straight line of *Figure 9*

$$\Delta S^* = -12 + 0{\cdot}66 E_D/T \qquad (16)$$

Alternatively the data may be represented by the line

$$\log D_0 = -4{\cdot}4 + 0{\cdot}14 E_D/T \qquad (17)$$

Table 6. E_D (kcal mole^{-1}), D_0 (cm^2 sec^{-1}), ΔS^* (cal mole^{-1} deg^{-1}), ΔH^* (kcal mole^{-1}), and ΔG^* (kcal mole^{-1}) for gases in copolymers (from D_L)

Polymer	T_{mean} °C	*Gas*	E_D	D_0	ΔS^*	ΔH^*	ΔG^*
100% TEGDM	60	He	6·2	$2{\cdot}22\times10^{-3}$	0·29	5·5	5·4
	60	Ne	9·1	$5{\cdot}4\times10^{-1}$	6·7	8·4	6·2
	60	Ar	14·1	$5{\cdot}0\times10^{1}$	15·7	13·4	8·2
	65	Kr	15·4	$8{\cdot}5\times10^{1}$	16·7	14·6	9·0
	60	H_2	7·1	$7{\cdot}3\times10^{-2}$	2·68	6·4	5·5
	45	O_2	8·8	$2{\cdot}3\times10^{-2}$	0·51	8·2	8·0
	65	N_2	15·8	$3{\cdot}8\times10^{2}$	19·6	15·1	8·5
	60	CO_2	12·4	4·2	10·7	11·7	8·2
	65	CH_4	16·7	$6{\cdot}4\times10^{2}$	20·7	16·0	9·0
80% TEGDM	60	He	4·8	$2{\cdot}0\times10^{-3}$	−4·44	4·1	5·6
	60	Ne	7·6	$2{\cdot}8\times10^{-2}$	0·75	6·7	6·5
	65	Ar	12·4	3·3	10·2	11·7	8·3
	60	H_2	7·1	$4{\cdot}2\times10^{-3}$	1·59	6·5	6·0
	51	O_2	7·1	$9{\cdot}5\times10$	−1·32	6·4	6·8
60% TEGDM	60	He	6·6	$8{\cdot}4\times10^{-3}$	−1·62	5·9	6·4
	60	Ne	7·1	$6{\cdot}5\times10^{-2}$	2·46	6·5	5·7
	60	Ar	11·9	3·2	10·2	11·2	7·8
	55	Kr†	14·0	$2{\cdot}2\times10^{1}$	14·1	13·6	9·0
	60	H_2	6·6	$5{\cdot}2\times10^{-2}$	2·00	5·9	5·3
	65	N_2	15·5	$4{\cdot}9\times10^{2}$	20·2	14·8	7·7
	60	CO_2	12·3	4·3	10·9	11·6	8·0
	50	CH_4†	13·8	$1{\cdot}3\times10^{1}$	13·1	13·2	8·9
40% TEGDM	45	Ne	6·5	$2{\cdot}8\times10^{-3}$	0·89	5·9	5·6
	60	Ar	10·2	$4{\cdot}2\times10^{-1}$	6·2	9·5	7·5
	60	Kr	13·0	7·0	11·8	12 3	8·4
	45	O_2	8·9	$9{\cdot}2\times10^{-3}$	3·24	8·3	7·2
	65	N_2	12·0	4·7	11·0	11·3	7·6
	60	CO_2	11·8	3·3	10·3	11·1	7·7
	53	CH_4†	14·0	$3{\cdot}0\times10^{1}$	14·7	13·5	8·7
20% TEGDM	45	Ne	6·9	$9{\cdot}3\times10^{-3}$	3·4	6·3	5·2
	60	Ar	12·3	$2{\cdot}5\times10^{1}$	14·3	11·6	6·9
	60	Kr	13·8	$7{\cdot}4\times10^{1}$	16·5	13·1	7·6
	45	O_2	11·3	8·6	12·3	10·7	6·8
	65	N_2	11·7	7·8	12·0	11·0	7·0
	60	CO_2	12·1	$1{\cdot}3\times10^{1}$	14·0	11·4	6·8
	60	CH_4	12·5	$1{\cdot}2\times10^{1}$	12·9	11·8	7·5
	E_D, D_0, ΔS^*, ΔH^* and ΔG^* for gases in copolymers (from D_s)						
100% TEGDM	50	Ne	7·8	$1{\cdot}7\times10^{-1}$	4·5	7·2	5·7
	65	Ar	11·3	1·1	8·0	10·6	7·9
	55	H_2	7·9	$3{\cdot}5\times10^{-1}$	5·9	7·5	5·6
	65	CO_2	11·6	1·1	8·0	10·9	8·2
60% TEGDM	40	Ne	7·4	$1{\cdot}3\times10^{-1}$	4·0	6·8	5·5
	65	Ar	10·9	$8{\cdot}5\times10^{-5}$	7·6	10·2	7·7
	63	Kr	11·8	$7{\cdot}7\times10^{-1}$	7·3	11·1	8·7
	63	CO_2	11·4	1·2	8·2	10·7	8·0
	65	CH_4	12·6	3·6	9·5	12·0	8·8

†In the temperature range below 60°.

which compares well with the equation

$$\log D_0 = -4{\cdot}2 + 0{\cdot}13_6 E_D/T \qquad (18)$$

found to correlate data for a large number of elastomers and liquids[28].

In terms of the activated zone treatment of diffusion[26]

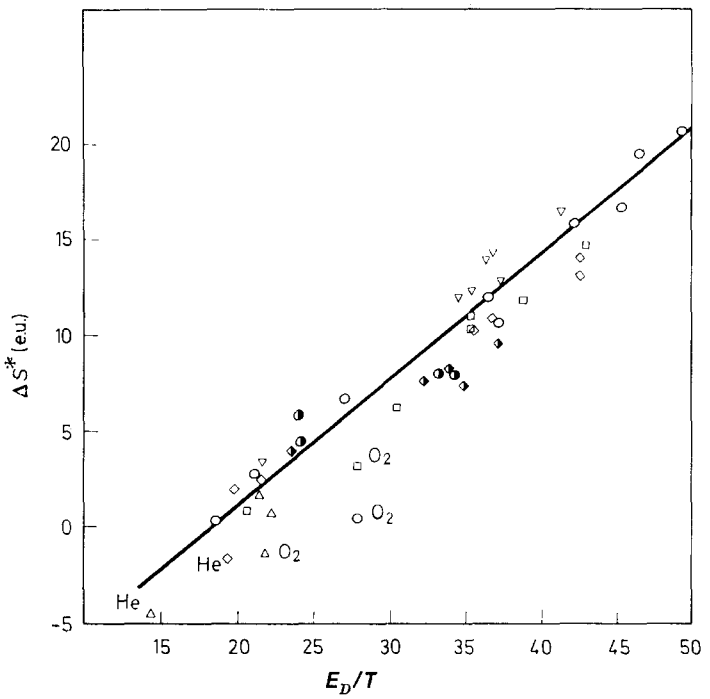

Figure 9—$\Delta\bar{S}^*$ versus E_D/T. ○, 100; △, 80; ◇, 60; □, 40 and △, 20 mole per cent TEGDM samples. Half shaded points are calculated from D_s data

$$\log D_0 = \log(\rho\bar{\nu}\lambda^2) + (f-1)\log[\{E_D + (f-1)RT\}/RT] - (f-1)\log(f-1) - \tfrac{1}{2}\log 2\pi(f-1) \quad (19)$$

The activation energy is shared amongst an optimum number of degrees of freedom, f. The factor ρ allows for any necessary synchronisation of the movements of penetrant and of the polymer segments for a successful unit diffusion step. $\bar{\nu}$ is the mean vibration frequency of penetrant relative to its environment and could be taken from *Table 5*. Since, however, ρ and λ are not known, a single value of $\rho\bar{\nu} = 0{\cdot}42 \times 10^{-12}$ sec has been taken, with $\lambda^2 = 10^{-15}$ cm^2 as before. The values of f (*Table 7*) are rather sensitive to that of $\rho\bar{\nu}\lambda^2$; even so it is probable that a considerable zone of activation is required for a unit diffusion step to occur.

Table 7. Number of degrees of freedom f

Per cent TEGDM	*Gas*							
	He	H_2	Ne	Ar	Kr	CH_4	N_2	CO_2
100	9	10	14	19	17	22	23	13
60	6	10	10	13	16	14	26	13
40	—	—	8	10	14	17	15	14
20	—	—	13	22	21	17	17	19

In vulcanized natural rubber E_D for a given penetrant increases with increased degree of crosslinking, and therefore as the polymer becomes less

rubbery[2]. In the TEGDM–EA copolymers of the present paper this behaviour is less clear. Inspection of *Table 6* will show no particular trend with helium or hydrogen and little with neon or carbon dioxide. The figure for argon, as a further example, tends to go through a minimum. However, it is also known that E_D in a given polymer is greater above the glass transition temperature T_g than below it[18,27], and we have already seen that T_g increases rapidly with per cent TEGDM. Thus a complex situation arises. Further complicating factors include the reduction of volume which accompanies crosslinking.

Permeability

For all copolymers in the temperature range 40° to 80°C the permeability increases in the order

$$N_2 < CH_4 < Kr < Ar < O_2 < Ne < CO_2 < H_2 < He$$

Stannett and Szwarc[28] expressed the permeability as a product of three factors

$$P(i,k) = F(\text{polymer } i)\, G(\text{gas } k)\, H(i,k) \tag{20}$$

where F is determined by the nature of the polymer, G by the nature of the gas and H by specific interactions between the gas and the polymer. Then for a pair of gases and a given polymer

$$\eta = \frac{P(i,k)}{P(i,l)} = \frac{G(\text{gas } k)}{G(\text{gas } l)} \cdot \frac{H(i,k)}{H(i,l)} \tag{21}$$

and for a single gas and a pair of polymers

$$\frac{P(i,k)}{P(j,k)} = \frac{F(\text{polymer } i)}{F(\text{polymer } j)} \cdot \frac{H(i,k)}{H(j,k)} \tag{22}$$

Equation (21) gives the steady state separation factor for the gas pair (k, l). The separation factors for the gas–polymer systems of this investigation are given in *Table 7* and do not show any strong dependence on the degree of crosslinking.

Rogers[29] evaluated the separation factor η of equation (21) for the gas pair (k, l) for 26 polymers at 30°C and found that η varied only by a factor of three while P changed 1200-fold. The values of P_O / P_{N_2} and P_{CO} / P_{N_2} in *Table 8* are in good agreement with average values of 3·8 and 24·2, respectively obtained from Rogers's data. In *Figures 10*(a), (b) and (c) are shown plots of P_{O_2}/P_{N_2}, P_{CO_2}/P_{N_2} and P_{He}/P_{N_2} respectively against $\log P_{N_2}$ for over 20 polymers representing semicrystalline and non-crystalline materials in the glassy or rubbery state. There is a tendency for the separation factor for a given gas pair to decrease with an increase in the permeability. This effect is most noticeable for the smaller gases such as helium. Stern *et al.*[30] have reported values for P_{He}/P_{N_2} and P_{He}/P_{CH_4} for 16 polymers which range from 1·5 to 370 and from 0·35 to 400 respectively. Again high permeation rates tend to be gained only at the expense of perm-selectivity. The separation factor P_{CO_2}/P_{N_2} at 30°C is approximately 45 for the 40 per cent TEGDM polymer and is the highest value reported for this

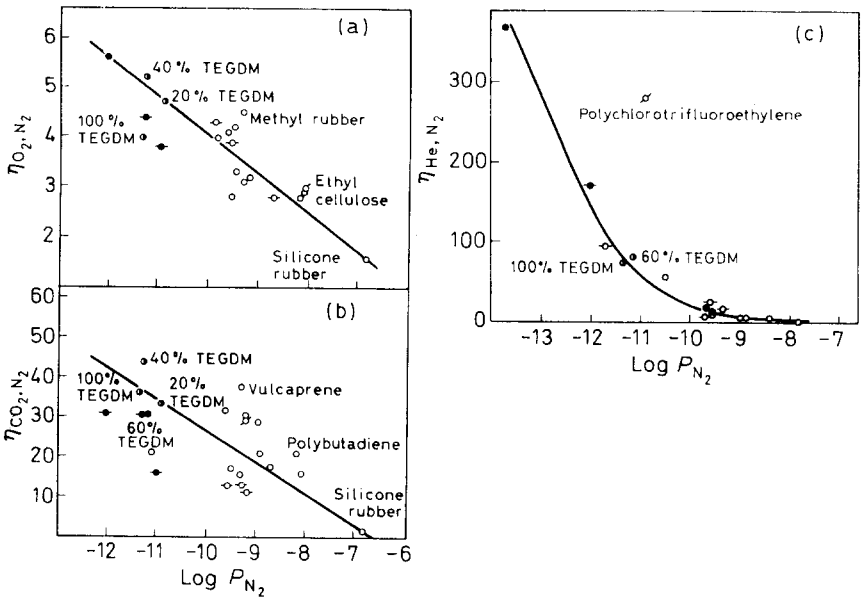

Figure 10—The separation factor η versus log P_{N_2} for several gas pairs at 30°C. ●, glassy; ◑, semi-glassy; ○, rubbery; ⌀, plasticized; ⊸○⊸, rubbery crystalline; ⊸●⊸, glassy crystalline. To avoid confusion the names of only a few materials are given

particular gas pair in polymer membranes. Favourable values of about 80 at 30°C are also obtained for P_{He}/P_{N_2} and P_{He}/P_{CH_4} for the 100 and 60 per cent TEGDM samples.

Table 8. Gas permeabilities of copolymer membranes at 60°C relative to nitrogen

Copolymer per cent TEGDM	$P_{N_2} \times 10^{11}$	$P_{(gas)}/P_{N_2}$							
		He	H_2	Ne	Ar	Kr	CH_4	CO_2	O_2
100	1·65	51	47	12	2·4	1·5	1·2	17	3·5
60	2·05	59	54	14	2·5	1·5	1·3	20	—
40	2·68	—	—	11	2·7	1·8	1·4	25	3·4
20	8·10	—	—	6·3	2·7	2·2	1·8	24	3·5

The permeability of all gases decreased as the number of crosslinks was increased, especially for those composed of larger molecules. In *Figure 11* the ratio P/P_{100} at 60°C, effectively the ratio $P(i,k)/P(j,k)$ of equation (22) is plotted as a function of the crosslink density C'. P_{100} is the permeability of the 100 per cent TEGDM polymer. The curves for the smaller gases helium, hydrogen and neon are practically coincident, with a slight minimum at around a composition of 90 per cent TEGDM. It may be that the 100 per cent TEGDM polymer contains defects or holes which facilitate the diffusion of these smaller gases but are not large enough to accommodate the larger molecules. It is also clear from *Figure 11* that equating the *H*

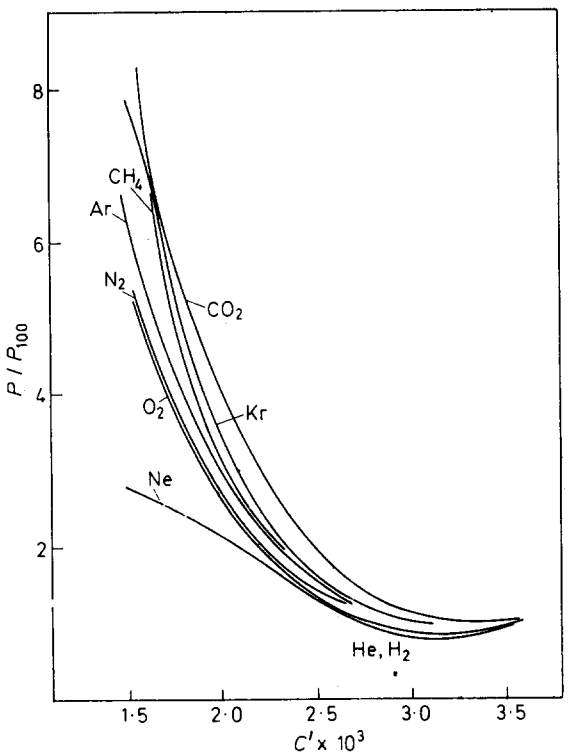

Figure 11—P/P_{100} versus crosslink density

ratio to unity is only a rough approximation so that the ratio $P(i, k)/P(j, k)$ is not dependent solely on the nature of the polymer.

One of us, P. S-L. Wong, is grateful to the Distillers Co. Ltd for the award of a bursary.

Physical Chemistry Laboratories,
Chemistry Department,
Imperial College, London, S.W.7.

(Received December 1967)

REFERENCES

[1] BARRER, R. M. *Trans. Faraday Soc.* 1940, **36,** 644
[2] BARRER, R. M. and SKIRROW, G. *J. Polym. Sci.* 1948, **3,** 549
[3] BARRER, R. M. and SKIRROW, G. *J. Polym. Sci.* 1948, **3,** 564
[4] AITKEN, A. and BARRER, R. M. *Trans. Faraday Soc.* 1955, **51,** 116
[5] VAN AMERONGEN, G. J. *Rubb. Chem. Technol.* 1947, **20,** 479
[6] CARPENTER, A. S. and TWISS, D. F. *Industr. Engng Chem. (Analyt. Ed),* 1940 **12,** 99
[7] REITLINGER, S. A., KUZININSKII, A. S. and FED'DSHTEIN, L. S. *Dokl. Akad. Nauk S.S.S.R.* 1958, **120,** 343
[8] SOBOLEV, I., MEYER, J. A., STANNETT, V. and SZWARC, M. *J. Polym. Sci.* 1955, **17,** 417
[9] LOSHAEK, S. and FOX, T. G. *J. Amer. chem. Soc.* 1953, **75,** 3544

[10] TOBOLSKY, A. V., KATZ, D., TAKAHASHI, M. and SCHAFFHAUSER, R. *J. Polym. Sci. A*, 1964, **2**, 2749
[11] BARRER, R. M., MALLINDER, R. and WONG, P. S-L. *Polymer, Lond.* 1967, **8**, 321
[12] MEARES, P. *Trans. Faraday Soc.* 1958, **54**, 40
[13] DRAISBASH, H., JESCHKE, D. and STUART, H. A. *Z. Naturf. A*, 1962, **17**, 447
[14] ROGERS, W. A., BURITZ, R. S. and ALPART, D. *J. appl. Phys.* 1954, **25**, 868
[15] CRANK, J. *The Mathematics of Diffusion*, Oxford University Press: London, 1957
[16] ASH, R., BARRER, R. M., BARRIE, J. A., PALMER, D. G. and WONG, P. S-L. *Chem. Commun.* 1966, 334
[17] MICHAELS, A. S., BIXLER, H. J. and FEIN, H. L. *J. appl. Phys.* 1964, **35**, 3165
[18] MEARES, P. *J. Amer. chem. Soc.* 1954, **76**, 3415
[19] MICHAELS, A. S. and BIXLER, H. J. *J. Polym. Sci.* 1961, **50**, 393
[20] GEE, G. *Quart. Rev. chem. Soc., Lond.* 1947, **1**, 265
[21] BARCLAY, I. M. and BUTLER, J. A. V. *Trans. Faraday Soc.* 1938, **34**, 1445
[22] BARRER, R. M. and CHIO, H. T. *J. Polym. Sci. C*, 1965, **10**, 111
[23] BARRER, R. M. *Trans. Faraday Soc.* 1947, **43**, 3
[24] HIRSCHFELDER, J. O., CURTISS, C. F. and BIRD, R. B. *Molecular Theory of Gases and Liquids*, Wiley: New York, 1954
[25] BARRER, R. M. *Diffusion in and through Solids*, Cambridge University Press: London, 1951
[26] BARRER, R. M. *Trans. Faraday Soc.* 1942, **38**, 322
[27] MICHAELS, A. S., VIETH, W. R. and BARRIE, J. A. *J. appl. Phys.* 1963, **34**, 13
[28] STANNETT, V. and SZWARC, M. *J. Polym. Sci.* 1955, **16**, 89
[29] ROGERS, C. E. *Physics and Chemistry of the Organic Solid State*, Vol. II, Interscience: New York, 1965
[30] STERN, S. A., SINCLAIR, T. F., GAREIS, P. J., VAHLDIECK, N. P. and MOHR, P. H. *Industr. Engng Chem. (Industr.)*, 1965, **57**, 49

The Polymerization of Crystalline Methacrylic Acid Initiated by Ultra-violet Radiation I—Radical Conformations and Reaction Mechanism

C. H. BAMFORD, A. BIBBY* and G. C. EASTMOND

A study has been made of the radicals produced during ultra-violet irradiation of methacrylic acid crystals at temperatures below −20°C. Under these conditions little polymerization occurs. Measurements of the radical concentration and conformation are reported, and from the results it is concluded that reaction is restricted to specific sites in imperfect regions of the crystals in which there is adequate molecular mobility. These sites have mobilities distributed over a wide range; as the temperature is raised the density of suitable sites increases. The distribution of mobilities is dependent on the conditions of crystallization.

Radicals are formed by irradiation in a specific conformation T giving rise to a 13-line e.s.r. spectrum, and subsequently relax to conformations N giving a 9-line spectrum. Evidence is adduced which indicates that this relaxation is a photo-assisted process. Termination is considered to result from radical formation in sites containing N radicals.

The implications of a simple theoretical model have been explored.

IN EARLIER papers[1–3] we have shown that crystalline methacrylic acid polymerizes when irradiated by ultra-violet light of $\lambda < 2\,500$ Å, approximately. When thin (20μ) single crystals are irradiated at temperatures close to 7°C, the conversion/time curve is sigmoid, as is observed in many solid phase reactions in which nucleation plays a significant part. The importance of crystal imperfections, probably dislocations, was demonstrated by the sensitivity of the reaction to comparatively low unidirectional mechanical stress (*ca.* 10 atm.) which greatly reduces the rate of polymerization, and suspends the after-effect[3]. Very recently, Thomas and Williams[4] have observed dislocations in sucrose crystals and have shown that thermal decomposition proceeds more rapidly in regions of high dislocation density. Earlier, Sella and Trillat[5], and Sella and Bensasson[6], studying the solid phase polymerization of acrylamide, reported that, in the initial stages, globules of polymer which appear at the crystal surface are aligned along preferred crystallographic directions. The globules probably correspond to the emergence of dislocation lines at the surface, and the lines may indicate the run of sub-grain boundaries. Bassett[7] has now identified the sites of initiation in the solid-phase polymerization of trioxan as imperfections at the {00·1} sub-grain boundaries; formerly it was considered that the ring-opening polymerizations of monomers such as trioxan occur only in the perfect crystals[8].

*Present address: North Staffordshire College of Technology, Stoke-on-Trent.

We have shown that at low temperatures (−30°C) the free radicals in crystalline methacrylic acid are formed in a single preferred conformation[9,10]; this is characterized by an electron spin resonance (e.s.r.) spectrum of 13 lines, different from the conventional methacrylate radical spectrum, which, for radicals in the amorphous solid phase, has 9 lines and corresponds to hindered rotation about the C_α—C_β bonds[11]. For radicals in the liquid phase the latter spectrum has been resolved into 16 lines, and indicates the existence of several preferred conformations[12]. As the temperature of the crystalline methacrylic acid is raised above −30°C the gradual onset of hindered rotation, accompanying increasing mobility in the dislocations, has been observed by a change in the e.s.r. spectrum to a mixture of the 13- and 9-line spectra[10]. 13-line spectra have also been observed in barium methacrylate by O'Donnell *et al.*[13]. In γ-irradiated acrylamide[14], acrylic acid[15] and barium methacrylate[13] a progressive change from anisotropic to isotropic spectra occurs with increasing temperature. Adler and Petropoulos[14] have attributed this type of change in acrylamide to the existence of a range of imperfections and consequently a range of radical environments.

In the present paper we consider the information about the nature of the imperfections in methacrylic acid crystals which is obtainable from studies of the concentrations and e.s.r. spectra of radicals formed by ultra-violet irradiation. We interpret the results in terms of the following postulates. (1) Radicals are formed by light only in crystal imperfections. (2) Polymerization occurs only in imperfections. (3) Imperfections may have various structures which will be associated with different properties, particularly different free volumes and molecular mobilities. (4) Radical formation and polymerization require adequate molecular mobilities. (5) The numbers of sites with suitable mobilities for radical formation and polymerization are functions of the temperature of the specimen. Subsequent papers in this series (Parts II and III) will deal with the effects of additives on the imperfections as deduced from e.s.r. studies and observations of the sensitivity of the polymerization to mechanical stress.

EXPERIMENTAL

Methacrylic acid, purchased from I.C.I. Ltd (Mond Division), was purified as described in an earlier paper[10]. It was stored frozen under nitrogen, and all subsequent handling was carried out in a dry-box.

Dilatometry was carried out on both powdered and bulk methacrylic acid, with mercury as the dilatometric fluid. The powdered acid was prepared in a dry-box by cooling in solid carbon dioxide with rapid stirring. It was introduced into the dilatometer bulb and degassed and the dilatometer was then filled with degassed mercury at −20°C. In experiments on bulk methacrylic acid, the monomer was degassed in the dilatometer bulb in the conventional manner and then frozen. In both cases the most reproducible results were obtained when the capillary of the dilatometer was open to the atmosphere. Dilatometers were maintained at each temperature for 24 h before a reading was taken. Corrections were applied for the thermal expansion of mercury. The two techniques gave similar results.

Optical retardations of methacrylic acid crystals were measured by using a Berek compensator in conjunction with a Leitz 'Ortholux' polarizing

microscope. The monomer samples, in the form of thin (10 to 20μ) single crystals, were prepared in a suitable cell, as described previously[3]; the temperature of the specimen was controlled by pumping cold methanol through a channel in the cell wall.

Specimens of methacrylic acid for e.s.r. studies were prepared according to the procedure already described[10]; crystallizations were carried out by plunging liquid monomer samples into either liquid nitrogen or a bath of methanol at the appropriate temperature. After two hours the specimens were removed to a low-temperature thermostat of the type described elsewhere[10] and irradiated by the light of a 250 W ME/D high pressure mercury arc.

In some experiments filters were interposed in the light beam to isolate certain wavelength regions. Aqueous copper sulphate and acetic acid filters were used. The former produces a reduction in intensity between 2 850 and 2 780 Å with a complete blackout below 2 780 Å, while with the latter the intensity is reduced between 2 500 and 2 450 Å with an almost complete blackout below 2 400 Å. The e.s.r. spectra were recorded on a Varian E-3 spectrometer operating at 9·5Gc/s, and employing 100kc/s field modulation. In all cases a microwave power of 1 mW and modulation amplitude of 1·6 gauss were used with the specimens maintained at -196°C. This modulation amplitude distorts the spectra slightly and reduces the resolution, but it was used for the purpose of enhancing the signal-to-noise ratio at short irradiation times (when radical concentrations are very low) as an alternative to longer scanning times and a longer time constant. In earlier papers[9,10] we have reported that irradiation of methacrylic acid for short times at low temperatures produces radicals giving a 13-line e.s.r. spectrum, while at higher temperatures, or on prolonged irradiation, the spectrum changes to the familiar 9-line type. We refer to the radical species responsible for these spectra as T and N, respectively. Most experimental spectra correspond to a mixture of the 13-line and 9-line types and a parameter X/Y has been defined (*Figure 1*) which indicates the contribution from the 13-line spectrum; $X/Y=0$ for the 9-line spectrum. (The definition of X/Y is slightly different from that used previously[10].)

For the purpose of determining relative radical concentrations all spectra were compared with that from a standard pitch sample. As the spectrum changes during irradiation, radical concentrations are not directly proportional to peak-to-peak heights. To allow for changes in the character of the spectrum a calibration curve was derived as follows. Spectra were constructed by mixing the normalized 'pure' 13- and 9-line spectra in proportions varying between 1: 9 and 9 : 1 with the aid of an English Electric KDF9 computer. Each spectrum then corresponded to the same radical concentration. The peak-to-peak heights of the central lines of the derivative spectra were plotted against X/Y; relative radical concentrations were then obtained from the experimental spectra by dividing the observed peak-to-peak height of the central line in each by the factor appropriate to the observed X/Y. In these calculations we assumed that a value of $X/Y=0{\cdot}35$ corresponds to a pure 13-line spectrum; this appeared to be the limiting value of X/Y at short irradiation times, within experimental error.

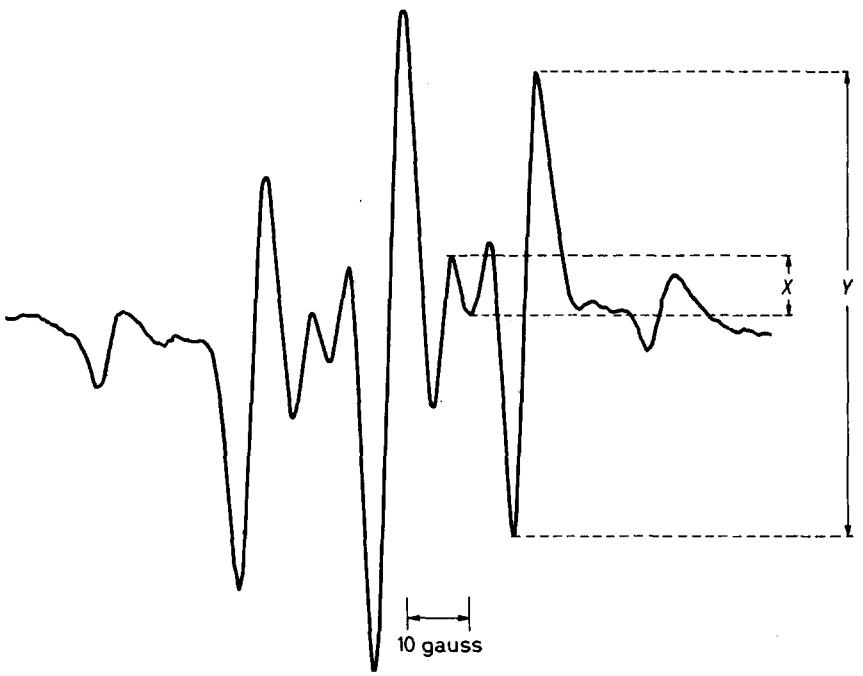

Figure 1—Typical e.s.r. spectrum of irradiated methacrylic acid crystals showing definitions of *X*, *Y*. The spectrum is a mixture of the 9- and 13- line types

RESULTS AND DISCUSSION

(1) *Molecular mobility*

When irradiation is carried out for a constant period at a series of temperatures it is found[9] that the radical concentration shows a peak at about $-5°C$; this suggested to us the possibility of a transition in the crystals near this temperature. Dilatometric observations in the temperature range $-15°$ to $+2°C$ demonstrate that below $-6°C$ the coefficient of thermal expansion decreases with decreasing temperature (*Figure 2*). Broad-line nuclear magnetic resonance (n.m.r.) studies by B. Arnold and G. C. Eastmond, to be reported in detail in a later paper, show that the second moment decreases as the temperature is raised above $-30°C$ in a way which indicates the gradual onset of new types of molecular motions without the appearance of a sharp transition. We have already reported[10] a decrease in line-width near $-6°C$, and in a private communication Y. Sakai has recorded a peak in the DTA spectrum at $-13°C$. There is also a steady decrease in optical retardation with increasing temperature above $-30°C$ (*Figure 3*). All these results are consistent with the gradual development of molecular mobility in the crystals with increasing temperature above $-30°C$ and we do not believe there is a sharp phase transition. The peak in radical concentration near $-5°C$ probably arises from the superposition of two opposing effects. As the temperature rises, the rate of radical formation increases on account of the growing number of suitable imperfections (postulates 4 and 5) while increasing radical mobility leads to an

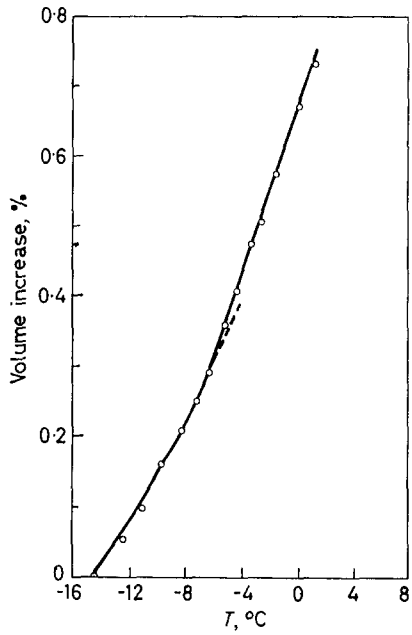

Figure 2—Change in volume of methacrylic acid crystals with temperature

increasing rate of mutual destruction of radicals, which predominates at the higher temperatures.

(2) *Effect of temperature of irradiation; the reaction mechanism at low temperatures*

The radical concentration is shown in *Figure 4* as a function of the time of photolysis for irradiation temperatures of −20°C, −30°C and −50°C. In these experiments the specimens were crystallized by plunging into liquid nitrogen.

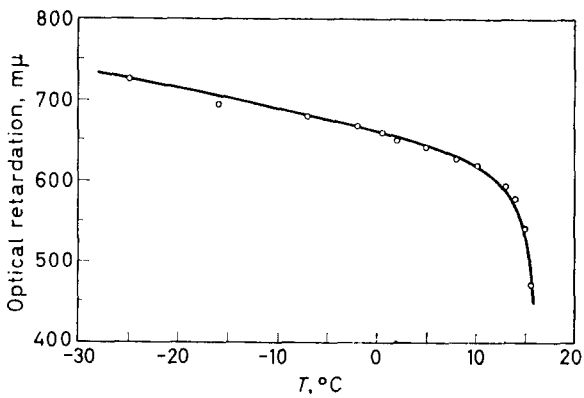

Figure 3—Optical retardation of a crystal of methacrylic acid as a function of temperature

As we have already recorded[3], the radical concentration reaches a steady value on prolonged irradiation; rates of polymerization are very low at these temperatures. There is little decay in radical concentration on storage in the dark and we have previously shown[3] that no marked decrease in concentration occurs when the light is turned off. The stationary radical concentration must arise from a balance between initiation and

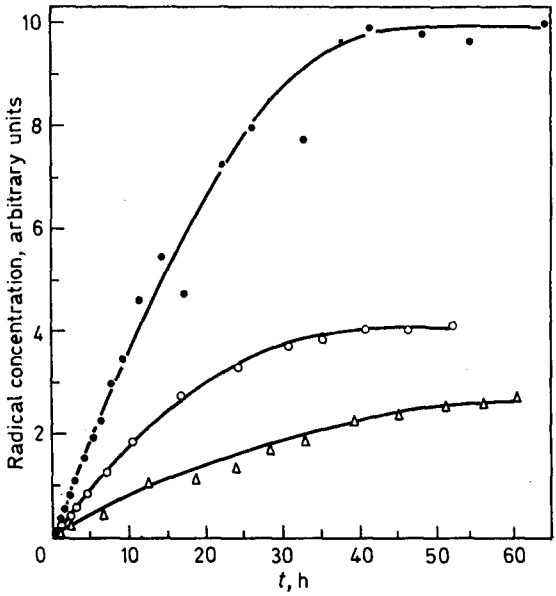

Figure 4—Variation of radical concentration with time of irradiation at: ●, −20°C; ○, −30°C; △, −50°C. Crystallizing bath at −196°C

termination, and as initiation occurs only during irradiation we conclude that the light must also facilitate termination. A mechanism of the termination process is suggested below.

Conformational data for the same samples are given in *Figure 5*. As irradiation proceeds, the value of X/Y decreases and ultimately reaches a limit which is characteristic of the temperature of irradiation. These results are consistent with the view that the methacrylic radicals arising from the initiation process are in the T conformation and are maintained in this

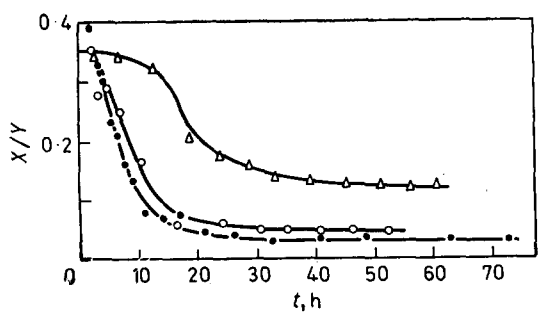

Figure 5—Variation of X/Y with time of irradiation at: ●, −20°C; ○, −30°C; △, −50°C. Crystallizing bath at −196°C

conformation by lattice forces, e.g. hydrogen bonds. The observed spectra show that such radicals must have propagated at least to the dimer stage, and are probably a mixture of dimers and trimers. Adler and Petropoulos[14] have considered the reactions of nearest neighbours in the crystal lattice and have concluded that radicals in acrylamide can only remain anisotropic up to the dimer or trimer stage. Restricted conformations have not been observed with acrylamide, but the radical anisotropy in that monomer and the restricted conformation of methacrylic radicals are both attributable to lattice forces and lack of mobility. Propagation requires the breaking of hydrogen bonds by thermal motions. This may happen in two ways; the T radical may become detached from the lattice and able to approach a neighbouring monomer molecule and achieve a configuration suitable for reaction, or, alternatively, a monomer molecule may acquire sufficient mobility to permit reaction with the attached radical. In either case the orderly arrangement of hydrogen bonds and the unique (T) conformation of the radical are lost, so that the active propagating species are of the N type. We shall refer to the T$\rightarrow$N change as relaxation, without wishing to imply that the process necessarily occurs by detachment of T radicals.

The processes we have so far considered account for a decrease in the ratio X/Y with increasing time of irradiation, since the initial T-type radicals are continuously converted to the N-type. It is now necessary to examine the significance of the limiting values of X/Y obtained at long irradiation times (*Figure 5*). T radicals must be formed by the light in pairs; after prolonged photolysis most sites capable of supporting reaction will contain N radicals, and there will be a high probability that a radical after relaxation from T to the N form will react with an N radical in the same site. The net result is that one N radical becomes replaced by T. This in turn can relax to N, so that a stationary value of T/N is obtained. Since, at long times, the total radical concentration T+N is constant, and T/N is constant, both T and N must be constant. The decreasing rate of relaxation T$\rightarrow$N with decreasing temperature in the range $-20°$ to $-50°$C, resulting from the reduced mobilities at the lower temperatures, explains both the increase in the stationary value of X/Y, and also the lower rate of decrease in X/Y during irradiation, as the temperature is lowered. An approximate kinetic treatment based on these ideas is developed in § 5.

All the samples referred to in *Figure 4* were crystallized at the same temperature and might be expected to have the same density of imperfections. For this reason it would be anticipated that the limiting radical concentration would be independent of irradiation temperature. However, *Figure 4* shows that both the initial rate of radical formation and the limiting concentration are higher at the higher temperatures. We take this to indicate that at any temperature the imperfections possess a spectrum of mobilities (postulate 3); only those imperfections in which the molecular mobility exceeds a threshold value are capable of supporting reaction (i.e. postulate 4). Further, the number of such imperfections increases with increasing temperature (cf. postulate 5). On this view, the limiting radical concentration is a measure of the density of imperfections in which reaction can occur (see § 5).

(3) *Effect of conditions of crystallization*

The results of a series of experiments with irradiation at −20°C, in which the temperature of the crystallizing bath was varied in the range −20° to −196°C, are shown in *Figure 6*. Changing the bath temperature

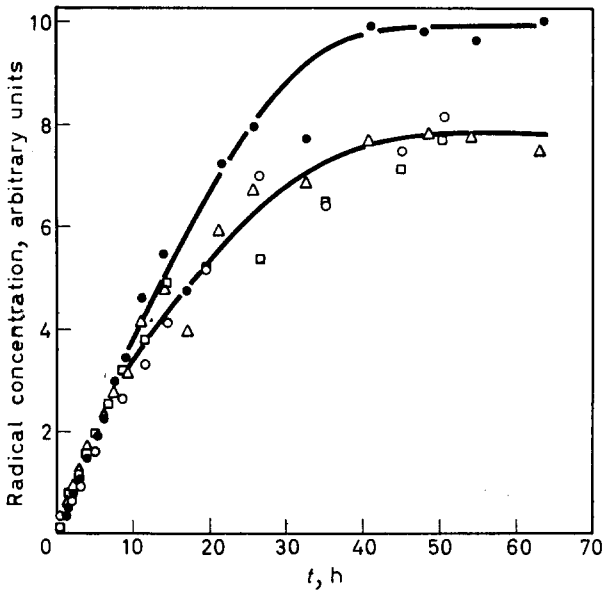

Figure 6—Dependence of radical concentration on temperature of crystallizing bath. ●, −196°C; □, −60°C; ○, −40°C; △, −20°C. Irradiation at −20°C

from −20° to −60°C has no effect on the limiting radical concentration, within experimental error, indicating that the density of imperfections is approximately the same in the crystals produced. Cooling at −196°C results in higher limiting concentrations, and must therefore introduce more imperfections. This would follow from an increased rate of nucleation at −196°C.

Values of X/Y for the same specimens are given in *Figure 7*. At long irradiation times X/Y approaches a limit which is the same for all samples, showing that at these times all the imperfections have the same character. For short irradiation times differences are perceptible; this is more easily seen from *Figure 8* which is an expanded version of the first ten hours of irradiation in *Figure 7*, with additional data for crystallization in a bath at −90°C. It appears that a higher value of X/Y is obtained when crystallization is carried out in a bath at a lower temperature; although there is a higher density of imperfections in these circumstances, the average molecular mobility in the imperfections is lower. Even at the start of irradiation the spectra of specimens crystallized in baths at higher temperatures contain a contribution from N radicals suggesting that the relaxation T⟶N in these samples can occur readily in at least some of the imperfections (postulates 3 and 4). We have previously reported[10] that

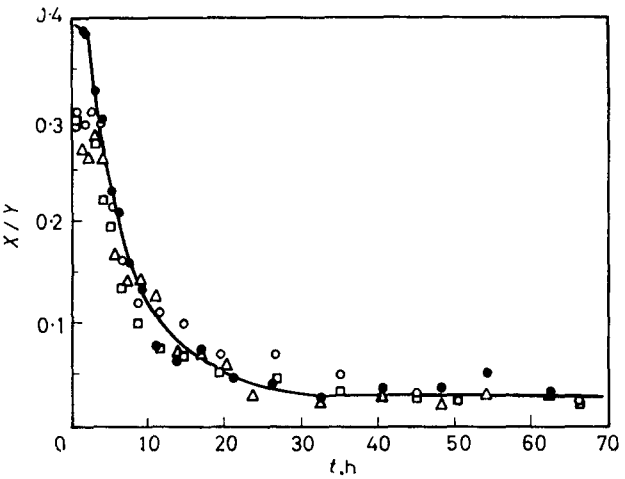

Figure 7—Dependence of X/Y on temperature of crystallizing bath. ●, −196°C; □, −60°C; ○, −40°C; △, −20°C. Irradiation at −20°C

crystallization in baths above 0°C with subsequent irradiation at lower temperatures gives rise only to radicals in the N form; clearly under these conditions there must be considerable mobility so that T radicals are never observed. These experiments substantiate the view that the mean properties of the imperfections at a given temperature can be changed by altering the conditions of crystallization.

As the specimens prepared under different crystallization conditions have imperfections with different average properties we might expect that the initial differences in X/Y (*Figure 7*) would be maintained throughout

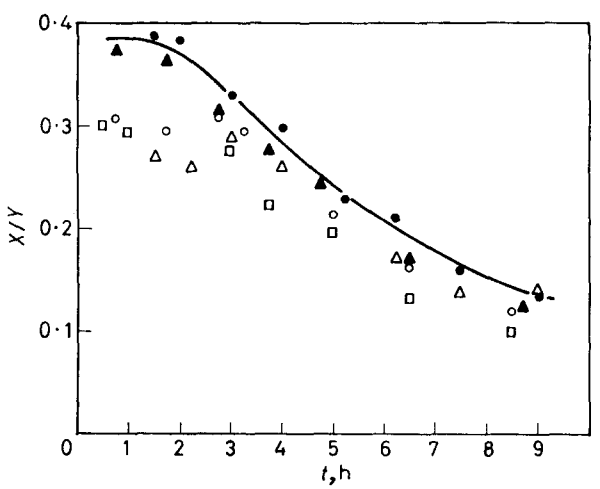

Figure 8—Results in *Figure 7* for first ten hours of irradiation on an expanded time scale. Temperatures of crystallizing baths: ●, −196°C; ▲, −90°C; □, −60°C; ○, −40°C; △, −20°C

irradiation. This is not so, hence it follows that all T radicals formed must be capable of ultimate relaxation under continuous irradiation (see §4). Similar behaviour is observed in the presence of additives and a fuller discussion is reserved for Part II.

(4) *Irradiation at different wavelengths*

Figure 9 shows corresponding values of the radical concentration and X/Y for a specimen subjected to irradiation with a series of different wavelengths at a constant temperature ($-20°C$). The original crystallization was carried out in a bath at $-196°C$.

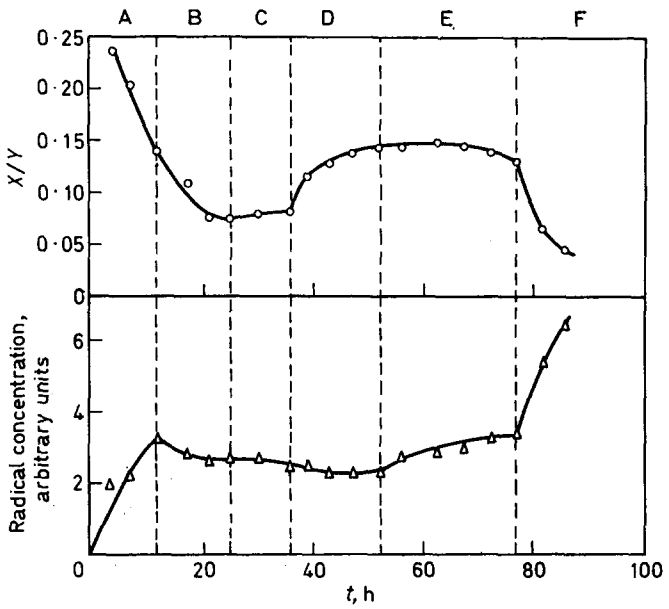

Figure 9—Values of radical concentration and X/Y under different conditions of illumination at $-20°C$, as described in text

In region A the specimen was irradiated by the full light of the mercury arc, and the behaviour observed is similar to that in *Figure 5* already discussed. On standing at $-20°C$ in the dark (region B) X/Y continues to fall showing that the relaxation T⟶N is occurring in the dark in a fraction of the sites (those in which the mobility is highest); eventually X/Y becomes constant, as some radicals are unable to relax under these conditions. As already shown in § 3, continued irradiation enables all T radicals to relax, hence relaxation in some sites must be assisted by irradiation. This is understandable if an exciton formed by absorption of radiation becomes localized and decays in an imperfection[16] in the neighbourhood of a T radical, thus enabling the constraints on the radical to be overcome by thermal motion.

In region B the radical concentration decreases by approximately 20 per cent; this decrease is comparable to the observed change in X/Y,

on the assumption that only T radicals decay. This arises because a pair of T radicals formed by the light will frequently be located in the neighbourhood of an N radical; relaxation of one T radical followed by combination with N would remove two radicals, and subsequent relaxation of the other T radical would replace the initial N radical. The net effect is therefore the loss of T radicals. The process may be depicted as shown below

$$\begin{matrix} TT \\ N \end{matrix} \rightarrow \begin{matrix} TN \\ N \end{matrix} \rightarrow T \rightarrow N \qquad (1)$$

In region C, corresponding to illumination with light of $\lambda > 3\,000$ Å, X/Y increases slightly and the radical concentration decreases slightly. These small changes appear to be quite reproducible. Separate experiments show that no radicals are formed by the light under these conditions. The changes in region C are consistent with a small loss of N radicals. This process may be assisted by irradiation, the trapping of excitons in the imperfections enhancing the mobility and facilitating propagation. (Unpublished results of G. C. Eastmond give independent evidence that propagation may be assisted by light of $\lambda > 3\,000$ Å at higher temperatures; the magnitude of the after-effect in methacrylic acid crystals following irradiation with the light of the full mercury arc is increased by illumination with wavelengths longer than 3 000 Å.) In region D ($\lambda > 2\,800$ Å) a small amount of radical formation occurs, but this could not account for the observed decrease in radical concentration (as radicals are formed in pairs). There is a considerable decrease in N radical concentration, so that the processes outlined for region C must also occur to a greater extent.

The acetic acid filter used in region E transmits freely light with $\lambda > 2\,500$ Å, but only transmits feebly in the range 2 400 to 2 500 Å. We have already noted that polymerization occurs on irradiation with light with λ in the range 2 500 Å to 2 800 Å, so that it is not surprising that a slow build-up in radical concentration occurs in this region. This is accompanied by a small decrease in X/Y, essentially similar to that in region A. Finally, in region F, with the full intensity of the shorter wavelengths, there is a rapid increase in radical concentration and also a rapid decrease in X/Y, as the processes we have so far considered operate at the normal rates corresponding to the high intensity.

(5) *Kinetics of radical formation under conditions of negligible polymerization*

The ideas described in the preceding sections suggest the exploration of a simple model for the processes occurring in irradiated methacrylic acid crystals. This is most likely to be applicable under conditions of negligible polymerization, so that reactions are restricted to suitable sites present initially, the properties of the sites being effectively independent of time. In practice, we believe these conditions are satisfied if the temperature of irradiation is below -20°C, approximately.

The kinetic mechanism must include the following steps: (i) initial photo-formation of T radicals; (ii) relaxation of these to N radicals; and (iii) a terminiation process involving light absorption. There appears to be

little radical decay in the dark, consequently under these conditions there is no significant overall bimolecular termination. These steps are represented in the equations below.

$$\underset{(\mathcal{T}_1)}{2S \xrightarrow{k_1 I_0} 2T} \tag{2}$$

$$\underset{(\mathcal{T}_1)\ (\mathcal{N}_1)}{T \xrightarrow{k_r} N} \tag{3}$$

$$\underset{(\mathcal{T}_2)}{\mathcal{N}_1 \xrightarrow{k_2 I_0} \begin{matrix} TT \\ N \end{matrix}} \tag{4}$$

$$\underset{(\mathcal{T}_2)}{\begin{matrix} TT \\ N \end{matrix}} \xrightarrow[(a)]{} \underset{(\mathcal{T}_1)}{\begin{matrix} TN \\ N \end{matrix}} \xrightarrow[(b)]{} T \tag{5}$$

Here S represents a vacant site in which there is sufficient mobility for radical formation to occur. A site which contains one T radical is designated $\mathcal{T}_1$. Equation (2) represents the photochemical formation of T radicals. Equation (3) corresponds to the relaxation T→N; a reaction site containing an N radical is designated $\mathcal{N}_1$. As there is some evidence that the relaxation is assisted by light (§4), k_r may include a photochemical contribution. As explained in §4, we assume that light absorption frequently leads to the formation of two T radicals in an $\mathcal{N}_1$ site; the result is the production of a $\mathcal{T}_2$ site containing two T and one N radicals [equation (4)]. Such a site may contain, after relaxation of one T radical, a TNN arrangement [equation (5a)]. This arrangement may react in two ways: N–N combination may occur, so that a $\mathcal{T}_1$ site is formed [equation (5b)], or, relaxation of the remaining T radical may take place, with formation of a site containing three N radicals, which after N–N recombination, becomes an $\mathcal{N}_1$ site. For simplicity we assume that equation (5b) is the predominant process; further, we assume that the transformation $\mathcal{T}_2 \rightarrow \mathcal{T}_1$ is characterized by a single rate constant k. Like k_r, k may possess a photochemical component.

The model we have described represents an oversimplification of the real system, since it assumes that radical formation and relaxation can occur at similar rates in all reaction sites. In fact this is not so, and the velocity coefficients will be average values. Further, the whole termination process is assumed to be light-assisted and of the cage-type [equations (4) and (5)], and no account is taken of non-cage bimolecular termination (see §4).

On the basis of the model we obtain the following equations for the concentrations of the various types of site.

$$-\mathrm{d}[S]/\mathrm{d}t = k_1 I_0 [S] \tag{6}$$

$$\mathrm{d}[\mathcal{T}_1]/\mathrm{d}t = k_1 I_0 [S] - k_r [\mathcal{T}_1] + k [\mathcal{T}_2] \tag{7}$$

$$d[\mathcal{N}_1]/dt = k_r[\mathcal{I}_1] - k_2 I_0[\mathcal{N}_1] \tag{8}$$

$$d[\mathcal{I}_2]/dt = k_2 I_0[\mathcal{N}_1] - k[\mathcal{I}_2] \tag{9}$$

From these equations we find that:

$$[S] = [S]_0 e^{-k_1 I_0 t} \tag{10}$$

$$[\mathcal{I}_2] = \frac{k_2 k_r I_0 [S]_0}{\alpha+\beta}\left\{e^{-pt}\left[-\frac{\beta}{\alpha}\left(\cos qt + \frac{p}{q}\sin qt\right) - \frac{k_1 I_0}{q}\sin qt\right] - e^{-k_1 I_0 t} + \frac{\alpha+\beta}{\alpha}\right\} \tag{11}$$

for $(k_r + k + k_2 I_0)^2 - 4k_r(k + k_2 I_0) - 4kk_2 I_0 < 0$;

$$[\mathcal{I}_2] = \frac{k_2 k_r I_0 [S]_0}{\alpha+\beta}\left\{\frac{1}{2q}\left(\frac{m_2\beta}{\alpha} - k_1 I_0\right) e^{(-p+q)t} - \frac{1}{2q}\left(\frac{m_1\beta}{\alpha} - k_1 I_0\right) e^{(-p-q)t} - e^{-k_1 I_0 t} + \frac{\alpha+\beta}{\alpha}\right\} \tag{12}$$

for $(k_r + k + k_2 I_0)^2 - 4k_r(k + k_2 I_0) - 4kk_2 I_0 > 0$.

Here

$$\left.\begin{aligned} \alpha &= k_r(k + k_2 I_0) + kk_2 I_0 \\ \beta &= k_1^2 I_0^2 - k_1 I_0(k_r + k + k_2 I_0) \\ p &= \tfrac{1}{2}(k_r + k + k_2 I_0) \\ q^2 &= \tfrac{1}{4}\left|\{k_r + k + k_2 I_0)^2 - 4k_r(k + k_2 I_0) - 4kk_2 I_0\}\right| \\ m_1 &= -p + q \\ m_2 &= -p - q \end{aligned}\right\} \tag{13}$$

Further,

$$[\mathcal{I}_1] = [S]_0(1 - e^{-k_1 I_0 t}) - [\mathcal{I}_2]\left(1 + \frac{k}{k_2 I_0}\right) - \frac{1}{k_2 I_0}\frac{d[\mathcal{I}_2]}{dt} \tag{14}$$

and

$$[\mathcal{N}_1] = [S]_0(1 - e^{-k_1 I_0 t}) - [\mathcal{I}_1] - [\mathcal{I}_2] \tag{15}$$

From equations (10) to (15) we may calculate the total radical concentration [R·] and the total T radical concentration with the aid of the relations:

$$[R\cdot] = [\mathcal{N}_1] + [\mathcal{I}_1] + 3[\mathcal{I}_2] \tag{16}$$

$$[T\cdot] = [\mathcal{I}_1] + 2[\mathcal{I}_2] \tag{17}$$

In the stationary state ($t \to \infty$) we see from equations (6) to (9) and (15) that for $I_0 \neq 0$ the values of [S], $[\mathcal{N}_1]$, $[\mathcal{I}_1]$, $[\mathcal{I}_2]$ are given by:

$$\left.\begin{aligned}
[\mathrm{S}]_s &= 0 \\
[\mathcal{N}_1]_s &= [\mathrm{S}]_0/\mathcal{D} \\
[\mathcal{T}_1]_s &= ([\mathrm{S}]_0/\mathcal{D})(k_2 I_0/k_r) \\
[\mathcal{T}_2]_s &= ([\mathrm{S}]_0/\mathcal{D})(k_2 I_0/k) \\
[\mathrm{R}\cdot]_s &= ([\mathrm{S}]_0/\mathcal{D})(1 + k_2 I_0/k_r + 3k_2 I_0/k) \\
[\mathrm{T}\cdot]_s &= (k_2 I_0\,[\mathrm{S}]_0/\mathcal{D})(1/k_r + 2/k)
\end{aligned}\right\} \qquad (18)$$

where $$\mathcal{D} = 1 + k_2 I_0(1/k_r + 1/k) \qquad (19)$$

Equations (10) to (17) may be used to calculate [R·] and [T·]/[R·]. The results of such calculations with the values of the parameters indicated are shown in *Figures 10* and *11*. The two sets of parameters might correspond to −50°C and −20°C, respectively. The form and general disposition of the curves in *Figures 10* and *11* may be compared to those found experimentally and shown in *Figures 4* and *5*. Clearly the calculated curves are in reasonable accord with observations; in view of the crudity

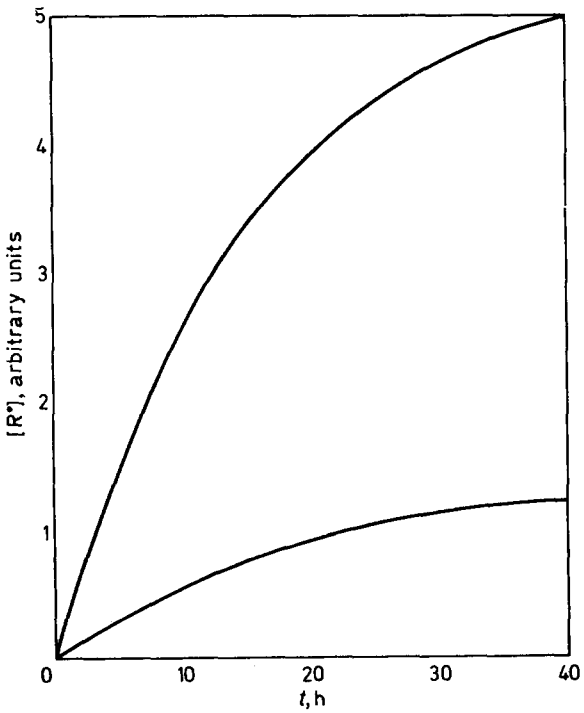

Figure 10—Calculated variation of radical concentration with time of irradiation. Lower curve: equations (11), (14), (15), (16) with $k = 0{\cdot}2$ h^{-1}, $k_r = 0{\cdot}1$ h^{-1}, $k_1 I_0 = k_2 I_0 = 0{\cdot}067$ h^{-1}, $[S]_0 = 1$. Upper curve: equations (12), (14), (15), (16) with $k = 2$ h^{-1}, $k_r = 1$ h^{-1}, $k_1 I_0 = k_2 I_0 = 0{\cdot}067$ h^{-1}, $[S]_0 = 5$

of our model no attempt has been made to obtain the 'best' values of the parameters for fitting the experimental results. At both temperatures it has been assumed that $k=2k_r$. The quantity $(k_2I_0)/k$ has a negative temperature coefficient; it seems likely that this arises from the increase in k with temperature, k_2 being less strongly dependent on temperature. The limiting radical concentrations, although somewhat in excess of the total

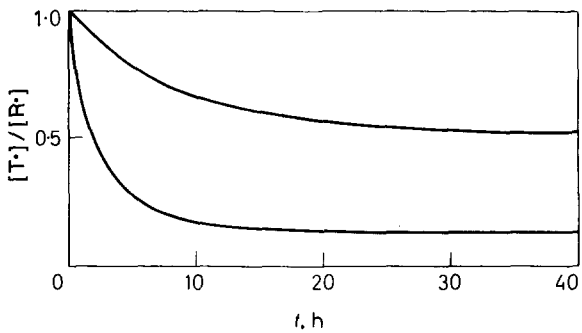

Figure 11—Calculated variations of [T·]/[R·] with time of irradiation. Lower curve: equations (12), (14), (15), (16) with $k=2$ h^{-1}, $k_r=1$ h^{-1}, $k_1I_0=k_2I_0=0{\cdot}067$ h^{-1}. Upper curve: equations (11), (14), (15), (16) with $k=0{\cdot}2$ h^{-1}, $k_r=0{\cdot}1$ h^{-1}, $k_1I_0=k_2I_0=0{\cdot}067$ h^{-1}

number of suitable sites at both temperatures [equations (18)], are clearly mainly determined by this quantity, as already inferred (§2), while the ratio [T·]/[R·] is independent of $[S]_0$, but is determined by the rates of relaxation (k, k_r) and $\mathcal{T}_2$ formation (k_2I_0).

The initial portions of the observed X/Y curves, especially at -50°C (*Figure 5*), are not matched by the calculated [T·]/[R·] relations (*Figure 11*). A possible reason for the form of the observed curves in this region is discussed in Part II, where it is suggested that the existence of sites with different molecular mobilities is responsible.

In its main features, the behaviour of our model, based on equations (2) to (5), resembles that of the real system at low temperatures. At higher temperatures the stresses set up by polymerization probably lead to dislocation multiplication, so that a much more complicated situation arises.

Department of Inorganic, Physical and Industrial Chemistry,
University of Liverpool, Liverpool.

(*Received March 1968*)

REFERENCES

[1] BAMFORD, C. H. JENKINS, A. D. and WARD, J. C. *J. Polym. Sci.* 1960, **48**, 37
[2] BAMFORD, C. H., EASTMOND, G. C. and WARD, J. C. *Nature, Lond.* 1961, **192**, 1036
[3] BAMFORD, C. H., EASTMOND, G. C. and WARD, J. C. *Proc. Roy. Soc. A*, 1963, **271**, 357
[4] THOMAS, J. M. and WILLIAMS, J. O. *Trans. Faraday Soc.* 1967, **63**, 1922
[5] SELLA, C. and TRILLAT, J. J. *C.R. Acad. Sci., Paris*, 1961, **253**, 1511
[6] SELLA, C. and BENSASSON, R. *J. Polym. Sci.* 1962, **56**, S1

[7] BASSETT, D. C. *Nature, Lond.* 1967, **215,** 731
[8] OKAMURA, S., HAYASHI, K. and KITANISHI, Y. *J. Polym. Sci.* 1962, **58,** 925
[9] BAMFORD, C. H., EASTMOND, G. C. and SAKAI, Y. *Nature, Lond.* 1963, **200,** 1284
[10] BAMFORD, C. H., BIBBY, A. and EASTMOND, G. C. *J. Polym. Sci. C,* 1967, **16,** 2417
[11] SYMONS, M. C. R. *J. chem. Soc.* **1963,** 1186
[12] FISCHER, H. *Z. Naturf.* 1964, **19a,** 866
[13] O'DONNELL, J. H., MCGARVEY, B. and MORAWETZ, H. *J. Amer. chem. Soc.* 1964, **86,** 2322
[14] ADLER, G. and PETROPOULOS, J. H. *J. phys. Chem.* 1965, **69,** 3712
[15] SHIOJI, Y., OHNISHI, S. I. and NITTA, I. *J. Polym. Sci. A,* 1963, **1,** 3373
[16] DAVYDOV, A. S. *Theory of Molecular Excitons,* translated by KASHA, M. and OPPENHEIMER, M. McGraw-Hill: New York and London, 1962

The Polymerization of Crystalline Methacrylic Acid Initiated by Ultra-violet Radiation II—The Effect of Added Isobutyric Acid on Radical Conformations and Rates of Reaction

C. H. BAMFORD, A. BIBBY* and G. C. EASTMOND

The influence of low concentrations of isobutyric acid in methacrylic acid crystals on the radical concentrations and conformations observed during irradiation with ultra-violet light at temperatures below −20°C has been studied. The additive, which is not chemically active, increases the density of sites in which there is adequate molecular mobility for reaction, and also changes the distribution of mobility in these sites. As a result, radical formation and relaxation occur more readily in the presence of the additive. At somewhat higher temperatures (−14°C), higher rates of polymerization, and higher molecular weights, are obtained in the presence of isobutyric acid.

IN Part I[1] we discussed the solid phase polymerization of methacrylic acid crystals in terms of radical formation and reaction in imperfect regions of the crystals. If these processes occur exclusively in such regions one would expect them to be very sensitive to the presence of trace impurities, which would be concentrated in the imperfections. There are various reports in the literature on the influence of chemically inert additives on the course of solid state polymerizations of vinyl monomers[2–5], but these usually refer to additive concentrations exceeding one per cent. The polymerizations of crystalline cyclic monomers have been shown to be sensitive to the presence of reactive impurities[6, 7] such as water, in low concentrations (~0·1 per cent), and the irreproducibility of the kinetics observed in the polymerization of crystalline trioxan[8] may be at least partly due to slight differences in purity. In this paper we discuss effects on the solid state polymerization of methacrylic acid resulting from the addition of low concentrations of isobutyric acid (the saturated analogue of methacrylic acid) before crystallization. This compound is relatively inert chemically, and any effect it produces must be physical in origin.

EXPERIMENTAL

Methacrylic acid, ICI Ltd (Mond Division), was purified as described previously[9]. Isobutyric acid, L. Light and Co. Ltd, was dried with molecular sieve type 4A and distilled; the fraction distilling at 154° to 155°C was collected.

Solutions of isobutyric acid in methacrylic acid were prepared in the dry-box. Samples for e.s.r. studies were prepared according to the procedure described in the previous paper[1]. The same procedure was adopted in

*Present address: North Staffordshire College of Technology, Stoke-on-Trent.

preparing specimens for estimations of polymer yields and reduced viscosities except that the e.s.r. tube was replaced by a silica tube of 1 cm internal diameter, and 5 ml samples of monomer were used. All samples were crystallized in a bath at − 196°C.

Ultra-violet irradiations were carried out as described previously[10]. Radical concentrations and values of the parameter X/Y quoted in *Figures 2* and *3* were determined from e.s.r. spectra obtained with the Varian E-3 spectrometer as described in the previous paper[1]. The data quoted in *Figure 1* were obtained from spectra recorded on a V 4500 spectrometer, employing 100 kc/s modulation, but an unknown modulation amplitude. The values of X/Y quoted in *Figure 1* of this paper cannot therefore be compared directly with those of *Figure 3* or of the previous paper[1].

Polymer yields were determined by extracting residual monomer with cold (− 14°C) ether containing pyrogallol as inhibitor.

Viscosities of 0·004% w/v solutions of polymer in 0·006 N aqueous sodium hydroxide solution were determined with a simple Ostwald viscometer.

The purity of methacrylic acid was examined by gas–liquid chromatography after conversion to the methyl ester by reaction with diazomethane. The chromatographic column was four feet long and contained 10% w/w polyethylene glycol adipate supported on 120 mesh Celite. All chromatograms showed a very small peak corresponding to the retention time of methyl isobutyrate. Addition of known amounts of isobutyric acid to the methacrylic acid showed that the quantity of the former present as impurity was significantly less than the amounts used in the experiments to be described.

Microscopic examination failed to show the presence of any liquid at − 15°C in specimens containing up to 3% v/v isobutyric acid.

RESULTS AND DISCUSSION

(1) *Effect on radical concentrations and conformations*

Figure 1 shows that the total radical concentration formed by irradiation for 11 h at − 14°C increases rapidly as the initial concentration of isobutyric acid is increased. At the same time the ratio X/Y falls off markedly, and becomes close to zero for an isobutyric acid concentration of one per cent by volume. Earlier experiments[10], over a limited range of concentrations and made with a less sensitive e.s.r. spectrometer, did not reveal this trend in X/Y. The development of the radical concentration with time of irradiation at − 50°C for different concentrations of isobutyric acid up to 0·1% v/v is indicated in *Figure 2*. Under these conditions polymerization is extremely slow and the results are not complicated by polymer formation. Although the limiting radical concentrations are not reached in *Figure 2*, it seems likely that these increase with the concentration of additive over the range studied. The addition of isobutyric acid must, therefore, increase the density of imperfections which are capable of supporting reaction; in terms of the model proposed in Part I (§5)[1], this is equivalent to an increase in $[S]_0$. However, the initial rates of radical formation are even more sensitive; for example, an isobutyric acid concentration of 0·02 per cent increases the rate approximately threefold. This implies that not only is there an increase in the number of active imperfections, but also that there are some imperfec-

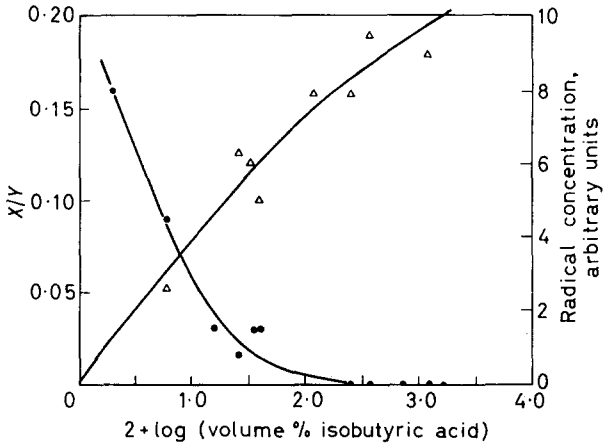

Figure 1—Dependence of radical concentration [R·], △, and X/Y, ●, on isobutyric acid concentration in crystals; 11 h irradition at −14°C

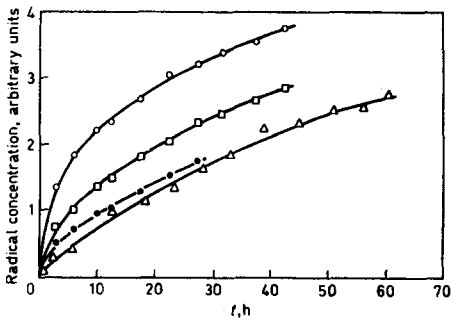

Figure 2—Radical concentration as a function of time of irradiation at −50°C. Isobutyric acid contents of crystals are: △ 0%; ● 0·02%; □0·06%; ○0·10%

Figure 3—Dependence of X/Y on time of irradiation at −50°C. Isobutyric acid contents of crystals: △ 0%; ● 0·02%; □ 0·06%; ○ 0·10%

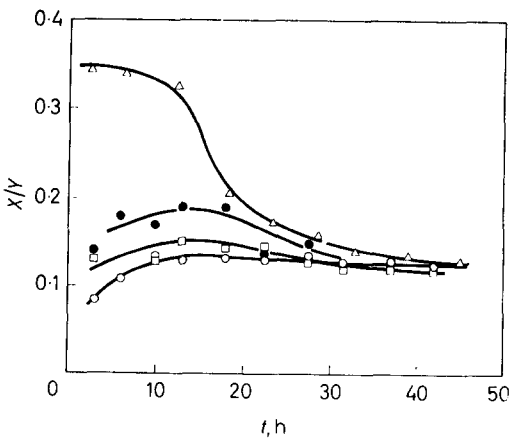

tions in which radical formation occurs extremely readily in the presence of isobutyric acid.

The high molecular mobility in these latter imperfections is shown by the low values of X/Y at short irradiation times (*Figure 3*). As the irradiation time is increased, all the samples in *Figure 3*, including that in which no isobutyric acid is present, approach the same value of X/Y, suggesting that under these conditions all the imperfections have the same character, within the limits of differentiation obtainable in this kind of experiment. The high mobility observable in the early stages of polymerization, e.g. with 0·10 per cent isobutyric acid present, must, therefore, disappear. There are at least two mechanisms by which this could occur. Initially, the additive is concentrated in the central regions of the imperfections but, as polymerization proceeds in these regions, it will become detached from the lattice and adsorbed on to the polymer to a steadily increasing extent. The interface between the polymer and the lattice will gradually extend into more ordered regions where the concentration of isobutyric acid is low, so that the additive has a progressively decreasing effect on the process of radical formation. In the limit, the formation of T radicals and their relaxation to the N form will be governed by the processes already described for the pure monomer[1], so that the same value of X/Y is reached in all cases. A possible, but less likely, alternative is that during reaction the isobutyric acid diffuses along imperfections into regions of low concentration, to give an average concentration that is too low to be detected in these experiments.

In the early stages of irradiation most of the radicals are formed in imperfections where the molecular mobility is highest. Probably these imperfections soon became saturated with radicals, new radicals formed entering into termination reactions as described in Part I[1], so that a stationary radical concentration and a low value of X/Y are achieved in a fraction of the imperfections. At intermediate times of irradiation (5 to 15 h) a significant fraction of the radicals originates in imperfections in which the mobility is lower and such radicals, having a high X/Y ratio, are responsible for the observed rise in X/Y in the presence of isobutyric acid. A similar phenomenon in the pure monomer would account for the retention of high values of X/Y during the first ten hours of irradiation (Part I, § 5)[1]. *Figure 2* shows that, in specimens containing isobutyric acid, the rapid increase in radical concentration soon gives way to a rate of increase which is comparable to that found in pure monomer. This observation also reflects the existence of reaction sites with molecular mobilities distributed over a wide range.

The high molecular mobility in reaction sites attributed to the presence of isobutyric acid would correspond to a large increase in the relaxation parameters k_r, k (Part I, § 5)[1]; from the calculations presented in Part I it is clear that at short irradiation times this would result in low values of [T·]/[R·], (i.e. X/Y), as observed. However, according to the views expressed above, the subsequent increase in X/Y as irradiation proceeds arises from decreases in k_r, k with increasing extent of reaction, and these are not allowed for in the model of Part I.

(2) *Effect on rates and degrees of polymerization*

The conversion and the reduced viscosities of the polymers formed after irradiation at − 14°C for 6 h are shown in *Figures 4* and *5*. We must point out that these experiments at − 14°C (unlike those at − 50°C) lead to comparatively high conversions, particularly in the presence of isobutyric acid. As the monomer absorbs the incident light strongly, polymerization at any instant is confined to a thin reaction zone which gradually traverses the specimen[9]. It is easily seen from the extents of conversion that in the polymerizations in *Figure 4* the reaction zone must have progressed into the

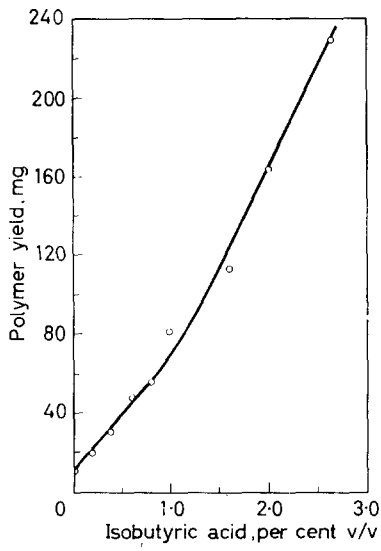

Figure 4—Dependence of polymer yield on isobutyric acid content of crystals. Irradiation of 5g of monomer at −14°C for 6 h

interior of the specimen. The mean rates of polymerization calculable from *Figure 4* are, therefore, lower than the initial rates. The complex nature of the reaction under conditions of high conversion makes quantitative discussion of the results pointless. Nevertheless, it is qualitatively clear that both the rates of polymerization and the molecular weights of the polymers are increased markedly by the addition of low concentrations of isobutyric acid. These results support the views already expressed. The higher molecular mobility in the neighbourhood of the radicals resulting from the presence of the additive would be expected greatly to increase the rate of propagation, i.e. the effective mean propagation coefficient, so that higher polymers and higher overall rates are produced. Some of the increase in rate may also be attributable to the increased density of imperfections. The possibility of chain transfer to polymer, leading to branching and crosslinking, cannot be excluded.

It is important to realize that at these low temperatures the molecular mobility in methacrylic acid crystals, even in imperfect regions, is low; consequently increases in mobility brought about by the addition of impurities have a dominating effect. At higher temperatures, when the molecular mobility is much greater (unpublished results of B. Arnold and G. C.

Eastmond), additives may not increase the rate of polymerization to a comparable extent. This is illustrated by the results at 4°C quoted in Part III of this series[11].

Other workers have examined the effects of additives on solid state polymerizations, but generally at much higher concentrations. However, the views expressed above may still be applicable to systems in which the

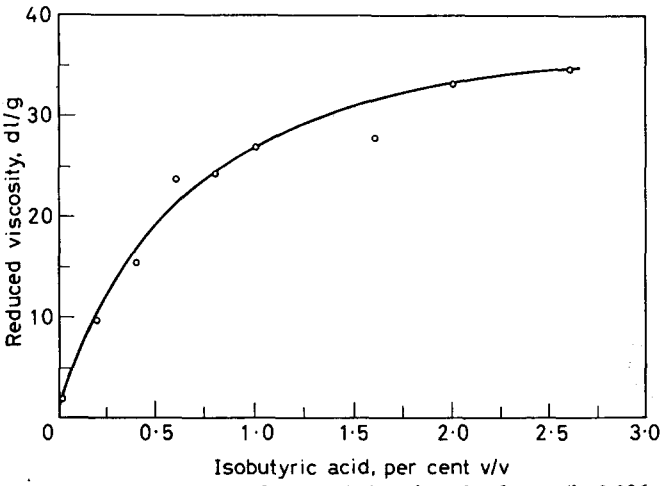

Figure 5—Dependence of reduced viscosity of polymer (in 0·006 N aqueous sodium hydroxide) on isobutyric acid content of crystals

additive is incorporated in the monomer lattice as a solid solution. The polymerization of acrylamide in its solid solutions with propionamide has been studied by Fadner and Morawetz[2], and by Adler and Reams[3]. The relevant work has been carried out at 25°C. Fadner and Morawetz found that the presence of ten per cent propionamide has no effect on the rate of fractional conversion in the post-irradiation polymerization, although the degrees of polymerization are greatly reduced. At higher concentrations—up to 50 per cent propionamide—the initial rates of conversion, expressed as fractions of the initial monomer present reacting in unit time, remain sensibly constant, but after about ten per cent conversion the rates are lower than those in the pure monomer. In all cases the degrees of polymerization are reduced. On the basis of these results Fadner and Morawetz proposed that, under their conditions, propionamide acts as an active transfer agent[2]; it was stated that the activity diminishes with increasing temperature. Adler and Reams[3] showed that in all solid solutions containing more than ten per cent acrylamide the conversion ultimately reached 100 per cent on irradiation; even solid solutions containing four per cent acylamide gave 60 per cent conversion. Adler and Reams isolated the polymers by extraction of residual monomer with methanol[3]. By using the same extraction procedure, Baysal *et al.*[12] failed to observe the formation of polymers with molecular weights less than 9 000 from pure acrylamide; Adler and Reams[3] therefore argued that if this arises from solubility of lower polymers in methanol, the

polymers obtained in the solid solution experiments must have had molecular weights in excess of 9 000. This result is clearly incompatible with extensive chain transfer.

It is necessary to consider the mechanism by which such low concentrations of monomer are able to polymerize so extensively in the crystals. Although diffusion of acrylamide through the perfect lattice is improbable, diffusion along the interface between the amorphous polymer and the lattice was postulated by Adler and Reams[3]; in this way the monomer could be brought into contact with radicals formed in imperfections and hence enabled to react. Another factor that could well be important in systems containing only low concentrations of acrylamide is the concentration of monomer around the dislocation lines, in the manner of a Cottrell cloud[13]. Acrylamide molecules in these regions may have sufficient mobility to allow polymerization to occur. Some of the monomer would be situated in the more perfect regions of the lattice and would be comparatively immobile; thus limiting conversions would be expected in systems containing low concentrations of acrylamide.

We suggest that the low molecular weights obtained in the presence of propionamide can be explained without invoking extensive transfer to the additive. It is generally agreed that γ-initiation is brought about by radiolytic hydrogen atoms, which can diffuse through the crystal and become trapped in imperfections. However, unlike the excitons in our studies of the u.v.-initiated polymerizations of crystalline methacrylic acid, these small hydrogen atoms may add to any acrylamide molecule in the lattice. If it is accepted that only radicals and monomer molecules in certain sites can give rise to high polymers, then many initial radicals situated in more ordered regions of the lattice will be unable to react. It might be expected that the number of such 'unreactive' radicals will be greater in the presence of propionamide, since it is known that this additive gives rise to high yields of radiolytic hydrogen[4] and high radical concentrations in the solid solutions[14]. These radicals, however, may be able to terminate and initiate polymerization as reaction proceeds to high conversion. Thus, if the rate of polymerization is related to the initial density of reactive sites the rate of polymerization may not be significantly affected by the presence of propionamide, but the degree of polymerization may be considerably reduced.

Department of Inorganic, Physical and Industrial Chemistry,
University of Liverpool, Liverpool.

(*Received March 1968*)

REFERENCES

[1] BAMFORD, C. H., BIBBY A. and EASTMOND, G. C. *Polymer, Lond.* 1968, **9**, 629
[2] FADNER, T. A. and MORAWETZ, H. *J. Polym. Sci.* 1960, **45**, 475
[3] ADLER, G. and REAMS, W. *J. Polym. Sci. A*, 1964, **2**, 2617
[4] ADLER, G., BALLANTINE, D., DAVIS, T. and RANGANTHAN, R. *J. phys. Chem.* 1964, **68**, 2184
[5] KAETSU, I., SAGANE, N., HAYASHI, K. and OKAMURA, S. *J. Polym. Sci. A-1*, 1966, **4**, 2241
[6] MARANS, N. S. and WESSELLS, F. A. *J. appl. Polym. Sci.* 1965, **9**, 3681
[7] KAGIYA, T., IZU, M. and FUKUI, F. *Makromol. Chem.* 1967, **102**, 39

[8] RAO, H. and BALLANTINE, D. S. *J. Polym. Sci. A*, 1965, **3**, 2579
[9] BAMFORD, C. H., EASTMOND, G. C. and WARD, J. *Proc. Roy. Soc. A*, 1963, **271**, 357
[10] BAMFORD, C. H., BIBBY, A. and EASTMOND, G. C. *J. Polym. Sci. C*, 1967, **16**, 2417
[11] BAMFORD, C. H., BIBBY, A. and EASTMOND, G. C. *Polymer, Lond.* 1968, **9**, 645
[12] BAYSAL, B., ADLER, G., BALLANTINE, D. and GLINES, A. *J. Polym. Sci. B*, 1963, **1**, 257
[13] COTTRELL, A. H. *Dislocations and Plastic Flow in Crystals*, Oxford University Press: London, 1953
[14] ADLER, G. and PETROPOULOS, J. H. *J. phys. Chem*, 1965, **69**, 3712

The Polymerization of Crystalline Methacrylic Acid Initiated by Ultra-violet Radiation III—The Pressure Effect

C. H. BAMFORD, A. BIBBY* and G. C. EASTMOND

The influences of low concentrations of isobutyric acid, and of changes of temperature, on the sensitivity of the photopolymerization of methacrylic acid crystals to small applied stresses have been examined. A concentration of approximately 0·3% v/v isobutyric acid effectively removes the pressure effect (for a pressure of approximately 10 atm) at 4°C. Reduction in temperature to −14°C also eliminates the pressure effect, but at this temperature addition of isobutyric acid causes its reappearance. It is envisaged that the reaction takes place in dislocations and that application of stress reduces the molecular mobility in the neighbourhood of propagating radicals, e.g. by movement of dislocations, to such an extent that reaction cannot occur. The additive counteracts the effect of stress by increasing the molecular mobility. At low temperatures, in the absence of additive, the crystals are too hard for the low stresses used to be effective. The pressure effect in the pure monomer is sensitive to the magnitude of the applied stress.

IN Part II[1] we have shown that low concentrations of isobutyric acid exercise a remarkable effect on the radical conformations and rates of polymerization observed during the ultra-violet irradiation of crystalline methacrylic acid. The results are consistent with the view that the additive is located in crystal imperfections which are also the sites of radical formation and polymerization. We reported in an earlier publication[2] that the sensitivity of the system to comparatively small unidirectional mechanical stresses demonstrates the important part played by imperfections, probably dislocations, in these solid phase reactions. Since this work there have been several investigations[3–6] of the effect of pressure on solid phase polymerization, generally with higher pressures, in the range 5 000 to 36 000 atm. Both increases and decreases in the rate of polymerization with applied stress have been recorded[3–6], and in some cases the effect changes sign with increasing conversion[4]. As a rule, the observations made at these pressures are considered to be consistent with previously expressed views about the nature of the reactions. Thus, when imperfections have been invoked, decreases in rate in the early stages of reaction have been attributed to the maintaining of crystallinity of the monomer[4]; the same factor has been held responsible for increases in the rate of reaction of monomers of which the polymerization was supposed to occur preferentially in the lattice[7]. In our opinion, the existence of this latter type of polymerization is now very doubtful. The relatively small effects of high pressures on the polymerization of monomers such as acrylamide[3–5], calcium acrylate[4], barium methacrylate[4], and methacrylonitrile[6] contrast with the sensitivity of the reactions of acrylic and methacrylic acids to low pressures under our conditions[2]. It would appear that high and low pressures affect the crystals and the course of polymeriza-

*Present address: North Staffordshire College of Technology, Stoke-on-Trent.

tion in different ways, which require different mechanisms for their interpretation.

In the present paper we describe a continuation of our low-pressure investigations, with particular reference to the effects of additives and changes in temperature on the sensitivity of the system to pressure. We have also made a few measurements with different magnitudes of the applied stress.

EXPERIMENTAL

Methacrylic acid and isobutyric acid were purified as described previously[1,2].

Experiments were carried out to determine the influence of small concentrations of isobutyric acid on the solid state polymerization of methacrylic acid crystals at various temperatures and under small mechanical stresses. For this purpose samples of monomer, with or without additive, in the form of thin (10 to 20μ) layers of non-overlapping single crystals were prepared by freezing degassed samples of monomer between a quartz plate and a cover-slip in a suitable cell which has been described in detail in an earlier paper[2]. With this cell only a rough estimate of the stresses applied to the crystals could be obtained. To obtain a more accurate estimate of the stresses and to investigate the effect of varying the stress a second cell (*Figure 1*) was constructed, as described below.

The main body of the cell A was fixed to the base E, with an O-ring to form a seal. A quartz window D was fixed to base E with a retaining ring; an O-ring formed the seal between D and E. Copper bellows F (maximum pressure 170 lb/in^2) were soft-soldered to E and to the ring G, which was fitted with a quartz window H fixed to G by the sample carriage J; the seal between H and G was made with an O-ring. The specimen consisted of a thin layer of single crystals situated between the quartz disc K and cover-slip L. Above the sample was situated a glass block P fixed to the top-plate O by a retaining ring N, with an O-ring forming a seal between O and P. The top-plate O was also fitted with a glass window Q, held in position by a retaining ring; an O-ring formed a seal between O and Q. The top-plate O was fixed to A, with an O-ring to form a seal. A channel M provided a means of cooling the cell to crystallize the monomer and also allowed cooling of the cell when situated on the microscope. The cell was evacuated through tube R which terminated in a standard cone and was fitted with a glass tap. The pressure in the interior of the bellows could be adjusted by means of the hole B and the needle-valve C. The cell was constructed so that the cover-slip L over the sample was situated just below the glass block P when the pressures in the body of the cell and inside the bellows were equal. During the degassing of monomer by the freeze, pump, thaw technique, the interiors of both the cell and the bellows were evacuated. After degassing, the monomer was finally frozen and the cell and bellows were filled with nitrogen to atmospheric pressure. Stresses were applied to the samples by increasing the nitrogen pressure in the bellows, i.e. between H and D, until cover-slip L made contact with P, and subsequently increasing the pressure in the bellows by the required amount. Samples of monomer were introduced into the cell and irradiation was carried out as described in an earlier paper[2]. A special carriage was constructed to allow the cell to

be used in conjunction with the mechanical stage of the polarizing microscope.

Measurements of the optical retardation of individual crystals were made using a Berek compensator in conjunction with a Leitz 'Ortholux' polarizing microscope.

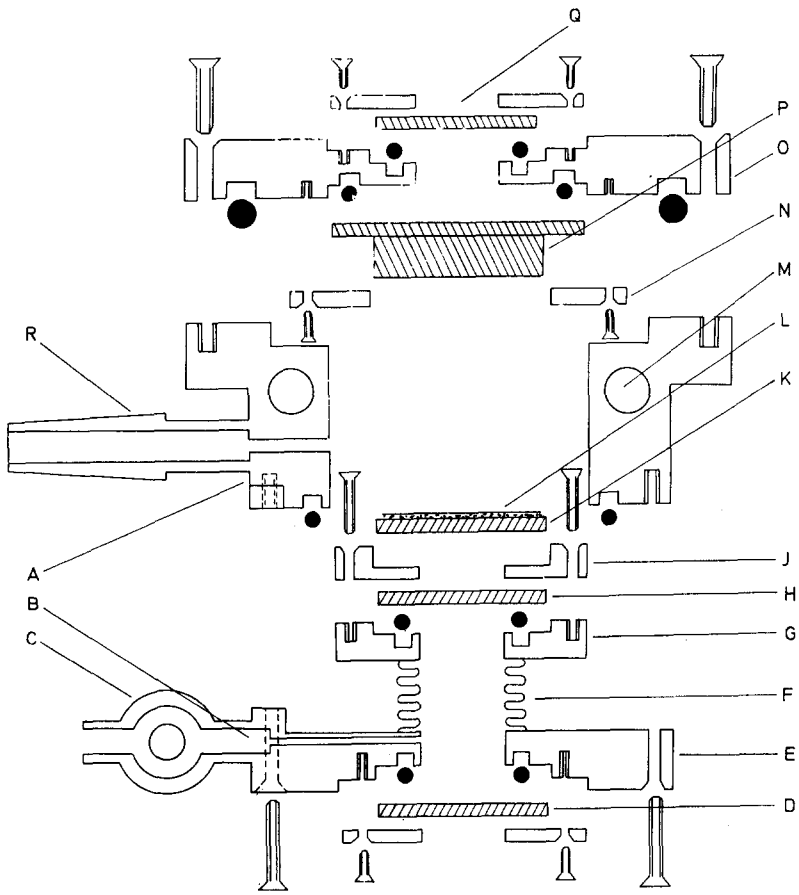

Figure 1—Apparatus for determination of pressure effects

RESULTS AND DISCUSSION

(1) *The effect of isobutyric acid at 4°C*

When a single crystal of methacrylic acid is irradiated by ultra-violet light, the optical retardation/time curve is sigmoid in shape. *Figure 2* shows the effect of applying a stress of approximately 10 atm in the early stages of reaction (approximately 20 per cent conversion) at points marked A. In the absence of any additive the reaction is almost brought to a halt immediately the stress is applied, and continues at a very low rate during continued irradiation. On removing the stress at point B the reaction rapidly resumes the rate observed just before the point A. These results are reminiscent of

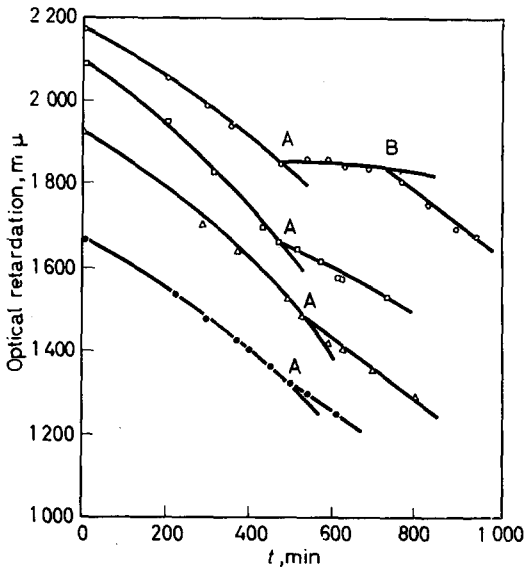

Figure 2—Dependence of pressure effect on isobutyric acid content of crystals. Pressure (approximately 10 atm) applied at points A and removed at B. Isobutyric acid contents: ○, 0%; □, 0·1%; △, 0·2%; ●, 0·3%

Table 1. The pressure effect at 4°C

Isobutyric acid concentration, % v/v	0	0·1	0·2	0·3
Pressure effect; pressure = 10 atm approximately	18·5	1·02	0·46	0·19

observations previously made at 7°C[2]. Addition of isobutyric acid before crystallization is seen to reduce the effect of stress dramatically (*Figure 2*). We may define the pressure effect quantitatively as the ratio ($\geqslant 1$) of the slopes of the curves close to and on either side of point A, minus one. According to this definition the value zero signifies the absence of a pressure effect. Numerical values of this quantity are given in *Table 1* for isobutyric acid concentrations up to 0·3% v/v. The extreme sensitivity of the pressure effect to the presence of isobutyric acid provides convincing evidence that the polymerization is associated with imperfections in the crystal. The origin of the pressure effect must lie in a reduction in the molecular mobility in the regions of propagating radicals brought about by the applied stress. We have previously suggested[2] that the imperfections with which we are concerned are dislocations, which can be moved away from growing chains by the application of stress. The polymer molecules must, of course, remain in imperfect regions of the crystal, but we assume that the monomer molecules in such regions are not sufficiently mobile to allow reaction at a significant rate. Possibly in absolutely pure methacrylic acid the pressure effect would be infinitely large, as previously reported for acrylic acid[2], in which no polymerization is observed when stress is applied. The dislocations that are displaced by stress will pile up against suitable obstacles, e.g. grain boundaries or perhaps non-propagating portions of polymer molecules, and in

these regions the monomer molecules would appear to have insufficient mobility for reaction. The overall effect of the stress is thus considered to be a reduction in molecular mobility.

Two types of explanation of the effect of isobutyric acid may be devised. The additive may effectively pin the dislocations by a Cottrell cloud mechanism[8], or, alternatively, it may induce the onset of pre-melting. This would have an effect similar to raising the temperature of the specimen; we have already shown[2] that with acrylic acid an increase in temperature from 4° to 7°C (the latter temperature being in the pre-melting region) reduces the pressure effect from infinity to zero. We shall see later that it is possible to distinguish experimentally between the two alternative hypotheses.

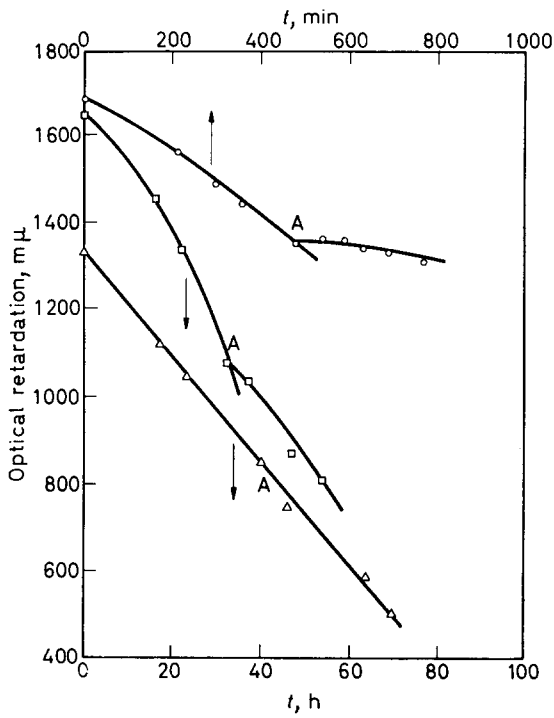

Figure 3—Dependence of pressure effect on temperature of irradiation. Pressure (approximately 10 atm) applied at points A. ○, +4° C; □, −10°C; △, −14°C

(2) *The influence of temperature on the pressure effect*

As the temperature of irradiation is reduced below 4°C the sensitivity of the polymerization to applied stress is found to decrease (*Figure 3*). *Table 2* gives numerical values derived from the results in *Figure 3*. This loss of

Table 2. The pressure effect at different temperatures

T, °C	4	−10	−14
Pressure effect; pressure = 10 atm approximately	18·5	1·9	0

sensitivity may be attributed to the increased hardness of the crystal at the lower temperatures. Larger stresses would be required to move dislocations at these lower temperatures and hence cause a reduction in the rate of reaction.

(3) *The effect of isobutyric acid at − 14°C*

It will be apparent from *Figure 4* and *Table 3* that the addition of 0·1 per cent isobutyric acid enables a pressure effect to be observed at − 14°C. Further addition of isobutyric acid up to 0·5 per cent brings about a diminution in the effect.

Table 3. The pressure effect at −14°C

Isobutyric acid concentration, % v/v	0	0·1	0·5
Pressure effect; pressure = 10 atm approximately	0	4·1	1·1

The reappearance of the pressure effect in the presence of isobutyric acid is difficult to explain if the additive immobilizes dislocations. Consequently we believe that the second alternative in § 1 is the correct one, and that the

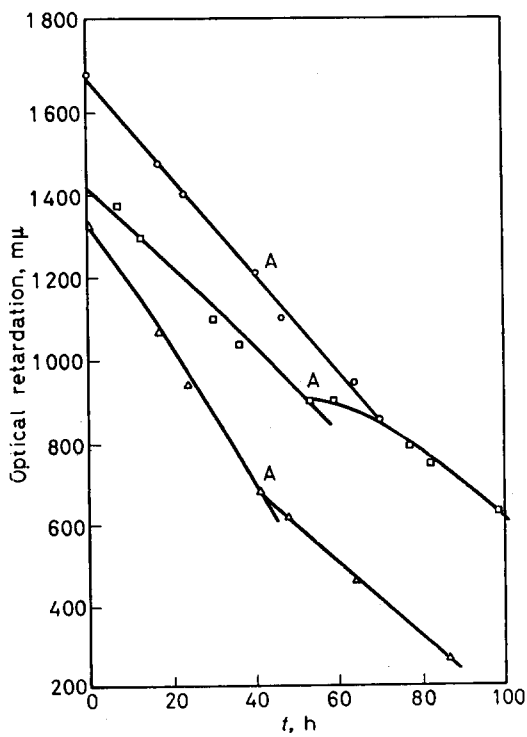

Figure 4—Dependence of pressure effect at −14°C on isobutyric acid content of crystals. Pressure (approximately 10 atm) applied at points A. Isobutyric acid contents: ○, 0%; □, 0·1%; △, 0·5%

effect of isobutyric acid is to increase the general molecular mobility and so reduce the hardness of the crystal. The failure of the Cottrell cloud mechanism to pin down the dislocations is probably a result of the fact that the temperatures are comparatively close to the melting point, so that thermal motions are large enough to permit dislocations to leave their impurity clouds[8]. At concentrations of isobutyric acid in the region of 0·5 per cent the high molecular mobility becomes of dominating importance, and the sensitivity of the reaction to stress falls according to the mechanism described in § 1.

(4) *Effect of magnitude of stress*

As would be expected, the pressure effect diminishes as the magnitude of the applied stress is reduced (*Figure 5*). Numerical values are given in

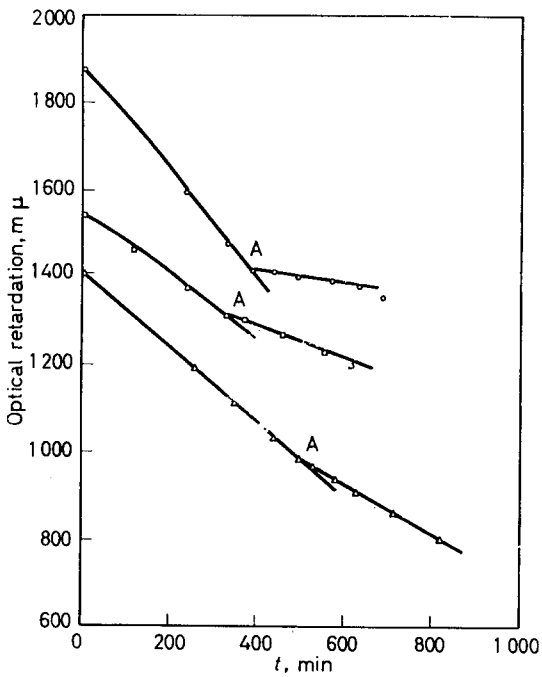

Figure 5—Effect of magnitude of stress on pressure effect at +4°C. Pressures applied at points A: ○, 165; □, 130; Δ, 85 lb/in²

Table 4; the conversions stated are those holding when the stress was first applied. The similarity of the conversions in the first and third experiments shows that the effects observed are not attributable to differences in conversion. It would seem that pressures of approximately 165 lb/in² are

Table 4. The pressure effect at different stresses at 4°C

Stress, lb/in²	*Pressure effect*	*Conversion %*
165	18·5	25
130	1·24	13
85	0·54	28

required to move the majority of dislocations in which the reaction is proceeding. Lower pressures are able to move only a small fraction of such dislocations—presumably those occurring in slip planes where movement is easiest.

Rather similar observations have already been reported[2] for acrylic acid crystals at 4°C, although in this case the estimated stresses were only approximate and were probably too small by a factor of two.

Isobutyric acid is commonly present as an impurity in commercial methacrylic acid and complete purification by physical methods is difficult. The monomer used for the above work probably contains a minute concentration of isobutyric acid, since it was just possible to observe a peak corresponding to this substance by vapour phase chromatography[1]. The concentration must have been much less than 0·1 per cent. In view of the sensitivity of the pressure effect to the presence of isobutyric acid it would seem possible that an infinite pressure effect would be obtained in absolutely pure monomer with a stress of 165 lb/in^2. The lower pressures might also be more effective.

GENERAL CONCLUSIONS (PARTS I[9], II[1], III)

(1) The addition before crystallization of low concentrations of isobutyric acid—a chemically inactive compound—has been shown to exert a large influence on the concentration and conformation of free radicals formed during irradiation of methacrylic acid crystals with ultra-violet light, and on the sensitivity of the polymerization to low applied stresses. These observations show that radical formation and reaction occur preferentially in regions of the crystals in which the additive is also located, and we believe these to be dislocations. The new data thus reinforce our earlier opinion that this solid phase polymerization is restricted to crystal imperfections[2].

(2) The rate of radical formation and the course of reaction are functions of the numbers of suitable sites (in crystal imperfections) and their character, in particular the associated molecular mobility.

(3) The rate of the radical relaxation T$\rightarrow$N is a measure of the local molecular mobility.

(4) Data on radical concentrations and conformations are consequently able to provide information about the density of suitable sites and the prevailing molecular mobility. It appears that, in a given crystal, an increase of temperature increases the density and mean mobility. These properties are influenced by the crystallization procedure; crystallization in a bath at -196°C gives a relatively high density of sites with rather low mobility.

(5) The incorporation of low concentrations of isobutyric acid in the crystals produces large increases in the molecular mobility in the reaction sites, and also increases the density of sites suitable for reaction. Under these conditions there is clear evidence for the existence of sites having very different mobilities. During irradiation the average mobility changes, due, we believe, to a tendency for isobutyric acid to become adsorbed on the polymers formed.

(6) Evidence has been adduced in support of the view that light of $\lambda > 3\,000$Å, which does not produce free radicals, increases the rates of some free radical processes in the crystal, notably relaxation and propaga-

tion. This phenomenon is probably the result of the localization of excitons at imperfections, followed by their decay to thermal energy[10] which accelerates the reactions.

(7) When conversion to polymer becomes appreciable, the stresses set up in the crystal probably lead to dislocation multiplication so that the site density is increased. Thus, ultimately, 100 per cent conversion to polymer becomes possible.

Department of Inorganic, Physical and Industrial Chemistry,
University of Liverpool, Liverpool.

(*Received March 1968*)

REFERENCES

[1] BAMFORD, C. H., BIBBY, A. and EASTMOND, G. C. *Polymer, Lond.* 1968, **9**, 645
[2] BAMFORD, C. H., EASTMOND, G. C. and WARD, J. C. *Proc. Roy. Soc. A*, 1963, **271**, 357
[3] TABATA, Y. and SUZUKI, T. *Polymer Preprints*, 1964, **5**, 997
[4] FYDELOR, P. J. and CHARLESBY, A. Paper presented at IUPAC Symposium, Prague, 1965
[5] PRINCE, M. and HORNYAK, J. *J. Polym. Sci. B*, 1966, **4**, 493; *J. Polym. Sci. A1*, 1967, **5**, 531
[6] SUZUKI, T., TABATA, Y. and OSHIMA, K. *J. Polym. Sci. C*, 1967, **16**, 1821
[7] LANDO, J. B. and MORAWETZ, H. *J. Polym. Sci. C*, 1964, **4**, 789
[8] COTTRELL, A. H. *Dislocations and Plastic Flow in Crystals*, Oxford University Press: London, 1953
[9] BAMFORD, C. H., BIBBY, A. and EASTMOND, G. C. *Polymer, Lond.* 1968, **9**, 629
[10] DAVYDOV, A. S. *Theory of Molecular Excitons*, translated by KASHA, M. and OPPENHEIMER, M. McGraw-Hill: New York and London, 1962

Classified Contents

Author Index

Author Index